DOE Award No: DE-FC26-08NT0005643

Final Report

Geomechanical Study of Bakken Formation for Improved Oil Recovery

Submitted by:

Kegang Ling (Principal Investigator, July 1, 2012-December 31, 2013)
Zhengwen Zeng* (Principal Investigator, October 1, 2008- June 30, 2012)
University of North Dakota
Department of Petroleum Engineering
243 Centennial Drive, Stop 8154
Grand Forks, ND 58202-8154
(* now with BP America, Inc.)

Major Contributors:
Jun He
Peng Pei
Xuejun Zhou
Hong Liu
Luke Huang
Mehdi Ostadhassan
Hadi Jabbari
Derrick J Blanksma
Harry Feilen
Salowah Ahmed

Senior Members
Steve Benson
Michael Mann
Richard LeFever
Will Gosnold

Period of Performance (10/1/2008 - 12/31/13)
Final Report Written by: Kegang Ling, Zhengwen Zeng, Jun He, and Peng Pei

Prepared for:

John R. Terneus (Project Manager)
U. S. Department of Energy
National Energy Technology Laboratory

December 31, 2013

FINAL REPORT

DOE Award No: DE-FC26-08NT0005643
Name of recipient: University of North Dakota
Department of Petroleum Engineering
243 Centennial Drive, Stop 8154
Grand Forks, ND 58202-8154
Project title: Geomechanical Study of Bakken Formation for Improved Oil Recovery
Principal investigators: Kegang Ling, Zhengwen Zeng
Date of report: December 31, 2013

DISCLAIMER

This report was prepared as an account of work sponsored by an agency of the United States Government. Neither the United States Government nor any agency thereof, nor any of their employees, makes any warranty, express or implied, or assumes any legal liability or responsibility for the accuracy, completeness, or usefulness of any information, apparatus, product, or process disclosed, or represents that its use would not infringe privately owned rights.

Reference herein to any specific commercial product, process, or service by trade name, trademark, manufacturer, or otherwise does not necessarily constitute or imply its endorsement, recommendation, or favoring by the United States Government or any agency thereof. The views and opinions of authors expressed herein do not necessarily state or reflect those of the

United States Government or any agency thereof.

ACKNOWLEDGEMENTS

This report is based upon work supported by the U.S. Department of Energy National Energy Technology Laboratory under Award Number DE-FC26-08NT0005643.

The project team at The University of North Dakota would like to thank U.S. Department of Energy National Energy Technology Laboratory for sponsoring this study, and the Wilson M. Laird Core and Sample Library,The North Dakota Geological Survey for providing core samples and other information for this study.

We also wish to expresses gratitude to Department of Petroleum Engineering and Department of Geology and Geological Engineering at The University of North Dakota for various administrative support to this project.

Table of Contents

ACKNOWLEDGEMENTS 4
EXECUTIVE SUMMARY 8
1. INTRODUCTION 9
1.1. Background 9
1.2. Williston Basin 9
1.3. Bakken Formation 11
1.4. Horizontal Drilling and Fracturing Technology 12
2. GOALS AND OBJECTIVES 13
2.1. Challenges in Exploration and Production 13
2.2. Current State-of-the-Art 13
2.3. Benefits and Inadequacies of Current Technology 13
2.4. Problems to be Addressed 14
2.5. Impact on the U.S. Oil and Gas Industry 16
3. Petroleum Geological Model of Bakken Formation 17
3.1. Study Area and Wells Used for Geological Model 17
3.2. Work Procedure 19
3.3. Geological Modelling 23
4. Minor and Micro Structures Analysis 29
4.1. Rock Quality Designation (RQD) Based Bakken Formation Minor and Micro Fracture System 29
4.2. Bakken Wells Production Performance and RQD 43
5. Mapping of Paleo In-Situ Stresses 53
5.1. Geological Settings 53
5.2. Tectonic History of the Basin 54
5.3. Tectonic History of the Nesson Anticline 57
5.4. Elastic Properties 60
5.5. Modeling of the Paleo In-Situ Stress 73
5.6. Modeling Results 76
5.7. Discussion and Conclusion 87
6. Mapping of Current In-Situ Stresses 90
6.1. Geological Settings 90
6.2. Tectonic History of the Basin 90
6.3. Tectonic History of the Nesson Anticline 90
6.4. Elastic Properties 90
6.5. Modeling of the Current In-Situ Stresses 91
6.6. Modeling Results 96
7. EXPERIMENTAL METHODS 104
7.1. Core Sampler and Rock Geomechanics Test System 104
7.2. Porosity 108
7.3. Permeability 110
7.4. Sonic Velocity 116
7.5. Dynamic Moduli and Poisson's Ratio 121
7.6. Static Moduli and Poisson's Ratio (Non-Destructive Strength Test) 122
7.7. Biot's Coefficient 126
7.8. Uniaxial/Triaxial Compressive Strength, Young's Modulus and Poisson's Ratio (Destructive) 129

7.9. Mohr's Circle, Angle of Internal Friction and Cohesive Strength 134
7.10. Uniaxial Tensile Strength 135
8. EXPERIMENTAL RESULTS 140
8.1. Porosity 140
8.2. Permeability 142
8.3. Sonic Velocity 145
8.4. Dynamic Young's Modulus and Poisson's Ratio 147
8.5. Static Young's Modulus and Poisson's Ratio 149
8.6. Biot's Coefficient 152
8.7. Rock Strength (Uni/Triaxial Destructive Test) 154
8.8. Cohesive Strength and Angle of Internal Friction Calculate from Uni/Triaxial Destructive Test 156
8.9. Uniaxial Tensile Strength Test 157
9. Application Guidelines for Horizontal Drilling and Hydraulic Fracturing 159
9.1. Guideline for Creating 3D RQD (or Other Geological Parameter) Model 159
9.2. In-Situ Stress Analysis and Guideline for Horizontal Drilling 159
9.3. Guideline for Horizontal Drilling- Impacts of Stresses on the Stability of Horizontal Wells 171
10. New Methodology for In-Situ Stresses and Fracture Toughness 184
10.1. Kaiser Effect Method for In-Situ Stresses 184
10.2. Kaiser Effect Method –Experiment Setup and Procedure 188
10.3. Kaiser Effect Method –Data Analysis 196
10.4. CDISK Method for Fracture Toughness-Background 201
10.5. CDISK Method-Fracture Toughness Measurement 201
10.6. CDISK Method-Concluding Remarks on Fracture Toughness 210
11. CONCLUSIONS 211
12. Technology Transfer 212
12.1. Journal and Conference Papers 212
12.2. Technical Presentations 213
12.3. Website databases 213
REFERENCES 214
ATTACHMENTS 220
A.1. Well 20 Bakken Samples Testing Results 220
A.1.1 Permeability 220
A.1.2 Sonic Velocity, Dynamic Moduli and Poisson's Ratio 229
A.1.3 Biot's Coefficient 249
A.1.4 Static Moduli and Poisson's Ratio (Non-destructive) 262
A.1.5 Uni/Triaxial Compressive Strength, Young's Modulus and Poisson's Ratio 268
A.1.6 Mohr's Circle 271
A.2. Well 96 Bakken Samples Testing Results 272
A.2.1 Permeability 272
A.2.2 Sonic Velocity, Dynamic Moduli and Poisson's Ratio 276
A.2.3 Biot's Coefficient 296
A.2.4 Static Moduli and Poisson's Ratio (Non-destructive) 301
A.2.5 Uni/Triaxial Compressive Strength, Young's Modulus and Poisson's Ratio 307
A.2.6 Mohr's Circle 308
A.3. Well 2 Bakken Samples Testing Results 310
A.3.1 Permeability 310
A.3.2 Sonic Velocity, Dynamic Moduli and Poisson's Ratio 314

A.3.3 Biot's Coefficient *321*
A.3.4 Static Moduli and Poisson's Ratio (Non-destructive) *329*
A.3.5 Uni/Triaxial Compressive Strength, Young's Modulus and Poisson's Ratio *333*
A.3.6 Mohr's Circle *336*
A.4. WELL 70 BAKKEN SAMPLES TESTING RESULTS 338
A.4.1 Permeability *338*
A.4.2 Sonic Velocity, Dynamic Moduli and Poisson's Ratio *344*
A.4.3 Biot's Coefficient *373*
A.4.4 Static Moduli and Poisson's Ratio (Non-destructive) *385*
A.4.5 Uni/Triaxial Compressive Strength, Young's Modulus and Poisson's Ratio *390*
A.4.6 Mohr's Circle *393*
A.5. WELL 72 BAKKEN SAMPLES TESTING RESULTS 398
A.5.1 Permeability *398*
A.5.2 Sonic Velocity, Dynamic Moduli and Poisson's Ratio *402*
A.5.3 Biot's Coefficient *408*
A.5.4 Static Moduli and Poisson's Ratio (Non-destructive) *411*
A.5.5 Uni/Triaxial Compressive Strength, Young's Modulus and Poisson's Ratio *414*
A.5.6 Mohr's Circle *414*
A.6. WELL 13 BAKKEN SAMPLES TESTING RESULTS 414
A.6.1 Permeability *414*
A.6.2 Sonic Velocity, Dynamic Moduli and Poisson's Ratio *417*
A.6.3 Biot's Coefficient *447*
A.6.4 Static Moduli and Poisson's Ratio (Non-destructive) *449*
A.6.5 Uni/Triaxial Compressive Strength, Young's Modulus and Poisson's Ratio *454*
A.6.6 Mohr's Circle *455*
A.7. WELL 86 BAKKEN SAMPLES TESTING RESULTS 456
A.7.1 Permeability *456*
A.7.2 Sonic Velocity, Dynamic Moduli and Poisson's Ratio *465*
A.7.3 Biot's Coefficient *492*
A.7.4 Static Moduli and Poisson's Ratio (Non-destructive) *512*
A.7.5 Uni/Triaxial Compressive Strength, Young's Modulus and Poisson's Ratio *519*
A.7.6 Mohr's Circle *522*
A.8. WELL 18 BAKKEN SAMPLES TESTING RESULTS 528
A.8.1 Permeability *528*
A.8.2 Sonic Velocity, Dynamic Moduli and Poisson's Ratio *529*
A.8.3 Biot's Coefficient *536*
A.8.4 Static Moduli and Poisson's Ratio (Non-destructive) *543*
A.8.5 Uni/Triaxial Compressive Strength, Young's Modulus and Poisson's Ratio *547*
A.8.6 Mohr's Circle *549*

EXECUTIVE SUMMARY

On October 1, 2008 US DOE-sponsored research project entitled "Geomechanical Study of Bakken Formation for Improved Oil Recovery" under agreement DE-FC26-08NT0005643 officially started at The University of North Dakota (UND). This is the final report of the project; it covers the work performed during the project period of October 1, 2008 to December 31, 2013.

The objectives of this project are to outline the methodology proposed to determine the in-situ stress field and geomechanical properties of the Bakken Formation in Williston Basin, North Dakota, USA to increase the success rate of horizontal drilling and hydraulic fracturing so as to improve the recovery factor of this unconventional crude oil resource from the current 3% to a higher level. The success of horizontal drilling and hydraulic fracturing depends on knowing local in-situ stress and geomechanical properties of the rocks. We propose a proactive approach to determine the in-situ stress and related geomechanical properties of the Bakken Formation in representative areas through integrated analysis of field and well data, core sample and lab experiments. Geomechanical properties are measured by AutoLab 1500 geomechanics testing system. By integrating lab testing, core observation, numerical simulation, well log and seismic image, drilling, completion, stimulation, and production data, in-situ stresses of Bakken formation are generated. These in-situ stress maps can be used as a guideline for future horizontal drilling and multi-stage fracturing design to improve the recovery of Bakken unconventional oil.

1. INTRODUCTION

1.1. Background

The objectives of this five-year research project are to determine the in-situ stresses and to measure the geomechanical properties of the Bakken Formation in Williston Basin, North Dakota, USA to increase the success rate of horizontal drilling and hydraulic fracturing so as to improve the recovery factor of this 200-400 billion original oil in place (OOIP) unconventional crude oil resource from the current 3% to a higher level. Horizontal drilling with hydraulic fracturing is a required well completion technique for economic exploitation of crude oil from Bakken Formation in the North Dakota Williston Basin. The success of horizontal drilling and hydraulic fracturing depends on knowing local in-situ stress and geomechanical properties of the rocks. Currently some areas experienced low success rate in drilling and multistage fracturing due to wellbore instability and unsuccessful fracturing with the cost of 5-10 million dollars per well due to the limited knowledge of in-situ stresses and geomechanical properties of the Bakken Formation. To increase the success rate of drilling and fracing, we determined the in-situ stress and related geomechanical properties of the Bakken Formation in representative areas through integrated analysis of field and well data, core sample, and lab experiments. By integrating lab testing, core observation, numerical simulation, well log drilling and completion, and production data, in-situ stresses were modeled and the in-situ stress maps were generated. A database of geomechanical properties of the Bakken formation rocks in the studied areas was generated. The results of this research can be used as a guideline and reference to optimize horizontal drilling and fracturing design to increase estimated ultimate recovery (EUR) in unconventional shale oil and gas productions.

The Bakken Formation in North Dakota is a significant portion of the largest contiguous oil reserve ever discovered in the lower 48 states. The U.S. Geological Survey's original study of the Bakken Formation found 4.3 billion barrels of recoverable oil in the Montana and North Dakota portion of the Williston Basin. According to federal testimony provided by the director of the North Dakota Department of Mineral Resources, Hydraulic fracturing is a critical component of developing the Bakken Formation, indeed every shale play throughout the U.S. and Canada. Without hydraulic fracturing, under regulation of the states, this resource could not be produced. Hydraulic fracturing is the process of improving the ability of oil to flow through a rock formation by creating fractures. The process involves pumping into the fractures a mixture of water and additives that include various sizes of sand or ceramic particles called proppants that are designed to "prop" the fractures open, creating greater conductivity of fluids to the wellbore. However, within the Bakken Formation, field data suggest that operators are unable to sustain propped fractures spatially or temporally (Vincent, 2011), resulting in decreased oil production. This research sought an improved understanding of performance and the factors that contribute to optimize horizontal drilling and hydraulic fracturing in the Bakken Formation.

1.2. Williston Basin

The Williston Basin is a roughly oval-shaped, sub-surface sedimentary basin with the deepest point near Williston, ND. The Williston Basin, an intracratonic basin, is a major structural feature of central North America that covers surface areas between 120,000 and 240,000 square miles (Landes, 1970). The basin reaches approximately 475 miles north-south from southern Saskatchewan to northern South Dakota and 300 miles east-west into western North Dakota and eastern Montana. It underlies most of North Dakota, western Montana, northwestern South Dakota, southeastern Saskatchewan and a small section of southwestern Manitoba (Heck et al., 2002). The Williston Basin began to subside during the Ordovician Period, around 495 million years ago and underwent episodic subsidence throughout the rest of the Phanerozoic Eon. The Phanerozoic Eon extends from approximately 600 million years ago to the present. Although the Williston Basin was subsiding, marine sediments were not deposited in it continuously. The basin contains a complete rock record compared to many basins (Heck et al., 2002). All sedimentary systems from Cambrian through Quaternary are presented in the basin, with a rock column more than 15,000 ft thick in the deepest section (Heck et al., 2002). This nearly continuous deposition of sediments shown in the geologic record makes the Williston Basin one of only a handful of basins worldwide with that distinction.

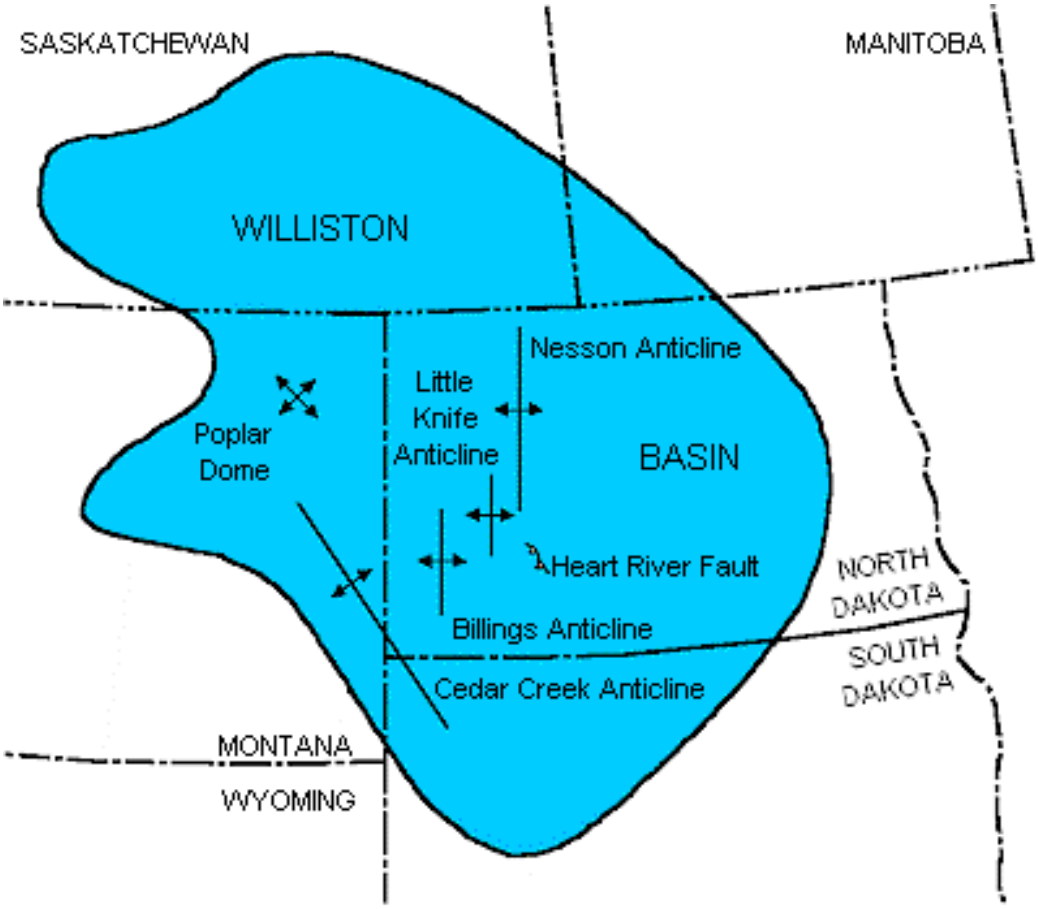

Figure 1-1 Williston basin and its major structures (Heck et al, 2002).

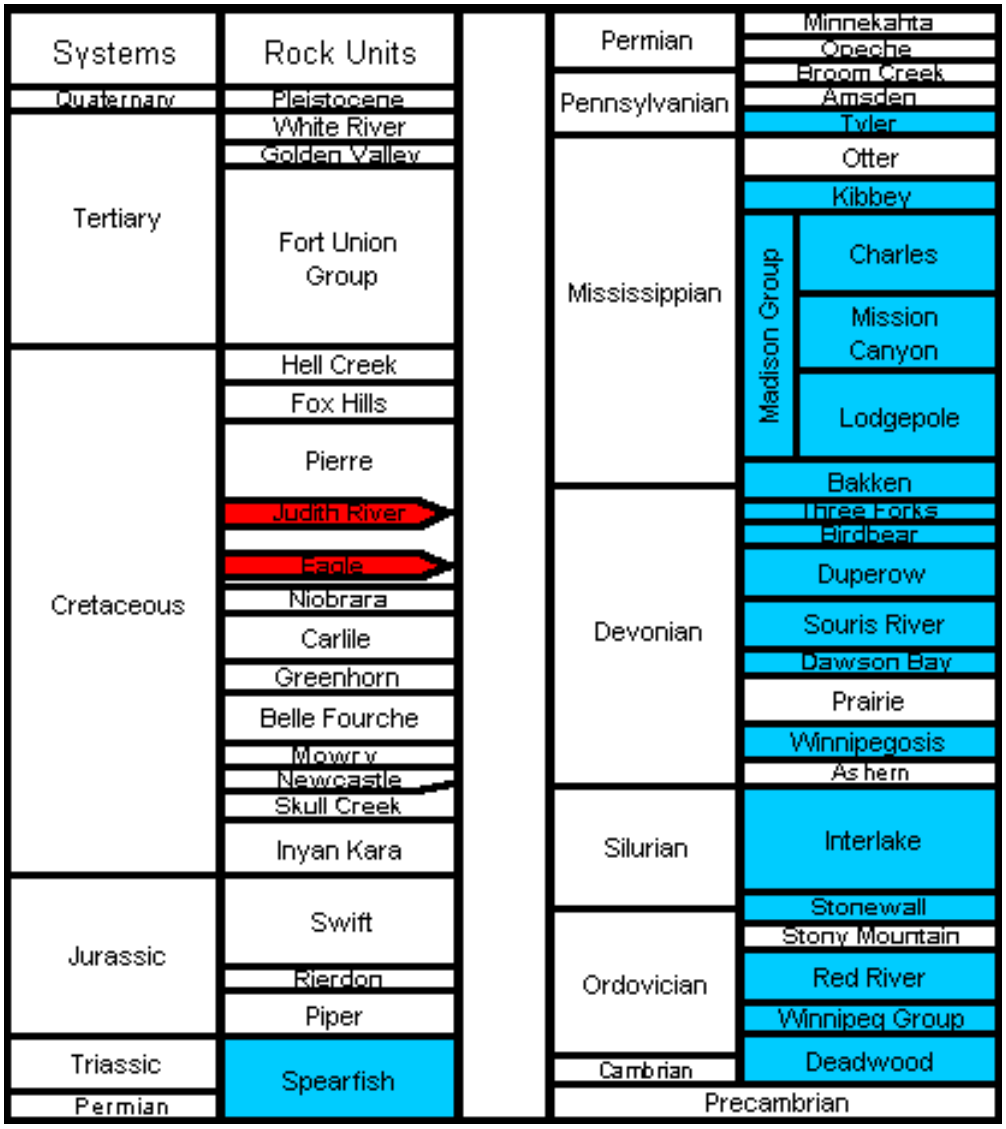

Figure 1-2. Generalized stratigraphic column for Williston basin with the oil producing horizons in blue and the two gas producing horizons in red (Heck et al, 2002).

1.3. Bakken Formation

Several companies explored for oil starting in 1917, and although several wells hit shallow gas, it was not until 1951 that Amerada's Clarence Iverson No. 1 well struck commercial quantities of oil south of Tioga, ND at a depth greater than 11,000 feet below the surface. This discovery led to a boom in leasing and drilling activities in the Williston Basin, especially along the prolific Nesson Anticline. The discovery well was completed in the Silurian Interlake Formation but subsequent development on the anticline focused on the Mississippian Madison Group. The basin became a major oil province in the 1950s. It has been experiencing a steady and substantial increase in oil production since 2004, when the application of horizontal drilling technologies and stage fracing facilitated the ability to extract oil from previously unviable deposits, the Bakken shales. The Bakken Formation, a large subsurface formation within the Williston Basin, is known for its rich petroleum deposits. Currently, the Bakken formation is considered the main reservoir and source of a large portion of the oil generated and produced in the Williston Basin. Formed during the late Devonian and early Mississippian age, Bakken shale is a thin, naturally fractured and considered both a source and reservoir. The Bakken formation consists of three members: the upper shale, the lithologically variable middle member, and the lower shale. The upper and lower shales have rich organic content with greater than one percent carbonaceous material, and are the source rocks for oil and gas in the Bakken Formation. In North Dakota,

the middle member is mainly gray interbedded siltstones and sandstones with a maximum thickness of 85 ft occurring at depths of approximately 9,500 to 10,000 ft (Heck et al., 2002). Located above the Bakken is the Lodgepole Formation, and below is the Three Forks formation. Although the Bakken Formation is very thin compared to other oil producing horizons, it has recently attracted much attention because its extremely high carbon content places it among the richest hydrocarbon source rocks in the world. Estimates of original oil in place (OOIP) range from 200 to more than 400 billion barrels (Price, 2000). For comparison, excluding these Bakken Formation reserves, so far the total US discovered OOIP is less than 600 billion barrels, of which only less than 200 billion barrels has been produced. With the growth rate of demand outpacing that of new reserves on oil and gas, the importance of these unconventional reserves in the Bakken Formation becomes increasingly important. Since 2001, a significant amount of oil has been successfully produced from the Bakken Formation in Richland County, Montana, USA. However, application of similar well construction technologies to the Bakken Formation in the North Dakota part of the basin has not achieved the expected success. This paper presents part of the ongoing efforts in improving the success rate of horizontal drilling and hydraulic fracturing in this thin, naturally fractured tight shale formation through geomechanical study.

From 1953 to 1987, vertical wells were drilled to recover the crude oil from Bakken Formation. Successful wells were those that encountered natural fractures which displayed high production at the beginning and soon dropped rapidly to a steady, low level production rate. The Bakken shale is oil-wet, and could not be waterflooded. Acidizing is prohibited because the injected fluid may react with the pyrite present in the shales, forming an iron hydroxide precipitate.

1.4. Horizontal Drilling and Fracturing Technology

The small formation thickness, the limited chance of hitting the natural fractures in a vertical well, the problem with hydraulically fracturing the vertical wells, and the restriction on using water flooding and acidizing led to the application of horizontal drilling (Joshi, 1987; Breit et al, 1992; Reisz, 1992). From 1987 to 2001, horizontal drilling was extensively practiced in the Bakken Formation (Carlisle et al., 1996). These wells performed quite well in the "Bakken Fairway" area in North Dakota. Due to the high investment, horizontal wells are usually drilled for two purposes: increasing the drainage area in thin layers, and/or connecting more fractures in naturally fractured reservoirs (Economides and Boney, 2000). The success of horizontal well depends on two factors: (1) vertical permeability and (2) wellbore orientation with respect to natural fractures (Karcher et al, 1987; Mukherjee and Economides, 1991; Hudson and Matson, 1992). Using horizontal drilling improved the performance, to a certain degree, especially with the successful production of oil from the upper shale. However, horizontal wells also encountered new challenges: borehole instability and wellbore interference. The large investment and high risk in drilling horizontal wells in the Bakken Formation kept the exploration and production activities at a low level until 2000 when new well construction technique was developed in Richland County, Montana (Lantz et al., 2007), which later extended to western North Dakota. This new technique combines horizontal drilling with hydraulic fracturing. However, in-situ stress field and geomechanical properties change not only along the axis of those horizontal wells that extends several thousand feet, but also from location to location in the basin. Well orientation with respect to the in-situ stresses is one of the controlling factors to the success of hydraulic fracturing and wellbore stability during drilling and production. Therefore, it is vitally important to know the in-situ stress field and fundamental geomechanical parameters for selecting the adequate orientation of horizontal wells and for designing successful hydraulic fracturing treatment.

2. GOALS AND OBJECTIVES

The objectives of the project are to determine the in-situ stresses and to measure the geomechanical properties of the Bakken Formation in Williston Basin, North Dakota, USA to increase the success rate of horizontal drilling and hydraulic fracturing so as to improve the recovery factor of this 200-400 billion OOIP unconventional crude oil resource from the current 3% to a higher level.

2.1. Challenges in Exploration and Production

Since the first Bakken discovery well was drilled in the 1950s (Anderson, 1953), thousands of wells have been drilled to produce oil from this formation (NDIC, 2008a). The Bakken Formation in the North Dakota Williston Basin is a thin layer of interbedded, naturally fractured low permeability black shale, siltstone, silty sandstone and silty carbonate rocks at about 10,000 ft depth (LeFever, 2005). Due to the high total organic carbon (TOC) content in the upper and lower shales, it is estimated to have 200 - 400 billion barrels of OOIP (Price, 2000). However, an April 2008 assessment by the US Geological Survey indicated that technical recoverable reserve is about 3.6 billion barrels of crude oil (Pollastro et al., 2008). A more recent research report released by North Dakota Geological Survey assessed the current recoverable reserve is 2.1 billion barrels (Brimberry, 2008a). Although there is a big gap between these two assessments, both indicate a recovery factor of about 3%, which is much lower than the US domestic average recovery factor of 30% (Lake, 1989; Green and Willhite, 2003).

The Bakken Formation in the North Dakota Williston Basin is a thin layer (maximum thickness 145 ft) of interbedded, naturally fractured low permeability black shale, siltstone, silty sandstone and silty carbonate rocks at about 10,000 ft depth. Due to the high carbon content in the upper and lower shales, it is estimated to have 200 - 400 billion barrel OOIP. However, an April 2008 assessment by the US Geological Survey indicated that technical recoverable reserve is about 3.6 billion barrel of crude oil, only 3% recovery, much lower than the normal recovery of 30%. The success of horizontal drilling and hydraulic fracturing depends on the local in-situ stress and geomechanical properties of formation rocks. Only limited information on these aspects is available. The geology heterogeneity and the special features of the Bakken Formation makes it impossible to drill and complete the well successfully without knowing the in-situ stress and geomechanical properties of the formation rocks. Currently some areas experienced success rate of less than 10% in drilling this type of wells due to wellbore instability and unsuccessful fracturing, each of these wells costing 3-6 million dollars.

2.2. Current State-of-the-Art

Currently horizontal drilling followed by hydraulic fracturing stimulations are being applied to produce the Bakken crude oil in the North Dakota Williston Basin. In building the horizontal wells, multilateral (single, dual and tri lateral) technologies were used. Similarly, different completion techniques (perforated liner or open hole, cased and cemented) were tried (Brimberry, 2008b). Corresponding to the above well schemes, different types of well spacing have been used, including: (1) long single lateral 1280 acres, (2) single 640 acres, (3) coplanar dual and tri lateral 1280 acres, and (4) coplanar 640 acres (Helms, 2007). In the hydraulic fracturing stimulation, both longitudinal and transverse fractures were tried. Different combinations of wellbore azimuth, length, and placement were tested (Cox, et al., 2008).

2.3. Benefits and Inadequacies of Current Technology

Maximum thickness of Bakken Formation is about 145 ft, including about 20 ft in Upper Bakken, 85 ft in Middle Bakken, and 40 ft in Lower Bakken. The Middle Bakken is further divided into 5 Lithofacies L1~5. Bakken oil is produced mainly from two central Lithofacies, L2, interbedded shale and silty sandstone, and L3, sandstone. These two Lithofacies are about 10 to 20 ft thick (LeFever, 2005). It is believed, and confirmed by recovered cores, that the Bakken Formation is naturally fractured due to the action of in-situ stress fields and internal pressure when hydrocarbon was generated in the low permeability shales. Combination of horizontal wells and hydraulic fracturing in the Bakken Formation has the following benefits:

(1) Horizontal wells increase the exposure to reservoir rock in thin formations. Vertical wells have only limited exposure to the reservoir rock, which is the formation thickness. Instead, exposure of horizontal wells equals the length of the horizontal sections.

(2) Horizontal wells increase the connection between wellbore and the natural fractures, and those laterally isolated fractures. Because horizontal wells have larger exposure to reservoir rock, it is more likely that they hit and connect more natural fractures in comparison with vertical wells.

(3) Hydraulic fracturing stimulation increases the reservoir drainage volume and speeds up the recovery, because the Bakken Formation has very low permeability.

However, due to the complex geological conditions in the Bakken Formation, the above technology has some serious limitations:

(1) Improper well orientation will cause wellbore instability (Roegiers, 2008a). In order to have the most stable wellbore, the optimized orientation is the one that has the most homogeneous stress distribution, or minimum stress difference, around the wellbore. Finding this optimized orientation needs the information of in-situ stresses: both orientation and magnitude.

(2) Improperly selected wellbore orientation may greatly reduce the well performance. Because one of the purposes of using horizontal wells is to connect laterally isolated natural fractures, which usually follow a patterned distribution controlled by in-situ stresses.

(3) Improperly designed hydraulic fracturing treatment may not only ruin the well, but also affect the nearby wells, and lose the reserves in the targeted drainage volume (Roegiers, 2008b). The orientation of the hydraulically induced fractures is controlled by local in-situ stresses. The geometry is partly controlled by the geomechanical properties of both the target formation (Bakken Formation) and the boundary formations.

2.4. Problems to be Addressed

In comparing to the success in producing crude oil from the Bakken Formation in eastern Montana, the horizontal drilling with hydraulic fracturing stimulation technology suffered many more difficulties in western North Dakota, and new completion and fracturing technologies were developed (LeFever, 2005; Powell et al, 2007; Phillips et al, 2007). The biggest challenges include: (1) the horizontal well could not hit the natural fracture, and (2) the hydraulically generated fractures did not develop longitudinally as designed, but more than often transversely instead (Wiley, 2004; Besler et al, 2007). This was attributed to the lack of in-situ stress knowledge and the geological heterogeneity in the Bakken Formation in the North Dakota portion (Powell et al, 2007). Recently, the US Geological Survey updated the technically recoverable crude oil reserve in the Bakken Formation from 151 million barrels to 3.65 billion barrels of oil (Pollastro et al, 2008). In the same report, the Bakken Formation was divided into five assessment units (AU): (1) Elm Coulee-Billings Nose AU, (2) Central Basin-Polar Dome AU, (3) Nesson-Little Knife Structural AU, (4) Eastern Expulsion Threshold AU, and (5) Northwest Expulsion Threshold AU, as shown in Figure 2-1. The boundaries of these assessment units are consistent with the major structures in this area, and support the aforementioned geological heterogeneity.

We propose an active approach to attack these problems: determine the in-situ stress and related geomechanical properties of the Bakken Formation in representative areas (Five assessment units in Figure 2-1) through integrated analysis of field and well data, core sample, and lab experiments. We use well data, core analyses, and lab testing to determine the direction and magnitude of the in-situ stresses. Geomechanical properties are measured using suggested methods by International Society for Rock Mechanics. A large scale in-situ stress field map of the targeted region is developed. A database of geomechanical properties of the Bakken formation rocks in the studied areas is generated.

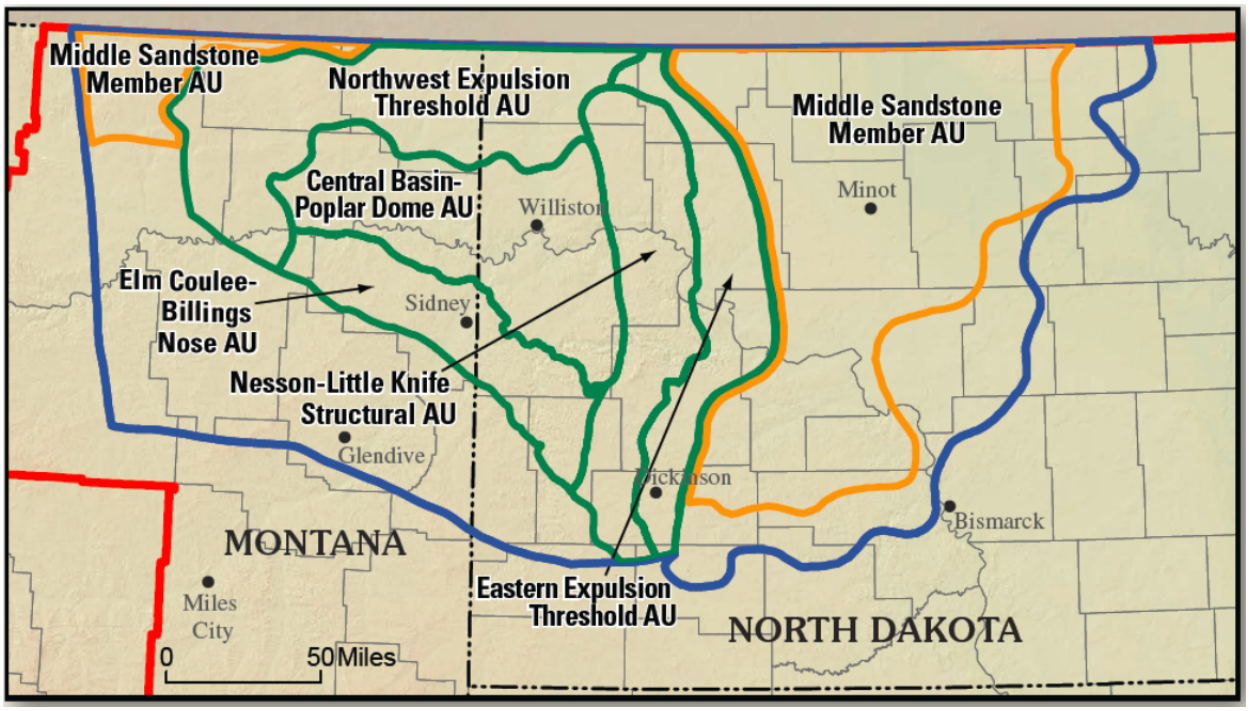

Figure 2-1. The five continuous assessment units of the Bakken Formation (Pollastro et al, 2008).

In-situ Stress Determination

Knowing the in-situ stress field is vitally important to any underground excavation, including petroleum drilling, mining, and tunneling (Jaeger et al, 2007). Many efforts have been made to determine the direction and magnitude of in-situ stresses (Hudson, 1993). Consequently many different methods were developed. After carefully reviewing the existing techniques and our conditions, we use the following methods to determine the orientation and magnitude of the in-situ stresses.

Stress orientation from analyzing discontinuities: When the rock is subjected to load, it deforms. When the load exceeds a certain limit, it fractures or fails. The failure surface is called discontinuity of the rock. The failure plane and the stress orientation have a certain relationship Narr et al, (2006). Following the geological guidelines, the feature of the discontinuity, i.e., tensile failure (joint) or shear failure (fault) or bedding plane, can be identified from core sample observation (Davis and Reynolds, 1996). Using the relationship between the in-situ stresses and the discontinuities, part of the direction(s) of the principal stresses can be derived. Similar method can be also applied to characterizing naturally fractured reservoirs by using surface lineaments and fractures (Guo et al, 1999). Recent development in this area is a new type of acoustic log for principal stress direction using the split waves (Nihei et al, 2002). Because the Bakken Formation in Williston Basin is at about 10,000 ft depth, no surface access is available. The North Dakota Geological Survey Core Library, which is located on the University of North Dakota campus, has a large collection of Bakken Formation core samples from the petroleum drilling activities, including some oriented core samples. With the recent booming drilling in the Bakken Formation, more samples are being delivered.

Geomechanical Properties of Bakken Formation

Geomechanical properties of rocks are important parameters for well design to avoid instability and for a hydraulic fracturing treatment plan (Fjaer et al, 1992, Zeng, 2002). However, the Bakken Formation hasn't been investigated very much in this aspect; only one reference was found with limited data (Kuhlman et al, 1992; Zhou et al, 2008); this is far behind the research on the petroleum geology of the Bakken Formation (LeFever, 1991; Webster, 1992; Gosnold, 1999). We conduct geomechanical experimental investigation on Bakken Formation rocks, including measurement of the following properties: (1) Uniaxial compressive and tensile strengths, (2) Cohesion and angle of internal friction, (3) Young's modulus and Poisson's ratio, (4) Triaxial strength at three different confining pressures, and (5) Biot's coefficient. We also measure rock porosity, permeability, and sonic velocity. International Society for

Rock Mechanics' (ISRM) suggested methods and other related guidelines are followed in specimen preparation and experiment (Zeng et al, 2004). Most of the testing methods for all these rock properties have been well developed.

Uniaxial compressive strengths, Young's modulus, Poisson's ratio and in-situ stresses: Uniaxial compressive strength is measured together with Young's modulus, and Poisson's ratio. Axial load, axial and lateral deformations are measured during the compression until failure of the specimen. Load-deformations curves are converted to stress-strain curves using the specimen's geometry, from which the Young's modulus and Poisson's ratio are obtained using the linear portion. Because the Williston Basin is very flatling, we can assume that one of the three principal stresses will be parallel to the vertical direction. With this assumption, using the measured historic stresses in three different directions in the bedding plane allows the determination of the two principal stresses in the bedding plane.

Tensile strength: Point load test or direct extension method are used to measure the tensile strength.

Triaxial strength, cohesion and angle of internal friction: Triaxial strength under three different confining pressures is measured. Using these results and the uniaxial compressive and tensile strengths, a Mohr envelope of this rock is developed, from which the cohesion and angle of internal friction is determined.

Biot's coefficient: Biot's coefficient defines the relationship among total stress, effective stress and pore fluid pressure (Biot and Willis, 1957; Geertsma, 1957). It describes how soon the matrix stress will respond when the pore fluid pressure is changed. It is more important to low permeability rocks, such as the Bakken Formation. This parameter is used in hydraulic fracturing treatment design and wellbore stability. It is measured using triaxial and hydrostatic compression (Azeemuddin et al, 2002).

2.5. Impact on the U.S. Oil and Gas Industry

Using the results from this research, the success rate of horizontal drilling and hydraulic fracturing will be greatly increased. For each saved well, the direct impact is 3-6 million dollars. More importantly, optimized well alignment in the Bakken Formation, due to the knowledge of in-situ stresses, will not only improve primary recovery, but also allow future application of enhanced oil recovery technology, such as CO2 flooding. An increase of 1% in recovery (a modest goal) will lead to increase of 2 - 4 billion barrels of domestic production, a direct impact of 200 - 400 billion dollars reduction in trade deficit at current oil price. New job opportunities and other benefits will be even larger.

Results from this research project will directly serve the technical demand on recovering oil and gas from the Bakken Formation in North Dakota Williston Basin. These results can also be used to help oil and gas development in many other naturally shale formations, such as the Antrim shale in the Michigan, the New Albany shale in Illinois, and the Eastern Devonian shale in Appalachian region (Kentucky, West Virginia, Ohio, and Pennsylvania), and Pierre shale in Colorado. In fact, it is the PI's belief that using the technologies developed in this project to improve gas recovery in the above mentioned shale formations will have huge impact on domestic gas supply and reduction of green house gas emission, due to the fact those formations are close to big population centers.

3. Petroleum Geological Model of Bakken Formation

The petroleum geological model provides an understanding to the hydrocarbon resources and special structural features of the Bakken Formation. It serves as a platform for future research works. Based on the investigation to the fundamentals on the aspect of geomechanics, geophysics, reservoir features, and recovery plan, the project targets at finding solutions which is suitable for the unique features of exploration and production in the Bakken formation (Figure 3-1). To build the geological model, geological, geophysical, petrophysical, geomechanical, and engineering data are analyzed, Laboratory test of core and fluid and field stress data are collected. The model constructed in this project can be further developed as more works will add information and more understandings will be obtained to update and calibrate the existing model.

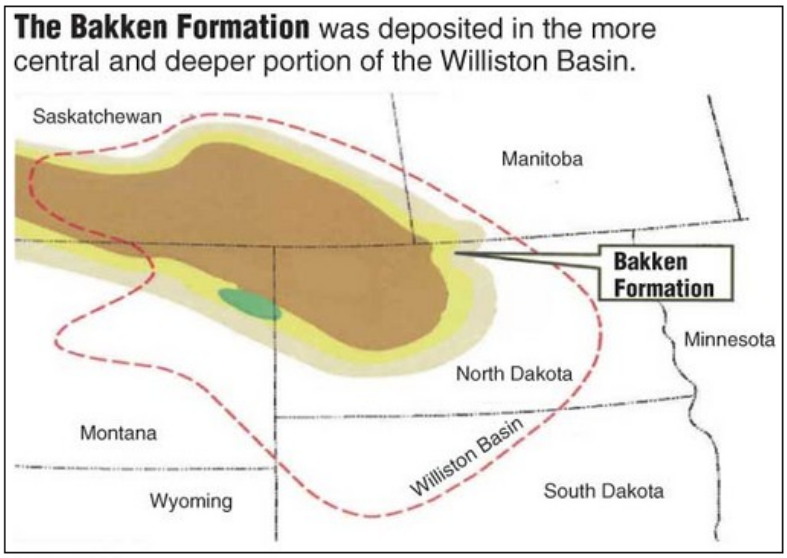

Figure 3-1: Map of the Bakken Formation (USGS, http://bakkenshale.com/home/attachment/bakken-formation-map-usgs-2/)

3.1. Study Area and Wells Used for Geological Model

The work is based on information from 65 wells drilled in five assessment units in the Williston Basin (Figure 3-2). The corresponding North Dakota Industrial Commission (NDIC) file# to Map# for these 65 wells are listed in Table 3-1. These wells are mainly located in the west side of North Dakota, most along the Nesson Anticline and north side of the Billings Anticline.

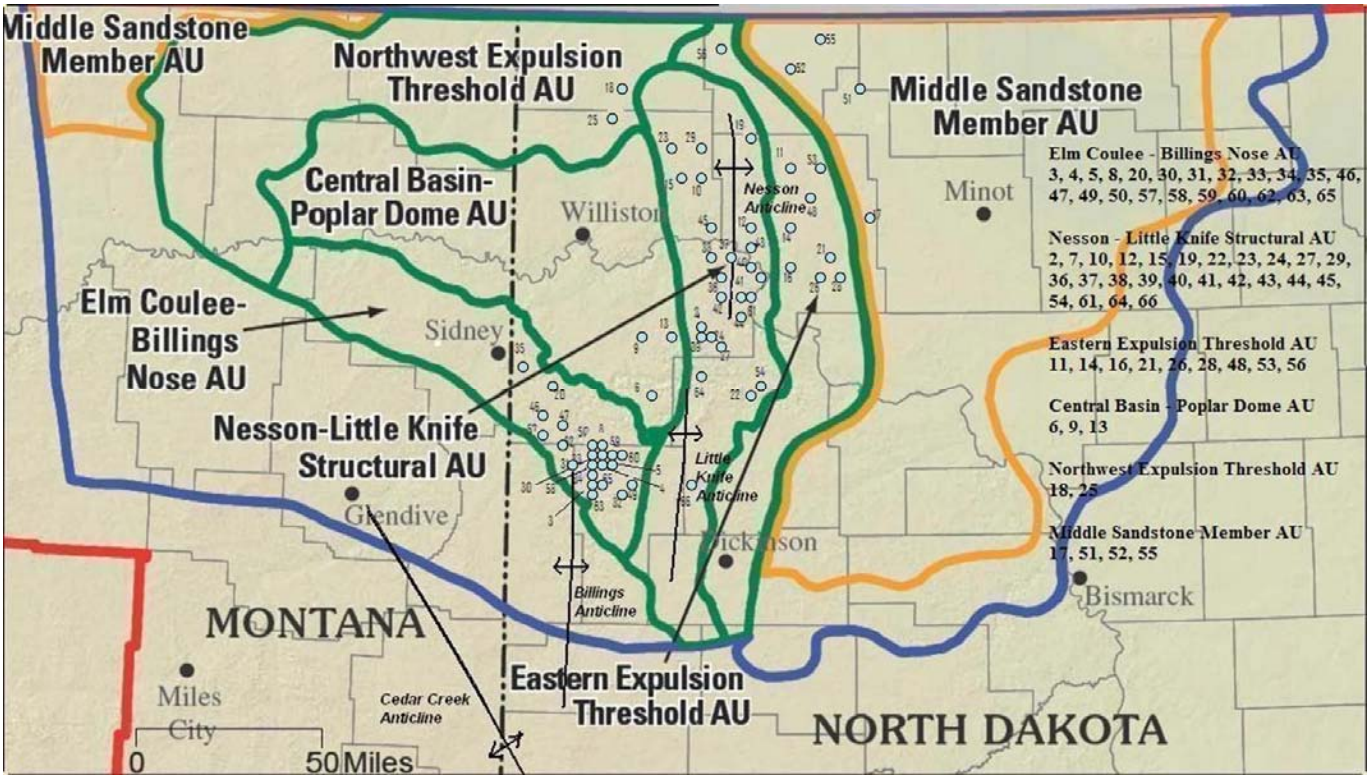

Figure 3-2: Location of the 65 wells and five assessment units in Williston Basin

Table 3-1. List of the corresponding NDIC file# to Map# in Figure 3-2 for 65 wells used in this study

File #	Map #	File #	Map #	File #	Map #	File #	Map #
11617	2	16160	19	1202	36	8699	53
12072	3	16174	20	1254	37	8709	54
12297	4	16324	21	1343	38	8824	55
12748	5	16333	22	1405	39	8850	56
12772	6	16405	23	1748	40	8902	57
12807	7	16433	24	1779	41	9426	58
12886	8	16458	25	1780	42	10077	59
13098	9	16532	26	2179	43	10989	60
15674	10	16652	27	2383	44	12019	61
15845	11	16743	28	4297	45	12160	62
15889	12	5656	29	6966	46	12494	63
15923	13	8251	30	7579	47	12785	64
15986	14	9033	31	7851	48	12873	65
16030	15	12162	32	7887	49	16466	66
16068	16	12331	33	8474	50		
16083	17	12558	34	8637	51		
16089	18	14974	35	8636	52		

3.2. Work Procedure

3.2.1 Data Collection

We have screened and collected available data for representative areas and wells within the study area. The data used in this project is mainly obtained from the information provided by companies who once drilled production wells and wildcat wells. Data collected include cores, core images, digitized geophysical well logs, monthly production, and available petrophysical testing results. A database containing information of the selected 65 wells is established. The database includes basic information of wells (longitude, latitude, depth, formation intervals, well path, core analytical data, sample lithology descriptions, and well logs), and derived results (lithology, porosity, hydrocarbon saturation, and water saturation). Most of this information can be accessed via the Premium Services on the website of North Dakota Department of Mineral Resource (DMR) (https://www.dmr.nd.gov/oilgas/), and Wilson M. Laird Core and Sample Library of the North Dakota Geologic Survey (Figure 3-3). RQD measurements of all the 65 wells are also conducted.

Figure 3-3: Photo of the core samples (https://www.dmr.nd.gov/oilgas/)

Well logs listed on the DMR website include gamma, resistivity, neutron, sonic, and density. However, it should be noticed that most of these 65 wells do not have all the above logs, and 45 wells' logs are originally in the form of image instead of digit format. These image files are digitized by using the Petra software (Figure 3-4), and the generated LAS files are ready to be read in Interactive Petrophysics software. The Interactive Petrophysics calculates parameters like clay volume, porosity, and saturation based on these log files. The second way to get the core parameters is collecting data from the well reports submitted by operators. Available core parameters in the well report are read and recorded in ASCII format, and imported into the database of Interactive Petrophysics. The core parameters obtained through the two approaches are compared and provide reference for later analysis. Details of the work using Interactive Petrophysics are described as the following part.

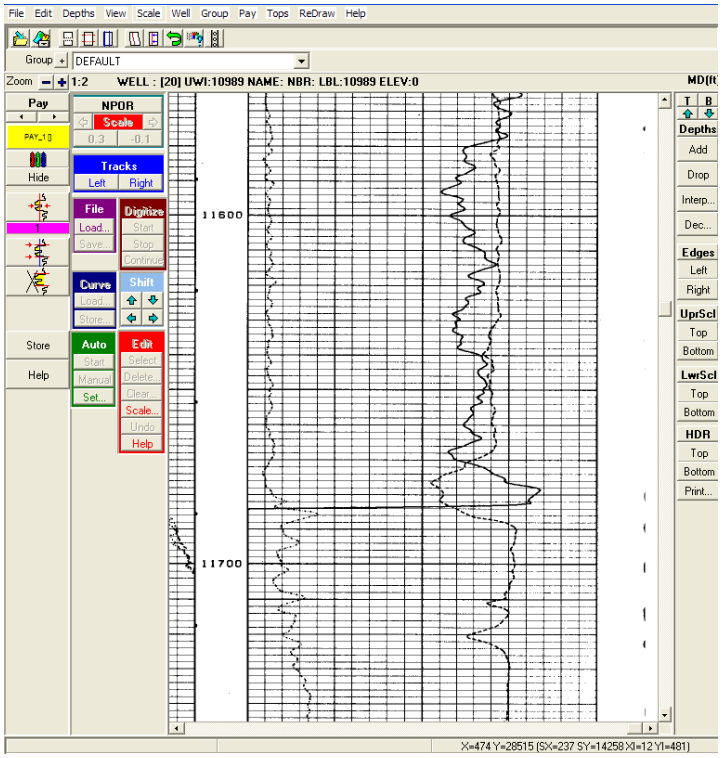

Figure 3-4: Digitizing of well logs

3.2.2 Data Analysis

We analyze field and well data to build a geological model of the study area to include factors affecting in-situ stresses such as structural features and basin stress history. Commercial software is used to analyze well logs. Interactive Petrophysics a product is developed by Schlumberger and is an ideal tool for well log interpretation and analysis. Using the gamma ray, density, sonic, neutron, resistivity curves, the software is able to calculate porosity, water saturation, and analyze lithology. The detail process follows 6 steps.

Identification of three member of the Bakken formation

The depth intervals are initially split into zones based on the value sparks of gamma ray curve. The Bakken Formation is split into three zones: upper, middle, and lower, as the different compositions among the middle sandstone and the upper and lower shale (Figure 3-5). To build the 3D skeleton model, the middle Bakken is divided into 5 layers, and the upper and lower members are kept as single layer for each.

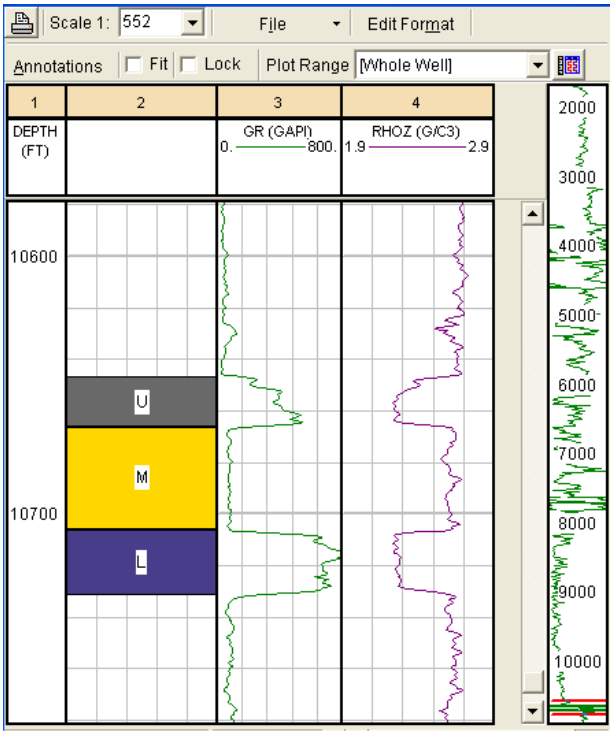

Figure 3-5: Identifying top and bottom for three members of the Bakken formation based on GR

Normalization of well logs

Well logs of different wells are recorded in various ranges. In order to setup a common basis for comparison, the well logs are normalized. Knowing the value of gamma ray of the pure sandstone and the pure shale, wells curves are normalized using the "normalize" function in the histogram module. Figure 3-6 shows the histograms of a gamma ray before and after normalization.

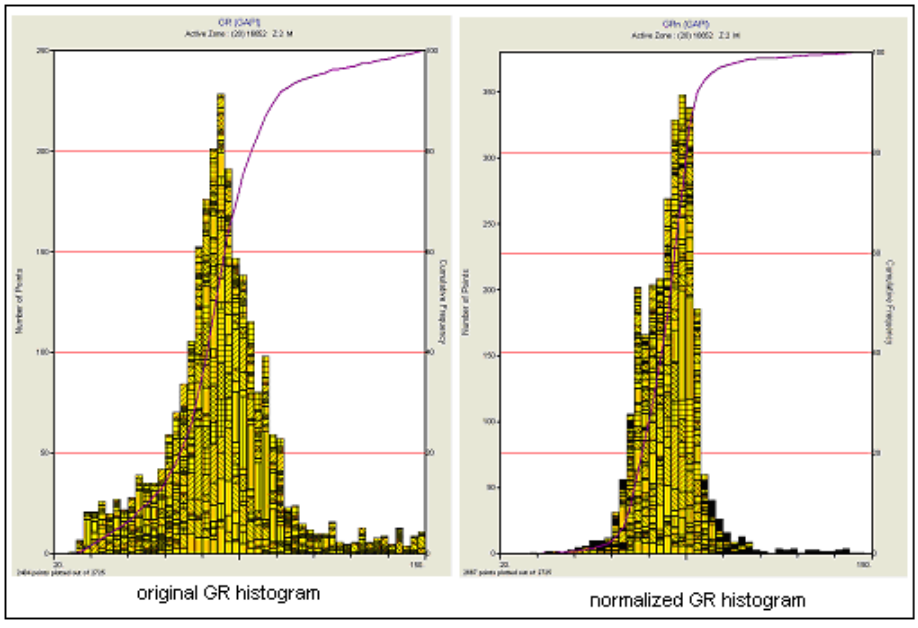

Figure 3-6: Histograms of GR before and after normalization

Calculation of clay volume

The volume of clay is the parameter for analyzing porosity and water saturation. Gamma ray is a good indicator and all wells have gamma ray curve, so it was used to analyze clay volume through:

$$VCL = \frac{GR - GR_{sand}}{GR_{shale} - GR_{sand}} \quad \text{.....(3-1)}$$

where VCL is the volume of the clay, GRsand is the gamma ray value of pure sandstone and GRshale is gamma ray value of pure shale. If one well has other logs like neutron, density and sonic curves, besides gamma ray, a function named "Dural Clay Indicator" can be used to analyze the volume of clay. Combining pares include neutron/density (Figure 3-7), neutron/sonic or density/sonic. However, using the combinations and equations also requires knowing the log values for pure sandstone and pure shale.

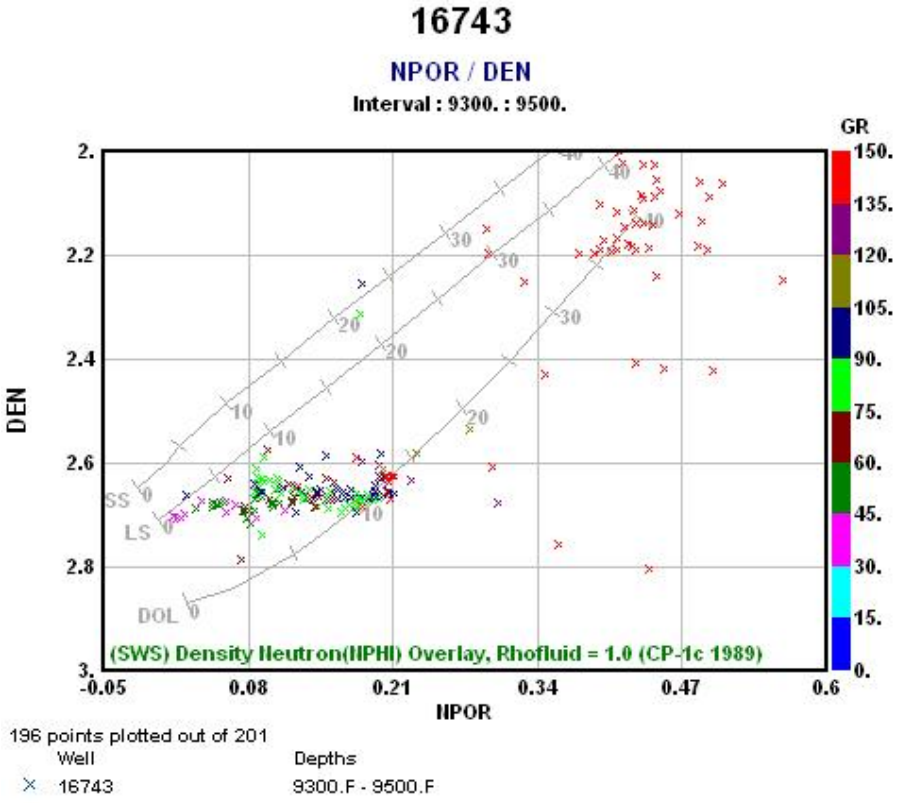

Figure 3-7: Neutron/density cross plot of Well#16743

Lithology and porosity analysis

The rock lithology and porosity can be determined by using the cross plots module. The cross plot function has different equations for calculation, such as Schlumberger Neutron/Sonic or Western Atlas Den/Neutron (Figure 3-8). Choosing of equations is based on available logs of each well. If more than one equation is available, multiple results are obtained and compared with the core analysis data given in the well report to determine the most suitable equation.

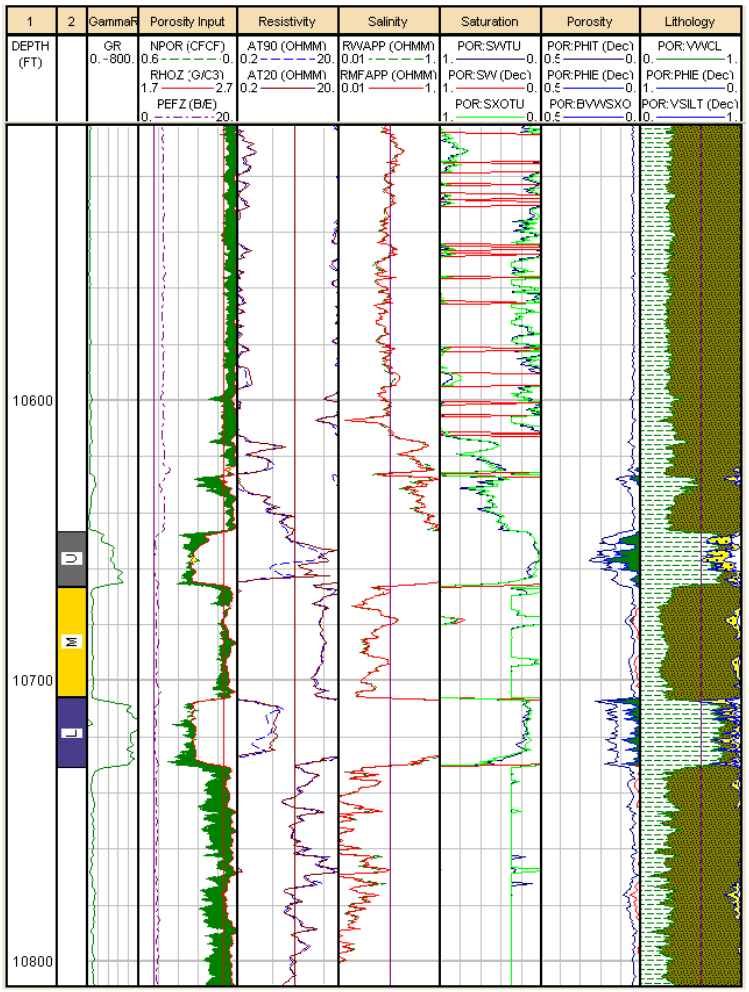

Figure 3-8: Well logs interpretation results: lithology, porosity, and saturation

Saturation analysis

The water saturation is determined by the resistivity/porosity cross plots and the Archie equation.

Sw = [(a / Fm)*(Rw / Rt)](1/n) .....(3-2)

where Sw is water saturation; F is porosity; Rw is formation water resistivity; Rt is bulk resistivity, a is a constant (often taken to be 1); m is cementation factor (varies around 2); and n is saturation exponent (generally 2).

Permeability analysis

The Interactive Petrophysics does not have a function to calculate the permeability. But some of core analysis records in the well reports contain the permeability values and we have measured core permeability in this study. In order to calculate the permeability values of all wells and the entire formation, a correlation (Equation 3-3) between the porosity and permeability is developed using experimental data. This correlation is used as an empirical equation to calculate Bakken formation permeability.

$$k = 0.0394Exp(0.5412\phi) \quad \text{.....(3-3)}$$

3.3. Geological Modelling

3.3.1 Data input and 3D skeleton model construction

First, the data of well tops are input into the Petrel. As divided by Petrophysics, there are 3 zones contained in the well data: upper, middle, and lower Bakkens. Once the top data are loaded into Petrel, two isodepth maps are generated: one is the top of the Upper Bakken, the other is the bottom of the Lower Bakken. Then the 3D skeleton model is created based on these two isodepth maps as shown in Figure 3-9. The 3D skeleton model has three horizons. The top and bottom horizons are actually the two isodepth maps. The middle horizon is generated automatically by the Petrel and bounded by the top bottom horizons. Figure 3-10 shows the isopachous map of Bakken formation. Each of the three horizontal surfaces is gridded by a pattern of 500×500. It should be noticed that the 3D skeleton model is just a physical model before any rock properties are loaded. The 3D skeleton serves as a platform for further modeling works.

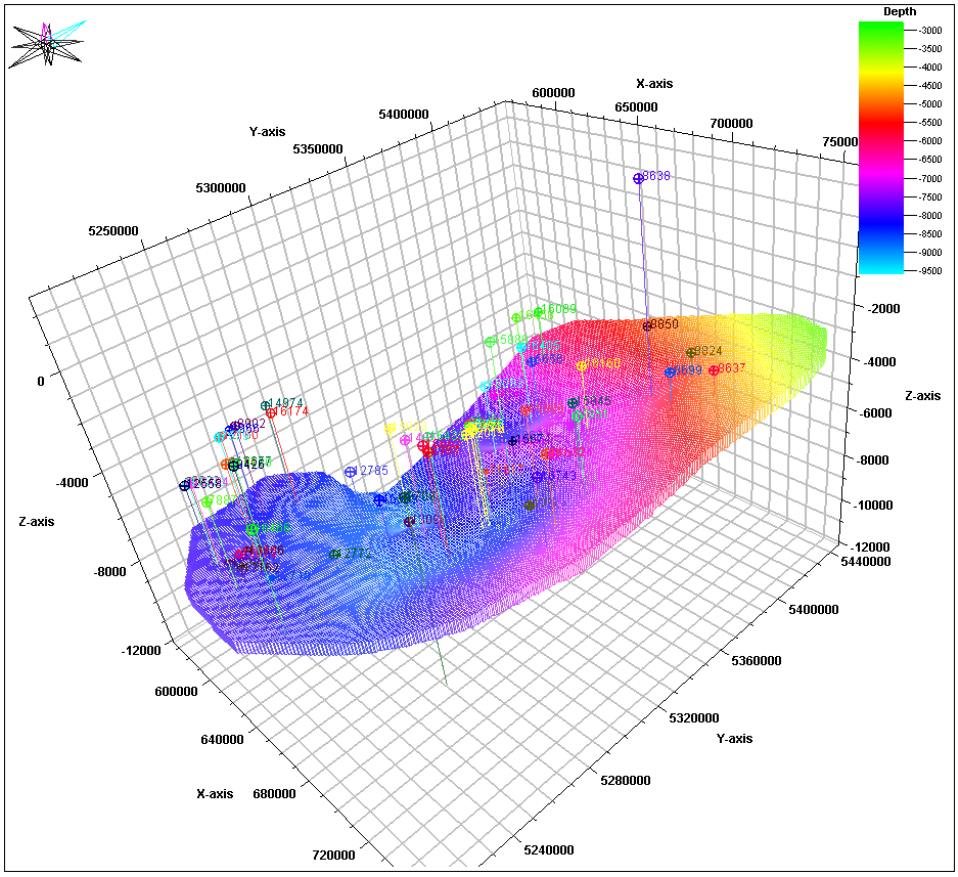

Figure 3-9. The 3D skeleton model

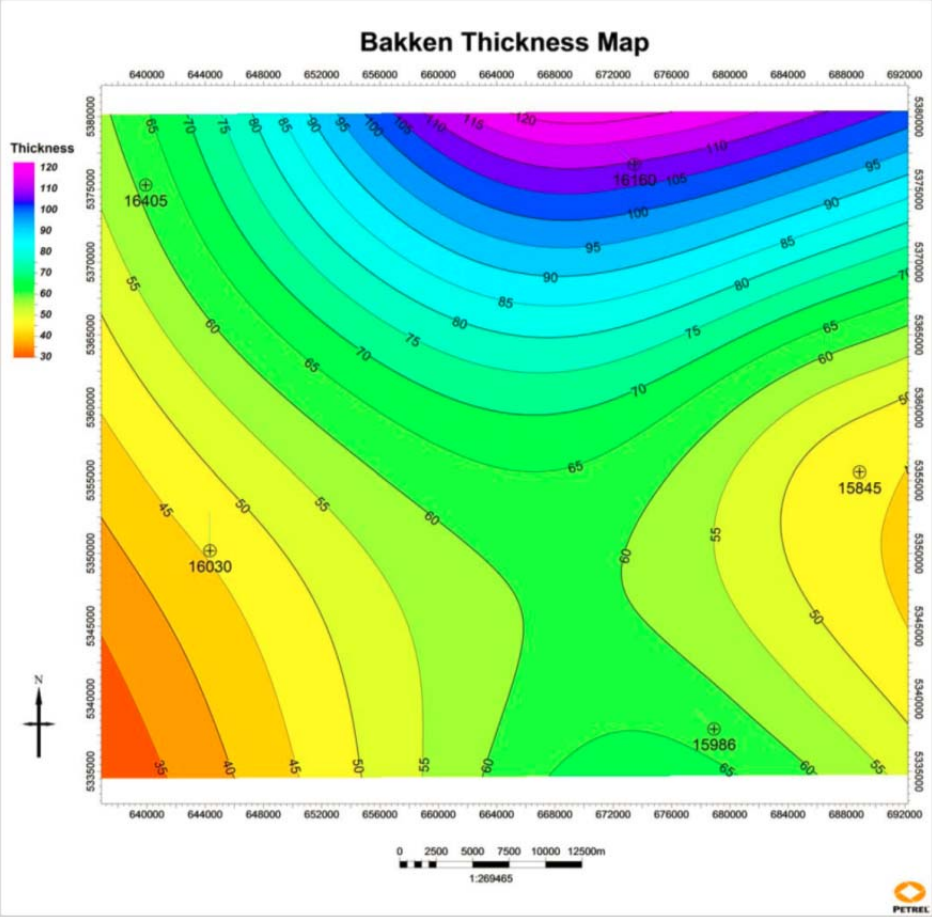

Figure 3-10. The isopachous map of Bakken formation

3.3.2 Geological modelling results

In current work, the Middle Bakken is again split into 5 layers, with the upper Bakken and lower Bakken are kept as one integrated layer, respectively, so there are 7 layers in total. However, the Lower Bakken Member pinches out since in some south parts of the formation, 7 is not a fixed number for the layers in the model. The formation model is later inserted with the rock and fluid parameters exported from Interactive Petrophysics. The parameters of each 65 wells are first added into the cells that are exactly located in the wells' position, and then the Petrel populates these parameters into all cells in the 3D grid based on the simulated formation geometry and on-site conditions. Currently, the parameter added in the model is porosity (Figure 3-11). In the future, more data including permeability, oil saturation, gas saturation, water saturation, fractures, et al, can be loaded into the model. The model can be updated as new data available.

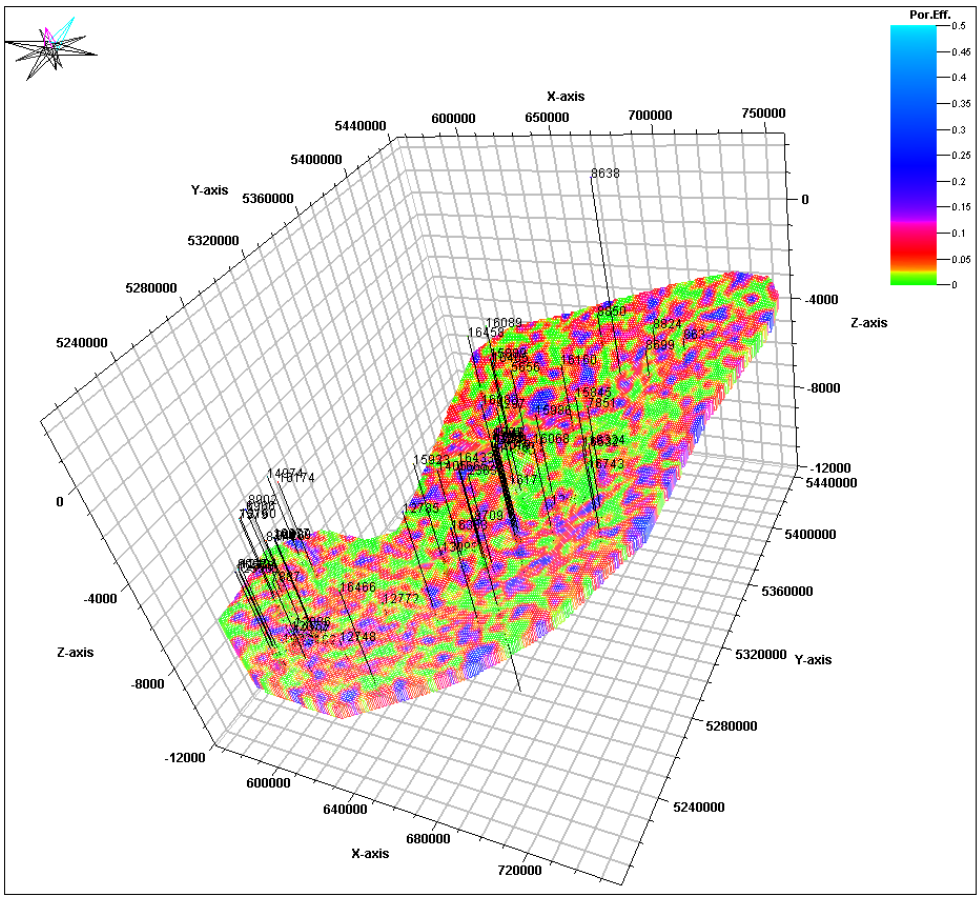

Figure 3-11: The 3D porosity model of the Bakken formation

In the 3D model, views of different layers can be obtained and used to indicate the variation of rock properties on these layers. Interested cross sectional profiles also can be easily obtained. By amplifying the interested spot on the cross sectional plot, one can see the distribution of property values, both geological and geometrical. For example, from the cross sectional profiles (Figures 3-12 through 3-15), it can be found that the north part of the formation is shallower than the south part, and the east part is shallower than the west part. In Figure 3-13, the enlarged parts indicates the low porosity of the middle Bakken member comparing with the upper and lower shales.

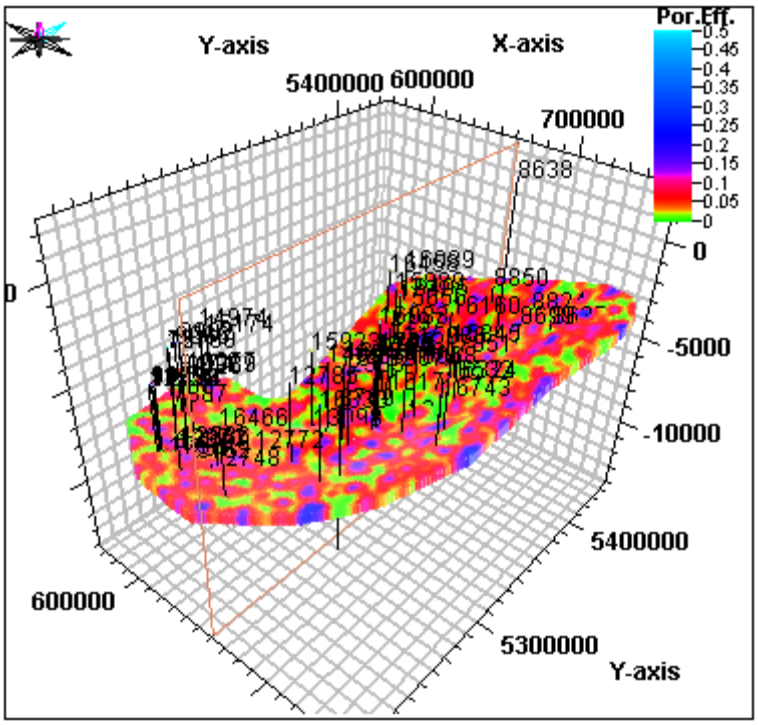

Figure 3-12. 3D model of the formation with north-south cross sectional cut

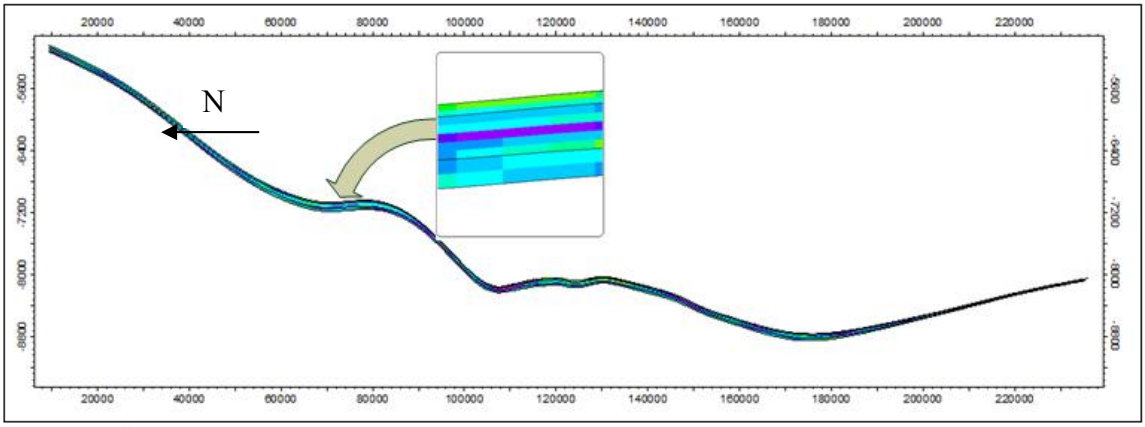

Figure 3-13. North-south cross sectional view

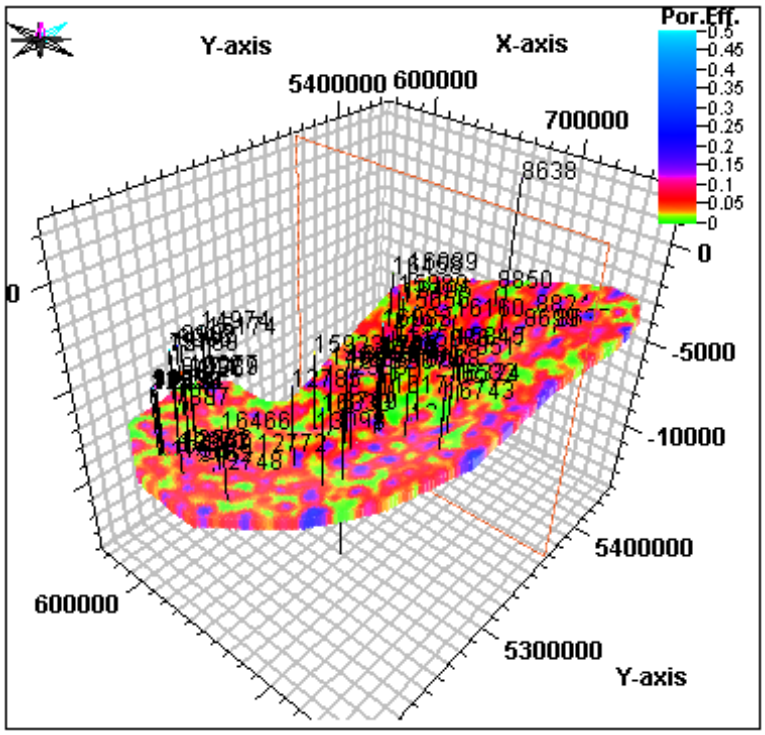

Figure 3-14. Model of the formation with east-west cross sectional cut

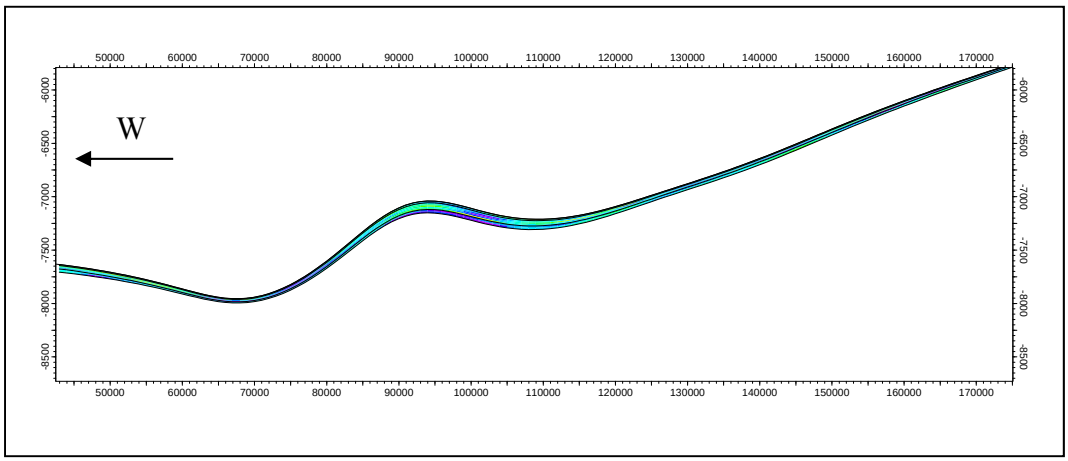

Figure 3-15: East-west cross sectional view

4. Minor and Micro Structures Analysis

4.1. RQD Based Bakken Formation Minor and Micro Fracture System

4.1.1 The RQD Index

The Bakken formation is a tight reservoir with extremely low matrix permeability. Fractures in the formation can significantly improve the permeability and therefore increase the oil production rate. Fractures and cracks are observed in the borehole cores from the Bakken Formation. These fractures and cracks can be either natural fractures or induced ones due to drilling and handling. In most cases, these induced cracks occur on the plans of weakness. Therefore, similar natural and induced fractures should also exist in the productions wells penetrating through the Bakken formation. Referring to the concept of Rock Quality Designation (RQD) in geomechanics, we have collected the statistic information about the fractures and cracks on the Bakken core samples, calculated the RQD index, and visualized the results in the Petrel 3D model. The RQD index is defined as the borehole core recovery percentage incorporating only pieces of solid core that are longer than or equal 10cm in length measured along the centerline of the core. Expressed mathematically,

$$RQD = 100\sum_{i=1}^{n}\frac{x_i}{L}\% \quad \text{.....(4-1)}$$

where x_i = length of cores greater than 10 cm (standard RQD distribution) or 5 cm (non-standard RQD distribution); n = the number of these core that are greater than 10 cm or 5 cm intersected by a borehole core or scanline of length L. The higher value of the RQD index, the higher integrity the core has. On the other hand, the lower RQD index values mean the rock tends to be broken or weak. In this project, we have two sets of RQD index: x_i greater than 10 cm, and x_i greater than 5 cm. Using the International Society for Rock Mechanics (ISRM) proposed method, the 10-cm based, standard rock quality designation (RQD) of 89 wells in the study area are measured. In addition, 5-cm based, non-standard RQD are determined.

4.1.2 Data Collection

The RQD information was collected from 89 Bakken borehole cores stored the Wilson M. Laird Core and Sample Library of the North Dakota Geologic Survey (Figure 4-1). Top depth of each piece of core which is longer than 10 cm is recorded in ft. The length of cores is recorded in cm. The measured data were input into the Excel sheet, and converted to the RQD index. The "L" in the RQD equation is set to be 100 cm, so the calculating interval for RQD is 100 cm. The calculation starts at the top of the measured sample, and the interval is moved down at a step of 5 cm, until the bottom of the sample. Through the calculation, a continuous RQD value along the depth was obtained for each core sample and the RQD index is presented in a form similar to the well logs used in reservoir modeling (Figure 4-2).

Figure 4-1. Photo of the borehole cores

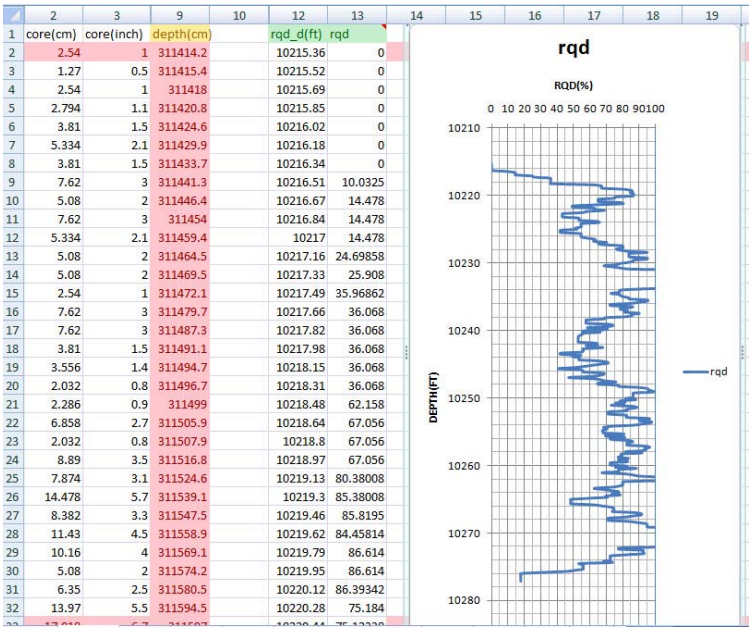

	2	3	9	10	12	13
1	core(cm)	core(inch)	depth(cm)		rqd_d(ft)	rqd
2	2.54	1	311414.2		10215.36	0
3	1.27	0.5	311415.4		10215.52	0
4	2.54	1	311418		10215.69	0
5	2.794	1.1	311420.8		10215.85	0
6	3.81	1.5	311424.6		10216.02	0
7	5.334	2.1	311429.9		10216.18	0
8	3.81	1.5	311433.7		10216.34	0
9	7.62	3	311441.3		10216.51	10.0325
10	5.08	2	311446.4		10216.67	14.478
11	7.62	3	311454		10216.84	14.478
12	5.334	2.1	311459.4		10217	14.478
13	5.08	2	311464.5		10217.16	24.69858
14	5.08	2	311469.5		10217.33	25.908
15	2.54	1	311472.1		10217.49	35.96862
16	7.62	3	311479.7		10217.66	36.068
17	7.62	3	311487.3		10217.82	36.068
18	3.81	1.5	311491.1		10217.98	36.068
19	3.556	1.4	311494.7		10218.15	36.068
20	2.032	0.8	311496.7		10218.31	36.068
21	2.286	0.9	311499		10218.48	62.158
22	6.858	2.7	311505.9		10218.64	67.056
23	2.032	0.8	311507.9		10218.8	67.056
24	8.89	3.5	311516.8		10218.97	67.056
25	7.874	3.1	311524.6		10219.13	80.38008
26	14.478	5.7	311539.1		10219.3	85.38008
27	8.382	3.3	311547.5		10219.46	85.8195
28	11.43	4.5	311558.9		10219.62	84.45814
29	10.16	4	311569.1		10219.79	86.614
30	5.08	2	311574.2		10219.95	86.614
31	6.35	2.5	311580.5		10220.12	86.39342
32	13.97	5.5	311594.5		10220.28	75.184

Figure 4-2. Example of RQD index log along the depth of a core sample

4.1.3 Calculation Procedure

The steps to calculate RQD index and generate the RQD log are as follows:

1) The records of core size were input to the Excel. There are 2 column values: one is the depth and another is core size.
2) It should be noted that recovery efficiency for coring is equal or less than 100%. Under the condition of <100% recovery efficiency, some cores were lost. To be able to calibrate the total core length to penetration footage during the coring operation, which is recorded in drilling operation, we assumed the lost cores' sizes are less than 5 cm.
3) The RQD is the total length of the rocks whose length are great or equal than 10 cm (or 5 cm) in the 100 cm range of penetration footage.
4) The first RQD index is calculated using step 3 from the top of the core interval. The RQD index is assigned in the middle of the 100cm range. Then changing the position through adding 5cm to get another RQD index.
5) Repeat step 4 until last RQD index is calculated.

4.1.4 Populating and Visualization in Petrel 3D Model

Two sets of the RQD index (x_i > 5 cm and x_i > 10 cm) of the 89 core samples were then input to the 3D Model of the Bakken formation which was constructed earlier in Petrel. The RQD logs were input as a continuous property (Figure 4-3). After inserting the RQD index along the corresponding well path (Figure 4-4), Petrel upscale the value in to the cells located in the well path (Figure 4-5), and then populates the parameters into all cells in the 3D grid based on the simulated formation geometry (Figure 4-6).

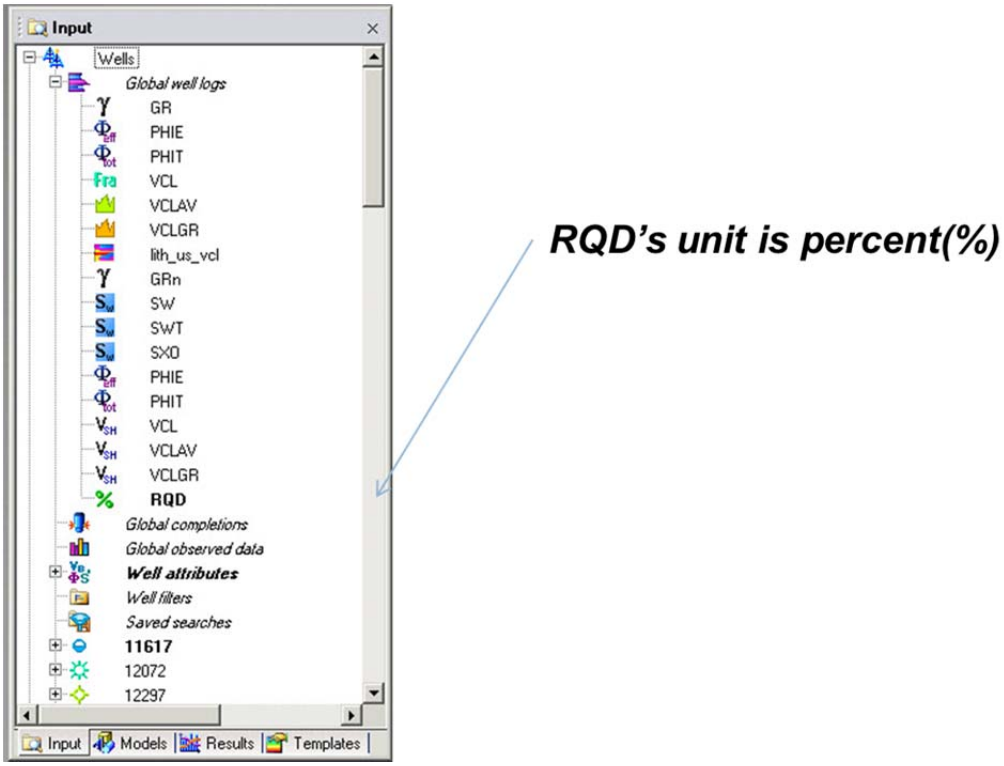

Figure 4-3. Generating RQD index as a new log type in global variable in Petrel

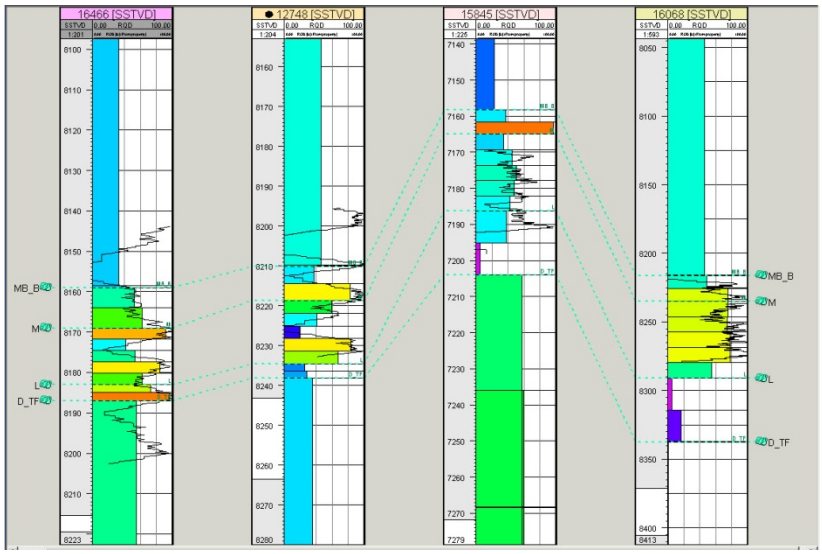

Figure 4-4. The RQD index along the corresponding well path in Petrel

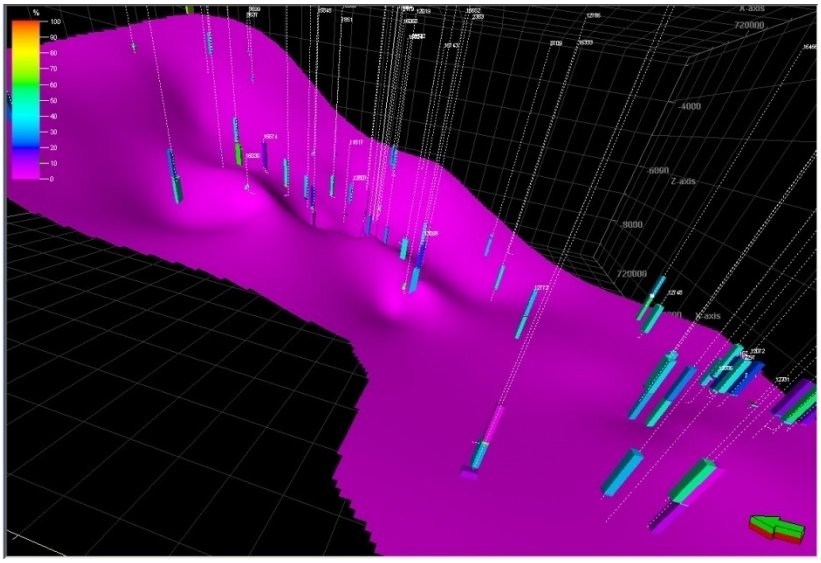

Figure 4-5. 3D geological model with the RQD index along the corresponding well path in Petrel

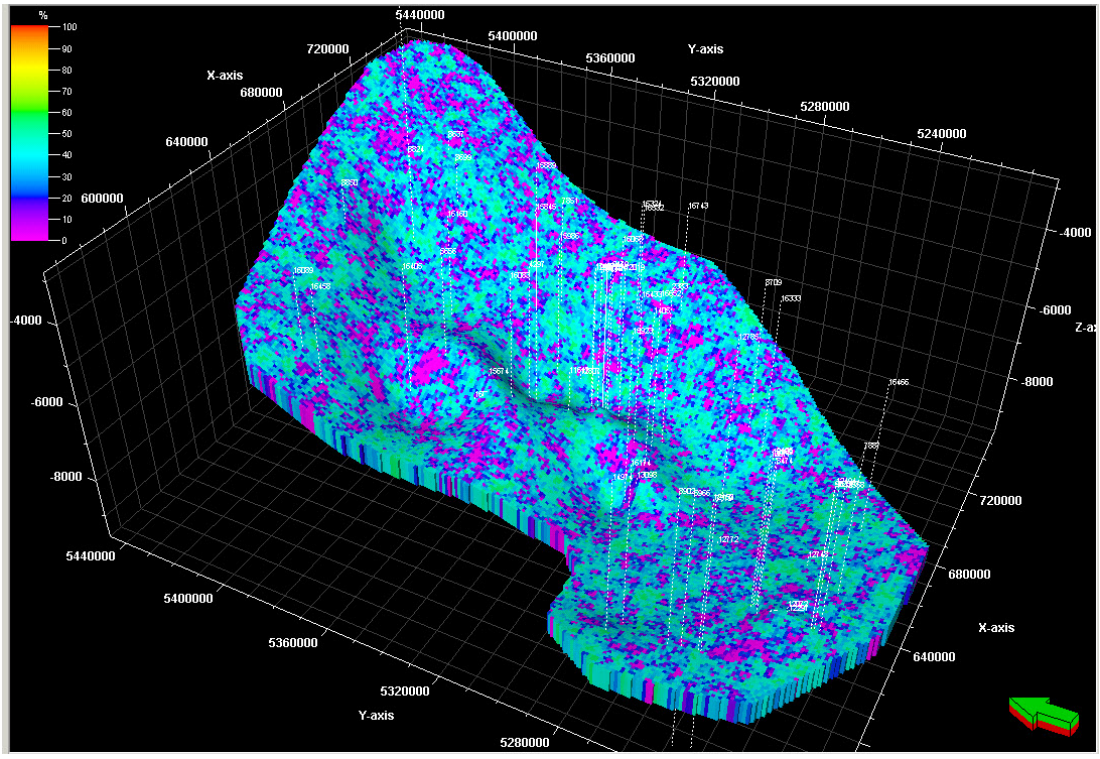

Figure 4-6. Populating RQD index in the 3D geological model in Petrel

4.1.5 RQD Results

10 cm based model

The statistical results of the RQD index of the 10 cm based model are summarized in Table 4-1. Figures 4-7, 4-8, and 4-9 show the RQD index presented in the 3D model for the upper, middle and low Bakken members, respectively. Figure 4-10 is the RQD profile of North-South cross-section view and Figure 4-11 is the RQD profile of West-East cross-section view.

Table 4-1. Statistic results of RQD index, 10 cm based

Member	Mean RQD	Std RQD
Upper Bakken	37%	25%
Middle Bakken	51%	25%
Lower Bakken	27%	24%
Total Bakken	35%	24%

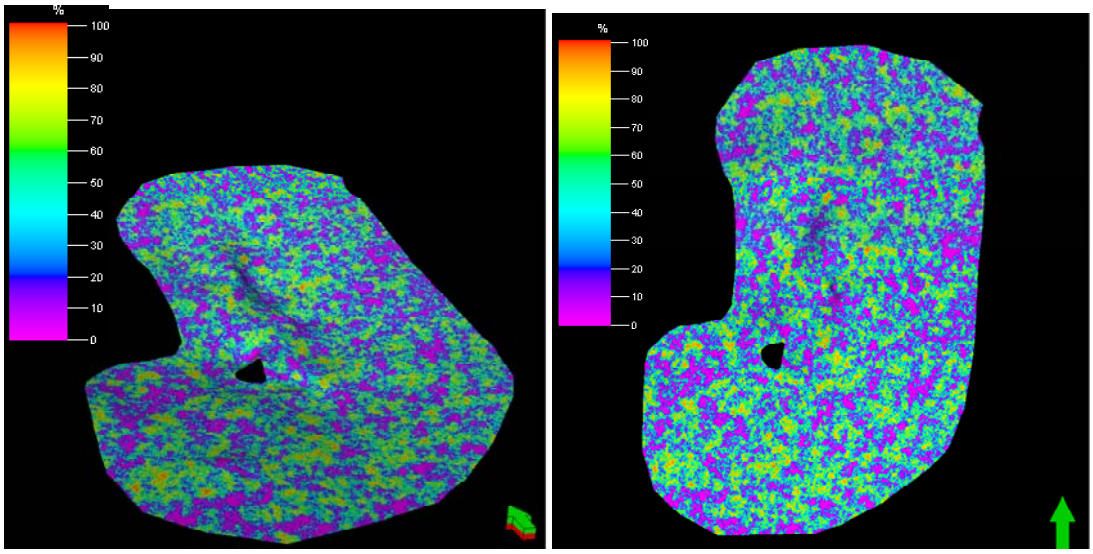

Figure 4-7. The RQD index (10 cm based) in upper Bakken Formation, green arrow pointing to north

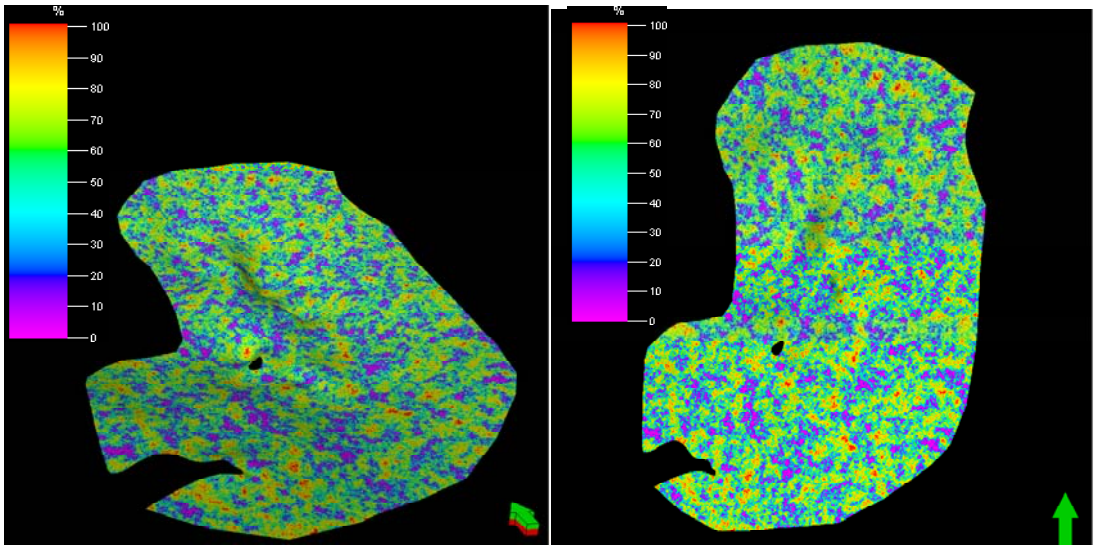

Figure 4-8. The RQD index (10 cm based) in middle Bakken Formation green arrow pointing to north

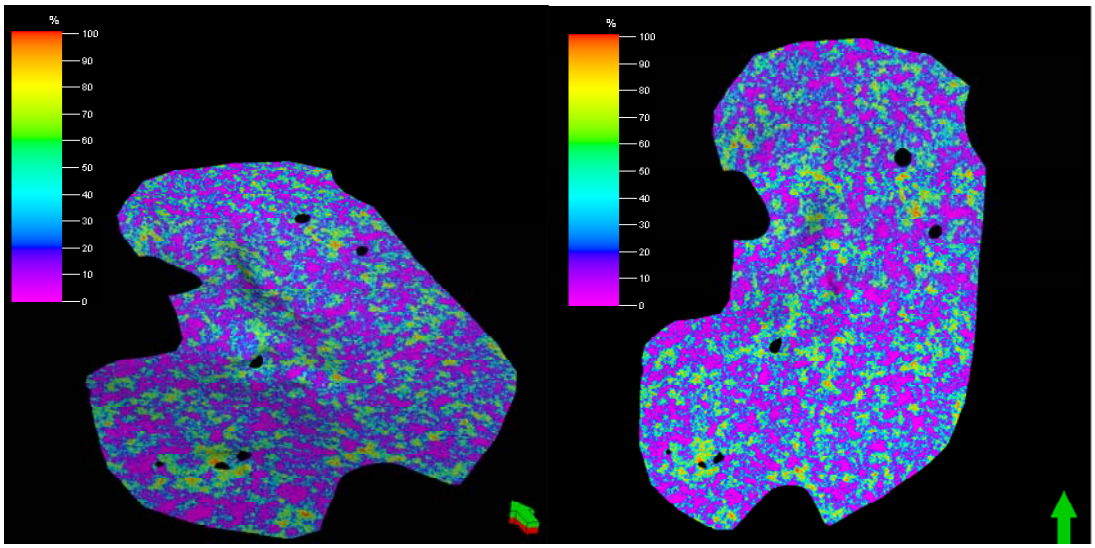

Figure 4-9. The RQD index (10 cm based) in lower Bakken Formation, green arrow pointing to north

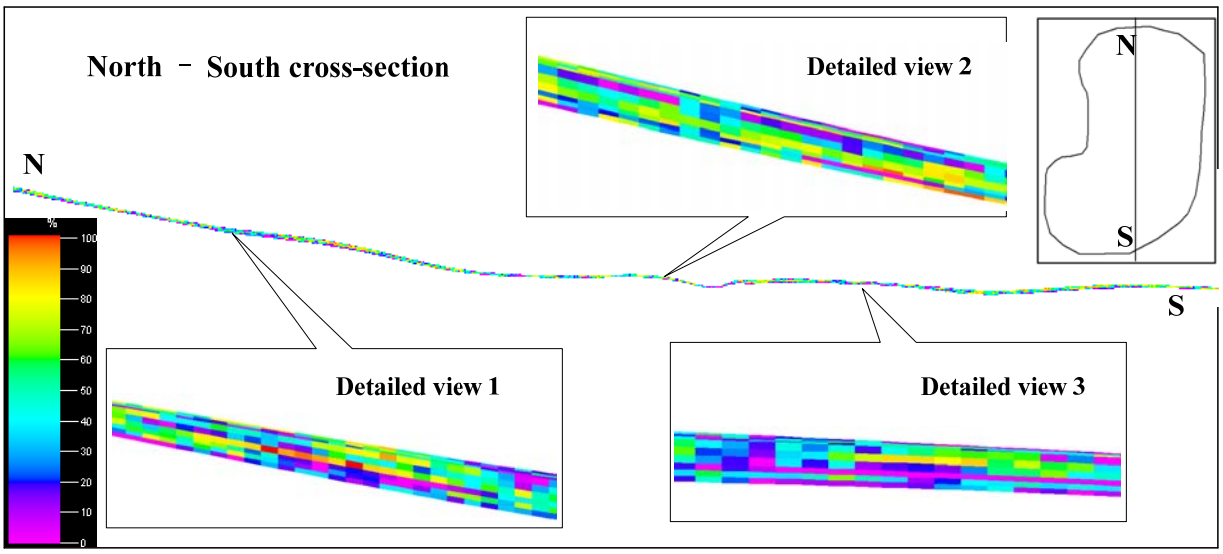

Figure 4-10. North-South cross-section view, 10 cm based RQD index

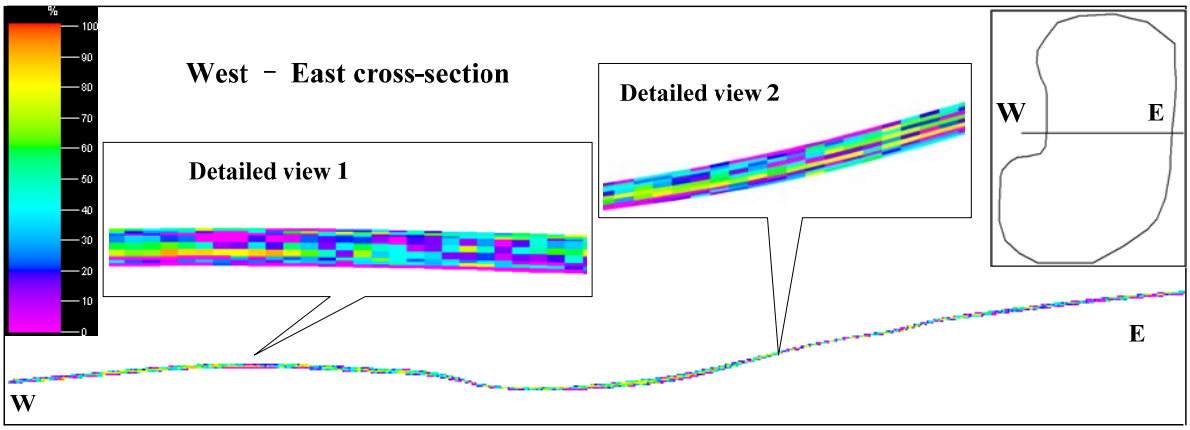

Figure 4-11: West-East cross-section view, 10 cm based RQD index

5 cm based model

The statistical results of the RQD index of the 10 cm based model are summarized in Table 4-2. Figures 4-12, 4-13, and 4-14 show the RQD index presented in the 3D model for the upper, middle and low members respectively. Figure 4-15 is the North-South intersectional view and Figure 4-16 is the West-East intersection view.

Table 4-2. Statistic results of RQD index, 5 cm based

Member	Mean RQD	Std RQD
Upper Bakken	54%	28%
Middle Bakken	64%	26%
Lower Bakken	46%	27%
Total Bakken	52%	27%

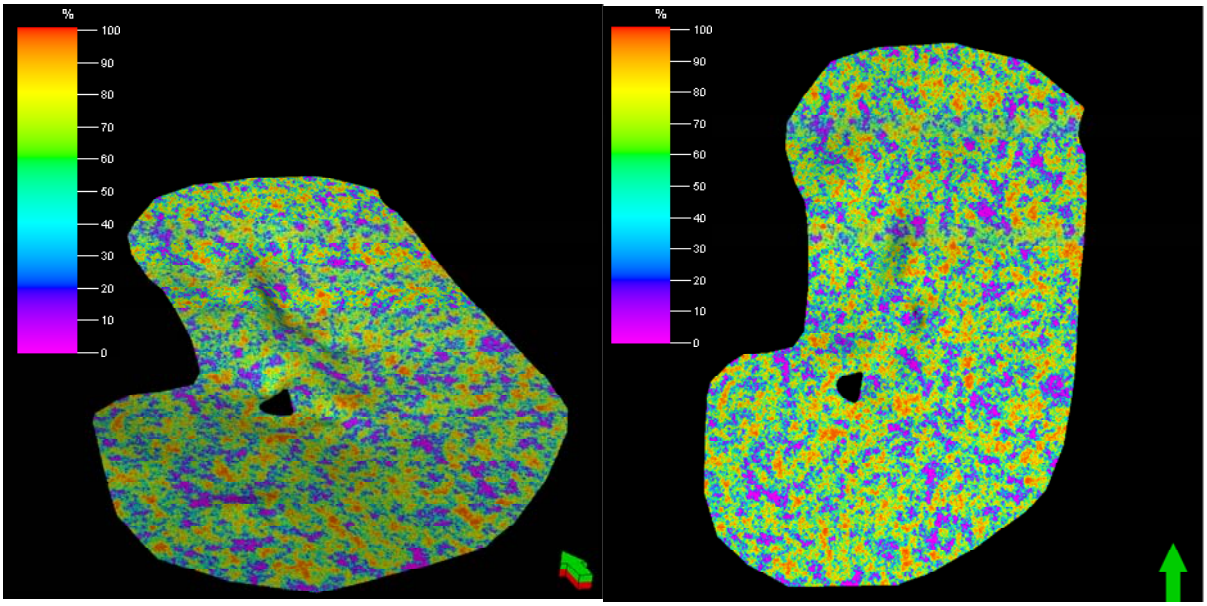

Figure 4-12. The RQD index (5cm based) in upper Bakken Formation, green arrow pointing to north

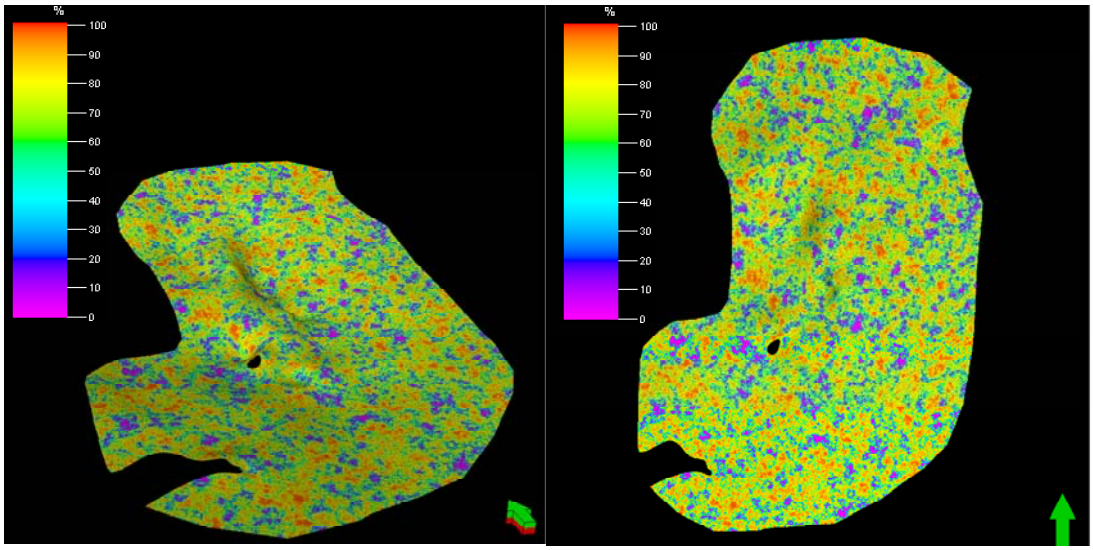

Figure 4-13. The RQD index (5cm based) in middle Bakken Formation, green arrow pointing to north

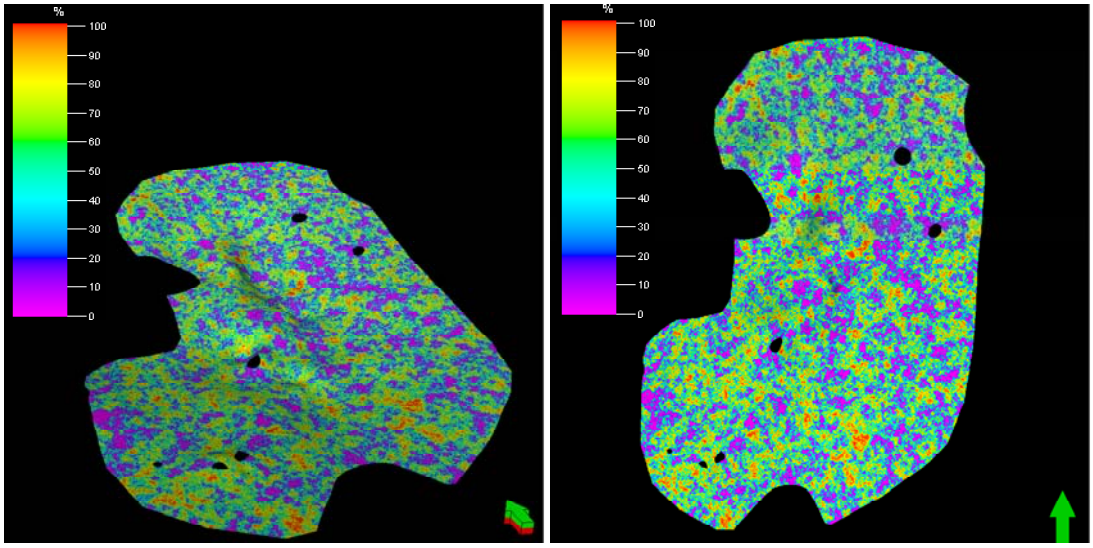

Figure 4-14. The RQD index (5cm based) in lower Bakken Formation, green arrow pointing to north

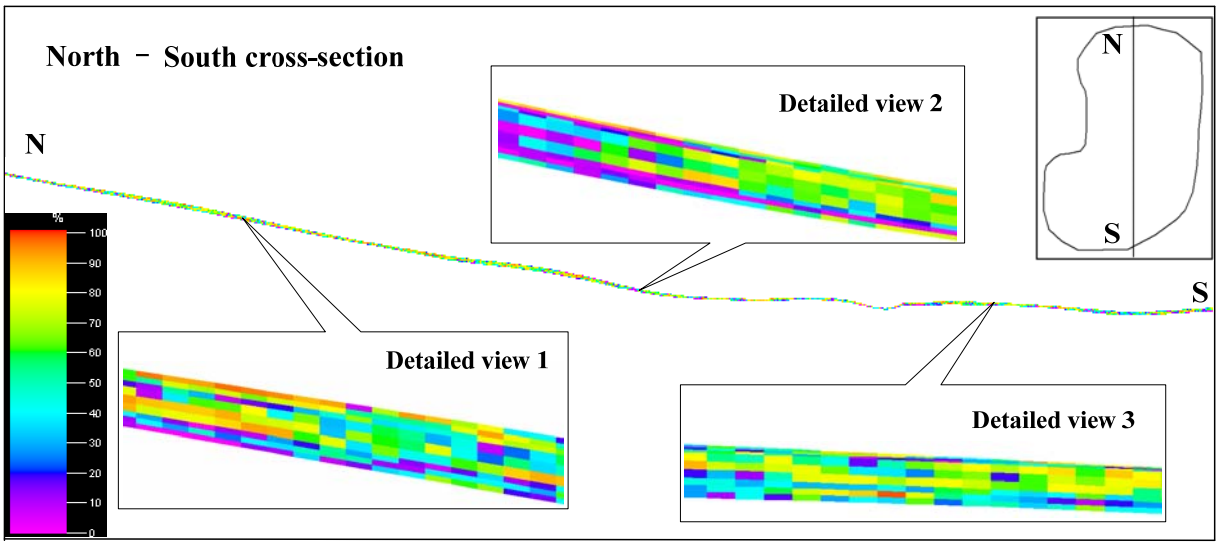

Figure 4-15. North-South cross-section view, 5cm based RQD index

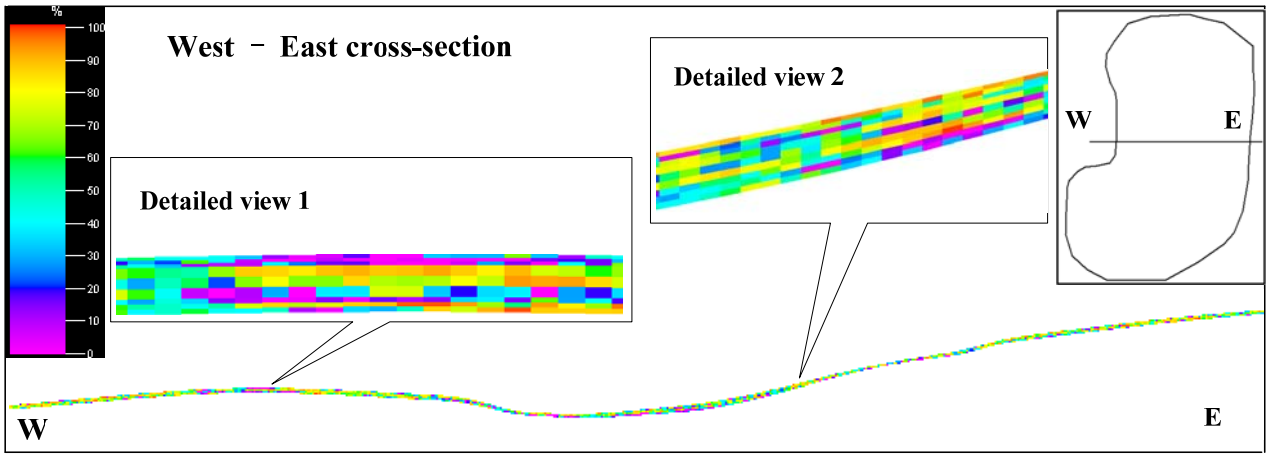

Figure 4-16. West-East cross-section view, 5cm based RQD index

4.1.6 Analysis of 3D RQD Model for Bakken Formation.

In the vertical direction, RQD index is low in upper and lower Bakken formations, while middle Bakken has the highest RQD index (Figure 4-17). It should be noted that upper and lower Bakken formations are black shale and middle Bakken formation is interbedded with limestone, siltstone, and dolomite. Therefore, it is reasonable that upper and lower Bakken formations contain more discontinuity (or lower RQD index) than middle formation. From the RQD index point of view, the lower Bakken formation is the "poorest rock" or the most uncompetitive rock and should be the target of multistage fracturing in the horizontal well completion to achieve economical oil and gas production rate. However, we notice that the RQD index in this study represents the discontinuity surface in horizontal direction. In other words, it is easier to create horizontal fracture in upper and lower Bakken than in middle Bakken. Considering the depth of Bakken formation in Williston Basin as target for multistage fracturing ranges from 7000 ft to 13000 ft, the artificial fractures generated from well stimulation are mainly vertical or high angle with rare case of horizontal. We also observe that as a result of the lithology and mineralogy differences, upper and lower Bakken become more brittle and weaker due to dehydration and weathering after the cores are extracted from subsurface, which can cause fracture or crack along the dispositional bedding. Therefore, RQD index developed in this study should not be applied without any calibration to each unique well when RQD is used to design fracturing stimulation in Bakken formation. Based on the observation and experience in the core plug preparation, we conclude that it is easier to drill the core plug or generate fracture in vertical direction for middle

Bakken than for upper and lower Bakkens. This is one of the reasons that the industry is targeting middle Bakken formation even it is more competitive than upper and lower Bakken formations. Of course, a higher permeability in middle Bakken than those in upper and lower Bakken is another driven force.

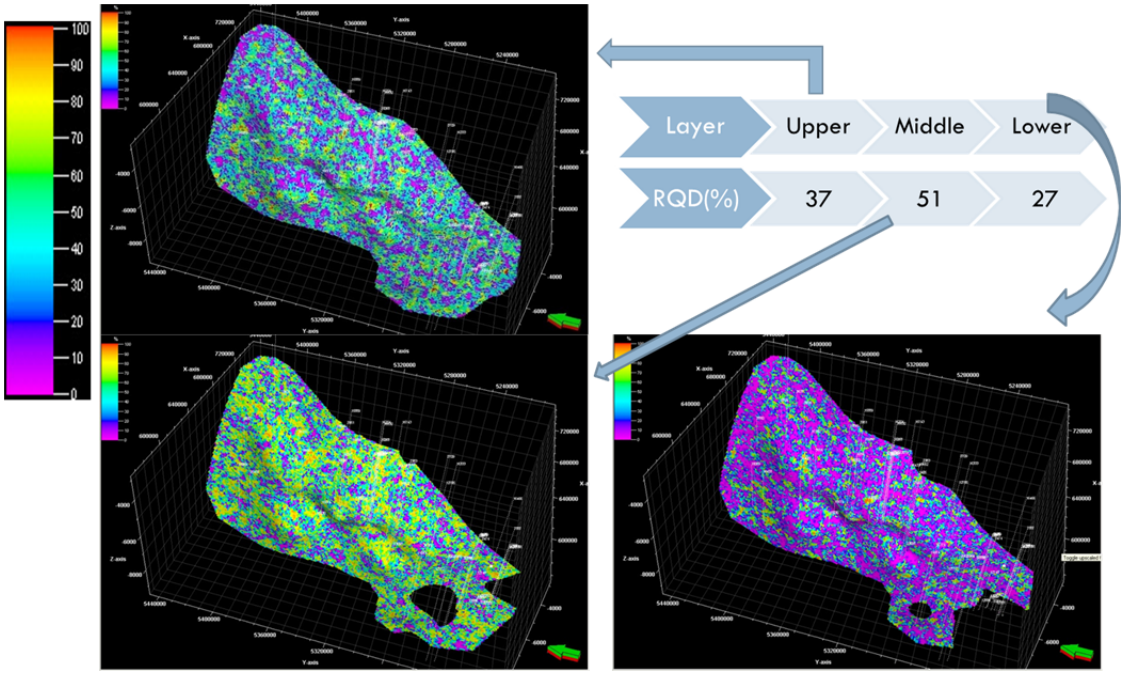

Figure 4-17. RQD index for upper, middle, and lower Bakken formations

In the horizontal direction, RQD index is low in the northern portion than in the southern portion as shown in (Figure 4-18). It should be noted that formation dip angle in north is higher than that in south, or the deformation in north is larger than that in the south, which agrees with the RQD index.

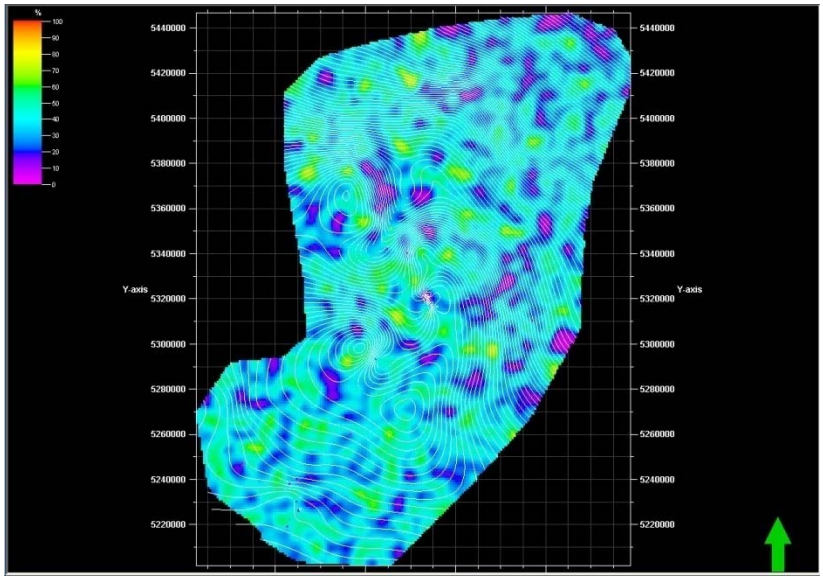

Figure 4-18. RQD index in north is lower than in south for Bakken formations

4.1.7 Correlating RQD to production history.

RQD index at the downdip (or flank) of the structure is lower than that at the updip (or the structure high). Figures 4-19 and 4-20 show the 2D and 3D structure map overlapped by RQD index. We believe the flank of the structure is

more productive than the updip of structure for Bakken formation. Two wells, Well#15923 drilled at the flank of structure and Well#13098 drilled at the top of structure (Figure 4-21), are compared to show that the structure is not the key element for well targeting Bakken formation. It is shown that Well#15923 is a productive well while Well#13098 is dry (Table 4-3). Horizontal well (Well#15845) has a higher cumulative production than that of vertical well (Table 4-4) because horizontal well contact more discontinuity surface comparing with vertical well. It seems that drilling along the long axis of anticline (Well#16532) results in a higher productivity than drilling along the short axis of anticline (Well#16333) as depicted in Figure 4-22 and Table 4-5.

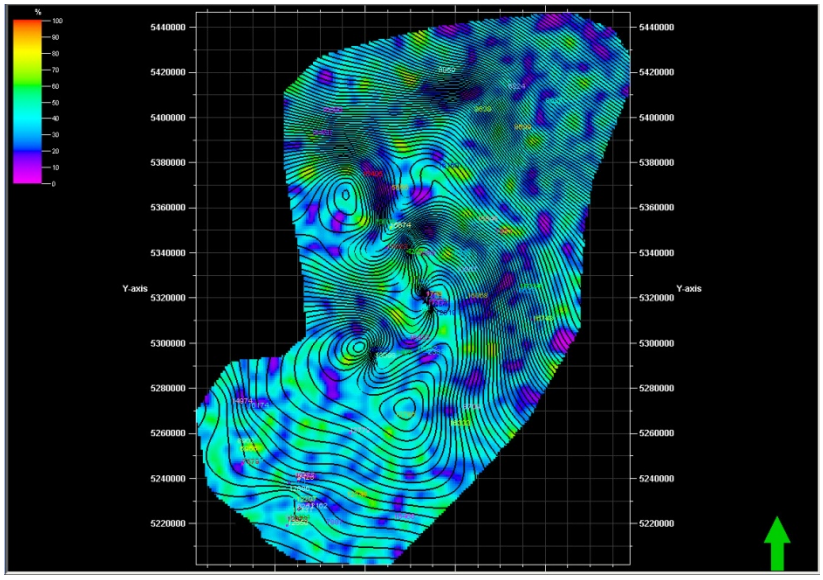

Figure 4-19. 2D structure map overlapped by RQD index for Bakken formation

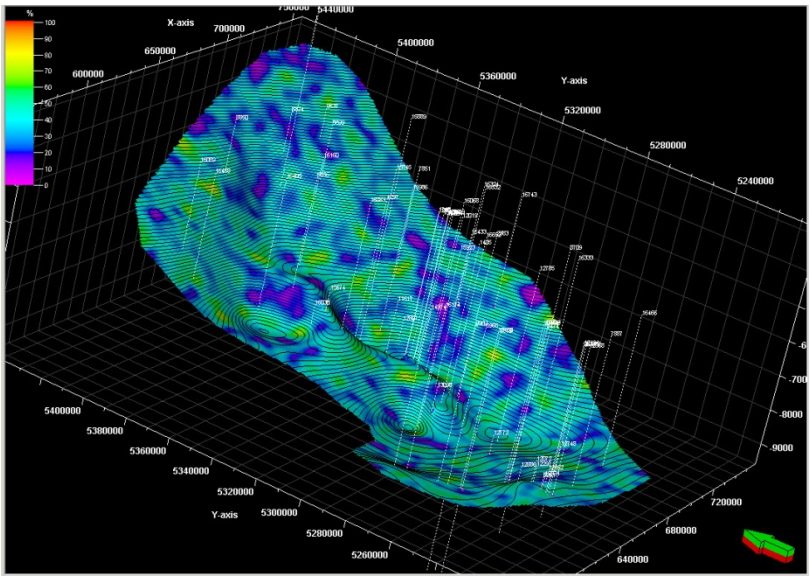

Figure 4-20. 3D structure map overlapped by RQD index for Bakken formation

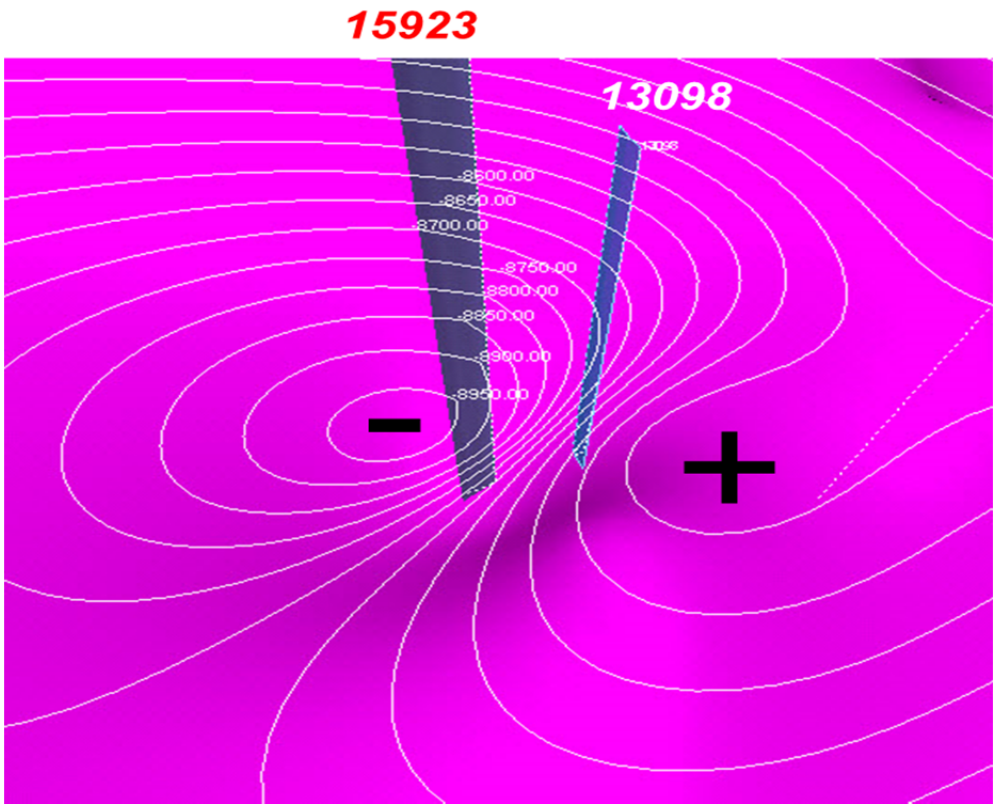

Figure 4-21. Locations of Well#15923 and Well#13098

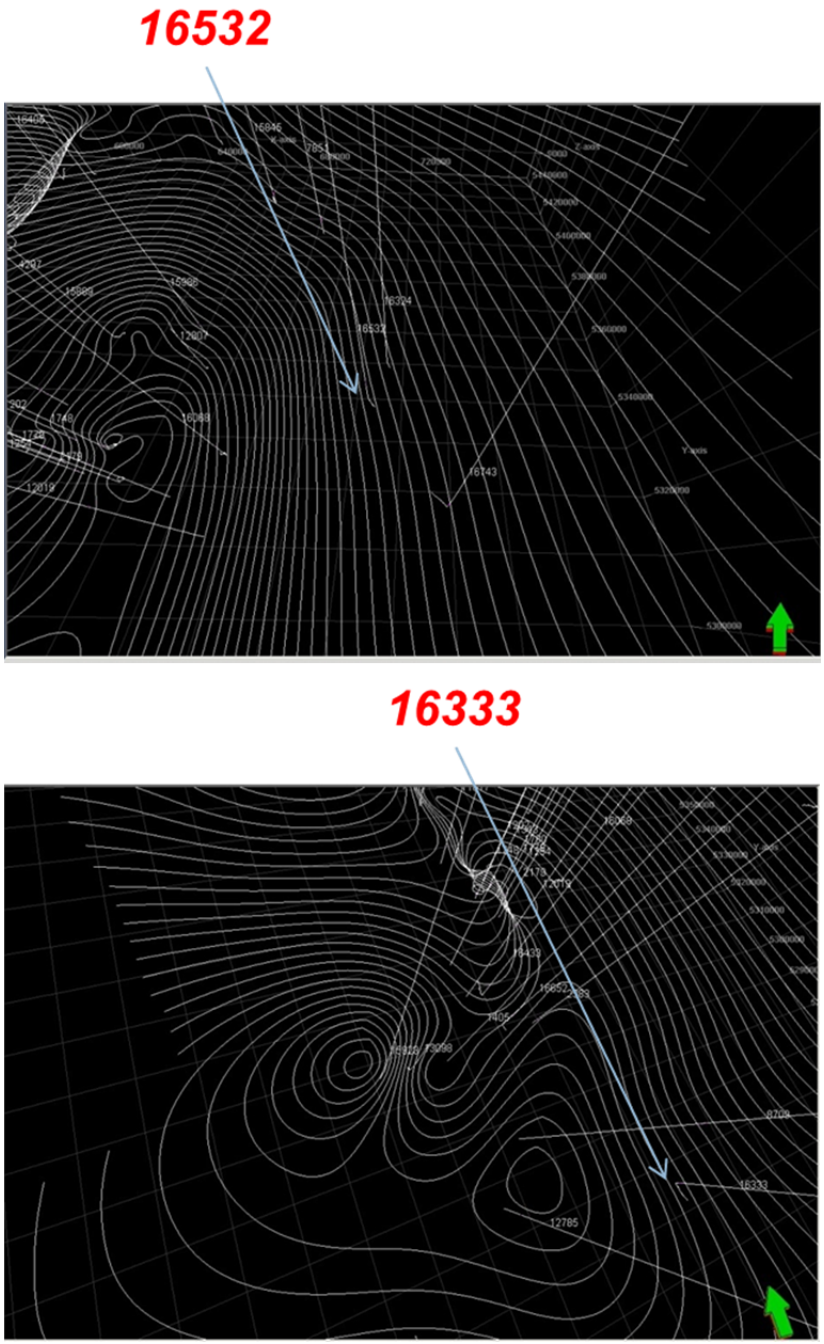

Figure 4-22. Locations of Well#16532 and Well#16333

Table 4-3. Cumulative productions of Well#15923 and Well#13098

Well	Cumulative oil (stb)	Cumulative gas (Mscf)	Cumulative oil (bbl)
15923	23,729	49,110	23,068
13098	0	0	0

Table 4-4. Cumulative productions of Well#15845 and Well#7851

Well	Cumulative oil (stb)	Cumulative gas (Mscf)	Cumulative oil (bbl)
15845	68,520	62,156	14,022
7851	1375	0	0

Table 4-5. Cumulative productions of Well#16532 and Well#16333

Well	Cumulative oil (stb)	Cumulative gas (Mscf)	Cumulative oil (bbl)
16532	280,840	117,161	11,330
16333	210,601	121,041	32,918

4.2. Bakken Wells Production Performance and RQD

4.2.1 Decline Curve Analysis

Decline curves are one of the most extensively used forms of data analysis employed in evaluating oil and gas reserves and predicting future production. The decline curve analysis technique is based on the assumption that the past production trend with its controlling factors will continue in the future and, therefore, can be extrapolated and described by a mathematical expression. The method of extrapolating a "trend" for the purpose of estimating future performance must satisfy the condition that the factors which caused changes in the past performance, i.e., decline in the flow rate, will operate in the same way in the future. These decline curves are characterized by three factors (Ahmed and McKinney, 2005):
(1) Initial production rate or the rate at some particular time;
(2) Curvature of the decline;
(3) Rate of decline.

These factors are a complex function of numerous parameters within the reservoir, wellbore, and surface-handling facilities. Certain conditions must prevail before we can analyze a production decline curve with any degree of reliability. The production must have been stable over the period being analyzed; that is, a flowing well must have been produced with constant choke size or constant wellhead pressure and a pumping well must have been pumped off or produced with constant fluid level. These indicate that the well must have been produced at capacity under a given set of conditions. The production decline observed should truly reflect reservoir productivity and not be the result of external causes, such as a change in production conditions, well damage, production controls, and equipment failure (Ahmed and McKinney, 2005). Stable reservoir conditions must also prevail in order to extrapolate decline curves with any degree of reliability. This condition will normally be met as long as the producing mechanism is not altered. However, when action is taken to improve the recovery of oil, such as infill drilling, fluid injection, fracturing, and acidizing, decline curve analysis can be used to estimate the performance of the well or reservoir in the absence of the change and compare it to the actual performance with the change. This comparison will enable us to determine the technical and economic success of our efforts (Ahmed and McKinney, 2005). Production decline curve analysis is used in the evaluation of new investments and the audit of previous expenditures. Associated with this is the sizing of equipment and facilities such as pipelines, plants, and treating facilities. Also associated with the economic analysis is the determination of reserves for a well, lease, or field. This is an independent method of reserve estimation, the result of which can be compared with volumetric or material balance estimates (Ahmed and McKinney, 2005).

The basic concept in decline curve analysis is that the "curvature" in the production rate versus time can be expressed mathematically by one of the hyperbolic family of equations. Arps (1945) recognized the following three types of rate decline behavior (Ahmed and McKinney, 2005):
(1) Exponential decline;
(2) Harmonic decline;
(3) Hyperbolic decline.

Nearly all conventional decline curve analysis is based on empirical relationships of production rate versus time given by Arps (1945) as:

$$q_t = \frac{q_i}{\left(1 + nD_i\Delta t\right)^{1/n}} \quad \text{.....(4-2)}$$

where:

q_t = gas flow rate at time t, MMscf/day

q_i = initial gas flow rate, MMscf/day
t = time, days
$D_i = bq_i^n$ =initial decline rate, 1/day
b =decline coefficient, 1/ (day (STB/day)^n)
n = Arps's decline curve exponent

Arps introduced this empirical relationship for a gas well, but with the use of linear and nonlinear regression techniques we can also use it for an oil well. The mathematical description of these production decline curves is greatly simplified with the use of the instantaneous (nominal) decline rate *D*. This decline rate is defined as the rate of change of the natural logarithm of the production rate, i.e., *ln(q)*, with respect to time *t* (Ahmed and McKinney, 2005):

$$D = -\frac{d\left(ln(q)\right)}{dt} = \frac{-1}{q}\frac{dq}{dt} \quad \text{.....(4-3)}$$

The parameters determined from the classical fit of the historical data, namely the decline rate *D* and the exponent *n*, can be used to predict future production. This type of decline curve analysis can be applied to individual wells or the entire reservoir. The accuracy of the entire reservoir application is sometimes better than for individual wells due to smoothing of the rate data. Based on the type of rate decline behavior of the hydrocarbon system, the value of *n* ranges from 0 to 1 and, accordingly, Arps's (1945) equation can be conveniently expressed in the following three forms (Ahmed and McKinney, 2005).

Table 4-6 Different types of rate-time relationship

Case	n	**Rate-time relationship**	
Exponential	$n=0$	$q_t = q_i \times e^{-D_i \Delta t}$	(3)
Harmonic	$n=1$	$q_t = \frac{q_i}{\left(1+D_i \Delta t\right)}$	(4)
Hyperbolic	$0 \prec n \prec 1$	$q_t = \frac{q_i}{\left(1+nD_i \Delta t\right)^{1/n}}$	(5)

where q_t is the oil production rate at time t, q_i is the initial oil production rate, and D_i is the initial decline rate (at t=0).

In this study we use the first two methods to analyze the relation between RQD and the decline trend of the wells producing from Bakken formation in Williston Basin. The use of hyperbolic method to analyze the decline rate of the Bakken wells failed because of the divergence of the solutions. The main characteristics of these decline curves are discussed below and can be used to select the flow rate decline model which is appropriate for describing the rate–time relationship of a hydrocarbon system:

In Williston Basin 25 wells, which are producing from Bakken formation, are studied in this research (the rest of the wells either lacked some data or were not Bakken-related). First, RQD data of the wells were obtained from the core laboratory measurements. Then, the decline curve analysis was done for estimating the decline trend of each well. Efforts were made to correlate the RQD measurements with the decline rate coefficient of the wells. It's been expected that the higher the RQD, the less prolific the well (no matter horizontal or vertical well). In the following, this hypothesis is examined through the use of sophisticated mathematical methods.

Table 4-7 Values of total RQD and Decline coefficient for each well

Well Name	10077	12160	12331	12494	12873	15674	15845	15889	15923
RQD_t	0.48	0.06	0.98	0.47	0.45	0.34	0.33	0.47	0.51
b	2.77E-05	2.97E-05	2.15E-05	2.63E-05	8.82E-05	2.08E-05	4.55E-05	1.10E-04	2.14E-04

15986	16030	16068	12162	16803	16089	16160	16174	16405
0.51	0.47	0.45	0.37	0.40	0.38	0.51	0.58	0.43
1.39E-04	1.16E-04	1.80E-05	7.85E-05	1.65E-05	9.11E-05	5.36E-04	1.61E-04	1.95E-04

16458	16532	16652	5656	7579	8251	8474	8709
0.17	0.19	0.38	0.14	0.39	0.36	0.29	0.26
1.74E-04	8.26E-06	5.38E-05	9.24E-05	3.24E-05	6.60E-05	1.57E-05	4.80E-04

4.2.2 Exponential Decline Analysis

A straight-line relationship will result when flow rate is plotted versus time on a semilog scale and also when the flow rate versus cumulative production is plotted on a Cartesian scale. Regarding exponential decline, using linear regression technique we may have:

$$D = b$$

$$x_i = \Delta t$$

$$y_i = \ln(\frac{q_t}{q_i})$$

$$y_i = -bx_i \quad \text{.....(4-4)}$$

The parameter b is approximated in such a way that the error function becomes minimal (least square method).

$$s = \sum_{i=1}^{N} \left(y_i + bx_i \right)^2 \quad \text{.....(4-5)}$$

$$\frac{\partial s}{\partial b} = \sum_{i=1}^{N} \left(y_i x_i + bx_i^2 \right) \quad \text{.....(4-6)}$$

Hence, b can be calculated by the following formula:

$$b = -\frac{\sum_{i=1}^{N} y_i x_i}{\sum_{i=1}^{N} x_i^2} \quad \text{.....(4-7)}$$

4.2.3 Harmonic Decline Analysis

Harmonic decline equation in Table 4-6 describes the rate-time relationship in harmonic decline case. Since it is not possible to build any linear relationship between rate and time neither in Cartesian nor in logarithmic system, we have to use another technique to approximate the decline coefficient of the wells. The method of nonlinear regression is used to determine the decline rate and the decline coefficient by analyzing the production data since the time point

at which the production rate of the wells started to decline. Therefore, the time difference (Δt) is defined as any time increment from that time onward. The following mathematical procedure has been coded by computer programs to obtain the decline coefficient for all the wells:

$$D_i = bq_i$$
$$x_i = \Delta t$$
$$y_i = \frac{q_t}{q_i} \quad \text{.....(4-8)}$$

where b is the decline coefficient, and D_i is the initial decline rate to be determined. We should obtain D_i such that the series in Equation 4-10 becomes minimal. This is the basic element of nonlinear regression technique. To obtain such value for D_i the following calculations are established:

$$s = \sum_{i=1}^{N} \left(y_i - (1 + D_i x_i)^{-1} \right)^2 \quad \text{.....(4-9)}$$

$$\frac{\partial s}{\partial D_i} = f(D_i) = \sum_{i=1}^{N} \left(\frac{x_i \left(y_i - (1 + D_i x_i)^{-1} \right)}{(1 + D_i x_i)^2} \right) \quad \text{.....(4-10)}$$

The Jacobian matrix of the objective function is also obtained by applying Equation 4-11.

$$J = [\frac{\partial f}{\partial D_i}] = [\sum_{i=1}^{N} x_i^2 \frac{\left(1 - 2(1 + D_i x_i)\left(y_i - (1 + D_i x_i)^{-1} \right)\right)}{(1 + D_i x_i)^4}] \quad \text{.....(4-11)}$$

and here is the objective function to be minimized:

$$f(D_i^*) = \sum_{i=1}^{N} \left(\frac{x_i \left(y_i - (1 + D_i x_i)^{-1} \right)}{(1 + D_i x_i)^2} \right) = 0 \quad \text{.....(4-12)}$$

$$D_i^* = D_i + dD_i \quad \text{.....(4-13)}$$

D_i is the first guess and dD_i is the difference between the first guess and the first result which can be obtained from Equation 4-15. To obtain this difference we use the Taylor series (in the following equations [ ] refers to matrix):

$$f(D_i^*) = f(D_i) + \frac{\partial f(D_i)}{\partial D_i} \times dD_i = f(D_i) + \left[\frac{\partial f(D_i)}{\partial D_i} \right] \left[dD_i \right] = 0$$

$$\Rightarrow \left[f(D_i) \right] = -\left[\frac{\partial f(D_i)}{\partial D_i} \right] \left[dD_i \right]$$

$$where:$$

$$\left[\frac{\partial f(D_i)}{\partial D_i} \right] = Jacob = J \quad \text{.....(4-14)}$$

From these equations we may have:

$$\left[f(D_i)\right] = -J\left[dD_i\right]$$
$$\Rightarrow \left[dD_i\right] = -J^{-1}\left[f(D_i)\right]$$
$$where:$$
$$\left[dD_i\right] = \left[D_i^*\right] - \left[D_i\right]$$
$$\Rightarrow \left[D_i^*\right] - \left[D_i\right] = -J^{-1}\left[f(D_i)\right] \quad \text{.....(4-15)}$$

where the definitions of $[D_i]$ and $[D_i^*]$ are as follows:

$$\left[D_i\right] = \left[D_i\right]^k \quad the\ first\ guess!$$
$$\left[D_i^*\right] = \left[D_i\right]^{k+1} \quad the\ first\ result!$$
$$\left[D_i\right]^{k+1} - \left[D_i\right]^k = -J^{-1}\left[f(D_i)\right] \quad \text{.....(4-16)}$$

Therefore, the following trial-error relationship can be established between the guesses and the results in many iterative steps of calculations:

$$\left[D_i\right]^{k+1} = \left[D_i\right]^k - J^{-1}\left[f(D_i)\right] \quad \text{.....(4-17)}$$

where J^{-1} is the inverse of Jacobian matrix, and k denotes the number of calculation steps after assuming a starting guess. This iterative computation is repeated until the relative difference between the values of D_i at any two consecutive computation steps becomes smaller than a specified value. To check this relative error the following is used:

$$norm = \sqrt{\sum_{i=1}^{N} f_i^2}$$
$$here\ N = 1$$
$$\Rightarrow norm = f \quad \text{.....(4-18)}$$

If the norm is higher than a specified value, the calculations proceed until an acceptable norm is achieved. There is also another criterion which should be fulfilled, that is:

$$norm_2 = f\left(\left[D_i\right]^{k+1}\right)$$
$$norm_1 = f\left(\left[D_i\right]^{k}\right)$$
$$\Rightarrow$$
$$norm_2 \prec norm_1 \quad \text{.....(4-19)}$$

At any step this condition should hold, unless otherwise Equation 4-17 should be modified as the following:

$$[D_i]^{k+1} = [D_i]^k - J^{-1} s[f(D_i)]$$

$$s = \frac{\sqrt{1+6\eta}-1}{3\eta}$$

where

$$\eta = \frac{norm_2}{norm_1} \qquad \text{.....(4-20)}$$

This process has been programmed in MATLab, and this procedure has been accomplished for all the wells listed in Table 4-7 and the results of a handful of the wells are illustrated in Figures 4-23 through 4-28 (in these figures q_o is oil production rate and q_{oi} is the initial oil production rate).

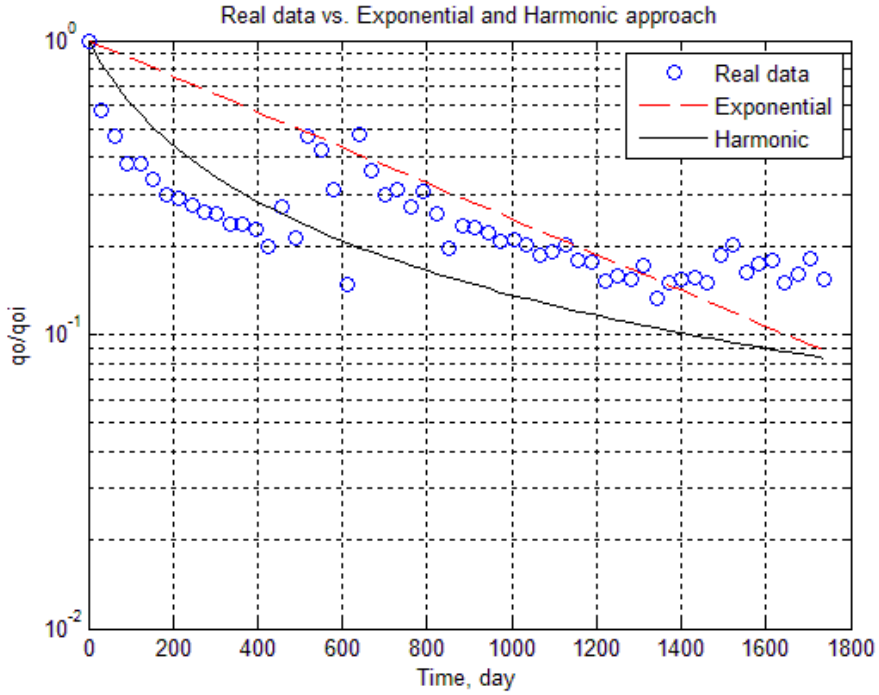

Figure 4-23. Real data vs. Exponential and Harmonic decline approach (well 15674)

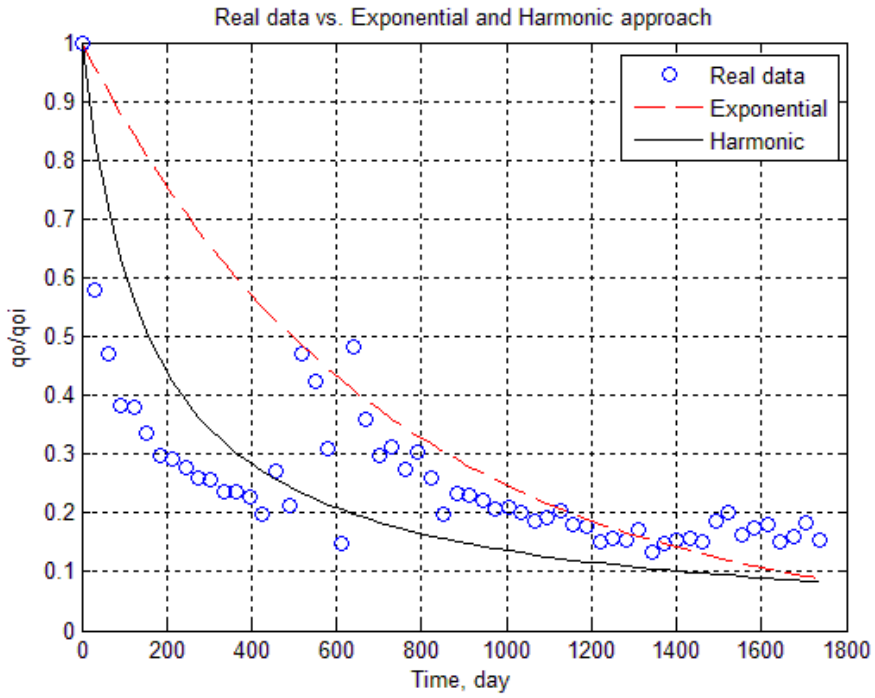

Figure 4-24. Real data vs. Exponential and Harmonic decline approach (well 15674)

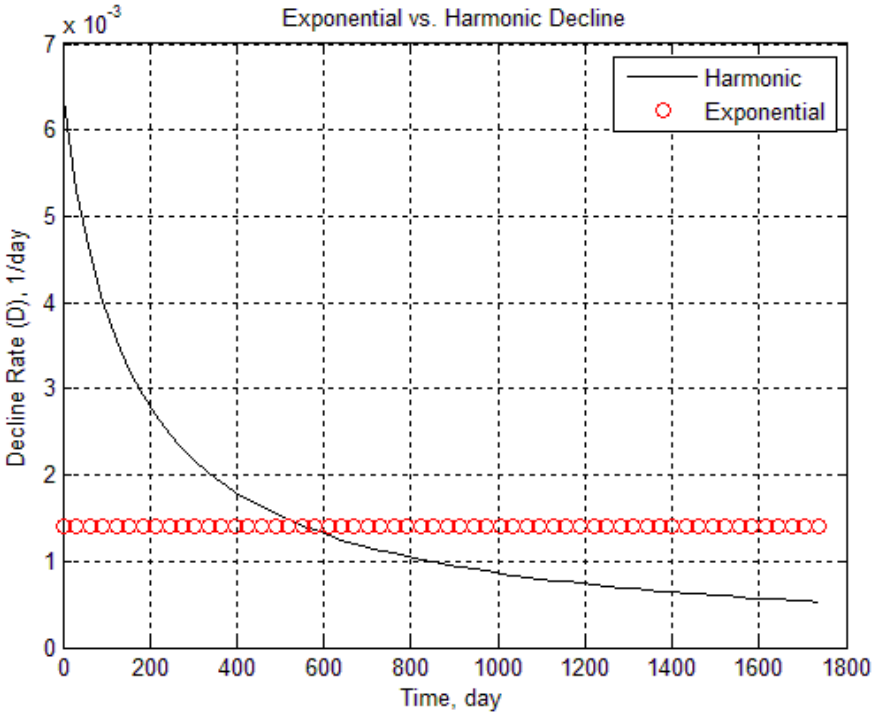

Figure 4-25. Exponential vs. Harmonic decline approach (well 15674)

The same results for another well (well 15986) are obtained and are shown below:

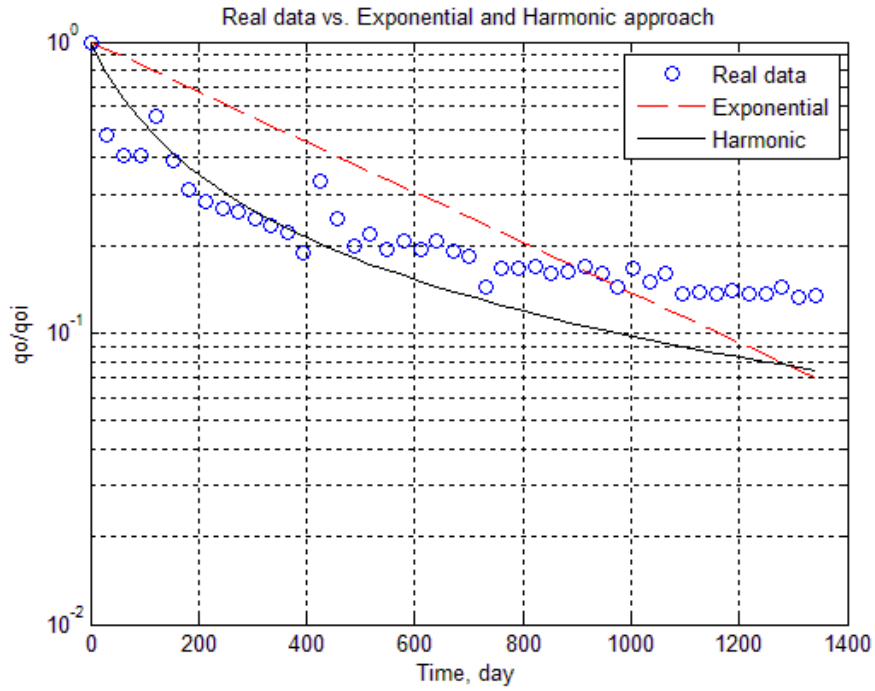

Figure 4-26. Real data vs. Exponential and Harmonic decline approach (well 15986)

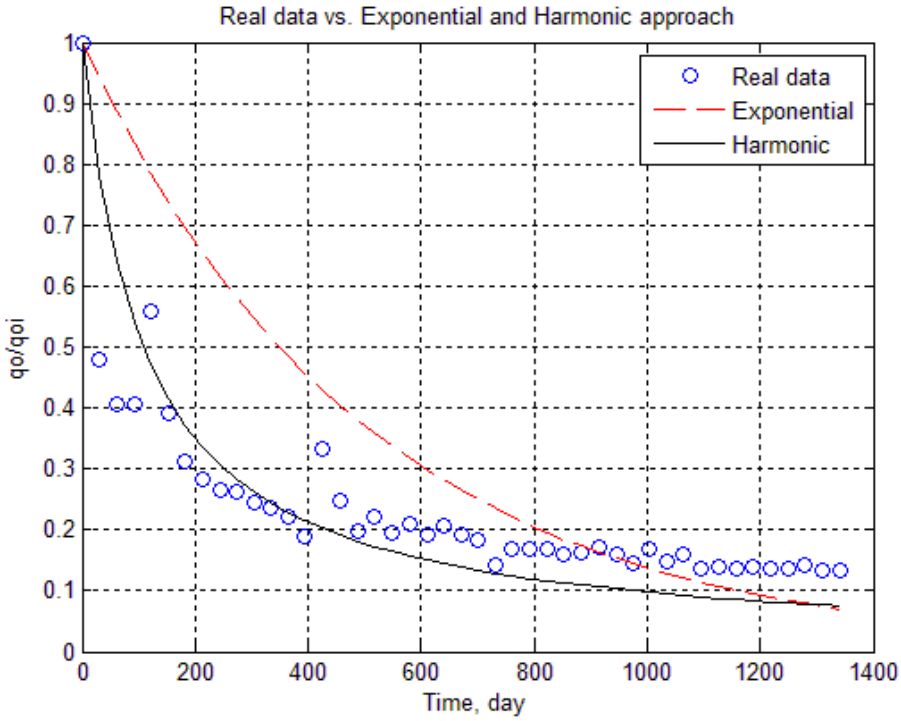

Figure 4-27. Real data vs. Exponential and Harmonic decline approach (well 15986)

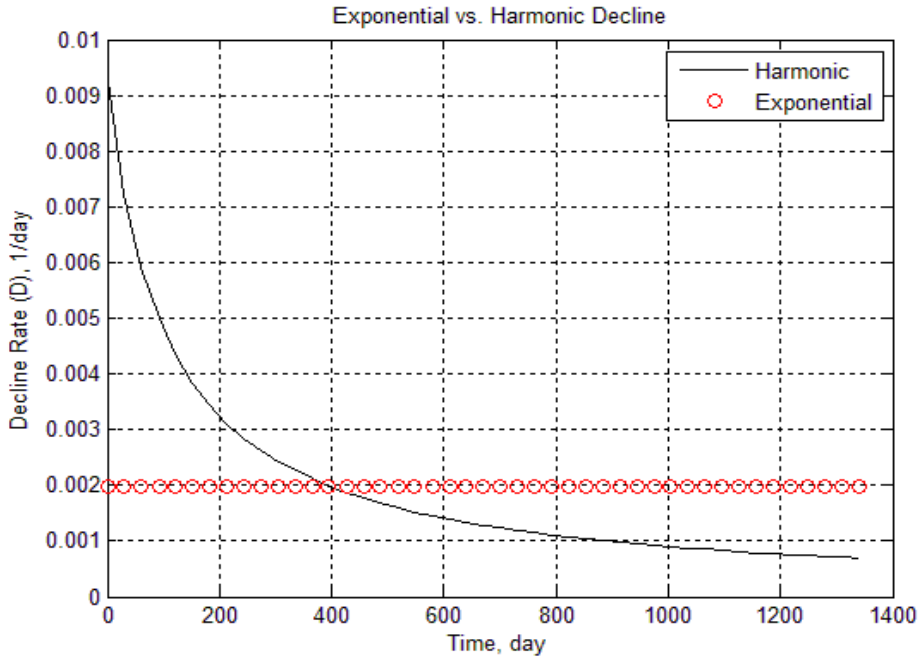

Figure 4-28. Exponential vs. Harmonic decline approach (well 15986)

Using Equation 4-3 and rearranging harmonic decline equation, led us to Equation 4-21. From this we may conclude that the more the decline coefficient (b), the more the decline rate (D). This is clearly illustrated in Figure 4-29.

$$D = \frac{bq_{oi}}{\left(1 + bq_{oi}\Delta t\right)} \quad \text{.....(4-21)}$$

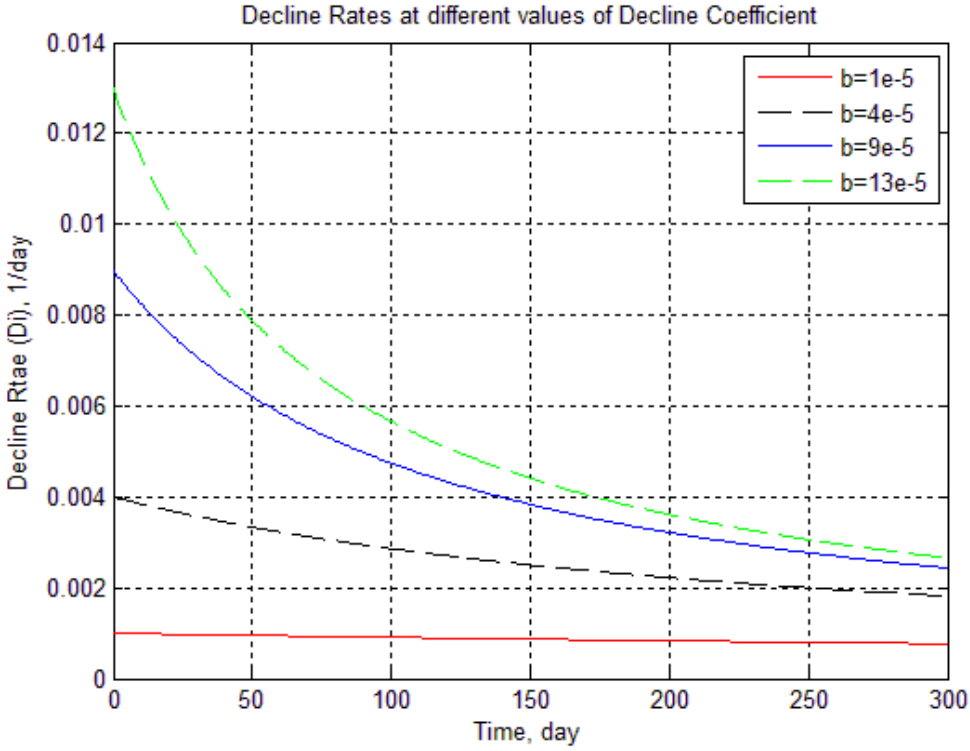

Figure 4-29. Effect of Decline coefficient on decline rate

4.2.4 Relation between Production Decline and RQD

Due to the reasons mentioned above, we may expect that the more the decline coefficient, the more the RQD of a well. This makes sense since the more RQD generally means the less number of fractures or fissures along the centerline of the core. In Figure 4-30 this hypothesis is investigated.

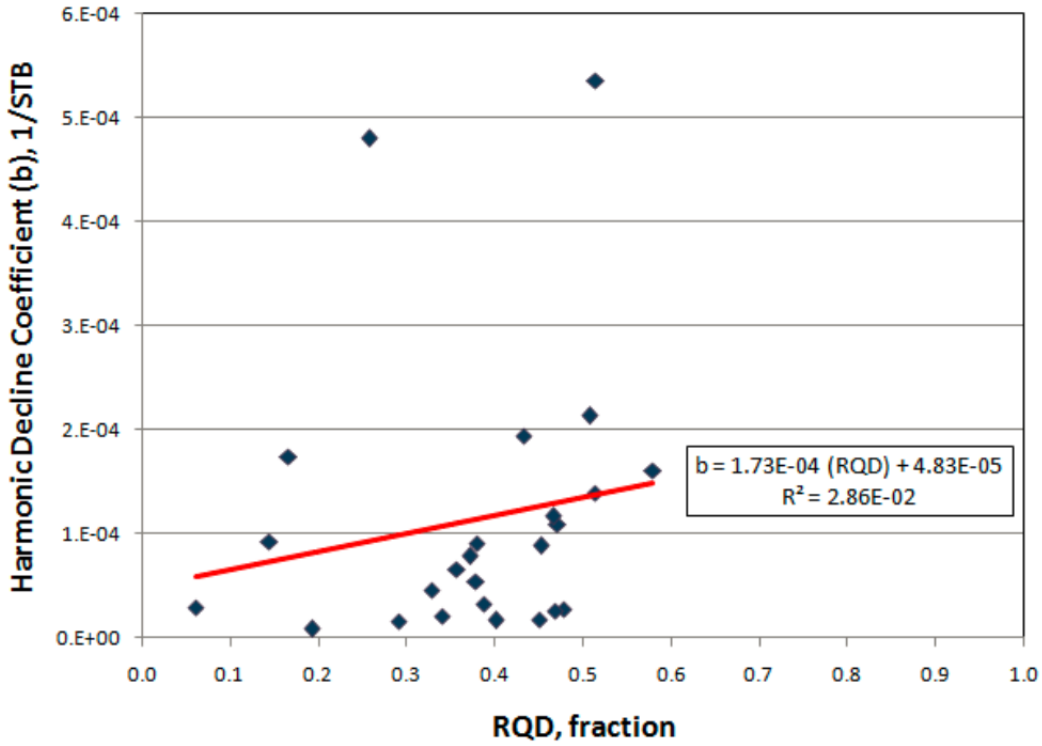

Figure 4-30. Decline coefficients of wells vs. RQD

In Figure 4-30 *b* is the decline coefficient which is shown on the ordinate. The values of this parameter for all the wells were obtained and are plotted versus their corresponding RQD values in Fig.8. The trend line in this graph is calculated by the linear curve fit method. It is clear that the relationship between decline coefficient and RQD conforms well to the linear trend line. It means that the higher RQD, the higher decline coefficient and the higher decline rate, accordingly.

Based on the study described above, we can now conclude that the value of RQD of the wells- producing from Bakken formation is related reversely to the wells performance. It might be applicable to delineate the degree of fracturing in the Bakken wells along with to make comparisons among the producing wells.

5. Mapping of Paleo In-Situ Stresses

5.1. Geological Settings

The Bakken formation is a tight oil play with continuous oil accumulation. Fractures play an important role in both exploration and production of the oil. As considered to be one of the most promising plays in the world, oil production from the Bakken largely depends on presence of natural or artificially-created fractures. There also exist arguments about the oil migration patterns in and out of the Bakken. This study reviews the tectonic history of the Williston basin, North Dakota, USA, and a numerical model of the study area has been built to reconstruct the paleostress under the far-field effect of the Laramide orogeny in late Cretaceous. The modeling results show that tensile horizontal stress was developed in most parts around the Nesson master fault in the study area during the Laramide event, and tensile fractures are very likely to be generated in the north and south sides of the fault. These tensile fractures could enhance the reservoir quality in both porosity and permeability. Zones of possible fracture development are identified based on the stress profile. In the fault zone, the paleostress has a lower magnitude of compressive stress than that in the host rock, so driving force may be provided to push the oil migrate from the host rock to the fault zone. However, after the hydrocarbon accumulated in the fault, fractures presented around the fault may function as additional pathways for migration again.

The Nesson anticline is a major north-trending structural feature located near the center of the Williston Basin (Figure 5-1). The anticline is created by a drag fold and its deformation is controlled mainly by movement on a major normal fault beneath the west side of the anticline crest. The Nesson anticline is about 175 km long, with nearly continuous production along a north-south line from just south of Canadian border (T163N) to the Killdeer Mountains (T146N), south of the Missouri River. Nesson master fault bounds the structure from Beaver Lodge Field (T156N) to just south of T150N, with its west side downthrown. (Lindsay et al., 1988). The Nesson anticline has a large bifurcation on its southeast side – the Antelope anticline (Figures 5-1 and 5-2). The Antelope anticline trends NW-SE, with a much smaller size comparing to the Nesson anticline. Antelope fault occurs along the northeast side of the Antelope anticline, with its northeast side downthrown. The Antelope fault is thought to have affected Devonian and younger strata (Lindsay et al., 1988).

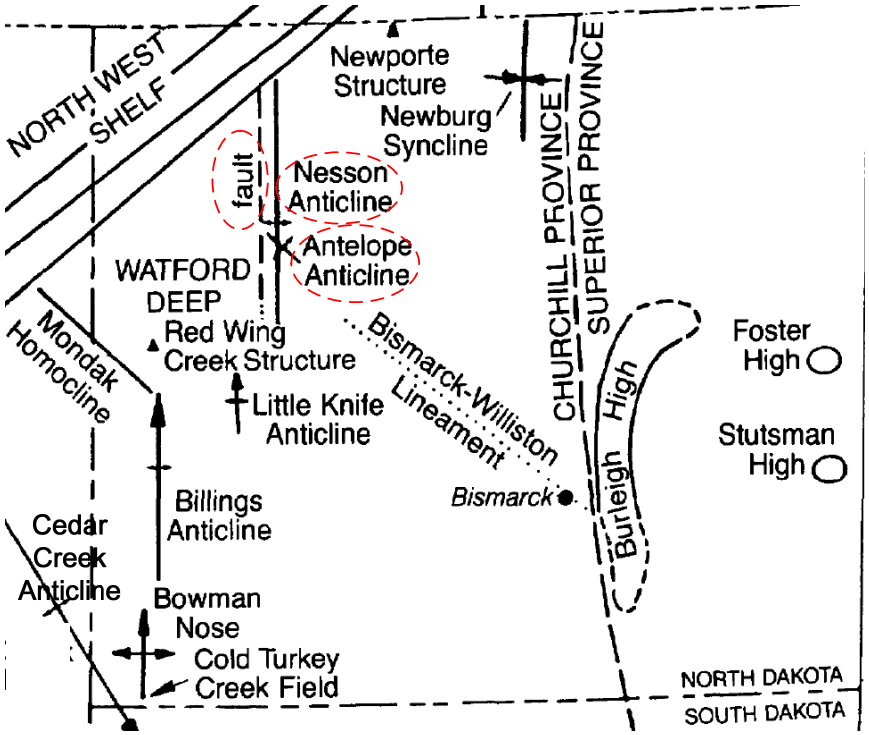

Figure 5-1. Major structural features of the Williston basin, North Dakota portion (After Gerhard et al., 1990).

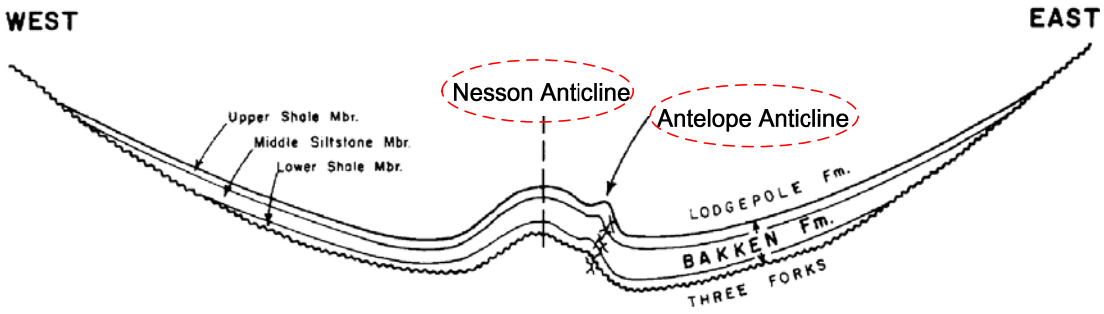

Figure 5-2. Cross section view of the Nesson anticline and Antelope anticline (after Meissner, 1978).

Presences of the Nesson master fault and the Antelope fault can influence the local in situ stress field. Both the magnitude and the direction of the in situ stress in the fault zone differ from those in the host rock (Gudmundsson et al., 2010). The Nesson anticline area has the most intensive oil production in the Williston basin. Horizontal drilling and hydraulic fracturing are extensively applied in this area. It is of great interest to understand the distribution of the natural fractures and the in situ stress in this region.

The characteristics of the natural fractures, especially origination mechanisms, in the Bakken formation have been investigated by many researchers (Pitman et al., 2001; Meissner 1978; Murray 1968; Druyff, 1991; Mullen et al., 2009; Stockton, 2009; Warner, 2011). As early as 1968, Murray (1968) applied the curvature method to study the fracture development in the Devonian Sanish pool in the Antelope field, and the contribution of the natural fractures to reservoir quality. In general, natural fractures in the Bakken formation can be categorized into three types according to different origination mechanisms: 1) fractures caused by tectonic stress; 2) fractures as a result of regional stress; and 3) fractures associated with super-lithostatic pressure increase due to the hydrocarbon expulsion during maturation. The Bakken is also regionally overpressured and featured with a very high pore pressure. Documented fluid-pressure gradient is as high as 0.73psi/ft (16.5 kPa/m) in the Antelope filed. These high pressures are discretely confined to the Bakken interval Meissner (1978) and are beneficial for oil production.

5.2. Tectonic History of the Basin

The Williston Basin is one of the four cratonic basins in North America (Bally, 1989). They are different from the other two types of Most basins were formed due to extensional and/or compressional deformation of the sedimentary rocks. Cratonic basins were formed mainly due to large scale deposition of sedimentary rocks that covers one or more cycles of complete marine transgressive-regressive process.

The basin is neither structurally complicated, nor tectonically active. To better understand the basin, it is essential to study its tectonics. From tectonic point of view, the Williston Basin is composed of two parts: the hard basement and the relatively soft sedimentary top deposits. The structural geology and part of the geomechanical properties (i.e., in-situ stress) of the sedimentary formations, including Bakken formation, are largely influenced (controlled) by the geological features of the basement.

5.2.1 The Basement

The Williston basin basement includes five major components. From east to west in a plan view, these five components are (Green, 1985; Fischer et al., 2005): (1) the Superior craton, (2) the Archean- Proterozoic Thompson boundary zone, (3) the Proterozoic island arc massifs, (4) the Trans-Hudson orogenic belt, and (5) the Wyoming craton, as shown in Figure 5-3.

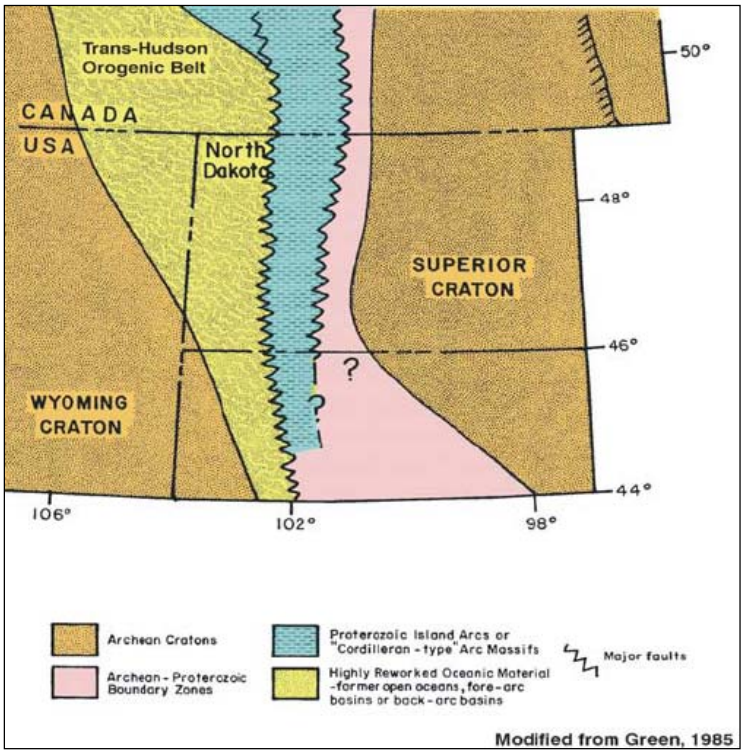

Figure 5-3. Basement terrain of the Williston basin (after Fischer et al., 2005).

The two cratons are of Archean Eon and represent proto-continents. They are separated by oceanic sediments in the Archean- Proterozoic Thompson boundary zone, the Proterozoic island arc massifs, and the Trans-Hudson orogenic belt. Rocks of the Superior craton underlie most of eastern North and South Dakota, as well as Manitoba, and consist primarily of granites and greenstones. The Wyoming craton underlies eastern Montana, western Saskatchewan, western South Dakota, and southwestern North Dakota. It consists of quartz-rich rocks, including gneisses. Both cratons are approximately the same age.

The Archean- Proterozoic Thompson boundary zone and the Trans-Hudson orogenic belt underlie most of western North Dakota. Sediments of these two components are composed of oceanic materials that accreted between the active continental margins the two cratons (Green et al., 1985).

The Proterozoic island arc massifs represent highly reformed oceanic materials from former open oceans and fore-arc or back-arc basins as well as rocks believed to be associated with island arc formation. Basement rocks in these massifs are interpreted as representing the initially rifting between the two cratons, and later their collision, which clearly shows the instability of the craton during that time. The collision formed a north–south oriented structure that comprises an underlying vertical and sub-vertical faulting system etching on the basement. The relatively strong massifs formed subsurface highs which initiated the anticlines in the overlying sedimentary rocks.

5.2.2 The Lineament Structures

The basement is can be further divided into blocks by a series of tectonic features, referred to as lineaments (Figure 5-4). Lineaments are best defined as linear zones of structural weakness. Similar to faults, lineaments are believed to be responsible for the origin of structures and depositional patterns within the sedimentary formations in the basin. Lineaments are important component in the formation of the basin. They were formed in response to external stresses and, once formed, served as conduits to transmit and release stresses through deformation.

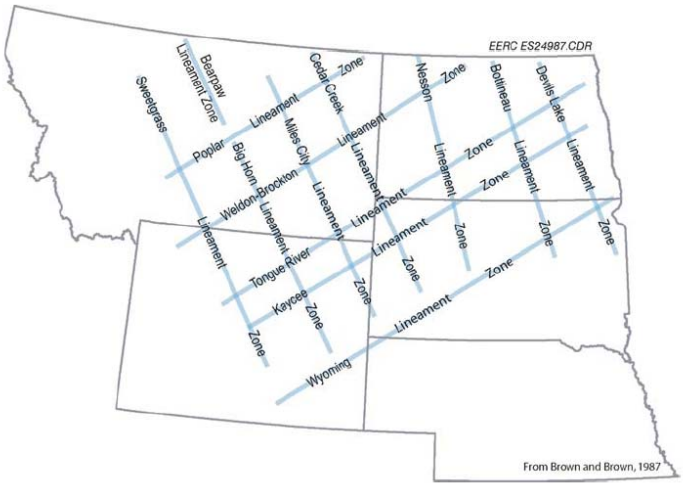

Figure 5-4. Major Paleozoic structural lineaments (after Fischer et al., 2005).

The Williston basin may have formed as a sag on the cratons in response to a left lateral shearing movement between two regional lineaments: the Weldon–Brockton and the Wyoming lineaments (Gerhard et al., 1982). Some in-depth study shows major structural lineaments were observed on the Landsat image with orientations of 70 degrees and 120 degrees (Figure 5-5). These observations confirmed the lineaments in Figure 5-4. The lineaments are surface expressions of major structural features in deep basement rocks of the Williston basin.

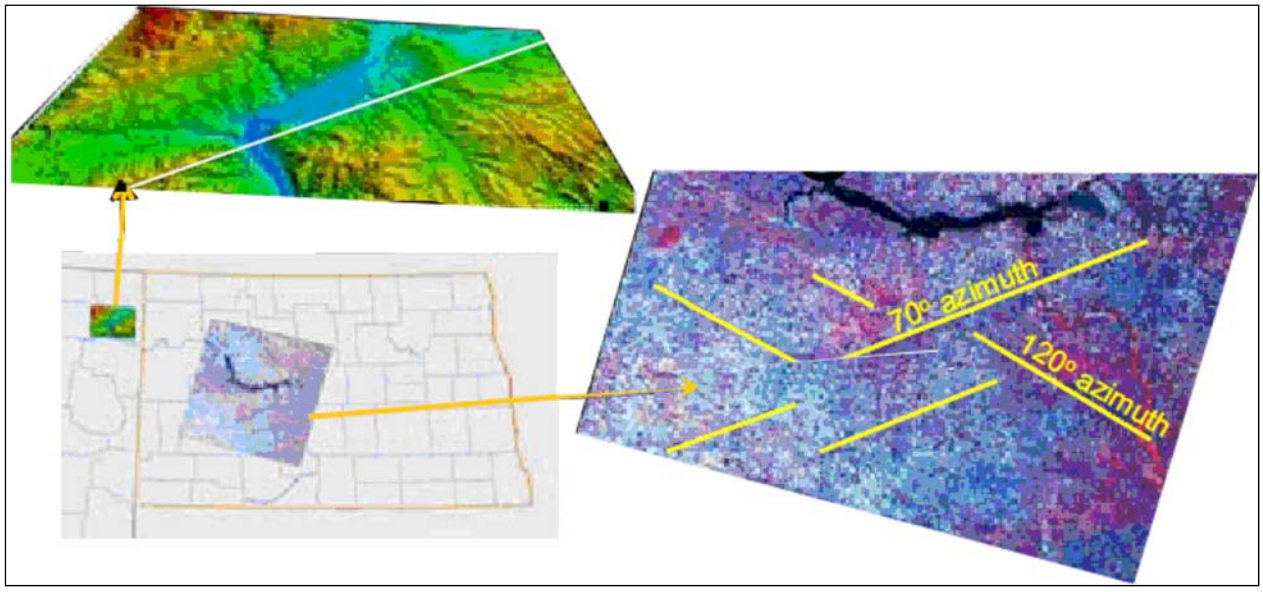

Figure 5-5. Major structural lineaments in satellite imagery (after Abbott et al., 2009).

Other tectonic features in the Williston basin include faulting and folding. These features formed in response to either subsidence or the sporadic movement of individual linearly-bounded basement blocks.

5.2.3 The Faults

Due to the cratonic feature, faulting in the Williston basin is less intensive in comparing to other Rocky Mountain basins. Some faults, such as those on the west flank of the Cedar Creek Anticline (Clement, 1987), the west flank of the Nesson Anticline, and the Heart River Anticline, are identifiable on a seismic survey (Figure 5-6). Seismic image

shows that these faults are near vertical. Clement (1987) further reported that faults along the Cedar Creek Anticline have undergone recurrent near-vertical shearing.

There might be two mechanisms for the vertical and sub-vertical faulting. The two cratons and the massifs are relatively strong terrains. While the two cratons defined the east and west boundaries of the basin, the massifs formed the subsurface highs. The Thompson boundary zone and the Trans-Hudson Orogenic belt are relatively soft rock bodies. Differential vertical movements might have been occurring during the Paleozoic eon in responding to the adjustment of the five basement components. On the other hand, during the deposition process, differential compaction of the sediments on top of the subsurface highs (massifs) and lows (the Thompson boundary zone and the Trans-Hudson Orogenic belt) could have been existing.

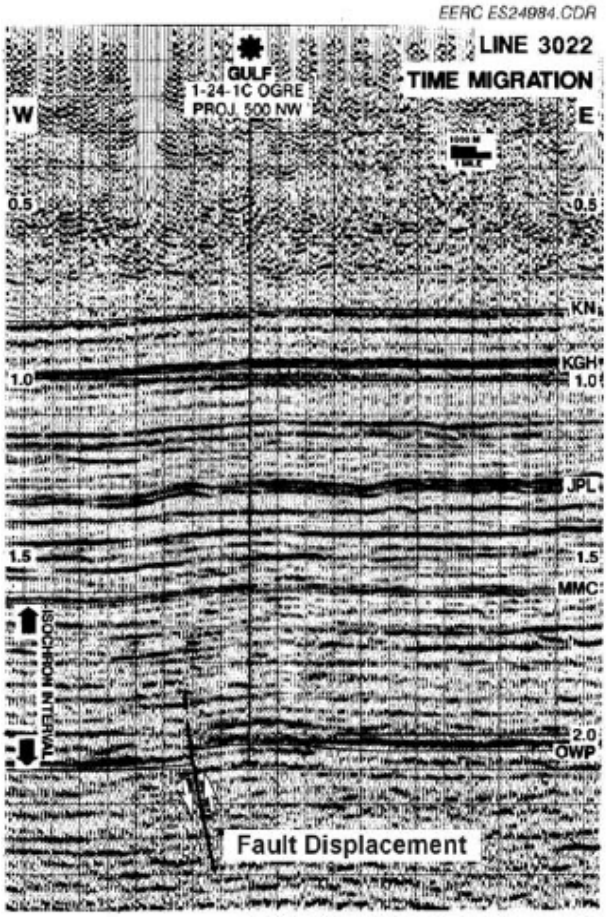

Figure 5-6. Seismic image across Heart River Anticline, Stark County, North Dakota (after Fischer et al., 2005).

5.2.4 The Folds

As mentioned above, the subsurface highs formed in the basement have initiated the formation of folding structures such as the Nesson Anticline, the Little Knife Anticline, the Billings Anticline, the Cedar Creek Anticline, and the Poplar Dome (Figure 1-1). Throughout time, the basin might have responded to local and regional orogenic events to further shape these folding structures.

5.3. Tectonic History of the Nesson Anticline

Different explanations have been proposed about the tectonic history of anticlines in the Williston basin. Redly and Hajnal (1995) proposed that these foldings are formed as a result of the subsidence of the basin. They considered that subsidence of a circular segment of a spherical surface, such as the Williston basin, gave rise to two types of folding:

circular folding at the dynamic rim, and radial folding at the central part. According to their description, the Cedar Creek anticline, with a proven ENE dipping (basin center direction) western boundary fault, is an example of circular folding. The Nesson anticline, which is toward to the center of the basin, is a radial folding. However, most of other studies consider that the fold structures in the basin are the result of deep basement-linked normal faults reactivated several times during the Paleozoic. We tend to agree with this explanation and follow this explanation in the modeling process presented in this paper. The tectonic history of the Nesson anticline is given as following.

The Nesson anticline is created by a drag fold and its deformation is controlled mainly by the vertical movement along the normal Nesson master fault beneath the west side of the anticline crest (Figure 5-1). This fault system has been present and active since Precambrian time. The Nesson anticline underwent periodic deformations through the history of the Williston basin. The most recent and strongest reactivation of the fault occurred in response to the Laramide orogeny during late Cretaceous (Gerhard et al., 1990; Lindsay et al., 1988; Meissner, 1978; Warner 2011; Thomas, 1974; Brown and Brown, 1987; Gerhard et al., 1987). This event is thought to have largely resulted in the current structure of the anticline, and the tectonic stress may have induced natural fractures. The detailed stress model used to explain the behavior of the fault and consequent deformation is described below.

In the Williston basin, a series of basement-weakness zone, represented as lineament at the surface, trend northeasterly and northwesterly. These weakness zones define a framework of basement blocks. These basement blocks and bounding weakness zones appear to have influenced the development of structural features in the basin. The Nesson fault is located on the Weldon basement which trends northeasterly (Figure 5-7). In late Cretaceous, the Laramide orogeny provided regional compressive stresses from the southwest, and the response of the basement blocks to the Laramide tectonics can be analyzed by analogy to a hypothesized cardboard model (Figure 5-8). According to the simple shear model proposed by Thomas (1974) and the wrench-style deformation model proposed by Brown (1978), the regional stress regime created the dominant left-lateral adjustment on the northwesterly trending blocks, and the subordinate right-lateral adjustment on the northeasterly trending blocks. Therefore, the Weldon block, where the Nesson anticline is set, subjected to a right-lateral adjustment and experienced right-lateral stress and tensile stress during the Laramide event (Figure 5-8). This stress profile in the block rejuvenated the vertical displacement along the Nesson master fault (Figure 5-9). Gerhard et al. (1987) described that during the event, the master fault has a down-to-the-west displacement of about 120 m, while the Antelope fault appears to have been relatively quiescent. The vertical offset resulted in the fold-drag deformation and set the current structure of the anticline. It is worthy of noticing the descriptions given by Pilcher et al. (2009) that the structural features with NW-SE trend, such as the Antelope and Cedar Creek anticlines, were oriented optimally and strongly inverted by the Laramide tectonics. However, in this modeling work, we consider that the Antelope anticline is relative quiescent with minor displacement.

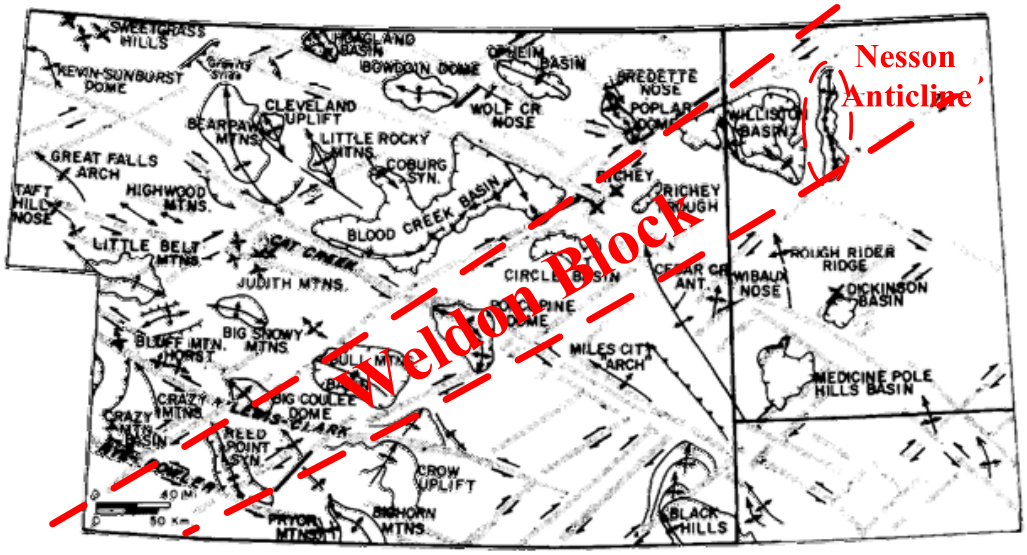

Figure 5-7. Basement blocks of the Williston-Blood Creek basin. Highlighted by the red dash lines is the northeasterly trending Weldon block, where the Nesson anticline lays on (After Warner, 2011; Thomas, 1974).

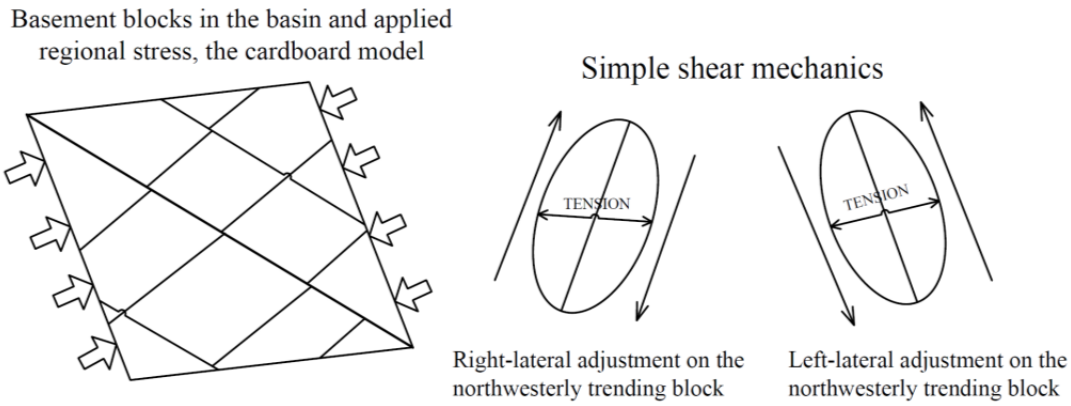

Figure 5-8. Regional stress applied on the basement blocks during the Laramide orogeny, and response of the northeasterly trending blocks and northwesterly trending blocks, according to the simple shear model (After Thomas, 1974).

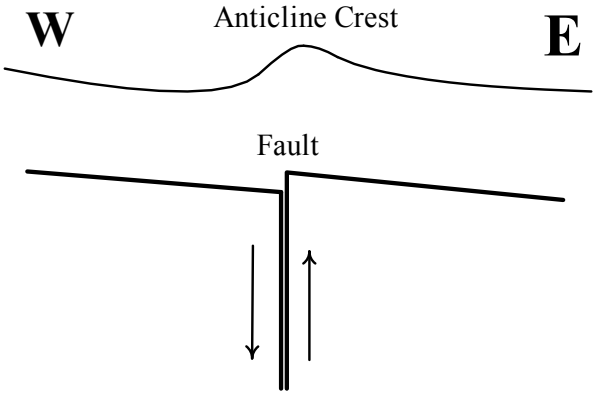

Figure 5-9. The Laramide orogeny tectonics rejuvenated the vertical movement of the Nesson master fault, and resulted in the drag-fold deformation.

It is also believed that, during late Cretaceous, or even until early Tertiary, the Bakken was buried to its maximum depth within the oil window, as shown in Figure 5-10 (Pitman et al., 2001; Flannery and Kraus, 2006; Warner, 2011). It is very possible that the fold deformation and oil maturation occurred at the same time, and it is likely that tensile fractures could be generated during the Laramide event. Comparing to shear fractures, tensile fractures are more beneficial to reservoir quality due to their higher conductivity. On the other hand, the presence of the Nesson master fault and Antelope fault would change both the direction and magnitude of the local principal stresses, influencing the distribution and orientation of natural fractures around the faults. The tensile fractures would also function as pathways for mature hydrocarbon to migrate out of the Bakken. This paper uses finite element method (FEM) to reconstruct the paleostress during the Laramide event in Nesson anticline area based on the information from previous studies. With the simulated paleostress profile, possibility of development of natural fractures is discussed.

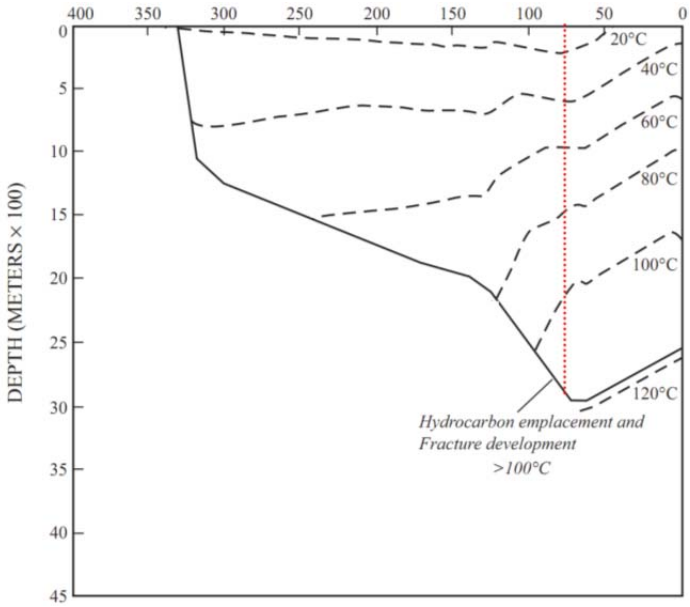

Figure 5-10. A Bakken Formation burial curve from the center of the Williston basin in North Dakota (After Pitman et al., 2001; Warner, 2011).

5.4. Elastic Properties

5.4.1 Overview of previous testing

Wells cored for testing

In order to study the geomechanical parameters of the Bakken formation: (1) uniaxial compressive strength (UCS); (2) cohesion and angle of internal friction; (3) Young's modulus and Poisson's ratio; (4) triaxial strength under different confining pressures; (5) Biot's coefficient; (6) fracture gradient; (7) dynamic elastic parameters; and (8) elastic wave velocities., we must select the specimen from different wells at different depth so as to make profound insights into this aspect. Among all the screened wells, Bakken shales in seven wells were cored and tested. The cored specimens from four wells were used for all-purpose parameter testing, and the core specimen from the other three wells were adopted to do the express geomechanical testing to gain UCS. Figure 5-11 indicate the geographic location of each testing well.

Table 5-1 Test contents for each well

Well #	Well Name	Testing contents	Well completion report
WT1	SARAG BARSTAD 6-44H	UCS*	15889 (NDIC, 2007a)
WT2	J.HORST 1-11 H	UCS	15986 (NDIC, 2006)
WT3	ANDERSON SMITH 1-26H	UCS	16083 (NDIC, 2007b)
WT4	NELSON FARMS 1-24H	All	15845 (NDIC, 2005)
WT5	NORDSTOG 14-23-161-98H	All**	16089 (NDIC, 2009)
WT6	PEGASUS 2-17H	all	16405 (NDIC, 2007c)
WT7	OLSON 10-15-1H	all	17513 (NDIC, 2010)

*UCS -- Uniaxial compressive strength, from express testing method;
**All-- all parameters from triaxial rock mechanics test.

Figure 5-11 Distribution of wells with cored specimens for testing.

5.4.2 Overview of testing methods and instruments

Procedures for triaxial compressive strength test with ultrasonic velocities

The general procedures for triaxial compressive test with ultrasonic velocities are summarized in the following:

(1) A right cylindrical plug is cut from the sample core and their ends ground parallel according to International Society for Rock Mechanics (ISRM) and American Society for Testing and Materials (ASTM) standards. A length to diameter ratio of 2:1 is recommended, to obtain representative geomechanical properties of the sample. Physical dimensions of the specimen are recorded and the specimen is saturated with simulated formation brine.
(2) The specimen is then placed between two endcaps and a thermal-shrink jacket is placed over the specimen.
(3) Devices for axial and radial strains are mounted in the endcaps and on the vertical surface of the specimen, respectively.
(4) The specimen assembly is placed into the pressure vessel and brought into contact with a loading piston that allows application of axial load.
(5) Confining pressure is applied to the desired hydrostatic testing pressure.
(6) Ultrasonic velocities are measured at the hydrostatic confining pressure.
(7) Increase axial load at a constant rate until the specimen fails or axial strain reached a desired amount of strain while confining pressure is held constant.
(8) Reduce axial stress to the initial hydrostatic condition after sample fails or reaches a desired axial strain.
(9) Reduce confining pressure to zero and disassemble sample.

Core-Based Strength (CBS) logging test

Benefits of using Brinell Hardness (BH) in identifying Core-Based Strength (CBS) logs include:

(1) Generates the relative strength along the length of the core;
(2) Identifies the weakest areas over large depth intervals;
(3) Provides a non-destructive strength profile vs. depth;
(4) Provides high resolution logs with multiple rock mechanical parameters (UCS, BH);
(5) A helpful guide in determining which areas require additional core analysis;

The Brinell Hardness test can be performed on samples with a variety of shapes and sizes. Brinell Hardness is a measure of the resistance of the rock to indentation and has a direct correlation to rock strength. The test apparatus is shown in Figure 5-12. The Brinell hardness test is performed by applying measured load to a spherical steel-ball (indenter) that is in contact with the sample. The depth of ball penetration is recorded along with applied load. The hardness value is determined from the ratio of applied load to the indentation area and is expressed as kg/mm^2 or in other units.

Figure 5-12. Brinell Hardness Test Apparatus.
(UCS as determined from Brinell Hardness using slabbed core sections)

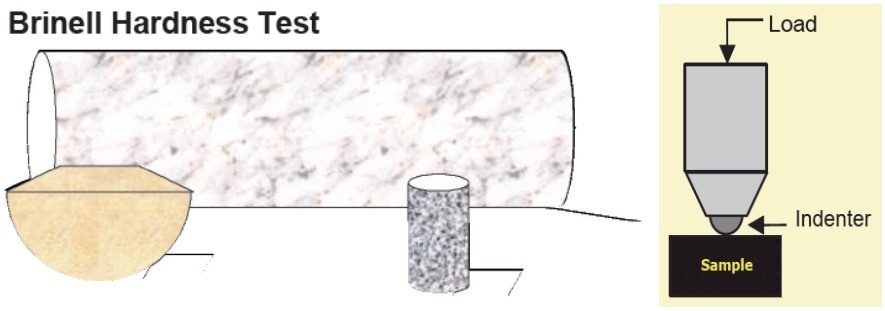

(a) Test samples (b) Test procedure

Figure 5-13. Brinell Hardness test sample and procedure.

5.4.3 Geomechanics properties

The following contents are the testing results for different kinds of parameters.

UCS compilation

The following contents are the testing results for UCS from test well WT1 (Figure 5-14), WT2 (Figure 5-15), and WT3 (Figure 5-16).

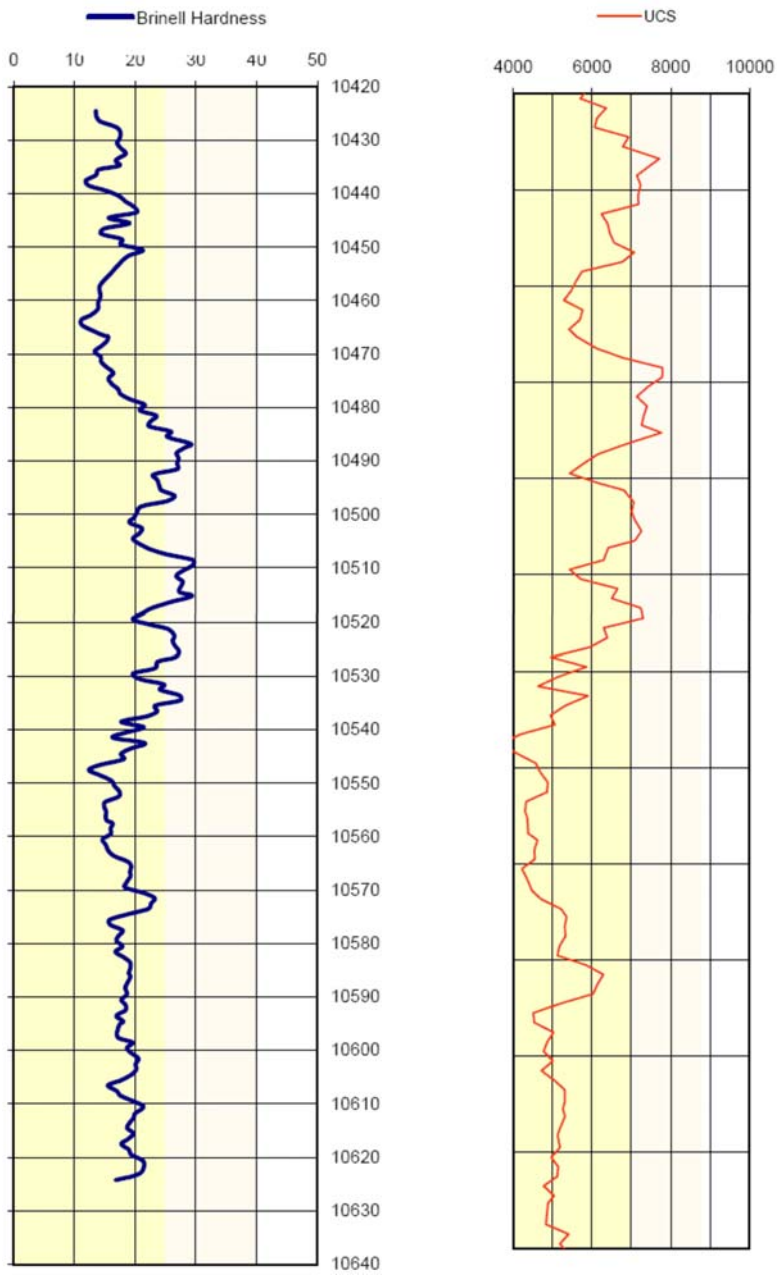

Figure 5-14. UCS and Brinell hardness curve in Well WT1(NDIC, 2007a)

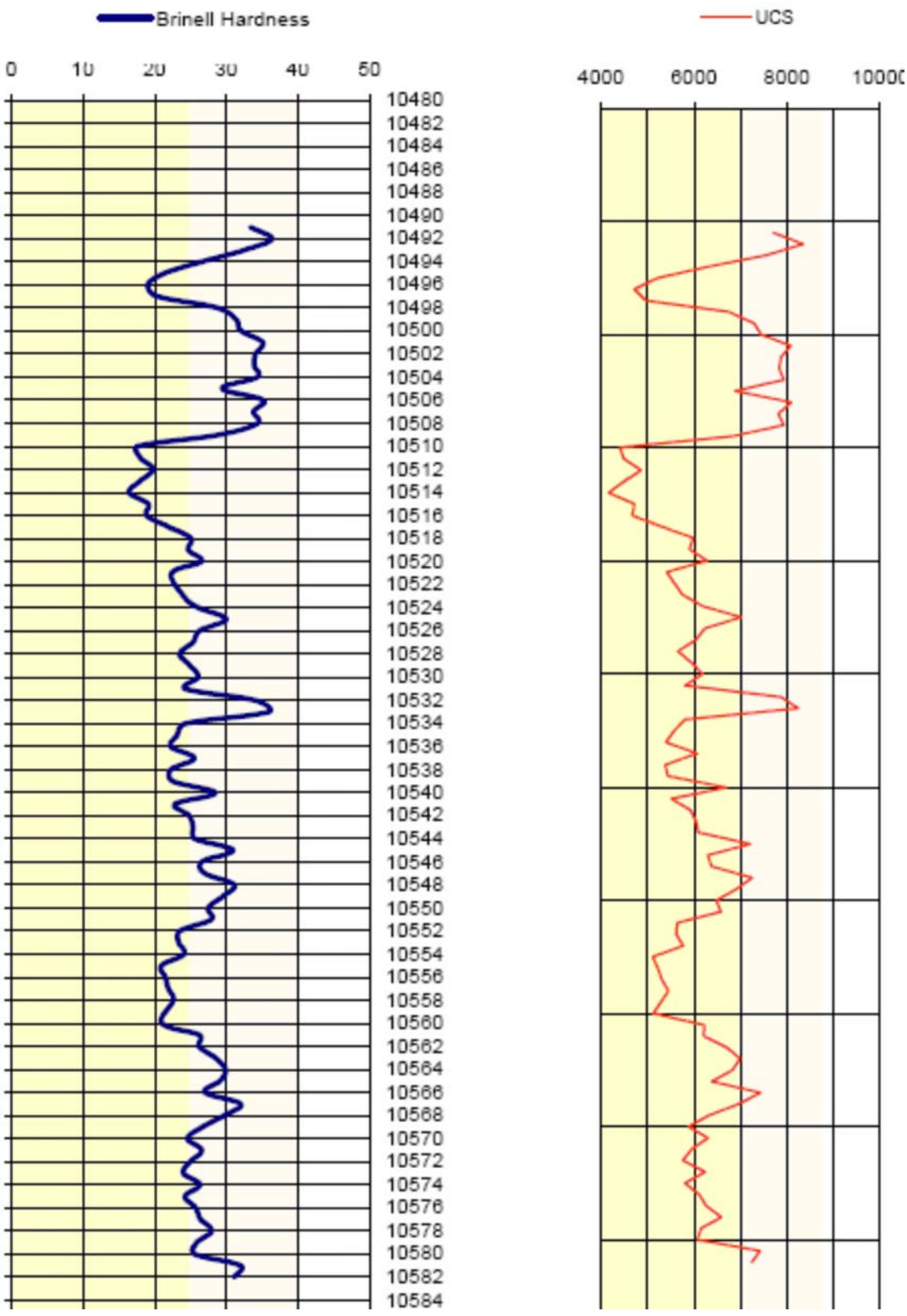

Figure 5-15. UCS and Brinell hardness curve in Well WT2 (NDIC, 2006)

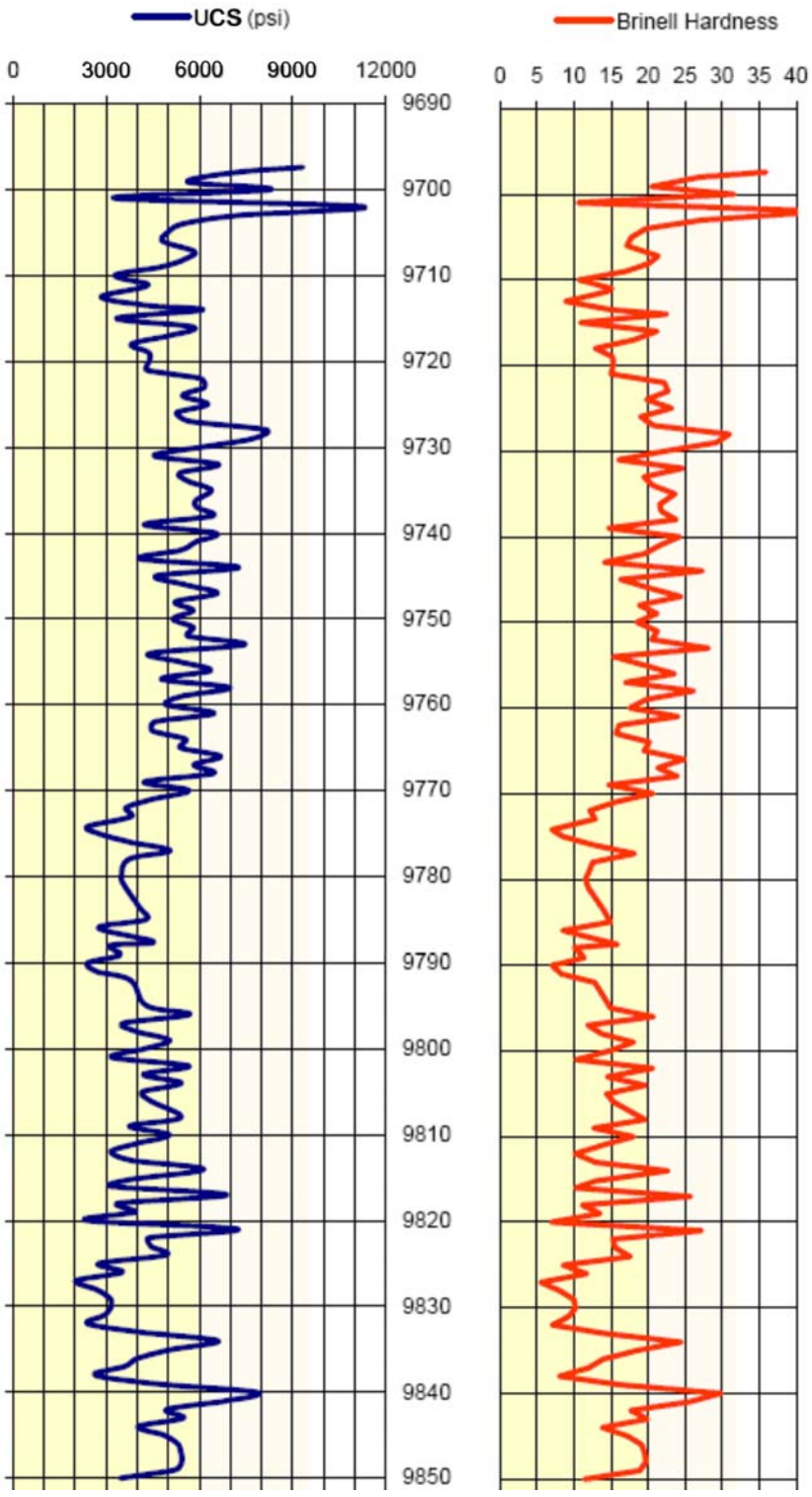

Figure 5-16. UCS and Brinell hardness curve in well WT3 (NDIC, 2007b)

All parameters compilation

Tables 5-2. through 5-4 summarize all the geomechanical properties from these tests.

Table 5-2. Summary of Triaxial Compressive Tests

Well No.	Sample No.	Depth (ft)	Confining Pressure (psi)	Compressive Strength (psi)	Static Young's Modulus ($\times 10^6$)	Static Poisson's Ratio	Biot's Constant
WT4	1-8VA-RM	9623.20	4600	31,065	4.09	0.42	0.62
	1-8VB-RM	9623.20	2700	27,070	3.89	0.40	
	1-20VA-RM	9635.30	4600	35,980	4.81	0.29	0.74
	1-20VB-RM	9635.30	2700	29,305	4.69	0.32	
	1-21VA-RM	9636.80	3040	35,875	6.11	0.47	
	1-21VB-RM	9636.80	2700	36,035	6.32	0.49	
	1-21VC-RM	9636.80	4600	43,380	6.62	0.49	
WT5	1V	8544.00	1450	31,413	5.37	0.28	0.77
	2V	8586.20	1450	35,785	9.49	0.31	0.83
	3V	8629.60	1450	23,160	4.58	0.24	0.69
	4V	8631.40	1450	22,491	4.30	0.24	0.68
	5V	8639.30	1450	26,876	4.90	0.24	0.79
	6V	8715.50	1450	19,627	4.35	0.26	0.79
	7V	8720.10	1450	49,650	9.81	0.27	0.74
	8V	8729.00	1450	22,676	6.45	0.26	0.71
	9V	8737.50	1450	15,762	3.61	0.26	0.75
WT6	1-6V-RM	10073.25	3400	40,815	6.86	0.36	
	1-35V-RM	10102.30	3400	28,860	5.35	0.33	
	1-49V-RM	10116.40	4000	24,520	3.20	0.39	
	1-57V-RM	10124.00	3400	33,000	4.66	0.26	
	2-9V-RM	10137.75	3400	36,265	4.98	0.31	
	2-21V-RM	10149.70	3400	28,215	4.35	0.27	
	2-43V-RM	10171.00	3400	29,910	4.43	0.31	
	2-54V-RM	10182.70	4000	22,705	2.67	0.25	
	3-11V-RM	10199.00	4000	33,610	3.43	0.27	
	3-21BV-RM	10209.90	3400	22,885	3.66	0.26	
	3-26V-RM	10214.90	3400	23,270	3.44	0.23	
	1-44-RM*	10111.60	4000	31,475	3.99	0.29	
	2-53B-RM*	10182.45	4000	31,525	4.23	0.34	
WT7	1-17VRM-C	10625.15	3900	33,593	4.39	0.32	
	2-24VRM-C	10693.25	3900	63,729	8.85	0.35	

Notes: *Horizontal sample

Table 5-3. Summary of ultrasonic velocities and dynamic elastic parameters

Well No.	Sample No.	Depth (ft)	Confining Pressure (psi)	Axial pressure	Bulk Density (g/cc)	Ultrasonic Wave Velocity				Dynamic Elastic Parameter			
						Compressional		Shear		Young's Modulus ($\times 10^6$ psi)	Poisson's Ratio	Bulk Modulus ($\times 10^6$ psi)	Shear Modulus ($\times 10^6$ psi)
						ft/sec	µsec/ft	ft/sec	µsec/ft				
WT4	1-8VA-RM	9623.20	4600	/	2.65	15,395	64.96	8921	112.10	7.08	0.25	4.67	2.84
	1-20VA-RM	9635.30	4600	/	2.65	15,981	62.58	9565	104.54	7.79	0.22	4.65	3.19
	1-21VC-RM	9636.80	4600	/	2.65	18,746	53.35	9907	100.94	9.18	0.31	7.89	3.51
WT5	1V	8544	1450	1450	2.69	17,580	56.88	9606	104.11	8.00	0.29	6.73	3.34
	1V	8544	1450	12,000	2.69	18,466	54.15	9970	100.30	9.31	0.29	7.55	3. 60
	2V	8586.2	1450	1450	2.57	20,663	48.40	10,654	92.13	11.11	0.31	9.72	4.24
	2V	8586.2	1450	13,000	2.57	21,066	47.42	11,010	90.63	11.46	0.31	10.10	4.36
	3V	8629.6	1450	5000	2.59	15,717	59.82	9688	103.43	8.16	0.25	5.41	3.27
	3V	8629.7	1450	10,000	2.59	17,201	58.14	9901	101.0	8.58	0.25	5.77	3.43
	4V	8631.4	1450	4000	2.55	15,724	63.60	9142	100.38	7.14	0.24	4.66	2.57
	4V	8631.4	1450	15,000	2.55	16,211	61.69	9248	108.13	7.39	0.26	5.10	2.93
	5V	8639.3	1450	5000	2.65	17,557	56.96	9496	105.31	8.32	0.29	6.71	3.22

	5V	8639.3	1450	15000	2.65	18303	54.64	9074	101.28	9.00	0.29	7.31	3.48
	6V	8715.5	1450	1450	2.62	14567	60.65	7857	127.27	5.64	0.29	4.58	2.18
	6V	8715.5	1450	9000	2.62	15751	60.49	8776	113.92	6.93	0.27	5.12	2.72
	7V	8720.1	1450	5000	2.72	19370	51.63	10782	92.75	10.89	0.28	6.09	4.27
	7V	8720.1	1450	10000	2.72	20076	49.81	11180	89.45	11.70	0.28	6.05	4.59
	8V	8729	1450	6000	2.67	18311	54.61	10433	95.85	9.86	0.26	6.83	3.91
	8V	8729	1450	12000	2.67	18702	53.47	10600	94.36	10.20	0.26	7.19	4.04
	9V	8737.5	1450	10000	2.57	15370	65.27	8481	117.91	6.38	0.28	4.51	2.49
	9V	8737.5	1450	10000	2.57	15676	63.79	8497	117.69	6.46	0.29	5.18	2.50
WT6	1-6V-RM	10073.25	3400		2.69	18923	52.85	9999	100.01	9.48	0.31	8.16	3.63
	1-35V-RM	10102.30	3400		2.64	17877	55.94	9612	104.03	8.54	0.30	7.00	3.29
	1-49V-RM	10116.40	4000		2.40	11939	83.78	7061	141.62	3.98	0.23	2.46	1.61
	1-57V-RM	10124. 0	3400		2.64	16253	61.53	9395	106.45	7.85	0.25	5.22	3.14
	2-9V-RM	10137.75	3400		2.66	16938	59.04	9083	110.09	7.68	0.30	6.34	2.96
	2-21V-RM	10149.70	3400		2.61	16000	62.50	9449	105.83	7.73	0.23	4.81	3.14
	2-43V-RM	10171.00	3400		2.62	15862	63.04	9231	108.33	7.48	0.24	4.87	3.01
	2-54V-RM	10182.70	4000		2.34	12051	82.98	6788	147.31	3.69	0.27	2.65	1.46
	3-11V-RM	10199.00	4000		2.36	12854	77.80	7849	127.41	4.71	0.20	2.64	1.96
	3-21BV-RM	10129.90	3400		2.65	15742	63.52	8430	118.63	6.59	0.30	5.46	2.54
	3-26V-RM	10214.90	3400		2.65	13789	72.52	8169	122.42	5.85	0.23	3.61	2.38
	1-44-RM*	10111.60	4000		2.30	14180	70.52	7946	125.84	4.98	0.27	3.63	1.96
	2-53B-RM*	10182.45	4000		2.31	14367	69.60	8684	115.15	5.70	0.21	3.30	2.35
WT7	1-17VRM-C	10625.15	3900		2.57	15757	63.46	9540	104.8	7.63	0.21	4.40	3.15
	2-24VRM-C	10693.25	3900		2.71	19506	51.27	11350	88.11	11.72	0.24	7.63	4.71

Notes: * Horizontal samples

Table 5-4. Result of Mohr-Coulomb Failure Analysis

Well No.	Sample No.	Depth (ft)	Confining pressure $Pc=\sigma_3$ (psi)	Differential Stress $\sigma_1.\sigma_3$ (psi)	Compressive Strength σ_1 (psi)	Slope on σ_1 vs Pc	Unconfined Compressive Strength (psi)	Angle of Internal Friction (deg)	Coeff. Of internal Friction	Cohesion (psi)
WT7	1-17VRM-A	10625.15	0	13746	13746	4.68	15578	40.4	0.85	3602
	1-17VRM-B	10625.15	1950	25886	27815					
	1-17VRM-C	10625.15	3900	29693	33593					
	1-17VRM-D	10625.15	4900	32525	37425					
WT7	2-24VRM-A	10693.25	0	17472	17472	8.92	23864	53.0	1.33	3995
	2-24VRM-B	10693.25	1950	48198	50148					
	2-24VRM-C	10693.25	3900	59829	63729					
	2-24VRM-D	10693.25	4900	55079	59979					

Figures 5-17 and 5-18 show the Mohr-Coulomb envelopes derived from triaxial tests, and the geomechanical properties from these tests.

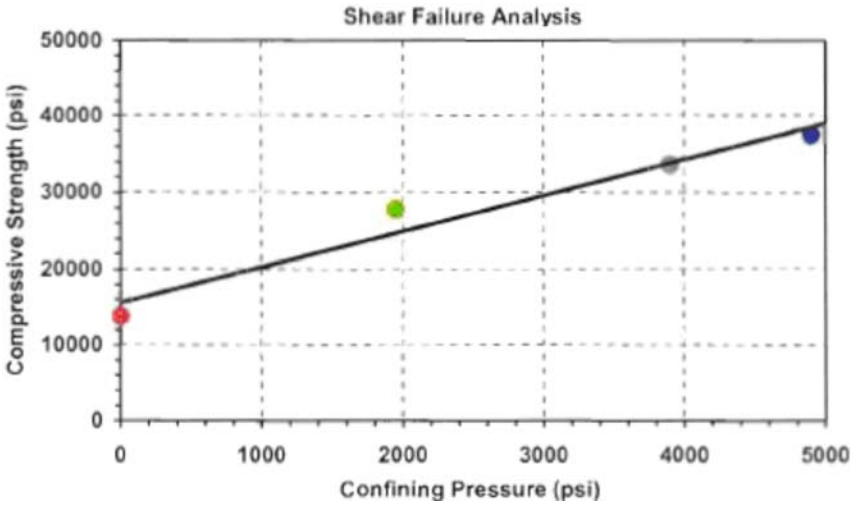

(a) Shear failure analysis for sample set 1-17VRM from WT7

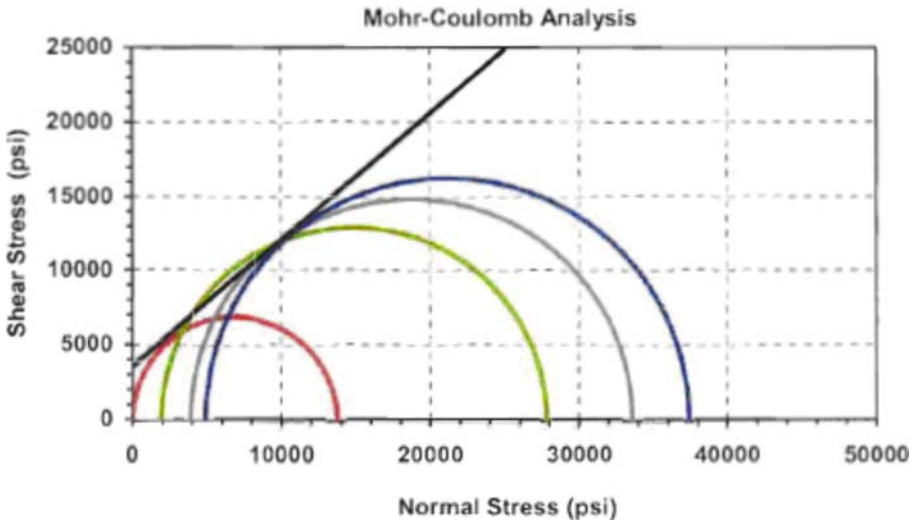

(b) Mohr-Coulomb analysis for sample set 1-17VRM from WT7

Figure 5-17. Shear and Mohr-Coulomb analysis for sample set 1-17VRM from WT7 (NDIC, 2010)

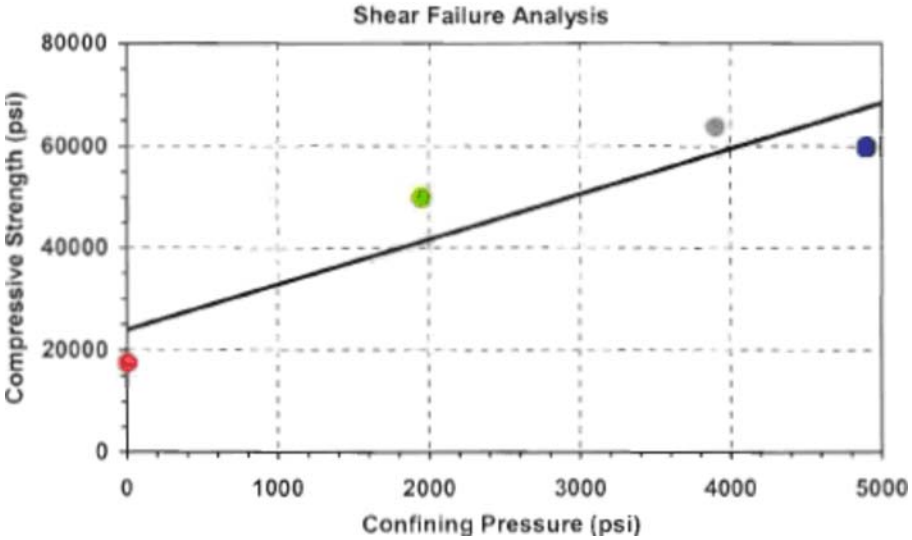

(a) Shear failure analysis for sample set 2-24VRM from WT7

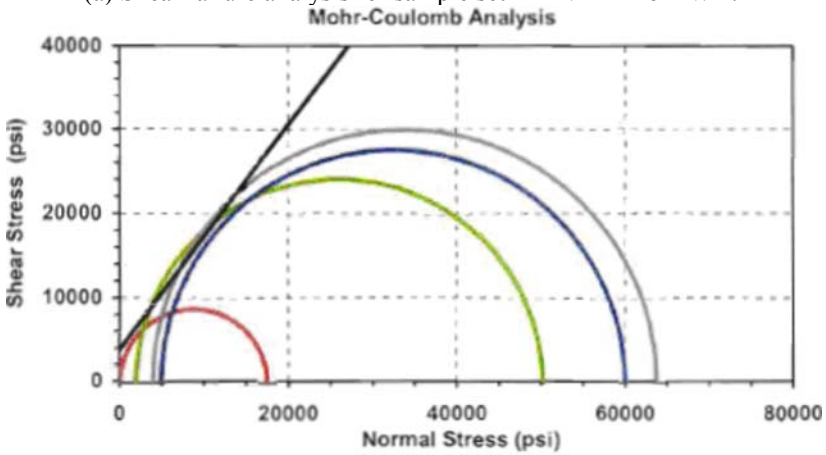

(b) Mohr-Coulomb analysis for sample set 2-24VRM from WT7

Figure 5-18. Shear and Mohr-Coulomb analysis for sample set 2-24VRM from WT7 (NDIC, 2010)

To check if there exists depth-dependent distribution of the measured geomechanical properties and depths, these properties are plotted against depth. Figures 5-19 through 5-25 show these results.

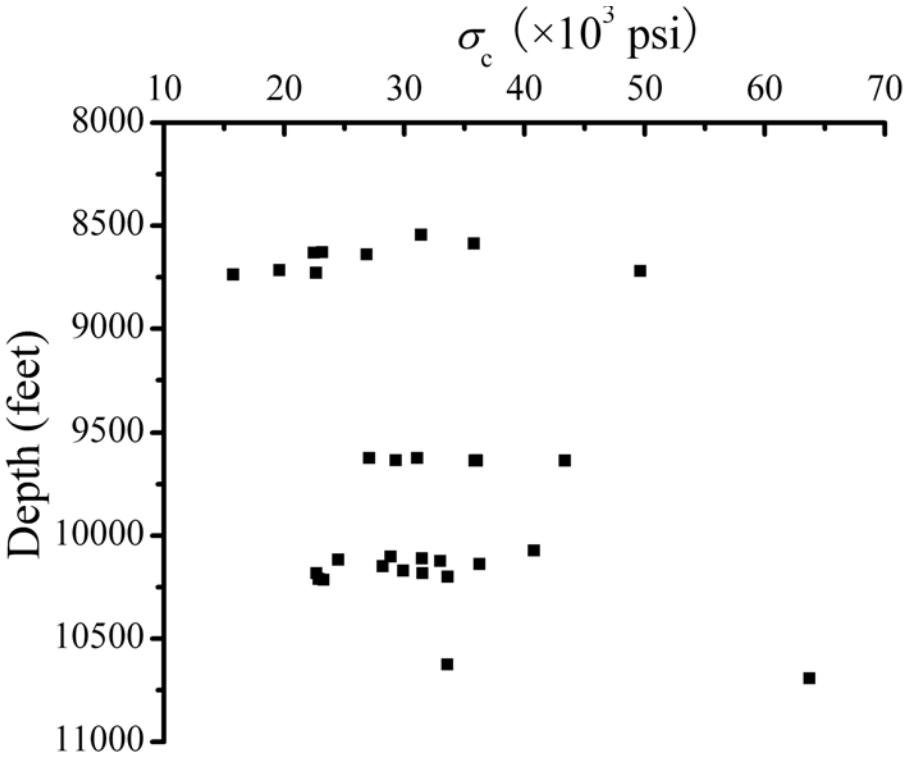

Figure 5-19 Uniaxial compressive strength vs. depth

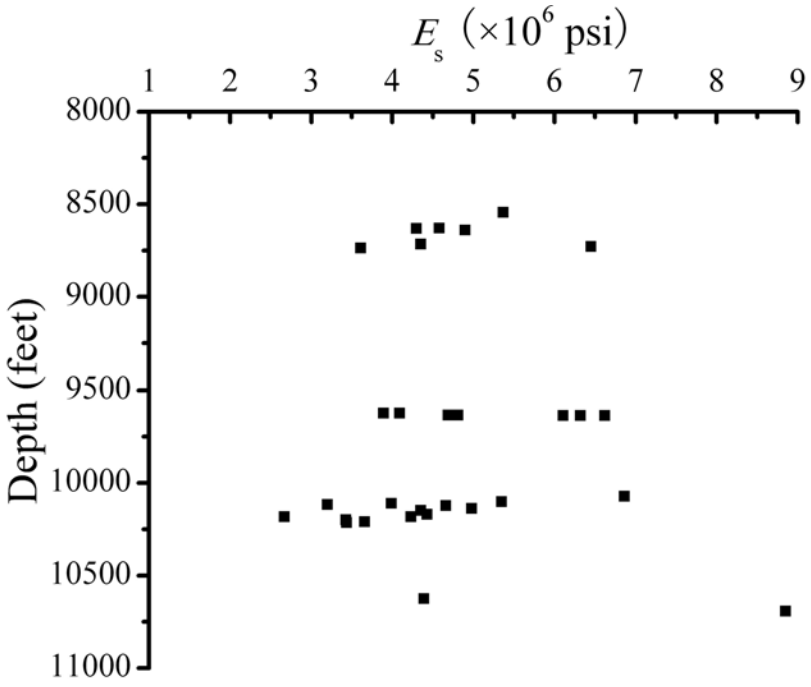

Figure 5-20. Elastic modulus vs. depth

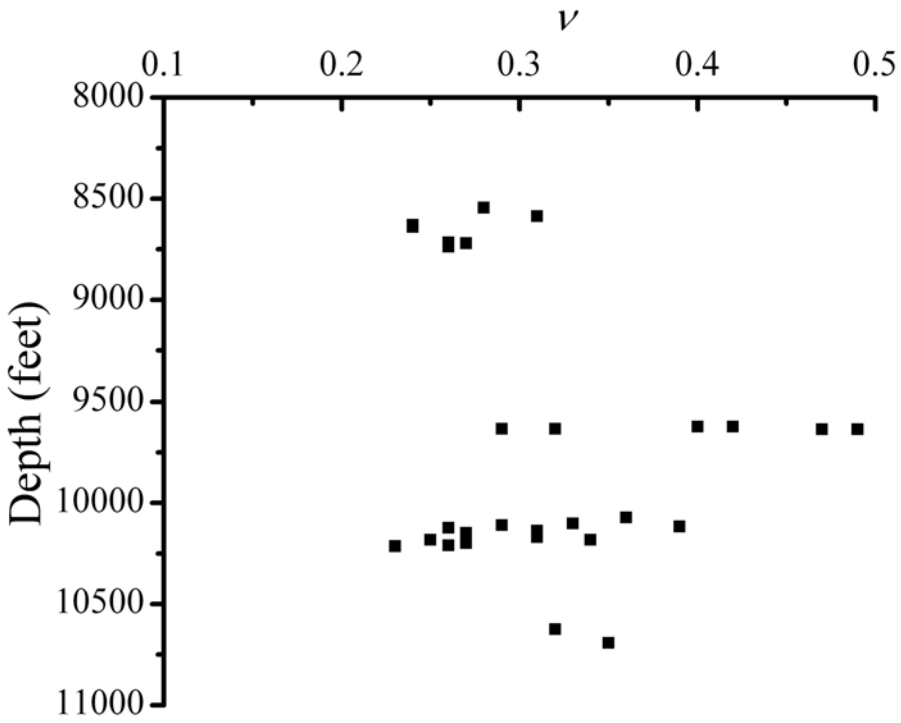

Figure 5-21. Poisson's ratio vs. depth

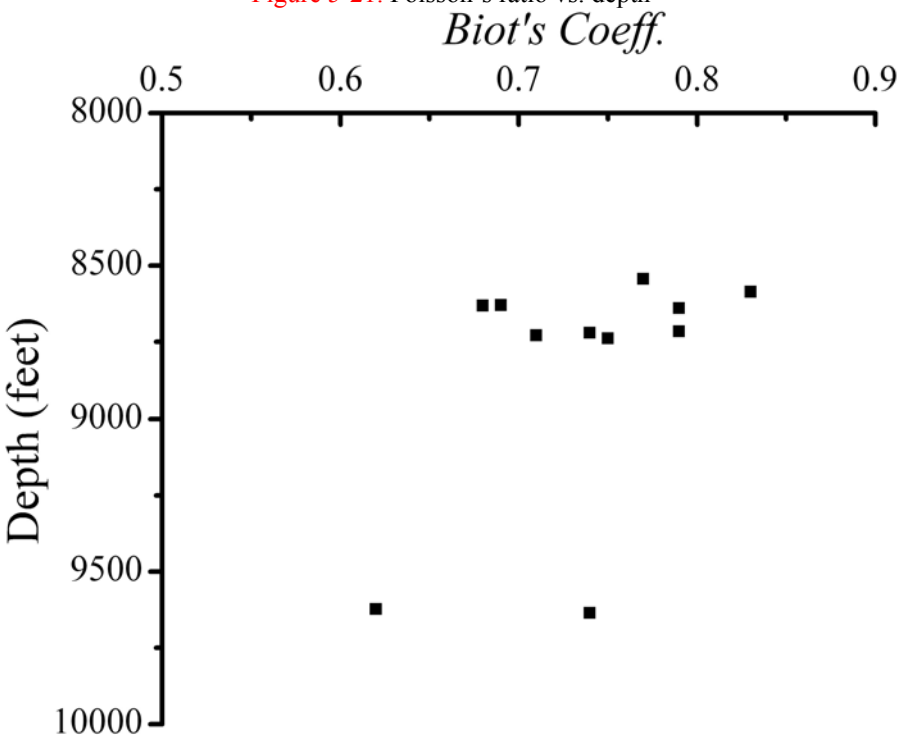

Figure 5-22. Biot's coefficient vs. depth

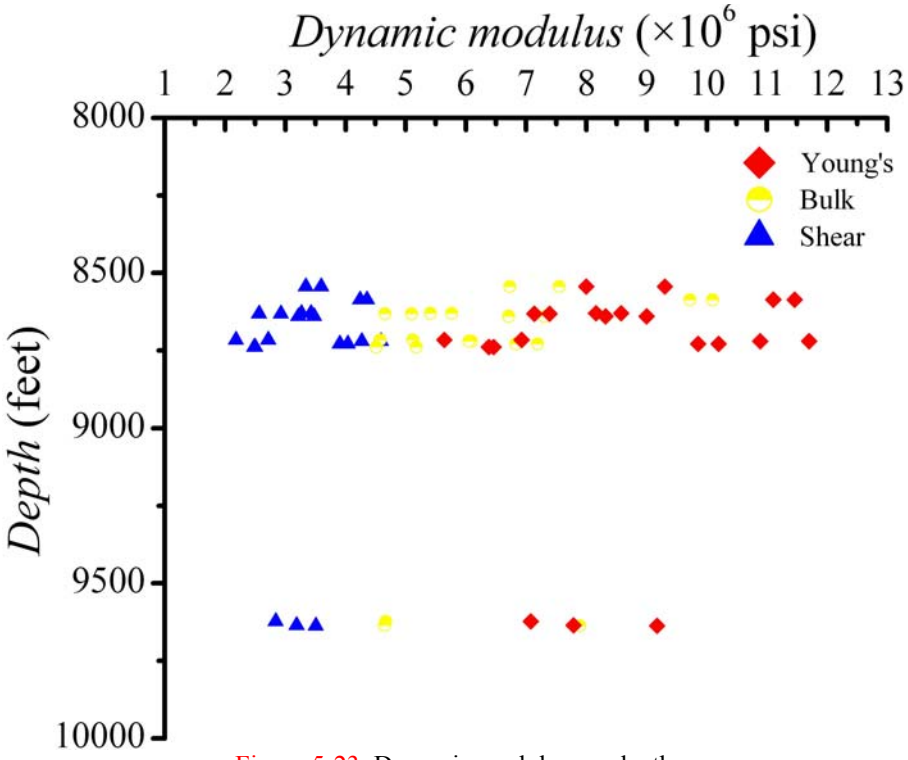

Figure 5-23. Dynamic modulus vs. depth

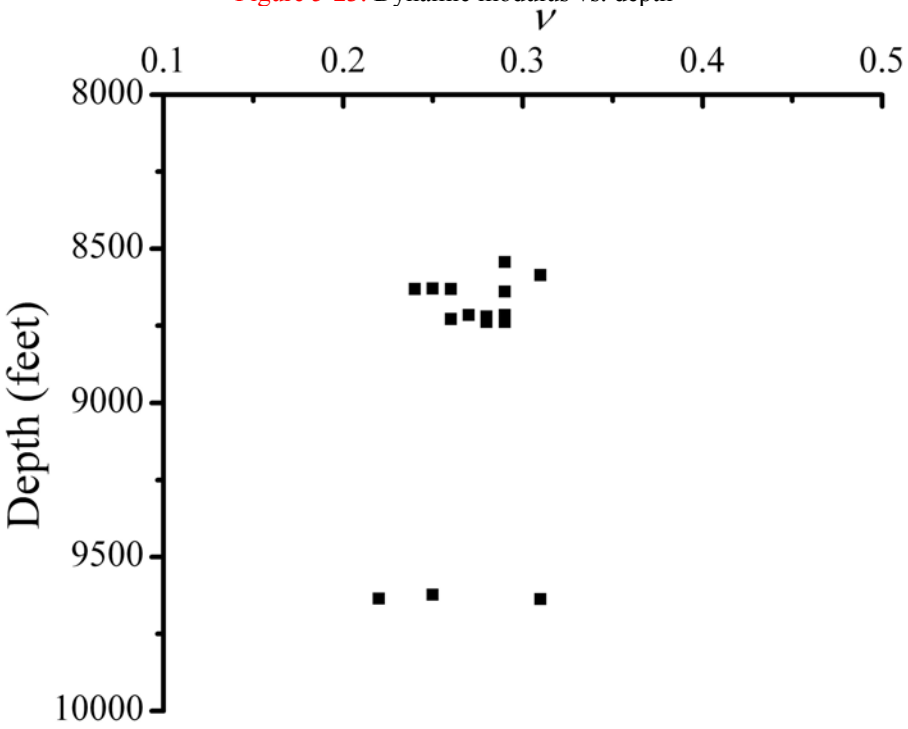

Figure 5-24. Dynamic Poisson's ratio vs depth

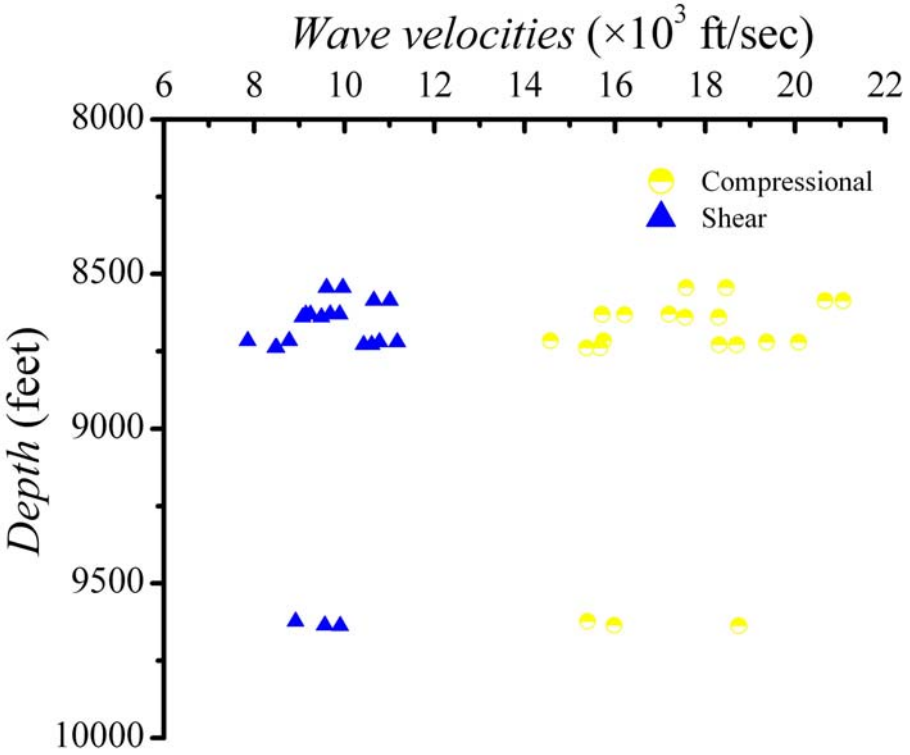

Figure 5-25. Ultrasonic wave velocities vs. depth

According to the analysis, all the measured geomechanical properties are rather scattered. There exist no correlation between the properties and depth directly. Because lithology and ingredients vary unpredictably, the scattering of all these parameters surely is the result of variation of lithology and anisotropy of the rock mass around these test wells. The ranges of these geomechanical properties of the Bakken shales are as follows.

(1) For UCS of Bakken shale, the value varies between 4,000 and 6,000 psi.
(2) For the triaxial compressive strengths, the value varies between 20,000 and 45,000 psi under confining pressures that corresponding the core depths.
(3) For the static Young's modulus determined with triaxial tests, the value varies between 3.5×10^6 and 6.5×10^6 psi.
(4) For the Poisson's ratio determined with triaxial tests, the values fall between 0.25 and 0.45.
(5) For the Biot's coefficient, although only limited number of values are available, most values are between 0.7 and 0.8.
(6) For the dynamic Poisson's ratio, most values are between 0.25 and 0.35.
(7) For the dynamic modulus, the shear modulus varies within a narrow range from 2×10^6 to 4.5×10^6 psi, but the dynamic bulk and Young's moduli vary in a rather large range.
(8) For the elastic wave velocities, the shear wave velocity varies between 0.7×10^4 and 1.1×10^4 ft/sec, and the compressional wave velocity varies between 1.4×10^4 and 2.1×10^4 ft/sec.

Other works to measure in situ stress and related properties of the Bakken formation include Jia et al., 1996; Chu et al., 2008; Fu et al., 2009; Beekman et al., 2000; Zhao and Muller, 2001; Gundmumdsson et al., 2010. Comparing the current experimental results on Bakken samples obtained by our group and other available information (Crammer, 1992; Spikes, 2011; Haven, 2011; Kuhlman et al., 1992; Reynolds et al., 2002; Wang and Zeng, 2011), Young's modulus and Poisson's ratio used in this model is determined as in Table 5-5.

Table 5-5. Elastic properties of different materials used in the model

Material No.	Geological portion	Young's modulus	Poisson's ratio
1	Fault core	5 GPa	0.32
2	Damage zone	10 GPa	0.27

3	Host rocks	45 GPa	0.27

5.5. Modeling of the Paleo In-Situ Stress

The finite element modeling package ANSYS (2010) is used in this study. The shell element provided by ANSYS can well model the stress and strain profile of the geological formation. In numerical modeling, the fault usually is modeled as a weak zone, with a lower Young's modulus and higher Poisson's ratio comparing to the host rock. Gundmundsson et al. (2010) suggest that a fault zone can be modeled as a core in the center, sandwiched by damage zones on both sides. The modeling area should be set large enough to offset the impact of boundary conditions to the results. The main modeling part of the three dimensional model is a rhomboid in plan view with a side length of 120 km, and a rectangle in side view with a thickness of 1 km, starting from the basement of the basin to the top of the Bakken formation. The structure of the main block is shown in Figure 5-26. As the cardboard model described above (Figure 5-8), the blocks in the basin interacted with each other under the far-field effect of the Laramide tectonics. The Weldon block would subject to compressive and frictional forces from its neighboring blocks. Therefore, two rectangular blocks, A and B, are added and contact with to rhombic block on its north and south sides. The two additional blocks provide compressive and frictional effects from the neighboring blocks (Figure 5-27).

The Nesson master fault (about 60 km long) and the Antelope fault (about 25 km long) are put in the center of the model. The Nesson fault is represented by a fault core sandwiched by two damage zones. The Antelope fault is modeled as a damage zone because of its smaller size. Material attributes are listed in Table 5-5 and shown in Figure 5-28. In the model, 6-node and 8-node shell elements are used.

Displacement constraints on X and Y directions are applied on the northeast and southwest corners of the additional blocks. A vertical pressure of 70 MPa is applied to simulate the overburden pressure. Horizontal stress is applied on the three lateral faces of the additional blocks A and B. Therefore, right lateral force, or frictional forces can be provided on the contact surface between the main rhombic block and the additional blocks. To account the driving force from the corners of neighboring blocks, we add four concentrated forces at each corner of the main block, pointing to the SE, SW, NW and NE directions respectively (Figure 5-27). The applied stresses and forces are adjusted until the offset between the east and west of the Nesson master fault reaches about 120 m as described in the literature (Gerhard et al., 1987).

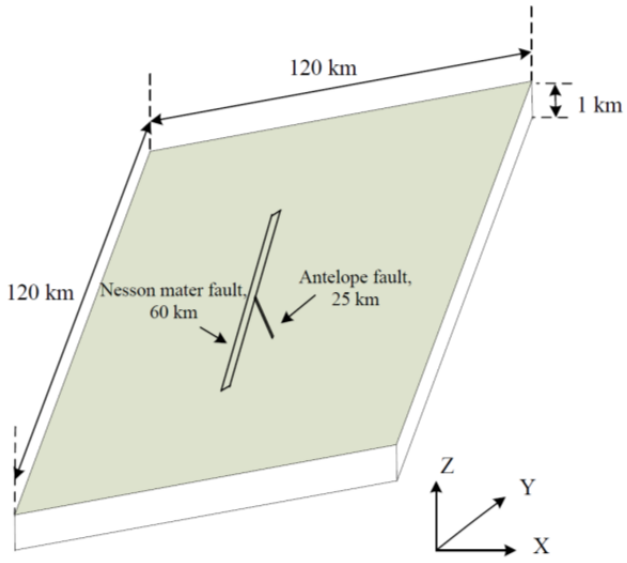

Figure 5-26. Structure of the main rhombic block in the three dimensional model, with exaggeration in the Z (vertical) direction.

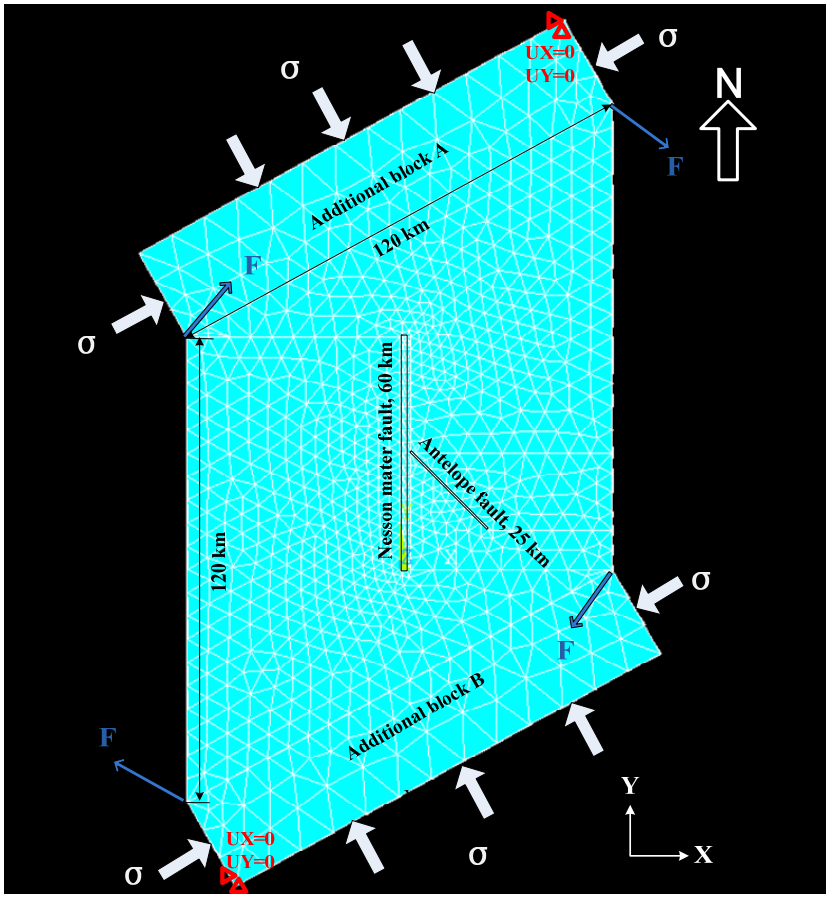

Figure 5-27. Plan view from Z (vertical) direction of the finite element model.

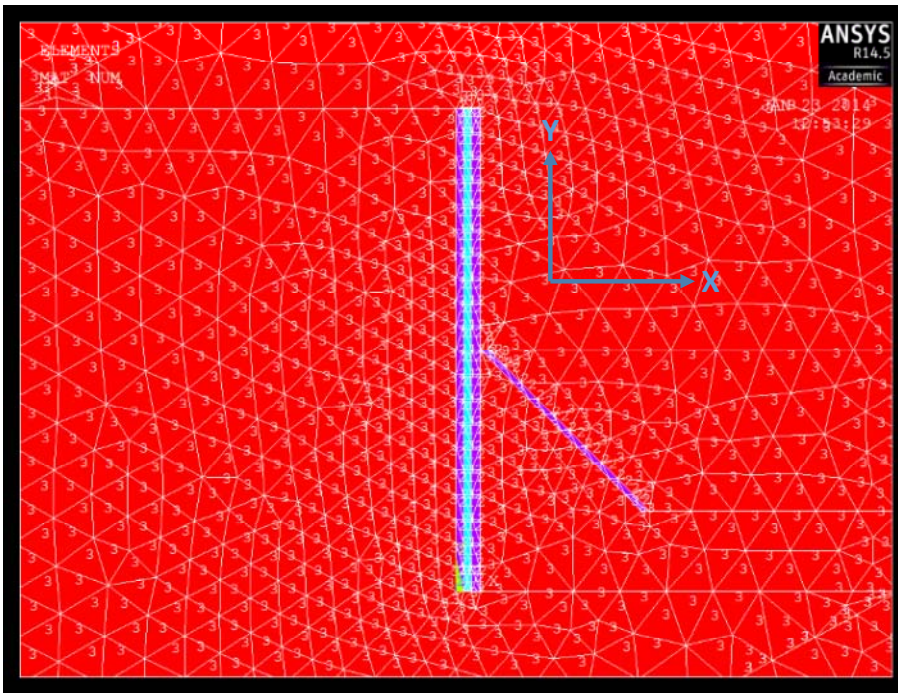

(a) 2D model

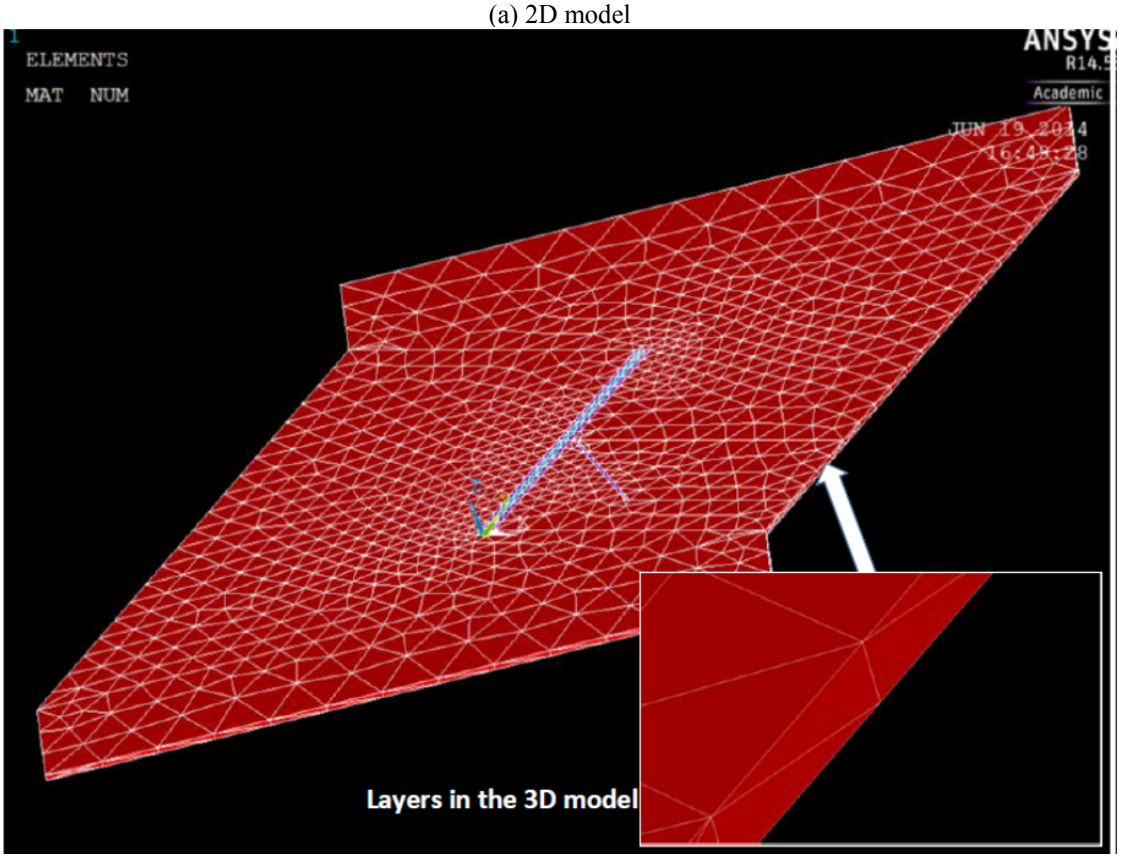

(b) 3D model

Figure 5-28. Different materials used for the elements: cyan (Material 1) – fault core, purple (Material 2) – damage zone, and red (Material 3) – host rock.

5.6. Modeling Results

The modeling results show that, during the Laramide event, the maximum principal stress is in the vertical direction, and the other two principal stresses are horizontal. Figure 5-29 shows the contour maps of the minimum horizontal stress, maximum horizontal stress, vertical stress and stress intensity. The stress intensity is defined as (σ_1-σ_3), corresponding to two times of the maximum shear stress in geological convention (ANSYS, 2010). For the horizontal stress from Figures 5-29a, 5-29b, 5-29c, and 5-29d, it can be seen that tensile stress (negative value) was developed in most parts around the fault. Stresses of lower magnitude (larger tensile stress) appear in north and south of the Nesson master fault. The lowest value (maximum tensile stress) is less than -12 MPa just next to the north and south ends of the fault. There is an obvious change of the stress magnitude in and out of the fault zone. The presence of the faults, especially the Nesson master fault, has a significant impact to the magnitude of the vertical and horizontal stresses. In general, stresses in the fault zone have a lower value than those in the host rock. This is consistent to other researchers' modeling results (Gudmundsson et al., 2010).

According to Kuhlman and Claiborne (1992) and Haven (2011), it can be assumed that the tensile strength of the Bakken shale is about 6 to 9 MPa. Based on the magnitude of the minimum horizontal stress, zones of possible tensile fracture development can be recognized. Due to the accuracy of the model, it is hard to say that fracture zones can be accurately identified. However, it is fair to say that the lower the tensile stress value, the more likely the tensile fractures could be generated. Therefore, we classify the possible fractural zones as Class I and II (Figure 5-31). Class I refers to areas with the very low value of minimum horizontal stress (< -6 MPa), so tensile factures are developed in this zone. Class II refers to areas with minimum principal stress between -3 and -6 MPa. Tensile fractures are less developed in this zone. In zones of Class I and II, porosity and permeability could be enhanced by the fractures, and these zones are likely form "sweet spots" in the reservoir. For other areas with minimum principal stress of negative values, some tensile fractures probably exist in this zone, but not in large scale.

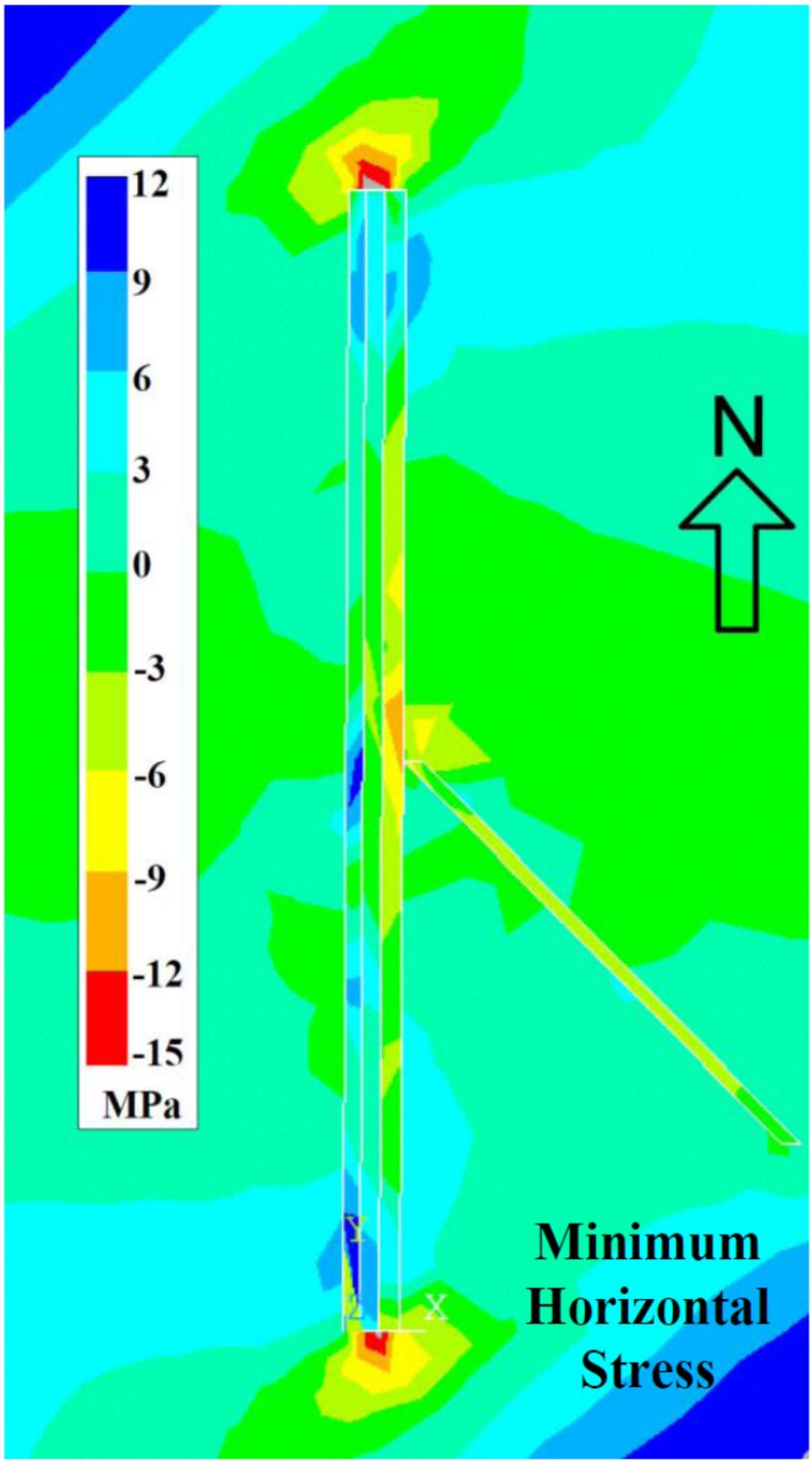

(a) 2D model

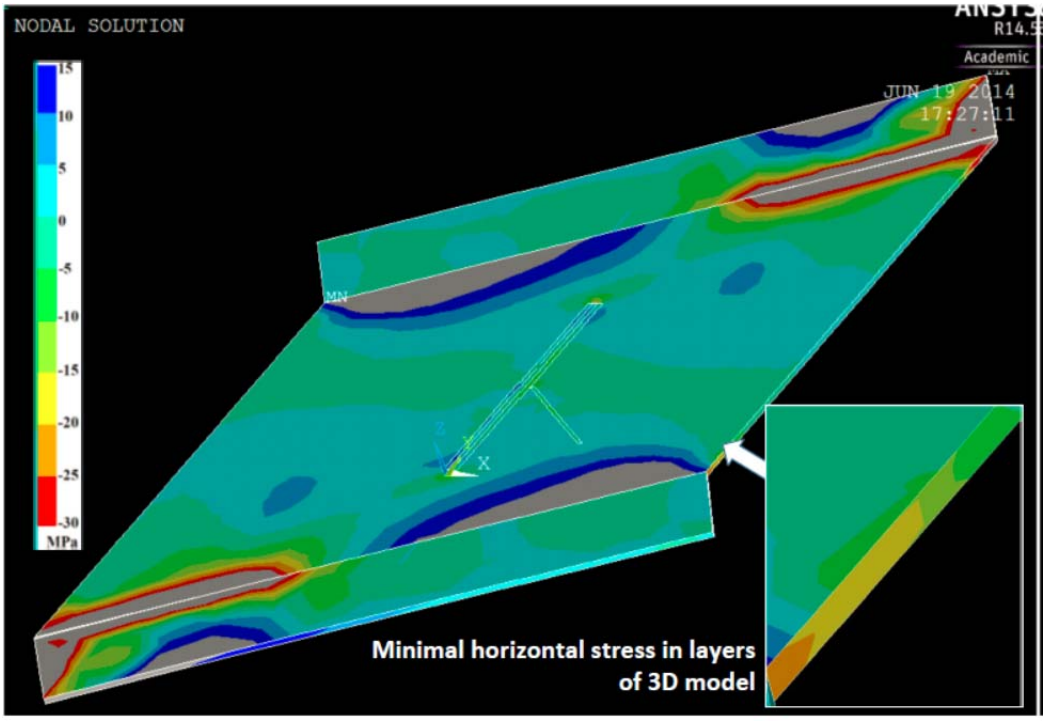

(b) 3D model

Figure 5-29a. Contour map of minimum horizontal stress.

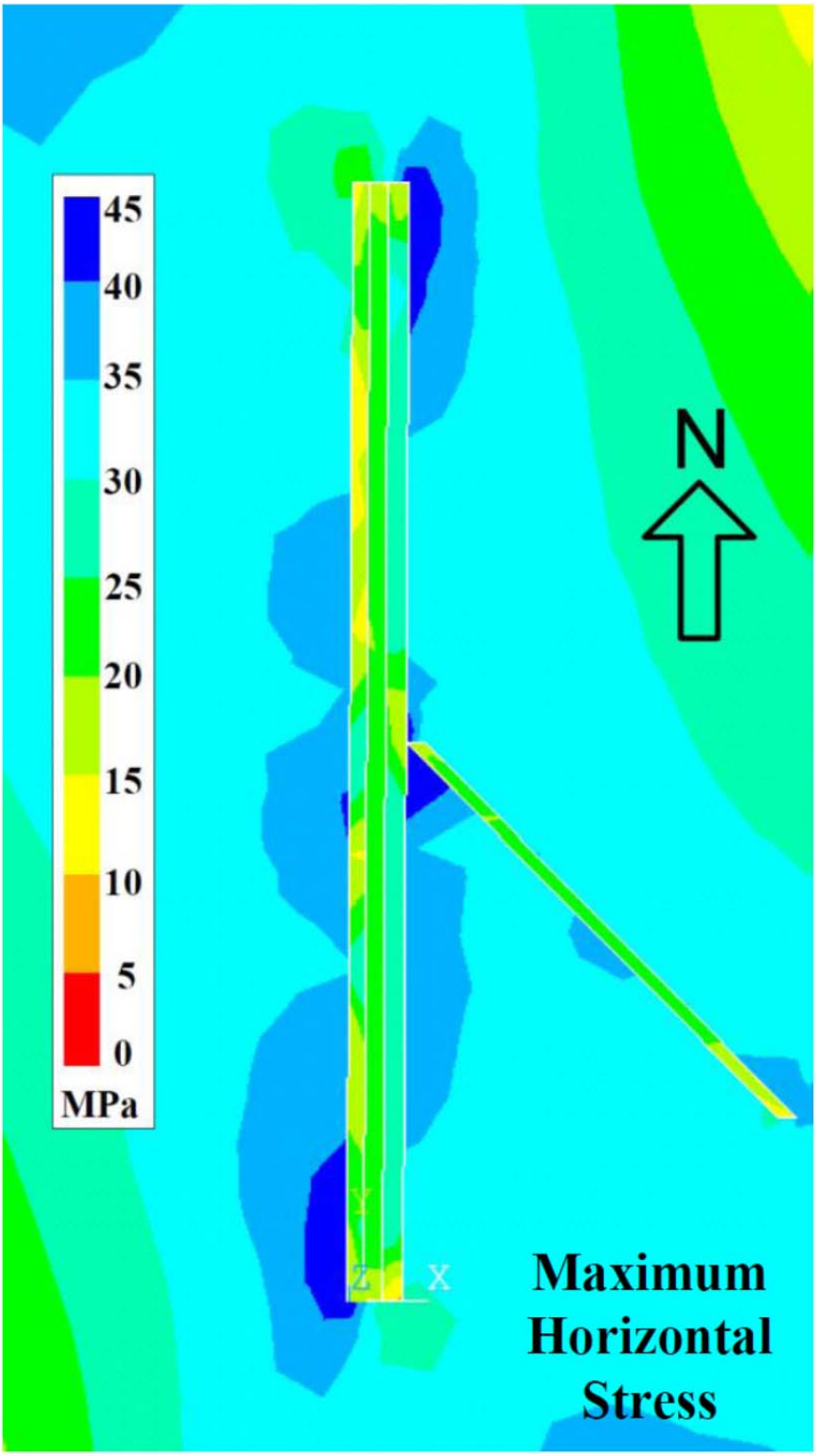
45
40
35
30
25
20
15
10
5
0
MPa
N
Z
X
Maximum
Horizontal
Stress

(a) 2D model

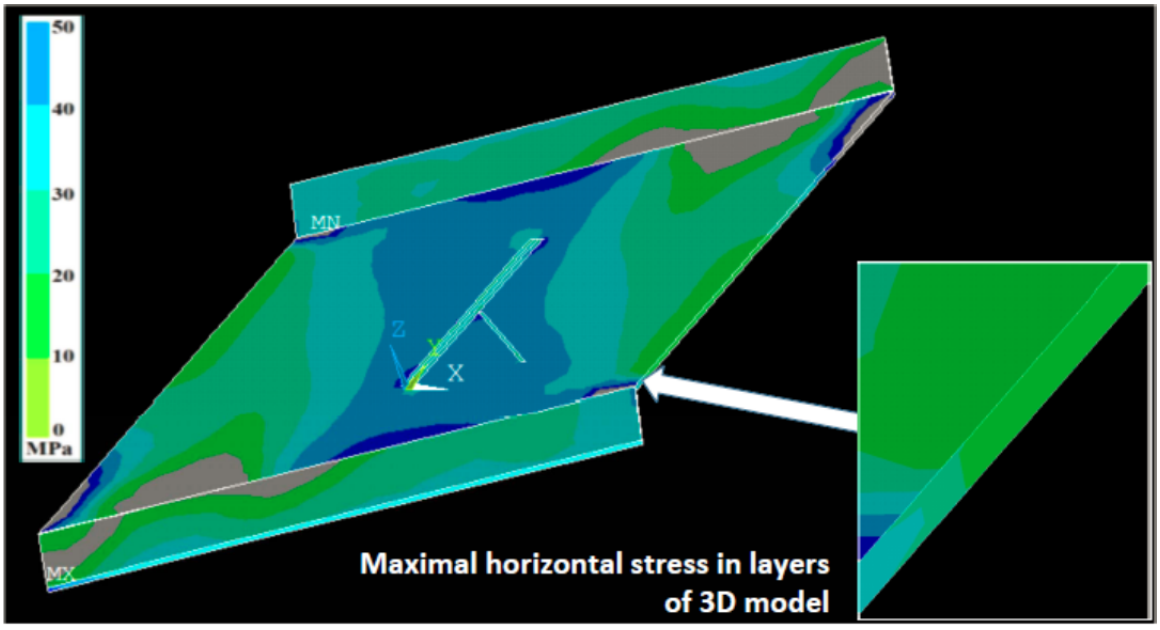

(b) 3D model

Figure 5-29b. Contour map of maximum horizontal stress.

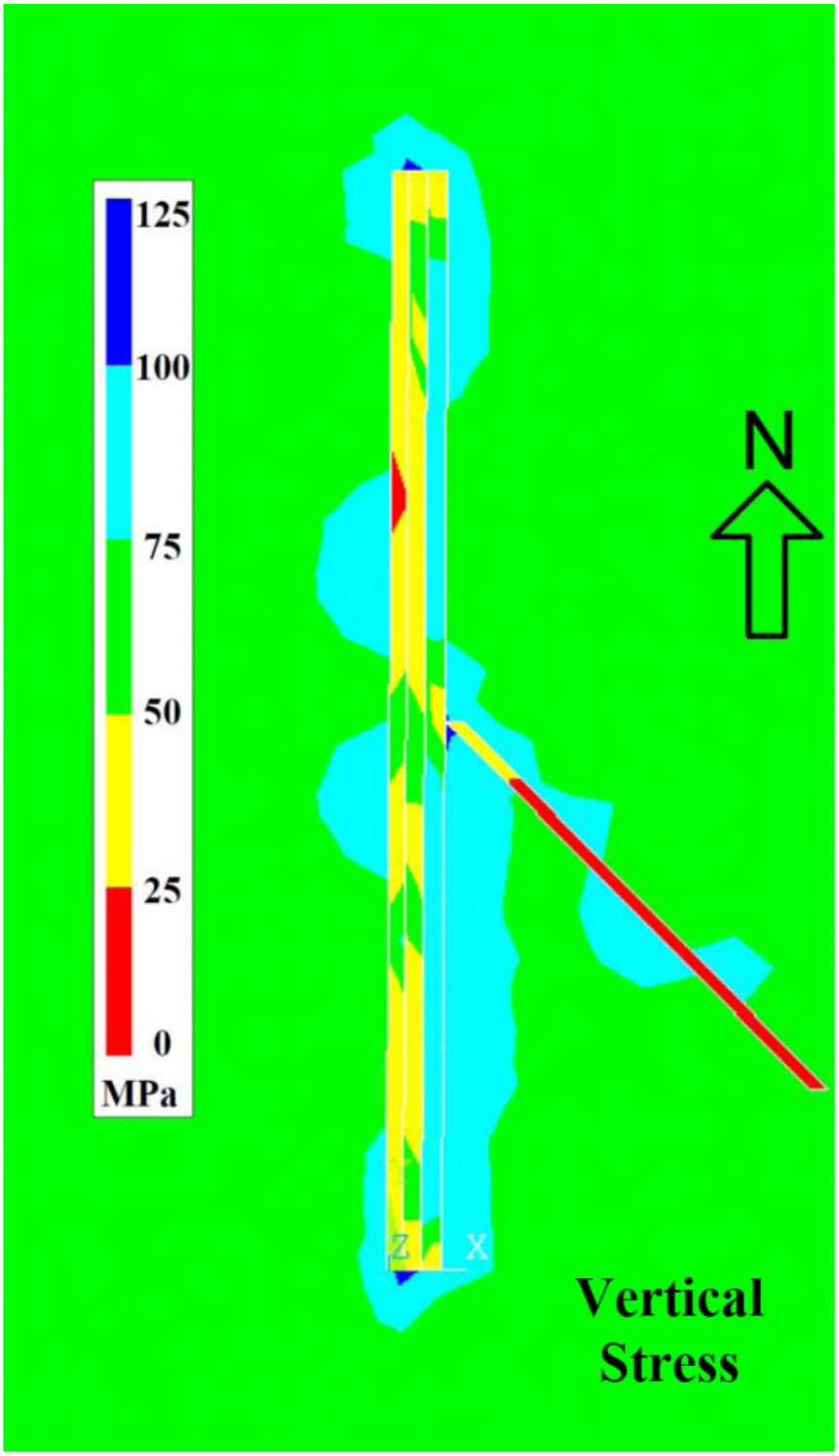
125
100
75
50
25
0
MPa
N
Z
X
Vertical
Stress

(a) 2D model

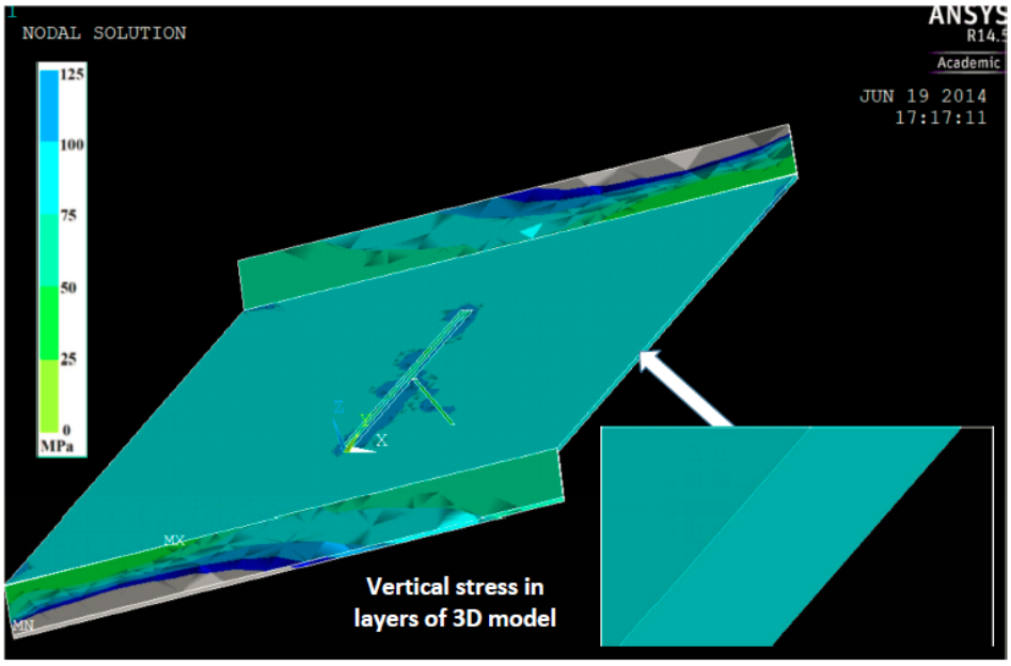

(b) 3D model

Figure 5-29c. Contour map of vertical stress.

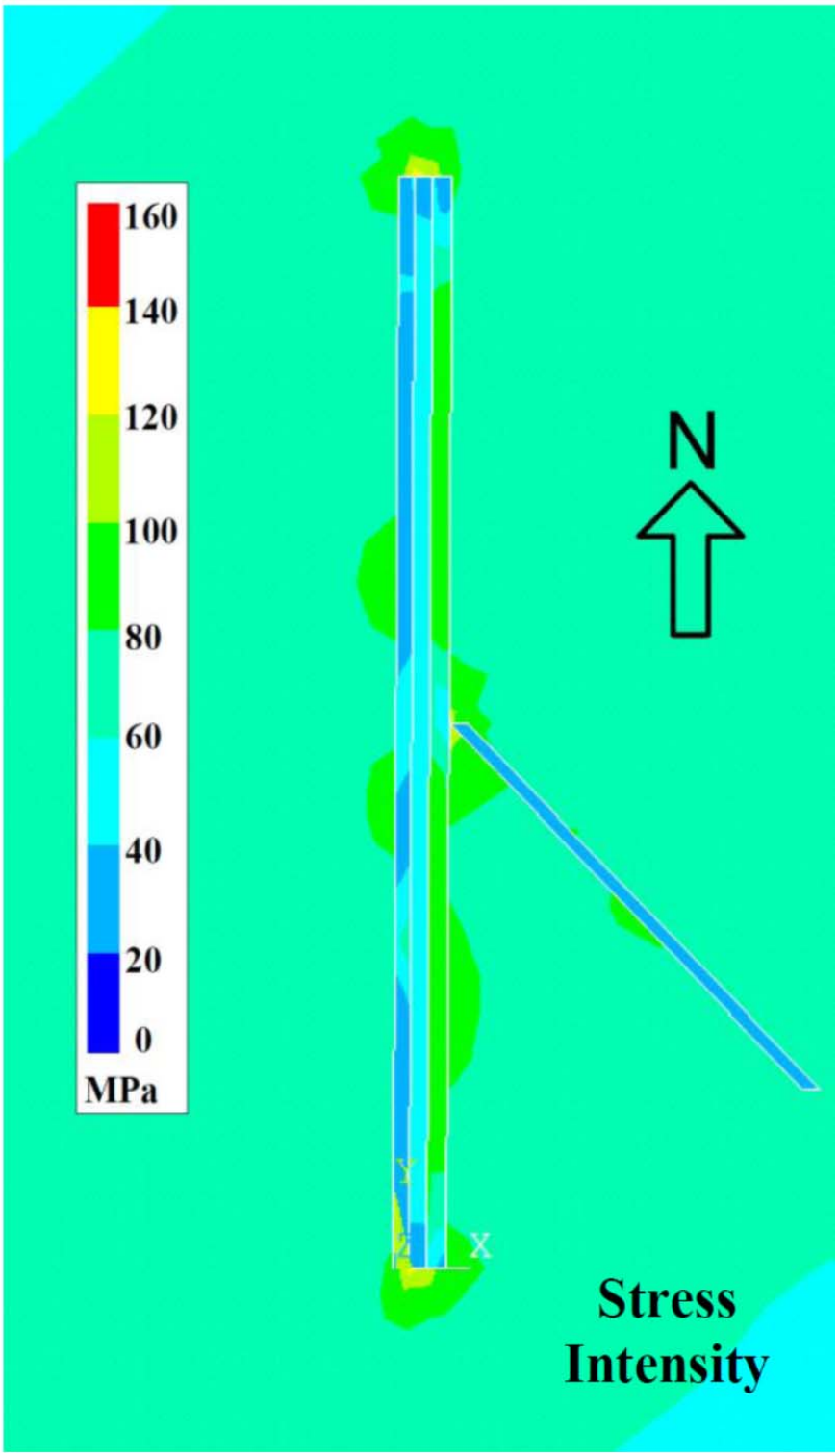

Figure 5-29d. Contour map of stress intensity.

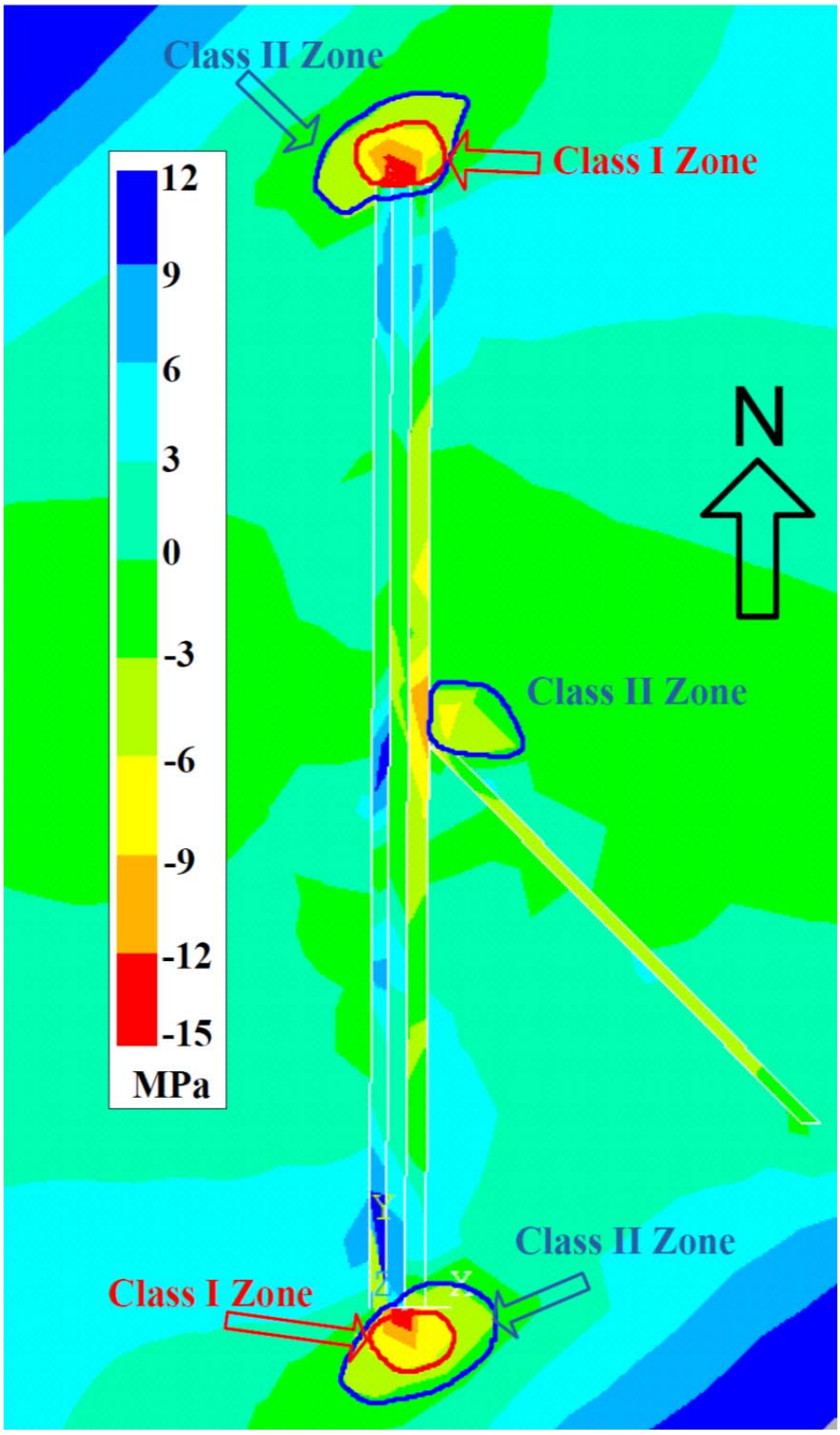

Figure 5-31. Possible zones for natural tensile fracture development.

Figures 5-32 to 5-34 show the maps of trajectories of maximum horizontal stress in areas around the north, middle and south portions of the Nesson master fault respectively. Due to the existence of the lateral force, the direction of the principal stresses varies across the study area. However, in general the maximum horizontal stress is in NNW direction, and the minimum horizontal stress is in ENE direction. Therefore, if any possible tensile fractures were generated under the effect of the Laramide event, the fracture should be in the NNW direction, parallel to the maximum horizontal paleostress. This modeling result agrees with the hydraulic fracturing test result conducted by the Bakken Research Consortium (Headington Oil LLC and XTO Energy Inc, 2008; Dow, 1974). The project area is in Section 36-T156N-R95W in eastern Williams County, North Dakota, which is on the eastern flank of Nesson anticline, next to the Nesson master fault on its northeast. Three horizontal wells were drilled and a hydraulic fracturing test was conducted. Natural fractures encountered in the drilling are primarily in the NW direction.

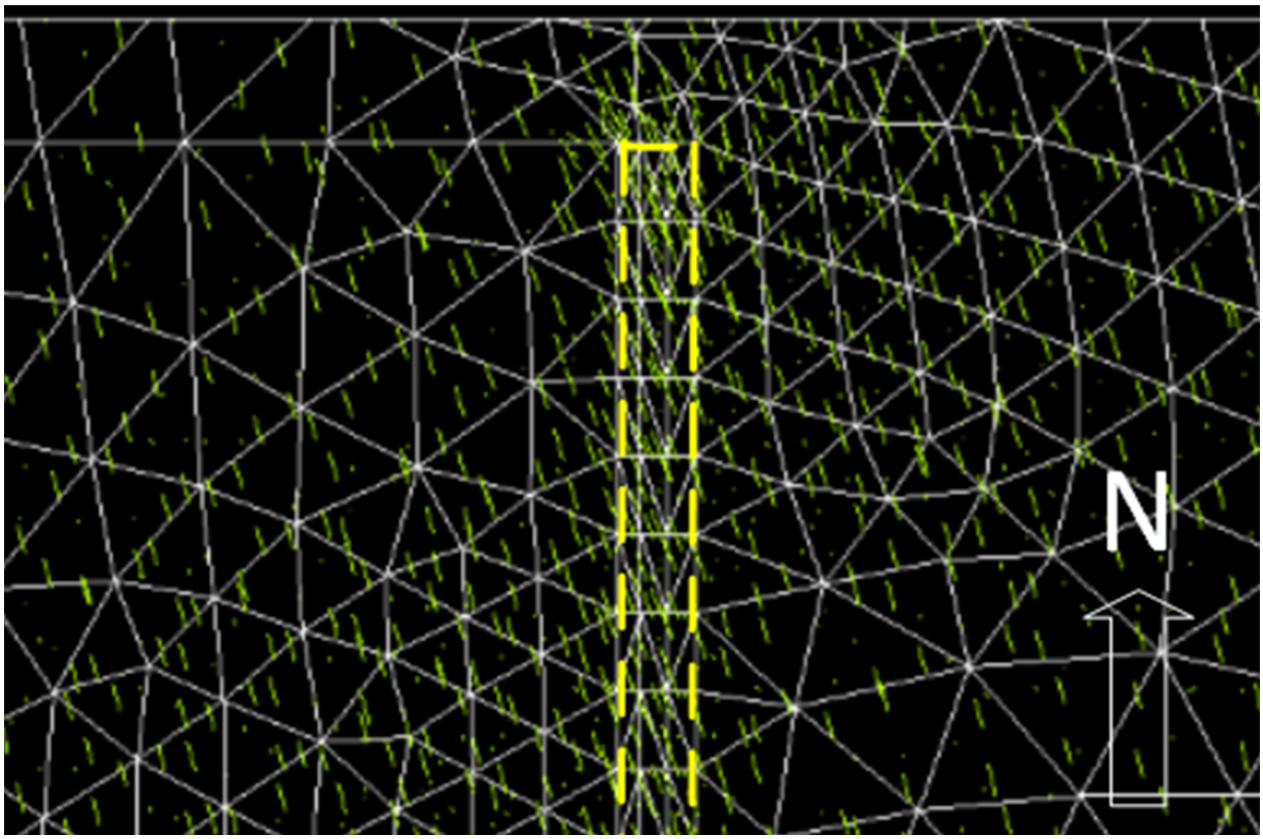

Figure 5-32. Trajectories of the maximum horizontal stress, north part of the Nesson master fault.

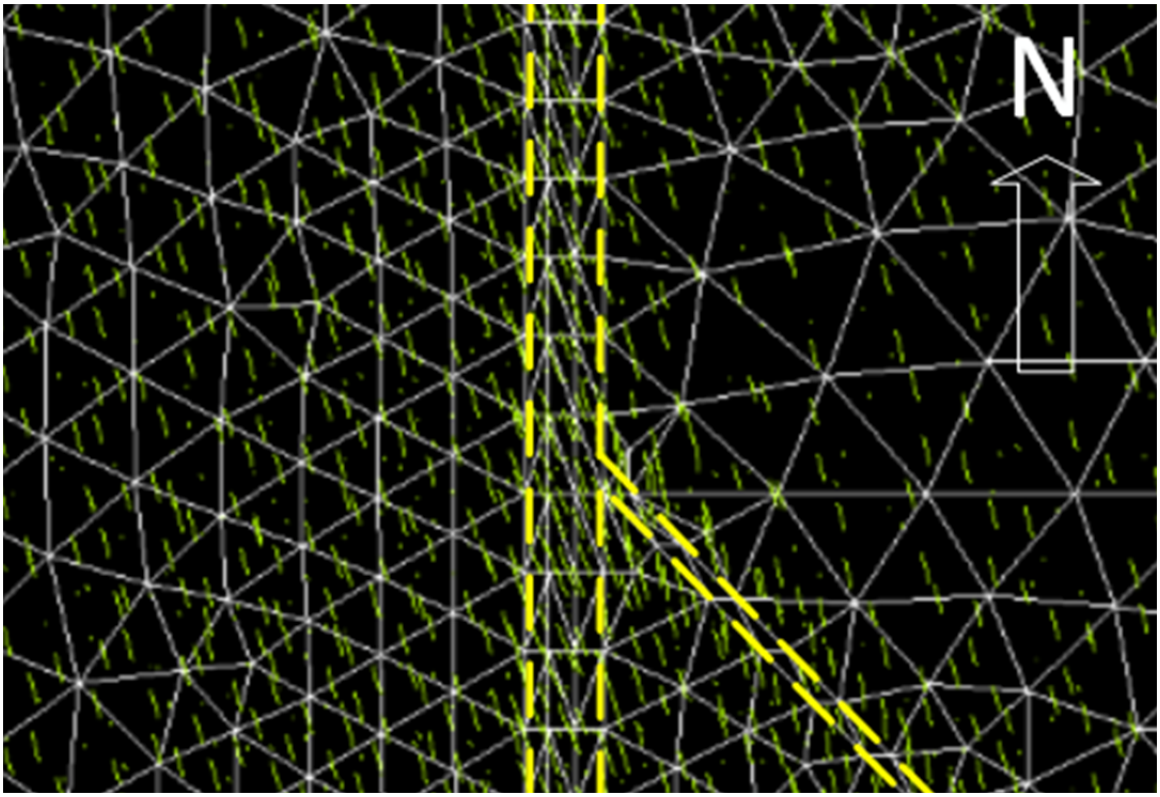

Figure 5-33. Trajectories of the maximum horizontal stress, middle part of the Nesson master fault.

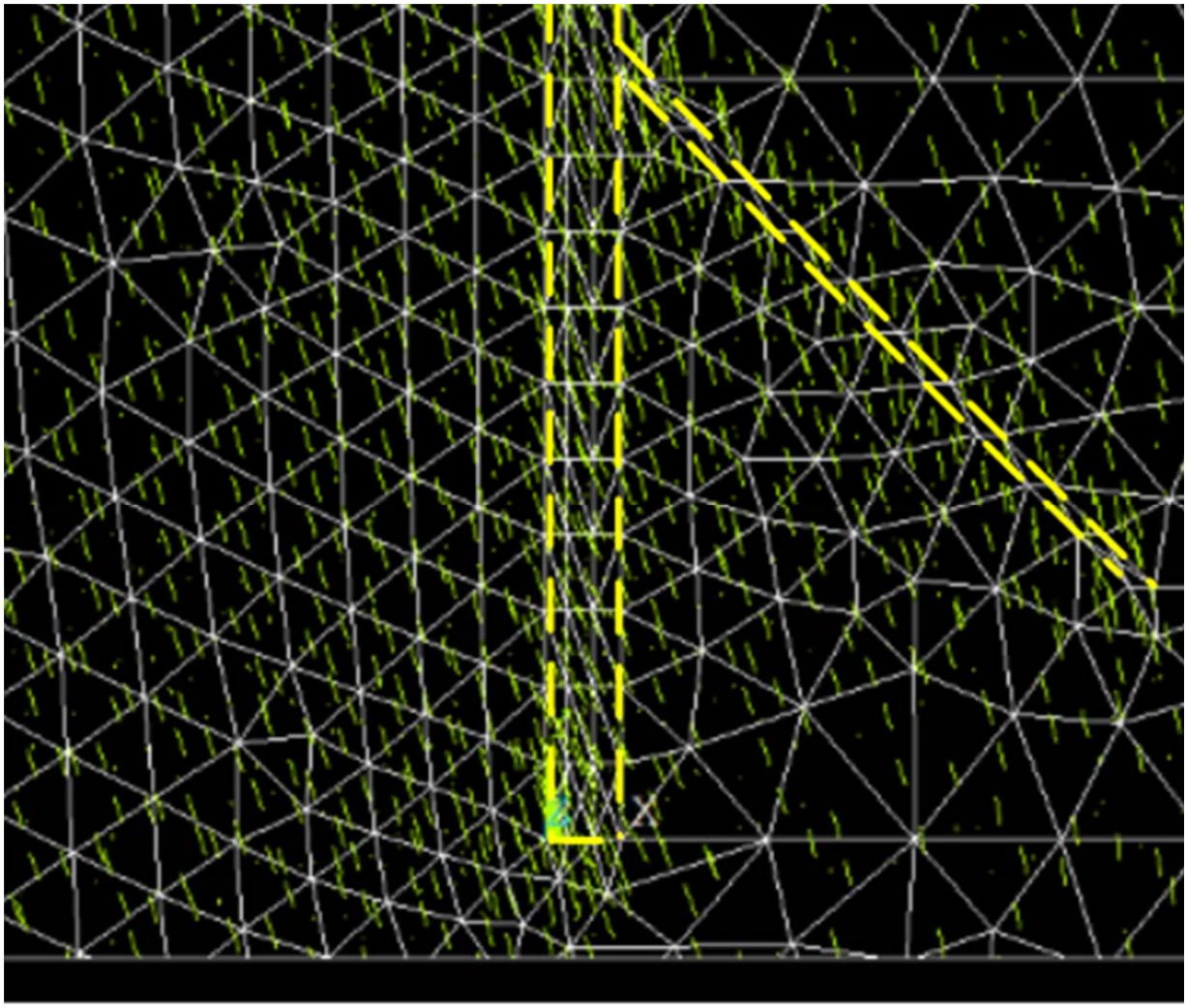

Figure 5-34. Trajectories of the maximum horizontal stress, south part of the Nesson master fault.

5.7. Discussion and Conclusion

The deformation of the Nesson anticline is controlled by the Nesson master fault beneath the west side of its crest. The vertical movement of the fault under the far-field effect of the Laramide orogeny largely determined the deformation of the fold. On the other hand, the Nesson master fault, and a secondary fault – the Antelope fault, have an obvious influence on the local in situ stress. The paleostress profile during the Laramide event has been reconstructed by using a three-dimensional finite element elastic model, which treats the geological formation as shell elements. The modeling result indicates that, in late Cretaceous, horizontal tensile stress was probably generated in areas around the Nesson master fault, and vertical stress was the maximum principal stress. On the north and south ends of the fault, the minimum principal stress reaches its lowest value; hence tensile factures are very likely developed. As a continuous, tight, self-sourced reservoir, natural tensile fractures can form "sweet spots" and greatly enhance the reservoir quality in terms of both porosity and permeability. According to the vector map of the principal stresses, the natural tensile fractures around the Nesson anticline should be in the NNW direction.

The modeling result also provides information for discussion of the oil migration and accumulation pattern. The Bakken shale is an excellent source rock in the Williston basin. There have been arguments that if the generated oil is confined in Bakken or the Bakken shale is also the source rock for other Mississippian reservoirs in the basin

(Meissner, 1978; Webster, 1984; Price et al., 1984; Osadetz and Snowdon, 1986; Price and LeFever, 1994). As shown in the contour maps of principal stresses (Figure 5-28), the fault zone generally present as an area of low stress magnitude comparing to the host rock. If the modeled paleostress regime had lasted until the post-maturation of hydrocarbon in the source rock, the stress regime should have an impact to the oil migration. It is known that the Bakken shale in the area around the Nesson anticline has generated the largest volume of oil comparing to other areas in the basin (Figure 5-35). The high compressive stresses in the host rock could provide driving force pushing the mature hydrocarbon to the low-stress zone in the fault from both sides. As the hydrocarbon accumulated in the fault zone, the vertical fractures may provide additional pathways for outward migration to overlying formations and other areas in the basin until suitable cap rock is encountered.

In previous literature, horizontal fractures on the Bakken core samples are reported, and it is doubted that these fractures were generated by the super-lithostatic pressure due to the hydrocarbon expulsion in the shale rocks when it reached the maturation window. Since the direction of the fractures is orthogonal to the minimum principal stress, the vertical stress had to be the minimum principal stress so that the horizontal fractures could be generated when the hydrocarbon reached maturation during late Cretaceous. Nevertheless, there is no sound evidence by far that the minimum stress was vertical stress during that time. Warner (2011) suspected that the contemporaneous Laramide orogeny far-field tectonics probably generated a maximum horizontal stress regime, then joint propagation in the Bakken at that time would have likely been horizontal. However, the modeling results in this paper show that the vertical stress was the maximum principal stress under the effect of Laramide orogeny. Therefore, these reported horizontal fractures are probably generated by other mechanisms, or just caused by pressure-release during coring.

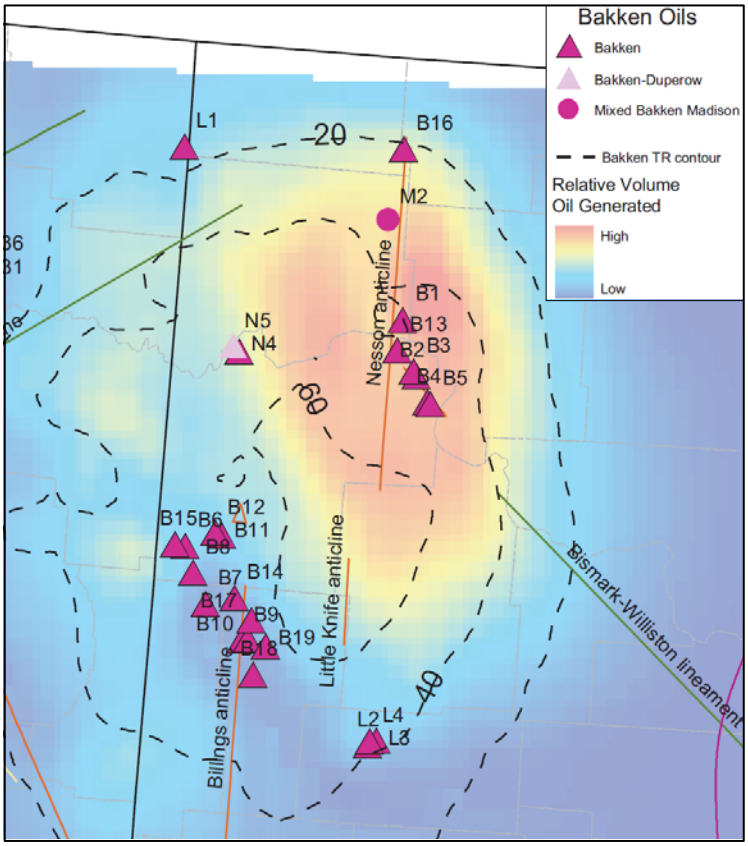

Figure 5-35. Relative volume oil generated from the Bakken shale (after Flannery and Kraus, 2006).

The modeling work presented in this study provides an alternative approach to reconstruct the paleostress in the Williston basin. As mentioned early in the above section, natural fractures in the Bakken have been generated by different mechanisms at different times in the history. This modeling work focus on the late Cretaceous period and gives an image where the tensile fractures were probably developed, as well as possible hydrocarbon migration

patterns based on the paleostress profile. The model can be improved if a more accurate three dimensional geological model could be built with seismic profile and a better well control. It is also suggested that some laboratory test can be carried out to investigate the effect of stress difference on hydrocarbon migration in tight formations.

6. Mapping of Current In-Situ Stresses

According to existing literature, in-situ stresses of the Bakken formation have not been investigated systematically. The objective of this study is to screen for geomechanical properties from exiting references and perform a preliminary research on the in-situ stress characteristics. The overall goal is to increase the success rate of horizontal drilling and hydraulic fracturing to expand the access to reservoir rocks, and consequently to improve the ultimate recovery factor of this 200-400 billion barrels unconventional crude oil resource. The following aspects related to the in-situ stresses of the Bakken formation in the Williston basin, North Dakota are touched: (1) the basin tectonics, (2) the orientation and magnitude of the principal stresses, and (3) distribution of in-situ stresses in the Bakken formations, and (4) stress concentration around a horizontal well at different orientations.

6.1. Geological Settings

The geological settings of the study area have been discussed in previous section.

6.2. Tectonic History of the Basin

The tectonic history of the Williston basin has been discussed in aforementioned section.

6.3. Tectonic History of the Nesson Anticline

The tectonic history of the Nesson anticline has been discussed in aforementioned section.

6.4. Elastic Properties

A review of literature has been conducted to investigate the modeling approach as discussed in aforementioned section.

There is not much information about the in situ stress data in the Williston Basin available. Most of the available data only give either the magnitude or direction of the principal stresses (Wang and Zeng, 2011; Kuhlman et al., 1992; Phillips et al., 2007; Cipolla et al., 2009; Heidbach et al., 2008). For this modeling work, we consider that the best information is the result of a hydraulic fracturing test provided by the Bakken Research Consortium (Headington Oil LLC and XTO Energy Inc, 2008; Sturm and Gomez, 2009). The project area is in Section 36-T156N-R95W in eastern Williams County, North Dakota, which is on the eastern flank of Nesson anticline. Three horizontal wells were drilled and hydraulic fracturing test was conducted. Figure 6-1 shows pump plot of two of the three wells. The horizontal principal stresses can be estimated using the equations of suggested calculation for stress determination (Hudson and Harrison, 1997; Kim and Franklin, 1987):

$$P_S = \sigma_h \quad (6\text{-}1)$$

$$P_B = 3\sigma_h - \sigma_H + \sigma_t \quad (6\text{-}2)$$

where P_s is the shut-in pressure, P_B is the break pressure, σ_t is the tensile strength of rock, σ_h is the minimum horizontal stress, and σ_H is the maximum horizontal stress.

The tensile strength is assigned a value of 1192 psi (8.2 MPa) according to Kuhlman et al. (1992). Using Equations (6-1) and (6-2), we estimated that the maximum horizontal principal stress is 41.4 MPa, and minimum horizontal principal stress is 27.6 MPa. Depth of the wells is between 10,200 and 10,400 ft, therefore the vertical stress is

assumed to be 70 MPa, or about 10,200 psi. Directions of the maximum horizontal stress determined by tests on these three wells are NE 41°, 34° and 45° respectively.

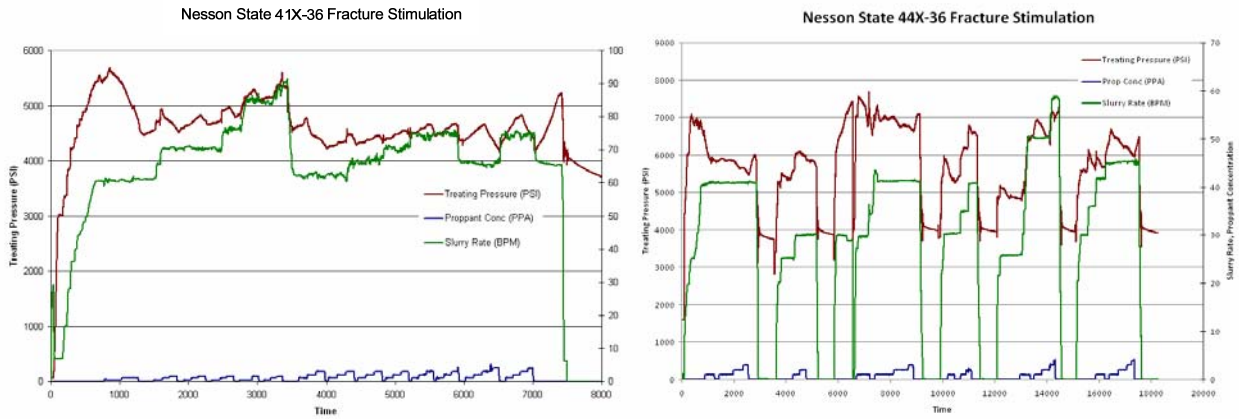

Figure 6-1. Pump plot of the hydraulic stimulation test (after Headington Oil LLC and XTO Energy Inc, 2008).

Elastic properties have appeared in previous literature (Crammer, 1992; Spikes, 2011; Haven, 2011; Kuhlman et al., 1992; Reynolds et al., 2002; Wang and Zeng, 2011), Over 200 core specimens have been tested at the University of North Dakota. The tested wells are selected to represent a decent geographical coverage. The test results were the database of elastic properties in the modeling work. In the modeling work, the modeled area was divided into several areas. Each area was assigned with its elastic properties based on the laboratory test results of nearby wells. Comparing the current experimental results on Bakken samples obtained by our study and other available information Young's modulus and Poisson's ratio used in this model are shown in Table 6-1.

Table 6-1. Elastic properties of different materials used in the model

Reference well	Material No.	Geological portion	Young's modulus, GPa	Poisson's ratio
16174	1	Lower Bakken	63	0.25
16174	2	Middle Bakken	75	0.23
16174	3	Upper Bakken	62	0.28
16089	4	Lower Bakken	67.8	0.2
17450	7	Lower Bakken	86	0.24
17450	8	Middle Bakken	65	0.2
17450	9	Upper Bakken	73	0.24
16862	11	Middle Bakken	60	0.2
16862	12	Upper Bakken	72	0.22
11617	13	Lower Bakken	68	0.18
15923	14	Middle Bakken	58	0.22
16985	15	Upper Bakken	63	0.19
Literature	16	Antelope fault	10	0.27
Literature	17	Nesson master fault	5	0.32

6.5. Modeling of the Current In-Situ Stresses

The numerical modeling package ANSYS is used in this study. ANSYS has already extensively been used in different fields of mechanical engineering, chemical engineering and civil engineering. It provides sound solutions for structure design, bridge and tunneling engineering, aviation and aerospace simulation etc. The shell element provided by ANSYS can well model the stress and strain profile of the geological formation.

In this study, the three-dimensional model has a thickness of 95 meters. The satellite map of the modeling area is shown in Figure 6-2. The lower Bakken member is modeled is 30 m thick; the middle Bakken member is modeled

as 50 m thick, and the upper Bakken member is modeled as 15 m thick. To eliminate the impact of the boundary condition to the results, the areas is set as a square of 200*200 km^2. The Nesson fault and the Antelope fault are put at the center of the model. The Nesson fault and the Antelope fault are modeled as damage zones of weak elastic properties. Material attributes are listed in Table 6-1. 8-node solid-shell elements are used. After meshing, the central part of the model, including the two faults, is shown in Figure 6-3. Figure 6-4 shows the different materials used for the elements.

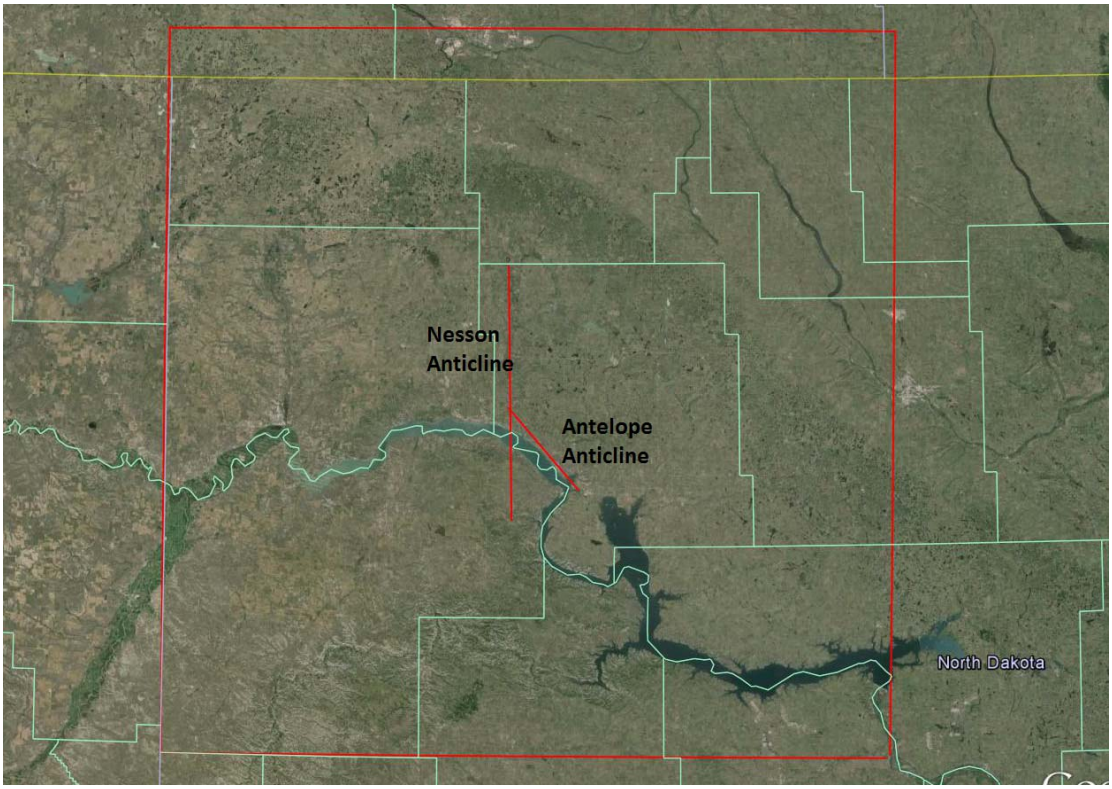

Figure 6-2. Satellite map of the modeling area

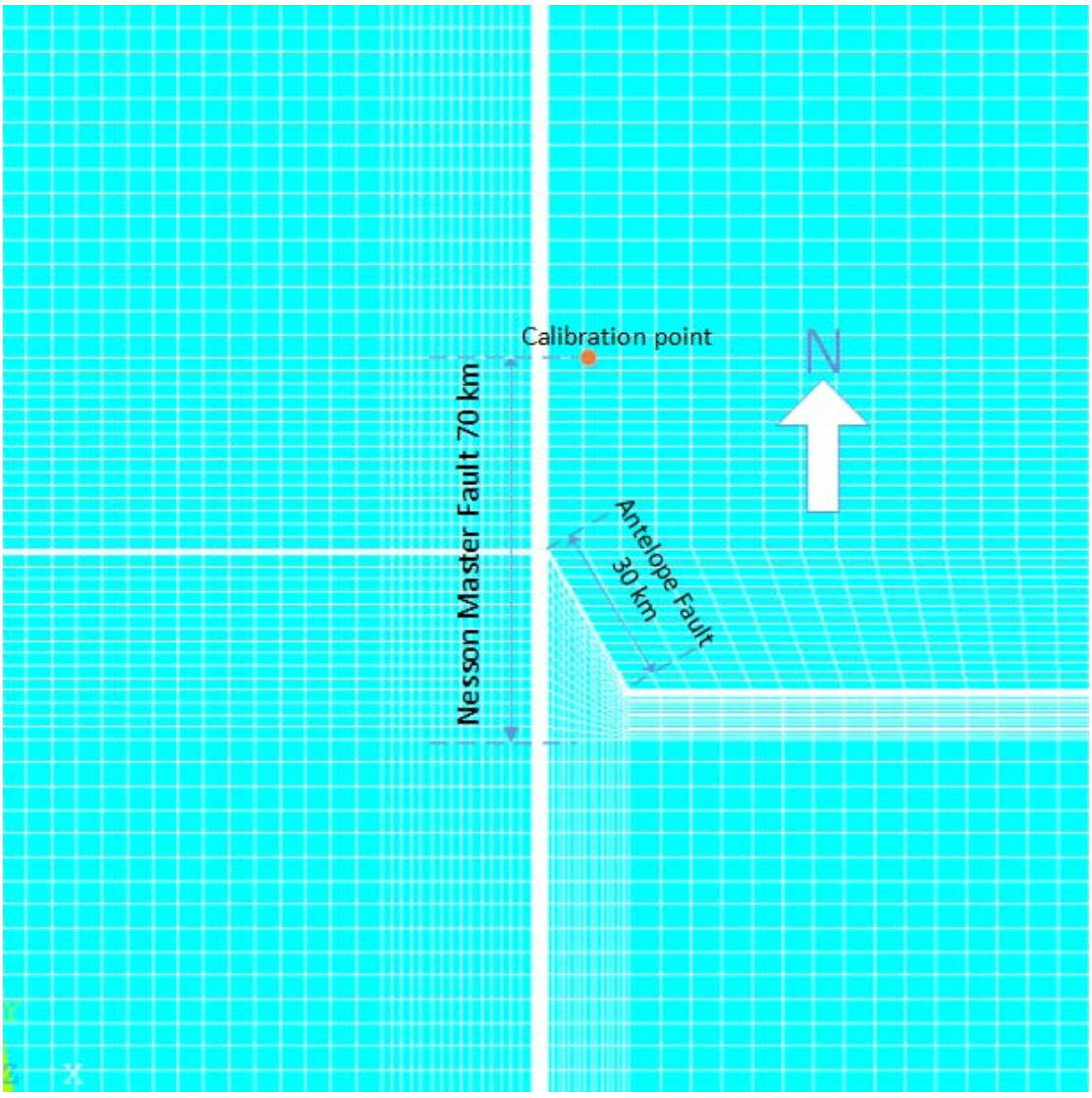
Calibration point
N
Nesson Master Fault 70 km
Antelope Fault
30 km

(a) 2D model

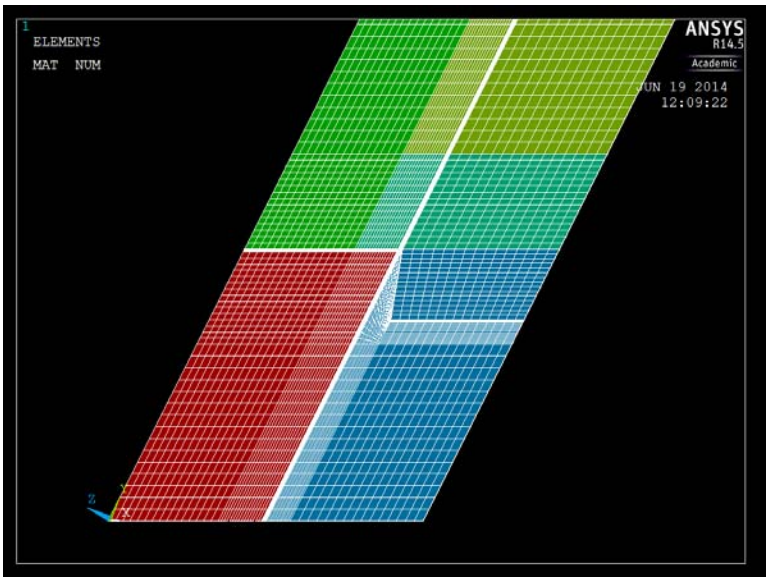

(b) 3D model

Figure 6-3. Meshed model

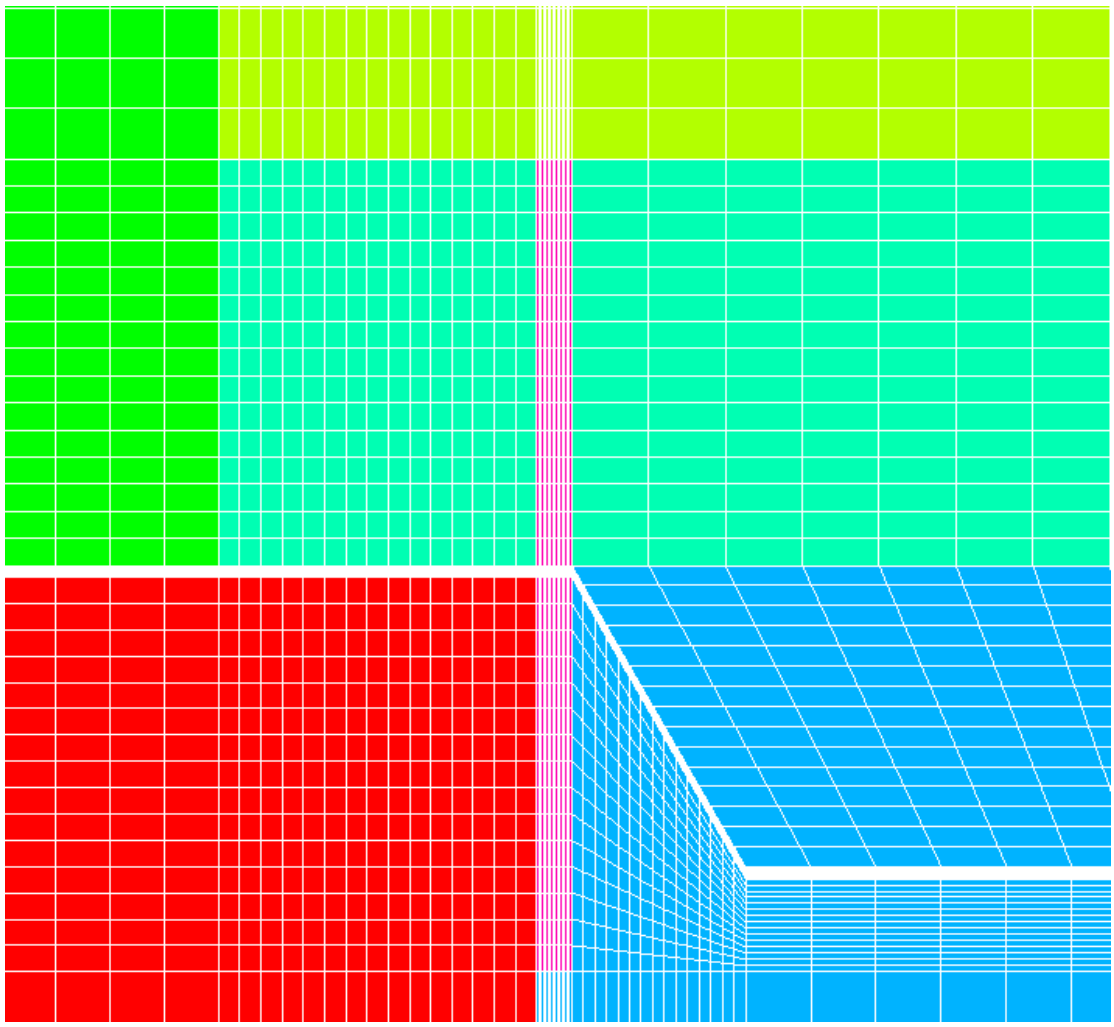

(a) 2D model

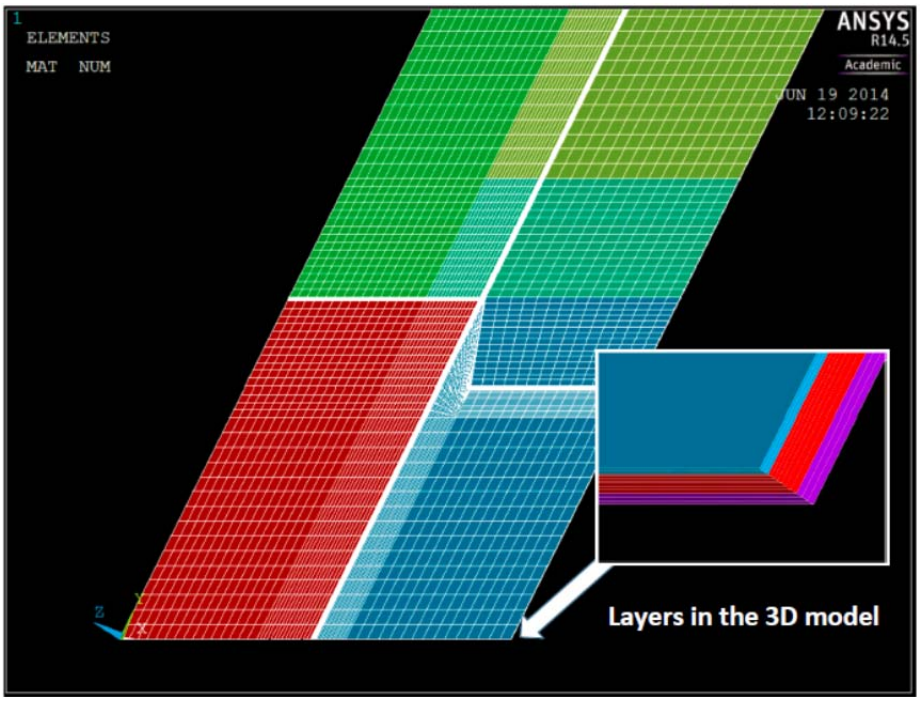

(b) 3D model

Figure 6-4. Different materials used for the elements. Different colors represent different materials in the model.

A vertical pressure of 70 MPa is applied on the model to simulate the vertical stress. Pressure is applied on the NE and SW boundaries of the model at the direction of NE 40^o. The NW and SE boundaries are fixed. The boundary pressure is adjusted until the values of the principal stresses on the calibrated point (Section 36-T156N-R95W, Williams County, ND) matches the measured values mentioned above.

6.6. Modeling Results

The contour maps of the minimal horizontal stress, maximum horizontal stress and vertical stress are shown in Figures 6-5, 6-6 and 6-7 respectively. It can be seen that due to the existence of the fault zone, the magnitude of the principal stresses varies from the faults to the host rocks. In general, the stresses in the fault zone have a lower value than those in the host rock. This is constant with the description of other researchers' modeling results.

The vector map of the maximum horizontal stress is shown in Figure 6-8. Figures 6-9 to 6-11 are plan views of the detailed vector map in the North, Central and South portions of the Nesson Anticline. It can be seen that there is a minor rotation of the direction of the maximum horizontal stress around the fault zone.

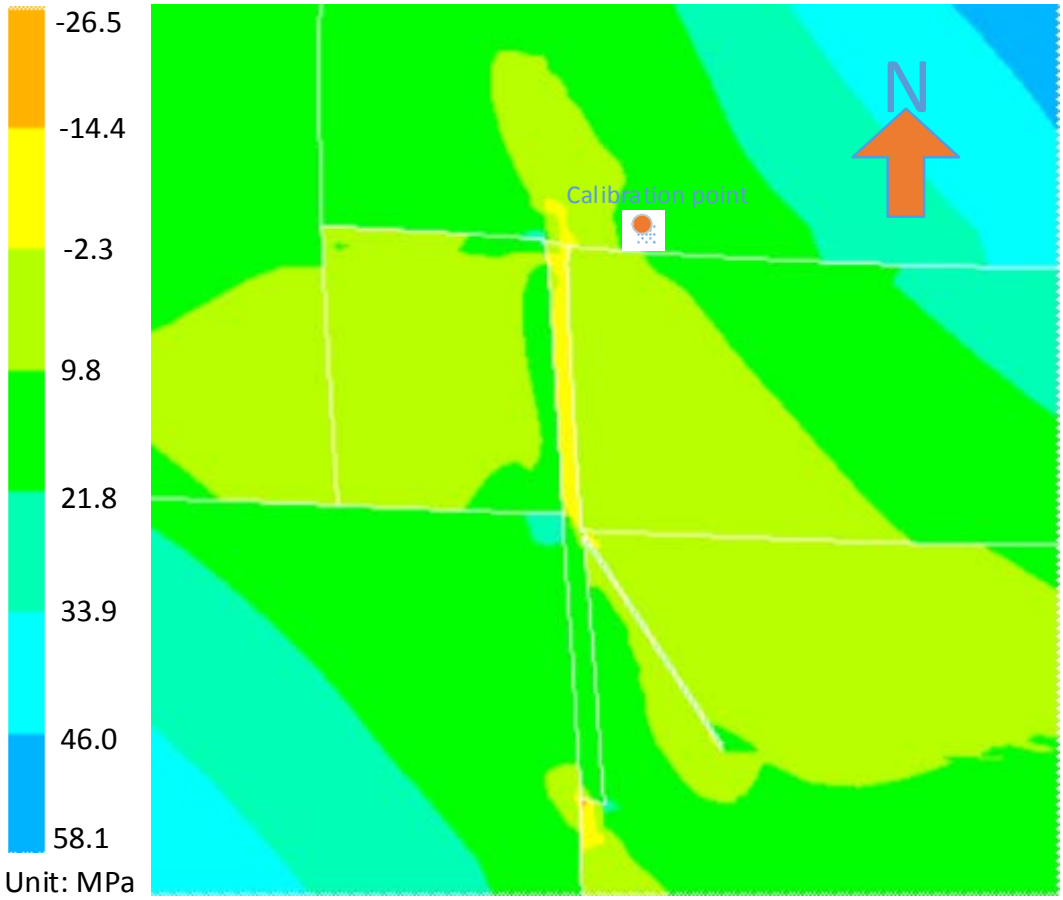

(a) 2D model

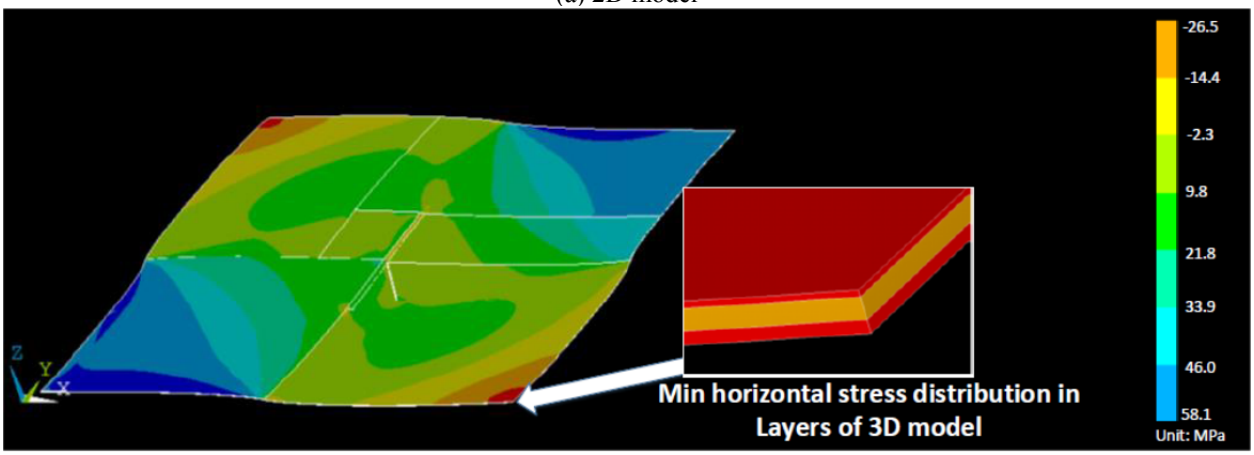

(b) 3D model

Figure 6-5. Contour map of the minimal horizontal stress

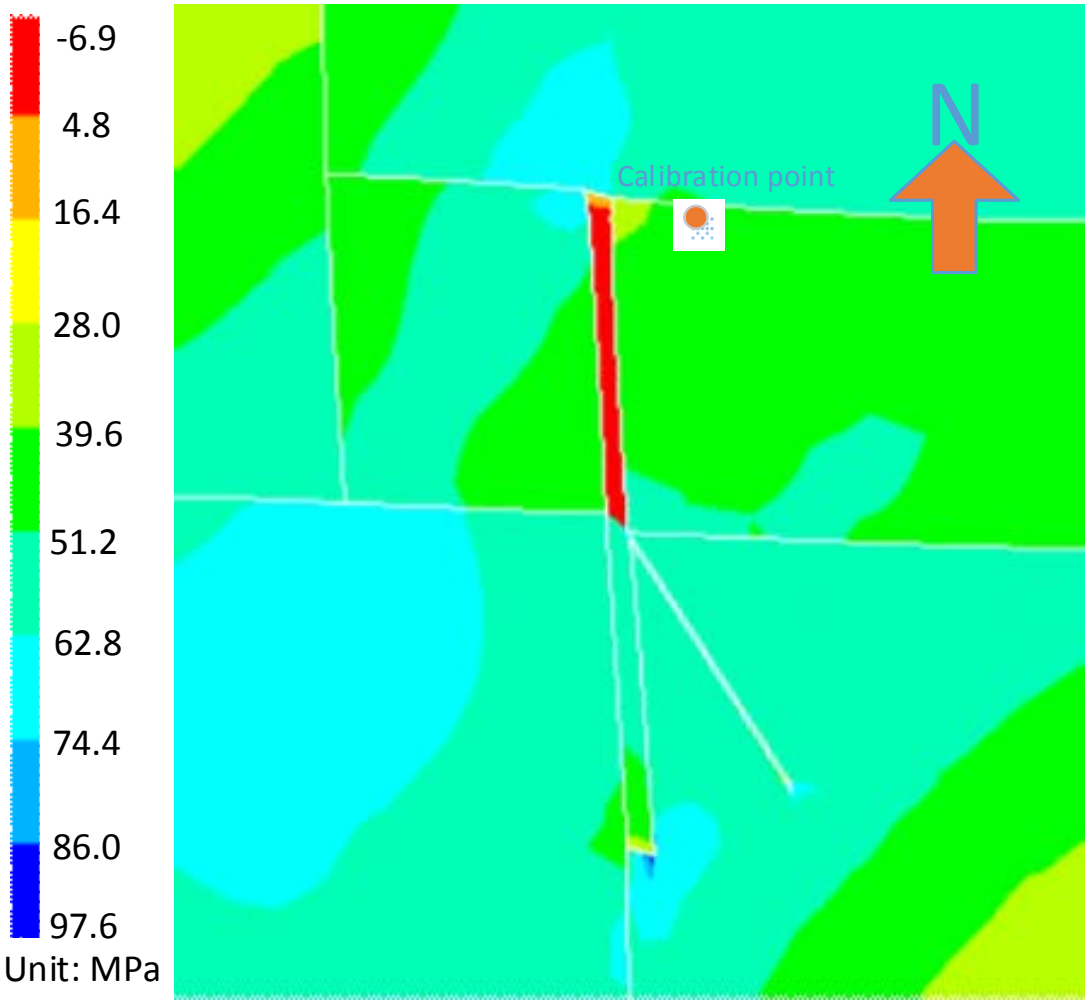

(a) 2D model

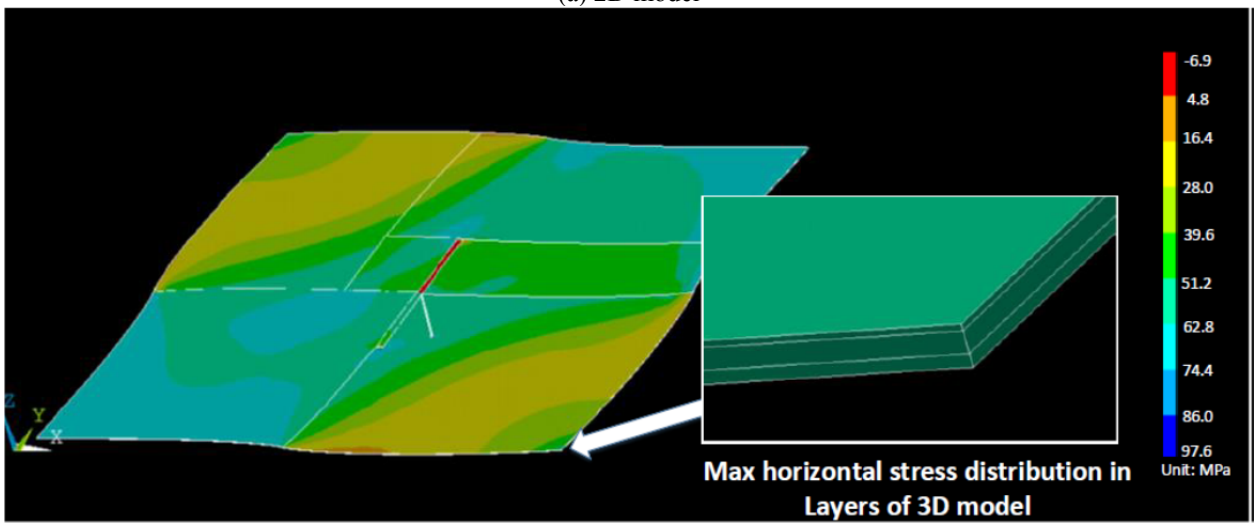

(b) 3D model

Figure 6-6. Contour map of the maximum horizontal stress

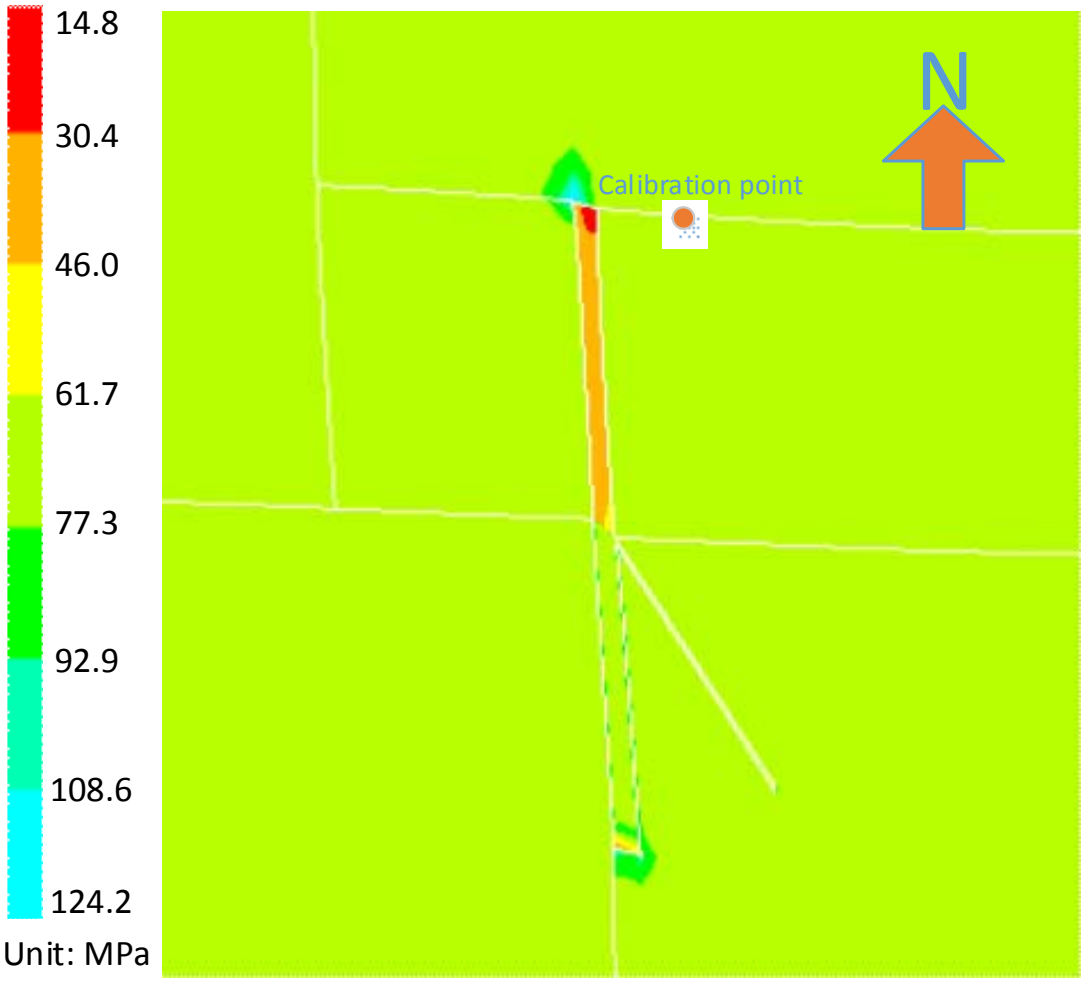

(a) 2D model

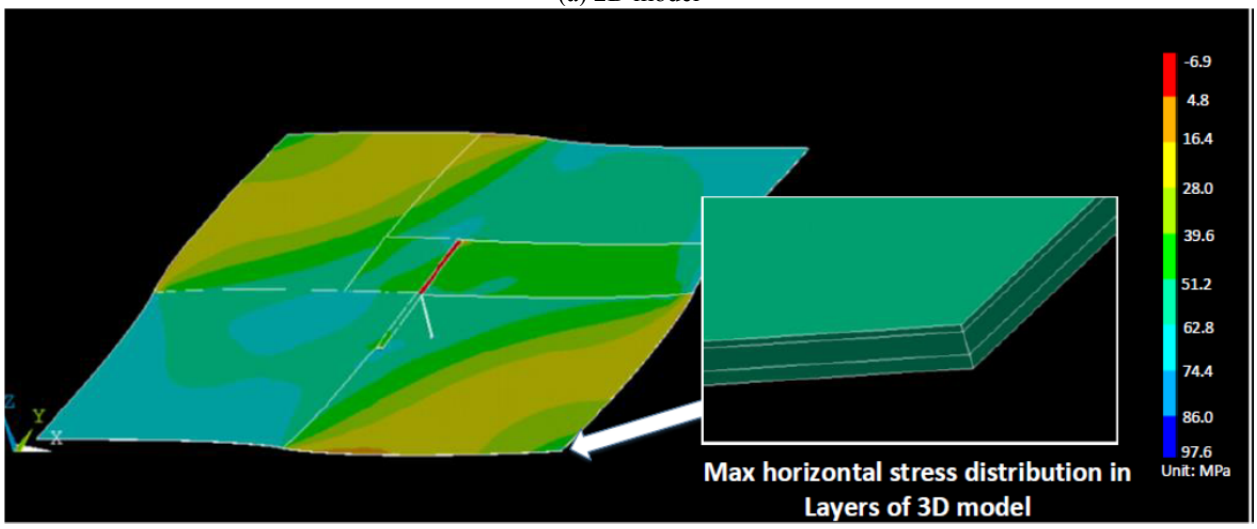

(b) 3D model

Figure 6-7. Contour map of the vertical stress in vertical direction

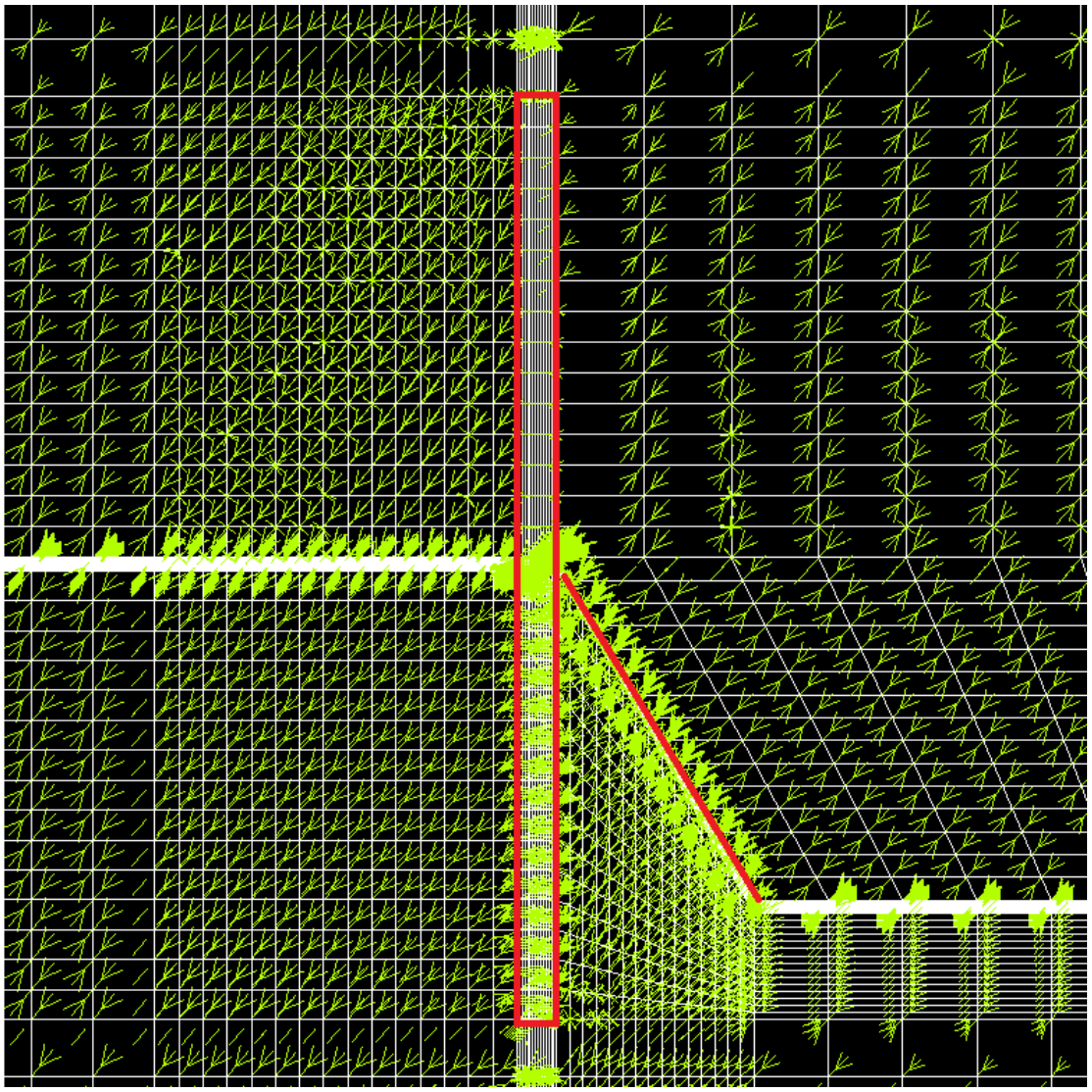

Figure 6-8. Vector map of the maximum principal stresses

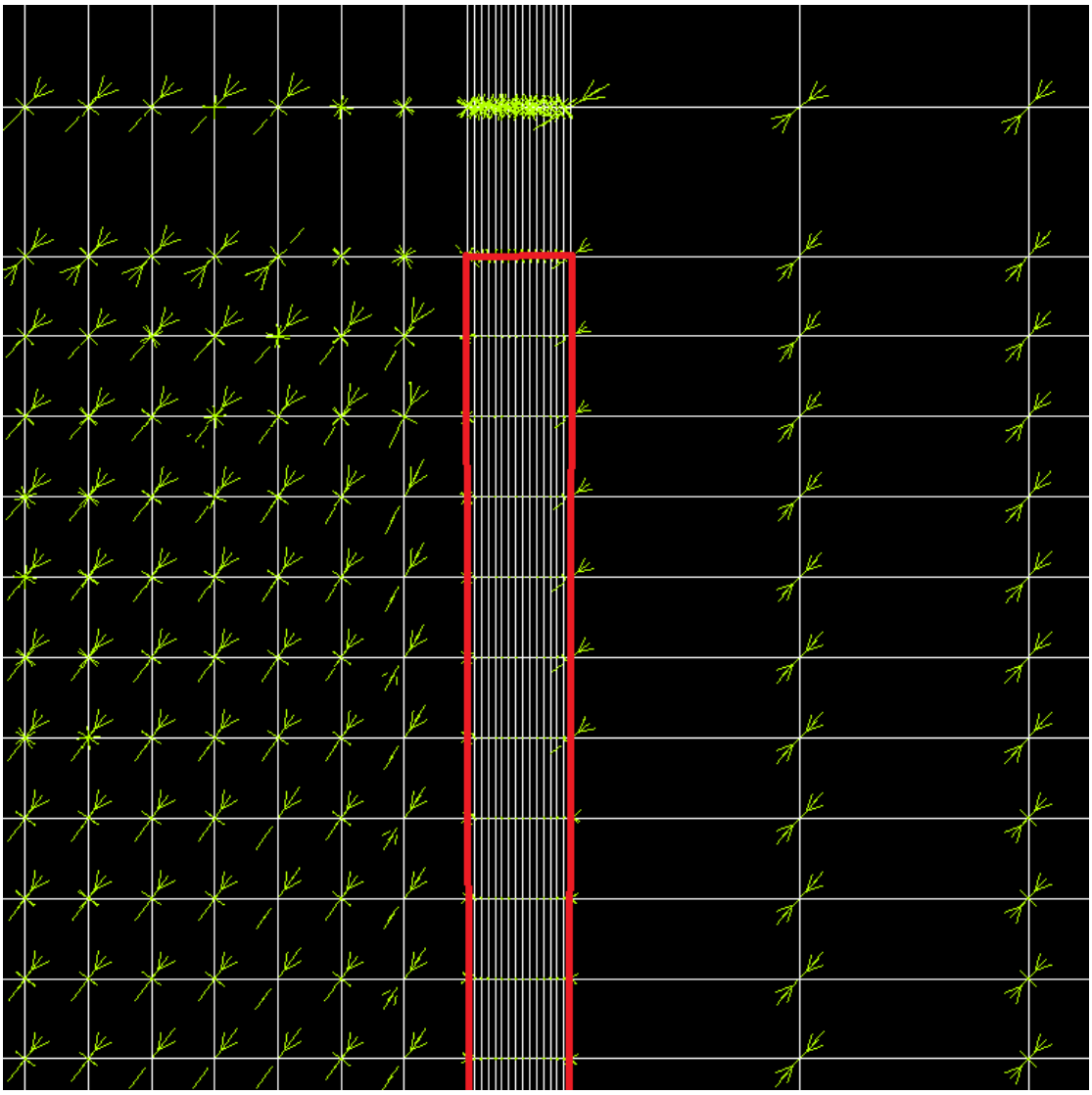

Figure 6-9. Vector map of the maximum horizontal stresses, North portion of Nesson Anticline.

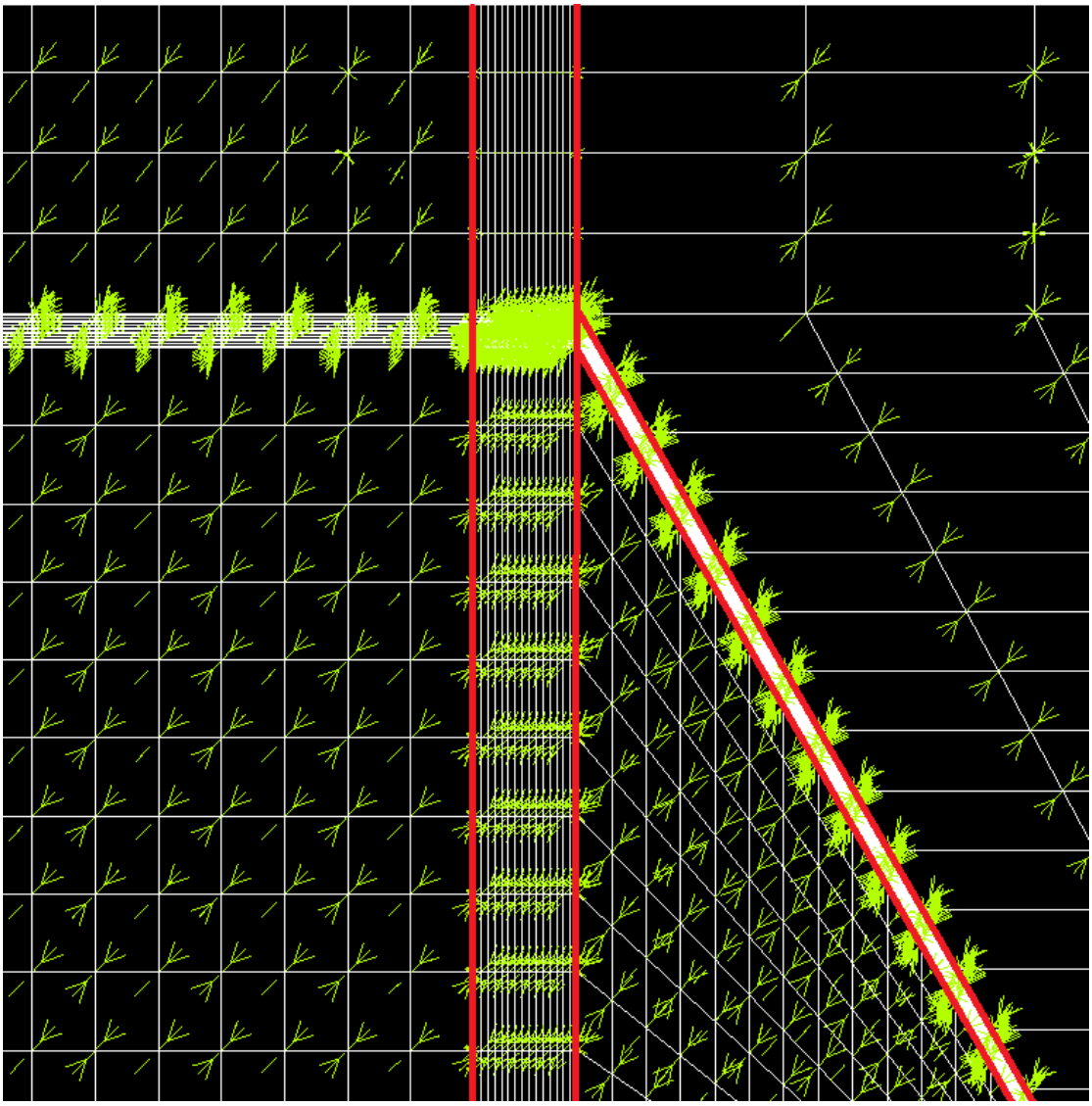

Figure 6-10. Vector map of the maximum principal stresses, Central portion of Nesson Anticline.

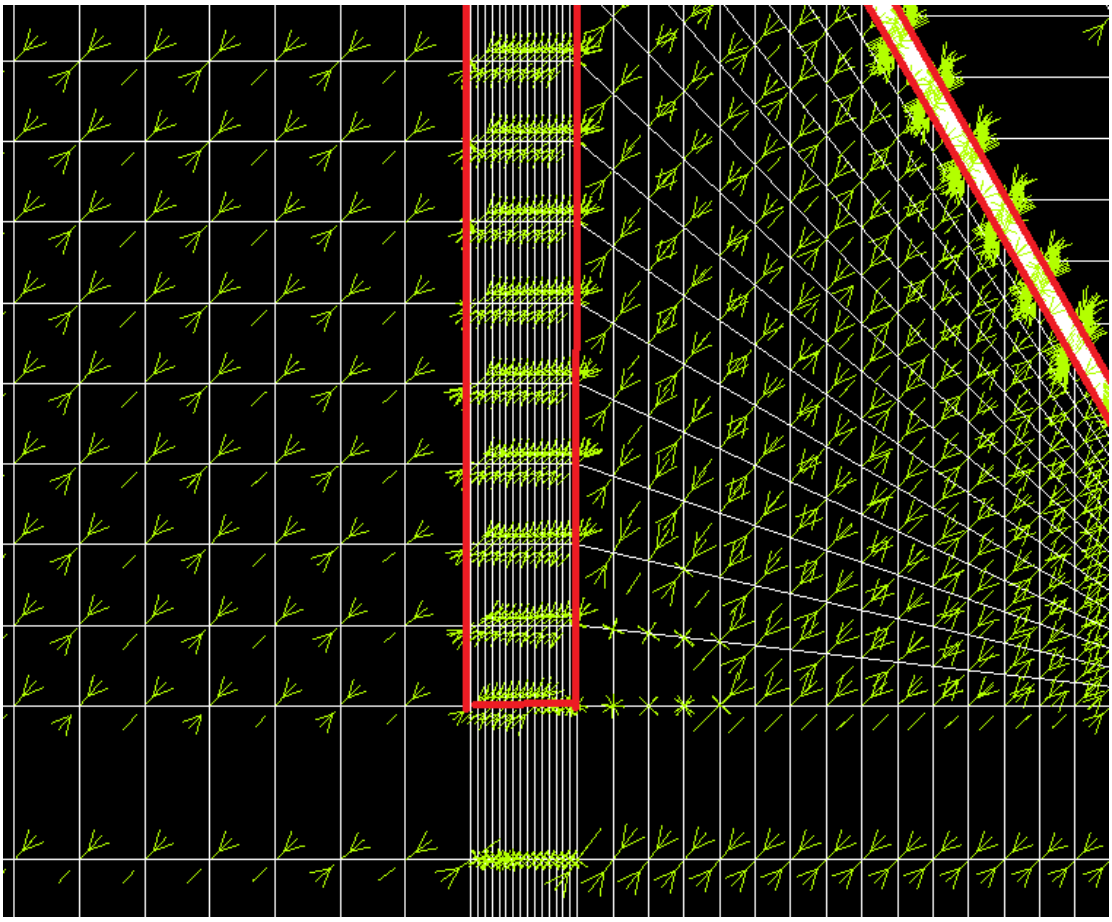

Figure 6-11. Vector map of the maximum horizontal stresses, South portion of Nesson Anticline.

7. EXPERIMENTAL METHODS

Middle, Upper, and Lower Bakken Formation cores were cut into rectangular cubes for performing rock strength testing with of a Brinell hardness tester. These samples were cut using a gas jet to attain the proper geometry without destroying the core

7.1. Core Sampler and Rock Geomechanics Test System

Bakken core samples, supplied by the North Dakota Geological Survey's Wilson M. Laird Core and Sample Library, were chosen as the specimens to represent the tight rocks. Due to the fragile nature of the core, we drilled the core plug with liquid N_2 as coolant (Figure 7-1). The core plugs are cylindrical with dimension of one inch in diameter and two inches long.

Figure 7- 1 Core plug sampling system used in this study

The equipment that is used to perform our experiments is AutoLab-1500, which is made by New England Research Inc. AutoLab 1500 supports a comprehensive suite of physical rock properties measurements as a function of the state of stress and temperature (AutoLab 1500, 2009). The system conveniently runs most standard rock mechanics test regimens, such as hydrostatic compression, pure shear, unconfined compression, confined compression, creep, and uniaxial strain. Each of these tests can be performed at pore pressures and temperatures representative of reservoir conditions. The system can also measure rock permeability, sonic velocity, and resistivity. Figure 7-2 is an image of AutoLab 1500 used in this study. Figure 7-3 presents the experimental setup and hydraulic diagram of AutoLab-1500. The cylindrical core plug was covered with copper sheet (Figure 7-4) in order to make a gas-tight

seal on the cylindrical wall of the sample, and for applying radial confining pressure. Then the core plug was mounted in a sample holder with flexible rubber sleeves at both ends of the plug (Figure 7-5). At last, the sample holder was put into a pressure vessel flooded with mineral oil, in which the sample can be hydrostatically compressed by applying force to plug by hydraulic means.

Figure 7-2 is an image of AutoLab 1500 used in this study.

Figure 7-2 AutoLab 1500 used in this study.

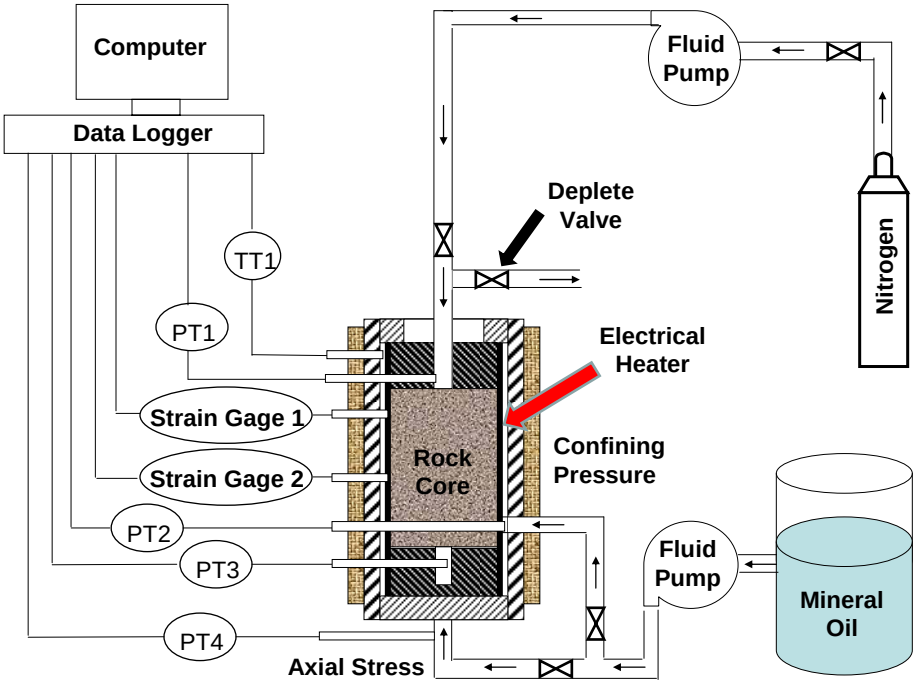

Figure 7-3 Experimental setup for permeability measurement under stresses

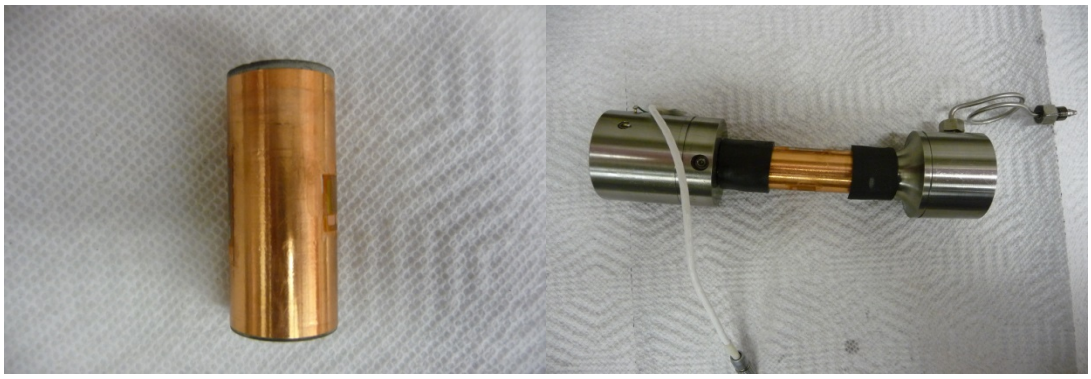

Figure 7-4 Images of core and core holder for rock properties test

Figure 7-5 Images of the end caps (left: downstream cap, right: upstream cap)

Figure 7-5 shows that the two end caps contain two axial ports for transporting test fluid to and from the sample and each of them has radial and circular grooves for distributing fluid to its entire surface. The upstream end-cap connects to a servo-controlled hydraulic intensifier, which is used to control and monitor the upstream pressure (p_1). The downstream pressure at the other end of the sample is monitored by a miniature pressure transducer, which is located in the downstream end-cap.

The experimental procedure is as follows:

1) A specimen of core plug was prepared using the core plug sampling system shown in Figure 7-1.

2) The dimension of core plug is measured and the volume of core plug is calculated

3) The weight of core plug is measured and the dry bulk density was calculated.

4) Porosity is measured using the facility shown in Figure 7-6.

5) Permeability, sonic velocity, uniaxial and triaxial strength (non-destructive), Biot's coefficient, and uniaxial and triaxial strength (destructive) are tested using AutoLab 1500.

The following is a step-by-step procedure for conducting the experiment in AutoLab 1500.

1) Prepare the specimen as a right circular cylinder and measure its dimensions.

2) Measure the dry bulk density of the specimen.

3) Measure the porosity of the specimen.

4) Insert the specimen into a pliable jacket. Cut the jacket approximately 20 mm longer than the test specimen. Insert the sample in the jacket and secure it to a transducer assembly using a double wrap of steel wire.

5) Insert the transducer assembly with the jacketed specimen into the pressure vessel.

6) Set the servo-controllers to panel mode. Turn the control knobs fully counterclockwise.

7) Turn on the hydraulic power supply.

8) Fill the pressure vessel with mineral oil.

9) Advance the axial piston inside the vessel approximately 5 mm and close the valve between the intensifier and the vessel.

10) Increase the confining pressure to desired level.

11) Expel air from the pore pressure lines to the sample assembly.

12) Fully charge both pore pressure intensifiers.

13) Connect the upstream and downstream pore pressure tubes to the specimen.

14) Open the valve on the upstream pore pressure system so that fluid can be injected into the specimen.

15) After several minutes or so, fluid will begin to flow out the downstream pore pressure reservoir. This indicates that all of the tubing and the specimen are fully saturated with pore fluid.

16) Wait for pressure reach equilibrium; adjust the upstream and downstream pressure to desired level

17) Close inlet valve at upstream reservoir.

18) Switch the servo-controls for both the confining pressure and pore pressure to computer. control. The system is fully charged now and ready to begin an experiment.

7.2. Porosity

Porosity is a measure of the void spaces in a rock, and is a fraction of the volume of voids over the total rock volume. For oil and gas reservoirs, porosity provides the space to store the fluid subsurface and is important to the permeability of rock. Porosity measurements were conducted to evaluate the storage ability of Bakken Formation. Gas compression method is used to measure the porosities of core plugs in this research. Helium is used as the test fluid due to its small molecular size and inertial property. Figure 7-6 (He et al., 2013) shows the setup to measure rock porosity. The system consists of gas source, three pressure gauges, and two chambers. The core is put in Chamber 2.

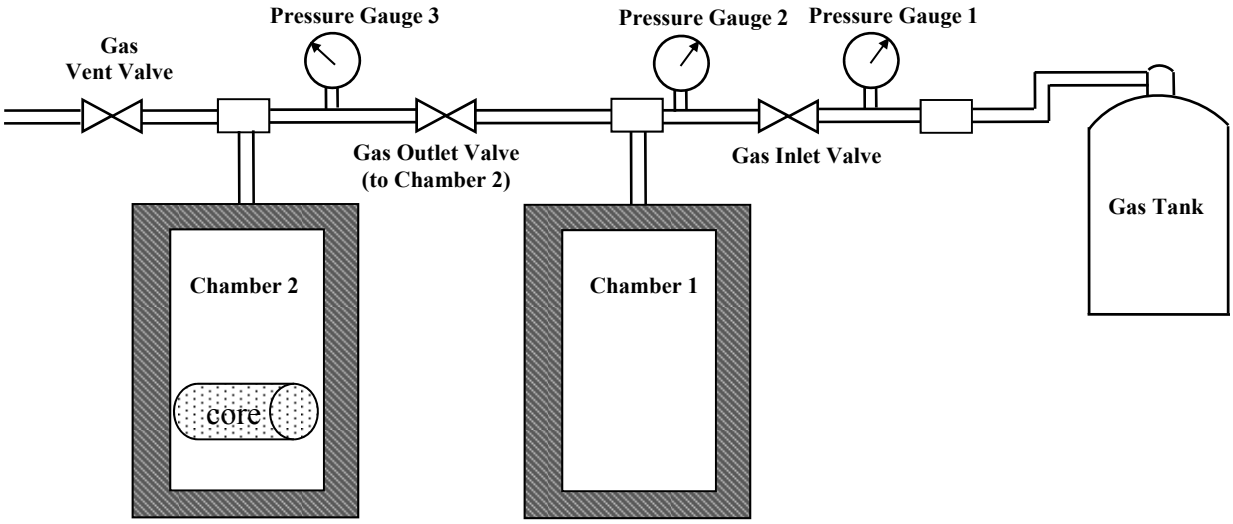

Figure 7-6. Schematic of facility to measure rock porosity

Measurement Principle

The measurement principle is based on real gas law. Followings are the derivation of governing equation to measure the core porosity.

Firstly, the sum of the volume of Chamber 1 and pipeline volume between Gas Inlet Valve and Gas Outlet Valve is denoted as Volume 1, V_1.

$$V_1 = V_{\text{chamber 1}} + V_{\text{pipeline between Gas Inlet Valve and Gas Inlet Valve}} \quad \text{(7-1)}$$

Similarly, the sum of the volume of Chamber 2 (without core) and pipeline volume between Gas Outlet Valve and Gas Vent Valve is denoted as Volume 2, V_2.

$$V_2 = V_{\text{chamber 2}} + V_{\text{pipeline between Gas Outlet Valve and Gas Vent Valve}} \quad \text{(7-2)}$$

The bulk volume of core is denoted as $V_{bulk,\ core}$, which is calculated by

$$V_{bulk,core} = \frac{\pi}{4} D_{core}^2 h_{\text{core}} \quad \text{..} \quad (7\text{-}3)$$

Initially the pressure in Chamber 1 is p_1 and pressure in Chamber 2 is p_2, where $p_1 > p_2$. Then Gas Outlet Valve is open to allow gas flow from Chamber 1 to Chamber 2 and reach equilibrium. The equilibrium pressure, p_3, is recorded. According to real gas law we have

$$p_1 V_1 = z_1 n_1 R T_1 \quad \text{..} \quad (7\text{-}4)$$

$$p_2 \left[V_2 - V_{bulk,core} \left(1 - \phi\right) \right] = z_2 n_2 R T_2 \quad \text{..} \quad (7\text{-}5)$$

$$p_3 \left\{ \left[V_2 - V_{bulk,core} \left(1 - \phi\right) \right] + V_1 \right\} = z_3 \left(n_1 + n_2\right) R T_3 \quad \text{..} \quad (7\text{-}6)$$

The temperature is kept constant and pressure is changed in a narrow range. Therefore we have

$$z_1 \cong z_2 \cong z_3 \quad \text{..} \quad (7\text{-}7)$$

Equations (7-4), (7-5), and (7-6) can be simplified into

$$p_1 V_1 = z_1 n_1 R T_1 \quad \text{..} \quad (7\text{-}8)$$

$$p_2 \left[V_2 - V_{bulk,core} \left(1 - \phi\right) \right] = z_1 n_2 R T_1 \quad \text{..} \quad (7\text{-}9)$$

$$p_3 \left\{ \left[V_2 - V_{bulk,core} \left(1 - \phi\right) \right] + V_1 \right\} = z_1 \left(n_1 + n_2\right) R T_1 \quad \text{..} \quad (7\text{-}10)$$

Summing Equations (7-8) and (7-9) we obtain

$$p_2 \left[V_2 - V_{bulk,core} \left(1 - \phi\right) \right] + p_1 V_1 = z_1 \left(n_1 + n_2\right) R T_1 \quad \text{..} \quad (7\text{-}11)$$

Comparing the right-hand-sides of Equations (7-10) and (7-11) gives us

$$p_2 \left[V_2 - V_{bulk,core} \left(1 - \phi\right) \right] + p_1 V_1 = p_3 \left\{ \left[V_2 - V_{bulk,core} \left(1 - \phi\right) \right] + V_1 \right\} \quad \text{..} \quad (7\text{-}12)$$

Rearranging Equation (7-12) yields

$$\phi = 1 - \frac{V_2}{V_{bulk,core}} + \frac{\left(p_1 - p_3\right) V_1}{\left(p_3 - p_2\right) V_{bulk,core}} \quad \text{..} \quad (7\text{-}13)$$

Equation (7-13) is the governing equation to measurement rock porosity. Three pressures are recorded in the measurement. Volume 1, V_1, and Volume 2, V_2 can be determined using standard volume samples made of stainless steel (zero porosity). The approach is also based on real gas law. The bulk volume of core can be readily calculated from core diameter and height.

Measurement Procedure

The measurement of porosity of a specimen includes following steps:

1) Put the core into Chamber 2, close Gas Vent Valve, and open Gas Inlet Valve and Gas Outlet Valve to allow gas from gas tank fill Chambers 1 and 2 until pressure reaches 100 psig

2) Open Gas Vent Valve and allow gas from gas tank purge Chambers 1 and 2, Wait for 10 to 20 minutes until the purity of gas in Chambers 1 and 2 is high enough.

3) Close Gas Vent Valve, Gas Inlet Valve, and Gas Outlet Valve, record the pressure of Chamber 2, p_2.

4) Keep Gas Vent Valve and Gas Outlet Valve close, Open Gas Inlet Valve and allow gas from gas tank fill Chamber 1 until its pressure reaches target pressure, close Gas Inlet Valve and record the pressure of Chamber 1, p_1.

5) Open Gas Outlet Valve to allow gas flow from Chamber 1 to Chamber 2 (because $p_1 > p_2$), wait until pressure reaches equilibrium, or pressure at Pressure Gauge 3 equates pressure at Pressure Gauge 2, record equilibrium pressure, p_3.

6) Now we finish the porosity measurement of specimen. Porosity can be calculated by Equation (7-13).

7.3. Permeability

Rock permeability is one of most important rock properties for fluid flow in reservoir according to Darcy's law. It is a measure of the ease with which a fluid, such as gas, oil and water in petroleum engineering, can move through a porous rock. Permeability is an inherent characteristic of the porous media only. It depends on rock type, the textural of rock, effective porosity, pore throat size, geometry of the pore, and connection and distribution of pore. Conventional methods of measuring permeability in the laboratory utilize steady-state flow. Steady-state flow, or a constant pressure gradient flow, is established through the core plug, and the permeability is calculated from the rate of the measured flow and the pressure gradient. But this method is not adequate when measuring permeability in the low permeability Bakken samples. Not only the low flow rates across the core plug are difficult to be measured and controlled, but the tests are also quite time consuming. Because of the disadvantage of the steady-state flow, unsteady state flow, a condition under which the pressure gradient is a function of time, was used. With the measurements of the volumetric flow rate, upstream, and downstream pressures, the permeability can be calculated. Three unsteady-state methods, which are oscillating pulse method, pulse decay method, and radius-of investigation method had been developed to measure permeability in this project.

Oscillating Pulse Method

The oscillating pulse method estimates rock permeability by interpreting the amplitude attenuation and the phase retardation in the sinusoidal oscillation of the pore pressure as it propagates through a sample. At the beginning of the experiment, the sample pore pressure, the upstream pressure, and the downstream pressure are stabilized. Then a sinusoidal pressure wave is generated in the upstream and propagates through a core plug. Using the information of the amplitude attenuation and phase shift between the upstream pressure wave and the derived downstream pressure wave at the downstream side of the sample, the permeability can be obtained (Figure 7-7). This method can measure the permeability of tight rock in a relative short time without destroying rock sample. The accuracy of permeability obtained from this method relies on the signal-to-noise ratio and data analysis techniques. The optimum frequency of the oscillation and the ratio of the downstream to upstream pore pressures depend upon the sample size and the magnitude of permeability (Kranz et al., 1990). Therefore, the calculated permeability contains large uncertainty when measured under the condition of low signal-to-noise ratio. Moreover, different analysis techniques can result in different permeabilities in the same experiment.

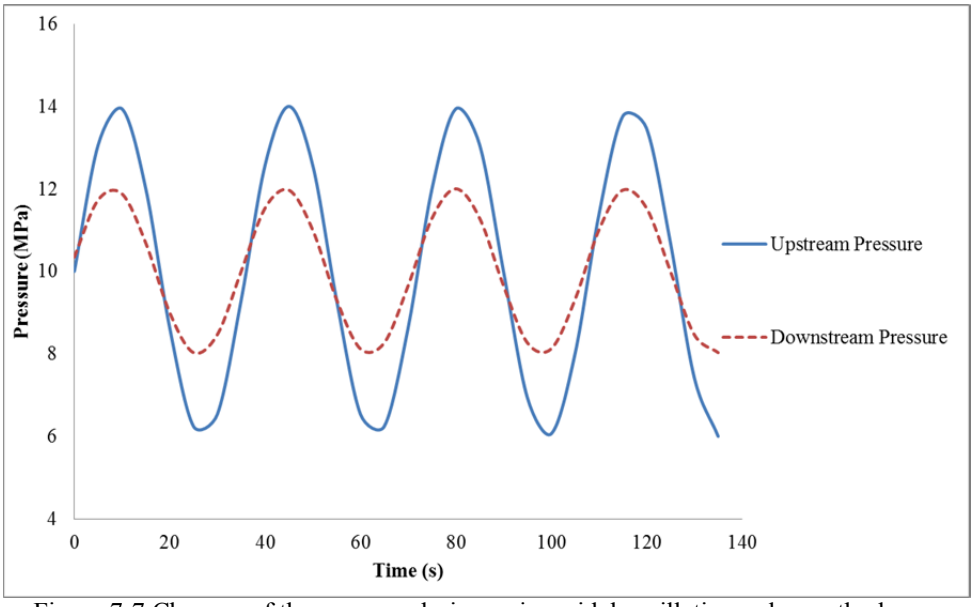

Figure 7-7 Changes of the pressure during a sinusoidal oscillation pulse method

Pulse Decay Method

The pulse decay method is a transient method. The experimental arrangement is shown schematically in Figure 7-8. The sample has both upstream reservoir and downstream reservoir with the initial condition of uniform pore, upstream and downstream pressures. When a pressure pulse is applied at the upstream end of a core plug and propagates through core to the downstream reservoir, the pressure pulse will decay over time. The decay characteristics depend on the permeability, size of the sample, volumes of upstream and downstream reservoirs, and physical characteristics of the fluid. Permeability is estimated by analyzing the decay characteristics of the pressure pulse.

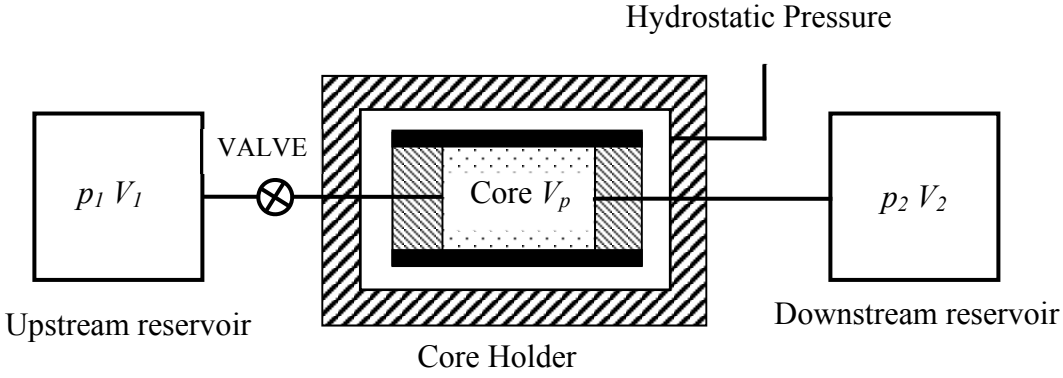

Figure 7-8 Schematic diagram for pulse decay permeability system

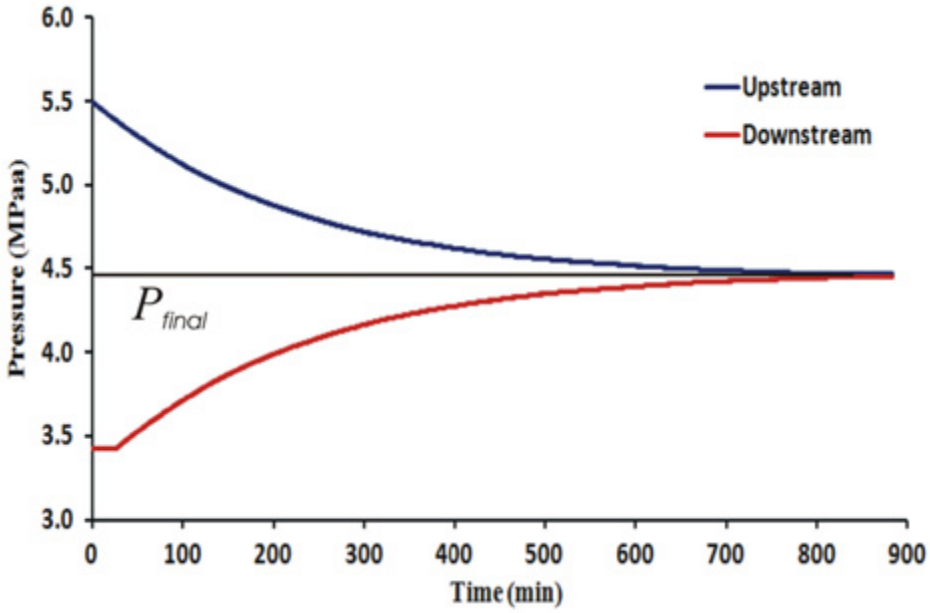

Figure 7-9 Changes of upstream and downstream pressures in pulse decay method

To calculate the permeability from the build-up curve of the measured downstream pressure, the solution of the diffusivity Equation (7-14) needs to be known. According to the solution of this problem from Hsieh et al. (1981) and Dicker and Smits (1988), the exact solution for the pressure in the downstream reservoir is

$$\frac{\partial^2}{\partial x^2}[m(p)] = \frac{\varphi \mu c_t}{k}\frac{\partial}{\partial t}[m(p)] \quad \text{..... (7-1)}$$

$$\frac{m[p_2(t)] - m[p_2(0)]}{m[p_1(0)] - m[p_2(0)]} = \frac{b}{a+b+ab} + 2\sum_{m=1}^{\infty} \frac{e^{-t_D \theta_m^2}\left(ab^2 - b\theta_m^2\right)}{[\theta_m^4 + \theta_m^2\left(a + a^2 + b + b^2\right) + ab(a+b+ab)]\cos\theta_m} \quad \text{..... (7-2)}$$

where θ_m can be calculated from the following equation

$$\tan\theta = \frac{(a+b)\theta}{\theta^2 - ab} \quad \text{..... (7-3)}$$

where a is the ratio of the sample pore volume (V_p) over the upstream reservoir volume (V_1), and b is the ratio of the sample pore volume over the downstream reservoir volume (V_2), $\left(a = \frac{V_p}{V_1}, b = \frac{V_p}{V_2}\right)$.

In the Equation (7-15) the dimensionless time, t_D, is defined as:

$$t_D = \frac{kt}{\varphi \mu c_t L^2} \quad \text{..... (7-17)}$$

The setup of the permeability test system in this study and measurement pressure and temperature allow us simplify Equation (7-15) to:

$$\frac{p_1^2(0)-p_2^2(t)}{p_1^2(0)-p_2^2(0)}=e^{-t_D\theta_1^2}\cdot\left(2\frac{b\sqrt{\theta_1^4+\theta_1^2b^2}}{\theta_1^4+\theta_1^2(b+b^2)}\right) \quad (7\text{-}4)$$

Let $\Delta p(t)=p_1^2(0)-p_2^2(t)$, we get

$$\frac{\Delta p(t)}{\Delta p(0)}=\left(2\frac{b\sqrt{\theta_1^4+\theta_1^2b^2}}{\theta_1^4+\theta_1^2(b+b^2)}\right)\cdot e^{-t_D\theta_1^2} \quad (7\text{-}5)$$

which can be written as

$$\Delta p(t)=\left(2\Delta p(0)\cdot\frac{b\sqrt{\theta_1^4+\theta_1^2b^2}}{\theta_1^4+\theta_1^2(b+b^2)}\right)\cdot e^{-t_D\theta_1^2} \quad (7\text{-}6)$$

Taking the natural log of Equation (7-20) yields

$$ln[\Delta p(t)]=ln\left(2\Delta p(0)\cdot\frac{b\sqrt{\theta_1^4+\theta_1^2b^2}}{\theta_1^4+\theta_1^2(b+b^2)}\right)+\left(-t_D\theta_1^2\right) \quad (7\text{-}7)$$

Substituting t_D from Equation (7-17) into Equation (7-21), we get

$$ln[\Delta p(t)]=ln\left(2\Delta p(0)\cdot\frac{b\sqrt{\theta_1^4+\theta_1^2b^2}}{\theta_1^4+\theta_1^2(b+b^2)}\right)-\frac{\theta_1^2k}{\varphi\mu c_tL^2}t \quad (7\text{-}8)$$

The determination of the permeability is a three-step process, namely installing the core plug into AutoLab-1500, running the test, and analyzing the resultant data.

1) Installing the core plug into AutoLab-1500
First, the core holder is placed into the vessel, then the vessel is filled with mineral oil and the confining pressure is increased to the desired level (p_c). The valve between the core plug and the upstream reservoir is closed. Dry nitrogen is used to fill the upstream reservoir and the upstream pressure is increased to the desired level (p_1). The downstream pressure is atmospheric pressure. Notice that the confining pressure must be greater than the upstream pressure.

2) Running the test
The starting time is recorded when the valve between the core plug and the upstream reservoir is opened. During the whole test, the upstream and the confining pressures are constant. The pressures are monitored and recorded at both the upstream and downstream ends of the sample. The test is end when the downstream pressure is equal to the upstream pressure, which is shown in Figure 7-9.

3) Analyzing the resultant data
First the pressure difference is calculated in a logarithm scale from equation:. Then form the plot by function fitting (Figure 7-10), we get the slope, *s*. Finally, using Equation (7-23), we can obtain the permeability of the rock.

$$k=\frac{2\varphi\mu c_tL^2s}{3-3\sqrt{1+\frac{4\varphi AL}{3V_2}}} \quad (7\text{-}23)$$

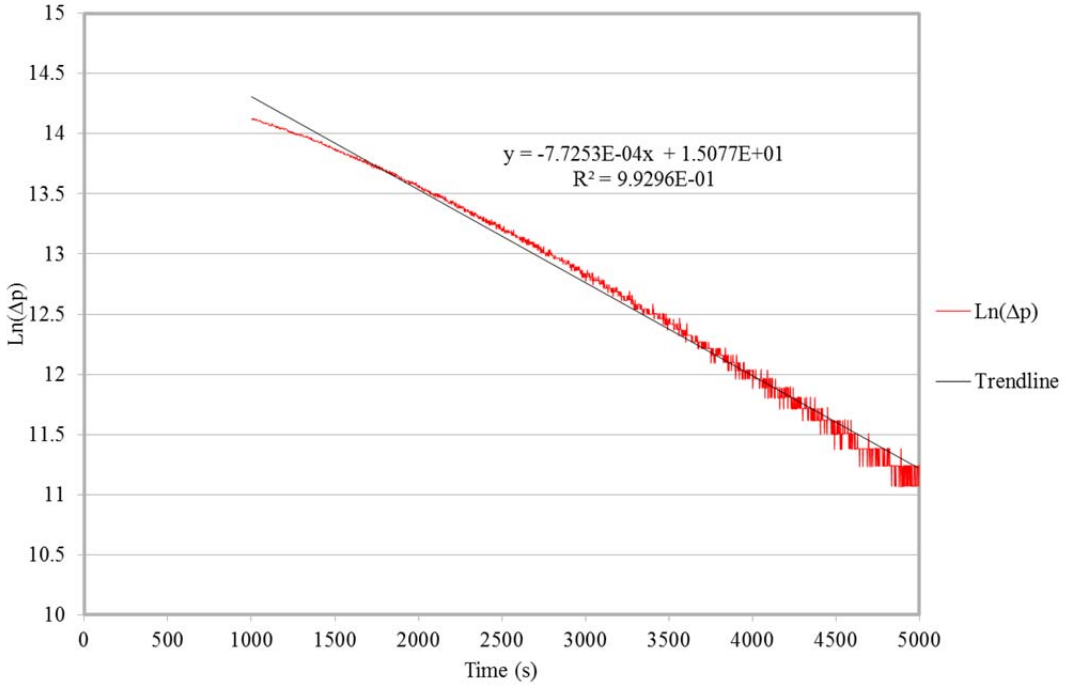

Figure 7-10 ln(Δ*p*) vs. time plot for core sample permeability measurement using pulse decay method

Radius-of-Investigation Method

Based on the radius-of-investigation concept (Lee, 1982), we proposed a new laboratory core permeability measurement method (Ling et al., 2013). When doing the permeability test using the downstream pressure build-up method, we observed that the downstream pressure did not increase immediately when the upstream reservoir connected with the core plug. The lower the permeability is, the longer delay time is observed. Based on this phenomenon, a correlation can be found between the permeability and the delaying time. Through this correlation, the permeability can be measured in a much shorter time (Figure 7-11) when compared with the previous method.

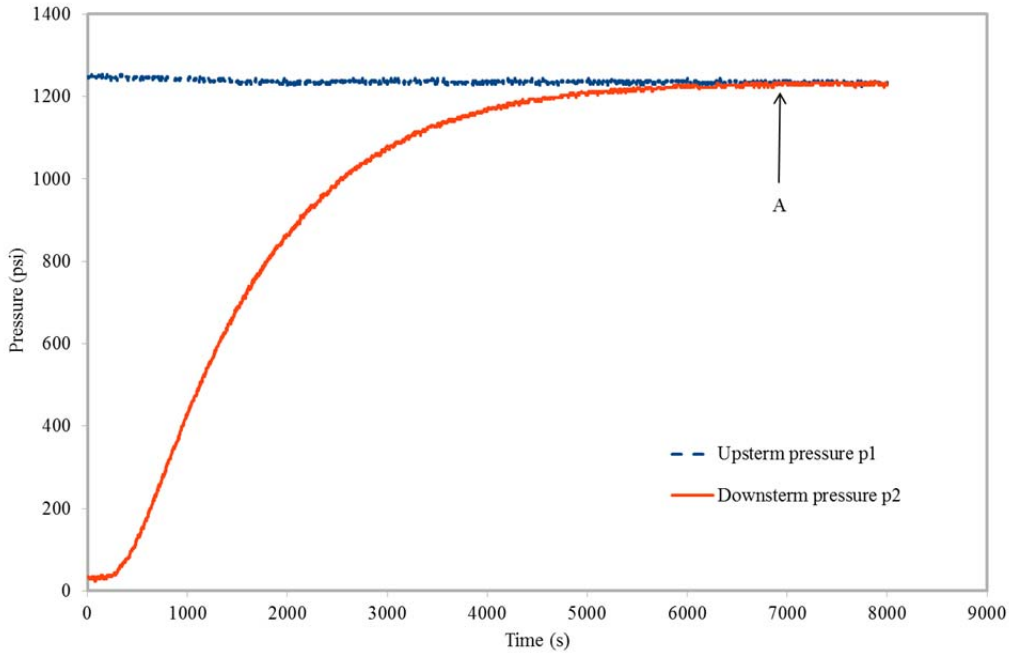

Figure 7-11 Changes of the downstream pressures while maintaining constant upstream pressure
The upstream pressure (p_1) is constant, and the downstream pressure (p_2) builds up through the time.

In our research, we discovered that the radius-of-investigation concept could be useful for uncovering the relationship between the permeability of rock and the waiting time before the downstream pressure increases. Radius of investigation is the distance that a pressure disturbance moves into a formation when it is caused from the well. Lee pointed out that it is possible to calculate the maximum distance that a pressure disturbance can reach at any time, if we know the properties of rock and fluid, such as the rock permeability and porosity, fluid viscosity, and the compression of both rock and fluid. This means that the maximum distance of pressure disturbance is a function of permeability and time, when other parameters are constants. Thus, the time that a pressure disturbance spends in a rock is a function of the permeability of the rock, if we know the length of the rock. Our hypothesis is that we can calculate the low permeability in laboratory by measuring the delaying time, which is the time that the pressure disturbance propagates from the upstream end of the core plug to the downstream end (in case pressure disturbance is generated in upstream), or the pressure disturbance propagates from the downstream end of the core plug to the upstream end (in case pressure disturbance is generated in downstream). Permeability can be calculated for given porosity, viscosity, total compressibility, location, and time, which is

$$k = \frac{\varphi \mu c_t x^2}{2 t_m} \quad \text{(7-24)}$$

Converting Equation (7-24) into the U.S. field units we have

$$k = \frac{1896 \varphi \mu c_t x^2}{t_m} \quad \text{(7-25)}$$

where permeability k is in mD, porosity φ is dimensionless (in fraction), viscosity μ is in cp, total compressibility c_t is in psi^{-1}, time t_m is in hour, and location (or distance) x is in ft. Equations (7-24) and (7-25) are the governing equations to measure the rock permeability. They are used to calculate the permeability of any rock that meets the aforementioned assumptions and can be used for high-permeability rocks as well. The proposed method evaluates the permeability under unsteady-state flow and requires short time period to determine the flow capacity of the low-permeability rock.

7.4. Sonic Velocity

Sonic velocity, or seismic velocity, is a measure of a formation's capacity to transmit seismic waves. It varies with lithology and rock textures, most notably decreasing with an increasing effective porosity. This means that a sonic log can be used to calculate the porosity of a formation if the seismic velocity of the rock matrix and pore fluid are known, which is very useful for hydrocarbon exploration. The velocity is calculated by measuring the travel time from the transmitter to the receiver. There are many types of seismic waves. Two types of wave, primary waves (P-waves) and secondary waves (S-waves), are used to test the sonic velocity in rock in this study. P-waves are compressional waves that are longitudinal in nature. P waves are pressure waves that travel faster than S-waves through the rock. S-waves are shear waves that are transverse in nature. P-waves can travel through any materials. S waves can travel only through solids, as fluids (liquids and gases) do not support shear stresses. S waves are slower than P waves.

AutoLab 1500 is used to test the sonic velocity of core plug. The following is a step-by-step procedure for conducting the experiment.

1) Prepare the specimen.

2) Measure the dry bulk density of the specimen.

3) Measure the porosity of the specimen.

4) Jacket the specimen with copper foil. Insert the specimen into a pliable jacket. Seal the jacket to the end plugs with a section of rubber tubing the same diameter as the test specimen. The rubber jacket is secured to the end plugs at two points with several wraps of steel wire.

5). Secure the test specimen to the PS2 ultrasonic velocity transducer assembly after applying shear wave couplant to the face of the transducers. Secure the specimen at one end of the assembly using a section of elastomer jacket with the same inside diameter as the test specimen. The rubber jacket is attached to the transducer assembly at two points with several warps of steel wire. Secure the other transducer to the specimen with a section of rubber tubing as described above. It is important that the vibration direction for the S1 and S2 components of the shear waves are aligned to obtain good shear wave data. The S1 component on each transducer is marked and indicated with a line ground into the transducer assembly.

6). Connect the PS2 ultrasonic velocity transducer output; make sure that the connections are in the correct position.

7) Insert the transducer assembly with the jacketed specimen into the pressure vessel.

8) Set the servo-controllers to panel mode. Turn the control knobs fully counterclockwise.

9) Turn on the hydraulic power supply.

10) Fill the pressure vessel with mineral oil.

11) Advance the axial piston inside the vessel approximately 5 mm and close the valve between the intensifier and the vessel.

12) Increase the confining pressure to desired level.

13) Initiate the AutoLab Software.

14) Select Acquire Data in the NER Laboratory Process Monitor.

15) Select the appropriate PS2 ultrasonic velocity transducer under the transducer selection. Set the gain and attenuation information for the pulse-receiver.

16) Check the waveforms for the compressional and shear wave velocities. Locate the oscilloscope panel and configure the scope to obtain a clear waveform for a P wave. Once you have obtained satisfactory waveforms for the compressional wave, subsequently check the S1 and S2 waveforms to make sure that there is sufficient amplitude near the first arrival of the shear wave to make accurate measurements of velocity. Select Accept Scope from the Commander window.

17) Set the Sampling Interval and click Collect a/d channels. axial strain as a function of differential stress.

18) In Commander, select Mode/Script.

19) A Scripter window file will appear. Once the Scripter window appears select File. A pop-down menu will appear. Select an existing file or choose Editable from the menu. A red box will appear in the window. Now you can generate a script file for the loading and data acquisition sequence. Save the file with a unique designation: the file will be reused for subsequent experiments, over the same loading path.

20) Make a final check of all of the servo-controls on the electronics console and the Analog Monitor. If all of the variables are within the appropriate range, select Run in the Scripter window to initiate the experiment. The experiment begins immediately.

21) Terminate the data acquisition at the end of the experiment by clicking the Collect a/d channels button on the Commander window to stop A/D data collection.

22) Select Stop Data Acquisition in the Commander window. Select Process/Print Existing Data from the NER Laboratory Process Monitor.

23) When File Browser appears, highlight the file name of the experiment that you have just completed. Select Process Traces.

24) Select the wave type to be displayed by clicking the mouse on the p, s1, or s2 buttons in the upper right hand corner of the Arrival Picker. The selected waveforms for each wave type will appear as a waterfall plot.

25) Process the P waves. The compressional waves that you have recorded during the experiment will appear. Using the mouse click the mouse at the approximate point of the first arrival (the onset of compressional wave energy) for each trace. Once all of the first arrivals for all of the compressional waveforms have been selected, save the data by selecting Save at the bottom of the window.

26) Process the shear wave data. Select s1 at the top of the window. The button will appear red and the shear wave data for the S1 component will appear on the screen. Repeat the procedure described above for compressional waves. When the data is processed select Save at the bottom of the screen. Then repeat the process for the S2 shear waveforms. When you have completed picking all of the waveforms for the P and the S waves select Save Changes and Exit.

27) Print a velocity report.

In the AutoLab 1500, the pulser-receiver is used to excite the ultrasonic transducer assembly and amplify the received signal. When making measurements on a sample, we increase the confining pressure to the maximum value expected during the test in order to properly set the pulser-receiver. The settings should be adequate for both the compressional and shear waves if both types are to be recorded. Once the experiment has been completed, the data is edited and plotted. The first step is to display the waveforms and pick the first arrivals for each wave type: compressional or polarized shear wave. After the times of first arrival of P (Figure 7-12), S1 (Figure 7-13), S2 (Figure 7-14) are selected. An example of the compression and shear wave velocities of core plug are shown in Figure 7-15.

Waveform waterfall for **p** arrivals	
Experiment:	velocity
Well:	16771
Depth:	3176.6 m
File name:	w16771-10422-velocity

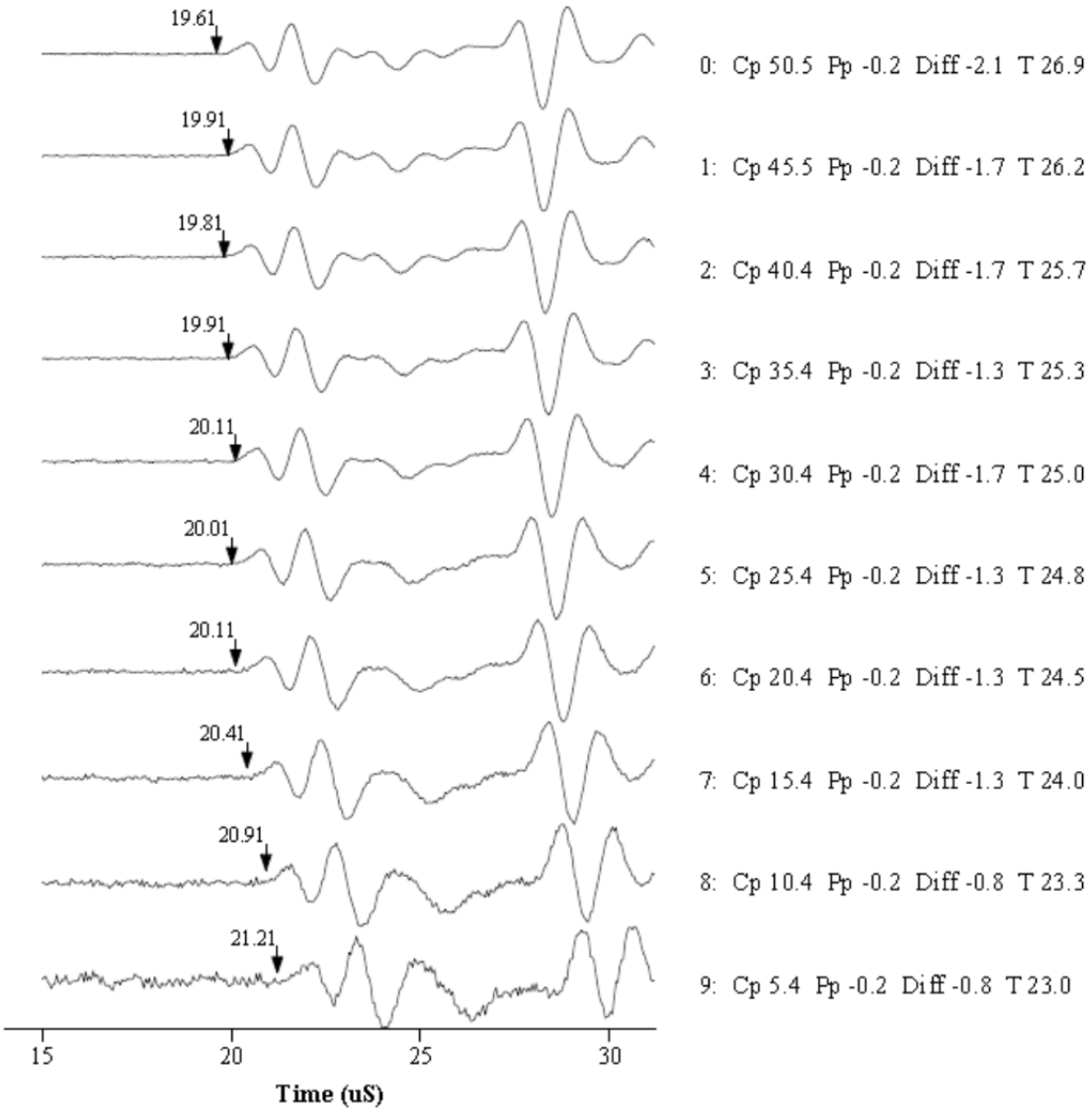

Figure 7-12 Waveform for P arrivals

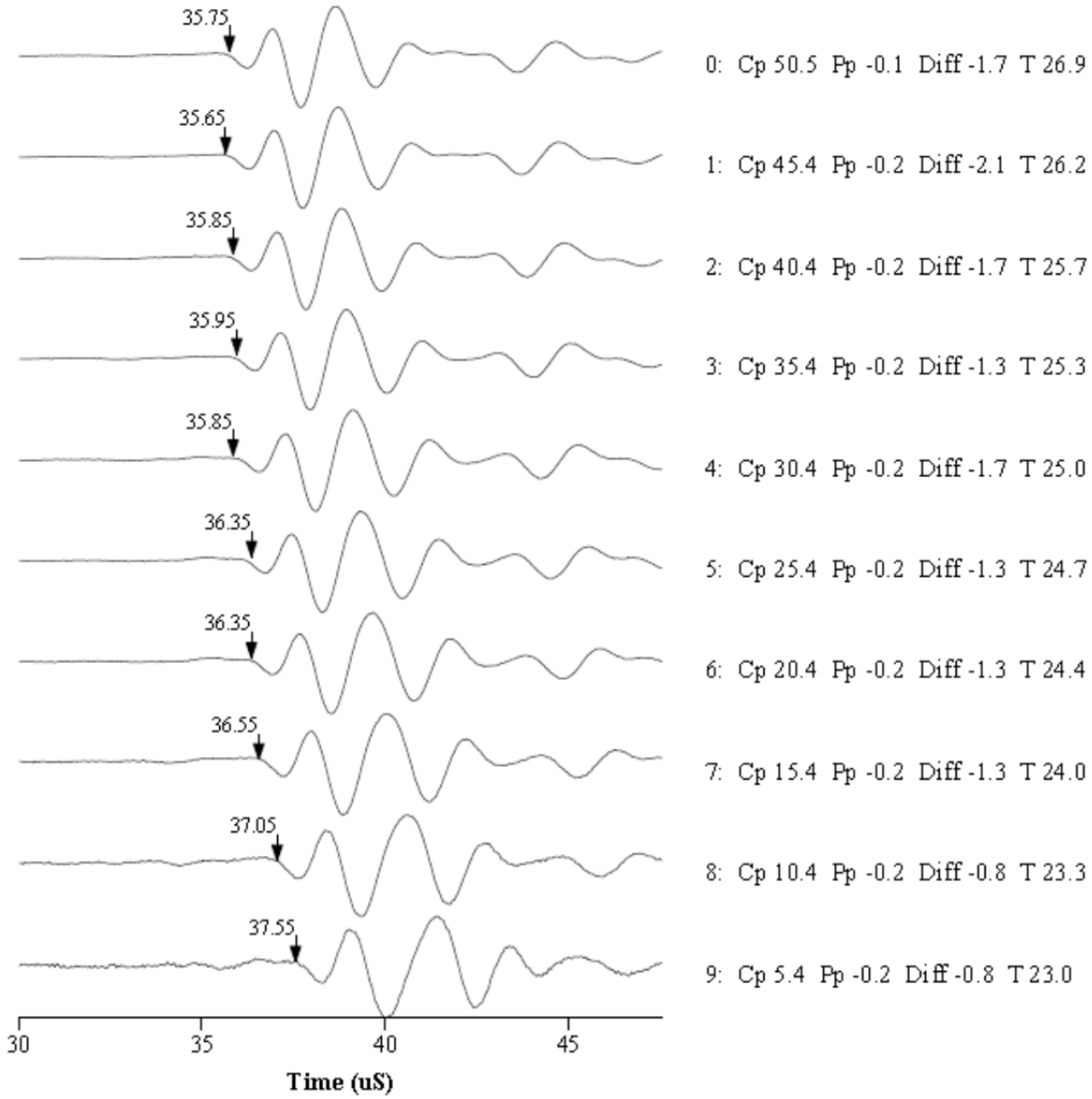

Figure 7-13 Waveform for S1 arrivals

Waveform waterfall for **s2** arrivals	
Experiment:	velocity
Well:	16771
Depth:	3176.6 m
File name:	w16771-10422-velocity

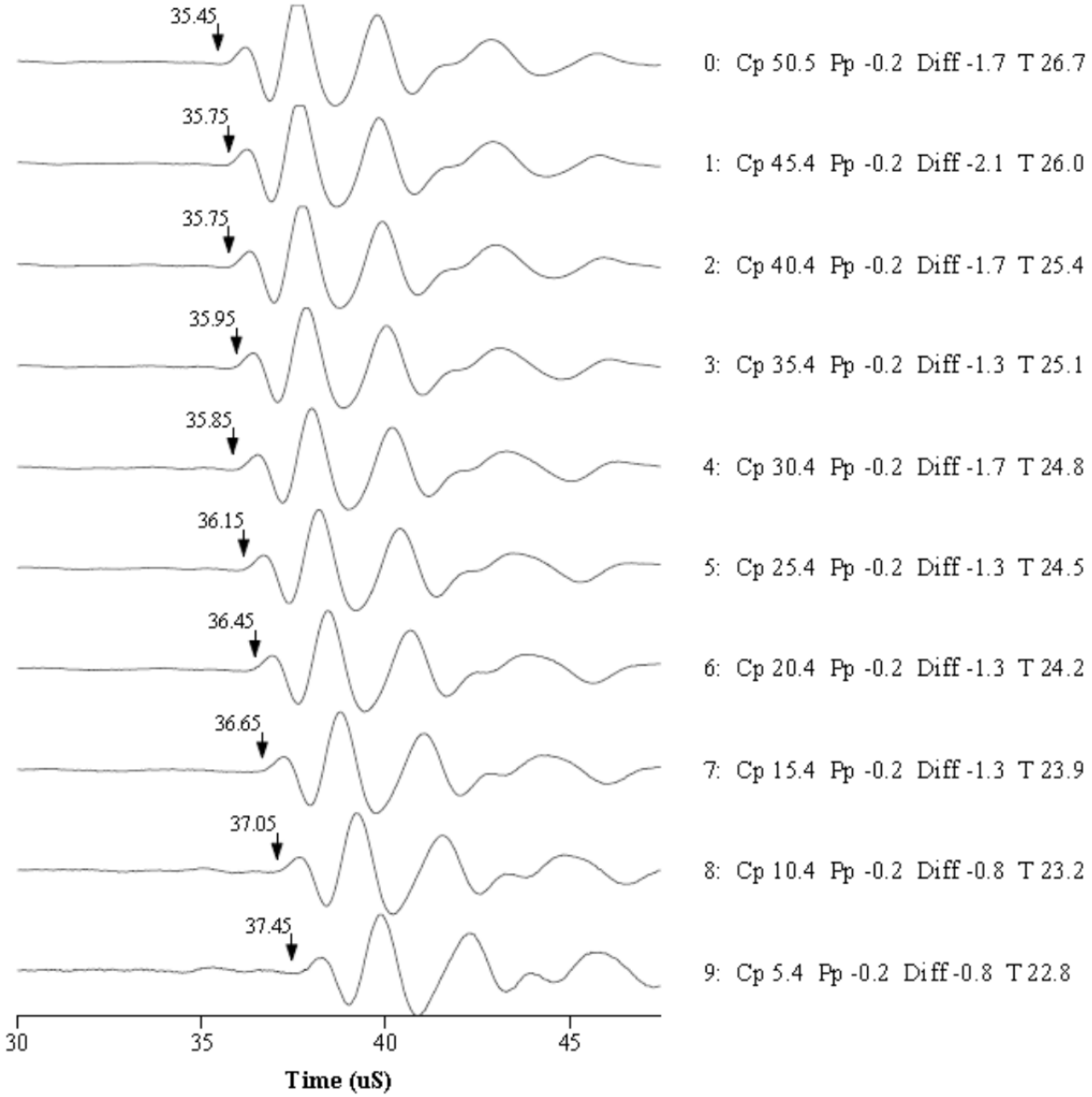

Figure 7-14 Waveform for S2 arrivals

7.5. Dynamic Moduli and Poisson's Ratio

By definition, dynamic moduli and Poisson's ratio are those calculated from the elastic wave velocity and density. They are different from static dynamic moduli and Poisson's ratio moduli, which are directly measured in a deformational experiment. The static and dynamic moduli of the same rock may significantly differ from each other. The main reason is likely to be the difference in the deformation, or strain, amplitude between the dynamic and static experiments. In this study, dynamic Young's modulus and Poisson's ratio are calculated from the P-waves and S-waves velocities and density.

$$E_{dyn} = \rho v_s^2 \frac{3v_p^2 - 4v_s^2}{v_p^2 - v_s^2} \quad \text{.....(7-26)}$$

$$\upsilon_{dyn} = \frac{v_p^2 - 2v_s^2}{2\left(v_p^2 - v_s^2\right)} \quad \text{.....(7-27)}$$

where E_{dyn} is the dynamic elastic modulus, ν_{dyn} is the dynamic Poisson's ratio, ρ is the density of rock sample, v_p is P-wave velocity, and v_s is S-wave velocity.

Dynamic Young's modulus and Poisson's ratio can be calculated from sonic velocity test. Figure 7-15 shows the dynamic properties calculated from sonic velocity measurement of a Bakken core plug.

Sample and Experiment Information for File w16771-10426.8-velocity			
Well:	16771	Organization:	UND
Depth:	3178.1 m	Transducer:	Vel_1in_new
Formation:	lower bakken	Rock type:	
Dry bulk density:	2.590 gm/cm^3	Porosity:	6.6%
Sat. bulk density:		Pore fluids:	Nitrogen
Diameter:	26.39 mm	Entered Length:	62.69 mm

Comments:	Geomechanics by Jun He
Expt name:	velocity
Expt date:	Tue Feb 19 13:13:46 2013
Print date:	Sun Apr 28 16:01:59 2013
A2D File:	

Observed Velocities and Moduli for File w16771-10426.8-velocity									
Event	Conf	Pore	Diff	Temp	V_p	$V_s^{(1)}$	$V_s^{(2)}$	Young's Modulus	Poisson's Ratio
	MPa	MPa	MPa	°C	m/s	m/s	m/s	GPa	
0	50.5	-0.2	-2.1	26.0	5189	3095	2965	59.03	0.241
1	45.4	-0.2	-2.1	25.4	5146	3095	2951	58.53	0.237
2	40.5	-0.1	-1.7	24.9	5276	3095	2979	59.83	0.252
3	35.4	-0.2	-1.7	24.6	5189	3080	2951	58.65	0.245
4	30.4	-0.2	-1.7	24.4	5232	3065	2910	58.17	0.258
5	25.4	-0.2	-1.6	24.2	5104	3080	2937	57.85	0.234
6	20.4	-0.2	-1.3	23.9	5104	3065	2910	57.30	0.239
7	15.5	-0.2	-0.7	22.5	5189	3050	2910	57.68	0.254
8	10.4	-0.2	-0.8	22.0	5232	3065	2883	57.79	0.261
9	5.4	-0.2	-0.4	21.4	5104	3065	2870	56.78	0.245

Figure 7-15 Dynamic properties calculated from sonic velocity

7.6. Static Moduli and Poisson's Ratio (Non-Destructive Strength Test)

Young's modulus, also known as the tensile modulus or elastic modulus, is a measure of the stiffness of an elastic material and is a quantity used to characterize materials. It is defined as the ratio of the stress along an axis over the strain along that axis in the range of stress in which Hooke's law holds. Young's modulus, *E*, can be calculated by dividing the tensile stress by the tensile strain in the elastic (linear) portion of the stress-strain curve (Figure 7-16).

$$E = \frac{\sigma}{\varepsilon} \quad \text{(7-28)}$$

where

E is the Young's modulus (modulus of elasticity)
σ is the axial stress exerted on specimen
ε is the strain of specimen in axial direction

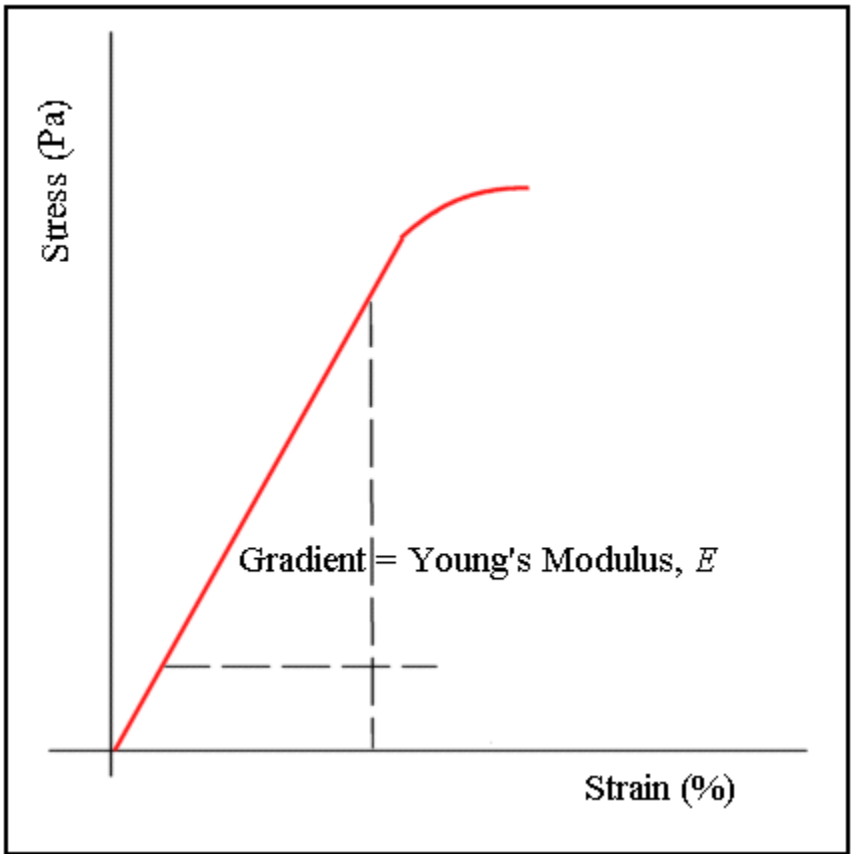

Figure 7-16 Static Young's modulus calculated from stress-stain relation

Poisson's ratio, ν, named after Siméon Poisson, is the negative ratio of transverse to axial strain. When a material is compressed in one direction, it usually tends to expand in the other two directions perpendicular to the direction of compression (Figure 7-17). This phenomenon is called the Poisson effect. The Poisson ratio is the ratio of the fraction of expansion divided by the fraction of compression, for small values of these changes.

$$\nu = \frac{\varepsilon_D}{\varepsilon_L} \quad \text{(7-29)}$$

where

$$\varepsilon_D = \frac{\Delta D}{D} \quad \text{(7-30)}$$

$$\varepsilon_L = \frac{\Delta L}{L} \quad \text{(7-31)}$$

ε_D is the strain of specimen in radial direction
ε_L is the strain of specimen in axial (or vertical) direction

If the material is stretched, it usually tends to contract in the directions transverse to the direction of stretching. The Poisson's ratio will be the ratio of relative contraction to relative stretching, and will have the same value as above. Due to the requirement that Young's modulus, the shear modulus and bulk modulus have positive values, Poisson's ratio can vary from initially 0 to about 0.5. Generally, "stiffer" materials will have lower Poisson's ratios than "softer" materials. If Poisson's ratios are larger than 0.5, it implies that the material was stressed to cracking, or caused by experimental error, etc.

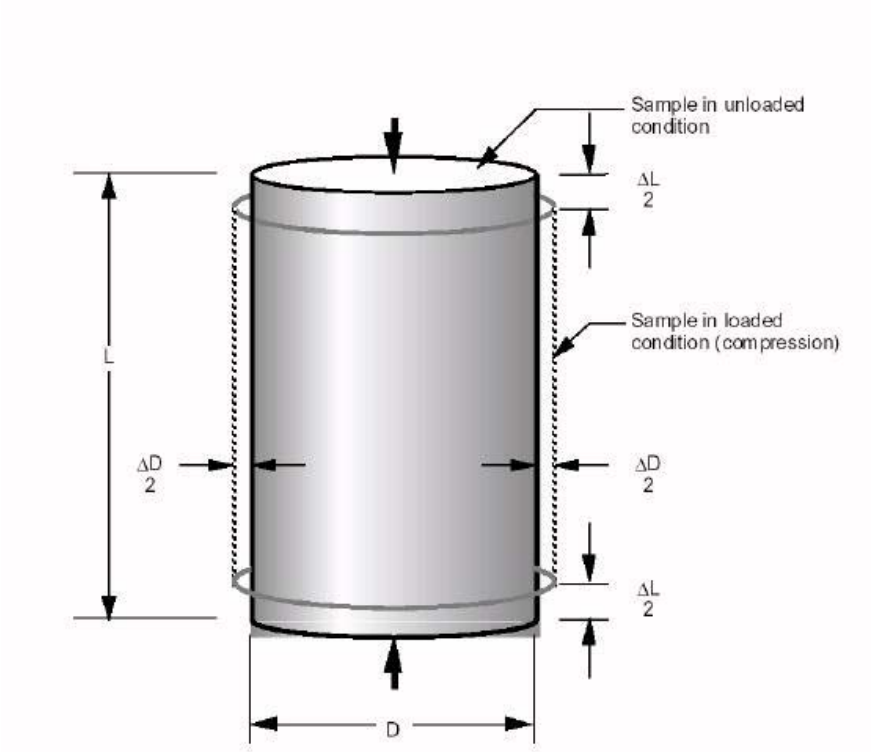

Figure 7-17 Poisson's ratio from a deformed cylinder-shape specimen
(http://classes.engr.oregonstate.edu/cce/winter2012/ce492/Modules/06_structural_design/poissons_ratio.htm)

Static dynamic moduli and Poisson's ratio moduli are directly measured in a deformational experiment. In this work we measured the strain in the axial and radial directions of core plug. The compressional stresses in the axial and radial directions are also recorded. We used the following procedure to conduct a uniaxial stress experiment.

1) Prepare the specimen.

2) Measure the dry bulk density of the specimen.

3) Jacket the specimen with thick copper.

4) Seat the jacket to specimen.

5) Attach strain gages to the test specimen.

6) Secure the sample to the end caps. Place the sample assembly on the base plug of the pressurization system.

7) Connect strain gage leads in the base plug. Make sure that the leads for the radial and axial gages are soldered to the appropriate connectors.

8) Insert the sample assembly into the pressure vessel. Fill the pressure vessel with oil.

9) Initiate the AutoLab software.

10) Check the Analog Channel Monitor to ensure that the strain gages are on scale.

11) Now calibrate the strain gages.

12) Increase the differential stress and the confining pressure to the initial value for the uniaxial stress measurement. Activate the window for the Uniaxial Stress measurement.

13) Fill in the appropriate values in the Uniaxial Stress experiment command module. Select the loading rate and set the amplitude of the shear stress cycle, and set the number of loading cycles for the experiment.

14) Select the portion of the stress-strain data that will be processed after the capture.

15) Once all the data is satisfactorily entered into the Uniaxial Stress experiment user interface, apply the load to conduct test.

16) At the conclusion of the test sequence, the processed data are presented.

17) Examine the data and accept them if they are acceptable. The data are now permanently stored.

18) Increase the mean stress to the next value and repeat the cyclic-loading experiment described above.

19) Step wise increase the confining pressure as desired to determine the elastic constants as a function of confining pressure.

20) At the termination of the test sequence, terminate the data acquisition and end the experiment.

21) Process and review the data that has been collected, recalculate the moduli for different portions of the load/unload cycles, and print a final report.

Figure 7-18 shows an example of stress and strain in a non-destructive strength test in this study.

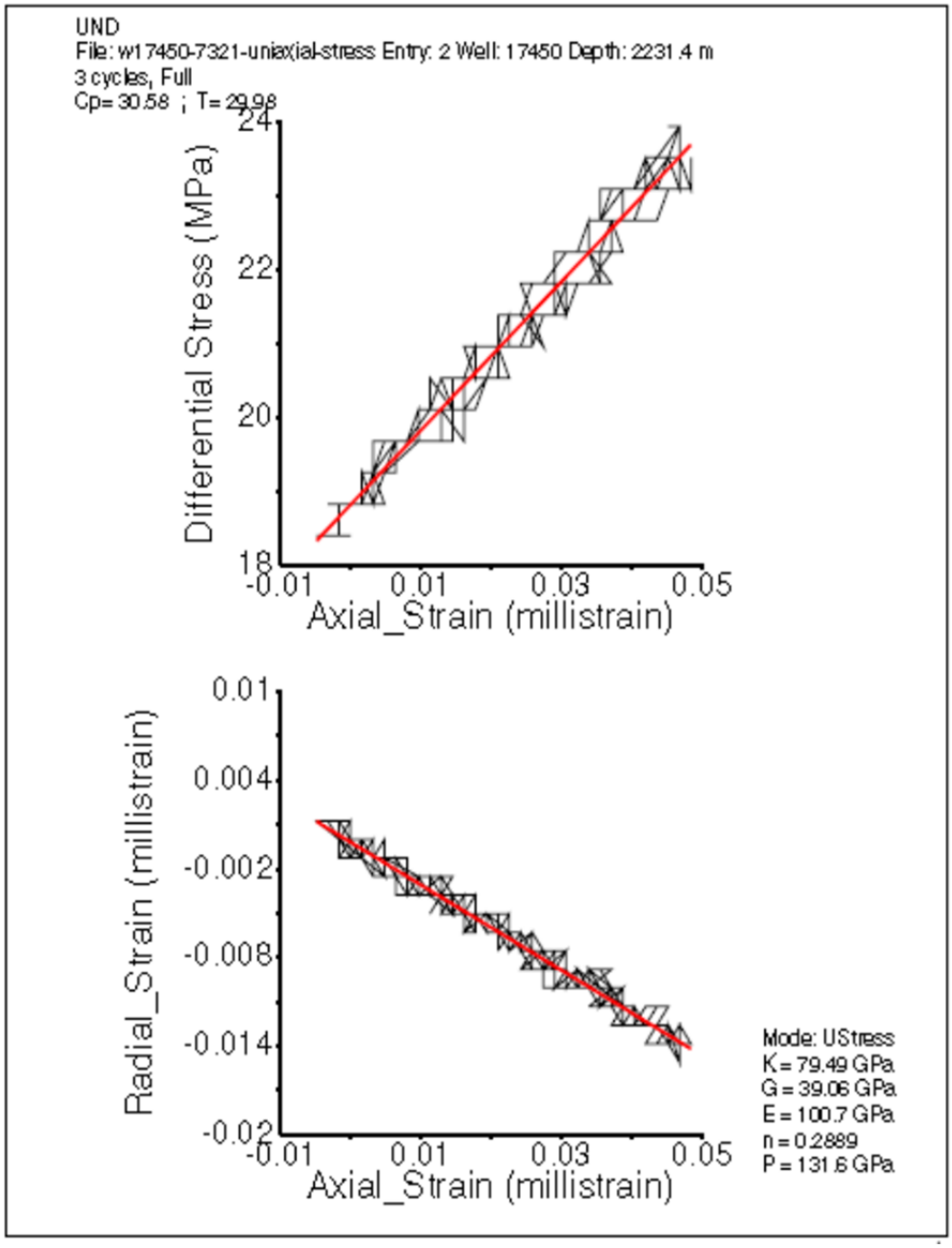

Figure 7-18 An example of stress and strain in a non-destructive strength test in this study

After the velocity test and non-destructive strength test, Young's modulus and Poisson's ratio from both test are compared.

7.7. Biot's Coefficient

Biot's coefficient is an important parameter used to determine the influence of pore pressure on rock deformation. Biot's coefficient defines the relationship among total stress, effective stress and pore fluid pressure (Biot and Willis, 1957; Geertsma, 1957). It describes how soon the matrix stress will respond when the pore fluid pressure is changed. It is more important to low permeability rocks, such as the Bakken Formation. This parameter is used in hydraulic fracturing treatment design and wellbore stability. Physical fracturing of these formations could enhance the overall

formation permeability and thus improve shale oil extraction. One of the outstanding issues in rock fracturing is to determine the magnitude of applied effective stress. The general effective-stress law is defined as

$$\sigma_{eff} = \sigma_c - \alpha\sigma_p \quad \text{(7-32)}$$

where
σ_c is total confining stress,
σ_p is fluid pore pressure,
σ_{eff} is effective stress,
α is Biot's coefficient,

Each physical quantity of rock responds to total stress and pore pressure in a different way, and thus each quantity has its own unique Biot's effective-stress coefficient. The main objective of this study is to experimentally determine the Biot's coefficient for Bakken formation. According to Equation (7-32), Biot's coefficient can be estimated by measuring two sets of fluid pore pressure and confining pressure under constant effective stress, or constant strains, which is achievable in the experiment. Therefore, Biot's coefficient, α, is the ratio between confining pressure difference and pore pressure difference under constant strains.

$$\alpha = \frac{\Delta \sigma}{\Delta p} \quad \text{at } \Delta\varepsilon=0 \text{ at both axial and radial directions} \quad \text{(7-33)}$$

The measurement consists of measuring the strains under a set of fluid pore pressure and confining pressure, and then fluid pore pressure is changed; meanwhile confining pressure is adjusted to keep the strains constant. Biot's coefficient can be obtained from these two set of pressures (Figure 7-19).

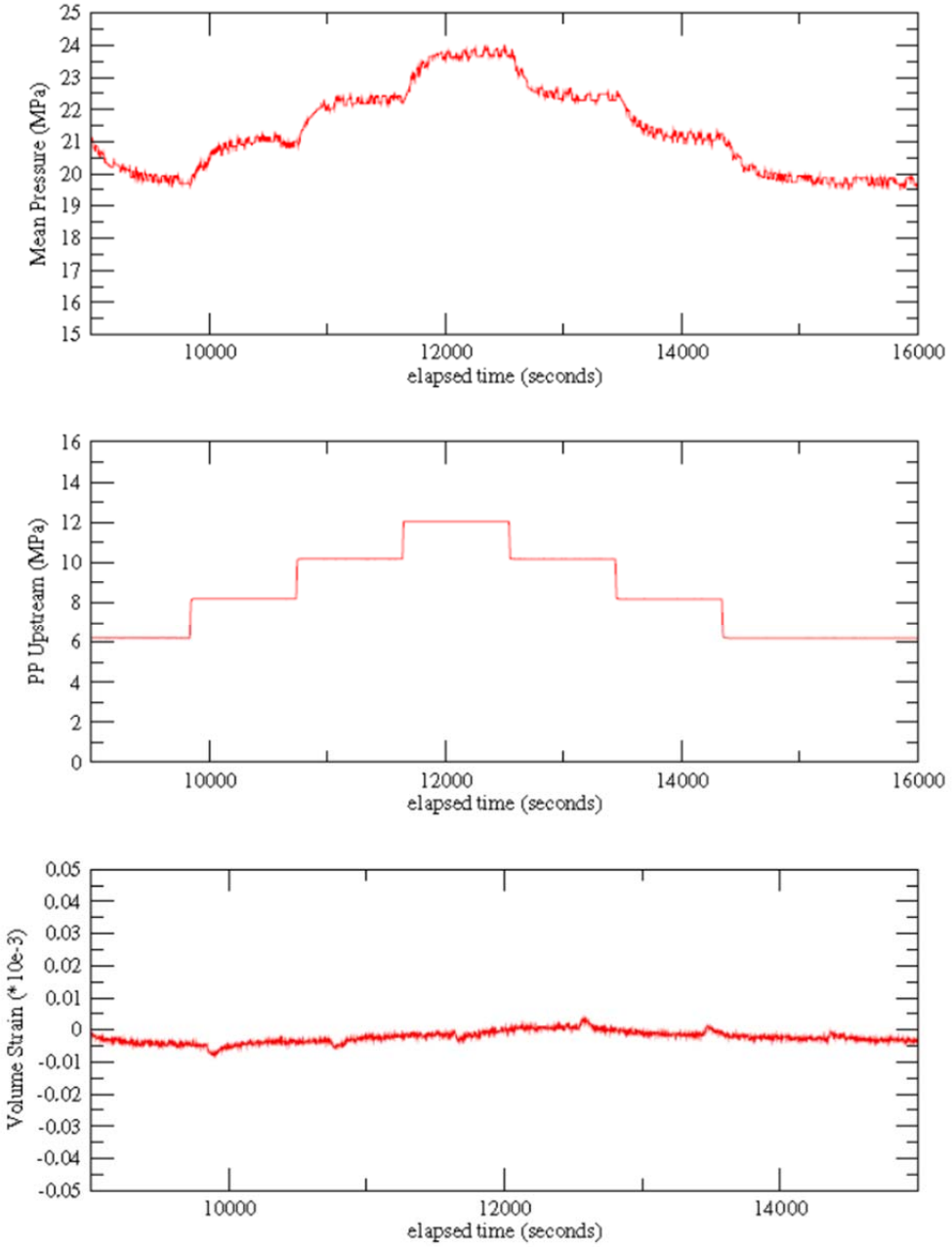

Figure 7-19 Biot's coefficient measurement using constant deformation under different confining pressure

The test procedure is similar to the stress-strain test. To obtain Biot's coefficient, several stress-strain tests are repeated by keeping the strains constant. Followings are steps for stress-strain test to calculate Biot's coefficient.
1) Prepare the specimen.

2) Measure the dry bulk density of the specimen.

3) Jacket the specimen with thick copper.

4) Seat the jacket to specimen.

5) Attach strain gages to the test specimen.

6) Secure the sample to the end caps. Place the sample assembly on the base plug of the pressurization system.

7) Connect strain gage leads in the base plug. Make sure that the leads for the radial and axial gages are soldered to the appropriate connectors.

8) Insert the sample assembly into the pressure vessel. Fill the pressure vessel with oil.

9) Initiate the AutoLab software.

10) Check the Analog Channel Monitor to ensure that the strain gages are on scale.

11) Now calibrate the strain gages.

12) Increase the differential stress and the confining pressure to the initial value for the uniaxial stress measurement. Activate the window for the Uniaxial Stress measurement.

13) Fill in the appropriate values in the Uniaxial Stress experiment command module.

14) Select the portion of the stress-strain data that will be processed after the capture.

15) Once all the data is satisfactorily entered into the Uniaxial Stress experiment user interface, apply the load to conduct test.

16) Record the strains and stresses.

17) Examine the data and accept them if they are acceptable. The data are now permanently stored.

18) Increase the pore pressure to the next value and adjust the confining pressure to keep strains constant. Record the strains and stresses.

19) Step wise increase the pore pressure and adjust confining pressure to keep strains constant.

20) At the termination of the test sequence, terminate the data acquisition and end the experiment.

21) Process and review the data that has been collected, calculate Biot's coefficient, and print a final report.

7.8. Uniaxial/Triaxial Compressive Strength, Young's Modulus and Poisson's Ratio (Destructive)

Uniaxial/triaxial compressive strength is measured together with Young's modulus and Poisson's ratio. Axial load, axial and lateral deformations are measured during the compression until failure of the specimen. Load-deformations curves are converted to stress-strain curves using the specimen's geometry, from which the Young's modulus and Poisson's ratio are obtained using the linear portion. Because the Williston Basin is very flat lying, we can assume that one of the three principal stresses will be parallel to the vertical direction. With this assumption, using the measured historic stresses in three different directions in the bedding plane would allow the determination of the two principal stresses in the bedding plane.

A detailed procedure for the experiment is given below. The recommended procedure for confined compression to failure experiments is as follows:

1) Prepare the specimens according to sample preparation.

2) Measure the dry bulk density of the specimen.

3) Jacket the specimen with 0.13 mm thick copper. The procedure is described as above.

4) Seat the jacket to the specimen. Insert hardened steel end-plugs into the extensions of the foil jacket at each end of the specimen. Seal the jacket to the end plugs with a section of rubber tubing the same diameter as the test specimen. The rubber jacket is secured to the end plug at two points with several wraps of #19 steel wire. Insert the jacketed test specimen into the pressure vessel and increase the pressure to approximately 7 MPa (1,000 psi).

5) Remove the jacketed test specimen from the pressure vessel and examine the surface of the copper jacket. There should be no punctures in the foil and the jacket should be tightly swaged to the specimen. If you observe small holes in the jacket, fill them with either epoxy or a spot of solder.

6) Position the supporting ring for the axial displacement transducer (LVDT) barrels approximately one specimen radius below the upper end of the specimen. Carefully center the ring so that it is concentric with the specimen.

7) Position the LVDT ring used to measure the radial displacement at the midpoint of the specimen. The supporting ring for the LVDT is positioned so that the line between the adjusting screw on the ring and the axis of the core barrel pass through the axis of the specimen and is perpendicular to the axis of the specimen.

8) Position the lower support ring for the axial LVDT concentrically about the specimen approximately one specimen diameter below the upper ring. This ring supports the stainless steel extension rods for the LVDT cores. (Note: Always use non-magnetic stainless steel or brass extension rods to support the LVDT cores.) Be sure that the axis of the LVDT core barrels are aligned parallel with the axis of the specimen. The extension rods are supported with adjusting screws that are secured with locking nuts.

9) Measure the center-to-center separation of the axial LVDT support rings with a caliper micrometer. Record this value in your notebook; this value will be used to compute the strain.

10) Place the specimen assembly on the base plug of the load frame. Connect the two axial LVDTs and the radial LVDT to the electrical leads in the base plug.

11) Make the final mechanical adjustments on the LVDT. Each LVDT is adjusted so that its initial amplified output is positive. All of the LVDTs are wired so that increasing the specimen diameter or shortening the specimen length results in an increasingly positive output voltage.

For specimens tested in confined compression, there is an initial volume reduction. The output voltage of the radial displacement gage will decrease. The proper initial setting in this case will be strongly positive to account for the reduction in diameter due to hydrostatic compression. The axial LVDTs will become increasingly positive with pressurization. Consequently, a slightly negative voltage may be required to insure that the LVDTs have sufficient range at the appropriate sensitivity to measure the deformation of

12) Insert the sample assembly into the pressure vessel.

13) Fill the pressure vessel with oil.

14) Set the limit switches for the fail-safe module according to the properties of the specimen being tested.

15) Turn the panel command knobs for the servo-controllers fully counterclockwise. Lock the differential pressure intensifier.

16) Turn on the hydraulic power supply.

17) Set the differential pressure intensifier to force feedback.

18) Unlock the differential pressure intensifier.

19) Slowly increase the command signal for the axial force until the piston begins to slowly move down to contact the specimen. Make sure that the vent valve for the confining pressure system is open.

20) Back off the axial force after it touches the specimen. When the force on the specimen drops to zero, lock the differential load intensifier.

21) Balance the displacement transducer monitoring the position of the piston. It is important that the LVDT is set exactly at 0.00 and that the output voltage read on the computer is also 0.00.

22) Switch the mode control for the differential pressure intensifier from force to displacement feedback.

23) Unlock the differential load intensifier. The piston will remain close to the top of the specimen assembly but exert no load on the specimen.

24) Lock the differential intensifier.

25) Initiate the AutoLab Software.

26) Select Acquire Data in the NER Laboratory Process Monitor.

27) Choose Deformation (without Velocity, Resistivity, or Permeability or any of the other experiment types) in the Experiment Type Panel and click OK.

28) Fill in the Experimental Information Panel. Under Channel File Selection, select a channel file where displacement is the feedback signal for the differential pressure intensifier. Click Done.

29) Change the mode selection switches on the servo-controllers from panel to computer once the Commander window appears. The computer is now controlling the servo-hydraulic intensifiers.

30) Check the Analog Channel Monitor panel to ensure that the displacement transducers have not shifted during set-up.

31) Close the vent valve on the confining pressure system.

32) Unlock the Failsafe for the differential pressure intensifier.

33) Increase the slide bar to the desired confining pressure, in this case 10.0 MPa.

34) Select a Ramp Time of two minutes and using the mouse, Send the command to the servo-amplifiers. The confining pressure on the specimen will increase. There is no change in the axial force measured with the force cell or the position of the moveable piston in the pressure vessel.

35) Wait until the confining pressure reaches 10.0 MPa and check the output of the LVDTs. Are they on scale, (i.e. between 0 and 10 volts)? Adjust the output offset on the appropriate signal-conditioning card between 0.250 and 0.750 volts.

36) Estimate the strain at which the specimen will fail based on previous measurements. From this information, compute the approximate displacement that the specimen will experience during the loading process. Triple this value to account for elastic deformation in the system and to compensate for excessively strong specimens.

37) Set the displacement slide bar in Commander to the value computed in step 36. Choose a strain rate for the experiment. Typically, the minimum recommended strain rate for confined compression to failure experiments is 10^{-5} s^{-1}. Compute the time that will result in an appropriate strain rate for the specimen. After several experiments

with the system you will be able to estimate the strain rate in the specimen from the displacement rate of the system. Since the system will behave identically from experiment to experiment, a simple chart of displacement rate versus strain rate can be used to apply the same loading rate for an entire suite of experiments.

38) Select a Sampling Interval. Depending on the duration of the test the frequency of data acquisition is selected. For most experiments, collecting data every two to five seconds is adequate. However, after you become experienced with the system and with performing experiments an appropriate data acquisition rate will become apparent. Click Collect a/d data.

39) It is frequently useful to monitor the experiment. Select the axis on the graph that will provide you with the most information concerning the experiment.

40) Leave the confining pressure at its existing value of 10.0 MPa and click Send to initiate loading.

41) Continue the experiment until the specimen fails. Monitor the output voltages of the LVDTs throughout the experiment. In many cases it is useful to use a graphical representation of the experiment as deformation proceeds. In this case you may wish to initiate the xmgrace graphical program and to monitor individual channels that are of interest to you. Typically, the most important data are obtained by monitoring one of the axial LVDTs as a function of force and one of the axial LVDTs as a function of the change in diameter (the radial LVDT).

42) Continue the loading to examine the post failure behavior of the specimen, if it is important. Since the system is operating in displacement feedback, failure will be accompanied by a drop in the force on the specimen. Most likely the specimen will not be completely unloaded and the piston will not unload the total elastic energy stored in the system into the specimen. By continuing the experiment the post failure behavior of the specimen can be observed. As the specimen continues to deform, it will support a lower stress than prior to failure. If the axial LVDTs have not been misaligned during failure, the shortening of the specimen may be observed in the post failure regime.

43) Terminate the experiment by first stopping the collection of A/D data. Click Collect a/d channels to terminate the data acquisition. Set the slide bars for displacement and confining pressure to zero and choose a Ramp Time of two minutes. Click the Send button.

44) Select Stop Data Acquisition from the NER Laboratory Process Monitor window.

45) Drain the confining fluid from the pressure vessel using the procedure outlined in Chapter 2. Remove the specimen from the pressure vessel and examine the failure characteristics and note any pertinent information in your laboratory notebook.

46) Select Process/Print Existing Data from the NER Laboratory Process Monitor window.

47) Select the file that you wish to process from the File Browser. For this experiment we will be processing the A/D analog data from the confined compression experiment on Berea sandstone. In order to process the data, we write the data file to a spreadsheet. Choose the file for the experiment that has just been completed. Make sure that the end of the line in the File Browser for the file you have chosen contains the designation ending with “A/D: yes”, indicating that this data file has an associated “.a2d” file.

48) Select A/D to Spreadsheet from the menu in the file browser. A pop-up panel will appear. This gives options for the configuration of the spreadsheet. Select the criteria that conform to the spread sheet you use. Select the directory that the data is to be stored in and click OK.

49) Transfer the data to a computer running your favorite spreadsheet program.

50) Open the file using your favorite spreadsheet program and process the data. The following data should be processed. The differential stress applied to the specimen is computed from the force data. Compute the cross-sectional area of the specimen and divide it by the force. Convert the stress to units of MPa or psi depending on your preference. For this experiment we selected MPa. Next, the strains are computed from the output voltages of the LVDTs. Computing the strains is straightforward. First, multiply the scale factors for the displacement transducer by the output voltage (after first correcting for the initial offset in the output voltage). This quantity is divided by the separation between the rings. For this experiment the separation between the rings was 50.08 mm (2.0 inches). The result of this calculation is the strain computed for one axial LVDT. Repeat the procedure for the other axial LVDT. To obtain the average axial strain, average the two strains. To compute the radial strain on the specimen, first calculate the change in the diameter of the specimen by multiplying the scale factor for the radial displacement transducer by the change in the output voltage of the devise. This value is then divided by the diameter of the specimen to obtain the strain normal to the loading axis.

51) Plot the data from the experiment. Figure 7-20 graphically displays the data collected on a sample. Strain, in millistrain, is plotted as a function of stress difference. In this diagram we plot three strains: axial, radial, and volumetric. Volumetric strain for a cylindrical sample is computed by summing the axial strain plus twice the radial strain. (Remember that the radial strain has a different sign than the axial strain.) The data collected on Berea sandstone are typical of most sandstones. The sample compacts to approximately two-thirds of its failure stress and then begins to dilate. The dilation is most apparent in the radial and volumetric strain. If Young's modulus and Poisson's ratio are to be computed, they should be computed over a linear portion of the stress–strain curve over a stress interval of between approximately 10 to 50% of the stress difference.

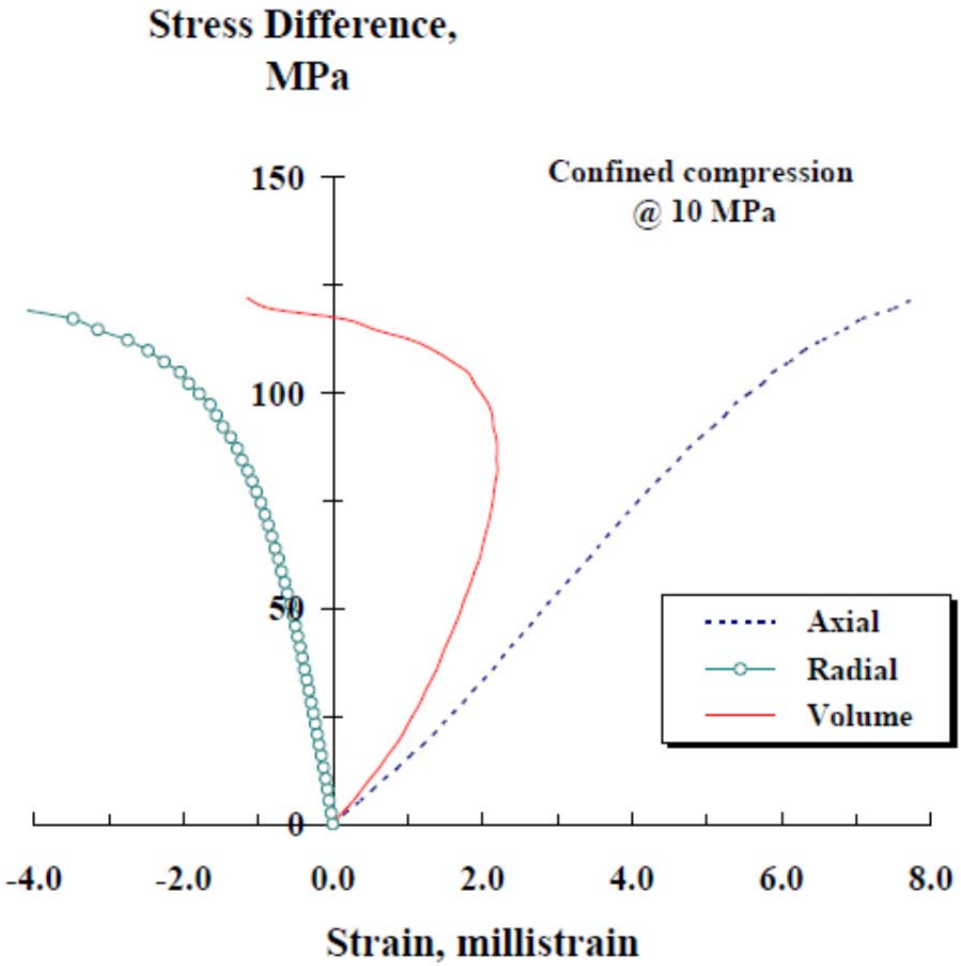

Figure 7-20. Strain and stress data collected on a sample

7.9. Mohr's Circle, Angle of Internal Friction and Cohesive Strength

With the decline in conventional oil and gas production worldwide, petroleum exploration and production from unconventional oil and gas resources have gained great momentum throughout the world to fill the gap between ever increasing demand of energy and decreasing production of conventional reservoirs. Knowledge of geomechanical properties of target reservoirs ensures producing hydrocarbons from unconventional resources safely, environmental friendly, and economically. Rock geomechanical properties are key parameters in designing oil and gas well drilling and completion, modeling fluids flow in reservoir, and forecasting well production. Direct measurement of rock strength parameters such as cohesive strength and angle of internal friction is accomplished through uniaxial or triaxial strength experiment (destructive test).

The Mohr Theory of Failure, also known as the Coulomb-Mohr criterion or internal-friction theory, is based on the famous Mohr's Circle. Mohr's theory is often used in predicting the failure of brittle materials, and is applied to cases of 2D stress. Mohr–Coulomb theory is a mathematical model describing the response of rock to shear stress as well as normal stress. Generally the theory applies to materials for which the compressive strength far exceeds the tensile strength. In geotechnical engineering it is used to define shear strength of soils and rocks at different effective stresses. In structural engineering it is used to determine failure load as well as the angle of fracture of a displacement fracture in concrete and similar materials. Coulomb's friction hypothesis is used to determine the combination of shear and normal stress that will cause a fracture of the material. Mohr's circle is used to determine which principal stresses that will produce this combination of shear and normal stress, and the angle of the plane in which this will occur. According to the principle of normality the stress introduced at failure will be perpendicular to the line describing the fracture condition. It can be shown that a material failing according to Coulomb's friction hypothesis will show the displacement introduced at failure forming an angle to the line of fracture equal to the angle of friction. This makes the strength of the material determinable by comparing the external mechanical work introduced by the displacement and the external load with the internal mechanical work introduced by the strain and stress at the line of failure. By conservation of energy the sum of these must be zero and this will make it possible to calculate the failure load.

Mohr's theory suggests that failure occurs when Mohr's Circle at a point in the body exceeds the envelope created by the two Mohr's circles for uniaxial tensile strength and uniaxial compression strength. This envelope is shown in the Figure 7-21.

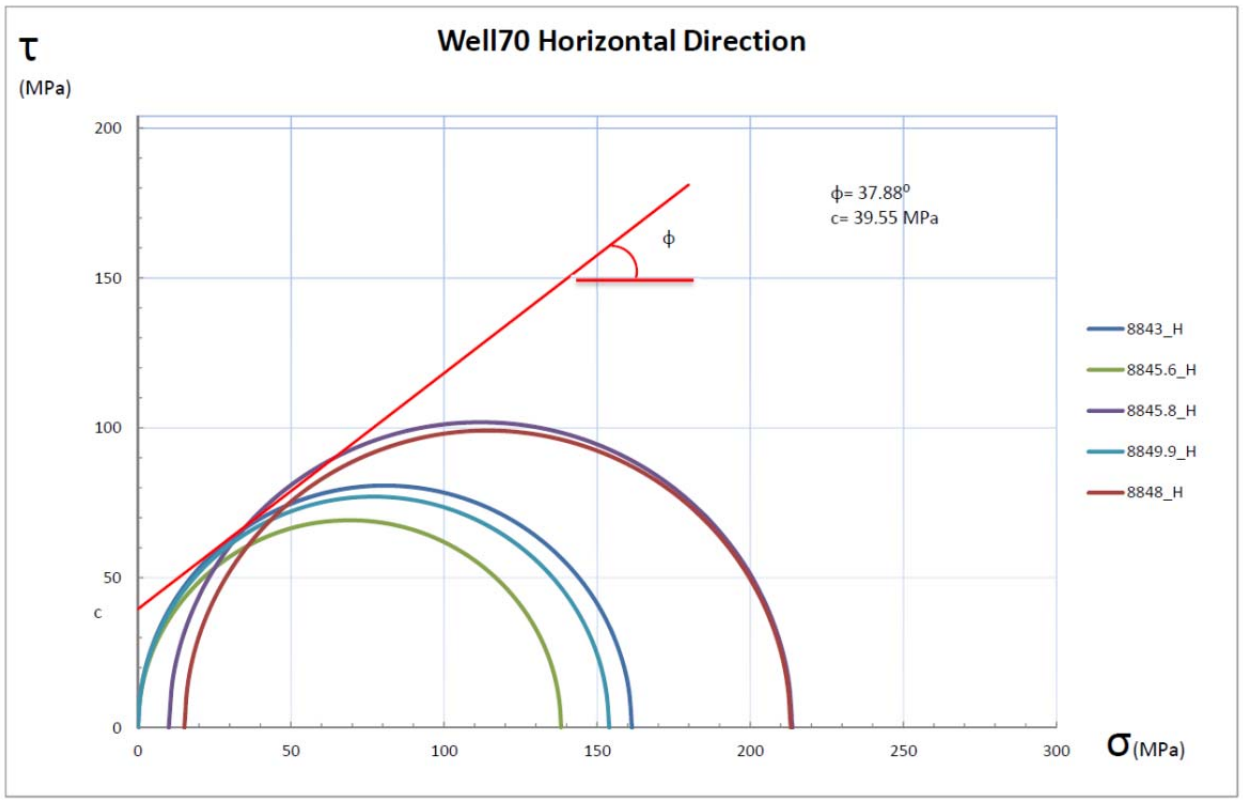

Figure 7-21 Mohr envelop for Bakken formation, established by drawing the best fit tangent to experimentally determined failure stresses at a range of confining pressures and isothermal conditions

7.10. Uniaxial Tensile Strength

Tensile strength of rocks is one of the most important parameters for drilling excavation in rocks, because rocks are much weaker in tension than in compression. There are two methods for determining the tensile strength of rock: indirect method such as Brazil Test, and direct method (ISRM, 1978). Because the cored Bakken samples can't meet the requirements of indirect testing methods for tensile strength in terms of size and quantities, we developed a uniaxial tensile strength tester that allows us to test 1-in diameter by 2-in length and 2-in diameter by 4-in length cylindrical rock specimens. This report introduces the apparatus and the verification testing results..

To perform direct measurement, an in-house tensile strength test apparatus (Figure 7-22) is set up. This uniaxial tensile strength tester was designed and developed following the ISRM (1978) suggested methods with references to some earlier literature (Fairhurst, 1961; Vutukuri et al., 1974). It is composed of a movable frame, a jack, a lever, upper and lower chains with swivel adaptors, a transparent bucket, and a dynamometer. A dynamometer (Figure 7-23) on the top is used to record the force where the specimen is loaded. Two steel caps are used to grip the specimen by gluing on each end of the specimen. A jack is used to increase the force.

Figure 7-22. Tensile strength test apparatus

Figure 7-23. Dynamometer on top of tensile strength test apparatus

During the measurement, it is important to mount the specimen in tension grips. Cylindrical specimen and epoxy based cements are used. The rock specimen is glued onto two caps in advance (Figure 7-24). During sample installation, the two caps are connected onto the upper and lower adaptors (Figures 7-25 and 7-26). The installed specimen is inside the center of a transparent bucket. The bucket allows observation during testing, and provides protection to the specimen at failure.

Figure 7-24. Specimen glued to steel caps

Figure 7-25. Tensile test apparatus (with upper side of the specimen is fixed)

Figure 7-26.Tensile test apparatus (with both sides of the specimen was fixed)

After the specimen installation is completed, the lower chain, the specimen, the upper chain, and the loading point of the dynamometer are all on a vertical line, without any torque and resistance, and each is free to rotation, the load force will be increased slowly with the jack until the specimen was crashed (Figure 7-27). At the testing, the jack applies load to the lever which pulls the rock specimen along the upper and lower chains until failure. The tensional force is showing on the dynamometer. At failure, the peak force can be recorded by the dynamometer (Figure 7-28).

Figure 7-27. Specimen is crashed

Figure 7-28. Reaching peak force as the specimen is crashed

The key for direct tensile strength test is to provide direct tension onto the sample. The criterion to verify if the apparatus, and thus the test, is successful is that the rock sample would fail in pure tension. This can be checked from the broken specimen. From Figure 7-27, it is obvious that the rock specimen is failure under pure tension, because the failure plane is flat and rough. Therefore, it can be concluded that this Uniaxial Tensile Strength Tests provides the capability of measuring the direct tensile strength.

8. EXPERIMENTAL RESULTS

We have tested 240 core plugs to obtain porosity, permeability, sonic velocity, static Young's modulus, static Poisson's ratio, Biot's coefficient, rock strength (destructive test), cohesive strength, and angle of internal friction. Information of 8 wells providing core plugs for test are shown in Table 8-1. The location of these wells can be found in Figure 3-2.

Table 8-1. Wells providing core plugs for test in this study

Well #	NDIC file #	Assessment Unit (USGS 2008)	Assessment Unit #	Top of Formation (ft)
96	16771	Nesson-Little Knife Structural AU	2	Upper Bakken (UB):10288 Middle Bakken (MB):10307 Lower Bakken (LB):10378
70	16862	Eastern Expulsion Threshold AU	3	Upper Bakken:8803 Middle Bakken:8820 Lower Bakken:8850
20	16174	Elm Coulee-Billings Nose AU	1	Upper Bakken:10673 Middle Bakken:10683 Lower Bakken:10712
13	15923	Central Basin-Poplar Dome AU	4	Upper Bakken:10985 Middle Bakken:11005 Lower Bakken:11050
86	17450	Northwest Expulsion Threshold AU	5	Upper Bakken:7300 Middle Bakken:7355 Lower Bakken:7415
18	16089	Northwest Expulsion Threshold AU	5	Upper Bakken:8595 Middle Bakken:8610 Lower Bakken:8675
72	16985	Central Basin-Poplar Dome AU	4	Upper Bakken:10486 Middle Bakken:10510 Lower Bakken:10550
2	11617	Nesson-Little Knife Structural AU	2	Upper Bakken:10310 Middle Bakken:10330 Lower Bakken:10380

8.1. Porosity

Porosities of core plugs from 8 wells have been measured. Measurement results are listed in Table 8-2.

Table 8-2. Porosities of core plugs tested in this study

Well #	Depth	Formation	Porosity	Well #	Depth	Formation	Porosity	Well #	Depth	Formation	Porosity
	(ft)		%		(ft)		%		(ft)		%
20	10673.6	UB	0.9	2	10371.8	MB	4.8	13	11035	MB	4.2
20	10678.3	UB	0.8	2	10372	MB	6.3	13	11004	UB	5.7
20	10682	UB	3.5	2	10373	MB	4.7	13	11006.8	MB	4.3
20	10729.5	LB	4.5	2	10374-13-1	MB	5.5	13	11007	MB	2.1
20	10732.3	LB	5.5	2	10374.1-13-2	MB	3.8	13	11008.5	MB	5.8
20	10727.2	LB	4.8	2	10375	MB	5.6	13	11012B	MB	4.6

20	10729.9	LB	5.6	2	10403-15-1	LB	6.1	13	11025H	MB	3.1
20	10733.3	LB	4.9	2	10403-15-2	LB	6.0	13	11031	MB	4.5
20	10731.4	LB	5.2	2	10412.8	LB	6.0	13	11033	MB	7.0
20	10726.9	LB	4.7	2	10415	LB	6.0	86	7308.1	UB	1.4
20	10728.1	LB	4.6	2	10416	LB	3.4	86	7313	UB	1.4
20	10718.7	LB	6.9	70	8823.8	MB	4.7	86	7320	UB	1.3
20	10729.1	LB	5.6	70	8824.7	MB	5.0	86	7321	UB	1.3
20	10715.7	LB	4.0	70	8826.2	MB	5.6	86	7321.2	UB	0.8
20	10716.5	LB	4.0	70	8826.3	MB	5.6	86	7323.6	UB	4.6
20	10723	LB	5.2	70	8827.6	MB	3.5	86	7326.5	UB	2.5
20	10728.8	LB	6.2	70	8832.9	MB		86	7327	UB	1.9
20	10716.4	LB	5.5	70	8833.8	MB	5.3	86	7328.8-1	UB	2.5
20	10731.4	LB	7.6	70	8834.2	MB	4.1	86	7330	UB	6.2
20	10714	LB	5.1	70	8834.4	MB	4.7	86	7332	UB	6.2
20	10712	LB	4.8	70	8834.6	MB	3.7	86	7348.8	UB	6.2
20	10687	MB	4.5	70	8835.2	MB	3.6	86	7351	UB	4.7
20	10697.7	MB	3.9	70	8836.7	MB	5.4	86	7353	UB	4.3
20	10700	MB	4.0	70	8837	MB	4.3	86	7354	UB	5.7
20	10700	MB	3.6	70	8837.8	MB	5.6	86	7354.5	UB	7.0
20	10705.9	MB	3.2	70	8838.5	MB	5.8	86	7401.9	MB	2.6
20	10683.5	MB	1.9	70	8839.4	MB	6.2	86	7402.8	MB	4.6
20	10685.9	MB	3.9	70	8840.8	MB	6.2	86	7403	MB	4.4
20	10689.3	MB	6.5	70	8841.4	MB	2.8	86	7404	MB	4.4
20	10696	MB	4.7	70	8841.9	MB	5.1	86	7404.3	MB	4.3
20	10696.8	MB	3.7	70	8842.7	MB	4.3	86	7405	MB	4.1
20	10704.7	MB	4.1	70	8845	MB	5.7	86	7405.8	MB	4.5
20	10705.5	MB	4.3	70	8848.5	MB	3.3	86	7406	MB	3.6
20	10712	LB	4.7	70	8843.8	MB	3.0	86	7407	MB	4.2
96	10422	LB	5.0	70	8850.3	LB	5.8	86	7407.8	MB	2.6
96	10426.8	LB	6.6	70	8849	MB	4.2	86	7408.3	MB	3.5
96	10431	LB	5.5	70	8843	MB	3.5	86	7409	MB	4.1
96	10432	LB	7.0	70	8845.6	MB	4.9	86	7409.8	MB	3.8
96	10436	LB	6.1	70	8845.8	MB	4.0	86	7410	MB	3.2
96	10436-2	LB	4.5	70	8848	MB	4.5	86	7445.1	LB	6.9
96	10437	LB	6.2	70	8849.5	MB	3.9	86	7448	LB	5.4
96	10441.6	LB	5.2	70	8849.9	MB	4.2	86	7449	LB	5.4
96	10443	LB	4.9	70	8844.9	MB	4.6	86	7451	LB	7.1
96	10445	LB	5.5	70	8842.3	MB	4.2	86	7397	MB	5.6
96	10446	LB	10.4	70	8843.4	MB	4.4	86	7379	MB	5.9

96	10449	LB	6.3	70	8846.2	MB	3.5	86	7374	MB	6.4
96	10449-2	LB	6.3	70	8847.3	MB	4.3	86	7355	MB	8.2
96	10452	LB	6.2	70	8846.6	MB	4.2	86	7355-2	MB	8.2
96	10456	LB	5.4	70	8847.7	MB	4.3	86	7393.5	MB	5.3
96	10456-2	LB	7.1	72	10487.5	UB	5.6	86	7363	MB	8.7
96	10456.5	LB	7.0	72	10487.5(2)	UB	5.6	86	7403.8	MB	3.2
96	10460.5	LB	8.4	72	10488	UB	7.9	86	7393.1	LB	6.0
96	10463	LB	7.5	72	10488.5	UB		86	7380	LB	5.2
96	10321	MB	2.4	72	10490	UB	6.8	86	7370	LB	2.2
96	10336	MB	5.7	72	10491	UB	6.0	86	7373	LB	5.5
96	10341.5	MB	6.6	72	10491(2)	UB	6.0	86	7355.9	LB	7.3
96	10348	MB	5.6	72	10492	UB	2.8	86	7389	LB	5.4
96	10357.7	MB	2.6	72	10492(2)	UB	2.8	86	7369	LB	2.6
96	10357.7	MB	2.8	72	10493	UB	3.1	86	7374	LB	6.5
96	10307.5	MB	2.4	72	10494	UB		86	7350	UB	5.5
96	10310	MB	6.4	72	10497	UB	7.3	18	8648.2	MB	5.7
96	10339	MB	6.3	72	10498	UB	7.4	18	8650.6	MB	5.8
96	10347	MB	6.6	72	10499.8	UB	5.9	18	8651.4	MB	5.7
96	10347.8	MB	5.5	72	10503	UB	2.9	18	8655	MB	5.2
96	10356.6	MB	5.9	72	10504	UB	3.7	18	8655.7	MB	5.5
96	10307	MB	2.3	72	10504(2)	UB	3.7	18	8657.2	MB	4.1
96	10311	MB	3.2	72	10504.8	UB	3.7	18	8657.4	MB	5.0
96	10321.1	MB	2.2	72	10504.8(2)	UB	3.7	18	8659.4	MB	7.8
96	10334.7	MB	6.1	72	10505.7	UB	5.4	18	8660.7	MB	7.3
96	10345	MB	6.2	72	10509	UB	5.9	18	8661.9	MB	7.5
2	10364	MB	4.9	72	10512.7	MB	6.4	18	8664.2	MB	7.2
2	10365	MB	5.8	72	10514.5	MB	6.2	18	8665	MB	5.6
2	10367	MB	6.1	72	10517.8	MB	2.8	18	8665.3	MB	6.5
2	10367	MB	6.9	13	11006	MB	5.5	18	8668	MB	3.2
2	10419	LB	6.6	13	11008(V1)	MB	3.6	18	8669	MB	6.1
2	10368.5	MB	6.1	13	11008(V2)	MB	2.2	18	8670.2	MB	3.7
2	10369	MB	5.5	13	11009	MB	4.6	18	8672	MB	5.0
2	10369.8	MB	4.3	13	11025V	MB	3.6	18	8673.2	MB	5.4
2	10370	MB	5.7	13	11034(V1)	MB	4.9	18	8674	MB	5.8
2	10371	MB	5.7	13	11034(V2)	MB	6.2	18	8677.4	LB	4.0

8.2. Permeability

Permeabilities of core plugs from 8 wells have been tested. Test results are listed in Table 8-3. More detail can be found in Attachments.

Table 8-3. Permeabilities of core plugs tested in this study

Well #	Depth	Formation	Permeability	Well #	Depth	Formation	Permeability	Well #	Depth	Formation	Permeability
	(ft)		uD		(ft)		uD		(ft)		uD
20	10673.6	UB	0.57	2	10371.8	MB	2.3800	13	11035	MB	
20	10678.3	UB		2	10372	MB	0.3350	13	11004	UB	
20	10682	UB	91.6	2	10373	MB	0.2920	13	11006.8	MB	0.413
20	10729.5	LB	0.493	2	10374-13-1	MB	24.30	13	11007	MB	0.63
20	10732.3	LB	0.0238	2	10374.1-13-2	MB	0.1590	13	11008.5	MB	
20	10727.2	LB	0.0265	2	10375	MB	0.1680	13	11012B	MB	0.0944
20	10729.9	LB	47.9	2	10403-15-1	LB	5.4600	13	11025H	MB	
20	10733.3	LB	19.4	2	10403-15-2	LB	0.2370	13	11031	MB	
20	10731.4	LB	0.0188	2	10412.8	LB		13	11033	MB	
20	10726.9	LB	1.62	2	10415	LB		86	7308.1	UB	
20	10728.1	LB	2.36	2	10416	LB	0.0772	86	7313	UB	1970
20	10718.7	LB	0.121	70	8823.8	MB	0.008	86	7320	UB	2120
20	10729.1	LB	6.15	70	8824.7	MB	0.02	86	7321	UB	1.18
20	10715.7	LB	0.035	70	8826.2	MB		86	7321.2	UB	2680
20	10716.5	LB	0.114	70	8826.3	MB		86	7323.6	UB	2720
20	10723	LB	1.77	70	8827.6	MB	0.01	86	7326.5	UB	10.9
20	10728.8	LB	625	70	8832.9	MB		86	7327	UB	4.96
20	10716.4	LB	0.024	70	8833.8	MB	0.012	86	7328.8-1	UB	20.6
20	10731.4	LB	0.261	70	8834.2	MB	0.044	86	7330	UB	3500
20	10714	LB	0.0137	70	8834.4	MB	0.095	86	7332	UB	2320
20	10712	LB	0.0903	70	8834.6	MB	313	86	7348.8	UB	33400
20	10687	MB	1.38	70	8835.2	MB	0.229	86	7351	UB	2980
20	10697.7	MB		70	8836.7	MB	1.87	86	7353	UB	0.175
20	10700	MB	0.204	70	8837	MB	0.025	86	7354	UB	0.12
20	10700	MB	0.114	70	8837.8	MB	0.093	86	7354.5	UB	2390
20	10705.9	MB	0.034	70	8838.5	MB	0.15	86	7401.9	MB	0.103
20	10683.5	MB	0.0241	70	8839.4	MB	74	86	7402.8	MB	0.39
20	10685.9	MB	11.2	70	8840.8	MB	0.132	86	7403	MB	0.267
20	10689.3	MB	1700	70	8841.4	MB	0.021	86	7404	MB	0.0973
20	10696	MB	6.03	70	8841.9	MB	0.093	86	7404.3	MB	15.6
20	10696.8	MB	30.6	70	8842.7	MB	0.0396	86	7405	MB	0.178
20	10704.7	MB	45	70	8845	MB	0.0671	86	7405.8	MB	0.046
20	10705.5	MB	0.606	70	8848.5	MB	0.015	86	7406	MB	0.0891
20	10712	LB	9.68	70	8843.8	MB	1.31	86	7407	MB	0.135
96	10422	LB		70	8850.3	LB	0.0478	86	7407.8	MB	0.027

96	10426.8	LB	7660	70	8849	MB	0.0601	86	7408.3	MB	0.0438
96	10431	LB	2630	70	8843	MB	0.0626	86	7409	MB	15.2
96	10432	LB		70	8845.6	MB	0.344	86	7409.8	MB	49.3
96	10436	LB	8020	70	8845.8	MB	0.0597	86	7410	MB	0.0729
96	10436-2	LB	1920	70	8848	MB	0.192	86	7445.1	LB	0.822
96	10437	LB	2000	70	8849.5	MB		86	7448	LB	1.46
96	10441.6	LB	2830	70	8849.9	MB	0.0578	86	7449	LB	2.25
96	10443	LB	26	70	8844.9	MB	0.224	86	7451	LB	96.9
96	10445	LB		70	8842.3	MB	0.299	86	7397	MB	0.15
96	10446	LB	25300	70	8843.4	MB	0.112	86	7379	MB	1.7
96	10449	LB		70	8846.2	MB	0.097	86	7374	MB	0.0465
96	10449-2	LB		70	8847.3	MB	0.0323	86	7355	MB	53.6
96	10452	LB	4120	70	8846.6	MB	0.0603	86	7355-2	MB	110
96	10456	LB	2159	70	8847.7	MB	0.0497	86	7393.5	MB	2.31
96	10456-2	LB	0.04	72	10487.5	UB		86	7363	MB	139
96	10456.5	LB	1270	72	10487.5(2)	UB	3340	86	7403.8	MB	0.0247
96	10460.5	LB	0.0593	72	10488	UB	6760	86	7393.1	LB	0.574
96	10463	LB	1680	72	10488.5	UB	6.79	86	7380	LB	0.228
96	10321	MB		72	10490	UB	12000	86	7370	LB	0.727
96	10336	MB	0.835	72	10491	UB		86	7373	LB	1.28
96	10341.5	MB		72	10491(2)	UB	42700	86	7355.9	LB	27.8
96	10348	MB	1.49	72	10492	UB		86	7389	LB	0.0648
96	10357.7	MB		72	10492(2)	UB	21900	86	7369	LB	1.48
96	10357.7	MB		72	10493	UB	1480	86	7374	LB	0.0051
96	10307.5	MB	0.896	72	10494	UB		86	7350	UB	0.0305
96	10310	MB	44	72	10497	UB	4660	18	8648.2	MB	3.6
96	10339	MB	8.01	72	10498	UB	5480	18	8650.6	MB	21.9
96	10347	MB	659	72	10499.8	UB	10300	18	8651.4	MB	9.4
96	10347.8	MB	173	72	10503	UB	0.001	18	8655	MB	0.27
96	10356.6	MB	984	72	10504	UB		18	8655.7	MB	1
96	10307	MB	0.253	72	10504(2)	UB	17800	18	8657.2	MB	0.4
96	10311	MB	0.868	72	10504.8	UB		18	8657.4	MB	0.3
96	10321.1	MB	0.183	72	10504.8(2)	UB	0.0169	18	8659.4	MB	1.46
96	10334.7	MB	1.42	72	10505.7	UB	27400	18	8660.7	MB	1.23
96	10345	MB	98.3	72	10509	UB	10200	18	8661.9	MB	1.08
2	10364	MB	1.8700	72	10512.7	MB	3230	18	8664.2	MB	0.11
2	10365	MB	0.3560	72	10514.5	MB	1250	18	8665	MB	
2	10367	MB	0.2220	72	10517.8	MB	0.371	18	8665.3	MB	
2	10367	MB	6310.0	13	11006	MB	1	18	8668	MB	0.6

2	10419	LB	0.0603	13	11008(V1)	MB		18	8669	MB	0.04
2	10368.5	MB	0.3710	13	11008(V2)	MB	4.68	18	8670.2	MB	0.0136
2	10369	MB	0.0835	13	11009	MB	4.02	18	8672	MB	0.0403
2	10369.8	MB	0.0098	13	11025V	MB	0.32	18	8673.2	MB	0.352
2	10370	MB	0.0267	13	11034(V1)	MB		18	8674	MB	0.695
2	10371	MB	0.0255	13	11034(V2)	MB		18	8677.4	LB	0.0838

8.3. Sonic Velocity

Sonic velocities of core plugs from 8 wells have been tested. Test results are listed in Table 8-4. More detail can be found in Attachments.

Table 8-4. Sonic velocities of core plugs tested in this study

ll #	Depth	Formation	Primary wave velocity	Secondary wave velocity	Well #	Depth	Formation	Primary wave velocity	Secondary wave velocity	Well #	Depth	Formation	Primary wave velocity	Secondary wave velocity
	(ft)		m/s	m/s		(ft)		m/s	m/s		(ft)		m/s	m/s
20	10673.6	UB	6227	3320	2	10371.8	MB	5256	3100	13	11035	MB	4877	3007
20	10678.3	UB	4603	2732	2	10372	MB	4737	2956	13	11004	UB	4974	3049
20	10682	UB	5192	3100	2	10373	MB	5402	3082	13	11006.8	MB	5299	3049
20	10729.5	LB	5155	2933	2	10374-13-1	MB	4878	3556	13	11007	MB	5733	3177
20	10732.3	LB	5221	3201	2	10374.1-13-2	MB	5460	3016	13	11008.5	MB	5126	2994
20	10727.2	LB	5934	3390	2	10375	MB	5216	2913	13	11012B	MB	4974	3058
20	10729.9	LB	5645	2716	2	10403-15-1	LB	4983	3013	13	11025H	MB	5395	3168
20	10733.3	LB	5197	2642	2	10403-15-2	LB	4949	2941	13	11031	MB	5256	3084
20	10731.4	LB	4585	3188	2	10412.8	LB	5376	3908	13	11033	MB	4797	2974
20	10726.9	LB	5169	3056	2	10415	LB		3500	86	7308.1	UB		
20	10728.1	LB	5542	3305	2	10416	LB			86	7313	UB	5802	3288
20	10718.7	LB	4655	2846	70	8823.8	MB	4907	2865	86	7320	UB	6392	3335
20	10729.1	LB	5294	3112	70	8824.7	MB	4857	2779	86	7321	UB	6125	3259
20	10715.7	LB	5321	3193	70	8826.2	MB			86	7321.2	UB	6125	3245
20	10716.5	LB	5419	3347	70	8826.3	MB	5132	3055	86	7323.6	UB	5515	3133
20	10723	LB	5857	3343	70	8827.6	MB	5143	3157	86	7326.5	UB	6221	3216
20	10728.8	LB	5079	2733	70	8832.9	MB			86	7327	UB	6306	3245
20	10716.4	LB	4705	3074	70	8833.8	MB	4943	2975	86	7328.8-1	UB	5706	3122
20	10731.4	LB	4480	2850	70	8834.2	MB	4869	2841	86	7330	UB	5775	3130
20	10714	LB	5200	3083	70	8834.4	MB	4879	2830	86	7332	UB	6414	3717
20	10712	LB	4846	2848	70	8834.6	MB	5073	3025	86	7348.8	UB	5369	3075
20	10687	MB	5286	3169	70	8835.2	MB	4874	2903	86	7351	UB	5365	3058
20	10697.7	MB			70	8836.7	MB	4841	2981	86	7353	UB	5406	3127

20	10700	MB	5018	3086	70	8837	MB	4995	2875	86	7354	UB	5281	3196
20	10700	MB	4880	2992	70	8837.8	MB	4923	3124	86	7354.5	UB	5110	3052
20	10705.9	MB	4799	2923	70	8838.5	MB	4784	2847	86	7401.9	MB	5400	3179
20	10683.5	MB	5934	3215	70	8839.4	MB	4723	2889	86	7402.8	MB	5117	3171
20	10685.9	MB	5303	3189	70	8840.8	MB	4560	2705	86	7403	MB	5280	3109
20	10689.3	MB	5565	3214	70	8841.4	MB	4937	3010	86	7404	MB	5118	3076
20	10696	MB	5347	3050	70	8841.9	MB	4449	2796	86	7404.3	MB	5032	3101.5
20	10696.8	MB	5415	3138	70	8842.7	MB	4643	2918	86	7405	MB	5153	3180
20	10704.7	MB	5226	3066	70	8845	MB	4567	2890	86	7405.8	MB	5166	3062
20	10705.5	MB	5106	3008	70	8848.5	MB	4685	2928	86	7406	MB	5321	3204
20	10712	LB	5290	3155	70	8843.8	MB	4699	2963	86	7407	MB	5158	3098
96	10422	LB	5771	3420	70	8850.3	LB	4456	2835	86	7407.8	MB	5414	3120
96	10426.8	LB	5232	3030	70	8849	MB	4563	2911	86	7408.3	MB	5426	3169
96	10431	LB	5303	3046	70	8843	MB	5015	3035	86	7409	MB	5179	3074
96	10432	LB	4942	2830	70	8845.6	MB	4978	3017	86	7409.8	MB	5111	3070
96	10436	LB	5618	3540	70	8845.8	MB	5025	3050	86	7410	MB	5337	3020
96	10436-2	LB	5638	3210	70	8848	MB	5031	3051	86	7445.1	LB	5223	2937
96	10437	LB	5261	2940	70	8849.5	MB	4988	3033	86	7448	LB	6101	3480
96	10441.6	LB	4231	2550	70	8849.9	MB	5004	3044	86	7449	LB	5927	3453
96	10443	LB	5679	3170	70	8844.9	MB	4955	2947	86	7451	LB	5291	3107
96	10445	LB	5845		70	8842.3	MB	4897	2970	86	7397	MB	4557	2972
96	10446	LB			70	8843.4	MB	4746	2933	86	7379	MB	4360	2929
96	10449	LB	4898	2725	70	8846.2	MB	4777	2970	86	7374	MB	4443	2881
96	10449-2	LB			70	8847.3	MB	4847	2973	86	7355	MB	4328	2852
96	10452	LB	5219	3125	70	8846.6	MB	4795	2971	86	7355-2	MB	4673	2950
96	10456	LB	4879	3012	70	8847.7	MB	4814	2988	86	7393.5	MB	4537	2967
96	10456-2	LB	4396	2790	72	10487.5	UB	4856	3050	86	7363	MB	4224	2797
96	10456.5	LB	4639	2940	72	10487.5(2)	UB	4856	3050	86	7403.8	MB	4939	3077
96	10460.5	LB	4773	2810	72	10488	UB	5187	2940	86	7393.1	LB	4936	3097
96	10463	LB	4942	2850	72	10488.5	UB	5105	3095	86	7380	LB	4809	3020
96	10321	MB	4673	2926	72	10490	UB	5055	3000	86	7370	LB	5350	3018
96	10336	MB	4497	2881	72	10491	UB	5025	3065	86	7373	LB	4694	2983
96	10341.5	MB	4531	2853	72	10491(2)	UB	5025	3065	86	7355.9	LB	4690	2926
96	10348	MB	4349	2809	72	10492	UB	5199	3040	86	7389	LB	4926	3087
96	10357.7	MB			72	10492(2)	UB	5199	3040	86	7369	LB	4880	2909
96	10357.7	MB			72	10493	UB	5273	3060	86	7374	LB	4736	2901
96	10307.5	MB	5152	2947	72	10494	UB	5291	4600	86	7350	UB	4873	3012
96	10310	MB			72	10497	UB	5019	3040	18	8648.2	MB	4635	2888
96	10339	MB	4702	2964	72	10498	UB	4791	3020	18	8650.6	MB	4764	2813

96	10347	MB	4693	2813	72	10499.8	UB	4926	2930	18	8651.4	MB	4541	2738
96	10347.8	MB	4700	2836	72	10503	UB	5269	3140	18	8655	MB	4700	2928
96	10356.6	MB	4568	2815	72	10504	UB	5065	3140	18	8655.7	MB	4782	2952
96	10307	MB	4914	3022	72	10504(2)	UB	5065	3140	18	8657.2	MB	5013	2983
96	10311	MB	4695	2864	72	10504.8	UB	5068	2960	18	8657.4	MB	4973	3014
96	10321.1	MB	5078	3047	72	10504.8(2)	UB	5068	2960	18	8659.4	MB	4812	2923
96	10334.7	MB	4477	2847	72	10505.7	UB	5055	2920	18	8660.7	MB	4725	2850
96	10345	MB	4530	2823	72	10509	UB	5190	3020	18	8661.9	MB	4836	2882
2	10364	MB	5232	3572	72	10512.7	MB	4911	3015	18	8664.2	MB	4232	2746
2	10365	MB	4806	2998	72	10514.5	MB	4995	3060	18	8665	MB	4656	2444
2	10367	MB	4711	3230	72	10517.8	MB	5395	3165	18	8665.3	MB	4676	2912
2	10367	MB	5012	3098	13	11006	MB	4858	2968	18	8668	MB	5336	3070
2	10419	LB	5332	3167	13	11008(V1)	MB	5176	3045	18	8669	MB	4879	2902
2	10368.5	MB	4687	2929	13	11008(V2)	MB	5596	3128	18	8670.2	MB	5412	3232
2	10369	MB	5046	2988	13	11009	MB	5099	2961	18	8672	MB	5122	3085
2	10369.8	MB	5236	3078	13	11025V	MB	5098	3075	18	8673.2	MB	5031	3085
2	10370	MB	4752	2962	13	11034(V1)	MB			18	8674	MB	5071	3080
2	10371	MB	4805	2966	13	11034(V2)	MB	4698	2954	18	8677.4	LB	4753	3002

8.4. Dynamic Young's Modulus and Poisson's Ratio

Dynamic Young's modulus and Poisson's ratio of core plugs calculated from sonic velocity are shown in Table 8-5. More detail can be found in Attachments.

Table 8-5. Dynamic Young's modulus and Poisson's ratio of core plugs calculated from sonic velocity

ll #	Depth	Formation	Dynamic Young's Modulus	Dynamic Poisson's Ratio	Well #	Depth	Formation	Dynamic Young's Modulus	Dynamic Poisson's Ratio	Well #	Depth	Formation	Dynamic Young's Modulus	Dynamic Poisson's Ratio
	(ft)		GPa	fraction		(ft)		GPa	fraction		(ft)		GPa	fraction
20	10673.6	UB	76.31	0.301	2	10371.8	MB	61.19	0.233	13	11035	MB	56.53	0.193
20	10678.3	UB	43.26	0.228	2	10372	MB	52.91	0.181	13	11004	UB	57.35	0.199
20	10682	UB	61.12	0.223	2	10373	MB	62.91	0.259	13	11006.8	MB	60.67	0.253
20	10729.5	LB	55.02	0.261	2	10374-13-1	MB	61.00	-0.067	13	11007	MB	68.75	0.278
20	10732.3	LB	64.71	0.199	2	10374.1-13-2	MB	61.30	0.280	13	11008.5	MB	57.81	0.241
20	10727.2	LB	76.85	0.258	2	10375	MB	55.80	0.273	13	11012B	MB	58.47	0.196
20	10729.9	LB	52.31	0.349	2	10403-15-1	LB	54.94	0.212	13	11025H	MB	65.94	0.237
20	10733.3	LB	48.48	0.326	2	10403-15-2	LB	52.29	0.227	13	11031	MB	61.19	0.237
20	10731.4	LB	54.53	0.032	2	10412.8	LB	73.37	-0.060	13	11033	MB	53.59	0.188
20	10726.9	LB	60.42	0.231	2	10415	LB	131.68	1.000	86	7308.1	UB		
20	10728.1	LB	70.65	0.224	2	10416	LB			86	7313	UB	72.15	0.263

20	10718.7	LB	50.35	0.202	70	8823.8	MB	52.52	0.241	86	7320	UB	78.19	0.313
20	10729.1	LB	62.96	0.236	70	8824.7	MB	49.99	0.257	86	7321	UB	74.17	0.303
20	10715.7	LB	65.87	0.219	70	8826.2	MB			86	7321.2	UB	73.40	0.305
20	10716.5	LB	70.69	0.192	70	8826.3	MB	59.86	0.226	86	7323.6	UB	64.45	0.262
20	10723	LB	74.88	0.258	70	8827.6	MB	62.55	0.198	86	7326.5	UB	72.49	0.318
20	10728.8	LB	49.97	0.296	70	8832.9	MB			86	7327	UB	73.95	0.320
20	10716.4	LB	55.28	0.128	70	8833.8	MB	55.61	0.216	86	7328.8-1	UB	66.60	0.286
20	10731.4	LB	48.31	0.160	70	8834.2	MB	51.99	0.242	86	7330	UB	65.57	0.292
20	10714	LB	61.46	0.229	70	8834.4	MB	51.58	0.246	86	7332	UB	89.26	0.247
20	10712	LB	53.06	0.236	70	8834.6	MB	58.20	0.224	86	7348.8	UB	61.53	0.256
20	10687	MB	63.56	0.219	70	8835.2	MB	53.04	0.225	86	7351	UB	60.94	0.259
20	10697.7	MB			70	8836.7	MB	54.80	0.195	86	7353	UB	64.21	0.249
20	10700	MB	59.91	0.196	70	8837	MB	53.81	0.252	86	7354	UB	64.27	0.211
20	10700	MB	56.16	0.199	70	8837.8	MB	56.99	0.163	86	7354.5	UB	58.26	0.223
20	10705.9	MB	54.10	0.205	70	8838.5	MB	50.68	0.226	86	7401.9	MB	66.27	0.235
20	10683.5	MB	71.52	0.292	70	8839.4	MB	50.88	0.201	86	7402.8	MB	61.98	0.188
20	10685.9	MB	65.09	0.217	70	8840.8	MB	45.29	0.229	86	7403	MB	61.90	0.235
20	10689.3	MB	65.36	0.250	70	8841.4	MB	56.79	0.204	86	7404	MB	59.66	0.217
20	10696	MB	61.68	0.259	70	8841.9	MB	46.72	0.174	86	7404.3	MB	59.42	0.194
20	10696.8	MB	64.15	0.247	70	8842.7	MB	51.56	0.174	86	7405	MB	62.80	0.192
20	10704.7	MB	61.04	0.238	70	8845	MB	50.03	0.166	86	7405.8	MB	59.85	0.229
20	10705.5	MB	58.70	0.234	70	8848.5	MB	52.22	0.180	86	7406	MB	65.02	0.216
20	10712	LB	64.89	0.224	70	8843.8	MB	53.35	0.170	86	7407	MB	61.44	0.218
96	10422	LB	75.75	0.229	70	8850.3	LB	47.00	0.160	86	7407.8	MB	64.43	0.251
96	10426.8	LB	59.40	0.248	70	8849	MB	50.42	0.157	86	7408.3	MB	65.03	0.241
96	10431	LB	59.77	0.254	70	8843	MB	57.89	0.211	86	7409	MB	60.01	0.228
96	10432	LB	51.82	0.256	70	8845.6	MB	56.72	0.210	86	7409.8	MB	59.78	0.218
96	10436	LB	75.75	0.171	70	8845.8	MB	58.20	0.208	86	7410	MB	60.96	0.264
96	10436-2	LB	67.90	0.260	70	8848	MB	58.16	0.209	86	7445.1	LB	56.98	0.269
96	10437	LB	56.90	0.273	70	8849.5	MB	56.96	0.207	86	7448	LB	81.01	0.259
96	10441.6	LB	40.62	0.215	70	8849.9	MB	57.28	0.206	86	7449	LB	77.90	0.243
96	10443	LB	67.13	0.274	70	8844.9	MB	55.43	0.226	86	7451	LB	58.29	0.237
96	10445	LB			70	8842.3	MB	55.22	0.209	86	7397	MB	51.12	0.130
96	10446	LB			70	8843.4	MB	52.64	0.191	86	7379	MB	47.64	0.089
96	10449	LB	48.26	0.276	70	8846.2	MB	53.92	0.185	86	7374	MB	47.83	0.137
96	10449-2	LB			70	8847.3	MB	54.82	0.198	86	7355	MB	45.47	0.116
96	10452	LB	62.11	0.221	70	8846.6	MB	54.03	0.188	86	7355-2	MB	51.90	0.169
96	10456	LB	55.07	0.192	70	8847.7	MB	54.64	0.187	86	7393.5	MB	50.97	0.126
96	10456-	LB	46.29	0.163	72	10487.5	UB	55.32	0.174	86	7363	MB	43.45	0.110

	2													
96	10456.5	LB	50.45	0.164	72	10487.5(2)	UB	55.47	0.174	86	7403.8	MB	59.16	0.183
96	10460.5	LB	49.16	0.235	72	10488	UB	55.65	0.263	86	7393.1	LB	57.78	0.175
96	10463	LB	51.78	0.251	72	10488.5	UB	59.40	0.209	86	7380	LB	54.71	0.174
96	10321	MB	53.04	0.178	72	10490	UB	55.65	0.228	86	7370	LB	61.20	0.267
96	10336	MB	48.03	0.152	72	10491	UB	57.04	0.204	86	7373	LB	52.86	0.161
96	10341.5	MB	48.43	0.172	72	10491(2)	UB	57.24	0.204	86	7355.9	LB	50.97	0.181
96	10348	MB	45.81	0.142	72	10492	UB	60.94	0.240	86	7389	LB	57.63	0.177
96	10357.7	MB			72	10492(2)	UB	61.12	0.240	86	7369	LB	54.69	0.224
96	10357.7	MB			72	10493	UB	58.89	0.246	86	7374	LB	51.23	0.200
96	10307.5	MB	57.27	0.257	72	10494	UB	-5.30	-1.048	86	7350	UB	55.28	0.191
96	10310	MB			72	10497	UB	55.92	0.210	18	8648.2	MB	49.88	0.183
96	10339	MB	51.62	0.170	72	10498	UB	52.83	0.170	18	8650.6	MB	49.41	0.232
96	10347	MB	48.57	0.220	72	10499.8	UB	52.73	0.226	18	8651.4	MB	46.11	0.214
96	10347.8	MB	49.40	0.214	72	10503	UB	62.94	0.225	18	8655	MB	51.42	0.183
96	10356.6	MB	47.66	0.194	72	10504	UB	59.65	0.188	18	8655.7	MB	52.61	0.192
96	10307	MB	57.77	0.196	72	10504(2)	UB	59.20	0.188	18	8657.2	MB	55.93	0.226
96	10311	MB	51.51	0.204	72	10504.8	UB	55.06	0.241	18	8657.4	MB	56.06	0.210
96	10321.1	MB	59.82	0.219	72	10504.8(2)	UB	54.96	0.241	18	8659.4	MB	52.55	0.208
96	10334.7	MB	47.28	0.161	72	10505.7	UB	53.68	0.250	18	8660.7	MB	50.09	0.214
96	10345	MB	47.70	0.183	72	10509	UB	58.26	0.244	18	8661.9	MB	51.54	0.225
2	10364	MB	70.69	0.063	72	10512.7	MB	54.42	0.198	18	8664.2	MB	43.33	0.136
2	10365	MB	54.36	0.181	72	10514.5	MB	56.53	0.200	18	8665	MB	40.05	0.310
2	10367	MB	56.63	0.056	72	10517.8	MB	64.69	0.238	18	8665.3	MB	51.83	0.183
2	10367	MB	57.87	0.191	13	11006	MB	54.71	0.202	18	8668	MB	60.08	0.253
2	10419	LB	63.33	0.227	13	11008(V1)	MB	60.10	0.235	18	8669	MB	53.37	0.226
2	10368.5	MB	51.39	0.180	13	11008(V2)	MB	66.15	0.273	18	8670.2	MB	67.32	0.223
2	10369	MB	57.25	0.230	13	11009	MB	57.08	0.246	18	8672	MB	59.63	0.215
2	10369.8	MB	60.73	0.236	13	11025V	MB	60.62	0.214	18	8673.2	MB	59.10	0.199
2	10370	MB	53.13	0.182	13	11034(V1)	MB			18	8674	MB	58.92	0.208
2	10371	MB	54.03	0.192	13	11034(V2)	MB	52.55	0.173	18	8677.4	LB	52.80	0.168

8.5. Static Young's Modulus and Poisson's Ratio

Static Young's modulus and Poisson's ratio of core plugs are measured through non-destructive strength test. The measurement results are shown in Table 8-6. More detail can be found in Attachments.

Table 8-6. Static Young's modulus and Poisson's ratio of core plugs measured by non-destructive strength test.

Well #	Depth	Formation	Static Young's Modulus	Static Poisson's Ratio	Well #	Depth	Formation	Static Young's Modulus	Static Poisson's Ratio	Well #	Depth	Formation	Static Young's Modulus	Static Poisson's Ratio

	(ft)		GPa	fraction		(ft)		GPa	fraction		(ft)		GPa	fraction
20	10673.6	UB	172.3	0.393	2	10371.8	MB	99.58	0.061	13	11035	MB		
20	10678.3	UB	41.62	0.178	2	10372	MB	106.28	0.015	13	11004	UB		
20	10682	UB	81.97	0.09	2	10373	MB	100.1	0.28	13	11006.8	MB	85.31	0.336
20	10729.5	LB	76.7	0.298	2	10374-13-1	MB	66.97	0.163	13	11007	MB	64.46	0.243
20	10732.3	LB	124.93	0.377	2	10374.1-13-2	MB	82.52	0.255	13	11008.5	MB	55.5	0.238
20	10727.2	LB	159.63	0.464	2	10375	MB	208.88		13	11012B	MB	56.41	0.172
20	10729.9	LB	79.41	0.254	2	10403-15-1	LB	167.75	0.317	13	11025H	MB	62.22	0.221
20	10733.3	LB	67.35	0.267	2	10403-15-2	LB	36.2	0.05	13	11031	MB	64.16	0.118
20	10731.4	LB	32.76	0.413	2	10412.8	LB			13	11033	MB	40.69	0.135
20	10726.9	LB	89.46	0.033	2	10415	LB			86	7308.1	UB		
20	10728.1	LB	87.14	0.199	2	10416	LB	187.51	0.347	86	7313	UB	78.5	0.26
20	10718.7	LB	62.62	0.241	70	8823.8	MB	81.44	0.112	86	7320	UB	68.34	0.324
20	10729.1	LB	74.76	0.15	70	8824.7	MB	79.64	0.022	86	7321	UB	100.68	0.289
20	10715.7	LB	72.55	0.169	70	8826.2	MB			86	7321.2	UB	83.29	0.299
20	10716.5	LB	79.46	0.233	70	8826.3	MB			86	7323.6	UB	84.78	0.299
20	10723	LB	82.69	0.136	70	8827.6	MB	100.73	0.289	86	7326.5	UB	94.4	0.321
20	10728.8	LB	37.61	0.484	70	8832.9	MB			86	7327	UB	75	0.255
20	10716.4	LB	46.63	0.168	70	8833.8	MB	83.39	0.183	86	7328.8-1	UB	89	0.26
20	10731.4	LB	70.88	0.116	70	8834.2	MB	62.63	0.2	86	7330	UB	80.6	0.229
20	10714	LB	82.22	0.362	70	8834.4	MB	42.86	0.24	86	7332	UB	159	0.628
20	10712	LB	106.54	0.387	70	8834.6	MB	87.87	0.214	86	7348.8	UB	76.43	0.192
20	10687	MB	50.58	0.113	70	8835.2	MB	68.07	0.24	86	7351	UB	72.2	0.205
20	10697.7	MB			70	8836.7	MB	72.62	0.202	86	7353	UB	65	0.186
20	10700	MB	82.36	0.238	70	8837	MB	88.38	0.309	86	7354	UB	80.1	0.106
20	10700	MB	68.98	0.194	70	8837.8	MB	653	0.486	86	7354.5	UB	63.5	0.148
20	10705.9	MB	54.57	0.177	70	8838.5	MB	36.36	0.205	86	7401.9	MB	45.71	0.49
20	10683.5	MB	75.57	0.234	70	8839.4	MB	76.4	0.294	86	7402.8	MB	51.75	0.19
20	10685.9	MB	82.14	0.148	70	8840.8	MB	70.19	0.096	86	7403	MB	124.59	0.19
20	10689.3	MB	88.4	0.258	70	8841.4	MB	97.85	0.13	86	7404	MB	53.77	0.155
20	10696	MB	63.58	0.209	70	8841.9	MB	78.88	0.247	86	7404.3	MB	63.4	0.167
20	10696.8	MB	63.53	0.189	70	8842.7	MB	59.4	0.183	86	7405	MB	143.56	0.167
20	10704.7	MB	78.33	0.129	70	8845	MB	53.97	0.186	86	7405.8	MB	122.65	0.167
20	10705.5	MB	69.12	0.181	70	8848.5	MB	58.89	0.162	86	7406	MB	83.86	0.167
20	10712	LB	67.31	0.16	70	8843.8	MB	53.78	0.142	86	7407	MB	113.8	0.418
96	10422	LB		-	70	8850.3	LB	49.08	0.156	86	7407.8	MB	45.25	0.418
96	10426.8	LB	106	0.129	70	8849	MB	50.07	0.15	86	7408.3	MB	42.3	0.304
96	10431	LB	49	0.181	70	8843	MB	75.16	0.11	86	7409	MB	116.86	0.334

96	10432	LB		-	70	8845.6	MB	62.04	0.303	86	7409.8	MB	69.09	0.157
96	10436	LB	114.5	0.255	70	8845.8	MB	81.72	0.126	86	7410	MB	64.7	0.22
96	10436-2	LB	60	0.227	70	8848	MB			86	7445.1	LB	49.5	0.08
96	10437	LB	86	0.23	70	8849.5	MB			86	7448	LB	219.23	0.232
96	10441.6	LB	67	0.19	70	8849.9	MB	57.2	0.197	86	7449	LB	70.96	0.232
96	10443	LB	74.2	0.289	70	8844.9	MB	67.87	0.225	86	7451	LB	76.89	0.232
96	10445	LB			70	8842.3	MB	63.54	0.165	86	7397	MB	73.5	0.249
96	10446	LB			70	8843.4	MB	57.2	0.162	86	7379	MB	53.89	0.186
96	10449	LB	54.7	0.463	70	8846.2	MB	55.49	0.151	86	7374	MB	46.39	0.166
96	10449-2	LB			70	8847.3	MB	61.09	0.215	86	7355	MB	54.1	0.162
96	10452	LB	185	0.465	70	8846.6	MB	79.47	0.27	86	7355-2	MB	34.71	0.174
96	10456	LB	54	0.18	70	8847.7	MB	59.5	0.184	86	7393.5	MB	52.36	0.183
96	10456-2	LB	80	0.16	72	10487.5	UB			86	7363	MB	45.03	0.112
96	10456.5	LB	52	0.348	72	10487.5(2)	UB	63	0.15	86	7403.8	MB	61.9	0.204
96	10460.5	LB	88	0.06	72	10488	UB	87	0.1	86	7393.1	LB	56.78	0.169
96	10463	LB	73.7	0.02	72	10488.5	UB	109.35	0.097	86	7380	LB	52.73	0.219
96	10321	MB	50.84	0.194	72	10490	UB	48.27	0.034	86	7370	LB	56.77	0.263
96	10336	MB	39.58	0.155	72	10491	UB			86	7373	LB	51.94	0.149
96	10341.5	MB			72	10491(2)	UB	87	0.403	86	7355.9	LB	67.29	0.13
96	10348	MB	38.99	0.15	72	10492	UB			86	7389	LB	58.56	0.139
96	10357.7	MB			72	10492(2)	UB	67	0.19	86	7369	LB	67.09	0.271
96	10357.7	MB			72	10493	UB	62.56	0.253	86	7374	LB	51.96	0.181
96	10307.5	MB	62.38	0.208	72	10494	UB			86	7350	UB	73.86	0.281
96	10310	MB	49.13	0.118	72	10497	UB	47.2	0.15	18	8648.2	MB	52	0.33
96	10339	MB	48.68	0.167	72	10498	UB	54	0.25	18	8650.6	MB	68.44	0.27
96	10347	MB	55	0.147	72	10499.8	UB			18	8651.4	MB	53.26	0.169
96	10347.8	MB	44.42	0.188	72	10503	UB	75.5	0.12	18	8655	MB	59.66	0.182
96	10356.6	MB	50.15	0.169	72	10504	UB			18	8655.7	MB	106.84	0.39
96	10307	MB	59.15	0.205	72	10504(2)	UB	60	0.3	18	8657.2	MB	42.33	0.02
96	10311	MB	52.67	0.22	72	10504.8	UB			18	8657.4	MB	78.83	0.159
96	10321.1	MB	63.29	0.224	72	10504.8(2)	UB	68	0.195	18	8659.4	MB	124.5	0.109
96	10334.7	MB	47.77	0.165	72	10505.7	UB	52.68	0.23	18	8660.7	MB	40.93	0.326
96	10345	MB	51.75	0.209	72	10509	UB	59	0.256	18	8661.9	MB	65.75	0.104
2	10364	MB	59.11	0.235	72	10512.7	MB	54.1	0.44	18	8664.2	MB	66.36	0.233
2	10365	MB	48.15	0.175	72	10514.5	MB	35.03	0.05	18	8665	MB		
2	10367	MB	68.11	0.167	72	10517.8	MB	48.7	0.07	18	8665.3	MB		
2	10367	MB	43.36	0.165	13	11006	MB	50.72	0.15	18	8668	MB	70.94	0.179
2	10419	LB	60.18	0.182	13	11008(V1)	MB	58.13	0.22	18	8669	MB	52.24	0.167
2	10368.5	MB	48.73	0.154	13	11008(V2)	MB	69.06	0.245	18	8670.2	MB	64.42	0.14

2	10369	MB	72.07	0.174	13	11009	MB	58.1	0.232	18	8672	MB	42.02	0.404
2	10369.8	MB	39.86	0.03	13	11025V	MB			18	8673.2	MB	84.93	0.33
2	10370	MB	54.91	0.003	13	11034(V1)	MB			18	8674	MB	65.64	0.306
2	10371	MB	71.28	0.225	13	11034(V2)	MB	30.6	0.128	18	8677.4	LB	106.89	0.004

8.6. Biot's Coefficient

Biot's coefficients of core plugs from 8 wells have been tested. Test results are listed in Table 8-7. More detail can be found in Attachments.

Table 8-7. Biot's coefficients of core plugs tested in this study

Well #	Depth	Formation	Biot's coefficients	Well #	Depth	Formation	Biot's coefficients	Well #	Depth	Formation	Biot's coefficients
	(ft)		fraction		(ft)		fraction		(ft)		fraction
20	10673.6	UB		2	10371.8	MB	0.7303	13	11035	MB	
20	10678.3	UB		2	10372	MB	0.7107	13	11004	UB	
20	10682	UB		2	10373	MB	0.654	13	11006.8	MB	0.674
20	10729.5	LB	0.7383	2	10374-13-1	MB	0.65	13	11007	MB	0.4173
20	10732.3	LB	0.4019	2	10374.1-13-2	MB	0.6996	13	11008.5	MB	
20	10727.2	LB	0.5732	2	10375	MB	0.7068	13	11012B	MB	0.703
20	10729.9	LB	0.65	2	10403-15-1	LB	0.6647	13	11025H	MB	
20	10733.3	LB	0.8312	2	10403-15-2	LB		13	11031	MB	
20	10731.4	LB	0.4141	2	10412.8	LB		13	11033	MB	
20	10726.9	LB	0.7703	2	10415	LB		86	7308.1	UB	
20	10728.1	LB	0.5469	2	10416	LB	0.91	86	7313	UB	
20	10718.7	LB	0.584	70	8823.8	MB	0.42	86	7320	UB	0.329
20	10729.1	LB	0.7838	70	8824.7	MB	0.53	86	7321	UB	0.374
20	10715.7	LB	0.3061	70	8826.2	MB		86	7321.2	UB	0.393
20	10716.5	LB	0.6586	70	8826.3	MB		86	7323.6	UB	0.8
20	10723	LB	0.8713	70	8827.6	MB	0.41	86	7326.5	UB	0.317
20	10728.8	LB	0.6378	70	8832.9	MB		86	7327	UB	0.03
20	10716.4	LB	0.5455	70	8833.8	MB	0.593	86	7328.8-1	UB	0.709
20	10731.4	LB		70	8834.2	MB	0.81	86	7330	UB	
20	10714	LB	0.9013	70	8834.4	MB	0.29	86	7332	UB	
20	10712	LB	0.8496	70	8834.6	MB	0.96	86	7348.8	UB	0.645
20	10687	MB	0.441	70	8835.2	MB	0.73	86	7351	UB	0.76
20	10697.7	MB		70	8836.7	MB		86	7353	UB	0.718
20	10700	MB	0.6112	70	8837	MB	0.72	86	7354	UB	0.707
20	10700	MB	0.5853	70	8837.8	MB	0.67	86	7354.5	UB	0.846
20	10705.9	MB		70	8838.5	MB	0.79	86	7401.9	MB	0.514
20	10683.5	MB	0.315	70	8839.4	MB	0.83	86	7402.8	MB	0.612

20	10685.9	MB	0.5086	70	8840.8	MB	0.779	86	7403	MB	0.614
20	10689.3	MB	0.664	70	8841.4	MB	0.79	86	7404	MB	0.609
20	10696	MB	0.7968	70	8841.9	MB	0.66	86	7404.3	MB	0.73
20	10696.8	MB	0.745	70	8842.7	MB	0.6518	86	7405	MB	0.971
20	10704.7	MB	0.5184	70	8845	MB	0.6617	86	7405.8	MB	0.614
20	10705.5	MB	0.583	70	8848.5	MB		86	7406	MB	0.526
20	10712	LB	0.62	70	8843.8	MB	0.517	86	7407	MB	0.697
96	10422	LB	-	70	8850.3	LB	0.597	86	7407.8	MB	0.653
96	10426.8	LB		70	8849	MB	0.57	86	7408.3	MB	0.611
96	10431	LB		70	8843	MB	0.587	86	7409	MB	0.67
96	10432	LB	-	70	8845.6	MB	0.669	86	7409.8	MB	0.568
96	10436	LB	0.837	70	8845.8	MB	0.6835	86	7410	MB	0.691
96	10436-2	LB		70	8848	MB	0.505	86	7445.1	LB	0.828
96	10437	LB		70	8849.5	MB		86	7448	LB	0.701
96	10441.6	LB		70	8849.9	MB	0.661	86	7449	LB	0.751
96	10443	LB	0.759	70	8844.9	MB	0.704	86	7451	LB	0.789
96	10445	LB		70	8842.3	MB	0.507	86	7397	MB	0.6125
96	10446	LB		70	8843.4	MB	0.648	86	7379	MB	0.625
96	10449	LB		70	8846.2	MB	0.641	86	7374	MB	
96	10449-2	LB		70	8847.3	MB	0.73	86	7355	MB	0.6561
96	10452	LB		70	8846.6	MB	0.6949	86	7355-2	MB	0.63
96	10456	LB		70	8847.7	MB	0.6057	86	7393.5	MB	0.585
96	10456-2	LB	0.692	72	10487.5	UB		86	7363	MB	
96	10456.5	LB		72	10487.5(2)	UB		86	7403.8	MB	0.507
96	10460.5	LB	0.326	72	10488	UB		86	7393.1	LB	0.68
96	10463	LB		72	10488.5	UB		86	7380	LB	0.699
96	10321	MB		72	10490	UB		86	7370	LB	0.688
96	10336	MB		72	10491	UB		86	7373	LB	0.678
96	10341.5	MB	0.743	72	10491(2)	UB		86	7355.9	LB	0.6886
96	10348	MB	0.58	72	10492	UB		86	7389	LB	0.665
96	10357.7	MB		72	10492(2)	UB		86	7369	LB	0.8252
96	10357.7	MB		72	10493	UB		86	7374	LB	
96	10307.5	MB	0.669	72	10494	UB		86	7350	UB	
96	10310	MB	0.743	72	10497	UB		18	8648.2	MB	0.7
96	10339	MB	0.754	72	10498	UB		18	8650.6	MB	0.81
96	10347	MB	0.759	72	10499.8	UB		18	8651.4	MB	0.8
96	10347.8	MB	0.805	72	10503	UB		18	8655	MB	0.85
96	10356.6	MB	0.818	72	10504	UB		18	8655.7	MB	0.73
96	10307	MB	0.668	72	10504(2)	UB		18	8657.2	MB	0.7

96	10311	MB	0.622	72	10504.8	UB		18	8657.4	MB	0.69
96	10321.1	MB	0.701	72	10504.8(2)	UB		18	8659.4	MB	0.74
96	10334.7	MB	0.576	72	10505.7	UB		18	8660.7	MB	0.78
96	10345	MB	0.703	72	10509	UB		18	8661.9	MB	0.78
2	10364	MB	-	72	10512.7	MB		18	8664.2	MB	0.09
2	10365	MB	0.585	72	10514.5	MB		18	8665	MB	
2	10367	MB	0.7273	72	10517.8	MB		18	8665.3	MB	
2	10367	MB	0.6481	13	11006	MB		18	8668	MB	
2	10419	LB	0.6211	13	11008(V1)	MB		18	8669	MB	0.85
2	10368.5	MB	0.6168	13	11008(V2)	MB	0.4231	18	8670.2	MB	
2	10369	MB	0.7221	13	11009	MB	0.6492	18	8672	MB	0.8713
2	10369.8	MB	0.6226	13	11025V	MB		18	8673.2	MB	0.7582
2	10370	MB		13	11034(V1)	MB		18	8674	MB	0.6298
2	10371	MB	0.6749	13	11034(V2)	MB		18	8677.4	LB	

8.7. Rock Strength (Uni/Triaxial Destructive Test)

Rock strength are measured through uni/triaxial destructive test. The measurement results are shown in Table 8-8. More detail can be found in Attachments.

Table 8-8. Rock strength by uni/triaxial destructive test.

Well #	Depth	Formation	Uni/Triaxial Peak Stress (Destructive test)	Confining pressure	Well #	Depth	Formation	Uni/Triaxial Peak Stress (Destructive test)	Confining pressure	Well #	Depth	Formation	Uni/Triaxial Peak Stress (Destructive test)	Confining pressure
	(ft)		Mpa	Mpa		(ft)		Mpa	Mpa		(ft)		Mpa	Mpa
20	10673.6	UB			2	10371.8	MB	146	0	13	11035	MB		
20	10678.3	UB			2	10372	MB	109.8	10.1	13	11004	UB		
20	10682	UB			2	10373	MB	54.3	19.1	13	11006.8	MB	159.1	0
20	10729.5	LB	156.3	20	2	10374-13-1	MB			13	11007	MB	232.3	20.3
20	10732.3	LB	123	10.2	2	10374.1-13-2	MB			13	11008.5	MB		
20	10727.2	LB	140.1	0	2	10375	MB			13	11012B	MB	106.6	0
20	10729.9	LB	103.8	20.2	2	10403-15-1	LB			13	11025H	MB		
20	10733.3	LB	125.5	10.2	2	10403-15-2	LB			13	11031	MB	149.9	11.3
20	10731.4	LB	27.4	0	2	10412.8	LB			13	11033	MB		
20	10726.9	LB			2	10415	LB			86	7308.1	UB		
20	10728.1	LB			2	10416	LB			86	7313	UB		
20	10718.7	LB	125.1	20.1	70	8823.8	MB	178.9	16	86	7320	UB	53	12.9
20	10729.1	LB			70	8824.7	MB	195.5	8	86	7321	UB	64.5	6.1
20	10715.7	LB			70	8826.2	MB			86	7321.2	UB	111.5	0
20	10716.5	LB			70	8826.3	MB			86	7323.6	UB	79.4	13.2
20	10723	LB			70	8827.6	MB	92.7	0	86	7326.5	UB	105.9	6.2

20	10728.8	LB			70	8832.9	MB			86	7327	UB	21.4	0
20	10716.4	LB	100.4	10.2	70	8833.8	MB	176.3	16	86	7328.8-1	UB	171.6	13.1
20	10731.4	LB			70	8834.2	MB	106.8	8	86	7330	UB		
20	10714	LB			70	8834.4	MB	134.5	0	86	7332	UB		
20	10712	LB	117	0	70	8834.6	MB	173.4	16.1	86	7348.8	UB	111.5	6.2
20	10687	MB	172.1	0	70	8835.2	MB	146.9	0	86	7351	UB	82.4	0
20	10697.7	MB			70	8836.7	MB			86	7353	UB	266	13.7
20	10700	MB	247.2	20.1	70	8837	MB	120.4	8	86	7354	UB	139.2	6.4
20	10700	MB	139.6	0	70	8837.8	MB	118.3	16.2	86	7354.5	UB	146.5	0
20	10705.9	MB	185.3	10.1	70	8838.5	MB	121.7	8.1	86	7401.9	MB		
20	10683.5	MB	209.9	0	70	8839.4	MB	77.3	0	86	7402.8	MB		
20	10685.9	MB			70	8840.8	MB	77.7	16	86	7403	MB		
20	10689.3	MB	274.1	20.2	70	8841.4	MB	186.2	8.1	86	7404	MB		
20	10696	MB	125.9	0	70	8841.9	MB	145.6	0	86	7404.3	MB		
20	10696.8	MB	193.8	10.2	70	8842.7	MB	148.3	0	86	7405	MB		
20	10704.7	MB	169.1	10.1	70	8845	MB			86	7405.8	MB		
20	10705.5	MB	149.4	20.1	70	8848.5	MB	228	15.2	86	7406	MB		
20	10712	LB	111.7	0	70	8843.8	MB	194.3	10	86	7407	MB		
96	10422	LB	-		70	8850.3	LB	154.4	0	86	7407.8	MB		
96	10426.8	LB			70	8849	MB			86	7408.3	MB		
96	10431	LB			70	8843	MB	161.4	0	86	7409	MB		
96	10432	LB	-		70	8845.6	MB	138.3	0	86	7409.8	MB		
96	10436	LB			70	8845.8	MB	203.7	10.1	86	7410	MB		
96	10436-2	LB			70	8848	MB	198.1	15.2	86	7445.1	LB		
96	10437	LB			70	8849.5	MB			86	7448	LB		
96	10441.6	LB			70	8849.9	MB	154	0	86	7449	LB		
96	10443	LB			70	8844.9	MB			86	7451	LB		
96	10445	LB			70	8842.3	MB	162.3	10.1	86	7397	MB	155.2	0
96	10446	LB			70	8843.4	MB	132.4	0	86	7379	MB	155.5	0
96	10449	LB			70	8846.2	MB			86	7374	MB		
96	10449-2	LB			70	8847.3	MB	145.1	0	86	7355	MB	188.3	15.1
96	10452	LB			70	8846.6	MB			86	7355-2	MB		
96	10456	LB			70	8847.7	MB	176.8	15.3	86	7393.5	MB	166.2	0
96	10456-2	LB			72	10487.5	UB			86	7363	MB	152.9	10.3
96	10456.5	LB			72	10487.5(2)	UB			86	7403.8	MB		
96	10460.5	LB			72	10488	UB			86	7393.1	LB	157	0
96	10463	LB			72	10488.5	UB			86	7380	LB	198.1	15
96	10321	MB	207.1	18	72	10490	UB			86	7370	LB		
96	10336	MB			72	10491	UB			86	7373	LB	198.5	10.1

96	10341.5	MB	103.4	0	72	10491(2)	UB			86	7355.9	LB	116.2	15.4
96	10348	MB	140.5	10.4	72	10492	UB			86	7389	LB	117.7	0
96	10357.7	MB			72	10492(2)	UB			86	7369	LB	76.9	0
96	10357.7	MB			72	10493	UB			86	7374	LB		
96	10307.5	MB	132	0	72	10494	UB			86	7350	UB	176.3	10.1
96	10310	MB			72	10497	UB			18	8648.2	MB	92.7	15.3
96	10339	MB	191.3	20.5	72	10498	UB			18	8650.6	MB	169.1	8
96	10347	MB	60.89	0	72	10499.8	UB			18	8651.4	MB	130.7	0
96	10347.8	MB			72	10503	UB			18	8655	MB	171.2	15.3
96	10356.6	MB	114.9	10.4	72	10504	UB			18	8655.7	MB	175.9	8
96	10307	MB	134.6	0	72	10504(2)	UB			18	8657.2	MB	102.9	0
96	10311	MB	172.1	20.4	72	10504.8	UB			18	8657.4	MB	192.6	15
96	10321.1	MB	148.2	0	72	10504.8(2)	UB			18	8659.4	MB	147.3	8
96	10334.7	MB			72	10505.7	UB			18	8660.7	MB	64.9	0
96	10345	MB	105.9	10.1	72	10509	UB			18	8661.9	MB	92.7	15
2	10364	MB	-		72	10512.7	MB			18	8664.2	MB	92.7	8
2	10365	MB	175.5	19	72	10514.5	MB			18	8665	MB		
2	10367	MB	193.4	10.1	72	10517.8	MB			18	8665.3	MB		
2	10367	MB	43.2	10.1	13	11006	MB			18	8668	MB		
2	10419	LB	116.2	0	13	11008(V1)	MB	148.3	0	18	8669	MB	124.7	0
2	10368.5	MB	137.9	0	13	11008(V2)	MB	234.8	20.2	18	8670.2	MB		
2	10369	MB	128.5	19.1	13	11009	MB			18	8672	MB		
2	10369.8	MB	131.9	10	13	11025V	MB	182.3	10	18	8673.2	MB		
2	10370	MB			13	11034(V1)	MB	113.2	0	18	8674	MB		
2	10371	MB	105.1	19.1	13	11034(V2)	MB			18	8677.4	LB		

8.8. Cohesive Strength and Angle of Internal Friction Calculate from Uni/Triaxial Destructive Test

Cohesive strength and angle of internal friction of rock can be calculated from peak stress and confining pressure in uni/triaxial destructive test. The calculated results are shown in Table 8-9. More detail can be found in Attachments.

Table 8-9. Cohesive strength and angle of internal friction calculated from uni/triaxial destructive test.

Well #	Cohesive strength	Angle of internal friction	Well #	Cohesive strength	Angle of internal friction	Well #	Cohesive strength	Angle of internal friction
	MPa	degree		MPa	degree		MPa	degree
20	21.06	51.75	70	39.55	37.88	86	16.38	52.78
20	26.76	46.75	70	30.5	45.28	86	40.59	35.31
20	21.6	47.71	70	33.27	36.64	86	46.33	29.52
96	9.88	49.34	70	13.6	57	86	26	40

96	19.88	47.93	70	20	43	86	26.8	39
96	39.95	28.62	70	15.8	45.5	86	15.8	48
2	32.9	31	13	23.63	45.82	86	13.8	53
2	29.4	44	13	36.07	39.2	18	29.8	41
			13	26.35	46.09	18	27.5	44
						18	32.2	38
						18	17.9	52
						18	21	46
						18	21.4	49
						18	35.4	31

8.9. Uniaxial Tensile Strength Test

Uniaxial tensile strength test is conducted on Hinckley sandstone sample only. The specimen diameter is 24.8 mm. The recorded peak force is 530 N. Therefore, the calculated tensile strength of this Hinckley sandstone is 10.97 MPa.

One vertical Bakken core plug from Well#96 was tested. The specimen diameter is 24.8 mm with a length of 52.27 mm. The recorded peak force is 3610 N. Therefore, the calculated tensile strength of this Bakken core plug is 74.7 MPa. Figure 8-1 shows the preparation of core plug for tensile strength test. Figure 8-2 illustrates the installation of core plug on tensile strength test apparatus. Figure 8-3 depicts the destruction of core plug after tensile strength test.

Figure 8-1. The preparation of core plug for tensile strength test

Figure 8-2 The installation of core plug on tensile strength test apparatus.

Figure 8-3 Pictures of the destruction of core plug after tensile strength test.

9. Application Guidelines for Horizontal Drilling and Hydraulic Fracturing

Several procedures and technologies have been developed through this project. We believe these procedures can play as guidelines or references for future exploration, development, and production of unconventional oil and gas resource like Bakken formation and depositional basin similar to Williston Basin. The technologies we propose here will benefit the energy sector through increasing experiment efficiency, shortening experimental test time, lowering experimental cost, optimizing drilling and stimulation design, reducing drilling and completion costs, and improving exploration and production efficiencies.

9.1. Guideline for Creating 3D RQD (or Other Geological Parameter) Model

A three dimensional RQD (or other geological parameter) model is very useful in revealing the geological features of the formation from different directions, at different levels, or in different angles. These models can be built using standard well logs or from self-defined well logs. If standard well logs are available, and the features of interest are directly or indirectly calculable from the logs, then the 3D model can be created directly using industrial software packages, such as PETREL.

Most old well logs were in image record. In this case, they need to be digitized at first. When the features of interest cannot be directly derived from standard well logs, self-defined well logs need to be used. This will include collecting the data from the cores, extrapolating the discrete data to a continuous distribution along the well, and create a digital self-defined well log. After that, PETREL or other similar software packages can be used to create the 3D geological model. The following steps show how a self-defined, three dimensional RQD (or other geological parameter) model is built.

1) Collect data through well logging or core laboratory measurement,
2) Self-define a well log,
3) Create and digitize well logs or RQD,
4) Calculate geological parameter if building other geological parameter model
5) Scale up the well logs or geological parameter,
6) Project the logs or geological parameter onto well cells,
7) Populate the logs or geological parameter from well cells into 3D space,
8) Application of the 3D model.

9.2. In-Situ Stress Analysis and Guideline for Horizontal Drilling

9.2.1 Orientation of the Principal Stresses

Because the Williston basin is a cratonic basin, and vertical and sub-vertical faulting occurred in the basement and extended to the sedimentary formations, the in-situ stress field in the basin is in normal faulting stress regime, meaning that the maximum principal stress, σ_1, is vertical or sub-vertical. Consequently, the intermediate and minimum principal stresses, σ_2 and σ_3, are horizontal, corresponding to the maximum and minimum horizontal principal stresses, σ_H and σ_h. The existence of some continuous lineament structures in the NE-SW direction, and some discontinuous, interrupted lineaments in the NW-SE direction indicates that in most area, the maximum horizontal principal stress, σ_H, is in the NE-SW direction, and the minimum horizontal principal stress, σ_h, is in the NW-SE direction. In some areas, this might be different due to local heterogeneity.

Because of the difficulties of measuring the in-situ stress tensors directly, the alternative way is to observe on oriented cores or on well walls. Unfortunately, there are no available conditions to carry out such kind of investigation. Therefore, we screened all the well completion reports available in North Dakota Geological Survey, and found 15 wells that contain some useful data for in-situ stress analysis. These in-situ stress data mainly relied on induced fractures in oriented cores, anelastic strain recovery, acoustic velocity anisotropy, and induced fractures in well walls, and the dip sonic method. At the same time, we searched all the related literatures for the in-situ stress of

the Bakken formation in the Williston Basin. These wells are scattered all over the southeastern part of the Williston Basin, the western part of North Dakota. Figure 9-1 shows the exact locations of these data wells on a North Dakota map.

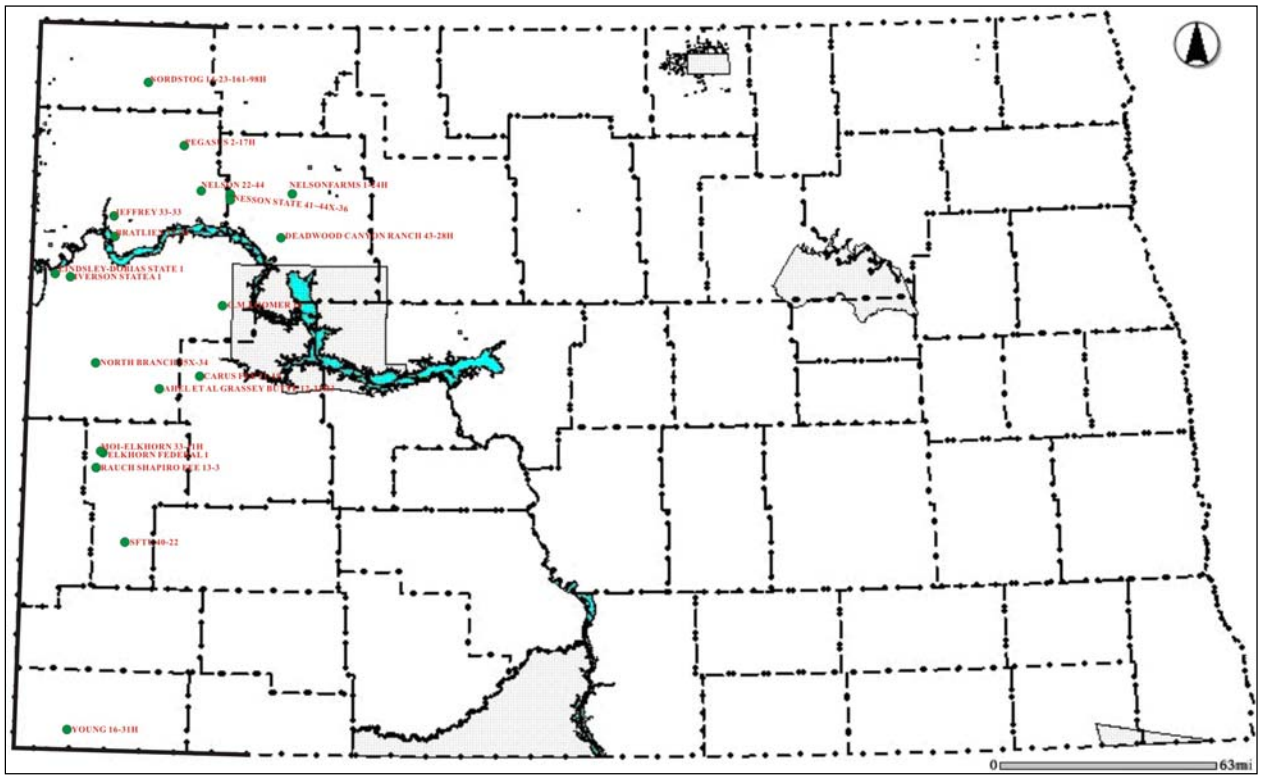

Figure 9-1. Distribution of data wells in North Dakota.

Table 9-1 shows all the collected data. Orientations of the maximum horizontal principal stress were plotted on a North Dakota map to show their change with geographic locations, as shown in Figure 9-2. From the data in Table 9-1 and Figure 9-2, we can conclude that the orientation of the maximum horizontal principal stress is between N30ºE to N70ºE, statistically.

Table 9-1 Summary of orientations of the maximum horizontal principal stresses in the Bakken formation

Serial No.	Well file No.	Well name	Depth	σ_H orientation	Method[1]	Formation	Lithology	Data quality[2]
1	12072	MOI-ELKHORN 33-11H	10388.0-10418.64	275º; 270~285 º	IF	Bakken	Limestone	G
2	12297	ELKHORN FEDERAL 1	10530.0-10531.0	49º, 34º, 42º	ASR	Bakken	Shale	G
3	12494	RAUCH SHAPIRO FEE 13-3	10472.0-10532.0	40~50º	IF	Lodgephole, Bakken, Three Forks	/	G
4	12772	AHEL ET AL GRASSEY BUTTE 12-31H3	11242.0-11284.0	330-340º; 290-300º	IF	Bakken	Limestone	F
5	12785	CARUS FEE 21-19	11261.0-11318.0	10-30º; 50-60º; 70-80º	IF	Three Forks and Bakken	Limestone	/
6	15845	NELSON FARMS 1-24H	9637.0-9675.85	300 º	AVA	Bakken	Shale, dolomite	/
7	16089	NORDTOG 14-23-161-98H	8629.82-8720.78	60 º, 30 º, 45 º, 75 º, 75 º, 105 º	AVA	Bakken, Three Forks	Limestone	/
8	16405	PEGASUS 2-17H	10088.70-10209.0	330 º, 315 º, 75 º, 75 º	AVA	Bakken, Three Forks	Limestone	/
9	12173	C. M. LOOMER 16	9328.0-9388.0	40-50 º	IF	Mission Canyon	/	G
10	14712	SFTU 40-22	9165.6-9168.9	40-50 º	IF	Fryburg	Limestone	G
11	16841	DEADWOOD CANYON RANCH 43-28H	10084.0-10204.4	30 º	IF	Bakken	Sandstone	G
12				60 º	Dip Sonic		Sandstone	G
13	16968	NESSON STATE 41X-36	10470-10860	49 º	IFWW	Bakken	Limestone	G
14	17015	NESSON STATE 42X-36	10440-10980	56 º	IFWW	Bakken	Limestone	G
15	17017	NESSON STATE 44X-36	10061-10620	45 º	IFWW	Bakken	Limestone	G
16	Kuhlman and Claiborne, 1992		9925	67.6±2.81º	ASR	Bakken	Shale	G, 10 samples
17	Kuhlman and Claiborne, 1992		9925	69±11.1º	DSA	Bakken	Shale	G, 6 samples
18	Roundtree, Eberhard and Barree, 2009,			NE		Bakken		

Notes: 1. IF-induced fractures in core, ASR - anelastic strain recovery, AVA-acoustic velocity anisotropy, DSA-differential strain analysis, and IFWW- induced fractures in well wall; 2. G - Good, F - Fair.

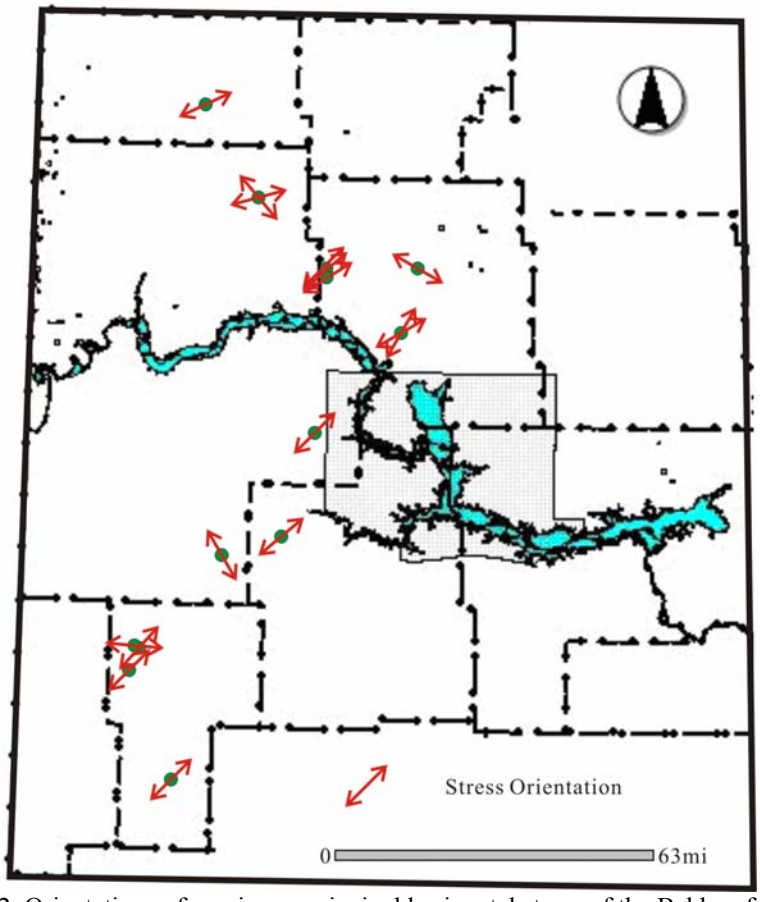

Figure 9-2. Orientations of maximum principal horizontal stress of the Bakken formation.

9.2.2 Stress Magnitude

In-situ stress magnitude can be determined through field test in the oil well, or in lab test on cores. These tests include micro hydraulic fracturing (μ-HF) test, anelastic strain recovery (ASR), differential strain analysis (DSA), etc. Different methods can offer different data types, for example, the μ-HF test can estimate stress magnitudes, but the ASR and DSA only can offer ratios among the three principal stresses. According to the previous section on the tectonics, the research area is under the dominant effect of normal faulting, with secondary strike-slip faulting. Based on the collected data, we have come to the uniform conclusion that the vertical principal stress is approximately equal to the overburden. Tables 9-2 and 9-3 summarize the data based on different methods and from different sources. According to these two tables, the stress gradients or magnitudes may differ a little bit with location and with formation. For the Bakken formation, the fracture gradient ranges from 0.75 to 0.85 psi/ft.

The ratios among three principal stresses, i.e., the vertical principal stress, the maximum horizontal principal stress and the minimum horizontal principal stress are 1:0.95-0.85:0.85-0.75, which means the stress conditions is favorable for normal faults and/or strike slip faults. Thus, the stress states should be $\sigma_V > \sigma_H > \sigma_h$.

For the orientation of the maximum horizontal principal stress, most data indicate a range between N30ºE to N70ºE; a few (four) data points show an orientation in NW. After examining these four data carefully, we found that three of the four data were based on the acoustic velocity anisotropy (AVA). According to Narr and Burruss (1984) (Figure 9-3) and Table 9-4, the secondary strike direction of natural fractures is NW. So for the three sets of data based on AVA, we intend to believe that the orientation very likely indicates the strike of micro natural fractures present in the oriented core, and represent a secondary orientation due to local heterogeneity. For the data serial No. 4, we checked the data quality and source carefully, and found that all these induced fractures in the oriented core are along with the orientation scribe line, so we think these fractures were created by the scribe groove.

We can get other evidence to support our estimated orientation of the maximum horizontal principal stress. The first reliable source comes from the World Stress Map (WSM) (Figure 9-4). According to the WSM, there are only a few data available in Williston basin, but the stress directions around this area is NE. The other source is the literatures. Several researchers (Haimson, 1978; Narr and Burruss, 1984) have compiled hydraulic fracturing in-situ stress measurement data onto a map (Figure 9-5), this map shows the stress orientation around this area is NE to NEE. In summary, the orientation of the maximum horizontal principal stress is mainly NE to NEE in the Bakken formation in the Williston Basin, North Dakota.

For the stress magnitudes, data shown in Tables 9-1 and 9-2 are rather scattered, which are reasonable. We can still extract some useful information from the above data sheets: i. e. the differences among three principal stresses are smaller than those calculated using Hooke's law; and the stress anisotropy is not remarkable. This is consistent with the analysis in the tectonics section in which the two slat layers neighboring the Bakken formation are considered responsible to this pseudo-lithostatic status.

Table 9-2 Summary of lab tests on stress magnitudes (Nordtog 14-23-161-98H, North Dakota)

Sample No.	Depth (ft)	Overburden stress (psi)	Pore Pressure (psi)	Min Horizontal Stress(psi)	Biot's Constant	Fracture Gradient (psi/ft)	Formation	Lithology	Fracture Toughness (psi-in$^{0.5}$)
1V	8544.00	8544	4443	6435	0.77	0.753	Bakken	Sandstone	2020
2V	8586.20	8586	4465	6657	0.83	0.775			2711
3V	8629.60	8630	4487	6235	0.69	0.723			1844
4V	8631.40	8631	4488	6250	0.68	0.724			1787
5V	8639.30	8639	4492	6100	0.79	0.706			1908
6V	8715.50	8716	4532	6336	0.79	0.727			1807
7V	8720.10	8720	4534	6519	0.74	0.748			2722
8V	8729.00	8729	4539	6474	0.71	0.742			2201
9V	8737.50	8738	4544	6416	0.75	0.734			1646

Table 9-3 Summary of research findings on stress magnitudes

Serial No.	Depth (ft)	Formation	Lithology	Vertical stress (psi)	Max. horizontal stress (psi)	Min. horizontal stress (psi)	Pore pressure or gradient	Fracture gradient (psi/ft)	Ref.
1	9925	Upper and lower Bakken	Shale	9925	8933	7950		0.795	Kuhlman & Perez, 1992
2	9600-10,400	Upper and Lower Bakken	Shale					0.80-0.86	Phillips et al., 2007
3		Middle Bakken	Sandstone and siltstone					0.60-0.65	Lolon & Cipolla, 2009
4		Upper and lower Bakken	Shale					0.70	Lolon & Cipolla, 2009
5		Bakken						>0.85	Russell et al., 2009
6	10,500	Bakken in Motana		10,500	7135	6735	4998	0.67	Russell et al., 2009
7	10,000	Bakken in Motana					0.5	0.69-0.75	Wiley et al., 2004
8	6765-7267	Winnepeg formation, Deadwood Formation, Precambrian basement						0.60	Roegiers & McLennan, 1979

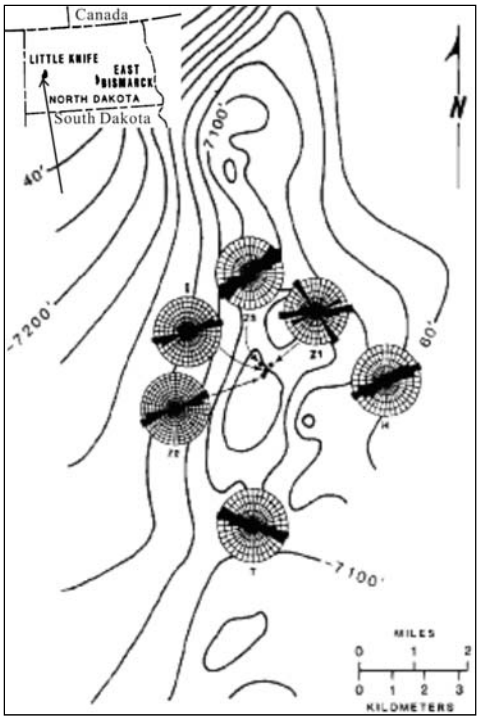

Figure 9-3. Strikes of natural fractures in the Little Knife field, based on five wells (Narr and Burruss, 1984).

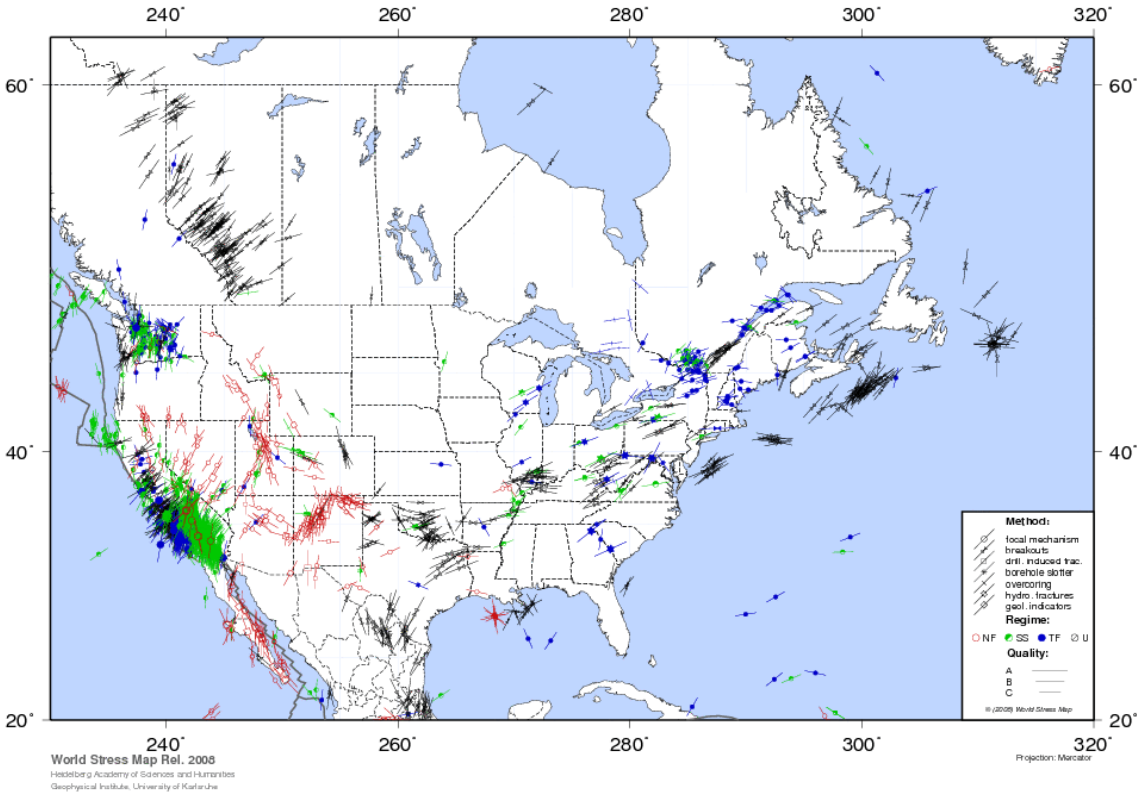

Figure 9-4 Stress map of North America from the World Stress Map (after Heidbach et al., 2008).

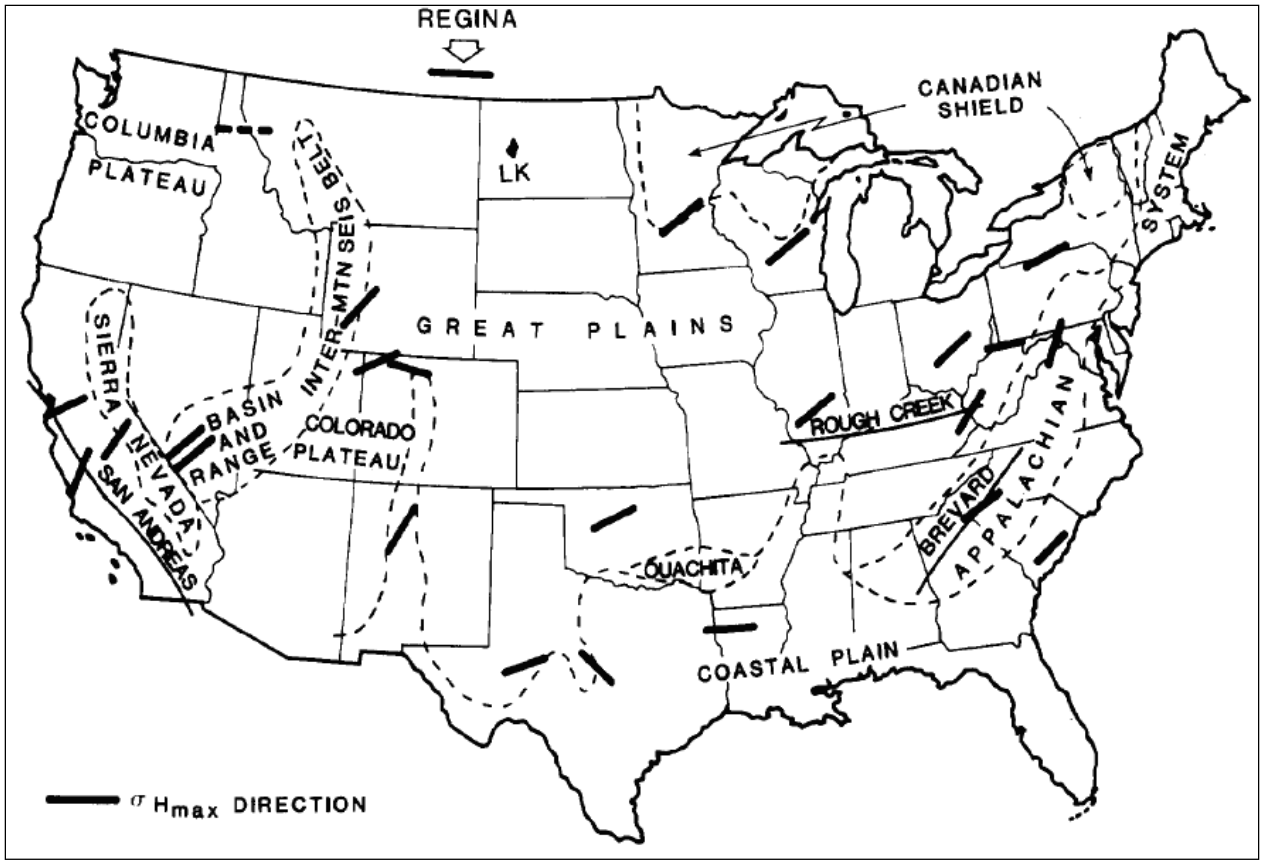

Figure 9-5 The maximum horizontal principal stress directions in continental United States based on the orientation of vertical hydrofractures (after Haimson, 1978; Narr and Burruss, 1984)

Such a conclusion can be proved by the structural characteristics of this region. Just as addressed above, in the Williston basin of North Dakota, most faults are normal faults, part are strike-slip faults, which means $\sigma_V \geqslant \sigma_H > \sigma_h$. However, according to the seismic investigation, there still exist some reverse fault, and the only possible explanation for this phenomenon is that the differential stress is very small, and such stress conditions can make all these things happen.

In summary, in the Bakken formation, the fracture gradient ranges from 0.75 to 0.85 psi/ft, and the ratios among three principal stresses, i.e. the vertical principal stress, the maximum horizontal principal stress, and the minimum horizontal principal stress are 1:0.95-0.85:0.85-0.75 (Table 9-4).

Table 9-4 Summary of strikes of natural fractures extracted from oriented cores

Serial No.	Well No.	Well name	Depth (ft)	Strikes	Formation	Lithology
1	12297	ELKHORN FEDERAL 1	10530.0-10531.0	N86ºW, N68ºE, N67ºE	Bakken	Shale
2	12772	AHEL ET AL GRASSEY BUTTE 12-31H3	11242.0-11284.0	330-340º; 50-70º	Bakken	Limestone
3	12785	CARUS FEE 21-19	11261.0-11318.0	290-300º; 20-30º; 40-50º	Three Forks and Bakken	Limestone
4	15845	NELSON FARMS 1-24H	9637.0-9675.85	280 º	Bakken	Shale, Dolomite
5	12173	C. M. LOOMER 16	9328.0-9388.0	40-60 º	Mission	

					Canyon	
6	14712	SFTU 40-22	9165.6-9168.9	40-60 º	Fryburg	Limestone
7	12831	NELSON 22-44	9840.0-9897.0	310-320º; 260-270º	Bakken	
8			11705.0-11762.0	320-330º; 300º-310º; 340-350º; 290-330 º	Interlake	
9	10103	IVERSON STATEA 1	9289.0-9423.50	60-70º; 50-70 º	Misson Canyon; Ratcliffe	Limestone
10	11157	LINDSLEY-DOBIAS STATE 1	8988.0-9035.0; 9035.0-9095.0; 9095.0-9130.0	0-20 º, 40-60 º, 40-50 º,	Misson Canyon; Ratcliffe	Limestone
11	14638	BRATLIEN 13-34	9528.6-9548.20	290-300 º	Misson Canyon;	Limestone
12	13841	YOUNG 16-31H	9169.60-9190.20	60 º-70 º	Red River	Limestone
13	12962	NORTH BRANCH 35X-34	10970.0-11006.0	270 º-290 º	Nisku	Limestone
14	14637	JEFFEY 33-33	9418.3-9433.80	290-320 º	Misson Canyon	Limestone
15	16968	NESSON STATE 41X-36	10470-10860	310-330º; 40-50º	Bakken	Limestone
16	17015	NESSON STATE 42X-36	10440-10980	310-320º; 40-50º	Bakken	Limestone
17	17017	NESSON STATE 44X-36	10061-10620	310-330º; 40-50º	Bakken	Limestone
18	Kuhlman and Claiborne, 1992		9925	315 º	Bakken	Shale

9.2.3. Numerical Modeling of Stress Distribution

The general technical route for numerical modeling is: (1) building the model to cover the target area, (2) obtaining data in some controlling points using direct measurement or other techniques, (3) determining the boundary conditions for the model; and (4) simulating the distribution of the properties in question in the whole area. Following these steps, we built a numerical model and simulated the in-situ stress field in the Bakken Formation using the data summarized in Tables 9-1 through 9-4.

Building the numerical model

The establishment of a numerical model includes determining the geometries and estimating physical parameters of the materials inside the model.

For the Bakken Formation, based on the figures of Fred (1978), we built the model as shown in Figures 9-6 and 9-7. Our objectives were to cover the maximum area with acceptable resolution in the depth direction. To achieve the objectives, we exaggerated the thickness and compress the lengths of the simulated block. The final numerical model was 217.1 miles long in the X-direction (SE-NW direction), 125.8 miles long in the Z-direction (SW-NE direction), and 270 ft in the Y-direction (vertical direction) which included the whole Bakken Formation (upper, middle and lower units), and part of Lodgepole formation on the top, and part of Three Forks formation at the bottom. The upper boundary was at the elevation of -10,000 feet, and the lower boundary plane is at the elevation plane of -10,270 feet. The six sides of this numerical model were rectangular planes. Figure 9-8 shows the geometry and the geological information in the depth direction.

The top layer of the model was the Lodgepole formation. It was limestone. The middle layer was Bakken formation, which include three parts: the upper Bakken, the middle Bakken, and the lower Bakken. The upper and lower Bakken are black shale; and the middle Bakken is sandstone, inter-bedded with siltstone, dolomite and limestone. The lower layer of the model is the Three Forks formation; it was dolomite. Because all these formations were at great depth, there is no mechanically significant fault and other discontinuities in the modeled area. Therefore, an

elastic and continuous model was assumed. Figures 9-8 and 9-9 show the numerical model; it contained 40,545 elements and 180,181 nodes. Element size was selected to reflect the deformation of the geological structural features.

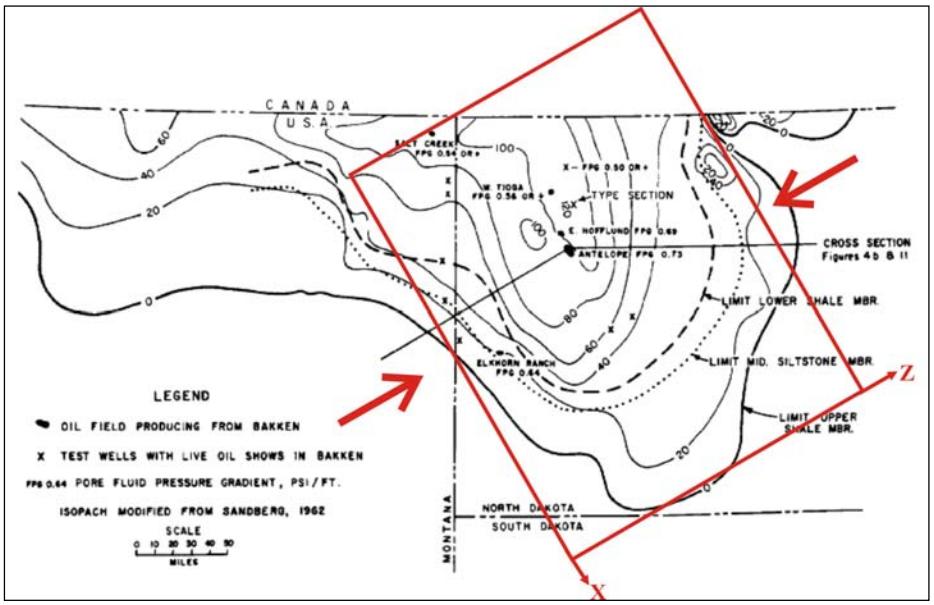

Figure 9-6. Schematic map for the numerical model of the Bakken Formation.

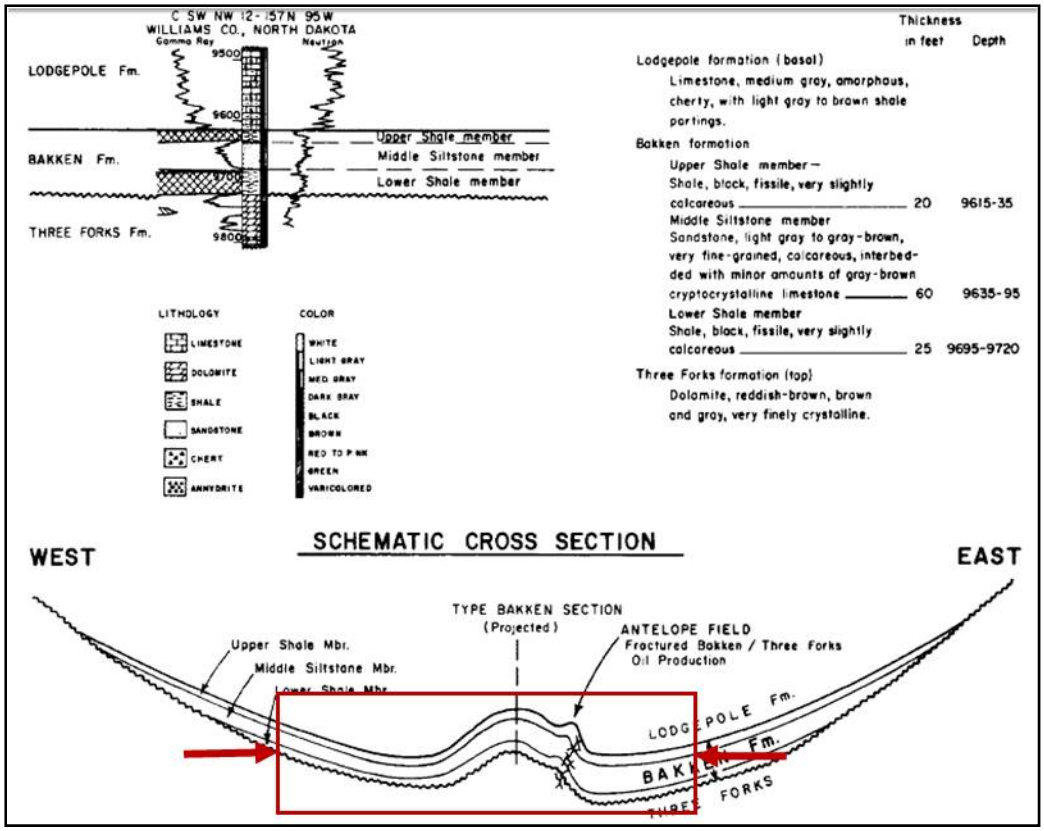

Figure 9-7. Schematic map of the numerical model for Bakken Formation in a typical cross-section through the Williston Basin (cross-section located in Figure 9-6).

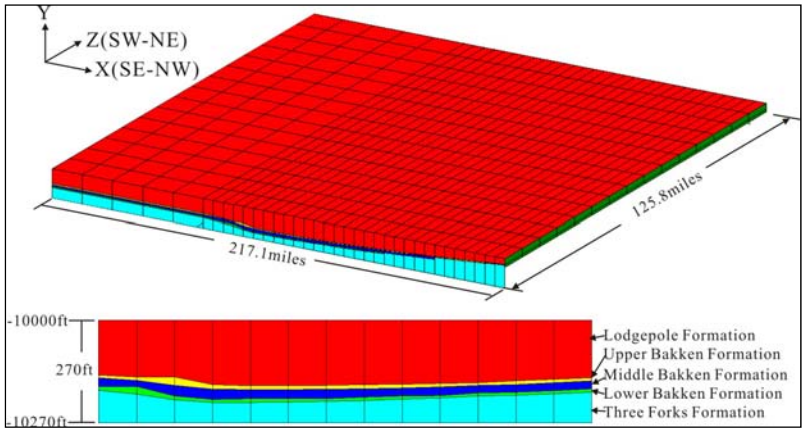

Figure 9-8. The numerical model with geometry and geology information.

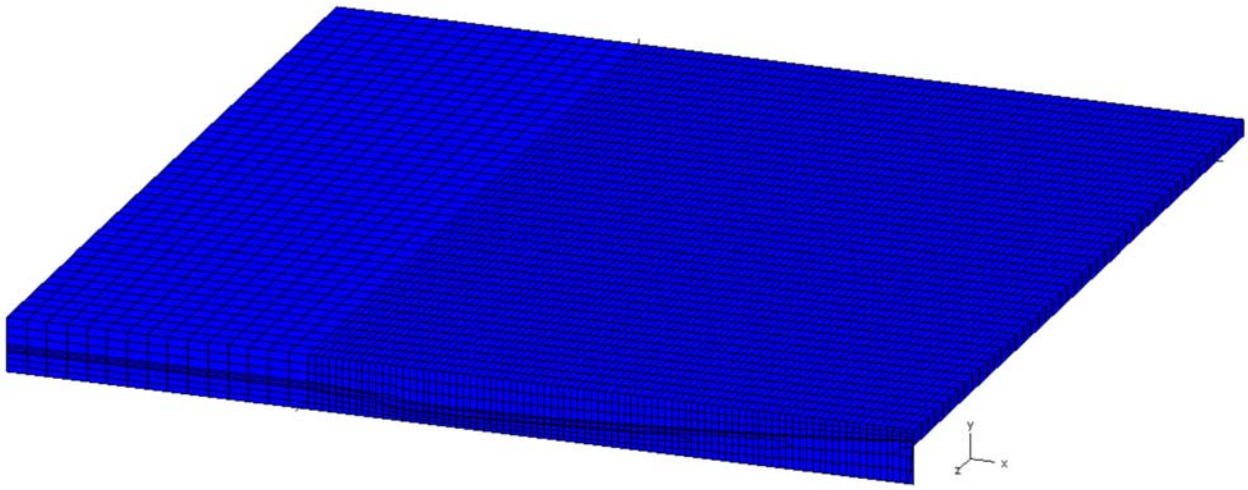

Figure 9-9. The Numerical model with grids.

Boundary conditions and input parameters

In finite element simulation, it is required to constrain the boundaries of a numerical model. Correct constraint conditions can help assure the reliability and rationality of the calculated results.

For this numerical modeling study, the bottom plane (i.e. Y = -10,270 ft plane) was constrained rigidly in the Y-direction; the right X-plane (i.e. X = +217.1 mile plane) was rigidly constrained in the X-direction, and the back Z-plane (i.e. Z = 0 mile plane) was under the rigid constraints in the Z-direction. Evenly distributed planar vertical load (overburden) of 10,000 psi was applied to the upper boundary (i.e. Y = -10,000 ft plane). The left X-plane (i.e. X = 0 mile plane) and the front Z-plane (i.e. Z = +125.8 mile plane) were loaded with linearly increased horizontal stresses, each at a stress gradient of 0.8 psi/ft and 0.9 psi/ft, respectively. Figure 9-10 shows the schematic boundary conditions.

Loads on the numerical model were classified into two categories. The first category included the gravitational load on the top plane, and the hydrostatic loads on the side planes due to the overburden pressure. The gravitational load was applied to the center of each element; the magnitude was determined by the weight of rock column above the element. The second category of the loads was the loads to be determined, which were applied onto the left X plane (X = 0 mile plane) and the front Z plane (Z = +125.8 mile plane), as indicated in Figure 9-10. During the back analysis process, the above-mentioned data in Table 9-4 were used as the stress constraint conditions. Using linear elasticity, the load magnitudes on the two side planes were determined. Finally, the loads on the entire numerical model were calculated.

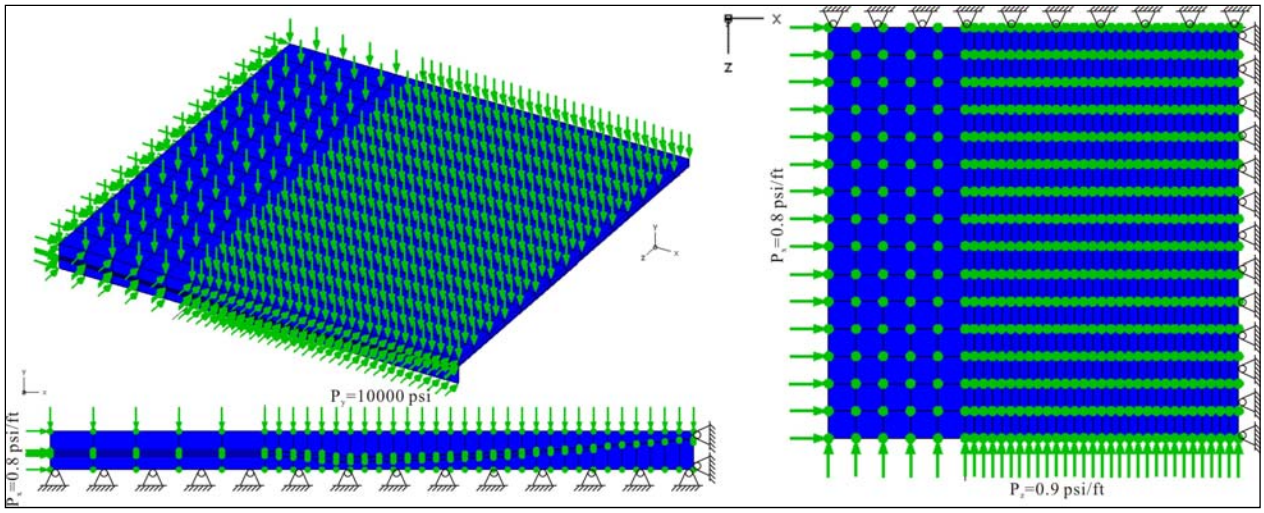

Figure 9-10. Boundary conditions for the numerical model.

Input parameters

Generally, lab tested strength parameters of rock specimens are different from that of real field rock-masses. How to apply the lab test results on intact rock specimens to represent reservoir rock-mass properties is one of the research topics in geomechanics. One of the widely accepted methods is the Hoek-Brown strength criterion. According to the physical and mechanical parameters summarized above, combined with the characteristics of this numerical model, the physical and mechanical properties of reservoir rock-masses in the research area were estimated with the new version of Hoek-Brown Criterion. All the input parameters are shown in Table 9-5.

Table 9-5 Input parameters for the numerical model

Formation	Rock type	E_m ($\times 10^6$psi)	σ_t (psi)	C (psi)	φ (º)	γ (psi/ft)	Lateral loading coefficient X	Lateral loading coefficient Z
Lodgephole	Limestone	3.88	87.46	785.4	37.7	1	0.8	0.9
Upper Bakken	Shale	1.35	12.62	229.2	28.1	1	0.8	0.9
Middle Bakkenn	Sandstone	2.24	71.79	876.89	41.3	1	0.8	0.9
Lower Bakken	Shale	1.35	12.62	229.2	28.1	1	0.8	0.9
Three Forks	Dolomite	6.53	162.87	1307.5	38.2	1	0.8	0.9

9.2.4 Results and Discussion

Numerical modeling serves two major functions: (1) as a numerical tester to find (define) the proper boundary conditions with some known (controlling) values, and (2) as a calculator to find the distribution of some properties inside the middle of some known (controlling) points.

First, we conducted the numerical modeling according to the above-mentioned boundary conditions and stress constraints to estimate the unknown loads. Then we calculated the stress magnitudes on the two lateral planes. After multiple backward calculations and parameter adjustments, the unknown loads were determined. The final loads on the X-plane start from 8000 psi at Y = -10,000 ft, and increase by 0.8 psi/ft downward to Y = -10,270 ft; the direction of the load is parallel to the X-axis, compressive to the X-plane. Similarly, the final loads on the Z-plane start from 9000 psi at Y = -10,000 ft, and increases by 0.9 psi/ft downward to Y = -10,270 ft; the direction of the load is parallel to the Z-axis, compressive to the Z-plane. Based on these geometric, material and load conditions, we got an estimated stress distribution in the Bakken Formation.

According to the modeling results and the actual engineering needs, Figures 9-11 through 9-15 show the distribution of the maximum and minimum stresses in the Bakken Formation. In all the figures, the stresses are in psi, and negative values represent compressive stresses. The maximum and minimum principal stresses are defined by their absolute values.

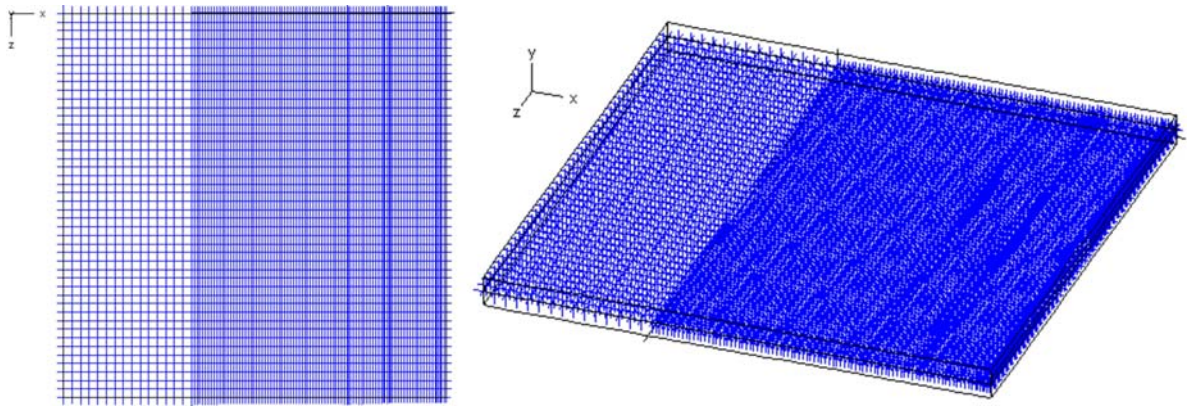

Figure 9-11. Orientations of principal stresses.

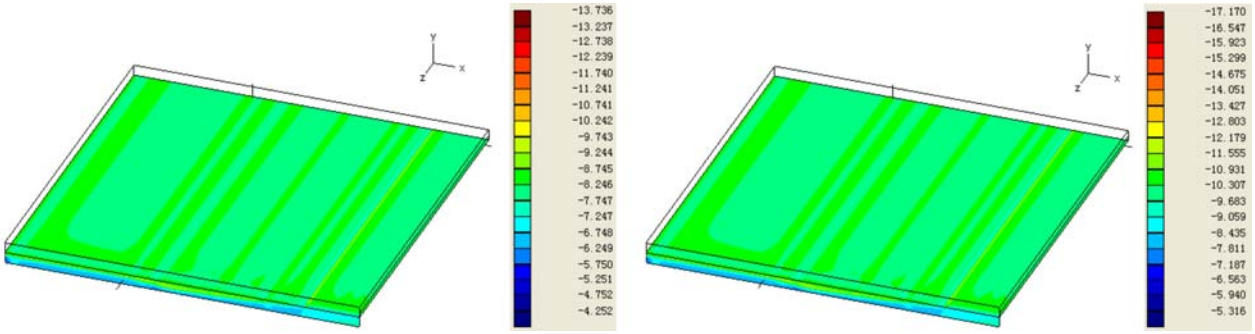

Figure 9-12. Distribution of minimum (left) and maximum (right) principal stresses in the Bakken Formation.

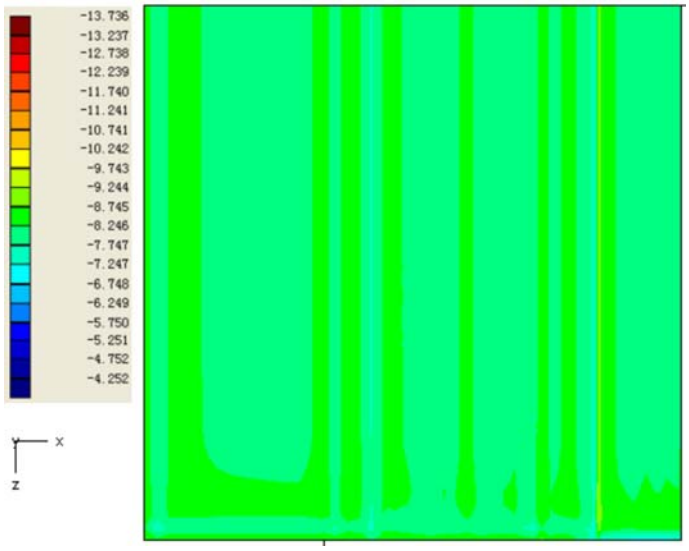

Figure 9-13. Distribution of minimum principal stress on the horizontal plane at Y = -10135ft.

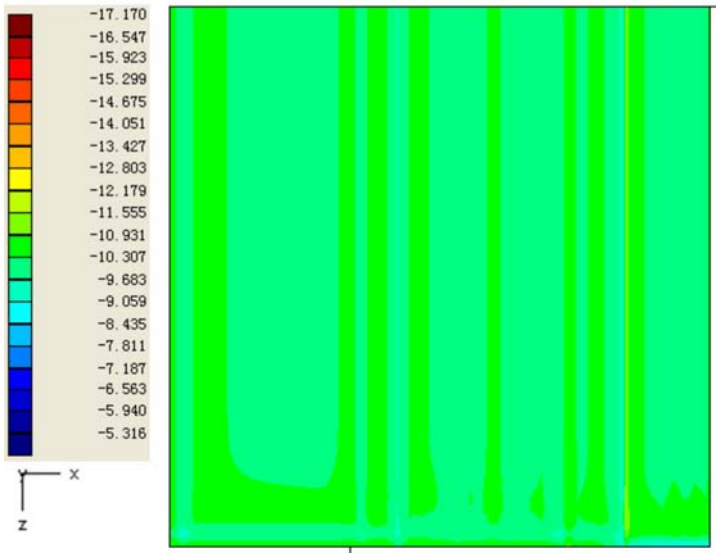

Figure 9-14. Distribution of maximum principal stress on the horizontal plane at Y = -10135ft.

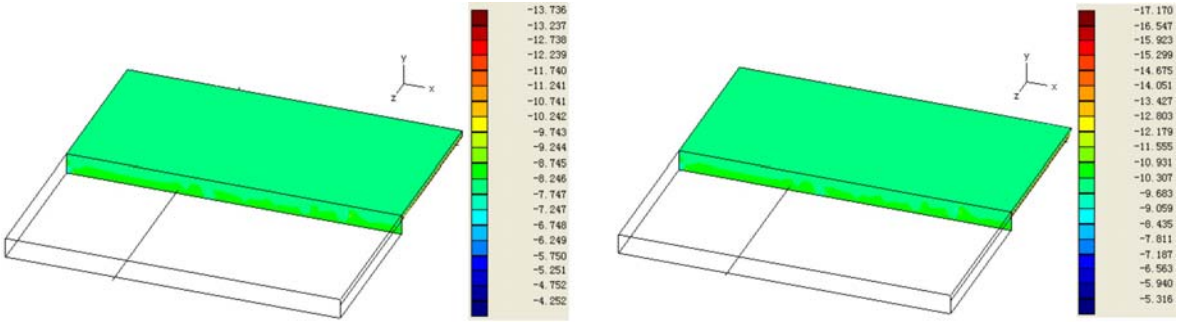

Figure 9-15. The min (left) and the max (right) principal stresses on the vertical plane at Z= 62.9 mile planes.

From the above numerical results, one can see that, under the assumed boundary conditions and material properties, the orientation of the principal stresses are stable and consistent across the simulated area (Figure 9-11). Change of the maximum and minimum principal stresses in the Bakken Formation is relatively homogeneous (Figures 9-12 to 9-14); their magnitudes are mainly influenced by the material properties of the rock-mass in these formations (Figure 9-15). In general, the principal stresses increase with the depth.

9.3. Guideline for Horizontal Drilling- Impacts of Stresses on the Stability of Horizontal Wells

9.3.1 Impacts of Stresses on the Stability of Horizontal Wells

After we know the stress field in the Bakken Formation, we can further study how the stress regime affects the stability of horizontal wells. After two months' screening on all the oil wells in Williston Basin, North Dakota, we found that most horizontal wells were parallel to the direction of the maximum horizontal principal stress (σ_H), some were perpendicular to σ_H, and a few were in an acute angle with σ_H. According to these facts, we designed three cases to simulate the impact of the in-situ stresses on the stability of horizontal wells: (1) well axis is parallel to σ_H; (2) well axis is perpendicular σ_H; and (3) well axis is 45º to σ_H.

9.3.2 Establishment of the Numerical Model

The establishment of a numerical model includes determining the boundary geometries and sizes of the interested area and estimating physical and mechanical parameters for the numerical model. To investigate the impact of in-

situ stresses on the stability of horizontal wells in the Bakken Formation, we built the models according to the well completion report, as shown in Figure 9-16. In order to get a better resolution at the current limitation of software and computational capacity, for Cases 1 and 2, we built a rectangular parallelepiped model of 36-inch X 36-inch X 100-inch, with a 6-inch diameter horizontal well through the center of the model. The six outer side surfaces of this model are flat, regular planes (Figure 9-17). For Case 3, we built a cubic model of 36-inch, with a 6-inch diameter horizontal well through, and counter-clockwise rotated 45^0 of the maximum and minimum horizontal principal stresses σ_H and σ_h with respect to the well axis, i.e., the Z-axis changed from SW-NE to S-N, and X-axis from SE-NW to E-W (Figure 9-18). Because the Middle Bakken Unit is currently the major production zone, our models focus on this unit. Again the model is simplified to be elastic and continuous.

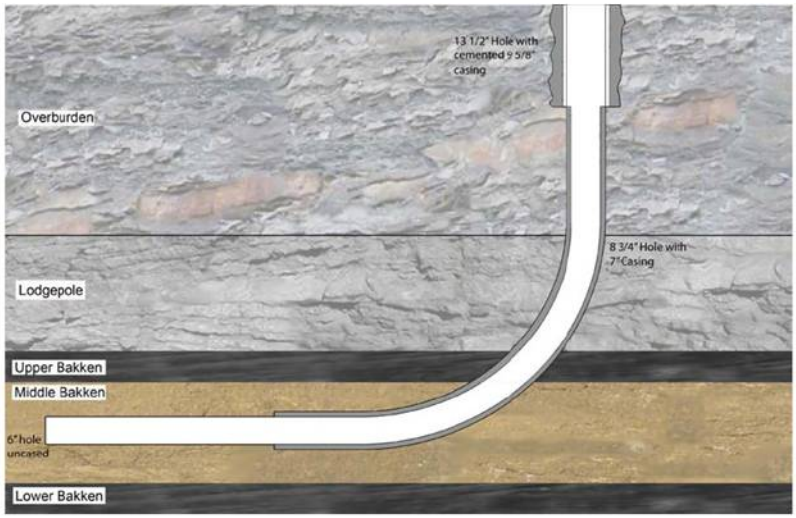

Figure 9-16. Generalized depiction of an open-hole completion in the Middle Bakken Unit (based on NDDMR-OGD well file).

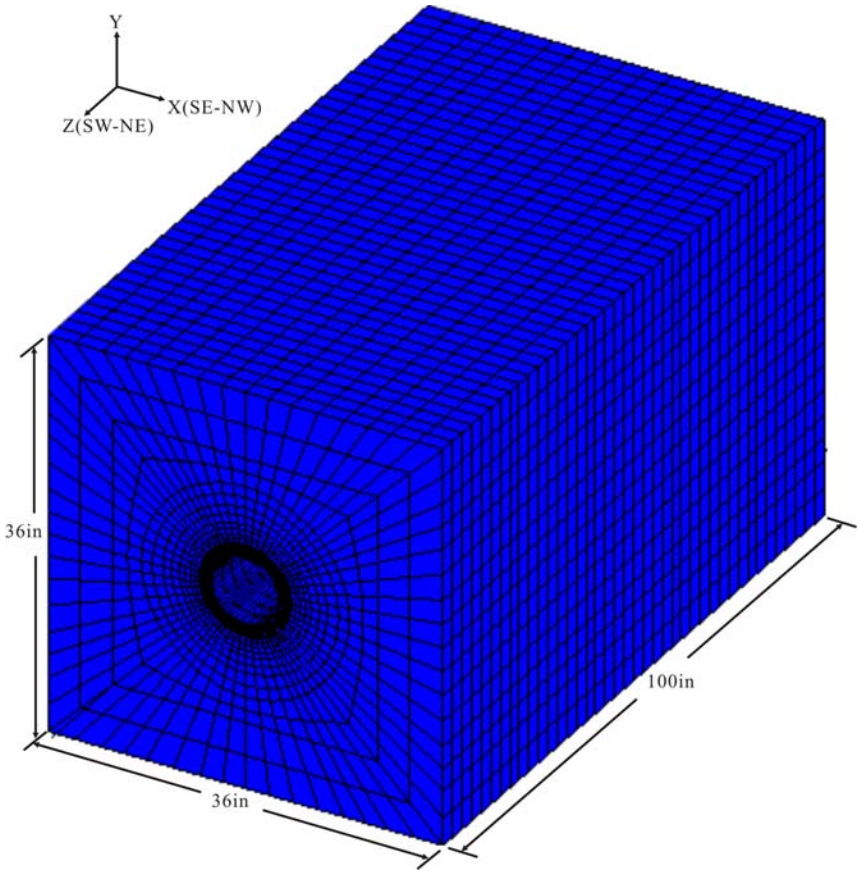

Figure 9-17. Model for the horizontal well parallel/perpendicular to the maximum horizontal principal stress, σ_H.

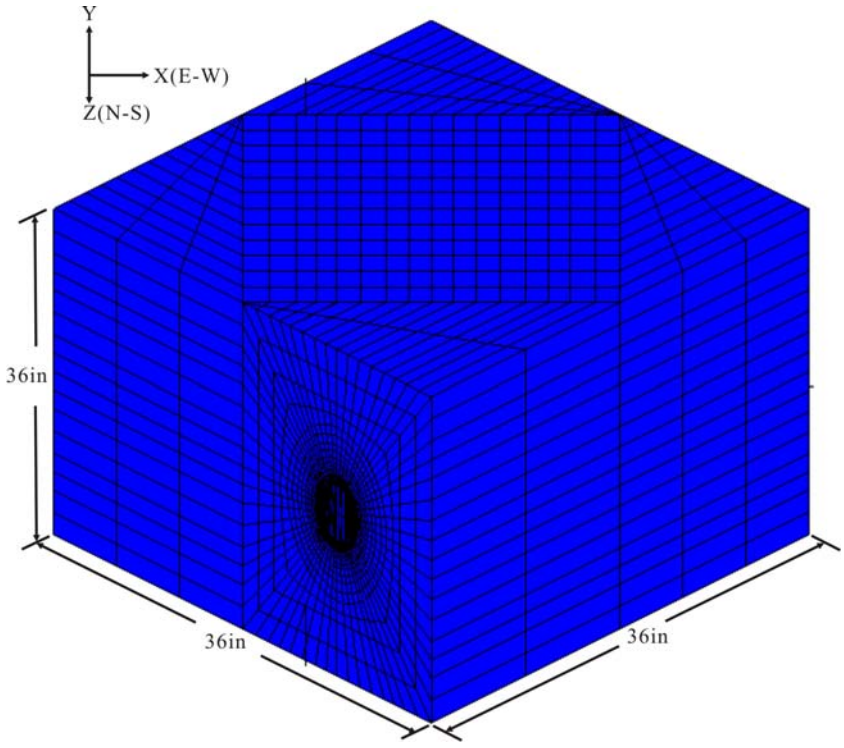

Figure 9-18. Model for a horizontal well at 45º angle to the maximum horizontal principal stress, σ_H.

9.3.3 Boundary Conditions and Input Parameters

Boundary conditions

During the finite element simulation, it is required to constrain the boundaries of the model. For Cases 1 and 2, the bottom boundary is constrained rigidly in the Y-direction; the right X plane is rigidly constrained in the X direction; and the back Z plane is under the rigid constraints in Z direction. Due to the relatively small size, evenly distributed loads were applied to the upper Y, left X, and front Z boundary planes. The schematic boundary conditions for these two cases are shown in Figures 9-19 and 9-20. For Case 3, the loads were applied on top and the four extended lateral planes (because it is hard to apply strain constrains on to these planes); the bottom boundary is constrained rigidly in Y direction, as shown in Figure 9-21.

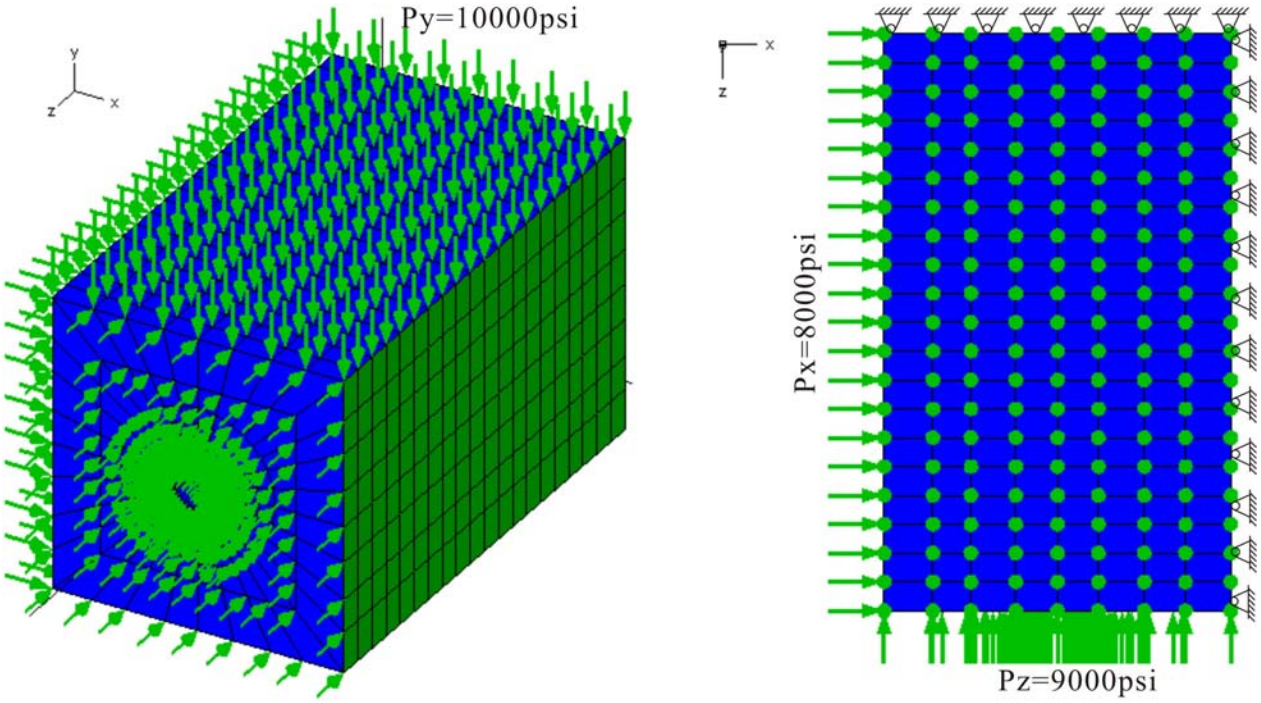

Figure 9-19. Boundary conditions for the Case 1, well axis parallel to σ_H.

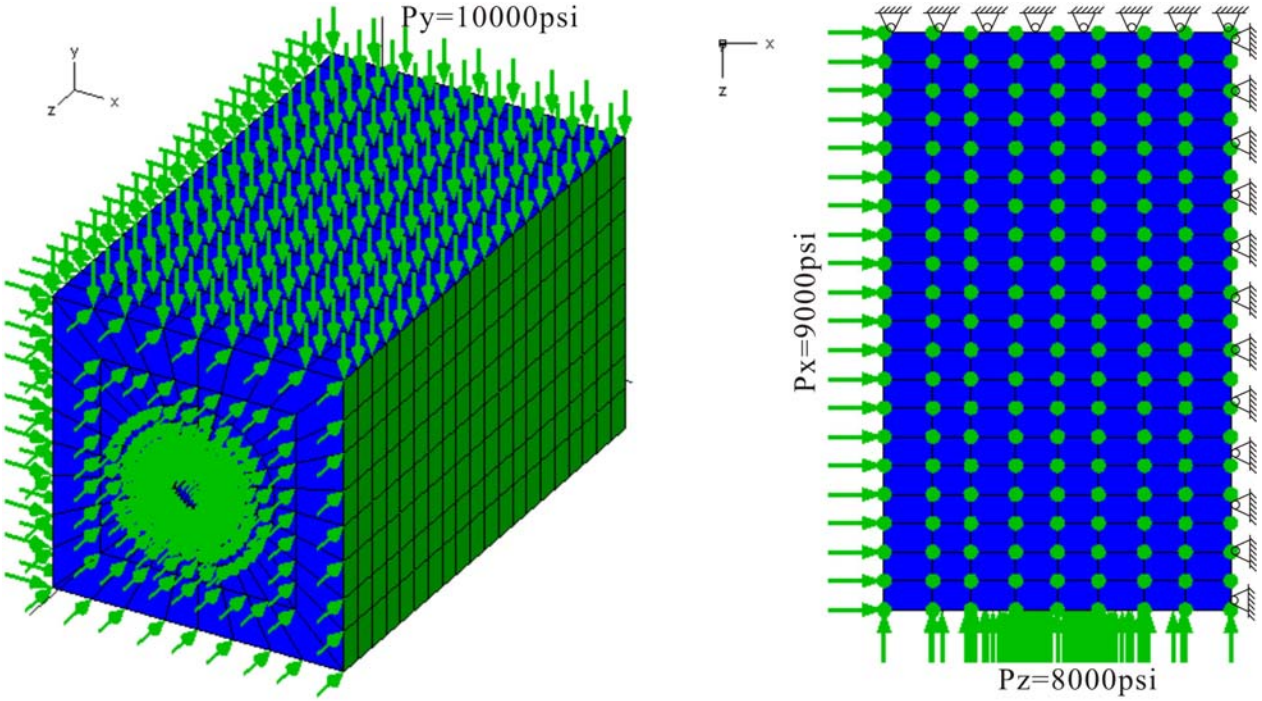

Figure 9-20. Boundary conditions for the Case 2, well axis perpendicular to σ_H.

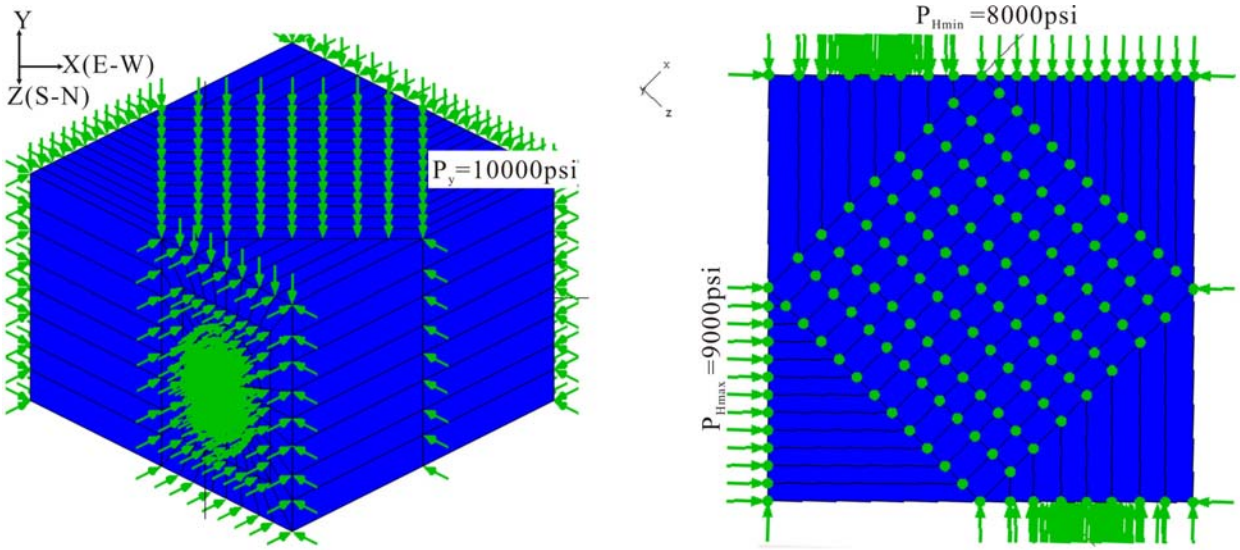

Figure 9-21. Boundary conditions for the Case 3, well axis is 45^0 to σ_H.

Input parameters

The procedures and rock properties used in the previous section were used here, as shown in Table 9-6.

Table 9-6. Input parameters for the Middle Bakken Unit numerical model

Formation	Rock type	E_m (10^6psi)	σ_t (psi)	C (psi)	φ (º)	γ (psi/ft)	Lateral loading coefficient X	Lateral loading coefficient Z
Middle Bakken	Sandstone	2.24	71.79	876.89	41.3	1	0.8	0.9

9.3.4 Case 1- Well Axis Parallel to the Maximum Horizontal Principal Stress

Figures 9-22 and 9-23 show the distribution of maximum and minimum stresses around the well section. The maximum and minimum stresses along the well axis are shown in Figures 9-24 and 9-25. According to these results, the compressive stress concentration will occur at the two middle lateral spots of the well wall, and the tensile stress concentration will occur at the top and bottom arch spots of the well. The concentration coefficient of the maximum principal stress is larger than that of the minimum principal stress. As indicated in Figure 9-26, tensile failures may occur at the top and bottom arch spots of the well wall. These two spots may tend to fail during the construction and operation of the horizontal well. So special attention should be given to this stability problem.

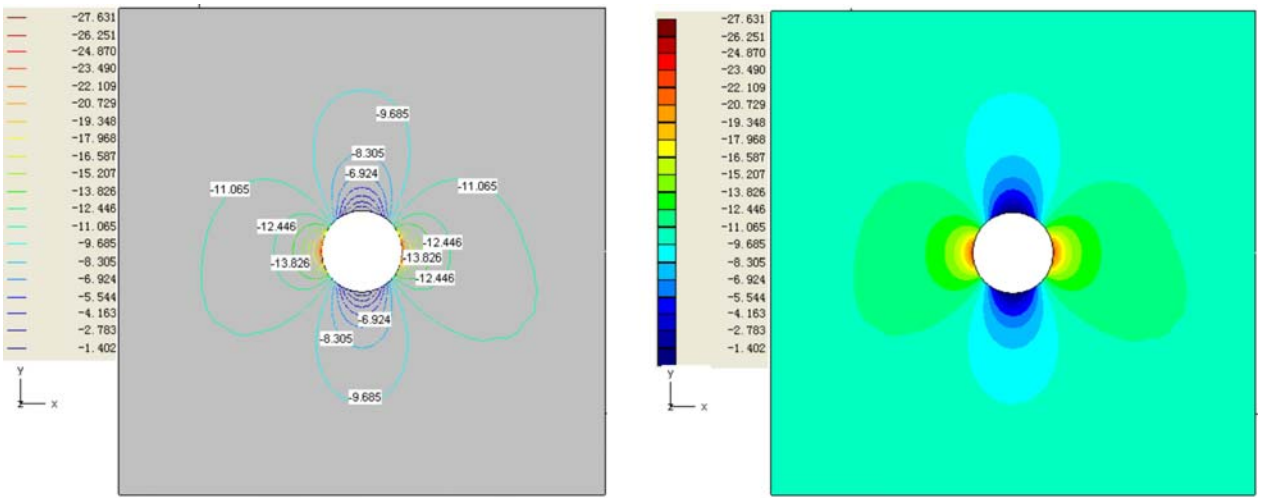

Figure 9-22. Case 1: The maximum principal stress σ_1 around the well bore section.

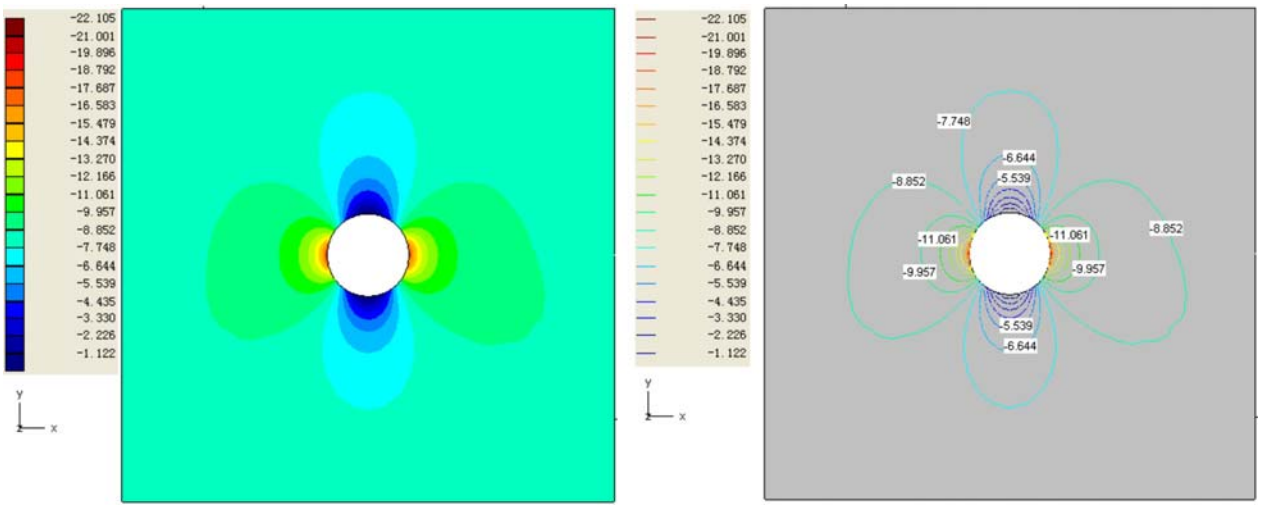

Figure 9-23. Case 1: The minimum principal stress σ_3 around the well bore section.

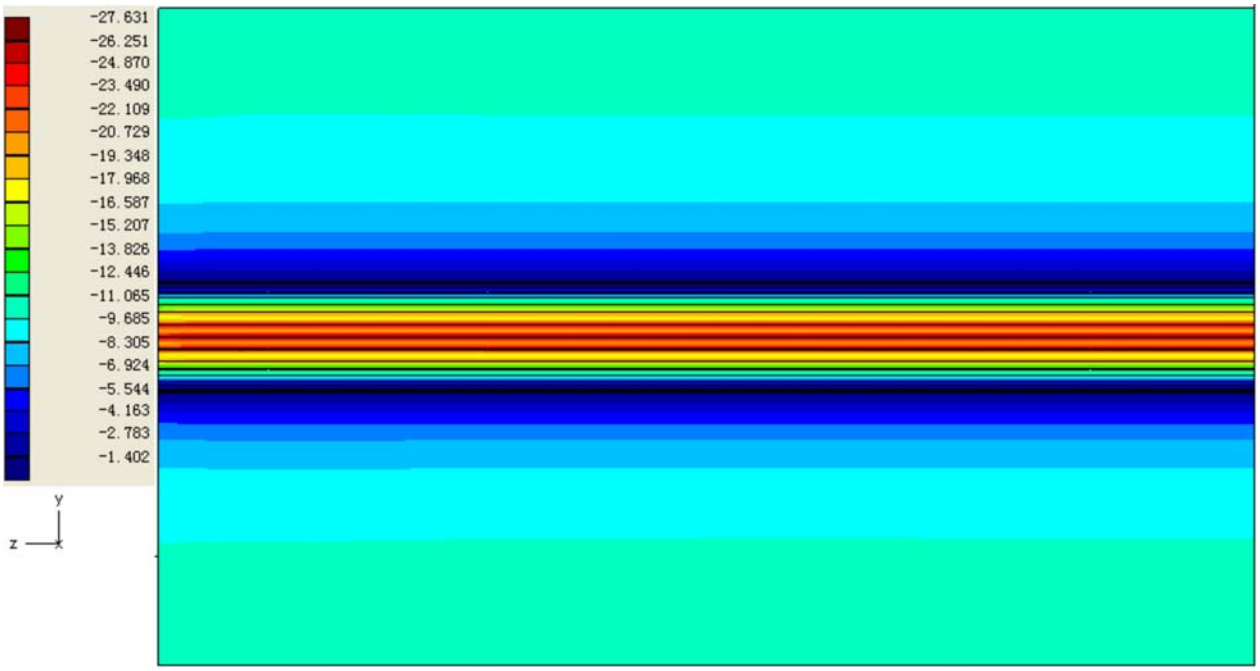

Figure 9-24. Case 1: The maximum principal stress along the well axis.

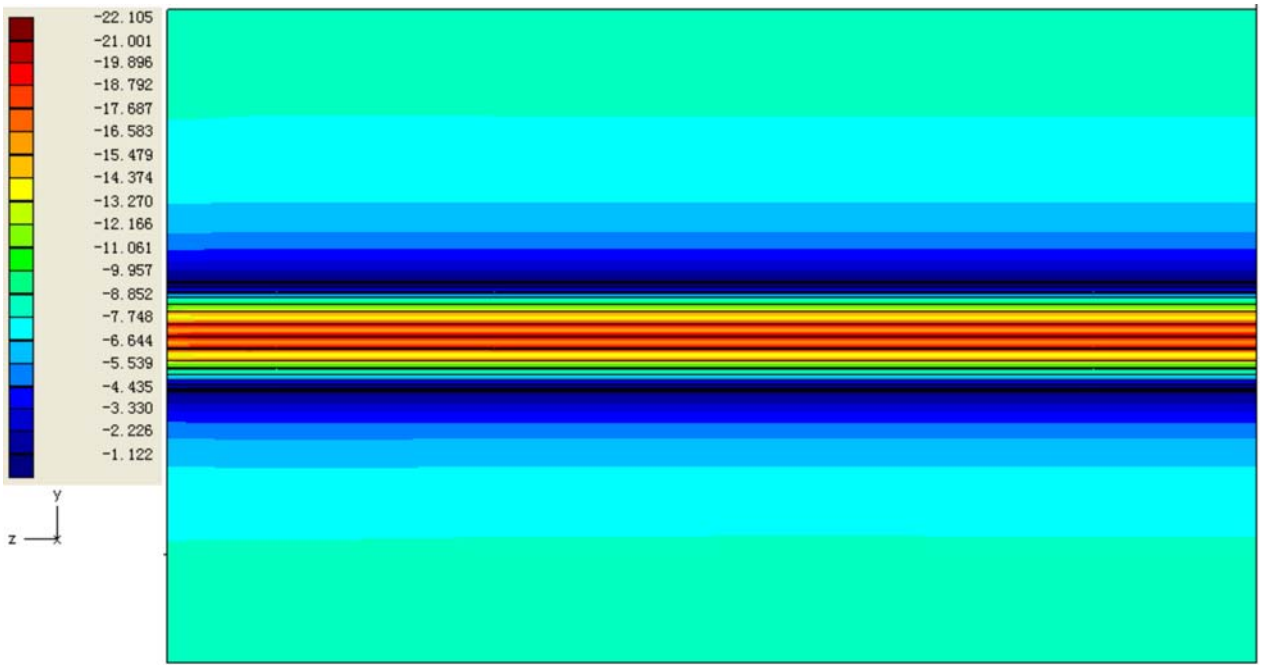

Figure 9-25. Case 1: The minimum principal stress along the well axis.

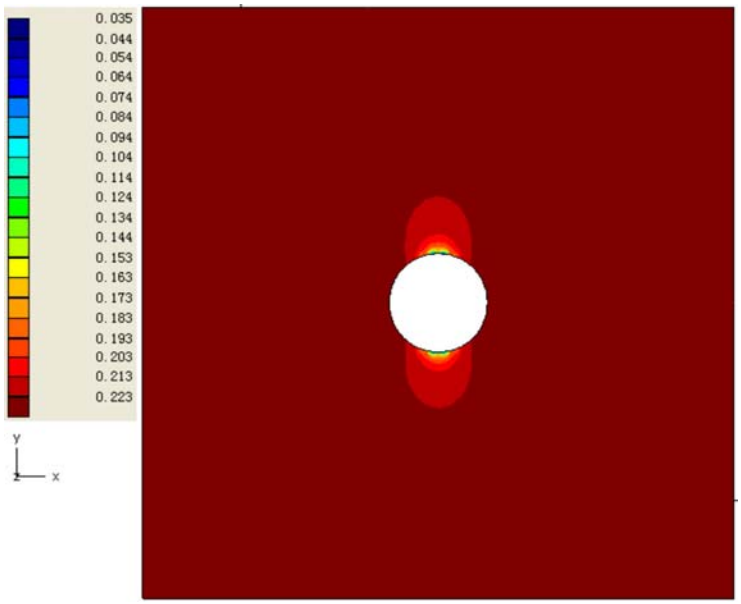

Figure 9-26. Case 1: Safety coefficient for minimum principal stresses. Possible tensile failure on top and bottom of the well bore.

9.3.5 Case 2- Well Axis Perpendicular to the Maximum Horizontal Principal Stress

The following figures show the stress distribution around the well section (Figures 9-27 and 9-28) and along the well axis (Figures 9-29 and 9-30). The tensile stress concentration also occurred at the top and bottom of the well bore (Figure 9-31). According to these results, these results are similar to those mentioned above, but here the stress magnitudes (absolute values) are lower than those in Case 1.

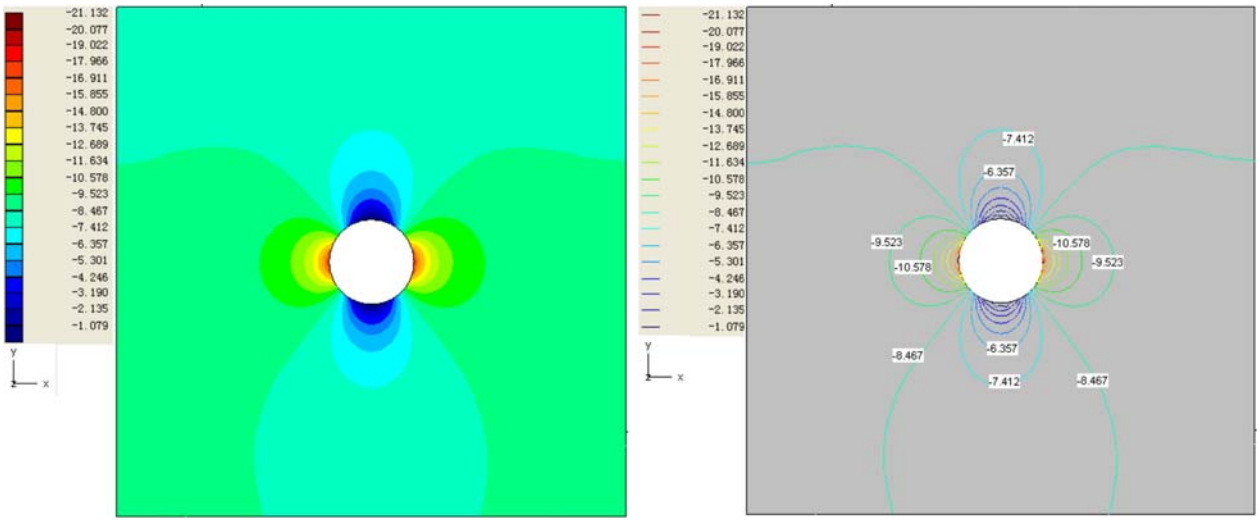

Figure 9-27. Case 2: The maximum principal stress σ_1 around the well bore section.

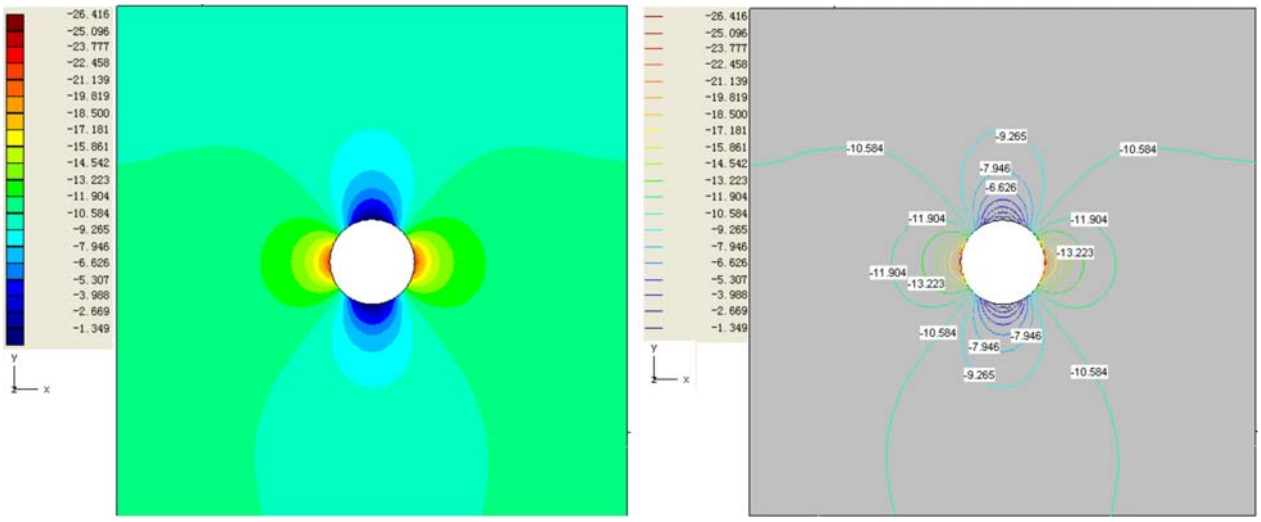

Figure 9-28. Case 2: The minimum principal stress σ_3 around the well bore section.

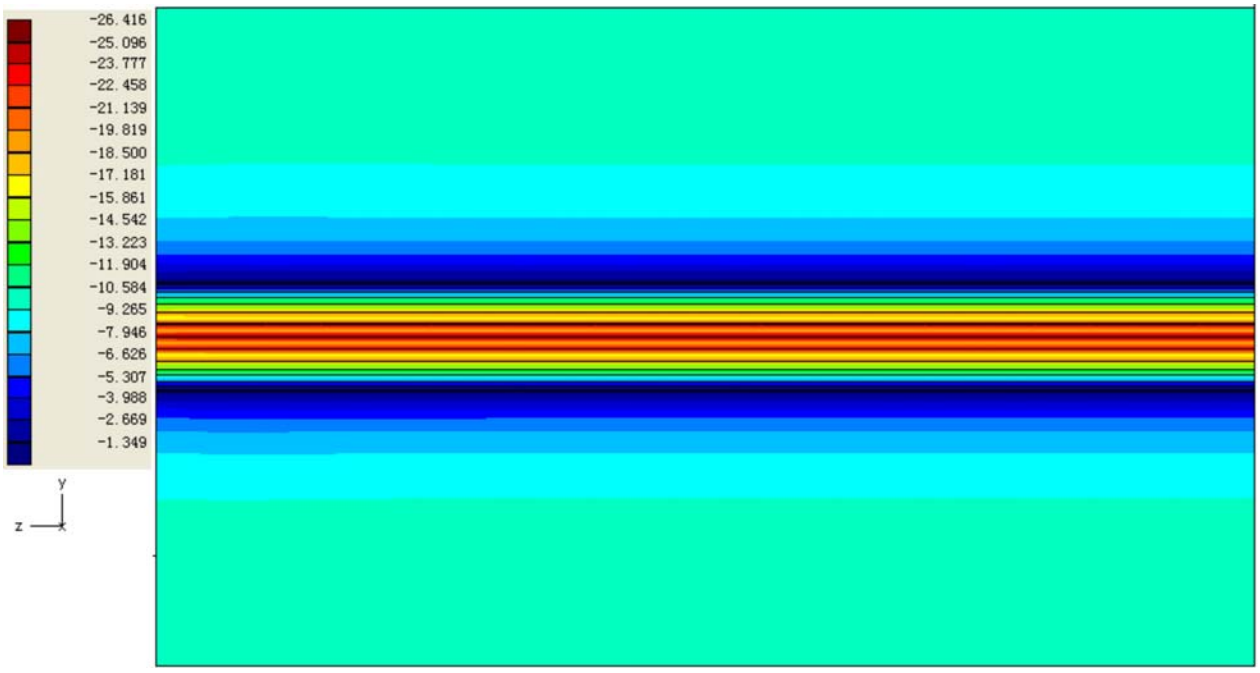

Figure 9-29. Case 2: The maximum principal stress along the well axis.

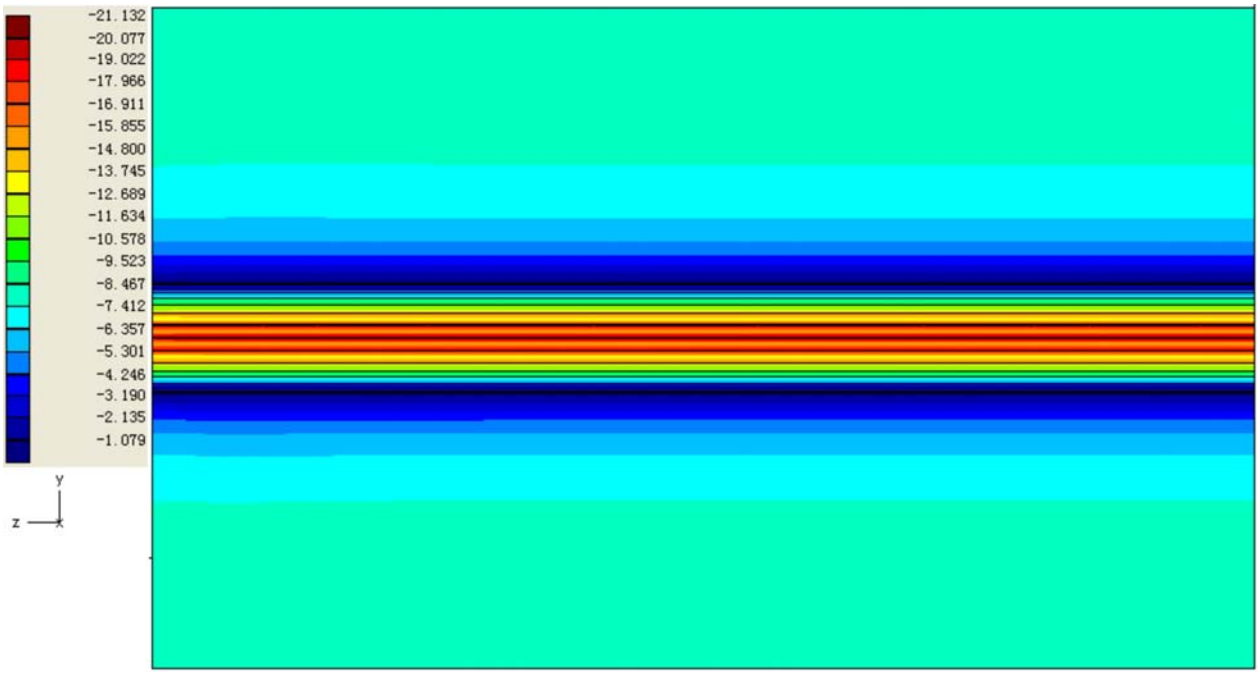

Figure 9-30. Case 2: The minimum principal stress along the well axis.

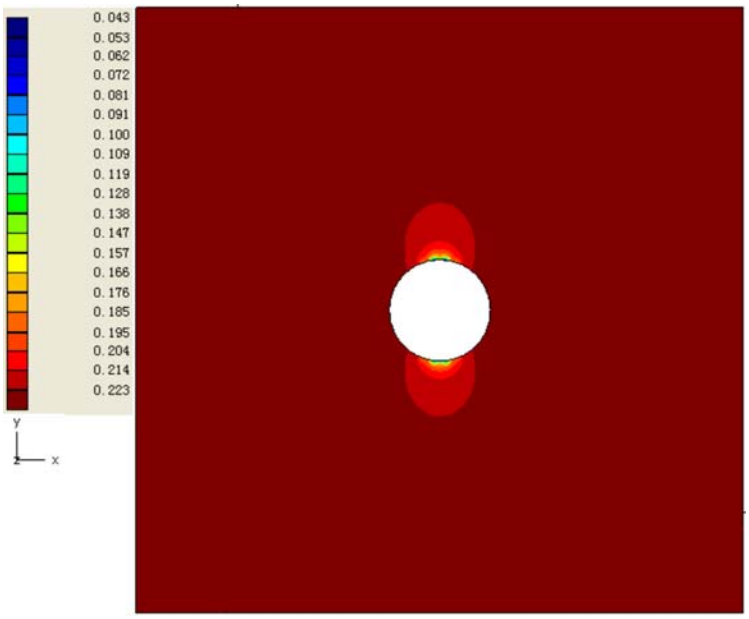

Figure 9-31. Case 2: Safety coefficient for minimum principal stresses. Possible tensile failure on top and bottom of the well bore.

9.3.6 Case 3- Well Axis 45-Degree to the Maximum Horizontal Principal Stress

The following figures show the stress distribution around the well section (Figures 9-32 and 9-33). The safety coefficient for Case 3 is shown in Figure 9-34. Comparing to the results in Cases 1 and 2, it is seen that the distribution of the maximum and minimum principal stresses are similar in all three cases, however, their magnitudes are different.

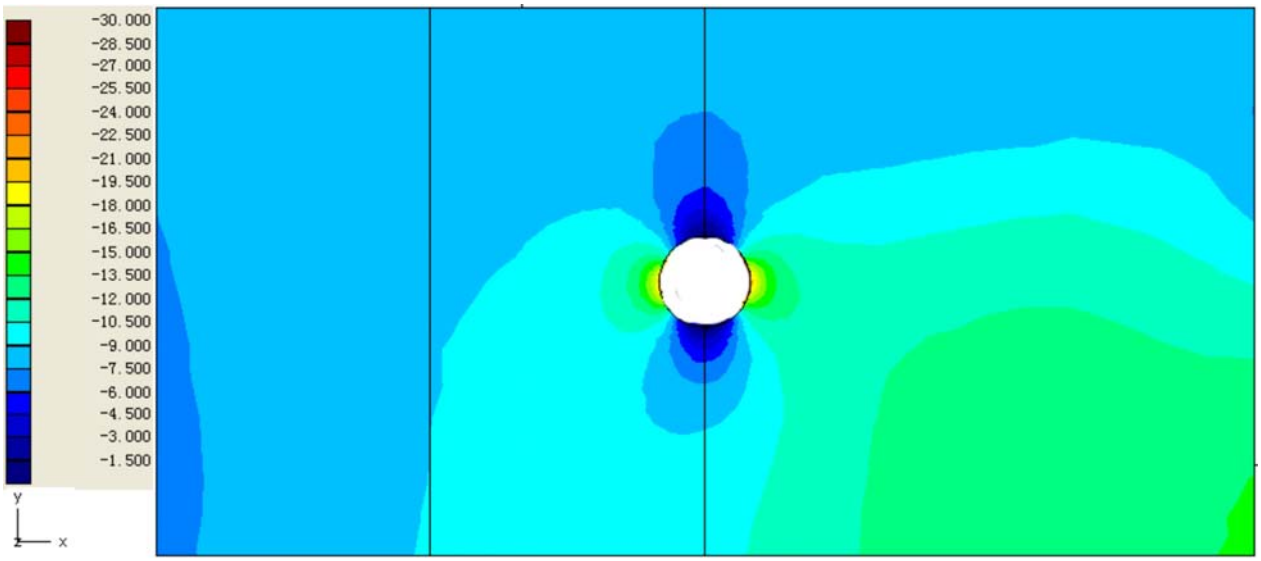

Figure 9-32. Case 3: The maximum principal stress σ_1 around the well bore section.

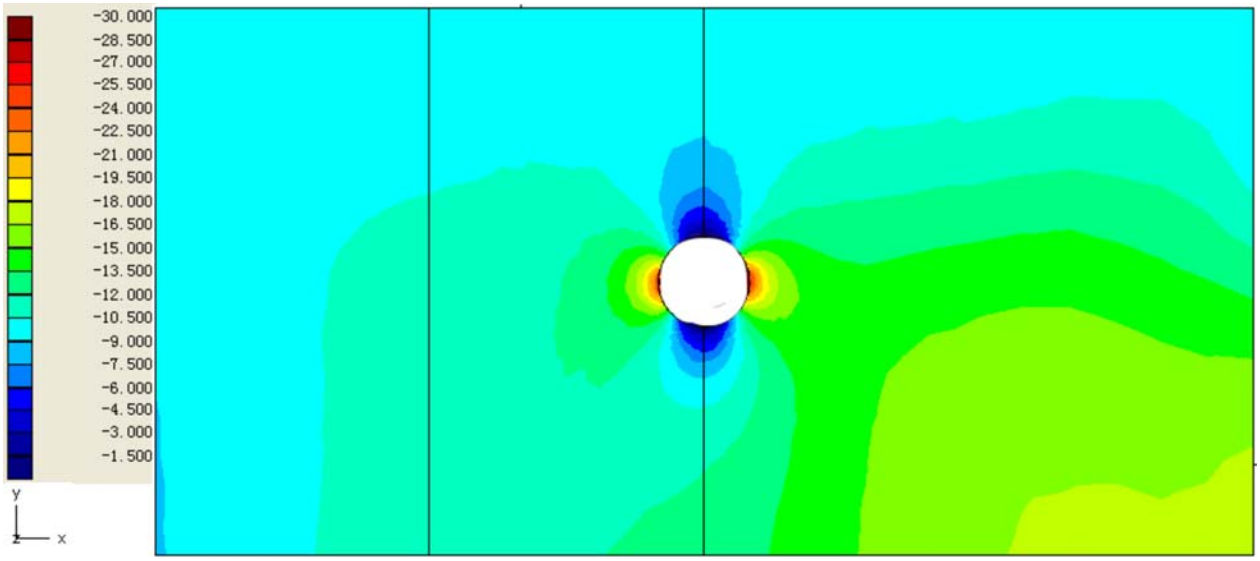

Figure 9-33. Case 3: The minimum principal stress σ_3 around the well bore section.

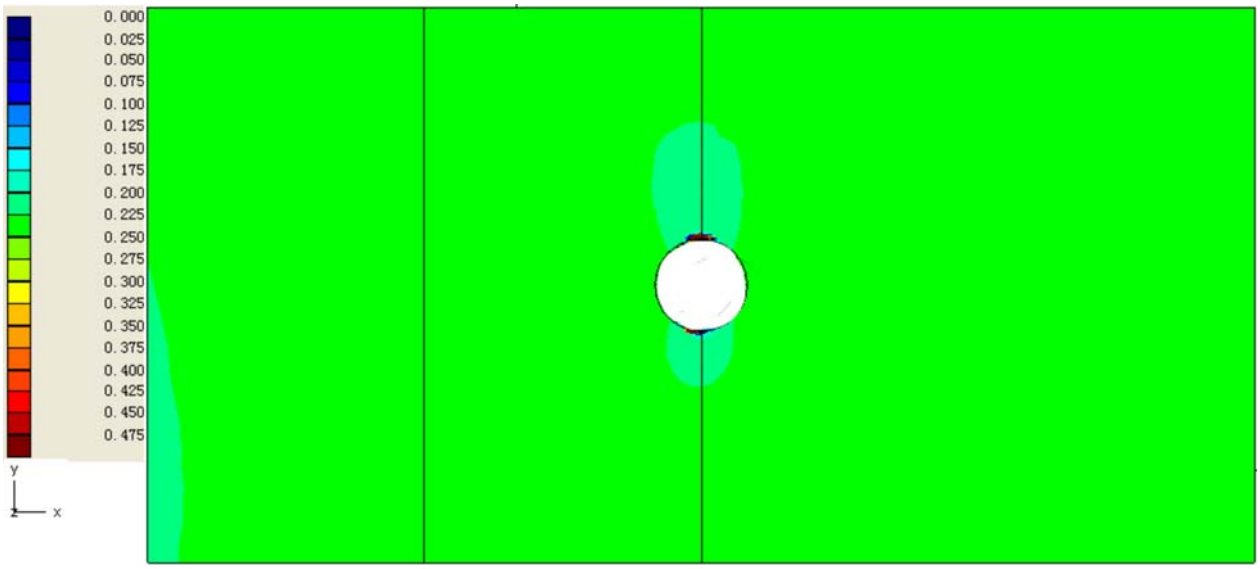

Figure 9-34. Case 3: Safety coefficient for minimum principal stresses. Possible tensile failure on top and bottom of the well bore.

9.3.7 Discussion

Actually, the above figures show the overall distribution of the maximum and minimum principal stresses for each of the studied each cases. However, to compare the differences among the three cases, we need to set up specific stress monitoring points around the well section to get the specific magnitudes of each case and compare them. From the above study, it is obvious that the top, bottom, and the middle spots of the well bore are the most stress-concentrated points, and need more attention on their detailed values (Figure 9-35).

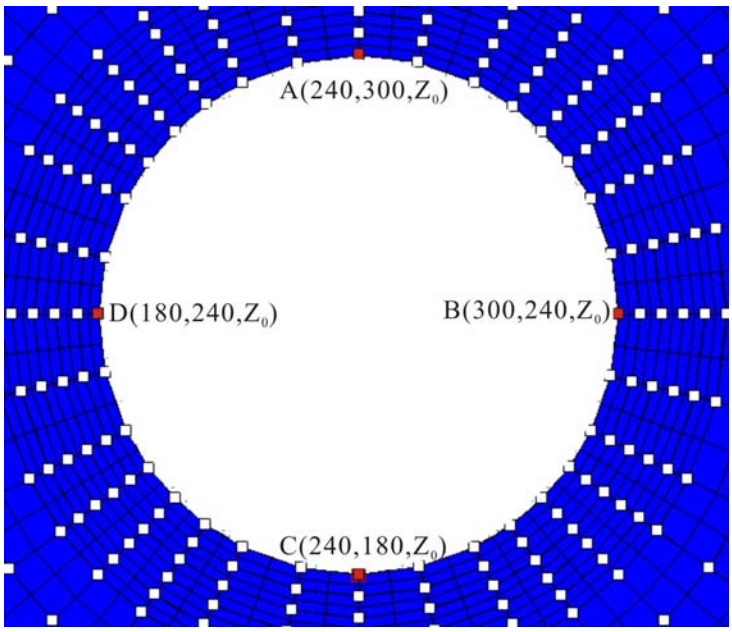

Figure 9-35. Stress monitoring points around the well section.

Table 9-7 summarizes all the data from these four stress-concentrated points. According to the data shown in Table 9-7, there are small differences among these three research cases. However, we can also find out that case 2 is good to the stability the horizontal well, and case 3 is the worst design among the three.

Table 9-7 Summary of stress data at the four monitoring points

Cases	Monitoring point	Coordinates		σ_1 (1000 psi)	σ_2 (1000 psi)	σ_3 (1000 psi)
		X	Y			
Case1	A	240	300	-0.049	-0.055	-0.061
	B	300	240	-22.104	-24.867	-27.63
	C	240	180	-0.05	-0.056	-0.062
	D	180	240	-21.901	-24.639	-27.376
Case2	A	240	300	-0.068	-0.076	-0.085
	B	300	240	-21.096	-23.733	-26.37
	C	240	180	-0.068	-0.076	-0.085
	D	180	240	-20.867	-23.475	-26.084
Case3	A	240	300	0.726	0.654	0.581
	B	300	240	-17.812	-20.039	-22.265
	C	240	180	0.801	0.721	0.64
	D	180	240	-19.166	-21.561	-23.957

9.3.8 Conclusion on In-Situ Stress on Stability of Horizontal Wells

From screening and reviewing previous work by oil companies, the orientation of the maximum horizontal principal stress is NE to NEE in the Bakken Formation, Williston Basin, North Dakota. For the Bakken Formation, the fracture gradient ranges from 0.75 to 0.85 psi/ft, and the ratios among three principal stresses, i.e. the vertical principal stress, the maximum horizontal principal stress and the minimum horizontal principal stress are approximately 1:0.95-0.85:0.85-0.75. Based on a simplified numerical modeling, distribution of in-situ stresses in the Bakken Formation is relatively homogeneous. The stress orientations are stable and consistent across the study area; and the magnitudes may be affected by the mechanical properties of the rock-mass in the formations. In general, the stress magnitude increases with the depth, i.e. the stress magnitudes will increase at a certain stress gradient. Impact of in-situ stress on stability of horizontal wells were numerically studied. Compressive stress concentration appeared at the middle of the well-bore side walls, and tensile stress concentration appeared at the top and bottom of the well bore. The magnitude varied with the relative orientation of the horizontal well axis with respect to the maximum horizontal stress. From the stability point of view, the case of the well axis perpendicular to the maximum horizontal principal stress is the best; and the case of the well axis at 45º angle with the maximum horizontal principal stress is worst.

In this study, we collected and compiled existing geomechanical data from previous work by others. After screening all reports of 4000+ Bakken wells, we found that there were only 18 points that have incomplete, sometimes problematic, geomechanical data. Based on these data and other tectonic and geological literatures, we derived the orientation and magnitude of the in-situ stress field in the Bakken Formation, and numerically modeled the impact on stability of horizontal wells in different directions. As a summary, we obtained the following insights about the basin and the geomechanical properties of the Bakken Formation:

1) The Williston Basin is a cratonic basin. There have been no major tectonic activities since Paleozoic eon.
2) The tectonics of the basement controls the geology in the sedimentary formations. The anticlines and domes in the sedimentary formations represent the subsurface highs in the basement.
3) Vertical and sub-vertical faulting was the dominant fracturing process. Strike-slip faulting in the NE-SW and NE-SW directions were secondary and tertiary fracturing processes.
4) The Bakken formation is around 10,000 ft below the surface. There are two major salt formations above and below the neighborhood of the Bakken formation. The salt formations changed the overburden-induced horizontal stress magnitude from dominated by Hooke's law to Pascal's law.
5) In-situ stresses in the Bakken formation is controlled by the above features, and can be estimated as follows:
    a. The maximum principle stress, σ_1, is in the vertical direction, and can be estimated with the overburden pressure, σ_V;
    b. The intermediate principle stress, σ_2, is in the horizontal direction. It is the maximum horizontal stress, σ_H. It is in the NE direction in general, but may vary due to local heterogeneity. The ratio of σ_H / σ_V is about 0.9, closer to the hydrostatic status than to the Hooke's status.

c. The minimum principle stress, σ_3, is in the horizontal direction. It is the minimum horizontal stress, σ_h. It is in the NW direction in general, but may vary due to local heterogeneity. The ratio of σ_h / σ_V is about 0.8, closer to the hydrostatic status than to the Hooke's status.

Using the collected geomechanical data from previous work by others and the above geological model, we conducted 3-dimensional numerical modeling to simulate the stress distribution inside the Bakken Formation and investigated the impact of in-situ stress orientation on wellbore stability. The results indicate that compressive and tensile stress concentration occurs around the wellbore at different points, and the magnitudes change with the orientation of the well with respect to the maximum horizontal stresses.

10. New Methodology for In-Situ Stresses and Fracture Toughness

10.1. Kaiser Effect Method for In-Situ Stresses

In this study we have designed the Kaiser In-Situ Stress (KISS) system. The KISS system's goal is to determine in-situ stresses in rock formations by means of stress-induced acoustic emission (AE) and the Kaiser effect. The KISS system is a non-destructive approach of in-situ stress determination and has received much attention in the past. To fully understand AE, the Kaiser effect and how it is used to determine stress we present the necessary theoretical background, available experimentation and results from other investigators to investigate the plausibility of AE and the Kaiser effect for in-situ stress determination. The final goal of the design is to investigate the uniaxial compression induced AE and the Kaiser effect in rock to determine the fundamental process of the Kaiser effect. Once confirmation of the Kaiser effect from the uniaxial compression method is achieved, more sophisticated experimentation with triaxial compression-induced AE and the Kaiser effect, which simulates the in-situ conditions, can be analyzed (Blanksma, 2011).

Besides only proposing the KISS system as a theoretical design we also presents results from an initial design KISS system. In order to find out the plausibility of using AE and the Kaiser effect for in-situ stress determination, experiments have to be conducted using fundamental processes. Theoretical work on AE and the Kaiser effect has been investigated extensively and the only way to determine scientific plausibility is by empirical observation and analysis. The process investigates uniaxial compression induced AE to determine the presence of the Kaiser effect. By actually performing the experiments that quantify physical phenomena comparisons can be made to see if uniaxial compression induced AE can determine in-situ stresses and be developed further to determine true states of in-situ stress (Blanksma, 2011).

10.1.1 Importance of Kaiser Effect Method

The in-situ stresses in rocks can be determined by means of compression induced acoustic emission (AE) and the Kaiser effect. AE is analogous to earthquakes. Earthquakes transmit energy by means of compression waves and shearing waves. Micro cracks transmit energy by means of compression waves in the form of acoustic emission. The Kaiser effect is an AE phenomenon defined as the absence of detectable acoustic emission until the previously applied stress level is exceeded (Norlund and Li). It is a measure of damage, specifically microcracks in a material subjected to loading. It is firstly investigated on metals by Joseph Kaiser (Kaiser, 1950).

10.1.2 Kaiser Effect Method- Problem Definition

Current methods for determining rock in-situ stresses used today can be classified into two categories: destructive method and non-destructive method. Destructive methods disturb the in-situ rock conditions, i.e. inducing strain, deformations or crack openings. Non-destructive methods are based on observation of the rock behavior without major influence on the rock. We focus on non-destructive method by developing a method to determine in-situ stresses in rock that is inexpensive, non-evasive and relatively accurate, based on the fundamental idea of induced acoustic emission. The work contains two stages: 1) development of the KISS system, 2) testing and improving.

The goal of the first stage is to develop the KISS system based on the theoretical framework of acoustic emission and the Kaiser effect. Hardware is set up and software is designed at this stage. Another goal in this step is to become familiar with coding the data acquisition system for the KISS system. National Instruments *LabVIEW* will be utilized for data acquisition and data analysis. Since substantial knowledge is required to use *LabVIEW*, designing the data acquisition code offers the opportunity to learn and use a powerful program. In addition, knowing how to code programs using different software is a vital part of all engineering disciplines. Once the in-situ stresses are experimentally obtained by the KISS system, stress transformation equations are implemented to determine the principle stress tensor. The stress tensor contains the magnitude of the principal stresses and the direction cosines for each stress (Blanksma, 2011).

The second stage involves all the testing and calibration of the hardware and software. Different rock samples that represent different oil containing formations will be analyzed to compare one against the other. Because the system relies on analog to digital processing, large amounts of data will need to be stripped down to reveal the physical properties that are useful to this design.

10.1.3 Kaiser Effect Method- Theory

Kaiser Effect in Rock

The Kaiser effect is a physical phenomenon prevalent in many materials as wells as rocks. The theoretical foundation of the Kaiser Effect can be demonstrated by many different physical phenomena including electromagnetic waves, seismic waves and important to this study, induced acoustic waves. AE (acoustic waves) is a property of wave mechanics and is the propagation of a lateral compression wave through a medium that is produced by an energetic event such as cracking or sudden deformation. The energy of the wave can range greatly. For example, large scale waves travelling through a rock mass are the source of what is commonly known as earthquakes. However, small scale waves are also produced by small strain. These small waves are nowhere near the magnitude of an earthquake, but the idea is logical that some induced AE waves represent “miniature” earthquakes travelling through a rock mass. Depending on the rate of change in the volume of a rock mass relative to its original volume, i.e. strain rate, energy may be transformed into a pressure wave travelling through the rock mass if cracking occurs. The propagating wave is identified as AE and it directly indicates an amount of damage in a rock specimen from the formation of a crack (Blanksma, 2011).

The Kaiser effect can be produced empirically numerous ways. One method for identifying damage in rock is to count acoustic events and look for any changes in time; changes of the number of AE in time represent an increase or decrease in crack growth. The empirical method that exploits the Kaiser effect takes place in rocks and materials subjected to cyclic loading/unloading. In the simplest case of cyclic, uniaxial loading with the cycles peak stress increasing from cycle to cycle, the acoustic emission is zero or close to the background level as long as the current stress remains below the largest previously reached stress value. As this peak stress value is attained, the AE activity increases dramatically (Lavrov, 2003). The change in AE activity at the point of previously applied maximum stress is the Kaiser Effect. A graph in Figure 10-1 of AE versus time for two cycles illustrates the concept (Blanksma, 2011).

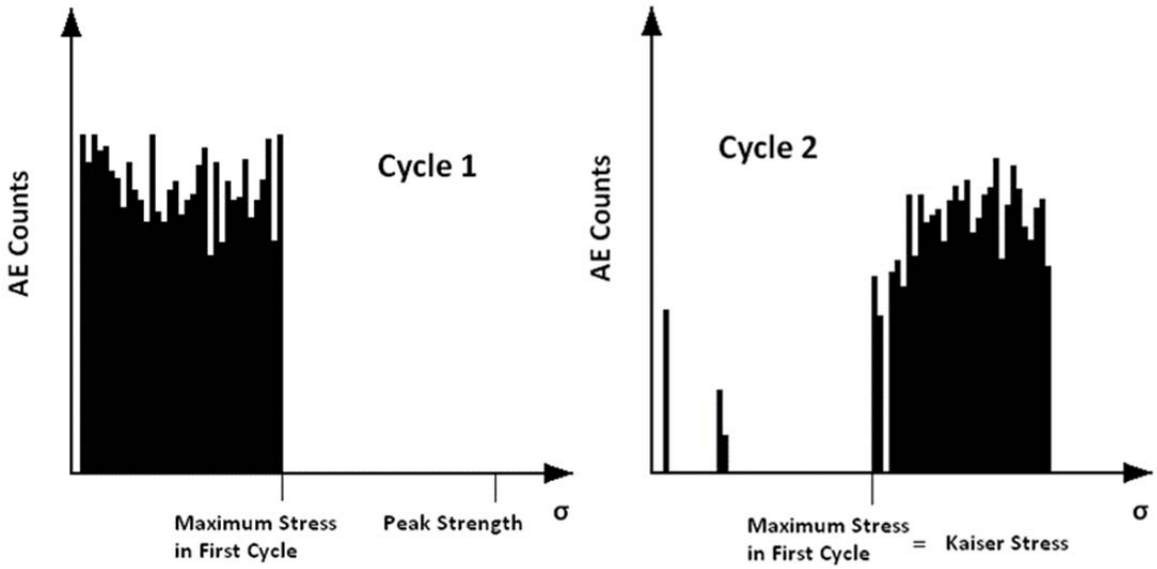

Figure 10-1. Two loading cycles showing AE counts versus stress. The absence of AE in cycle 2 indicates the Kaiser Effect

The rate of AE is a function of stress on a rock and most importantly the time the rock has been under stress. Because of this relationship rock have the ability to "remember" the largest previous stress that had once acted upon it. The theory is that the first cycle of compression is actually the in-situ stress state of a rock in the subsurface and by extracting a sample of the rock and reloading can be completed in a lab to determine the previously applied maximum stress. This maximum "memorized" stress is a direct consequence of the Kaiser effect and can be determined experimentally. By verifying that the memorized stress is in fact the maximum previously applied stress may allow for determination of the entire in-situ stress regime of the rock. Determining the "memorized" stress (σ_m) requires mathematical analysis of the second cycle cumulative AE hits versus stress. The Kaiser effect can be recognized as an inflection point (change in slope) on the graph of cumulative AE versus stress (Lavrov, 2003). Figures 10-2 and 10-3 show the location of σ_m. Finding the inflection point can be performed by bilinear regression, or by drawing tangents to the two parts of the curve and searching for their intersection (Lavrov A. , 2003)

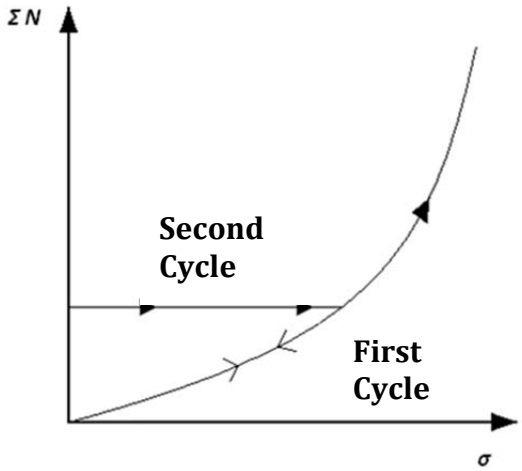

Figure 10-2. A graph of the cumulative AE hits (Σ N) versus stress (σ) for two loading cycles subject to uniaxial compression.

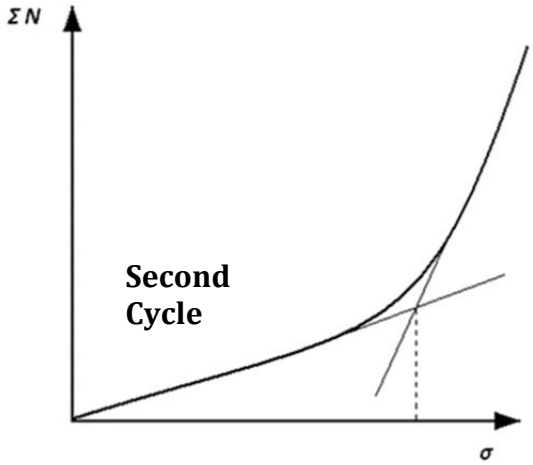

Figure 10-3. Inflection in the cumulative AE hits (Σ N) versus stress (σ) graph indicates the previous maximum stress state.

Determining the inflection point as the peak memorized stress level requires high resolution equipment and therefore is not always evident when comparing cumulative AE hits versus stress. A technique developed by Yoshikawa and Mogi (1989) can be used by comparing the AE hit *rate* versus stress. Figure 10-4 gives a graphical example of this method. This graph shows a better indication of where the Kaiser point is located. The Kaiser point will be indicated by the separation of the two lines corresponding to different loading cycles. In the first cycle AE hit rate increases as stress increases. In the second cycle AE hit rate will be the same as in cycle one. However, once the stress level in cycle two reaches the previous applied stress level in cycle one, AE hit rate will no longer be the same for both cycle one and two. The bifurcation point is the Kaiser point (Blanksma, 2011).

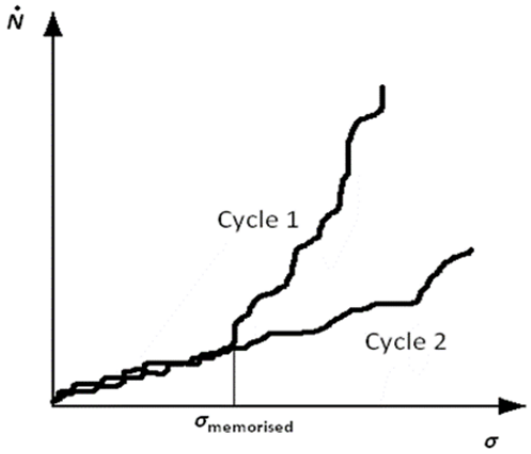

Figure 10-4. AE hit rate versus stress (σ) reveals the Kaiser point at the bifurcation of the two different loading cycles.

Physical Models for the Kaiser Effect

Empirical evidence for the Kaiser effect clearly shows the physical phenomenon and has been extensively investigated prior to the 1980's. However an accepted physical model was not fully developed until much later and still receives changes to this day. The Kaiser effect was first investigated by Joseph Kaiser in the early 1950's. His initial experiments were conducted on metals, woods and sandstones (Kaiser, 1953). Since the work of Joseph Kaiser many physical models have been suggested to explain the Kaiser effect.

For practical purposes the physical model that best explains AE and the Kaiser effect is analogous to the mechanics of an earthquake. During an earthquake deformation of crustal material occurs rapidly and releases energy in the form of shearing (S-waves) and compression (P-waves) waves. In small rock mass, on the order of inches and feet,

rapid deformation takes place when exposed to a force. The deformation exists in the form of microcracks. The microcracks can be related to earthquakes but have orders of magnitude less energy. Figure 10-5 shows a schematic of the microcrack model (Blanksma, 2011). Many more sophisticated models have been investigated for AE and the Kaiser effect. Stevens and Holcomb (1980) presented a sliding crack model to account for stress memory in rock. Holcomb (1980) also suggested a reversible Griffith crack model to explain the Kaiser effect. Later suggested models by Lavrov (1997) used Fairhurst-Cook wing crack models to interpret the Kaiser effect in uniaxial compression (cycle 2) after true triaxial compression (cycle 1) (Blanksma, 2011).

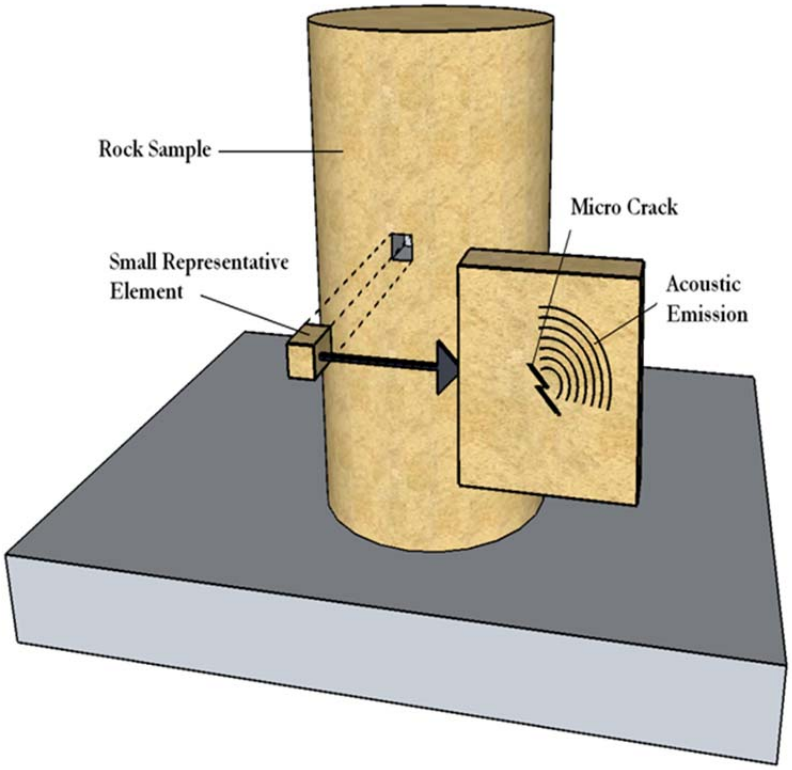

Figure 10-5. The microcrack model for AE

10.2. Kaiser Effect Method –Experiment Setup and Procedure

10.2.1 Design Constraints

Obtaining a rock specimen that has been cored from a rock formation can be accomplished directly or indirectly. Direct coring of a rock formation, especially oil containing rock formation is expensive and problematic for the KISS system. For example core from the Bakken Formation in North Dakota is highly valuable and difficult to obtain. Also, obtaining core samples directly disturbs the in-situ stress on the rock and results in damage caused by tensile and shear stresses near the drill bit, thus complicating any Kaiser Effect observation on the sample core (Lavrov A. , 2003). An indirect approach can be considered by using rock with known characteristics that resemble oil containing rocks. Acquiring theses rocks is usually inexpensive; however the accuracy of the results depends completely on the similarity of the rock being tested to oil bearing rock. In this study indirect measurement on various rock types will be implemented to ensure the system works properly, if oil containing core can be obtained it will be tested by the KISS system. Rock type has a profound effect on AE. Most Kaiser effect experiments were performed on brittle rocks because they produce more micro cracks upon compression and thus have a higher AE frequency compared to softer rocks. Results obtained by Filimonov et al. (2002) on rock salt, a very ductile rock, revealed a well pronounced Kaiser effect. Results by Dunning et al. (1989) revealed a clear Kaiser effect on sandstone if the sample was preloaded to about 60% of its peak strength and inclined at an angle to simulate a fault zone (Blanksma, 2011).

After obtaining a suitable core sample to test, time is of the essence. Like humans, the ability for a rock to retain its memorized stress history fades with time. Once the rock is removed from the rock mass, AE activity decays exponentially to the point where the Kaiser effect is indistinguishable (Lavrov , 2003). The reason for the crack "healing" has been an issue that needs further investigation. By receiving a core sample as soon as it is cored will result in a better analysis of the in-situ stresses in the rock formation. Another issue that must be addressed is the type of testing. When the Kaiser effect was first being investigated most lab measurements involved a uniaxial compression test on the sample. However, Holcomb (1993) showed that it is impossible to determine a rock's stress history by uniaxial compression when it was stressed in a triaxial environment. The only way a Uniaxial Load Method (ULM) will work effectively in determining stress history is if the primary principle stress (σ_1) during reloading is parallel by no more than 10° to the primary principle stress during preloading (Lavrov , 2003). This requires an estimate of which direction σ_1 acted on the rock sample while it was in-situ. In the case of the KISS system and in most lab methods σ_1 is considered to be in the vertical direction, as a result of the overlying rock mass. If obtaining the preloaded σ_1 stress direction is accomplished and the sample is reloaded by the ULM, the very best results are only a linear combination of the in-situ stress tensor of the rock in question (Lavrov , 2003).

After determining which method of compression is better suited for the experiment, determining how to conduct the experiment is crucial. During the cyclic loading test it is best to ensure that the preloading cycle does to reach the maximum strength of the rock. The closer the preloading stress to the ultimate strength of the rock, the less pronounced the Kaiser effect is during reloading (Kurita & Fujii, 1979). According to Lavrov, in order to obtain a well – pronounced Kaiser effect, the preload stress should be in a range from about 30% to about 80% of the ultimate strength (Lavrov, 2003). Experiments have shown that the longer the duration of loading on soft rocks in the first cycle creates a clearer Kaiser effect in the reloading cycle (Michihiro, Yoshioka, & Hata, 1989). On brittle rocks experiments have shown little influence of the duration of loading on the Kaiser effect (Yoshikawa & Mogi, 1989). However, a study on brittle rocks has found that if the loading rate in the first cycle is fast compared to that of the second cycle, then the Kaiser effect occurred at 67% of the peak stress of the first cycle. When the order was reversed (first cycle slow, second cycle fast) the Kaiser effect occurred at the peak stress of the first cycle. The dependency of the Kaiser Effect on the loading rate has not been determined for soft rocks and plastic rocks (Lavrov, 2001).

The KISS system is intended to provide a more cost effective rock in-situ stress testing method than its predecessors without sacrificing accuracy. For example, in the majority of rock testing methods used today an expensive piece of equipment has to be placed down the borehole into the rock formation and analyzed on site. These methods do work; however, the KISS system eliminates the need to send equipment into the borehole. The KISS system requires only obtaining core samples of the rock formation that can then be brought back to a lab for analysis (Blanksma, 2011).

10.2.2 Software

Software is a crucial component of the KISS system. While many programs exist for other rock testing systems the KISS system is unique in the way that it will need its own data acquisition program. Creating a program for the KISS system will require substantial knowledge about coding. In industry, a practical solution may be to hire a software engineer or computer scientist. However, in an industry that also hinges on technical application and economic practicality, being able to create your own code for projects that require customized data acquisition eliminates the need to hire a software engineer or computer scientist.

All programs in this system have been designed by the author. Proficiency in coding for data acquisition and correlation is necessary to create and understand programs that record reliably. The software used in the KISS system is National Instruments LabVIEW 8.2. Because of its superior data analysis and ease of coding using G-language, LabVIEW is excellent software for coding customizable programs. The three important programs for the KISS system include; 1 – The data acquisition program that will be used during experimentation, 2 – a waveform analysis program to determine AE and its corresponding times and, 3 – a correlating program to match force data with AE data to construct a cumulative AE versus stress/force graph (Blanksma, 2011).

10.2.3 Preliminary Design Options

The KISS system can be designed two ways: The first using the uniaxial load method (ULM), and the second using a triaxial load method. The ULM requires applying a load along the axis of the rock sample in a direction that is no more than 10 degrees different from the in-situ principal stress direction (Lavrov A. , 2003). The method relies on

the estimation that the in-situ principal stress is directed along the vertical axis (see Figure 10-6) of the rock sample. Upon loading, acoustic transducers will record analog signals of the AE activity and run the signal to a high-speed digitizer. The digital signals will be recorded and analyzed by signal analyzing software. At the same time the uniaxial compression system will also have force transducers to record the stress data along with the corresponding time of each stress level. By comparing the stress values and acoustic emission values with the corresponding times, the memorized stress level can be deduced on principles described in the Section 3. However, the limit of finding the memorized stress level for the ULM is only a linear combination and the entire stress tensor can never be achieved using the ULM, as described in previous section. (Blanksma, 2011).

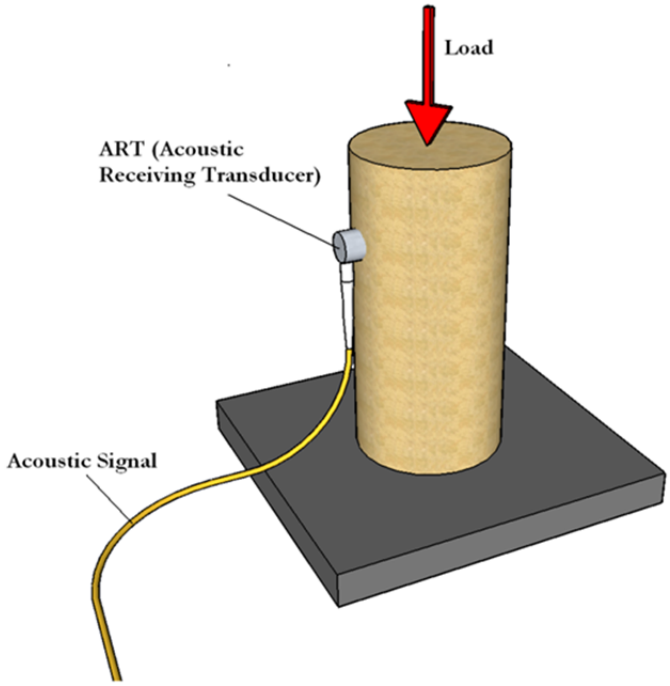

Figure 10-6. Rock sample showing direction of vertical stress and attachment of ART's (Acoustic Receiving Transducers)

The triaxial design option includes similar but much more sophisticated waveform analysis software, and very different hardware. A triaxial load method requires a compression machine that can achieve three degrees of pressure. In the case of a triaxial KISS system, axisymmetric ($\sigma_1 > \sigma_2 = \sigma_3$) or true triaxial ($\sigma_1 > \sigma_2 > \sigma_3$) compression is needed to exploit the Kaiser Effect. Operating a triaxial compression machine that can be either axisymmetric or triaxial requires a high degree of operating knowledge and maintenance. However, finding the complete stress tenor requires a device that can achieve true triaxial compression (Holcomb, 1993).

10.2.4 Selected Design

The KISS system will use the Uniaxial Loading Method (see Figure 10-7). While using a triaxial compression machine is ideal, the fundamental concept of uniaxial compression and the Kaiser Effect needs to be experimentally evaluated before triaxial experimentation can continue. An MTS 816 Rock Mechanics Testing system will provide the uniaxial compression. This rock testing system was chosen because it provides servo-controlled loading for highly stabilized loading rates.

The components of the uniaxial rock testing system include a pump which controls the compression hydraulics, the uniaxial compression machine, two acoustic receiving transducers (ARTS), a pre-amplifier, a high-speed digitizer, and two computers; one to control the uniaxial compression machine and the other for the AE acquisition (Blanksma, 2011). A schematic of the entire MTS 816 Rock Testing System is shown below in Figure 10-8.

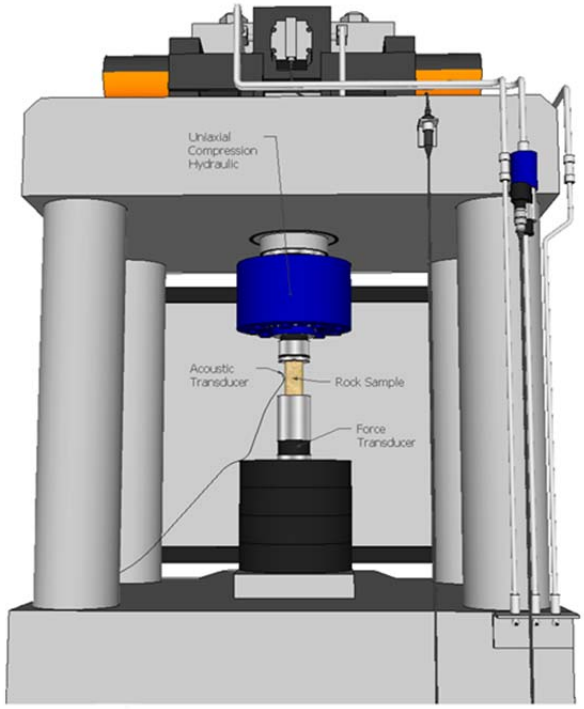

Figure 10-7. A close-up picture of the Uniaxial Loading Method (816 Rock Test System)

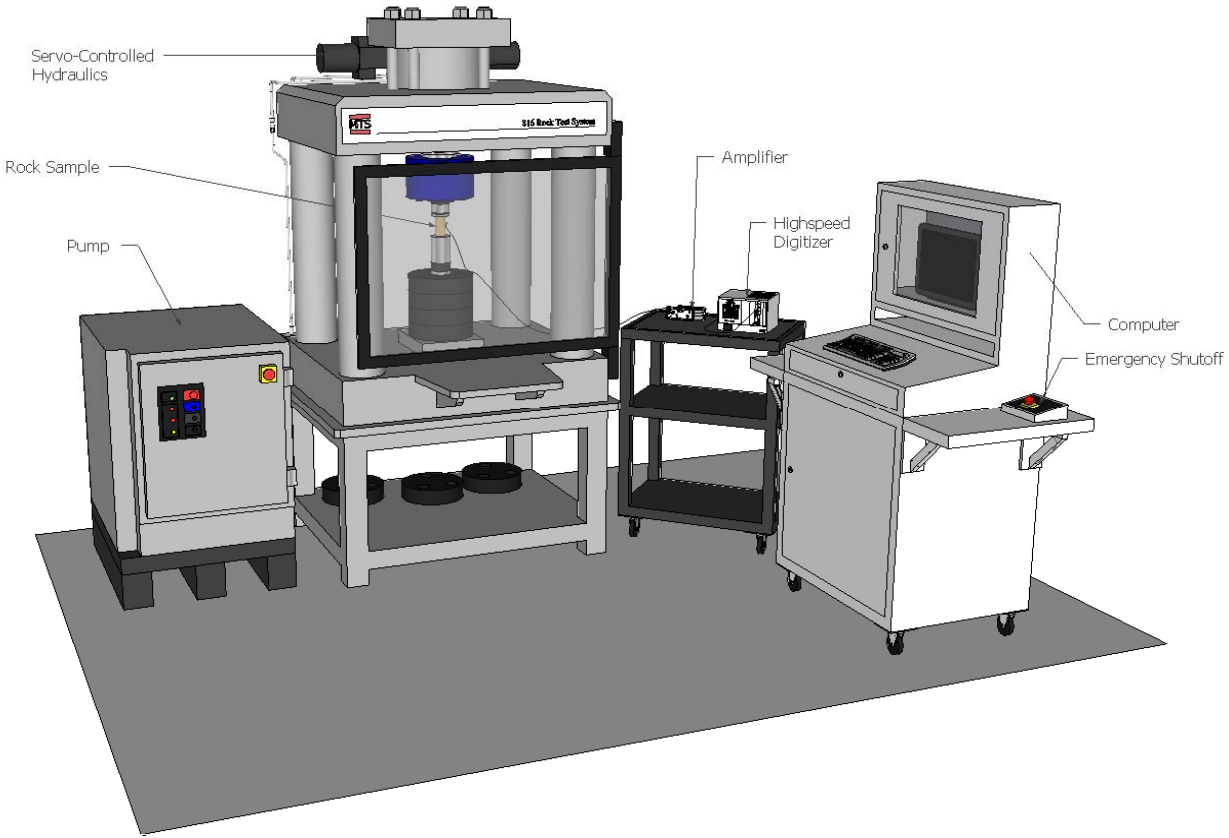

Figure 10-8. A layout of the 816 Rock Test System (MTS). Other components include an amplifier and a high-resolution digitizer. This system uses a uniaxial loading method on the rock sample.

Another reason the ULM has been chosen is because one of the KISS system goals is to investigate the possibility of using the ULM in a new way. A way that may result in determining the entire in-situ stress tensor rather than just a linear combination of the principal in-situ stresses. The new method hinges on the idea that if the orientation of the maximum principal in-situ stress in known, the in-situ stress tensor can be determined from four different specimens cut at four different orientations from one another that are cut from a single core sample (Fa, et al., 2010). Figure 10-9 shows how the sample would be cut. Mathematical techniques for determining the principal in-situ stresses are given in below. Equations for determining the principle stresses are given by Fa et al. (2010):

$$\sigma_v = \sigma_{v0} + \alpha p_p \quad \text{(10-1)}$$

$$\sigma_H = \frac{\sigma_{0^\circ}+\sigma_{90^\circ}}{2} + \frac{\sigma_{0^\circ}-\sigma_{90^\circ}}{2}(1+tan^2 2\theta)^{1/2} + \alpha p_p \quad \text{(10-2)}$$

$$\sigma_h = \frac{\sigma_{0^\circ}+\sigma_{90^\circ}}{2} - \frac{\sigma_{0^\circ}-\sigma_{90^\circ}}{2}(1+tan^2 2\theta)^{1/2} + \alpha p_p \quad \text{(10-3)}$$

$$tan2\theta = \frac{\sigma_{0^\circ}+\sigma_{90^\circ}-2\sigma_{45^\circ}}{\sigma_{0^\circ}+\sigma_{90^\circ}} \quad \text{(10-4)}$$

σ_v = vertical principal stress
σ_H = maximum horizontal principal stress
σ_h = minimum horizontal principal stress
α = effective stress coefficient
p_p = pore pressure
σ_{v0} = Kaiser stress in the vertical direction
σ_{0°, σ_{45°, σ_{90° = Kaiser stress in the plugs orientated at directions 0, 45 and 90 respectively (Figure 10-9).
θ = angle between the 0° direction and the maximum horizontal principal stress direction

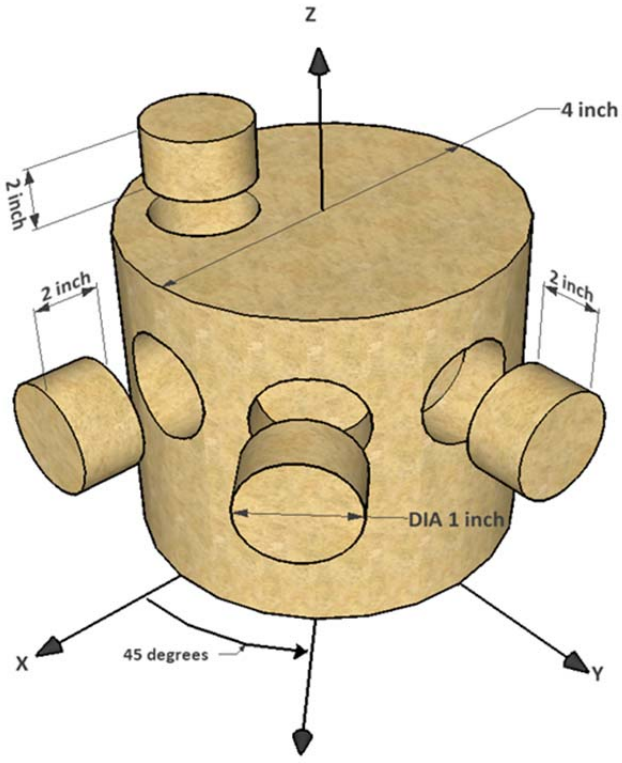

Figure 10-9. Kaiser stress in the plugs orientated at directions 0, 45 and 90, respectively.

The data acquisition portion of the KISS system includes Acoustic Receiving Transducers (ARTs) that will receive waveforms generated during AE activity that send analog signals to a wide band width AE Amplifier. After signal amplification a *National Instruments* high-speed Digitizer will convert all incoming analog signals into digital signals that the selected software can receive and analyze. The selected software will be National Instruments *LabVIEW* because of its ease of graphical coding and signal analysis capabilities.

The high-speed digitizer has a resolution of 16 bit to 24 bit. The advantage of having variable resolution allows a higher sampling rate at a lower resolution or a lower sampling rate at a higher resolution (Fa, et al., 2010). This becomes important when different kinds of rocks are tested. Previous section explained that brittle rocks have more frequent AE events than soft rocks. Therefore, the sampling rate can be lowered to allow for higher resolution for soft rocks that require higher resolution to detect any AE activity, and a higher sampling rate for brittle rocks that do not require such high resolution. A picture of the data acquisition components is given in Figure 10-10.

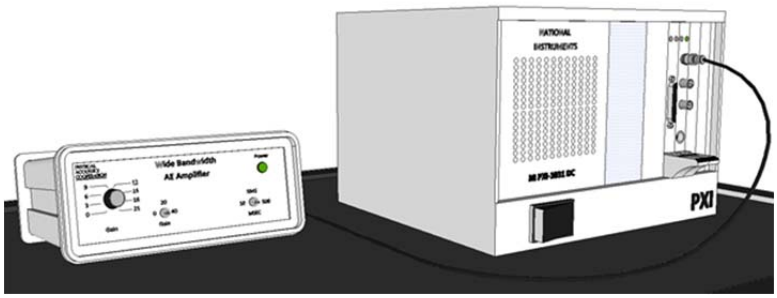

Figure 10-10. Wide band width amplifier (left) and NI Chassis (right) with a high-resolution digitizer and interface card installed.

In the first stage of experimentation the KISS system tests Hinckley sandstone, obtained from Hinckley Minnesota. Some of the physical characteristics of Hinckley sandstone are shown in Table 10-1.

Physical Properties of Hinckley Sandstone

Table 10-1. Physical properties of Hinckley sandstone

Porosity	10.57%
Degree of Saturation	3.85%
Point Load Strength	0.0386 (lbf/mm^2)
Uniaxial Compressive Strength	2500 psi
Young's Modulus	6250000 (psi)
Cohesion Coefficient	722 psi
Internal Angle of Friction	31 °

The sandstone is a good representation for sandstone oil reservoirs and past experimentation has shown sandstone to have a well pronounced Kaiser point (Dunning, et al., 1989). Since the Hinckley sandstone has not been under any forces for a long period of time it will serve as a good control and calibration experiment for the KISS system to verify the ULM for AE and the Kaiser effect. By preloading the sandstone to a desired point below its ultimate strength the KISS system will attempt to replicate the previous known stress via the AE detection rates outlined in previous section. If the determined Kaiser stress in the second loading cycle correlates with the known stress in the first cycle, then the KISS system is functional and may be expanded further to triaxial testing (Blanksma, 2011).

10.2.5 KISS test procedure

Procedural guideline for the KISS system – uniaxial loading is as follows:

Sample Preparation

1) Core out a right cylindrical sample. Coring is completed in the sample preparation lab. The diameter of the sample should be approximately 1.5 inches and the length of the sample approximately 3 inches. Record the length and diameter with calipers.

2) Ensure the ends of the samples are cut smoothly and equally as possible. Ideally within 0.005 mm of being parallel. Also, be sure there are no undesired joints or fractures that may create a plane of weakness when the sample is loaded.
3) Use a file or sand paper to create a small flattened surface on one side of the rock sample and 180 degrees on the other side of the sample. This is where the ART's (Acoustic Receiving Transducers) attach. Be sure not to sand off too much rock material as it may diminish the structural integrity of the rock sample. Figure 10-6 shows a picture of a rock sample with an attached ART.

Hardware Setup

1) Set up the digitizer and amplifier as illustrated in Figures 10-11 and 10-12.
2) One or two ART's need to be attached to the sample. Usually the ART's are attached with super glue located at the area's that have been slightly flattened. A rubber band is also a good way to attach the ART's to the rock sample.
3) If you are using a single ART attach the connector to the Preamplifier port on the AE amplifier. A second ART may be wired directly to the digitizer.
4) Once the setup in part c is complete turn on the NI Digitizer and amplifier followed by the computer with the *LabVIEW* data acquisition (DAQ) program.
5) See Figures 10-7, 10-8, 10-11, and 10-12 for a full picture of the set up including the computer for detecting AE, the computer for controlling loading, digitizer, and amplifier.

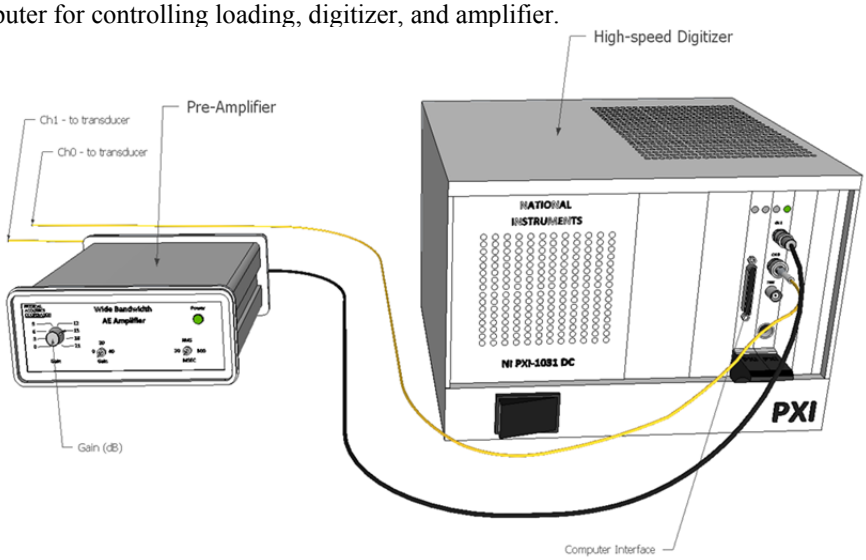

Figure 10-11. Setup of pre-amplifier and digitizer

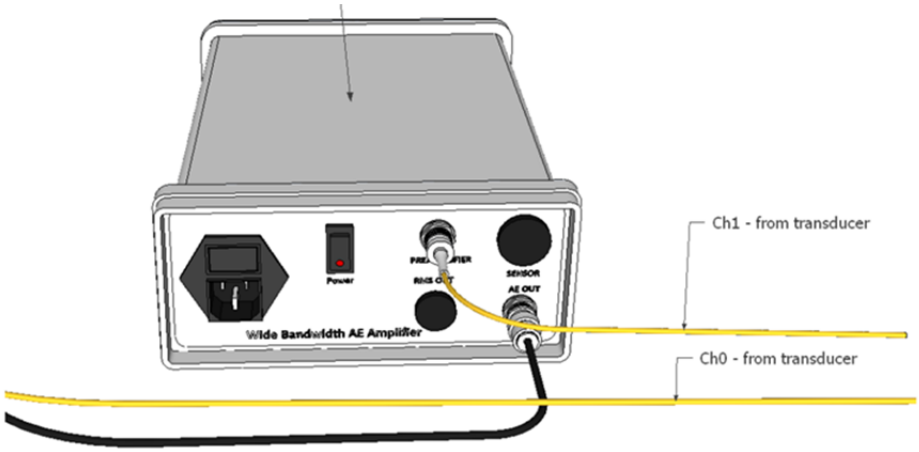

Figure 10-12. Picture of back side of pre-amplifier

Test Preparation

1) Acoustic Detection Program – *LabVIEW*
Open the folder labeled KISS on the desktop. Next, open the folder labeled *DAQ_programs* and the *DAQ_Kaiser_effect.vi*:

2) Amplification – Table 10-2 shows values of amplification for different triggering threshold voltages. These are only suggested values and determining the correct triggering and amplification depends on the level of noise during experimentation and the type of rock.

Table 10-2. Values of amplification for different triggering threshold voltages

GAIN (dB)	Threshold Voltage (mV)
20	-
35	20
40	90
55	120
61	150

3) Running a Test

This is a two cycle test. The first cycle simply loads the rock specimen to a desired force level, but below its peak strength. The only necessary piece of information in the first cycle is obtaining the maximum force.

CYCLE 1

Step 1: Load the specimen to within 30% – 80 % of its peak strength. Determining the peak strength will require a failure test or knowledge of the rock properties of the specimen.
Step 2: All the uniaxial loading data will be saved and stored for later analysis. Once cycle 1 is complete unload the sample.

CYCLE 2

Step 1: Prepare the 816 Rock Test System (Figures 10-7, 10-8, 10-11, and 10-12) by moving the compression platen to the point where it just touches the rock sample. DO NOT apply a load at this point to the rock sample.
Step 2: Click the run icon on the Front Panel of the *DAQ_Kaiser_effect_op1.vi* program. You will be asked to select or create a TDMS file to save your data to. Create the file and save it to the *waveform_data* folder in the *Data* folder.
Step 3: Begin the procedure of loading the rock sample with the 816 MTS Rock Test System and press the START button on the front panel of the DAQ program. Once the start button is pressed the initial time dialogue box will show the time data acquisition began. Be sure to make a note of this time.
Step 4: Monitor the program as it is running. Once the second cycle of compression is completed, click STOP on the Front Panel of the *DAQ_Kaiser_effect_op1.vi.*
Step 5: A window will appear asking if you would like to view your data in the TDMS viewer. Select cancel to end the test or OK to view your data in the *TDMSviewer.vi*.

4) Analyzing the Data

5) Correlating AE data and Force Data

Step 1: Open the file *data_time_finder.vi* in the *Analysis* folder. Select the box icon to the right of AE Time file and find the AE time data from the *ae_time_data* folder. Also select the MTS Force/Time file button and select the file from the 793.61 Rock Mechanics Software that contains all the displacement, force and time data from the experiment.
Step 2: These two sets of data contain both time data in seconds. The program searches the MTS Force/Time file for the equivalent time from the AE Time file and returns the force level for that particular acoustic event.
Step 3: Run the program – You will be asked to create a *Correlated Time file*. This file contains all the necessary information to construct a cumulative AE graph versus time. Save the file in the *correlated_data* folder found in the *Data* folder.
Step 4: Since both the AE data and the force data are functions of time the cumulative number of acoustic events in cycle 2 can be plotted against the force data. The resulting graph is similar to Figure 10-13. The Kaiser stress is indicated as the inflection point. Figure 10-14 shows a sample of cumulative AE versus force for a Hinckley Sandstone specimen loaded twice.

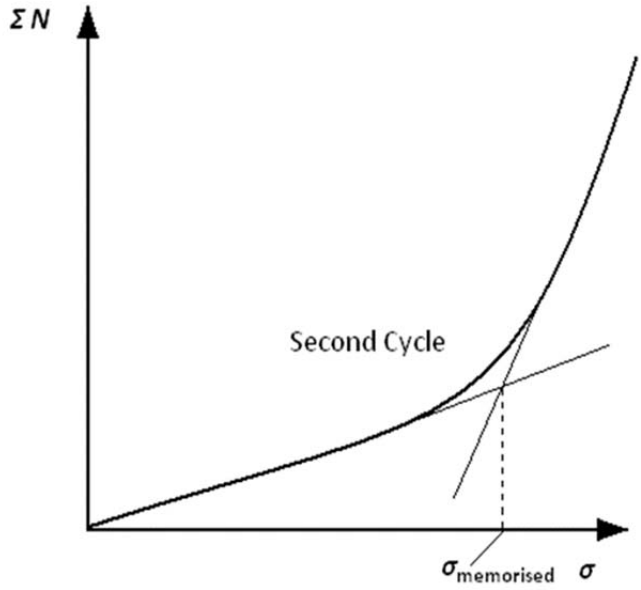

Figure 10-13. Inflection in the cumulative AE hits (Σ N) versus stress (σ) graph indicates the previous maximum stress state.

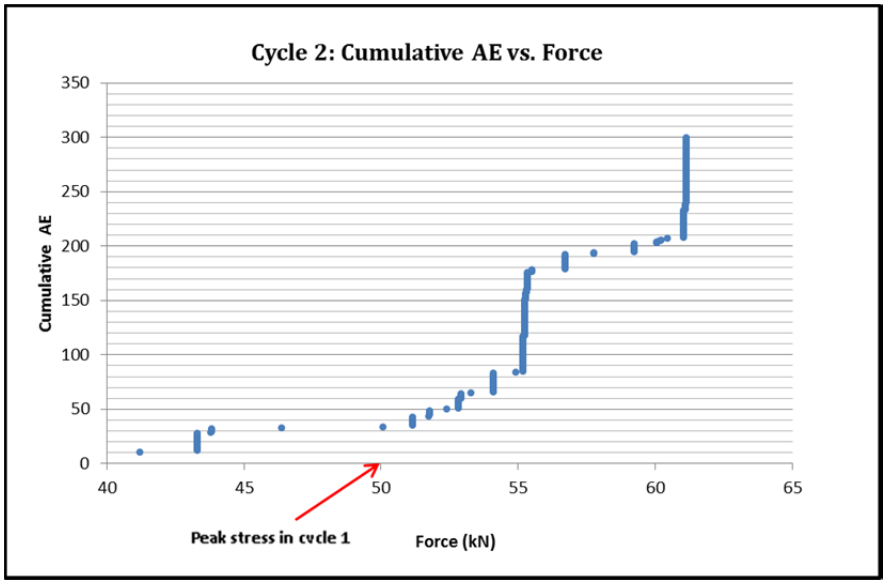

Figure 10-14. Sample graph of Cumulative AE counts versus Force for Hinckley Sandstone in the second cycle of compression

10.3. Kaiser Effect Method –Data Analysis

10.3.1 Experiment on Hinckley Sandstone

The data presented in this section has been obtained to investigate the plausibility of the KISS system using the ULM. Figure 10-15 shows that Hinckley sandstone has identifiable Kaiser Effect point. Figures 10-16 through 10-19 show that at different stages of deformation, the induced acoustic emissions will have different waveforms, and different frequency features.

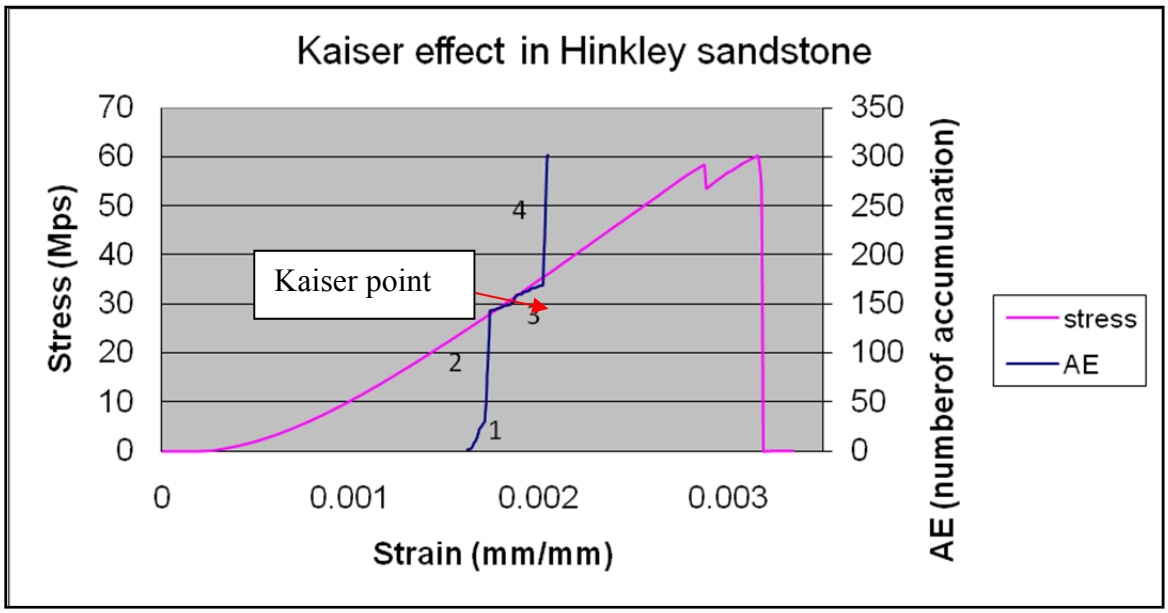

Figure 10-15 Kaiser point on the stress & cumulative AE vs. strain curves in Hinckley sandstone.

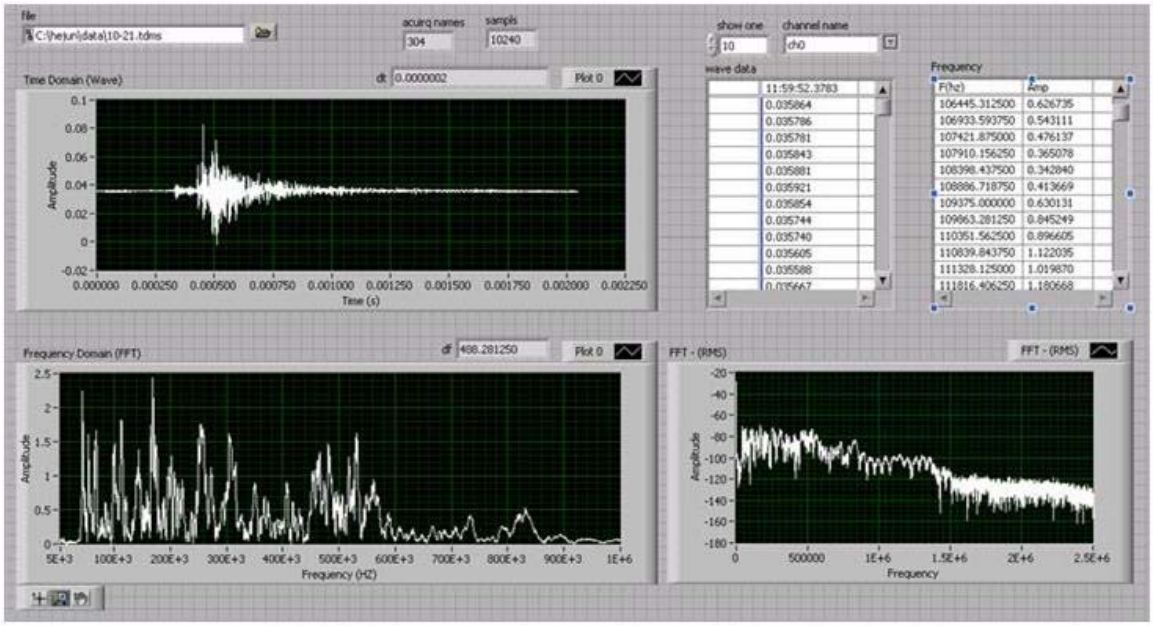

Figure 10-16. Full waveforms and frequency spectrum of AE events in Stage 1 of Figure 10-15.

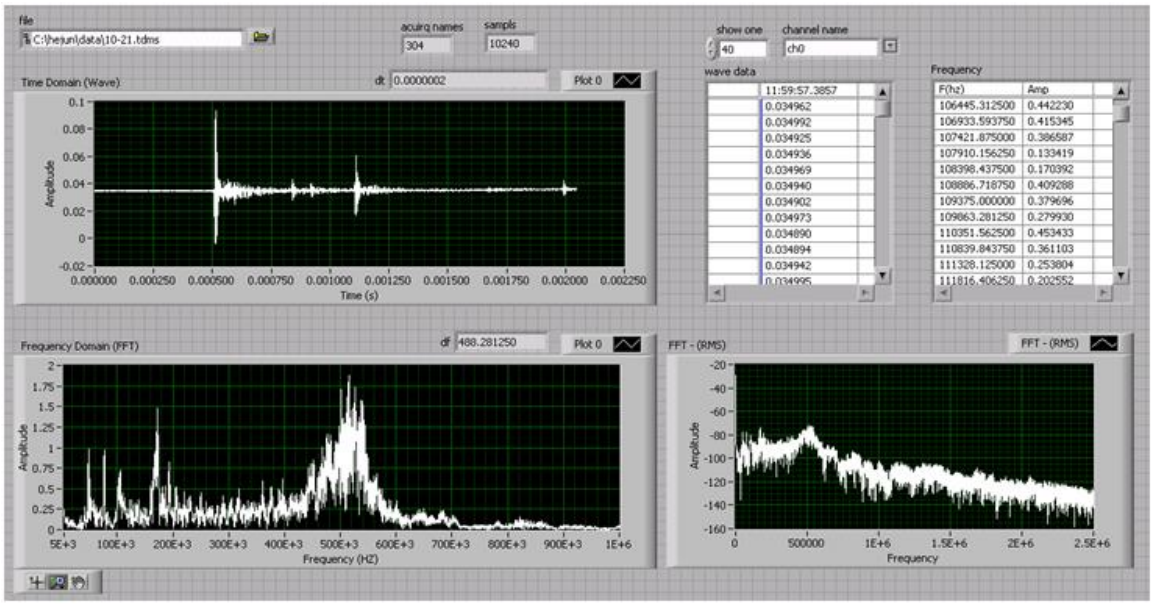

Figure 10-17. Full waveform and frequency spectrum of AE events in Stage 2 of Figure 10-15.

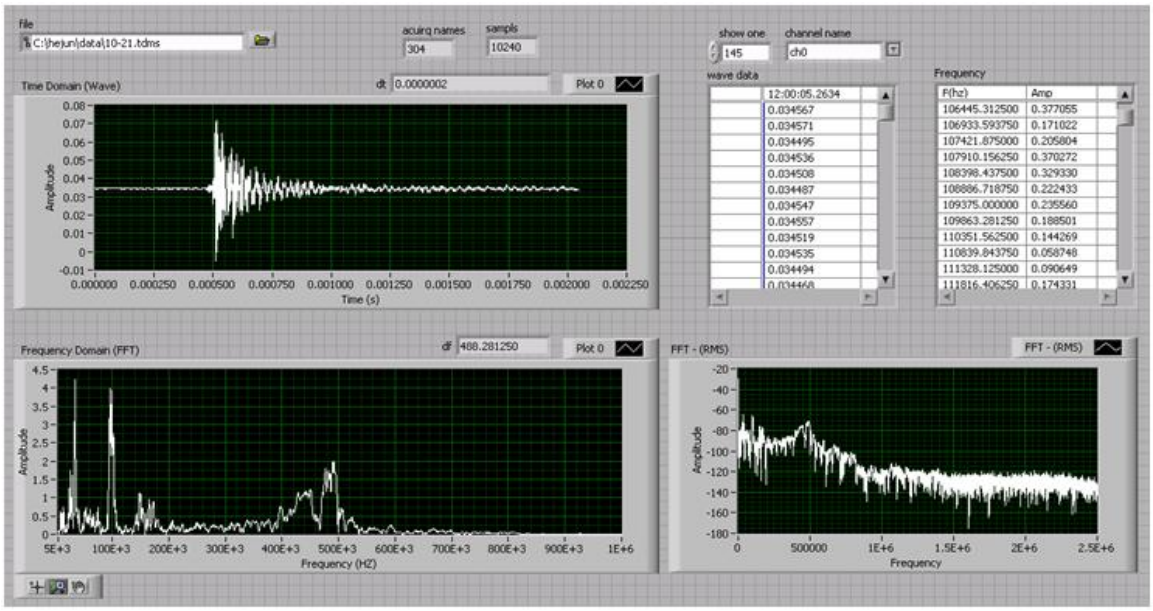

Figure 10-18 Full waveform and frequency spectrum of AE events in Stage 3 of Figure 10-15.

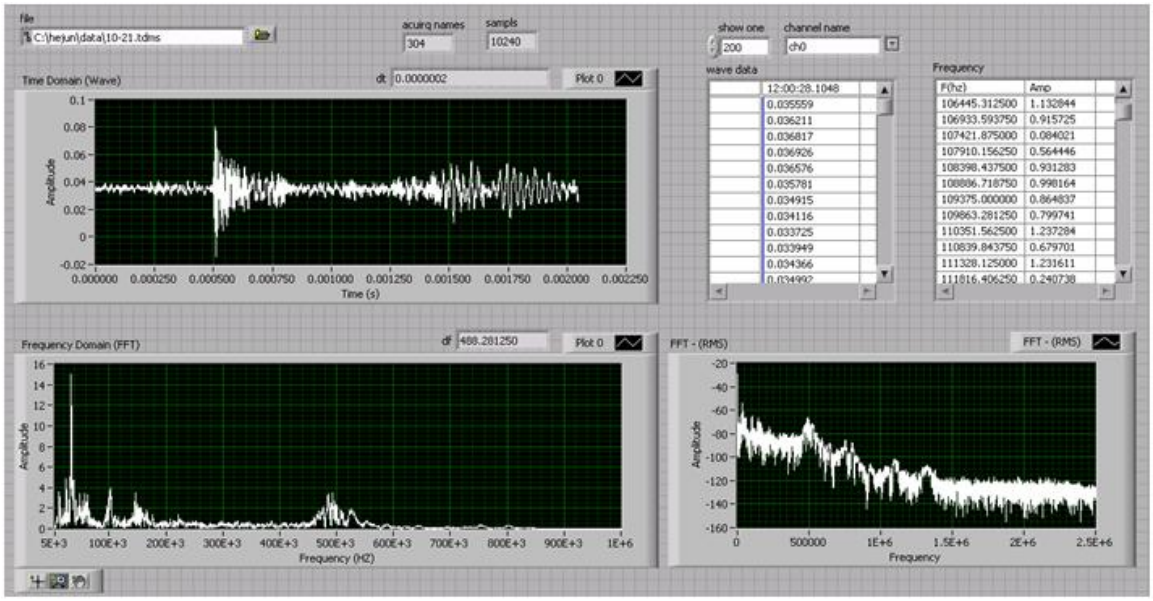

Figure 10-19. Full waveform and frequency spectrum of AE events in Stage 4 of Figure 10-15.

Figure 10-20 shows cumulative AE for 126 acoustic events gathered over a time of 22.78 minutes at a loading rate of 0.0003658 mm/s for channel 0. Figure 10-14 shows cumulative AE versus time considering over 1800 acoustic events. All acoustic events in Figure 10-14 where considered to have amplitudes of 0.001 v or more.

All programs to correlate time data with force data where creates and used by the author. Error between correlating the MTS Force/Time data with the AE data is on the order of 0.001 seconds since that was the range for matching time data.

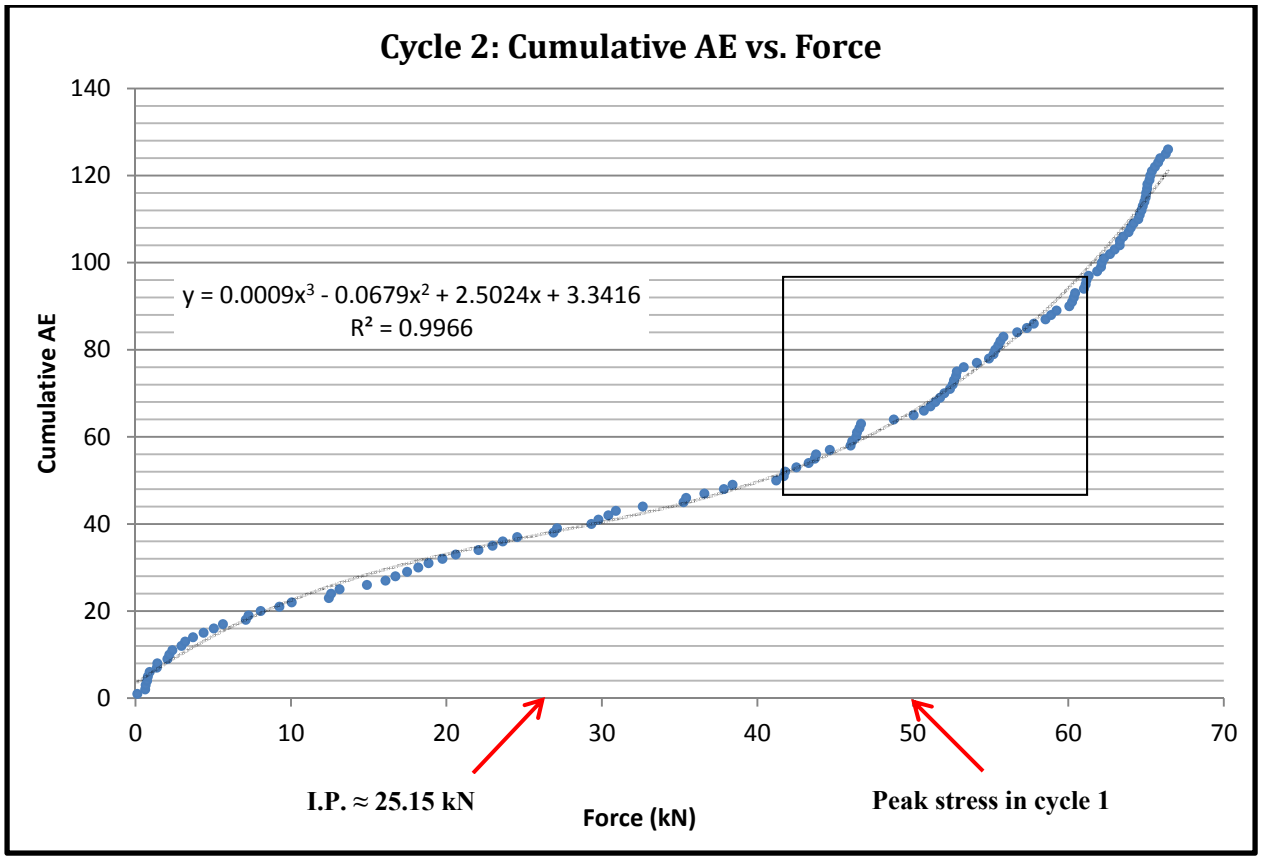

Figure 10-20. Cumulative AE for 126 acoustic events gathered over a time of 22.78 minutes in cycle 2

Figure 10-20 indicates that there is an inflection point at approximately 25.15 kN. This has about a 50% error since the true stress achieved in cycle one was 50 kN. The reason for this discrepancy may be acoustic events that are associated with frictional sliding rather than microcracking has been recorded in Figure 10-20. Another issue is that Figure 10-20 contains only 126 acoustic events. This is a product of the LabVIEW program that recorded the AE. In the program, triggers were considered as the AE event and data that recorded one second after each trigger was ignored. However, considering the boxed section in Figure 10-20 small inflection points in the range of approximately 45 kN to 60 kN are discernible.

In order to mitigate this lack of resolution the entire data set was reanalyzed for over 1800 acoustic events each of which was defined as having amplitude of 0.001 volts. Figure 10-14 shows the results of cycle 2 after analyzing over 1800 acoustic events. After close inspection it can be seen in Figure 10-14 that from 0 kN to approximately 50 kN the cumulative AE remains between 0 and 40. However, once the 50 kN point is reached, cumulative AE increase rapidly, especially at the 55 kN point and approximately the 62 kN point. The 50 kN point was the maximum stress level achieved in cycle 1 and thus in cycle 2 the Kaiser effect is observed.

10.3.2 Conclusion on KISS System

The KISS system offers the capabilities of determining in-situ stresses in rocks that are non-evasive, relatively cheap and capable of delivering accurate results. AE and the Kaiser effect have been extensively studied and analyzed to determine in-situ stresses in rocks. Many of these attempts to use AE and the Kaiser effect have fallen short due to the lack of sophisticated computing technology. However, the KISS system incorporates the use of high resolution digitizers, servo-controlled compression and a faster computing process to identify stress memory in rocks, where before, computing capabilities could not yield high enough resolution to distinguish stress memory.

Many fundamental problems must be addressed in order for this system to work, however by following the design proposal this system is the initial step to creating a system that can one day calculate the entire stress tensor. Using the KISS system with the uniaxial compression method revealed the Kaiser effect on cyclically loaded Hinckley

sandstone, as shown in section 6. The knowledge gained and methods used created a fundamental starting point for more sophisticated experimentation such as, triaxial compression. It is clear that the only way to recreate the entire stress state of a subsurface rock mass is to reload a rock specimen in a triaxial environment. Little work has been produced on this subject, however new ideas and methods are being developed and the first stage of development has been laid out in this project.

There is much promise for the KISS system. As far as improving the system better waveform filtering techniques such as Fourier transforms, Nyquist frequency and analysis in the frequency domain offers better noise reduction and identification of AE associated with microcracking. Also, better software development would help with time synchronization and data recording. All of these developments will help the KISS system find more accurate and better results.

10.4. CDISK Method for Fracture Toughness-Background

Rock fracture toughness is a property which describes the ability of a rock containing a crack to resist fracture, and is one of the most important properties of rock for oil and gas well drilling and stimulation. To determine the fracture toughness of rocks, the International Society for Rock Mechanics (ISRM) recommended two methods with three types of core-based specimens: chevron bend and short rod specimens (Ouchterlony 1988), and cracked chevron notched Brazilian disc (CCNBD) specimen (Fowell, 1995). The cracked chevron notch Brazilian disc (CCNBD) method is one of the widely used techniques to characterize rock fracture toughness. The CCNBD is an ideal specimen for rock fracture toughness measurement. The good features are large failure load, simple loading fixture, convenient and flexible specimen preparation.

We developed the tools and method on sample preparation, and compared the test results of Indiana limestone and Pierre shale using 2-in and 1-in diameters. It seems that results of 1-in diameter samples are systematically lower than that from 2-in samples, but the difference is within 5%.

10.5. CDISK Method-Fracture Toughness Measurement

10.5.1 Fracture toughness measurement on Indiana limestone

Fracture toughness is the resistance offered by a material against preexisting crack's propagation. It is an important material property which describes the critical states of stresses or energy near the crack tip required for the initiation of fracturing (Krishnan et al., 1997; Ayatollahi and Aliha, 2008). The International Society for Rock Mechanics (ISRM) suggested method (ISRM, 1995), CCNBD is used to measure fracture toughness of Indiana limestone. This method uses a specimen with a chevron shaped notch cut along the core diameter, as shown in the following figure.

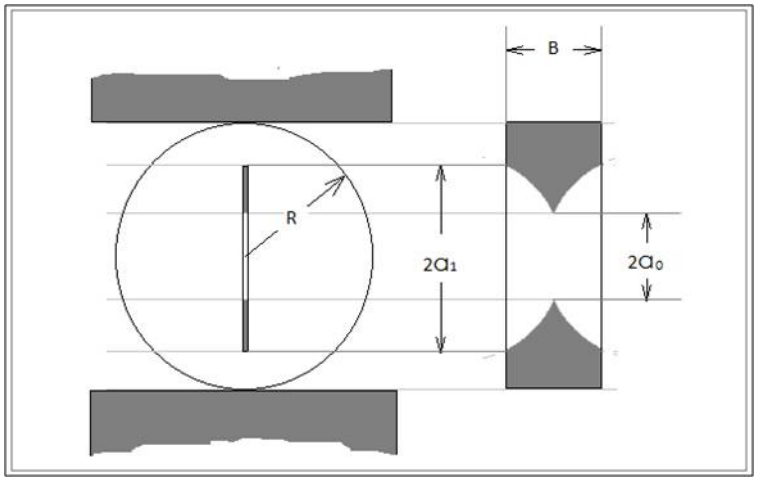

Figure 10-21. The cracked chevron notched Brazilian disc specimen (modified after ISRM, 1995)

The chevron notch causes crack propagation to start at the tip of the V alignment and to proceed outwards in a stable fashion. All the dimensions of the geometry should be converted into dimensionless parameters with respect to the specimen radius R as follows:

$$\alpha_0 = a_0/R; \quad \alpha_1 = a_1/R; \quad \alpha_B = B/R \qquad (10\text{-}5)$$

The selected dimensions should satisfy the following restrictions:

$$\alpha_1 \geq 0.4; \quad \alpha_1 \geq \alpha_B/2; \quad \alpha_1 \geq 0.4$$

$$\alpha_B \leq 1.04; \quad \alpha_B \geq 1.1729 \cdot \alpha_1^{1.6666}; \quad \alpha_B \geq 0.44 \qquad (10\text{-}6)$$

With the help from the Technology department of UND, a circular diamond saw mounted on a computer controlled lathe was used to cut the required notch, in which the flanks of the chevron notch was straight by a linear cutting motion. As programmed, the chevron notches were ensured to be exactly in the center of the disc and the geometrical dimensions conformed to the given tolerances, as shown in the following figures.

Figure 10-22. CCNBD specimen preparation

After finishing the sample preparation, the MTS rock tester was used to compress the sample to develop a failure surface for further measurements, and at the same time, the force versus displacement curve was recorded, as shown in the following figures.

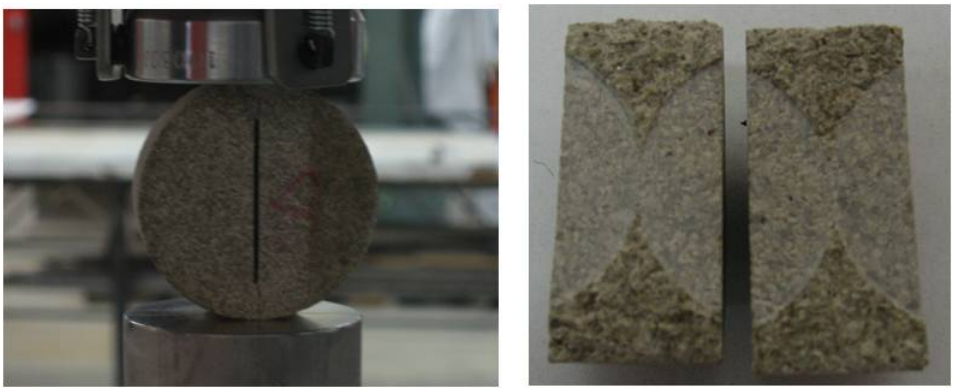

Figure 10-23. Sample compressed by MTS rock tester and the fracture surface after failure

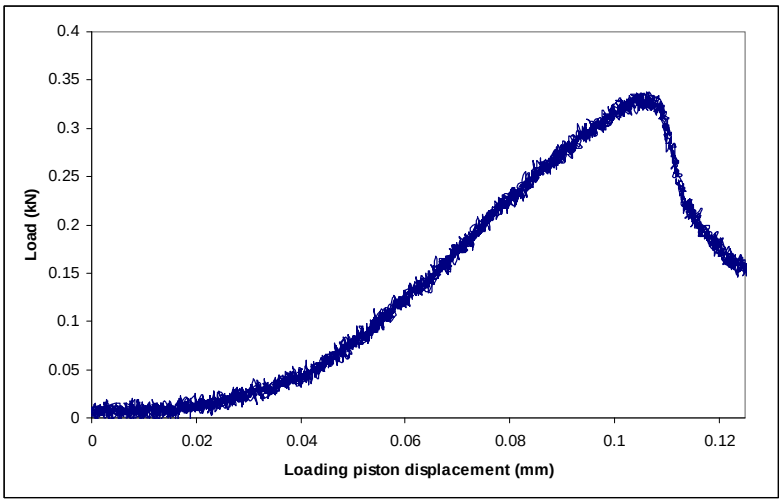

Figure 10-24. Load versus displacement of loading piston (sample T10L06).

The fracture toughness of the specimen is calculated by the following formula (ISRM, 1995):

$$K_{IC} = \frac{P_{\max}}{B \cdot \sqrt{D}} \cdot Y^*_{\min} \text{ ; where } Y^*_{\min} = u \cdot e^{v \cdot \alpha_1} \quad \text{..... (10-7)}$$

where P_{max} is the maximum load that breaks the sample, and Y^*_{min} is called the critical dimensionless stress intensity value, which is determined by the specimen geometry, and u and v are constants interpolated by α_0 and α_B from Table 2 of ISRM (1995). It was noted that some minor modifications to this formula and the "u", "v" values were suggested in the past few years (Zeng and Roegiers, 2000; Wang et al., 2004; Wang, 2010), however, before a formal standard is published by the ISRM, this formula is followed to keep the test results consistent. The test results are shown in the Table 10-3.

From the tests results, one can see that these results are insensitive to the sample sizes as fracture toughness is an intrinsic mechanical property of materials. However, the diameter of the sample should be related to the size of the largest grain in the rock by the ratio of at least 10:1 (ISRM, 1995); obviously, this criterion is believed to be sufficiently satisfied by considering the fine grain nature of limestone. All the tested samples were in the valid geometrical range as shown in the following figure.

Table 10-3. Fracture toughness tests on Indiana limestone

Sample ID	Diameter D (mm)	Thickness B (mm)	$2a_1$ (mm)	$2a_0$ (mm)	Y^*_{min}	Pmax (kN)	K_{IC} $MPa\sqrt{m}$
10F03	50.35	20.38	33.90	17.12	0.930878	1.463	0.298
10F04	50.18	16.81	30.06	9.08	0.772534	1.455	0.299
10F11	50.34	17.82	31.07	9.46	0.831154	0.942	0.196
10F07	50.48	19.56	36.69	19.48	1.019895	0.962	0.223
Average							0.261
Standard deviation							0.052
T10L03	24.73	11.82	17.60	0.00	0.890603	0.626	0.300
T10L04	24.45	11.26	17.89	2.43	0.900698	0.588	0.301
T10L05	24.78	11.70	18.29	4.27	0.930112	0.485	0.245
T10L06	24.80	12.14	17.97	2.78	0.889921	0.338	0.157
T10L07	24.78	11.38	18.41	3.83	0.936906	0.574	0.300
T10L08	24.52	12.02	17.28	2.76	0.860530	0.668	0.305
T10L09	24.50	11.28	18.09	4.36	0.935208	0.546	0.289
Average							0.271
Standard deviation							0.054

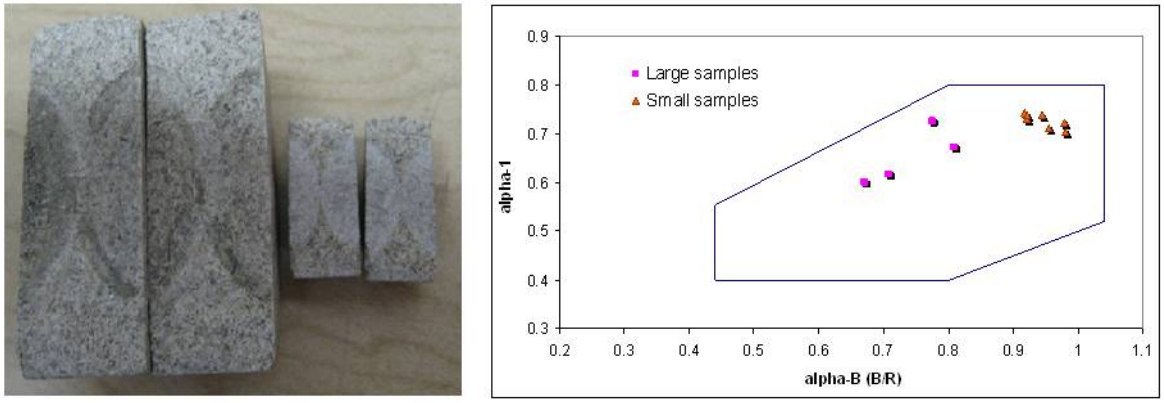

Figure 10-25. Both large and small samples (left) are in the valid geometrical range (right).

Some experimental studies support the assumption that fractures, once initiated, will propagate as long as the stress intensity at the crack tip exceeds the fracture toughness of the material (Warpinski et al., 1979).

10.5.2 Fracture toughness measurement on Pierre shale

Following similar method and procedure for the testing on Indiana limestone, we conducted fracture toughness test on Pierre shale. After a test, a typical load versus displacement curve based on loading piston is shown in the following figure.

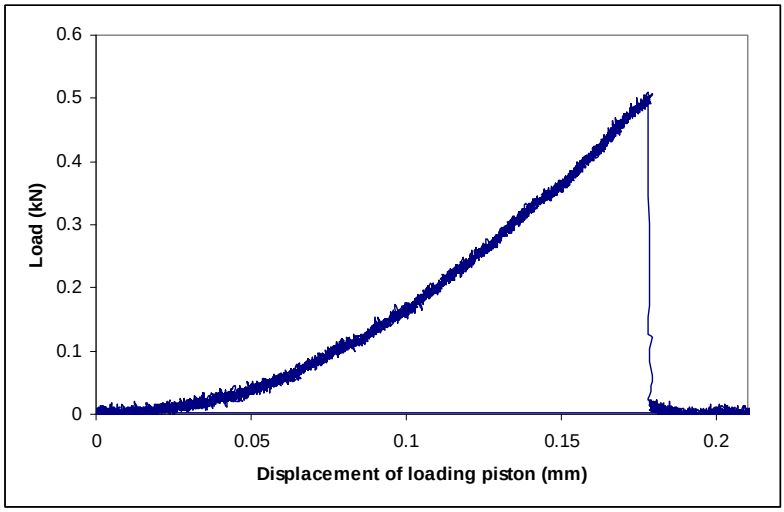

Figure 10-26. Load versus displacement of loading piston (sample T10S01).

Similarly, both large and small samples were tested, and it was found that the fracture surfaces were all very well developed (Figure 10-27). Thus the anisotropy of shale seems to be overcome by the induced fractures.

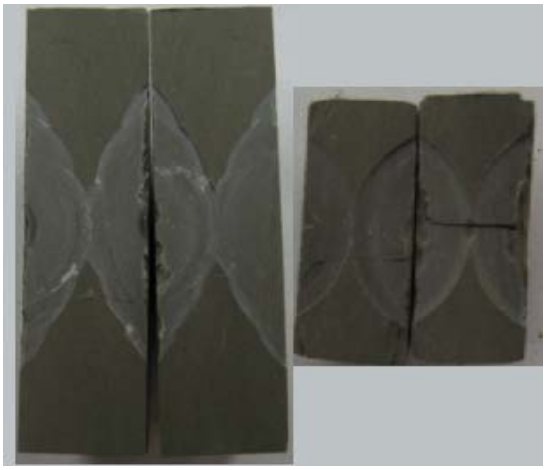

Figure 10-27. Both large and small samples show well defined fracture surfaces.

Also note all the shale samples tested were in the valid geometrical range as shown in the following figure.

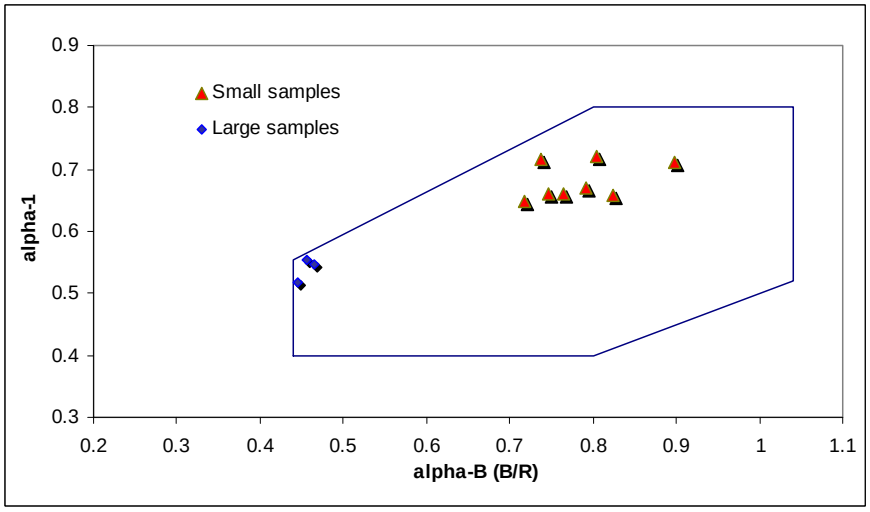

Figure 10-28. Verification of sample geometry qualification.

The test results are shown in the Table 10-4.

Table 10-4. Fracture toughness tests on Pierre shale

Sample ID	Diameter D (mm)	Thickness B (mm)	2a1 (mm)	2a0 (mm)	Y*min	Pmax (kN)	KIC $MPa\sqrt{m}$
T10S01	25.84	9.65	17.05	2.42	0.826497	0.510	0.272
T10S02	25.59	9.78	16.92	0.00	0.812046	0.436	0.226
T10S03	25.02	11.24	17.80	1.75	0.875578	0.421	0.207
T10S04	25.92	9.30	16.80	0.00	0.808306	0.487	0.263
T10S05	25.00	9.22	17.88	6.30	0.945540	0.395	0.256
T10S06	26.20	10.38	17.53	5.52	0.854318	0.555	0.282
T10S07	24.88	10.00	17.92	7.12	0.956106	0.428	0.259
T10S08	25.02	10.32	16.45	0.00	0.787968	0.487	0.235
Average							0.250

Standard deviation							0.025
T10SB1	51.21	11.69	28.37	3.65	0.733445	0.868	0.241
T10SB2	51.20	11.93	27.97	9.63	0.737625	0.701	0.191
T10SB4	50.77	11.30	26.30	6.38	0.693323	1.305	0.355
Average							0.262
Standard deviation							0.084

One can see that the fracture toughness of Pierre shale is smaller than that of Indiana limestone. Besides, its deviation is smaller. Figure 10-29 and 10-30 show the test and fractured surface of rock samples. Note due to the smaller sample size, a steel cylinder was added for the test. Figure 10-31 shows fractured surfaces after tests for the test samples.

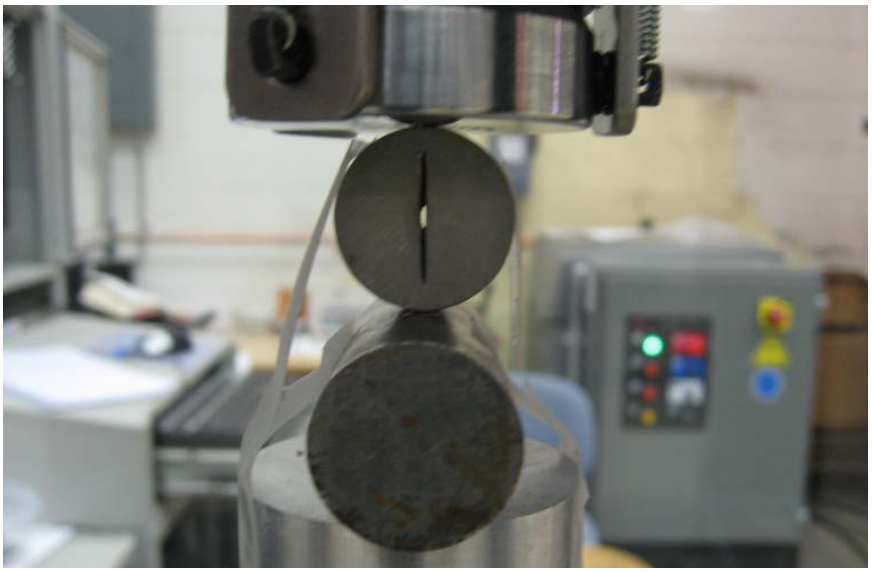

Figure 10-29. Shale sample under compression at MTS station

Figure 10-30. Fractured surface after tests

T10L01

T10L03

T10L04

T10L05

T10L06	T10L07
T10L08	T10L09
	10F07
T10S01	T10S02

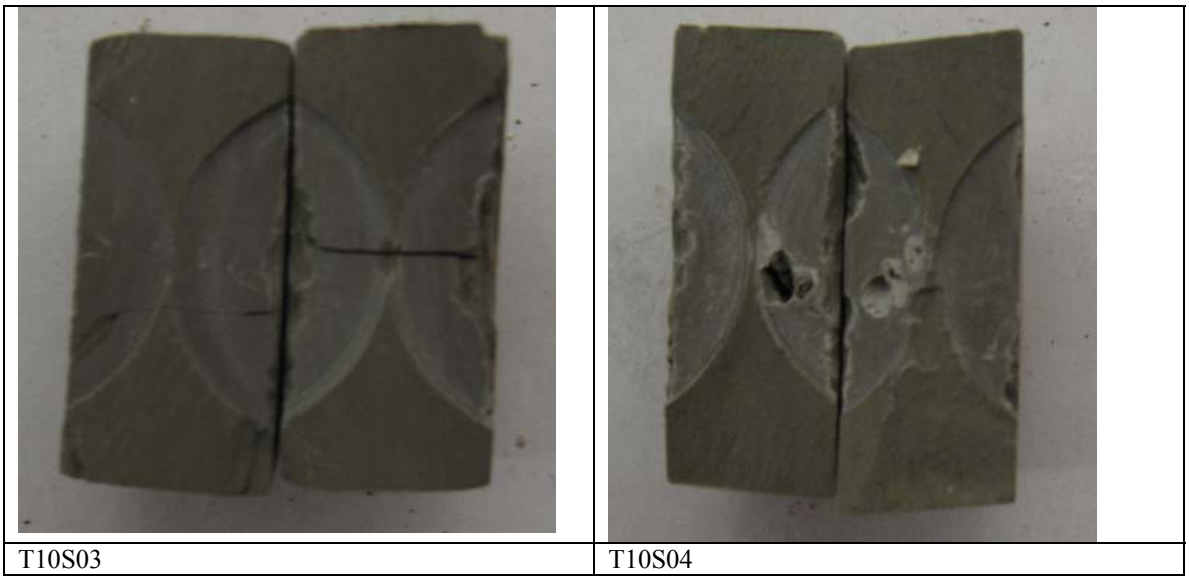

T10S03	T10S04

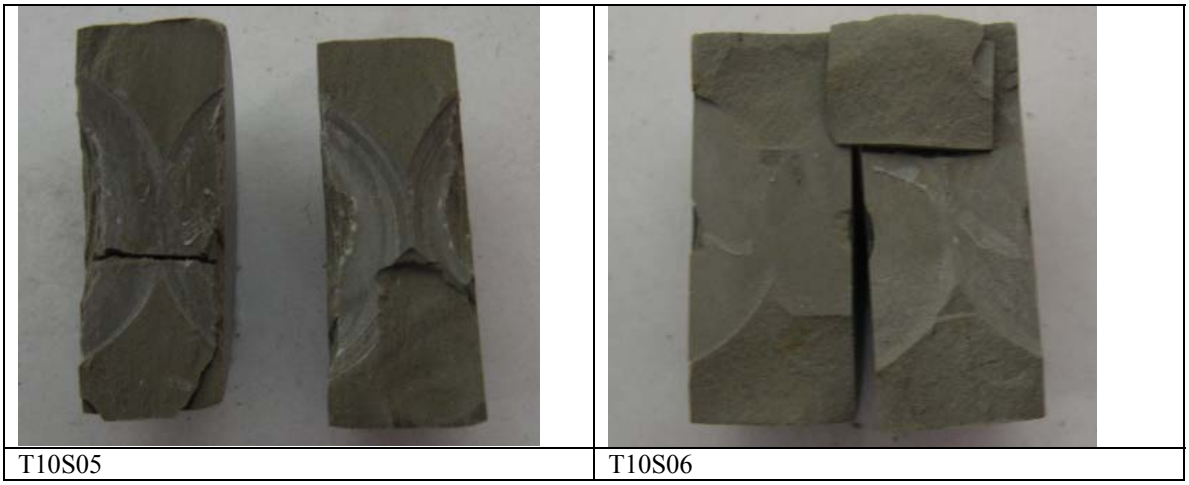

T10S05	T10S06

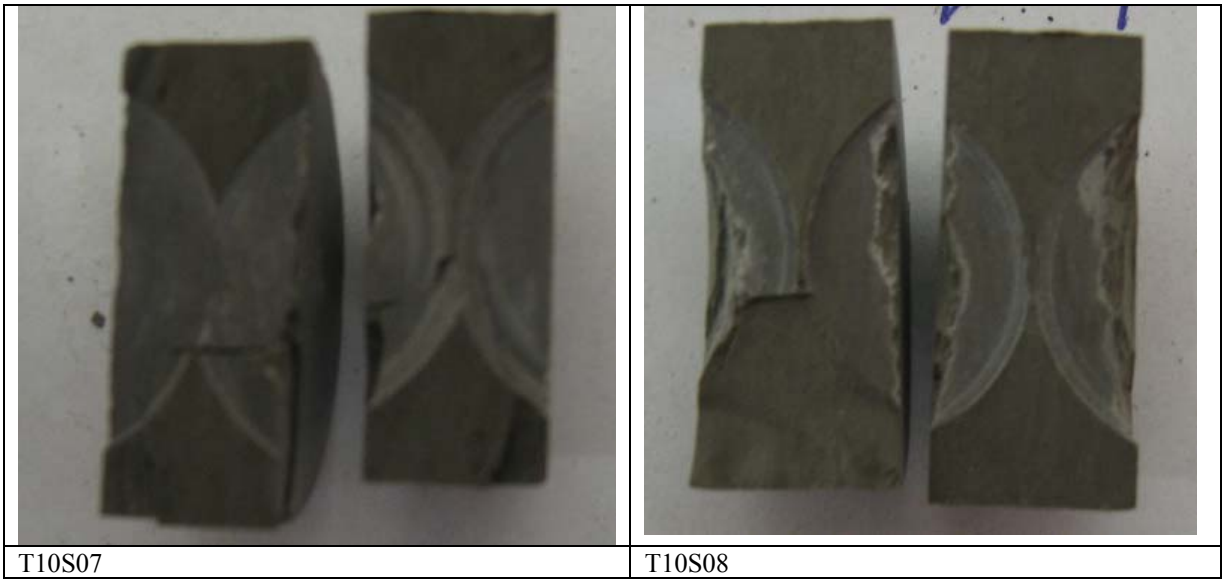

T10S07	T10S08

Figure 10-31. Fractured surfaces after tests for the test samples

10.6. CDISK Method-Concluding Remarks on Fracture Toughness

We have developed a set of procedure that allow us to prepare the fracture toughness sample for cracked Chevron notched Brazilian disc (CCNBD) in any direction at samples as small as 1-in diameter.

Comparison test on Indiana limestone and Pierre shale of both 2-in and 1-in disc samples indicated that tested fracture toughness of larger samples is systematically higher than those form small samples. However, the difference is only about 5%. In addition, fracture toughness of Indiana limestone is higher than that of Pierre shale, which is reasonable.

11. CONCLUSIONS

By finishing this project, we have trained locally sustainable technical team in petroleum geomechanics and petrophysics. We have built local capability in lab testing in related areas. We also have made progresses in understanding Bakken geomechanics, which includes

1) built a 3D Bakken geological model using thickness data.
2) developed a method that can help build 3D Bakken model of any petrophysical and geomechanical properties as long as adequate amount data is available from lab testing and field correlation, with the possibility of improving model using updated data.
3) developed a conceptual model that allows integration of plug-scale lab-testing data, core-scale data and field scale data.
4) set up the foundation of testing various of petrophysical and geomechanical properties, and have completed test of middle, upper, and middle Bakken core plugs from 8 wells.
5) published more than 25 technical papers and presented more than 30 presentations to transfer technology.

12. Technology Transfer

The technologies developed in this project have been transferred to the public through journal papers, conference papers, and technical presentations. We have developed a website database for public access.

12.1. Journal and Conference Papers

K. Ling, J. He, P. Pei, G. Han, H. Zhang, "Determining the Permeability of Tight Rock with Gas Transient Flow", *Journal of Natural Gas Science and Engineering*. Vol.15, November 2013.

J. He, P. Pei, K. Ling, Z. Zeng, H. Liu, "Quantification of Rock Porosity Change before and after Freezing", *Journal of Petroleum Science Research*. July 2013

J. He, K. Ling, P. Pei, X. Ni, "Calculation of Rock Compressibility by Use of Pressure Buildup in Permeability Experiment", URTeC:1928297, the Unconventional Resources Technology Conference held in Denver, Colorado, USA, 25-27 August 2014.

K. Ling, Z. Shen, G. Han, J. He, P. Pei, "A Review of Enhanced Oil Recovery Methods Applied in Williston Basin", URTeC:1891560, the Unconventional Resources Technology Conference held in Denver, Colorado, USA, 25-27 August 2014.

K. Ling, J. He, P. Pei, X. Ni, "Identifying Fractures in Tight Rocks Using Permeability Test Data", ARMA 14-6984, the 48th US Rock Mechanics / Geomechanics Symposium held in Minneapolis, MN, USA, 1-4 June 2014.

K. Ling, J. He, P. Pei, X. Ni, "A New Method to Determine Pore Compressibility", ARMA 14-6964, the 48th US Rock Mechanics / Geomechanics Symposium held in Minneapolis, MN, USA, 1-4 June 2014.

J. He, K. Ling, "A New Method to Determine Biot Coefficients of Bakken Samples", ARMA 14-7022, the 48th US Rock Mechanics / Geomechanics Symposium held in Minneapolis, MN, USA, 1-4 June 2014.

P. Pei, J. He, K. Ling, "Correlating Geomechanical Properties of the Bakken Formation Rocks with Lithofacies and Sequence", ARMA 14-7437, the 48th US Rock Mechanics / Geomechanics Symposium held in Minneapolis, MN, USA, 1-4 June 2014.

K. Ling, G. Han, Z. Shen, A. Ghalambor, J. He, P. Pei, "Calculating Pore Size Distribution by Using Capillary Pressure", paper SPE 168183, SPE International Symposium and Exhibition on Formation Damage Control held in Lafayette, Louisiana, USA, 26–28 February 2014.

J. He, K. Ling, P. Pei, J. Ge, W. Qin, "A Correlation to Evaluate the Fracture Permeability Changes as Reservoir is Depleted", paper SPE 165709, SPE Eastern Regional Meeting held in Pittsburgh, Pennsylvania, USA, 20–22 August 2013.

Zhou, X. and Zeng, Z. 2014. The Development of Stylolites in Carbonate Formation: Implication for CO2 sequestration. Acta Geologica Sinica, Vol. 88, No.1:238-247.

Jabbari, H., Zeng, Z., Korom, S. and Khavanin, M. 2012. Well Test Analysis in Dual-Porosity Aquifers with Stress-Dependent Conductivity. Research Journal of Environmental and Earth Sciences, Vol. 4, No. 11:962-981.

Fa, L., Castagna, J.P., Zeng, Z., Brown, R.L., and Zhao, M. 2010. Effects of anisotropy on time-depth relation in transversely isotropic medium with a vertical axis of symmetry. Chinese Science Bulletin, Vol. 55, No. 21:2243-2251.

Fa, L. , Zeng, Z. , Deng, C. and Zhao, M. 2010. Effects of geometrical-size of cylindrical-shell transducer on acoustic-beam steering efficiency for a slim-hole acoustic-logging tool. The Open Acoustics Journal, No. 3, p.21-29.

Zeng, Z. and Jiang, A. 2010. Geomechanics key in Bakken success. The American Oil & Gas Reporter. April issue. 123-127.

Jabbari, H. and Zeng, Z. and Ostadhassan, M. Decline-Curve Analysis of Naturally Fractured Reservoirs Considering Geomechanics. Paper SPE 147008, Proc. SPE Annual Technical Conference and Exhibition held in Denver, Colorado, USA, 30 October–2 November, 2011. 13 p.

Pei, P., Zeng, Z., and He, J. Characterization of the Harmon Lignite for Underground Coal Gasification, Proc. 28th Int. Pittsburgh Coal Conf., held in Pittsburgh, Pennsylvania, September 12-15, 2011. 13 p.

Jabbari, H., Zeng, Z., and Ostadhassan, M. Impact of In-Situ Stress Change on Fracture Conductivity in Naturally Fractured Reservoirs: Bakken Case Study. Paper ARMA11-239, Proc. 45th US Rock Mechanics / Geomechanics Symp. held in San Francisco, CA, June 26–29, 2011. 8 p.

Ostadhassan, M. , Zeng, Z. and Jabbari, H. Using Advance Acoustic Data to Determine Stress State Around Wellbore, paper ARMA 11-319, Proc. 45th US Rock Mechanics / Geomechanics Symp. held in San Francisco, CA, June 26–29, 2011. 7 p.

Wang, C. and Zeng, Z. Overview of geomechanical properties of Bakken Formation in Williston Basin, North Dakota, Paper ARMA 11-199, Proc. 45th US Rock Mechanics / Geomechanics Symp. held in San Francisco, CA, June 26–29, 2011. 11 p.

Zhou, X.J., Zeng, Z. and Liu, H. Stress-dependent permeability of carbonate rock and the implication to CO2 sequestration, paper ARMA 11-135, Proc. 45th US Rock Mechanics / Geomechanics Symp. held in San Francisco, CA, June 26–29, 2011. 7 p.

Jabbari, H. and Zeng, Z. A Three-Parameter Dual Porosity Model for Naturally Fractured Reservoirs. Paper SPE 144560, Proc. SPE Western North American Regional Meeting held in Anchorage, Alaska, USA, 7–11 May, 2011. 20 p.

Fa, L., Zeng, Z. and Liu, H. A new device for measuring in-situ stresses by using acoustic emissions in rocks, paper ARMA10-160, Proc. 44th U.S. and 5th U.S.-Canada Rock Mech. Symp., Salt Lake City, UT, USA. June 27-30, 2010. 7 p.

Pei, P., Zeng, Z. and He, J. Feasibility study of underground coal gasification combined with CO2 capture and sequestration in Williston Basin, North Dakota, paper ARMA10-240, Proc. 44th U.S. and 5th U.S.-Canada Rock Mech. Symp., Salt Lake City, UT, USA. June 27-30, 2010. 8 p.

Zhou, X. , Zeng, Z. and Liu, H. Laboratory testing on Pierre shale for CO2 sequestration under clayey caprock, paper ARMA10-107, Proc. 44th U.S. and 5th U.S.-Canada Rock Mech. Symp., Salt Lake City, UT, USA. June 27-30, 2010. 12 p.

Zeng, Z, He, J., Pei, P. and Wang, Y. 2009. Development of a Three Dimensional Bakken Formation Model for Improved Oil Recovery, presented at Geol. Soc. Of Amer. Abstracts with Programs Vol. 41, No. 7.

Jiang, A., Zeng, Z., Zhou, X. and Han, Y. 2009. A strain-softening model for drilling-induced damage on boreholes in Williston Basin, paper ARMA09-026, Proc. 43rd U.S. and 4th U.S.-Canada Rock Mech. Symp., Ashville, NC, USA. June 28-July 1. 8 p.

Zeng, Z. and Jiang, A. 2009. Geomechanical Study of Bakken Formation for Improved Oil Recovery, SINOROCK2009 paper No. 341, Proc. ISRM Int. Symp. Rock Mech., Hong Kong, China. May 19-22. 5 p.

Zhou, X., Zeng, Z., Liu, H. and Boock, A. 2009. Laboratory testing on geomechanical properties of carbonate rocks for CO2 sequestration, paper ARMA09-011, Proc. 43rd U.S. and 4th U.S.-Canada Rock Mech. Symp., Ashville, NC, USA. June 28-July 1. 9 p.

12.2. Technical Presentations

We have presented more than 50 presentations in technical professional conferences, industrial workshops, and seminars.

12.3. Website databases

The link to the website database is
http://www.petrodata.und.edu/

REFERENCES

Abbott, D., Williams-Stroud, S. & R. Shaffer, 2009, Surface Microseismic Monitoring of Hydraulic Fracture Stimulations, Bakken Formation, Nesson Anticline, Williston Basin, North Dakota, AAPG Annual Convention, Denver, Colorado, June 7-10, 2009.

Ahmed T. and McKinney P. 2005. *Advanced Reservoir Engineering*. Gulf Professional Publishing.

Anderson, S.B. 1953. Summary of the Henry O. Bakken No. 1 Williams County, North Dakota. North Dakota Geological Survey Circular No. 16. 1-26.

ANSYS, version 13.0., Canonsburg, Pennsylvania: The ANSYS, Inc, 2010.

Arps, J. 1945. Analysis of decline curve, *Trans. AIME*, 160, 228–231.

AutoLab 1500 Manual, New England Research Inc. 2009

Ayatollahi, M.R., and M.R.M. Aliha, 2008. On the use of Brazilian disc specimen for calculating mixed mode I-II fracture toughness of rock materials. Engineering Fracture Mechanics 75:4631-4641.

Bally, A.W., 1989, Phanerozoic basins of North America, *in* The Geology of North America – An Overview (Bally & Palmer eds.). The Geological Society of America. Vol. A:397-446.

Beekman, F., Badsi, M. and van Weesl, J. 2000. Faulting, Fracturing and in-Situ Stress Prediction in the Ahnet Basin, Algeria – a Finite Element Approach. Tectonophysics, vol.320, p.311-329.

Besler, M. R., Steele, J.W., Egan, T. and Wagner, J. 2007. Improving Well Productivity and Profitability in the Bakken. Paper SPE 110679, SPE Annual Technical Conference and Exhibition, Anaheim, California USA Nov. 11-14.

Biot, M.A. and Willis, D.G. 1957. The Elastic Theory of Consolidation. *J. Appl. Mech.*, December.

Blanksma, D.J. 2011. Investigation of In-Situ Stresses in Rocks via Acoustic Emission and the Kaiser Effect, Geological Engineering Senior Design proposal, University of North Dakota.

Breit, V.S., Stright, D.H. Jr., and Dozzo, J.A. 1992. Reservoir Characterization of Bakken Shale from Modeling of Horizontal Well Production Interference Data. Paper SPE 24320. SPE Rocky Mountain Regional Meeting, Casper, Wyoming. May 18-21.

Brimberry, D. 2007. An Operator's View of the Bakken Play Investigation. *The Bakken Shale Forum*. University of North Dakota Energy and Environmental Research Center, Grand Forks, ND USA. November 6.

Brimberry, D. 2008a. Bakken Geologic and Reservoir Engineering Technical Evaluation Methods, Leading Edge Earth and Planetary Sciences (LEEPS) Lecture Series, University of North Dakota, Grand Forks, North Dakota. November 21.

Brimberry, D. 2008b. Resource Estimation Approaches (Bakken Examples), Leading Edge Earth and Planetary Sciences (LEEPS) Lecture Series, University of North Dakota, Grand Forks, North Dakota. November 21.

Brown, D.L. 1987. Wrench-Style Deformational Patterns Associated with a Meridional Stress Axis Recognized in Paleozoic Rocks in Parts of Montana, South Dakota, and Wyoming, in: D. Rehrig, (Eds.), Economic Geology of the Williston Basin: the 24th Montana Geological Society Annual Conference and Williston Basin Symposium, Montana Geological Society, Billings, Montana, 1978, pp. 17-31.

Brown, D. L., and Brown, D. L., 1987, Wrench-Style Deformation and Paleostructural Influence on Sedimentation in and around a Cratonic Basin, in Longman, M. W., ed., Williston Basin: Anatomy of a Cratonic Oil Province: Rocky Mountain Association of Geologists, p. 57-70.

Carlisle, W.J., Dryff, L., Fryt, M.S., Artindale, J.S., and Von Der Dick, H. 1996. The Bakken Formation – an Integrated Geologic Approach to Horizontal Drilling. In *Production from Fractured Shales*, SPE Reprint Series No. 45, Society of Petroleum Engineers, Texas.

Chu, D., Tong, H., Li, Q., Zhang, Y., Wang, H. and Xu, D. 2008. Analysis of tectonic stress field modeling based on ANSYS – A Case Study Based on Conditions of Coalbed 7_2 in Renlou Coal Mine. Journal of Anhui University of Science and Technology (Natural Science), vol.28, no.1, p.16-19.

Cipolla, C.L., E.P. Lolon, M.J. Mayerhofer and N.R. Warpinski. 2009. The Effect of Proppant Distribution and Un-propped Fracture Conductivity on Well Performance in Unconventional Gas Reservoirs, Paper SPE119368, SPE Hydraulic Fracturing Technology Conference, Woodlands, Texas, USA, January 19-21.

Clement, J.H., 1987, Cedar Creek: A significant paleotectonic feature of the Williston Basin, in Longman, M.W., ed., Williston Basin: Anatomy of a cratonic oil province: Rocky Mountain Association of Geologists, p.p. 323–336.

Cox, S.A., Cook, D.M., Dunek, K. Daniels, R. Jump, C. and Barree, B. 2008. Unconventional Resource Play Evaluation: A Look at the Bakken Shale Play of North Dakota. Paper SPE 114171, SPE Unconventional Reservoirs Conference, keystone, CO. February 10-12.

Crammer, D. 1992. Treating-Pressure Analysis in the Bakken Formation. *Journal of Petroleum Technology*, vol. 44, no.1, p.20-27.

Davis, G.H. and Reynolds, S.J. 1996. *Structural Geology of Rocks and Regions* (2nd edition). John Wiley and Sons, Inc., New York, USA.

Dicker, A. I., and Smits, R. M. 1988. A Practical Approach for Determining Permeability from Laboratory Pressure-Pulse Decay Measurements. SPE 17578, p. 285-292.

Dow, W.G. 1974. Application of Oil Correlation and Source-Rock Data to Exploration in the Williston Basin, *AAPG Bulletin*. 58(1974) 1253-1262.

Druyff, L. 1991. Reservoir Properties of the Bakken Shale (abstract), in: B. Hansen, (Eds.), Geology and Horizontal Drilling of the Bakken Formation, Montana Geological Society, Billings, 1991, pp. 91.

Dunning, J. D., Leaird, J. D., and Miller, M. E. 1989. The Kaiser effect and frictional deformation. *Fourth Conference on AE/MA in Geologic Structures and Materials* (pp. 3-13). Clausthal-Zellerfeld: Trans Tech Publications.

Economides, M.J. and Boney, C. 2000. Reservoir Stimulation in Petroleum Production. In *Reservoir Stimulation* (Economides and Nolte, eds.), Wiley and Sons, New York.

Fa, L., Zeng, Z., and Liu, H. 2010. A New Device for Measuring In-situ Stresses by Using Acoustic Emission in Rocks. *44th US Rock Mechanics Symposium.* Salt Lake: American Rock Mechanics Association.

Fairhurst, C. 1961. Laboratory Measurement of Some Physical Properties of Rock. Proc. 4th Symp. Rock Mech. Univ. Park, Penn. pp.105-118.

Filimonov, Y., Lavrov, A., Shafarenko, Y., and Shkuratnik, V. 2002. Observation of post-failure Kaiser effect in a plastic rock. *Pure Applied Geophysics* , 1321-1331.

Fischer, D.D., LeFever, J.A., LeFever, R.D., and et al., 2005, Overview of Williston Basin Geology as it relates to CO2 sequestration, UND EERC report.

Fjaer, E., R.M. Holt, P. Horsrud, A.M. Raaen, and R. Risnes. 1992. *Petroleum Related Rock Mechanics*. Amsterdam: ELSEVIER.

Flannery, J. and Kraus, J. 2006. Integrated Analysis of the Bakken Petroleum System, U.S. Williston Basin, in: Search and Discovery Article #10105, AAPG Annual Convention, Houston, Texas, April 10-12, 2006.

Fowell RJ, Hudson JA, Xu C, Chen JF. 1995. Suggested method for determining mode- I fracture toughness using cracked chevron-notched Brazilian disc (CCNBD) specimens. Int J Rock Mech Min Sci Geomech Abstr 1995; 32(1): 57–64.

Fu, Y., Wang, X. and Yuang, H. 2009. Finite Element Inverse Analysis of Boundary Load for Tectonic Stress Field. *Journal of Rock and Soil Mechanics*, vol. 30, no.6, 1850-1855.

Geertsma, J. 1957. The Effect of Fluid Pressure Decline on Volumetric Changes of Porous Rock, *Trans. AIME.* 210, 331-339.

Gerhard, L. C., Anderson, S. B., and LeFever, J. A., 1987, Structural History of the Nesson Anticline, in Longman, M. W., ed., Williston Basin: Anatomy of a Cratonic Oil Province: Rocky Mountain Association of Geologists, p. 337-353.

Gerhard, L. C., Anderson, S.B. and Fischer, D.W. 1990, Petroleum Geology of the Williston Basin: in Leighton, M., Kolata, D., Oltz, D., and Eidel, J., eds., Petroleum Geology of Interior Cratonic Basins: American Association of Petroleum Geologists Memoir 51, p.507-559.

Gosnold, W.D. 1999. Basin-Scale Groundwater Flow and Advective Heat Flow: An Example from the Northern Great Plains. In *Geothermics in Basin Analysis (Forster and Merriam, eds.)*, Kluwer Academic / Plenum Publishers, 1999.

Green, A.G., Weber, W., and Hajnal, Z., 1985, Evolution of proterozoic terranes beneath the Williston Basin: Geology, v. 13, p. 624–628.

Green, D.W. and Willhite, G.P. 2003. *Enhanced Oil Recovery*. Society of Petroleum Engineers, Richardson, TX.

Gudmundsson, A., Simmenes, T.H., Larsen, B. and Philipp, S.L., 2009. Effects of Internal Structure and Local Stresses on Fracture Propagation, Deflection, and Arrest in Fault Zones. *Journal of Structural Geology*, vol.32, p.1643–1655.

Guo G., George, S.A., and Lindsey, R.P. 1999. Statistical Analysis of Surface Lineaments and Fractures for Characterizing Naturally Fractured Reservoirs. In *Reservoir Characterization Recent Advances* (Schatzinger and Jordan, eds.), American Association of Petroleum Geologists, Tulsa, OK, USA.

Haven, J. 2011. Mechanic Properties of the Bakken Formation, Mater Thesis, Department of Geophysics, Colorado School of Mines.

He, J., Pei, P., Ling, K., Zeng, Z., and Liu, H. 2013. Quantification of Rock Porosity Change before and after Freezing, *Journal of Petroleum Science Research*. July 2013

Headington Oil LLC and XTO Energy Inc. 2008. Hydraulic Fracturing and Microseismic Monitoring Project. Final Report Submitted to the North Dakota Industrial Commission. Contract No. G-015-028

Heck, T.J., LeFever, R.D., Fischer, D.W. and LeFever, J. 2002. *Overview of the Petroleum Geology of the North Dakota Williston Basin*. North Dakota Geological Survey, Bismarck, ND.

Heidbach, O., Tingay, M., Barth, A., Reinecker, J., Kurfeß, D. and Müller, B. 2009. The World Stress Map (Based on the Database Release 2008), Commission for the Geological Map of the World, Paris, France.

Holcomb, D. J. 1993. General Theory of the Kaiser Effect. *International Journal of Rock Mechanics and Mining Sciences* , 929-935.

Hsieh, P. A., Tracy, J. V., Neuzil, C. E., Bredehoeft, J. D., and Silliman, S. E. (1981). A Transient Laboratory Method for Determining the Hydraulic Properties of 'Tight' Rocks-I. Theory. *International Journal of Rock Mechanics and Mining Sciences and Geomechanics Abstracts, 18*, p. 245-252.

Hudson, J.A. (ed.) 1993. *Comprehensive Rock Engineering Volume 3 Rock Testing and Site Characterization*. Pergamon Press Ltd, Oxford, England.

Hudson, J.A., and Harrison, J.P. 1997. Engineering Rock Mechanics, An Introduction to the Principles. 1st ed. London: Pergamon.

Hudson, P.J. and Matson, R.P. 1992. Hydraulic Fracturing in Horizontal Wellbores. Paper SPE 23950, SPE Permian Basin Oil and Gas Recovery Conference, March 18-20, Midland, TX.

ISRM, 1978. Suggested Methods for Determining Tensile Strength of Rock Materials. International Society for Rock Mechanics. Int. J. Rock Mech. Min. Sci. & Geomech. Abstr. Vol. 15, pp.99-103.

ISRM Testing Commission, 1995. Suggested method for determining Mode-I fracture toughness using cracked chevron-notched Brazilian disc (CCNBD) specimens, Int. J. Rock Mech. Min. Sci. Geomech. Abstr., Vol. 32 (1):57–64.

Jaeger, J.C., Cook, N.G.W. and Zimmerman, R.W. 2007. Fundamentals of Rock Mechanics (4th edition), Blackwell publishing, Malden, MA, USA.

Jia, Y., Ji, C., Li, X., Xu, J., Zhou, Y., Zhang, L., Gao, X., Gao, P., Zeng, Z., Yang, Y., Wang, C. and Qu, G. 1996. Research of the Fault Characteristics and Petroleum Accumulation in the Southern Portion of Central Highs. Project Report, Institute of Geology, State Seismological Bureau of China and Liaohe Petroleum Exploration Bureau.

Joshi, S.D. 1987. A Review of Horizontal Well and Drainhole Technology. Paper SPE 16868, Proc. 62nd Annual Technical Conf., Dallas, Texas, Sept 27-30.

Kaiser, J. 1953. Erkenntnisse und Folgerungen aus der Messung von Gerauschen bei Zugbeanspruchung von metallischen Werkstoffen. *Archiv Eisenhuttenwesen* , 43-45.

Kim, K. and Franklin, J.A. 1987. Suggested Methods for Rock Stress Determination. *Int.J. Rock Mech. Min. Sci. and Geomech.* Abstr. Vol. 24, no.1, p.53-74.

Kranz, R. L., Saltzman, J. S., and Blacic, J. D. (1990). Hydraulic Diffusivity Measurements on Laboratory Rock Samples Using an Oscillating Pore Pressure Method. *International Journal of Rock Mechanics and Mining Sciences and Geomechanics Abstracts 27*, P 345-352.

Krishnan, G.R., X.L. Zhao, M. Zaman, and J.-C. Roegiers, 1998. Fracture toughness of a soft sandstone. Int. J. Rock Mech, Min. Sci. Vol. 35, No. 6:695-710.

Kuhlman, R. D., and Claiborne, E. B. Jr. 1992. Microfracture Stress Tests, An Elastic Strain Recovery and Differential Strain Analysis Assist in Bakken Shale Horizontal Drilling Program, Paper SPE24379. SPE Rocky Mountain Regional Meeting, Casper, Wyoming, USA, May 18-21.

Kurita, K., and Fujii, N. 1979. Stress memory of crystalline rocks in acoustic emission. *Geophysical Research Letters* , 9 - 12.

Lake, L.W. 1989. *Enhanced Oil Recovery*. Prentice Hall Inc., Upper Saddle River, NJ.

Landes, K. 1970. *Petroleum Geology of the United States*. John Wiley and Sons, New York.

Lantz, T. Greene, D. Eberhard, M., Norrid, S. and Pershall, R. 2007. Refracturing Treatments

Lavrov. 2001. Kaiser effect observation in brittle rock cyclically loaded with different loading rates. *Mech Mater* , 669-677.

Lavrov, A. 2003. The Kaiser effect in rocks: principles and stress estimation techniques. *International Journal of Rock Mechanics and Mining Sciences* , 151-171.

Lavrov, A. (1997). Three-dimensional simulation of memory effects in rock samples. In: Rock Stress. *Proceedings of the International Symposium on Rock Stress* (pp. 197-202). Rotterdam: A.A. Balkema.

Lee, W. J. (1982). Well Testing. *SPE Text book Series V1*, P13-15.

LeFever, J.A. 1991. History of Oil Production from Bakken Formation, North Dakota, in Montana Geological Society 1991 Guidebook to Geology and Horizontal Drilling of the Bakken Formation (Hansen, ed.), Billings, MT pp3-17.

LeFever, J.A. 2005. Oil Production from the Bakken Formation: a Short History. NDGS Newsletter, Vol 32, No. 1.

Lindsay, R.F., Anderson, S.B., Gerhard, L.C. and LeFever, R.D. 1988. Structural History and Reservoir Characteristics (Mississippian) of Nesson Anticline, North Dakota. In Giant Oil and Gas Fields Edited by Anthony J. Lomando and Paul M. Harris, vol. no12, p.741 -802.

Ling, K., He, J., Pei, P., Han, G., and Zhang, H. 2013. Determining the Permeability of Tight Rock with Gas Transient Flow, *Journal of Natural Gas Science and Engineering*. Vol.15, November 2013

Ljunggren, C., Chang, Y., Janson, T., and Christiansson, R. 2003. An overview of rock stress measurement methods. *International Journal of Rock Mechanics and Mining Sciences* , 975-989.

Meissner, F.F. 1978. Petroleum Geology of the Bakken Formation Williston Basin, North Dakota and Monta. In Proceedings of the Williston Basin Symposium and the 24th Annual Conference of Montana Geological Society, Billings, Montana.

Michihiro, K., Yoshioka, H., and Hata, K. F. 1989. Strain dependence of the Kaiser Effect for various rocks. *Fourth Conference on AE/MA* (pp. 87-95). Clausthal-Zellerfeld: Trans Tech Publication.

Mullen, M., Pitcher, J., Hinz, D., Everts, M., Dunbar, D., Calstrom, G., and Brenize, G. 2009. Does the Presence of Natural Fractures have an Impact on Production? A Case Study from the Middle Bakken Dolomite, North Dakota, in: Society of Petroleum Engineers Annual Technical Conference and Exhibition, Florence, Italy, September 19-22, 2009.

Murray, G.H. 1968. Quantitative Facture Study: Sanish Pool, McKenzie County, North Dakota, AAPG Bulletin. 52 (1968) 57-65.

Narr, W., and Burruss, R.C. 1984, Origin of Reservoir Fractures in Little Knife Field, North Dakota, The American Association of Petroleum Geologists Bulletin, V. 68 No.9, P.1087-1100.

Narr, W. Schechter, D.W. and Thompson, L.B. 2006. Naturally Fractured Reservoir Characterization. Society of Petroleum Engineers, Richardson, TX, USA

NDIC, 2006. Well File No. 15986. North Dakota Industrial Commission Oil and Gas Division, Bismarck, ND.

NDIC, 2007a. Well File No. 15889. North Dakota Industrial Commission Oil and Gas Division, Bismarck, ND.

NDIC, 2007b. Well File No. 16083. North Dakota Industrial Commission Oil and Gas Division, Bismarck, ND.

NDIC, 2008a. Bakken Formation Wells (Two 42-in by 96-in Maps). North Dakota Industrial Commission, Bismarck, ND.

NDIC, 2008b. Hydraulic Fracturing and Microseismic Monitoring Project — Bakken Research Consortium (Contract No. G015-028) Technical Summaries, North Dakota Industrial Commission Oil and Gas Research Program, Bismarck, ND.

NDIC, 2010. Well File No. 17513. North Dakota Industrial Commission Oil and Gas Division, Bismarck, ND.

Nihei, K.T., Nakagawa, S., Myer L.R. and Majer, E.L. 2002. Fracture Imaging with Elastic Waves, Proc. 5th International Workshop on the Application of Geophysics in Rock Engineering, Toronto, Canada, July 7.

Osadetz, K.G. and Snowdon, L.R. 1986. Speculation on the Petroleum Source Rock Potential of Portions of the Lodgepole Formation (Mississippian) of Southern Saskatchewan, in: Current Research, Part B, Geological Survey of Canada, Paper 86-1 B, Ottawa, 1986, p. 647-651.

Ouchterlony F. 1988. Suggested methods for determining the fracture toughness of rock. Int J Rock Mech Min Sci Geomech Abstr 1988; 25(2): 71–96.

Phillips, Z. D., Halverson, R.J., Strauss, S.R., Layman, J.M., Green. T.W. 2007. A Case Study in the Bakken Formation: Changes to Hydraulic Fracture Stimulation Treatments Results in Improved Oil Production and Reduced Treatment Costs, Paper SPE108045, SPE Rocky Mountain Oil and Gas Technology Symposium, Denver, Colorado, USA, April 16-18,.

Pilcher, R.S., Coisek, J.M., McArthur, K., Homan, J., and Schmitz, P.J. 2009. Ranking Production Potential Based on Key Geological Drivers—Bakken Case Study, in: International Petroleum Technology Conference, Bangkok, Thailand, February 7-9, 2009.

Pitman, J.K., Price, L.C., and LeFever, J.A. 2001. Diagenesis and Fracture Development in the Bakken Formation, Williston Basin: Implication for Reservoir Quality in the Middle Member, Professional Paper 1653: U.S. Geological Survey.

Pollastro, R.M., Cook, T.A. , Roberts, L.N.R., Schenk, C.J. Lewan, M.D., Anna, L.O., Gaswirth, S.B., Lillis, P.G., Klett, T.R., and Charpentier, R.R. 2008. Assessment of Undiscovered Oil Reserves in the Devonian-Mississippian Bakken Formation, Williston Basin Province, Montana and North Dakota, 2008. *US Geological Survey Fact Sheet 2008-3021*, April 2008.

Powell, A., Bustos, O., Kordziel, W., Olsen, T., Sobernheim, D and Vizurraga, T. 2007. Fiberladen Fracturing Fluid Improves Production in the Bakken Shale Multilateral Play. Paper SPE 107979, Rocky Mountain Oil and Gas Tech. Symp., Denver, Colorado, USA. April 16-18.

Price, L.C. 2000. Origin and Characteristics of the Basin-Centered Continuous-Reservoir Unconventional Oil-resource Base of Bakken Source System, Williston Basin. Energy and 62.

Price, L.C., Ging, T., Daws, T., Love, A., Pawlewicz, M. and Anders, D. 1984. Organic metamorphism in the Mississippian-Devonian Bakken Shale North Dakota Portion of the Williston Basin, in: J. Woodward, F.S. Meissner and J.L. Clayton, (Eds.), Hydrocarbon source rocks of the greater Rocky Mountain Region: Rocky Mountain Association of Geologists, Billings, 1984, pp. 83-133.

Price, L.C. and LeFever, J.A. 1994. Dysfunctionalism in the Williston Basin: the Bakken/mid-Madison Petroleum System, *Canadian Petroleum Geology Bulletin*. 42 (1994) 187-219.

Redly, P. and Hajnal, Z. 1995. Tectono-Stratigraphic Evolution of the Williston Basin — a Regional Seismic Stratigraphic Study, in: L.D. Hunter and R.A. Schalla, (Eds.), Proceedings of Seventh International Williston Basin Symposium: Montana Geological Society, Billings, 1995, pp. 341-350.

Reisz, M.R. 1992. Reservoir Evaluation of Horizontal Bakken Well Performance on the Southwestern Flank of Williston Basin. Paper SPE 22389, SPE International Meeting, Beijing, China. 24-27 March.

Reynolds, S.D., Coblentz, D.D. and Hills, R.R. 2002. Tectonic Forces Controlling the Regional Intraplate Stress Field in Continental Australia: Results from New Finite Element Modeling. *Journal of Geophysical Research*, vol.107, no.B7, p.2131-2146.

Roegiers, J.-C. 2008a. Importance of Geomechanics to Petroleum Engineering, Leading Edge Earth and Planetary Sciences (LEEPS) Lecture Series, University of North Dakota, Grand Forks, North Dakota. November 14.

Roegiers, J.-C. 2008b. Some Mysteries about Shales, Leading Edge Earth and Planetary Sciences (LEEPS) Lecture Series, University of North Dakota, Grand Forks, North Dakota. November 14.

Roundtree, R., Eberhard, M., and Barree, R., Horizontal, Near-Wellbore Stress Effects on Fracture Initiation, SPE Rocky Mountain Petroleum Technology Conference held in Denver, Colorado, USA, 14-16 April, 2009.

Spikes, K.T. 2011, Modeling Elastic Properties and Assessing Uncertainty of Fracture Parameters in the Middle Bakken Siltstone. Geophysics, Vol.76, no.4, p.117-126.

Stevens, J., and Holcomb, D. 1980. A theoretical investigation of the sliding crack model of dilatancy. *Journal of Geophysical Research* , 7091-7100.

Stockton, S.L. 2009. The Use of 3-component Seismic Data to Identify Sweet Spots in Fractured Bakken Reservoirs, in: AAPG International Conference and Exhibition, Calgary, Canada, September 12-15, 2009.

Sturm, S.D. and Gomez, E. 2009. Role of Natural Fracturing in Production from the Bakken Formation, Williston Basin, North Dakota. Adapted from Poster Presentation at AAPG Annual Convention and Exhibition, Denver, Colorado, USA, June 7-10.

Thomas, G.E. 1974. Lineament-Block Tectonics: Williston-Blood Creek Basin. *The American Association of Petroleum Geologists Bulletin*, vol. 58, no. 7 (July 1974), P. 1305-1322

Vincent, M.C. 2011. Optimizing Transverse Fractures in Liquid-Rich Formations. SPE 146376, SPE Annual Technical Conference and Exhibition held in Denver, Colorado, USA, 30 October–2 November 2011

Vutukuri, V.S., Lama, R.D. and Saluja, S.S., 1974. Handbook on Mechanical properties of Rocks, Vol. I. Trans Tech Publications, Clausthal, Germany. pp. 87-95.

Warner, T.B. 2011. Subsurface Horizontal Microfracture Propagation within the Middle Member of the Bakken Formation, Williston Basin, North Dakota: Evidence and Implications. Master Thesis, Department of Geology and Geography, West Virginia University.

Wang, C. and Zeng, Z. 2011. Overview of Geomechanical Properties of Bakken Formation in Williston Basin, North Dakota. In Proceedings of the 45th US Rock Mechanics Symposium and 5th US-Canada Rock Mechanics Symposium in San Francisco, CA, June 26–29.

Wang, Q.Z., X.M. Jia and L.Z. Wu, 2004. Wide-range stress intensity factors for the ISRM suggested method using CCNBD specimens for rock fracture toughness tests. Int. J. Rock Mech, Min. Sci. Vol. 41:709-716.

Wang, Q.Z., 2010. Formula for calculating the critical stress intensity factor in rock fracture toughness tests using cracked chevron notched Brazilian disc (CCNBD) specimens. Int. J. Rock Mech, Min. Sci. Vol. 47:1006-1011.

Warpinski, N.R., Schmidt, R.A., Cooper, P.W., Walling, H, C., and Northrop, D.A., 1979, High-Energy Gas Frac: Multiple Fracturing in a Wellbore. Proc. 20th US Symp. on Rock Mechanics, pp.143-151.

Webster, R.L. 1982. *Analysis of Petroleum Source Rocks of the Bakken Formation (Devonian and Mississippian) in North Dakota*. MS Thesis, University of North Dakota, Grand forks, ND.

Webster, R.L. 1984. Petroleum Source Rocks and Stratigraphy of the Bakken Formation in North Dakota, in: J. Woodward, F.S. Meissner, and J.L. Clayton, (Eds.), Hydrocarbon Source Rocks of the Greater Rocky Mountain Region, Rocky Mountain Association of Geologists, Billings, 1984, pp. 5781.

WGEPSS (Working Group for Estimating Primary State of Stress in a Rock Using the Acoustic Technique). 2002. Suggested Method for In-Situ Stress Measurement from a Rock Core Using the Acoustic Emission Technique. Proc. 5th International Workshop on the application of Geophysics in Rock Engineering, Toronto, Canada, July 7.

Wiley, C., Barree, B., Eberhard, M., and Lantz, T. 2004. Improved Horizontal Well Stimulation in Bakken Formation, Williston Basin. Montana. Paper SPE 90697, SPE Annual Technical Conference, Houston TX, USA 26-29 September.

Yoshikawa, S., and Mogi, K. 1989. Experimental studies on the effect of stress history on acoustic emission activity - a possibility for estiamtion of rock stress. *Journal of Acoustic Emission* , 113-123.

Zeng, Z. 2002. *Laboratory Imaging of Hydraulic Fracturing Using Microseismicity*. PhD Dissertation, University of Oklahoma, Norman, OK, USA.

Zeng, Z., and J.C. Roegiers, 2000. Derivation of formulae for fracture toughness determination by CDISK test. Internal Report, The University of Oklahoma.

Zhao, S. and Muller, R.D. 2001. Three-Dimensional Finite-Element Modeling of the Tectonic Stress Field in Continental Australia. Geological Society of Australia Special Publication 22, p.65–83.

Zhou, X., Zeng, Z., Belobraydic, M., and Han, Y. 2008. Geomechanical Stability Assessment of Williston Basin Formations for Petroleum Production and CO2 Sequestration. Paper ARMA08-211, *Proc. 42nd US Rock Mech. Symp. and 2nd U.S.-Canada Rock Mech. Symp.*, San Francisco, California, USA. June 29-July 2.

ATTACHMENTS

A.1. Well 20 Bakken Samples Testing Results

A.1.1 Permeability

Permeability and Specific Storage for File w20-mb-10689.3H-perm							
Event	Type	Conf	Pore Top	Diff	Temp	Perm	Storage
		MPa	MPa	MPa	°C	μD	m^{-1}
0	aspike	30.4	7.8	-5.2	33.6	1.46e+03	8.81e-05
1	aspike	30.5	7.8	-5.2	33.5	1.70e+03	0.000110
2	aspike	25.5	7.8	-4.8	33.3	1.92e+03	0.000113
3	aspike	25.5	7.8	-4.8	33.3	1.78e+03	0.000109
4	aspike	20.4	7.8	-4.8	33.0	1.97e+03	0.000109
5	aspike	20.4	7.8	-4.8	33.7	1.89e+03	0.000110
6	aspike	15.3	7.8	-4.8	33.1	2.01e+03	9.73e-05
7	aspike	15.4	7.8	-3.9	33.1	2.06e+03	0.000109

Permeability and Specific Storage for File w20-mb-10696H-perm							
Event	Type	Conf	Pore Top	Diff	Temp	Perm	Storage
		MPa	MPa	MPa	°C	μD	m^{-1}
0	multipulse	30.6	7.8	-4.8	33.6	5.96	2.38e-12
1	multipulse	30.5	7.8	-4.3	33.6	6.03	2.76e-11
2	multipulse	25.5	7.8	-4.3	33.5	6.44	5.94e-12
3	multipulse	20.5	7.8	-3.9	33.3	7.28	1.92e-10
4	multipulse	15.4	7.8	-3.9	33.2	11.5	9.07e-11
5	aspike	20.4	6.3	-4.3	33.3	9.98	4.17e-12
6	aspike	20.5	6.3	-3.9	33.3	12.6	1.84e-11

Permeability and Specific Storage for File w20-mb-10700V1-perm							
Event	Type	Conf	Pore Top	Diff	Temp	Perm	Storage
		MPa	MPa	MPa	°C	μD	m^{-1}
0	multipulse	30.5	7.9	-4.3	31.9	0.182	4.47e-07
1	multipulse	30.5	7.9	-4.3	31.7	0.204	4.43e-07
2	multipulse	25.5	7.9	-3.9	31.6	0.218	4.61e-07
3	multipulse	20.4	7.8	-3.9	31.5	0.239	4.33e-07
4	multipulse	15.4	7.8	-3.9	31.5	0.279	3.00e-07

Permeability and Specific Storage for File w20-mb-10700V2-perm							
Event	Type	Conf	Pore Top	Diff	Temp	Perm	Storage
		MPa	MPa	MPa	°C	μD	m^{-1}
0	multipulse	30.4	7.8	-4.3	32.0	0.114	6.65e-07
1	multipulse	25.5	7.8	-3.9	32.4	0.146	5.08e-07
2	multipulse	20.5	7.8	-3.9	32.4	0.198	1.21e-08
3	multipulse	15.4	7.8	-3.5	33.1	0.924	1.20e-12

Permeability and Specific Storage for File w20-mb-10705.5V45-perm							
Event	Type	Conf	Pore Top	Diff	Temp	Perm	Storage
		MPa	MPa	MPa	°C	μD	m^{-1}
0	multipulse	30.4	7.8	-5.2	33.6	0.606	7.18e-08
1	multipulse	25.5	7.8	-4.8	33.7	0.692	5.16e-12
2	multipulse	20.5	7.8	-4.3	34.3	0.940	5.32e-12
3	multipulse	15.4	7.8	-4.3	33.8	1.66	1.95e-13
4	multipulse	20.7	6.3	-4.3	34.0	1.42	1.10e-12
5	multipulse	20.7	6.3	-4.3	33.9	0.948	4.47e-11
6	multipulse	20.7	6.3	-4.3	34.0	1.24	1.97e-13

Permeability and Specific Storage for File w20-mb-10705.9V-perm							
Event	Type	Conf	Pore Top	Diff	Temp	Perm	Storage
		MPa	MPa	MPa	°C	μD	m^{-1}
0	multipulse	15.5	7.8	-3.9	35.1	0.150	1.42e-05
1	multipulse	30.4	7.8	-4.3	36.1	0.0338	2.89e-06
2	multipulse	20.4	7.8	-4.3	36.2	0.0109	5.77e-07

Permeability and Specific Storage for File w20-mb-10712V45-perm							
Event	Type	Conf	Pore Top	Diff	Temp	Perm	Storage
		MPa	MPa	MPa	°C	μD	m^{-1}
0	multipulse	30.4	7.8	-4.8	33.6	7.97	5.77e-10
1	multipulse	30.4	7.8	-4.8	33.6	9.68	1.86e-11
2	sine6	30.4	7.8	-4.8	33.6	9.47	1.51e-12
3	aspike	20.5	7.7	-4.8	33.1	13.8	5.37e-12
4	aspike	20.5	7.8	-4.3	33.3	19.4	2.07e-07
5	aspike	15.4	7.7	-3.9	33.3	26.2	1.09e-11

Permeability and Specific Storage for File w16174-10715.2-pluse-perm							
Event	Type	Conf	Pore Top	Diff	Temp	Perm	Storage
		MPa	MPa	MPa	°C	μD	m^{-1}
21	multipulse	30.4	8.5	-4.8	23.4	0.188	0.000109
22	multipulse	40.6	8.5	-5.2	23.5	0.00133	4.86e-08
23	multipulse	50.5	8.5	-6.0	23.3	0.0371	2.07e-05

Permeability and Specific Storage for File w16174-10721.4-pluse-perm							
Event	Type	Conf	Pore Top	Diff	Temp	Perm	Storage
		MPa	MPa	MPa	°C	μD	m^{-1}
0	multipulse	20.6	4.0	-3.9	24.3	1.16	8.93e-11
1	multipulse	30.5	3.8	-4.8	24.5	1.16	9.73e-11
2	multipulse	40.5	3.7	-4.8	24.6	517.	2.28e-06
3	multipulse	50.6	3.5	-5.6	24.6	16.9	2.86e-10
4	multipulse	20.6	12.5	-4.3	23.9	0.0393	4.42e-07
5	multipulse	30.5	12.6	-4.8	23.9	0.0355	5.30e-07
6	multipulse	40.6	12.5	-5.2	24.1	0.0294	4.84e-07
7	multipulse	50.6	12.5	-5.6	24.3	0.0223	3.41e-07
8	multipulse	50.5	11.5	-5.6	25.7	0.0234	4.65e-07
9	multipulse	40.5	11.5	-5.2	25.7	0.0256	5.46e-07
10	multipulse	30.5	11.5	-4.8	25.8	0.0267	5.86e-07
11	multipulse	20.6	11.5	-3.9	25.3	0.0385	7.10e-07
12	multipulse	20.5	10.4	-3.9	25.3	0.0342	4.95e-07
13	multipulse	30.5	10.4	-4.8	25.3	0.0213	3.02e-07
14	multipulse	40.5	10.5	-4.8	25.3	0.0224	3.54e-07
15	multipulse	50.5	10.5	-5.6	25.1	0.0179	2.99e-07
16	multipulse	50.5	8.5	-5.6	26.4	0.0176	3.72e-07
17	multipulse	40.6	8.5	-4.8	26.4	0.0214	4.94e-07
18	multipulse	30.5	8.5	-4.3	26.6	0.0276	7.00e-07
19	multipulse	20.5	8.4	-4.3	26.4	0.0275	4.98e-07

Permeability and Specific Storage for File w16174-10730.6-pluse-perm							
Event	Type	Conf	Pore Top	Diff	Temp	Perm	Storage
		MPa	MPa	MPa	°C	μD	m^{-1}
0	multipulse	20.4	10.3	-3.9	25.2	0.0207	1.12e-06
1	multipulse	20.5	10.3	-3.9	25.5	0.277	5.29e-05
2	multipulse	30.5	10.3	-3.9	25.5	0.0280	8.44e-06
3	multipulse	40.5	10.3	-4.8	25.6	0.0176	1.46e-05
4	multipulse	50.5	10.3	-5.6	25.8	0.00474	2.95e-07
5	multipulse	20.5	10.4	-3.5	25.7	0.00720	3.61e-07
6	multipulse	30.5	10.4	-3.9	25.9	0.00263	8.77e-08
7	multipulse	40.5	10.4	-4.8	26.0	0.00170	1.04e-07
8	multipulse	50.5	10.4	-5.6	25.9	0.00279	1.50e-07
9	multipulse	20.5	8.4	-3.9	25.3	0.0139	7.07e-06
10	multipulse	30.5	8.4	-4.3	25.4	0.0138	5.77e-06
11	multipulse	40.5	8.5	-4.8	25.4	0.168	0.000106
12	multipulse	50.5	8.4	-5.2	25.3	0.0157	5.05e-06
13	multipulse	20.5	12.1	-3.5	25.4	0.00612	3.98e-07
14	multipulse	30.4	12.1	-4.8	25.4	0.000850	1.14e-07
15	multipulse	40.5	12.1	-4.8	25.5	0.000634	1.40e-07
16	multipulse	50.5	12.1	-5.6	25.4	0.181	0.000103
17	multipulse	20.5	10.9	-4.3	25.0	0.00288	1.24e-07
18	multipulse	30.4	10.9	-4.8	25.0	0.127	0.000107
19	multipulse	40.5	11.0	-5.2	25.1	0.000109	1.22e-07
20	multipulse	50.5	11.0	-6.0	25.0	0.0197	1.45e-05

Permeability and Specific Storage for File w16174-10712-vertical-perm-biot							
Event	Type	Conf	Pore Top	Diff	Temp	Perm	Storage
		MPa	MPa	MPa	°C	μD	m^{-1}
0	multipulse	20.6	7.6	-0.8	23.4	0.121	5.58e-07
1	multipulse	30.6	7.6	-1.3	23.5	0.0903	5.75e-07
2	multipulse	40.7	7.6	-1.7	27.3	0.0735	6.35e-07

Permeability and Specific Storage for File w16174-10714-perm-biot							
Event	Type	Conf	Pore Top	Diff	Temp	Perm	Storage
		MPa	MPa	MPa	°C	μD	m^{-1}
0	multipulse	20.7	7.6	-0.8	23.1	0.0302	1.67e-11
1	multipulse	30.7	7.7	-0.8	23.4	0.0137	1.73e-11
2	multipulse	40.7	7.6	-2.1	23.5	0.00906	7.37e-11

Permeability and Specific Storage for File w16174-10715.7-perm-biot							
Event	Type	Conf	Pore Top	Diff	Temp	Perm	Storage
		MPa	MPa	MPa	°C	μD	m^{-1}
0	multipulse	20.7	7.5	-0.4	22.8	0.0415	2.22e-07
1	multipulse	30.6	7.5	-1.3	22.8	0.0350	1.84e-07

Permeability and Specific Storage for File w16174-10716.4-vertical-perm-biot							
Event	Type	Conf	Pore Top	Diff	Temp	Perm	Storage
		MPa	MPa	MPa	°C	μD	m^{-1}
0	multipulse	20.7	7.5	-0.4	28.8	0.0396	1.34e-07
1	multipulse	30.7	7.5	-0.8	29.0	0.0240	8.43e-08
2	multipulse	40.7	7.5	-1.7	29.0	0.0259	5.87e-08

Permeability and Specific Storage for File w16174-10716.5-perm-biot							
Event	Type	Conf	Pore Top	Diff	Temp	Perm	Storage
		MPa	MPa	MPa	°C	μD	m^{-1}
0	multipulse	20.7	7.5	-0.8	23.5	0.137	2.98e-12
1	multipulse	30.7	7.5	-0.8	23.7	0.114	1.90e-12
2	multipulse	40.7	7.5	-1.7	24.1	0.102	1.15e-12
3	multipulse	50.7	7.6	-1.7	23.7	0.0903	1.64e-11

Permeability and Specific Storage for File w16174-10718.7-vertical-perm-biot							
Event	Type	Conf	Pore Top	Diff	Temp	Perm	Storage
		MPa	MPa	MPa	°C	μD	m^{-1}
0	multipulse	20.7	7.6	-1.3	24.7	0.239	4.80e-07
1	multipulse	30.7	7.6	-1.7	24.8	0.121	2.98e-07
2	multipulse	40.7	7.6	-2.1	24.3	0.0978	2.65e-07
3	multipulse	50.7	7.6	-2.5	23.7	0.0789	3.31e-07

Permeability and Specific Storage for File w16174-10723-perm-biot							
Event	Type	Conf	Pore Top	Diff	Temp	Perm	Storage
		MPa	MPa	MPa	°C	μD	m^{-1}
0	multipulse	20.7	7.6	-0.8	29.7	3.04	1.84e-10
1	multipulse	20.7	7.6	-0.8	29.8	2.01	2.55e-07
2	multipulse	30.7	7.6	-0.8	30.6	1.77	1.62e-07
3	multipulse	40.7	7.6	-1.3	31.4	0.263	8.15e-12
4	multipulse	40.7	7.6	-1.3	31.1	0.929	1.15e-06
5	multipulse	50.7	7.6	-1.7	30.0	0.811	3.79e-06

Permeability and Specific Storage for File w16174-10726.9-perm-biot							
Event	Type	Conf	Pore Top	Diff	Temp	Perm	Storage
		MPa	MPa	MPa	°C	μD	m^{-1}
0	multipulse	20.7	7.5	-0.8	24.6	1.59	3.57e-09
1	multipulse	30.6	7.6	-0.8	25.7	1.62	1.35e-07
2	multipulse	40.7	7.6	-1.3	27.4	1.37	1.86e-07

Permeability and Specific Storage for File w16174-10727.2-perm-biot							
Event	Type	Conf	Pore Top	Diff	Temp	Perm	Storage
		MPa	MPa	MPa	°C	μD	m^{-1}
0	multipulse	20.7	7.6	-1.3	23.8	0.0320	1.36e-12
1	multipulse	30.6	7.5	-1.7	25.7	0.0265	6.13e-13
2	multipulse	40.7	7.5	-2.5	46.1	0.0265	1.13e-12

Permeability and Specific Storage for File w16174-10728.1-perm-biot							
Event	Type	Conf	Pore Top	Diff	Temp	Perm	Storage
		MPa	MPa	MPa	°C	μD	m^{-1}
0	multipulse	20.7	7.5	-1.3	25.4	3.0	7.67e-11
1	multipulse	30.6	7.5	-1.7	25.6	2.36	3.62e-11
2	multipulse	40.7	7.5	-1.7	25.7	2.05	7.07e-11
3	multipulse	50.7	7.6	-2.1	27.2	1.80	1.08e-12

Permeability and Specific Storage for File w16174-10728.8-perm-biot							
Event	Type	Conf	Pore Top	Diff	Temp	Perm	Storage
		MPa	MPa	MPa	°C	μD	m^{-1}
0	aspike	20.7	7.5	-0.4	23.9	567.	3.27e-09
1	aspike	30.6	7.5	-1.3	26.1	625.	1.62e-06
2	aspike	40.7	7.5	-1.3	27.5	309.	7.07e-11

Permeability and Specific Storage for File w16174-10729.1-perm-biot							
Event	Type	Conf	Pore Top	Diff	Temp	Perm	Storage
		MPa	MPa	MPa	°C	μD	m^{-1}
0	multipulse	20.7	7.5	-0.8	23.3	6.88	3.12e-11
1	multipulse	30.0	7.6	-1.3	24.6	6.15	2.34e-07
2	multipulse	40.1	7.6	-1.7	25.6	6.27	1.84e-08

Permeability and Specific Storage for File w16174-10729.5-perm-biot							
Event	Type	Conf	Pore Top	Diff	Temp	Perm	Storage
		MPa	MPa	MPa	°C	μD	m^{-1}
0	multipulse	20.6	7.5	-1.3	23.8	10.7	1.12e-10
1	multipulse	30.7	7.6	-1.3	23.5	0.493	2.76e-11
2	multipulse	40.7	7.6	-2.1	23.9	0.383	4.08e-12
3	multipulse	50.7	7.6	-2.5	23.7	0.409	1.55e-10

Permeability and Specific Storage for File w16174-10729.9-perm-biot							
Event	Type	Conf	Pore Top	Diff	Temp	Perm	Storage
		MPa	MPa	MPa	°C	μD	m^{-1}
0	aspike	20.7	7.7	-0.8	34.4	70.6	1.50e-07
1	aspike	30.4	7.7	-1.3	34.8	47.9	4.44e-11
2	aspike	40.2	7.8	-1.7	35.2	43.1	7.29e-08

Permeability and Specific Storage for File w16174-10731.4-horizontal-perm-biot							
Event	Type	Conf	Pore Top	Diff	Temp	Perm	Storage
		MPa	MPa	MPa	°C	μD	m^{-1}
0	multipulse	20.7	7.5	-0.8	25.0	0.486	4.75e-12
1	multipulse	30.6	7.5	-1.3	25.2	0.261	1.70e-11

Permeability and Specific Storage for File w16174-10731.4-vertical-perm-biot							
Event	Type	Conf	Pore Top	Diff	Temp	Perm	Storage
		MPa	MPa	MPa	°C	μD	m^{-1}
0	multipulse	20.7	7.5	-0.8	23.0	2.0	0.000115
1	multipulse	30.7	7.6	-1.3	24.3	0.0188	6.28e-07

Permeability and Specific Storage for File w16174-10732.3-perm-biot							
Event	Type	Conf	Pore Top	Diff	Temp	Perm	Storage
		MPa	MPa	MPa	°C	μD	m^{-1}
0	multipulse	20.7	7.6	-1.3	22.6	0.912	3.23e-11
1	multipulse	30.7	7.6	-1.3	22.8	0.0238	1.77e-12
2	multipulse	40.7	7.6	-1.7	22.8	0.0272	1.11e-07

Permeability and Specific Storage for File w16174-10733.3-perm-biot							
Event	Type	Conf	Pore Top	Diff	Temp	Perm	Storage
		MPa	MPa	MPa	°C	μD	m^{-1}
0	multipulse	20.7	7.5	-1.3	23.5	28.4	6.51e-12
1	multipulse	30.6	7.5	-1.3	23.3	19.4	1.71e-12
2	multipulse	40.7	7.6	-2.1	23.8	12.5	2.76e-12
3	multipulse	50.7	7.6	-2.1	23.4	10.9	2.36e-09

A.1.2 Sonic Velocity, Dynamic Moduli and Poisson's Ratio

Observed Velocities and Moduli for File Middle_Bakken-W20-10700V1-Velocity									
Event	Conf	Pore	Diff	Temp	V_p	$V_s^{(1)}$	$V_s^{(2)}$	Young's Modulus	Poisson's Ratio
	MPa	MPa	MPa	°C	m/s	m/s	m/s	GPa	
0	2.5	-0.2	-1.7	22.3	4381	2953	2981	49.84	0.076
1	4.4	-0.2	-2.1	22.3	4606	2977	2992	53.32	0.138
2	6.4	-0.2	-2.1	22.4	4601	2988	2999	53.40	0.133
3	8.5	-0.2	-1.9	22.5	4664	2999	2999	54.29	0.148
4	10.5	-0.2	-2.1	22.6	4697	3010	3015	54.92	0.151
5	12.4	-0.2	-2.2	22.6	4763	3015	3019	55.78	0.165
6	14.4	-0.2	-2.4	22.7	4786	3028	3033	56.30	0.165
7	16.5	-0.2	-2.1	22.8	4837	3035	3042	57.02	0.174
8	18.4	-0.2	-2.9	22.8	4855	3042	3049	57.35	0.176
9	20.5	-0.2	-2.5	22.9	4872	3049	3067	57.79	0.175
10	22.4	-0.2	-2.9	22.8	4878	3060	3065	57.95	0.175
11	24.5	-0.2	-2.5	22.9	4884	3065	3072	58.14	0.174
12	26.4	-0.2	-2.7	22.9	4914	3073	3084	58.67	0.177
13	28.4	-0.2	-3.4	22.9	4938	3076	3088	59.00	0.181
14	30.4	-0.2	-2.9	23.0	5018	3086	3093	59.99	0.195

Observed Velocities and Moduli for File Middle_Bakken-W20-10705.9V-Velocity									
Event	Conf	Pore	Diff	Temp	V_p	$V_s^{(1)}$	$V_s^{(2)}$	Young's Modulus	Poisson's Ratio
	MPa	MPa	MPa	°C	m/s	m/s	m/s	GPa	
0	2.5	-0.2	-1.7	22.1	4590	2877	2872	51.17	0.177
1	4.5	-0.2	-1.7	22.2	4614	2879	2894	51.65	0.178
2	6.5	-0.2	-2.1	22.2	4648	2897	2898	52.21	0.182
3	8.4	-0.2	-2.5	22.3	4669	2897	2902	52.45	0.186
4	10.5	-0.2	-2.1	22.4	4667	2892	2904	52.40	0.186
5	12.5	-0.2	-2.1	22.4	4672	2896	2911	52.56	0.185
6	14.5	-0.2	-2.1	22.5	4667	2902	2913	52.60	0.183
7	16.5	-0.2	-2.5	22.6	4648	2904	2923	52.53	0.176
8	18.4	-0.2	-2.8	22.5	4692	2908	2931	53.09	0.184
9	20.5	-0.2	-2.8	22.6	4712	2908	2917	53.14	0.191
10	22.5	-0.2	-2.5	22.6	4742	2913	2927	53.58	0.195
11	24.4	-0.2	-3.1	22.6	4763	2911	2931	53.79	0.199
12	26.4	-0.2	-2.9	22.6	4737	2915	2936	53.65	0.192
13	28.5	-0.2	-2.9	23.0	4773	2921	2936	54.05	0.198
14	30.4	-0.2	-3.1	22.9	4799	2923	2940	54.35	0.202

Observed Velocities and Moduli for File Middle_Bakken-w20-10689.3H-velocity									
Event	Conf	Pore	Diff	Temp	V_p	$V_s^{(1)}$	$V_s^{(2)}$	Young's Modulus	Poisson's Ratio
	MPa	MPa	MPa	°C	m/s	m/s	m/s	GPa	
0	2.5	-0.2	-1.5	22.8	5245	3072	3059	58.99	0.241
1	4.4	-0.2	-1.8	22.8	5294	3081	3089	59.85	0.243
2	6.5	-0.2	-2.1	23.0	5321	3093	3095	60.29	0.245
3	8.4	-0.2	-2.1	23.0	5393	3114	3111	61.29	0.250
4	10.5	-0.2	-2.1	23.1	5338	3128	3126	61.29	0.239
5	12.5	-0.2	-2.1	23.2	5393	3142	3126	61.88	0.245
6	14.4	-0.2	-2.5	23.2	5390	3143	3137	62.02	0.243
7	16.5	-0.2	-2.2	23.4	5453	3153	3146	62.73	0.250
8	18.4	-0.2	-2.9	23.4	5449	3173	3161	63.18	0.245
9	20.4	-0.2	-2.9	23.4	5437	3187	3163	63.31	0.241
10	22.4	-0.2	-2.8	23.4	5439	3187	3165	63.36	0.241
11	24.5	-0.2	-2.7	23.4	5474	3192	3177	63.85	0.244
12	26.4	-0.2	-2.9	23.4	5460	3194	3182	63.84	0.241
13	28.5	-0.2	-2.8	23.5	5503	3207	3194	64.50	0.244
14	30.4	-0.2	-2.9	23.5	5565	3214	3209	65.25	0.250

Observed Velocities and Moduli for File Middle_Bakken-w20-10700V2-velocity									
Event	Conf	Pore	Diff	Temp	V_p	$V_s^{(1)}$	$V_s^{(2)}$	Young's Modulus	Poisson's Ratio
	MPa	MPa	MPa	°C	m/s	m/s	m/s	GPa	
0	2.4	-0.2	-1.7	25.0	4363	2854	2867	48.15	0.123
1	4.4	-0.2	-1.7	25.1	4436	2875	2874	49.28	0.138
2	6.4	-0.2	-2.1	25.1	4498	2882	2886	50.16	0.151
3	8.4	-0.2	-2.1	25.2	4530	2894	2902	50.77	0.154
4	10.4	-0.2	-2.2	25.3	4591	2906	2912	51.64	0.165
5	12.5	-0.2	-2.1	25.3	4616	2917	2924	52.12	0.166
6	14.5	-0.2	-2.2	25.4	4630	2927	2934	52.46	0.166
7	16.5	-0.2	-2.2	25.4	4672	2936	2941	53.06	0.173
8	18.4	-0.2	-2.5	25.5	4672	2948	2950	53.26	0.169
9	20.5	-0.2	-2.1	25.5	4702	2958	2964	53.82	0.171
10	22.4	-0.2	-2.5	25.4	4727	2961	2971	54.18	0.175
11	24.5	-0.2	-2.5	25.5	4780	2972	2978	54.90	0.184
12	26.4	-0.2	-2.9	25.5	4809	2979	2988	55.37	0.187
13	28.5	-0.2	-2.5	25.5	4813	2985	2989	55.48	0.187
14	30.4	-0.2	-2.9	25.6	4880	2992	2995	56.27	0.198

Observed Velocities and Moduli for File Middle_Bakken-w20-10705.5V45-Velocity									
Event	Conf	Pore	Diff	Temp	V_p	$V_s^{(1)}$	$V_s^{(2)}$	Young's Modulus	Poisson's Ratio
	MPa	MPa	MPa	°C	m/s	m/s	m/s	GPa	
0	2.4	-0.2	-1.7	25.6	4919	2959	3019	56.74	0.207
1	4.4	-0.2	-1.9	25.6	4941	2969	3030	57.18	0.208
2	6.4	-0.2	-1.7	25.7	4953	2977	3041	57.51	0.208
3	8.4	-0.2	-2.1	25.8	4949	2978	3045	57.53	0.206
4	10.4	-0.2	-2.1	25.8	4994	2980	3047	57.97	0.214
5	12.4	-0.2	-2.1	25.8	4989	2986	3058	58.14	0.210
6	14.4	-0.2	-2.4	25.9	5005	2988	3057	58.29	0.213
7	16.4	-0.2	-2.5	25.8	4996	2988	3059	58.23	0.211
8	18.4	-0.2	-2.2	25.9	5009	2996	3066	58.53	0.211
9	20.5	-0.2	-2.5	25.9	4998	2995	3068	58.44	0.209
10	22.4	-0.2	-2.2	26.0	5051	2997	3074	59.00	0.217
11	24.5	-0.2	-2.5	26.0	5087	3001	3078	59.40	0.222
12	26.4	-0.2	-2.5	26.0	5091	3005	3079	59.50	0.222
13	28.4	-0.2	-2.8	26.0	5091	3005	3081	59.52	0.222
14	30.4	-0.2	-2.7	26.0	5106	3008	3082	59.70	0.224

Observed Velocities and Moduli for File Middle_Bakken-w20-10712V45-velocity									
Event	Conf	Pore	Diff	Temp	V_p	$V_s^{(1)}$	$V_s^{(2)}$	Young's Modulus	Poisson's Ratio
	MPa	MPa	MPa	°C	m/s	m/s	m/s	GPa	
0	2.4	-0.2	-2.1	24.3	5105	3081	3089	61.38	0.212
1	4.4	-0.2	-1.9	24.4	5146	3089	3075	61.67	0.220
2	6.4	-0.2	-1.8	24.5	5184	3104	3081	62.26	0.224
3	8.4	-0.2	-2.4	24.5	5192	3110	3084	62.45	0.224
4	10.4	-0.2	-2.5	24.5	5196	3115	3089	62.61	0.223
5	12.5	-0.2	-2.1	24.6	5217	3116	3101	62.96	0.225
6	14.4	-0.2	-2.5	24.6	5230	3127	3101	63.22	0.225
7	16.5	-0.2	-2.5	24.6	5243	3133	3098	63.36	0.227
8	18.4	-0.2	-2.5	24.7	5264	3135	3113	63.77	0.228
9	20.4	-0.2	-2.9	24.6	5277	3136	3123	64.02	0.229
10	22.4	-0.2	-2.9	24.6	5273	3142	3132	64.19	0.226
11	24.4	-0.2	-3.2	24.7	5273	3141	3125	64.08	0.227
12	26.4	-0.2	-2.9	24.7	5299	3154	3119	64.39	0.230
13	28.5	-0.2	-2.9	24.9	5282	3150	3126	64.29	0.227
14	30.4	-0.2	-3.4	25.3	5290	3155	3129	64.47	0.227

Observed Velocities and Moduli for File Middle_Bakkn-w20-10687V-velocity									
Event	Conf	Pore	Diff	Temp	V_p	$V_s^{(1)}$	$V_s^{(2)}$	Young's Modulus	Poisson's Ratio
	MPa	MPa	MPa	°C	m/s	m/s	m/s	GPa	
0	2.5	-0.2	-1.7	22.3	4523	2951	2953	50.96	0.129
1	4.4	-0.2	-2.1	22.3	4561	2959	2970	51.64	0.134
2	6.4	-0.2	-2.1	22.4	4608	2984	2984	52.53	0.139
3	8.4	-0.2	-2.1	22.5	4704	3000	3005	53.99	0.156
4	10.4	-0.2	-2.1	22.5	4704	3017	3017	54.25	0.151
5	12.4	-0.2	-2.5	22.6	4830	3034	3047	56.11	0.172
6	14.4	-0.2	-2.5	22.6	4849	3051	3070	56.72	0.169
7	16.4	-0.2	-2.8	22.6	4868	3072	3088	57.31	0.166
8	18.4	-0.2	-2.9	22.7	4896	3090	3103	57.95	0.167
9	20.5	-0.2	-2.7	22.7	4975	3103	3112	59.03	0.180
10	22.4	-0.2	-2.9	22.7	4983	3115	3125	59.38	0.178
11	24.4	-0.2	-3.2	22.7	5039	3132	3136	60.27	0.185
12	26.4	-0.2	-2.9	23.4	5077	3141	3162	61.05	0.187
13	28.4	-0.2	-3.4	23.0	5166	3152	3161	62.04	0.202
14	30.4	-0.2	-3.4	22.9	5286	3169	3173	63.49	0.219

Observed Velocities and Moduli for File w20-mb-10683.5H-velocity									
Event	Conf	Pore	Diff	Temp	V_p	$V_s^{(1)}$	$V_s^{(2)}$	Young's Modulus	Poisson's Ratio
	MPa	MPa	MPa	°C	m/s	m/s	m/s	GPa	
0	30.4	-0.2	-3.2	28.9	5934	3215	3223	71.73	0.292
1	28.4	-0.2	-2.9	28.7	5865	3214	3221	71.29	0.285
2	26.4	-0.2	-2.5	28.5	5868	3215	3216	71.24	0.285
3	24.5	-0.2	-2.5	28.2	5841	3212	3218	71.06	0.283
4	22.4	-0.2	-2.5	28.0	5825	3210	3208	70.77	0.282
5	20.4	-0.2	-2.8	27.8	5833	3206	3213	70.83	0.283
6	18.4	-0.2	-2.2	27.7	5833	3206	3211	70.80	0.283
7	16.4	-0.2	-2.5	27.5	5794	3207	3214	70.63	0.278
8	14.4	-0.2	-2.1	27.5	5794	3206	3219	70.70	0.278
9	12.4	-0.2	-2.1	27.5	5922	3206	3226	71.56	0.291
10	10.4	-0.2	-2.5	27.3	5817	3202	3210	70.62	0.282
11	8.4	-0.2	-2.5	27.2	5801	3201	3214	70.57	0.280
12	6.4	-0.2	-2.1	27.2	5809	3198	3205	70.42	0.282
13	4.4	-0.2	-1.7	27.1	5794	3185	3208	70.17	0.281
14	2.4	-0.2	-1.7	27.1	5778	3179	3179	69.49	0.283

Observed Velocities and Moduli for File w20-mb-10685.9H-velocity									
Event	Conf	Pore	Diff	Temp	V_p	$V_s^{(1)}$	$V_s^{(2)}$	Young's Modulus	Poisson's Ratio
	MPa	MPa	MPa	°C	m/s	m/s	m/s	GPa	
0	30.5	-0.2	-2.5	22.6	5303	3189	3121	64.19	0.226
1	28.5	-0.2	-2.5	22.4	5290	3184	3118	63.98	0.225
2	26.4	-0.2	-2.7	22.3	5296	3184	3116	64.00	0.226
3	24.4	-0.2	-2.7	22.0	5258	3177	3110	63.51	0.222
4	22.4	-0.2	-2.7	22.5	5246	3175	3105	63.32	0.221
5	20.5	-0.2	-2.5	22.1	5233	3206	3101	63.55	0.215
6	18.4	-0.2	-2.5	21.9	5184	3166	3101	62.60	0.212
7	16.5	-0.2	-2.2	21.8	5190	3161	3096	62.53	0.215
8	14.5	-0.2	-2.1	22.2	5178	3154	3092	62.29	0.214
9	12.4	-0.2	-2.5	21.8	5159	3145	3081	61.87	0.214
10	10.4	-0.2	-2.4	21.7	5171	3141	3051	61.54	0.221
11	8.4	-0.2	-2.5	21.6	5093	3127	3034	60.47	0.212
12	6.5	-0.2	-2.1	22.2	5087	3114	3028	60.19	0.213
13	4.4	-0.2	-2.1	21.7	5082	3101	3009	59.75	0.217
14	2.5	-0.2	-1.7	21.6	5018	3092	2999	58.96	0.208

Observed Velocities and Moduli for File w20-mb-10696.8H-velocity									
Event	Conf	Pore	Diff	Temp	V_p	$V_s^{(1)}$	$V_s^{(2)}$	Young's Modulus	Poisson's Ratio
	MPa	MPa	MPa	°C	m/s	m/s	m/s	GPa	
0	30.4	-0.2	-2.8	24.1	5415	3138	3199	64.97	0.240
1	28.5	-0.2	-2.5	24.3	5401	3134	3206	64.90	0.237
2	26.4	-0.2	-2.7	23.9	5366	3131	3191	64.38	0.234
3	24.4	-0.2	-2.7	23.7	5366	3129	3201	64.49	0.233
4	22.4	-0.2	-2.5	23.6	5360	3124	3201	64.37	0.233
5	20.4	-0.2	-2.7	23.4	5339	3120	3189	63.99	0.232
6	18.4	-0.2	-2.2	23.3	5325	3113	3179	63.64	0.232
7	16.5	-0.2	-2.2	23.2	5305	3092	3172	63.11	0.232
8	14.5	-0.2	-2.1	23.2	5265	3083	3162	62.54	0.229
9	12.5	-0.2	-2.1	23.6	5251	3080	3167	62.45	0.226
10	10.4	-0.2	-2.5	23.1	5238	3065	3160	62.05	0.227
11	8.4	-0.2	-1.9	23.1	5219	3038	3155	61.48	0.228
12	6.4	-0.2	-2.4	23.0	5176	3031	3143	60.89	0.224
13	4.4	-0.2	-2.1	22.9	5125	2998	3138	59.98	0.221
14	2.4	-0.2	-2.1	22.9	5085	2966	3122	59.05	0.221

Observed Velocities and Moduli for File w20-mb-10696H-velocity									
Event	Conf	Pore	Diff	Temp	V_p	$V_s^{(1)}$	$V_s^{(2)}$	Young's Modulus	Poisson's Ratio
	MPa	MPa	MPa	°C	m/s	m/s	m/s	GPa	
0	30.4	-0.2	-2.5	26.7	5347	3050	3175	63.38	0.244
1	28.4	-0.2	-2.8	26.4	5315	3043	3165	62.90	0.241
2	26.4	-0.2	-2.9	26.1	5302	3041	3163	62.75	0.240
3	24.5	-0.2	-2.5	26.0	5269	3043	3163	62.52	0.235
4	22.4	-0.2	-2.5	25.9	5263	3034	3154	62.23	0.236
5	20.4	-0.2	-2.7	25.7	5256	3030	3149	62.06	0.236
6	18.4	-0.2	-2.5	25.6	5276	3026	3142	62.06	0.240
7	16.5	-0.2	-2.2	25.5	5237	3022	3138	61.65	0.236
8	14.4	-0.2	-2.5	25.4	5165	3013	3133	60.90	0.226
9	12.4	-0.2	-2.5	25.3	5162	3003	3129	60.69	0.227
10	10.4	-0.2	-2.1	25.2	5144	2999	3122	60.40	0.226
11	8.4	-0.2	-2.5	25.0	5119	2984	3117	59.94	0.225
12	6.5	-0.2	-1.8	25.0	5126	2976	3102	59.70	0.229
13	4.5	-0.2	-1.8	24.9	5071	2957	3095	58.93	0.224
14	2.4	-0.2	-2.1	24.7	5071	2945	3087	58.68	0.226

Observed Velocities and Moduli for File w20-mb-10704.7V45-velocity									
Event	Conf	Pore	Diff	Temp	V_p	$V_s^{(1)}$	$V_s^{(2)}$	Young's Modulus	Poisson's Ratio
	MPa	MPa	MPa	°C	m/s	m/s	m/s	GPa	
0	30.4	-0.2	-2.9	25.1	5226	3066	3122	61.71	0.230
1	28.5	-0.2	-2.5	24.9	5131	3068	3115	60.85	0.215
2	26.4	-0.2	-2.5	24.7	5118	3066	3113	60.69	0.213
3	24.4	-0.2	-2.5	24.5	5106	3061	3113	60.52	0.212
4	22.4	-0.2	-2.4	24.3	5100	3063	3108	60.43	0.211
5	20.5	-0.2	-2.4	24.2	5094	3055	3111	60.31	0.211
6	18.4	-0.2	-2.4	24.0	5082	3055	3104	60.12	0.210
7	16.5	-0.2	-2.1	24.6	5088	3053	3104	60.15	0.211
8	14.4	-0.2	-2.5	24.1	5100	3048	3099	60.13	0.215
9	12.5	-0.2	-2.1	24.0	5106	3045	3097	60.12	0.217
10	10.5	-0.2	-1.9	23.9	5058	3051	3097	59.77	0.207
11	8.5	-0.2	-1.7	23.8	5058	3049	3106	59.86	0.206
12	6.4	-0.2	-2.1	23.7	5076	3043	3104	59.92	0.211
13	4.4	-0.2	-2.1	23.6	5058	3032	3085	59.40	0.212
14	2.4	-0.2	-1.9	23.6	5017	3025	3082	58.91	0.206

Observed Velocities and Moduli for File w16174-10673.6-velociy									
Event	Conf	Pore	Diff	Temp	V_p	$V_s^{(1)}$	$V_s^{(2)}$	Young's Modulus	Poisson's Ratio
	MPa	MPa	MPa	°C	m/s	m/s	m/s	GPa	
0	50.6	-0.2	-3.8	22.2	6279	3324	3329	76.82	0.305
1	45.6	-0.2	-3.9	21.9	6279	3321	3338	76.93	0.304
2	40.5	-0.2	-4.2	21.3	6256	3318	3325	76.52	0.304
3	35.6	-0.2	-3.8	21.5	6237	3316	3322	76.33	0.302
4	30.5	-0.2	-3.4	20.8	6227	3314	3322	76.24	0.302
5	25.5	-0.2	-3.5	21.2	6223	3310	3320	76.11	0.302
6	20.6	-0.2	-2.9	20.5	6212	3308	3319	76.00	0.301
7	15.5	-0.2	-2.5	20.3	6196	3301	3313	75.68	0.301
8	10.5	-0.2	-2.4	20.0	6155	3299	3312	75.41	0.297
9	5.5	-0.2	-2.5	19.0	6146	3281	3301	74.85	0.299

Observed Velocities and Moduli for File w16174-10678.3-velocity									
Event	Conf	Pore	Diff	Temp	V_p	$V_s^{(1)}$	$V_s^{(2)}$	Young's Modulus	Poisson's Ratio
	MPa	MPa	MPa	°C	m/s	m/s	m/s	GPa	
0	50.5	-0.2	-3.7	24.2	4658	2602	2899	44.00	0.232
1	45.5	-0.2	-2.9	23.4	4621	2597	2896	43.68	0.227
2	40.4	-0.2	-3.4	22.7	4615	2595	2885	43.51	0.228
3	35.4	-0.2	-3.4	22.3	4618	2592	2883	43.48	0.229
4	30.4	-0.2	-2.9	21.9	4603	2587	2877	43.26	0.228
5	25.4	-0.2	-2.8	21.4	4600	2586	2868	43.14	0.229
6	20.5	-0.2	-2.2	20.3	4592	2579	2868	43.02	0.229
7	15.4	-0.2	-2.1	19.8	4539	2573	2862	42.55	0.221
8	10.4	-0.2	-1.9	19.1	4533	2563	2859	42.38	0.222
9	5.4	-0.2	-1.9	19.3	4490	2557	2844	41.88	0.217

Observed Velocities and Moduli for File w16174-10682-velocity									
Event	Conf	Pore	Diff	Temp	V_p	$V_s^{(1)}$	$V_s^{(2)}$	Young's Modulus	Poisson's Ratio
	MPa	MPa	MPa	°C	m/s	m/s	m/s	GPa	
0	50.5	-0.2	-3.8	23.9	5297	3105	3130	62.42	0.235
1	45.5	-0.2	-3.8	23.5	5237	3099	3125	61.79	0.227
2	40.4	-0.2	-3.7	23.1	5214	3101	3123	61.61	0.223
3	35.4	-0.2	-3.4	22.9	5222	3093	3119	61.52	0.226
4	30.4	-0.2	-3.8	22.6	5192	3090	3115	61.18	0.222
5	25.4	-0.2	-3.1	22.5	5166	3085	3113	60.87	0.219
6	20.5	-0.2	-2.9	22.3	5166	3076	3106	60.67	0.221
7	15.4	-0.2	-2.8	22.0	5113	3069	3092	59.96	0.215
8	10.4	-0.2	-2.9	21.7	5098	3054	3092	59.65	0.215
9	5.4	-0.2	-2.5	21.5	5080	3042	3079	59.18	0.215

Observed Velocities and Moduli for File w16174-10715.2-velocity									
Event	Conf	Pore	Diff	Temp	V_p	$V_s^{(1)}$	$V_s^{(2)}$	Young's Modulus	Poisson's Ratio
	MPa	MPa	MPa	°C	m/s	m/s	m/s	GPa	
0	50.5	-0.2	-3.9	20.6	5247	3131	3169	62.62	0.218
1	45.5	-0.2	-4.2	20.5	5225	3127	3158	62.24	0.217
2	40.5	-0.2	-3.8	20.1	5221	3120	3152	62.04	0.218
3	35.5	-0.2	-3.4	20.1	5203	3115	3141	61.68	0.217
4	30.5	-0.2	-3.4	20.5	5203	3110	3136	61.56	0.218
5	25.5	-0.2	-3.4	19.9	5182	3106	3128	61.22	0.217
6	20.5	-0.2	-3.2	19.9	5158	3099	3124	60.88	0.214
7	15.5	-0.2	-2.5	19.7	5116	3092	3128	60.47	0.207
8	10.5	-0.2	-2.5	19.7	5070	3082	3120	59.83	0.201
9	5.5	-0.2	-2.1	20.1	5043	3055	3105	59.09	0.203

Observed Velocities and Moduli for File w16174-10721.4-velocity									
Event	Conf	Pore	Diff	Temp	V_p	$V_s^{(1)}$	$V_s^{(2)}$	Young's Modulus	Poisson's Ratio
	MPa	MPa	MPa	°C	m/s	m/s	m/s	GPa	
0	50.4	-0.2	-3.8	23.7	4925	2737	2971	52.62	0.247
1	45.5	-0.2	-3.7	23.2	4919	2731	2970	52.49	0.247
2	40.4	-0.2	-3.5	22.8	4896	2729	2963	52.23	0.245
3	35.4	-0.2	-3.4	22.5	4886	2721	2954	51.95	0.246
4	30.4	-0.2	-3.2	22.2	4870	2719	2943	51.68	0.245
5	25.5	-0.2	-2.7	21.9	4870	2711	2937	51.50	0.247
6	20.5	-0.2	-2.5	21.6	4832	2701	2934	51.09	0.242
7	15.5	-0.2	-2.5	20.0	4827	2692	2930	50.89	0.243
8	10.5	-0.2	-2.1	18.6	4796	2670	2909	50.16	0.244
9	5.4	-0.2	-2.2	17.6	4757	2611	2893	48.98	0.248

Observed Velocities and Moduli for File w16174-10730.6-velocity									
Event	Conf	Pore	Diff	Temp	V_p	$V_s^{(1)}$	$V_s^{(2)}$	Young's Modulus	Poisson's Ratio
	MPa	MPa	MPa	°C	m/s	m/s	m/s	GPa	
0	50.5	-0.2	-3.5	23.3	5224	2931	3086	58.69	0.252
1	45.5	-0.2	-3.7	22.6	5182	2920	3083	58.22	0.248
2	40.5	-0.2	-3.2	22.1	5180	2923	3084	58.26	0.247
3	35.5	-0.2	-3.4	21.7	5170	2925	3073	58.07	0.246
4	30.5	-0.2	-3.1	21.3	5186	2910	3072	57.96	0.251
5	25.5	-0.2	-2.5	20.8	5105	2911	3072	57.41	0.239
6	20.5	-0.2	-2.8	20.6	5124	2912	3066	57.48	0.242
7	15.4	-0.2	-2.8	20.1	5118	2918	3056	57.39	0.242
8	10.5	-0.2	-2.1	19.1	5099	2903	3057	57.07	0.241
9	5.5	-0.2	-2.1	18.7	5044	2890	3037	56.25	0.236

Observed Velocities and Moduli for File W16174-10712-velocity									
Event	Conf	Pore	Diff	Temp	V_p	$V_s^{(1)}$	$V_s^{(2)}$	Young's Modulus	Poisson's Ratio
	MPa	MPa	MPa	°C	m/s	m/s	m/s	GPa	
0	10.1	-0.2	0.2	23.6	4681	2801	2838	51.20	0.215
1	20.1	-0.2	-0.8	23.7	4824	2829	2848	52.75	0.235
2	30.0	-0.2	-0.8	24.0	4846	2848	2866	53.37	0.234
3	40.0	-0.2	-1.4	24.5	4868	2869	2876	53.92	0.233
4	50.0	-0.2	-2.3	24.2	4924	2892	2884	54.72	0.238

Observed Velocities and Moduli for File W16174-10714-velocity									
Event	Conf	Pore	Diff	Temp	V_p	$V_s^{(1)}$	$V_s^{(2)}$	Young's Modulus	Poisson's Ratio
	MPa	MPa	MPa	°C	m/s	m/s	m/s	GPa	
0	10.2	-0.2	-0.4	25.3	5004	2904	3093	57.69	0.220
1	20.1	-0.2	-0.4	25.6	5188	3052	3105	61.23	0.228
2	30.0	-0.2	-0.8	25.9	5200	3083	3131	62.07	0.222
3	40.1	-0.2	-1.4	26.1	5245	3083	3125	62.36	0.230
4	49.9	-0.2	-2.1	26.3	5239	3116	3118	62.66	0.226

Observed Velocities and Moduli for File W16174-10715.7-velocity									
Event	Conf	Pore	Diff	Temp	V_p	$V_s^{(1)}$	$V_s^{(2)}$	Young's Modulus	Poisson's Ratio
	MPa	MPa	MPa	°C	m/s	m/s	m/s	GPa	
0	10.1	-0.2	-0.1	20.8	5178	3143	3090	62.60	0.216
1	20.0	-0.2	-0.4	21.3	5303	3176	3112	64.39	0.229
2	30.0	-0.2	-0.8	21.6	5321	3193	3136	65.09	0.226
3	40.0	-0.2	-1.7	22.1	5441	3193	3148	66.22	0.243
4	50.0	-0.2	-2.0	22.4	5410	3210	3159	66.37	0.235

Observed Velocities and Moduli for File W16174-10716.4vertical-velocity									
Event	Conf	Pore	Diff	Temp	V_p	$V_s^{(1)}$	$V_s^{(2)}$	Young's Modulus	Poisson's Ratio
	MPa	MPa	MPa	°C	m/s	m/s	m/s	GPa	
0	9.9	-0.2	-0.3	26.7	4348	2911	2907	47.99	0.095
1	20.0	-0.2	-0.8	26.6	4648	3001	3006	53.34	0.142
2	30.1	-0.2	-1.0	26.5	4705	3074	3085	55.28	0.125
3	40.1	-0.2	-1.4	26.7	4872	3110	3130	58.11	0.152
4	49.9	-0.2	-2.1	26.9	4901	3156	3152	59.08	0.147

Observed Velocities and Moduli for File W16174-10716.5-velocity									
Event	Conf	Pore	Diff	Temp	V_p	$V_s^{(1)}$	$V_s^{(2)}$	Young's Modulus	Poisson's Ratio
	MPa	MPa	MPa	°C	m/s	m/s	m/s	GPa	
0	10.0	-0.2	0.0	19.7	5219	3249	3143	64.96	0.200
1	20.0	-0.2	-0.6	20.2	5331	3306	3207	67.58	0.202
2	29.9	-0.2	-1.1	20.5	5419	3347	3253	69.57	0.205
3	40.1	-0.2	-1.6	20.2	5482	3367	3288	70.91	0.208
4	50.1	-0.2	-1.8	20.4	5552	3384	3318	72.22	0.213

Observed Velocities and Moduli for File W16174-10718.7vertical-velocity									
Event	Conf	Pore	Diff	Temp	V_p	$V_s^{(1)}$	$V_s^{(2)}$	Young's Modulus	Poisson's Ratio
	MPa	MPa	MPa	°C	m/s	m/s	m/s	GPa	
0	10.2	-0.2	0.0	26.5	4512	2794	2797	48.11	0.188
1	20.1	-0.2	-0.4	26.8	4720	2827	2829	50.54	0.220
2	29.9	-0.2	-1.1	27.0	4655	2846	2850	50.46	0.201
3	40.0	-0.2	-1.7	27.2	4760	2864	2864	51.68	0.216
4	50.1	-0.2	-2.0	27.4	4780	2872	2884	52.16	0.216

Observed Velocities and Moduli for File W16174-10723-velocity									
Event	Conf	Pore	Diff	Temp	V_p	$V_s^{(1)}$	$V_s^{(2)}$	Young's Modulus	Poisson's Ratio
	MPa	MPa	MPa	°C	m/s	m/s	m/s	GPa	
0	10.1	-0.2	-0.3	23.1	5351	3180	3277	67.31	0.214
1	20.1	-0.2	-0.6	24.2	5656	3287	3340	72.35	0.239
2	30.0	-0.2	-1.0	24.5	5857	3343	3395	75.65	0.253
3	40.1	-0.2	-1.4	24.7	6017	3384	3444	78.29	0.263
4	50.0	-0.2	-2.1	24.7	6103	3429	3478	80.23	0.264

Observed Velocities and Moduli for File W16174-10726.9-velocity									
Event	Conf	Pore	Diff	Temp	V_p	$V_s^{(1)}$	$V_s^{(2)}$	Young's Modulus	Poisson's Ratio
	MPa	MPa	MPa	°C	m/s	m/s	m/s	GPa	
0	10.2	-0.2	0.4	24.9	5045	3014	2986	58.06	0.226
1	20.0	-0.2	-0.3	24.9	5127	3048	3001	59.33	0.233
2	30.0	-0.2	-0.7	25.0	5169	3056	3017	59.97	0.237
3	40.1	-0.2	-1.7	25.0	5147	3066	3014	59.89	0.232
4	50.0	-0.2	-1.8	25.2	5183	3073	3031	60.49	0.235

Observed Velocities and Moduli for File W16174-10727.2-velocity									
Event	Conf	Pore	Diff	Temp	V_p	$V_s^{(1)}$	$V_s^{(2)}$	Young's Modulus	Poisson's Ratio
	MPa	MPa	MPa	°C	m/s	m/s	m/s	GPa	
0	10.0	-0.2	0.3	24.2	5794	3288	3388	74.19	0.252
1	20.1	-0.2	-0.8	24.4	5956	3360	3430	77.22	0.259
2	29.9	-0.2	-1.3	24.6	5934	3390	3469	78.17	0.249
3	40.1	-0.2	-1.3	24.8	6021	3397	3472	79.00	0.259
4	50.0	-0.3	-2.3	24.9	5985	3416	3499	79.47	0.250

Observed Velocities and Moduli for File W16174-10728.8-velocity									
Event	Conf	Pore	Diff	Temp	V_p	$V_s^{(1)}$	$V_s^{(2)}$	Young's Modulus	Poisson's Ratio
	MPa	MPa	MPa	°C	m/s	m/s	m/s	GPa	
0	10.0	-0.2	-0.4	26.8	4966	2654	2981	51.72	0.263
1	19.9	-0.2	-0.8	27.0	5009	2696	3000	52.78	0.261
2	30.0	-0.2	-1.1	27.2	5079	2733	3012	53.85	0.265
3	40.1	-0.2	-1.3	27.2	5085	2741	3018	54.08	0.264
4	50.1	-0.2	-1.8	27.3	5074	2734	3033	54.12	0.261

Observed Velocities and Moduli for File W16174-10729.1-velocity									
Event	Conf	Pore	Diff	Temp	V_p	$V_s^{(1)}$	$V_s^{(2)}$	Young's Modulus	Poisson's Ratio
	MPa	MPa	MPa	°C	m/s	m/s	m/s	GPa	
0	10.1	-0.2	-0.4	21.8	5300	3094	3108	62.71	0.240
1	20.0	-0.2	-0.8	22.0	5278	3109	3120	62.91	0.233
2	30.0	-0.2	-1.3	22.2	5294	3112	3124	63.13	0.234
3	40.1	-0.2	-1.3	22.1	5378	3126	3137	64.14	0.244
4	50.0	-0.2	-2.3	22.2	5390	3137	3141	64.44	0.243

Observed Velocities and Moduli for File W16174-10729.5-velocity									
Event	Conf	Pore	Diff	Temp	V_p	$V_s^{(1)}$	$V_s^{(2)}$	Young's Modulus	Poisson's Ratio
	MPa	MPa	MPa	°C	m/s	m/s	m/s	GPa	
0	10.1	-0.2	0.3	22.6	5061	2897	3013	55.07	0.241
1	20.0	-0.2	-0.4	23.0	5303	2947	3032	57.53	0.267
2	30.0	-0.2	-0.8	23.0	5155	2933	3043	56.56	0.247
3	39.9	-0.2	-1.3	23.2	5155	2928	3061	56.73	0.245
4	50.1	-0.2	-1.4	23.3	5253	2939	3061	57.52	0.258

Observed Velocities and Moduli for File W16174-10729.9-velocity									
Event	Conf	Pore	Diff	Temp	V_p	$V_s^{(1)}$	$V_s^{(2)}$	Young's Modulus	Poisson's Ratio
	MPa	MPa	MPa	°C	m/s	m/s	m/s	GPa	
0	10.1	-0.2	0.0	24.5	5429	2632	3158	57.37	0.301
1	20.0	-0.2	-0.7	24.6	5436	2680	3207	58.91	0.293
2	30.1	-0.2	-1.3	24.7	5645	2716	3254	61.21	0.306
3	40.1	-0.2	-1.7	24.9	5703	2729	3285	62.18	0.307
4	49.9	-0.2	-1.7	25.0	5762	2735	3298	62.76	0.311

Observed Velocities and Moduli for File W16174-10731.4-Velocity									
Event	Conf	Pore	Diff	Temp	V_p	$V_s^{(1)}$	$V_s^{(2)}$	Young's Modulus	Poisson's Ratio
	MPa	MPa	MPa	°C	m/s	m/s	m/s	GPa	
0	10.0	-0.2	-0.4	21.3	3805	2994	3013	31.59	-0.327
1	20.1	-0.2	-0.4	21.7	4272	3088	3156	46.98	-0.073
2	29.9	-0.2	-1.3	21.8	4585	3188	3279	54.65	0.005
3	40.1	-0.2	-1.7	21.8	4454	3250	3384	50.20	-0.123
4	50.0	-0.2	-2.1	22.0	5027	3308	3407	64.32	0.097

Observed Velocities and Moduli for File W16174-10731.4horizontal-velocity									
Event	Conf	Pore	Diff	Temp	V_p	$V_s^{(1)}$	$V_s^{(2)}$	Young's Modulus	Poisson's Ratio
	MPa	MPa	MPa	°C	m/s	m/s	m/s	GPa	
0	10.1	-0.2	-0.4	24.6	4436	2831	2899	48.00	0.142
1	20.0	-0.2	-0.6	24.7	4448	2844	2913	48.35	0.140
2	29.9	-0.2	-1.0	24.9	4480	2850	2925	48.87	0.145
3	40.0	-0.2	-1.4	25.3	4492	2863	2932	49.16	0.144
4	50.1	-0.2	-2.0	25.3	4525	2870	2939	49.66	0.150

Observed Velocities and Moduli for File W16174-10732.3-Velocity									
Event	Conf	Pore	Diff	Temp	V_p	$V_s^{(1)}$	$V_s^{(2)}$	Young's Modulus	Poisson's Ratio
	MPa	MPa	MPa	°C	m/s	m/s	m/s	GPa	
0	10.0	-0.2	0.4	23.9	4923	3078	3095	58.94	0.176
1	20.0	-0.2	-0.6	24.0	5086	3155	3170	62.33	0.185
2	30.0	-0.2	-1.0	24.2	5221	3201	3221	64.85	0.196
3	40.1	-0.2	-1.4	24.4	5307	3225	3251	66.37	0.203
4	50.0	-0.2	-2.0	24.5	5353	3240	3273	67.29	0.206

Observed Velocities and Moduli for File W16174-10733.3-Velocity									
Event	Conf	Pore	Diff	Temp	V_p	$V_s^{(1)}$	$V_s^{(2)}$	Young's Modulus	Poisson's Ratio
	MPa	MPa	MPa	°C	m/s	m/s	m/s	GPa	
0	10.0	-0.2	0.0	25.6	5111	2622	3052	53.87	0.277
1	20.1	-0.2	-0.8	25.8	5138	2630	3110	54.95	0.273
2	30.0	-0.2	-0.7	26.1	5197	2642	3149	56.01	0.275
3	40.0	-0.2	-1.7	26.2	5264	2656	3147	56.55	0.282
4	50.1	-0.2	-1.7	26.2	5366	2670	3162	57.50	0.290

Observed Velocities and Moduli for File W16174-1728.1-velocity									
Event	Conf	Pore	Diff	Temp	V_p	$V_s^{(1)}$	$V_s^{(2)}$	Young's Modulus	Poisson's Ratio
	MPa	MPa	MPa	°C	m/s	m/s	m/s	GPa	
0	10.1	-0.2	0.2	23.5	5261	3193	3054	63.25	0.228
1	20.1	-0.2	-0.8	23.7	5392	3255	3117	66.02	0.232
2	30.0	-0.2	-1.3	23.8	5542	3305	3174	68.74	0.240
3	40.0	-0.2	-1.7	23.9	5600	3338	3222	70.37	0.239
4	50.0	-0.2	-2.1	24.0	5749	3356	3255	72.29	0.253

A.1.3 Biot's Coefficient

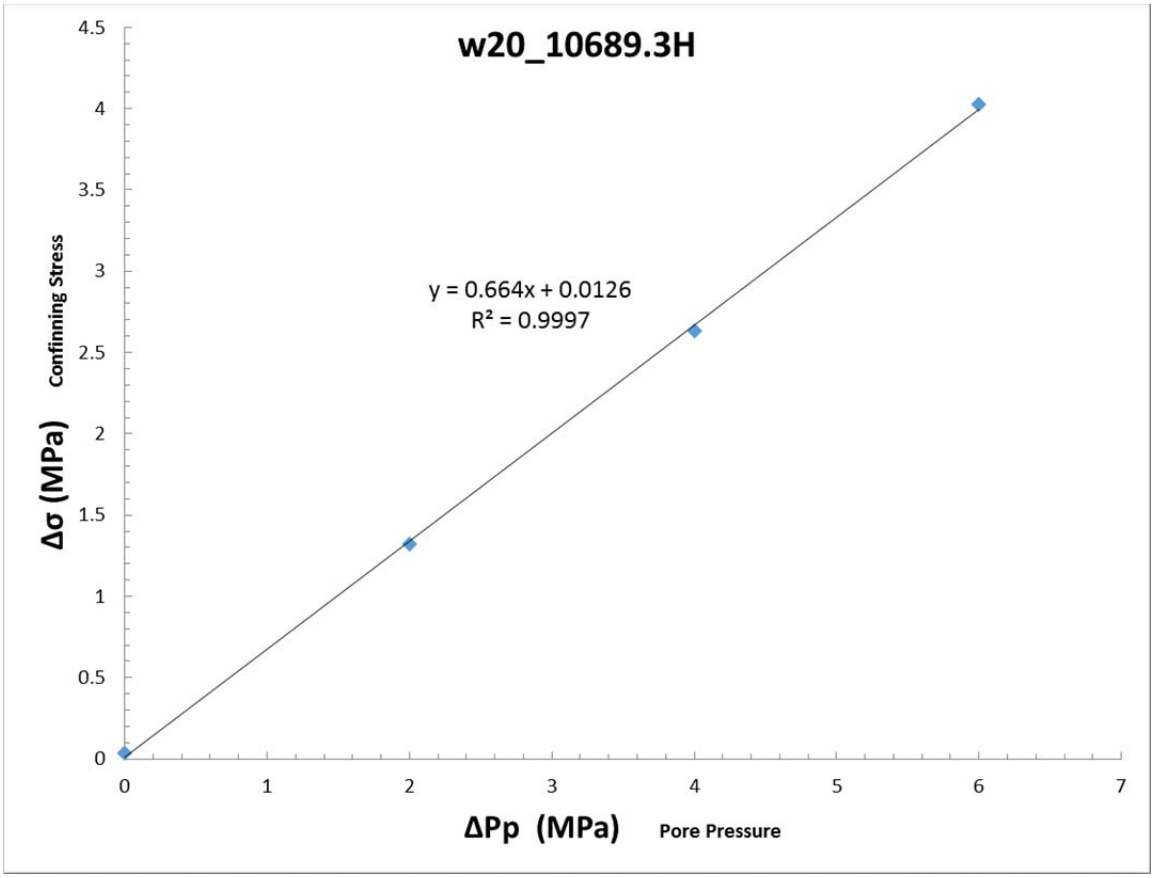

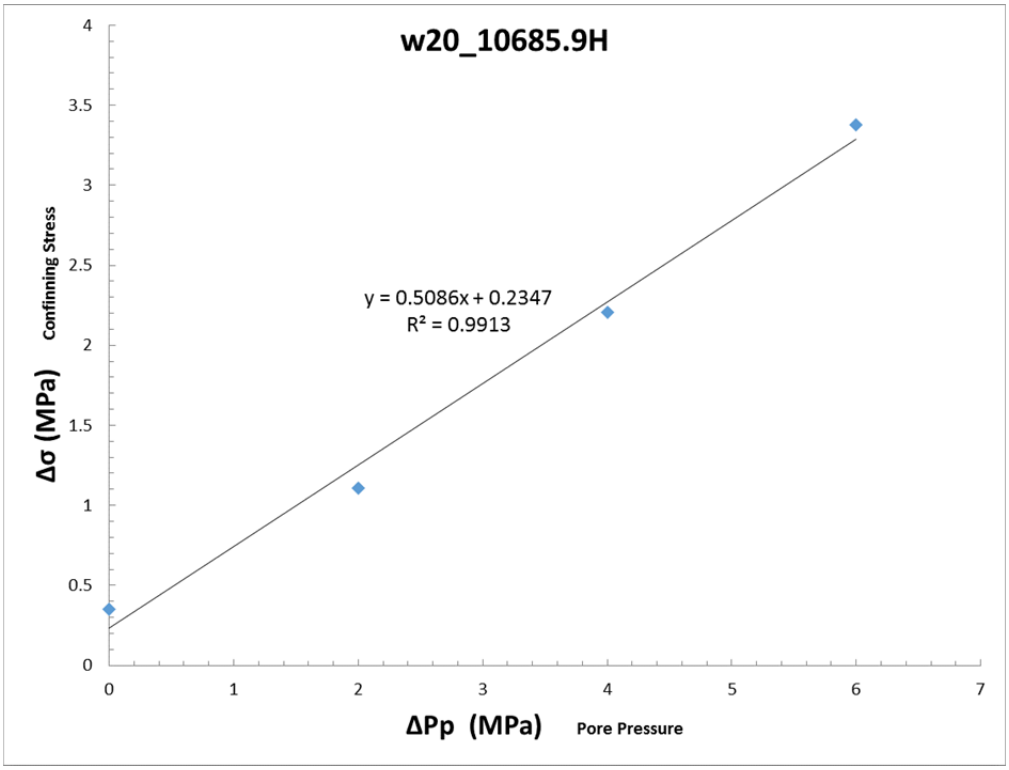
w20_10685.9H
y = 0.5086x + 0.2347
R² = 0.9913
Δσ (MPa) Confinning Stress
ΔPp (MPa) Pore Pressure
0
0.5
1
1.5
2
2.5
3
3.5
4
0
1
2
3
4
5
6
7

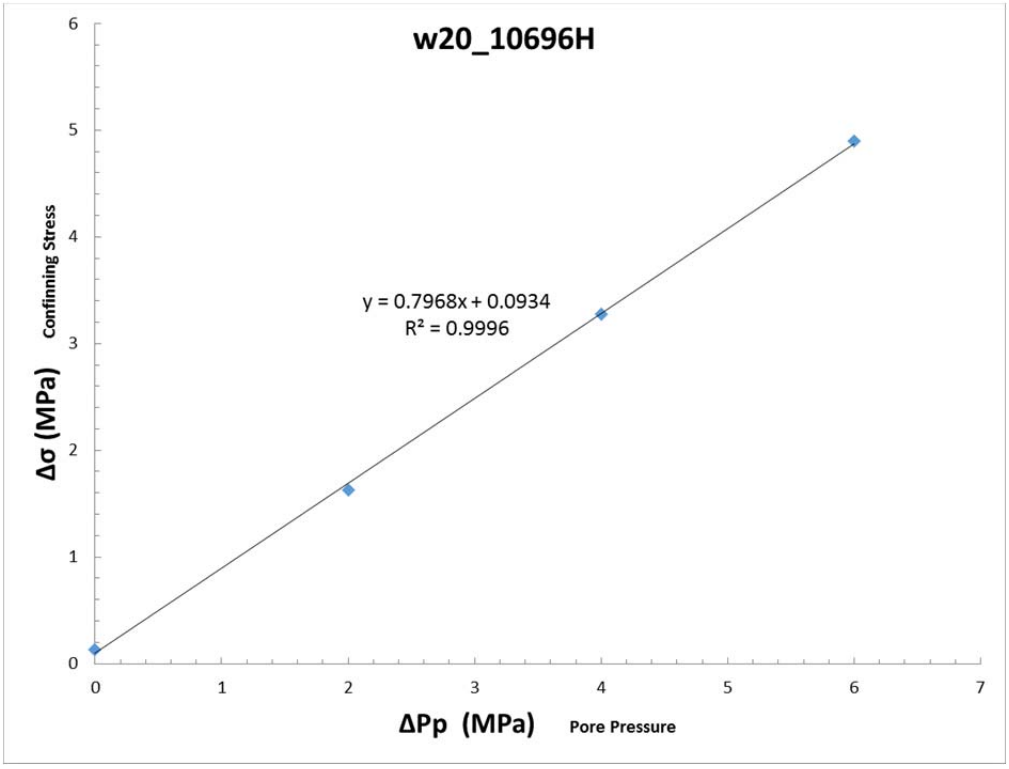
w20_10696H
y = 0.7968x + 0.0934
R² = 0.9996
Δσ (MPa) Confinning Stress
ΔPp (MPa) Pore Pressure
0
1
2
3
4
5
6
0
1
2
3
4
5
6
7

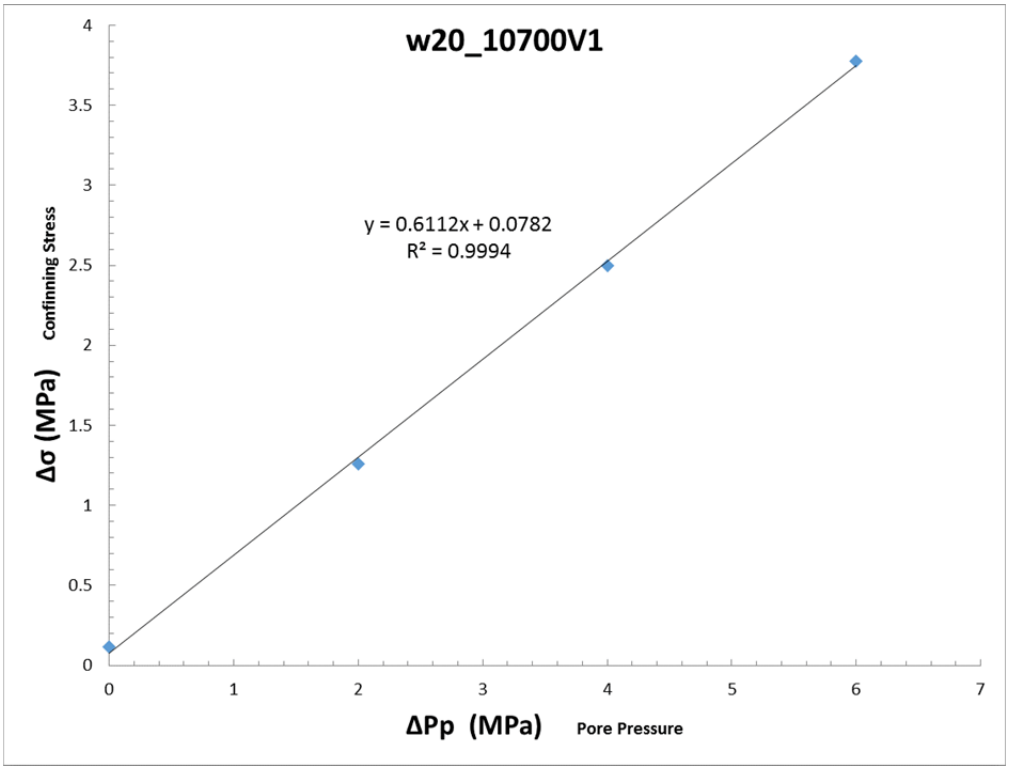
w20_10700V1
y = 0.6112x + 0.0782
R² = 0.9994
Δσ (MPa) Confinning Stress
ΔPp (MPa) Pore Pressure
0
0.5
1
1.5
2
2.5
3
3.5
4
0
1
2
3
4
5
6
7

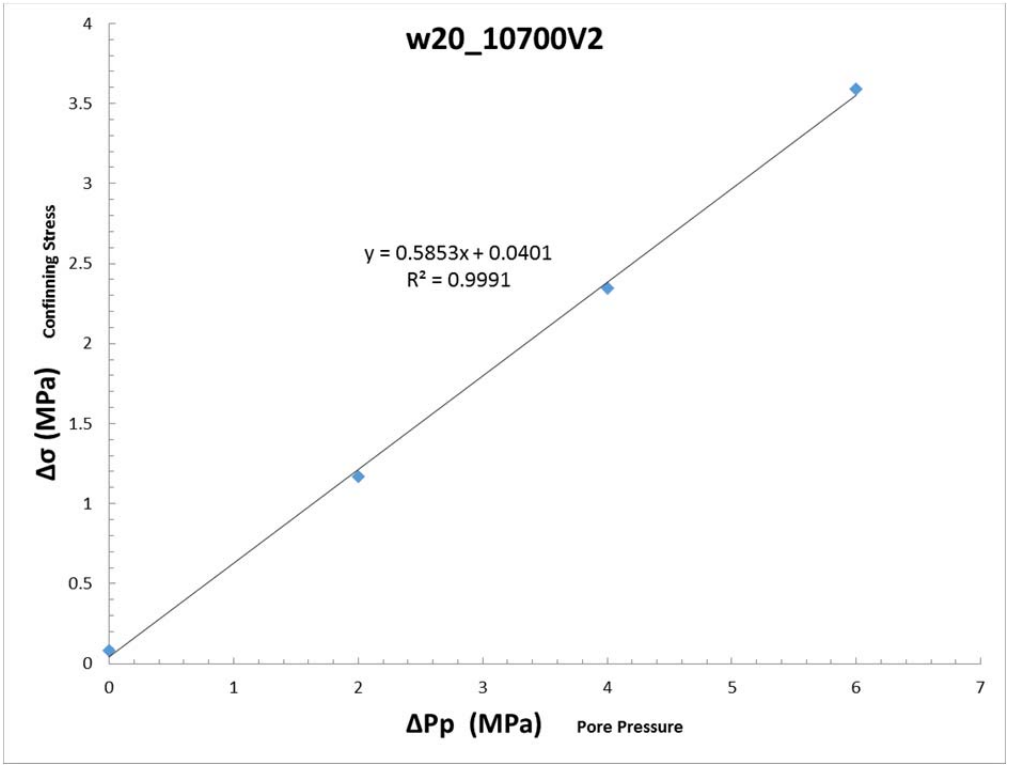
w20_10700V2
y = 0.5853x + 0.0401
R² = 0.9991
Δσ (MPa) Confinning Stress
ΔPp (MPa) Pore Pressure
0
0.5
1
1.5
2
2.5
3
3.5
4
0
1
2
3
4
5
6
7

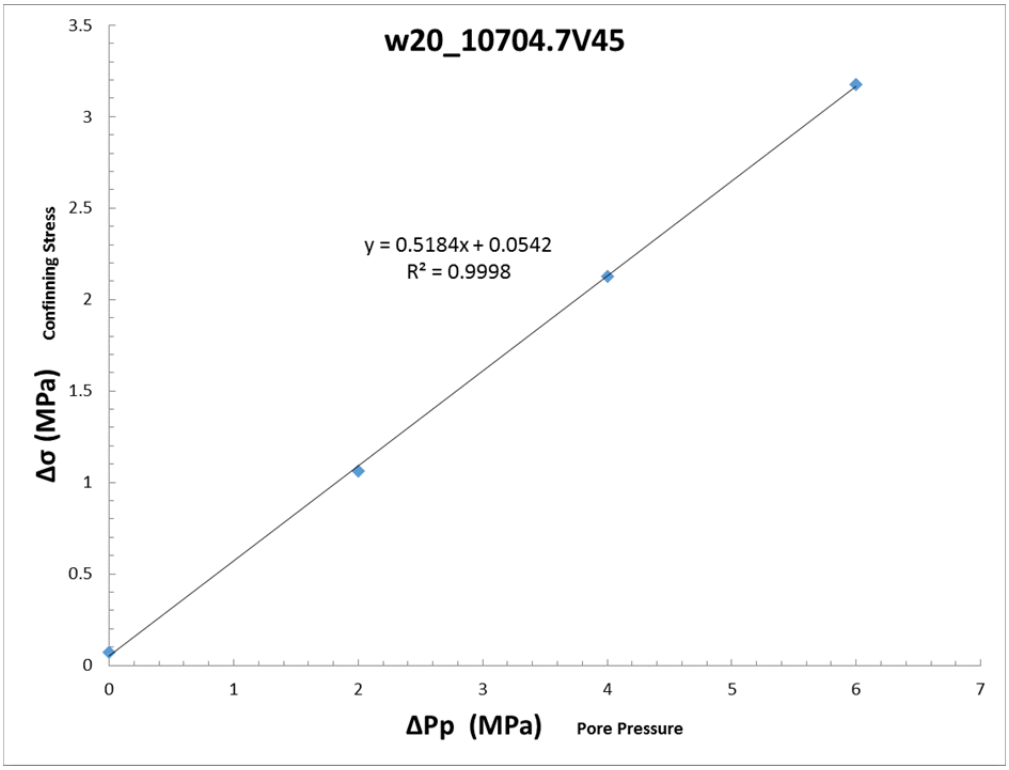
w20_10704.7V45
y = 0.5184x + 0.0542
R² = 0.9998
Δσ (MPa) Confinning Stress
ΔPp (MPa) Pore Pressure
0
0.5
1
1.5
2
2.5
3
3.5
0
1
2
3
4
5
6
7

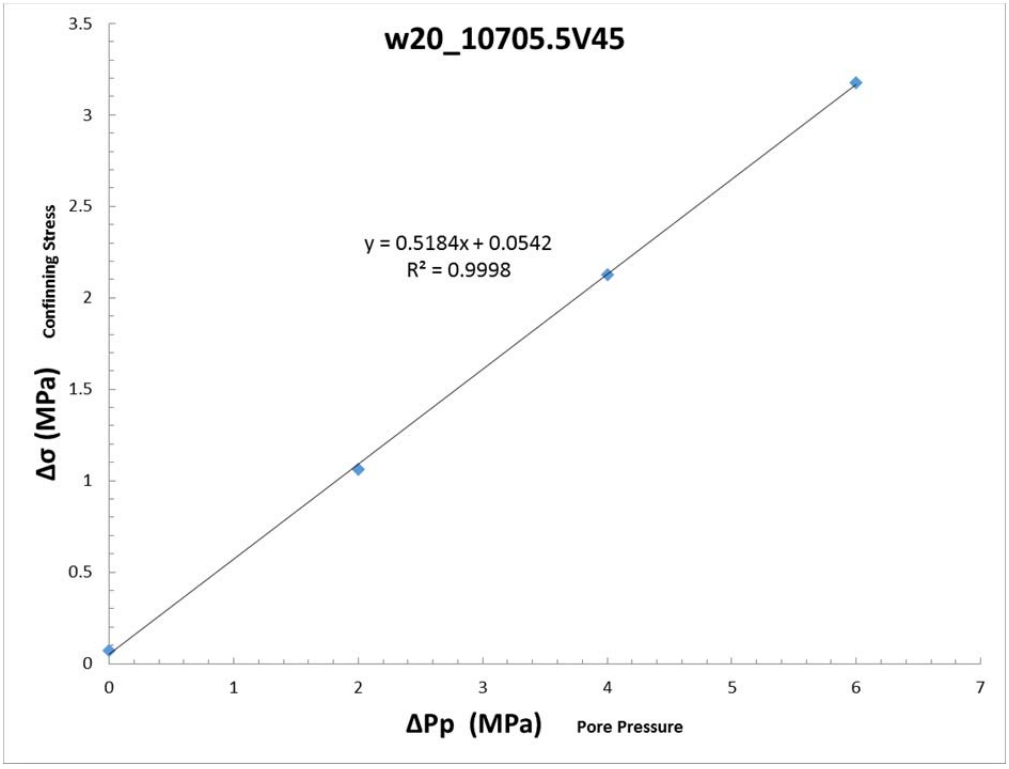
w20_10705.5V45
y = 0.5184x + 0.0542
R² = 0.9998
Δσ (MPa) Confinning Stress
ΔPp (MPa) Pore Pressure
0
0.5
1
1.5
2
2.5
3
3.5
0
1
2
3
4
5
6
7

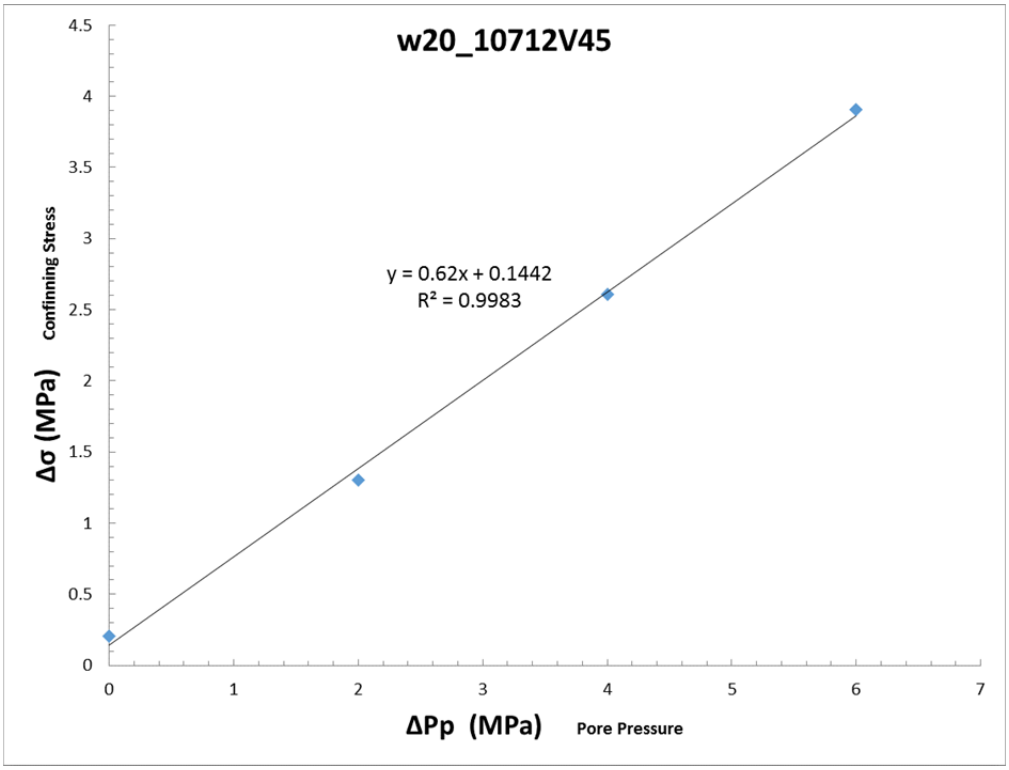
w20_10712V45
y = 0.62x + 0.1442
R² = 0.9983
Δσ (MPa) Confinning Stress
ΔPp (MPa) Pore Pressure
0
0.5
1
1.5
2
2.5
3
3.5
4
4.5
0
1
2
3
4
5
6
7

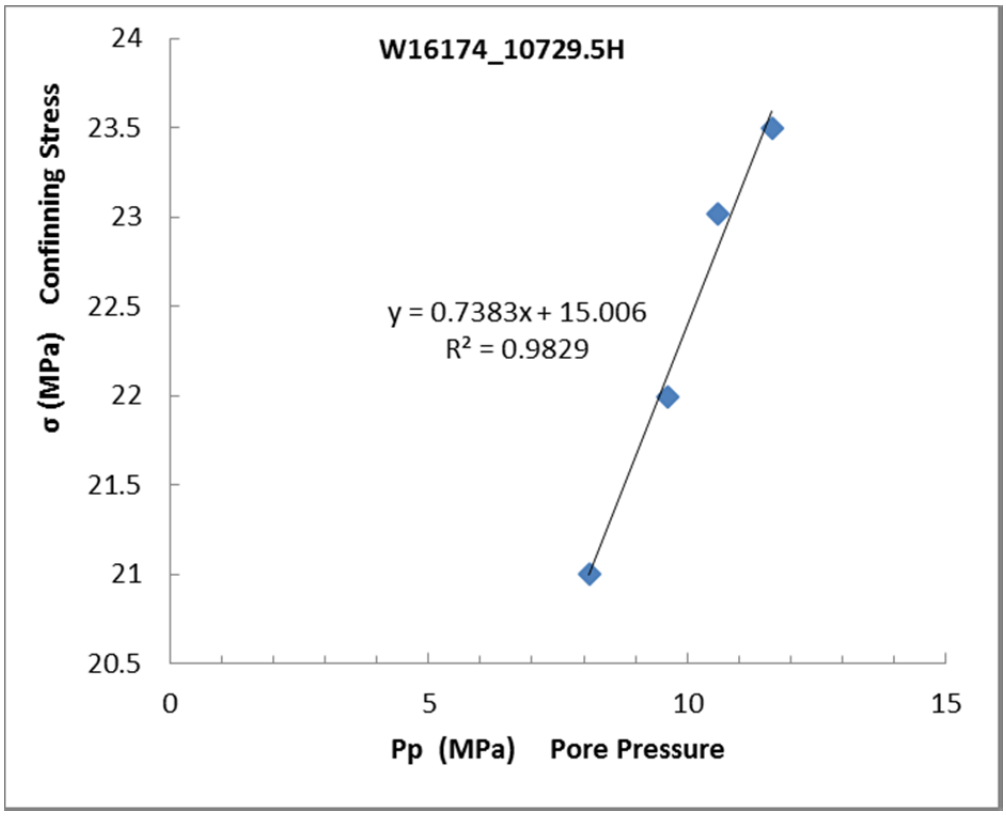
W16174_10729.5H
y = 0.7383x + 15.006
R² = 0.9829
σ (MPa) Confinning Stress
Pp (MPa) Pore Pressure
20.5
21
21.5
22
22.5
23
23.5
24
0
5
10
15

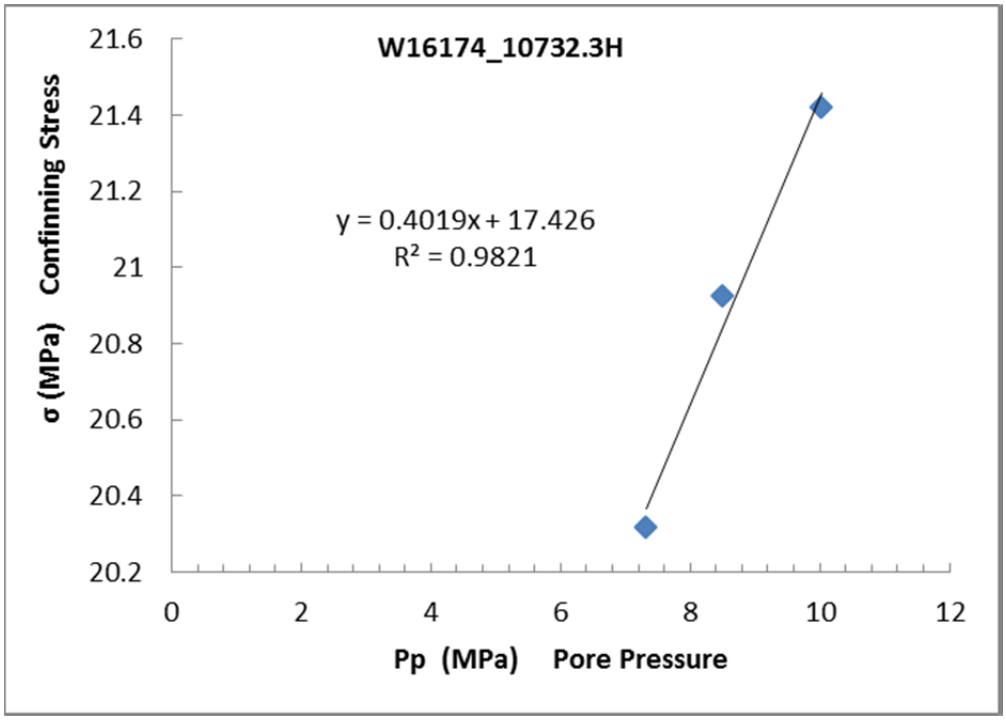
W16174_10732.3H
y = 0.4019x + 17.426
R² = 0.9821
σ (MPa) Confinning Stress
Pp (MPa) Pore Pressure
21.6
21.4
21.2
21
20.8
20.6
20.4
20.2
0
2
4
6
8
10
12

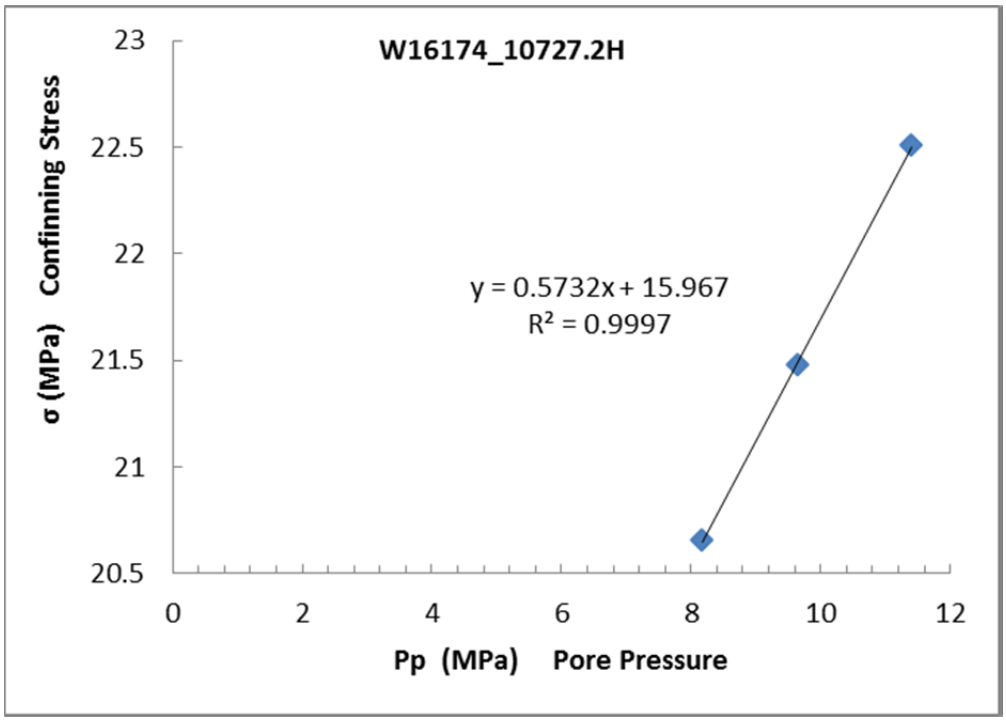
W16174_10727.2H
y = 0.5732x + 15.967
R² = 0.9997
σ (MPa) Confinning Stress
Pp (MPa) Pore Pressure
23
22.5
22
21.5
21
20.5
0
2
4
6
8
10
12

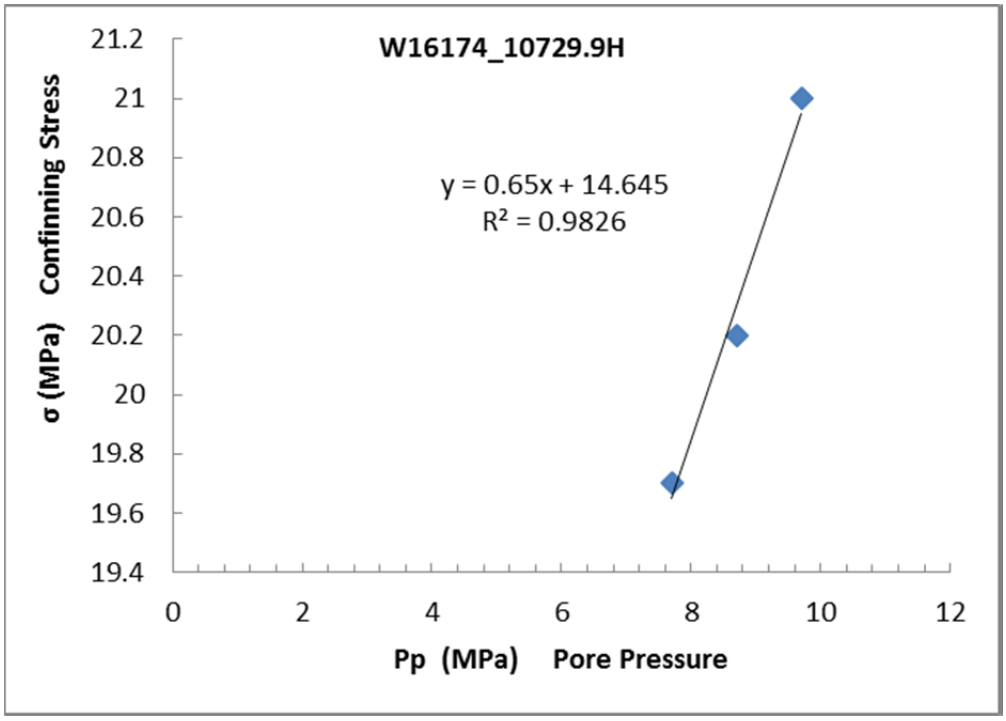
W16174_10729.9H
y = 0.65x + 14.645
R² = 0.9826
σ (MPa) Confinning Stress
Pp (MPa) Pore Pressure
21.2
21
20.8
20.6
20.4
20.2
20
19.8
19.6
19.4
0
2
4
6
8
10
12

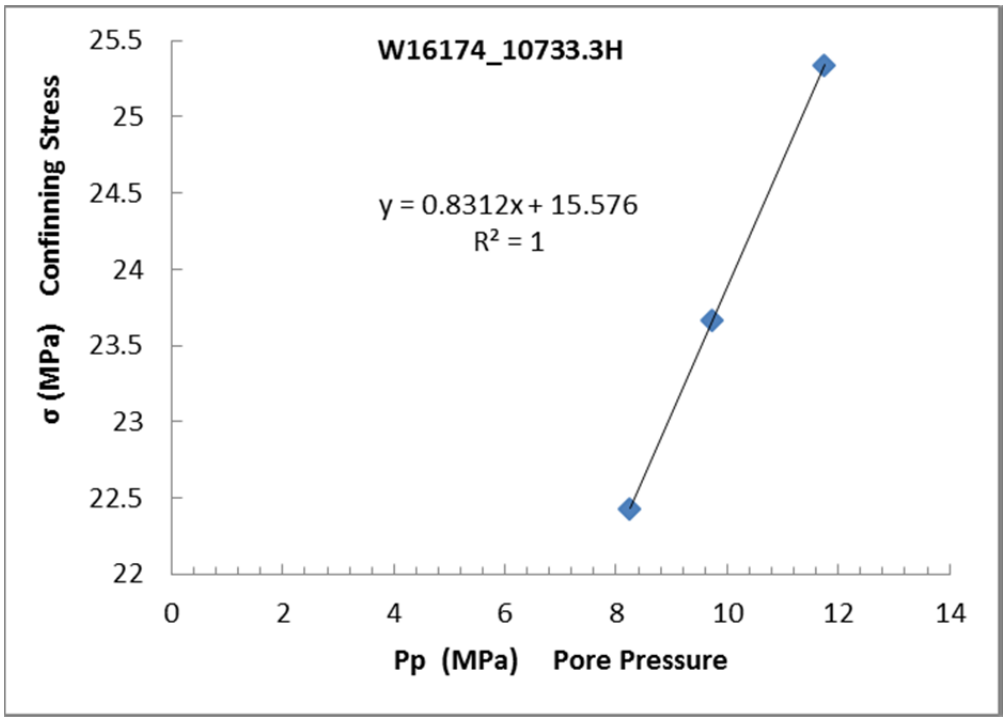
W16174_10733.3H
y = 0.8312x + 15.576
R² = 1
σ (MPa) Confinning Stress
Pp (MPa) Pore Pressure
25.5
25
24.5
24
23.5
23
22.5
22
0
2
4
6
8
10
12
14

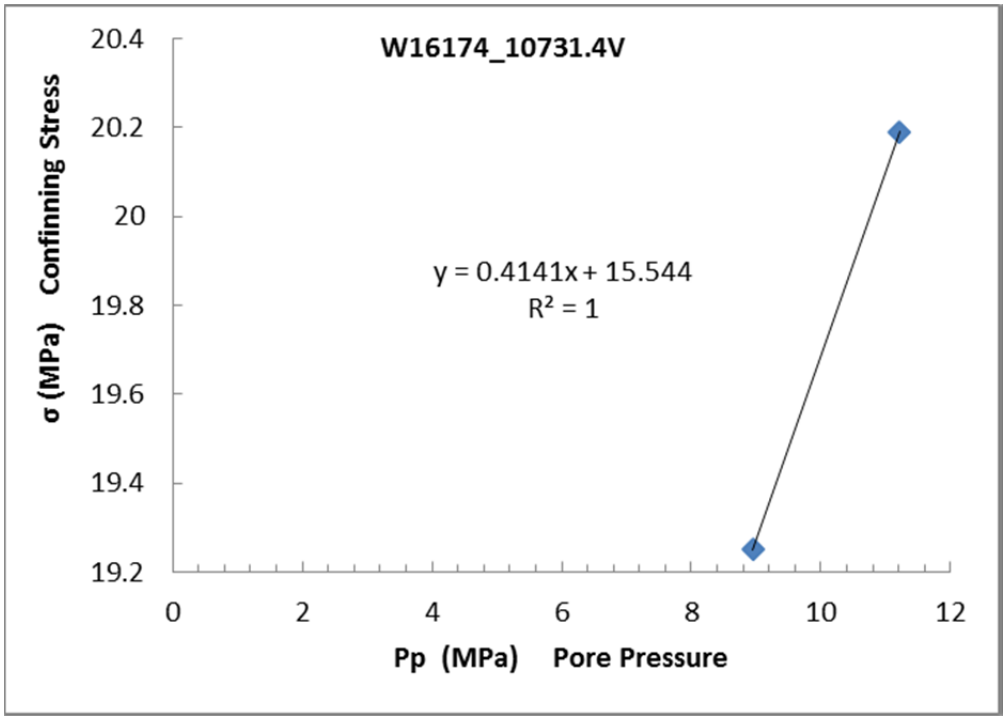
W16174_10731.4V
y = 0.4141x + 15.544
R² = 1
σ (MPa) Confinning Stress
Pp (MPa) Pore Pressure
20.4
20.2
20
19.8
19.6
19.4
19.2
0
2
4
6
8
10
12

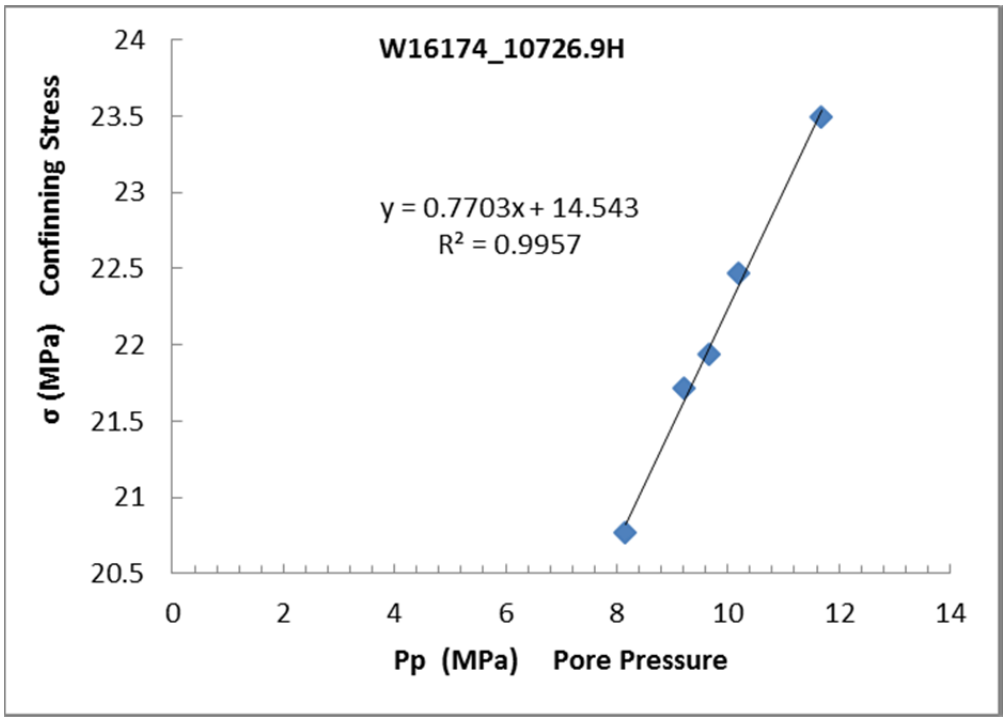
W16174_10726.9H
y = 0.7703x + 14.543
R² = 0.9957
σ (MPa) Confinning Stress
Pp (MPa) Pore Pressure
24
23.5
23
22.5
22
21.5
21
20.5
0
2
4
6
8
10
12
14

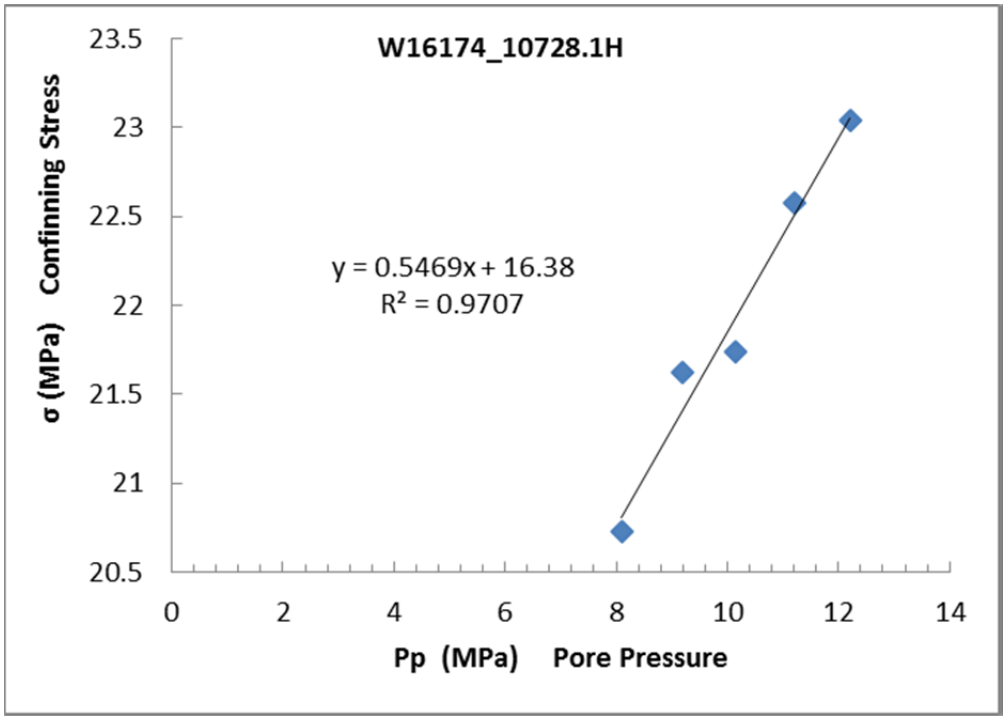
W16174_10728.1H
y = 0.5469x + 16.38
R² = 0.9707
σ (MPa) Confinning Stress
Pp (MPa) Pore Pressure
23.5
23
22.5
22
21.5
21
20.5
0
2
4
6
8
10
12
14

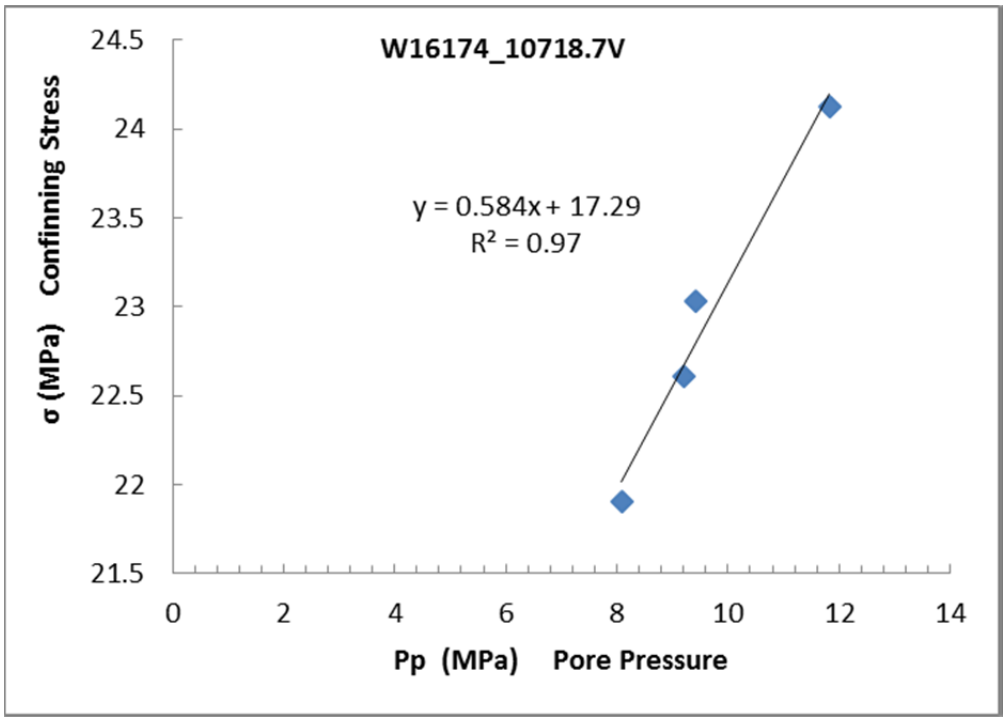
W16174_10718.7V
y = 0.584x + 17.29
R² = 0.97
σ (MPa) Confinning Stress
Pp (MPa) Pore Pressure
24.5
24
23.5
23
22.5
22
21.5
0
2
4
6
8
10
12
14

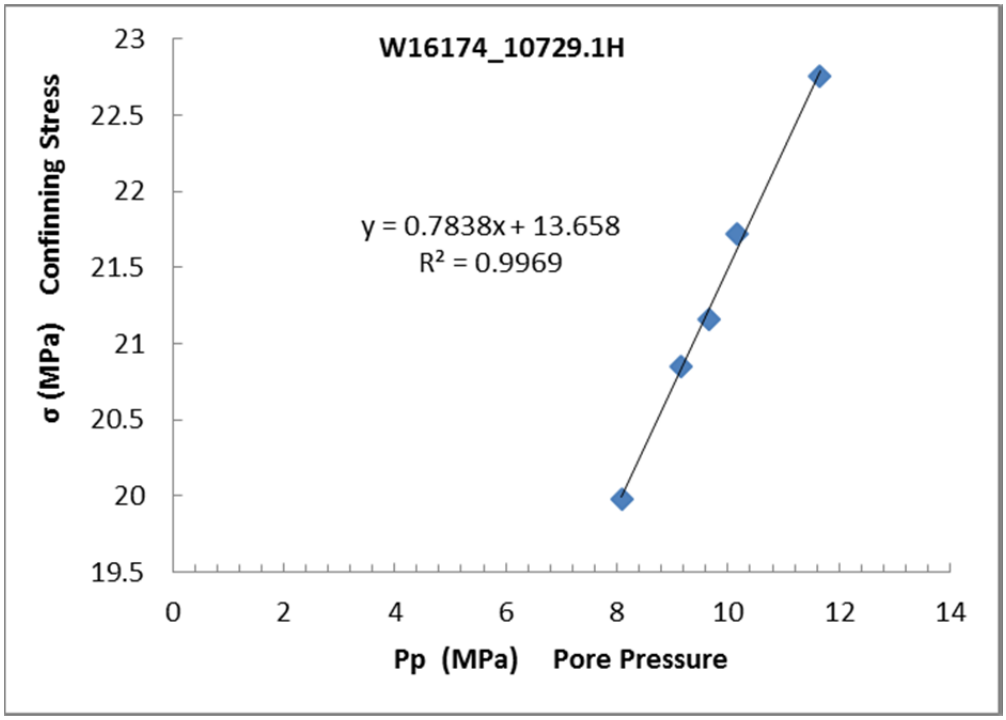
W16174_10729.1H
y = 0.7838x + 13.658
R² = 0.9969
σ (MPa) Confinning Stress
Pp (MPa) Pore Pressure
23
22.5
22
21.5
21
20.5
20
19.5
0
2
4
6
8
10
12
14

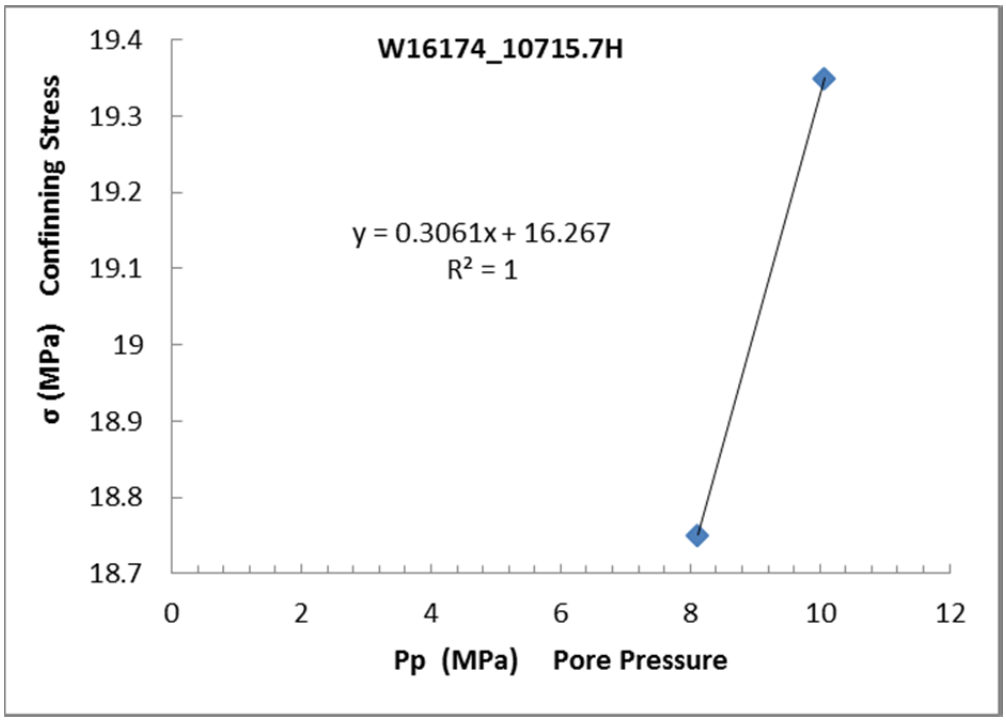
W16174_10715.7H
y = 0.3061x + 16.267
R² = 1
σ (MPa) Confinning Stress
Pp (MPa) Pore Pressure
19.4
19.3
19.2
19.1
19
18.9
18.8
18.7
0
2
4
6
8
10
12

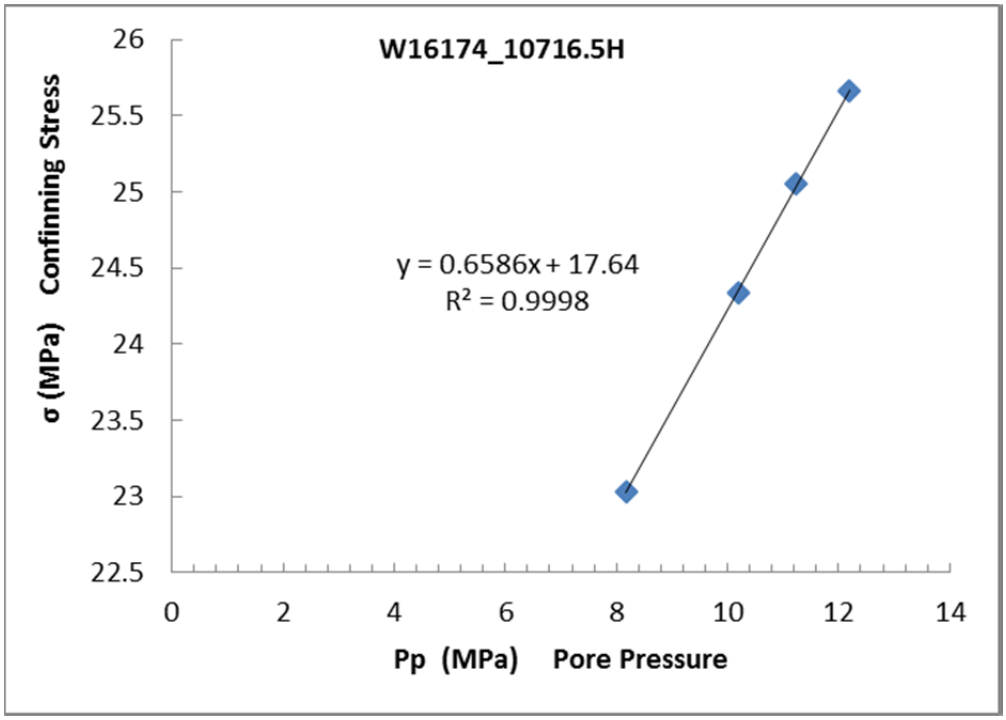
W16174_10716.5H
y = 0.6586x + 17.64
R² = 0.9998
σ (MPa) Confinning Stress
Pp (MPa) Pore Pressure
26
25.5
25
24.5
24
23.5
23
22.5
0
2
4
6
8
10
12
14

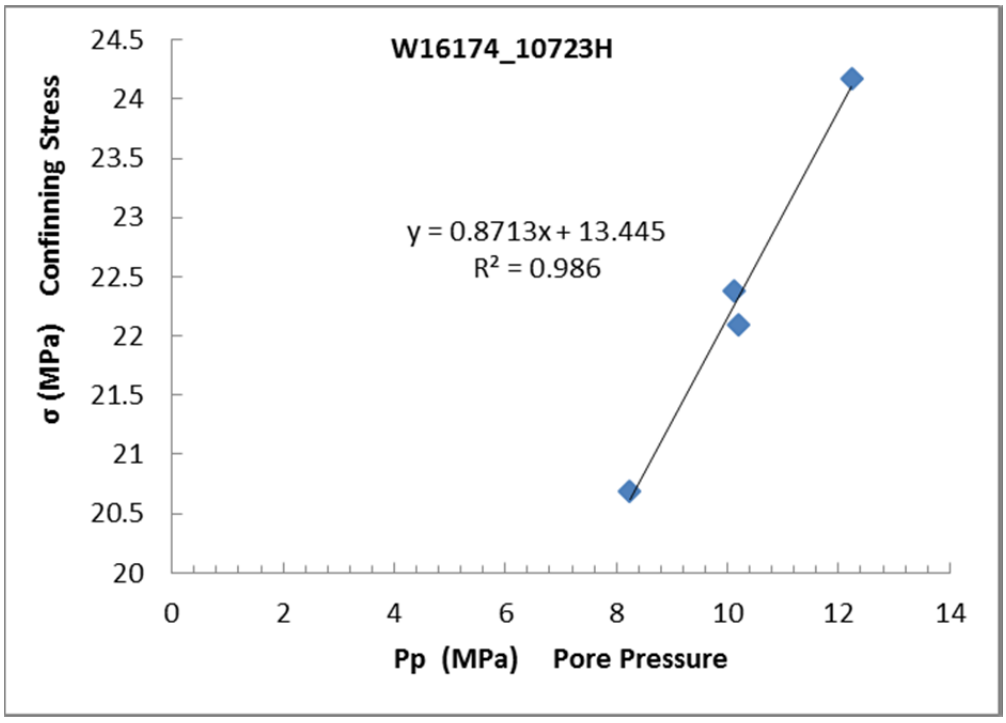
W16174_10723H
y = 0.8713x + 13.445
R² = 0.986
σ (MPa) Confinning Stress
Pp (MPa) Pore Pressure
24.5
24
23.5
23
22.5
22
21.5
21
20.5
20
0
2
4
6
8
10
12
14

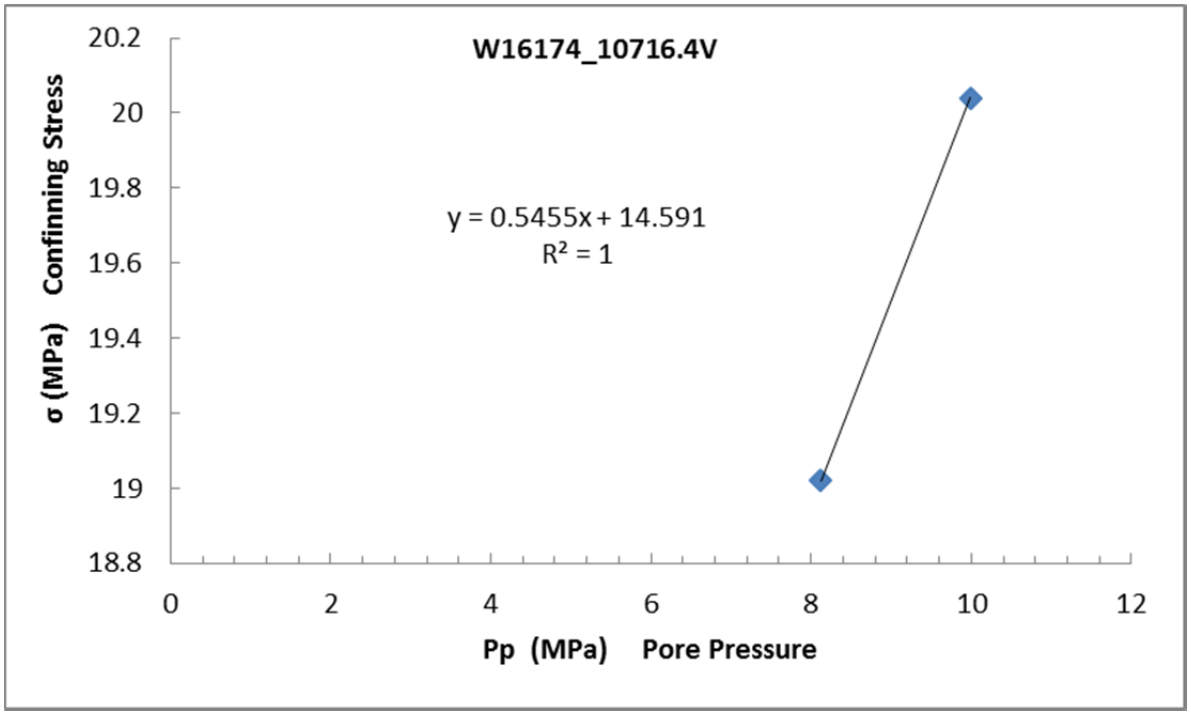
W16174_10716.4V
y = 0.5455x + 14.591
R² = 1
σ (MPa) Confinning Stress
Pp (MPa) Pore Pressure
20.2
20
19.8
19.6
19.4
19.2
19
18.8
0
2
4
6
8
10
12

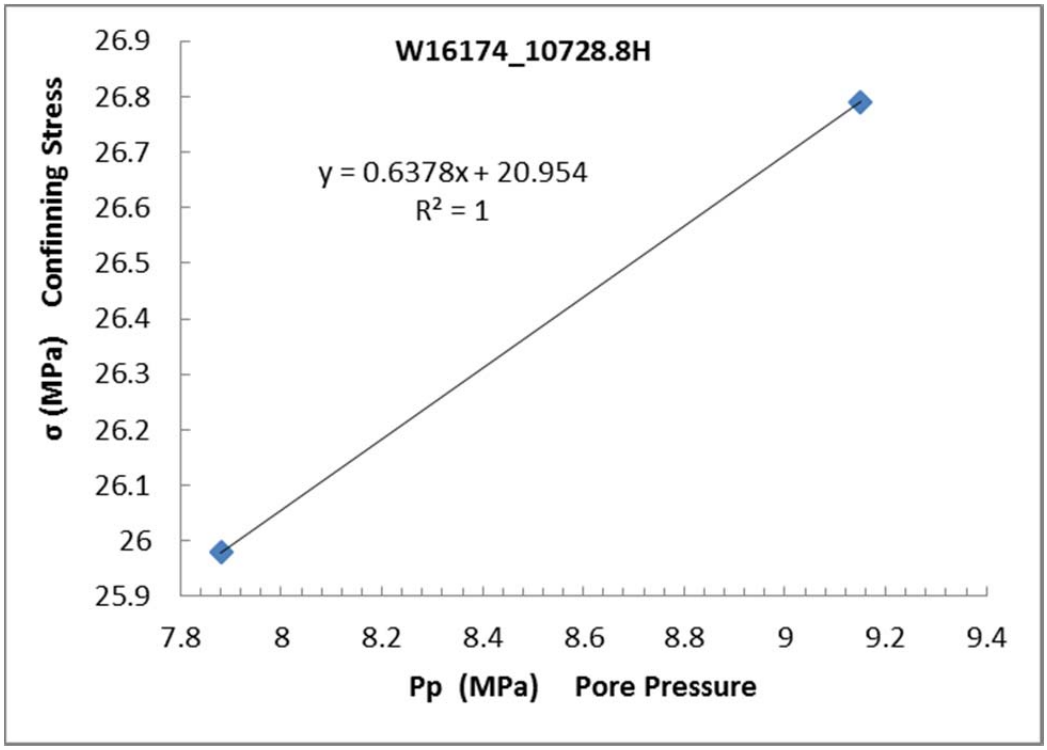
W16174_10728.8H
y = 0.6378x + 20.954
R² = 1
σ (MPa) Confinning Stress
Pp (MPa) Pore Pressure
26.9
26.8
26.7
26.6
26.5
26.4
26.3
26.2
26.1
26
25.9
7.8
8
8.2
8.4
8.6
8.8
9
9.2
9.4

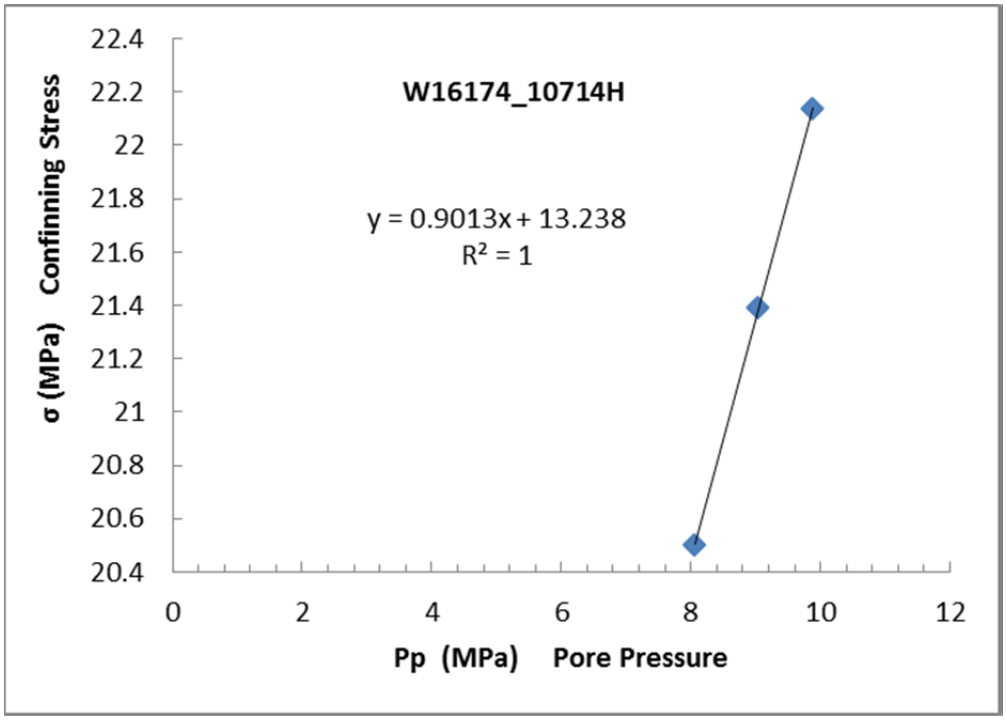
W16174_10714H
y = 0.9013x + 13.238
R² = 1
σ (MPa) Confinning Stress
Pp (MPa) Pore Pressure
22.4
22.2
22
21.8
21.6
21.4
21.2
21
20.8
20.6
20.4
0
2
4
6
8
10
12

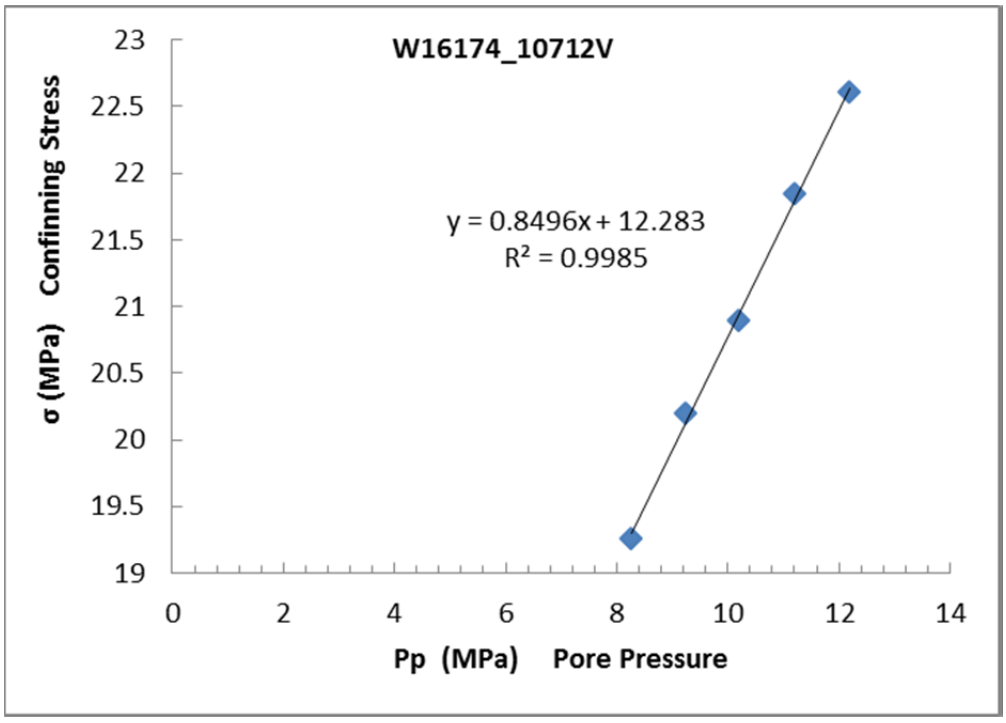
W16174_10712V
y = 0.8496x + 12.283
R² = 0.9985
σ (MPa) Confinning Stress
Pp (MPa) Pore Pressure
23
22.5
22
21.5
21
20.5
20
19.5
19
0
2
4
6
8
10
12
14

A.1.4 Static Moduli and Poisson's Ratio (Non-destructive)

Uniaxial Stress for File w16174-10730.6-uniaxial-stress									
Event	Conf	Pore	Diff	Temp	E	n	K	G	P
	MPa	MPa	MPa	°C	GPa		GPa	GPa	GPa
0	30.5	-0.2	52.1	29.0	81.83	0.046	30.01	39.13	82.18
1	25.5	-0.2	52.1	28.7	86.26	0.051	32.04	41.02	86.74
2	10.4	-0.2	52.6	28.5	86.20	0.057	32.45	40.77	86.81

Uniaxial Stress for File w16174-10721.4-uniaxial-stress									
Event	Conf	Pore	Diff	Temp	E	n	K	G	P
	MPa	MPa	MPa	°C	GPa		GPa	GPa	GPa
0	50.6	-0.2	51.3	28.6	39.98	0.236	25.28	16.17	46.83
1	50.5	-0.2	50.0	29.0	48.96	0.241	31.48	19.73	57.79
2	40.5	-0.2	45.3	29.1	47.48	0.261	33.07	18.83	58.17
3	30.5	-0.2	45.7	29.6	46.59	0.252	31.28	18.61	56.10
4	20.6	-0.2	46.6	29.2	46.17	0.250	30.81	18.47	55.43
5	10.5	-0.2	46.6	29.1	48.23	0.253	32.48	19.25	58.16

Uniaxial Stress for File w16174-10715.2-uniaxial-stress									
Event	Conf	Pore	Diff	Temp	E	n	K	G	P
	MPa	MPa	MPa	°C	GPa		GPa	GPa	GPa
0	50.5	-0.2	45.3	28.0	50.57	0.224	30.55	20.66	58.09
1	40.6	-0.2	46.6	27.7	61.77	0.242	39.87	24.87	73.03
2	30.5	-0.2	47.0	27.5	61.10	0.247	40.25	24.50	72.91
3	20.6	-0.2	47.0	27.3	60.23	0.249	40.03	24.11	72.18
4	10.5	-0.2	47.4	26.3	60.87	0.259	42.16	24.17	74.38

Uniaxial Stress for File w16174-10682-uniaxial-stress									
Event	Conf	Pore	Diff	Temp	E	n	K	G	P
	MPa	MPa	MPa	°C	GPa		GPa	GPa	GPa
0	50.6	-0.2	56.4	29.5	76.21	0.056	28.62	36.07	76.72
1	40.5	-0.2	56.4	29.2	80.00	0.089	32.44	36.73	81.42
2	30.5	-0.2	56.8	29.1	81.97	0.090	33.31	37.60	83.45
3	20.5	-0.2	57.2	29.5	79.28	0.088	32.06	36.44	80.65
4	10.5	-0.2	58.1	29.0	79.56	0.086	32.01	36.64	80.86

Uniaxial Stress for File w16174-10678.3-uniaxial-stress									
Event	Conf	Pore	Diff	Temp	E	n	K	G	P
	MPa	MPa	MPa	°C	GPa		GPa	GPa	GPa
0	50.5	-0.2	36.3	29.7	36.05	0.164	17.90	15.48	38.54
1	50.5	-0.2	36.3	30.0	35.74	0.166	17.83	15.33	38.26
2	40.5	-0.2	36.8	29.7	28.25	0.126	12.60	12.54	29.32
3	30.4	-0.2	37.2	29.2	41.62	0.178	21.53	17.67	45.09
4	20.5	-0.2	37.6	29.5	41.40	0.171	20.99	17.67	44.56
5	10.5	-0.2	38.0	29.5	41.97	0.167	21.01	17.98	44.98
6	40.5	-0.2	36.8	30.5	42.34	0.200	23.53	17.64	47.05

Uniaxial Stress for File w16174-10673.6-uniaxial-stress									
Event	Conf	Pore	Diff	Temp	E	n	K	G	P
	MPa	MPa	MPa	°C	GPa		GPa	GPa	GPa
0	50.6	-0.2	45.7	28.8	177.13	0.385	255.87	63.96	341.15
1	50.5	-0.2	45.3	28.6	177.94	0.394	280.26	63.81	365.35
2	40.5	-0.2	45.7	28.6	167.95	0.381	235.90	60.79	316.96
3	30.5	-0.2	46.6	28.4	172.28	0.393	267.71	61.85	350.17
4	20.5	-0.2	46.6	28.5	175.43	0.383	249.08	63.44	333.67

Uniaxial Stress for File w20-mb-10689.3H-uniaxial_stress								
Event	Conf	Diff	Temp	E	n	K	G	P
	MPa	MPa	°C	GPa		GPa	GPa	GPa
0	25.4	29.5	31.0	88.40	0.258	60.83	35.14	107.69
1	15.4	15.0	31.0	93.36	0.275	69.11	36.62	117.93
2	5.4	10.7	31.5	75.62	0.243	49.00	30.42	89.57

Uniaxial Stress for File w20-mb-10696H-uniaxial_stress								
Event	Conf	Diff	Temp	E	n	K	G	P
	MPa	MPa	°C	GPa		GPa	GPa	GPa
0	25.5	29.9	32.8	63.58	0.209	36.47	26.28	71.52
1	15.4	15.8	32.8	69.36	0.210	39.87	28.66	78.08
2	5.4	11.1	32.7	68.61	0.205	38.74	28.47	76.70

Uniaxial Stress for File w20-mb-10700V1-uniaxial_stress								
Event	Conf	Diff	Temp	E	n	K	G	P
	MPa	MPa	°C	GPa		GPa	GPa	GPa
0	25.5	31.2	31.7	82.36	0.238	52.40	33.26	96.75
1	15.4	16.3	31.5	81.72	0.259	56.40	32.47	99.69
2	5.4	11.6	31.3	69.22	0.223	41.65	28.30	79.38

Uniaxial Stress for File w20-mb-10700V2-uniaxial_stress								
Event	Conf	Diff	Temp	E	n	K	G	P
	MPa	MPa	°C	GPa		GPa	GPa	GPa
0	25.5	30.8	28.3	68.98	0.194	37.51	28.90	76.04
1	15.5	16.3	27.2	81.23	0.241	52.18	32.74	95.84
2	5.5	12.0	27.5	68.57	0.206	38.91	28.42	76.80

Uniaxial Stress for File w20-mb-10705.5V45-uniaxial_stress								
Event	Conf	Diff	Temp	E	n	K	G	P
	MPa	MPa	°C	GPa		GPa	GPa	GPa
0	25.5	29.9	31.9	69.12	0.181	36.11	29.26	75.13
1	15.4	15.0	32.0	58.10	0.181	30.33	24.60	63.13
2	5.4	10.3	32.8	52.18	0.178	27.04	22.14	56.56

Uniaxial Stress for File w20-mb-10705.9V-uniaaxial_stress								
Event	Conf	Diff	Temp	E	n	K	G	P
	MPa	MPa	°C	GPa		GPa	GPa	GPa
0	25.5	30.4	35.3	54.57	0.177	28.19	23.18	59.09
1	15.4	15.4	35.1	67.07	0.202	37.47	27.91	74.68
2	5.4	11.1	34.9	64.91	0.203	36.48	26.97	72.43

Uniaxial Stress for File w20-mb-10712V45-uniaxial_stress								
Event	Conf	Diff	Temp	E	n	K	G	P
	MPa	MPa	°C	GPa		GPa	GPa	GPa
0	25.5	30.4	32.6	67.31	0.150	32.08	29.25	71.09
1	15.4	15.4	32.5	78.37	0.114	33.80	35.19	80.72
2	5.4	11.1	32.5	68.51	0.120	30.03	30.59	70.82

Uniaxial Stress for File w16174-10712-vertical-uniaxial-stress									
Event	Conf	Pore	Diff	Temp	E	n	K	G	P
	MPa	MPa	MPa	°C	GPa		GPa	GPa	GPa
0	40.6	-0.2	20.1	29.4	112.08	0.400	186.81	40.03	240.18
1	50.6	-0.2	24.8	29.6	111.16	0.387	164.20	40.07	217.62
2	30.6	-0.2	20.5	28.9	106.54	0.387	156.71	38.41	207.93

Uniaxial Stress for File w16174-10714-uniaxial-stress									
Event	Conf	Pore	Diff	Temp	E	n	K	G	P
	MPa	MPa	MPa	°C	GPa		GPa	GPa	GPa
0	40.7	-0.2	20.1	25.5	82.91	0.323	78.25	31.32	120.02
1	50.7	-0.2	25.2	25.8	75.34	0.248	49.89	30.18	90.13
2	30.6	-0.2	20.5	23.9	82.22	0.362	99.52	30.18	139.75

Uniaxial Stress for File w16174-10715.7-uniaxial-stress									
Event	Conf	Pore	Diff	Temp	E	n	K	G	P
	MPa	MPa	MPa	°C	GPa		GPa	GPa	GPa
0	40.7	-0.2	20.1	25.2	75.26	0.199	41.68	31.38	83.53
1	50.7	-0.2	25.2	25.7	80.66	0.174	41.26	34.35	87.06
2	30.6	-0.2	21.0	23.4	72.55	0.169	36.49	31.04	77.88

Uniaxial Stress for File w16174-10716.4-vertical-uniaxial-stress									
Event	Conf	Pore	Diff	Temp	E	n	K	G	P
	MPa	MPa	MPa	°C	GPa		GPa	GPa	GPa
0	40.6	-0.2	20.1	30.2	46.75	0.164	23.16	20.09	49.95
1	50.6	-0.2	29.5	30.6	37.50	0.227	22.85	15.28	43.23
2	30.6	-0.2	21.0	29.0	46.63	0.168	23.42	19.96	50.03

Uniaxial Stress for File w16174-10716.5-uniaxial-stress									
Event	Conf	Pore	Diff	Temp	E	n	K	G	P
	MPa	MPa	MPa	°C	GPa		GPa	GPa	GPa
0	40.7	-0.2	20.5	26.3	84.17	0.220	50.04	34.50	96.04
1	50.6	-0.2	24.8	26.2	84.66	0.181	44.28	35.83	92.06
2	30.6	-0.2	21.0	23.9	79.46	0.233	49.54	32.23	92.52

Uniaxial Stress for File w16174-10718.7-vertica-uniaxial-stress									
Event	Conf	Pore	Diff	Temp	E	n	K	G	P
	MPa	MPa	MPa	°C	GPa		GPa	GPa	GPa
0	40.7	-0.2	19.7	25.3	68.35	0.244	44.45	27.48	81.09
1	50.7	-0.2	24.4	25.7	62.98	0.224	38.05	25.73	72.35
2	30.7	-0.2	20.5	23.7	62.62	0.241	40.26	25.24	73.91

Uniaxial Stress for File w16174-10723-uniaxail-stress									
Event	Conf	Pore	Diff	Temp	E	n	K	G	P
	MPa	MPa	MPa	°C	GPa		GPa	GPa	GPa
0	40.6	-0.2	19.7	27.0	85.56	0.140	39.66	37.51	89.68
1	50.7	-0.2	24.4	27.0	94.50	0.161	46.45	40.70	100.72
2	30.7	-0.2	20.5	25.1	82.69	0.136	37.87	36.39	86.39

Uniaxial Stress for File w16174-10726.9-uniaxial-stress									
Event	Conf	Pore	Diff	Temp	E	n	K	G	P
	MPa	MPa	MPa	°C	GPa		GPa	GPa	GPa
0	40.6	-0.2	20.1	29.9	89.35	-0.010	29.22	45.11	89.37
1	50.6	-0.2	24.4	29.8	89.46	0.033	31.91	43.31	89.66
2	30.6	-0.2	20.5	28.6	92.68	-0.015	29.98	47.05	92.72

Uniaxial Stress for File w16174-10727.2-uniaxial-stress									
Event	Conf	Pore	Diff	Temp	E	n	K	G	P
	MPa	MPa	MPa	°C	GPa		GPa	GPa	GPa
0	40.6	-0.2	20.5	77.0	159.63	0.464	733.65	54.53	806.35
1	50.1	-0.2	29.9	73.8	166.07	0.460	698.66	56.86	774.47

Uniaxial Stress for File w16174-10728.1-uniaxial-stress									
Event	Conf	Pore	Diff	Temp	E	n	K	G	P
	MPa	MPa	MPa	°C	GPa		GPa	GPa	GPa
0	40.6	-0.2	19.7	29.3	82.77	0.189	44.33	34.81	90.74
1	50.6	-0.2	29.5	28.2	75.97	0.178	39.30	32.25	82.30
2	30.6	-0.2	20.5	25.5	87.14	0.199	48.19	36.35	96.65

Uniaxial Stress for File w16174-10729.1-uniaxil-stress									
Event	Conf	Pore	Diff	Temp	E	n	K	G	P
	MPa	MPa	MPa	°C	GPa		GPa	GPa	GPa
0	40.7	-0.2	20.1	25.3	74.03	0.155	35.80	32.04	78.52
1	50.7	-0.2	24.8	25.9	78.21	0.161	38.42	33.69	83.35
2	30.6	-0.2	20.5	23.9	74.76	0.150	35.57	32.51	78.92

Uniaxial Stress for File w16174-10729.5-uniaxial-stress									
Event	Conf	Pore	Diff	Temp	E	n	K	G	P
	MPa	MPa	MPa	°C	GPa		GPa	GPa	GPa
0	40.6	-0.2	19.7	24.9	78.00	0.275	57.88	30.58	98.65
1	50.7	-0.2	24.8	25.9	75.28	0.251	50.34	30.10	90.47
2	30.7	-0.2	21.0	23.0	76.70	0.298	63.22	29.55	102.62

Uniaxial Stress for File w16174-10729.9-uniaxial-stress									
Event	Conf	Pore	Diff	Temp	E	n	K	G	P
	MPa	MPa	MPa	°C	GPa		GPa	GPa	GPa
0	40.6	-0.2	20.1	35.7	77.48	0.230	47.80	31.50	89.79
1	49.9	-0.2	29.9	35.5	86.41	0.263	60.80	34.20	106.40
2	30.0	-0.2	21.0	34.6	79.41	0.254	53.71	31.67	95.94

Uniaxial Stress for File w16174-10731.4-horizontal-uniaxial-stress									
Event	Conf	Pore	Diff	Temp	E	n	K	G	P
	MPa	MPa	MPa	°C	GPa		GPa	GPa	GPa
0	40.6	-0.2	20.1	26.2	69.68	0.129	31.33	30.85	72.46
1	50.7	-0.2	29.9	26.5	74.61	0.171	37.81	31.85	80.28
2	30.6	-0.2	20.5	24.2	70.88	0.116	30.74	31.77	73.10

Uniaxial Stress for File w16174-10731.4-vertical-uniaxial-stress									
Event	Conf	Pore	Diff	Temp	E	n	K	G	P
	MPa	MPa	MPa	°C	GPa		GPa	GPa	GPa
0	40.6	-0.2	20.5	25.3	30.55	0.427	69.75	10.70	84.02
1	50.7	-0.2	30.4	25.0	33.64	0.471	191.64	11.44	206.89
2	30.0	-0.2	31.2	22.8	32.76	0.413	62.95	11.59	78.40

Uniaxial Stress for File w16174-10732.3-uniaxial-stress									
Event	Conf	Pore	Diff	Temp	E	n	K	G	P
	MPa	MPa	MPa	°C	GPa		GPa	GPa	GPa
0	40.6	-0.2	20.5	26.4	114.50	0.314	102.69	43.56	160.78
1	50.1	-0.2	20.1	26.2	118.13	0.319	109.01	44.77	168.70
2	30.2	-0.2	21.0	23.2	124.93	0.377	168.68	45.38	229.19

Uniaxial Stress for File w16174-10733.3-uniaxial-stress									
Event	Conf	Pore	Diff	Temp	E	n	K	G	P
	MPa	MPa	MPa	°C	GPa		GPa	GPa	GPa
0	40.6	-0.2	21.0	26.2	63.67	0.210	36.64	26.30	71.71
1	50.6	-0.2	29.9	26.0	60.76	0.234	38.12	24.61	70.93
2	30.6	-0.2	21.4	23.7	67.35	0.267	48.26	26.57	83.69

A.1.5 Uni/Triaxial Compressive Strength, Young's Modulus and Poisson's Ratio

Strength for File w20-mb-10689.3H-strength					
Event	Conf	Temp	E	n	peak_stress
	MPa	°C	GPa		MPa
0	20.2	33.2	52.03	0.286	274.1

Strength for File w20-mb-10700V1-strength					
Event	Conf	Temp	E	n	peak_stress
	MPa	°C	GPa		MPa
0	20.1	32.7	47.96	0.135	67.1
1	20.1	33.1	37.68	0.220	247.2

Strength for File w20-mb-10705.5V45-strength					
Event	Conf	Temp	E	n	peak_stress
	MPa	°C	GPa		MPa
0	20.1	27.1	37.19	0.200	149.4

Strength for File w16174-10712-vertical-strength						
Event	Conf	Diff	Temp	E	n	peak_stress
	MPa	MPa	°C	GPa		MPa
0	0.9	36.3	34.0	71.30	0.708	117.0

Strength for File w16174-10716.4-vertical-strength						
Event	Conf	Diff	Temp	E	n	peak_stress
	MPa	MPa	°C	GPa		MPa
0	10.2	14.1	28.3	112.22	1.225	100.4

Strength for File w16174-10718.7-vertical-strength						
Event	Conf	Diff	Temp	E	n	peak_stress
	MPa	MPa	°C	GPa		MPa
0	20.1	22.2	37.4	115.63	0.618	125.1

Strength for File w16174-10727.2-stregth						
Event	Conf	Diff	Temp	E	n	peak_stress
	MPa	MPa	°C	GPa		MPa
0	0.8	31.2	28.3	106.42	0.362	140.1

Strength for File w16174-10729.5-strength						
Event	Conf	Diff	Temp	E	n	peak_stress
	MPa	MPa	°C	GPa		MPa
0	20.0	8.6	35.1	156.69	0.451	156.3

Strength for File w16174-10729.9-strength						
Event	Conf	Diff	Temp	E	n	peak_stress
	MPa	MPa	°C	GPa		MPa
0	20.2	4.7	32.2	112.84	0.511	103.8

Strength for File w16174-10731.4-vertical-strength						
Event	Conf	Diff	Temp	E	n	peak_stress
	MPa	MPa	°C	GPa		MPa
0	0.9	9.9	22.1	12.16	0.632	27.4

Strength for File w16174-10732.3-strength						
Event	Conf	Diff	Temp	E	n	peak_stress
	MPa	MPa	°C	GPa		MPa
0	10.2	8.2	39.8	165.08	0.811	123.0

Strength for File w16174-10733.3-strength						
Event	Conf	Diff	Temp	E	n	peak_stress
	MPa	MPa	°C	GPa		MPa
0	10.2	3.5	37.2	96.06	0.847	125.5

A.1.6 Mohr's Circle

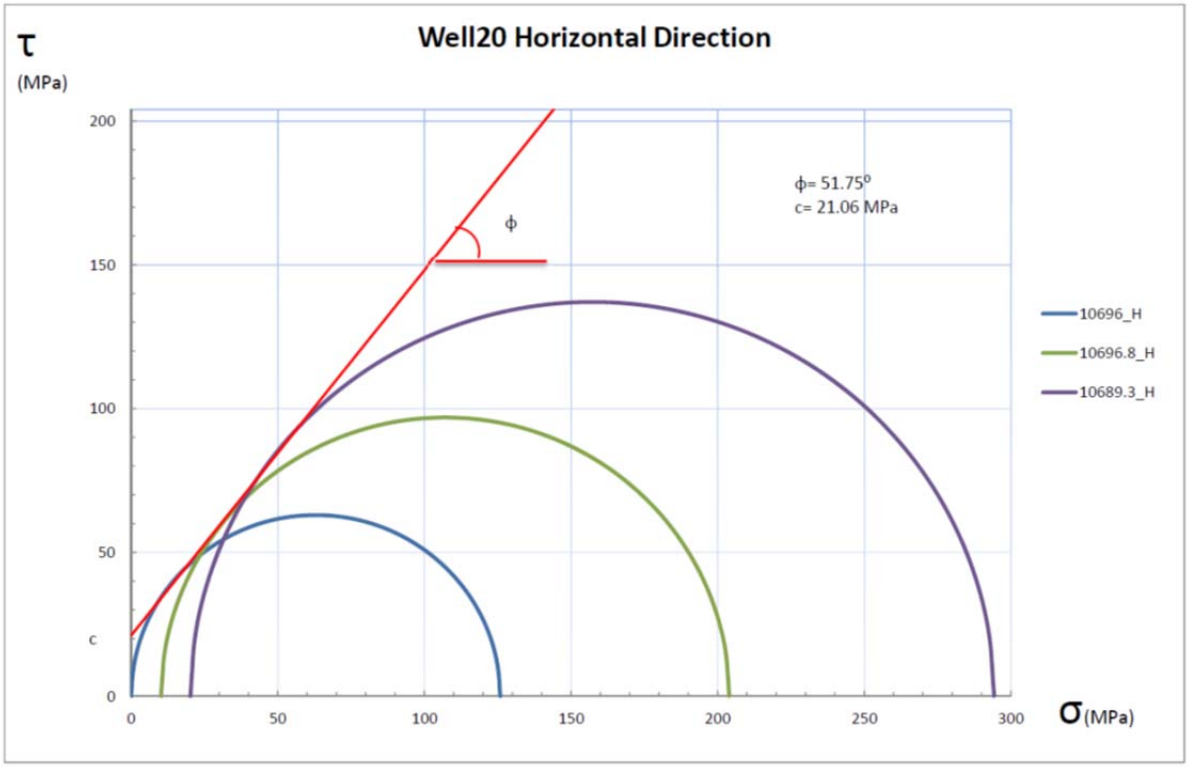

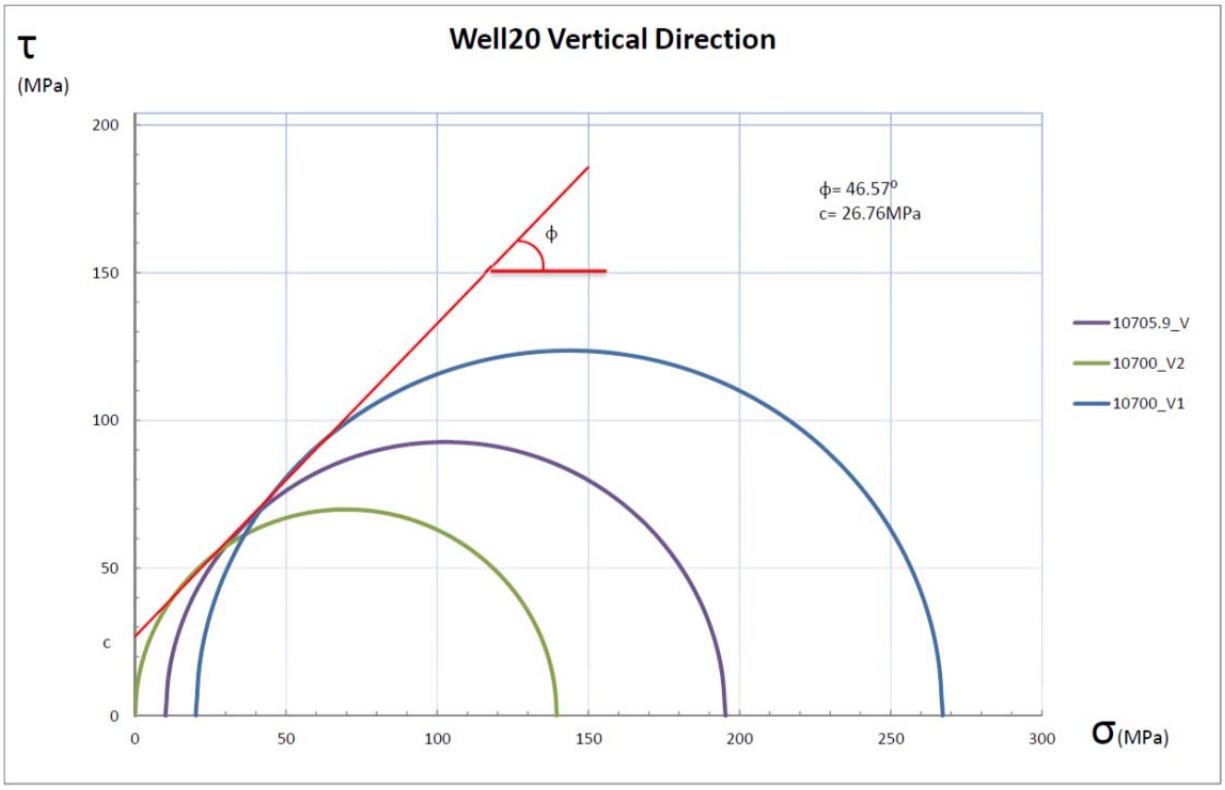

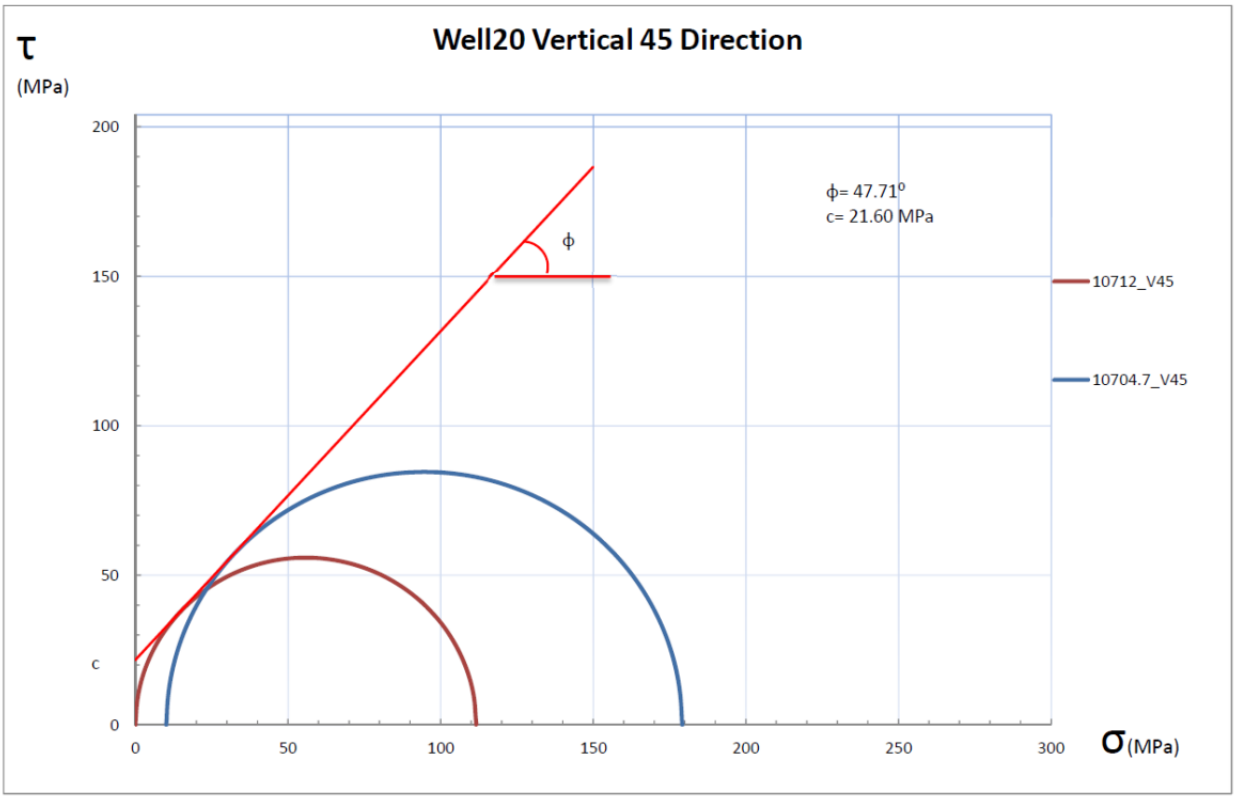

A.2. Well 96 Bakken Samples Testing Results

A.2.1 Permeability

Permeability and Specific Storage for File W16771-10446-Permeability							
Event	Type	Conf	Pore Top	Diff	Temp	Perm	Storage
		MPa	MPa	MPa	°C	μD	m^{-1}
0	steady-state	20.3	8.0	-1.3	24.3	4.64e+04	0.00
1	steady-state	29.9	8.5	-1.3	24.6	1.47e+05	0.00
2	steady-state	40.4	8.4	-2.1	24.9	2.53e+04	0.00
3	steady-state	50.2	8.0	-2.1	25.1	1.96e+04	0.00

Permeability and Specific Storage for File well-16771-10437-Permeability							
Event	Type	Conf	Pore Top	Diff	Temp	Perm	Storage
		MPa	MPa	MPa	°C	μD	m^{-1}
0	steady-state	5.0	4.6	0.4	27.7	-	0.00
1	steady-state	20.5	8.2	-0.4	28.8	3.27e+03	0.00
2	steady-state	30.4	8.8	-1.3	29.1	2.00e+03	0.00
3	steady-state	40.5	8.8	-2.1	29.4	3.88e+03	0.00
4	steady-state	40.5	8.3	-1.7	29.4	3.09e+03	0.00
5	steady-state	40.5	8.9	-1.7	29.7	2.35e+03	0.00
6	steady-state	50.5	8.3	-2.1	30.0	1.87e+03	0.00

Permeability and Specific Storage for File w16771-10460.5-plus-perm							
Event	Type	Conf	Pore Top	Diff	Temp	Perm	Storage
		MPa	MPa	MPa	°C	μD	m^{-1}
0	multipulse	20.5	7.9	-3.9	27.3	0.0601	1.99e-08
1	multipulse	25.5	7.9	-4.3	27.3	0.0640	1.18e-08
2	multipulse	30.4	7.9	-4.8	27.3	0.0593	5.45e-09
3	multipulse	35.5	7.9	-4.8	27.3	0.0578	3.60e-11

Permeability and Specific Storage for File w16771-10456-2-perm							
Event	Type	Conf	Pore Top	Diff	Temp	Perm	Storage
		MPa	MPa	MPa	°C	μD	m^{-1}
0	multipulse	20.5	7.9	-0.4	27.8	0.171	3.74e-06
1	multipulse	30.4	7.9	-1.3	28.5	0.0450	6.54e-07
2	multipulse	40.5	7.9	-1.7	28.8	0.0296	4.29e-07

Permeability and Specific Storage for File w16771-10452-permeability							
Event	Type	Conf	Pore Top	Diff	Temp	Perm	Storage
		MPa	MPa	MPa	°C	μD	m^{-1}
0	steady-state	20.3	8.9	-0.8	23.2	9.93e+03	0.00
1	steady-state	20.3	9.3	-0.8	23.0	3.40e+03	0.00
2	steady-state	20.2	8.3	-1.3	23.3	4.55e+03	0.00
3	steady-state	30.1	9.1	-1.7	23.6	4.12e+03	0.00
4	steady-state	30.2	9.2	-1.3	23.2	2.26e+03	0.00
5	steady-state	40.0	8.6	-1.7	23.0	2.52e+03	0.00
6	steady-state	50.2	8.8	-2.1	23.3	2.15e+03	0.00

Permeability and Specific Storage for File w16771-10443-plus-perm							
Event	Type	Conf	Pore Top	Diff	Temp	Perm	Storage
		MPa	MPa	MPa	°C	μD	m^{-1}
0	aspike	20.5	7.9	-4.3	26.3	32.4	2.58e-11
1	aspike	25.5	7.8	-4.8	26.3	29.4	5.52e-11
2	aspike	30.4	7.8	-4.8	26.4	26.3	5.76e-08
3	aspike	35.5	7.9	-4.8	26.3	21.1	1.01e-07

Permeability and Specific Storage for File W16771-10463-Permeability							
Event	Type	Conf	Pore Top	Diff	Temp	Perm	Storage
		MPa	MPa	MPa	°C	μD	m^{-1}
0	steady-state	10.5	8.5	0.4	24.6	1.64e+03	0.00
1	steady-state	20.5	8.9	-0.4	25.1	1.60e+03	0.00
2	steady-state	30.4	8.5	-1.3	25.4	1.68e+03	0.00
3	steady-state	40.6	8.7	-1.3	25.6	1.53e+03	0.00
4	steady-state	50.5	8.1	-1.7	25.6	1.61e+03	0.00

Permeability and Specific Storage for File W16771-10456.5-Permeability							
Event	Type	Conf	Pore Top	Diff	Temp	Perm	Storage
		MPa	MPa	MPa	°C	μD	m^{-1}
0	steady-state	20.5	8.2	-0.4	27.3	1.45e+03	0.00
1	steady-state	30.4	8.8	-1.3	27.4	1.27e+03	0.00
2	steady-state	40.4	8.8	-2.1	28.1	1.28e+03	0.00
3	steady-state	50.5	8.9	-2.1	27.8	2.59e+03	0.00
4	steady-state	50.5	8.3	-2.1	27.7	1.56e+03	0.00

Permeability and Specific Storage for File W16771-10456-Permeability							
Event	Type	Conf	Pore Top	Diff	Temp	Perm	Storage
		MPa	MPa	MPa	°C	μD	m^{-1}
0	steady-state	20.5	8.7	-0.8	24.6	2.19e+03	0.00
1	steady-state	30.4	8.9	-1.7	24.9	2.10e+03	0.00
2	steady-state	40.5	8.2	-2.1	24.9	2.15e+03	0.00
3	steady-state	50.5	8.2	-2.5	25.0	1.96e+03	0.00

Permeability and Specific Storage for File W16771-10441.6-Permeability							
Event	Type	Conf	Pore Top	Diff	Temp	Perm	Storage
		MPa	MPa	MPa	°C	μD	m^{-1}
0	steady-state	20.6	8.4	-0.8	26.8	3.13e+03	0.00
1	steady-state	30.5	8.2	-1.7	26.9	2.83e+03	0.00
2	steady-state	40.6	8.2	-2.1	27.4	2.53e+03	0.00
3	steady-state	50.5	8.9	-3.0	26.8	2.54e+03	0.00

Permeability and Specific Storage for File W16771-10436-2-Permeability							
Event	Type	Conf	Pore Top	Diff	Temp	Perm	Storage
		MPa	MPa	MPa	°C	μD	m^{-1}
0	steady-state	20.5	8.2	-1.3	26.6	1.89e+03	0.00
1	steady-state	30.5	8.9	-1.7	26.9	1.92e+03	0.00
2	steady-state	40.5	8.8	-2.5	27.1	1.93e+03	0.00
3	steady-state	50.6	8.1	-2.1	27.3	1.87e+03	0.00

Permeability and Specific Storage for File W16771-10431-permeability							
Event	Type	Conf	Pore Top	Diff	Temp	Perm	Storage
		MPa	MPa	MPa	°C	μD	m^{-1}
0	steady-state	20.8	8.7	0.4	31.3	2.81e+03	0.00
1	steady-state	30.6	8.8	0.4	31.5	2.63e+03	0.00
2	steady-state	40.6	8.9	0.9	31.7	2.31e+03	0.00
3	steady-state	50.6	8.2	0.0	31.8	1.73e+03	0.00

Permeability and Specific Storage for File Bakken-w96-10357v-perm							
Event	Type	Conf	Pore Top	Diff	Temp	Perm	Storage
		MPa	MPa	MPa	°C	μD	m^{-1}
0	aspike	20.1	9.5	-0.1	23.8	0.00723	2.11e-06
1	multipulse	20.1	9.2	-0.1	24.1	0.0133	2.02e-06
2	multipulse	20.1	9.2	0.8	24.4	0.0105	1.95e-06
3	multipulse	20.1	9.2	0.4	24.0	0.0118	2.86e-06
4	multipulse	20.1	9.2	-0.1	24.6	0.0116	2.65e-06

A.2.2 Sonic Velocity, Dynamic Moduli and Poisson's Ratio

Observed Velocities and Moduli for File Middle_Bakken-W96-10307V45-Velocity									
Event	Conf	Pore	Diff	Temp	V_p	$V_s^{(1)}$	$V_s^{(2)}$	Young's Modulus	Poisson's Ratio
	MPa	MPa	MPa	°C	m/s	m/s	m/s	GPa	
0	2.5	-0.2	-1.7	24.1	4355	2718	2798	46.80	0.165
1	4.4	-0.2	-1.8	22.8	4417	2832	2811	48.56	0.155
2	6.4	-0.2	-2.2	23.0	4458	2803	2818	48.80	0.170
3	8.4	-0.2	-2.4	23.1	4525	2832	2829	49.86	0.179
4	10.4	-0.2	-2.5	23.1	4519	2862	2875	50.51	0.163
5	12.4	-0.2	-2.1	23.2	4571	2862	2895	51.25	0.171
6	14.4	-0.2	-2.2	23.2	4642	2893	2926	52.58	0.176
7	16.4	-0.2	-2.4	23.3	4655	2877	2926	52.56	0.182
8	18.4	-0.2	-2.8	23.2	4726	2908	2926	53.57	0.192
9	20.4	-0.2	-2.9	23.3	4682	2893	2958	53.31	0.180
10	22.3	-0.2	-2.9	23.3	4764	2908	2967	54.37	0.193
11	24.4	-0.2	-2.5	23.4	4764	2940	2971	54.75	0.187
12	26.4	-0.2	-2.9	23.4	4880	2972	3007	56.61	0.200
13	28.4	-0.2	-3.2	23.3	4886	3005	3004	57.00	0.196
14	30.4	-0.2	-2.9	23.4	4914	3022	3015	57.59	0.197

Observed Velocities and Moduli for File Middle_Bakken-W96-10311V45-velocity									
Event	Conf	Pore	Diff	Temp	V_p	$V_s^{(1)}$	$V_s^{(2)}$	Young's Modulus	Poisson's Ratio
	MPa	MPa	MPa	°C	m/s	m/s	m/s	GPa	
0	2.5	-0.2	-2.1	25.3	3836	2572	2568	37.68	0.093
1	4.5	-0.2	-1.7	25.4	3957	2598	2587	39.43	0.124
2	6.5	-0.2	-2.4	25.6	4085	2612	2600	41.01	0.157
3	8.5	-0.2	-2.1	25.7	4053	2653	2627	41.17	0.132
4	10.4	-0.2	-2.5	25.7	4153	2681	2655	42.68	0.149
5	12.5	-0.2	-2.5	25.7	4223	2681	2697	43.75	0.159
6	14.4	-0.2	-2.5	25.8	4223	2696	2742	44.22	0.146
7	16.5	-0.2	-2.8	26.0	4258	2710	2751	44.79	0.151
8	18.4	-0.2	-2.9	26.0	4332	2755	2787	46.24	0.154
9	20.5	-0.2	-3.1	26.2	4369	2785	2818	47.15	0.151
10	22.4	-0.2	-3.1	26.2	4446	2785	2834	48.11	0.168
11	24.4	-0.2	-3.4	26.2	4486	2816	2834	48.80	0.171
12	26.4	-0.2	-2.9	26.8	4526	2832	2850	49.50	0.175
13	28.5	-0.2	-2.9	26.4	4567	2832	2876	50.16	0.180
14	30.4	-0.2	-3.5	26.4	4695	2864	2910	52.03	0.196

Observed Velocities and Moduli for File Middle_Bakken-W96-10321.1V45-Velocity									
Event	Conf	Pore	Diff	Temp	V_p	$V_s^{(1)}$	$V_s^{(2)}$	Young's Modulus	Poisson's Ratio
	MPa	MPa	MPa	°C	m/s	m/s	m/s	GPa	
0	2.4	-0.2	-1.4	26.3	4749	2921	2848	53.06	0.208
1	4.3	-0.2	-2.1	26.4	4798	2942	2866	53.92	0.211
2	6.4	-0.2	-1.8	26.5	4833	2951	2893	54.64	0.212
3	8.4	-0.2	-1.7	26.6	4840	2961	2911	55.02	0.209
4	10.4	-0.2	-2.1	26.7	4881	2967	2915	55.49	0.215
5	12.4	-0.2	-1.9	26.8	4927	2975	2924	56.07	0.221
6	14.4	-0.2	-2.1	26.9	4854	2993	2935	55.79	0.203
7	16.4	-0.2	-2.2	26.9	4927	2992	2955	56.65	0.214
8	18.4	-0.2	-2.2	27.0	4969	3009	2939	57.02	0.221
9	20.4	-0.2	-2.7	27.0	4971	3009	2954	57.22	0.219
10	22.4	-0.2	-2.7	27.1	5009	3019	2971	57.87	0.222
11	24.4	-0.2	-2.5	27.1	5017	3023	2971	57.98	0.223
12	26.4	-0.2	-2.8	27.1	5009	3043	2995	58.46	0.215
13	28.4	-0.2	-2.8	27.2	5061	3043	3001	58.97	0.223
14	30.4	-0.2	-2.9	27.1	5078	3047	3005	59.21	0.225

Observed Velocities and Moduli for File Middle_Bakken-W96-10334.7V45-Velocity									
Event	Conf	Pore	Diff	Temp	V_p	$V_s^{(1)}$	$V_s^{(2)}$	Young's Modulus	Poisson's Ratio
	MPa	MPa	MPa	°C	m/s	m/s	m/s	GPa	
0	2.4	-0.2	-1.7	26.0	3936	2609	2511	37.29	0.133
1	4.4	-0.2	-1.7	26.1	3943	2622	2542	37.64	0.125
2	6.4	-0.2	-2.1	26.2	4055	2650	2574	39.23	0.145
3	8.4	-0.2	-1.8	26.3	4103	2673	2598	40.06	0.149
4	10.4	-0.2	-1.9	26.4	4161	2694	2611	40.89	0.158
5	12.4	-0.2	-2.2	26.5	4206	2717	2645	41.78	0.158
6	14.4	-0.2	-2.2	26.5	4226	2734	2658	42.21	0.157
7	16.4	-0.2	-2.4	26.6	4238	2750	2686	42.67	0.151
8	18.4	-0.2	-2.5	26.7	4292	2773	2709	43.59	0.156
9	20.4	-0.2	-2.9	26.7	4344	2789	2731	44.42	0.162
10	22.4	-0.2	-2.5	26.7	4380	2796	2756	45.04	0.164
11	24.4	-0.2	-2.9	26.7	4405	2825	2762	45.59	0.164
12	26.3	-0.2	-3.1	26.8	4455	2832	2773	46.23	0.173
13	28.4	-0.2	-3.1	26.7	4501	2836	2792	46.87	0.179
14	30.4	-0.2	-2.9	27.4	4477	2847	2801	46.82	0.170

Observed Velocities and Moduli for File Middle_Bakken-W96-10339H-Velocity									
Event	Conf	Pore	Diff	Temp	V_p	$V_s^{(1)}$	$V_s^{(2)}$	Young's Modulus	Poisson's Ratio
	MPa	MPa	MPa	°C	m/s	m/s	m/s	GPa	
0	2.4	-0.2	-1.7	22.7	4231	2719	2495	40.74	0.194
1	4.4	-0.2	-1.7	22.8	4214	2746	2524	41.09	0.179
2	6.4	-0.2	-2.1	22.8	4257	2766	2553	41.89	0.180
3	8.4	-0.2	-2.1	22.9	4347	2781	2580	43.04	0.193
4	10.4	-0.2	-2.1	22.9	4363	2813	2609	43.74	0.186
5	12.4	-0.2	-2.5	23.0	4391	2834	2647	44.52	0.181
6	14.4	-0.2	-2.5	23.1	4419	2844	2684	45.20	0.179
7	16.4	-0.2	-2.4	23.2	4509	2867	2707	46.44	0.191
8	18.4	-0.2	-2.8	23.1	4548	2893	2721	47.16	0.192
9	20.4	-0.2	-2.9	23.2	4573	2909	2744	47.76	0.191
10	22.4	-0.2	-2.7	23.3	4619	2921	2770	48.54	0.194
11	24.4	-0.2	-2.7	23.3	4657	2935	2788	49.19	0.197
12	26.4	-0.2	-2.9	23.3	4660	2957	2803	49.59	0.191
13	28.4	-0.2	-3.4	23.3	4702	2960	2820	50.16	0.196
14	30.4	-0.2	-3.2	23.3	4702	2964	2830	50.31	0.194

Observed Velocities and Moduli for File Middle_Bakken-W96-10345V45-velocity									
Event	Conf	Pore	Diff	Temp	V_p	$V_s^{(1)}$	$V_s^{(2)}$	Young's Modulus	Poisson's Ratio
	MPa	MPa	MPa	°C	m/s	m/s	m/s	GPa	
0	2.4	-0.2	-1.7	23.6	3900	2601	2544	37.33	0.115
1	4.4	-0.2	-1.7	23.7	3964	2613	2553	38.18	0.131
2	6.4	-0.2	-2.2	23.7	4053	2639	2569	39.41	0.149
3	8.4	-0.2	-2.1	23.8	4076	2649	2602	39.95	0.145
4	10.4	-0.2	-2.4	23.9	4091	2678	2629	40.50	0.137
5	12.4	-0.2	-2.5	24.5	4170	2687	2651	41.56	0.153
6	14.4	-0.2	-2.5	24.6	4239	2710	2674	42.61	0.162
7	16.4	-0.2	-2.9	24.6	4272	2727	2693	43.23	0.163
8	18.4	-0.2	-2.8	24.6	4314	2741	2707	43.87	0.168
9	20.4	-0.2	-2.9	24.7	4345	2764	2719	44.47	0.169
10	22.4	-0.2	-2.9	24.7	4406	2771	2736	45.25	0.180
11	24.4	-0.2	-3.1	24.3	4442	2783	2746	45.78	0.184
12	26.4	-0.2	-3.1	24.4	4451	2803	2760	46.18	0.180
13	28.4	-0.2	-3.4	24.4	4484	2816	2769	46.69	0.183
14	30.3	-0.2	-3.4	24.4	4530	2823	2782	47.29	0.190

Observed Velocities and Moduli for File Middle_Bakken-W96-10347.8H-Velocity									
Event	Conf	Pore	Diff	Temp	V_p	$V_s^{(1)}$	$V_s^{(2)}$	Young's Modulus	Poisson's Ratio
	MPa	MPa	MPa	°C	m/s	m/s	m/s	GPa	
0	2.5	-0.1	-0.4	23.1	4182	2604	2652	41.02	0.174
1	4.5	-0.1	-0.5	23.2	4235	2687	2670	42.35	0.167
2	6.5	-0.1	-0.9	23.4	4284	2675	2701	42.97	0.175
3	8.5	-0.1	-0.9	23.6	4354	2682	2708	43.71	0.189
4	10.5	-0.2	-0.9	23.9	4390	2708	2729	44.46	0.189
5	12.5	-0.2	-1.2	24.5	4427	2718	2743	45.01	0.193
6	14.5	-0.2	-1.1	24.7	4491	2737	2762	45.91	0.200
7	16.6	-0.2	-1.1	24.3	4534	2759	2779	46.66	0.203
8	18.5	-0.2	-1.4	24.5	4541	2764	2791	46.89	0.201
9	20.5	-0.2	-1.2	24.7	4568	2779	2806	47.41	0.202
10	22.4	-0.2	-1.7	24.7	4628	2791	2816	48.13	0.210
11	24.5	-0.2	-1.9	24.9	4633	2808	2836	48.56	0.205
12	26.5	-0.2	-1.7	25.1	4674	2817	2847	49.10	0.210
13	28.5	-0.2	-2.1	25.5	4721	2819	2854	49.57	0.218
14	30.5	-0.2	-1.9	25.3	4700	2836	2859	49.65	0.210

Observed Velocities and Moduli for File Middle_Bakken-W96-10347H-velocity									
Event	Conf	Pore	Diff	Temp	V_p	$V_s^{(1)}$	$V_s^{(2)}$	Young's Modulus	Poisson's Ratio
	MPa	MPa	MPa	°C	m/s	m/s	m/s	GPa	
0	2.4	-0.2	-1.7	26.5	4262	2634	2695	42.19	0.179
1	4.4	-0.2	-1.5	26.5	4294	2660	2703	42.78	0.180
2	6.5	-0.2	-1.7	26.6	4346	2707	2716	43.77	0.181
3	8.4	-0.2	-1.8	26.7	4422	2738	2729	44.84	0.191
4	10.5	-0.2	-1.7	26.7	4482	2752	2745	45.64	0.199
5	12.4	-0.2	-2.4	26.8	4491	2766	2772	46.12	0.193
6	14.4	-0.2	-2.2	26.9	4557	2794	2779	47.01	0.201
7	16.5	-0.2	-2.1	26.9	4572	2800	2801	47.42	0.200
8	18.4	-0.2	-2.8	27.0	4591	2815	2809	47.82	0.200
9	20.5	-0.2	-2.5	27.0	4601	2830	2817	48.13	0.198
10	22.4	-0.2	-2.7	27.0	4643	2830	2830	48.62	0.204
11	24.5	-0.2	-2.5	27.1	4651	2837	2848	48.94	0.202
12	26.4	-0.2	-2.7	27.1	4661	2833	2854	49.05	0.204
13	28.5	-0.2	-2.7	27.1	4676	2840	2863	49.34	0.204
14	30.4	-0.2	-2.9	27.1	4693	2813	2875	49.32	0.210

Observed Velocities and Moduli for File Middle_Bakken-W96-10356.6H-velocity									
Event	Conf	Pore	Diff	Temp	V_p	$V_s^{(1)}$	$V_s^{(2)}$	Young's Modulus	Poisson's Ratio
	MPa	MPa	MPa	°C	m/s	m/s	m/s	GPa	
0	2.4	-0.2	-1.7	26.6	4111	2627	2166	35.97	0.243
1	4.4	-0.2	-1.8	26.8	4203	2651	2183	36.89	0.253
2	6.5	-0.2	-1.7	27.0	4237	2674	2205	37.55	0.252
3	8.4	-0.2	-2.1	27.0	4301	2687	2228	38.28	0.258
4	10.4	-0.2	-1.9	27.1	4310	2701	2247	38.69	0.254
5	12.5	-0.2	-1.8	27.2	4324	2729	2275	39.39	0.248
6	14.4	-0.2	-2.2	27.3	4345	2735	2297	39.81	0.248
7	16.4	-0.2	-2.5	27.3	4396	2757	2317	40.56	0.250
8	18.4	-0.2	-2.1	27.3	4402	2771	2335	40.95	0.247
9	20.4	-0.2	-2.8	27.3	4418	2771	2349	41.20	0.247
10	22.4	-0.2	-2.7	27.4	4438	2780	2367	41.61	0.247
11	24.4	-0.2	-2.8	27.4	4489	2794	2380	42.21	0.251
12	26.4	-0.2	-2.5	27.5	4507	2801	2398	42.60	0.251
13	28.4	-0.2	-2.9	27.4	4543	2810	2410	43.04	0.254
14	30.4	-0.2	-2.9	27.5	4568	2815	2421	43.37	0.255

Observed Velocities and Moduli for File Middle_Bakken-w96-10307.5H-velocity									
Event	Conf	Pore	Diff	Temp	V_p	$V_s^{(1)}$	$V_s^{(2)}$	Young's Modulus	Poisson's Ratio
	MPa	MPa	MPa	°C	m/s	m/s	m/s	GPa	
0	2.5	-0.2	-1.7	19.4	4580	2713	2797	48.38	0.217
1	4.5	-0.2	-1.8	19.9	4583	2730	2831	48.97	0.209
2	6.5	-0.2	-1.7	20.3	4618	2744	2834	49.44	0.213
3	8.4	-0.2	-2.1	20.3	4637	2766	2858	50.10	0.209
4	10.5	-0.2	-1.8	21.0	4721	2791	2873	51.23	0.219
5	12.5	-0.2	-2.1	20.6	4723	2810	2890	51.66	0.214
6	14.4	-0.2	-2.2	20.6	4762	2827	2905	52.34	0.216
7	16.5	-0.2	-2.5	21.3	4841	2844	2926	53.41	0.225
8	18.4	-0.2	-2.4	20.9	4864	2862	2940	53.97	0.224
9	20.5	-0.2	-2.5	20.9	4911	2879	2959	54.78	0.227
10	22.4	-0.2	-2.8	21.5	4911	2890	2962	54.95	0.225
11	24.4	-0.2	-2.9	21.2	4950	2907	2983	55.72	0.226
12	26.4	-0.2	-2.9	21.2	4999	2918	2989	56.31	0.232
13	28.5	-0.2	-3.2	21.8	5057	2940	3002	57.19	0.236
14	30.4	-0.2	-3.2	21.4	5152	2947	3027	58.29	0.247

Observed Velocities and Moduli for File Middle_Bakken-w96-10336V-velocity									
Event	Conf	Pore	Diff	Temp	V_p	$V_s^{(1)}$	$V_s^{(2)}$	Young's Modulus	Poisson's Ratio
	MPa	MPa	MPa	°C	m/s	m/s	m/s	GPa	
0	2.4	-0.2	-1.7	24.9	3969	2689	2679	39.01	0.079
1	4.3	-0.2	-2.1	25.0	3975	2696	2708	39.23	0.071
2	6.4	-0.2	-1.7	25.2	3999	2717	2716	39.70	0.072
3	8.3	-0.2	-2.1	25.2	4064	2727	2736	40.75	0.088
4	10.4	-0.2	-2.2	25.3	4123	2743	2738	41.63	0.104
5	12.4	-0.2	-1.8	25.9	4157	2764	2761	42.32	0.105
6	14.3	-0.2	-2.4	25.5	4170	2777	2773	42.62	0.103
7	16.4	-0.2	-2.1	25.6	4235	2797	2799	43.73	0.113
8	18.4	-0.2	-2.5	25.7	4265	2809	2811	44.26	0.116
9	20.4	-0.2	-2.5	25.7	4296	2825	2828	44.85	0.118
10	22.4	-0.2	-2.5	25.8	4330	2837	2839	45.42	0.123
11	24.4	-0.2	-2.5	26.4	4376	2856	2846	46.16	0.131
12	26.3	-0.2	-3.2	26.4	4436	2863	2860	47.01	0.144
13	28.4	-0.2	-2.9	26.5	4472	2872	2874	47.59	0.149
14	30.3	-0.2	-3.4	26.1	4497	2881	2889	48.06	0.150

Observed Velocities and Moduli for File w16771-10422-velocity									
Event	Conf	Pore	Diff	Temp	V_p	$V_s^{(1)}$	$V_s^{(2)}$	Young's Modulus	Poisson's Ratio
	MPa	MPa	MPa	°C	m/s	m/s	m/s	GPa	
0	50.5	-0.2	-1.8	26.8	6034	3371	3462	77.61	0.264
1	45.4	-0.2	-2.0	26.2	5873	3388	3408	75.82	0.248
2	40.4	-0.2	-1.7	25.6	5926	3354	3408	75.68	0.259
3	35.4	-0.2	-1.3	25.3	5873	3337	3373	74.47	0.258
4	30.4	-0.2	-1.7	24.9	5771	3354	3391	74.23	0.241
5	25.4	-0.2	-1.3	24.7	5822	3271	3339	72.52	0.262
6	20.4	-0.2	-1.3	24.4	5771	3271	3289	71.38	0.261
7	15.4	-0.2	-1.3	24.0	5623	3239	3257	69.34	0.250
8	10.4	-0.2	-0.8	23.3	5394	3161	3194	65.55	0.234
9	5.4	-0.2	-0.8	22.9	5265	3087	3133	62.68	0.232

Observed Velocities and Moduli for File w16771-10426.8-velocity									
Event	Conf	Pore	Diff	Temp	V_p	$V_s^{(1)}$	$V_s^{(2)}$	Young's Modulus	Poisson's Ratio
	MPa	MPa	MPa	°C	m/s	m/s	m/s	GPa	
0	50.5	-0.2	-2.1	26.0	5189	3095	2965	59.03	0.241
1	45.4	-0.2	-2.1	25.4	5146	3095	2951	58.53	0.237
2	40.5	-0.1	-1.7	24.9	5276	3095	2979	59.83	0.252
3	35.4	-0.2	-1.7	24.6	5189	3080	2951	58.65	0.245
4	30.4	-0.2	-1.7	24.4	5232	3065	2910	58.17	0.258
5	25.4	-0.2	-1.6	24.2	5104	3080	2937	57.85	0.234
6	20.4	-0.2	-1.3	23.9	5104	3065	2910	57.30	0.239
7	15.5	-0.2	-0.7	22.5	5189	3050	2910	57.68	0.254
8	10.4	-0.2	-0.8	22.0	5232	3065	2883	57.79	0.261
9	5.4	-0.2	-0.4	21.4	5104	3065	2870	56.78	0.245

Observed Velocities and Moduli for File Middle_Bakken-w96-10348V-velocity									
Event	Conf	Pore	Diff	Temp	V_p	$V_s^{(1)}$	$V_s^{(2)}$	Young's Modulus	Poisson's Ratio
	MPa	MPa	MPa	°C	m/s	m/s	m/s	GPa	
0	2.4	-0.2	-1.7	28.0	3841	2625	2663	37.28	0.050
1	4.4	-0.2	-1.9	28.0	3884	2648	2668	38.03	0.060
2	6.4	-0.2	-2.1	28.1	3925	2664	2676	38.73	0.069
3	8.4	-0.2	-2.4	28.2	3992	2671	2683	39.73	0.091
4	10.4	-0.2	-2.2	28.3	4025	2686	2706	40.36	0.093
5	12.4	-0.2	-2.4	28.4	4060	2709	2706	40.95	0.100
6	14.4	-0.2	-2.5	28.6	4094	2718	2723	41.53	0.105
7	16.4	-0.2	-2.4	28.6	4165	2729	2741	42.60	0.121
8	18.4	-0.2	-2.8	28.6	4165	2742	2747	42.71	0.116
9	20.5	-0.2	-2.5	28.3	4208	2762	2759	43.44	0.122
10	22.4	-0.2	-2.9	28.2	4287	2767	2780	44.55	0.140
11	24.5	-0.2	-2.5	28.3	4292	2778	2790	44.76	0.137
12	26.4	-0.2	-2.7	28.3	4335	2789	2800	45.40	0.144
13	28.4	-0.2	-2.7	28.3	4331	2794	2806	45.44	0.141
14	30.4	-0.2	-3.4	28.3	4349	2809	2815	45.82	0.141

Observed Velocities and Moduli for File w16771-10431-velocity									
Event	Conf	Pore	Diff	Temp	V_p	$V_s^{(1)}$	$V_s^{(2)}$	Young's Modulus	Poisson's Ratio
	MPa	MPa	MPa	°C	m/s	m/s	m/s	GPa	
0	50.4	-0.2	-2.5	25.9	5480	3074	3062	61.53	0.272
1	45.4	-0.2	-2.1	24.9	5573	3103	3076	62.71	0.278
2	40.4	-0.2	-2.0	23.7	5303	3074	3048	60.21	0.250
3	35.5	-0.2	-1.3	22.8	5303	3060	3048	60.02	0.252
4	30.4	-0.2	-1.7	22.0	5303	3046	3048	59.82	0.254
5	25.5	-0.2	-1.0	22.0	5390	3074	3019	60.36	0.265
6	20.5	-0.2	-1.3	21.0	5260	3032	3019	58.94	0.253
7	15.4	-0.2	-1.1	20.5	5303	3032	2978	58.65	0.264
8	10.4	-0.2	-1.0	20.0	5260	3004	3006	58.38	0.258
9	5.5	-0.1	-0.3	19.6	5136	2990	2951	56.63	0.249

Observed Velocities and Moduli for File w16771-10432-velocity									
Event	Conf	Pore	Diff	Temp	V_p	$V_s^{(1)}$	$V_s^{(2)}$	Young's Modulus	Poisson's Ratio
	MPa	MPa	MPa	°C	m/s	m/s	m/s	GPa	
0	50.4	-0.2	2.6	27.1	5073	2768	2895	52.08	0.274
1	45.5	-0.2	3.0	26.1	4985	2755	2924	51.81	0.260
2	40.4	-0.2	2.6	25.4	4942	2768	2910	51.53	0.254
3	35.4	-0.2	2.7	24.8	5073	2755	2895	51.90	0.275
4	30.4	-0.2	3.0	24.4	4942	2768	2910	51.53	0.254
5	25.5	-0.2	2.9	24.0	4985	2755	2910	51.62	0.262
6	20.5	-0.2	3.1	23.4	5118	2742	2895	51.95	0.282
7	15.4	-0.2	2.9	22.6	5029	2755	2895	51.67	0.269
8	10.4	-0.2	2.7	21.4	5029	2703	2881	50.78	0.277
9	5.4	-0.2	2.9	21.0	4985	2716	2881	50.72	0.270

Observed Velocities and Moduli for File w16771-10436-2-velocity									
Event	Conf	Pore	Diff	Temp	V_p	$V_s^{(1)}$	$V_s^{(2)}$	Young's Modulus	Poisson's Ratio
	MPa	MPa	MPa	°C	m/s	m/s	m/s	GPa	
0	50.6	-0.1	-1.7	23.0	5742	3195	3316	69.88	0.263
1	45.5	-0.1	-1.4	22.8	5742	3195	3334	70.16	0.261
2	40.5	-0.2	-1.7	22.4	5638	3179	3316	68.91	0.252
3	35.5	-0.2	-1.4	22.1	5638	3147	3264	67.65	0.261
4	30.4	-0.2	-1.3	22.1	5638	3131	3281	67.66	0.261
5	25.5	-0.2	-1.3	21.6	5489	3115	3247	65.88	0.247
6	20.5	-0.1	-0.6	21.6	5348	3084	3214	63.91	0.235
7	15.4	-0.2	-0.8	21.1	5258	3054	3181	62.35	0.229
8	10.5	-0.1	-0.4	20.6	5214	2981	3086	59.76	0.244
9	5.5	-0.2	-0.4	20.0	4965	2871	2983	55.17	0.234

Observed Velocities and Moduli for File w16771-10436-velocity									
Event	Conf	Pore	Diff	Temp	V_p	$V_s^{(1)}$	$V_s^{(2)}$	Young's Modulus	Poisson's Ratio
	MPa	MPa	MPa	°C	m/s	m/s	m/s	GPa	
0	50.5	-0.2	-2.3	25.8	5912	4062	3139	80.62	0.205
1	45.5	-0.2	-1.7	25.3	5975	4062	3156	81.51	0.213
2	40.4	-0.2	-2.1	24.8	5791	3948	3139	77.80	0.201
3	35.4	-0.2	-1.8	24.5	5791	4033	3104	78.45	0.194
4	30.4	-0.2	-1.7	24.2	5618	3976	3104	75.70	0.171
5	25.5	-0.2	-1.3	24.0	5732	3894	3037	75.10	0.212
6	20.5	-0.2	-1.3	23.9	5791	3690	2973	71.74	0.253
7	15.5	-0.2	-0.4	22.7	5352	3666	2942	67.15	0.192
8	10.4	-0.2	-0.8	21.2	5156	3596	2868	63.41	0.176
9	5.4	-0.2	-0.4	20.5	4725	3401	3445	57.30	-0.052

Observed Velocities and Moduli for File w16771-10437-velocity									
Event	Conf	Pore	Diff	Temp	V_p	$V_s^{(1)}$	$V_s^{(2)}$	Young's Modulus	Poisson's Ratio
	MPa	MPa	MPa	°C	m/s	m/s	m/s	GPa	
0	50.5	-0.1	-1.7	26.6	5310	3029	3031	59.85	0.259
1	45.5	-0.2	-1.7	26.0	5359	3013	3000	59.48	0.270
2	40.5	-0.2	-1.4	25.1	5310	3029	3015	59.63	0.260
3	35.4	-0.2	-1.7	24.7	5165	3029	3015	58.65	0.240
4	30.5	-0.2	-1.4	24.4	5261	3013	2968	58.43	0.261
5	25.4	-0.2	-1.6	24.2	5359	2982	2856	56.90	0.289
6	20.5	-0.2	-0.8	24.0	5213	3013	2984	58.35	0.253
7	15.5	-0.2	-0.7	23.8	5074	2998	2953	56.77	0.238
8	10.4	-0.2	-0.8	23.5	5029	2936	2968	55.84	0.237
9	5.5	-0.1	-0.4	23.3	4817	2921	2938	53.64	0.207

Observed Velocities and Moduli for File w16771-10441.6-velocity									
Event	Conf	Pore	Diff	Temp	V_p	$V_s^{(1)}$	$V_s^{(2)}$	Young's Modulus	Poisson's Ratio
	MPa	MPa	MPa	°C	m/s	m/s	m/s	GPa	
0	50.4	-0.2	-2.0	25.9	4298	2517	2628	41.53	0.221
1	45.4	-0.2	-1.7	25.0	4231	2505	2628	40.93	0.209
2	40.5	-0.2	-1.3	24.3	4298	2505	2628	41.40	0.223
3	35.4	-0.2	-1.3	24.1	4231	2494	2603	40.57	0.215
4	30.4	-0.2	-1.3	23.5	4231	2505	2603	40.68	0.213
5	25.4	-0.2	-1.3	23.0	4198	2482	2578	39.97	0.215
6	20.4	-0.2	-0.8	22.4	4264	2505	2566	40.53	0.227
7	15.4	-0.2	-0.8	21.4	4231	2482	2566	40.07	0.224
8	10.4	-0.1	-0.4	20.8	4134	2460	2554	39.06	0.209
9	5.4	-0.2	-0.4	21.5	4072	2449	2590	38.82	0.190

Observed Velocities and Moduli for File w16771-10443-velocity									
Event	Conf	Pore	Diff	Temp	V_p	$V_s^{(1)}$	$V_s^{(2)}$	Young's Modulus	Poisson's Ratio
	MPa	MPa	MPa	°C	m/s	m/s	m/s	GPa	
0	50.5	-0.2	-5.6	24.6	5679	3260	3180	68.62	0.263
1	45.5	-0.2	-5.5	23.7	5629	3276	3149	68.06	0.258
2	40.4	-0.2	-5.6	22.8	5943	3260	3118	69.16	0.298
3	35.4	-0.2	-5.2	22.3	6056	3243	3118	69.41	0.310
4	30.5	-0.1	-4.8	22.1	5679	3227	3118	67.15	0.273
5	25.5	-0.2	-4.8	21.4	5782	3243	3073	67.28	0.287
6	20.5	-0.1	-4.3	21.2	5580	3194	2987	64.00	0.279
7	15.5	-0.1	-4.2	21.3	5484	3163	3001	63.17	0.269
8	10.4	-0.2	-4.3	20.5	5216	3147	2879	59.44	0.250
9	5.5	-0.1	-3.5	20.3	5051	3057	2755	55.43	0.253

Observed Velocities and Moduli for File w16771-10449-velocity									
Event	Conf	Pore	Diff	Temp	V_p	$V_s^{(1)}$	$V_s^{(2)}$	Young's Modulus	Poisson's Ratio
	MPa	MPa	MPa	°C	m/s	m/s	m/s	GPa	
0	50.5	-0.2	-5.3	27.9	5011	2893	2596	49.39	0.286
1	45.4	-0.2	-5.3	27.1	5011	2855	2575	48.58	0.292
2	40.4	-0.2	-5.6	26.6	4935	2880	2575	48.57	0.280
3	35.4	-0.2	-4.8	26.3	4935	2855	2596	48.51	0.281
4	30.4	-0.2	-5.2	25.9	4898	2880	2575	48.38	0.275
5	25.4	-0.2	-4.8	25.5	4935	2843	2565	47.93	0.285
6	20.4	-0.2	-4.8	25.2	4935	2893	2565	48.61	0.280
7	15.4	-0.2	-4.3	23.8	4935	2868	2565	48.27	0.283
8	10.4	-0.2	-3.9	23.4	4972	2855	2565	48.27	0.289
9	5.4	-0.2	-3.8	23.0	4935	2868	2535	47.87	0.286

Observed Velocities and Moduli for File w16771-10452-velocity									
Event	Conf	Pore	Diff	Temp	V_p	$V_s^{(1)}$	$V_s^{(2)}$	Young's Modulus	Poisson's Ratio
	MPa	MPa	MPa	°C	m/s	m/s	m/s	GPa	
0	50.4	-0.2	-5.6	27.8	5310	3085	3213	63.60	0.229
1	45.4	-0.2	-5.6	26.9	5403	3085	3213	64.33	0.243
2	40.4	-0.2	-5.5	26.6	5403	3100	3196	64.30	0.243
3	35.4	-0.2	-5.2	26.4	5264	3069	3163	62.36	0.230
4	30.3	-0.2	-5.2	26.2	5219	3100	3147	62.18	0.221
5	25.4	-0.2	-4.9	26.1	5310	3069	3147	62.50	0.239
6	20.5	-0.2	-4.3	26.0	5219	3085	3163	62.19	0.221
7	15.4	-0.2	-3.9	25.9	5310	3054	3163	62.51	0.239
8	10.4	-0.2	-3.9	25.8	5219	2957	3131	60.08	0.242
9	5.4	-0.2	-3.6	25.8	5175	3069	3131	61.21	0.220

Observed Velocities and Moduli for File w16771-10456-2-velocity									
Event	Conf	Pore	Diff	Temp	V_p	$V_s^{(1)}$	$V_s^{(2)}$	Young's Modulus	Poisson's Ratio
	MPa	MPa	MPa	°C	m/s	m/s	m/s	GPa	
0	50.5	-0.2	-1.8	27.5	4511	2808	2833	48.02	0.179
1	45.5	-0.1	-1.7	26.9	4482	2808	2809	47.52	0.177
2	40.4	-0.2	-2.0	26.4	4453	2797	2809	47.14	0.172
3	35.4	-0.2	-1.4	26.1	4368	2819	2798	46.35	0.148
4	30.4	-0.2	-1.3	25.8	4396	2785	2798	46.37	0.162
5	25.5	-0.2	-1.3	25.5	4453	2797	2809	47.14	0.172
6	20.5	-0.2	-1.0	25.3	4396	2774	2798	46.27	0.164
7	15.4	-0.2	-1.0	25.1	4396	2763	2775	45.98	0.171
8	10.4	-0.2	-0.7	24.9	4424	2785	2798	46.65	0.169
9	5.4	-0.1	-0.3	24.8	4453	2752	2775	46.41	0.187

Observed Velocities and Moduli for File w16771-10456-velocity									
Event	Conf	Pore	Diff	Temp	V_p	$V_s^{(1)}$	$V_s^{(2)}$	Young's Modulus	Poisson's Ratio
	MPa	MPa	MPa	°C	m/s	m/s	m/s	GPa	
0	50.5	-0.2	-2.1	26.1	4917	2998	3042	55.68	0.197
1	45.5	-0.1	-1.7	24.5	4993	2984	3014	55.86	0.218
2	40.5	-0.2	-2.1	23.2	4879	3012	3028	55.33	0.189
3	35.5	-0.1	-1.7	22.8	4842	3012	3042	55.11	0.179
4	30.5	-0.1	-1.3	21.6	4879	3012	3014	55.18	0.192
5	25.6	-0.1	-1.3	21.2	4954	3026	3028	56.17	0.202
6	20.5	-0.2	-1.3	21.2	4954	2984	3014	55.54	0.211
7	15.5	-0.2	-0.8	20.3	4954	2984	3014	55.54	0.211
8	10.4	-0.2	-0.8	19.9	4806	2970	3000	53.89	0.186
9	5.5	-0.1	-0.4	19.7	4879	2984	2986	54.57	0.201

Observed Velocities and Moduli for File w16771-10456.5-velocity									
Event	Conf	Pore	Diff	Temp	V_p	$V_s^{(1)}$	$V_s^{(2)}$	Young's Modulus	Poisson's Ratio
	MPa	MPa	MPa	°C	m/s	m/s	m/s	GPa	
0	50.5	-0.2	-2.3	25.1	4888	2926	2914	52.33	0.223
1	45.5	-0.2	-2.3	24.3	4778	2926	2928	51.59	0.200
2	40.4	-0.2	-2.1	23.8	4743	2926	2914	51.14	0.195
3	35.4	-0.2	-2.0	23.4	4708	2926	2914	50.82	0.187
4	30.4	-0.2	-1.3	23.2	4639	2953	2928	50.53	0.164
5	25.5	-0.2	-1.4	22.9	4814	2940	2928	52.05	0.205
6	20.5	-0.2	-1.3	22.6	4673	2926	2914	50.49	0.180
7	15.5	-0.2	-0.6	22.2	4743	2940	2914	51.29	0.192
8	10.5	-0.1	-0.1	21.9	4743	2899	2928	51.01	0.197
9	5.4	-0.2	-0.1	21.6	4540	2899	2928	49.00	0.150

Observed Velocities and Moduli for File w16771-10460.5-velocity									
Event	Conf	Pore	Diff	Temp	V_p	$V_s^{(1)}$	$V_s^{(2)}$	Young's Modulus	Poisson's Ratio
	MPa	MPa	MPa	°C	m/s	m/s	m/s	GPa	
0	50.4	-0.2	-5.6	28.1	4773	2740	2955	50.01	0.224
1	45.4	-0.2	-5.2	27.2	4704	2740	2941	49.33	0.213
2	40.4	-0.2	-5.2	26.5	4704	2740	2941	49.33	0.213
3	35.4	-0.2	-5.2	26.0	4773	2740	2915	49.55	0.230
4	30.4	-0.2	-4.8	25.6	4773	2717	2902	49.13	0.235
5	25.4	-0.2	-4.6	25.1	4738	2706	2928	49.06	0.227
6	20.4	-0.2	-4.5	24.3	4773	2717	2915	49.28	0.233
7	15.4	-0.2	-4.3	24.1	4738	2717	2902	48.89	0.229
8	10.4	-0.2	-4.2	23.4	4670	2706	2902	48.27	0.218
9	5.4	-0.2	-3.6	24.0	4704	2706	2902	48.52	0.224

Observed Velocities and Moduli for File w16771-10463-velocity									
Event	Conf	Pore	Diff	Temp	V_p	$V_s^{(1)}$	$V_s^{(2)}$	Young's Modulus	Poisson's Ratio
	MPa	MPa	MPa	°C	m/s	m/s	m/s	GPa	
0	50.4	-0.2	-5.8	26.7	4985	3014	2756	52.98	0.248
1	45.4	-0.2	-5.8	26.3	4942	2999	2770	52.69	0.242
2	40.4	-0.2	-5.2	26.0	4985	2999	2770	52.97	0.248
3	35.4	-0.2	-5.0	25.8	4942	2968	2783	52.46	0.244
4	30.4	-0.2	-5.0	25.5	4942	2968	2743	51.96	0.249
5	25.4	-0.2	-4.8	25.2	4942	2999	2783	52.85	0.240
6	20.5	-0.2	-4.3	24.3	4942	2983	2797	52.83	0.240
7	15.4	-0.2	-4.1	23.2	4942	2999	2717	52.02	0.249
8	10.4	-0.2	-3.9	22.7	4985	2983	2756	52.59	0.252
9	5.4	-0.2	-3.5	23.2	4942	2937	2730	51.39	0.255

A.2.3 Biot's Coefficient

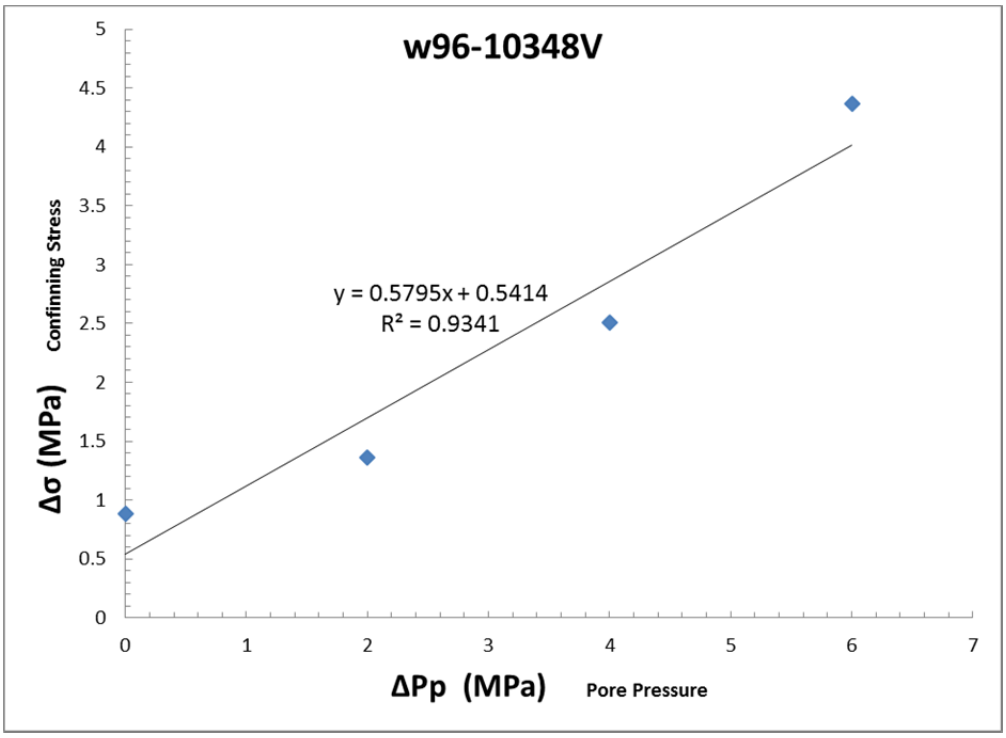

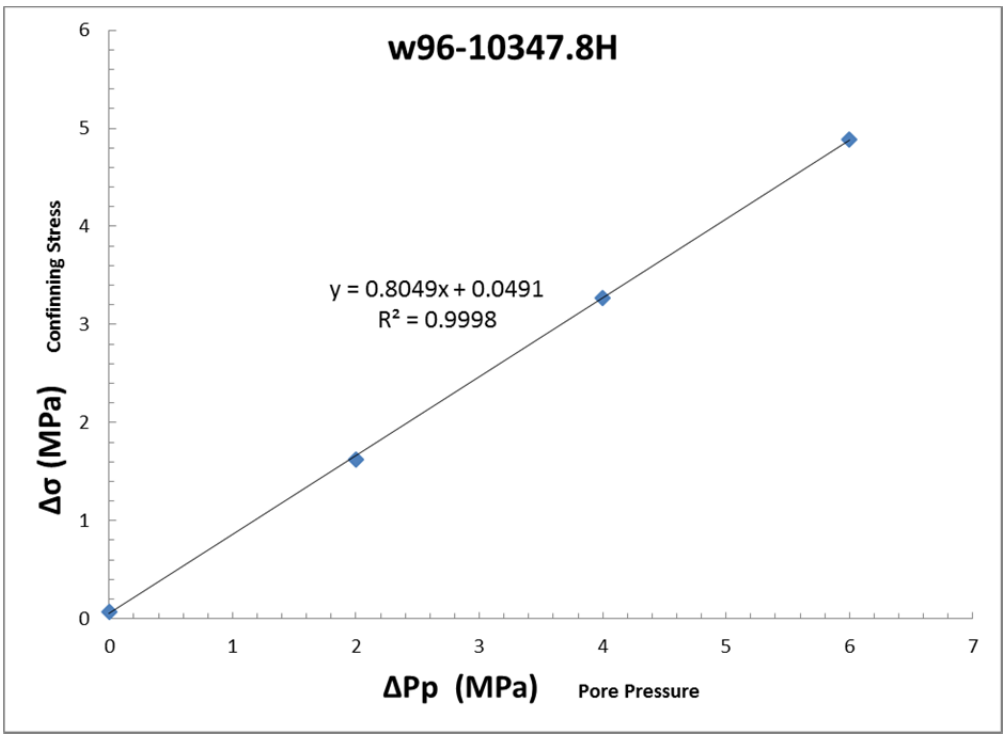

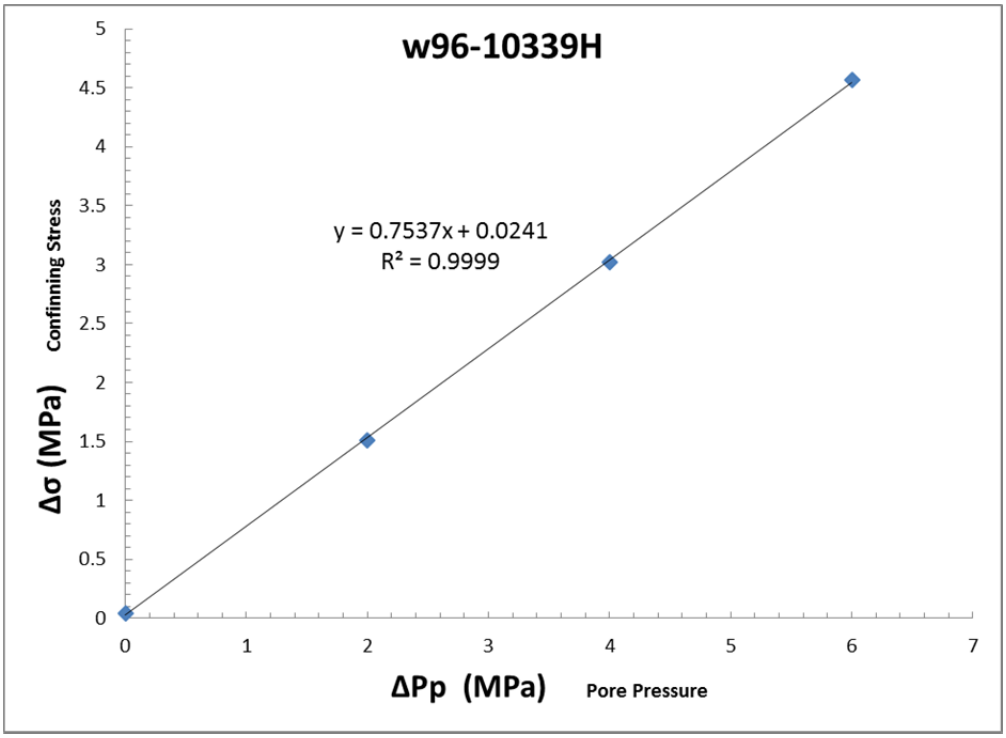
w96-10339H
y = 0.7537x + 0.0241
R² = 0.9999
Confinning Stress
Δσ (MPa)
ΔPp (MPa)
Pore Pressure
0
0.5
1
1.5
2
2.5
3
3.5
4
4.5
5
0
1
2
3
4
5
6
7

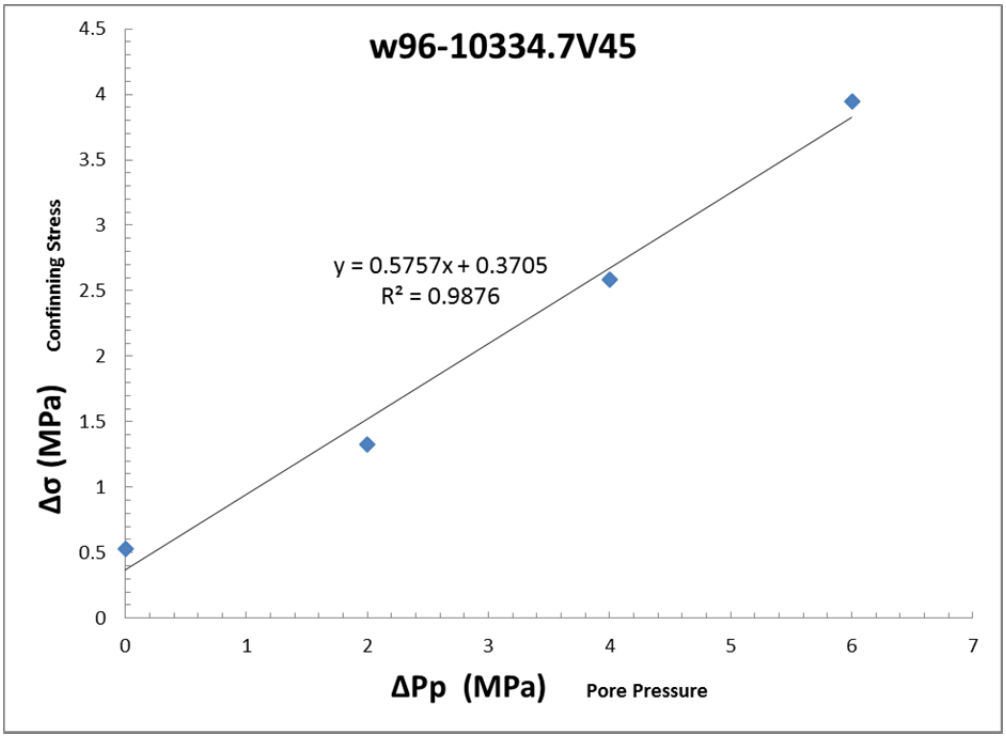
w96-10334.7V45
y = 0.5757x + 0.3705
R² = 0.9876
Confinning Stress
Δσ (MPa)
ΔPp (MPa)
Pore Pressure
0
0.5
1
1.5
2
2.5
3
3.5
4
4.5
0
1
2
3
4
5
6
7

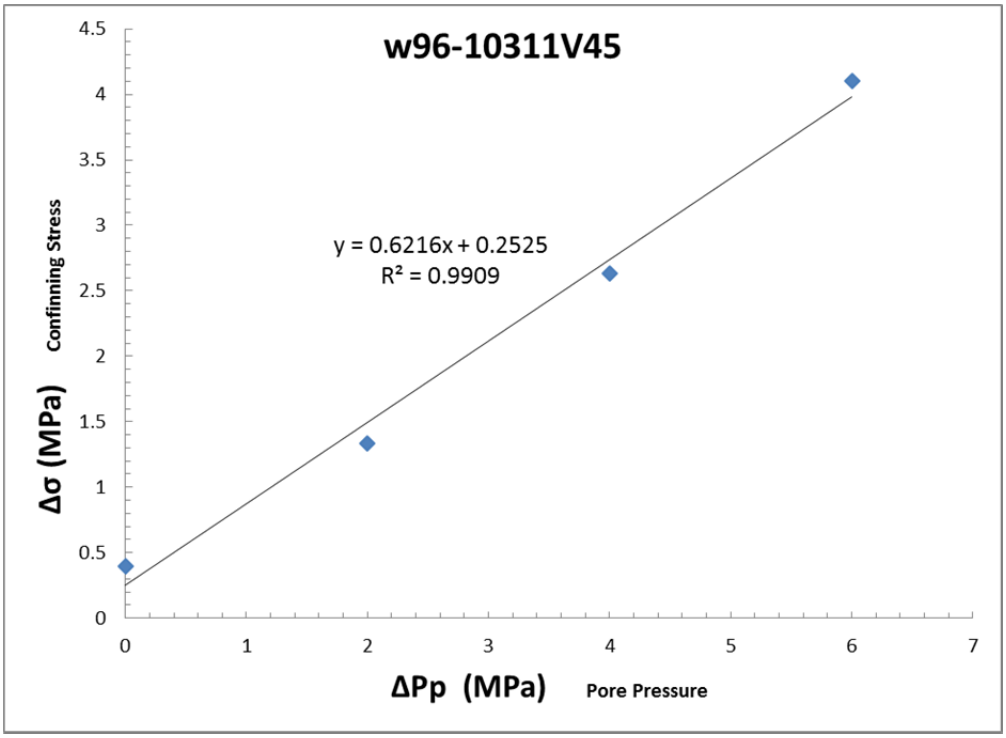
w96-10311V45
y = 0.6216x + 0.2525
R² = 0.9909
Confinning Stress
Δσ (MPa)
ΔPp (MPa)
Pore Pressure
0
0.5
1
1.5
2
2.5
3
3.5
4
4.5
0
1
2
3
4
5
6
7

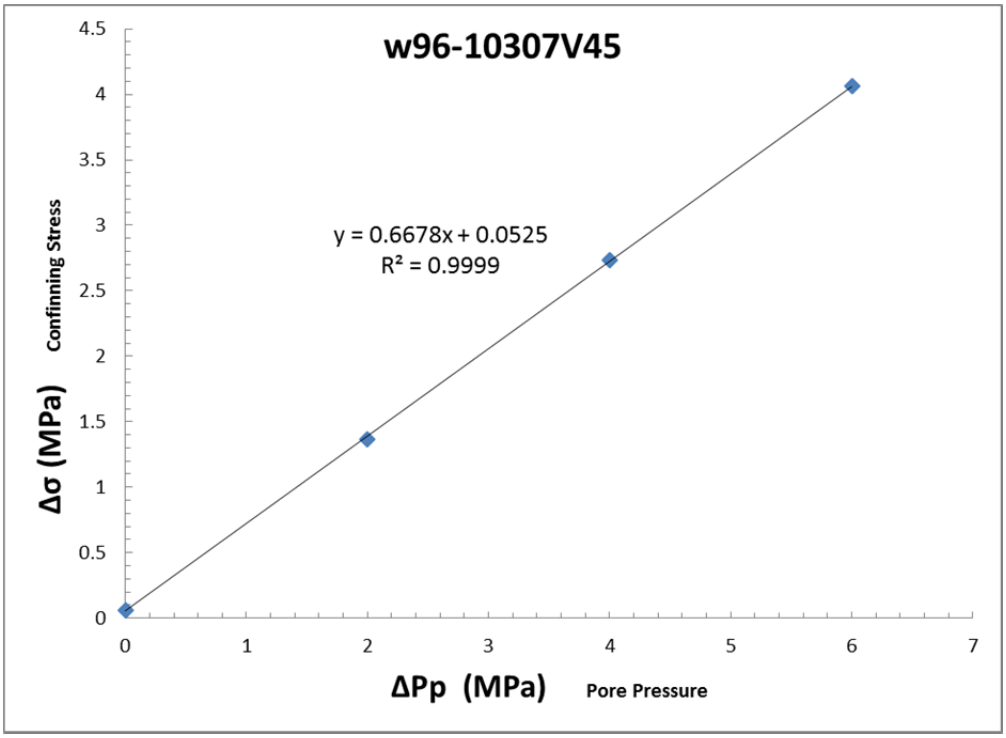
w96-10307V45
y = 0.6678x + 0.0525
R² = 0.9999
Confinning Stress
Δσ (MPa)
ΔPp (MPa)
Pore Pressure
0
0.5
1
1.5
2
2.5
3
3.5
4
4.5
0
1
2
3
4
5
6
7

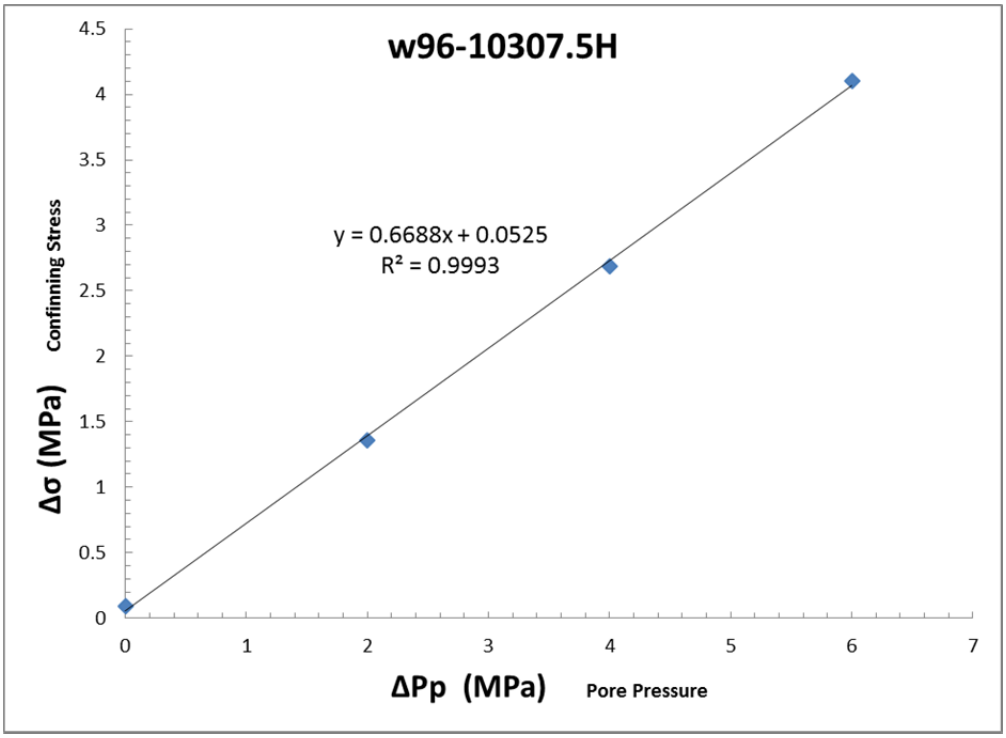
w96-10307.5H
y = 0.6688x + 0.0525
R² = 0.9993
Δσ (MPa) Confinning Stress
ΔPp (MPa) Pore Pressure
0
0.5
1
1.5
2
2.5
3
3.5
4
4.5
0
1
2
3
4
5
6
7

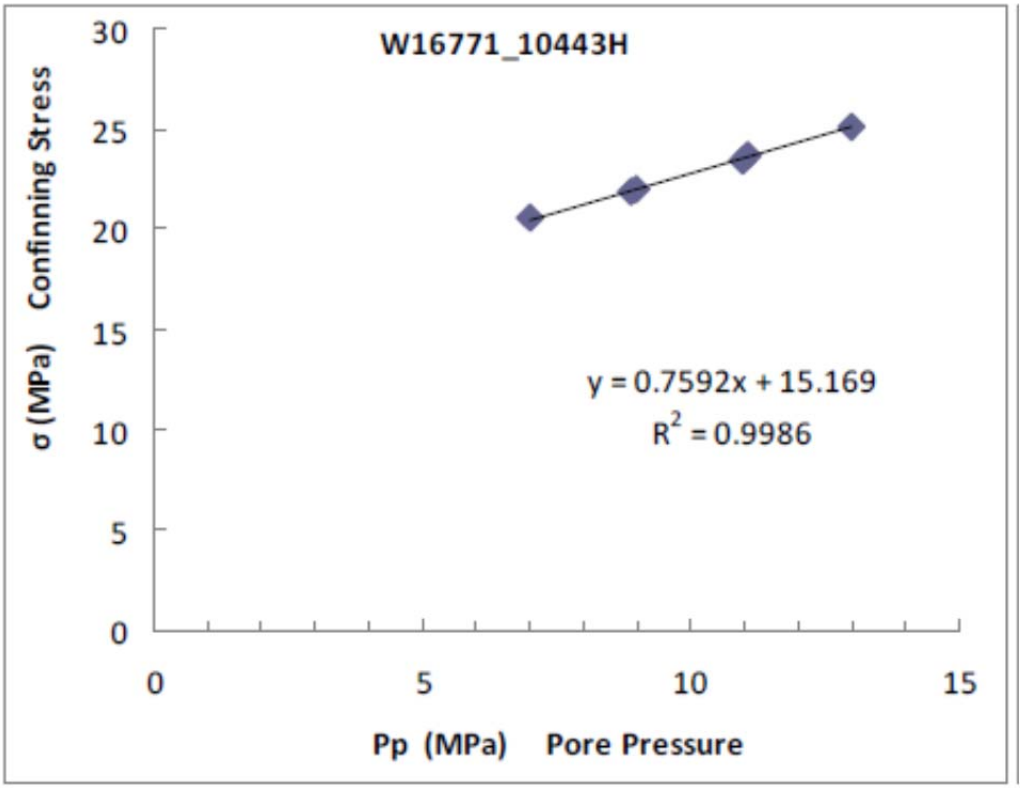
W16771_10443H
y = 0.7592x + 15.169
R² = 0.9986
σ (MPa) Confinning Stress
Pp (MPa) Pore Pressure
0
5
10
15
20
25
30
0
5
10
15

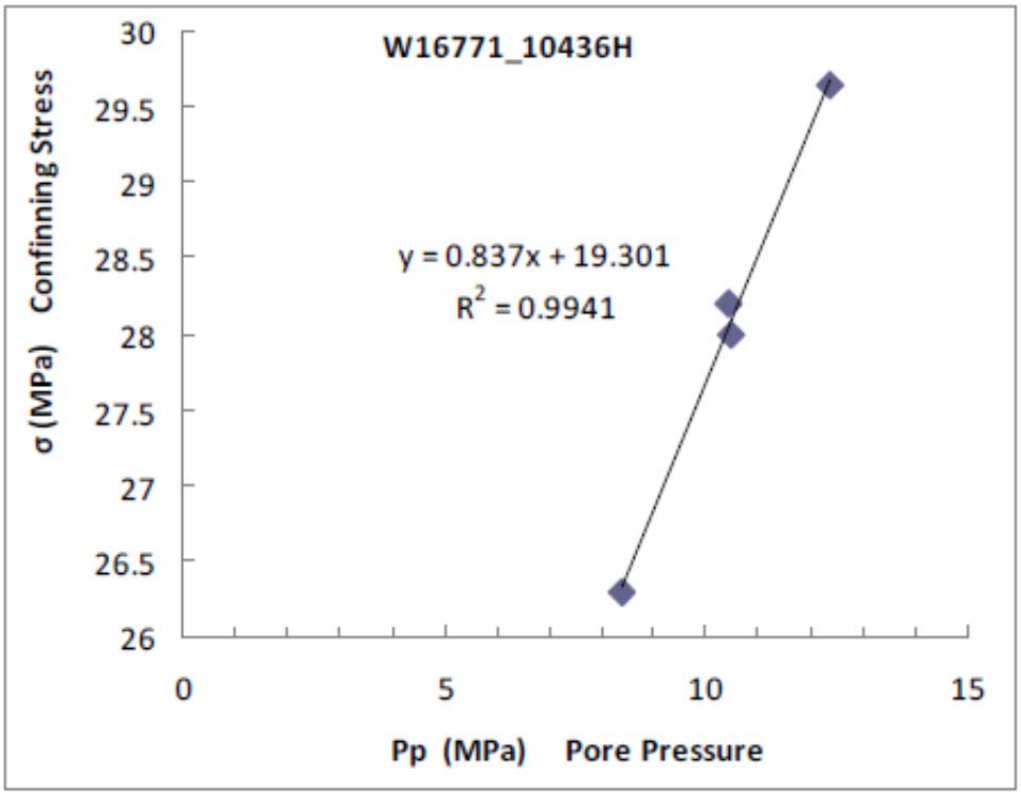
W16771_10436H
y = 0.837x + 19.301
R2 = 0.9941
σ (MPa) Confinning Stress
Pp (MPa) Pore Pressure
30
29.5
29
28.5
28
27.5
27
26.5
26
0
5
10
15

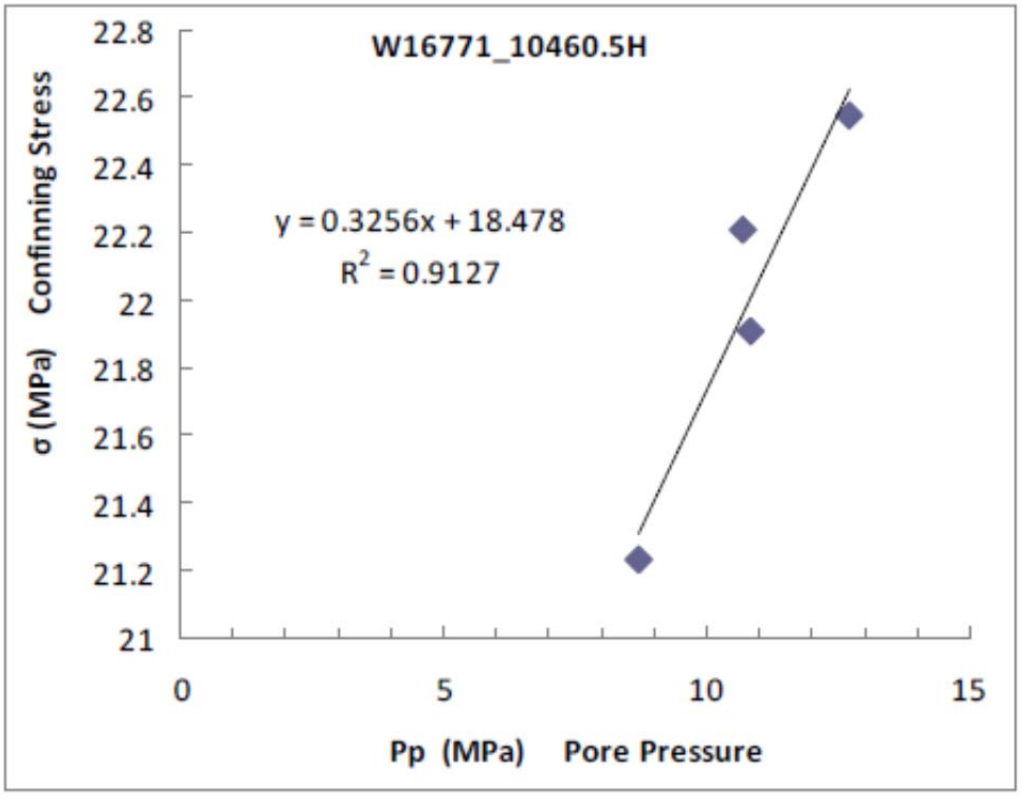
W16771_10460.5H
y = 0.3256x + 18.478
R2 = 0.9127
σ (MPa) Confinning Stress
Pp (MPa) Pore Pressure
22.8
22.6
22.4
22.2
22
21.8
21.6
21.4
21.2
21
0
5
10
15

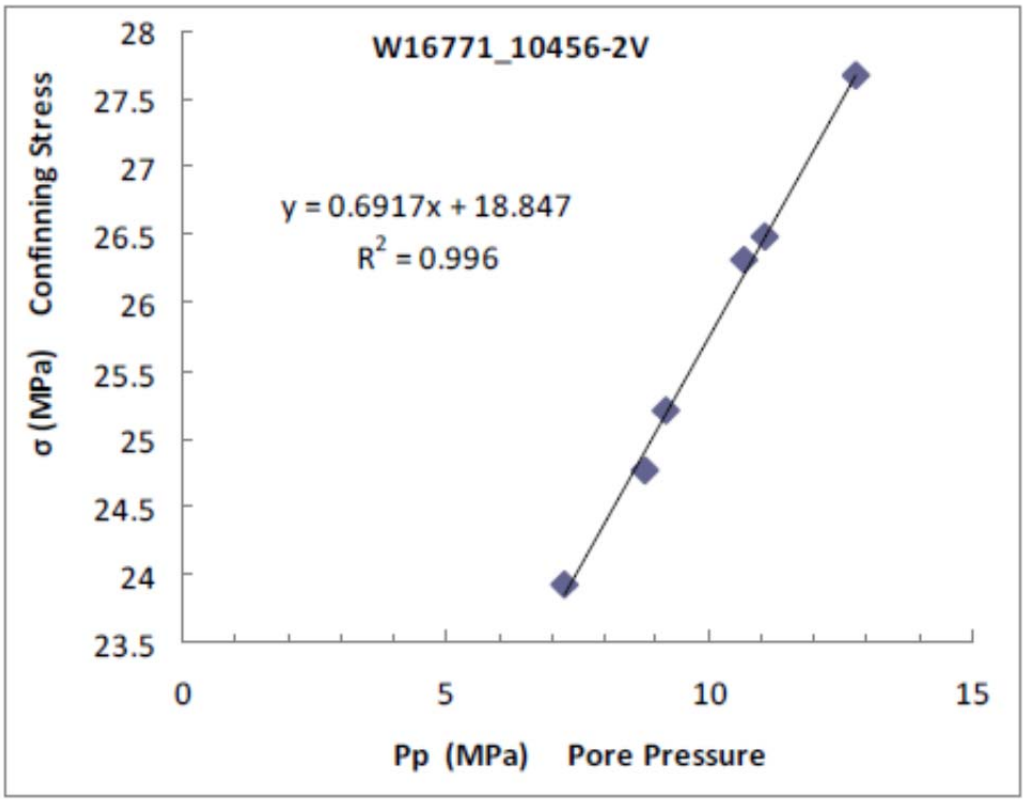

A.2.4 Static Moduli and Poisson's Ratio (Non-destructive)

Uniaxial Stress for File w16771-10463-uniaxial-stress									
Event	Conf	Pore	Diff	Temp	E	n	K	G	P
	MPa	MPa	MPa	°C	GPa		GPa	GPa	GPa
0	50.5	-0.2	41.5	31.6	73.73	0.020	25.60	36.15	73.79

Uniaxial Stress for File w16771-10460.5-uniaxial-stress									
Event	Conf	Pore	Diff	Temp	E	n	K	G	P
	MPa	MPa	MPa	°C	GPa		GPa	GPa	GPa
0	50.5	-0.2	23.5	31.3	81.05	0.051	30.10	38.55	81.50
1	50.4	-0.2	12.0	31.1	95.71	0.066	36.78	44.88	96.62

Uniaxial Stress for File w16771-10456.5-uniaxial-stress									
Event	Conf	Pore	Diff	Temp	E	n	K	G	P
	MPa	MPa	MPa	°C	GPa		GPa	GPa	GPa
0	50.4	-0.2	16.7	31.2	47.28	0.317	43.11	17.95	67.04
1	50.4	-0.2	13.3	31.0	53.16	0.343	56.53	19.79	82.91
2	50.5	-0.2	18.0	31.2	51.98	0.348	57.08	19.28	82.78

Uniaxial Stress for File w16771-10456-uniaxial-stress									
Event	Conf	Pore	Diff	Temp	E	n	K	G	P
	MPa	MPa	MPa	°C	GPa		GPa	GPa	GPa
0	50.4	-0.2	13.7	32.6	52.17	0.181	27.23	22.09	56.69
1	50.4	-0.2	19.7	32.3	56.16	0.177	28.97	23.86	60.78

Uniaxial Stress for File w16771-10456-2-uniaxial-stress									
Event	Conf	Pore	Diff	Temp	E	n	K	G	P
	MPa	MPa	MPa	°C	GPa		GPa	GPa	GPa
0	50.2	-0.2	15.8	31.5	80.52	0.151	38.43	34.99	85.08
1	50.2	-0.2	12.4	31.2	79.42	0.162	39.19	34.17	84.74

Uniaxial Stress for File w16771-10452-uniaxial-stress									
Event	Conf	Pore	Diff	Temp	E	n	K	G	P
	MPa	MPa	MPa	°C	GPa		GPa	GPa	GPa
0	50.5	-0.2	11.1	33.0	179.71	0.471	1044.58	61.07	1126.01
1	50.5	-0.2	15.8	32.8	191.50	0.462	831.84	65.51	919.18

Uniaxial Stress for File w16771-10449-uniaxial-stress									
Event	Conf	Pore	Diff	Temp	E	n	K	G	P
	MPa	MPa	MPa	°C	GPa		GPa	GPa	GPa
0	50.5	-0.2	17.5	28.6	38.39	1.104	-10.59	9.12	1.57
1	50.5	-0.2	13.3	28.8	58.13	0.289	45.94	22.54	76.00
2	50.4	-0.2	17.5	29.2	54.68	0.463	244.10	18.69	269.02

Uniaxial Stress for File w16771-10441.6-uniaxial-stress									
Event	Conf	Pore	Diff	Temp	E	n	K	G	P
	MPa	MPa	MPa	°C	GPa		GPa	GPa	GPa
0	49.6	-0.2	12.9	30.6	64.07	0.191	34.53	26.90	70.39
1	49.6	-0.2	18.0	30.9	70.61	0.190	37.90	29.68	77.48

Uniaxial Stress for File w16771-10437-uniaxial-stress									
Event	Conf	Pore	Diff	Temp	E	n	K	G	P
	MPa	MPa	MPa	°C	GPa		GPa	GPa	GPa
0	50.5	-0.2	17.1	27.9	86.09	-0.033	26.94	44.50	86.27
1	50.5	-0.2	13.3	27.9	93.11	-0.039	28.78	48.45	93.39
2	50.5	-0.2	18.0	28.6	81.14	-0.022	25.92	41.47	81.22
3	50.4	-0.2	12.9	30.4	91.17	-0.026	28.91	46.79	91.29

Uniaxial Stress for File w16771-10436-uniaxial-stress									
Event	Conf	Pore	Diff	Temp	E	n	K	G	P
	MPa	MPa	MPa	°C	GPa		GPa	GPa	GPa
0	50.5	-0.2	17.1	29.9	115.13	0.259	79.51	45.74	140.50
1	50.6	-0.2	13.7	29.9	110.54	0.231	68.60	44.88	128.45
2	50.6	-0.2	18.4	30.1	114.51	0.255	77.82	45.63	138.66

Uniaxial Stress for File w16771-10436-2-uniaxial-stress									
Event	Conf	Pore	Diff	Temp	E	n	K	G	P
	MPa	MPa	MPa	°C	GPa		GPa	GPa	GPa
0	50.5	-0.2	14.1	29.1	58.70	0.225	35.63	23.95	67.56
1	50.5	-0.2	9.9	28.9	62.19	0.230	38.45	25.27	72.14

Uniaxial Stress for File w16771-10431-uniaxial-stress									
Event	Conf	Pore	Diff	Temp	E	n	K	G	P
	MPa	MPa	MPa	°C	GPa		GPa	GPa	GPa
0	50.5	-0.2	19.3	31.9	48.44	0.234	30.32	19.63	56.50
1	50.5	-0.2	18.8	32.0	49.05	0.181	25.61	20.77	53.30
2	50.5	-0.2	26.9	32.1	50.18	0.141	23.32	21.98	52.63

Uniaxial Stress for File w16771-10426.8-uniaxial-stress									
Event	Conf	Pore	Diff	Temp	E	n	K	G	P
	MPa	MPa	MPa	°C	GPa		GPa	GPa	GPa
0	50.5	-0.2	18.0	27.2	103.74	0.140	48.03	45.50	108.70
1	50.5	-0.2	12.9	27.9	113.73	0.137	52.24	50.00	118.91
2	50.5	-0.2	17.1	28.4	106.04	0.129	47.65	46.96	110.26

Uniaxial Stress for File W16771-10443-Uniaxial-Stress									
Event	Conf	Pore	Diff	Temp	E	n	K	G	P
	MPa	MPa	MPa	°C	GPa		GPa	GPa	GPa
0	50.1	-0.2	18.0	31.9	63.34	0.250	42.16	25.34	75.95
1	50.1	-0.2	10.7	31.8	85.13	0.326	81.39	32.11	124.20

Uniaxial Stress for File W96-10307.5H-UStress								
Event	Conf	Diff	Temp	E	n	K	G	P
	MPa	MPa	°C	GPa		GPa	GPa	GPa
0	25.5	25.7	20.8	60.39	0.193	32.84	25.30	66.58
1	25.5	30.8	20.7	62.38	0.208	35.62	25.82	70.05
2	15.5	16.7	20.2	54.64	0.180	28.48	23.15	59.34
3	15.4	21.0	20.5	56.73	0.182	29.74	23.99	61.73
4	5.5	12.0	20.0	46.01	0.159	22.47	19.85	48.94

Uniaxial Stress for File W96-10307V45-UStress								
Event	Conf	Diff	Temp	E	n	K	G	P
	MPa	MPa	°C	GPa		GPa	GPa	GPa
0	25.5	32.1	21.7	59.15	0.205	33.40	24.55	66.13
1	25.5	37.2	21.4	59.93	0.211	34.51	24.75	67.51
2	15.4	22.2	20.8	56.89	0.203	31.95	23.64	63.46
3	15.4	27.4	20.9	57.03	0.205	32.19	23.67	63.75
4	5.5	18.0	20.7	53.20	0.189	28.56	22.36	58.37

Uniaxial Stress for File W96-10311V45-UStress								
Event	Conf	Diff	Temp	E	n	K	G	P
	MPa	MPa	°C	GPa		GPa	GPa	GPa
0	25.5	32.5	23.2	50.93	0.220	30.34	20.87	58.16
1	25.5	36.8	23.3	52.67	0.220	31.34	21.59	60.12
2	15.5	22.7	18.4	47.42	0.209	27.16	19.61	53.31
3	15.4	27.4	18.7	48.53	0.214	28.24	19.99	54.90
4	5.4	18.0	18.0	41.78	0.202	23.33	17.39	46.51

Uniaxial Stress for File W96-10334.7V45-UStress								
Event	Conf	Diff	Temp	E	n	K	G	P
	MPa	MPa	°C	GPa		GPa	GPa	GPa
0	25.4	31.6	30.1	47.77	0.165	23.74	20.51	51.09
1	15.5	23.1	28.6	51.38	0.147	24.28	22.39	54.13
2	5.4	12.4	21.1	43.48	0.138	20.00	19.11	45.47
3	15.4	27.4	21.6	46.94	0.144	21.98	20.51	49.33
4	25.4	37.2	25.5	46.89	0.150	22.30	20.39	49.49

Uniaxial Stress for File W96-10336V-UStress								
Event	Conf	Diff	Temp	E	n	K	G	P
	MPa	MPa	°C	GPa		GPa	GPa	GPa
0	25.5	32.1	24.2	39.58	0.155	19.14	17.13	41.98
1	15.4	22.2	22.3	40.69	0.164	20.19	17.47	43.49
2	5.5	12.9	21.5	41.26	0.161	20.32	17.76	44.00

Uniaxial Stress for File W96-10339H-UStress								
Event	Conf	Diff	Temp	E	n	K	G	P
	MPa	MPa	°C	GPa		GPa	GPa	GPa
0	25.4	31.6	23.2	48.68	0.167	24.38	20.85	52.19
1	25.5	37.2	23.2	49.57	0.168	24.91	21.21	53.20
2	15.5	22.7	21.6	47.97	0.168	24.07	20.54	51.45
3	15.4	27.4	21.5	48.65	0.165	24.17	20.89	52.03
4	5.4	18.0	20.8	44.43	0.161	21.81	19.14	47.34

Uniaxial Stress for File W96-10347.8H-UStress								
Event	Conf	Diff	Temp	E	n	K	G	P
	MPa	MPa	°C	GPa		GPa	GPa	GPa
0	25.5	32.1	22.6	43.04	0.186	22.88	18.14	47.06
1	25.5	37.2	22.3	44.42	0.188	23.69	18.70	48.63
2	15.4	22.7	21.6	43.03	0.184	22.71	18.17	46.94
3	15.4	27.4	21.7	43.53	0.185	23.03	18.37	47.52
4	5.4	18.0	21.3	39.46	0.184	20.84	16.66	43.05

Uniaxial Stress for File W96-10348V-UStress								
Event	Conf	Diff	Temp	E	n	K	G	P
	MPa	MPa	°C	GPa		GPa	GPa	GPa
0	25.5	30.8	20.3	38.99	0.150	18.57	16.95	41.18
1	25.5	36.3	20.9	38.23	0.152	18.32	16.59	40.44
2	15.5	22.2	20.3	36.83	0.147	17.40	16.05	38.81
3	15.5	26.9	20.1	38.15	0.153	18.30	16.55	40.37
4	5.5	17.1	20.2	32.11	0.138	14.79	14.11	33.60

Uniaxial Stress for File w96-b-10310H-uniaxial-stress								
Event	Conf	Diff	Temp	E	n	K	G	P
	MPa	MPa	°C	GPa		GPa	GPa	GPa
0	25.5	25.2	25.5	49.13	0.118	21.42	21.97	50.72
1	15.4	10.7	24.6	42.20	0.105	17.81	19.10	43.27
2	10.4	5.6	24.4	41.11	0.090	16.73	18.85	41.86

Uniaxial Stress for File w96-mb-10321.1V45-uniaxial-stress								
Event	Conf	Diff	Temp	E	n	K	G	P
	MPa	MPa	°C	GPa		GPa	GPa	GPa
0	25.5	25.2	26.1	63.29	0.224	38.17	25.86	72.65
1	15.4	10.7	25.3	55.38	0.258	38.20	22.00	67.54
2	10.4	5.6	24.4	49.75	0.257	34.18	19.78	60.56

Uniaxial Stress for File w96-mb-10345V45-uiaxial-stress								
Event	Conf	Diff	Temp	E	n	K	G	P
	MPa	MPa	°C	GPa		GPa	GPa	GPa
0	25.5	26.1	22.1	51.75	0.209	29.64	21.40	58.17
1	15.5	10.7	21.3	42.58	0.216	24.95	17.52	48.31
2	10.5	6.0	21.3	37.33	0.201	20.78	15.55	41.51

Uniaxial Stress for File w96-mb-10347H-uniaxial-stress								
Event	Conf	Diff	Temp	E	n	K	G	P
	MPa	MPa	°C	GPa		GPa	GPa	GPa
0	25.5	25.7	24.7	55.00	0.147	25.94	23.98	57.92
1	15.4	10.3	24.0	44.34	0.139	20.47	19.46	46.42
2	10.4	5.2	24.1	40.75	0.131	18.42	18.01	42.44

Uniaxial Stress for File w96-mb-10356.6H-uniaxial-stress								
Event	Conf	Diff	Temp	E	n	K	G	P
	MPa	MPa	°C	GPa		GPa	GPa	GPa
0	25.5	25.7	24.1	50.15	0.169	25.25	21.45	53.85
1	15.5	10.7	23.3	43.14	0.162	21.27	18.56	46.02
2	10.4	5.6	23.1	38.73	0.162	19.07	16.67	41.30

A.2.5 Uni/Triaxial Compressive Strength, Young's Modulus and Poisson's Ratio

Strength for File w96-mb-10311V45-strength						
Event	Conf	Diff	Temp	E	n	peak_stress
	MPa	MPa	°C	GPa		MPa
0	20.4	94.0	24.1	32.94	0.442	172.1

Strength for File w96-mb-10339H-strength						
Event	Conf	Diff	Temp	E	n	peak_stress
	MPa	MPa	°C	GPa		MPa
0	20.5	90.1	23.3	25.34	0.375	191.3

Strength for File w96-mb-10345V45-strength						
Event	Conf	Diff	Temp	E	n	peak_stress
	MPa	MPa	°C	GPa		MPa
0	10.1	56.0	23.0	27.84	0.213	105.9

Strength for File w96-mb-10348V-strength						
Event	Conf	Diff	Temp	E	n	peak_stress
	MPa	MPa	°C	GPa		MPa
0	10.4	54.3	22.6	20.12	0.318	140.5

Strength for File w96-mb-10356.6-strength						
Event	Conf	Diff	Temp	E	n	peak_stress
	MPa	MPa	°C	GPa		MPa
0	10.4	49.6	23.1	28.30	0.281	114.9

A.2.6 Mohr's Circle

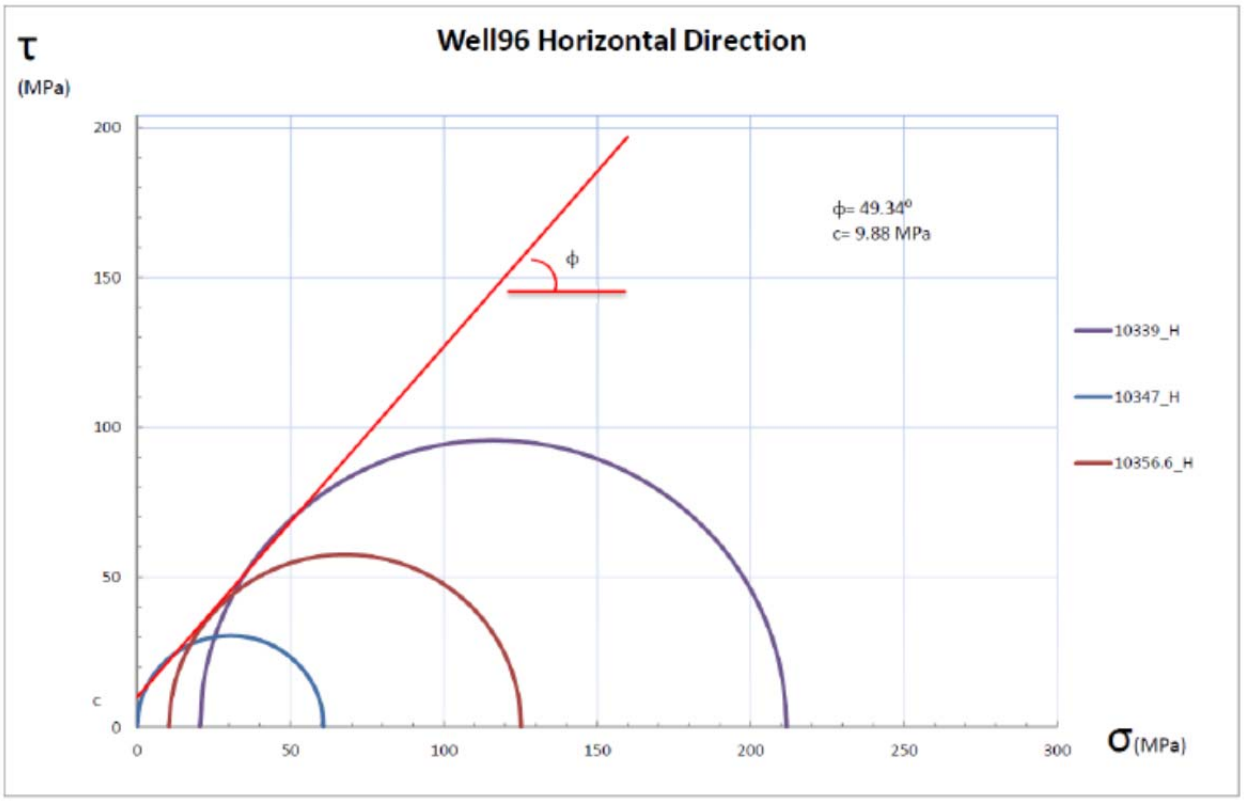

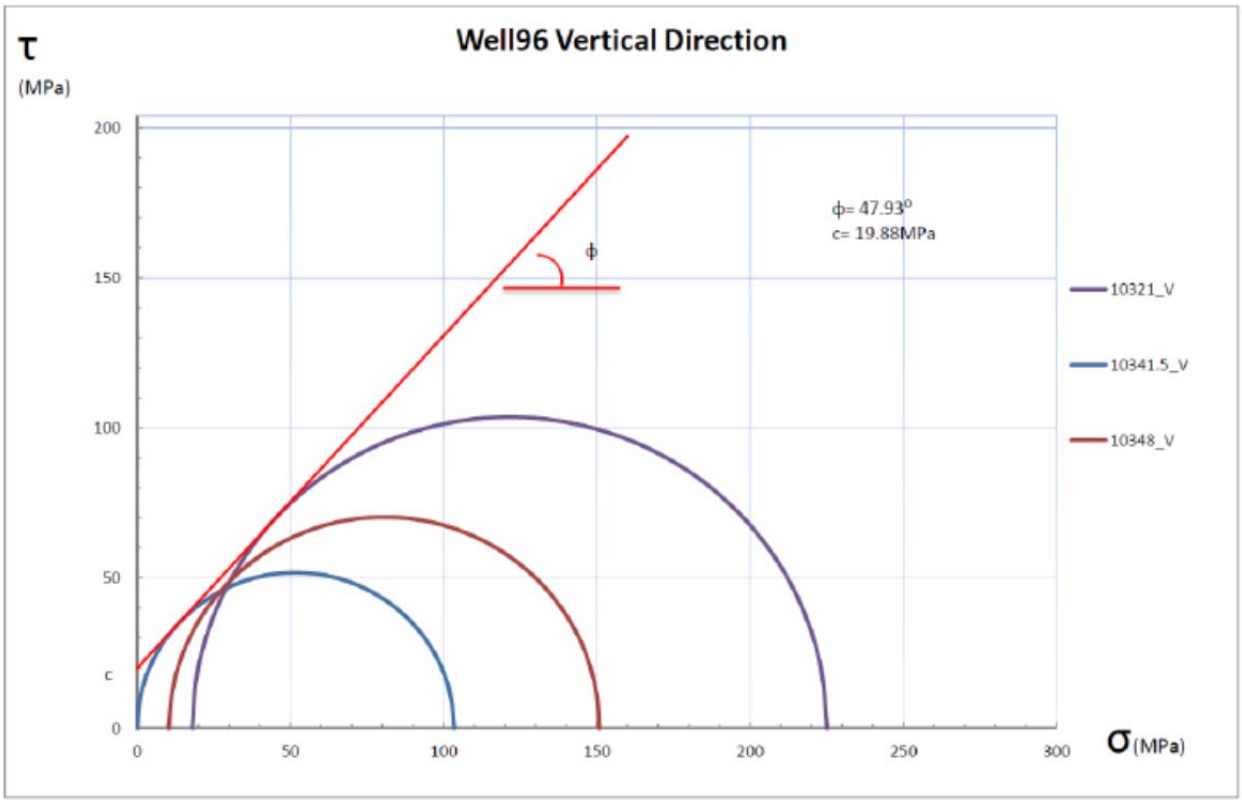
Well96 Vertical Direction
τ
(MPa)
200
150
100
50
c
0
0
50
100
150
200
250
300
σ (MPa)
ϕ= 47.93°
c= 19.88MPa
ϕ
10321_V
10341.5_V
10348_V

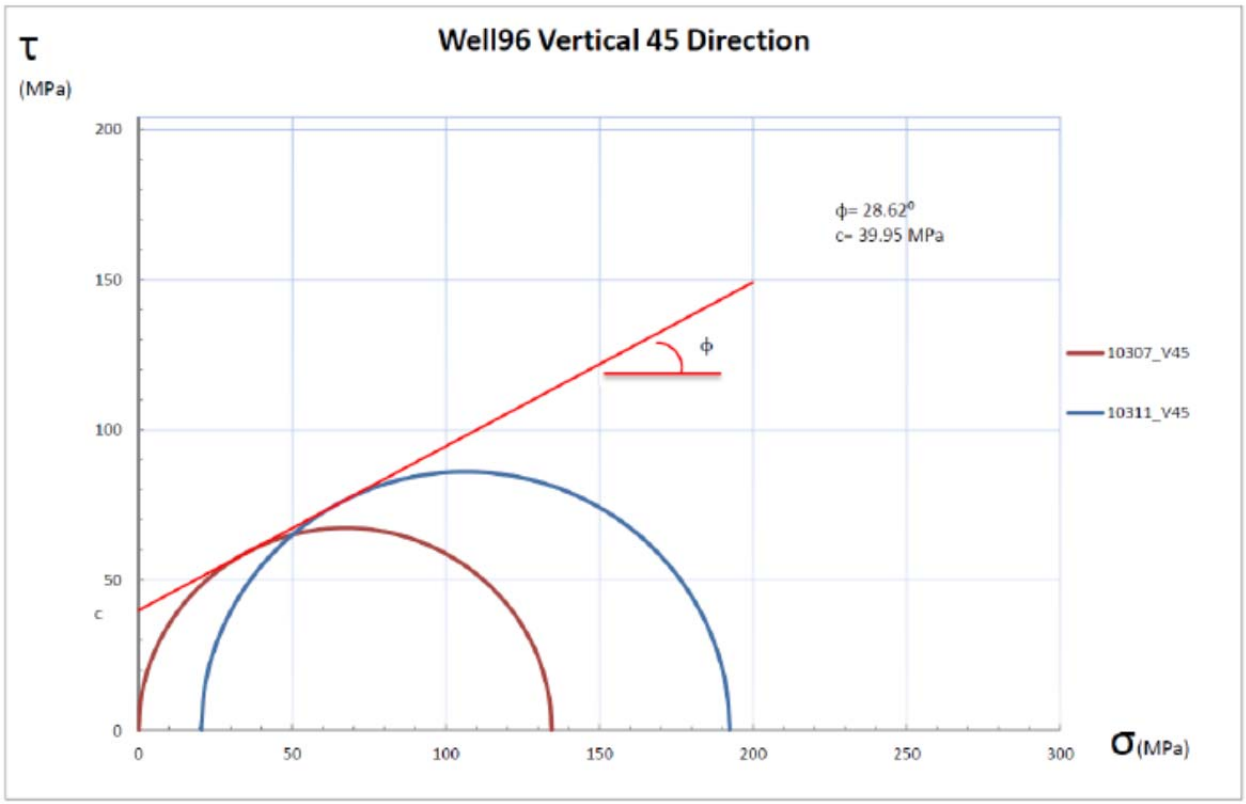
Well96 Vertical 45 Direction
τ
(MPa)
200
150
100
50
c
0
0
50
100
150
200
250
300
σ (MPa)
ϕ= 28.62°
c= 39.95 MPa
ϕ
10307_V45
10311_V45

A.3. Well 2 Bakken Samples Testing Results

A.3.1 Permeability

Permeability and Specific Storage for File w11617-10364-perm-biot							
Event	Type	Conf	Pore Top	Diff	Temp	Perm	Storage
		MPa	MPa	MPa	°C	μD	m^{-1}
0	aspike	20.3	7.5	-0.8	31.4	1.87	1.52e-07

Permeability and Specific Storage for File w11617-10365-perm-biot							
Event	Type	Conf	Pore Top	Diff	Temp	Perm	Storage
		MPa	MPa	MPa	°C	μD	m^{-1}
0	multipulse	20.7	7.5	-0.8	23.9	0.405	5.20e-12
1	multipulse	30.6	7.6	-1.7	24.4	0.356	1.36e-12
2	multipulse	40.7	7.6	-1.7	25.3	0.351	5.97e-13

Permeability and Specific Storage for File w11617-10367-horizontal-perm-biot							
Event	Type	Conf	Pore Top	Diff	Temp	Perm	Storage
		MPa	MPa	MPa	°C	μD	m^{-1}
0	steady-state	20.7	8.1	-1.3	26.8	5.10e+03	0.00
1	steady-state	30.6	8.5	-1.7	27.9	6.31e+03	0.00
2	steady-state	40.6	8.6	-2.5	28.3	4.79e+03	0.00
3	steady-state	50.6	9.1	-3.0	28.9	5.47e+03	0.00

Permeability and Specific Storage for File w11617-10367-vertical-perm-biot							
Event	Type	Conf	Pore Top	Diff	Temp	Perm	Storage
		MPa	MPa	MPa	°C	μD	m^{-1}
0	multipulse	20.7	7.6	-0.8	22.8	0.527	1.79e-06
1	multipulse	29.9	7.5	-1.7	23.5	0.222	4.32e-06
2	multipulse	40.1	7.6	-2.1	24.1	0.0501	6.13e-08

Permeability and Specific Storage for File w11617-10368.5-vertical-uniaxial-stress							
Event	Type	Conf	Pore Top	Diff	Temp	Perm	Storage
		MPa	MPa	MPa	°C	μD	m^{-1}
0	multipulse	20.8	7.6	-0.8	23.2	0.418	4.95e-11
1	multipulse	30.6	7.5	-1.7	23.4	0.371	5.60e-08
2	multipulse	40.7	7.6	-2.1	23.5	0.327	6.63e-12
3	multipulse	50.7	7.7	-2.5	23.7	0.313	1.65e-10

Permeability and Specific Storage for File w11617-10369-perm-biot							
Event	Type	Conf	Pore Top	Diff	Temp	Perm	Storage
		MPa	MPa	MPa	°C	μD	m^{-1}
0	multipulse	20.7	7.6	-0.8	26.7	0.0878	1.76e-07
1	multipulse	30.6	7.5	-1.7	27.1	0.0835	1.14e-07

Permeability and Specific Storage for File w11617-10369.8-perm-biot							
Event	Type	Conf	Pore Top	Diff	Temp	Perm	Storage
		MPa	MPa	MPa	°C	μD	m^{-1}
0	multipulse	20.7	7.6	-1.3	28.3	0.0688	2.76e-06
1	multipulse	30.7	7.6	-1.3	29.0	0.00981	1.36e-11
2	multipulse	40.6	7.6	-2.1	29.3	0.00905	5.95e-08

Permeability and Specific Storage for File w11617-10370-vertical-perm-biot-leak							
Event	Type	Conf	Pore Top	Diff	Temp	Perm	Storage
		MPa	MPa	MPa	°C	μD	m^{-1}
0	multipulse	20.7	7.6	-0.8	29.5	0.0469	1.14e-05
1	multipulse	30.7	7.6	-1.3	29.6	0.0267	9.95e-06
2	multipulse	20.7	7.5	-0.8	28.1	0.00140	9.19e-08
3	multipulse	30.7	7.5	-1.3	29.5	0.0218	3.49e-06
4	multipulse	40.7	7.6	-2.1	29.5	0.129	3.92e-05

Permeability and Specific Storage for File w11617-10371-v-perm-biot							
Event	Type	Conf	Pore Top	Diff	Temp	Perm	Storage
		MPa	MPa	MPa	°C	μD	m^{-1}
0	multipulse	20.7	7.5	-1.3	24.8	2.17	0.000114
1	multipulse	30.7	7.6	-1.3	24.8	0.0255	3.13e-07
2	multipulse	40.7	7.6	-1.7	26.6	0.0202	7.30e-08

Permeability and Specific Storage for File w11617-10371.8-perm-biot							
Event	Type	Conf	Pore Top	Diff	Temp	Perm	Storage
		MPa	MPa	MPa	°C	μD	m^{-1}
0	multipulse	20.7	8.1	-0.8	22.4	2.38	9.48e-13

Permeability and Specific Storage for File w11617-10372-vertical-perm-biot							
Event	Type	Conf	Pore Top	Diff	Temp	Perm	Storage
		MPa	MPa	MPa	°C	μD	m^{-1}
0	multipulse	20.7	7.6	-0.8	28.6	0.254	1.25e-07
1	multipulse	30.6	7.5	-1.7	28.8	0.335	7.33e-07
2	multipulse	40.7	7.5	-2.1	29.0	0.323	7.21e-07

Permeability and Specific Storage for File w11617-10373-perm-biot							
Event	Type	Conf	Pore Top	Diff	Temp	Perm	Storage
		MPa	MPa	MPa	°C	μD	m^{-1}
0	multipulse	20.7	7.6	-0.8	26.7	0.363	4.77e-08
1	multipulse	30.7	7.6	-1.7	23.4	0.292	1.12e-07

Permeability and Specific Storage for File w11617-10374-13-1-perm-biot							
Event	Type	Conf	Pore Top	Diff	Temp	Perm	Storage
		MPa	MPa	MPa	°C	μD	m^{-1}
0	multipulse	20.7	7.6	-0.8	32.2	21.8	6.08e-12
1	multipulse	30.1	7.5	-1.3	32.6	24.3	3.59e-11

Permeability and Specific Storage for File w11617-10374.1-13-2-perm-biot							
Event	Type	Conf	Pore Top	Diff	Temp	Perm	Storage
		MPa	MPa	MPa	°C	μD	m^{-1}
0	multipulse	20.7	7.6	-1.3	32.2	0.159	3.17e-06

Permeability and Specific Storage for File w11617-10375-perm-biot							
Event	Type	Conf	Pore Top	Diff	Temp	Perm	Storage
		MPa	MPa	MPa	°C	μD	m^{-1}
0	multipulse	20.7	7.5	-0.8	23.9	0.0383	1.31e-06
1	multipulse	30.6	7.6	-1.3	24.3	0.168	0.000113
2	multipulse	40.7	7.6	-1.7	25.2	0.147	3.43e-05

Permeability and Specific Storage for File w11617-10403-15-1-perm_biot							
Event	Type	Conf	Pore Top	Diff	Temp	Perm	Storage
		MPa	MPa	MPa	°C	μD	m^{-1}
0	multipulse	20.5	7.6	-1.3	23.3	7.87	3.63e-08
1	multipulse	30.5	7.6	-1.7	24.5	5.46	4.70e-08
2	multipulse	40.2	7.6	-2.1	25.5	3.84	6.54e-08
3	multipulse	50.5	7.6	-2.5	26.5	2.35	5.45e-11

Permeability and Specific Storage for File w11617-10403-15-2-perm-biot							
Event	Type	Conf	Pore Top	Diff	Temp	Perm	Storage
		MPa	MPa	MPa	°C	μD	m^{-1}
0	multipulse	20.7	7.5	-1.3	24.0	0.291	9.19e-12
1	multipulse	30.7	7.5	-1.7	24.5	0.237	1.90e-08
2	multipulse	40.7	7.5	-2.1	24.1	0.186	1.44e-07

Permeability and Specific Storage for File w11617-10416-perm-biot							
Event	Type	Conf	Pore Top	Diff	Temp	Perm	Storage
		MPa	MPa	MPa	°C	μD	m^{-1}
0	multipulse	20.7	7.6	-0.8	23.2	0.327	3.08e-06
1	multipulse	30.7	7.6	-1.3	23.5	0.0772	7.44e-07
2	multipulse	40.7	7.6	-1.7	23.7	0.0158	1.29e-07
3	multipulse	50.7	7.6	-2.1	23.7	0.0132	1.40e-07

Permeability and Specific Storage for File w11617-10419-perm-biot							
Event	Type	Conf	Pore Top	Diff	Temp	Perm	Storage
		MPa	MPa	MPa	°C	μD	m^{-1}
0	multipulse	20.7	7.6	-1.3	23.0	0.0603	6.74e-07

A.3.2 Sonic Velocity, Dynamic Moduli and Poisson's Ratio

Observed Velocities and Moduli for File W11617-10364-velocity									
Event	Conf	Pore	Diff	Temp	V_p	$V_s^{(1)}$	$V_s^{(2)}$	Young's Modulus	Poisson's Ratio
	MPa	MPa	MPa	°C	m/s	m/s	m/s	GPa	
0	10.0	-0.2	0.4	19.4	5025	3504	3132	63.74	0.113
1	20.1	-0.2	0.0	19.9	5136	3482	3132	65.17	0.146
2	30.1	-0.2	0.0	20.3	5232	3572	3205	67.99	0.139
3	40.2	-0.2	-0.6	21.2	5332	3540	3223	69.19	0.164
4	50.1	-0.2	-1.3	21.4	5332	5093	3242	64.57	-0.285

Observed Velocities and Moduli for File W11617-10365-velocity									
Event	Conf	Pore	Diff	Temp	V_p	$V_s^{(1)}$	$V_s^{(2)}$	Young's Modulus	Poisson's Ratio
	MPa	MPa	MPa	°C	m/s	m/s	m/s	GPa	
0	10.0	-0.2	0.4	20.8	4607	2894	2908	50.48	0.171
1	20.1	-0.2	0.0	21.3	4671	2958	2986	52.45	0.160
2	30.1	-0.2	-0.1	21.4	4806	2998	3027	54.66	0.176
3	40.0	-0.2	-1.0	21.6	4913	3039	3041	56.30	0.190
4	50.0	-0.2	-1.4	21.7	4986	3067	3069	57.61	0.195

Observed Velocities and Moduli for File W11617-10367Horizontal-velocity									
Event	Conf	Pore	Diff	Temp	V_p	$V_s^{(1)}$	$V_s^{(2)}$	Young's Modulus	Poisson's Ratio
	MPa	MPa	MPa	°C	m/s	m/s	m/s	GPa	
0	10.1	-0.2	0.9	22.4	4882	2999	2985	54.32	0.199
1	20.0	-0.2	0.4	23.0	4925	3048	3017	55.59	0.195
2	30.0	-0.2	0.0	22.7	5012	3098	3017	56.94	0.204
3	40.2	-0.2	-0.4	22.8	5057	3098	3050	57.71	0.207
4	50.1	-0.2	-1.1	22.8	5150	3115	3050	58.70	0.221

Observed Velocities and Moduli for File W11617-10367vertical-velocity									
Event	Conf	Pore	Diff	Temp	V_p	$V_s^{(1)}$	$V_s^{(2)}$	Young's Modulus	Poisson's Ratio
	MPa	MPa	MPa	°C	m/s	m/s	m/s	GPa	
0	10.1	-0.2	0.4	21.5	4552	2963	3084	51.93	0.105
1	20.1	-0.2	0.4	22.4	4711	3191	3156	56.15	0.085
2	30.1	-0.2	-0.4	22.3	4711	3230	3271	56.79	0.046
3	40.1	-0.2	-0.8	22.9	4881	3269	3311	60.29	0.084
4	50.0	-0.2	-1.3	22.7	5064	3289	3395	63.96	0.114

Observed Velocities and Moduli for File W11617-10368.5-vertical-velocity									
Event	Conf	Pore	Diff	Temp	V_p	$V_s^{(1)}$	$V_s^{(2)}$	Young's Modulus	Poisson's Ratio
	MPa	MPa	MPa	°C	m/s	m/s	m/s	GPa	
0	10.1	-0.2	0.4	23.4	4545	2859	2889	48.96	0.167
1	20.1	-0.2	0.4	23.7	4579	2915	2917	50.06	0.159
2	29.9	-0.2	-0.6	23.7	4687	2929	2931	51.43	0.179
3	40.1	-0.2	-0.7	24.0	4839	2988	2975	53.92	0.194
4	50.0	-0.2	-1.6	24.1	4839	3018	2990	54.39	0.186

Observed Velocities and Moduli for File W11617-10369-velocity									
Event	Conf	Pore	Diff	Temp	V_p	$V_s^{(1)}$	$V_s^{(2)}$	Young's Modulus	Poisson's Ratio
	MPa	MPa	MPa	°C	m/s	m/s	m/s	GPa	
0	10.1	-0.2	0.7	24.9	5091	2941	3121	58.77	0.225
1	19.9	-0.2	-0.1	25.3	5137	2988	3087	59.30	0.231
2	30.0	-0.2	-0.4	25.6	5046	2988	3138	59.17	0.208
3	40.1	-0.2	-1.1	25.9	5330	3019	3191	62.56	0.243
4	50.0	-0.2	-1.3	26.2	5281	3036	3191	62.42	0.234

Observed Velocities and Moduli for File W11617-10369.8-velocity									
Event	Conf	Pore	Diff	Temp	V_p	$V_s^{(1)}$	$V_s^{(2)}$	Young's Modulus	Poisson's Ratio
	MPa	MPa	MPa	°C	m/s	m/s	m/s	GPa	
0	10.1	-0.2	-0.1	20.5	5027	2962	3079	57.54	0.217
1	20.1	-0.2	-0.6	21.1	5370	3019	3110	61.22	0.259
2	30.0	-0.2	-1.3	21.5	5236	3078	3095	60.88	0.234
3	40.0	-0.2	-1.4	21.8	5280	3093	3125	61.82	0.235
4	50.0	-0.2	-1.8	22.5	5370	3093	3141	62.70	0.246

Observed Velocities and Moduli for File W11617-10370-vertical-velocity									
Event	Conf	Pore	Diff	Temp	V_p	$V_s^{(1)}$	$V_s^{(2)}$	Young's Modulus	Poisson's Ratio
	MPa	MPa	MPa	°C	m/s	m/s	m/s	GPa	
0	10.1	-0.2	0.2	22.3	4534	2885	2890	49.47	0.159
1	20.0	-0.2	-0.3	22.8	4649	2921	2928	51.35	0.173
2	30.1	-0.2	-1.3	23.0	4752	2962	2962	53.11	0.182
3	40.0	-0.2	-1.3	23.1	4850	2981	2984	54.47	0.196
4	50.0	-0.2	-1.7	23.3	4887	3002	3007	55.29	0.196

Observed Velocities and Moduli for File W11617-10371-vertical-velocity									
Event	Conf	Pore	Diff	Temp	V_p	$V_s^{(1)}$	$V_s^{(2)}$	Young's Modulus	Poisson's Ratio
	MPa	MPa	MPa	°C	m/s	m/s	m/s	GPa	
0	10.0	-0.2	-0.3	28.8	4682	2894	2991	52.43	0.174
1	20.2	-0.2	-0.4	28.6	4771	2936	2973	53.55	0.189
2	30.0	-0.2	-1.1	28.8	4805	2966	3005	54.53	0.186
3	40.0	-0.2	-1.7	28.9	4880	2994	3045	55.98	0.190
4	50.1	-0.2	-1.7	29.0	4945	3012	3046	56.80	0.200

Observed Velocities and Moduli for File W11617-10371.8-velocity									
Event	Conf	Pore	Diff	Temp	V_p	$V_s^{(1)}$	$V_s^{(2)}$	Young's Modulus	Poisson's Ratio
	MPa	MPa	MPa	°C	m/s	m/s	m/s	GPa	
0	10.1	-0.2	-0.1	27.4	5016	3044	2972	56.92	0.219
1	19.9	-0.2	-0.6	27.7	5128	3069	3000	58.47	0.231
2	30.1	-0.2	-1.1	28.0	5256	3100	3039	60.34	0.241
3	40.1	-0.2	-1.7	28.0	5296	3127	3058	61.26	0.241
4	50.1	-0.2	-2.1	27.9	5296	3149	3079	61.83	0.236

Observed Velocities and Moduli for File W11617-10372-vertical-velocity									
Event	Conf	Pore	Diff	Temp	V_p	$V_s^{(1)}$	$V_s^{(2)}$	Young's Modulus	Poisson's Ratio
	MPa	MPa	MPa	°C	m/s	m/s	m/s	GPa	
0	10.0	-0.2	0.0	25.3	4552	2869	2905	49.65	0.164
1	20.1	-0.2	-0.7	26.3	4660	2915	2932	51.44	0.175
2	30.1	-0.2	-1.3	26.2	4737	2956	2967	52.95	0.179
3	40.0	-0.2	-1.3	26.6	4812	2978	2991	54.15	0.187
4	50.2	-0.2	-1.7	26.8	4859	3003	3012	55.09	0.189

Observed Velocities and Moduli for File W11617-10373-velocity									
Event	Conf	Pore	Diff	Temp	V_p	$V_s^{(1)}$	$V_s^{(2)}$	Young's Modulus	Poisson's Ratio
	MPa	MPa	MPa	°C	m/s	m/s	m/s	GPa	
0	10.0	-0.2	0.0	27.8	5159	3011	3055	59.80	0.236
1	20.2	-0.2	-0.7	27.5	5226	3053	3063	60.98	0.240
2	30.1	-0.2	-1.3	28.4	5402	3082	3088	62.98	0.258
3	40.1	-0.2	-1.6	28.3	5384	3098	3115	63.47	0.250
4	50.0	-0.2	-1.8	28.5	5420	3112	3147	64.39	0.250

Observed Velocities and Moduli for File W11617-10374-13-1-velocity									
Event	Conf	Pore	Diff	Temp	V_p	$V_s^{(1)}$	$V_s^{(2)}$	Young's Modulus	Poisson's Ratio
	MPa	MPa	MPa	°C	m/s	m/s	m/s	GPa	
0	10.2	-0.2	0.0	24.5	4772	4577	3536	16.84	-0.802
1	20.1	-0.2	-0.4	26.0	4819	4611	3556	19.58	-0.773
2	30.1	-0.2	-0.7	26.6	4878	4668	3556	23.85	-0.728
3	40.1	-0.2	-0.8	27.9	4912	4708	3576	23.96	-0.730
4	50.0	-0.2	-2.1	28.3	4893	4732	3576	18.73	-0.790

Observed Velocities and Moduli for File W11617-10374.1-velocity									
Event	Conf	Pore	Diff	Temp	V_p	$V_s^{(1)}$	$V_s^{(2)}$	Young's Modulus	Poisson's Ratio
	MPa	MPa	MPa	°C	m/s	m/s	m/s	GPa	
0	10.3	-0.2	0.3	24.0	5149	2925	3004	57.88	0.252
1	20.2	-0.2	-0.3	24.5	5259	2976	3032	59.71	0.258
2	30.2	-0.2	-0.8	25.8	5460	3016	3056	61.87	0.276
3	40.2	-0.2	-1.7	27.3	5528	3046	3082	63.12	0.278
4	50.0	-0.2	-1.8	27.2	5619	3068	3099	64.24	0.285

Observed Velocities and Moduli for File W11617-10375-velocity									
Event	Conf	Pore	Diff	Temp	V_p	$V_s^{(1)}$	$V_s^{(2)}$	Young's Modulus	Poisson's Ratio
	MPa	MPa	MPa	°C	m/s	m/s	m/s	GPa	
0	10.1	-0.2	0.0	28.1	5089	2858	3073	56.40	0.243
1	20.1	-0.2	-0.4	28.1	5151	2885	3092	57.44	0.246
2	30.1	-0.2	-0.6	28.6	5216	2913	3111	58.51	0.250
3	40.0	-0.2	-1.3	28.6	5210	2930	3125	58.89	0.245
4	50.1	-0.2	-2.1	28.9	5241	2943	3133	59.39	0.247

Observed Velocities and Moduli for File W11617-10403-15-2-velocity									
Event	Conf	Pore	Diff	Temp	V_p	$V_s^{(1)}$	$V_s^{(2)}$	Young's Modulus	Poisson's Ratio
	MPa	MPa	MPa	°C	m/s	m/s	m/s	GPa	
0	10.1	-0.2	0.0	22.5	4788	3010	2935	51.58	0.186
1	20.0	-0.2	-0.4	24.4	4829	3018	2939	52.07	0.193
2	30.1	-0.2	-1.1	25.8	4949	2941	2955	52.38	0.225
3	40.1	-0.2	-1.3	26.3	4978	2991	2972	53.37	0.220
4	50.1	-0.2	-2.0	26.6	4921	3003	2977	53.11	0.207

Observed Velocities and Moduli for File W11617-10412.8-velocity									
Event	Conf	Pore	Diff	Temp	V_p	$V_s^{(1)}$	$V_s^{(2)}$	Young's Modulus	Poisson's Ratio
	MPa	MPa	MPa	°C	m/s	m/s	m/s	GPa	
0	10.1	-0.2	0.0	25.7	5213	3793	3019	66.97	0.128
1	19.9	-0.2	-0.8	25.9	5245	3771	3033	67.37	0.137
2	30.0	-0.2	-1.0	26.5	5376	3908	3416	73.27	0.067
3	39.9	-0.2	-1.4	26.6	5261	4044	4508	49.32	-0.473
4	50.0	-0.2	-2.1	26.8	5304	3979	—	69.42	-0.144

Observed Velocities and Moduli for File W11617-10415vertical-velocity									
Event	Conf	Pore	Diff	Temp	V_p	$V_s^{(1)}$	$V_s^{(2)}$	Young's Modulus	Poisson's Ratio
	MPa	MPa	MPa	°C	m/s	m/s	m/s	GPa	
0	10.1	-0.2	0.4	25.3	—	3338	3342	—	—
1	20.3	-0.2	-0.8	25.6	—	3414	3441	—	—
2	30.1	-0.2	-1.0	25.8	—	3500	3513	—	—
3	40.0	-0.2	-1.3	26.1	—	3568	3554	—	—
4	50.1	-0.2	-1.6	26.3	—	3591	3595	—	—

Transducer calibration ranges failures: vp-0 vp-1 vp-2 vp-3 vp-4

Observed Velocities and Moduli for File W11617-10419-velocity									
Event	Conf	Pore	Diff	Temp	V_p	$V_s^{(1)}$	$V_s^{(2)}$	Young's Modulus	Poisson's Ratio
	MPa	MPa	MPa	°C	m/s	m/s	m/s	GPa	
0	10.1	-0.2	0.6	20.7	5332	3139	2975	60.29	0.255
1	20.1	-0.2	0.0	21.1	5352	3153	2987	60.79	0.255
2	30.0	-0.2	-0.8	21.0	5332	3167	2987	60.85	0.250
3	40.1	-0.2	-1.3	21.3	5359	3179	3003	61.42	0.251
4	50.1	-0.2	-1.6	21.8	5373	3174	3019	61.67	0.251

Observed Velocities and Moduli for File W116617-10403-15-1-velocity									
Event	Conf	Pore	Diff	Temp	V_p	$V_s^{(1)}$	$V_s^{(2)}$	Young's Modulus	Poisson's Ratio
	MPa	MPa	MPa	°C	m/s	m/s	m/s	GPa	
0	10.1	-0.2	0.3	25.0	4937	2972	3000	54.01	0.212
1	20.0	-0.2	-0.7	25.4	4989	2992	3020	54.90	0.215
2	30.0	-0.2	-0.8	25.7	4983	3013	3033	55.23	0.209
3	40.1	-0.2	-1.6	26.5	5036	3020	3051	55.96	0.215
4	50.0	-0.2	-2.0	26.2	5066	3039	3052	56.44	0.217

A.3.3 Biot's Coefficient

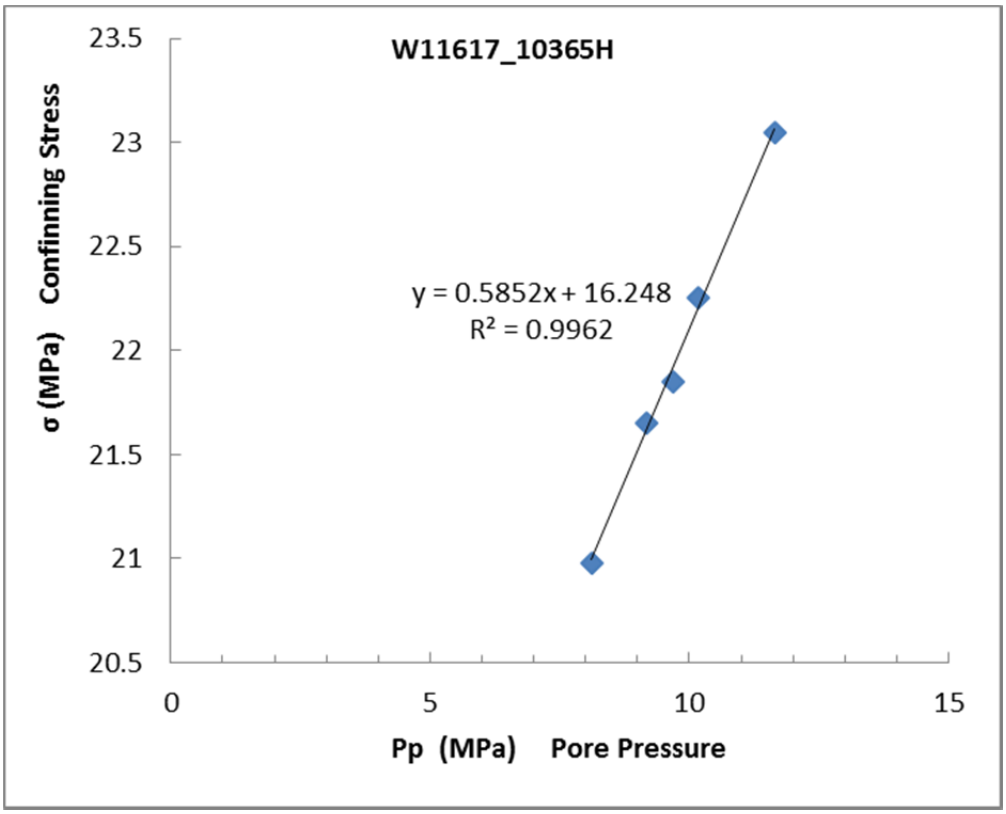

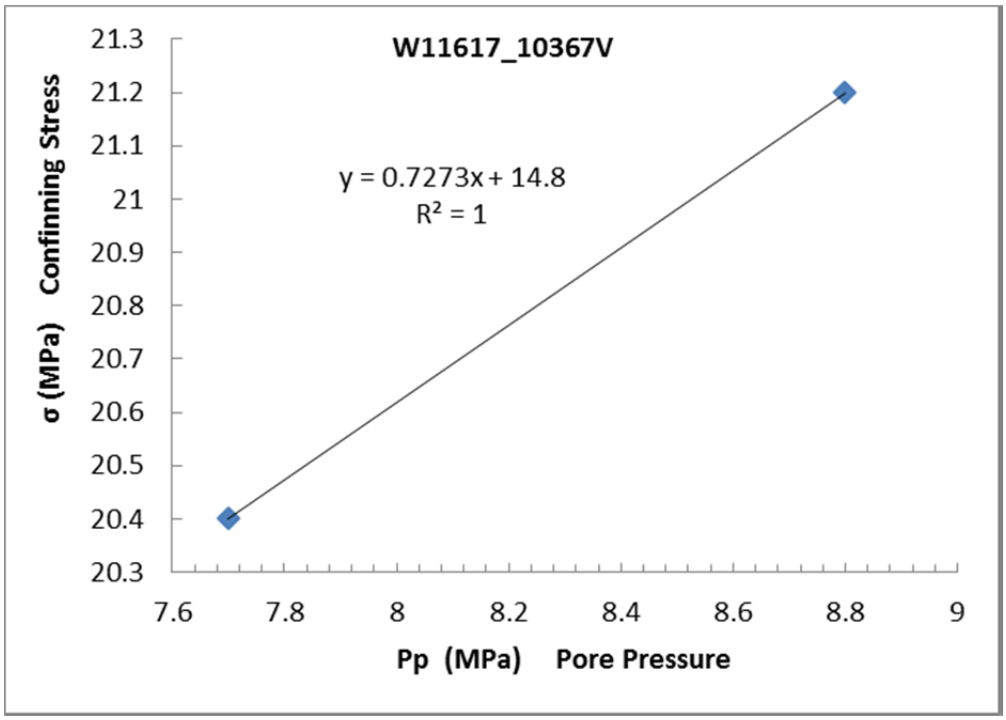

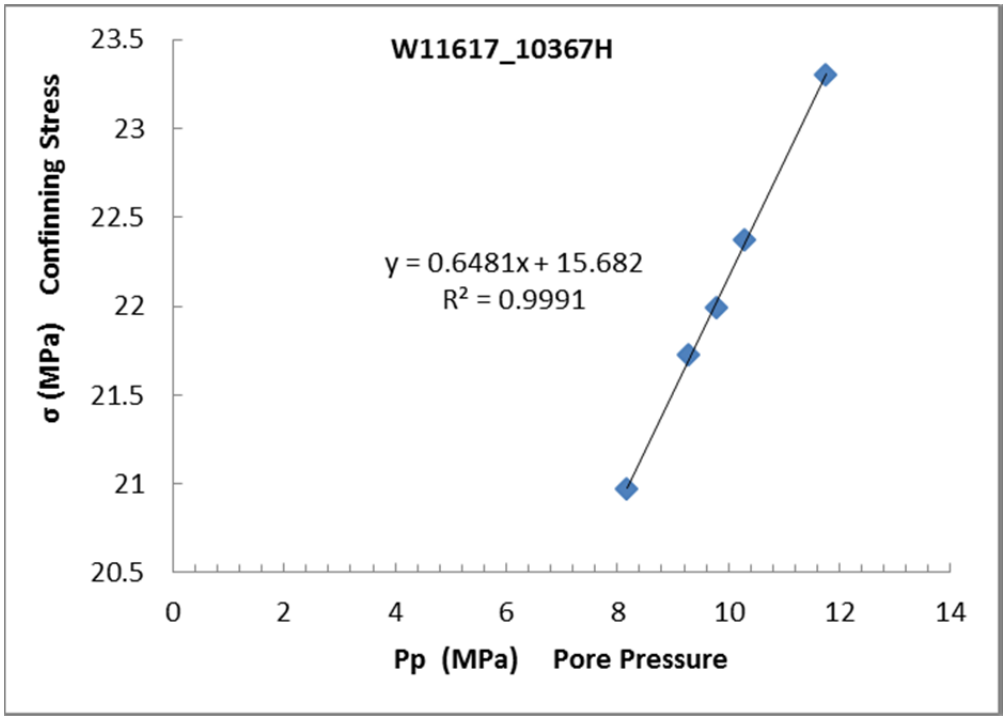
W11617_10367H
y = 0.6481x + 15.682
R² = 0.9991
σ (MPa) Confinning Stress
Pp (MPa) Pore Pressure
23.5
23
22.5
22
21.5
21
20.5
0
2
4
6
8
10
12
14

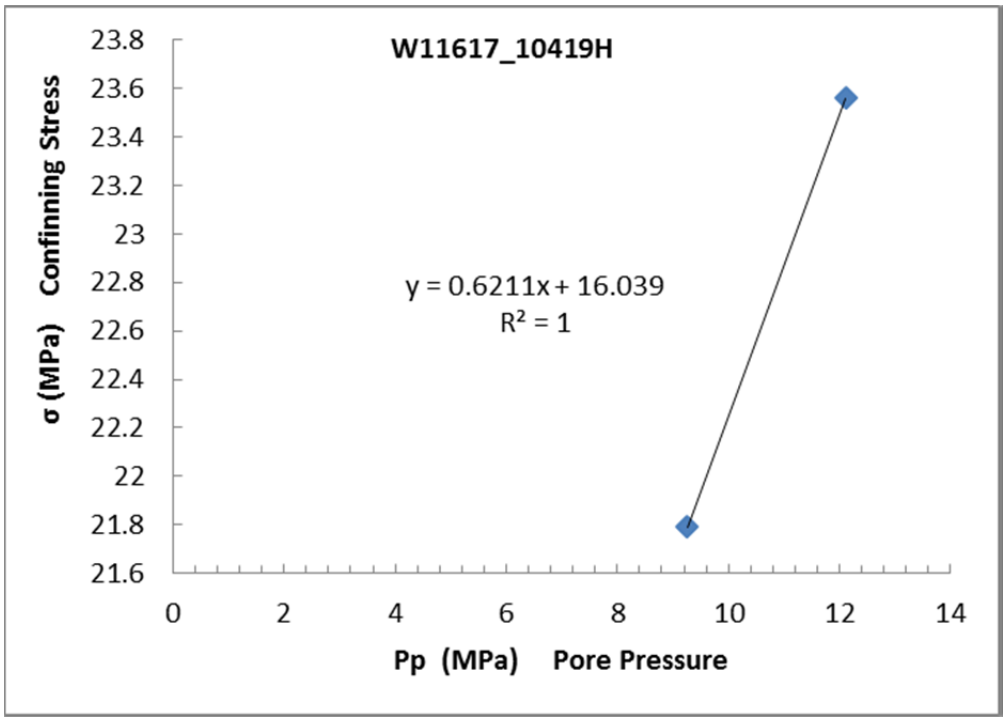
W11617_10419H
y = 0.6211x + 16.039
R² = 1
σ (MPa) Confinning Stress
Pp (MPa) Pore Pressure
23.8
23.6
23.4
23.2
23
22.8
22.6
22.4
22.2
22
21.8
21.6
0
2
4
6
8
10
12
14

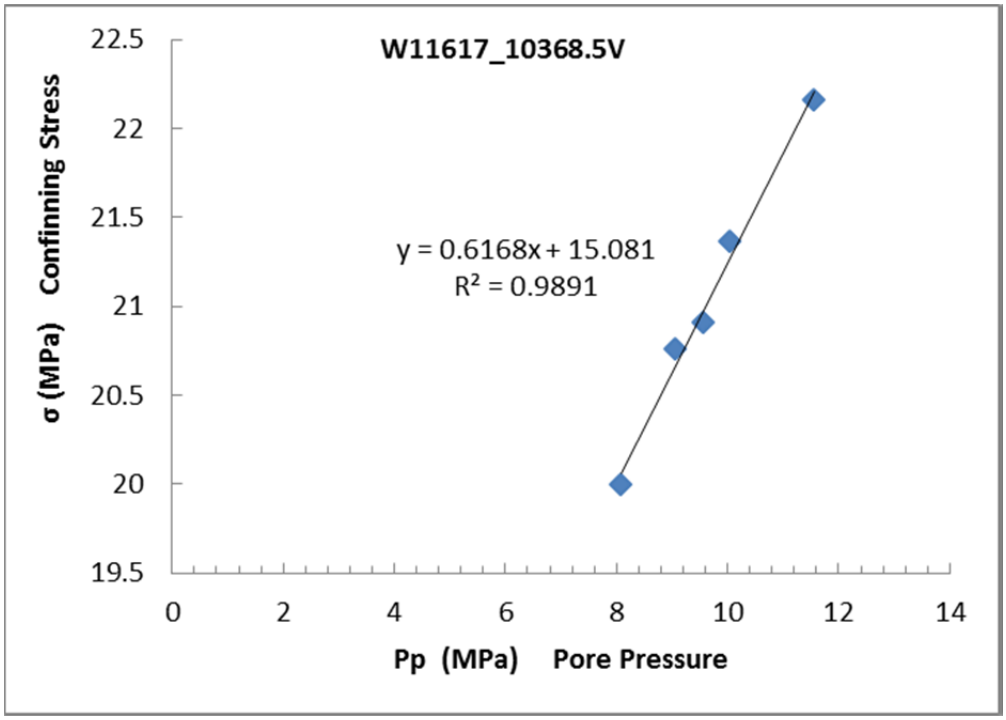
W11617_10368.5V
y = 0.6168x + 15.081
R² = 0.9891
σ (MPa) Confinning Stress
Pp (MPa) Pore Pressure
22.5
22
21.5
21
20.5
20
19.5
0
2
4
6
8
10
12
14

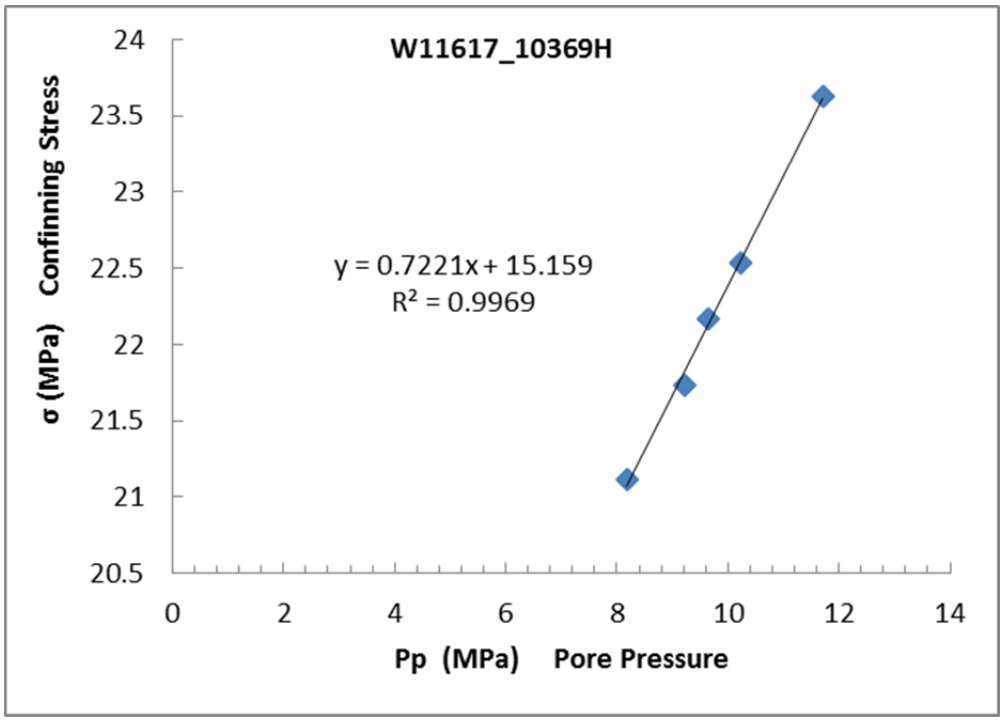
W11617_10369H
y = 0.7221x + 15.159
R² = 0.9969
σ (MPa) Confinning Stress
Pp (MPa) Pore Pressure
24
23.5
23
22.5
22
21.5
21
20.5
0
2
4
6
8
10
12
14

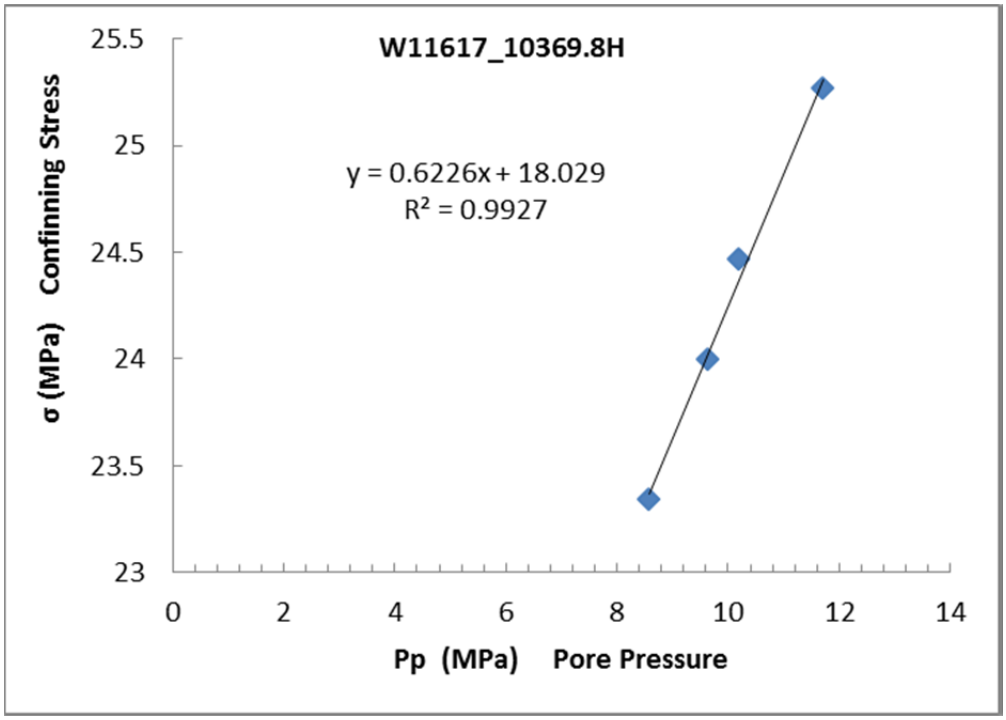
W11617_10369.8H
y = 0.6226x + 18.029
R² = 0.9927
σ (MPa) Confinning Stress
Pp (MPa) Pore Pressure
25.5
25
24.5
24
23.5
23
0
2
4
6
8
10
12
14

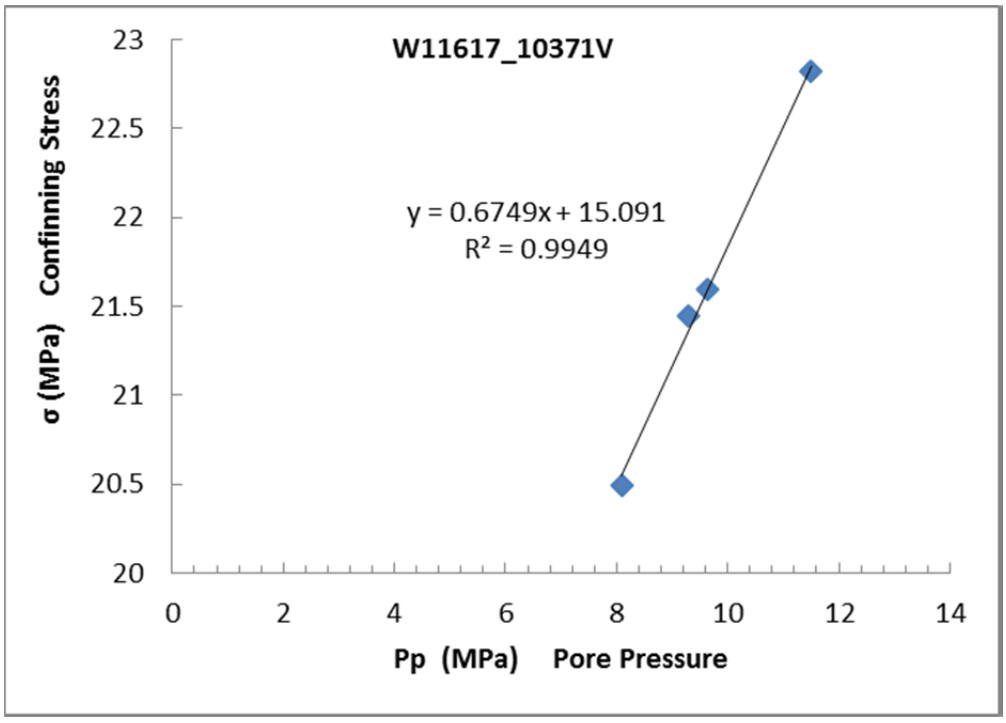
W11617_10371V
y = 0.6749x + 15.091
R² = 0.9949
σ (MPa) Confinning Stress
Pp (MPa) Pore Pressure
23
22.5
22
21.5
21
20.5
20
0
2
4
6
8
10
12
14

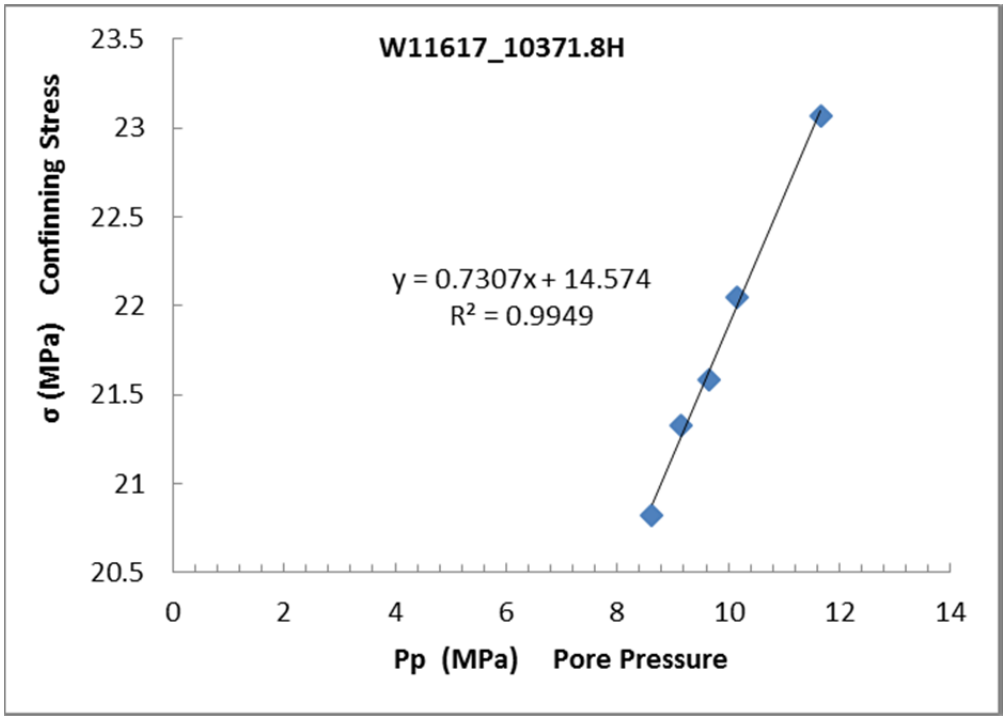
W11617_10371.8H
y = 0.7307x + 14.574
R² = 0.9949
σ (MPa) Confinning Stress
Pp (MPa) Pore Pressure
23.5
23
22.5
22
21.5
21
20.5
0
2
4
6
8
10
12
14

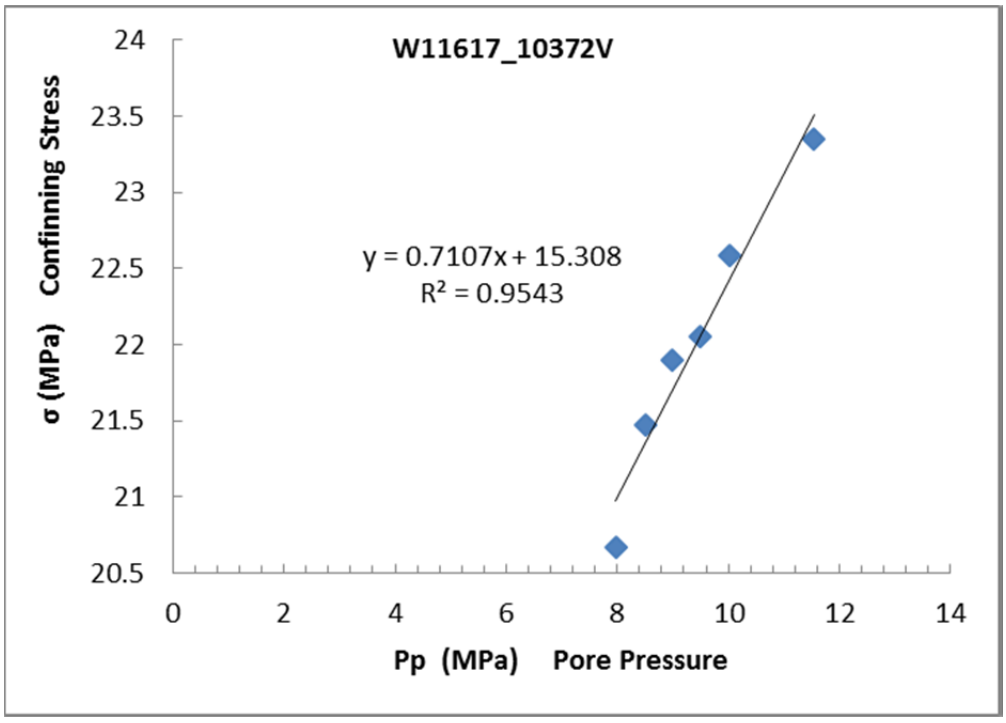
W11617_10372V
y = 0.7107x + 15.308
R² = 0.9543
σ (MPa) Confinning Stress
Pp (MPa) Pore Pressure
24
23.5
23
22.5
22
21.5
21
20.5
0
2
4
6
8
10
12
14

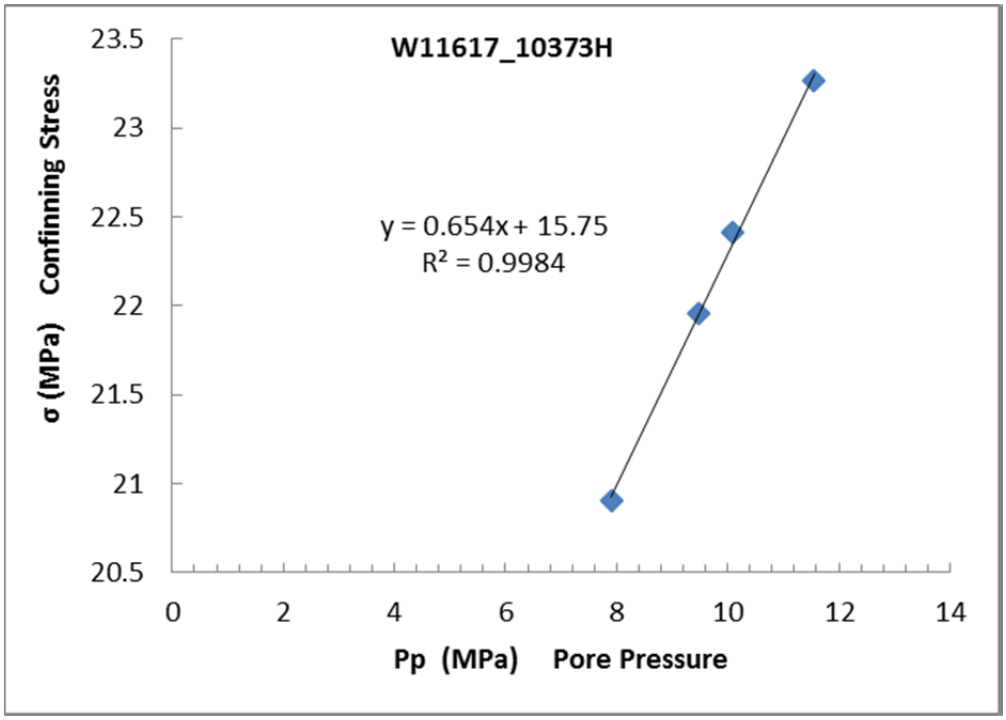
W11617_10373H
y = 0.654x + 15.75
R² = 0.9984
σ (MPa) Confinning Stress
Pp (MPa) Pore Pressure
23.5
23
22.5
22
21.5
21
20.5
0
2
4
6
8
10
12
14

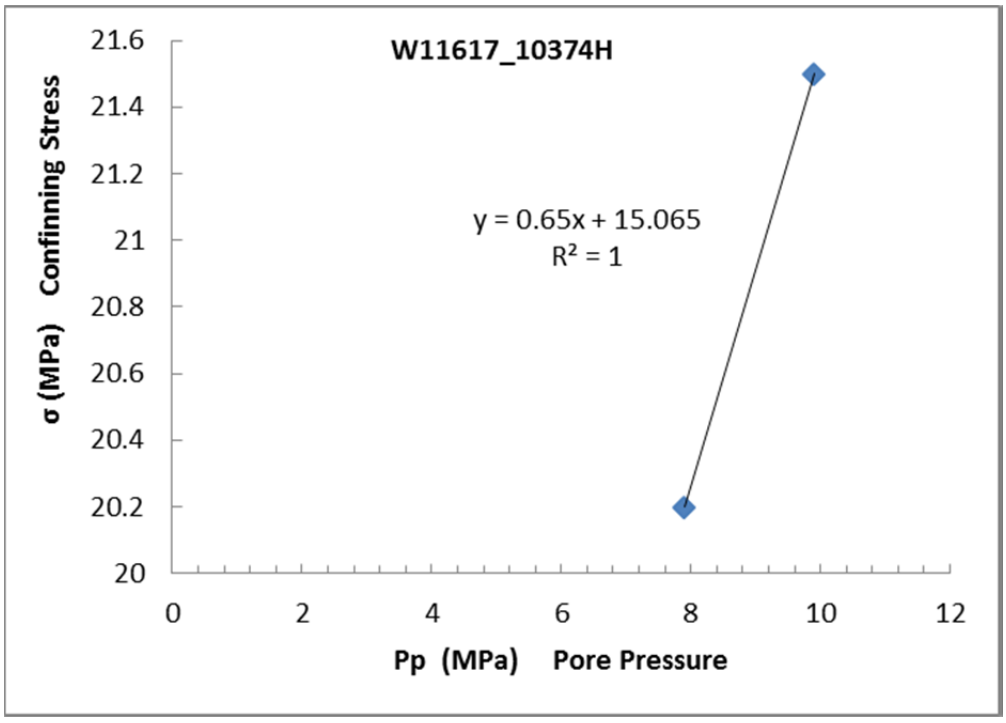
W11617_10374H
y = 0.65x + 15.065
R² = 1
σ (MPa) Confinning Stress
Pp (MPa) Pore Pressure
21.6
21.4
21.2
21
20.8
20.6
20.4
20.2
20
0
2
4
6
8
10
12

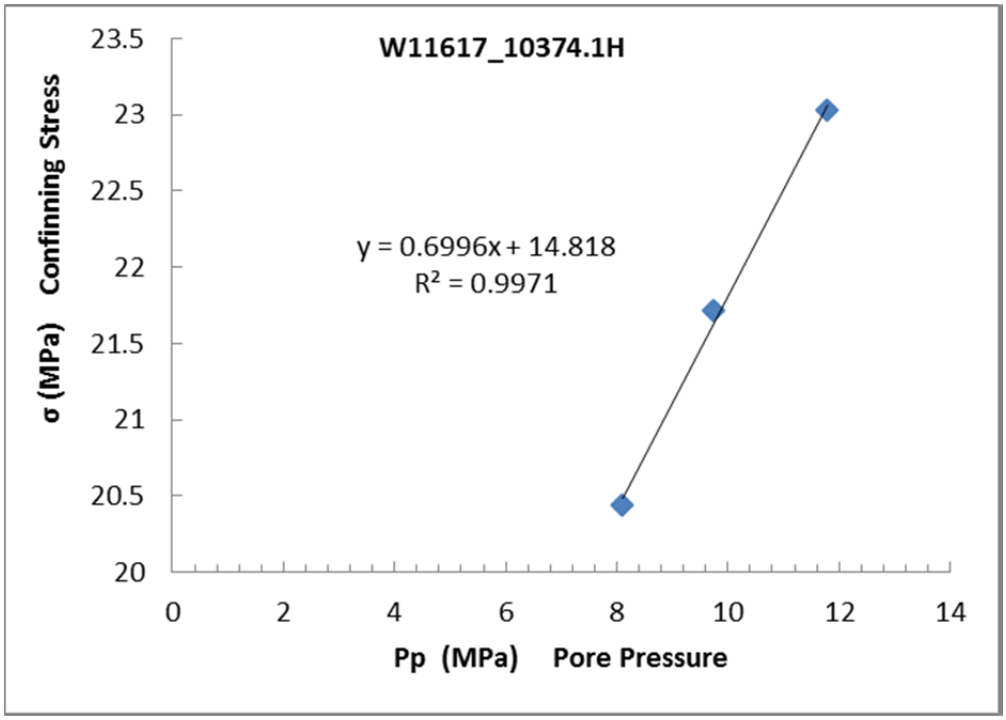
W11617_10374.1H
y = 0.6996x + 14.818
R² = 0.9971
σ (MPa) Confinning Stress
Pp (MPa) Pore Pressure
23.5
23
22.5
22
21.5
21
20.5
20
0
2
4
6
8
10
12
14

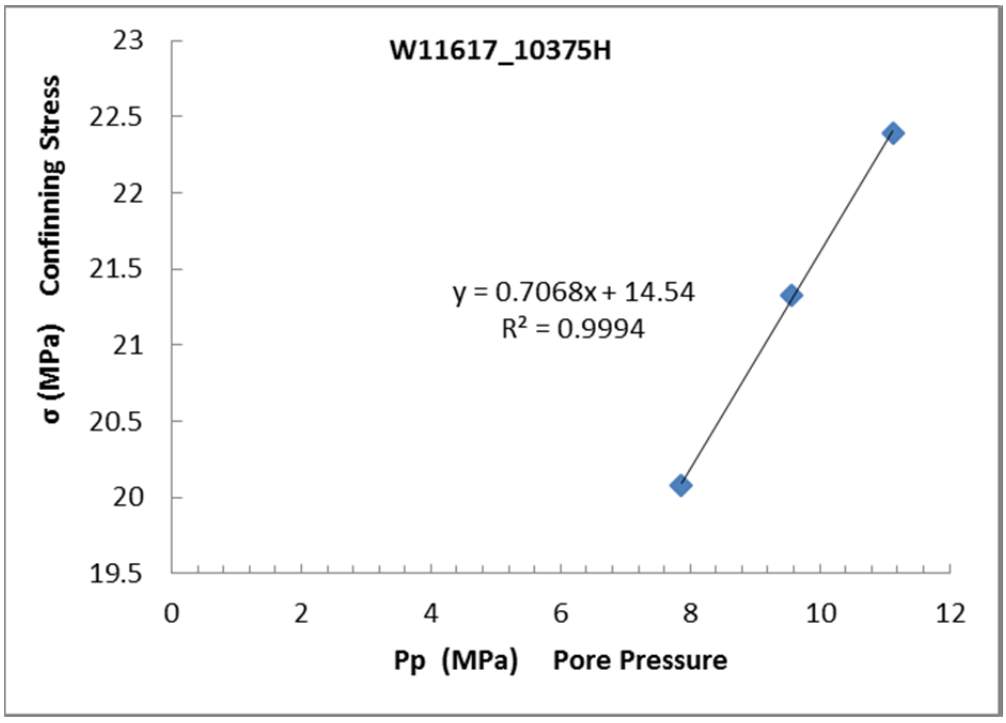
W11617_10375H
y = 0.7068x + 14.54
R² = 0.9994
σ (MPa) Confinning Stress
Pp (MPa) Pore Pressure
23
22.5
22
21.5
21
20.5
20
19.5
0
2
4
6
8
10
12

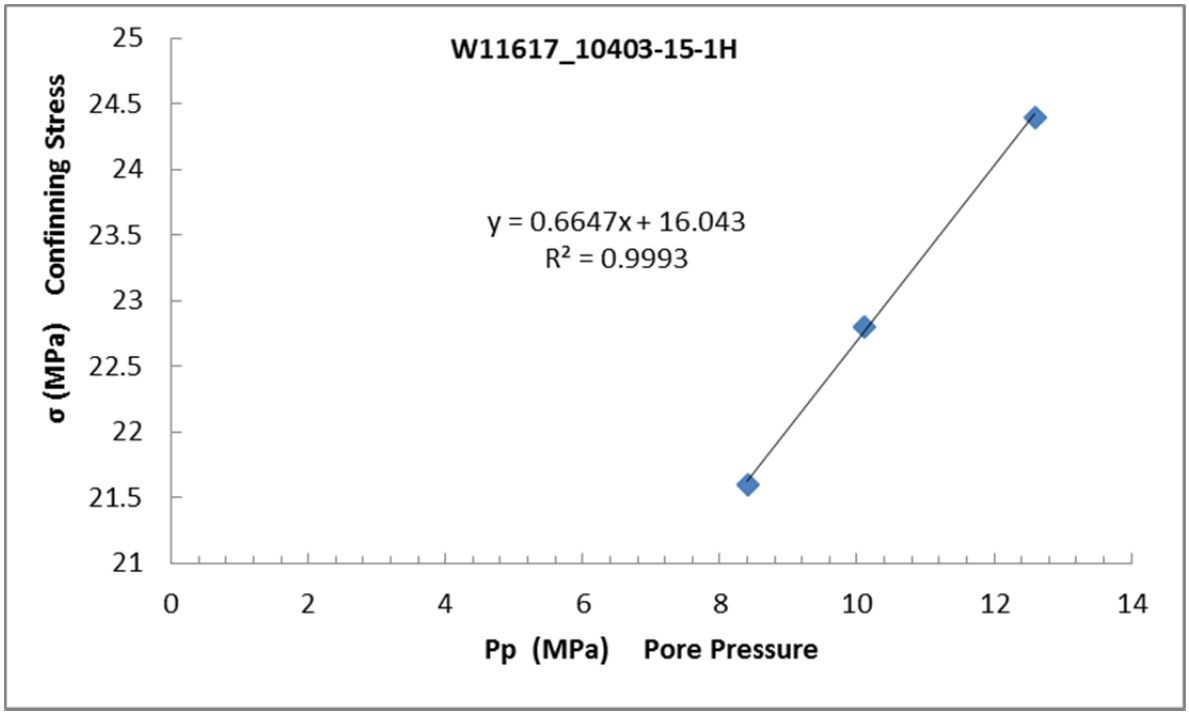
W11617_10403-15-1H
y = 0.6647x + 16.043
R² = 0.9993
σ (MPa) Confinning Stress
Pp (MPa) Pore Pressure
25
24.5
24
23.5
23
22.5
22
21.5
21
0
2
4
6
8
10
12
14

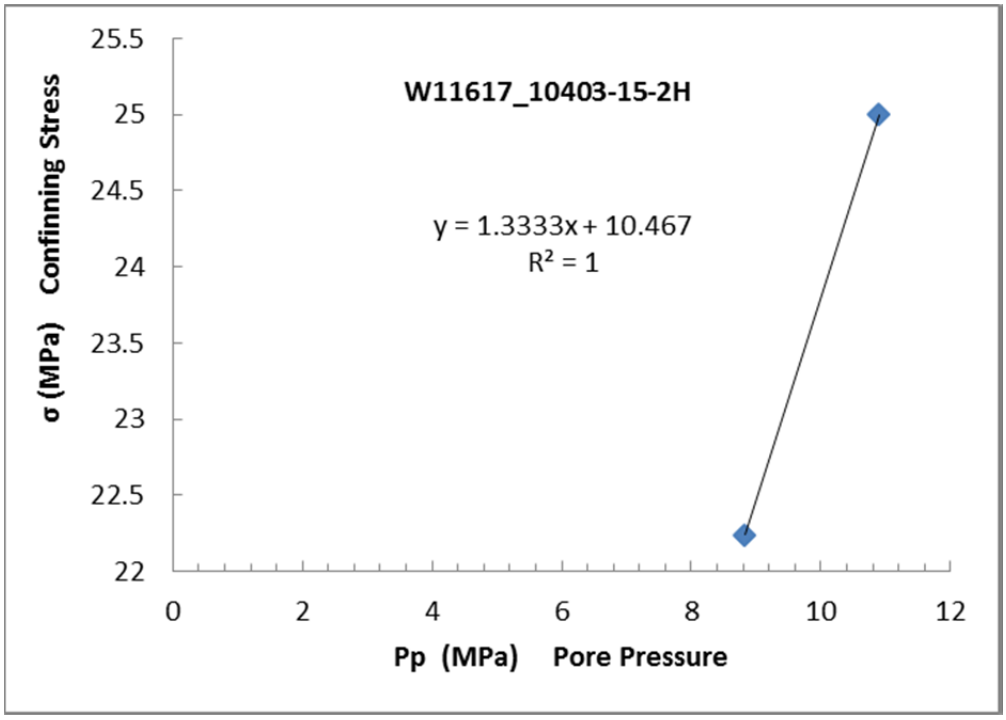
W11617_10403-15-2H
y = 1.3333x + 10.467
R² = 1
σ (MPa) Confinning Stress
Pp (MPa) Pore Pressure
25.5
25
24.5
24
23.5
23
22.5
22
0
2
4
6
8
10
12

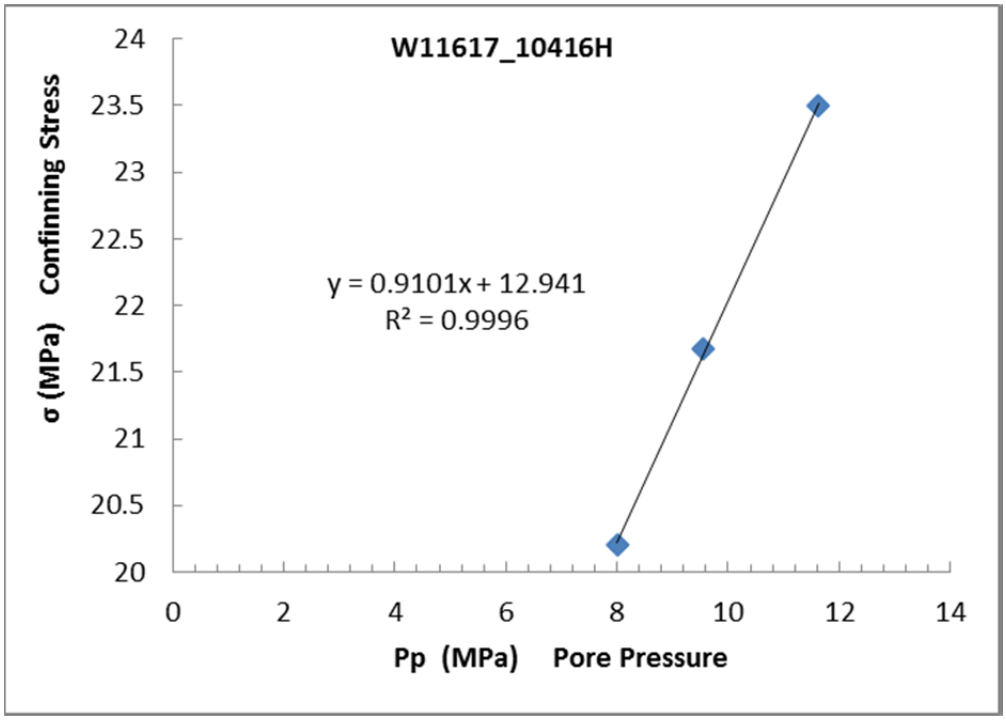

A.3.4 Static Moduli and Poisson's Ratio (Non-destructive)

Uniaxial Stress for File w11617-10364-uniaxial-stress									
Event	Conf	Pore	Diff	Temp	E	n	K	G	P
	MPa	MPa	MPa	°C	GPa		GPa	GPa	GPa
0	40.3	-0.2	21.0	35.4	60.69	0.258	41.78	24.12	73.94
1	50.2	-0.2	30.4	35.4	77.55	0.290	61.51	30.06	101.59
2	30.1	-0.2	21.0	34.3	59.11	0.235	37.13	23.94	69.05

Uniaxial Stress for File w11617-10365-uniaxial-stress									
Event	Conf	Pore	Diff	Temp	E	n	K	G	P
	MPa	MPa	MPa	°C	GPa		GPa	GPa	GPa
0	40.4	-0.2	20.1	28.9	24.25	0.059	9.17	11.45	24.44
1	40.4	-0.2	20.5	28.6	44.33	0.160	21.74	19.11	47.22
2	50.6	-0.2	29.9	29.1	39.97	0.148	18.93	17.41	42.14
3	29.8	-0.2	21.0	26.9	48.15	0.175	24.70	20.49	52.01

Uniaxial Stress for File w11617-10367-horizontal-uniaxial-stress									
Event	Conf	Pore	Diff	Temp	E	n	K	G	P
	MPa	MPa	MPa	°C	GPa		GPa	GPa	GPa
0	40.7	-0.2	21.8	28.8	40.91	0.137	18.77	18.00	42.76
1	50.3	-0.2	31.2	28.5	36.03	0.120	15.81	16.08	37.25
2	29.9	-0.2	21.8	27.1	43.36	0.165	21.55	18.62	46.37

Uniaxial Stress for File w11617-10367-vertical-uniaxial-stress									
Event	Conf	Pore	Diff	Temp	E	n	K	G	P
	MPa	MPa	MPa	°C	GPa		GPa	GPa	GPa
0	40.0	-0.2	21.0	27.2	46.07	0.154	22.18	19.96	48.80
1	50.0	-0.2	29.9	27.0	54.05	0.121	23.78	24.10	55.92
2	29.8	-0.2	21.0	24.1	68.11	0.167	34.06	29.19	72.98

Uniaxial Stress for File w11617-10368.5-verttcal-uniaxial-stress									
Event	Conf	Pore	Diff	Temp	E	n	K	G	P
	MPa	MPa	MPa	°C	GPa		GPa	GPa	GPa
0	41.1	-0.2	21.0	27.6	38.71	0.124	17.14	17.22	40.11
1	50.3	-0.2	30.4	27.7	41.04	0.132	18.60	18.12	42.76
2	30.5	-0.2	20.5	24.0	48.73	0.154	23.44	21.12	51.60

Uniaxial Stress for File w11617-10369-uniaxial-stress									
Event	Conf	Pore	Diff	Temp	E	n	K	G	P
	MPa	MPa	MPa	°C	GPa		GPa	GPa	GPa
0	40.5	-0.2	20.1	32.5	71.26	0.151	33.99	30.97	75.28
1	50.6	-0.2	29.9	29.7	61.89	0.125	27.50	27.51	64.17
2	29.8	-0.2	20.1	26.4	72.07	0.174	36.80	30.71	77.74

Uniaxial Stress for File w11617-10369.8-uniaxial-stress									
Event	Conf	Pore	Diff	Temp	E	n	K	G	P
	MPa	MPa	MPa	°C	GPa		GPa	GPa	GPa
0	40.7	-0.2	30.8	29.0	39.86	0.030	14.14	19.34	39.93
1	50.7	-0.2	30.8	29.1	43.77	0.034	15.64	21.17	43.87

Uniaxial Stress for File w11617-10370-vertical-uniaxial-stress									
Event	Conf	Pore	Diff	Temp	E	n	K	G	P
	MPa	MPa	MPa	°C	GPa		GPa	GPa	GPa
0	40.0	-0.2	21.0	29.3	44.67	-0.059	13.32	23.73	44.96
1	49.9	-0.2	30.8	29.9	41.57	-0.057	12.44	22.04	41.83

Uniaxial Stress for File w11617-10370-vertical-uniaxial-stress-leak									
Event	Conf	Pore	Diff	Temp	E	n	K	G	P
	MPa	MPa	MPa	°C	GPa		GPa	GPa	GPa
0	40.7	-0.2	20.5	30.5	54.91	0.003	18.42	27.37	54.91

Uniaxial Stress for File w11617-10371-v-uniaxial-stress									
Event	Conf	Pore	Diff	Temp	E	n	K	G	P
	MPa	MPa	MPa	°C	GPa		GPa	GPa	GPa
0	40.1	-0.2	20.1	28.6	67.80	0.202	37.91	28.21	75.52
1	50.1	-0.2	29.9	29.0	62.63	0.165	31.12	26.89	66.98
2	30.0	-0.2	21.0	28.3	71.28	0.225	43.12	29.10	81.93

Uniaxial Stress for File w11617-10371.8-uniaxial-stress									
Event	Conf	Pore	Diff	Temp	E	n	K	G	P
	MPa	MPa	MPa	°C	GPa		GPa	GPa	GPa
0	40.0	-0.2	20.5	28.6	81.32	0.066	31.20	38.16	82.08
1	50.0	-0.2	30.4	29.3	84.40	0.082	33.62	39.01	85.64
2	30.2	-0.2	21.4	27.7	99.58	0.061	37.78	46.94	100.37

Uniaxial Stress for File w11617-10372-vertical-uniaxial-stress									
Event	Conf	Pore	Diff	Temp	E	n	K	G	P
	MPa	MPa	MPa	°C	GPa		GPa	GPa	GPa
0	40.4	-0.2	24.0	25.9	106.95	0.028	37.78	52.01	107.12
1	50.2	-0.2	30.4	26.1	99.30	0.030	35.22	48.20	99.49
2	30.2	-0.2	21.8	25.3	106.28	0.015	36.51	52.36	106.33

Uniaxial Stress for File w11617-10373-uniaxial-stress									
Event	Conf	Pore	Diff	Temp	E	n	K	G	P
	MPa	MPa	MPa	°C	GPa		GPa	GPa	GPa
0	40.7	-0.2	21.4	30.9	105.66	0.299	87.45	40.68	141.69
1	50.7	-0.2	25.7	25.7	104.59	0.302	88.16	40.16	141.70
2	30.6	-0.2	21.4	22.9	100.10	0.280	75.90	39.10	128.03

Uniaxial Stress for File w11617-10374-13-1-uniaxial-stress									
Event	Conf	Pore	Diff	Temp	E	n	K	G	P
	MPa	MPa	MPa	°C	GPa		GPa	GPa	GPa
0	40.3	-0.2	20.1	34.8	66.58	0.076	26.18	30.94	67.43
1	50.4	-0.2	19.7	34.8	68.92	0.167	34.51	29.53	73.88
2	30.4	-0.2	21.0	33.4	66.97	0.163	33.10	28.80	71.50

Uniaxial Stress for File w11617-10374.1-13-2-uniaxial-stress									
Event	Conf	Pore	Diff	Temp	E	n	K	G	P
	MPa	MPa	MPa	°C	GPa		GPa	GPa	GPa
0	40.1	-0.2	20.5	34.9	73.46	0.218	43.34	30.17	83.56
1	50.1	-0.2	29.9	34.9	71.93	0.198	39.74	30.02	79.76
2	30.0	-0.2	20.5	33.8	82.52	0.255	56.23	32.87	100.05

Uniaxial Stress for File w11617-10375-uniaxial-stress									
Event	Conf	Pore	Diff	Temp	E	n	K	G	P
	MPa	MPa	MPa	°C	GPa		GPa	GPa	GPa
0	40.6	-0.2	20.5	28.8	238.31	0.647	-270.73	72.36	-174.25
1	50.4	-0.2	30.4	29.4	201.84	0.533	-1029.57	65.85	-941.77
2	30.3	-0.2	21.0	27.8	208.88	0.668	-207.68	62.63	-124.18

Uniaxial Stress for File w11617-10403-15-1-uniaxial-stress									
Event	Conf	Pore	Diff	Temp	E	n	K	G	P
	MPa	MPa	MPa	°C	GPa		GPa	GPa	GPa
0	40.6	-0.2	20.5	26.2	154.82	0.321	143.98	58.61	222.13
1	50.5	-0.2	29.9	26.4	142.15	0.280	107.65	55.53	181.69
2	30.4	-0.2	21.4	23.7	167.75	0.317	153.12	63.67	238.01

Uniaxial Stress for File w11617-10403-15-2-uniaxial-stress									
Event	Conf	Pore	Diff	Temp	E	n	K	G	P
	MPa	MPa	MPa	°C	GPa		GPa	GPa	GPa
0	39.8	-0.2	15.8	26.0	36.20	0.050	13.40	17.24	36.39
1	49.8	-0.2	15.8	26.4	38.17	0.060	14.47	18.00	38.47

Uniaxial Stress for File w11617-10416-uniaxial-stress									
Event	Conf	Pore	Diff	Temp	E	n	K	G	P
	MPa	MPa	MPa	°C	GPa		GPa	GPa	GPa
0	40.1	-0.2	20.5	27.1	176.44	0.305	150.88	67.60	241.01
1	50.3	-0.2	30.4	27.0	152.09	0.243	98.69	61.17	180.25
2	30.7	-0.2	21.4	23.7	187.51	0.347	204.66	69.59	297.45

Uniaxial Stress for File w11617-10419-uniaxial-stress									
Event	Conf	Pore	Diff	Temp	E	n	K	G	P
	MPa	MPa	MPa	°C	GPa		GPa	GPa	GPa
0	40.7	-0.2	20.5	26.2	62.27	0.190	33.45	26.17	68.34
1	50.7	-0.2	25.7	26.8	60.67	0.171	30.72	25.91	65.26
2	30.6	-0.2	21.4	23.2	60.18	0.182	31.56	25.45	65.50

A.3.5 Uni/Triaxial Compressive Strength, Young's Modulus and Poisson's Ratio

Strength for File w11617-10365-strength						
Event	Conf	Diff	Temp	E	n	peak_stress
	MPa	MPa	°C	GPa		MPa
0	19.0	18.8	39.8	70.03	0.531	175.5

Strength for File w11617-10367-horizontl-strength						
Event	Conf	Diff	Temp	E	n	peak_stress
	MPa	MPa	°C	GPa		MPa
0	10.1	12.4	33.1	19.48	0.189	43.2

Strength for File w11617-10367vertical-strength						
Event	Conf	Diff	Temp	E	n	peak_stress
	MPa	MPa	°C	GPa		MPa
0	10.1	29.1	29.8	114.58	1.057	193.4

Strength for File w11617-10368.5vertical-strength						
Event	Conf	Diff	Temp	E	n	peak_stress
	MPa	MPa	°C	GPa		MPa
0	0.7	3.5	32.8	52.29	0.199	137.9

Strength for File w11617-10369-strength						
Event	Conf	Diff	Temp	E	n	peak_stress
	MPa	MPa	°C	GPa		MPa
0	19.1	18.8	34.1	120.86	1.119	128.5

Strength for File w11617-10369.8-strength						
Event	Conf	Diff	Temp	E	n	peak_stress
	MPa	MPa	°C	GPa		MPa
0	10.0	18.8	41.1	57.79	0.036	131.9

Strength for File w11617-10371.8-strength						
Event	Conf	Diff	Temp	E	n	peak_stress
	MPa	MPa	°C	GPa		MPa
0	0.9	29.5	34.5	76.05	0.264	146.0

Strength for File w11617-10371vertical-strength						
Event	Conf	Diff	Temp	E	n	peak_stress
	MPa	MPa	°C	GPa		MPa
0	19.1	30.4	35.0	57.48	0.425	105.1

Strength for File w11617-10372vertical-strength						
Event	Conf	Diff	Temp	E	n	peak_stress
	MPa	MPa	°C	GPa		MPa
0	10.1	8.2	30.4	46.65	0.058	109.8

Strength for File w11617-10373-strength						
Event	Conf	Diff	Temp	E	n	peak_stress
	MPa	MPa	°C	GPa		MPa
0	19.1	30.8	34.7	87.89	2.999	54.3

Strength for File w11617-10419-strength						
Event	Conf	Diff	Temp	E	n	peak_stress
	MPa	MPa	°C	GPa		MPa
0	0.9	23.5	29.8	88.41	0.302	116.2

A.3.6 Mohr's Circle

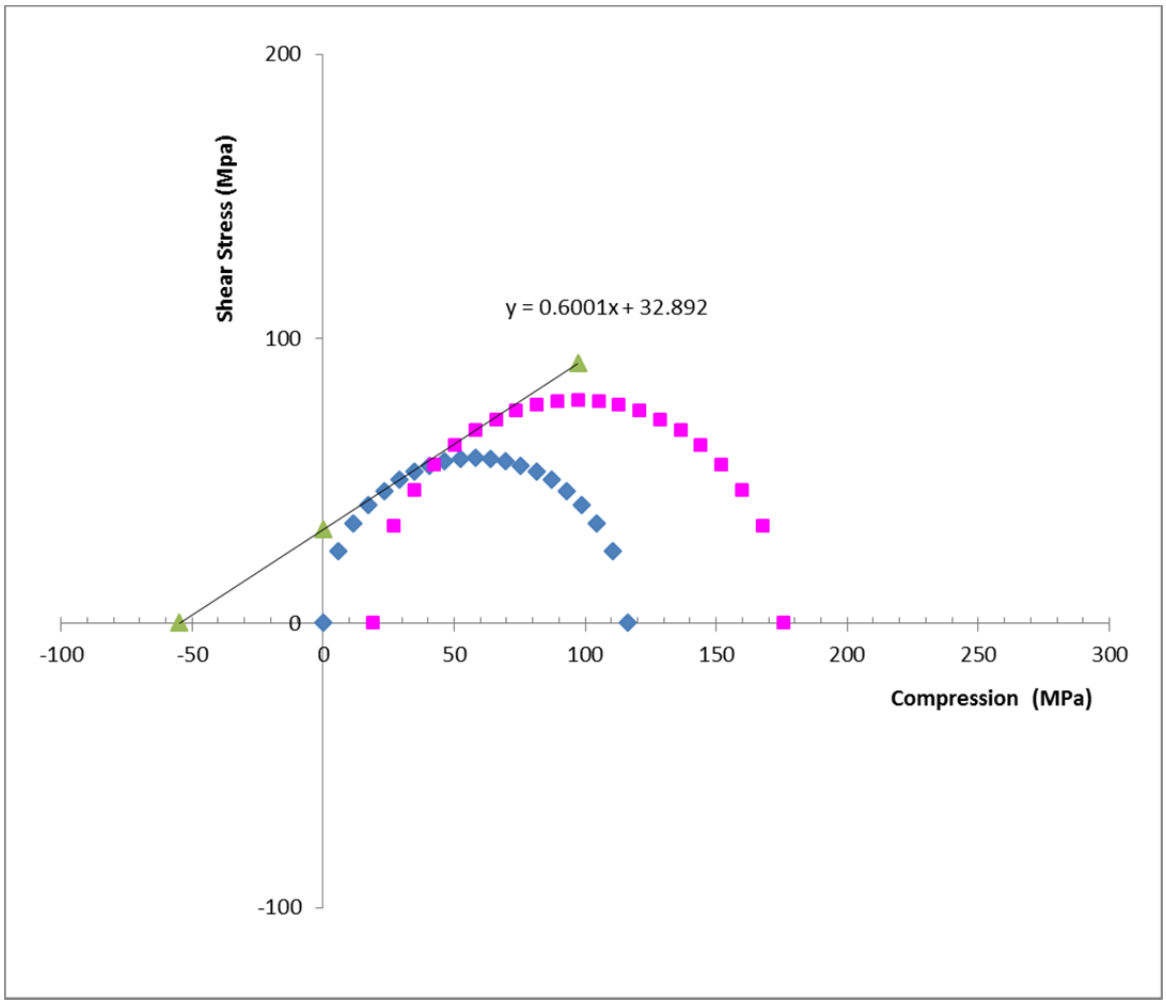

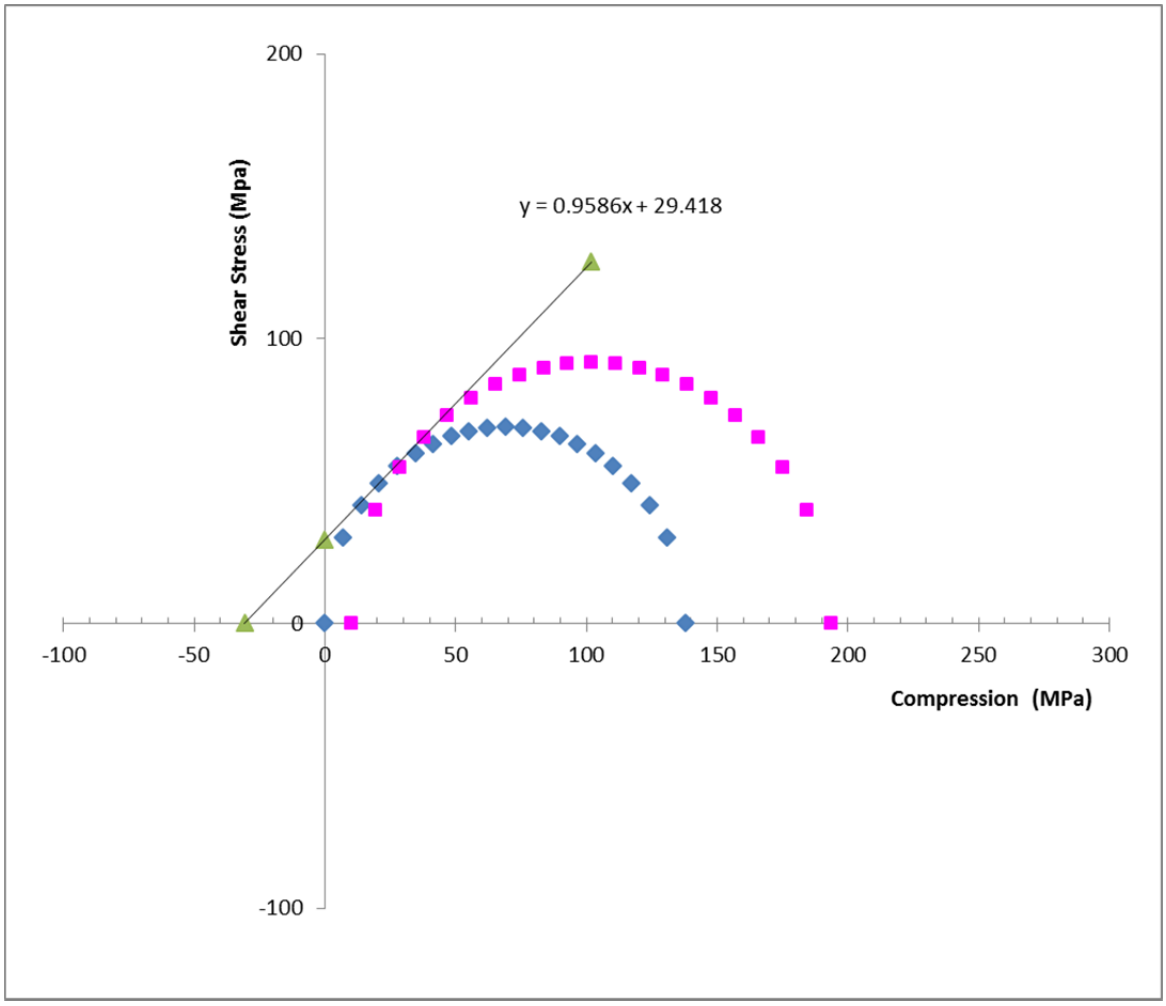
y = 0.9586x + 29.418
Shear Stress (Mpa)
Compression (MPa)
200
100
0
-100
-100
-50
0
50
100
150
200
250
300

A.4. Well 70 Bakken Samples Testing Results

A.4.1 Permeability

Permeability and Specific Storage for File w70-mb-8842.7V-perm							
Event	Type	Conf	Pore Top	Diff	Temp	Perm	Storage
		MPa	MPa	MPa	°C	μD	m^{-1}
0	multipulse	30.2	7.7	-4.8	28.8	0.0396	1.48e-07
1	multipulse	25.3	7.7	-4.8	28.6	0.0438	1.62e-07
2	multipulse	20.3	7.8	-3.9	28.6	0.0463	1.53e-07
3	multipulse	15.2	7.7	-3.9	28.5	0.0561	1.55e-07
4	multipulse	10.3	7.2	-3.1	28.4	0.140	1.68e-07

Permeability and Specific Storage for File w70-mb-8843H-perm							
Event	Type	Conf	Pore Top	Diff	Temp	Perm	Storage
		MPa	MPa	MPa	°C	μD	m^{-1}
0	multipulse	30.2	7.7	-4.8	24.7	0.0626	4.87e-07
1	multipulse	25.4	7.7	-4.3	24.5	0.0711	5.82e-07
2	multipulse	20.3	7.7	-3.9	25.2	0.0863	5.87e-07
3	multipulse	15.2	7.7	-4.3	20.7	0.111	5.86e-07
4	multipulse	10.2	7.2	-3.5	21.2	1.06e+03	6.28e-07

Permeability and Specific Storage for File w70-mb-8845.8H-perm							
Event	Type	Conf	Pore Top	Diff	Temp	Perm	Storage
		MPa	MPa	MPa	°C	μD	m^{-1}
0	multipulse	30.3	7.8	-3.9	23.3	0.0597	6.02e-07
1	multipulse	25.4	7.7	-3.5	24.1	0.0652	5.46e-07
2	multipulse	20.4	7.7	-3.1	23.6	0.0753	5.92e-07
3	multipulse	15.3	7.8	-2.6	24.0	0.0893	5.33e-07

Permeability and Specific Storage for File w70-mb-8845V-perm							
Event	Type	Conf	Pore Top	Diff	Temp	Perm	Storage
		MPa	MPa	MPa	°C	μD	m^{-1}
0	multipulse	30.3	7.7	-4.8	28.1	0.0671	1.26e-06
1	multipulse	25.3	7.7	-4.3	27.9	0.0711	1.28e-06
2	multipulse	20.3	7.8	-3.9	28.0	0.0834	1.36e-06
3	multipulse	15.3	7.8	-3.5	27.8	0.0946	1.35e-06
4	multipulse	10.3	7.2	-3.1	26.0	1.24e+03	9.71e-07

Permeability and Specific Storage for File w70-mb-8846.6V45-perm							
Event	Type	Conf	Pore Top	Diff	Temp	Perm	Storage
		MPa	MPa	MPa	°C	μD	m^{-1}
0	multipulse	30.3	7.8	-4.3	27.2	0.0603	9.81e-07
1	multipulse	25.3	7.7	-3.9	27.5	0.0659	9.15e-07
2	multipulse	20.3	7.7	-3.5	27.3	0.0731	8.77e-07
3	multipulse	15.3	7.7	-3.1	25.5	0.0915	8.38e-07
4	multipulse	10.3	6.3	-3.1	22.9	0.389	1.17e-07

Permeability and Specific Storage for File w70-mb-8847.3V45-perm							
Event	Type	Conf	Pore Top	Diff	Temp	Perm	Storage
		MPa	MPa	MPa	°C	μD	m^{-1}
0	multipulse	30.3	7.8	-3.9	23.3	0.0323	6.13e-08
1	multipulse	25.4	7.7	-4.3	23.5	0.0356	3.50e-08
2	multipulse	20.3	7.8	-3.5	23.7	0.0402	1.55e-08
3	multipulse	15.2	7.7	-3.5	23.7	0.0463	7.02e-08
4	multipulse	10.3	7.2	-3.1	23.0	0.0684	1.52e-11

Permeability and Specific Storage for File w70-mb-8847.3V45-perm(low-one)							
Event	Type	Conf	Pore Top	Diff	Temp	Perm	Storage
		MPa	MPa	MPa	°C	μD	m^{-1}
0	multipulse	15.2	7.7	-3.5	24.3	0.0528	5.42e-08

Permeability and Specific Storage for File w70-mb-8847.7V45-perm							
Event	Type	Conf	Pore Top	Diff	Temp	Perm	Storage
		MPa	MPa	MPa	°C	μD	m^{-1}
0	multipulse	30.3	7.7	-3.9	23.6	0.0497	4.62e-07
1	multipulse	25.3	7.8	-3.5	23.3	0.0573	5.40e-07
2	multipulse	20.3	7.7	-2.6	22.6	0.0569	4.04e-07
3	multipulse	15.3	7.7	-2.6	22.1	0.0740	4.29e-07
4	multipulse	10.3	6.3	-1.8	22.1	1.73	1.06e-10

Permeability and Specific Storage for File w70-mb-8848.5V-perm							
Event	Type	Conf	Pore Top	Diff	Temp	Perm	Storage
		MPa	MPa	MPa	°C	μD	m^{-1}
0	multipulse	15.0	7.8	-3.5	24.0	0.000197	2.10e-07
1	multipulse	15.0	7.8	-3.1	24.5	0.00560	3.31e-07
2	multipulse	10.5	7.7	-3.1	24.3	18.3	4.92e-12
3	multipulse	15.1	7.7	-3.5	24.5	0.0151	8.78e-07

Permeability and Specific Storage for File w70-mb-8848.5V-perm(fault)							
Event	Type	Conf	Pore Top	Diff	Temp	Perm	Storage
		MPa	MPa	MPa	°C	μD	m^{-1}
0	multipulse	30.3	7.8	-4.3	25.5	0.000217	3.51e-07
1	multipulse	25.4	7.7	-3.9	25.4	0.0302	2.59e-06
2	multipulse	20.3	7.7	-3.9	25.3	1.14	0.000114

Permeability and Specific Storage for File w70-mb-8848H-perm							
Event	Type	Conf	Pore Top	Diff	Temp	Perm	Storage
		MPa	MPa	MPa	°C	μD	m^{-1}
0	multipulse	30.3	7.7	-4.8	21.4	0.192	1.00e-05
1	multipulse	25.2	7.7	-4.8	21.7	0.0399	3.23e-07
2	multipulse	20.3	7.7	-4.3	22.0	0.0423	1.69e-07
3	multipulse	15.2	7.7	-3.9	22.3	0.0539	5.22e-08
4	multipulse	10.2	7.2	-3.5	23.0	1.12e+06	2.61e-07

Permeability and Specific Storage for File w16862-8823.8-perm&biot							
Event	Type	Conf	Pore Top	Diff	Temp	Perm	Storage
		MPa	MPa	MPa	°C	μD	m^{-1}
0	multipulse	20.6	7.9	-0.4	32.5	0.0109	2.02e-07
1	multipulse	30.6	8.0	-0.8	32.1	0.00826	4.66e-08
2	multipulse	40.6	8.0	-0.8	32.1	0.00343	5.16e-07

Permeability and Specific Storage for File w16862-8824.7-perm&biot							
Event	Type	Conf	Pore Top	Diff	Temp	Perm	Storage
		MPa	MPa	MPa	°C	μD	m^{-1}
0	multipulse	20.6	7.9	0.0	25.8	0.0475	4.46e-07
1	multipulse	30.6	8.0	-0.4	28.3	0.0195	7.48e-08

Permeability and Specific Storage for File w16862-8827.6-perm							
Event	Type	Conf	Pore Top	Diff	Temp	Perm	Storage
		MPa	MPa	MPa	°C	μD	m^{-1}
0	multipulse	20.6	7.9	-0.4	27.0	0.417	0.000111
1	multipulse	20.6	7.9	-0.4	28.4	0.0204	1.38e-07
2	multipulse	30.5	7.9	-0.8	27.0	0.00965	6.03e-08
3	multipulse	40.6	7.9	-1.3	27.3	0.0105	1.26e-07

Permeability and Specific Storage for File w16862-8833.8-perm&biot							
Event	Type	Conf	Pore Top	Diff	Temp	Perm	Storage
		MPa	MPa	MPa	°C	μD	m^{-1}
0	multipulse	20.6	7.9	-0.4	25.3	0.0222	2.75e-07
1	multipulse	30.5	7.9	-0.8	27.8	0.0118	3.79e-06
2	multipulse	40.6	7.9	-1.3	28.7	1.08	0.000100
3	multipulse	50.6	8.0	-1.3	29.1	0.00834	5.64e-07

Permeability and Specific Storage for File w16862-8834.2-perm&biot							
Event	Type	Conf	Pore Top	Diff	Temp	Perm	Storage
		MPa	MPa	MPa	°C	μD	m^{-1}
0	multipulse	20.6	8.0	0.0	28.5	0.0638	5.24e-07
1	multipulse	30.6	8.0	0.0	28.6	0.0438	3.40e-07
2	multipulse	40.6	8.0	-0.4	28.3	0.0721	8.05e-07
3	multipulse	50.7	8.0	-0.8	29.0	0.0475	9.09e-06

Permeability and Specific Storage for File w16862-8834.4-perm							
Event	Type	Conf	Pore Top	Diff	Temp	Perm	Storage
		MPa	MPa	MPa	°C	μD	m^{-1}
0	multipulse	20.5	7.9	-0.4	27.5	0.114	2.99e-07
1	multipulse	30.5	7.9	-0.8	27.7	0.0953	3.80e-07
2	multipulse	40.5	7.9	-1.3	27.8	0.0694	2.99e-07
3	multipulse	50.6	7.9	-1.7	27.7	0.0714	4.17e-07

Permeability and Specific Storage for File w16862-8834.6-perm&biot							
Event	Type	Conf	Pore Top	Diff	Temp	Perm	Storage
		MPa	MPa	MPa	°C	μD	m^{-1}
0	aspike	20.7	7.9	0.4	25.7	398.	8.23e-12
1	aspike	30.5	7.9	-0.4	27.2	313.	5.87e-13
2	aspike	50.7	8.0	-0.4	29.5	231.	3.25e-11

Permeability and Specific Storage for File w16862-8835.2-perm&biot							
Event	Type	Conf	Pore Top	Diff	Temp	Perm	Storage
		MPa	MPa	MPa	°C	μD	m^{-1}
0	multipulse	20.6	8.0	0.9	30.5	0.257	1.29e-07
1	multipulse	30.5	8.0	0.0	30.2	0.229	1.47e-07

Permeability and Specific Storage for File w16862-8836.7-perm&biot							
Event	Type	Conf	Pore Top	Diff	Temp	Perm	Storage
		MPa	MPa	MPa	°C	μD	m^{-1}
0	aspike	20.6	7.9	0.0	27.7	2.96	3.49e-06
1	aspike	30.5	7.9	-0.8	27.9	1.87	1.38e-06
2	aspike	40.6	7.9	-0.8	27.6	0.846	2.72e-09

Permeability and Specific Storage for File w16862-8837-perm&biot							
Event	Type	Conf	Pore Top	Diff	Temp	Perm	Storage
		MPa	MPa	MPa	°C	μD	m^{-1}
0	multipulse	20.6	7.9	0.4	31.8	0.0376	2.99e-07
1	multipulse	30.6	8.0	0.9	32.5	0.0251	1.58e-07

Permeability and Specific Storage for File w16862-8837.8-perm&biot							
Event	Type	Conf	Pore Top	Diff	Temp	Perm	Storage
		MPa	MPa	MPa	°C	μD	m^{-1}
0	multipulse	20.7	8.0	0.9	30.3	0.125	6.68e-07
1	multipulse	30.6	8.0	0.0	29.6	0.0934	4.39e-07
2	multipulse	40.7	8.0	-0.4	29.3	0.0694	3.37e-07
3	multipulse	50.6	8.0	-0.8	29.2	0.0752	4.17e-07

Permeability and Specific Storage for File w16862-8838.5-perm&biot							
Event	Type	Conf	Pore Top	Diff	Temp	Perm	Storage
		MPa	MPa	MPa	°C	μD	m^{-1}
0	multipulse	20.7	8.0	0.9	28.1	0.151	5.16e-07
1	multipulse	30.6	7.9	-0.4	28.8	0.150	6.95e-07
2	multipulse	40.7	8.0	-0.4	28.8	0.124	5.22e-07
3	multipulse	50.7	8.0	-0.8	29.1	0.121	6.01e-07

Permeability and Specific Storage for File w16862-8839.4-perm&biot							
Event	Type	Conf	Pore Top	Diff	Temp	Perm	Storage
		MPa	MPa	MPa	°C	μD	m^{-1}
0	aspike	20.6	7.9	0.0	29.8	69.0	5.72e-10
1	aspike	20.6	7.9	0.0	29.9	83.9	4.51e-13
2	aspike	30.6	7.9	0.0	31.3	74.0	3.95e-11
3	aspike	50.7	7.9	-0.8	31.5	57.3	1.69e-11

Permeability and Specific Storage for File w16862-8840.8-perm&biot							
Event	Type	Conf	Pore Top	Diff	Temp	Perm	Storage
		MPa	MPa	MPa	°C	μD	m^{-1}
0	multipulse	20.6	7.9	0.9	30.8	0.133	5.54e-07
1	multipulse	30.6	7.9	0.4	30.9	0.132	7.12e-07
2	multipulse	40.6	7.9	-0.4	31.1	0.0876	4.38e-07

Permeability and Specific Storage for File w16862-8841.4-perm&biot							
Event	Type	Conf	Pore Top	Diff	Temp	Perm	Storage
		MPa	MPa	MPa	°C	μD	m^{-1}
0	multipulse	20.7	8.0	1.3	32.6	0.0299	4.20e-07
1	multipulse	30.5	7.9	0.4	32.0	0.0212	3.71e-07

Permeability and Specific Storage for File w16862-8841.9-perm&biot							
Event	Type	Conf	Pore Top	Diff	Temp	Perm	Storage
		MPa	MPa	MPa	°C	μD	m^{-1}
0	multipulse	20.6	7.9	0.0	33.4	0.0881	1.95e-07
1	multipulse	30.6	8.0	-0.4	33.5	0.0931	3.82e-07
2	multipulse	40.6	7.9	-1.3	33.8	0.104	4.73e-07
3	multipulse	50.6	8.0	-1.7	33.9	0.0902	4.88e-07

A.4.2 Sonic Velocity, Dynamic Moduli and Poisson's Ratio

Observed Velocities and Moduli for File w16862-8837.8-vel									
Event	Conf	Pore	Diff	Temp	V_p	$V_s^{(1)}$	$V_s^{(2)}$	Young's Modulus	Poisson's Ratio
	MPa	MPa	MPa	°C	m/s	m/s	m/s	GPa	
0	10.5	0.6	0.7	28.5	4644	3117	2899	51.72	0.139
1	20.6	0.7	0.6	29.3	4721	3186	2974	53.79	0.129
2	30.6	0.6	0.0	30.2	4923	3259	2989	56.97	0.163
3	40.6	0.6	-0.8	30.8	4923	3277	3021	57.43	0.154
4	50.6	0.6	-1.1	30.9	5054	3354	3053	59.98	0.164

Observed Velocities and Moduli for File w16862-8837.8-vel									
Event	Conf	Pore	Diff	Temp	V_p	$V_s^{(1)}$	$V_s^{(2)}$	Young's Modulus	Poisson's Ratio
	MPa	MPa	MPa	°C	m/s	m/s	m/s	GPa	
0	10.5	0.6	0.7	28.5	4644	3117	2899	51.72	0.139
1	20.6	0.7	0.6	29.3	4721	3186	2974	53.79	0.129
2	30.6	0.6	0.0	30.2	4923	3259	2989	56.97	0.163
3	40.6	0.6	-0.8	30.8	4923	3277	3021	57.43	0.154
4	50.6	0.6	-1.1	30.9	5054	3354	3053	59.98	0.164

Observed Velocities and Moduli for File w16862-8837.8-vel									
Event	Conf	Pore	Diff	Temp	V_p	$V_s^{(1)}$	$V_s^{(2)}$	Young's Modulus	Poisson's Ratio
	MPa	MPa	MPa	°C	m/s	m/s	m/s	GPa	
0	10.5	0.6	0.7	28.5	4644	3117	2899	51.72	0.139
1	20.6	0.7	0.6	29.3	4721	3186	2974	53.79	0.129
2	30.6	0.6	0.0	30.2	4923	3259	2989	56.97	0.163
3	40.6	0.6	-0.8	30.8	4923	3277	3021	57.43	0.154
4	50.6	0.6	-1.1	30.9	5054	3354	3053	59.98	0.164

Observed Velocities and Moduli for File w16862-8837.8-vel									
Event	Conf	Pore	Diff	Temp	V_p	$V_s^{(1)}$	$V_s^{(2)}$	Young's Modulus	Poisson's Ratio
	MPa	MPa	MPa	°C	m/s	m/s	m/s	GPa	
0	10.5	0.6	0.7	28.5	4644	3117	2899	51.72	0.139
1	20.6	0.7	0.6	29.3	4721	3186	2974	53.79	0.129
2	30.6	0.6	0.0	30.2	4923	3259	2989	56.97	0.163
3	40.6	0.6	-0.8	30.8	4923	3277	3021	57.43	0.154
4	50.6	0.6	-1.1	30.9	5054	3354	3053	59.98	0.164

Observed Velocities and Moduli for File w16862-8837.8-vel									
Event	Conf	Pore	Diff	Temp	V_p	$V_s^{(1)}$	$V_s^{(2)}$	Young's Modulus	Poisson's Ratio
	MPa	MPa	MPa	°C	m/s	m/s	m/s	GPa	
0	10.5	0.6	0.7	28.5	4644	3117	2899	51.72	0.139
1	20.6	0.7	0.6	29.3	4721	3186	2974	53.79	0.129
2	30.6	0.6	0.0	30.2	4923	3259	2989	56.97	0.163
3	40.6	0.6	-0.8	30.8	4923	3277	3021	57.43	0.154
4	50.6	0.6	-1.1	30.9	5054	3354	3053	59.98	0.164

Observed Velocities and Moduli for File w16862-8837.8-vel									
Event	Conf	Pore	Diff	Temp	V_p	$V_s^{(1)}$	$V_s^{(2)}$	Young's Modulus	Poisson's Ratio
	MPa	MPa	MPa	°C	m/s	m/s	m/s	GPa	
0	10.5	0.6	0.7	28.5	4644	3117	2899	51.72	0.139
1	20.6	0.7	0.6	29.3	4721	3186	2974	53.79	0.129
2	30.6	0.6	0.0	30.2	4923	3259	2989	56.97	0.163
3	40.6	0.6	-0.8	30.8	4923	3277	3021	57.43	0.154
4	50.6	0.6	-1.1	30.9	5054	3354	3053	59.98	0.164

Observed Velocities and Moduli for File w16862-8837.8-vel									
Event	Conf	Pore	Diff	Temp	V_p	$V_s^{(1)}$	$V_s^{(2)}$	Young's Modulus	Poisson's Ratio
	MPa	MPa	MPa	°C	m/s	m/s	m/s	GPa	
0	10.5	0.6	0.7	28.5	4644	3117	2899	51.72	0.139
1	20.6	0.7	0.6	29.3	4721	3186	2974	53.79	0.129
2	30.6	0.6	0.0	30.2	4923	3259	2989	56.97	0.163
3	40.6	0.6	-0.8	30.8	4923	3277	3021	57.43	0.154
4	50.6	0.6	-1.1	30.9	5054	3354	3053	59.98	0.164

Observed Velocities and Moduli for File w16862-8837.8-vel									
Event	Conf	Pore	Diff	Temp	V_p	$V_s^{(1)}$	$V_s^{(2)}$	Young's Modulus	Poisson's Ratio
	MPa	MPa	MPa	°C	m/s	m/s	m/s	GPa	
0	10.5	0.6	0.7	28.5	4644	3117	2899	51.72	0.139
1	20.6	0.7	0.6	29.3	4721	3186	2974	53.79	0.129
2	30.6	0.6	0.0	30.2	4923	3259	2989	56.97	0.163
3	40.6	0.6	-0.8	30.8	4923	3277	3021	57.43	0.154
4	50.6	0.6	-1.1	30.9	5054	3354	3053	59.98	0.164

Observed Velocities and Moduli for File w16862-8837.8-vel									
Event	Conf	Pore	Diff	Temp	V_p	$V_s^{(1)}$	$V_s^{(2)}$	Young's Modulus	Poisson's Ratio
	MPa	MPa	MPa	°C	m/s	m/s	m/s	GPa	
0	10.5	0.6	0.7	28.5	4644	3117	2899	51.72	0.139
1	20.6	0.7	0.6	29.3	4721	3186	2974	53.79	0.129
2	30.6	0.6	0.0	30.2	4923	3259	2989	56.97	0.163
3	40.6	0.6	-0.8	30.8	4923	3277	3021	57.43	0.154
4	50.6	0.6	-1.1	30.9	5054	3354	3053	59.98	0.164

Observed Velocities and Moduli for File w16862-8837.8-vel									
Event	Conf	Pore	Diff	Temp	V_p	$V_s^{(1)}$	$V_s^{(2)}$	Young's Modulus	Poisson's Ratio
	MPa	MPa	MPa	°C	m/s	m/s	m/s	GPa	
0	10.5	0.6	0.7	28.5	4644	3117	2899	51.72	0.139
1	20.6	0.7	0.6	29.3	4721	3186	2974	53.79	0.129
2	30.6	0.6	0.0	30.2	4923	3259	2989	56.97	0.163
3	40.6	0.6	-0.8	30.8	4923	3277	3021	57.43	0.154
4	50.6	0.6	-1.1	30.9	5054	3354	3053	59.98	0.164

Observed Velocities and Moduli for File w16862-8837.8-vel									
Event	Conf	Pore	Diff	Temp	V_p	$V_s^{(1)}$	$V_s^{(2)}$	Young's Modulus	Poisson's Ratio
	MPa	MPa	MPa	°C	m/s	m/s	m/s	GPa	
0	10.5	0.6	0.7	28.5	4644	3117	2899	51.72	0.139
1	20.6	0.7	0.6	29.3	4721	3186	2974	53.79	0.129
2	30.6	0.6	0.0	30.2	4923	3259	2989	56.97	0.163
3	40.6	0.6	-0.8	30.8	4923	3277	3021	57.43	0.154
4	50.6	0.6	-1.1	30.9	5054	3354	3053	59.98	0.164

Observed Velocities and Moduli for File w16862-8837.8-vel									
Event	Conf	Pore	Diff	Temp	V_p	$V_s^{(1)}$	$V_s^{(2)}$	Young's Modulus	Poisson's Ratio
	MPa	MPa	MPa	°C	m/s	m/s	m/s	GPa	
0	10.5	0.6	0.7	28.5	4644	3117	2899	51.72	0.139
1	20.6	0.7	0.6	29.3	4721	3186	2974	53.79	0.129
2	30.6	0.6	0.0	30.2	4923	3259	2989	56.97	0.163
3	40.6	0.6	-0.8	30.8	4923	3277	3021	57.43	0.154
4	50.6	0.6	-1.1	30.9	5054	3354	3053	59.98	0.164

Observed Velocities and Moduli for File w16862-8837.8-vel									
Event	Conf	Pore	Diff	Temp	V_p	$V_s^{(1)}$	$V_s^{(2)}$	Young's Modulus	Poisson's Ratio
	MPa	MPa	MPa	°C	m/s	m/s	m/s	GPa	
0	10.5	0.6	0.7	28.5	4644	3117	2899	51.72	0.139
1	20.6	0.7	0.6	29.3	4721	3186	2974	53.79	0.129
2	30.6	0.6	0.0	30.2	4923	3259	2989	56.97	0.163
3	40.6	0.6	-0.8	30.8	4923	3277	3021	57.43	0.154
4	50.6	0.6	-1.1	30.9	5054	3354	3053	59.98	0.164

Observed Velocities and Moduli for File w70-mb-8842.3V45-vel									
Event	Conf	Pore	Diff	Temp	V_p	$V_s^{(1)}$	$V_s^{(2)}$	Young's Modulus	Poisson's Ratio
	MPa	MPa	MPa	°C	m/s	m/s	m/s	GPa	
0	30.2	5.6	-4.8	24.0	4897	2970	2926	54.73	0.216
1	28.3	5.6	-4.8	23.9	4866	2967	2917	54.34	0.212
2	26.3	5.6	-4.8	23.7	4855	2963	2915	54.17	0.211
3	24.3	5.6	-4.5	23.6	4820	2958	2908	53.74	0.206
4	22.2	5.6	-4.6	23.4	4805	2949	2902	53.44	0.205
5	20.2	5.6	-4.6	23.3	4794	2941	2891	53.14	0.206
6	18.2	5.6	-4.3	23.2	4787	2933	2886	52.93	0.207
7	16.2	5.6	-3.9	23.1	4759	2932	2875	52.56	0.204
8	14.2	5.6	-3.6	22.9	4744	2915	2861	52.09	0.206
9	12.3	5.6	-3.5	22.7	4704	2902	2855	51.53	0.201
10	10.2	5.6	-4.1	22.4	4667	2887	2847	50.96	0.197
11	8.1	5.6	-3.9	21.6	4637	2870	2835	50.39	0.196
12	6.2	5.6	-3.9	20.5	4574	2859	2809	49.44	0.188
13	4.2	5.6	-3.5	21.0	4537	2832	2787	48.62	0.189
14	2.2	5.6	-3.5	20.2	4446	2808	2706	46.76	0.188

Observed Velocities and Moduli for File w70-mb-8842.7V-vel									
Event	Conf	Pore	Diff	Temp	V_p	$V_s^{(1)}$	$V_s^{(2)}$	Young's Modulus	Poisson's Ratio
	MPa	MPa	MPa	°C	m/s	m/s	m/s	GPa	
0	30.2	5.6	-4.3	26.0	4643	2918	2909	51.48	0.175
1	28.3	5.6	-4.2	25.8	4588	2914	2906	50.84	0.163
2	26.2	5.6	-4.2	25.5	4560	2912	2901	50.47	0.158
3	24.3	5.6	-3.9	25.4	4552	2909	2898	50.33	0.157
4	22.2	5.6	-4.2	25.2	4548	2906	2893	50.22	0.158
5	20.3	5.6	-3.5	25.1	4541	2900	2887	50.04	0.158
6	18.2	5.6	-3.6	24.7	4516	2891	2881	49.63	0.155
7	16.2	5.6	-3.9	24.3	4509	2887	2876	49.48	0.155
8	14.2	5.6	-3.6	24.0	4492	2876	2867	49.12	0.154
9	12.2	5.6	-3.6	23.7	4464	2867	2859	48.67	0.151
10	10.2	5.6	-3.3	23.5	4431	2857	2851	48.15	0.145
11	8.2	5.7	-3.2	23.3	4401	2847	2838	47.62	0.142
12	6.2	5.6	-3.5	22.8	4380	2833	2832	47.22	0.141
13	4.2	5.6	-3.2	22.3	4350	2822	2817	46.67	0.138
14	2.2	5.6	-2.8	22.1	4269	2797	2802	45.40	0.123

Observed Velocities and Moduli for File w70-mb-8843.4V45-vel									
Event	Conf	Pore	Diff	Temp	V_p	$V_s^{(1)}$	$V_s^{(2)}$	Young's Modulus	Poisson's Ratio
	MPa	MPa	MPa	°C	m/s	m/s	m/s	GPa	
0	30.3	5.7	-4.3	25.0	4746	2933	3007	53.42	0.178
1	28.3	5.6	-4.5	24.8	4733	2931	3002	53.22	0.176
2	26.2	5.6	-4.8	24.6	4719	2925	2997	52.97	0.175
3	24.2	5.6	-4.5	24.4	4706	2920	2995	52.76	0.174
4	22.3	5.6	-4.2	24.3	4700	2913	2988	52.57	0.175
5	20.2	5.6	-4.3	24.1	4660	2909	2982	52.06	0.167
6	18.2	5.6	-4.3	24.0	4650	2903	2974	51.82	0.168
7	16.2	5.6	-4.3	23.9	4637	2898	2965	51.55	0.167
8	14.2	5.6	-3.9	23.8	4616	2894	2958	51.23	0.164
9	12.2	5.6	-3.6	23.7	4585	2884	2948	50.72	0.160
10	10.2	5.6	-3.8	23.6	4542	2873	2940	50.08	0.153
11	8.2	5.6	-3.5	23.5	4498	2861	2936	49.44	0.145
12	6.2	5.6	-3.9	23.4	4478	2855	2923	49.06	0.144
13	4.2	5.6	-3.6	23.4	4464	2847	2912	48.74	0.144
14	2.3	5.6	-3.2	22.3	4385	2810	2896	47.40	0.133

Observed Velocities and Moduli for File w70-mb-8843.8V-vel									
Event	Conf	Pore	Diff	Temp	V_p	$V_s^{(1)}$	$V_s^{(2)}$	Young's Modulus	Poisson's Ratio
	MPa	MPa	MPa	°C	m/s	m/s	m/s	GPa	
0	30.2	5.6	-4.3	26.5	4699	2963	2969	53.47	0.169
1	28.3	5.6	-3.9	26.3	4691	2957	2959	53.23	0.170
2	26.3	5.6	-3.9	26.1	4686	2953	2957	53.12	0.170
3	24.3	5.6	-3.9	25.9	4678	2949	2954	52.97	0.169
4	22.2	5.6	-4.1	25.7	4660	2943	2948	52.66	0.167
5	20.2	5.6	-4.1	25.6	4635	2937	2946	52.32	0.163
6	18.2	5.6	-3.6	25.4	4607	2931	2938	51.88	0.159
7	16.2	5.6	-3.6	25.0	4583	2928	2933	51.54	0.154
8	14.2	5.6	-3.9	24.0	4544	2917	2922	50.90	0.149
9	12.2	5.6	-3.6	24.2	4525	2911	2912	50.55	0.147
10	10.3	5.6	-3.1	24.0	4515	2900	2907	50.30	0.147
11	8.2	5.7	-3.1	23.9	4508	2890	2901	50.09	0.149
12	6.3	5.6	-3.1	24.0	4496	2881	2894	49.81	0.149
13	4.2	5.6	-3.5	23.7	4473	2865	2887	49.36	0.148
14	2.2	5.6	-3.1	23.4	4408	2835	2862	48.16	0.141

Observed Velocities and Moduli for File w70-mb-8843H-vel									
Event	Conf	Pore	Diff	Temp	V_p	$V_s^{(1)}$	$V_s^{(2)}$	Young's Modulus	Poisson's Ratio
	MPa	MPa	MPa	°C	m/s	m/s	m/s	GPa	
0	30.3	5.6	-4.8	22.1	5015	3035	3023	57.64	0.213
1	28.3	5.6	-4.8	21.6	4997	3034	3020	57.44	0.210
2	26.3	5.6	-4.8	21.4	4983	3031	3019	57.27	0.208
3	24.3	5.6	-4.5	21.7	4978	3030	3015	57.17	0.208
4	22.2	5.7	-4.5	21.0	4964	3027	3010	56.95	0.207
5	20.2	5.6	-4.8	20.7	4954	3024	3005	56.77	0.206
6	18.2	5.7	-4.3	20.5	4945	3017	3001	56.56	0.206
7	16.2	5.6	-4.5	20.2	4928	3015	2999	56.36	0.203
8	14.2	5.6	-4.3	20.0	4903	3009	2994	56.01	0.200
9	12.3	5.6	-3.9	19.7	4876	3001	2992	55.65	0.197
10	10.2	5.6	-4.1	19.5	4865	2997	2987	55.45	0.196
11	8.2	5.6	-4.1	19.7	4842	2992	2980	55.11	0.193
12	6.3	5.6	-3.6	19.7	4818	2975	2976	54.65	0.192
13	4.2	5.6	-3.9	19.2	4799	2953	2968	54.15	0.193
14	2.3	5.6	-3.5	18.8	4740	2928	2955	53.19	0.187

Observed Velocities and Moduli for File w70-mb-8844.9H-vel									
Event	Conf	Pore	Diff	Temp	V_p	$V_s^{(1)}$	$V_s^{(2)}$	Young's Modulus	Poisson's Ratio
	MPa	MPa	MPa	°C	m/s	m/s	m/s	GPa	
0	30.2	5.6	-5.2	24.0	4955	2947	3036	56.46	0.213
1	28.2	5.6	-4.8	23.8	4943	2942	3032	56.25	0.212
2	26.3	5.6	-4.5	23.6	4918	2935	3027	55.89	0.210
3	24.3	5.6	-4.5	23.3	4890	2932	3022	55.56	0.206
4	22.3	5.6	-4.3	23.2	4879	2929	3016	55.36	0.205
5	20.2	5.6	-4.6	23.0	4868	2927	3009	55.16	0.204
6	18.2	5.6	-4.5	22.8	4844	2920	3004	54.81	0.201
7	16.2	5.6	-4.2	22.6	4825	2910	3000	54.48	0.200
8	14.2	5.6	-4.1	22.4	4798	2904	2990	54.06	0.197
9	12.2	5.6	-4.3	22.1	4766	2821	2979	52.74	0.206
10	10.2	5.6	-4.1	21.7	4734	2800	2971	52.15	0.204
11	8.1	5.6	-4.2	20.4	4707	2780	2953	51.50	0.205
12	6.2	5.6	-3.8	20.6	4693	2744	2940	50.84	0.210
13	4.2	5.6	-3.5	20.5	4593	2718	2923	49.53	0.197
14	2.2	5.6	-3.8	20.4	4436	2688	2895	47.50	0.172

Observed Velocities and Moduli for File w70-mb-8845.6H-vel									
Event	Conf	Pore	Diff	Temp	V_p	$V_s^{(1)}$	$V_s^{(2)}$	Young's Modulus	Poisson's Ratio
	MPa	MPa	MPa	°C	m/s	m/s	m/s	GPa	
0	30.2	5.6	-2.9	24.8	4978	3017	3032	56.99	0.207
1	28.3	5.6	-2.9	24.5	4936	3014	3029	56.55	0.200
2	26.2	5.6	-2.9	24.0	4934	3011	3024	56.44	0.201
3	24.3	5.6	-2.9	23.5	4917	3008	3021	56.22	0.199
4	22.2	5.6	-3.4	23.1	4912	3003	3015	56.05	0.200
5	20.3	5.6	-2.8	22.7	4912	3001	3014	56.01	0.200
6	18.2	5.6	-2.9	22.4	4893	2994	3009	55.71	0.198
7	16.2	5.6	-3.1	22.1	4869	2989	3006	55.40	0.195
8	14.2	5.6	-2.9	21.8	4858	2986	3001	55.21	0.194
9	12.2	5.6	-2.9	21.4	4845	2979	2998	54.98	0.193
10	10.2	5.6	-2.5	21.2	4829	2978	2994	54.77	0.190
11	8.2	5.6	-2.4	20.9	4826	2972	2984	54.57	0.193
12	6.2	5.6	-2.5	20.7	4813	2959	2975	54.21	0.194
13	4.2	5.6	-2.1	20.5	4800	2942	2966	53.82	0.195
14	2.2	5.6	-1.9	20.2	4779	2936	2960	53.49	0.193

Observed Velocities and Moduli for File w70-mb-8845.8H-vel									
Event	Conf	Pore	Diff	Temp	V_p	$V_s^{(1)}$	$V_s^{(2)}$	Young's Modulus	Poisson's Ratio
	MPa	MPa	MPa	°C	m/s	m/s	m/s	GPa	
0	30.3	5.6	-3.2	24.9	5025	3050	2897	56.36	0.231
1	28.3	5.6	-2.9	24.7	4999	3041	2890	55.96	0.229
2	26.3	5.6	-3.2	24.4	4994	3038	2887	55.85	0.229
3	24.3	5.6	-2.9	24.2	4969	3036	2883	55.58	0.225
4	22.2	5.6	-3.4	24.1	4960	3032	2878	55.40	0.225
5	20.3	5.6	-2.8	24.0	4938	3024	2873	55.07	0.223
6	18.3	5.6	-2.7	23.8	4930	3022	2867	54.91	0.223
7	16.3	5.6	-2.8	23.7	4919	3021	2861	54.74	0.222
8	14.3	5.6	-2.7	23.5	4908	3015	2854	54.50	0.222
9	12.3	5.6	-2.7	23.1	4926	3011	2845	54.48	0.227
10	10.2	5.6	-2.7	22.2	4914	3010	2834	54.24	0.227
11	8.2	5.6	-2.4	21.5	4884	2992	2823	53.67	0.226
12	6.3	5.6	-2.2	21.3	4838	2987	2811	53.11	0.220
13	4.2	5.6	-2.5	21.1	4797	2972	2796	52.43	0.217
14	2.3	5.6	-2.1	20.9	4756	2960	2777	51.75	0.214

Observed Velocities and Moduli for File w70-mb-8845V-vel									
Event	Conf	Pore	Diff	Temp	V_p	$V_s^{(1)}$	$V_s^{(2)}$	Young's Modulus	Poisson's Ratio
	MPa	MPa	MPa	°C	m/s	m/s	m/s	GPa	
0	30.3	5.6	-4.6	22.2	4567	2890	2896	50.11	0.165
1	28.3	5.7	-4.3	22.6	4528	2888	2885	49.58	0.158
2	26.2	5.6	-4.8	21.9	4525	2882	2879	49.44	0.159
3	24.2	5.6	-4.3	21.8	4503	2878	2875	49.14	0.155
4	22.2	5.7	-3.9	21.5	4489	2872	2871	48.90	0.154
5	20.2	5.6	-4.2	21.9	4473	2867	2866	48.64	0.152
6	18.2	5.7	-4.1	21.4	4444	2864	2861	48.24	0.145
7	16.2	5.7	-3.8	21.2	4418	2852	2855	47.80	0.142
8	14.2	5.7	-3.5	21.1	4407	2846	2848	47.57	0.142
9	12.2	5.6	-4.1	21.5	4379	2836	2846	47.15	0.137
10	10.2	5.6	-3.5	21.0	4370	2826	2830	46.85	0.140
11	8.2	5.6	-3.5	20.8	4352	2817	2826	46.54	0.137
12	6.2	5.6	-3.6	20.6	4290	2804	2808	45.58	0.126
13	4.2	5.6	-3.3	21.1	4249	2786	2797	44.87	0.120
14	2.2	5.6	-3.5	20.4	4191	2773	2777	43.92	0.110

Observed Velocities and Moduli for File w70-mb-8846.2V45-vel									
Event	Conf	Pore	Diff	Temp	V_p	$V_s^{(1)}$	$V_s^{(2)}$	Young's Modulus	Poisson's Ratio
	MPa	MPa	MPa	°C	m/s	m/s	m/s	GPa	
0	30.2	5.6	-4.8	24.6	4777	2970	2932	53.54	0.191
1	28.3	5.6	-4.3	24.5	4764	2967	2927	53.33	0.190
2	26.3	5.6	-3.9	24.2	4729	2964	2922	52.91	0.184
3	24.3	5.6	-4.1	24.0	4713	2961	2920	52.71	0.181
4	22.3	5.6	-3.9	23.8	4703	2959	2916	52.55	0.180
5	20.2	5.6	-4.2	23.7	4662	2955	2912	52.05	0.172
6	18.2	5.6	-3.9	23.5	4654	2949	2905	51.85	0.173
7	16.2	5.6	-3.9	23.2	4640	2942	2898	51.57	0.172
8	14.2	5.6	-3.5	23.1	4628	2939	2894	51.38	0.171
9	12.3	5.6	-3.6	22.8	4613	2930	2882	51.03	0.171
10	10.2	5.6	-3.5	22.6	4589	2921	2876	50.64	0.168
11	8.2	5.6	-3.5	21.5	4573	2911	2867	50.30	0.168
12	6.3	5.6	-3.1	21.6	4537	2903	2857	49.76	0.163
13	4.2	5.6	-3.5	21.4	4494	2887	2847	49.07	0.157
14	2.2	5.5	-3.5	21.1	4423	2878	2832	48.07	0.143

Observed Velocities and Moduli for File w70-mb-8846.6V45-vel									
Event	Conf	Pore	Diff	Temp	V_p	$V_s^{(1)}$	$V_s^{(2)}$	Young's Modulus	Poisson's Ratio
	MPa	MPa	MPa	°C	m/s	m/s	m/s	GPa	
0	30.3	5.6	-4.3	24.9	4795	2971	2911	53.49	0.198
1	28.3	5.6	-4.6	24.6	4731	2965	2905	52.77	0.187
2	26.2	5.6	-4.6	24.7	4720	2963	2901	52.60	0.186
3	24.3	5.6	-4.1	23.9	4710	2953	2894	52.33	0.187
4	22.2	5.6	-4.3	23.7	4704	2950	2890	52.20	0.187
5	20.2	5.6	-4.2	23.6	4695	2946	2885	52.03	0.186
6	18.2	5.6	-4.2	23.4	4684	2944	2880	51.85	0.185
7	16.2	5.6	-4.1	23.0	4668	2942	2875	51.63	0.183
8	14.2	5.6	-3.6	22.5	4654	2939	2873	51.44	0.180
9	12.3	5.6	-3.5	22.2	4648	2933	2861	51.20	0.182
10	10.2	5.6	-3.5	21.6	4637	2931	2855	51.02	0.181
11	8.2	5.6	-3.5	21.6	4622	2922	2854	50.77	0.180
12	6.2	5.6	-3.9	21.5	4592	2915	2848	50.35	0.175
13	4.2	5.5	-3.6	21.0	4550	2892	2827	49.52	0.174
14	2.3	5.6	-3.5	21.2	4499	2859	2810	48.54	0.171

Observed Velocities and Moduli for File w70-mb-8847.3V45-vel									
Event	Conf	Pore	Diff	Temp	V_p	$V_s^{(1)}$	$V_s^{(2)}$	Young's Modulus	Poisson's Ratio
	MPa	MPa	MPa	°C	m/s	m/s	m/s	GPa	
0	30.3	5.6	-4.3	24.8	4847	2973	3008	55.25	0.193
1	28.3	5.6	-4.6	24.6	4836	2968	3005	55.06	0.192
2	26.3	5.6	-4.2	24.4	4825	2965	3001	54.88	0.191
3	24.3	5.6	-4.3	24.1	4822	2962	2995	54.76	0.192
4	22.3	5.6	-3.9	23.9	4811	2959	2993	54.60	0.190
5	20.2	5.6	-4.5	23.6	4797	2955	2986	54.35	0.189
6	18.2	5.6	-4.3	23.5	4782	2949	2980	54.08	0.188
7	16.2	5.6	-4.2	23.3	4776	2944	2976	53.93	0.188
8	14.2	5.6	-3.5	22.3	4755	2939	2967	53.58	0.186
9	12.3	5.6	-3.5	21.4	4731	2939	2962	53.29	0.182
10	10.2	5.6	-3.5	21.4	4704	2929	2958	52.88	0.178
11	8.2	5.6	-3.5	20.8	4681	2922	2954	52.54	0.175
12	6.2	5.6	-3.6	20.5	4645	2913	2946	52.00	0.170
13	4.2	5.5	-3.9	21.1	4638	2908	2936	51.79	0.171
14	2.3	5.6	-3.5	20.9	4585	2889	2919	50.89	0.165

Observed Velocities and Moduli for File w70-mb-8847.7V45-vel									
Event	Conf	Pore	Diff	Temp	V_p	$V_s^{(1)}$	$V_s^{(2)}$	Young's Modulus	Poisson's Ratio
	MPa	MPa	MPa	°C	m/s	m/s	m/s	GPa	
0	30.3	5.6	-4.3	24.2	4814	2988	2929	54.04	0.197
1	28.3	5.6	-4.3	24.0	4806	2984	2921	53.84	0.197
2	26.2	5.6	-4.5	23.7	4788	2981	2918	53.61	0.194
3	24.3	5.6	-4.8	23.5	4785	2977	2914	53.50	0.195
4	22.2	5.6	-4.3	23.2	4777	2973	2910	53.34	0.195
5	20.3	5.6	-3.9	23.1	4761	2967	2910	53.12	0.192
6	18.2	5.6	-4.3	22.9	4746	2963	2908	52.92	0.190
7	16.3	5.6	-3.9	22.3	4728	2958	2903	52.65	0.188
8	14.2	5.6	-3.9	21.5	4710	2955	2897	52.38	0.186
9	12.1	5.6	-3.9	20.9	4694	2950	2891	52.12	0.184
10	10.2	5.6	-3.8	20.6	4666	2940	2879	51.63	0.182
11	8.1	5.6	-3.9	20.1	4649	2928	2859	51.14	0.184
12	6.2	5.6	-3.9	20.6	4634	2920	2846	50.79	0.184
13	4.2	5.6	-3.5	20.4	4565	2910	2833	49.89	0.173
14	2.3	5.6	-3.1	20.7	4490	2888	2821	48.81	0.161

Observed Velocities and Moduli for File w70-mb-8848.5V-vel									
Event	Conf	Pore	Diff	Temp	V_p	$V_s^{(1)}$	$V_s^{(2)}$	Young's Modulus	Poisson's Ratio
	MPa	MPa	MPa	°C	m/s	m/s	m/s	GPa	
0	30.3	5.6	-4.3	23.2	4685	2928	2921	52.11	0.181
1	28.3	5.6	-4.8	23.0	4672	2923	2914	51.86	0.180
2	26.2	5.6	-4.3	22.8	4657	2916	2913	51.64	0.178
3	24.3	5.7	-3.9	22.6	4637	2915	2906	51.36	0.175
4	22.3	5.6	-3.9	23.1	4624	2913	2905	51.20	0.172
5	20.2	5.6	-3.9	22.9	4604	2908	2902	50.92	0.169
6	18.2	5.6	-3.9	22.8	4594	2903	2898	50.73	0.169
7	16.2	5.6	-4.1	22.6	4587	2895	2897	50.57	0.169
8	14.2	5.6	-3.5	22.1	4564	2888	2893	50.23	0.165
9	12.2	5.6	-3.9	21.9	4535	2884	2884	49.81	0.160
10	10.2	5.6	-3.5	21.7	4524	2878	2875	49.56	0.161
11	8.1	5.6	-3.9	21.3	4494	2867	2867	49.07	0.157
12	6.2	5.6	-3.3	20.8	4473	2859	2860	48.71	0.154
13	4.2	5.6	-3.5	20.7	4436	2849	2847	48.11	0.149
14	2.3	5.6	-3.1	20.6	4392	2828	2836	47.35	0.144

Observed Velocities and Moduli for File w70-mb-8848H-vel									
Event	Conf	Pore	Diff	Temp	V_p	$V_s^{(1)}$	$V_s^{(2)}$	Young's Modulus	Poisson's Ratio
	MPa	MPa	MPa	°C	m/s	m/s	m/s	GPa	
0	30.4	5.6	-4.5	21.4	5031	3051	2996	57.42	0.217
1	28.4	5.7	-4.3	20.9	5022	3050	2995	57.32	0.216
2	26.3	5.6	-4.6	21.0	4998	3048	2992	57.06	0.212
3	24.3	5.6	-4.3	20.2	4992	3045	2990	56.95	0.212
4	22.3	5.6	-4.2	20.4	4992	3041	2990	56.90	0.213
5	20.3	5.7	-3.9	19.7	4987	3038	2980	56.71	0.214
6	18.3	5.6	-4.3	19.4	4975	3037	2979	56.58	0.212
7	16.3	5.6	-3.9	19.3	4952	3031	2978	56.30	0.209
8	14.2	5.6	-4.2	19.0	4937	3025	2975	56.07	0.207
9	12.3	5.6	-3.5	19.4	4920	3018	2973	55.81	0.205
10	10.2	5.6	-3.9	18.7	4906	3014	2970	55.61	0.204
11	8.2	5.6	-3.8	18.4	4883	3008	2968	55.32	0.201
12	6.3	5.6	-3.6	18.4	4869	2995	2960	54.96	0.201
13	4.3	5.6	-3.3	18.2	4830	2984	2952	54.39	0.197
14	2.3	5.6	-3.1	17.9	4800	2964	2928	53.64	0.198

Observed Velocities and Moduli for File w70-mb-8849.5H-vel									
Event	Conf	Pore	Diff	Temp	V_p	$V_s^{(1)}$	$V_s^{(2)}$	Young's Modulus	Poisson's Ratio
	MPa	MPa	MPa	°C	m/s	m/s	m/s	GPa	
0	30.3	5.6	-4.8	22.4	4988	3033	2884	55.28	0.229
1	28.3	5.6	-4.5	22.2	4979	3031	2881	55.15	0.228
2	26.3	5.6	-4.6	22.2	4982	3029	2880	55.13	0.229
3	24.3	5.6	-4.3	21.4	4959	3026	2874	54.85	0.226
4	22.2	5.6	-4.2	20.9	4933	3023	2870	54.56	0.223
5	20.3	5.6	-4.1	20.6	4927	3019	2866	54.42	0.223
6	18.2	5.6	-4.3	20.2	4922	3018	2861	54.31	0.223
7	16.2	5.6	-4.2	19.9	4911	3011	2853	54.04	0.223
8	14.2	5.6	-3.9	19.6	4894	3008	2847	53.80	0.221
9	12.2	5.6	-3.9	19.3	4874	3001	2841	53.49	0.220
10	10.2	5.6	-3.9	19.1	4847	2999	2833	53.16	0.216
11	8.1	5.6	-3.9	18.8	4828	2991	2823	52.80	0.216
12	6.2	5.6	-3.6	18.6	4825	2978	2811	52.49	0.219
13	4.2	5.6	-3.3	19.0	4802	2972	2798	52.09	0.218
14	2.2	5.6	-3.6	18.7	4745	2946	2780	51.14	0.214

Observed Velocities and Moduli for File w70-mb-8849.9H-vel									
Event	Conf	Pore	Diff	Temp	V_p	$V_s^{(1)}$	$V_s^{(2)}$	Young's Modulus	Poisson's Ratio
	MPa	MPa	MPa	°C	m/s	m/s	m/s	GPa	
0	30.2	5.6	-4.8	23.5	5004	3044	3010	56.83	0.211
1	28.3	5.6	-4.3	23.2	4984	3039	3006	56.56	0.209
2	26.2	5.6	-4.3	22.6	4967	3037	3005	56.37	0.206
3	24.3	5.6	-4.2	22.1	4953	3035	3002	56.19	0.205
4	22.3	5.6	-3.9	21.7	4947	3031	3001	56.08	0.204
5	20.2	5.6	-3.9	21.3	4925	3028	2997	55.81	0.201
6	18.2	5.6	-4.1	21.1	4917	3030	2995	55.74	0.200
7	16.2	5.6	-4.3	20.7	4911	3026	2993	55.62	0.199
8	14.2	5.6	-3.9	20.4	4906	3021	2993	55.51	0.199
9	12.1	5.6	-3.9	20.1	4892	3015	2990	55.29	0.198
10	10.2	5.6	-3.5	19.9	4862	3010	2984	54.89	0.194
11	8.2	5.6	-3.5	19.7	4834	3006	2981	54.55	0.189
12	6.2	5.6	-3.6	19.4	4827	2997	2975	54.33	0.190
13	4.2	5.6	-3.6	19.2	4798	2988	2967	53.87	0.187
14	2.3	5.6	-3.2	19.1	4772	2963	2950	53.19	0.189

Observed Velocities and Moduli for File w70-mb-8849V-vel									
Event	Conf	Pore	Diff	Temp	V_p	$V_s^{(1)}$	$V_s^{(2)}$	Young's Modulus	Poisson's Ratio
	MPa	MPa	MPa	°C	m/s	m/s	m/s	GPa	
0	30.2	5.6	-4.8	25.8	4563	2911	2913	50.40	0.156
1	28.3	5.6	-4.5	25.7	4551	2904	2908	50.17	0.156
2	26.2	5.6	-4.5	25.5	4544	2902	2906	50.06	0.155
3	24.3	5.6	-4.6	25.4	4534	2899	2904	49.90	0.153
4	22.3	5.6	-3.9	25.3	4526	2895	2901	49.75	0.153
5	20.2	5.6	-4.3	25.2	4522	2891	2897	49.64	0.153
6	18.2	5.6	-3.9	25.1	4510	2883	2895	49.42	0.152
7	16.2	5.6	-4.3	25.0	4501	2879	2890	49.25	0.152
8	14.2	5.6	-3.5	24.9	4461	2871	2885	48.68	0.144
9	12.3	5.6	-3.5	24.8	4422	2868	2875	48.12	0.135
10	10.2	5.6	-3.5	24.6	4413	2861	2870	47.92	0.135
11	8.2	5.6	-3.5	24.6	4393	2852	2865	47.58	0.133
12	6.2	5.6	-3.9	24.1	4348	2840	2855	46.87	0.125
13	4.2	5.6	-3.3	23.6	4324	2826	2839	46.36	0.124
14	2.2	5.6	-3.5	22.5	4264	2800	2827	45.34	0.114

Observed Velocities and Moduli for File w70-mb-8850.3V-vel									
Event	Conf	Pore	Diff	Temp	V_p	$V_s^{(1)}$	$V_s^{(2)}$	Young's Modulus	Poisson's Ratio
	MPa	MPa	MPa	°C	m/s	m/s	m/s	GPa	
0	30.3	5.6	-4.3	25.3	4456	2835	2840	47.03	0.159
1	28.3	5.6	-4.3	25.1	4438	2831	2836	46.77	0.156
2	26.3	5.6	-4.2	24.9	4436	2830	2834	46.73	0.156
3	24.3	5.6	-4.2	24.7	4427	2829	2830	46.59	0.155
4	22.2	5.6	-4.3	24.6	4409	2827	2827	46.36	0.151
5	20.2	5.6	-4.3	24.5	4383	2819	2823	45.98	0.146
6	18.2	5.7	-3.9	24.3	4365	2814	2817	45.70	0.144
7	16.2	5.6	-4.2	24.2	4361	2811	2814	45.61	0.144
8	14.2	5.6	-3.9	24.0	4333	2805	2809	45.21	0.138
9	12.2	5.6	-3.8	23.8	4329	2800	2803	45.08	0.140
10	10.2	5.6	-3.9	23.5	4316	2795	2800	44.88	0.138
11	8.1	5.6	-3.6	23.3	4269	2791	2792	44.24	0.127
12	6.2	5.6	-3.3	23.2	4218	2778	2784	43.48	0.116
13	4.2	5.6	-3.3	23.1	4178	2763	2772	42.81	0.109
14	2.3	5.6	-3.1	22.9	4177	2741	2752	42.55	0.119

Observed Velocities and Moduli for File w16862-8826.3-vel									
Event	Conf	Pore	Diff	Temp	V_p	$V_s^{(1)}$	$V_s^{(2)}$	Young's Modulus	Poisson's Ratio
	MPa	MPa	MPa	°C	m/s	m/s	m/s	GPa	
0	10.5	0.6	1.0	29.1	5092	2967	2995	57.71	0.239
1	20.6	0.6	0.3	30.0	5172	3062	3022	59.91	0.236
2	30.6	0.6	0.0	30.9	5132	3062	3050	59.96	0.225
3	40.6	0.6	-0.6	31.2	5253	3091	3064	61.47	0.239
4	50.6	0.6	-1.3	31.6	5381	3120	3093	63.21	0.250

Observed Velocities and Moduli for File w16862-8827.6-vel									
Event	Conf	Pore	Diff	Temp	V_p	$V_s^{(1)}$	$V_s^{(2)}$	Young's Modulus	Poisson's Ratio
	MPa	MPa	MPa	°C	m/s	m/s	m/s	GPa	
0	10.5	0.7	1.2	29.6	5185	3124	3126	62.16	0.215
1	20.6	0.6	0.6	30.0	5143	3124	3142	61.98	0.205
2	30.6	0.6	0.3	30.6	5143	3140	3174	62.55	0.198
3	40.6	0.7	-0.1	31.5	5273	3124	3174	63.54	0.223
4	50.6	0.6	-1.1	31.6	5273	3172	3190	64.37	0.214

Observed Velocities and Moduli for File w16862-8833.8-vel									
Event	Conf	Pore	Diff	Temp	V_p	$V_s^{(1)}$	$V_s^{(2)}$	Young's Modulus	Poisson's Ratio
	MPa	MPa	MPa	°C	m/s	m/s	m/s	GPa	
0	10.5	0.6	0.9	28.3	4693	2915	2916	52.01	0.186
1	20.6	0.7	0.4	29.5	4762	2928	2943	53.07	0.194
2	30.5	0.6	0.0	30.4	4943	2968	2983	55.55	0.216
3	40.6	0.6	-0.7	30.9	4869	3023	3011	55.82	0.188
4	50.6	0.6	-0.8	31.6	5058	3037	3025	57.83	0.220

Observed Velocities and Moduli for File w16862-8837.8-vel									
Event	Conf	Pore	Diff	Temp	V_p	$V_s^{(1)}$	$V_s^{(2)}$	Young's Modulus	Poisson's Ratio
	MPa	MPa	MPa	°C	m/s	m/s	m/s	GPa	
0	10.5	0.6	0.7	28.5	4644	3117	2899	51.72	0.139
1	20.6	0.7	0.6	29.3	4721	3186	2974	53.79	0.129
2	30.6	0.6	0.0	30.2	4923	3259	2989	56.97	0.163
3	40.6	0.6	-0.8	30.8	4923	3277	3021	57.43	0.154
4	50.6	0.6	-1.1	30.9	5054	3354	3053	59.98	0.164

Observed Velocities and Moduli for File w16862-8823.8-vel									
Event	Conf	Pore	Diff	Temp	V_p	$V_s^{(1)}$	$V_s^{(2)}$	Young's Modulus	Poisson's Ratio
	MPa	MPa	MPa	°C	m/s	m/s	m/s	GPa	
0	10.6	-0.0	1.6	27.3	4836	2865	2939	53.16	0.219
1	20.5	-0.1	0.7	28.3	4863	2893	2948	53.81	0.218
2	30.5	-0.1	0.0	28.9	4907	2910	2962	54.53	0.221
3	40.5	-0.1	-0.4	29.3	4934	2910	2968	54.81	0.225
4	50.6	-0.1	-0.7	29.5	4948	2921	2985	55.26	0.223

Observed Velocities and Moduli for File w16862-8824.7-vel									
Event	Conf	Pore	Diff	Temp	V_p	$V_s^{(1)}$	$V_s^{(2)}$	Young's Modulus	Poisson's Ratio
	MPa	MPa	MPa	°C	m/s	m/s	m/s	GPa	
0	10.5	0.6	0.4	25.1	4739	2748	2965	51.14	0.215
1	20.5	0.6	0.0	26.7	4815	2764	2965	51.91	0.226
2	30.5	0.6	-0.4	27.4	4857	2779	2977	52.55	0.229
3	40.5	0.6	-1.0	27.9	4888	2790	2993	53.10	0.231
4	50.5	0.6	-1.6	28.1	4950	2804	2993	53.72	0.239

Observed Velocities and Moduli for File w16862-8834.2-vel									
Event	Conf	Pore	Diff	Temp	V_p	$V_s^{(1)}$	$V_s^{(2)}$	Young's Modulus	Poisson's Ratio
	MPa	MPa	MPa	°C	m/s	m/s	m/s	GPa	
0	10.6	0.7	1.3	26.7	4737	2774	2930	51.22	0.216
1	20.6	0.6	0.4	27.6	4797	2815	2967	52.59	0.215
2	30.5	0.7	0.4	28.4	4869	2841	2987	53.70	0.221
3	40.6	0.6	-0.3	29.1	4891	2861	3004	54.32	0.219
4	50.6	0.6	-1.0	29.2	4928	2880	3020	55.03	0.221

Observed Velocities and Moduli for File w16862-8834.4-vel									
Event	Conf	Pore	Diff	Temp	V_p	$V_s^{(1)}$	$V_s^{(2)}$	Young's Modulus	Poisson's Ratio
	MPa	MPa	MPa	°C	m/s	m/s	m/s	GPa	
0	10.6	0.7	1.2	26.9	4671	2731	2900	49.68	0.215
1	20.6	0.7	0.6	27.8	4831	2783	2954	52.13	0.228
2	30.6	0.7	0.2	28.5	4879	2830	2990	53.48	0.224
3	40.5	0.6	-0.6	28.8	4946	2859	3007	54.55	0.229
4	50.6	0.6	-1.0	28.9	5011	2885	3023	55.55	0.234

Observed Velocities and Moduli for File w16862-8834.6-vel									
Event	Conf	Pore	Diff	Temp	V_p	$V_s^{(1)}$	$V_s^{(2)}$	Young's Modulus	Poisson's Ratio
	MPa	MPa	MPa	°C	m/s	m/s	m/s	GPa	
0	10.5	-0.1	1.6	27.1	4954	2947	2981	55.79	0.221
1	20.6	-0.1	0.9	28.2	5015	2999	2997	57.11	0.222
2	30.5	-0.1	0.2	28.9	5073	3025	3025	58.25	0.224
3	40.6	-0.1	0.0	29.4	5079	3048	3045	58.83	0.219
4	50.5	-0.1	-0.8	29.7	5108	3076	3057	59.57	0.218

Observed Velocities and Moduli for File w16862-8835.2-vel									
Event	Conf	Pore	Diff	Temp	V_p	$V_s^{(1)}$	$V_s^{(2)}$	Young's Modulus	Poisson's Ratio
	MPa	MPa	MPa	°C	m/s	m/s	m/s	GPa	
0	10.5	0.7	0.4	24.4	4662	2830	2891	50.39	0.198
1	20.5	0.7	0.0	25.2	4803	2866	2942	52.53	0.212
2	30.4	0.6	-0.8	25.9	4874	2903	2982	53.99	0.213
3	40.5	0.7	-0.8	26.4	4960	2930	3009	55.33	0.221
4	50.6	0.7	-1.3	26.6	5020	2950	3030	56.30	0.225

Observed Velocities and Moduli for File w16862-8836.7-vel									
Event	Conf	Pore	Diff	Temp	V_p	$V_s^{(1)}$	$V_s^{(2)}$	Young's Modulus	Poisson's Ratio
	MPa	MPa	MPa	°C	m/s	m/s	m/s	GPa	
0	10.5	-0.1	1.0	26.5	4616	2874	2717	48.81	0.210
1	20.5	-0.1	0.4	27.5	4758	2939	2777	51.33	0.218
2	30.5	-0.1	0.0	28.9	4841	2981	2829	53.07	0.219
3	40.6	-0.1	0.0	29.0	4958	3009	2854	54.60	0.231
4	50.5	-0.1	-0.8	29.1	4979	3032	2882	55.38	0.228

Observed Velocities and Moduli for File w16862-8837-vel									
Event	Conf	Pore	Diff	Temp	V_p	$V_s^{(1)}$	$V_s^{(2)}$	Young's Modulus	Poisson's Ratio
	MPa	MPa	MPa	°C	m/s	m/s	m/s	GPa	
0	10.5	-0.1	1.4	27.2	4805	2769	2973	52.39	0.222
1	20.6	-0.1	1.0	28.6	4934	2826	2994	54.31	0.233
2	30.6	-0.1	0.7	29.1	4995	2875	3016	55.65	0.233
3	40.6	-0.1	0.0	29.7	5111	2905	3046	57.26	0.244
4	50.6	-0.1	-0.4	30.0	5201	2934	3070	58.59	0.250

Observed Velocities and Moduli for File w16862-8838.5-vel									
Event	Conf	Pore	Diff	Temp	V_p	$V_s^{(1)}$	$V_s^{(2)}$	Young's Modulus	Poisson's Ratio
	MPa	MPa	MPa	°C	m/s	m/s	m/s	GPa	
0	10.6	-0.0	1.3	27.0	4441	2645	2825	45.57	0.194
1	20.6	-0.1	0.9	28.0	4678	2768	2886	49.41	0.212
2	30.5	-0.1	0.0	28.7	4784	2847	2945	51.79	0.211
3	40.6	-0.1	-0.4	28.8	4886	2899	2990	53.72	0.215
4	50.6	-0.1	-0.6	29.0	4992	2927	3003	55.03	0.227

Observed Velocities and Moduli for File w16862-8839.4-vel									
Event	Conf	Pore	Diff	Temp	V_p	$V_s^{(1)}$	$V_s^{(2)}$	Young's Modulus	Poisson's Ratio
	MPa	MPa	MPa	°C	m/s	m/s	m/s	GPa	
0	10.5	-0.1	1.3	27.1	4466	2782	2809	46.76	0.178
1	20.6	-0.1	0.9	28.2	4566	2837	2858	48.68	0.182
2	30.6	-0.1	0.4	29.0	4723	2889	2893	50.97	0.200
3	40.6	-0.1	-0.4	29.4	4754	2912	2909	51.65	0.200
4	50.6	-0.1	-0.4	29.6	4792	2929	2927	52.35	0.202

Observed Velocities and Moduli for File w16862-8840.8-vel									
Event	Conf	Pore	Diff	Temp	V_p	$V_s^{(1)}$	$V_s^{(2)}$	Young's Modulus	Poisson's Ratio
	MPa	MPa	MPa	°C	m/s	m/s	m/s	GPa	
0	10.6	-0.0	1.6	27.4	4175	2497	2692	40.22	0.185
1	20.6	-0.1	0.6	28.2	4431	2607	2779	44.12	0.207
2	30.5	-0.1	0.4	29.0	4560	2705	2843	46.78	0.206
3	40.5	-0.1	-0.4	29.2	4630	2813	2877	48.82	0.197
4	50.6	-0.1	-0.8	29.2	4680	2830	2899	49.65	0.200

Observed Velocities and Moduli for File w16862-8841.4-vel									
Event	Conf	Pore	Diff	Temp	V_p	$V_s^{(1)}$	$V_s^{(2)}$	Young's Modulus	Poisson's Ratio
	MPa	MPa	MPa	°C	m/s	m/s	m/s	GPa	
0	10.5	-0.1	1.0	27.2	4742	2919	2807	51.71	0.213
1	20.6	-0.1	0.9	28.3	4805	2966	2863	53.40	0.209
2	30.5	-0.1	0.0	28.9	4937	3010	2911	55.57	0.219
3	40.5	-0.1	-0.4	29.2	5008	3036	2955	56.99	0.221
4	50.6	-0.1	-0.8	29.6	5082	3058	2980	58.17	0.227

Observed Velocities and Moduli for File w16862-8841.9-vel									
Event	Conf	Pore	Diff	Temp	V_p	$V_s^{(1)}$	$V_s^{(2)}$	Young's Modulus	Poisson's Ratio
	MPa	MPa	MPa	°C	m/s	m/s	m/s	GPa	
0	10.6	-0.0	1.3	27.3	4047	2653	2667	40.40	0.120
1	20.6	-0.1	0.9	28.3	4290	2736	2740	44.21	0.156
2	30.5	-0.1	0.2	29.1	4449	2796	2805	46.87	0.172
3	40.6	-0.1	0.0	29.5	4528	2830	2837	48.24	0.178
4	50.5	-0.1	-0.8	29.8	4592	2859	2861	49.36	0.183

A.4.3 Biot's Coefficient

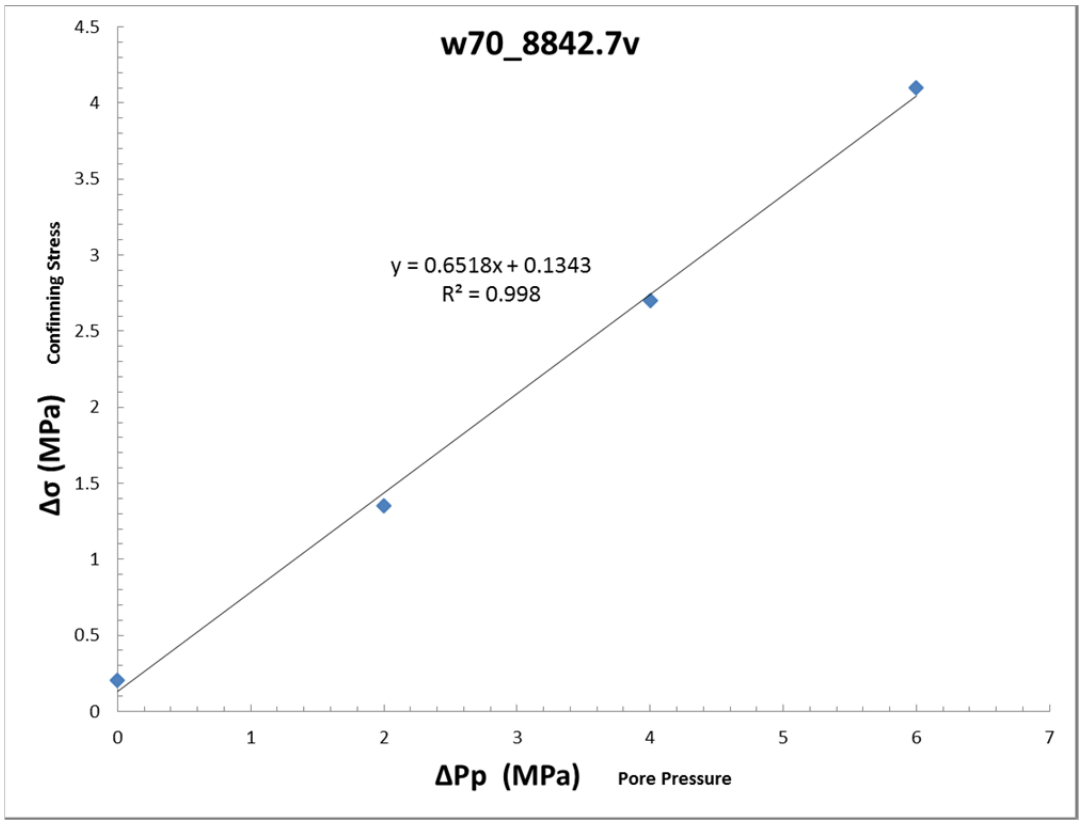

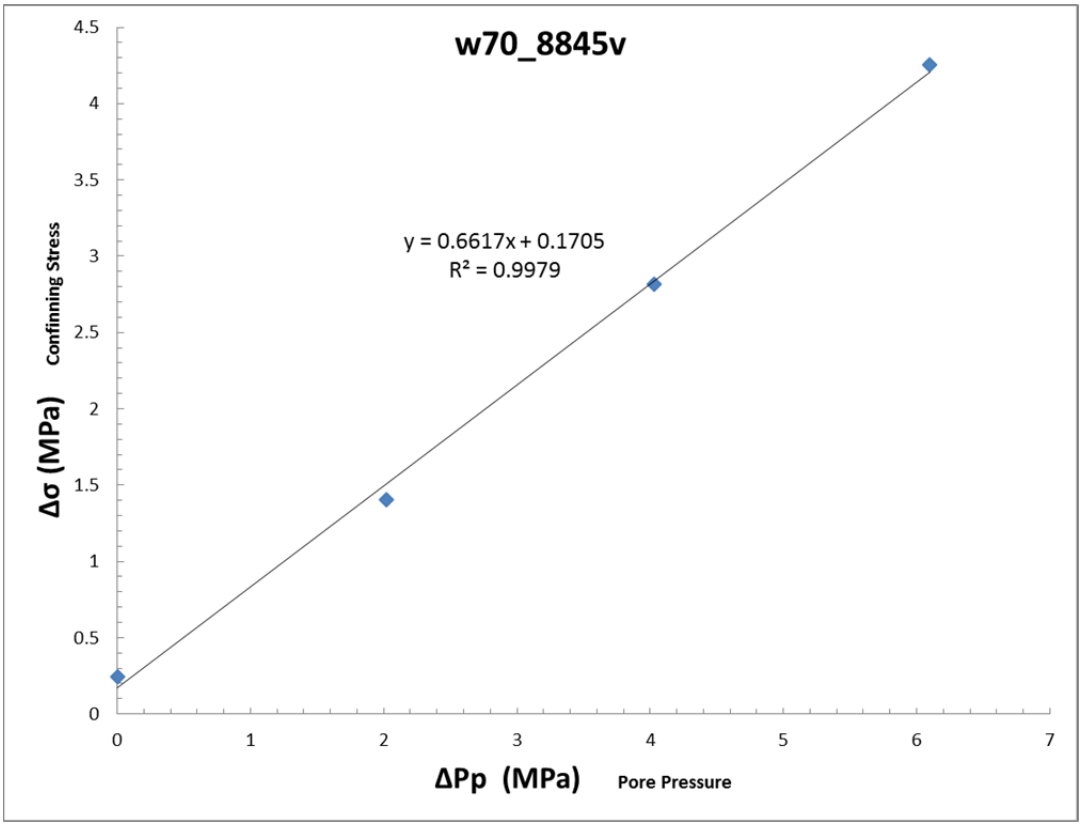
w70_8845v
y = 0.6617x + 0.1705
R² = 0.9979
Δσ (MPa) Confinning Stress
ΔPp (MPa) Pore Pressure
0
0.5
1
1.5
2
2.5
3
3.5
4
4.5
0
1
2
3
4
5
6
7

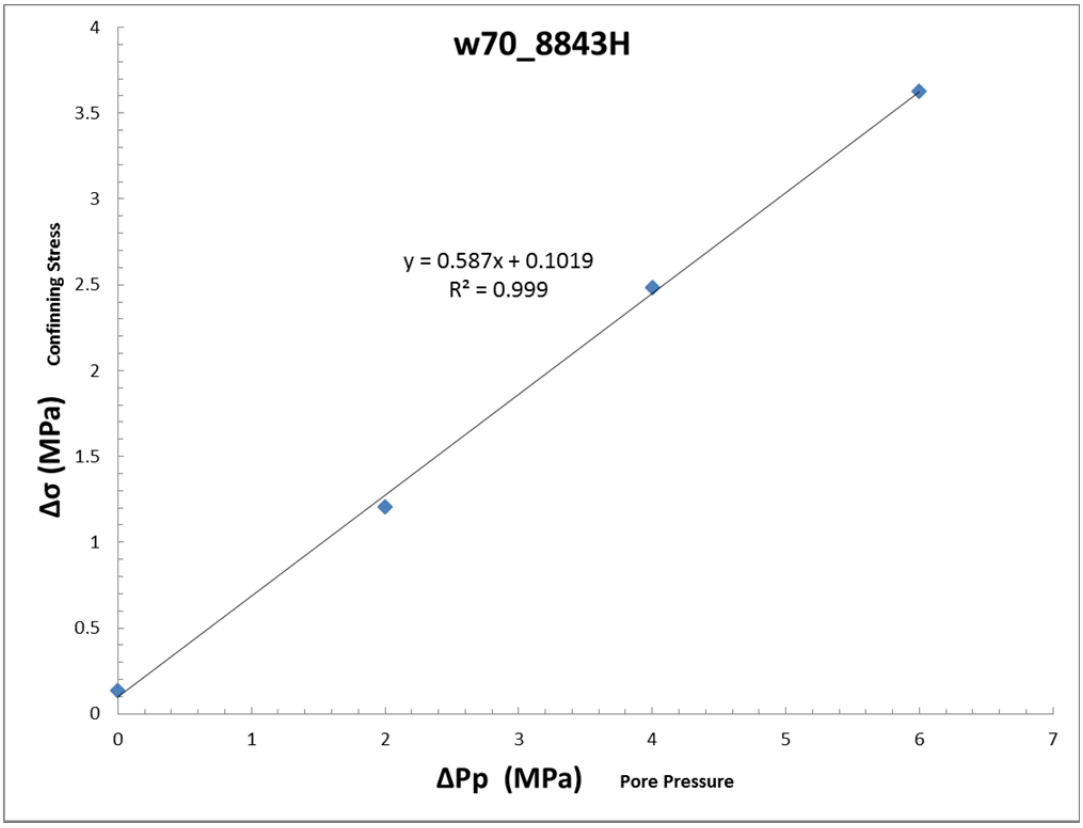
w70_8843H
y = 0.587x + 0.1019
R² = 0.999
Δσ (MPa) Confinning Stress
ΔPp (MPa) Pore Pressure
0
0.5
1
1.5
2
2.5
3
3.5
4
0
1
2
3
4
5
6
7

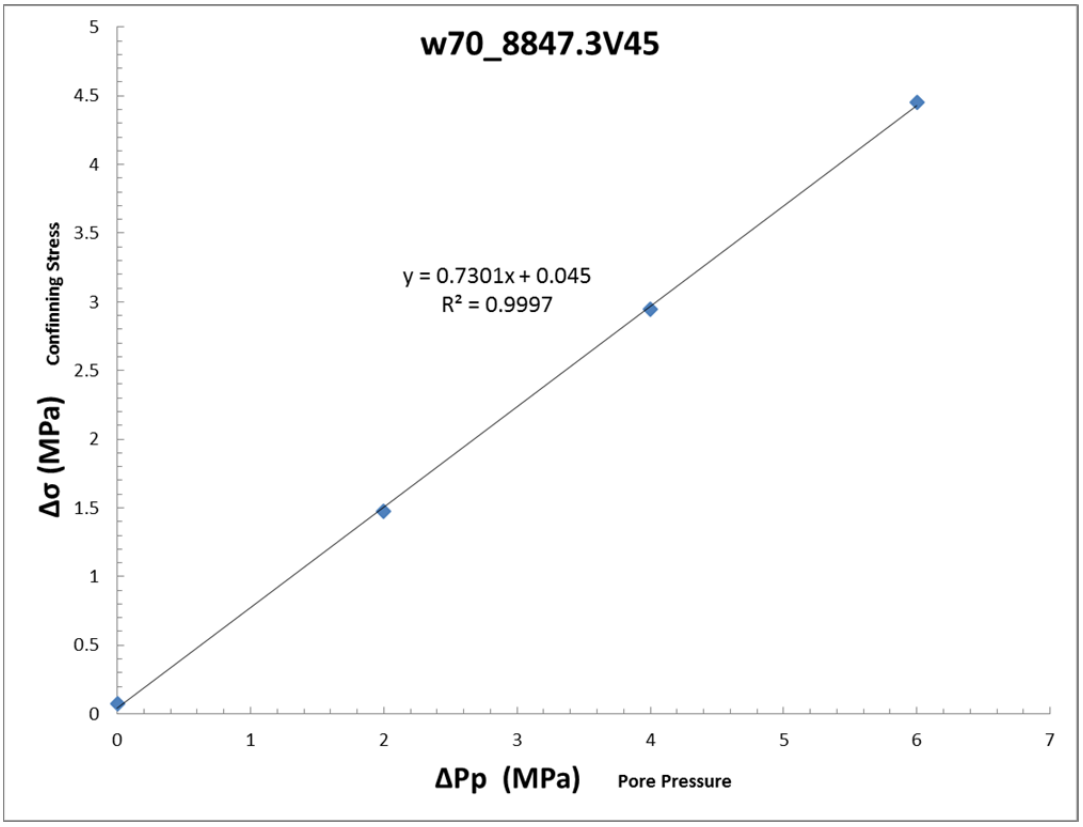
w70_8847.3V45
y = 0.7301x + 0.045
R² = 0.9997
Δσ (MPa) Confinning Stress
ΔPp (MPa) Pore Pressure
0
0.5
1
1.5
2
2.5
3
3.5
4
4.5
5
0
1
2
3
4
5
6
7

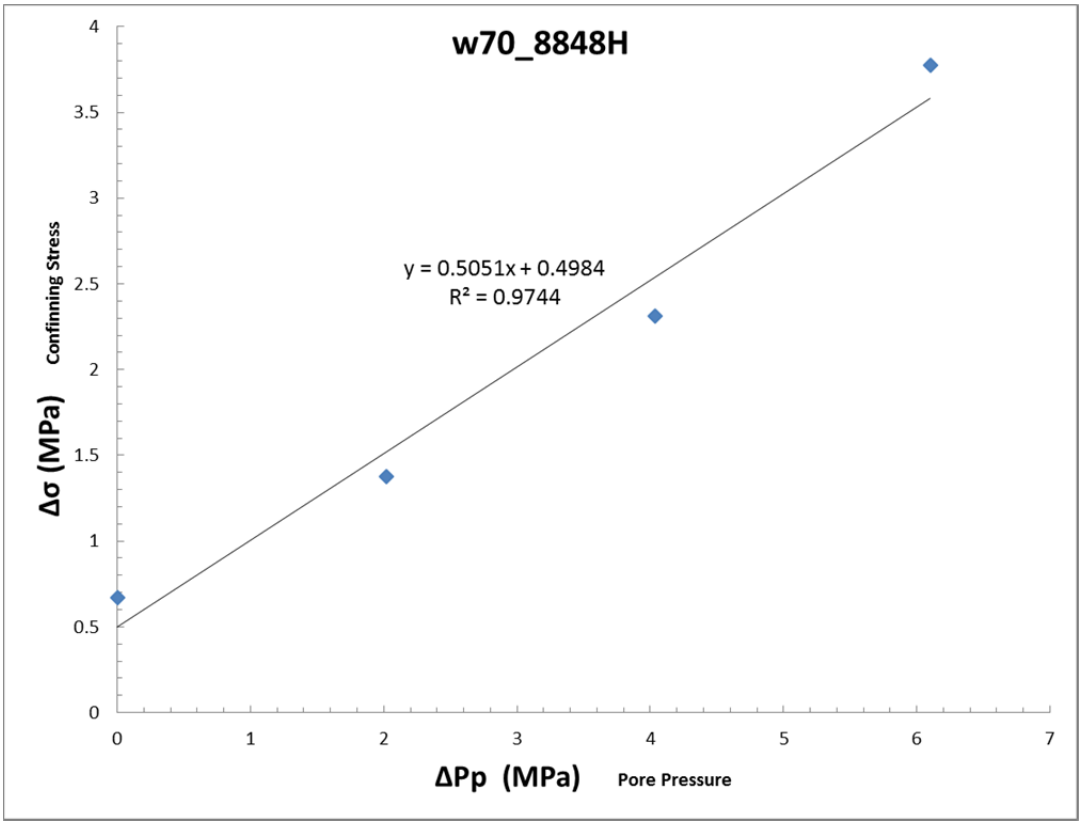
w70_8848H
y = 0.5051x + 0.4984
R² = 0.9744
Δσ (MPa) Confinning Stress
ΔPp (MPa) Pore Pressure
0
0.5
1
1.5
2
2.5
3
3.5
4
0
1
2
3
4
5
6
7

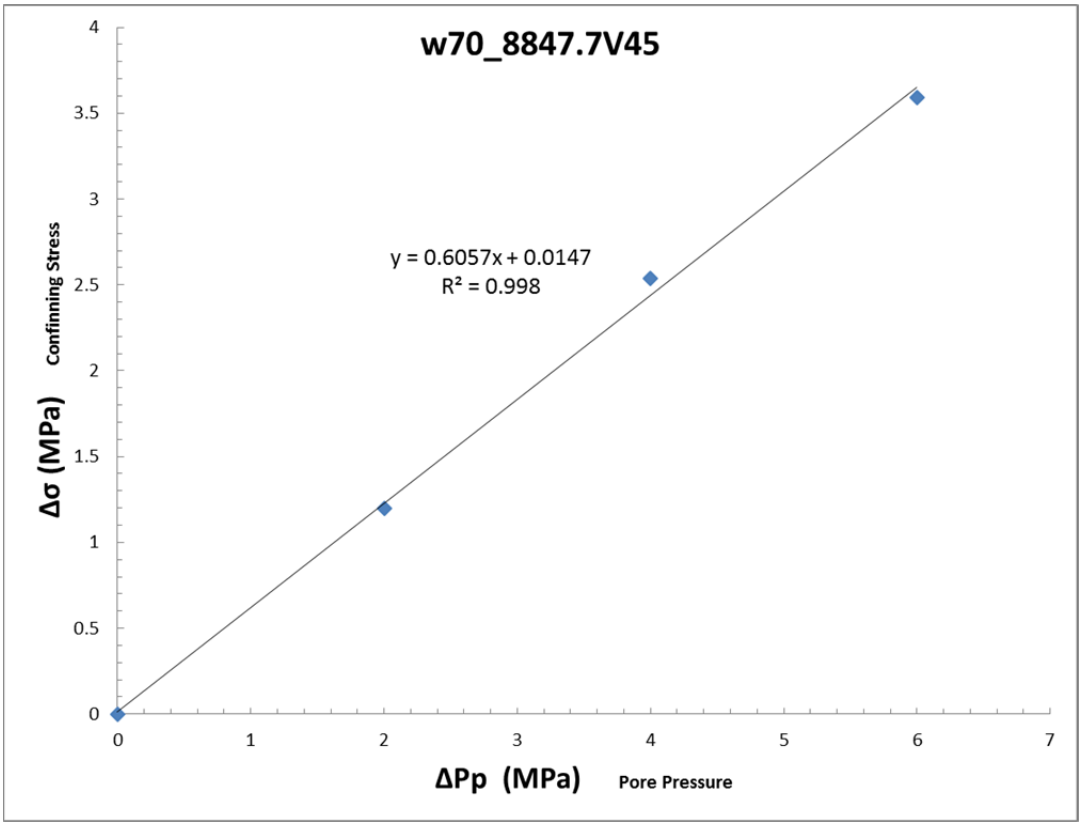
w70_8847.7V45
y = 0.6057x + 0.0147
R² = 0.998
Δσ (MPa) Confinning Stress
ΔPp (MPa) Pore Pressure
0
0.5
1
1.5
2
2.5
3
3.5
4
0
1
2
3
4
5
6
7

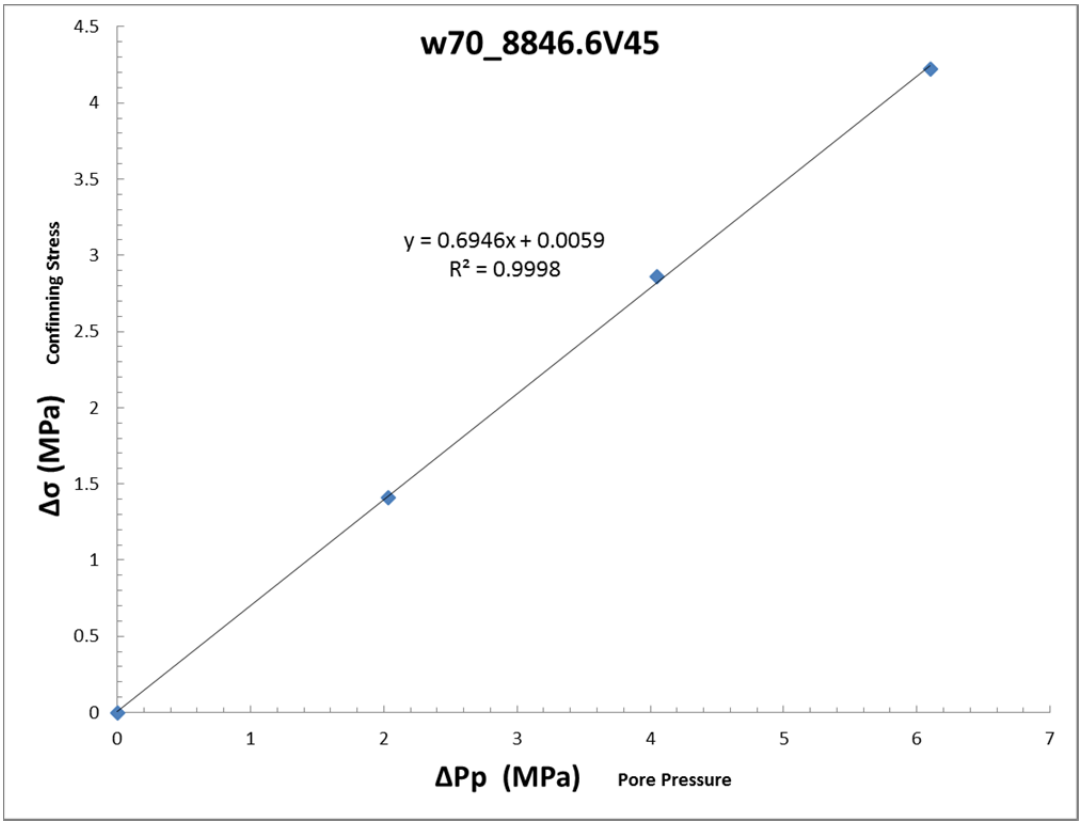
w70_8846.6V45
y = 0.6946x + 0.0059
R² = 0.9998
Δσ (MPa) Confinning Stress
ΔPp (MPa) Pore Pressure
0
0.5
1
1.5
2
2.5
3
3.5
4
4.5
0
1
2
3
4
5
6
7

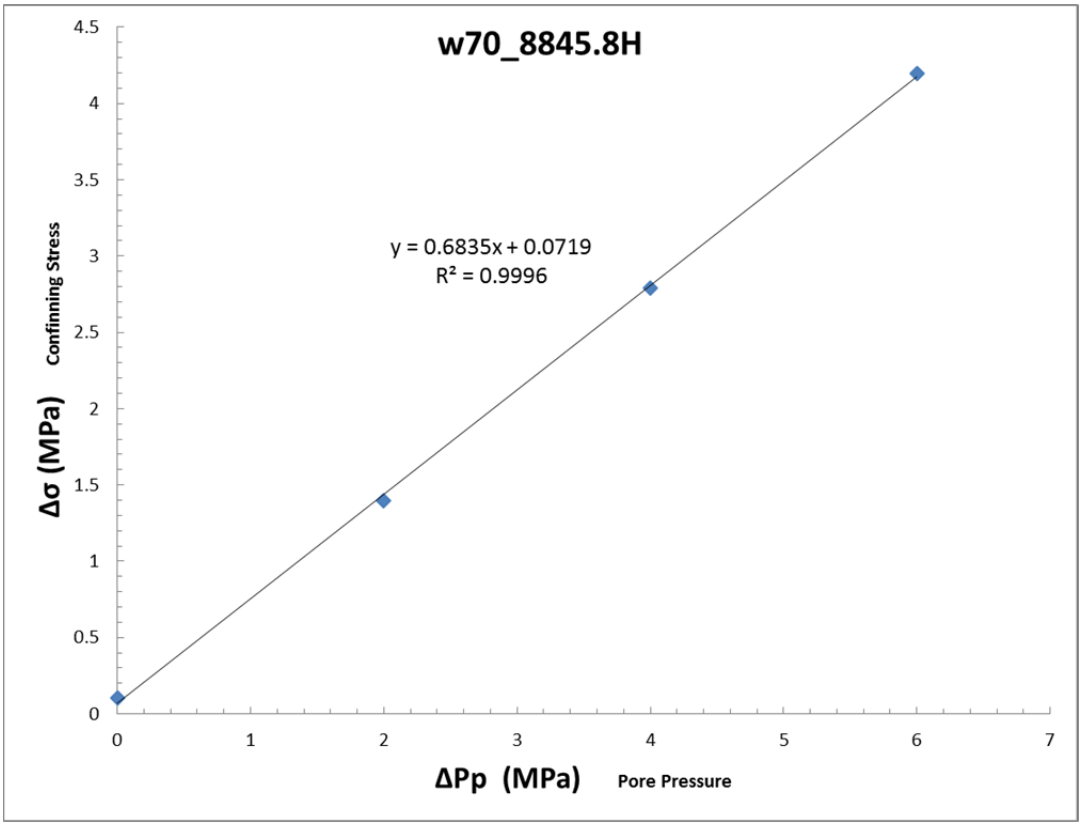
w70_8845.8H
y = 0.6835x + 0.0719
R² = 0.9996
Δσ (MPa) Confinning Stress
ΔPp (MPa) Pore Pressure
0
0.5
1
1.5
2
2.5
3
3.5
4
4.5
0
1
2
3
4
5
6
7

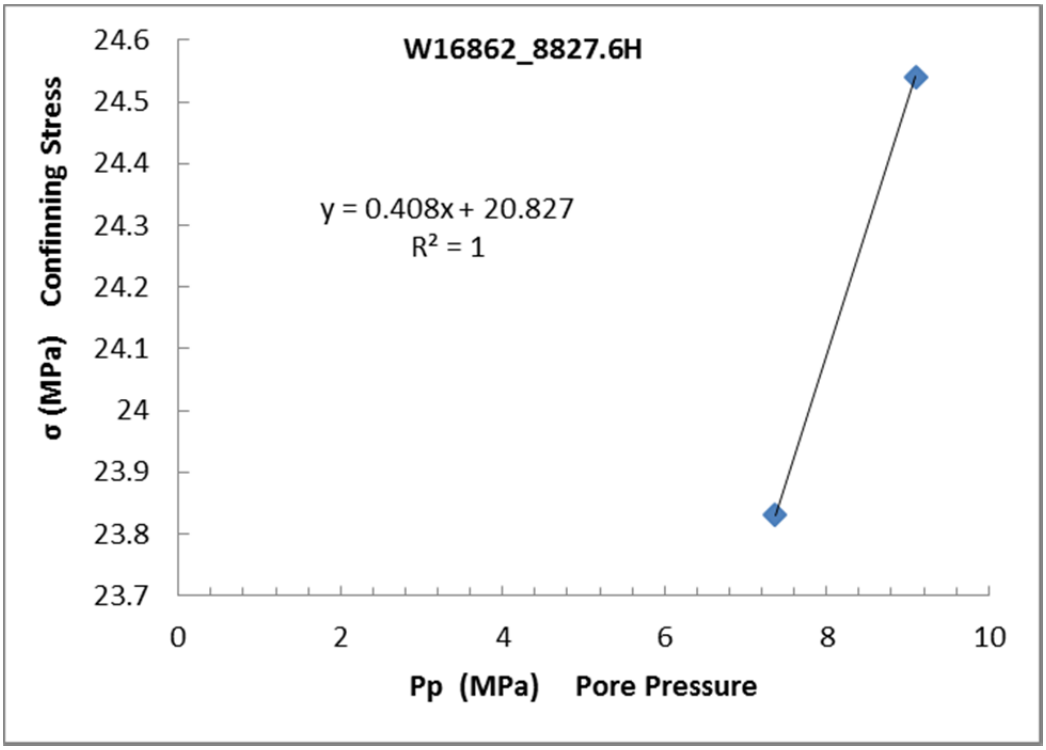
W16862_8827.6H
y = 0.408x + 20.827
R² = 1
σ (MPa) Confinning Stress
Pp (MPa) Pore Pressure
23.7
23.8
23.9
24
24.1
24.2
24.3
24.4
24.5
24.6
0
2
4
6
8
10

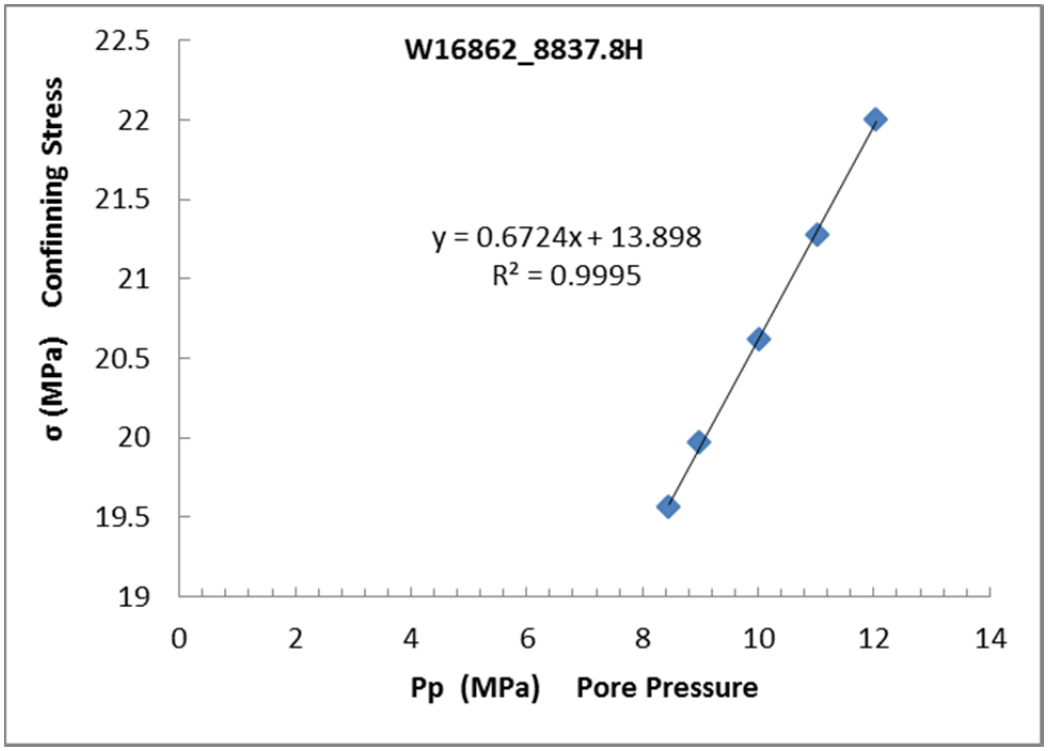
W16862_8837.8H
y = 0.6724x + 13.898
R² = 0.9995
σ (MPa) Confinning Stress
Pp (MPa) Pore Pressure
22.5
22
21.5
21
20.5
20
19.5
19
0
2
4
6
8
10
12
14

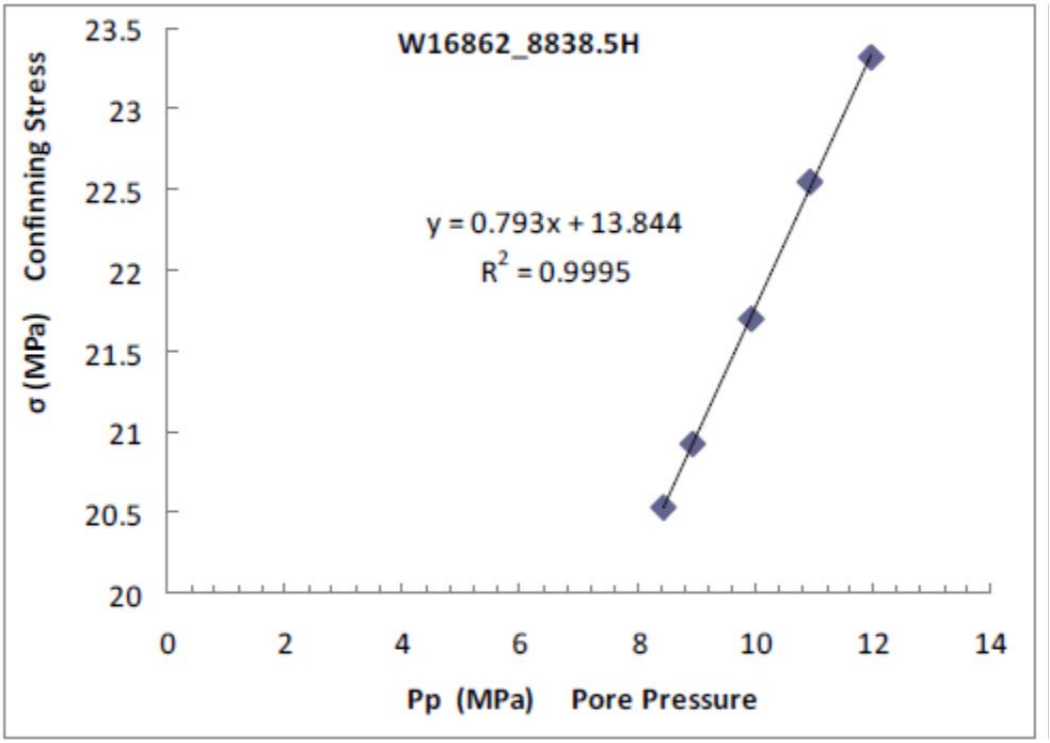
W16862_8838.5H
y = 0.793x + 13.844
R² = 0.9995
σ (MPa) Confinning Stress
Pp (MPa) Pore Pressure
23.5
23
22.5
22
21.5
21
20.5
20
0
2
4
6
8
10
12
14

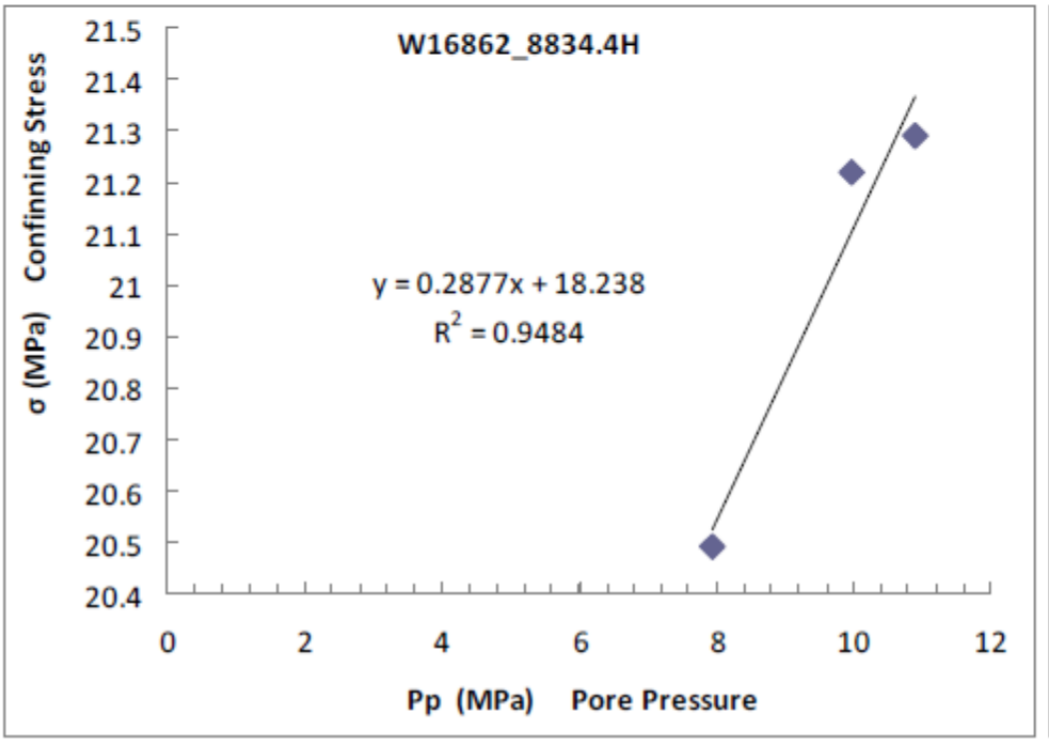
W16862_8834.4H
y = 0.2877x + 18.238
R2 = 0.9484
σ (MPa) Confinning Stress
Pp (MPa) Pore Pressure
21.5
21.4
21.3
21.2
21.1
21
20.9
20.8
20.7
20.6
20.5
20.4
0
2
4
6
8
10
12

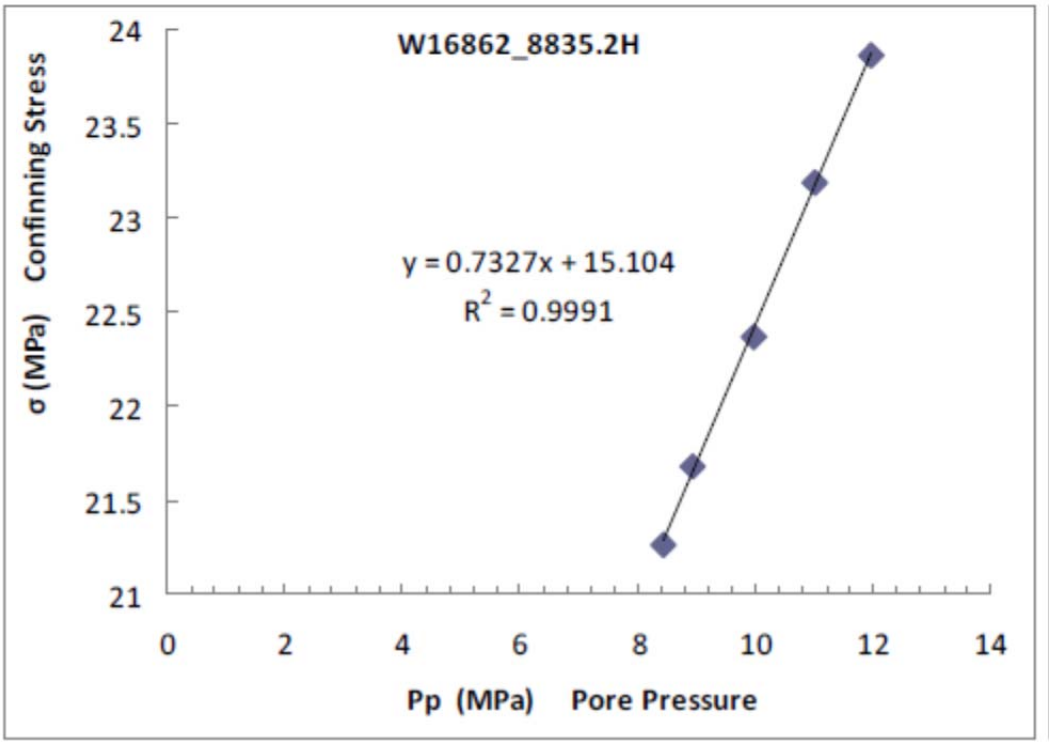
W16862_8835.2H
y = 0.7327x + 15.104
R2 = 0.9991
σ (MPa) Confinning Stress
Pp (MPa) Pore Pressure
24
23.5
23
22.5
22
21.5
21
0
2
4
6
8
10
12
14

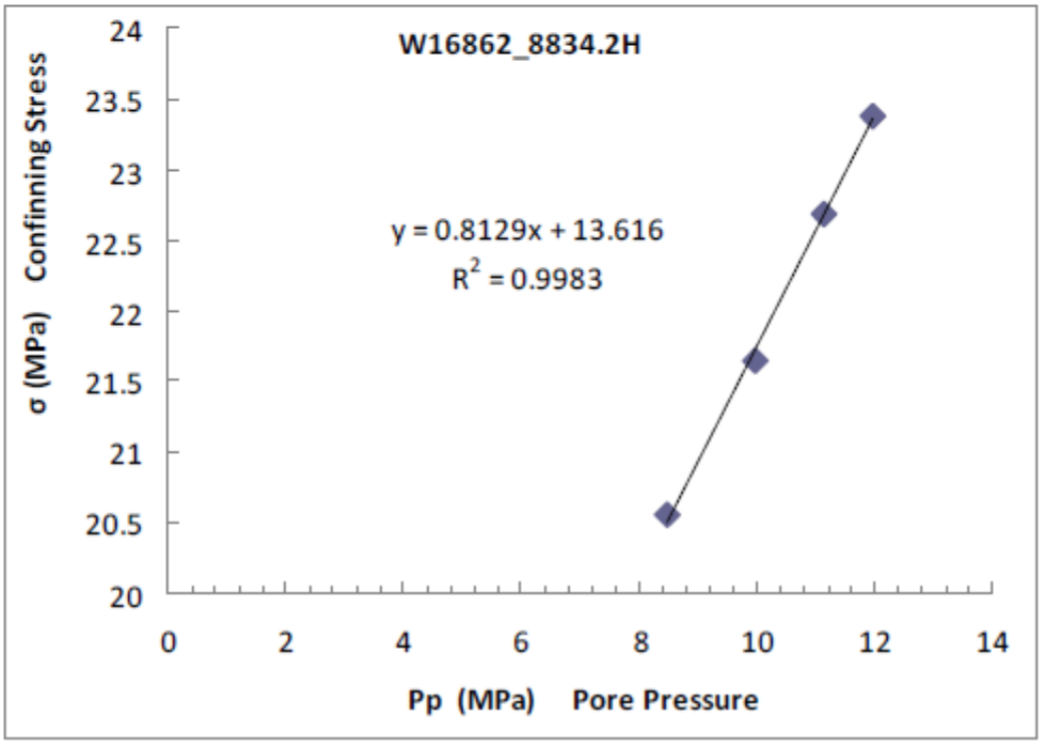
W16862_8834.2H
y = 0.8129x + 13.616
R2 = 0.9983
σ (MPa) Confinning Stress
Pp (MPa) Pore Pressure
24
23.5
23
22.5
22
21.5
21
20.5
20
0
2
4
6
8
10
12
14

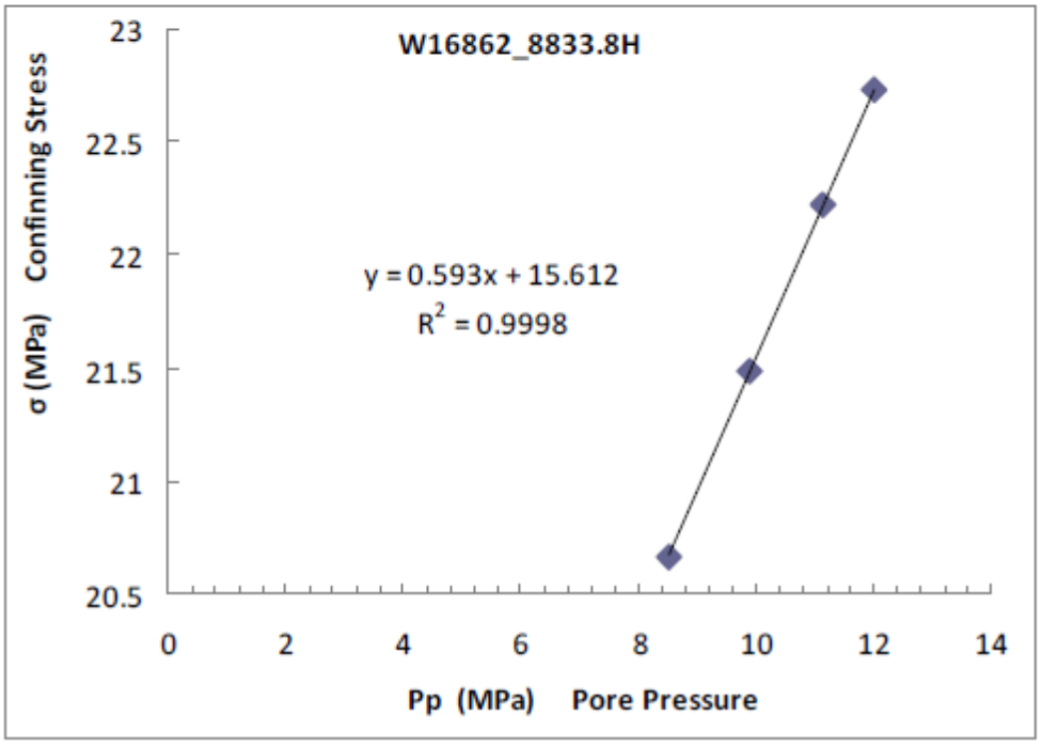
W16862_8833.8H
y = 0.593x + 15.612
R2 = 0.9998
σ (MPa) Confinning Stress
Pp (MPa) Pore Pressure
23
22.5
22
21.5
21
20.5
0
2
4
6
8
10
12
14

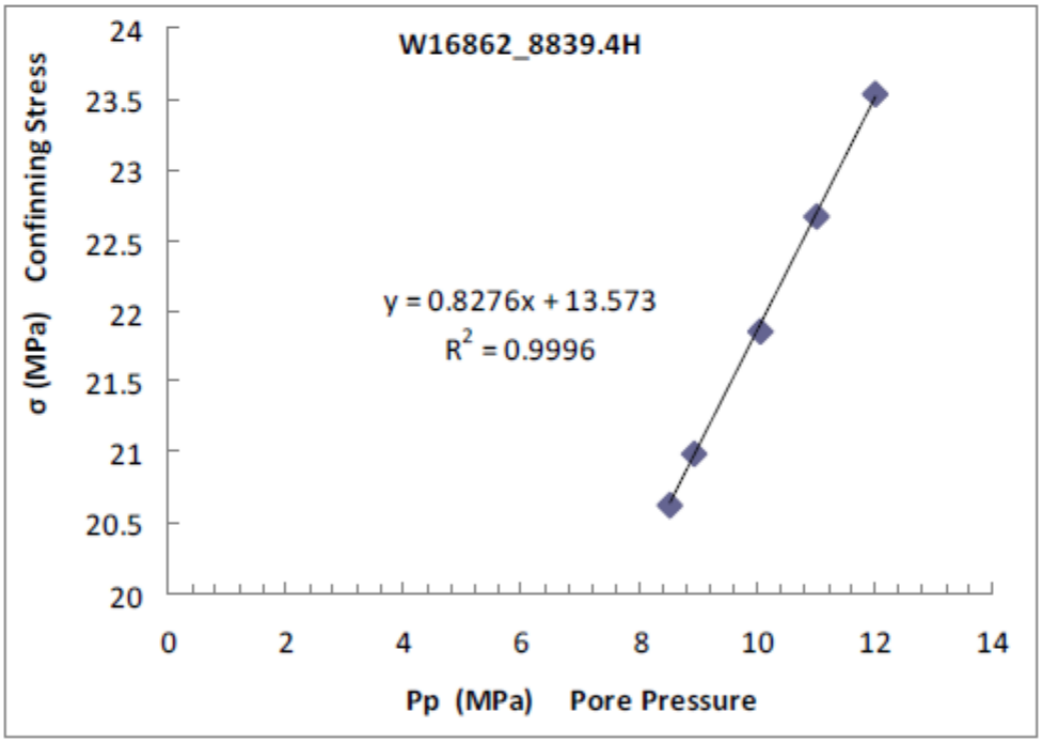
W16862_8839.4H
y = 0.8276x + 13.573
R2 = 0.9996
σ (MPa) Confinning Stress
Pp (MPa) Pore Pressure
24
23.5
23
22.5
22
21.5
21
20.5
20
0
2
4
6
8
10
12
14

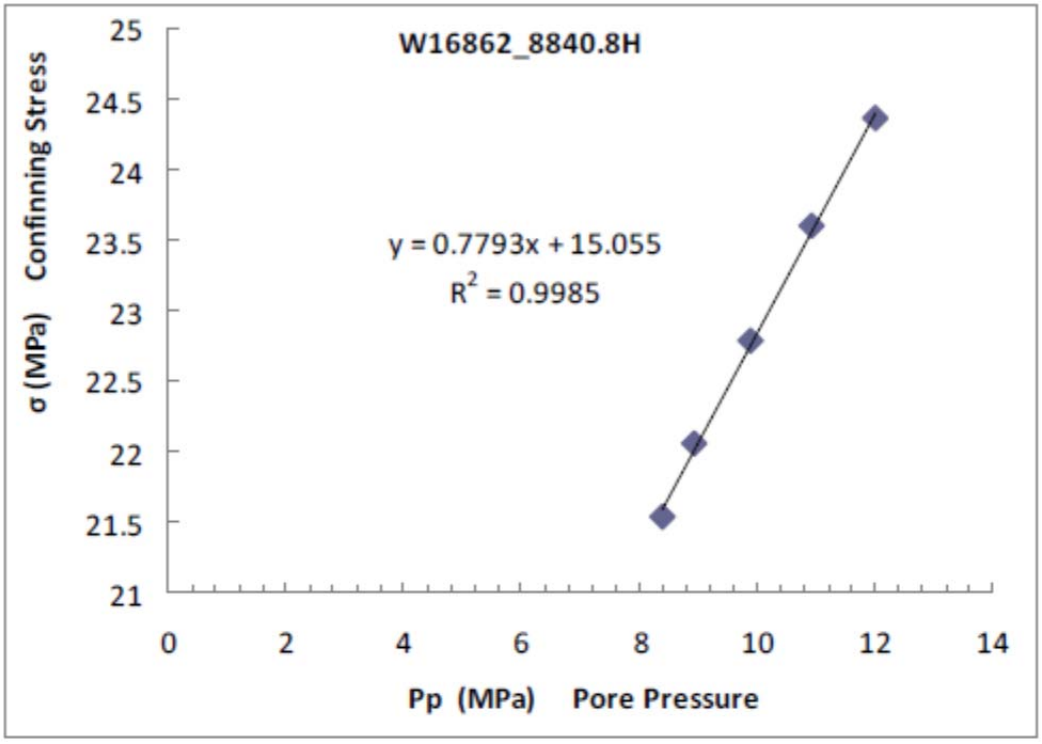
W16862_8840.8H
y = 0.7793x + 15.055
R2 = 0.9985
σ (MPa) Confinning Stress
Pp (MPa) Pore Pressure
25
24.5
24
23.5
23
22.5
22
21.5
21
0
2
4
6
8
10
12
14

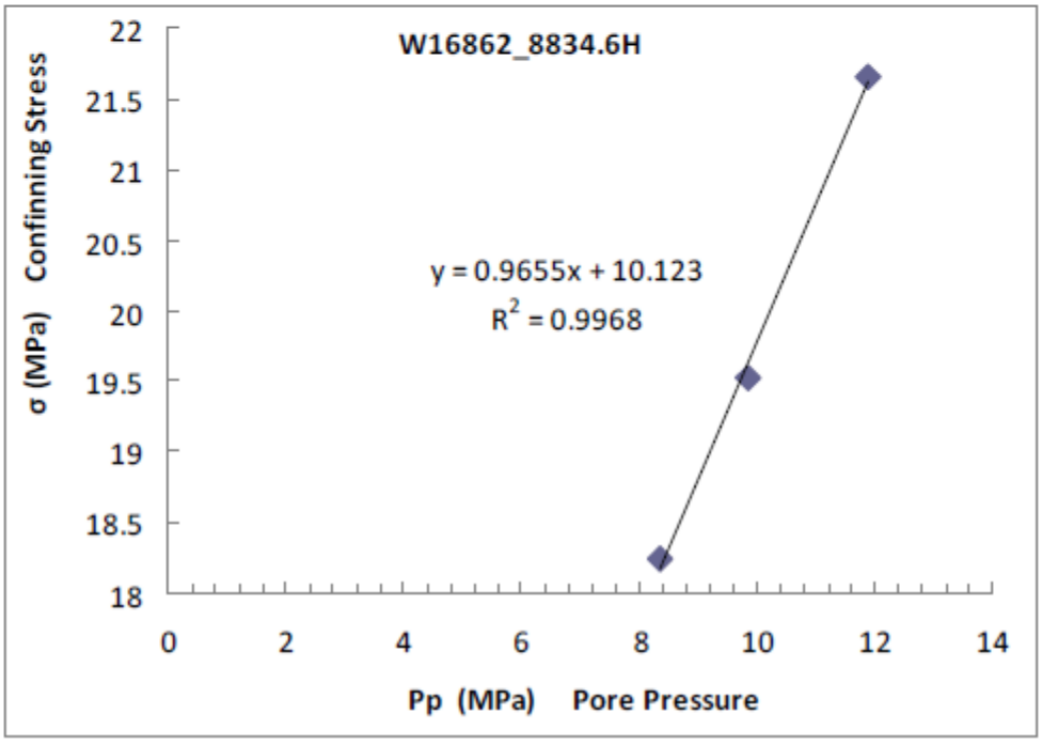
W16862_8834.6H
y = 0.9655x + 10.123
R2 = 0.9968
σ (MPa) Confinning Stress
Pp (MPa) Pore Pressure
22
21.5
21
20.5
20
19.5
19
18.5
18
0
2
4
6
8
10
12
14

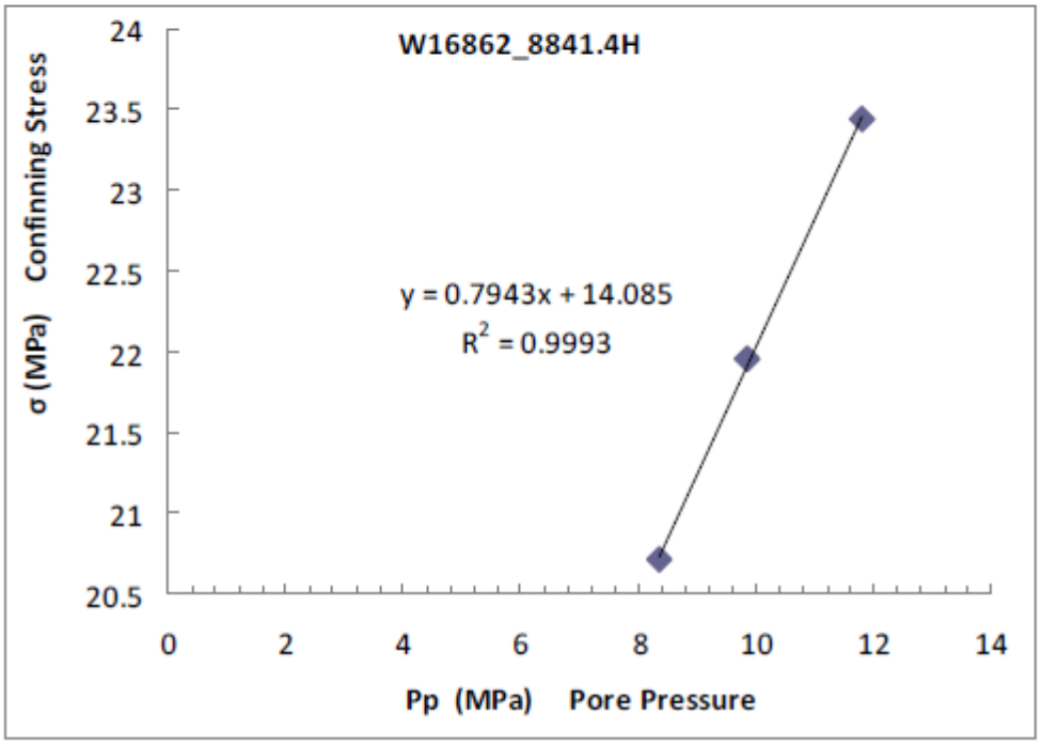
W16862_8841.4H
y = 0.7943x + 14.085
R2 = 0.9993
σ (MPa) Confinning Stress
Pp (MPa) Pore Pressure
24
23.5
23
22.5
22
21.5
21
20.5
0
2
4
6
8
10
12
14

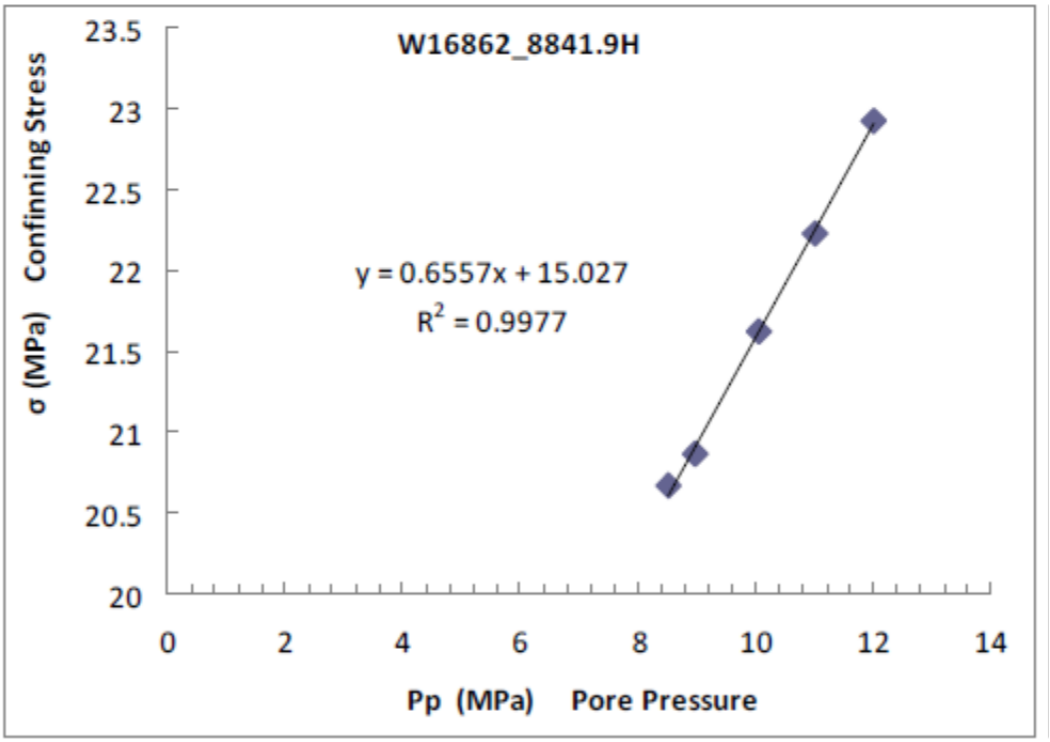
W16862_8841.9H
y = 0.6557x + 15.027
R2 = 0.9977
σ (MPa) Confinning Stress
Pp (MPa) Pore Pressure
23.5
23
22.5
22
21.5
21
20.5
20
0
2
4
6
8
10
12
14

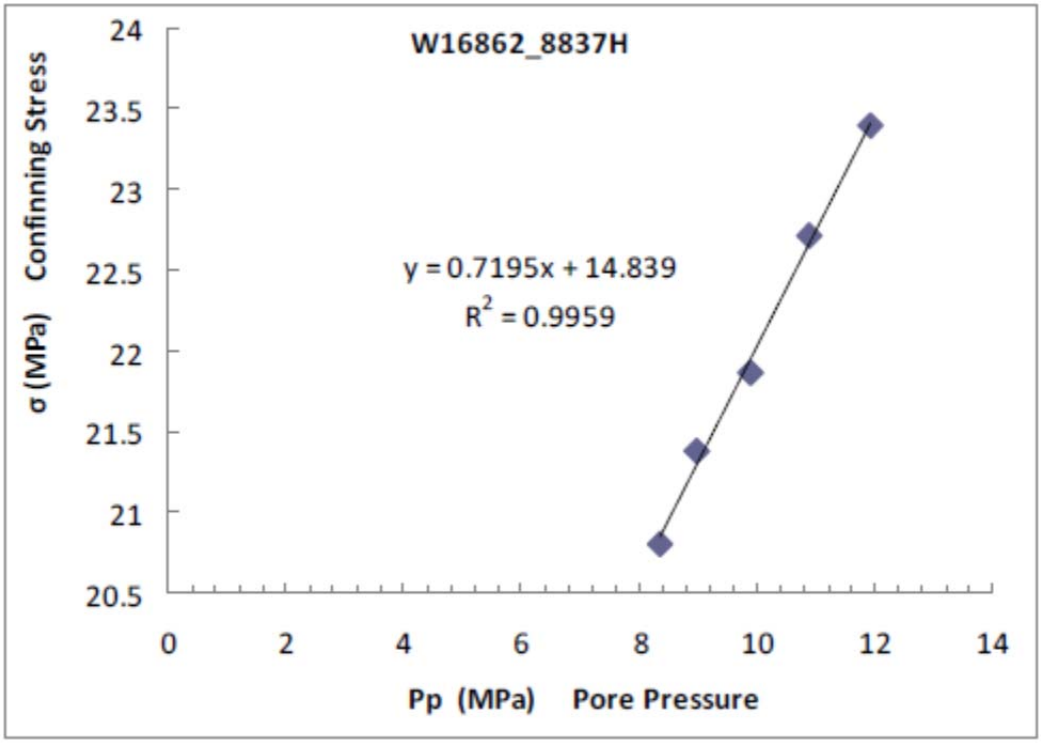
W16862_8837H
y = 0.7195x + 14.839
R2 = 0.9959
σ (MPa) Confinning Stress
Pp (MPa) Pore Pressure
24
23.5
23
22.5
22
21.5
21
20.5
0
2
4
6
8
10
12
14

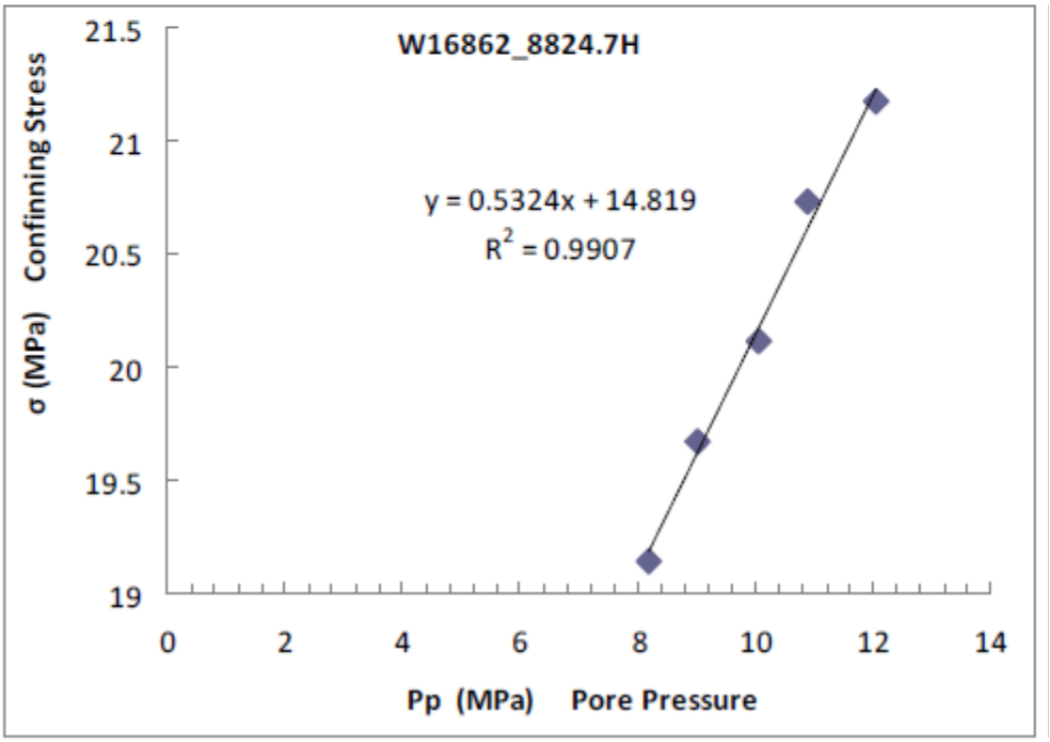
W16862_8824.7H
y = 0.5324x + 14.819
R2 = 0.9907
σ (MPa) Confinning Stress
Pp (MPa) Pore Pressure
21.5
21
20.5
20
19.5
19
0
2
4
6
8
10
12
14

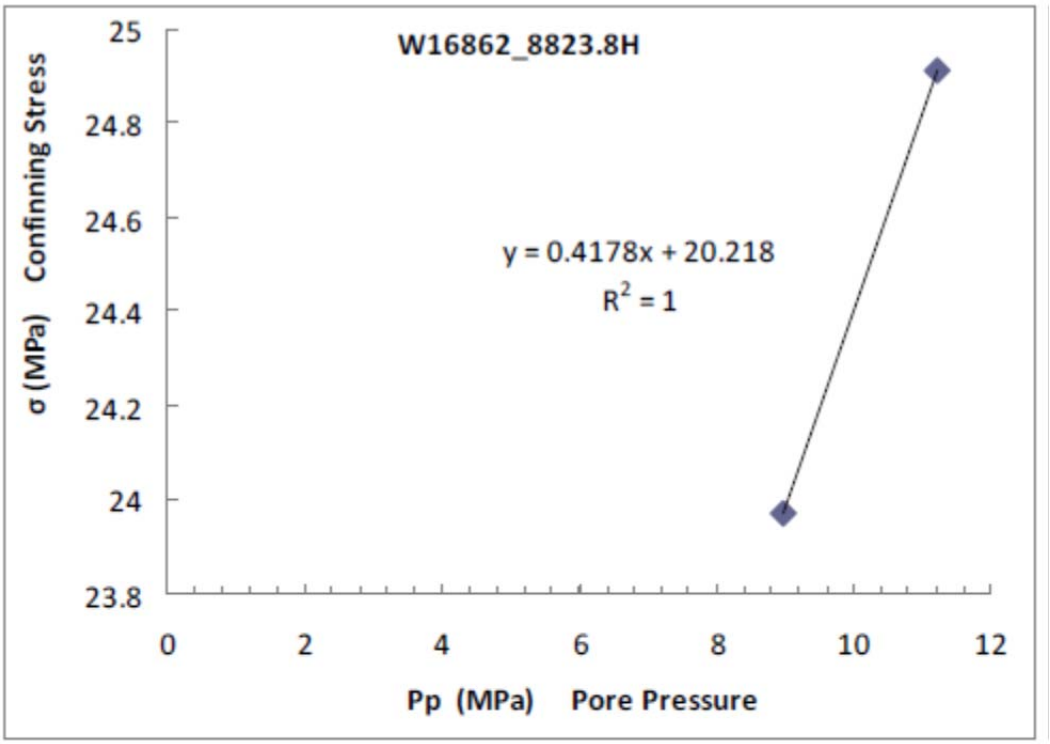
W16862_8823.8H
y = 0.4178x + 20.218
R2 = 1
σ (MPa) Confinning Stress
Pp (MPa) Pore Pressure
25
24.8
24.6
24.4
24.2
24
23.8
0
2
4
6
8
10
12

A.4.4 Static Moduli and Poisson's Ratio (Non-destructive)

Uniaxial Stress for File w70-mb-8842.7V-uniaxial_stress								
Event	Conf	Diff	Temp	E	n	K	G	P
	MPa	MPa	°C	GPa		GPa	GPa	GPa
0	25.3	25.7	28.2	59.40	0.183	31.24	25.10	64.71
1	15.3	12.0	28.0	61.80	0.184	32.56	26.11	67.37
2	5.2	6.9	27.5	49.83	0.190	26.81	20.93	54.72

Uniaxial Stress for File w70-mb-8843H-uniaxial_stress								
Event	Conf	Diff	Temp	E	n	K	G	P
	MPa	MPa	°C	GPa		GPa	GPa	GPa
0	25.4	26.9	25.3	75.16	0.110	32.10	33.86	77.25
1	15.3	11.1	25.4	64.90	0.120	28.45	28.98	67.09
2	5.3	6.9	24.3	55.56	0.131	25.08	24.57	57.83
3	25.3	25.7	26.1	74.74	0.111	31.98	33.65	76.85
4	15.3	11.6	23.5	63.73	0.117	27.74	28.52	65.77
5	5.2	6.9	19.2	57.15	0.128	25.60	25.33	59.38

Uniaxial Stress for File w70-mb-8845.8H-uniaxial_stress								
Event	Conf	Diff	Temp	E	n	K	G	P
	MPa	MPa	°C	GPa		GPa	GPa	GPa
0	25.3	26.5	25.0	81.72	0.126	36.39	36.30	84.78
1	15.3	12.4	24.1	81.34	0.097	33.64	37.07	83.07
2	5.3	7.7	23.7	66.92	0.120	29.35	29.88	69.18

Uniaxial Stress for File w70-mb-8845V-uniaxial_stress								
Event	Conf	Diff	Temp	E	n	K	G	P
	MPa	MPa	°C	GPa		GPa	GPa	GPa
0	25.4	26.9	28.5	53.97	0.186	28.68	22.74	59.00
1	15.3	12.0	28.2	61.17	0.207	34.76	25.35	68.55
2	5.3	7.7	21.4	52.66	0.214	30.67	21.69	59.59

Uniaxial Stress for File w70-mb-8846.6V45-uniaxial_stress								
Event	Conf	Diff	Temp	E	n	K	G	P
	MPa	MPa	°C	GPa		GPa	GPa	GPa
0	25.4	26.9	26.0	79.47	0.270	57.52	31.29	99.25
1	15.3	12.4	26.0	65.43	0.284	50.55	25.48	84.52
2	5.2	7.3	19.4	57.69	0.276	42.87	22.61	73.01

Uniaxial Stress for File w70-mb-8847.3V45-uniaxial_stress								
Event	Conf	Diff	Temp	E	n	K	G	P
	MPa	MPa	°C	GPa		GPa	GPa	GPa
0	25.3	26.9	23.2	61.09	0.215	35.69	25.15	69.22
1	15.2	12.0	22.4	62.75	0.240	40.19	25.31	73.93
2	5.3	7.7	22.0	55.31	0.223	33.24	22.62	63.40

Uniaxial Stress for File w70-mb-8847.7V45-uniaxial_stress								
Event	Conf	Diff	Temp	E	n	K	G	P
	MPa	MPa	°C	GPa		GPa	GPa	GPa
0	25.3	26.5	25.8	59.50	0.184	31.38	25.13	64.88
1	15.3	12.4	22.6	60.20	0.192	32.54	25.26	66.22
2	5.3	8.2	22.1	56.17	0.186	29.86	23.67	61.42

Uniaxial Stress for File w70-mb-8848.5V-uniaxial_stress								
Event	Conf	Diff	Temp	E	n	K	G	P
	MPa	MPa	°C	GPa		GPa	GPa	GPa
0	25.3	26.5	26.1	58.89	0.162	29.03	25.34	62.81
1	15.3	12.9	24.0	57.92	0.158	28.22	25.01	61.56
2	5.3	8.2	21.1	46.68	0.153	22.45	20.24	49.43

Uniaxial Stress for File w16862-8823.8-uniaxial-stress									
Event	Conf	Pore	Diff	Temp	E	n	K	G	P
	MPa	MPa	MPa	°C	GPa		GPa	GPa	GPa
0	40.6	-0.2	18.4	33.0	81.44	0.112	34.96	36.63	83.80
1	50.6	-0.2	23.1	33.0	85.24	0.150	40.65	37.05	90.04
2	30.6	-0.2	19.3	32.4	87.28	0.074	34.15	40.63	88.32

Uniaxial Stress for File w16862-8824.7-uniaxial-stress									
Event	Conf	Pore	Diff	Temp	E	n	K	G	P
	MPa	MPa	MPa	°C	GPa		GPa	GPa	GPa
0	40.5	-0.2	18.4	28.7	73.99	0.060	28.05	34.89	74.57
1	50.6	-0.2	23.5	28.4	68.75	-0.010	22.45	34.73	68.76
2	30.5	-0.2	18.8	25.2	79.64	0.022	27.78	38.95	79.72
3	30.5	-0.2	18.8	26.1	81.23	0.022	28.35	39.72	81.31

Uniaxial Stress for File w16862-8827.6-uniaxial-stress									
Event	Conf	Pore	Diff	Temp	E	n	K	G	P
	MPa	MPa	MPa	°C	GPa		GPa	GPa	GPa
0	40.6	-0.2	19.7	28.2	92.40	1.985	-10.37	15.47	10.27
1	50.6	-0.2	24.8	27.9	98.87	0.450	329.88	34.09	375.33
2	30.6	-0.2	20.5	26.6	100.73	0.289	79.41	39.09	131.52

Uniaxial Stress for File w16862-8833.8-uniaxial-stress									
Event	Conf	Pore	Diff	Temp	E	n	K	G	P
	MPa	MPa	MPa	°C	GPa		GPa	GPa	GPa
0	40.6	-0.2	18.8	30.4	71.89	0.120	31.54	32.09	74.33
1	50.6	-0.2	23.1	30.3	86.29	0.144	40.43	37.71	90.71
2	30.5	-0.2	19.3	29.1	83.39	0.183	43.88	35.24	90.87

Uniaxial Stress for File w16862-8834.2-uniaxial-stress									
Event	Conf	Pore	Diff	Temp	E	n	K	G	P
	MPa	MPa	MPa	°C	GPa		GPa	GPa	GPa
0	40.6	-0.2	18.8	29.4	61.28	0.207	34.89	25.38	68.73
1	50.6	-0.2	23.1	29.4	63.88	0.204	35.92	26.54	71.30
2	30.5	-0.2	18.4	27.3	62.63	0.201	34.88	26.08	69.65

Uniaxial Stress for File w16862-8834.4-uniaxial-stress									
Event	Conf	Pore	Diff	Temp	E	n	K	G	P
	MPa	MPa	MPa	°C	GPa		GPa	GPa	GPa
0	40.6	-0.2	19.7	28.2	36.18	0.240	23.18	14.59	42.63
1	50.6	-0.2	24.8	28.1	45.34	0.217	26.73	18.63	51.56
2	30.6	-0.2	20.5	26.8	42.86	0.241	27.60	17.27	50.62

Uniaxial Stress for File w16862-8834.6-uniaxial-stress									
Event	Conf	Pore	Diff	Temp	E	n	K	G	P
	MPa	MPa	MPa	°C	GPa		GPa	GPa	GPa
0	40.7	-0.2	20.1	29.5	77.58	0.249	51.50	31.06	92.91
1	30.5	-0.2	19.7	27.9	87.87	0.214	51.16	36.20	99.43
2	50.6	-0.2	28.6	28.8	79.96	0.242	51.68	32.18	94.60

Uniaxial Stress for File w16862-8835.2-uniaxial-stress									
Event	Conf	Pore	Diff	Temp	E	n	K	G	P
	MPa	MPa	MPa	°C	GPa		GPa	GPa	GPa
0	40.6	-0.2	23.1	33.2	55.69	0.192	30.17	23.35	61.31
1	30.5	-0.2	18.4	31.5	68.07	0.240	43.69	27.44	80.28
2	50.6	-0.2	32.5	33.3	68.46	0.142	31.91	29.96	71.87

Uniaxial Stress for File w16862-8836.7-uniaxial-stress									
Event	Conf	Pore	Diff	Temp	E	n	K	G	P
	MPa	MPa	MPa	°C	GPa		GPa	GPa	GPa
0	40.6	-0.2	18.0	29.7	71.82	0.153	34.53	31.14	76.05
1	50.5	-0.2	22.7	29.7	72.62	0.202	40.65	30.20	80.91
2	30.6	-0.2	4.7	27.9	57.20	0.085	22.97	26.36	58.12

Uniaxial Stress for File w16862-8837-uniaxial-stress									
Event	Conf	Pore	Diff	Temp	E	n	K	G	P
	MPa	MPa	MPa	°C	GPa		GPa	GPa	GPa
0	40.6	-0.2	18.4	32.2	86.41	0.301	72.35	33.21	116.63
1	50.7	-0.2	24.0	32.3	87.26	0.285	67.59	33.96	112.87
2	30.6	-0.2	19.7	30.2	88.38	0.309	77.25	33.75	122.25

Uniaxial Stress for File w16862-8838.5-uniaxial-stress									
Event	Conf	Pore	Diff	Temp	E	n	K	G	P
	MPa	MPa	MPa	°C	GPa		GPa	GPa	GPa
0	40.6	-0.2	20.1	29.8	34.03	0.168	17.10	14.57	36.52
1	50.6	-0.2	29.5	30.0	36.16	0.133	16.43	15.95	37.70
2	20.6	-0.2	20.1	26.3	36.36	0.205	20.56	15.08	40.67

Uniaxial Stress for File w16862-8839.4-uniaxial-stress									
Event	Conf	Pore	Diff	Temp	E	n	K	G	P
	MPa	MPa	MPa	°C	GPa		GPa	GPa	GPa
0	40.6	-0.2	18.4	34.1	77.56	0.279	58.39	30.33	98.83
1	50.6	-0.2	23.1	34.3	70.25	0.194	38.32	29.41	77.52
2	20.6	-0.2	16.3	29.8	76.40	0.294	61.77	29.52	101.13

Uniaxial Stress for File w16862-8840.8-uniaxial-stress									
Event	Conf	Pore	Diff	Temp	E	n	K	G	P
	MPa	MPa	MPa	°C	GPa		GPa	GPa	GPa
0	40.6	-0.2	18.4	32.0	66.22	0.084	26.51	30.55	67.25
1	50.6	-0.2	23.5	32.3	64.13	0.088	25.97	29.46	65.25
2	30.5	-0.2	18.8	29.9	70.19	0.096	28.98	32.01	71.67

Uniaxial Stress for File w16862-8841.4-uniaxial-stress									
Event	Conf	Pore	Diff	Temp	E	n	K	G	P
	MPa	MPa	MPa	°C	GPa		GPa	GPa	GPa
0	40.6	-0.2	18.4	32.5	84.07	0.098	34.85	38.29	85.90
1	30.5	-0.2	27.8	30.8	97.85	0.130	44.13	43.28	101.84
2	50.6	-0.2	37.6	32.4	85.39	0.080	33.92	39.52	86.61

Uniaxial Stress for File w16862-8841.9-uniaxial-stress									
Event	Conf	Pore	Diff	Temp	E	n	K	G	P
	MPa	MPa	MPa	°C	GPa		GPa	GPa	GPa
0	40.7	-0.2	18.8	33.7	63.72	0.171	32.26	27.21	68.54
1	50.6	-0.2	23.1	33.3	61.88	0.124	27.42	27.53	64.13
2	30.5	-0.2	18.4	32.9	78.88	0.247	52.04	31.62	94.19

A.4.5 Uni/Triaxial Compressive Strength, Young's Modulus and Poisson's Ratio

Strength for File w70-mb-8847.7V45-strength					
Event	Conf	Temp	E	n	peak_stress
	MPa	°C	GPa		MPa
0	15.3	21.8	60.60	0.520	176.8

Strength for File w70-mb-8848.5V-strength					
Event	Conf	Temp	E	n	peak_stress
	MPa	°C	GPa		MPa
0	15.2	27.9	33.83	0.299	228.0

Strength for File w70-mb-8848H-strength					
Event	Conf	Temp	E	n	peak_stress
	MPa	°C	GPa		MPa
0	15.2	25.3	64.10	0.639	198.1

Strength for File w16862-8823.8-strength						
Event	Conf	Diff	Temp	E	n	peak_stress
	MPa	MPa	°C	GPa		MPa
0	15.7	16.7	34.8	46.13	0.228	178.9

Strength for File w16862-8824.7-strength						
Event	Conf	Diff	Temp	E	n	peak_stress
	MPa	MPa	°C	GPa		MPa
0	8.0	15.0	35.7	41.29	0.159	195.5

Strength for File w16862-8827.6-strength						
Event	Conf	Diff	Temp	E	n	peak_stress
	MPa	MPa	°C	GPa		MPa
0	0.3	44.0	33.8	73.94	10.421	92.7

Strength for File w16862-8833.8-strength						
Event	Conf	Diff	Temp	E	n	peak_stress
	MPa	MPa	°C	GPa		MPa
0	15.8	33.3	39.5	46.54	0.300	176.3

Strength for File w16862-8834.2-strength						
Event	Conf	Diff	Temp	E	n	peak_stress
	MPa	MPa	°C	GPa		MPa
0	7.9	17.5	35.8	116.32	0.644	106.8

Strength for File w16862-8834.4-strength						
Event	Conf	Diff	Temp	E	n	peak_stress
	MPa	MPa	°C	GPa		MPa
0	0.6	28.2	35.1	43.01	0.352	134.5

Strength for File w16862-8834.6-strength						
Event	Conf	Diff	Temp	E	n	peak_stress
	MPa	MPa	°C	GPa		MPa
0	16.1	26.1	40.5	78.05	0.927	173.4

Strength for File w16862-8835.2-strength						
Event	Conf	Diff	Temp	E	n	peak_stress
	MPa	MPa	°C	GPa		MPa
0	0.7	9.4	37.0	38.76	0.259	146.9

Strength for File w16862-8837-strength						
Event	Conf	Diff	Temp	E	n	peak_stress
	MPa	MPa	°C	GPa		MPa
0	8.0	18.0	38.0	40.29	0.692	120.4

Strength for File w16862-8837.8-strength						
Event	Conf	Diff	Temp	E	n	peak_stress
	MPa	MPa	°C	GPa		MPa
0	16.2	19.3	34.3	145.98	5.010	118.3

Strength for File w16862-8838.5-strength						
Event	Conf	Diff	Temp	E	n	peak_stress
	MPa	MPa	°C	GPa		MPa
0	8.1	10.7	34.1	36.70	0.278	121.7

Strength for File w16862-8839.4-strength						
Event	Conf	Diff	Temp	E	n	peak_stress
	MPa	MPa	°C	GPa		MPa
0	0.7	0.0	32.8	30.54	1.091	77.3

Strength for File w16862-8840.8-strength						
Event	Conf	Diff	Temp	E	n	peak_stress
	MPa	MPa	°C	GPa		MPa
0	16.0	31.2	38.6	54.95	0.373	77.7

Strength for File w16862-8841.4-strength						
Event	Conf	Diff	Temp	E	n	peak_stress
	MPa	MPa	°C	GPa		MPa
0	8.1	14.1	34.6	52.61	0.491	186.2

Strength for File w16862-8841.9-strength						
Event	Conf	Diff	Temp	E	n	peak_stress
	MPa	MPa	°C	GPa		MPa
0	0.9	-1.2	33.8	37.71	0.196	145.6

A.4.6 Mohr's Circle

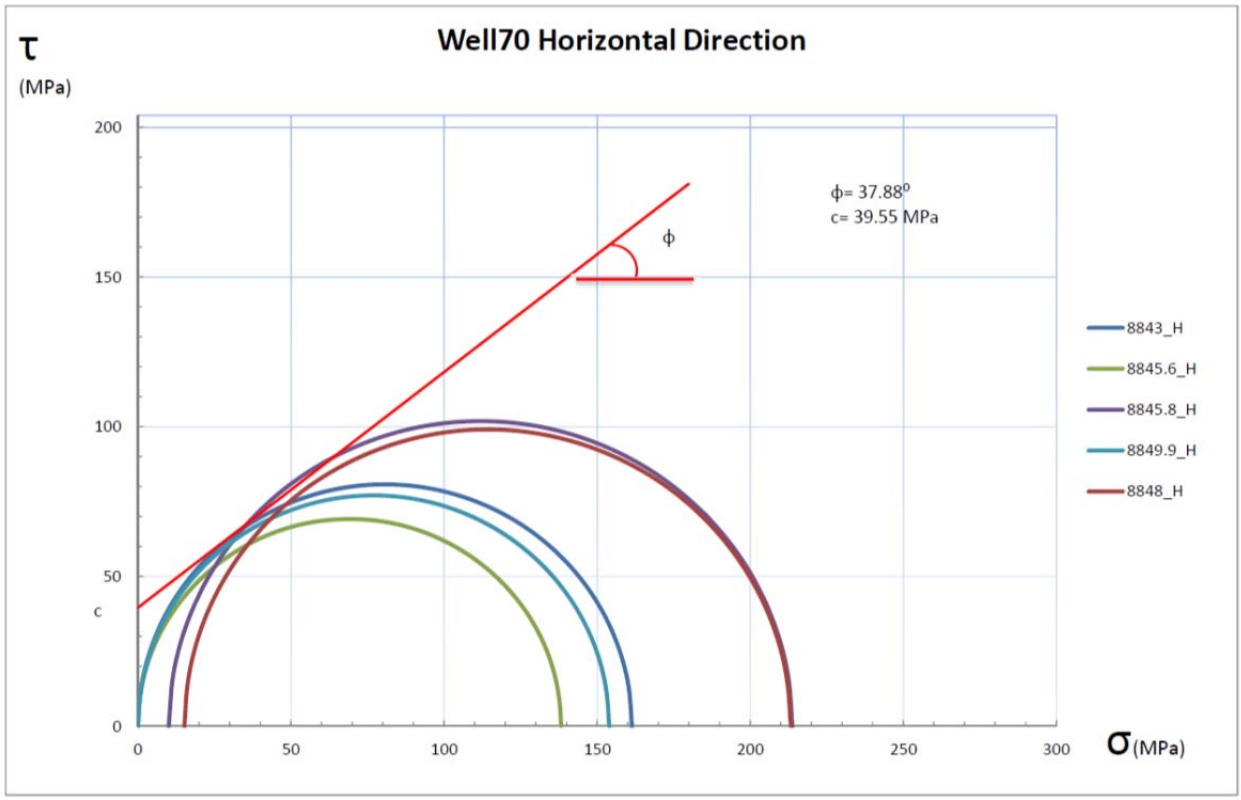

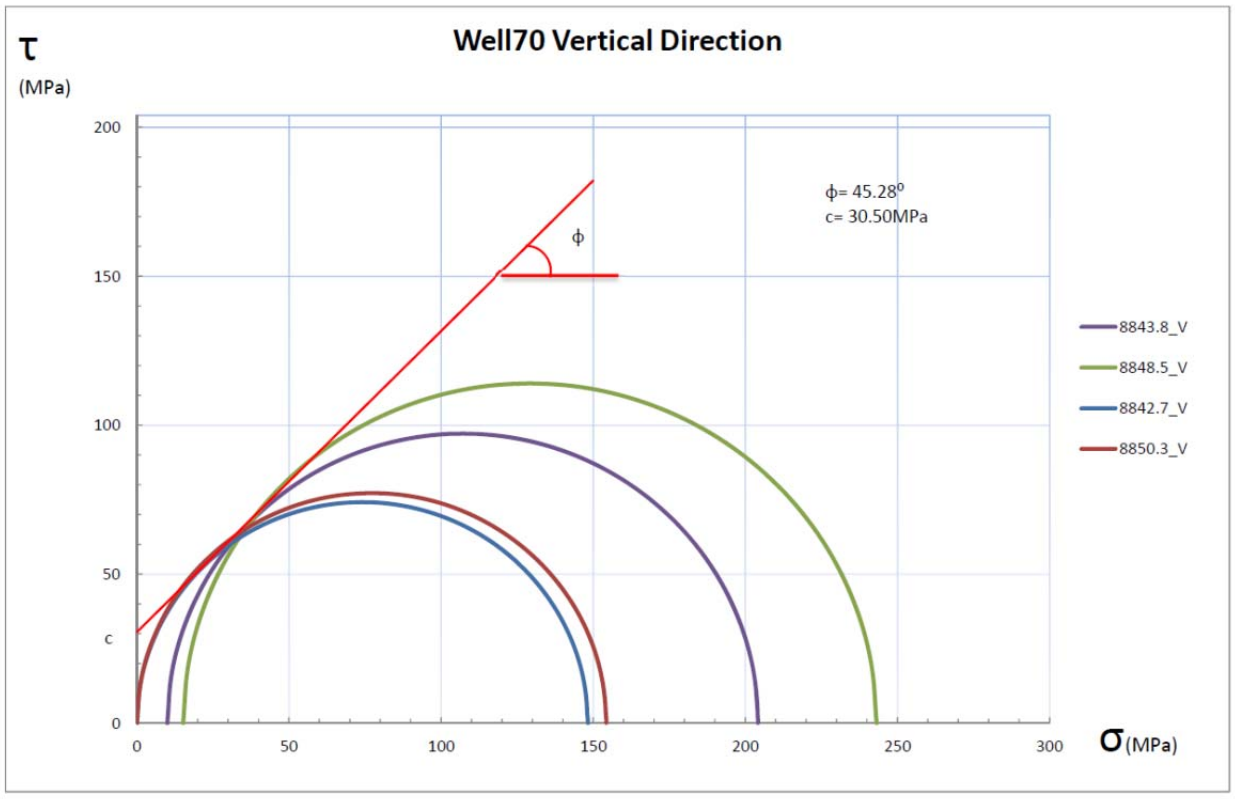
Well70 Vertical Direction
τ
(MPa)
200
150
100
50
c
0
0
50
100
150
200
250
300
σ (MPa)
ϕ= 45.28°
c= 30.50MPa
ϕ
8843.8_V
8848.5_V
8842.7_V
8850.3_V

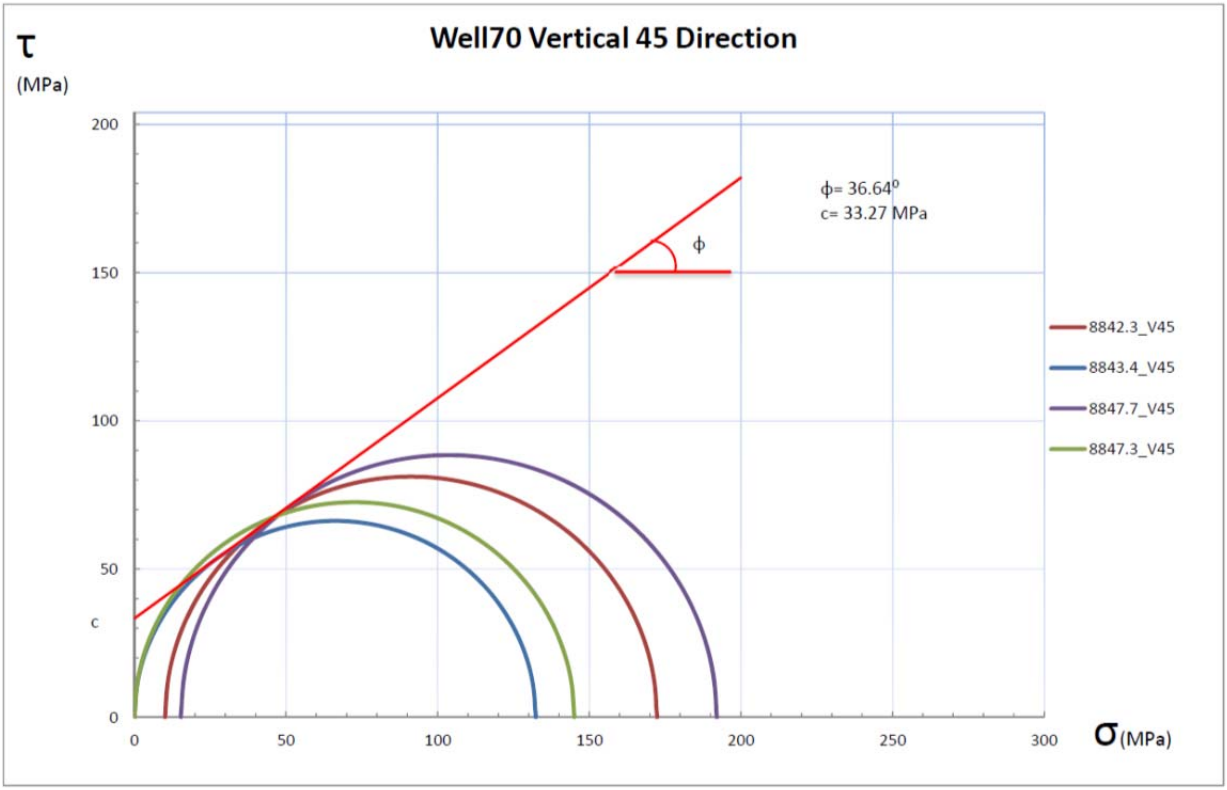
Well70 Vertical 45 Direction
τ
(MPa)
200
150
100
50
c
0
0
50
100
150
200
250
300
σ (MPa)
ϕ= 36.64°
c= 33.27 MPa
ϕ
8842.3_V45
8843.4_V45
8847.7_V45
8847.3_V45

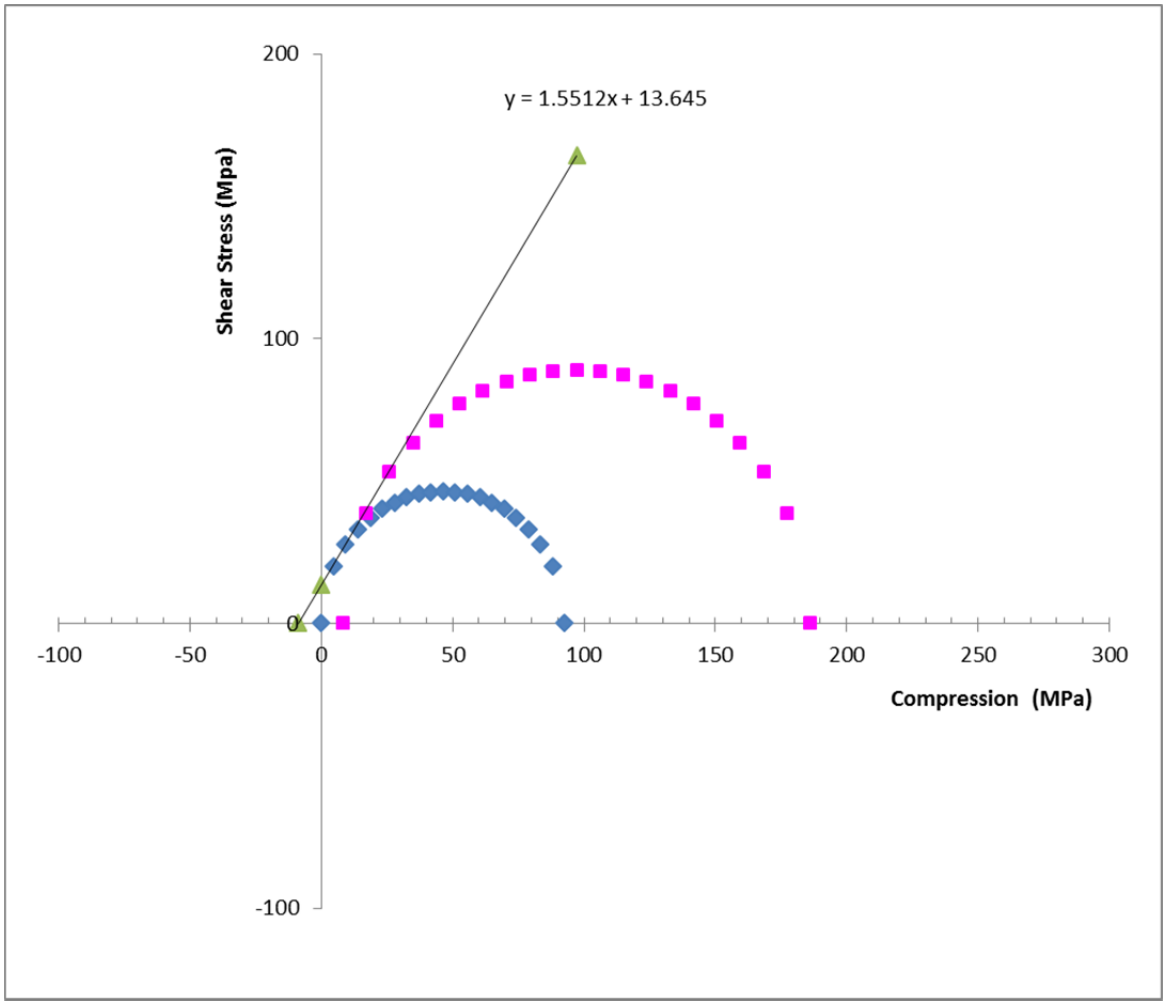
y = 1.5512x + 13.645
Shear Stress (Mpa)
Compression (MPa)
200
100
0
-100
-100
-50
0
50
100
150
200
250
300

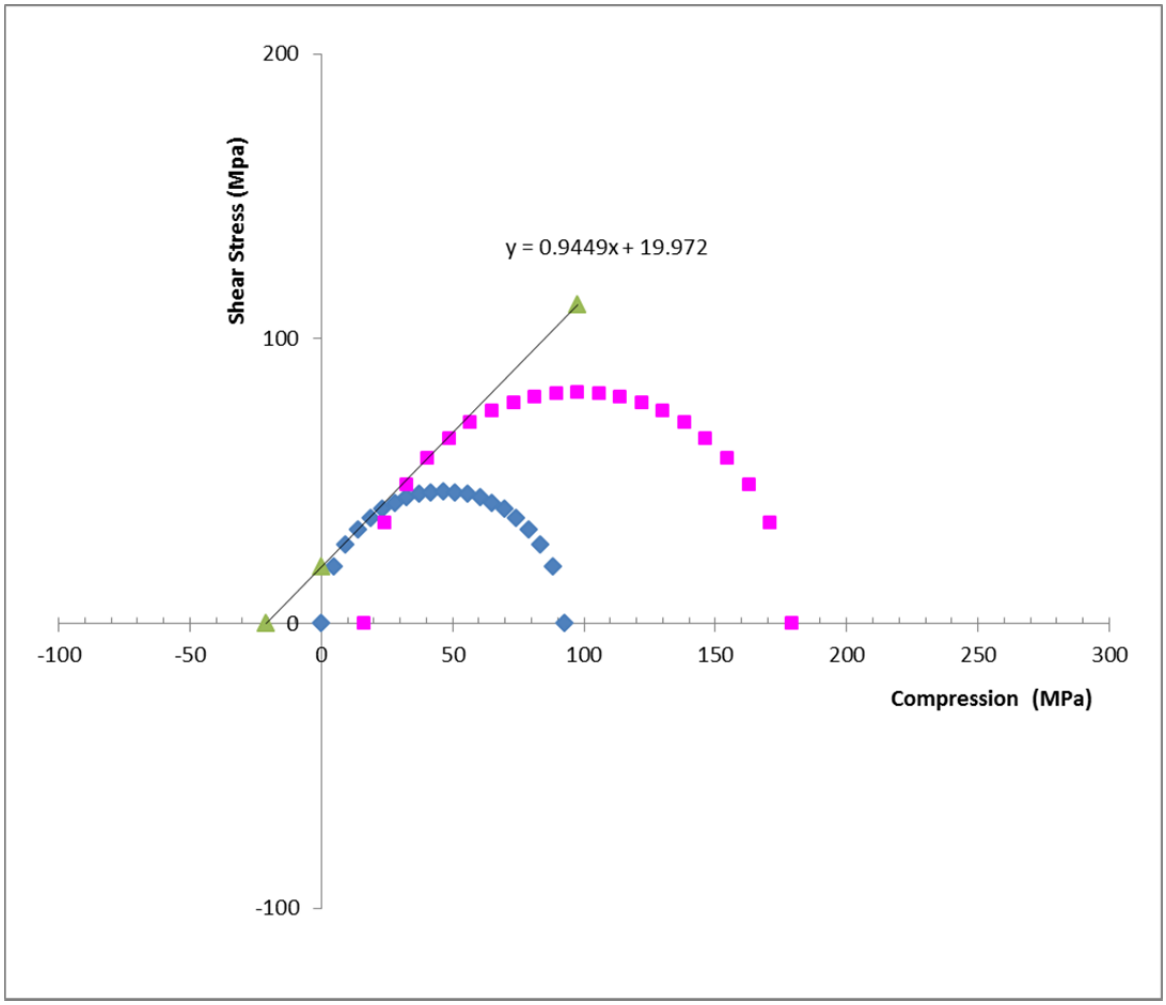
200
100
0
-100
Shear Stress (Mpa)
y = 0.9449x + 19.972
-100
-50
0
50
100
150
200
250
300
Compression (MPa)

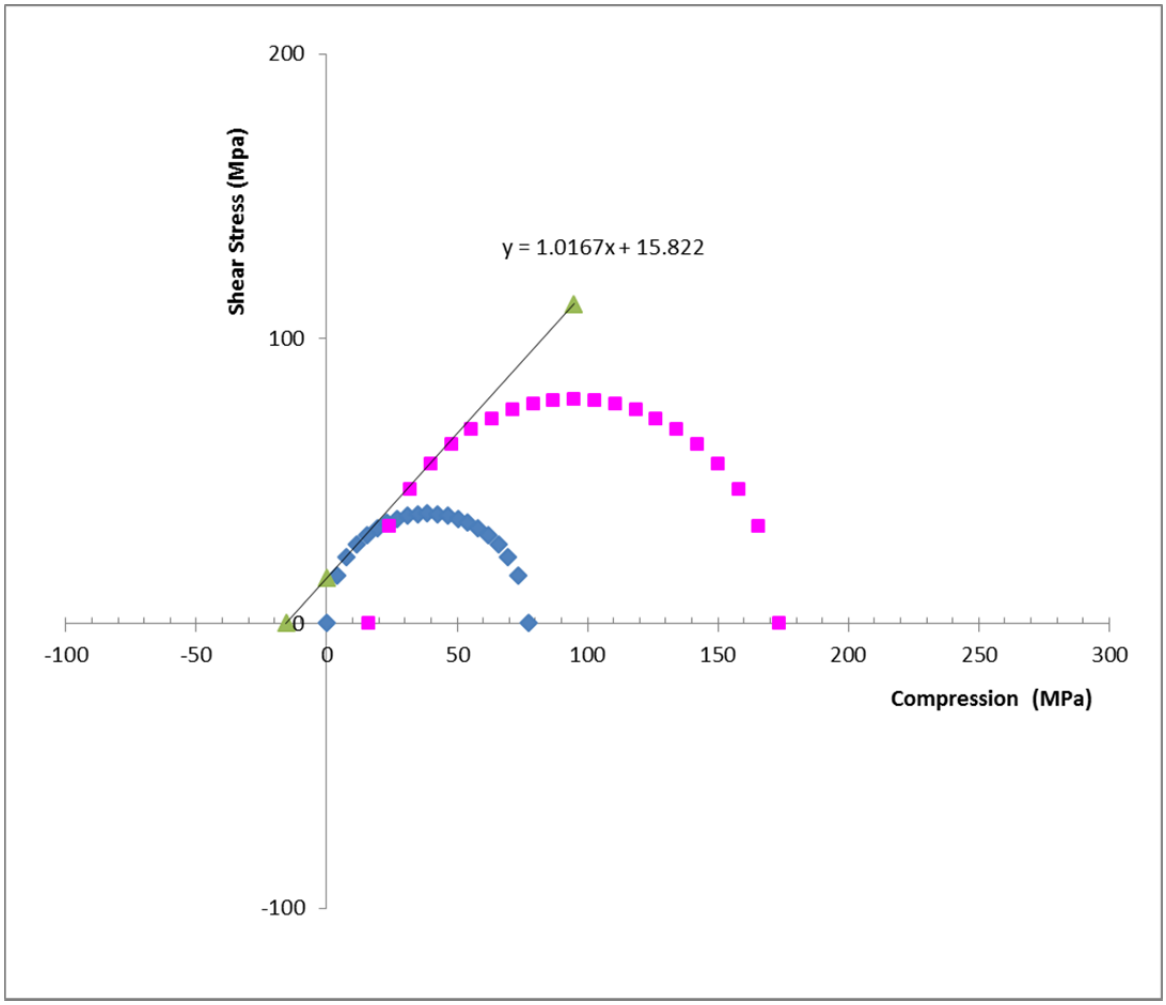
200
100
0
-100
-100
-50
0
50
100
150
200
250
300
Shear Stress (Mpa)
Compression (MPa)
y = 1.0167x + 15.822

A.5. Well 72 Bakken Samples Testing Results

A.5.1 Permeability

Permeability and Specific Storage for File W16985-10491-Permeability							
Event	Type	Conf	Pore Top	Diff	Temp	Perm	Storage
		MPa	MPa	MPa	°C	μD	m^{-1}
0	steady-state	20.6	7.7	-0.8	24.6	2.59e+04	0.00
1	steady-state	30.5	8.5	-1.3	25.4	4.27e+04	0.00
2	steady-state	40.5	7.6	-2.1	24.8	4.20e+04	0.00
3	steady-state	50.6	8.1	-2.5	24.9	1.56e+04	0.00

Permeability and Specific Storage for File W16985-10492-2-Permeability							
Event	Type	Conf	Pore Top	Diff	Temp	Perm	Storage
		MPa	MPa	MPa	°C	μD	m^{-1}
0	steady-state	20.5	7.7	-1.3	26.6	2.22e+04	0.00
1	steady-state	30.5	8.5	-1.3	26.7	2.19e+04	0.00
2	steady-state	40.5	7.8	-2.1	26.8	3.61e+03	0.00
3	steady-state	50.6	7.7	-2.5	26.8	3.02e+03	0.00

Permeability and Specific Storage for File W16985-10493-Permeability							
Event	Type	Conf	Pore Top	Diff	Temp	Perm	Storage
		MPa	MPa	MPa	°C	μD	m^{-1}
0	steady-state	20.6	8.1	-1.3	22.6	1.47e+03	0.00
1	steady-state	30.5	8.9	-2.1	22.6	1.48e+03	0.00
2	steady-state	40.6	9.0	-2.1	23.1	1.50e+03	0.00
3	steady-state	50.6	9.0	-2.5	23.2	1.45e+03	0.00

Permeability and Specific Storage for File W16985-10497-Permeability							
Event	Type	Conf	Pore Top	Diff	Temp	Perm	Storage
		MPa	MPa	MPa	°C	μD	m^{-1}
0	steady-state	20.5	8.5	-1.3	31.0	8.54e+03	0.00
1	steady-state	30.5	8.9	-1.7	31.7	4.66e+03	0.00
2	steady-state	40.6	8.9	-2.1	31.4	3.48e+03	0.00
3	steady-state	50.6	9.0	-2.5	31.3	2.54e+03	0.00

Permeability and Specific Storage for File W16985-10499.8-Permeability							
Event	Type	Conf	Pore Top	Diff	Temp	Perm	Storage
		MPa	MPa	MPa	°C	μD	m^{-1}
0	steady-state	20.6	8.8	-1.3	26.6	2.28e+04	0.00
1	steady-state	30.5	8.2	-1.7	27.1	1.03e+04	0.00
2	steady-state	40.6	8.2	-2.5	27.3	1.12e+04	0.00
3	steady-state	50.7	8.2	-2.5	27.6	6.48e+03	0.00

Permeability and Specific Storage for File W16985-10504-2-Permeability							
Event	Type	Conf	Pore Top	Diff	Temp	Perm	Storage
		MPa	MPa	MPa	°C	μD	m^{-1}
0	steady-state	20.6	7.8	-0.8	30.0	1.78e+04	0.00

Permeability and Specific Storage for File W16985-10505.7-Permeability							
Event	Type	Conf	Pore Top	Diff	Temp	Perm	Storage
		MPa	MPa	MPa	°C	μD	m^{-1}
0	steady-state	20.6	8.1	-0.8	24.3	5.67e+04	0.00
1	steady-state	30.5	8.7	-1.7	24.5	2.74e+04	0.00
2	steady-state	50.6	9.0	-3.0	24.7	1.49e+05	0.00
3	steady-state	40.6	8.4	-2.1	24.6	3.84e+04	0.00

Permeability and Specific Storage for File W16985-10509-Permeability							
Event	Type	Conf	Pore Top	Diff	Temp	Perm	Storage
		MPa	MPa	MPa	°C	μD	m^{-1}
0	steady-state	30.5	8.8	-2.1	27.1	1.02e+04	0.00
1	steady-state	40.5	8.7	-2.5	27.1	1.31e+04	0.00
2	steady-state	50.6	8.1	-3.0	27.1	3.09e+04	0.00

Permeability and Specific Storage for File W16985-10512.7-Permeability							
Event	Type	Conf	Pore Top	Diff	Temp	Perm	Storage
		MPa	MPa	MPa	°C	μD	m^{-1}
0	steady-state	20.6	9.0	-0.8	25.9	4.60e+03	0.00
1	steady-state	30.5	9.0	-1.7	26.0	3.23e+03	0.00
2	steady-state	40.6	8.9	-2.1	26.3	2.59e+03	0.00
3	steady-state	50.6	9.0	-3.0	26.4	2.35e+03	0.00

Permeability and Specific Storage for File W16985-10514.5-Permeability							
Event	Type	Conf	Pore Top	Diff	Temp	Perm	Storage
		MPa	MPa	MPa	°C	μD	m^{-1}
0	steady-state	20.5	8.6	-1.3	27.0	1.24e+03	0.00
1	steady-state	30.5	8.8	-1.3	27.2	1.25e+03	0.00
2	steady-state	40.5	8.9	-2.1	27.5	1.26e+03	0.00
3	steady-state	50.6	9.0	-2.5	27.6	1.23e+03	0.00

Permeability and Specific Storage for File w16985-10488-permeability							
Event	Type	Conf	Pore Top	Diff	Temp	Perm	Storage
		MPa	MPa	MPa	°C	μD	m^{-1}
0	steady-state	20.6	8.9	-0.8	23.2	8.30e+03	0.00
1	steady-state	30.4	8.9	-2.1	23.3	6.76e+03	0.00
2	steady-state	40.5	8.9	-2.5	23.2	4.89e+03	0.00
3	steady-state	50.6	8.9	-3.0	22.7	3.85e+03	0.00

Permeability and Specific Storage for File w16985-10488.5-permeability							
Event	Type	Conf	Pore Top	Diff	Temp	Perm	Storage
		MPa	MPa	MPa	°C	μD	m^{-1}
0	aspike	20.6	7.9	-0.8	26.2	6.20	2.30e-11
1	aspike	20.5	7.8	-1.7	26.1	8.89	4.03e-11
2	aspike	30.5	7.8	-2.1	26.7	6.79	6.16e-12
3	aspike	40.6	7.9	-2.5	26.9	6.93	7.76e-12
4	aspike	50.6	7.9	-2.5	27.1	6.97	1.17e-12

Permeability and Specific Storage for File w16985-10490-permeability							
Event	Type	Conf	Pore Top	Diff	Temp	Perm	Storage
		MPa	MPa	MPa	°C	μD	m^{-1}
0	steady-state	20.5	9.2	-1.3	27.5	2.33e+04	0.00
1	steady-state	30.5	8.4	-2.1	27.6	1.20e+04	0.00
2	steady-state	40.5	8.8	-2.5	27.7	1.02e+04	0.00
3	steady-state	50.6	9.2	-2.5	27.8	8.14e+03	0.00

Permeability and Specific Storage for File w16985-10498-permeability							
Event	Type	Conf	Pore Top	Diff	Temp	Perm	Storage
		MPa	MPa	MPa	°C	μD	m^{-1}
0	steady-state	20.5	8.2	-1.3	26.2	0.00	0.00
1	steady-state	20.5	9.5	-1.3	26.5	1.09e+04	0.00
2	steady-state	30.5	9.4	-1.7	27.0	5.48e+03	0.00
3	steady-state	40.5	9.5	-2.5	27.3	3.55e+03	0.00
4	steady-state	50.5	9.2	-3.0	27.6	7.45e+03	0.00

Permeability and Specific Storage for File w16985-10503-permeability							
Event	Type	Conf	Pore Top	Diff	Temp	Perm	Storage
		MPa	MPa	MPa	°C	μD	m^{-1}
0	multipulse	20.5	7.8	-1.3	28.2	0.0164	3.95e-07
1	multipulse	30.5	7.9	-1.3	25.3	0.00592	1.05e-07
2	multipulse	40.6	7.9	-1.7	25.3	0.414	0.000103

Permeability and Specific Storage for File w16985-10504.8-2-permeability							
Event	Type	Conf	Pore Top	Diff	Temp	Perm	Storage
		MPa	MPa	MPa	°C	μD	m^{-1}
0	multipulse	20.5	7.9	-1.3	28.5	0.265	0.000110
1	multipulse	30.5	7.9	-1.3	29.2	0.0169	6.60e-06
2	multipulse	40.5	8.0	-1.7	29.5	0.00468	6.01e-08

Permeability and Specific Storage for File w16985-10517.8-permeability							
Event	Type	Conf	Pore Top	Diff	Temp	Perm	Storage
		MPa	MPa	MPa	°C	μD	m^{-1}
0	aspike	20.5	7.9	-0.8	27.2	0.419	2.46e-06
1	aspike	20.5	7.9	-1.3	27.3	0.0631	3.36e-08
2	multipulse	20.5	7.9	-0.8	27.6	0.443	1.03e-06
3	multipulse	30.5	7.9	-1.3	28.1	0.371	9.75e-07
4	multipulse	40.5	7.9	-2.1	28.2	0.269	7.10e-07
5	multipulse	50.6	7.9	-2.5	28.4	0.242	8.74e-07

A.5.2 Sonic Velocity, Dynamic Moduli and Poisson's Ratio

Observed Velocities and Moduli for File W16985-10487.5-Velocity									
Event	Conf	Pore	Diff	Temp	V_p	$V_s^{(1)}$	$V_s^{(2)}$	Young's Modulus	Poisson's Ratio
	MPa	MPa	MPa	°C	m/s	m/s	m/s	GPa	
0	50.5	-0.2	-3.8	24.6	4856	3121	3034	55.80	0.164
1	40.5	-0.2	-3.7	23.7	4828	3099	3045	55.39	0.160
2	30.4	-0.2	-3.8	23.7	4856	3110	3012	55.49	0.170
3	20.5	-0.2	-3.4	23.0	4828	3099	2991	54.88	0.170
4	10.5	-0.2	-2.4	22.9	4695	3065	2950	52.73	0.152

Observed Velocities and Moduli for File W16985-10488.5-Velocity									
Event	Conf	Pore	Diff	Temp	V_p	$V_s^{(1)}$	$V_s^{(2)}$	Young's Modulus	Poisson's Ratio
	MPa	MPa	MPa	°C	m/s	m/s	m/s	GPa	
0	50.5	-0.2	-4.6	33.4	5182	3144	3132	61.03	0.210
1	40.5	-0.2	-3.8	32.6	5182	3130	3118	60.69	0.215
2	30.5	-0.2	-3.1	32.0	5105	3102	3090	59.34	0.209
3	20.5	-0.2	-2.9	31.3	4959	3061	3104	57.66	0.185
4	10.5	-0.2	-2.4	30.5	4924	3008	3090	56.60	0.189

Observed Velocities and Moduli for File W16985-10497-Velocity									
Event	Conf	Pore	Diff	Temp	V_p	$V_s^{(1)}$	$V_s^{(2)}$	Young's Modulus	Poisson's Ratio
	MPa	MPa	MPa	°C	m/s	m/s	m/s	GPa	
0	50.6	-0.2	-4.5	27.9	4933	3073	3092	56.05	0.180
1	40.5	-0.2	-4.2	27.1	5019	3024	3075	56.14	0.207
2	30.5	-0.2	-3.4	26.7	5019	3009	3075	55.97	0.210
3	20.5	-0.2	-3.4	26.3	4850	2993	3059	54.08	0.181
4	10.5	-0.2	-2.9	25.8	4653	2817	2949	49.39	0.188

Observed Velocities and Moduli for File W16985-10503-Velocity									
Event	Conf	Pore	Diff	Temp	V_p	$V_s^{(1)}$	$V_s^{(2)}$	Young's Modulus	Poisson's Ratio
	MPa	MPa	MPa	°C	m/s	m/s	m/s	GPa	
0	50.5	-0.2	-4.1	30.1	5269	3199	3126	63.61	0.218
1	40.5	-0.2	-3.7	28.2	5311	3199	3126	63.97	0.225
2	30.5	-0.2	-3.5	26.6	5269	3184	3098	63.05	0.224
3	20.6	-0.2	-2.7	25.2	5188	3169	3098	62.16	0.213
4	10.5	-0.2	-2.8	23.5	5032	3154	2948	58.76	0.209

Observed Velocities and Moduli for File W16985-10505.7-Velocity									
Event	Conf	Pore	Diff	Temp	V_p	$V_s^{(1)}$	$V_s^{(2)}$	Young's Modulus	Poisson's Ratio
	MPa	MPa	MPa	°C	m/s	m/s	m/s	GPa	
0	49.2	-0.2	-4.2	28.5	5055	3139	2740	54.20	0.245
1	47.8	-0.2	-4.4	27.9	5216	3119	2740	54.91	0.270
2	47.0	-0.2	-4.2	27.7	5216	3119	2740	54.91	0.270
3	46.4	-0.2	-4.6	27.5	5216	3119	2755	55.12	0.268
4	46.2	-0.2	-4.4	27.5	5108	3119	2755	54.48	0.253
5	40.6	-0.2	-4.2	27.3	5108	3119	2725	54.08	0.257
6	30.5	-0.2	-3.8	26.9	5055	3159	2710	54.07	0.246
7	20.6	-0.2	-3.4	26.6	5004	3180	2710	53.99	0.235
8	10.5	-0.2	-2.4	26.4	3959	3024	2637	39.46	-0.023

Observed Velocities and Moduli for File W16985-10509-Velocity									
Event	Conf	Pore	Diff	Temp	V_p	$V_s^{(1)}$	$V_s^{(2)}$	Young's Modulus	Poisson's Ratio
	MPa	MPa	MPa	°C	m/s	m/s	m/s	GPa	
0	50.5	-0.2	-4.6	28.5	5292	2935	3200	60.31	0.247
1	40.5	-0.2	-3.8	27.8	5190	2935	3200	59.56	0.232
2	30.4	-0.2	-3.8	27.5	5190	2903	3143	58.40	0.243
3	20.5	-0.2	-3.1	27.2	5140	2872	3107	57.16	0.244
4	10.5	-0.2	-3.2	26.7	5140	2872	3054	56.46	0.251

Observed Velocities and Moduli for File W16985-10514.5-Velocity									
Event	Conf	Pore	Diff	Temp	V_p	$V_s^{(1)}$	$V_s^{(2)}$	Young's Modulus	Poisson's Ratio
	MPa	MPa	MPa	°C	m/s	m/s	m/s	GPa	
0	50.6	-0.2	-4.2	27.0	5085	3054	3072	57.46	0.215
1	40.6	-0.2	-4.2	26.0	5085	3070	3124	58.26	0.205
2	30.5	-0.2	-4.2	25.3	4995	3037	3089	56.68	0.199
3	20.6	-0.2	-3.4	24.8	4865	3054	3056	55.25	0.174
4	10.5	-0.2	-3.1	24.2	4865	2957	3023	53.91	0.196

Observed Velocities and Moduli for File w16985-10488-velocity									
Event	Conf	Pore	Diff	Temp	V_p	$V_s^{(1)}$	$V_s^{(2)}$	Young's Modulus	Poisson's Ratio
	MPa	MPa	MPa	°C	m/s	m/s	m/s	GPa	
0	50.5	-0.2	-4.1	29.0	5242	3141	2834	57.33	0.259
1	40.5	-0.2	-3.7	26.9	5242	3161	2801	57.15	0.261
2	30.5	-0.2	-3.4	25.3	5187	3121	2754	55.62	0.264
3	20.5	-0.2	-3.2	24.1	5132	3101	2739	54.82	0.261
4	10.5	-0.2	-2.5	23.0	5079	3101	2679	53.70	0.261

Observed Velocities and Moduli for File w16985-10490-velocity									
Event	Conf	Pore	Diff	Temp	V_p	$V_s^{(1)}$	$V_s^{(2)}$	Young's Modulus	Poisson's Ratio
	MPa	MPa	MPa	°C	m/s	m/s	m/s	GPa	
0	50.5	-0.2	-4.1	28.2	5134	3117	2937	56.97	0.234
1	40.5	-0.2	-3.5	27.4	5094	3117	2911	56.35	0.231
2	30.4	-0.2	-3.4	26.8	5055	3087	2911	55.68	0.228
3	20.5	-0.2	-2.8	26.2	5094	3073	2872	55.30	0.242
4	20.5	-0.2	-2.8	26.3	5016	3073	2872	54.75	0.229
5	0.3	-0.2	-1.9	25.1	—	—	—	—	—

Observed Velocities and Moduli for File w16985-10491-velocity									
Event	Conf	Pore	Diff	Temp	V_p	$V_s^{(1)}$	$V_s^{(2)}$	Young's Modulus	Poisson's Ratio
	MPa	MPa	MPa	°C	m/s	m/s	m/s	GPa	
0	50.5	-0.2	-4.6	23.7	5178	3102	3081	58.91	0.223
1	40.5	-0.2	-4.2	23.0	5147	3102	3070	58.53	0.219
2	30.5	-0.2	-3.8	22.7	5025	3068	3059	56.96	0.204
3	20.5	-0.2	-3.2	22.3	4937	3079	3026	55.91	0.191
4	10.4	-0.2	-2.9	21.4	4880	3035	2994	54.57	0.191

Observed Velocities and Moduli for File w16985-10492-velocity									
Event	Conf	Pore	Diff	Temp	V_p	$V_s^{(1)}$	$V_s^{(2)}$	Young's Modulus	Poisson's Ratio
	MPa	MPa	MPa	°C	m/s	m/s	m/s	GPa	
0	50.5	-0.2	-4.6	26.8	5495	3088	3153	65.38	0.262
1	40.5	-0.2	-4.1	26.1	5343	3040	3102	62.88	0.253
2	30.4	-0.2	-3.8	25.8	5199	3028	3053	60.99	0.240
3	20.5	-0.2	-2.9	25.6	5030	2947	2994	57.84	0.232
4	10.5	-0.2	-2.5	24.1	4965	2870	2904	55.19	0.245

Observed Velocities and Moduli for File w16985-10493-velocity									
Event	Conf	Pore	Diff	Temp	V_p	$V_s^{(1)}$	$V_s^{(2)}$	Young's Modulus	Poisson's Ratio
	MPa	MPa	MPa	°C	m/s	m/s	m/s	GPa	
0	50.5	-0.2	-4.4	28.8	5333	3092	3116	60.40	0.244
1	40.5	-0.2	-3.5	27.1	5394	3092	3095	60.53	0.255
2	30.4	-0.2	-3.8	25.4	5273	3092	3035	58.90	0.245
3	20.5	-0.2	-3.1	24.2	5100	2974	2958	55.18	0.244
4	10.5	-0.2	-2.7	23.1	4836	2865	2850	50.69	0.232

Observed Velocities and Moduli for File w16985-10498-velocity									
Event	Conf	Pore	Diff	Temp	V_p	$V_s^{(1)}$	$V_s^{(2)}$	Young's Modulus	Poisson's Ratio
	MPa	MPa	MPa	°C	m/s	m/s	m/s	GPa	
0	50.5	-0.2	-4.4	26.5	4940	3143	3039	55.61	0.178
1	40.5	-0.2	-4.2	26.0	4828	3112	2996	53.75	0.166
2	30.5	-0.2	-3.5	25.7	4791	3052	2996	52.80	0.169
3	20.5	-0.2	-3.4	25.5	4755	3008	2968	51.77	0.174
4	10.5	-0.2	-2.2	25.3	4551	2885	2927	48.22	0.156

Observed Velocities and Moduli for File w16985-10499.8-velocity									
Event	Conf	Pore	Diff	Temp	V_p	$V_s^{(1)}$	$V_s^{(2)}$	Young's Modulus	Poisson's Ratio
	MPa	MPa	MPa	°C	m/s	m/s	m/s	GPa	
0	50.5	-0.2	-4.1	25.6	5015	3069	2896	54.55	0.226
1	40.5	-0.2	-3.8	24.6	4970	3052	2881	53.83	0.223
2	30.4	-0.2	-3.7	24.5	4926	3019	2851	52.75	0.225
3	20.5	-0.2	-2.9	23.5	4841	2971	2822	51.23	0.221
4	10.5	-0.2	-2.5	21.9	4718	2924	2766	49.14	0.214

Observed Velocities and Moduli for File w16985-10504-velocity									
Event	Conf	Pore	Diff	Temp	V_p	$V_s^{(1)}$	$V_s^{(2)}$	Young's Modulus	Poisson's Ratio
	MPa	MPa	MPa	°C	m/s	m/s	m/s	GPa	
0	50.5	-0.2	-4.6	25.4	5127	3140	3153	60.48	0.198
1	40.5	-0.2	-3.9	24.9	5035	3128	3153	59.44	0.182
2	30.5	-0.2	-3.4	24.8	5065	3140	3141	59.74	0.188
3	20.5	-0.2	-2.9	24.6	4946	3105	3106	57.77	0.175
4	10.5	-0.2	-2.4	24.7	4888	3093	3083	56.80	0.168

Observed Velocities and Moduli for File w16985-10504.8-velocity									
Event	Conf	Pore	Diff	Temp	V_p	$V_s^{(1)}$	$V_s^{(2)}$	Young's Modulus	Poisson's Ratio
	MPa	MPa	MPa	°C	m/s	m/s	m/s	GPa	
0	50.6	-0.2	-3.8	25.5	5038	3046	2942	55.65	0.227
1	50.5	-0.2	-4.6	24.9	5038	3046	2942	55.65	0.227
2	40.5	-0.2	-4.2	24.5	5099	3046	2912	55.72	0.241
3	30.5	-0.2	-3.4	24.1	5068	3014	2902	54.97	0.242
4	20.5	-0.2	-3.4	24.4	4950	2993	2892	53.75	0.227
5	10.5	-0.2	-2.5	23.7	4838	2951	2853	51.95	0.219

Observed Velocities and Moduli for File w16985-10512.7-velocity									
Event	Conf	Pore	Diff	Temp	V_p	$V_s^{(1)}$	$V_s^{(2)}$	Young's Modulus	Poisson's Ratio
	MPa	MPa	MPa	°C	m/s	m/s	m/s	GPa	
0	50.0	-0.2	-3.8	23.1	4986	3007	3066	55.56	0.205
1	40.0	-0.2	-4.1	22.5	4948	3021	3080	55.53	0.193
2	40.0	-0.2	-3.7	22.0	5063	2994	3080	56.22	0.219
3	40.0	-0.2	-4.1	22.6	5024	3007	3051	55.71	0.214
4	40.1	-0.2	-3.8	22.2	4986	3007	3066	55.56	0.205
5	30.5	-0.2	-3.4	22.1	4911	2980	3051	54.44	0.197
6	20.5	-0.2	-3.2	22.2	4875	2967	3009	53.53	0.199
7	10.4	-0.2	-2.9	21.6	4803	2914	2995	52.18	0.196

Observed Velocities and Moduli for File w16985-10517.8-velocity									
Event	Conf	Pore	Diff	Temp	V_p	$V_s^{(1)}$	$V_s^{(2)}$	Young's Modulus	Poisson's Ratio
	MPa	MPa	MPa	°C	m/s	m/s	m/s	GPa	
0	0.7	-0.2	-2.1	23.7	—	—	—	—	—
1	50.5	-0.2	-3.9	27.2	5545	3150	3219	66.38	0.254
2	40.4	-0.2	-4.1	26.4	5494	3183	3236	66.73	0.241
3	30.5	-0.2	-3.4	26.0	5396	3117	3219	64.81	0.237
4	20.5	-0.2	-2.9	24.9	5348	3133	3168	63.95	0.234
5	10.5	-0.2	-2.7	23.3	5348	3069	3087	61.93	0.252

A.5.3 Biot's Coefficient

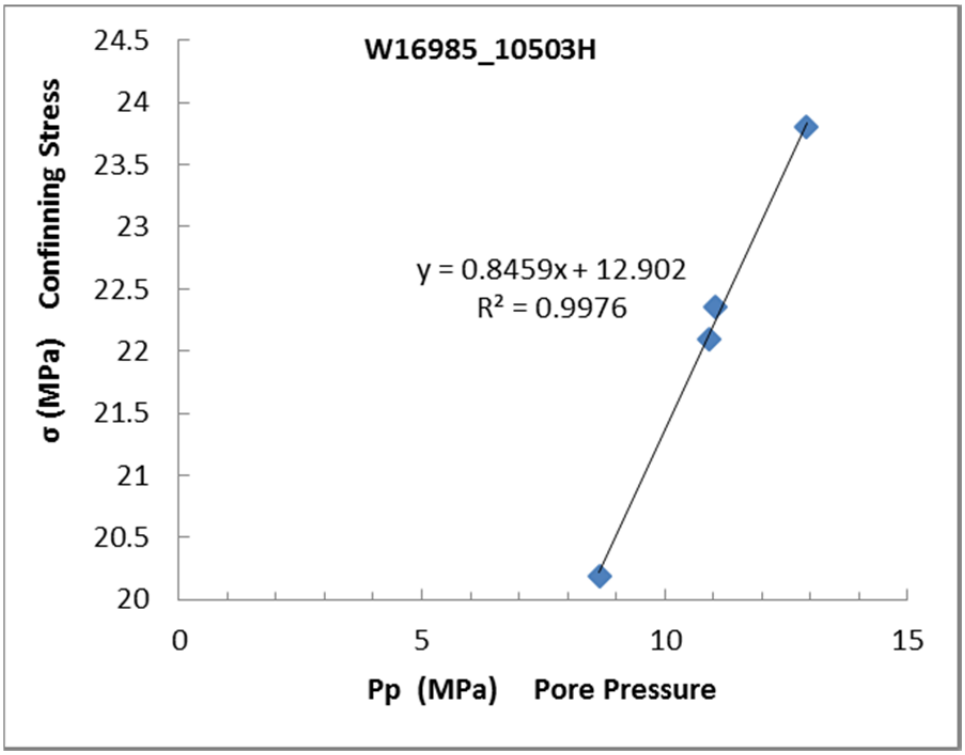

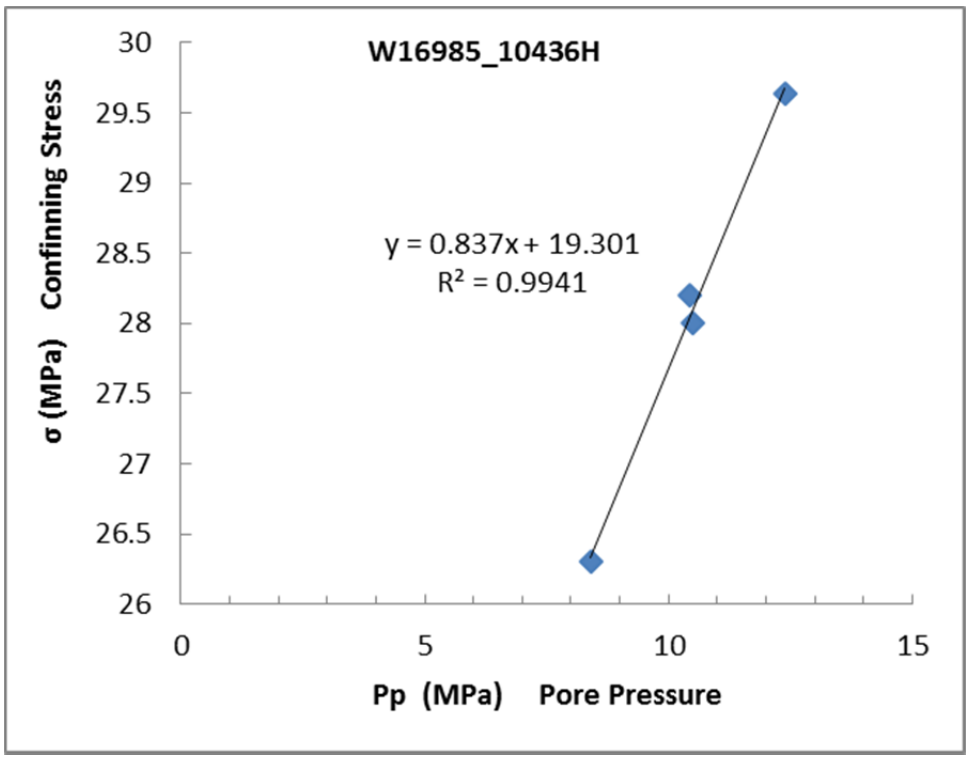
W16985_10436H
y = 0.837x + 19.301
R² = 0.9941
σ (MPa) Confinning Stress
Pp (MPa) Pore Pressure
30
29.5
29
28.5
28
27.5
27
26.5
26
0
5
10
15

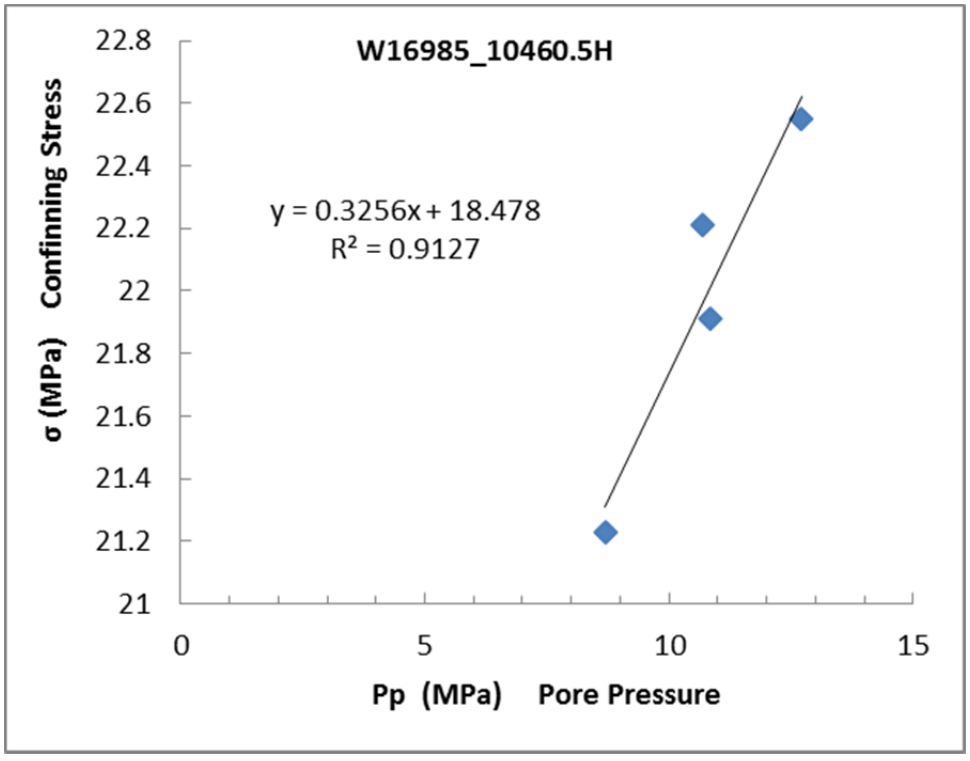
W16985_10460.5H
y = 0.3256x + 18.478
R² = 0.9127
σ (MPa) Confinning Stress
Pp (MPa) Pore Pressure
22.8
22.6
22.4
22.2
22
21.8
21.6
21.4
21.2
21
0
5
10
15

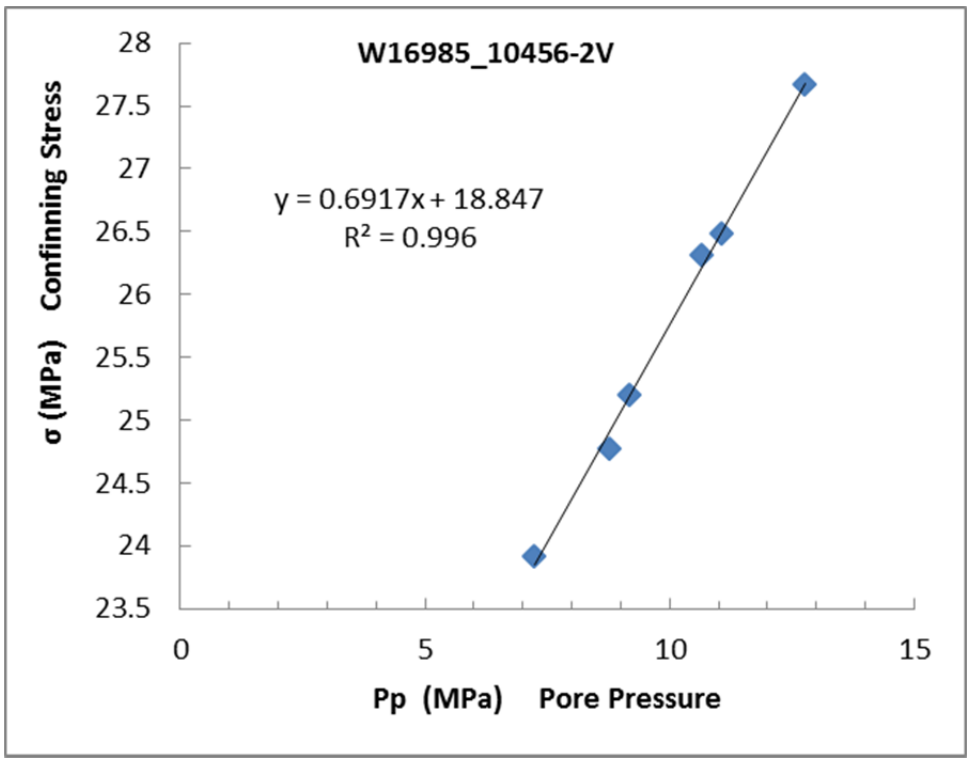
W16985_10456-2V
y = 0.6917x + 18.847
R² = 0.996
σ (MPa) Confinning Stress
Pp (MPa) Pore Pressure
28
27.5
27
26.5
26
25.5
25
24.5
24
23.5
0
5
10
15

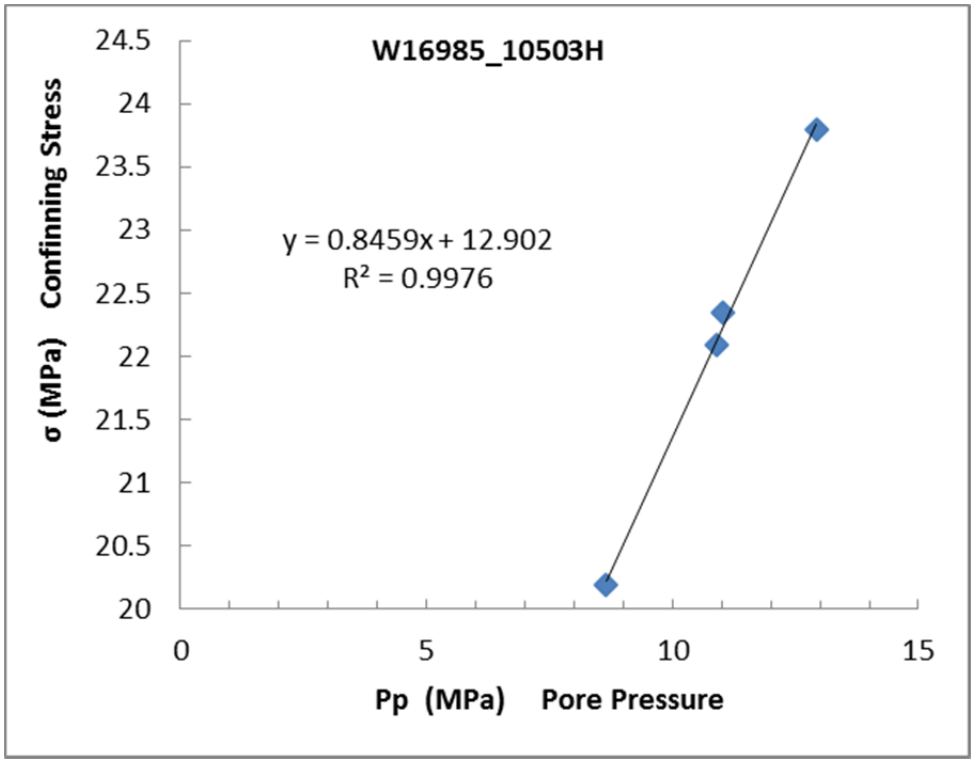
W16985_10503H
y = 0.8459x + 12.902
R² = 0.9976
σ (MPa) Confinning Stress
Pp (MPa) Pore Pressure
24.5
24
23.5
23
22.5
22
21.5
21
20.5
20
0
5
10
15

A.5.4 Static Moduli and Poisson's Ratio (Non-destructive)

Uniaxial Stress for File W16985-10488.5-Uniaxial_Stress									
Event	Conf	Pore	Diff	Temp	E	n	K	G	P
	MPa	MPa	MPa	°C	GPa		GPa	GPa	GPa
0	50.6	-0.2	34.2	33.7	109.35	0.097	45.21	49.85	111.67

Uniaxial Stress for File W16985-10490-uniaxial_stress									
Event	Conf	Pore	Diff	Temp	E	n	K	G	P
	MPa	MPa	MPa	°C	GPa		GPa	GPa	GPa
0	50.5	-0.2	29.5	34.0	48.27	0.034	17.25	23.35	48.38

Uniaxial Stress for File W16985-10492(2)-uniaxial_stress									
Event	Conf	Pore	Diff	Temp	E	n	K	G	P
	MPa	MPa	MPa	°C	GPa		GPa	GPa	GPa
0	30.3	-0.2	14.6	31.0	68.93	0.175	35.33	29.33	74.44
1	30.3	-0.2	20.1	30.9	66.08	0.219	39.13	27.11	75.28

Uniaxial Stress for File W16985-10498-Uniaxial_Stress									
Event	Conf	Pore	Diff	Temp	E	n	K	G	P
	MPa	MPa	MPa	°C	GPa		GPa	GPa	GPa
0	30.4	-0.2	14.6	32.3	52.94	0.249	35.18	21.19	63.44
1	30.4	-0.2	20.5	32.1	55.01	0.256	37.56	21.90	66.76

Uniaxial Stress for File W16985-10503-Uniaxial_Stress									
Event	Conf	Pore	Diff	Temp	E	n	K	G	P
	MPa	MPa	MPa	°C	GPa		GPa	GPa	GPa
0	50.4	-0.2	29.9	31.1	75.39	0.119	33.00	33.68	77.90
1	50.4	-0.2	29.5	31.0	76.25	0.138	35.12	33.50	79.78

Uniaxial Stress for File W16985-10504(2)-uniaxial_stress									
Event	Conf	Pore	Diff	Temp	E	n	K	G	P
	MPa	MPa	MPa	°C	GPa		GPa	GPa	GPa
0	20.6	-0.2	15.8	31.0	68.56	0.319	63.25	25.98	97.90
1	20.6	-0.2	20.1	30.8	56.01	0.278	42.06	21.91	71.27

Uniaxial Stress for File w16985-10487.5-2-uniaxial-stress									
Event	Conf	Pore	Diff	Temp	E	n	K	G	P
	MPa	MPa	MPa	°C	GPa		GPa	GPa	GPa
0	30.5	-0.2	15.4	26.4	64.77	0.141	30.08	28.38	67.92
1	30.4	-0.2	22.2	26.1	61.42	0.184	32.43	25.93	67.01

Uniaxial Stress for File w16985-10491-2-uniaxial-stress									
Event	Conf	Pore	Diff	Temp	E	n	K	G	P
	MPa	MPa	MPa	°C	GPa		GPa	GPa	GPa
0	30.5	-0.2	15.4	26.5	85.36	0.403	146.91	30.42	187.47
1	30.5	-0.2	18.4	25.9	89.20	0.390	135.41	32.08	178.19

Uniaxial Stress for File w16985-10493-uniaxial-stress									
Event	Conf	Pore	Diff	Temp	E	n	K	G	P
	MPa	MPa	MPa	°C	GPa		GPa	GPa	GPa
0	32.4	-0.2	22.2	33.9	62.56	0.253	42.28	24.95	75.56

Uniaxial Stress for File w16985-10497-uniaxial-stress									
Event	Conf	Pore	Diff	Temp	E	n	K	G	P
	MPa	MPa	MPa	°C	GPa		GPa	GPa	GPa
0	30.6	-0.2	15.8	27.9	45.45	0.143	21.23	19.88	47.73
1	30.6	-0.2	19.7	27.5	49.15	0.152	23.55	21.33	51.99

Uniaxial Stress for File w16985-10504.8-uniaxial-stress									
Event	Conf	Pore	Diff	Temp	E	n	K	G	P
	MPa	MPa	MPa	°C	GPa		GPa	GPa	GPa
0	30.4	-0.2	15.0	27.0	63.59	0.183	33.42	26.88	69.26
1	30.5	-0.2	19.7	26.1	70.77	0.209	40.52	29.27	79.55

Uniaxial Stress for File w16985-10505.7-uniaxial-stress									
Event	Conf	Pore	Diff	Temp	E	n	K	G	P
	MPa	MPa	MPa	°C	GPa		GPa	GPa	GPa
0	30.4	-0.2	18.0	32.1	52.68	0.230	32.54	21.41	61.09
1	40.4	-0.2	16.3	32.6	67.68	0.222	40.53	27.70	77.46
2	50.5	-0.2	16.3	32.9	60.42	0.213	35.04	24.91	68.26
3	20.7	-0.2	12.4	32.1	57.37	0.201	32.02	23.88	63.86

Uniaxial Stress for File w16985-10509-uniaxial-stress									
Event	Conf	Pore	Diff	Temp	E	n	K	G	P
	MPa	MPa	MPa	°C	GPa		GPa	GPa	GPa
0	30.2	-0.2	14.6	31.3	59.02	0.256	40.38	23.49	71.70

Uniaxial Stress for File w16985-10512.7-uniaxial-stress									
Event	Conf	Pore	Diff	Temp	E	n	K	G	P
	MPa	MPa	MPa	°C	GPa		GPa	GPa	GPa
0	30.3	-0.2	15.0	24.1	54.75	0.444	161.98	18.96	187.26
1	30.3	-0.2	18.8	26.6	53.61	0.455	197.14	18.43	221.71

Uniaxial Stress for File w16985-10514.5-uniaxial-stress									
Event	Conf	Pore	Diff	Temp	E	n	K	G	P
	MPa	MPa	MPa	°C	GPa		GPa	GPa	GPa
0	30.3	-0.2	9.4	31.0	35.03	0.050	12.97	16.68	35.21

Uniaxial Stress for File w16985-10517.8-uniaxial-stress									
Event	Conf	Pore	Diff	Temp	E	n	K	G	P
	MPa	MPa	MPa	°C	GPa		GPa	GPa	GPa
0	30.3	-0.2	16.3	26.3	44.55	0.064	17.02	20.94	44.94
1	30.3	-0.2	16.7	25.9	53.20	0.075	20.89	24.74	53.87

A.5.5 Uni/Triaxial Compressive Strength, Young's Modulus and Poisson's Ratio

No data is available.

A.5.6 Mohr's Circle

No data is available.

A.6. Well 13 Bakken Samples Testing Results

A.6.1 Permeability

Permeability and Specific Storage for File w13-mb-11006.8H-perm							
Event	Type	Conf	Pore Top	Diff	Temp	Perm	Storage
		MPa	MPa	MPa	°C	μD	m^{-1}
0	multipulse	30.2	7.7	-5.2	28.5	0.413	5.02e-07
1	multipulse	25.3	7.7	-4.3	28.6	0.487	4.25e-07

Permeability and Specific Storage for File w13-mb-11006.8H-perm(all)							
Event	Type	Conf	Pore Top	Diff	Temp	Perm	Storage
		MPa	MPa	MPa	°C	μD	m^{-1}
0	multipulse	30.2	7.7	-4.8	28.3	0.508	4.15e-07
1	multipulse	30.2	7.7	-4.8	28.4	0.507	4.12e-07
2	multipulse	30.2	7.7	-4.8	29.0	0.497	2.89e-07
3	multipulse	30.2	7.7	-4.8	29.0	0.532	3.99e-07
4	multipulse	30.2	7.2	-4.3	29.0	0.154	1.02e-07
5	multipulse	25.3	7.7	-4.3	28.9	0.568	3.97e-07
6	multipulse	20.3	7.7	-3.9	28.8	0.643	4.38e-07
7	multipulse	15.2	7.7	-3.9	28.1	0.713	2.76e-07
8	multipulse	10.3	7.2	-3.1	28.1	1.16	4.11e-07

Permeability and Specific Storage for File w13-mb-11006v-perm-biot(drain-undrain)							
Event	Type	Conf	Pore Top	Diff	Temp	Perm	Storage
		MPa	MPa	MPa	°C	μD	m^{-1}
0	multipulse	20.2	15.2	0.8	29.5	1.00	2.24e-09
1	aspike	20.2	15.1	0.8	29.0	2.87	9.00e-06

Permeability and Specific Storage for File w13-mb-11007H-perm							
Event	Type	Conf	Pore Top	Diff	Temp	Perm	Storage
		MPa	MPa	MPa	°C	μD	m^{-1}
0	multipulse	30.2	7.7	-4.8	29.3	0.627	1.73e-06
1	multipulse	25.2	7.7	-4.3	29.3	0.704	1.60e-06
2	multipulse	20.3	7.7	-3.9	29.5	0.865	1.73e-06
3	multipulse	15.2	7.7	-3.5	29.5	1.27	1.87e-06
4	multipulse	10.3	7.2	13.2	29.4	99.9	9.77e-11

Permeability and Specific Storage for File w13-mb-11008V2-perm							
Event	Type	Conf	Pore Top	Diff	Temp	Perm	Storage
		MPa	MPa	MPa	°C	μD	m^{-1}
0	multipulse	20.2	15.1	-3.9	25.8	4.68	4.80e-12
1	multipulse	20.1	15.1	-3.9	26.2	4.33	2.51e-07
2	multipulse	20.1	15.1	-4.3	26.2	4.52	3.27e-07

Permeability and Specific Storage for File w13-mb-11008V2-perm(all)							
Event	Type	Conf	Pore Top	Diff	Temp	Perm	Storage
		MPa	MPa	MPa	°C	μD	m^{-1}
0	multipulse	30.2	7.7	-5.2	27.6	2.89	1.06e-06
1	multipulse	25.3	7.7	-4.8	27.0	3.18	9.92e-07
2	multipulse	20.3	7.7	-4.3	27.7	4.09	1.47e-06
3	multipulse	15.3	7.7	-3.9	27.9	4.43	6.71e-07
4	multipulse	10.2	7.7	-4.3	27.3	99.6	1.13e-11

Permeability and Specific Storage for File w13-mb-11009V-perm							
Event	Type	Conf	Pore Top	Diff	Temp	Perm	Storage
		MPa	MPa	MPa	°C	μD	m^{-1}
0	multipulse	30.2	7.7	-5.2	27.2	4.02	5.00e-06
1	multipulse	25.3	7.7	-4.8	27.0	3.57	3.43e-06
2	multipulse	20.3	7.6	-4.8	27.5	3.73	2.41e-06
3	multipulse	15.3	7.7	-3.9	27.1	5.11	2.61e-06
4	multipulse	10.3	7.7	-3.9	27.0	1.33e+03	9.54e-10

Permeability and Specific Storage for File w13-mb-11025V2(small)-perm							
Event	Type	Conf	Pore Top	Diff	Temp	Perm	Storage
		MPa	MPa	MPa	°C	μD	m^{-1}
0	aspike	20.4	5.1	2.5	19.5	420.	4.96e-11
1	multipulse	20.3	5.1	2.1	20.0	393.	1.06e-10
2	multipulse	20.3	5.1	2.1	19.6	375.	2.17e-09
3	multipulse	15.2	5.1	2.1	20.3	515.	2.36e-10
4	aspike	15.2	5.1	2.1	19.9	860.	7.43e-08
5	multipulse	15.2	5.1	2.1	19.9	412.	1.03e-09

Permeability and Specific Storage for File w13-mb-11025v-perm							
Event	Type	Conf	Pore Top	Diff	Temp	Perm	Storage
		MPa	MPa	MPa	°C	μD	m^{-1}
0	multipulse	15.0	5.0	2.1	21.9	0.321	1.31e-05
1	multipulse	15.0	5.1	0.4	22.0	0.113	3.33e-06

Permeability and Specific Storage for File w13-mb-11025v-perm(2)							
Event	Type	Conf	Pore Top	Diff	Temp	Perm	Storage
		MPa	MPa	MPa	°C	μD	m^{-1}
0	multipulse	20.2	15.0	-0.5	27.9	0.181	2.21e-06

Permeability and Specific Storage for File w13-mb-11025v-perm-biot							
Event	Type	Conf	Pore Top	Diff	Temp	Perm	Storage
		MPa	MPa	MPa	°C	μD	m^{-1}
0	multipulse	20.2	15.1	0.8	27.9	0.187	1.42e-06

A.6.2 Sonic Velocity, Dynamic Moduli and Poisson's Ratio

Waveform waterfall for p arrivals	
Experiment:	MB-W13-11004V1-Vel
Well:	13
Depth:	3354.0 m
File name:	w13-mb-11004V1-vel

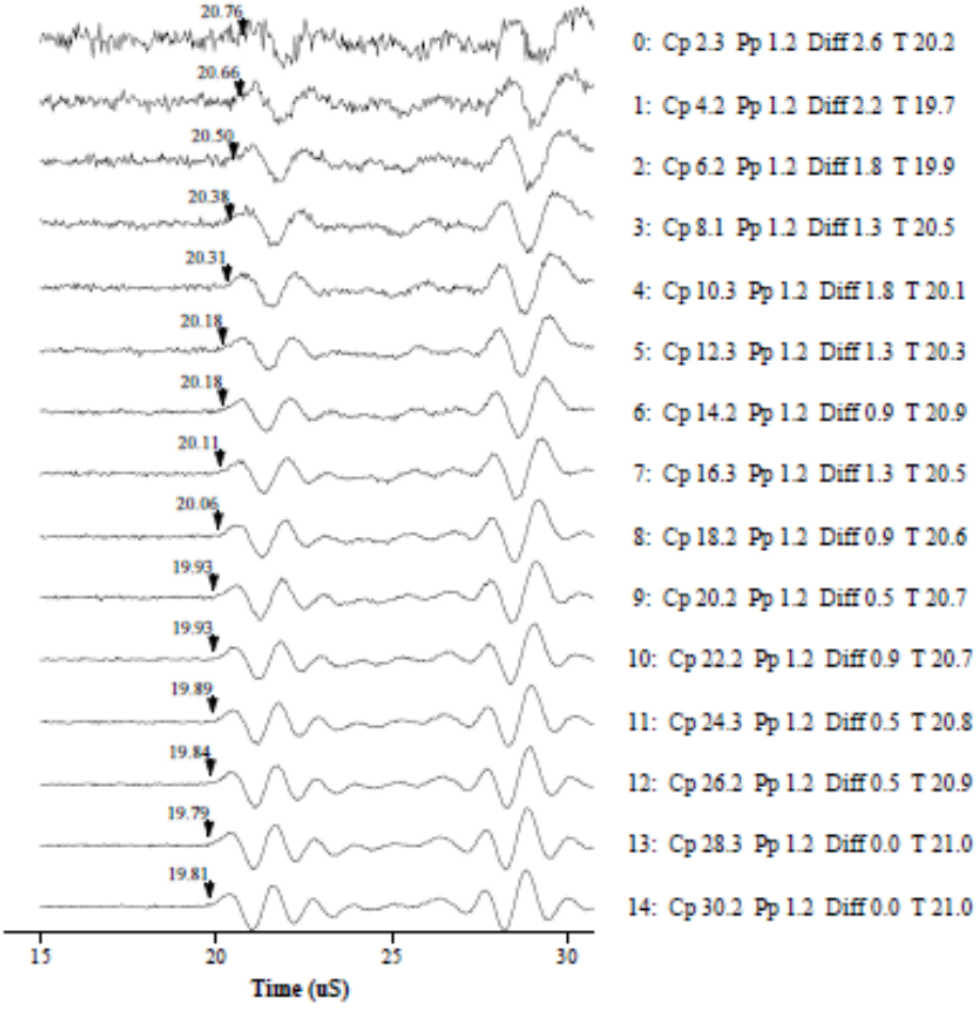

Waveform waterfall for s1 arrivals	
Experiment:	MB-W13-11004V1-Vel
Well:	13
Depth:	3354.0 m
File name:	w13-mb-11004V1-vel

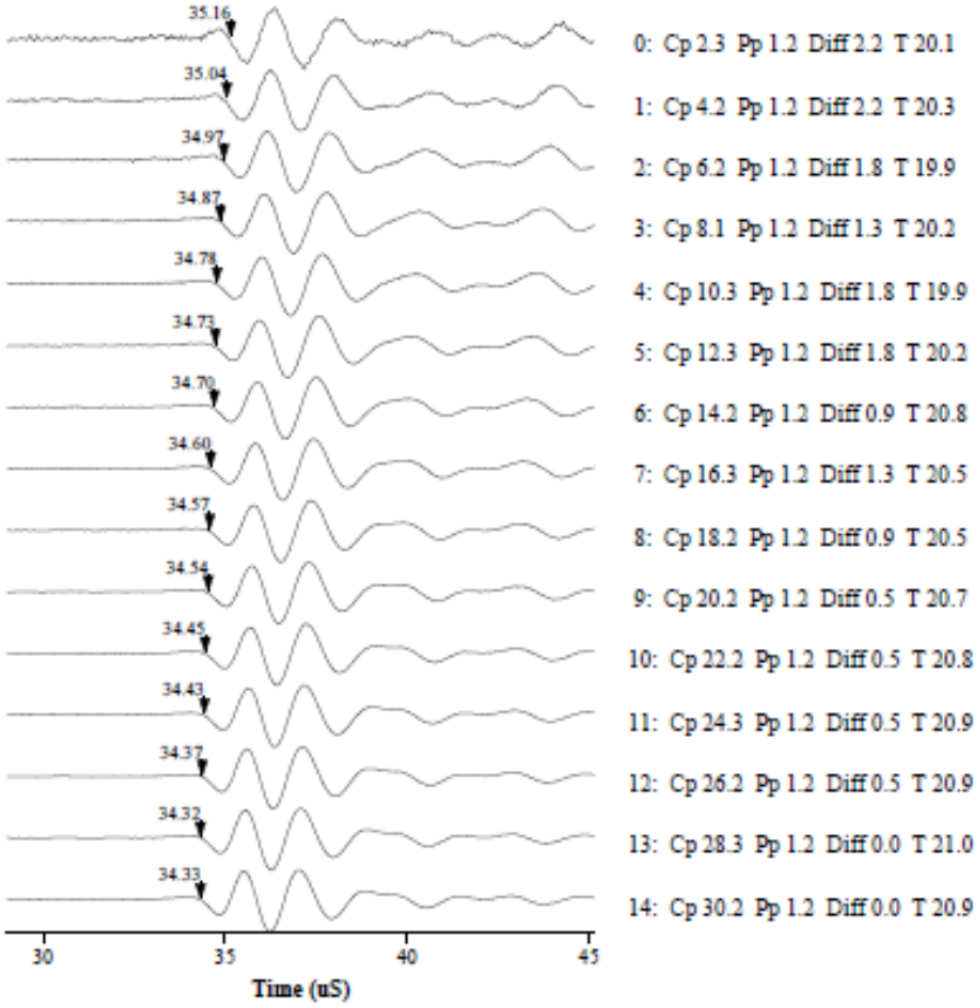

Waveform waterfall for p arrivals	
Experiment:	MB-W13-11006.8-Vel
Well:	#13
Depth:	3354.9 m
File name:	w13-mb-11006.8H-vel

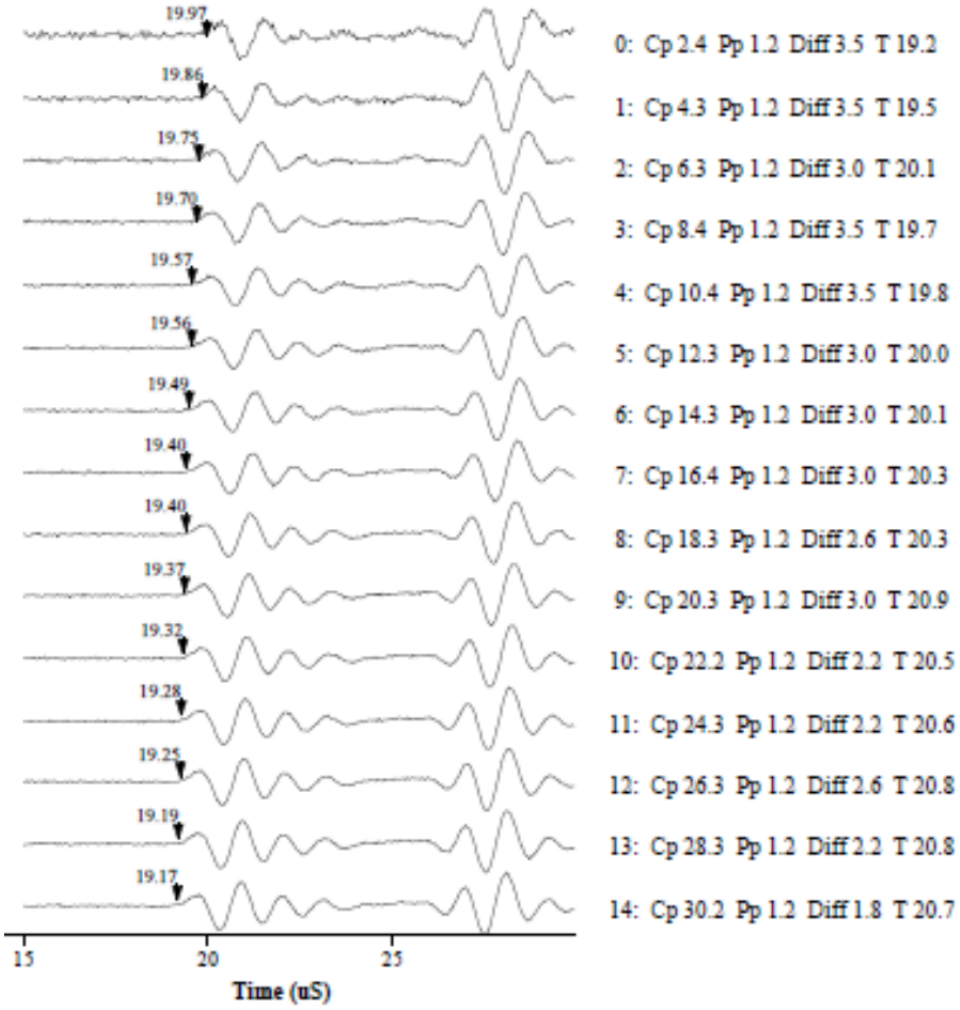

Waveform waterfall for s1 arrivals	
Experiment:	MB-W13-11006.8-Vel
Well:	#13
Depth:	3354.9 m
File name:	w13-mb-11006.8H-vel

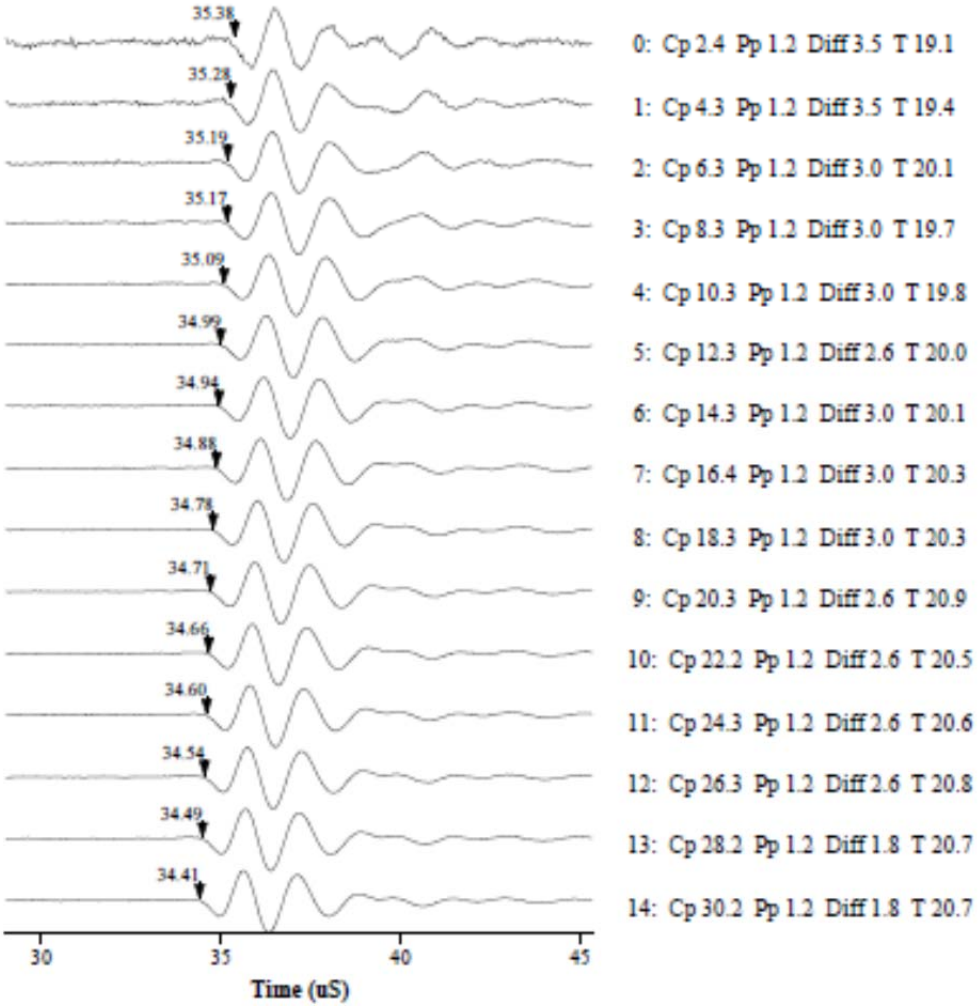

Waveform waterfall for p arrivals	
Experiment:	w13-11006-velocity
Well:	#13
Depth:	3354.6 m
File name:	w13-mb-11006v-vel

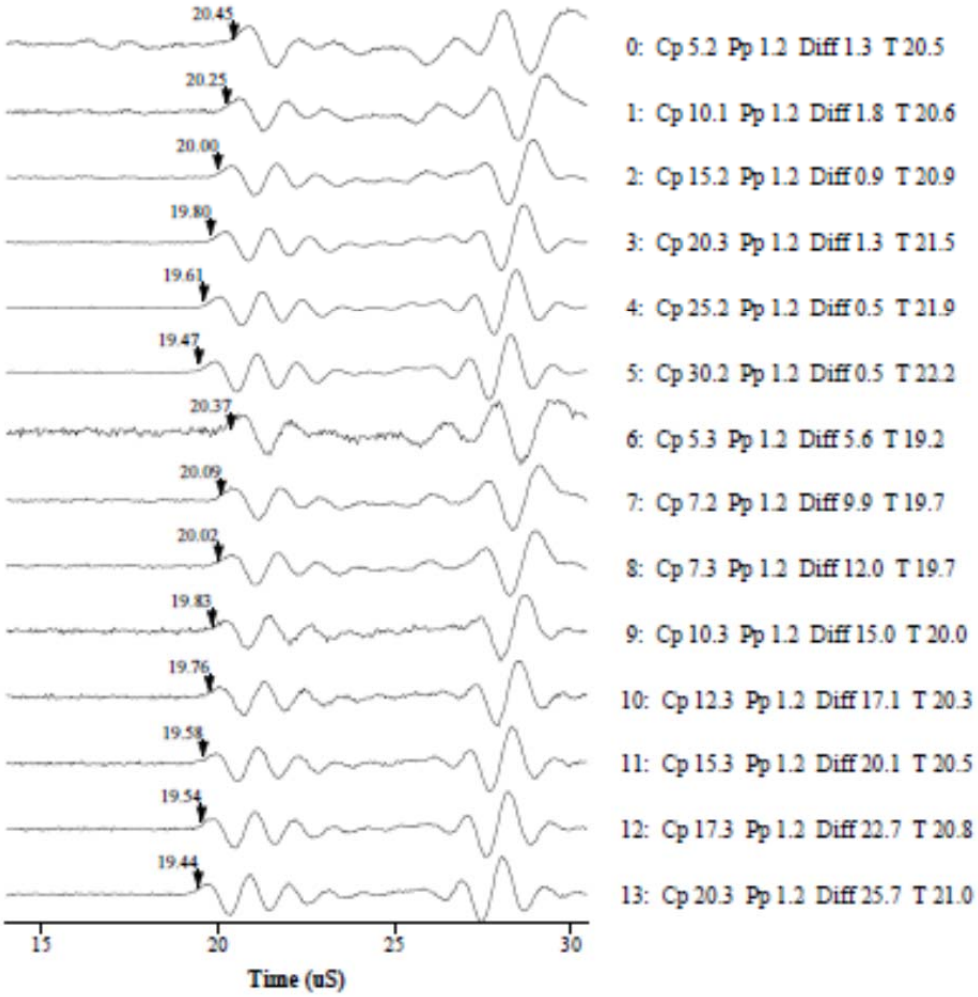

Waveform waterfall for s1 arrivals	
Experiment:	w13-11006-velocity
Well:	#13
Depth:	3354.6 m
File name:	w13-mb-11006v-vel

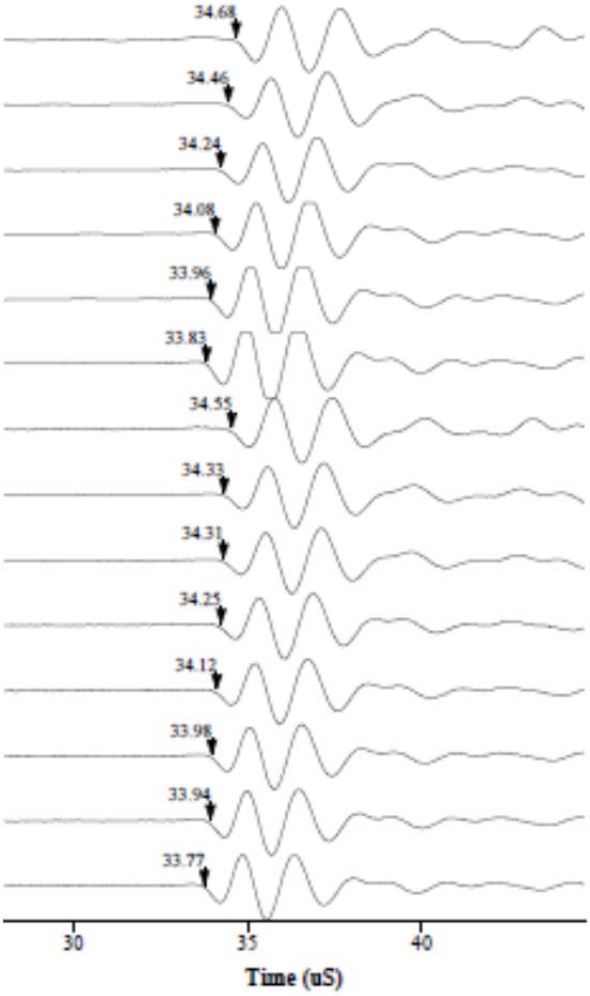

0: Cp 5.2 Pp 1.2 Diff 1.8 T 20.4

1: Cp 10.1 Pp 1.2 Diff 1.8 T 20.6

2: Cp 15.2 Pp 1.2 Diff 0.9 T 20.9

3: Cp 20.2 Pp 1.2 Diff 0.5 T 21.4

4: Cp 25.2 Pp 1.2 Diff 0.5 T 21.9

5: Cp 30.2 Pp 1.2 Diff 0.5 T 22.3

6: Cp 5.2 Pp 1.2 Diff 5.2 T 19.2

7: Cp 7.3 Pp 1.2 Diff 10.3 T 19.7

8: Cp 7.3 Pp 1.2 Diff 12.0 T 19.7

9: Cp 10.3 Pp 1.2 Diff 15.0 T 20.1

10: Cp 12.3 Pp 1.2 Diff 17.1 T 20.3

11: Cp 15.3 Pp 1.2 Diff 20.1 T 20.6

12: Cp 17.2 Pp 1.2 Diff 22.2 T 20.7

13: Cp 20.3 Pp 1.2 Diff 25.7 T 21.0

Waveform waterfall for p arrivals	
Experiment:	MB-W13-11007H-Vel
Well:	13
Depth:	3354.9 m
File name:	w13-mb-11007H-vel

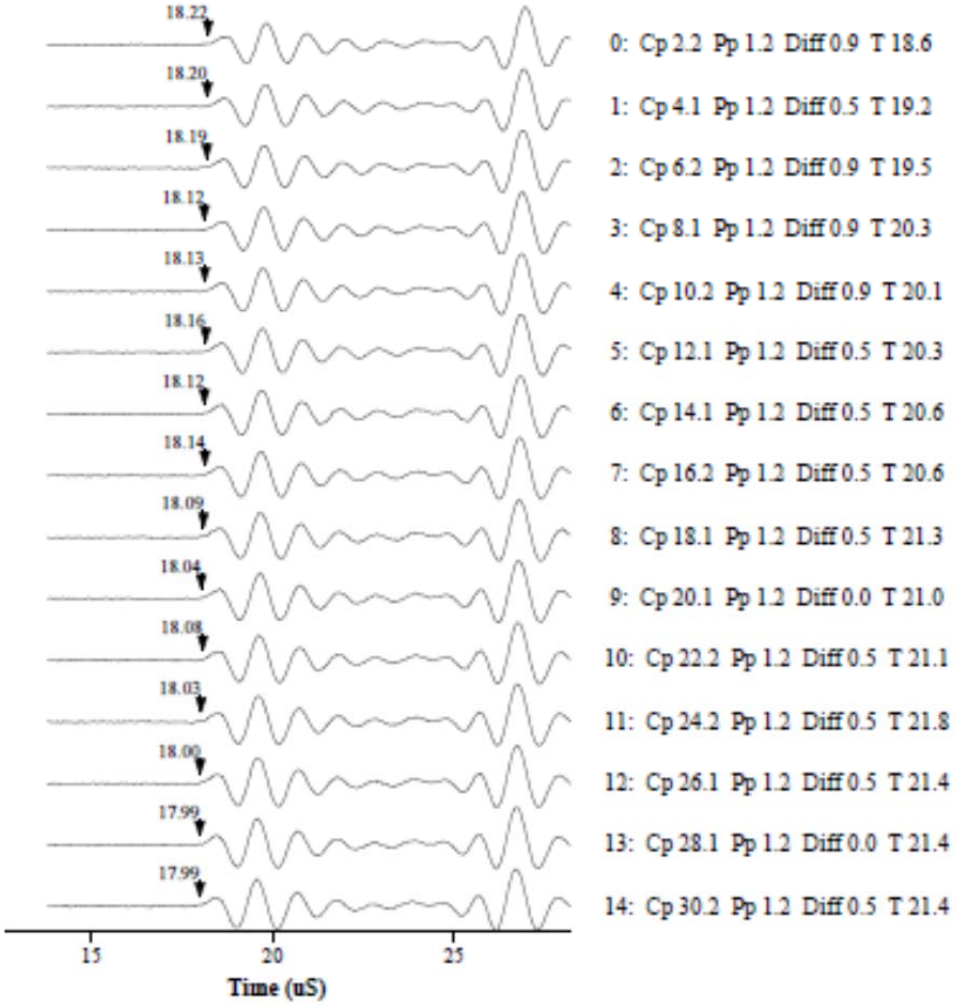

Waveform waterfall for s1 arrivals	
Experiment:	MB-W13-11007H-Vel
Well:	13
Depth:	3354.9 m
File name:	w13-mb-11007H-vel

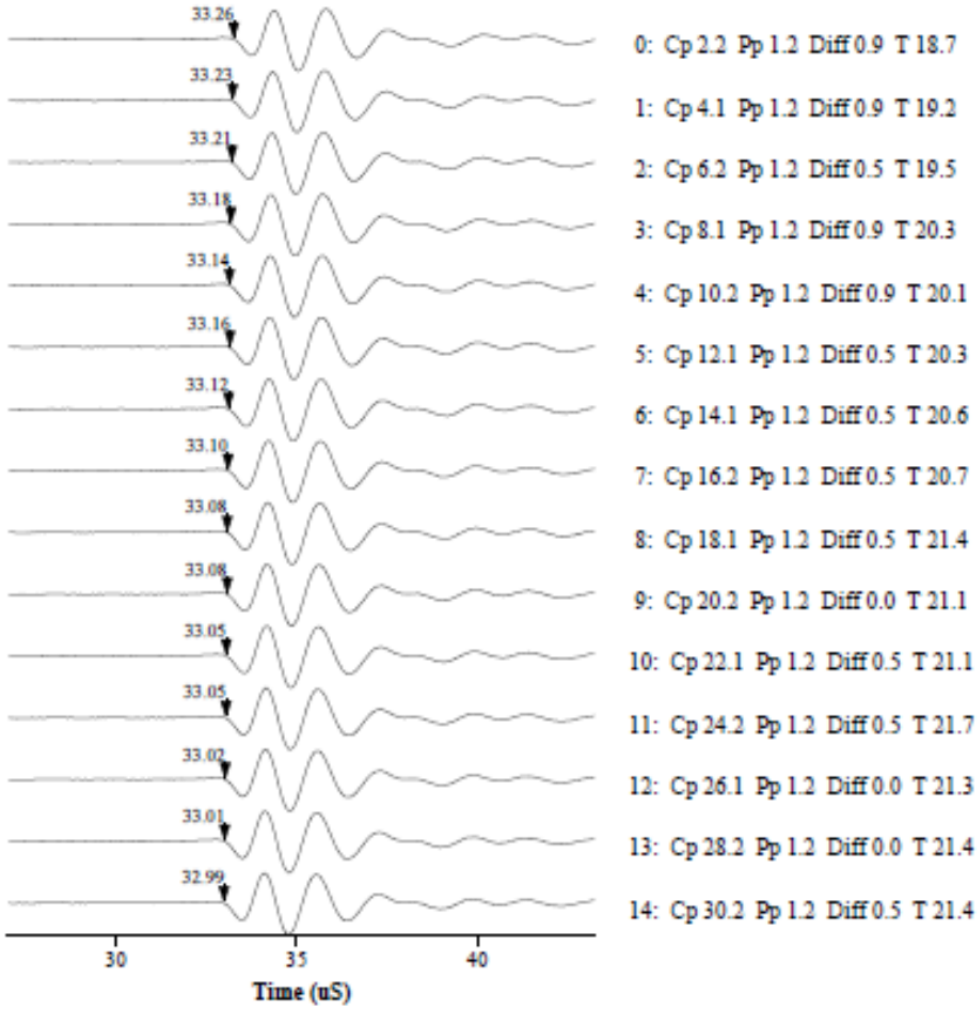

Waveform waterfall for p arrivals	
Experiment:	MB-W13-11008.5H-Vel
Well:	13
Depth:	3355.4 m
File name:	w13-mb-11008.5H-vel

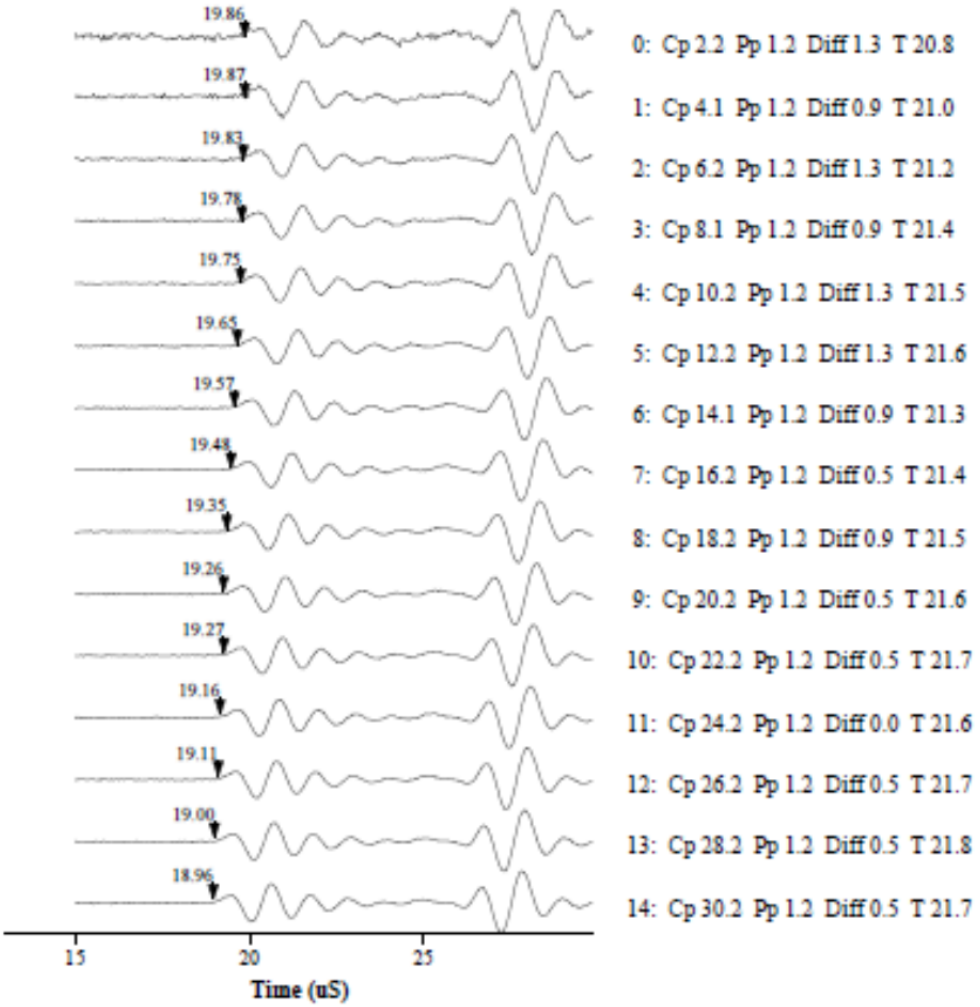

Waveform waterfall for s1 arrivals	
Experiment:	MB-W13-11008.5H-Vel
Well:	13
Depth:	3355.4 m
File name:	w13-mb-11008.5H-vel

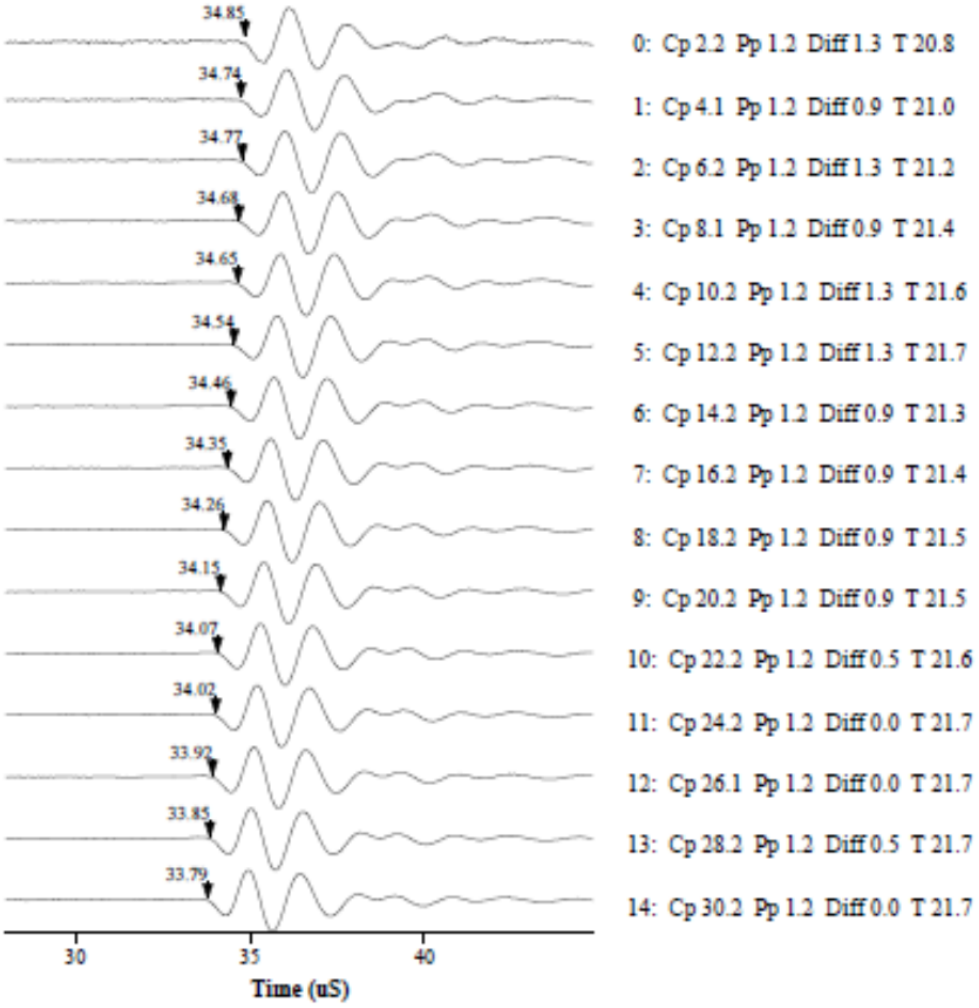

Waveform waterfall for p arrivals	
Experiment:	MB-W13-11008V1-Vel.
Well:	#13
Depth:	3355.2 m
File name:	w13-mb-11008V1-vel

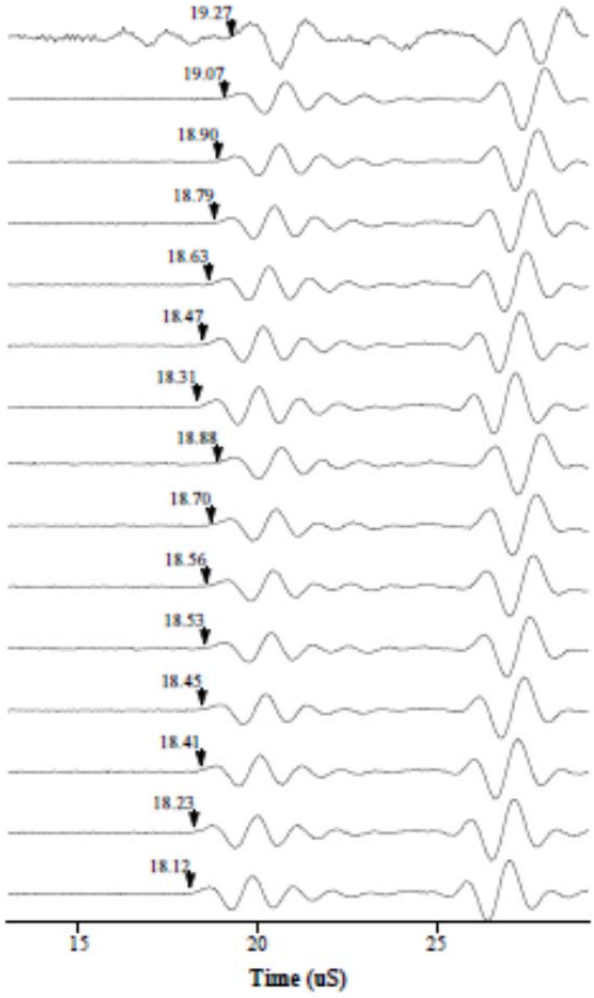

0: Cp 0.3 Pp 1.2 Diff 1.8 T 20.0
1: Cp 5.3 Pp 1.2 Diff 1.3 T 20.4
2: Cp 10.3 Pp 1.2 Diff 1.8 T 20.7
3: Cp 15.2 Pp 1.2 Diff 1.8 T 20.9
4: Cp 20.3 Pp 1.2 Diff 1.8 T 21.0
5: Cp 25.2 Pp 1.2 Diff 1.3 T 21.0
6: Cp 30.2 Pp 1.2 Diff 1.3 T 21.3
7: Cp 5.2 Pp 1.2 Diff 5.2 T 18.6
8: Cp 7.3 Pp 1.2 Diff 10.3 T 19.4
9: Cp 7.2 Pp 1.2 Diff 15.0 T 19.5
10: Cp 10.2 Pp 1.2 Diff 14.6 T 20.8
11: Cp 12.3 Pp 1.2 Diff 20.1 T 20.1
12: Cp 15.2 Pp 1.2 Diff 24.4 T 20.5
13: Cp 17.2 Pp 1.2 Diff 26.9 T 20.5
14: Cp 20.3 Pp 1.2 Diff 30.4 T 20.8

Waveform waterfall for s1 arrivals	
Experiment:	MB-W13-11008V1-Vel.
Well:	#13
Depth:	3355.2 m
File name:	w13-mb-11008V1-vel

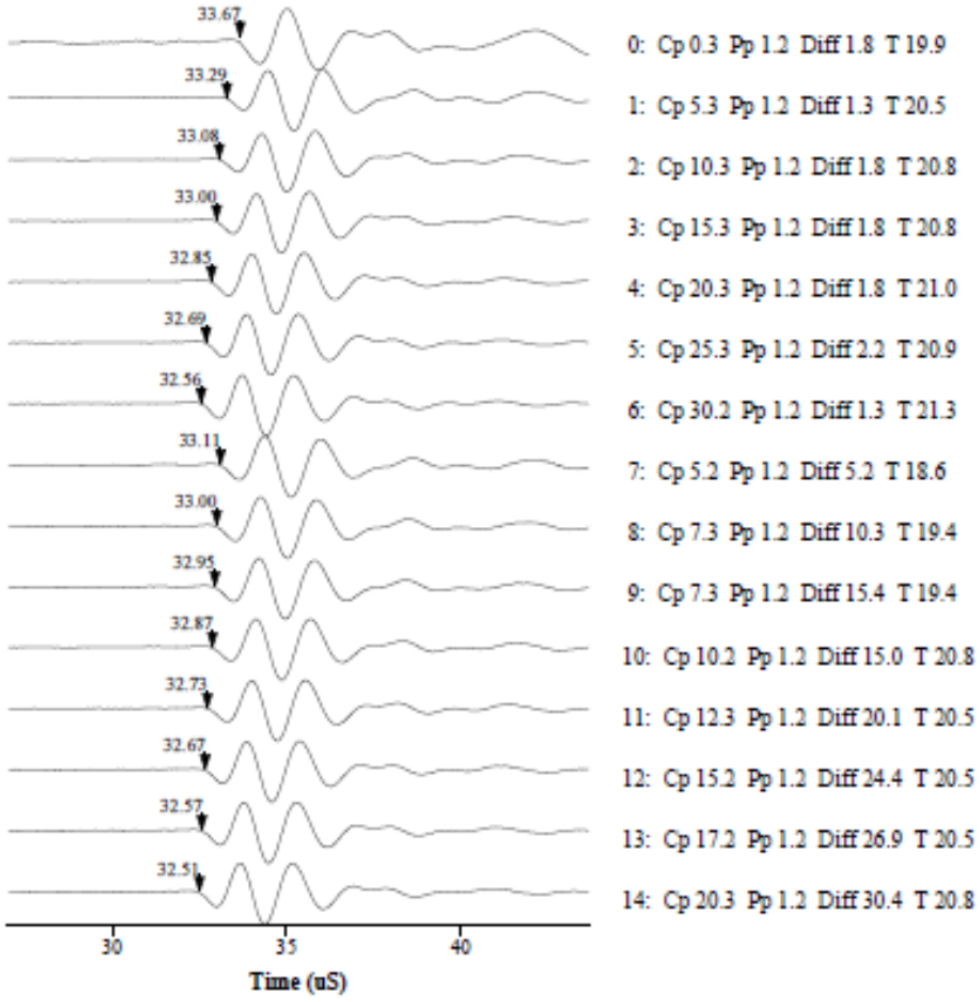

Waveform waterfall for p arrivals	
Experiment:	MB-W13-11008V2
Well:	13
Depth:	3355.2 m
File name:	w13-mb-11008V2-vel

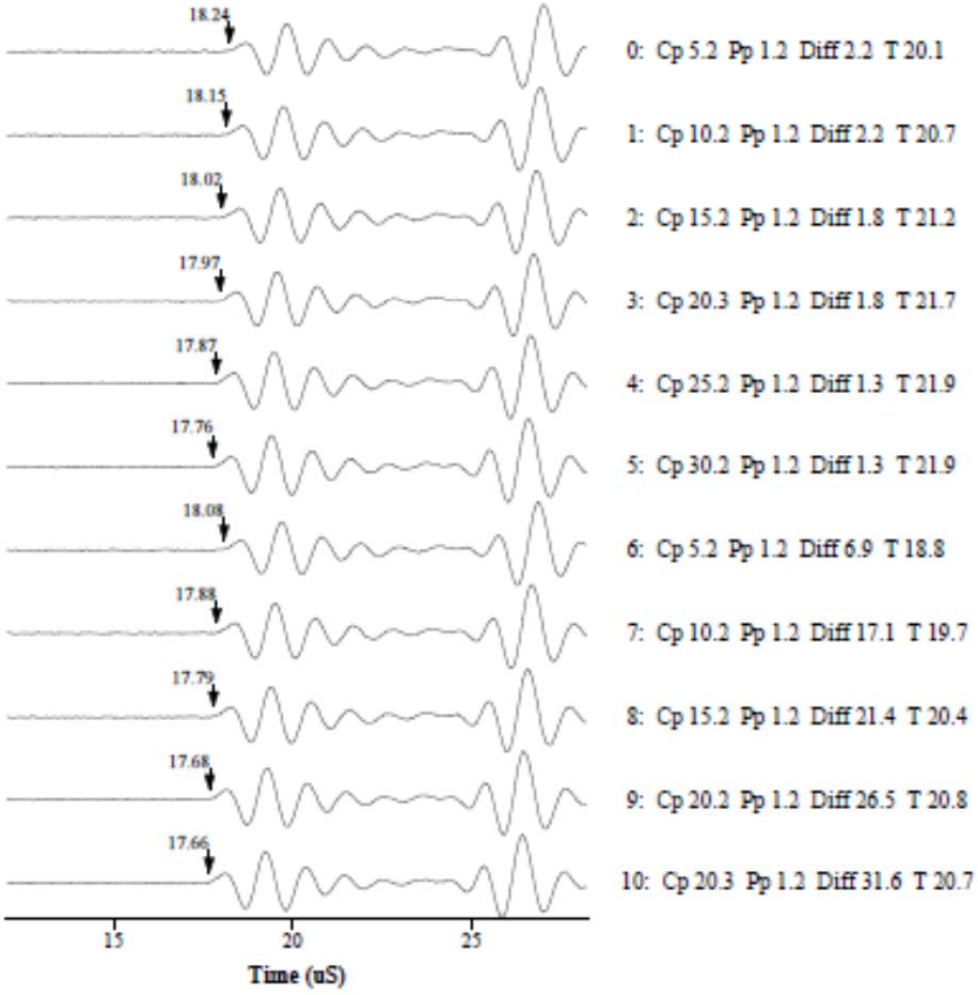

Waveform waterfall for s1 arrivals	
Experiment:	MB-W13-11008V2
Well:	13
Depth:	3355.2 m
File name:	w13-mb-11008V2-vel

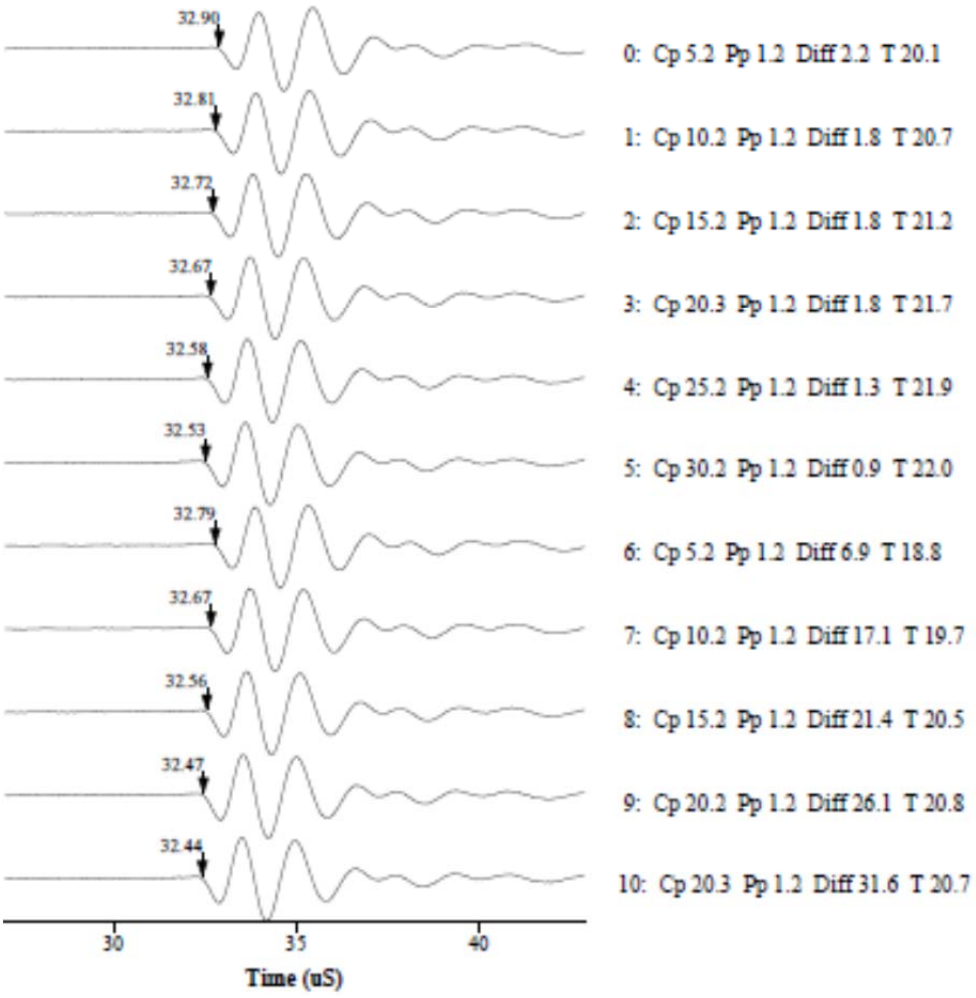

Waveform waterfall for p arrivals	
Experiment:	W13-11009V-Velocity
Well:	13
Depth:	3355.5 m
File name:	w13-mb-11009V-vel

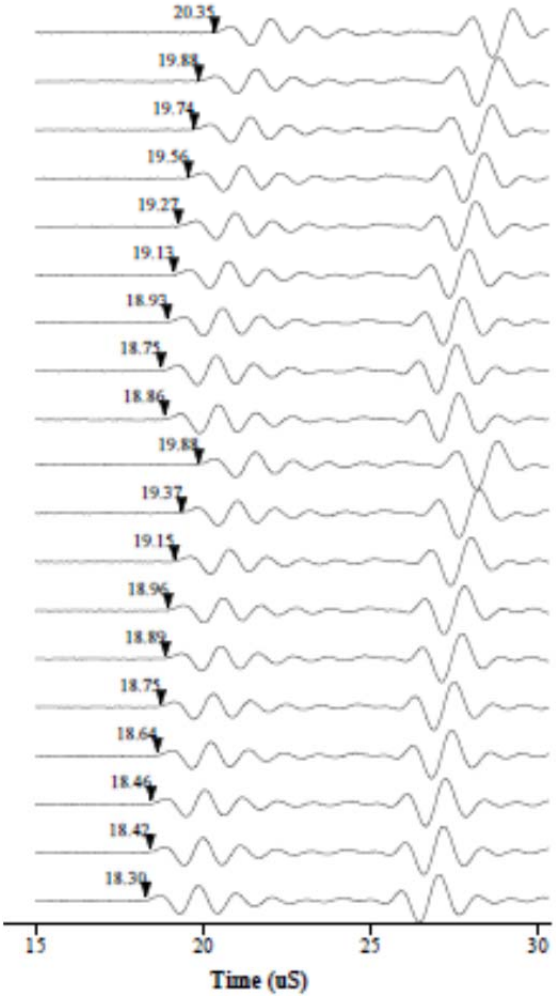

0: Cp 0.9 Pp 1.2 Diff 2.6 T 18.7
1: Cp 5.3 Pp 1.2 Diff 2.6 T 18.1
2: Cp 10.2 Pp 1.2 Diff 2.2 T 19.4
3: Cp 15.2 Pp 1.2 Diff 1.8 T 19.5
4: Cp 20.2 Pp 1.2 Diff 1.3 T 19.9
5: Cp 25.2 Pp 1.2 Diff 1.3 T 20.6
6: Cp 30.1 Pp 1.2 Diff 0.9 T 20.8
7: Cp 35.2 Pp 1.2 Diff 0.9 T 21.6
8: Cp 30.4 Pp 1.2 Diff -2.9 T 20.5
9: Cp 5.2 Pp 1.2 Diff 5.6 T 17.5
10: Cp 5.2 Pp 1.2 Diff 15.0 T 18.0
11: Cp 10.3 Pp 1.2 Diff 15.0 T 18.7
12: Cp 10.2 Pp 1.2 Diff 20.5 T 18.7
13: Cp 15.2 Pp 1.2 Diff 15.0 T 19.4
14: Cp 15.2 Pp 1.2 Diff 24.8 T 19.8
15: Cp 20.2 Pp 1.2 Diff 20.1 T 19.9
16: Cp 20.3 Pp 1.2 Diff 30.8 T 19.9
17: Cp 25.3 Pp 1.2 Diff 25.2 T 20.3
18: Cp 25.3 Pp 1.2 Diff 35.1 T 20.2

Waveform waterfall for s1 arrivals	
Experiment:	W13-11009V-Velocity
Well:	13
Depth:	3355.5 m
File name:	w13-mb-11009V-vel

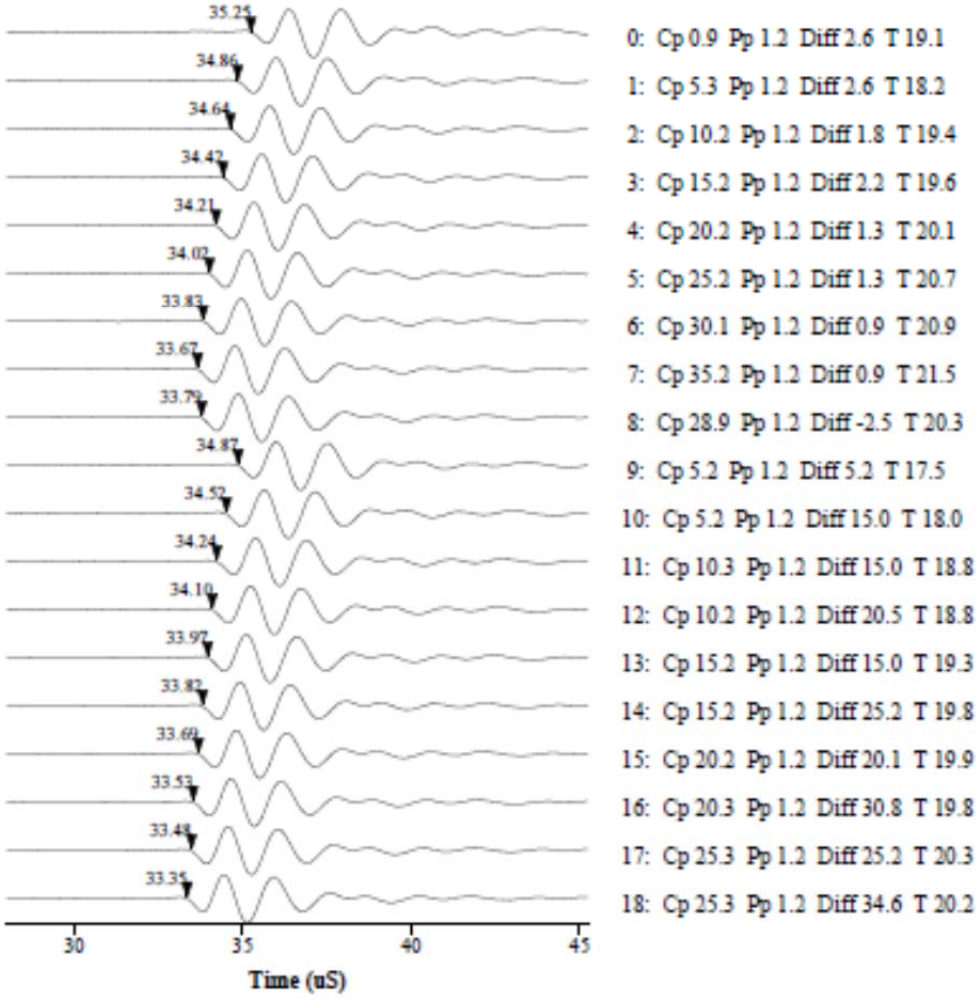

Waveform waterfall for p arrivals	
Experiment:	MB-W13-11012B(H)-Vel
Well:	13
Depth:	3356.5 m
File name:	w13-mb-11012B(H)-vel

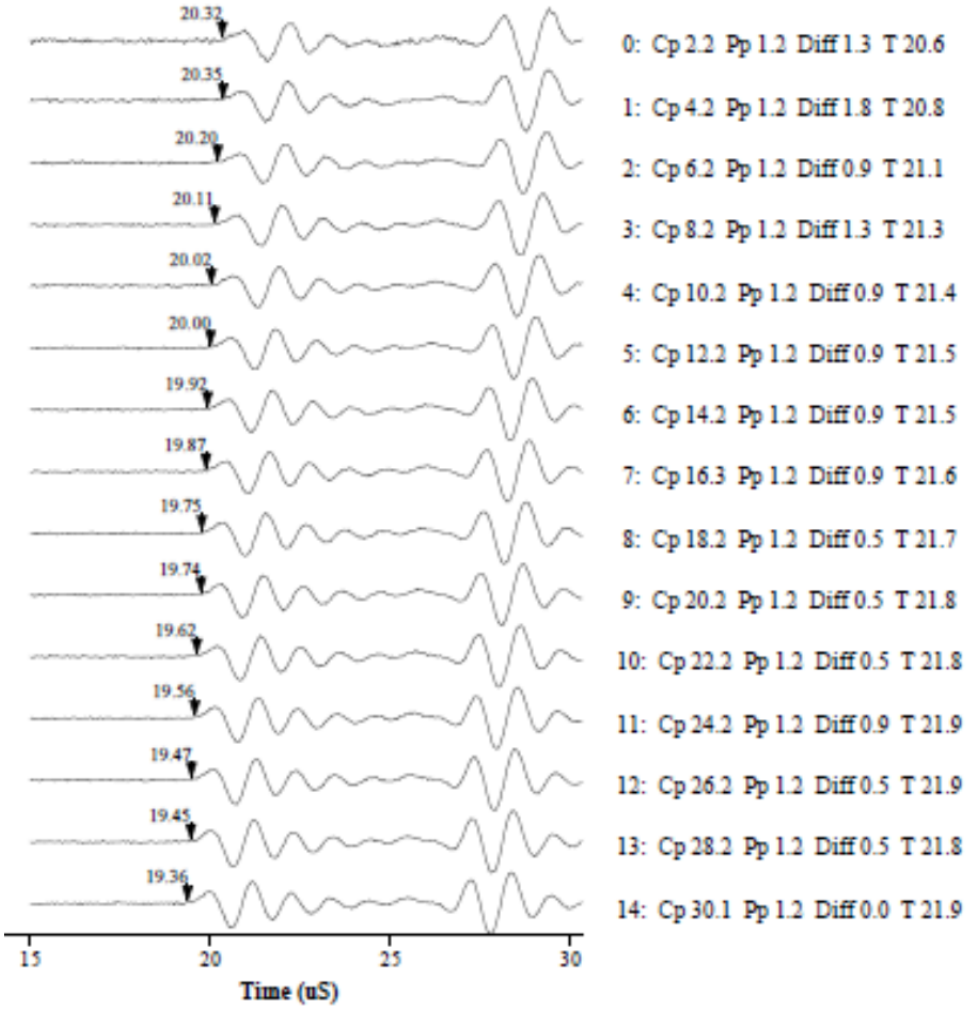

Waveform waterfall for s1 arrivals	
Experiment:	MB-W13-11012B(H)-Vel
Well:	13
Depth:	3356.5 m
File name:	w13-mb-11012B(H)-vel

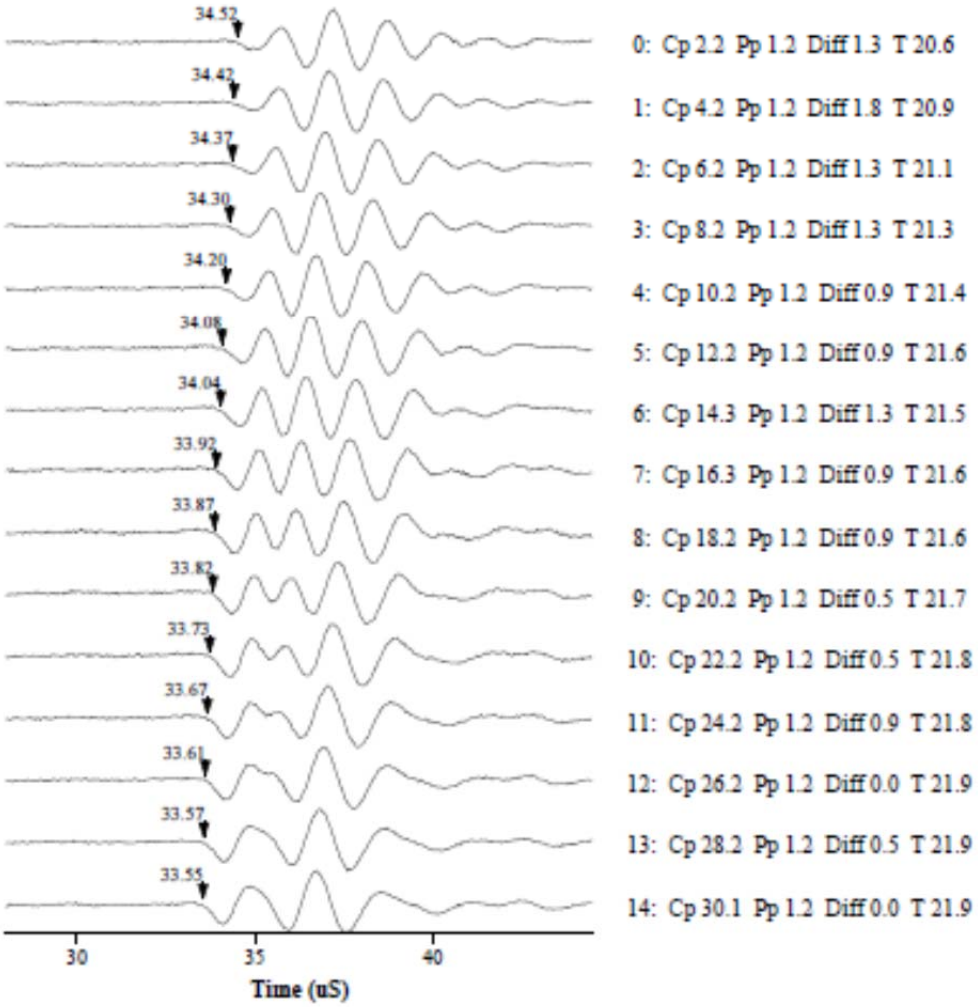

Waveform waterfall for p arrivals	
Experiment:	MB-W13-11025H-Vel
Well:	13
Depth:	3360.4 m
File name:	w13-mb-11025H-vel

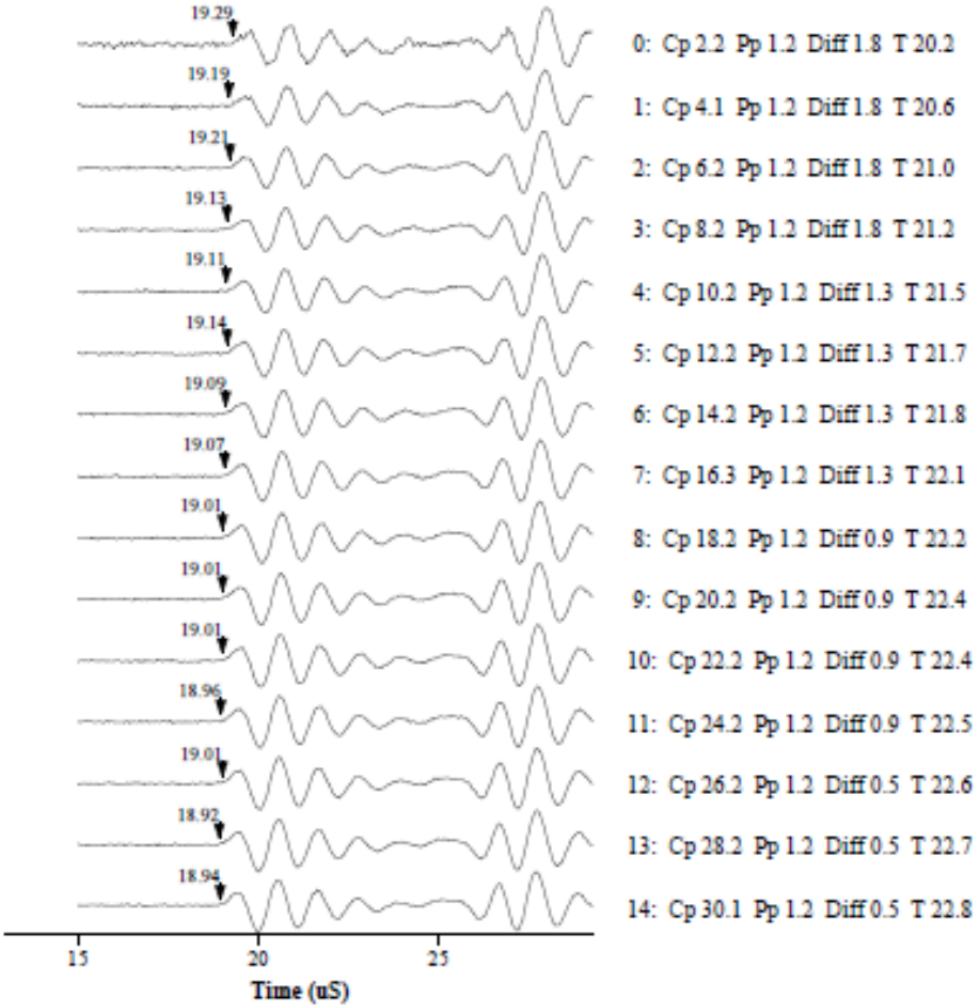

Waveform waterfall for s1 arrivals	
Experiment:	MB-W13-11025H-Vel
Well:	13
Depth:	3360.4 m
File name:	w13-mb-11025H-vel

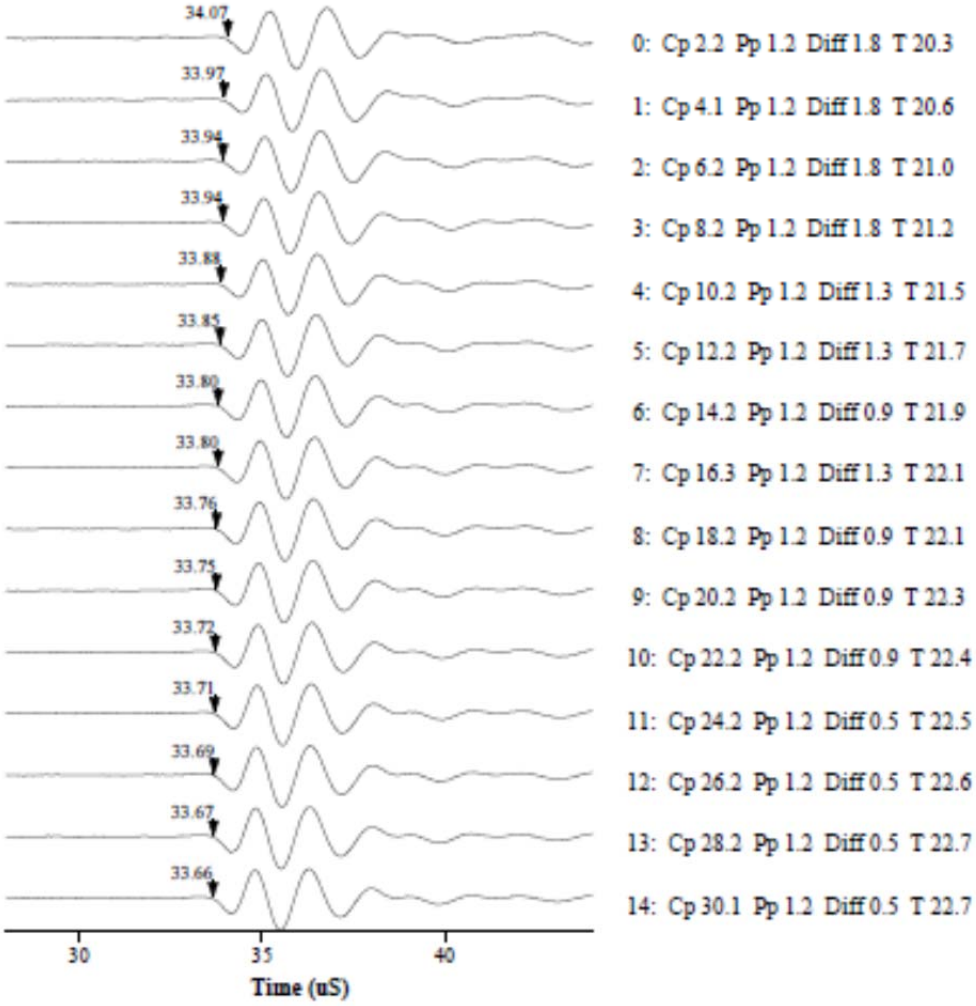

Waveform waterfall for p arrivals	
Experiment:	MB-#13-11025V
Well:	13
Depth:	3360.4 m
File name:	w13-mb-11025V-vel

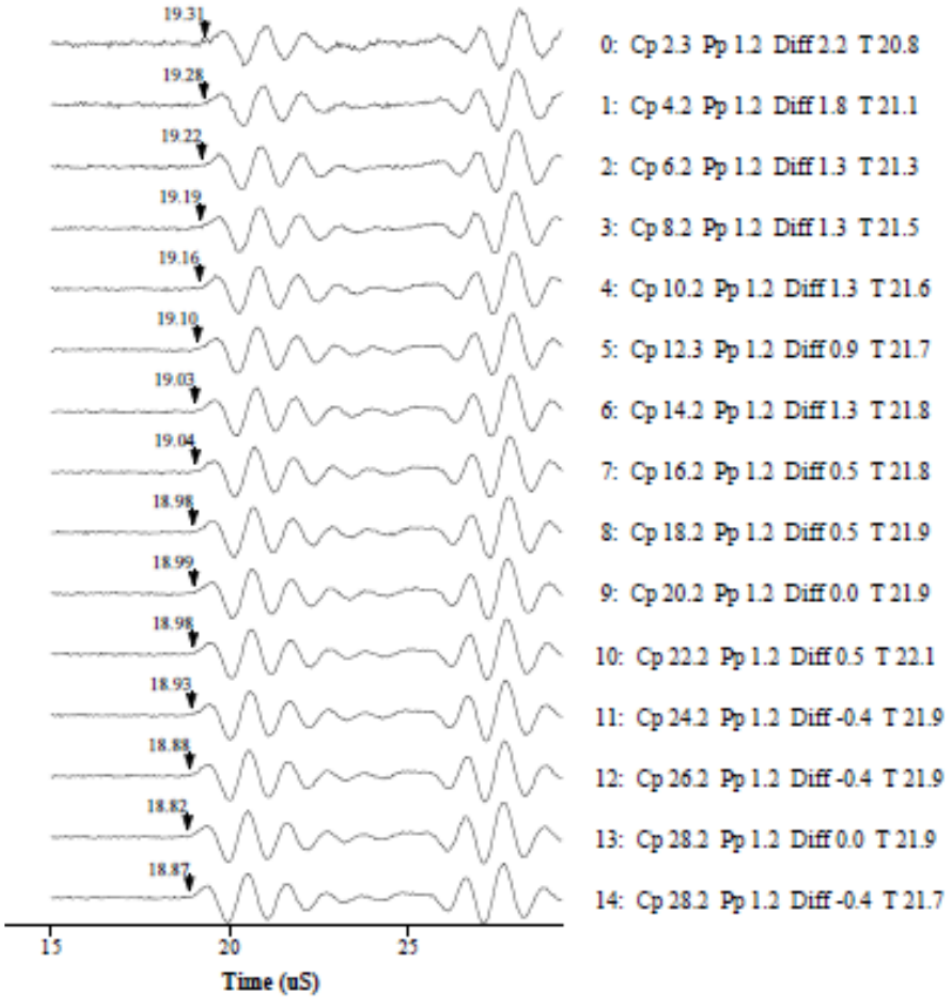

Waveform waterfall for s1 arrivals	
Experiment:	MB-#13-11025V
Well:	13
Depth:	3360.4 m
File name:	w13-mb-11025V-vel

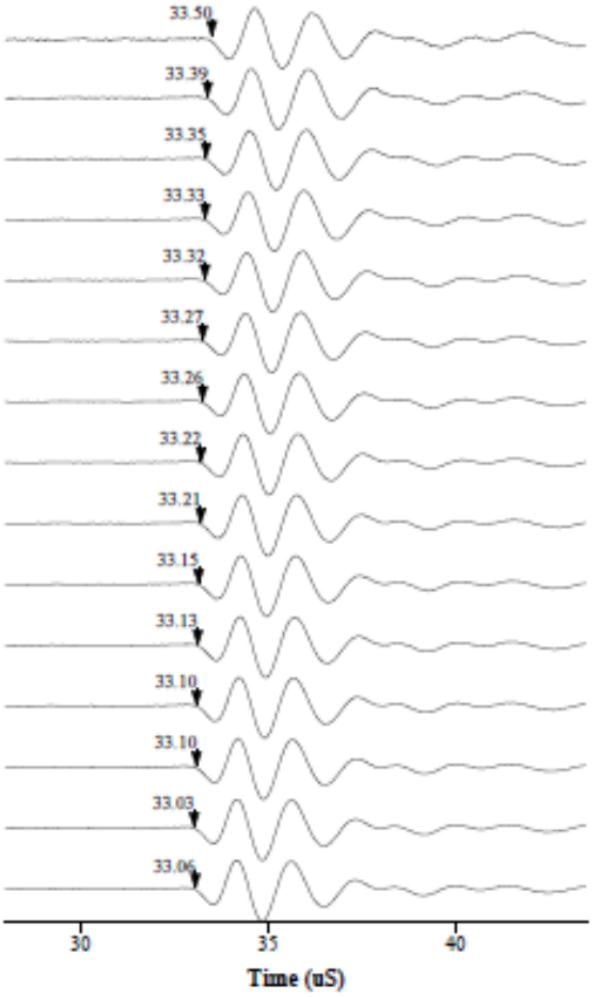

0: Cp 2.3 Pp 1.2 Diff 2.2 T 20.9
1: Cp 4.2 Pp 1.2 Diff 1.8 T 21.1
2: Cp 6.2 Pp 1.2 Diff 1.3 T 21.3
3: Cp 8.2 Pp 1.2 Diff 1.3 T 21.5
4: Cp 10.2 Pp 1.2 Diff 1.3 T 21.6
5: Cp 12.2 Pp 1.2 Diff 0.9 T 21.7
6: Cp 14.2 Pp 1.2 Diff 1.3 T 21.8
7: Cp 16.2 Pp 1.2 Diff 0.5 T 21.8
8: Cp 18.2 Pp 1.2 Diff 0.5 T 21.9
9: Cp 20.2 Pp 1.2 Diff 0.0 T 21.9
10: Cp 22.2 Pp 1.2 Diff 0.5 T 22.0
11: Cp 24.2 Pp 1.2 Diff -0.4 T 21.9
12: Cp 26.2 Pp 1.2 Diff -0.4 T 21.9
13: Cp 28.2 Pp 1.2 Diff 0.0 T 21.9
14: Cp 28.2 Pp 1.2 Diff 0.0 T 21.7

Waveform waterfall for p arrivals	
Experiment:	MB-W13-11031H-Vel
Well:	13
Depth:	3362.2 m
File name:	w13-mb-11031H-vel

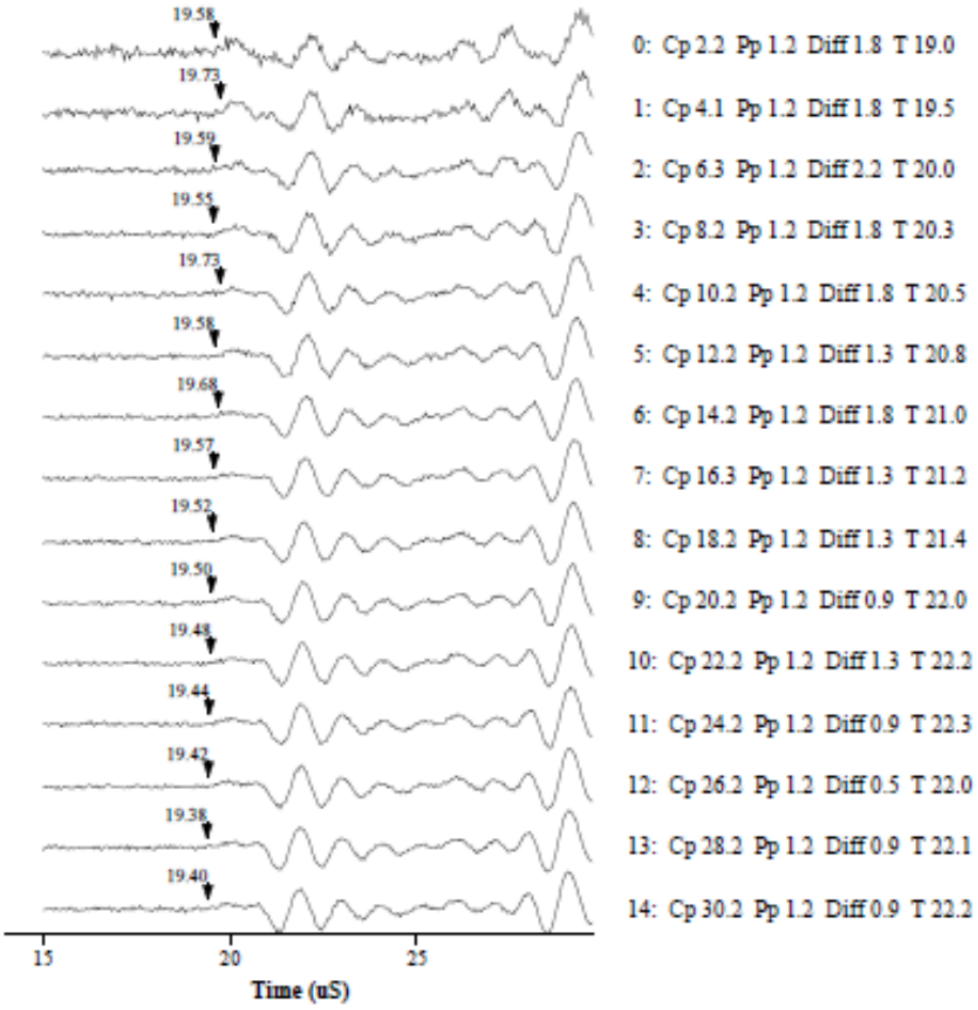

Waveform waterfall for s1 arrivals	
Experiment:	MB-W13-11031H-Vel
Well:	13
Depth:	3362.2 m
File name:	w13-mb-11031H-vel

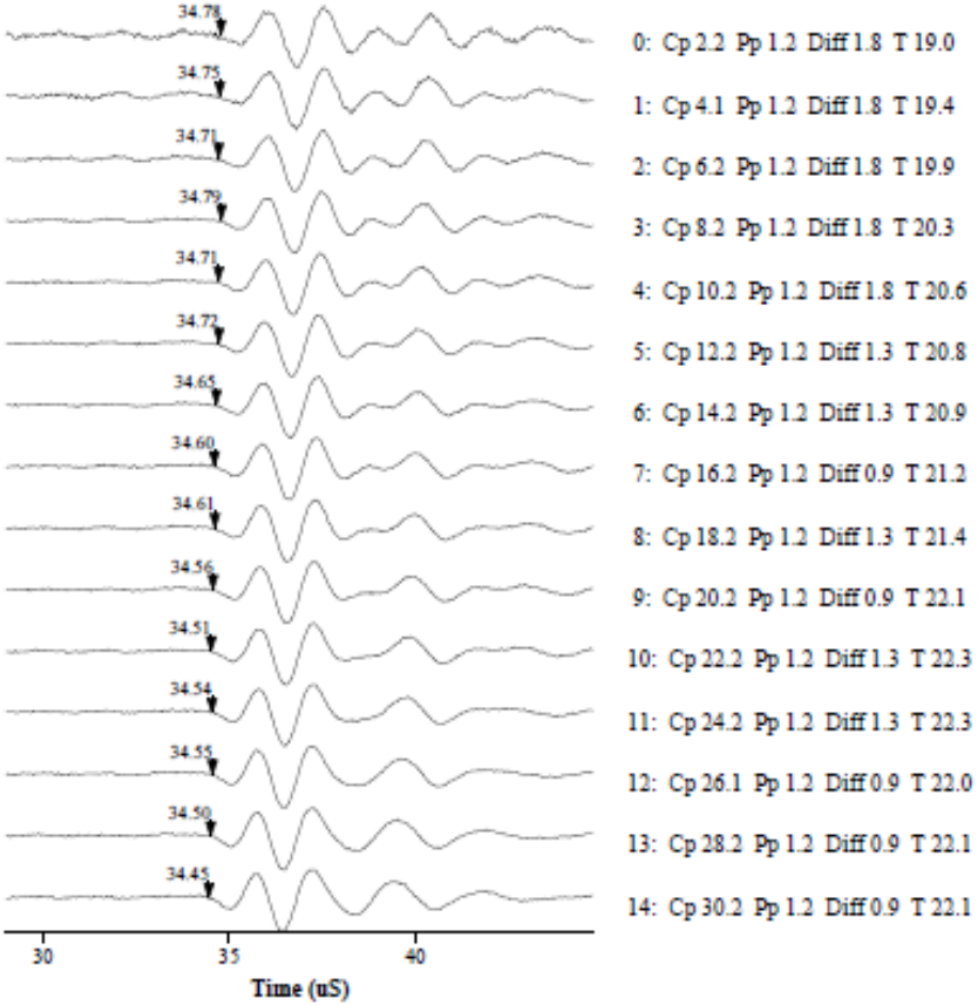

Waveform waterfall for p arrivals	
Experiment:	MB-W13-11033H-Vel
Well:	13
Depth:	3362.9 m
File name:	w13-mb-11033H-vel

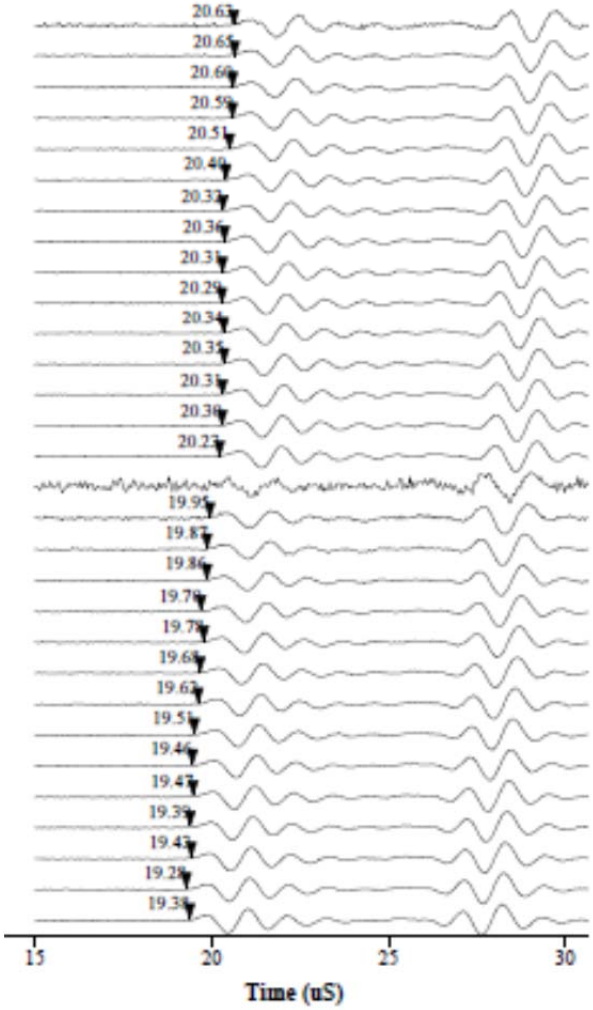

0: Cp 2.2 Pp 1.2 Diff 1.3 T 19.9
1: Cp 4.1 Pp 1.2 Diff 1.8 T 20.3
2: Cp 6.2 Pp 1.2 Diff 1.3 T 20.7
3: Cp 8.1 Pp 1.2 Diff 1.3 T 21.1
4: Cp 10.2 Pp 1.2 Diff 1.8 T 21.4
5: Cp 12.3 Pp 1.2 Diff 1.3 T 21.6
6: Cp 14.2 Pp 1.2 Diff 1.3 T 21.8
7: Cp 16.3 Pp 1.2 Diff 1.3 T 22.0
8: Cp 18.2 Pp 1.2 Diff 1.3 T 22.1
9: Cp 20.3 Pp 1.2 Diff 1.3 T 22.2
10: Cp 22.2 Pp 1.2 Diff 0.5 T 22.3
11: Cp 24.2 Pp 1.2 Diff 0.5 T 22.4
12: Cp 26.1 Pp 1.2 Diff 0.5 T 22.5
13: Cp 28.2 Pp 1.2 Diff 0.5 T 22.5
14: Cp 30.1 Pp 1.2 Diff 0.5 T 22.6
15: Cp 2.2 Pp 1.2 Diff 1.8 T 20.6
16: Cp 4.2 Pp 1.2 Diff 1.8 T 21.1
17: Cp 6.2 Pp 1.2 Diff 1.8 T 21.4
18: Cp 8.2 Pp 1.2 Diff 1.8 T 21.7
19: Cp 10.2 Pp 1.2 Diff 1.3 T 21.9
20: Cp 12.2 Pp 1.2 Diff 1.3 T 22.2
21: Cp 14.2 Pp 1.2 Diff 0.9 T 22.3
22: Cp 16.2 Pp 1.2 Diff 0.9 T 22.4
23: Cp 18.2 Pp 1.2 Diff 0.9 T 22.6
24: Cp 20.2 Pp 1.2 Diff 0.9 T 22.6
25: Cp 22.2 Pp 1.2 Diff 0.5 T 22.8
26: Cp 24.2 Pp 1.2 Diff 0.5 T 22.8
27: Cp 26.2 Pp 1.2 Diff 0.9 T 23.0
28: Cp 28.3 Pp 1.2 Diff 0.9 T 23.0
29: Cp 30.2 Pp 1.2 Diff 0.5 T 23.0

Waveform waterfall for s1 arrivals	
Experiment:	MB-W13-11033H-Vel
Well:	13
Depth:	3362.9 m
File name:	w13-mb-11033H-vel

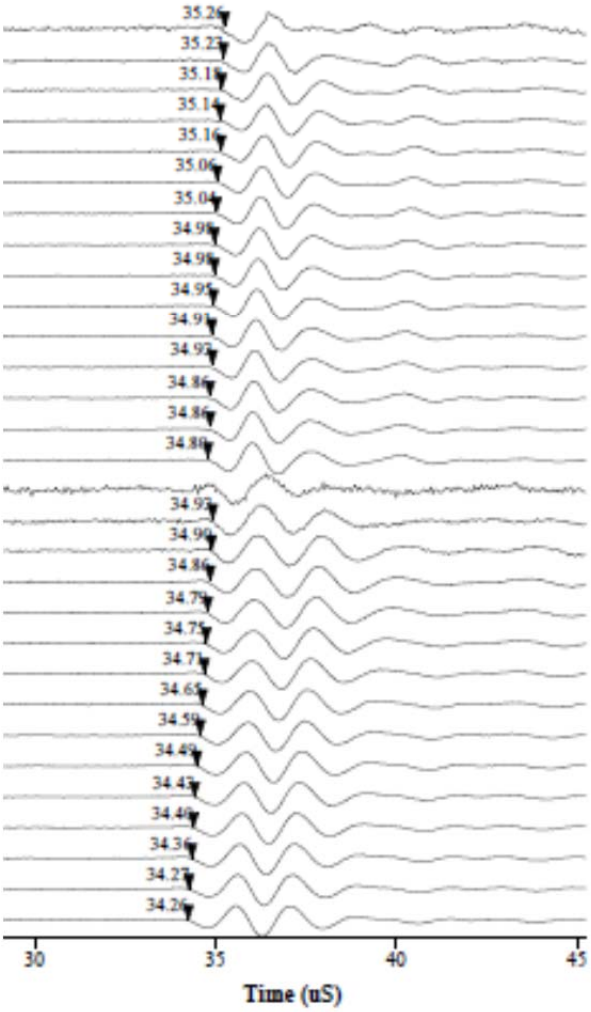

0: Cp 2.2 Pp 1.2 Diff 1.8 T 20.0
1: Cp 4.1 Pp 1.2 Diff 1.8 T 20.4
2: Cp 6.2 Pp 1.2 Diff 1.3 T 20.8
3: Cp 8.1 Pp 1.2 Diff 1.3 T 21.1
4: Cp 10.2 Pp 1.2 Diff 1.3 T 21.4
5: Cp 12.3 Pp 1.2 Diff 1.3 T 21.7
6: Cp 14.2 Pp 1.2 Diff 1.3 T 21.8
7: Cp 16.3 Pp 1.2 Diff 1.3 T 22.0
8: Cp 18.2 Pp 1.2 Diff 1.3 T 22.2
9: Cp 20.3 Pp 1.2 Diff 1.3 T 22.3
10: Cp 22.1 Pp 1.2 Diff 0.5 T 22.3
11: Cp 24.2 Pp 1.2 Diff 0.5 T 22.4
12: Cp 26.2 Pp 1.2 Diff 0.5 T 22.4
13: Cp 28.2 Pp 1.2 Diff 0.5 T 22.6
14: Cp 30.1 Pp 1.2 Diff 0.5 T 22.5
15: Cp 2.2 Pp 1.2 Diff 1.3 T 20.6
16: Cp 4.2 Pp 1.2 Diff 1.8 T 21.1
17: Cp 6.2 Pp 1.2 Diff 1.3 T 21.4
18: Cp 8.2 Pp 1.2 Diff 1.8 T 21.7
19: Cp 10.2 Pp 1.2 Diff 1.3 T 21.9
20: Cp 12.2 Pp 1.2 Diff 0.9 T 22.1
21: Cp 14.2 Pp 1.2 Diff 0.9 T 22.3
22: Cp 16.2 Pp 1.2 Diff 0.9 T 22.4
23: Cp 18.2 Pp 1.2 Diff 0.9 T 22.5
24: Cp 20.2 Pp 1.2 Diff 0.5 T 22.7
25: Cp 22.2 Pp 1.2 Diff 0.9 T 22.8
26: Cp 24.2 Pp 1.2 Diff 0.5 T 22.9
27: Cp 26.2 Pp 1.2 Diff 0.9 T 23.0
28: Cp 28.3 Pp 1.2 Diff 0.9 T 23.0
29: Cp 30.2 Pp 1.2 Diff 0.5 T 23.0

Waveform waterfall for p arrivals	
Experiment:	MB-W13-11034V2-Vel
Well:	13
Depth:	3363.2 m
File name:	w13-mb-11034(V2)-vel

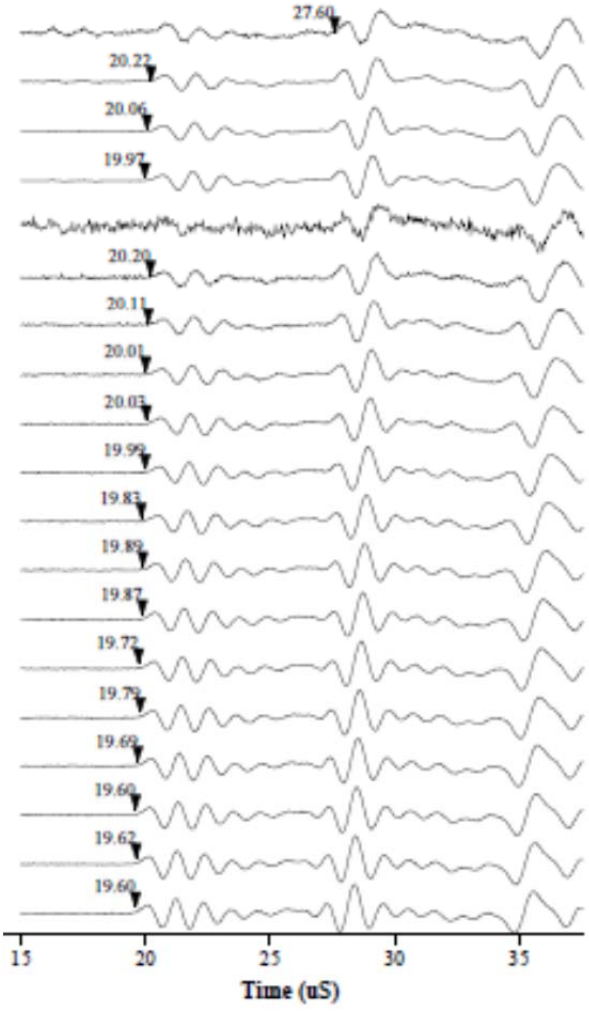

0: Cp 2.2 Pp 1.2 Diff 3.5 T 20.6
1: Cp 4.2 Pp 1.2 Diff 3.5 T 21.0
2: Cp 6.2 Pp 1.2 Diff 3.5 T 21.1
3: Cp 8.2 Pp 1.2 Diff 3.5 T 21.4
4: Cp 2.2 Pp 1.2 Diff 3.5 T 20.3
5: Cp 4.1 Pp 1.2 Diff 3.0 T 20.5
6: Cp 6.2 Pp 1.2 Diff 3.0 T 20.6
7: Cp 8.1 Pp 1.2 Diff 3.0 T 20.8
8: Cp 10.2 Pp 1.2 Diff 2.6 T 21.0
9: Cp 12.2 Pp 1.2 Diff 3.0 T 21.2
10: Cp 14.2 Pp 1.2 Diff 2.6 T 21.3
11: Cp 16.3 Pp 1.2 Diff 3.0 T 21.5
12: Cp 18.2 Pp 1.2 Diff 3.0 T 21.6
13: Cp 20.2 Pp 1.2 Diff 2.2 T 21.6
14: Cp 22.2 Pp 1.2 Diff 2.6 T 22.3
15: Cp 24.3 Pp 1.2 Diff 2.6 T 21.9
16: Cp 26.2 Pp 1.2 Diff 2.2 T 22.0
17: Cp 28.3 Pp 1.2 Diff 2.6 T 22.1
18: Cp 30.1 Pp 1.2 Diff 2.2 T 22.0

Waveform waterfall for s1 arrivals	
Experiment:	MB-W13-11034V2-Vel
Well:	13
Depth:	3363.2 m
File name:	w13-mb-11034(V2)-vel

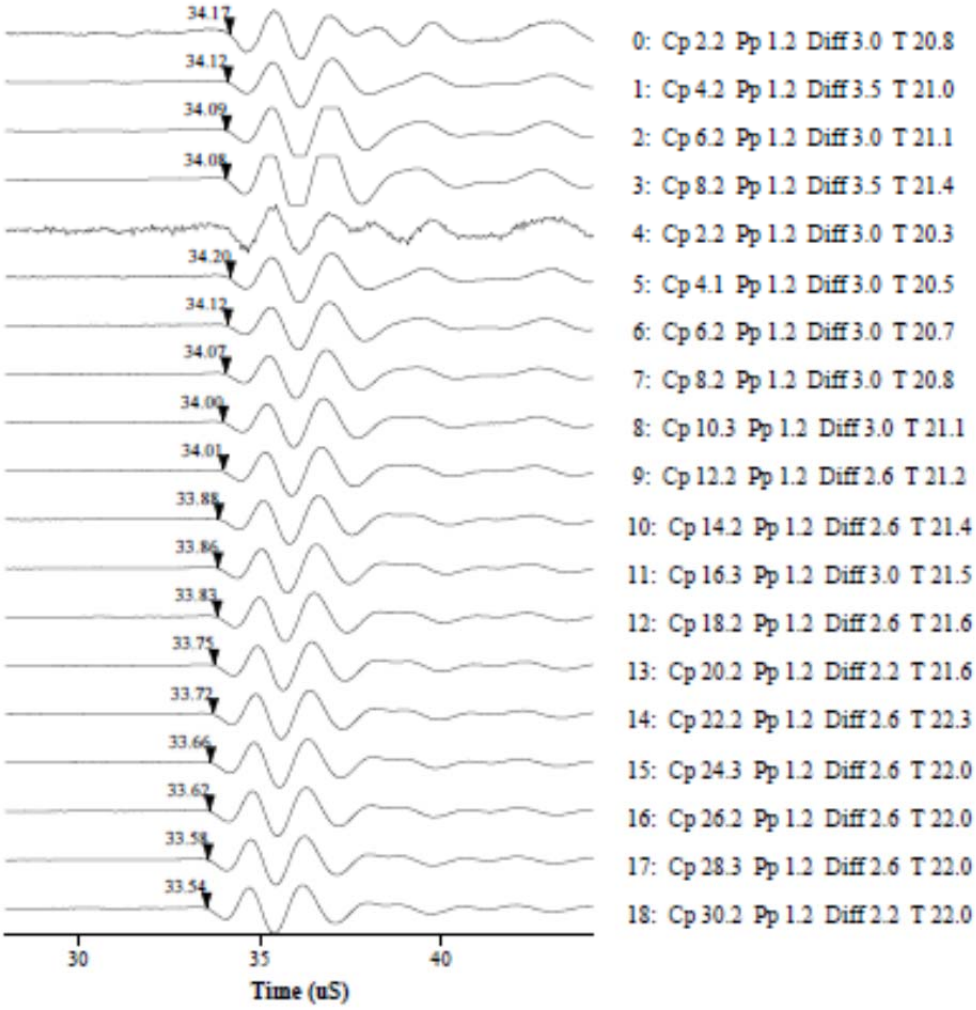

Waveform waterfall for p arrivals	
Experiment:	MB-W13-11025V-Vel
Well:	13
Depth:	3363.5 m
File name:	w13-mb-11035V-vel

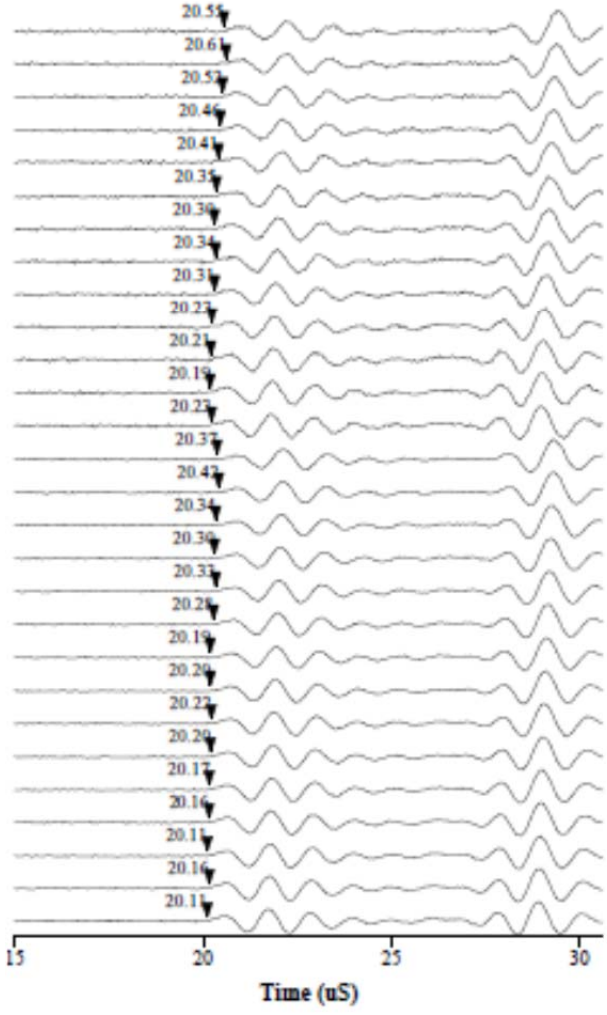

0: Cp 2.2 Pp 1.2 Diff 2.6 T 21.4
1: Cp 4.2 Pp 1.2 Diff 2.6 T 21.5
2: Cp 6.2 Pp 1.2 Diff 2.2 T 21.8
3: Cp 8.1 Pp 1.2 Diff 1.8 T 21.9
4: Cp 10.2 Pp 1.2 Diff 1.8 T 21.7
5: Cp 12.3 Pp 1.2 Diff 2.2 T 21.8
6: Cp 14.2 Pp 1.2 Diff 1.8 T 21.9
7: Cp 16.2 Pp 1.2 Diff 1.8 T 22.1
8: Cp 18.2 Pp 1.2 Diff 1.8 T 22.1
9: Cp 20.3 Pp 1.2 Diff 1.8 T 22.2
10: Cp 22.2 Pp 1.2 Diff 1.8 T 22.2
11: Cp 24.3 Pp 1.2 Diff 1.8 T 22.3
12: Cp 26.2 Pp 1.2 Diff 1.3 T 22.3
13: Cp 2.2 Pp 1.2 Diff 2.2 T 19.3
14: Cp 4.2 Pp 1.2 Diff 2.6 T 19.7
15: Cp 6.2 Pp 1.2 Diff 2.2 T 20.0
16: Cp 8.2 Pp 1.2 Diff 2.2 T 20.4
17: Cp 10.2 Pp 1.2 Diff 2.2 T 20.6
18: Cp 12.3 Pp 1.2 Diff 2.2 T 20.9
19: Cp 14.2 Pp 1.2 Diff 1.8 T 21.2
20: Cp 16.2 Pp 1.2 Diff 1.3 T 21.4
21: Cp 18.2 Pp 1.2 Diff 1.8 T 21.6
22: Cp 20.2 Pp 1.2 Diff 1.3 T 21.7
23: Cp 22.2 Pp 1.2 Diff 1.8 T 21.9
24: Cp 24.2 Pp 1.2 Diff 1.3 T 21.9
25: Cp 26.2 Pp 1.2 Diff 1.3 T 22.1
26: Cp 28.2 Pp 1.2 Diff 1.3 T 22.1
27: Cp 30.1 Pp 1.2 Diff 0.9 T 22.1

Waveform waterfall for s1 arrivals	
Experiment:	MB-W13-11025V-Vel
Well:	13
Depth:	3363.5 m
File name:	w13-mb-11035V-vel

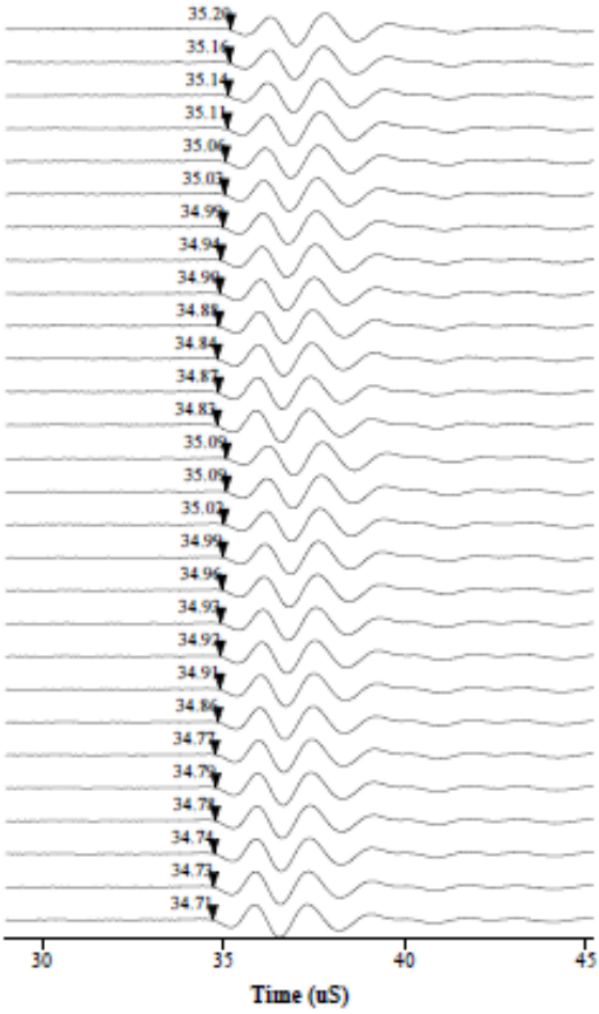

0: Cp 2.2 Pp 1.2 Diff 2.6 T 21.4
1: Cp 4.2 Pp 1.2 Diff 2.6 T 21.5
2: Cp 6.2 Pp 1.2 Diff 2.2 T 21.7
3: Cp 8.2 Pp 1.2 Diff 2.2 T 21.8
4: Cp 10.2 Pp 1.2 Diff 1.8 T 21.7
5: Cp 12.3 Pp 1.2 Diff 2.2 T 21.8
6: Cp 14.2 Pp 1.2 Diff 1.8 T 22.0
7: Cp 16.3 Pp 1.2 Diff 1.8 T 22.0
8: Cp 18.2 Pp 1.2 Diff 1.8 T 22.1
9: Cp 20.3 Pp 1.2 Diff 1.8 T 22.2
10: Cp 22.2 Pp 1.2 Diff 1.8 T 22.3
11: Cp 24.2 Pp 1.2 Diff 1.8 T 22.3
12: Cp 26.1 Pp 1.2 Diff 1.3 T 22.3
13: Cp 2.2 Pp 1.2 Diff 2.2 T 19.2
14: Cp 4.2 Pp 1.2 Diff 2.6 T 19.7
15: Cp 6.2 Pp 1.2 Diff 2.6 T 20.0
16: Cp 8.2 Pp 1.2 Diff 2.2 T 20.4
17: Cp 10.2 Pp 1.2 Diff 2.2 T 20.7
18: Cp 12.3 Pp 1.2 Diff 2.2 T 20.9
19: Cp 14.2 Pp 1.2 Diff 1.8 T 21.1
20: Cp 16.2 Pp 1.2 Diff 1.3 T 21.4
21: Cp 18.2 Pp 1.2 Diff 1.8 T 21.6
22: Cp 20.2 Pp 1.2 Diff 1.3 T 21.7
23: Cp 22.2 Pp 1.2 Diff 1.8 T 21.9
24: Cp 24.2 Pp 1.2 Diff 1.3 T 21.9
25: Cp 26.2 Pp 1.2 Diff 0.9 T 22.0
26: Cp 28.2 Pp 1.2 Diff 0.9 T 22.1
27: Cp 30.2 Pp 1.2 Diff 0.9 T 22.2

A.6.3 Biot's Coefficient

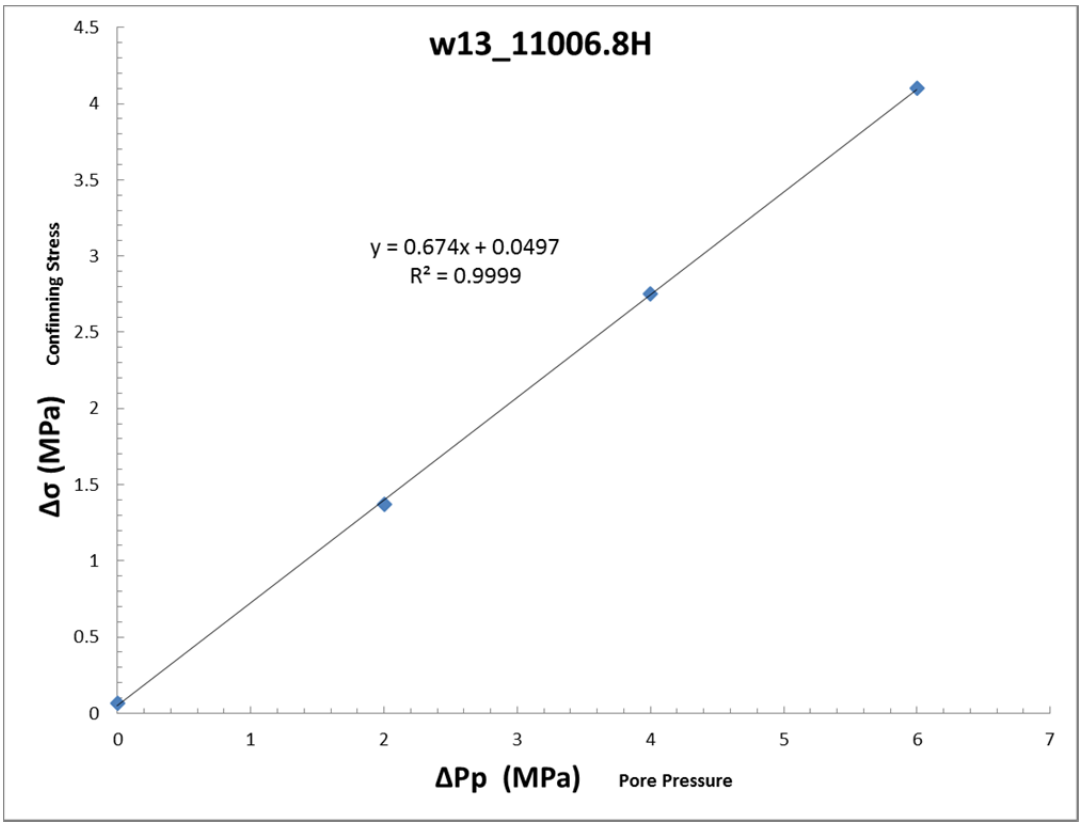

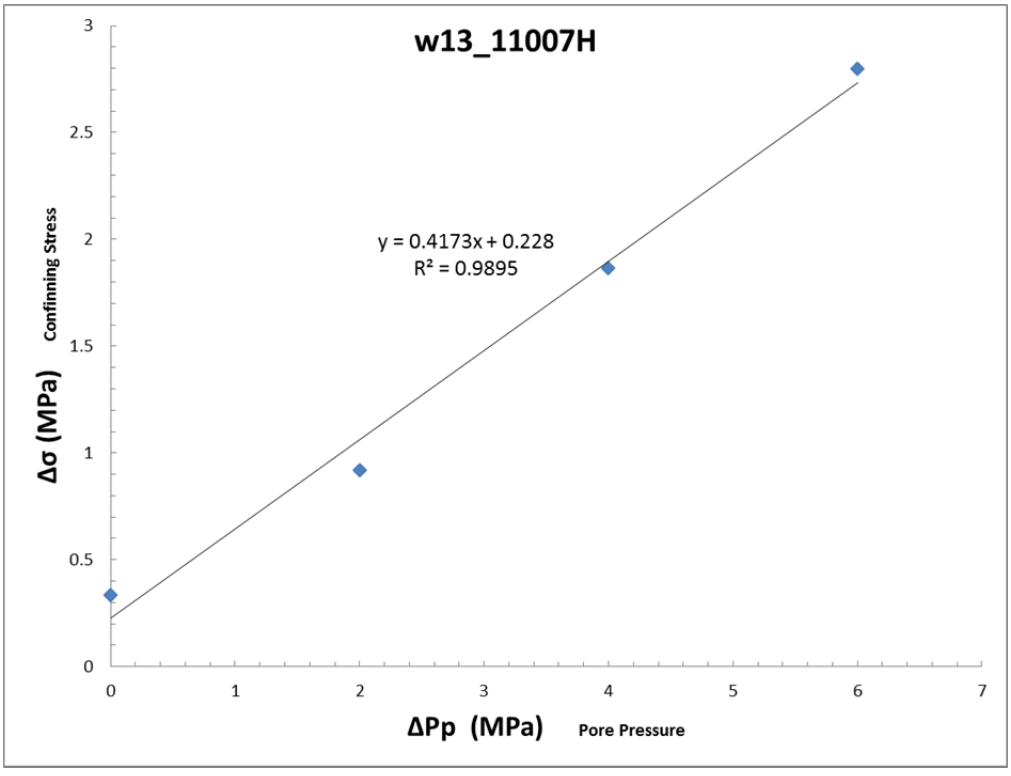

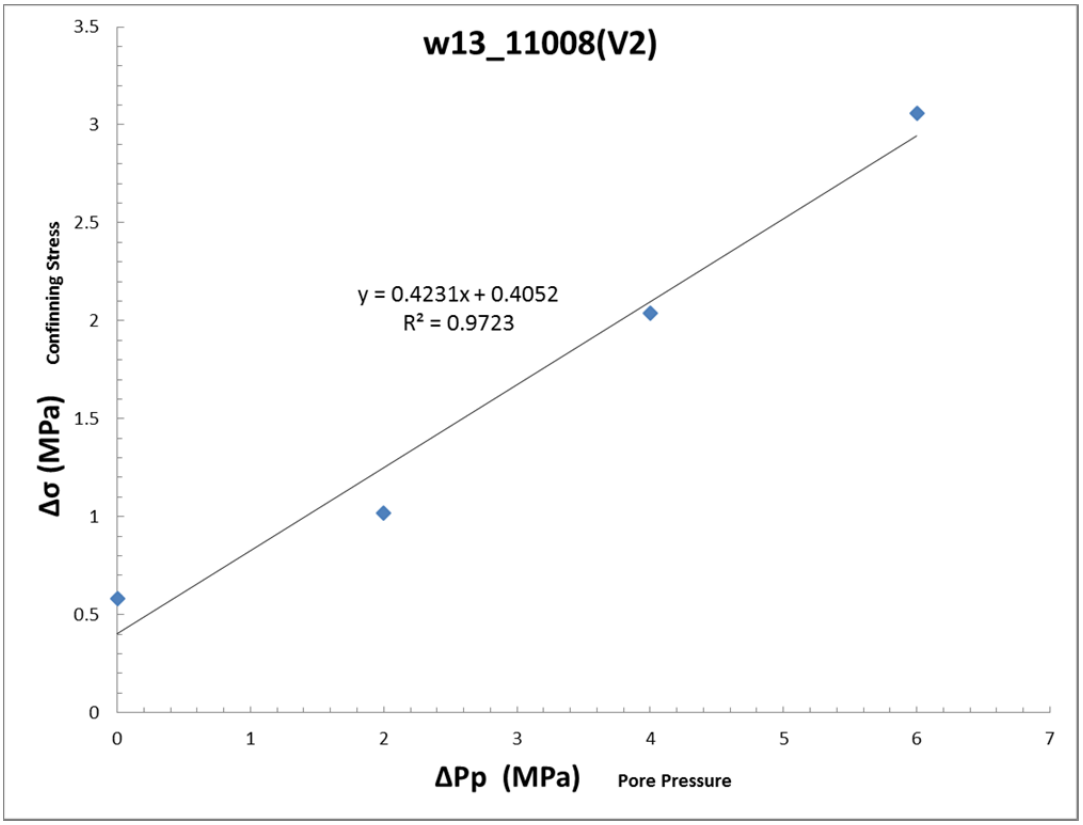
w13_11008(V2)
y = 0.4231x + 0.4052
R² = 0.9723
Δσ (MPa) Confinning Stress
ΔPp (MPa) Pore Pressure
0
0.5
1
1.5
2
2.5
3
3.5
0
1
2
3
4
5
6
7

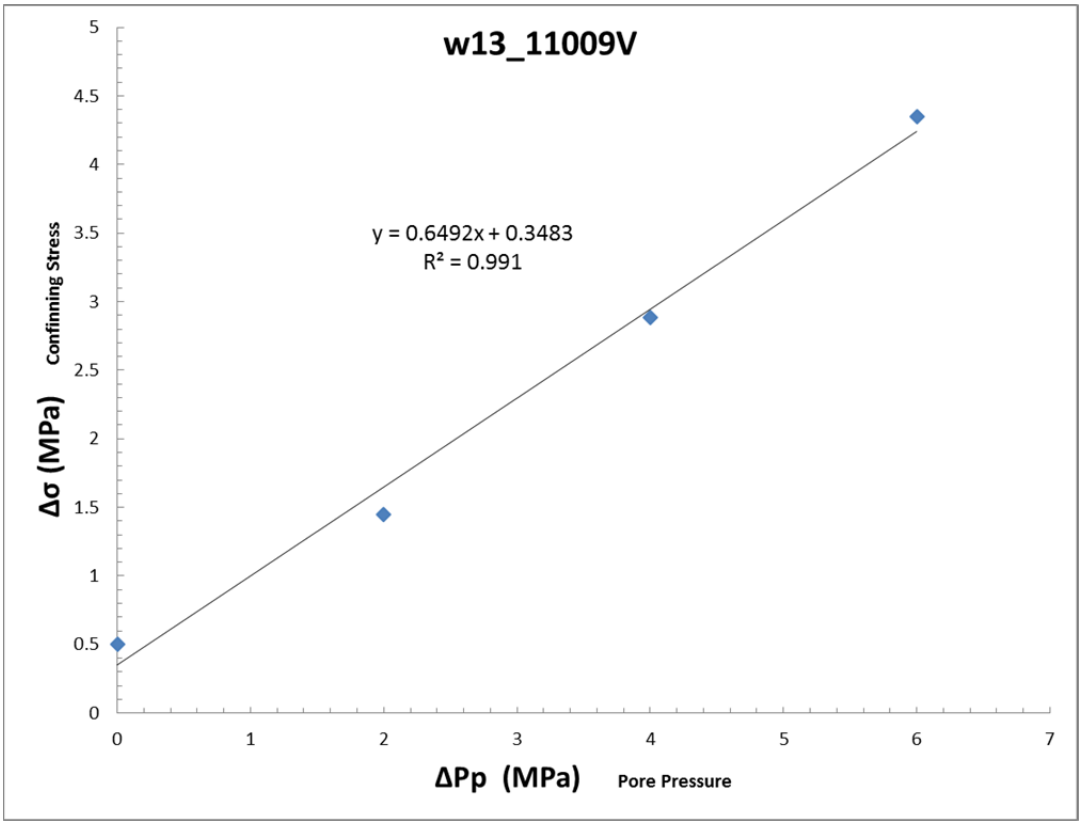
w13_11009V
y = 0.6492x + 0.3483
R² = 0.991
Δσ (MPa) Confinning Stress
ΔPp (MPa) Pore Pressure
0
0.5
1
1.5
2
2.5
3
3.5
4
4.5
5
0
1
2
3
4
5
6
7

A.6.4 Static Moduli and Poisson's Ratio (Non-destructive)

Uniaxial Stress for File w13-mb-11006.8H-uniaxial_stress								
Event	Conf	Diff	Temp	E	n	K	G	P
	MPa	MPa	°C	GPa		GPa	GPa	GPa
0	25.3	25.5	28.5	85.31	0.336	86.89	31.92	129.45
1	15.2	11.5	27.8	70.18	0.307	60.47	26.86	96.28
2	5.2	6.8	27.5	53.95	0.247	35.54	21.63	64.38

Uniaxial Stress for File w13-mb-11006V-uniaxial_stress								
Event	Conf	Diff	Temp	E	n	K	G	P
	MPa	MPa	°C	GPa		GPa	GPa	GPa
0	25.1	25.2	27.1	50.72	0.150	24.15	22.05	53.55
1	15.1	15.4	26.7	47.23	0.130	21.25	20.91	49.12
2	5.1	5.2	26.5	32.65	0.118	14.24	14.60	33.71

Uniaxial Stress for File w13-mb-11007H-uniaxial_stress								
Event	Conf	Diff	Temp	E	n	K	G	P
	MPa	MPa	°C	GPa		GPa	GPa	GPa
0	30.0	25.2	23.4	64.46	0.243	41.84	25.92	76.40
1	27.9	24.8	24.1	65.71	0.263	46.12	26.02	80.81
2	25.9	24.8	24.5	66.60	0.263	46.88	26.36	82.02
3	24.0	25.2	24.8	66.50	0.262	46.61	26.34	81.73
4	22.0	24.8	25.2	66.34	0.260	46.16	26.32	81.25
5	19.9	24.8	25.4	65.60	0.270	47.60	25.82	82.03
6	18.0	25.2	25.9	65.62	0.264	46.32	25.96	80.93
7	16.0	24.8	25.6	66.10	0.259	45.72	26.25	80.72
8	14.0	25.2	25.8	66.69	0.260	46.25	26.47	81.54
9	12.0	25.7	26.2	66.35	0.257	45.50	26.39	80.69
10	10.0	10.3	26.4	61.86	0.248	40.88	24.79	73.93
11	8.0	9.9	26.0	60.72	0.244	39.52	24.40	72.06
12	6.0	5.2	26.0	54.80	0.241	35.24	22.08	64.68
13	3.9	4.7	26.1	54.72	0.235	34.47	22.14	64.00
14	2.1	5.6	26.0	53.38	0.246	35.09	21.41	63.64

Uniaxial Stress for File w13-mb-11008.5H-uniaxial_stress								
Event	Conf	Diff	Temp	E	n	K	G	P
	MPa	MPa	°C	GPa		GPa	GPa	GPa
0	30.2	25.2	25.1	55.50	0.238	35.35	22.41	65.23
1	28.0	25.2	25.2	56.92	0.243	36.91	22.90	67.44
2	26.0	24.8	25.3	56.78	0.248	37.60	22.74	67.92
3	24.1	25.2	26.1	56.62	0.251	37.95	22.62	68.12
4	22.0	25.2	26.2	56.26	0.244	36.61	22.61	66.76
5	20.1	25.2	25.7	55.96	0.246	36.71	22.46	66.66
6	18.0	24.8	25.6	55.85	0.246	36.67	22.41	66.54
7	16.0	24.8	25.8	54.61	0.246	35.86	21.91	65.07
8	14.0	24.8	25.8	54.27	0.245	35.48	21.79	64.54
9	12.0	25.2	26.3	53.10	0.249	35.25	21.26	63.59
10	10.1	10.7	26.3	47.01	0.199	26.00	19.61	52.15
11	8.0	9.9	26.3	46.33	0.198	25.55	19.34	51.33
12	6.0	5.2	26.2	56.38	0.131	25.46	24.92	58.69
13	4.0	5.2	25.8	56.05	0.117	24.38	25.09	57.84
14	2.0	4.7	25.7	52.45	0.093	21.50	23.98	53.48

Uniaxial Stress for File w13-mb-11008V1-uniaxial_stress								
Event	Conf	Diff	Temp	E	n	K	G	P
	MPa	MPa	°C	GPa		GPa	GPa	GPa
0	30.2	24.8	27.0	58.13	0.220	34.57	23.83	66.34
1	28.0	24.8	26.8	66.00	0.260	45.81	26.19	80.73
2	26.1	25.2	26.7	62.52	0.268	44.82	24.66	77.71
3	24.2	25.2	26.6	63.95	0.272	46.75	25.14	80.27
4	22.1	25.2	26.6	65.07	0.269	46.94	25.64	81.12
5	20.1	25.2	27.0	60.88	0.268	43.78	24.00	75.78
6	30.1	25.2	26.9	60.57	0.229	37.29	24.63	70.14
7	28.1	24.8	26.9	62.89	0.251	42.17	25.13	75.68
8	26.0	24.8	27.0	64.31	0.261	44.77	25.51	78.79
9	24.1	24.8	26.9	64.83	0.260	44.94	25.74	79.26
10	22.0	25.2	26.9	63.56	0.259	43.93	25.25	77.60
11	20.1	24.8	26.9	65.20	0.259	45.15	25.88	79.66
12	18.1	25.2	26.8	62.73	0.261	43.72	24.87	76.89
13	16.1	25.7	26.9	62.50	0.258	43.13	24.83	76.24
14	14.0	24.8	26.8	64.94	0.257	44.52	25.83	78.96
15	10.0	25.2	26.7	67.58	0.270	49.03	26.60	84.49
16	10.1	10.3	26.8	56.79	0.213	33.03	23.40	64.23
17	8.0	9.9	26.8	58.30	0.219	34.54	23.92	66.44
18	6.1	5.2	26.8	50.82	0.196	27.83	21.25	56.17
19	4.0	4.7	26.8	52.72	0.185	27.91	22.24	57.56
20	2.1	5.2	27.0	50.78	0.163	25.09	21.83	54.21

Uniaxial Stress for File w13-mb-11008V2-uniaxial_strss								
Event	Conf	Diff	Temp	E	n	K	G	P
	MPa	MPa	°C	GPa		GPa	GPa	GPa
0	25.0	24.7	25.7	69.06	0.245	45.05	27.75	82.05
1	25.0	14.9	27.3	71.13	0.230	43.84	28.93	82.41
2	15.1	14.9	27.2	72.81	0.217	42.87	29.92	82.75
3	5.0	6.3	27.0	76.64	0.119	33.54	34.24	79.19

Uniaxial Stress for File w13-mb-11009V-uniaxial_stress								
Event	Conf	Diff	Temp	E	n	K	G	P
	MPa	MPa	°C	GPa		GPa	GPa	GPa
0	25.3	26.4	26.2	58.10	0.232	36.14	23.58	67.57
1	15.3	12.3	26.1	56.85	0.213	33.04	23.43	64.28
2	5.2	7.6	26.3	65.58	0.223	39.43	26.81	75.18

Uniaxial Stress for File w13-mb-11025H-uniaxial_stress								
Event	Conf	Diff	Temp	E	n	K	G	P
	MPa	MPa	°C	GPa		GPa	GPa	GPa
0	30.0	24.8	26.9	62.22	0.221	37.12	25.49	71.10
1	28.2	25.2	26.2	63.88	0.225	38.76	26.07	73.51
2	26.0	25.2	26.8	65.74	0.225	39.82	26.84	75.60
3	24.1	25.2	26.2	65.46	0.223	39.38	26.76	75.07
4	22.0	24.8	26.4	64.73	0.226	39.42	26.39	74.61
5	20.1	24.8	26.4	65.97	0.230	40.77	26.81	76.52
6	18.0	24.8	26.2	65.68	0.222	39.35	26.88	75.19
7	16.0	24.8	26.4	66.18	0.220	39.45	27.11	75.60
8	14.1	25.2	26.3	64.16	0.219	38.02	26.32	73.11
9	12.0	25.2	26.5	65.21	0.218	38.56	26.77	74.25
10	10.1	10.3	26.9	59.88	0.206	33.97	24.82	67.06
11	8.1	10.3	26.8	59.74	0.205	33.80	24.78	66.84
12	6.1	5.6	27.3	48.34	0.178	25.05	20.51	52.40
13	4.0	5.2	27.2	47.60	0.171	24.14	20.32	51.23
14	2.0	5.2	27.2	48.18	0.170	24.33	20.59	51.79

Uniaxial Stress for File w13-mb-11031H-uniaxial_stress								
Event	Conf	Diff	Temp	E	n	K	G	P
	MPa	MPa	°C	GPa		GPa	GPa	GPa
0	25.2	26.0	77.6	64.16	0.118	27.97	28.70	66.24
1	15.2	10.6	77.0	62.83	0.120	27.54	28.06	64.95
2	5.2	5.9	77.4	49.67	0.112	21.32	22.34	51.10

Uniaxial Stress for File w13-mb-11033H-uniaxial_stress								
Event	Conf	Diff	Temp	E	n	K	G	P
	MPa	MPa	°C	GPa		GPa	GPa	GPa
0	30.0	24.8	27.4	40.69	0.135	18.60	17.92	42.49
1	28.1	24.8	27.2	44.14	0.166	22.04	18.93	47.28
2	26.0	24.8	27.1	46.05	0.168	23.13	19.71	49.41
3	24.0	24.8	26.9	45.46	0.173	23.15	19.38	48.99
4	22.0	24.8	27.0	45.88	0.167	22.97	19.66	49.18
5	20.1	25.2	27.0	46.76	0.168	23.46	20.02	50.15
6	18.0	24.4	26.8	45.84	0.168	23.01	19.63	49.18
7	16.0	24.8	26.8	44.18	0.166	22.07	18.94	47.32
8	14.0	24.8	26.7	45.21	0.167	22.61	19.38	48.44
9	12.0	24.8	26.7	45.12	0.165	22.43	19.37	48.25
10	10.1	10.3	26.6	40.08	0.146	18.85	17.49	42.17
11	8.0	9.4	26.2	40.85	0.148	19.36	17.78	43.07
12	6.0	4.7	26.2	39.79	0.122	17.53	17.74	41.18
13	4.0	5.6	26.1	40.59	0.114	17.50	18.23	41.81
14	2.0	5.2	26.1	40.09	0.101	16.76	18.20	41.03
15	30.0	25.2	27.0	43.47	0.150	20.72	18.89	45.91

Uniaxial Stress for File w13-mb-11034V2-uniaxial_stress								
Event	Conf	Diff	Temp	E	n	K	G	P
	MPa	MPa	°C	GPa		GPa	GPa	GPa
0	30.0	25.2	26.1	30.60	0.128	13.72	13.56	31.80
1	28.0	25.7	25.9	38.71	0.145	18.16	16.91	40.70
2	26.1	25.2	25.8	36.95	0.142	17.21	16.18	38.78
3	24.1	25.2	26.3	36.54	0.140	16.90	16.03	38.27
4	22.0	25.2	26.4	36.31	0.139	16.75	15.95	38.01
5	20.1	25.2	25.9	36.60	0.141	16.99	16.04	38.37
6	18.0	25.2	26.5	35.61	0.139	16.43	15.63	37.28
7	16.0	25.2	26.5	36.58	0.134	16.67	16.13	38.17
8	13.9	25.2	26.4	35.96	0.134	16.37	15.86	37.52
9	12.0	25.2	26.6	35.97	0.135	16.41	15.85	37.55
10	10.0	9.9	26.5	33.64	0.118	14.66	15.05	34.72
11	8.0	9.9	26.4	33.63	0.123	14.86	14.97	34.83
12	6.0	4.7	26.0	38.29	0.122	16.89	17.06	39.64
13	4.0	4.7	25.9	40.49	0.123	17.92	18.02	41.95
14	2.0	5.2	25.9	37.53	0.129	16.88	16.62	39.04

A.6.5 Uni/Triaxial Compressive Strength, Young's Modulus and Poisson's Ratio

Strength for File w13-mb-11007H-strength					
Event	Conf	Temp	E	n	peak_stress
	MPa	°C	GPa		MPa
0	20.3	23.0	49.59	0.305	232.3

Strength for File w13-mb-11008V2-strength					
Event	Conf	Temp	E	n	peak_stress
	MPa	°C	GPa		MPa
0	20.2	26.8	48.97	0.318	234.8

A.6.6 Mohr's Circle

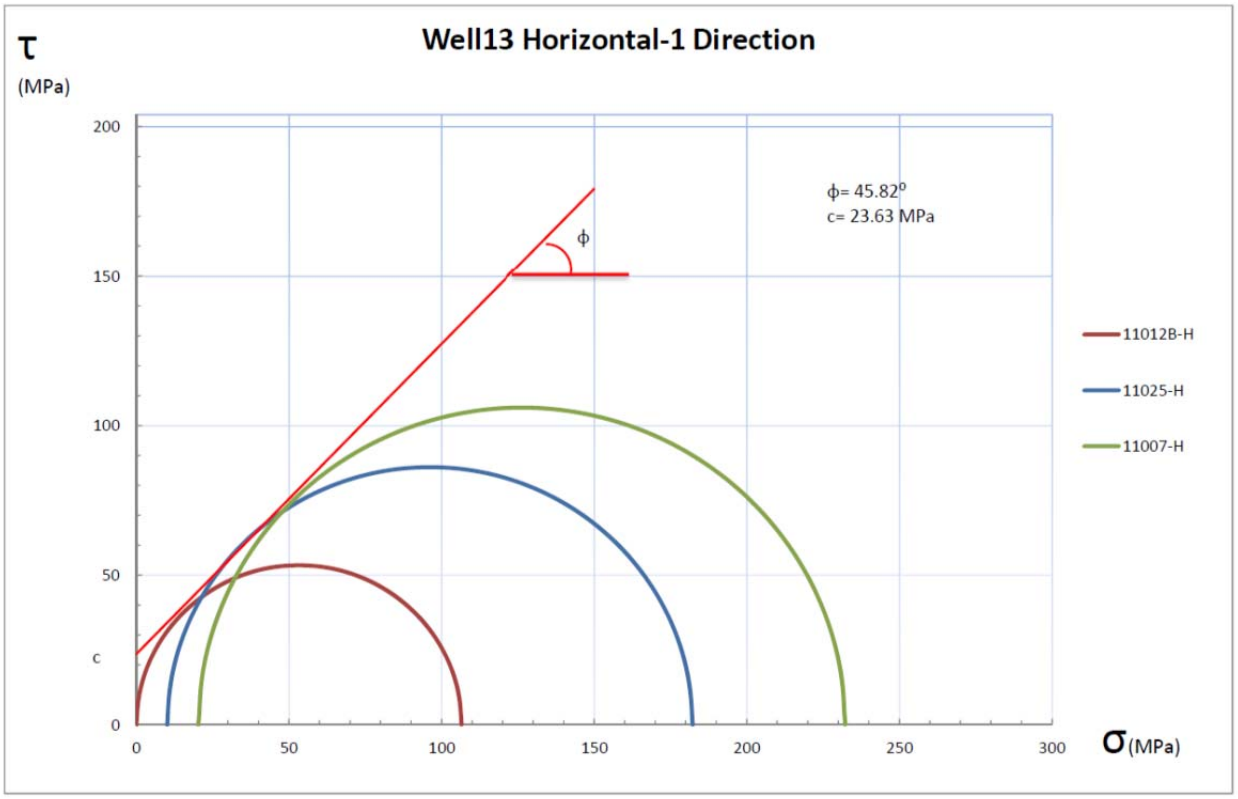

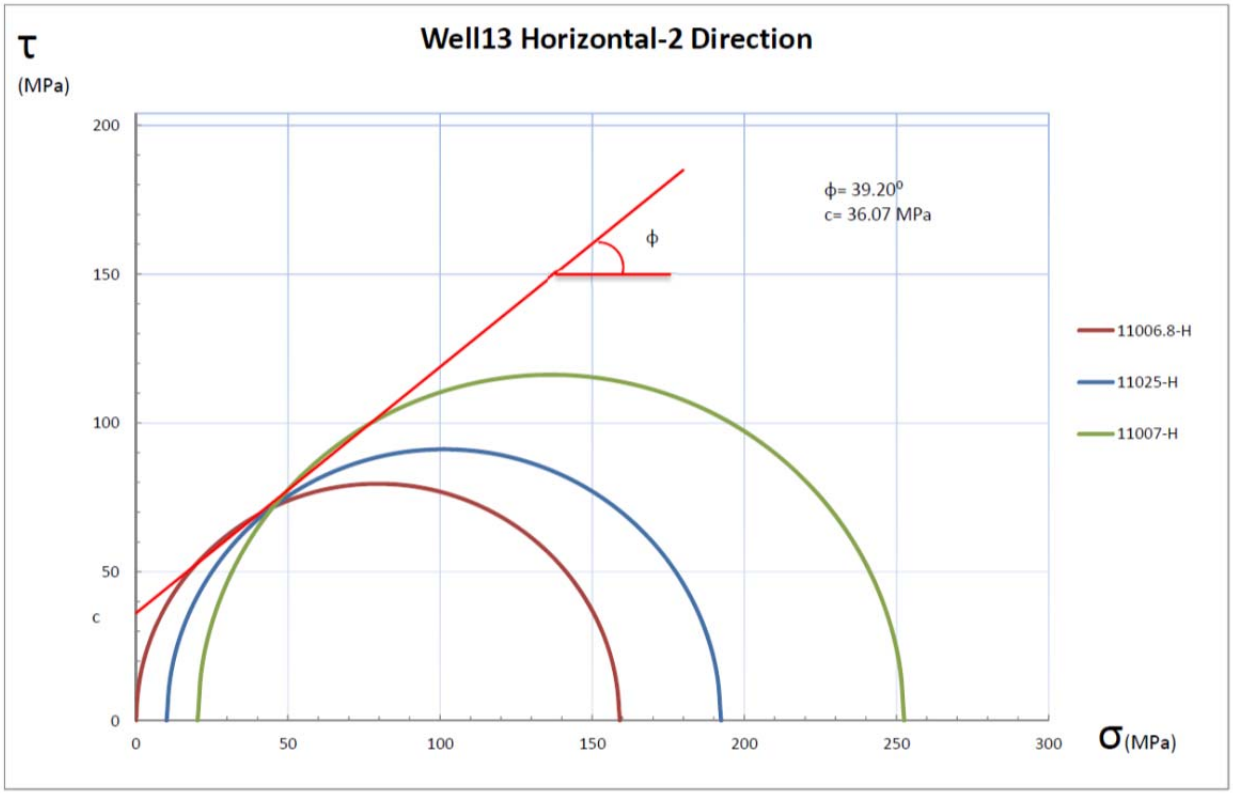

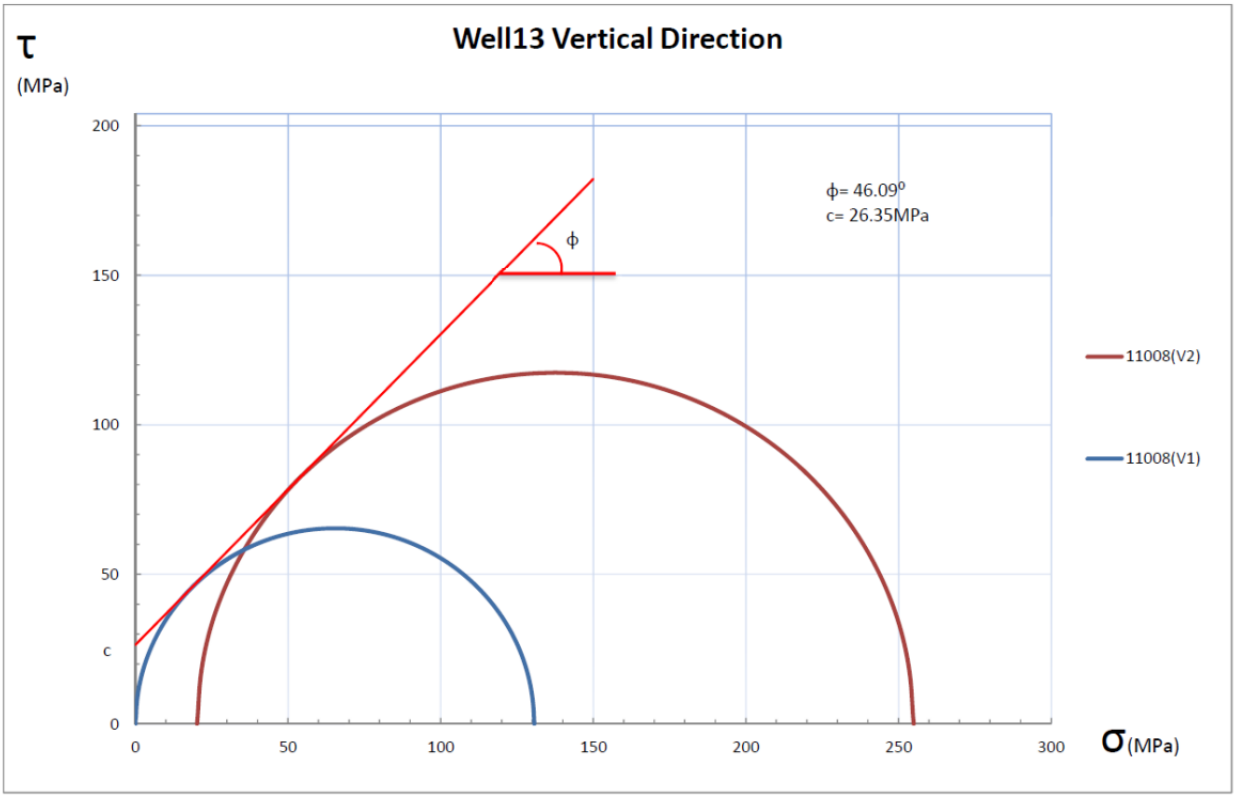

A.7. Well 86 Bakken Samples Testing Results

A.7.1 Permeability

Permeability and Specific Storage for File w86-mb-7350H-perm							
Event	Type	Conf	Pore Top	Diff	Temp	Perm	Storage
		MPa	MPa	MPa	°C	μD	m^{-1}
0	multipulse	30.4	7.8	-4.3	30.8	0.0305	1.21e-06
1	multipulse	25.5	7.8	-4.3	31.0	0.0335	8.44e-07
2	multipulse	20.5	7.8	-4.3	31.1	0.0569	1.45e-06
3	multipulse	15.4	7.8	-3.5	31.2	0.0793	1.74e-06

Permeability and Specific Storage for File w86-mb-7355.9H-perm							
Event	Type	Conf	Pore Top	Diff	Temp	Perm	Storage
		MPa	MPa	MPa	°C	μD	m^{-1}
0	multipulse	30.3	7.8	-5.2	25.1	27.8	0.000104
1	multipulse	25.3	7.8	-4.8	25.2	4.0	3.97e-06
2	multipulse	20.3	7.7	-4.3	25.2	4.68	3.74e-06
3	multipulse	15.3	7.8	-3.9	22.3	0.577	1.80e-12

Permeability and Specific Storage for File w86-mb-7355V-perm							
Event	Type	Conf	Pore Top	Diff	Temp	Perm	Storage
		MPa	MPa	MPa	°C	μD	m^{-1}
0	aspike	30.4	8.2	-3.9	27.4	53.6	1.91e-08
1	aspike	25.0	8.1	-3.9	26.6	61.6	2.84e-11
2	aspike	15.0	7.2	-3.1	23.0	147.	4.65e-12

Permeability and Specific Storage for File w86-mb-7369H-perm							
Event	Type	Conf	Pore Top	Diff	Temp	Perm	Storage
		MPa	MPa	MPa	°C	μD	m^{-1}
0	multipulse	30.3	7.8	-4.8	25.3	1.48	1.34e-06
1	multipulse	30.3	7.8	-4.3	25.1	1.45	1.27e-06
2	multipulse	25.4	7.8	-4.3	24.8	1.88	1.44e-06
3	multipulse	20.4	7.8	-4.3	24.8	2.49	1.30e-06
4	multipulse	15.3	7.8	-3.9	24.5	3.44	8.92e-07

Permeability and Specific Storage for File w86-mb-7374H-perm							
Event	Type	Conf	Pore Top	Diff	Temp	Perm	Storage
		MPa	MPa	MPa	°C	μD	m^{-1}
0	multipulse	15.4	7.8	-3.5	23.5	0.00508	5.15e-08
1	multipulse	30.4	7.8	-4.3	24.3	0.0807	4.27e-05
2	multipulse	30.4	7.9	-4.3	25.1	0.00509	2.15e-07

Permeability and Specific Storage for File w86-mb-7380H90-perm							
Event	Type	Conf	Pore Top	Diff	Temp	Perm	Storage
		MPa	MPa	MPa	°C	μD	m^{-1}
0	multipulse	30.4	7.8	-4.3	30.2	0.228	1.29e-06
1	multipulse	25.4	7.8	-3.9	29.9	0.190	7.30e-07
2	multipulse	20.4	7.8	-3.9	29.9	0.227	7.93e-07
3	multipulse	15.4	7.8	-3.1	29.7	0.310	1.37e-08

Permeability and Specific Storage for File w86-mb-7393.1H90-perm							
Event	Type	Conf	Pore Top	Diff	Temp	Perm	Storage
		MPa	MPa	MPa	°C	μD	m^{-1}
0	multipulse	30.3	7.8	-3.9	32.3	0.574	1.63e-06
1	multipulse	25.3	7.8	-3.9	32.7	0.690	2.15e-06
2	multipulse	20.4	7.8	-3.1	31.9	0.714	2.03e-06
3	multipulse	15.3	7.8	-2.6	23.4	0.913	2.01e-06

Permeability and Specific Storage for File w86-mb-7397V-perm							
Event	Type	Conf	Pore Top	Diff	Temp	Perm	Storage
		MPa	MPa	MPa	°C	μD	m^{-1}
0	multipulse	30.4	7.8	-4.8	26.5	0.150	1.03e-06
1	multipulse	25.4	7.8	-4.3	27.0	0.157	8.96e-07
2	multipulse	20.4	7.7	-3.5	26.9	0.185	9.18e-07
3	multipulse	15.3	7.8	-3.5	25.3	0.203	7.49e-07

Permeability and Specific Storage for File w86-mb-7403.8V-perm							
Event	Type	Conf	Pore Top	Diff	Temp	Perm	Storage
		MPa	MPa	MPa	°C	μD	m^{-1}
0	multipulse	30.4	7.8	-5.2	28.7	0.0247	1.51e-06
1	multipulse	25.4	7.8	-5.2	28.8	0.00993	5.32e-07
2	multipulse	20.5	7.8	-4.3	28.9	0.00377	1.80e-07
3	multipulse	15.4	7.8	-3.9	28.2	0.00681	1.39e-06
4	multipulse	15.4	7.8	-3.9	28.1	0.00376	5.62e-07

Permeability and Specific Storage for File W17450-7330-Permeability							
Event	Type	Conf	Pore Top	Diff	Temp	Perm	Storage
		MPa	MPa	MPa	°C	μD	m^{-1}
0	steady-state	20.1	7.8	-0.8	26.0	3.64e+03	0.00
1	steady-state	29.9	8.2	-1.7	26.0	3.50e+03	0.00
2	steady-state	40.1	8.4	-2.1	26.2	2.73e+03	0.00
3	steady-state	50.1	8.1	-2.5	26.6	2.37e+03	0.00

Permeability and Specific Storage for File W17450-7332-Permeability							
Event	Type	Conf	Pore Top	Diff	Temp	Perm	Storage
		MPa	MPa	MPa	°C	μD	m^{-1}
0	steady-state	20.1	8.0	-0.8	25.6	2.57e+03	0.00
1	steady-state	29.9	7.9	-1.3	26.4	2.32e+03	0.00
2	steady-state	40.1	8.5	-2.1	26.2	3.84e+03	0.00
3	steady-state	50.1	8.1	-2.5	26.3	3.49e+03	0.00

Permeability and Specific Storage for File W17450-7348.8-Permeability							
Event	Type	Conf	Pore Top	Diff	Temp	Perm	Storage
		MPa	MPa	MPa	°C	μD	m^{-1}
0	steady-state	20.4	8.2	-0.8	27.9	3.36e+04	0.00
1	steady-state	30.2	7.8	-1.7	27.5	3.34e+04	0.00
2	steady-state	40.1	8.5	-1.7	27.5	1.26e+04	0.00
3	steady-state	50.2	7.8	-2.5	27.1	5.33e+03	0.00

Permeability and Specific Storage for File W17450-7351-Permeability							
Event	Type	Conf	Pore Top	Diff	Temp	Perm	Storage
		MPa	MPa	MPa	°C	μD	m^{-1}
0	steady-state	20.1	8.0	-0.8	26.8	2.44e+03	0.00
1	steady-state	29.9	8.2	-1.3	27.3	2.98e+03	0.00
2	steady-state	40.2	8.5	-2.1	27.7	2.93e+03	0.00
3	steady-state	50.1	8.5	-2.5	27.8	2.47e+03	0.00

Permeability and Specific Storage for File W17450-7405-Permeability							
Event	Type	Conf	Pore Top	Diff	Temp	Perm	Storage
		MPa	MPa	MPa	°C	μD	m^{-1}
0	multipulse	20.0	7.3	-0.8	24.5	2.82	2.09e-09
1	multipulse	30.0	7.5	-0.8	24.8	0.178	7.20e-10
2	multipulse	40.1	7.5	-1.7	25.1	0.326	3.02e-05

Permeability and Specific Storage for File W17450-7407-Permeability							
Event	Type	Conf	Pore Top	Diff	Temp	Perm	Storage
		MPa	MPa	MPa	°C	μD	m^{-1}
0	aspike	20.1	7.3	-0.8	25.9	0.0338	7.25e-10
1	aspike	30.0	7.3	-0.8	25.9	0.135	4.35e-11
2	aspike	40.1	7.3	-1.3	25.9	0.903	1.82e-10

Permeability and Specific Storage for File W17450-7407.8-Permeability							
Event	Type	Conf	Pore Top	Diff	Temp	Perm	Storage
		MPa	MPa	MPa	°C	μD	m^{-1}
0	multipulse	20.0	7.5	-0.8	24.2	4.21	2.20e-09
1	multipulse	30.1	7.5	-1.3	24.1	0.0270	6.02e-07

Permeability and Specific Storage for File W17450-7409-Permeability							
Event	Type	Conf	Pore Top	Diff	Temp	Perm	Storage
		MPa	MPa	MPa	°C	μD	m^{-1}
0	aspike	20.2	7.5	-0.4	27.9	19.	1.71e-12
1	aspike	30.0	7.5	-0.8	28.2	15.2	1.78e-12
2	aspike	40.1	7.4	-1.3	28.1	10.9	4.40e-11

Permeability and Specific Storage for File W17450-7409.8-Permeability							
Event	Type	Conf	Pore Top	Diff	Temp	Perm	Storage
		MPa	MPa	MPa	°C	μD	m^{-1}
0	aspike	20.1	7.4	-0.4	26.0	55.6	1.07e-11
1	aspike	30.0	7.4	-0.8	26.7	49.3	5.13e-12
2	aspike	40.0	7.4	-1.7	27.2	21.8	5.46e-12

Permeability and Specific Storage for File W17450-7445.1-Permeability							
Event	Type	Conf	Pore Top	Diff	Temp	Perm	Storage
		MPa	MPa	MPa	°C	μD	m^{-1}
0	aspike	20.0	7.5	-0.4	27.2	1.49	1.68e-12
1	aspike	30.0	7.5	-0.8	27.5	0.822	9.85e-12
2	aspike	40.0	7.5	-1.7	27.4	0.426	1.30e-10

Permeability and Specific Storage for File W17450-7448-Permeability							
Event	Type	Conf	Pore Top	Diff	Temp	Perm	Storage
		MPa	MPa	MPa	°C	μD	m^{-1}
0	aspike	19.9	7.5	-0.4	26.6	0.767	4.61e-07
1	aspike	29.9	7.5	-0.8	27.1	1.46	1.26e-06
2	aspike	40.0	7.5	-1.3	28.0	0.449	1.57e-10

Permeability and Specific Storage for File W17450-7451-Permeability							
Event	Type	Conf	Pore Top	Diff	Temp	Perm	Storage
		MPa	MPa	MPa	°C	μD	m^{-1}
0	aspike	19.9	7.4	-1.3	22.8	72.5	6.90e-10
1	aspike	30.0	7.5	-1.3	22.8	96.9	1.55e-10
2	aspike	40.1	7.4	-2.1	23.8	69.	4.33e-09

Permeability and Specific Storage for File w17450-7321-permeability							
Event	Type	Conf	Pore Top	Diff	Temp	Perm	Storage
		MPa	MPa	MPa	°C	μD	m^{-1}
0	multipulse	20.6	7.4	-0.8	27.5	1.41	2.87e-10
1	multipulse	30.6	7.4	-1.3	27.3	1.18	1.07e-08
2	multipulse	40.6	7.4	-1.7	27.7	0.741	9.33e-08

Permeability and Specific Storage for File w17450-7326.5-permeability							
Event	Type	Conf	Pore Top	Diff	Temp	Perm	Storage
		MPa	MPa	MPa	°C	μD	m^{-1}
0	aspike	20.6	8.4	-0.8	24.0	5.21	2.54e-06
1	aspike	30.5	8.4	-1.3	24.6	213.	0.000112
2	aspike	40.6	8.4	-2.1	24.8	0.0231	3.59e-08
3	aspike	20.6	8.4	-0.8	25.5	16.6	0.000110
4	aspike	30.6	8.4	-1.3	26.1	0.0957	1.10e-05
5	aspike	40.6	8.4	-1.7	26.8	0.00292	7.34e-09

Permeability and Specific Storage for File w17450-7327-permeability							
Event	Type	Conf	Pore Top	Diff	Temp	Perm	Storage
		MPa	MPa	MPa	°C	μD	m^{-1}
0	aspike	20.6	7.9	-0.4	29.4	4.96	1.93e-07

Permeability and Specific Storage for File w17450-7328.8-1-permeability							
Event	Type	Conf	Pore Top	Diff	Temp	Perm	Storage
		MPa	MPa	MPa	°C	μD	m^{-1}
0	aspike	20.6	7.9	-0.4	22.9	23.2	6.12e-12
1	aspike	20.6	7.9	-0.4	22.9	18.1	3.01e-11

Permeability and Specific Storage for File w17450-7353-permeability							
Event	Type	Conf	Pore Top	Diff	Temp	Perm	Storage
		MPa	MPa	MPa	°C	μD	m^{-1}
0	multipulse	20.6	7.9	-0.8	25.5	0.244	5.50e-07
1	multipulse	30.6	7.9	-1.3	26.9	0.175	4.80e-07
2	multipulse	40.5	7.9	-2.1	27.7	0.134	4.33e-07
3	multipulse	50.6	7.9	-2.5	28.2	0.110	4.41e-07

Permeability and Specific Storage for File w17450-7401.9-permeability							
Event	Type	Conf	Pore Top	Diff	Temp	Perm	Storage
		MPa	MPa	MPa	°C	μD	m^{-1}
0	multipulse	30.5	7.9	-0.8	25.9	0.103	3.41e-07

Permeability and Specific Storage for File w17450-7402.8-permeability							
Event	Type	Conf	Pore Top	Diff	Temp	Perm	Storage
		MPa	MPa	MPa	°C	μD	m^{-1}
0	multipulse	30.5	7.9	-0.4	27.9	0.390	5.26e-05
1	multipulse	25.6	7.9	-0.4	28.0	0.0355	1.46e-06
2	multipulse	20.6	7.9	0.4	27.9	0.0220	4.82e-07
3	multipulse	15.5	7.9	0.4	27.9	0.0287	5.31e-07

Permeability and Specific Storage for File w17450-7403-permeability							
Event	Type	Conf	Pore Top	Diff	Temp	Perm	Storage
		MPa	MPa	MPa	°C	μD	m^{-1}
0	aspike	20.6	7.9	-0.4	26.7	0.412	3.22e-07
1	aspike	25.6	7.8	-0.8	27.0	1.57	2.95e-06
2	aspike	30.6	7.8	-0.8	27.7	0.267	3.03e-08

Permeability and Specific Storage for File w17450-7404-permeability							
Event	Type	Conf	Pore Top	Diff	Temp	Perm	Storage
		MPa	MPa	MPa	°C	μD	m^{-1}
0	multipulse	20.6	7.9	-0.4	25.1	0.108	1.21e-07
1	multipulse	25.6	7.9	-0.8	24.8	0.109	1.77e-07
2	multipulse	30.6	7.9	-0.8	25.3	0.0973	1.95e-07

Permeability and Specific Storage for File w17450-7404.3-permeability							
Event	Type	Conf	Pore Top	Diff	Temp	Perm	Storage
		MPa	MPa	MPa	°C	μD	m^{-1}
0	aspike	30.5	7.8	-1.3	26.9	10.8	1.46e-07
1	aspike	30.6	7.9	-0.8	26.9	15.6	1.89e-11
2	aspike	40.5	7.8	-2.1	27.2	18.6	4.06e-07
3	aspike	20.6	7.8	-0.8	26.2	18.0	7.41e-08

Permeability and Specific Storage for File w17450-7405.8-permeability							
Event	Type	Conf	Pore Top	Diff	Temp	Perm	Storage
		MPa	MPa	MPa	°C	μD	m^{-1}
0	multipulse	30.6	7.9	-1.3	23.8	0.0460	3.71e-07
1	multipulse	25.7	7.9	-0.8	24.3	0.0559	3.74e-07

Permeability and Specific Storage for File w17450-7406-permeability							
Event	Type	Conf	Pore Top	Diff	Temp	Perm	Storage
		MPa	MPa	MPa	°C	μD	m^{-1}
0	multipulse	20.6	7.9	0.0	26.8	0.110	9.41e-12
1	multipulse	25.6	7.9	-0.4	27.0	0.102	6.21e-12
2	multipulse	30.6	7.9	0.0	27.2	0.0891	2.25e-08
3	multipulse	15.5	7.9	0.0	27.2	0.120	3.15e-11

Permeability and Specific Storage for File w17450-7408.3-permeabiliy							
Event	Type	Conf	Pore Top	Diff	Temp	Perm	Storage
		MPa	MPa	MPa	°C	μD	m^{-1}
0	multipulse	30.5	7.9	-1.7	27.1	0.0438	1.58e-06

Permeability and Specific Storage for File w17450-7410-permeability							
Event	Type	Conf	Pore Top	Diff	Temp	Perm	Storage
		MPa	MPa	MPa	°C	μD	m^{-1}
0	multipulse	30.5	7.9	-1.7	26.2	0.0724	6.68e-07
1	multipulse	25.6	7.9	-0.8	26.5	0.0929	6.38e-07

Permeability and Specific Storage for File w17450-7449-permeability							
Event	Type	Conf	Pore Top	Diff	Temp	Perm	Storage
		MPa	MPa	MPa	°C	μD	m^{-1}
0	aspike	30.5	7.8	-1.3	26.3	2.25	4.00e-07
1	aspike	25.6	7.8	-0.4	26.2	3.07	6.92e-07

A.7.2 Sonic Velocity, Dynamic Moduli and Poisson's Ratio

Observed Velocities and Moduli for File Middle_Bakken-W86-7355V2-Velcity									
Event	Conf	Pore	Diff	Temp	V_p	$V_s^{(1)}$	$V_s^{(2)}$	Young's Modulus	Poisson's Ratio
	MPa	MPa	MPa	°C	m/s	m/s	m/s	GPa	
0	2.3	3.5	-2.1	22.1	3809	2621	2632	36.83	0.047
1	4.3	3.5	-1.9	22.2	3884	2670	2654	38.20	0.057
2	6.3	3.5	-2.1	22.3	3976	2688	2684	39.75	0.080
3	8.2	3.5	-2.5	22.4	3994	2728	2715	40.29	0.067
4	10.3	3.5	-2.2	22.5	4140	2747	2742	42.56	0.108
5	12.3	3.5	-2.7	22.6	4202	2781	2770	43.73	0.113
6	14.3	3.5	-2.7	22.7	4289	2801	2801	45.14	0.128
7	16.4	3.5	-2.5	22.7	4389	2826	2823	46.65	0.147
8	18.3	3.5	-2.9	22.8	4417	2846	2846	47.30	0.145
9	20.4	3.5	-2.5	22.9	4475	2874	2860	48.29	0.152
10	22.3	3.5	-2.9	22.9	4559	2885	2888	49.52	0.165
11	24.3	3.5	-3.1	23.0	4603	2903	2897	50.22	0.171
12	26.3	3.5	-2.9	23.0	4618	2908	2911	50.55	0.171
13	28.4	3.5	-2.9	23.0	4651	2927	2926	51.20	0.172
14	30.3	3.5	-3.4	23.0	4673	2950	2940	51.78	0.171

Observed Velocities and Moduli for File Middle_Bakken-W86-7369H-Velocity									
Event	Conf	Pore	Diff	Temp	V_p	$V_s^{(1)}$	$V_s^{(2)}$	Young's Modulus	Poisson's Ratio
	MPa	MPa	MPa	°C	m/s	m/s	m/s	GPa	
0	2.3	3.5	-2.1	20.7	4039	2541	2546	40.01	0.171
1	4.2	3.5	-2.1	21.6	4134	2568	2580	41.40	0.183
2	6.3	3.5	-1.9	21.2	4200	2615	2611	42.69	0.184
3	8.2	3.5	-2.1	21.1	4252	2641	2645	43.71	0.185
4	10.3	3.5	-2.5	21.6	4349	2673	2673	45.14	0.196
5	12.3	3.5	-2.2	21.2	4405	2703	2705	46.24	0.198
6	14.3	3.5	-2.4	21.5	4471	2733	2730	47.36	0.202
7	16.3	3.5	-2.7	21.8	4554	2764	2758	48.68	0.209
8	18.3	3.5	-2.5	22.2	4589	2786	2781	49.46	0.209
9	20.3	3.5	-2.9	22.6	4640	2818	2809	50.54	0.209
10	22.3	3.5	-3.1	23.0	4698	2837	2830	51.47	0.214
11	24.3	3.5	-3.2	23.2	4762	2851	2849	52.36	0.221
12	26.3	3.5	-3.4	23.3	4790	2877	2869	53.13	0.219
13	28.3	3.5	-3.2	23.4	4863	2893	2885	54.08	0.227
14	30.3	3.5	-3.5	23.4	4880	2909	2901	54.61	0.226
15	2.3	3.5	-1.7	20.4	4703	3018	2997	55.12	0.154
16	4.2	3.5	-2.2	21.8	4730	3021	3010	55.58	0.158
17	6.3	3.5	-2.5	21.2	4735	3036	3021	55.88	0.154
18	8.3	3.5	-2.4	21.0	4762	3050	3027	56.38	0.157

Observed Velocities and Moduli for File Middle_Bakken-W86-7370H90-Velocity									
Event	Conf	Pore	Diff	Temp	V_p	$V_s^{(1)}$	$V_s^{(2)}$	Young's Modulus	Poisson's Ratio
	MPa	MPa	MPa	°C	m/s	m/s	m/s	GPa	
0	2.4	3.5	-1.9	21.2	4549	2672	2731	47.48	0.228
1	4.3	3.5	-1.9	21.5	4558	2720	2758	48.41	0.217
2	6.3	3.5	-2.5	21.5	4659	2773	2781	50.05	0.224
3	8.3	3.5	-2.5	21.9	4754	2807	2804	51.43	0.233
4	10.4	3.5	-2.2	21.9	4805	2844	2832	52.60	0.232
5	12.4	3.5	-2.5	22.0	4895	2860	2856	53.74	0.241
6	14.3	3.5	-2.5	22.3	4950	2884	2892	54.90	0.242
7	16.3	3.5	-2.9	22.3	5011	2903	2909	55.80	0.247
8	18.3	3.5	-3.2	22.6	5069	2917	2945	56.86	0.249
9	20.4	3.5	-2.8	22.6	5121	2932	2965	57.69	0.252
10	22.3	3.5	-3.4	22.6	5181	2957	2981	58.66	0.256
11	24.4	3.5	-2.9	22.9	5248	2977	3003	59.69	0.260
12	26.3	3.5	-3.2	22.9	5255	2991	3019	60.16	0.257
13	28.3	3.5	-3.4	22.9	5318	3008	3028	60.94	0.262
14	30.3	3.5	-3.7	23.1	5350	3018	3034	61.38	0.265

Observed Velocities and Moduli for File Middle_Bakken-W86-7373H90-Velocity									
Event	Conf	Pore	Diff	Temp	V_p	$V_s^{(1)}$	$V_s^{(2)}$	Young's Modulus	Poisson's Ratio
	MPa	MPa	MPa	°C	m/s	m/s	m/s	GPa	
0	2.4	3.5	-1.7	21.3	4133	2734	2722	42.45	0.114
1	4.3	3.5	-2.1	21.5	4165	2759	2741	43.12	0.114
2	6.3	3.5	-2.1	21.8	4226	2773	2755	44.05	0.126
3	8.3	3.5	-2.1	22.0	4277	2795	2773	44.94	0.132
4	10.3	3.5	-1.8	22.2	4324	2813	2796	45.78	0.137
5	12.3	3.5	-2.4	22.4	4372	2834	2811	46.61	0.143
6	14.3	3.5	-2.5	22.6	4417	2851	2829	47.39	0.148
7	16.4	3.5	-2.1	22.8	4458	2873	2852	48.21	0.149
8	18.3	3.5	-2.8	22.9	4476	2888	2867	48.66	0.148
9	20.4	3.5	-2.9	23.0	4537	2909	2882	49.64	0.156
10	22.4	3.5	-2.5	23.2	4580	2924	2897	50.37	0.161
11	24.5	3.5	-2.5	23.2	4595	2942	2907	50.78	0.160
12	26.4	3.5	-2.9	23.3	4634	2956	2925	51.48	0.163
13	28.4	3.5	-2.9	23.4	4674	2969	2937	52.14	0.168
14	30.3	3.5	-3.4	23.5	4694	2983	2949	52.59	0.168

Observed Velocities and Moduli for File Middle_Bakken-W86-7374V-velocity									
Event	Conf	Pore	Diff	Temp	V_p	$V_s^{(1)}$	$V_s^{(2)}$	Young's Modulus	Poisson's Ratio
	MPa	MPa	MPa	°C	m/s	m/s	m/s	GPa	
0	2.4	3.5	-1.7	22.2	5830	2498	2489	43.67	0.388
1	4.3	3.5	-1.7	22.4	3563	2523	2530	32.12	-0.006
2	6.3	3.5	-2.4	22.5	3665	2554	2553	33.93	0.028
3	8.3	3.5	-2.1	22.7	3705	2586	2580	34.68	0.027
4	10.3	3.5	-2.5	22.8	3803	2622	2611	36.39	0.051
5	12.3	3.5	-2.5	22.9	3855	2669	2646	37.42	0.047
6	14.3	3.5	-2.5	23.0	3944	2707	2678	39.01	0.064
7	16.3	3.5	-2.5	23.1	4009	2735	2710	40.21	0.072
8	18.3	3.5	-2.4	23.3	4084	2747	2749	41.51	0.086
9	20.4	3.5	-2.9	23.3	4191	2779	2775	43.26	0.109
10	22.3	3.5	-2.9	23.4	4212	2799	2799	43.79	0.105
11	24.4	3.5	-2.9	23.5	4278	2828	2822	44.96	0.113
12	26.4	3.5	-2.5	23.6	4345	2843	2843	46.04	0.126
13	28.3	3.5	-3.2	24.2	4391	2867	2859	46.88	0.130
14	30.3	3.5	-3.4	24.2	4443	2881	2871	47.69	0.139

Observed Velocities and Moduli for File Middle_Bakken-W86-7380H90-velocity									
Event	Conf	Pore	Diff	Temp	V_p	$V_s^{(1)}$	$V_s^{(2)}$	Young's Modulus	Poisson's Ratio
	MPa	MPa	MPa	°C	m/s	m/s	m/s	GPa	
0	2.3	3.5	-2.1	22.6	4310	2804	2791	45.34	0.136
1	4.2	3.5	-2.1	22.6	4345	2821	2807	45.99	0.139
2	6.3	3.5	-1.7	22.8	4394	2841	2832	46.89	0.143
3	8.2	3.5	-2.5	22.9	4435	2860	2847	47.62	0.147
4	10.3	3.5	-2.1	23.2	4486	2880	2861	48.47	0.153
5	12.3	3.5	-2.1	23.2	4553	2897	2878	49.48	0.164
6	14.3	3.5	-2.1	23.3	4582	2923	2895	50.17	0.162
7	16.3	3.5	-2.9	23.3	4617	2939	2907	50.79	0.166
8	18.3	3.5	-2.5	23.4	4647	2960	2927	51.48	0.165
9	20.4	3.5	-2.5	23.4	4693	2964	2940	52.12	0.173
10	22.3	3.5	-2.5	23.5	4726	2978	2945	52.63	0.177
11	24.4	3.5	-2.7	23.5	4735	2996	2962	53.06	0.172
12	26.3	3.5	-3.1	23.5	4772	3005	2970	53.61	0.178
13	28.4	3.5	-2.9	23.6	4809	3014	2978	54.15	0.183
14	30.3	3.5	-3.1	23.6	4809	3020	2984	54.27	0.181

Observed Velocities and Moduli for File Middle_Bakken-W86-7389H0-velocity									
Event	Conf	Pore	Diff	Temp	V_p	$V_s^{(1)}$	$V_s^{(2)}$	Young's Modulus	Poisson's Ratio
	MPa	MPa	MPa	°C	m/s	m/s	m/s	GPa	
0	2.3	3.5	-1.8	24.6	4589	2945	2965	51.43	0.146
1	4.2	3.5	-2.1	24.6	4605	2967	2991	52.01	0.140
2	6.3	3.5	-2.2	24.7	4642	2980	2998	52.62	0.146
3	8.2	3.5	-2.5	24.8	4648	2994	3012	52.92	0.142
4	10.2	3.5	-2.5	24.8	4686	3003	3022	53.54	0.148
5	12.3	3.5	-2.1	24.9	4681	3007	3033	53.61	0.143
6	14.2	3.5	-2.5	24.9	4719	3021	3039	54.23	0.149
7	16.3	3.5	-2.8	25.0	4759	3033	3046	54.87	0.156
8	18.3	3.5	-2.5	25.0	4776	3040	3059	55.25	0.156
9	20.4	3.5	-2.7	25.0	4799	3046	3065	55.62	0.159
10	22.3	3.5	-2.9	25.0	4822	3053	3075	56.04	0.161
11	24.3	3.5	-3.4	25.0	4840	3058	3084	56.38	0.163
12	26.3	3.5	-3.4	25.0	4864	3068	3082	56.72	0.167
13	28.3	3.5	-3.1	25.0	4893	3079	3096	57.29	0.169
14	30.3	3.5	-3.2	25.1	4926	3087	3107	57.84	0.173

Observed Velocities and Moduli for File Middle_bakken-W86-7350H-Velocity									
Event	Conf	Pore	Diff	Temp	V_p	$V_s^{(1)}$	$V_s^{(2)}$	Young's Modulus	Poisson's Ratio
	MPa	MPa	MPa	°C	m/s	m/s	m/s	GPa	
0	2.3	3.5	-1.9	24.4	4329	2753	2776	45.22	0.156
1	4.3	3.5	-1.9	24.5	4389	2767	2794	46.11	0.165
2	6.3	3.5	-1.7	23.8	4442	2818	2813	47.25	0.164
3	8.3	3.5	-1.9	22.6	4490	2840	2831	48.09	0.168
4	10.3	3.5	-2.5	22.6	4562	2855	2854	49.16	0.178
5	12.3	3.5	-2.5	22.7	4616	2876	2879	50.12	0.182
6	14.3	3.5	-2.5	23.3	4644	2897	2894	50.74	0.182
7	16.3	3.5	-2.4	23.3	4695	2913	2913	51.57	0.187
8	18.3	3.5	-2.8	22.9	4730	2932	2931	52.28	0.188
9	20.3	3.5	-2.9	23.0	4752	2941	2943	52.70	0.189
10	22.3	3.5	-2.8	22.9	4783	2958	2954	53.28	0.191
11	24.4	3.5	-2.9	23.0	4802	2976	2968	53.80	0.190
12	26.3	3.5	-3.1	23.0	4822	2987	2976	54.19	0.191
13	28.3	3.5	-3.4	23.0	4838	2990	2987	54.48	0.192
14	30.3	3.5	-3.4	23.6	4873	3012	2998	55.17	0.193
15	2.3	3.5	-1.9	24.0	3801	2500	2525	35.94	0.112
16	4.2	3.5	-2.1	24.1	3875	2513	2551	37.01	0.127
17	6.3	3.5	-1.9	24.2	3921	2540	2577	37.85	0.129
18	8.2	3.5	-2.1	24.2	3986	2584	2602	39.01	0.133

Observed Velocities and Moduli for File Middle_bakken-W86-7355.9H-velocity									
Event	Conf	Pore	Diff	Temp	V_p	$V_s^{(1)}$	$V_s^{(2)}$	Young's Modulus	Poisson's Ratio
	MPa	MPa	MPa	°C	m/s	m/s	m/s	GPa	
0	2.3	3.5	-2.1	23.7	3933	2582	2615	37.87	0.113
1	4.3	3.5	-1.7	23.8	3999	2606	2640	38.92	0.122
2	6.3	3.5	-2.2	23.9	4063	2637	2675	40.07	0.127
3	8.2	3.5	-2.4	23.9	4137	2682	2712	41.44	0.130
4	10.3	3.5	-2.1	24.1	4197	2720	2749	42.63	0.131
5	12.3	3.5	-2.7	24.1	4276	2766	2788	44.13	0.135
6	14.3	3.5	-2.2	24.2	4337	2791	2822	45.25	0.140
7	16.3	3.5	-2.5	24.2	4390	2818	2858	46.32	0.141
8	18.3	3.5	-2.5	24.3	4449	2837	2886	47.34	0.147
9	20.4	3.5	-2.9	24.9	4514	2867	2912	48.51	0.153
10	22.3	3.5	-2.7	24.5	4561	2880	2927	49.26	0.159
11	24.4	3.5	-2.7	24.5	4606	2895	2948	50.05	0.163
12	26.3	3.5	-2.9	24.6	4641	2912	2960	50.67	0.166
13	28.3	3.5	-3.4	24.5	4666	2912	2982	51.13	0.168
14	30.3	3.5	-3.4	24.6	4690	2926	2993	51.61	0.169

Observed Velocities and Moduli for File Middle_bakken-W86-7355V-Velocity									
Event	Conf	Pore	Diff	Temp	V_p	$V_s^{(1)}$	$V_s^{(2)}$	Young's Modulus	Poisson's Ratio
	MPa	MPa	MPa	°C	m/s	m/s	m/s	GPa	
0	2.3	3.5	-1.7	24.3	3448	2472	2479	29.66	-0.032
1	4.3	3.5	-1.7	24.4	3487	2496	2513	30.33	-0.033
2	6.3	3.5	-1.8	24.5	3520	2527	2536	30.90	-0.036
3	8.2	3.5	-2.1	24.6	3595	2559	2568	32.29	-0.017
4	10.3	3.5	-2.4	24.6	3680	2602	2601	33.86	0.001
5	12.3	3.5	-2.4	24.7	3758	2630	2633	35.28	0.019
6	14.3	3.5	-2.5	24.7	3848	2652	2666	36.87	0.043
7	16.4	3.5	-2.4	24.8	3911	2689	2696	38.04	0.050
8	18.3	3.5	-2.5	24.8	3980	2720	2724	39.29	0.061
9	20.4	3.5	-2.5	24.9	4095	2748	2753	41.19	0.089
10	22.3	3.5	-2.9	24.9	4125	2772	2780	41.85	0.086
11	24.3	3.5	-3.1	24.9	4172	2795	2799	42.71	0.092
12	26.3	3.5	-2.7	24.9	4273	2816	2818	44.27	0.116
13	28.3	3.5	-3.2	24.9	4314	2839	2842	45.08	0.117
14	30.3	3.5	-3.4	24.9	4328	2852	2858	45.43	0.115

Observed Velocities and Moduli for File Middle_bakken-W86-7363V-velocity									
Event	Conf	Pore	Diff	Temp	V_p	$V_s^{(1)}$	$V_s^{(2)}$	Young's Modulus	Poisson's Ratio
	MPa	MPa	MPa	°C	m/s	m/s	m/s	GPa	
0	2.3	3.5	-1.9	19.8	2549	1893	1888	15.88	-0.111
1	4.3	3.5	-1.8	20.9	2683	1981	1981	17.67	-0.099
2	6.3	3.5	-2.2	20.5	2825	2067	2066	19.74	-0.075
3	8.3	3.5	-2.1	20.5	2995	2151	2153	22.38	-0.034
4	10.3	3.5	-2.2	20.7	3122	2238	2236	24.33	-0.028
5	12.4	3.5	-2.5	21.4	3278	2309	2324	26.86	0.001
6	14.3	3.5	-2.8	21.2	3415	2387	2398	29.14	0.018
7	16.3	3.5	-2.7	21.3	3526	2460	2465	31.05	0.024
8	18.3	3.5	-2.8	21.4	3656	2520	2531	33.28	0.044
9	20.3	3.5	-2.9	21.5	3775	2576	2588	35.35	0.060
10	22.3	3.5	-2.9	21.7	3881	2638	2646	37.28	0.068
11	24.4	3.5	-2.8	22.4	3999	2688	2689	39.31	0.088
12	26.3	3.5	-3.4	22.5	4062	2726	2731	40.53	0.089
13	28.3	3.5	-3.4	22.5	4151	2763	2774	42.13	0.099
14	30.3	3.5	-3.1	22.2	4224	2797	2805	43.45	0.108

Observed Velocities and Moduli for File Middle_bakken-W86-7374H0-Velocity									
Event	Conf	Pore	Diff	Temp	V_p	$V_s^{(1)}$	$V_s^{(2)}$	Young's Modulus	Poisson's Ratio
	MPa	MPa	MPa	°C	m/s	m/s	m/s	GPa	
0	2.3	3.5	-2.1	24.1	4486	2623	2792	45.19	0.214
1	4.2	3.5	-2.1	24.3	4272	2641	2811	43.66	0.157
2	6.2	3.5	-2.5	24.4	4361	2669	2842	45.04	0.168
3	8.2	3.5	-2.1	24.0	4401	2685	2860	45.73	0.171
4	10.3	3.5	-2.1	24.1	4419	2716	2876	46.31	0.166
5	12.2	3.5	-2.5	24.2	4451	2733	2898	46.97	0.166
6	14.2	3.5	-2.7	24.2	4498	2761	2911	47.81	0.170
7	16.2	3.5	-2.8	24.3	4541	2781	2929	48.58	0.173
8	18.2	3.5	-2.5	24.3	4565	2806	2941	49.16	0.172
9	20.3	3.5	-3.1	24.4	4599	2828	2951	49.79	0.174
10	22.3	3.5	-2.9	24.4	4654	2841	2970	50.63	0.181
11	24.3	3.5	-3.2	24.4	4689	2864	2986	51.35	0.181
12	26.3	3.5	-3.4	24.4	4710	2880	2991	51.76	0.182
13	28.3	3.5	-3.1	24.5	4731	2889	3006	52.20	0.183
14	30.2	3.5	-3.4	24.5	4736	2901	3017	52.48	0.180

Observed Velocities and Moduli for File Middle_bakken-W86-7379V-Velocity									
Event	Conf	Pore	Diff	Temp	V_p	$V_s^{(1)}$	$V_s^{(2)}$	Young's Modulus	Poisson's Ratio
	MPa	MPa	MPa	°C	m/s	m/s	m/s	GPa	
0	2.4	3.5	-1.7	24.4	3795	2702	2698	36.71	-0.013
1	4.3	3.5	-1.7	24.5	3828	2723	2723	37.36	-0.012
2	6.3	3.5	-2.1	24.6	3859	2740	2744	37.97	-0.010
3	8.2	3.5	-2.1	24.7	3913	2755	2758	39.04	0.007
4	10.3	3.5	-2.1	24.9	3944	2769	2771	39.65	0.013
5	12.3	3.5	-2.5	25.0	3996	2783	2791	40.66	0.026
6	14.3	3.5	-2.5	25.0	4038	2803	2805	41.48	0.034
7	16.3	3.5	-2.9	25.1	4072	2821	2822	42.15	0.038
8	18.3	3.5	-2.9	25.1	4132	2838	2840	43.28	0.053
9	20.4	3.5	-2.5	25.1	4195	2853	2855	44.41	0.069
10	22.3	3.5	-2.5	25.1	4222	2875	2870	44.99	0.069
11	24.4	3.5	-2.8	25.2	4278	2890	2885	45.99	0.082
12	26.3	3.5	-2.9	25.2	4328	2904	2894	46.85	0.093
13	28.3	3.5	-3.4	25.2	4365	2916	2915	47.57	0.097
14	30.2	3.5	-3.4	25.2	4360	2929	2925	47.62	0.090

Observed Velocities and Moduli for File Middle_bakken-W86-7393.1H90-Velocity									
Event	Conf	Pore	Diff	Temp	V_p	$V_s^{(1)}$	$V_s^{(2)}$	Young's Modulus	Poisson's Ratio
	MPa	MPa	MPa	°C	m/s	m/s	m/s	GPa	
0	2.3	3.5	-1.8	21.5	4658	2941	2923	51.58	0.172
1	4.3	3.5	-1.9	21.6	4641	2967	2937	51.77	0.160
2	6.3	3.5	-1.7	21.7	4728	2969	2946	52.78	0.179
3	8.2	3.5	-2.1	21.8	4707	2979	2951	52.71	0.171
4	10.3	3.5	-2.2	21.9	4740	2997	2962	53.33	0.173
5	12.4	3.5	-2.1	21.9	4763	3004	2975	53.77	0.175
6	14.3	3.5	-2.4	22.0	4738	3011	2985	53.66	0.166
7	16.3	3.5	-2.5	22.1	4794	3023	2984	54.36	0.177
8	18.3	3.5	-2.4	22.1	4889	3034	3001	55.59	0.192
9	20.4	3.5	-2.4	22.1	4836	3050	3010	55.32	0.177
10	22.3	3.5	-2.5	22.1	4939	3052	3026	56.52	0.195
11	24.4	3.5	-2.7	22.2	4966	3066	3026	56.93	0.198
12	26.3	3.5	-3.2	22.1	4868	3074	3035	56.14	0.175
13	28.4	3.5	-2.9	22.2	4966	3083	3041	57.28	0.193
14	30.3	3.5	-3.4	22.2	4936	3097	3039	57.12	0.185

Observed Velocities and Moduli for File Middle_bakken-W86-7393.5V-Velocity									
Event	Conf	Pore	Diff	Temp	V_p	$V_s^{(1)}$	$V_s^{(2)}$	Young's Modulus	Poisson's Ratio
	MPa	MPa	MPa	°C	m/s	m/s	m/s	GPa	
0	2.3	3.5	-1.7	21.7	3971	2773	2771	40.47	0.025
1	4.3	3.5	-1.7	22.1	4053	2791	2789	42.00	0.050
2	6.3	3.5	-2.1	22.9	4086	2801	2809	42.64	0.054
3	8.3	3.5	-2.1	23.4	4138	2823	2831	43.64	0.062
4	10.3	3.5	-2.1	23.7	4181	2833	2847	44.43	0.072
5	12.3	3.5	-2.2	23.8	4225	2842	2853	45.17	0.084
6	14.2	3.5	-2.5	23.8	4249	2857	2868	45.68	0.084
7	16.3	3.5	-2.2	24.0	4272	2876	2878	46.16	0.085
8	18.3	3.5	-2.5	24.1	4333	2893	2899	47.26	0.096
9	20.3	3.5	-2.9	24.1	4366	2901	2910	47.84	0.103
10	22.3	3.5	-2.7	24.2	4425	2921	2925	48.88	0.113
11	24.3	3.5	-3.1	24.1	4435	2931	2940	49.17	0.110
12	26.3	3.5	-2.9	24.2	4455	2947	2949	49.61	0.111
13	28.4	3.5	-2.9	24.2	4516	2953	2964	50.57	0.124
14	30.3	3.5	-2.9	24.2	4537	2967	2969	50.98	0.126

Observed Velocities and Moduli for File Middle_bakken-W86-7397V-velocity									
Event	Conf	Pore	Diff	Temp	V_p	$V_s^{(1)}$	$V_s^{(2)}$	Young's Modulus	Poisson's Ratio
	MPa	MPa	MPa	°C	m/s	m/s	m/s	GPa	
0	2.3	3.5	-2.1	24.6	4066	2781	2764	41.77	0.066
1	4.3	3.5	-1.9	24.6	4056	2796	2792	41.74	0.048
2	6.3	3.5	-2.1	24.7	4098	2800	2810	42.50	0.059
3	8.2	3.5	-2.5	24.7	4114	2822	2823	42.88	0.055
4	10.3	3.5	-2.1	24.8	4174	2834	2839	43.95	0.071
5	12.3	3.5	-2.5	24.8	4211	2853	2840	44.60	0.079
6	14.2	3.5	-2.7	24.9	4245	2872	2868	45.33	0.079
7	16.3	3.5	-2.5	25.0	4292	2891	2884	46.20	0.087
8	18.2	3.5	-2.9	25.0	4353	2892	2890	47.12	0.105
9	20.4	3.5	-2.5	25.0	4389	2913	2913	47.88	0.106
10	22.4	3.5	-2.5	25.0	4411	2933	2925	48.38	0.106
11	24.3	3.5	-3.2	25.0	4443	2948	2931	48.95	0.111
12	26.3	3.5	-3.2	25.0	4504	2952	2953	49.94	0.123
13	28.4	3.5	-2.9	25.1	4519	2960	2959	50.23	0.125
14	30.3	3.5	-3.2	25.0	4557	2972	2978	50.94	0.129

Observed Velocities and Moduli for File Middle_bakken-W86-7403.8V-velocity									
Event	Conf	Pore	Diff	Temp	V_p	$V_s^{(1)}$	$V_s^{(2)}$	Young's Modulus	Poisson's Ratio
	MPa	MPa	MPa	°C	m/s	m/s	m/s	GPa	
0	2.3	3.5	-1.7	20.8	4649	2971	2979	53.89	0.153
1	4.3	3.5	-1.8	20.9	4686	2985	2992	54.57	0.157
2	6.3	3.5	-2.1	21.0	4697	3005	3009	55.03	0.153
3	8.3	3.5	-2.1	21.1	4699	3006	3017	55.14	0.151
4	10.3	3.5	-2.1	21.2	4746	3010	3029	55.84	0.160
5	12.3	3.5	-2.5	21.3	4740	3025	3033	55.95	0.155
6	14.3	3.5	-2.7	21.3	4779	3029	3040	56.51	0.162
7	16.4	3.5	-2.4	21.4	4796	3036	3047	56.84	0.164
8	18.3	3.5	-2.5	21.4	4813	3044	3059	57.22	0.164
9	20.4	3.5	-2.5	21.5	4824	3055	3063	57.50	0.164
10	22.3	3.5	-2.5	21.5	4864	3054	3064	57.95	0.173
11	24.3	3.5	-3.1	21.4	4881	3061	3072	58.29	0.174
12	26.3	3.5	-2.9	21.5	4835	3070	3074	57.88	0.162
13	28.3	3.5	-2.9	21.5	4916	3072	3083	58.90	0.178
14	30.3	3.5	-3.2	21.5	4939	3077	3088	59.25	0.181

Observed Velocities and Moduli for File W17450-7326.5-Velocity									
Event	Conf	Pore	Diff	Temp	V_p	$V_s^{(1)}$	$V_s^{(2)}$	Young's Modulus	Poisson's Ratio
	MPa	MPa	MPa	°C	m/s	m/s	m/s	GPa	
0	10.0	-0.2	0.3	30.9	5871	2920	2960	61.28	0.333
1	20.1	-0.2	-0.1	31.1	6163	3200	3186	71.41	0.317
2	30.1	-0.2	-0.4	31.1	6221	3215	3217	72.50	0.318
3	40.1	-0.2	-1.0	31.1	6052	3200	3248	71.99	0.302
4	50.1	-0.2	-1.4	31.3	6107	3262	3248	73.37	0.302

Observed Velocities and Moduli for File W17450-7332-Velocity									
Event	Conf	Pore	Diff	Temp	V_p	$V_s^{(1)}$	$V_s^{(2)}$	Young's Modulus	Poisson's Ratio
	MPa	MPa	MPa	°C	m/s	m/s	m/s	GPa	
0	9.9	-0.2	0.0	27.8	6274	3500	3659	83.54	0.259
1	20.1	-0.2	-0.1	27.7	6414	3633	3731	88.08	0.254
2	30.2	-0.2	-0.7	28.2	6414	3704	3731	89.27	0.247
3	40.0	-0.2	-1.6	28.4	6343	3752	3707	89.04	0.236
4	50.1	-0.2	-1.7	28.8	6343	3802	3780	90.98	0.222

Observed Velocities and Moduli for File W17450-7354-Velocity									
Event	Conf	Pore	Diff	Temp	V_p	$V_s^{(1)}$	$V_s^{(2)}$	Young's Modulus	Poisson's Ratio
	MPa	MPa	MPa	°C	m/s	m/s	m/s	GPa	
0	10.0	-0.2	0.3	29.9	5104	3065	3282	62.05	0.185
1	20.0	-0.2	-0.4	30.1	5020	3144	3282	61.90	0.153
2	30.0	-0.2	-0.8	30.3	5281	3128	3264	64.32	0.211
3	40.1	-0.2	-1.3	30.6	5236	3160	3317	64.91	0.190
4	50.1	-0.2	-2.0	30.6	5281	3160	3299	65.15	0.201

Observed Velocities and Moduli for File W17450-7401.9-velocity									
Event	Conf	Pore	Diff	Temp	V_p	$V_s^{(1)}$	$V_s^{(2)}$	Young's Modulus	Poisson's Ratio
	MPa	MPa	MPa	°C	m/s	m/s	m/s	GPa	
0	10.2	-0.2	1.0	27.5	5161	3150	3109	63.01	0.209
1	20.0	-0.2	0.0	27.4	5318	3164	3137	64.93	0.230
2	30.1	-0.2	0.0	27.7	5400	3193	3166	66.40	0.235
3	40.0	-0.2	-0.4	27.8	5442	3222	3180	67.35	0.235
4	49.9	-0.2	-1.4	28.0	5528	3237	3224	68.88	0.241

Observed Velocities and Moduli for File W17450-7405-velocity									
Event	Conf	Pore	Diff	Temp	V_p	$V_s^{(1)}$	$V_s^{(2)}$	Young's Modulus	Poisson's Ratio
	MPa	MPa	MPa	°C	m/s	m/s	m/s	GPa	
0	10.1	-0.1	1.0	26.4	5114	3084	3115	60.43	0.210
1	19.9	-0.2	0.0	26.4	5037	3127	3144	60.51	0.184
2	29.9	-0.2	-0.4	26.8	5153	3172	3189	62.72	0.192
3	40.1	-0.2	-0.7	26.9	5153	3202	3250	63.73	0.178
4	49.9	-0.2	-1.3	27.4	5233	3202	3235	64.41	0.196

Observed Velocities and Moduli for File W17450-7405.8-velocity									
Event	Conf	Pore	Diff	Temp	V_p	$V_s^{(1)}$	$V_s^{(2)}$	Young's Modulus	Poisson's Ratio
	MPa	MPa	MPa	°C	m/s	m/s	m/s	GPa	
0	10.1	-0.1	0.9	28.6	4944	3065	2936	56.57	0.208
1	20.1	-0.2	0.4	28.4	5016	3121	3000	58.62	0.203
2	30.1	-0.2	-0.4	28.7	5166	3121	3013	60.06	0.228
3	40.0	-0.2	-0.7	29.5	5166	3149	3026	60.58	0.222
4	50.0	-0.2	-1.3	29.0	5285	3178	3094	62.81	0.228

Observed Velocities and Moduli for File W17450-7407.8-velocity									
Event	Conf	Pore	Diff	Temp	V_p	$V_s^{(1)}$	$V_s^{(2)}$	Young's Modulus	Poisson's Ratio
	MPa	MPa	MPa	°C	m/s	m/s	m/s	GPa	
0	10.0	-0.2	0.4	27.6	5320	2997	3153	62.36	0.249
1	20.1	-0.2	0.0	27.7	5367	3072	3153	63.77	0.247
2	30.1	-0.2	-0.4	27.5	5414	3072	3169	64.33	0.251
3	40.1	-0.2	-0.7	27.7	5462	3103	3186	65.37	0.252
4	50.0	-0.2	-1.6	27.9	5462	3167	3253	67.26	0.236

Observed Velocities and Moduli for File W17450-7408.3-Velocity									
Event	Conf	Pore	Diff	Temp	V_p	$V_s^{(1)}$	$V_s^{(2)}$	Young's Modulus	Poisson's Ratio
	MPa	MPa	MPa	°C	m/s	m/s	m/s	GPa	
0	10.1	-0.2	0.4	24.9	5193	3167	3073	61.87	0.218
1	20.0	-0.2	0.0	25.7	5238	3201	3073	62.69	0.220
2	30.0	-0.2	-0.8	26.2	5426	3218	3120	65.06	0.241
3	40.0	-0.2	-0.8	26.6	5378	3218	3120	64.69	0.234
4	50.0	-0.2	-1.4	26.8	5426	3253	3169	66.23	0.231

Observed Velocities and Moduli for File W17450-7451-velocity									
Event	Conf	Pore	Diff	Temp	V_p	$V_s^{(1)}$	$V_s^{(2)}$	Young's Modulus	Poisson's Ratio
	MPa	MPa	MPa	°C	m/s	m/s	m/s	GPa	
0	10.2	-0.1	0.9	27.3	4851	2701	2858	47.34	0.256
1	20.0	-0.2	-0.1	27.4	5163	2922	3048	54.31	0.249
2	30.1	-0.2	-0.6	28.1	5291	3046	3168	58.27	0.237
3	40.1	-0.2	-0.4	28.0	5424	3120	3232	61.00	0.239
4	50.1	-0.2	-1.3	28.6	5565	3214	3232	63.25	0.248

Observed Velocities and Moduli for File w17450-7313-vecolity									
Event	Conf	Pore	Diff	Temp	V_p	$V_s^{(1)}$	$V_s^{(2)}$	Young's Modulus	Poisson's Ratio
	MPa	MPa	MPa	°C	m/s	m/s	m/s	GPa	
0	50.6	-0.2	-3.8	30.9	5864	3356	3239	72.84	0.269
1	40.5	-0.2	-3.4	30.5	5928	3377	3259	73.93	0.272
2	30.5	-0.2	-2.9	30.1	5802	3356	3220	72.12	0.263
3	20.6	-0.2	-2.5	29.9	5864	3336	3239	72.52	0.271
4	10.5	-0.2	-1.9	29.5	5864	3296	3201	71.24	0.279

Observed Velocities and Moduli for File w17450-7320-velocity									
Event	Conf	Pore	Diff	Temp	V_p	$V_s^{(1)}$	$V_s^{(2)}$	Young's Modulus	Poisson's Ratio
	MPa	MPa	MPa	°C	m/s	m/s	m/s	GPa	
0	50.5	-0.2	-4.2	31.4	6463	3324	3308	77.88	0.321
1	40.5	-0.2	-3.8	30.7	6392	3344	3365	79.01	0.310
2	30.5	-0.2	-2.9	30.4	6392	3324	3346	78.27	0.313
3	20.5	-0.2	-2.9	30.1	6322	3344	3289	77.24	0.310
4	10.5	-0.2	-1.9	29.8	6187	3324	3289	76.19	0.300

Observed Velocities and Moduli for File w17450-7321-velocity									
Event	Conf	Pore	Diff	Temp	V_p	$V_s^{(1)}$	$V_s^{(2)}$	Young's Modulus	Poisson's Ratio
	MPa	MPa	MPa	°C	m/s	m/s	m/s	GPa	
0	50.6	-0.2	-3.8	29.5	6299	3290	3259	75.57	0.315
1	40.5	-0.2	-3.8	28.4	6182	3290	3244	74.73	0.306
2	30.5	-0.2	-3.2	28.2	6125	3290	3228	74.15	0.303
3	20.5	-0.2	-2.9	28.1	6182	3273	3259	74.69	0.306
4	10.5	-0.2	-2.5	27.9	6069	3290	3228	73.86	0.297

Observed Velocities and Moduli for File w17450-7321.2-velocity									
Event	Conf	Pore	Diff	Temp	V_p	$V_s^{(1)}$	$V_s^{(2)}$	Young's Modulus	Poisson's Ratio
	MPa	MPa	MPa	°C	m/s	m/s	m/s	GPa	
0	50.6	-0.2	-1.8	32.2	6232	3288	3216	74.14	0.313
1	40.5	-0.2	-1.7	31.6	6178	3303	3216	74.16	0.307
2	30.5	-0.2	-1.3	31.3	6125	3288	3201	73.36	0.305
3	20.5	-0.2	-0.6	31.1	6021	3273	3245	73.32	0.293
4	10.5	-0.2	-0.4	30.8	6178	3243	3187	72.54	0.314

Observed Velocities and Moduli for File w17450-7323.6-velocity									
Event	Conf	Pore	Diff	Temp	V_p	$V_s^{(1)}$	$V_s^{(2)}$	Young's Modulus	Poisson's Ratio
	MPa	MPa	MPa	°C	m/s	m/s	m/s	GPa	
0	50.6	-0.2	-1.8	29.1	5560	3118	3191	65.34	0.263
1	40.5	-0.2	-1.8	28.6	5650	3146	3162	65.88	0.274
2	30.4	-0.2	-1.6	28.2	5515	3118	3148	64.40	0.262
3	20.5	-0.2	-1.3	28.1	5605	3132	3177	65.62	0.268
4	10.5	-0.2	-0.1	28.0	5560	3118	3092	63.84	0.273

Observed Velocities and Moduli for File w17450-7327-velocity									
Event	Conf	Pore	Diff	Temp	V_p	$V_s^{(1)}$	$V_s^{(2)}$	Young's Modulus	Poisson's Ratio
	MPa	MPa	MPa	°C	m/s	m/s	m/s	GPa	
0	10.1	-0.2	-1.9	32.2	5994	3190	3234	71.27	0.299
1	20.1	-0.2	-2.1	32.4	6067	3190	3213	71.27	0.307
2	20.1	-0.2	-2.1	32.3	6226	3213	3215	72.45	0.318
3	30.1	-0.2	-2.5	32.5	6306	3234	3257	73.96	0.320
4	40.0	-0.2	-3.4	32.7	6306	3234	3257	73.96	0.320
5	50.2	-0.2	-3.7	32.9	6557	3255	3279	75.80	0.335

Observed Velocities and Moduli for File w17450-7328.8-1-velocity									
Event	Conf	Pore	Diff	Temp	V_p	$V_s^{(1)}$	$V_s^{(2)}$	Young's Modulus	Poisson's Ratio
	MPa	MPa	MPa	°C	m/s	m/s	m/s	GPa	
0	50.6	-0.2	-1.7	32.2	5706	3163	3108	67.14	0.284
1	40.5	-0.2	-1.7	31.6	5800	3163	3094	67.42	0.295
2	30.5	-0.2	-0.8	31.3	5706	3163	3081	66.70	0.286
3	20.5	-0.2	-1.0	31.0	5706	3134	3067	66.00	0.291
4	10.5	-0.2	-0.4	30.8	5356	3093	3027	62.65	0.258

Observed Velocities and Moduli for File w17450-7330-velocity									
Event	Conf	Pore	Diff	Temp	V_p	$V_s^{(1)}$	$V_s^{(2)}$	Young's Modulus	Poisson's Ratio
	MPa	MPa	MPa	°C	m/s	m/s	m/s	GPa	
0	50.6	-0.2	-3.8	31.9	5990	3156	3189	68.04	0.305
1	40.5	-0.2	-3.7	31.2	5775	3156	3189	66.94	0.284
2	30.5	-0.2	-2.9	30.9	5775	3110	3158	65.70	0.291
3	20.6	-0.2	-2.4	30.6	5624	3096	3127	64.16	0.279
4	10.5	-0.2	-2.1	30.2	5434	3051	3068	61.48	0.268

Observed Velocities and Moduli for File w17450-7348.8-velocity									
Event	Conf	Pore	Diff	Temp	V_p	$V_s^{(1)}$	$V_s^{(2)}$	Young's Modulus	Poisson's Ratio
	MPa	MPa	MPa	°C	m/s	m/s	m/s	GPa	
0	50.6	-0.2	-3.9	25.5	5326	3198	2994	61.81	0.245
1	40.5	-0.2	-3.8	25.3	5326	3198	2980	61.61	0.247
2	30.5	-0.2	-2.9	25.2	5369	3182	2967	61.50	0.256
3	20.5	-0.2	-3.1	25.8	5282	3182	2967	60.90	0.244
4	10.4	-0.2	-2.4	25.3	5117	3167	2789	57.14	0.244

Observed Velocities and Moduli for File w17450-7351-velocity									
Event	Conf	Pore	Diff	Temp	V_p	$V_s^{(1)}$	$V_s^{(2)}$	Young's Modulus	Poisson's Ratio
	MPa	MPa	MPa	°C	m/s	m/s	m/s	GPa	
0	50.6	-0.2	-1.8	30.8	5410	3043	3044	60.86	0.268
1	40.5	-0.2	-1.6	30.1	5454	3043	3030	60.91	0.275
2	30.5	-0.2	-0.8	29.8	5365	3071	3044	60.99	0.259
3	20.5	-0.2	-0.8	29.7	5322	3071	3030	60.51	0.255
4	10.5	-0.2	0.0	29.2	5410	3057	3044	61.07	0.267

Observed Velocities and Moduli for File w17450-7353-velocity									
Event	Conf	Pore	Diff	Temp	V_p	$V_s^{(1)}$	$V_s^{(2)}$	Young's Modulus	Poisson's Ratio
	MPa	MPa	MPa	°C	m/s	m/s	m/s	GPa	
0	50.5	-0.2	-1.7	31.6	5317	3224	3089	64.35	0.228
1	40.5	-0.2	-1.3	31.0	5406	3257	3104	65.73	0.235
2	30.5	-0.2	-1.1	30.7	5406	3209	3045	64.22	0.249
3	20.5	-0.2	-0.8	30.5	5274	3177	3045	62.78	0.233
4	10.5	-0.2	-0.4	30.4	5149	3177	2976	60.86	0.222

Observed Velocities and Moduli for File w17450-7354.5-velocity									
Event	Conf	Pore	Diff	Temp	V_p	$V_s^{(1)}$	$V_s^{(2)}$	Young's Modulus	Poisson's Ratio
	MPa	MPa	MPa	°C	m/s	m/s	m/s	GPa	
0	50.5	-0.2	-2.4	26.5	5318	3044	3075	60.03	0.253
1	40.5	-0.2	-1.7	26.0	5191	3073	3060	59.31	0.232
2	30.5	-0.2	-1.3	25.6	5110	3044	3060	58.31	0.223
3	20.5	-0.2	-0.8	25.3	5150	3002	3004	57.36	0.242
4	10.4	-0.2	-0.8	22.0	4808	2934	2923	52.92	0.205

Observed Velocities and Moduli for File w17450-7403-velocity									
Event	Conf	Pore	Diff	Temp	V_p	$V_s^{(1)}$	$V_s^{(2)}$	Young's Modulus	Poisson's Ratio
	MPa	MPa	MPa	°C	m/s	m/s	m/s	GPa	
0	9.9	-0.2	0.6	28.4	5068	3093	2950	57.90	0.224
1	20.0	-0.2	0.4	28.8	5027	3108	2992	58.24	0.209
2	30.1	-0.2	-0.4	29.1	5280	3154	3064	61.82	0.235
3	40.1	-0.2	-0.8	29.3	5068	3186	3079	60.53	0.191
4	50.0	-0.2	-1.4	29.5	5280	3186	3095	62.65	0.226

Observed Velocities and Moduli for File w17450-7404-velocity									
Event	Conf	Pore	Diff	Temp	V_p	$V_s^{(1)}$	$V_s^{(2)}$	Young's Modulus	Poisson's Ratio
	MPa	MPa	MPa	°C	m/s	m/s	m/s	GPa	
0	10.1	-0.2	0.7	27.4	4973	2896	3075	56.25	0.218
1	20.1	-0.2	0.3	28.5	5045	2969	3102	58.05	0.216
2	29.9	-0.2	-0.4	29.7	5118	2995	3157	59.66	0.217
3	40.0	-0.2	-0.8	30.2	5118	3020	3172	60.15	0.211
4	50.0	-0.2	-1.6	30.7	5232	3086	3172	61.95	0.222

Observed Velocities and Moduli for File w17450-7404.3-velocity									
Event	Conf	Pore	Diff	Temp	V_p	$V_s^{(1)}$	$V_s^{(2)}$	Young's Modulus	Poisson's Ratio
	MPa	MPa	MPa	°C	m/s	m/s	m/s	GPa	
0	10.1	-0.2	0.4	28.9	4814	3003	3018	55.34	0.179
1	20.0	-0.2	0.3	29.3	5149	3044	3046	59.13	0.231
2	30.0	-0.2	-0.4	29.6	5032	3115	3088	59.48	0.194
3	40.1	-0.2	-0.7	30.0	5149	3130	3117	61.09	0.209
4	50.0	-0.2	-1.1	30.3	5149	3175	3132	61.81	0.200

Observed Velocities and Moduli for File w17450-7406-velocity									
Event	Conf	Pore	Diff	Temp	V_p	$V_s^{(1)}$	$V_s^{(2)}$	Young's Modulus	Poisson's Ratio
	MPa	MPa	MPa	°C	m/s	m/s	m/s	GPa	
0	10.2	-0.2	0.7	27.2	5122	3108	3153	61.48	0.202
1	20.1	-0.2	0.4	28.5	5280	3166	3182	64.00	0.217
2	30.0	-0.2	-0.4	30.0	5321	3195	3212	65.13	0.216
3	40.1	-0.2	-0.8	30.5	5492	3225	3227	67.18	0.237
4	50.1	-0.2	-0.8	31.0	5363	3210	3258	66.29	0.214

Observed Velocities and Moduli for File w17450-7407-velocity									
Event	Conf	Pore	Diff	Temp	V_p	$V_s^{(1)}$	$V_s^{(2)}$	Young's Modulus	Poisson's Ratio
	MPa	MPa	MPa	°C	m/s	m/s	m/s	GPa	
0	10.3	-0.1	0.4	24.7	5037	3073	2935	58.10	0.224
1	20.2	-0.2	-0.4	25.6	5117	3133	3017	60.55	0.217
2	29.9	-0.2	-0.8	27.0	5158	3164	3032	61.48	0.218
3	40.0	-0.2	-1.3	27.3	5200	3195	3060	62.59	0.217
4	50.0	-0.2	-1.3	28.0	5242	3195	3120	63.73	0.215

Observed Velocities and Moduli for File w17450-7409-velocity									
Event	Conf	Pore	Diff	Temp	V_p	$V_s^{(1)}$	$V_s^{(2)}$	Young's Modulus	Poisson's Ratio
	MPa	MPa	MPa	°C	m/s	m/s	m/s	GPa	
0	10.5	-0.2	0.7	25.8	4988	3072	2992	57.48	0.207
1	20.5	-0.2	0.0	26.9	5063	3115	3033	59.13	0.208
2	30.5	-0.2	-0.1	27.6	5179	3115	3033	60.11	0.228
3	40.6	-0.2	-0.6	28.1	5140	3129	3046	60.13	0.218
4	50.5	-0.2	-1.4	28.2	5101	3144	3102	60.64	0.200

Observed Velocities and Moduli for File w17450-7409.8-velocity									
Event	Conf	Pore	Diff	Temp	V_p	$V_s^{(1)}$	$V_s^{(2)}$	Young's Modulus	Poisson's Ratio
	MPa	MPa	MPa	°C	m/s	m/s	m/s	GPa	
0	10.2	-0.2	0.9	27.3	5231	3102	2927	59.13	0.251
1	19.9	-0.2	0.0	28.4	5111	3146	2953	59.17	0.224
2	30.0	-0.2	0.0	29.8	5111	3161	2979	59.68	0.218
3	40.1	-0.2	-0.8	30.6	5272	3176	3006	61.51	0.238
4	50.2	-0.2	-0.8	31.2	5272	3206	3019	62.09	0.232

Observed Velocities and Moduli for File w17450-7410-velocity									
Event	Conf	Pore	Diff	Temp	V_p	$V_s^{(1)}$	$V_s^{(2)}$	Young's Modulus	Poisson's Ratio
	MPa	MPa	MPa	°C	m/s	m/s	m/s	GPa	
0	50.6	-0.2	-1.3	27.2	5337	3081	3027	61.88	0.257
1	40.5	-0.2	-1.0	26.1	5337	3053	3014	61.29	0.261
2	30.5	-0.2	-0.7	25.7	5337	3039	3000	60.88	0.265
3	20.5	-0.2	-0.4	24.6	5295	3026	2974	60.05	0.264
4	10.5	-0.2	0.2	23.5	5254	2999	2897	58.29	0.270

Observed Velocities and Moduli for File w17450-7445.1-velocity									
Event	Conf	Pore	Diff	Temp	V_p	$V_s^{(1)}$	$V_s^{(2)}$	Young's Modulus	Poisson's Ratio
	MPa	MPa	MPa	°C	m/s	m/s	m/s	GPa	
0	10.6	-0.2	0.4	25.3	4602	2778	2603	46.69	0.240
1	20.6	-0.2	-0.1	25.9	5034	2917	2779	53.34	0.265
2	30.5	-0.2	-0.4	26.5	5223	2967	2907	56.91	0.269
3	40.2	-0.2	-0.6	27.0	5646	3018	2968	60.77	0.305
4	50.1	-0.2	-1.3	27.4	5646	3071	3060	63.09	0.291

Observed Velocities and Moduli for File w17450-7448-velocity									
Event	Conf	Pore	Diff	Temp	V_p	$V_s^{(1)}$	$V_s^{(2)}$	Young's Modulus	Poisson's Ratio
	MPa	MPa	MPa	°C	m/s	m/s	m/s	GPa	
0	10.2	-0.2	0.4	26.0	5554	3159	3211	67.73	0.255
1	10.2	-0.2	0.9	25.9	5554	3159	3227	67.97	0.253
2	10.2	-0.2	0.9	25.7	5655	3192	3244	69.45	0.261
3	10.2	-0.2	0.4	25.6	5505	3159	3227	67.61	0.247
4	10.2	-0.2	0.4	25.7	5655	3159	3279	69.48	0.260
5	10.3	-0.1	1.3	25.6	5604	3159	3227	68.32	0.260
6	20.2	-0.2	0.4	26.6	5870	3384	3424	76.85	0.247
7	30.1	-0.2	0.0	28.0	6101	3459	3501	81.11	0.259
8	40.1	-0.2	-0.8	28.9	6224	3559	3603	85.45	0.253
9	50.0	-0.2	-1.3	29.5	6162	3559	3582	84.59	0.247

Observed Velocities and Moduli for File w17450-7449-velocity									
Event	Conf	Pore	Diff	Temp	V_p	$V_s^{(1)}$	$V_s^{(2)}$	Young's Modulus	Poisson's Ratio
	MPa	MPa	MPa	°C	m/s	m/s	m/s	GPa	
0	10.4	-0.2	0.0	25.2	5428	3169	3162	65.48	0.242
1	20.1	-0.2	-0.4	26.3	5809	3354	3356	73.99	0.250
2	30.1	-0.2	-0.4	27.6	5927	3461	3445	77.96	0.243
3	40.0	-0.2	-1.3	28.3	5981	3535	3519	80.71	0.233
4	50.1	-0.2	-1.7	28.9	6093	3574	3557	82.89	0.240

Observed Velocities and Moduli for File w71450-7402.8-velocity									
Event	Conf	Pore	Diff	Temp	V_p	$V_s^{(1)}$	$V_s^{(2)}$	Young's Modulus	Poisson's Ratio
	MPa	MPa	MPa	°C	m/s	m/s	m/s	GPa	
0	9.9	-0.2	0.3	28.8	4920	3093	3140	58.61	0.165
1	20.1	-0.2	-0.3	29.1	5117	3138	3125	60.99	0.201
2	30.1	-0.2	-0.4	29.5	5117	3154	3187	61.88	0.188
3	40.0	-0.2	-0.4	29.8	5201	3170	3203	63.09	0.200
4	50.2	-0.2	-1.0	30.0	5159	3170	3203	62.67	0.192

A.7.3 Biot's Coefficient

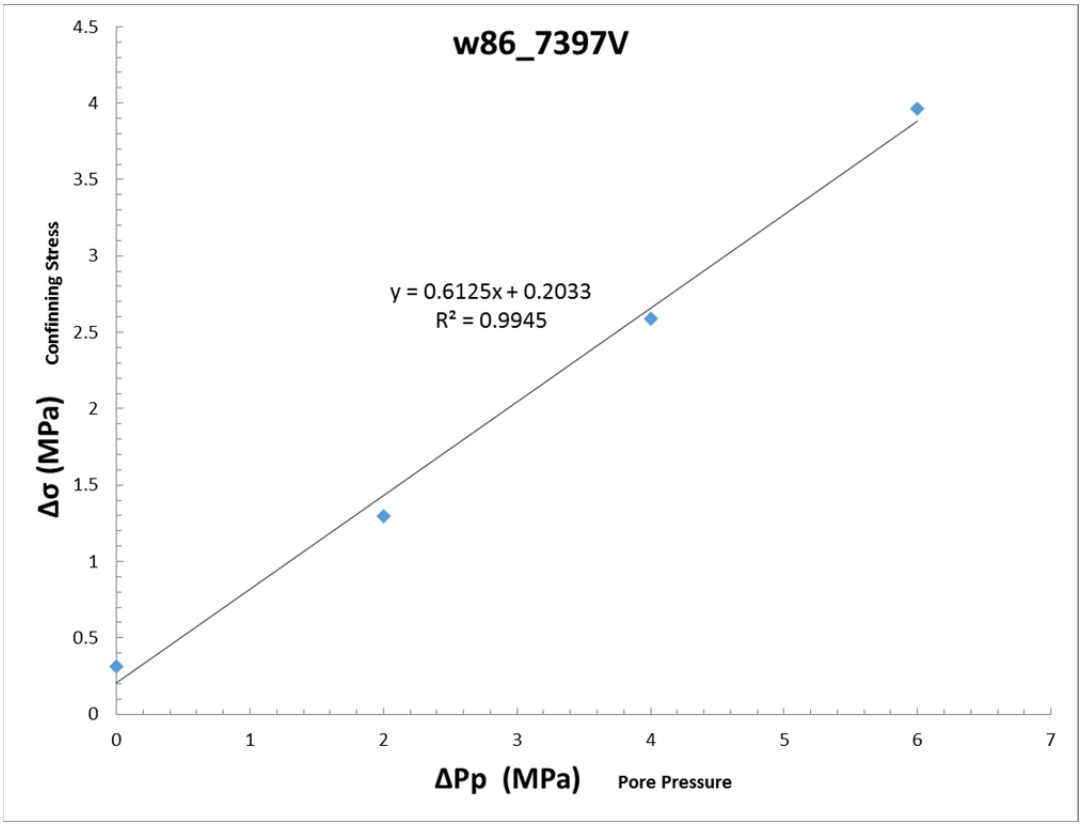
w86_7397V
y = 0.6125x + 0.2033
R² = 0.9945
Δσ (MPa) Confinning Stress
ΔPp (MPa) Pore Pressure
0
0.5
1
1.5
2
2.5
3
3.5
4
4.5
0
1
2
3
4
5
6
7

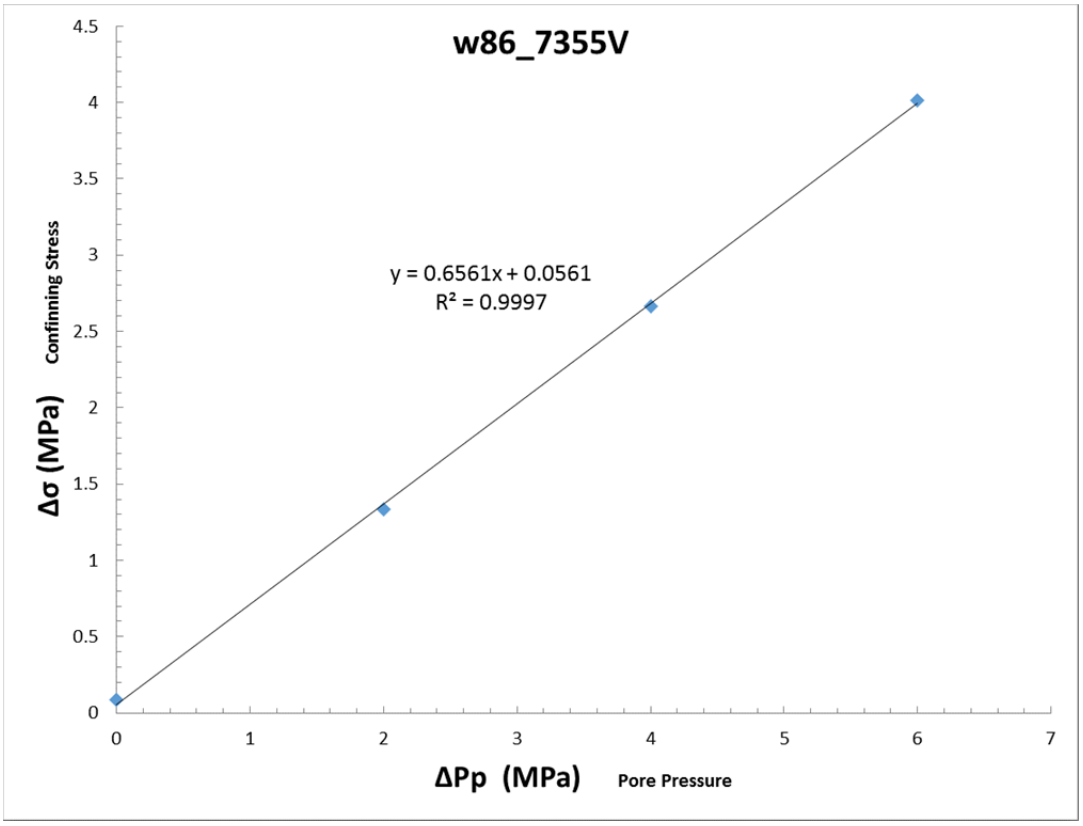
w86_7355V
y = 0.6561x + 0.0561
R² = 0.9997
Δσ (MPa) Confinning Stress
ΔPp (MPa) Pore Pressure
0
0.5
1
1.5
2
2.5
3
3.5
4
4.5
0
1
2
3
4
5
6
7

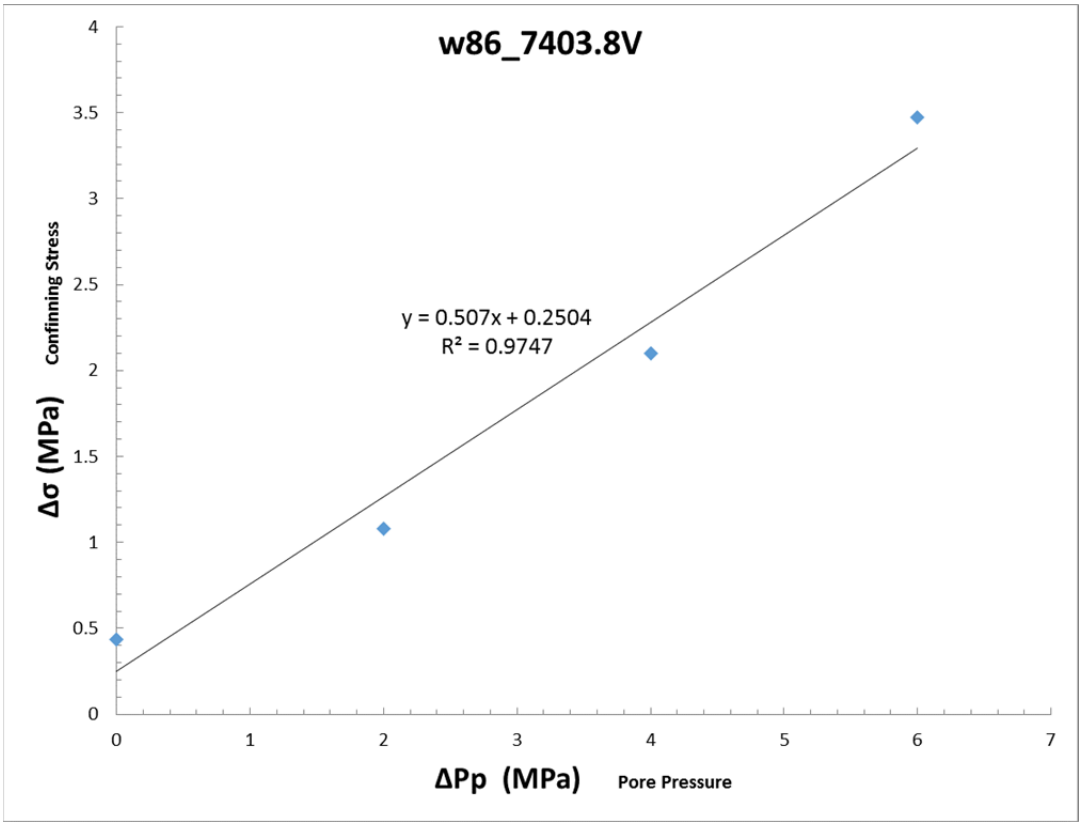
w86_7403.8V
y = 0.507x + 0.2504
R² = 0.9747
Δσ (MPa) Confinning Stress
ΔPp (MPa) Pore Pressure
0
0.5
1
1.5
2
2.5
3
3.5
4
0
1
2
3
4
5
6
7

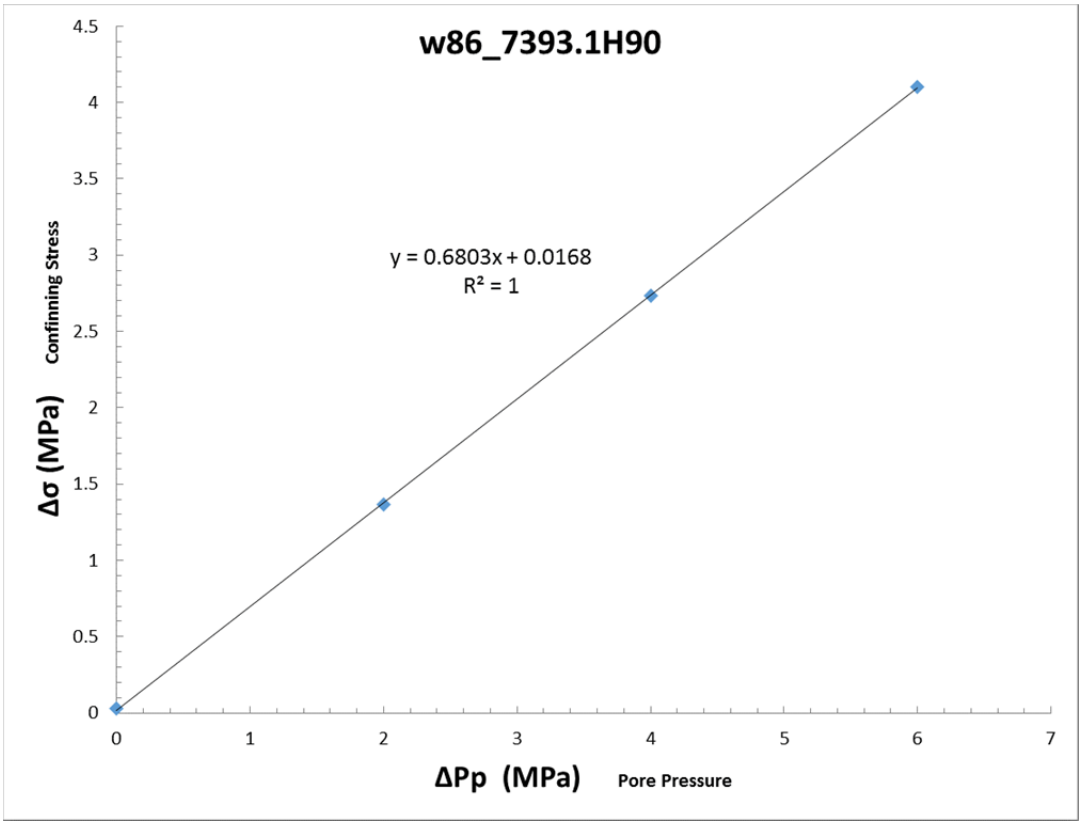
w86_7393.1H90
y = 0.6803x + 0.0168
R² = 1
Δσ (MPa) Confinning Stress
ΔPp (MPa) Pore Pressure
0
0.5
1
1.5
2
2.5
3
3.5
4
4.5
0
1
2
3
4
5
6
7

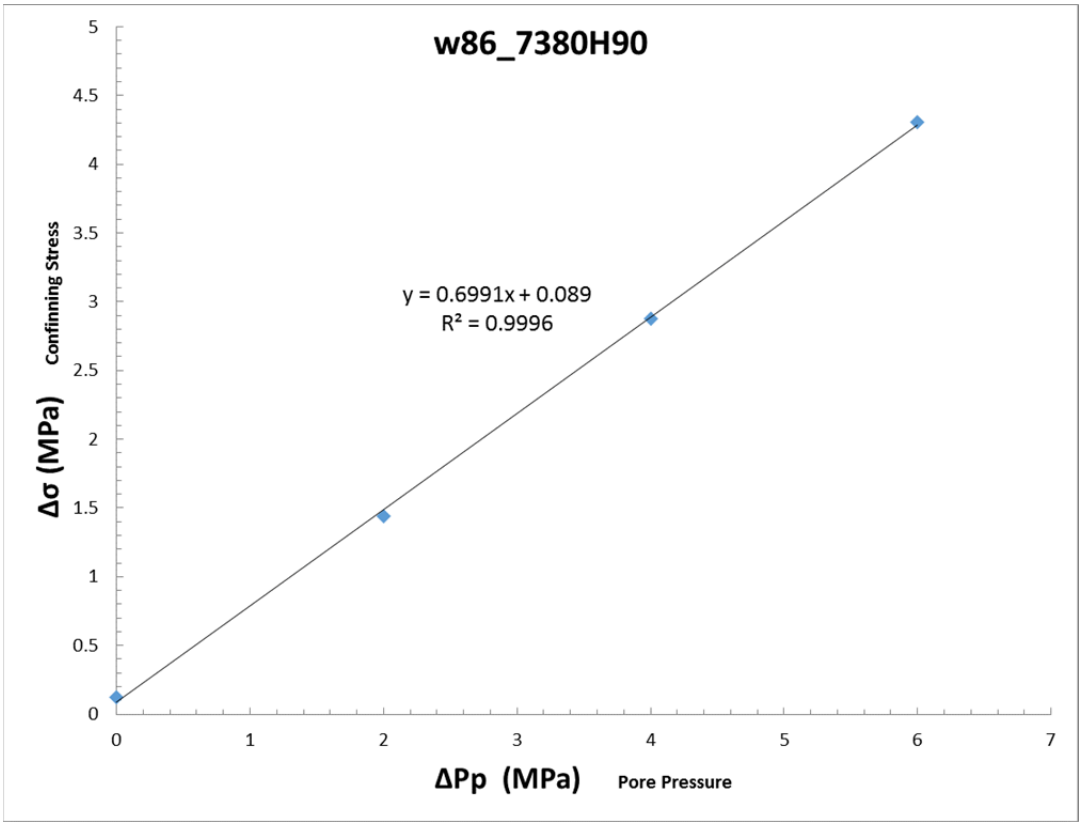
w86_7380H90
y = 0.6991x + 0.089
R² = 0.9996
Δσ (MPa) Confinning Stress
ΔPp (MPa) Pore Pressure
0
0.5
1
1.5
2
2.5
3
3.5
4
4.5
5
0
1
2
3
4
5
6
7

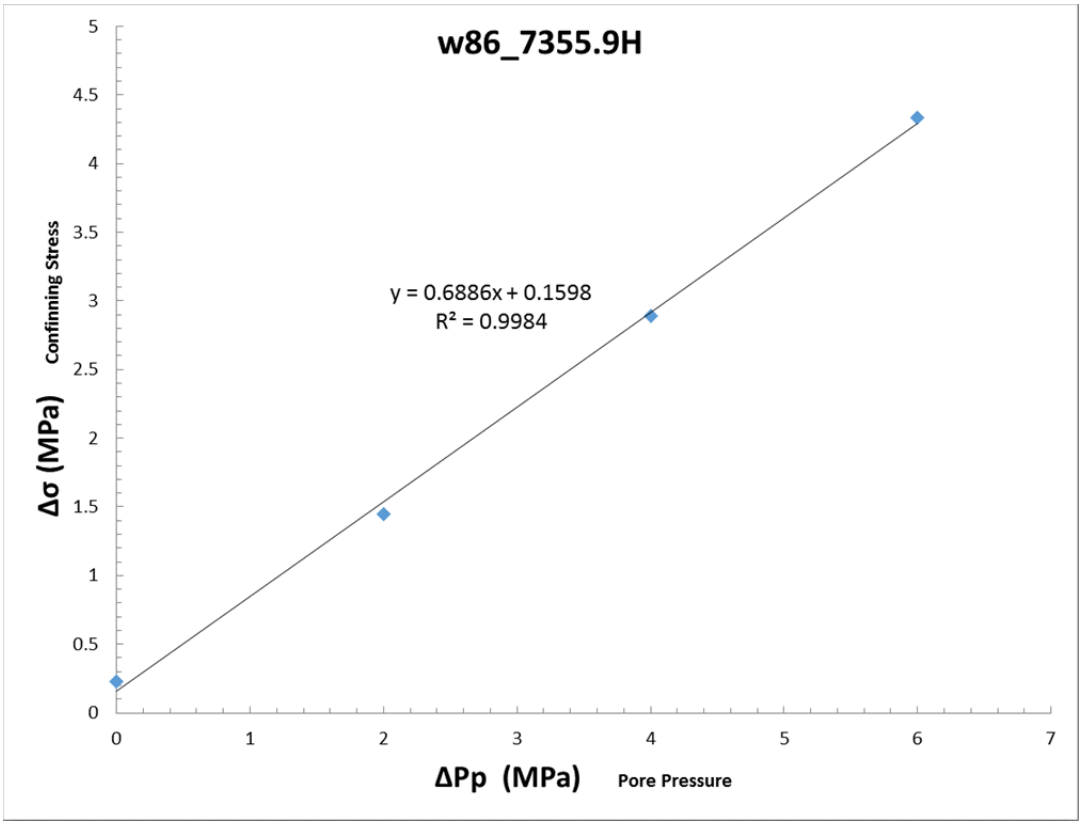
w86_7355.9H
y = 0.6886x + 0.1598
R² = 0.9984
Δσ (MPa) Confinning Stress
ΔPp (MPa) Pore Pressure
0
0.5
1
1.5
2
2.5
3
3.5
4
4.5
5
0
1
2
3
4
5
6
7

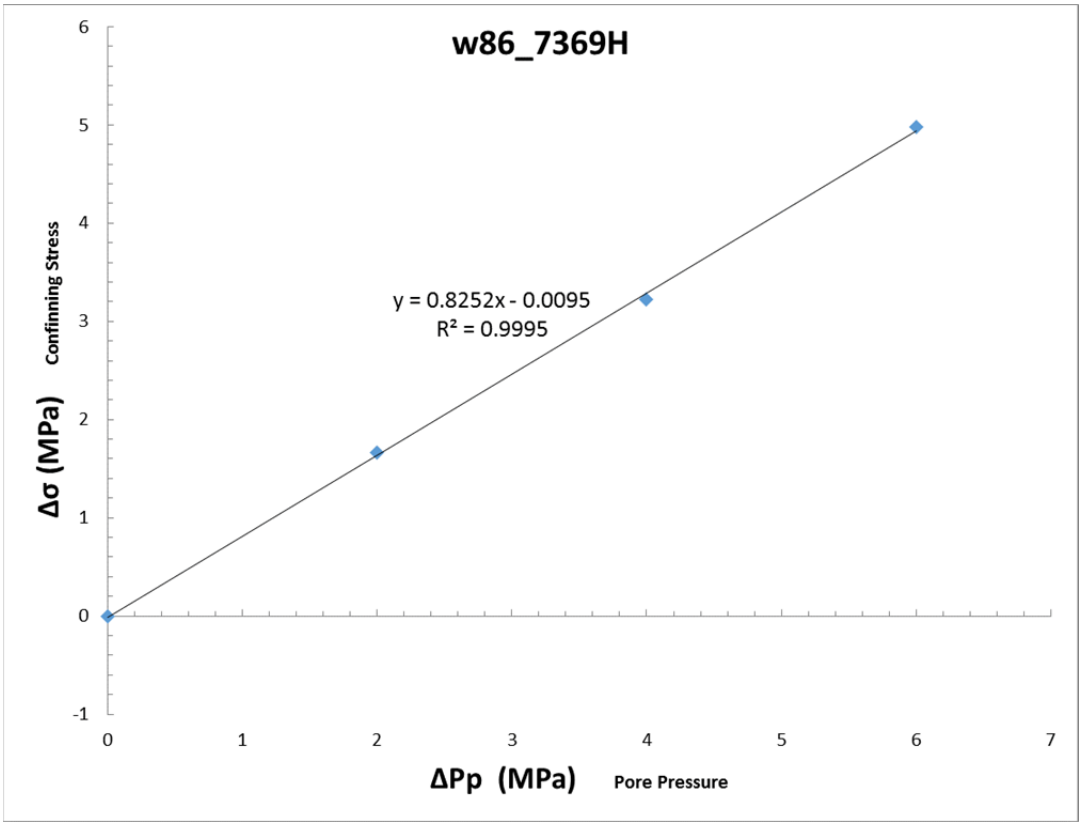
w86_7369H
y = 0.8252x - 0.0095
R² = 0.9995
Δσ (MPa) Confinning Stress
ΔPp (MPa) Pore Pressure
6
5
4
3
2
1
0
-1
0
1
2
3
4
5
6
7

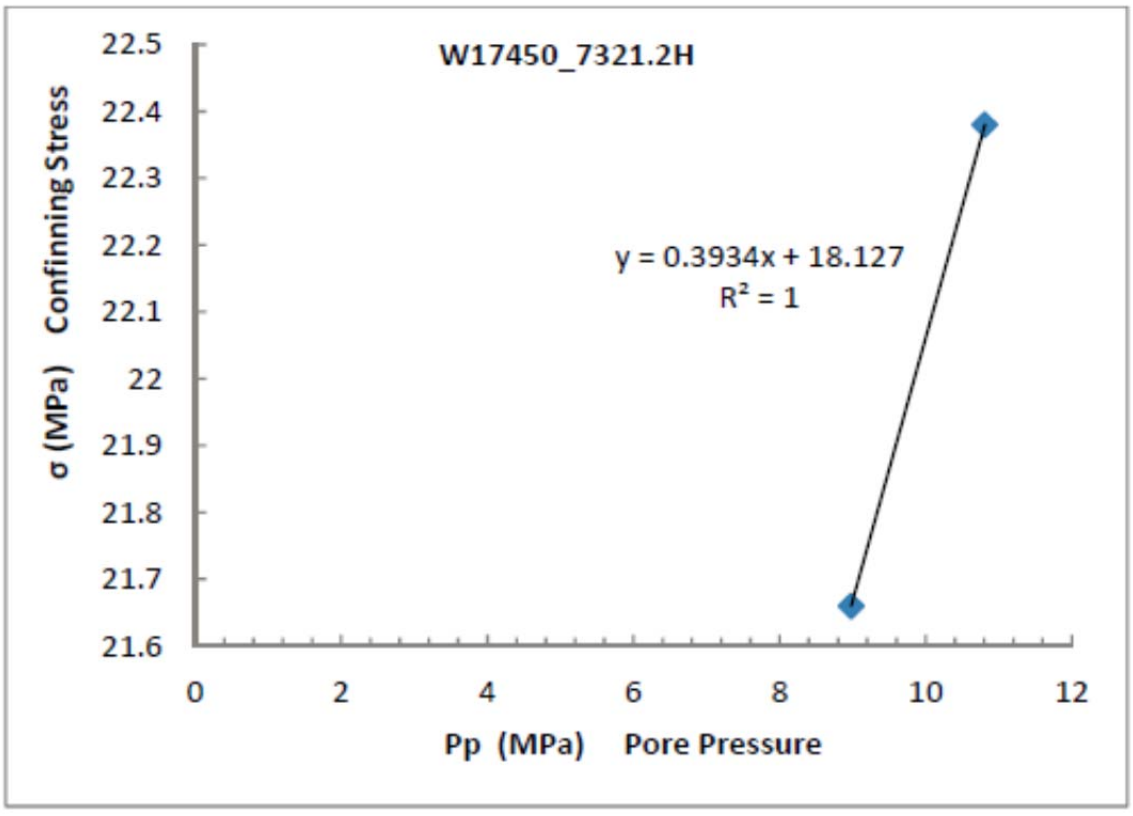
W17450_7321.2H
y = 0.3934x + 18.127
R² = 1
σ (MPa) Confinning Stress
Pp (MPa) Pore Pressure
22.5
22.4
22.3
22.2
22.1
22
21.9
21.8
21.7
21.6
0
2
4
6
8
10
12

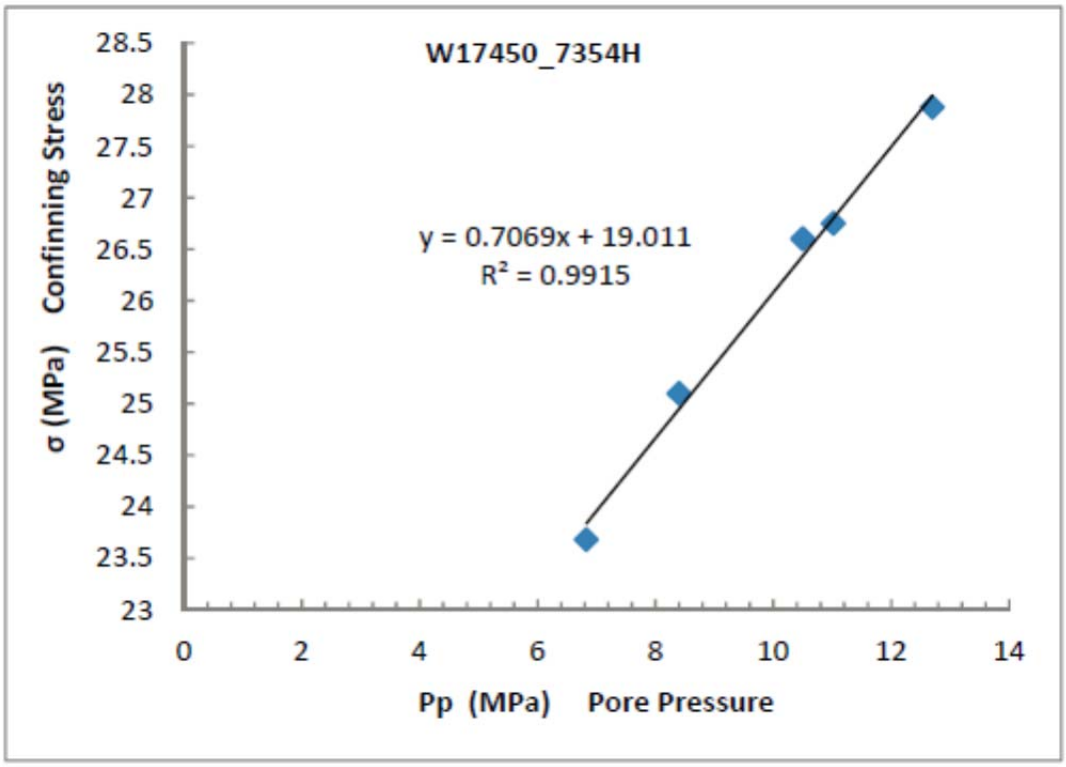
W17450_7354H
y = 0.7069x + 19.011
R² = 0.9915
σ (MPa) Confinning Stress
Pp (MPa) Pore Pressure
28.5
28
27.5
27
26.5
26
25.5
25
24.5
24
23.5
23
0
2
4
6
8
10
12
14

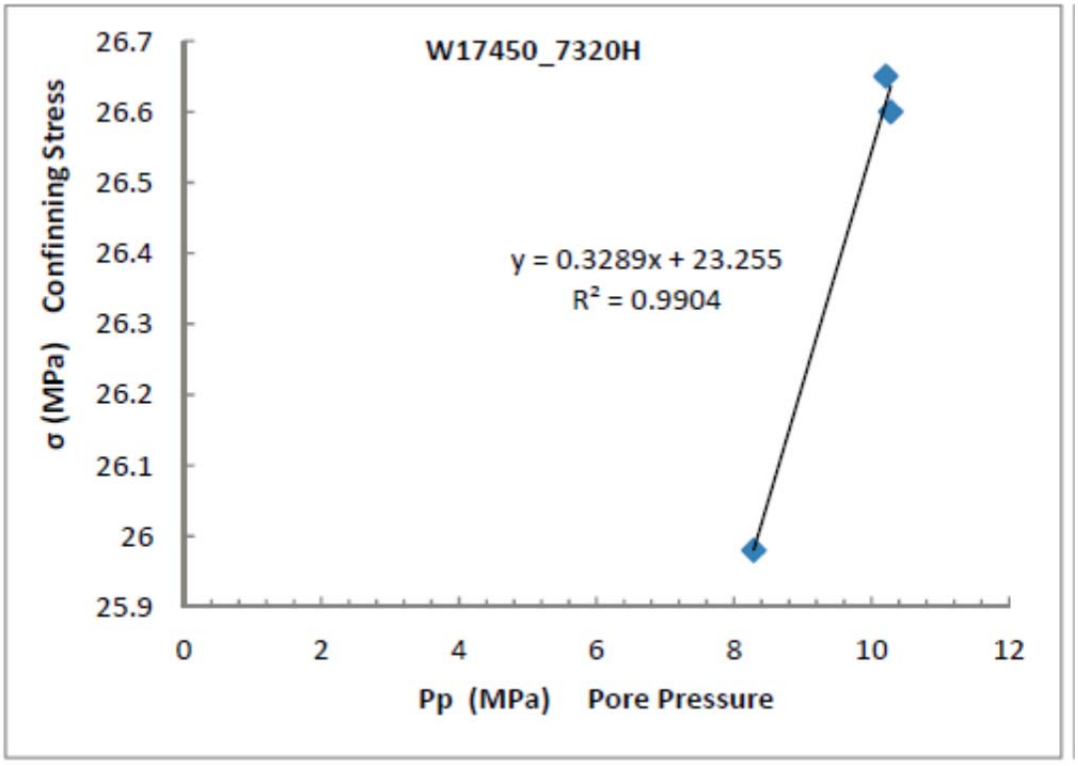
W17450_7320H
y = 0.3289x + 23.255
R² = 0.9904
σ (MPa) Confinning Stress
Pp (MPa) Pore Pressure
26.7
26.6
26.5
26.4
26.3
26.2
26.1
26
25.9
0
2
4
6
8
10
12

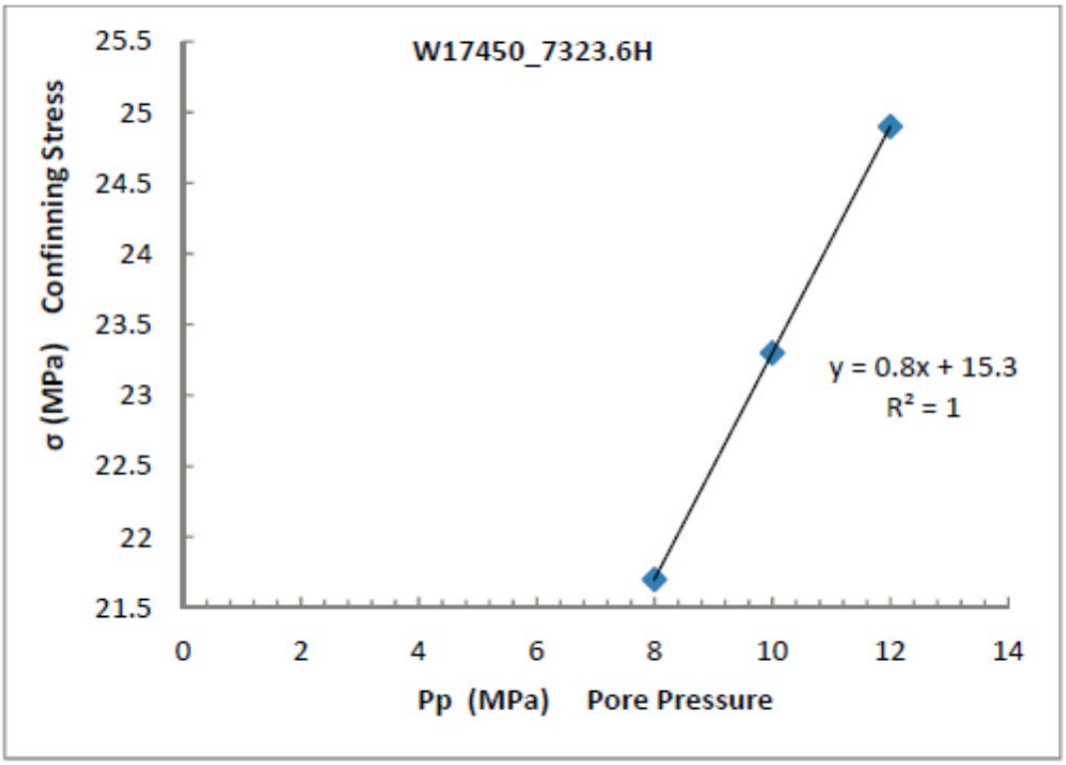
W17450_7323.6H
σ (MPa) Confinning Stress
Pp (MPa) Pore Pressure
y = 0.8x + 15.3
R² = 1
25.5
25
24.5
24
23.5
23
22.5
22
21.5
0
2
4
6
8
10
12
14

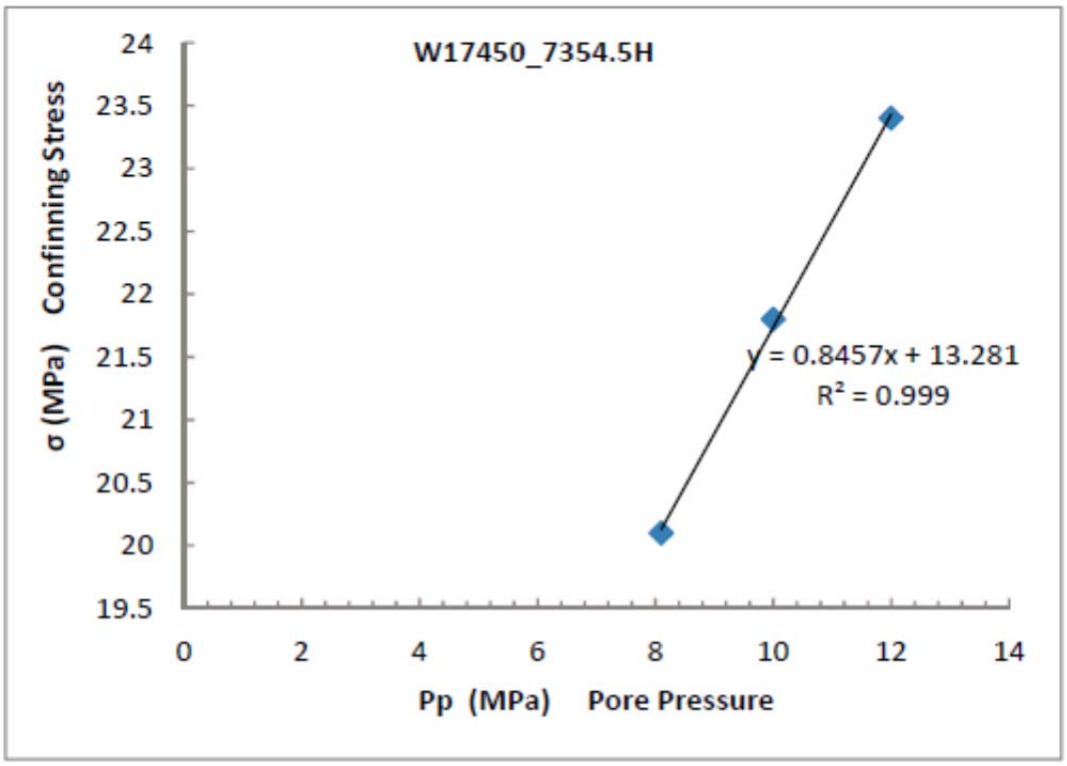
W17450_7354.5H
σ (MPa) Confinning Stress
Pp (MPa) Pore Pressure
y = 0.8457x + 13.281
R² = 0.999
24
23.5
23
22.5
22
21.5
21
20.5
20
19.5
0
2
4
6
8
10
12
14

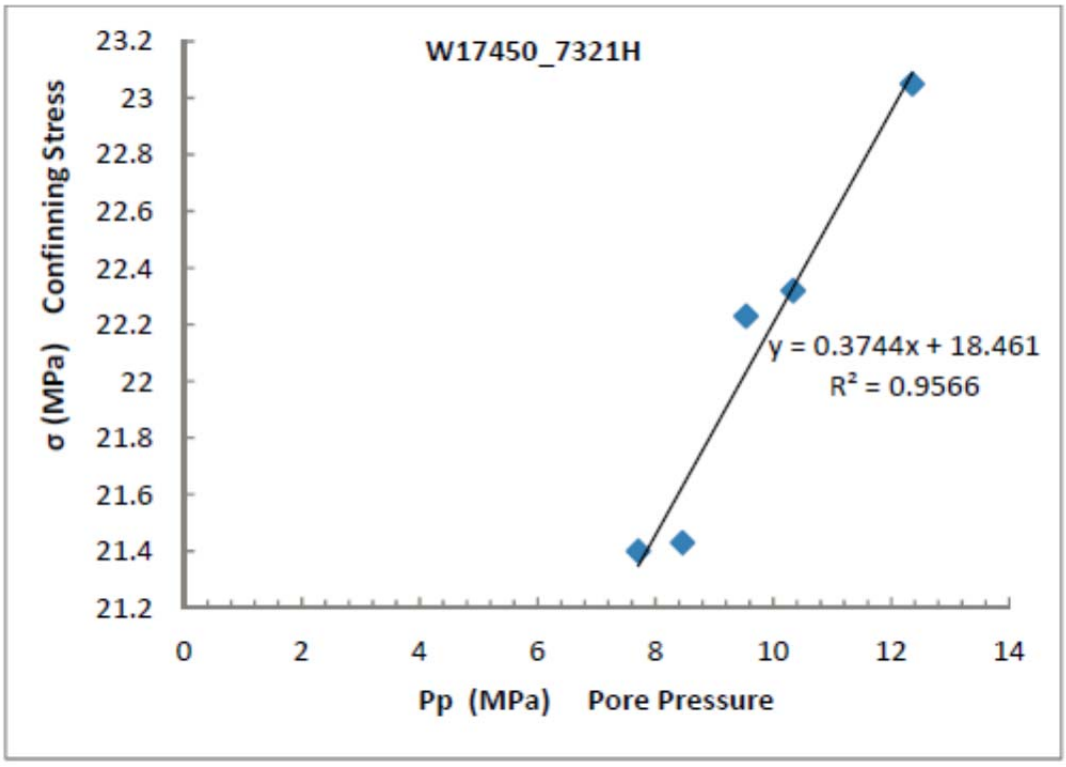
W17450_7321H
σ (MPa) Confinning Stress
Pp (MPa) Pore Pressure
y = 0.3744x + 18.461
R² = 0.9566
23.2
23
22.8
22.6
22.4
22.2
22
21.8
21.6
21.4
21.2
0
2
4
6
8
10
12
14

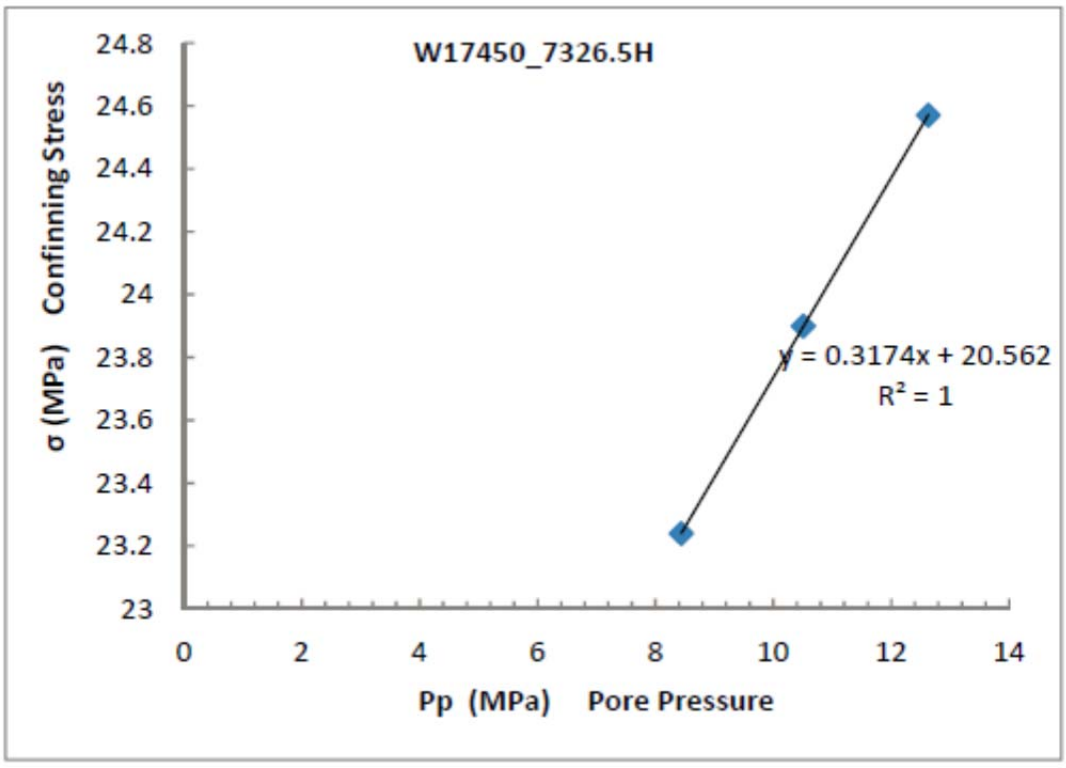
W17450_7326.5H
σ (MPa) Confinning Stress
Pp (MPa) Pore Pressure
y = 0.3174x + 20.562
R² = 1
24.8
24.6
24.4
24.2
24
23.8
23.6
23.4
23.2
23
0
2
4
6
8
10
12
14

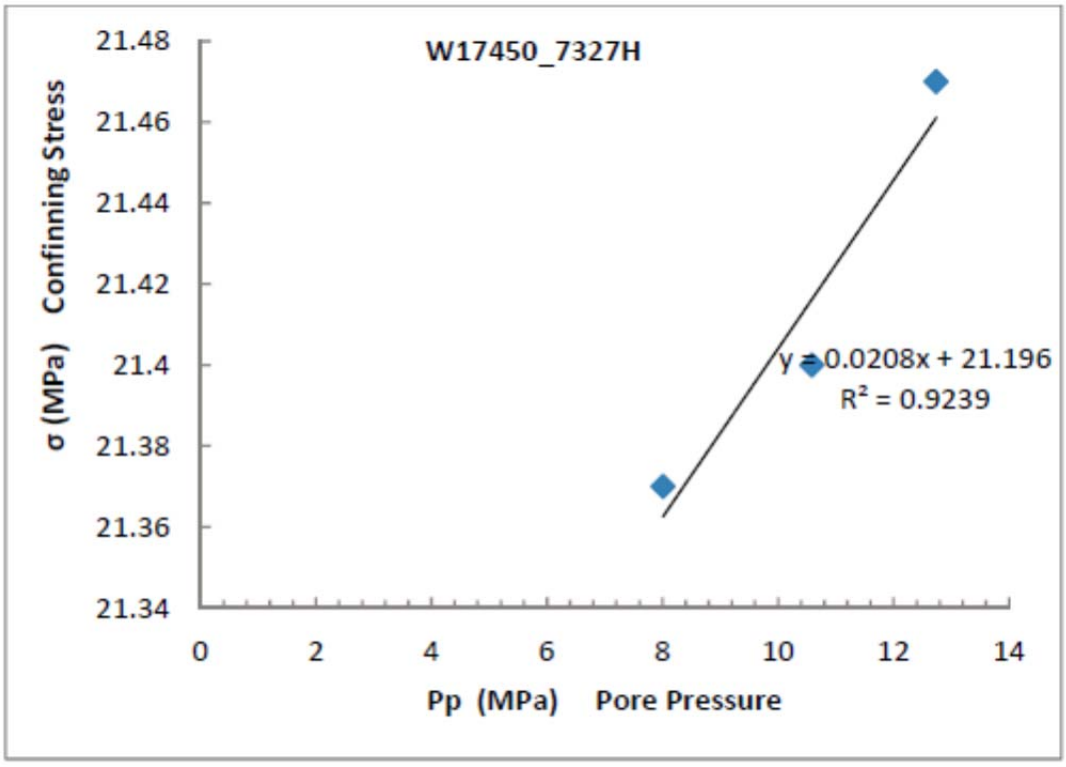
W17450_7327H
σ (MPa) Confinning Stress
21.48
21.46
21.44
21.42
21.4
21.38
21.36
21.34
y = 0.0208x + 21.196
R² = 0.9239
0
2
4
6
8
10
12
14
Pp (MPa) Pore Pressure

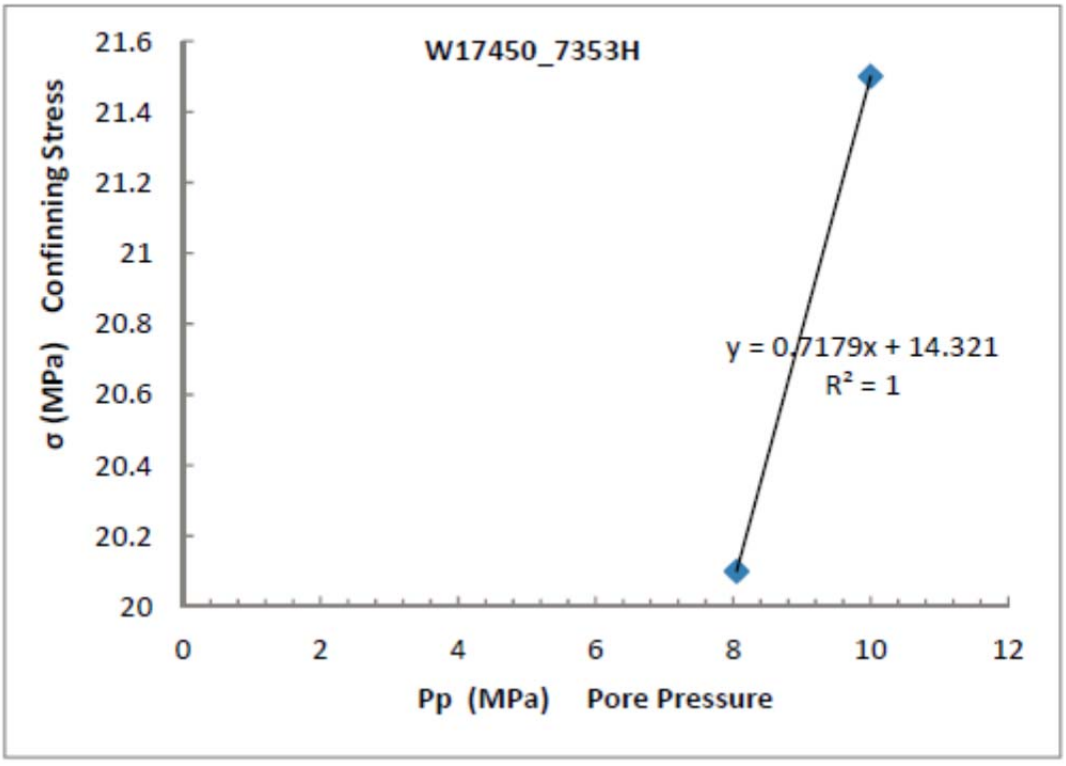
W17450_7353H
σ (MPa) Confinning Stress
21.6
21.4
21.2
21
20.8
20.6
20.4
20.2
20
y = 0.7179x + 14.321
R² = 1
0
2
4
6
8
10
12
Pp (MPa) Pore Pressure

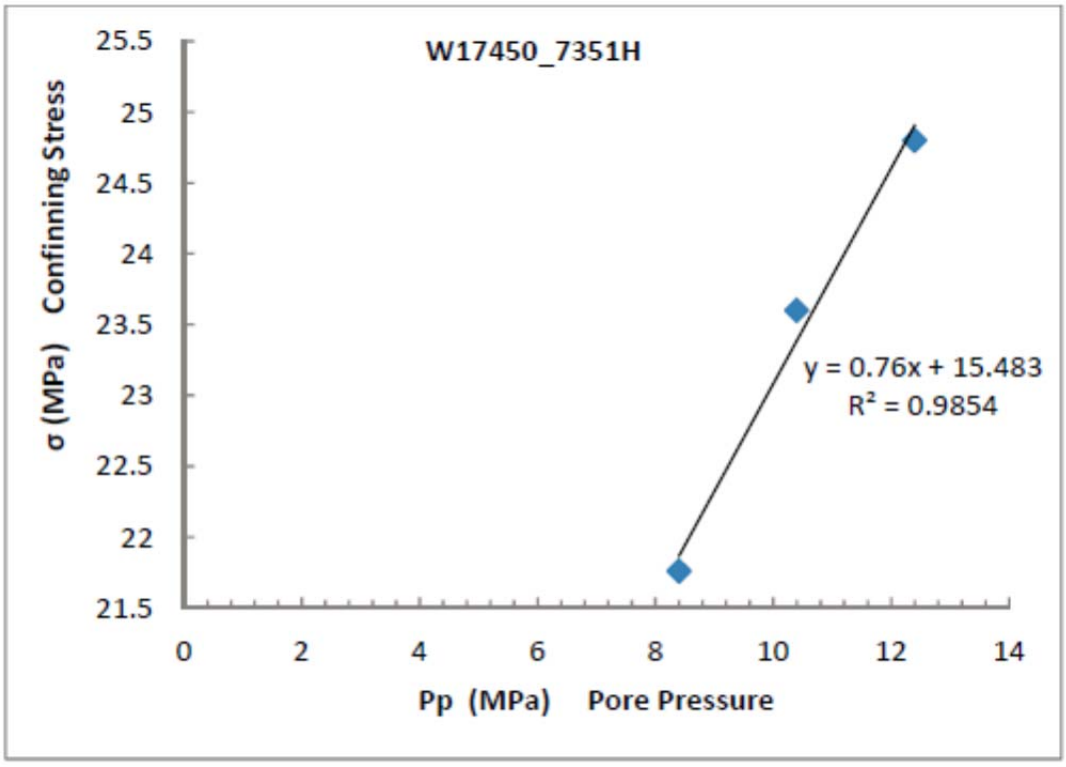
W17450_7351H
σ (MPa) Confinning Stress
Pp (MPa) Pore Pressure
y = 0.76x + 15.483
R² = 0.9854
25.5
25
24.5
24
23.5
23
22.5
22
21.5
0
2
4
6
8
10
12
14

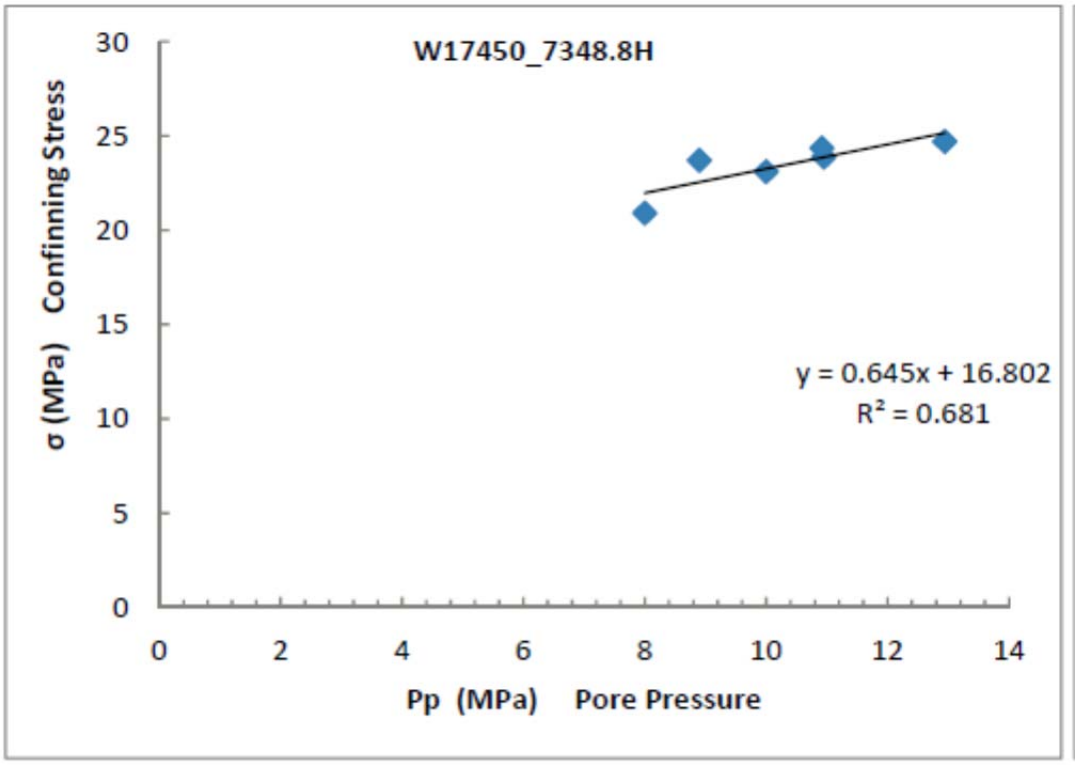
W17450_7348.8H
σ (MPa) Confinning Stress
Pp (MPa) Pore Pressure
y = 0.645x + 16.802
R² = 0.681
30
25
20
15
10
5
0
0
2
4
6
8
10
12
14

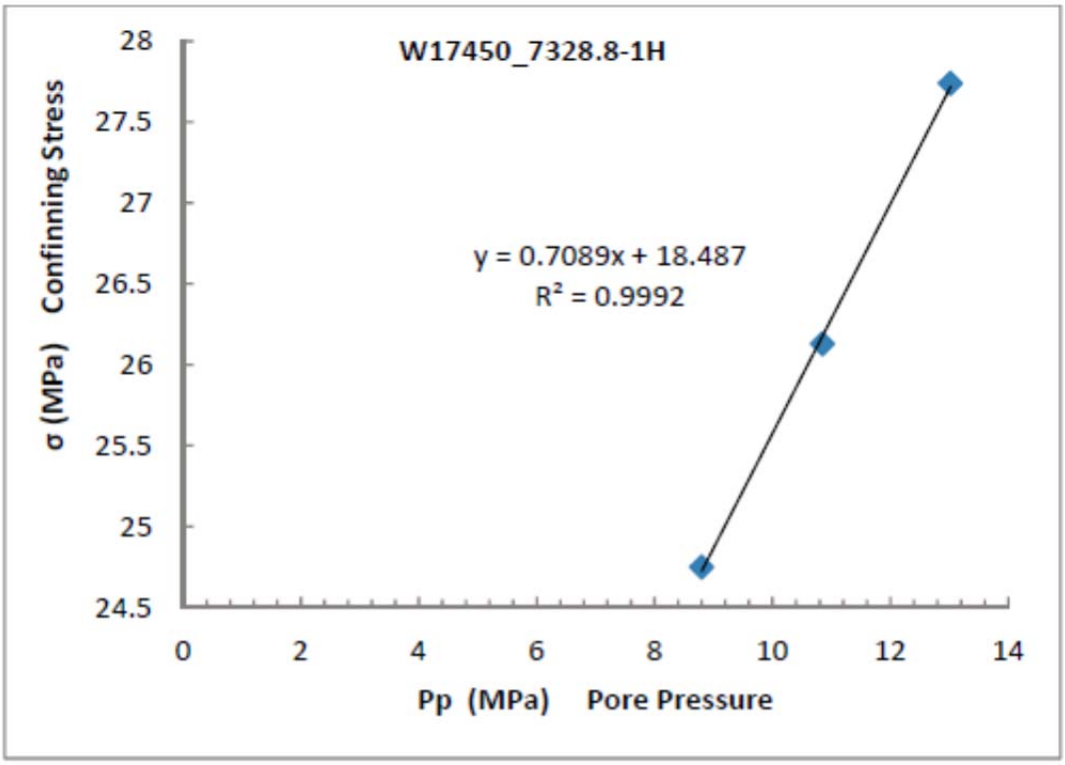
W17450_7328.8-1H
y = 0.7089x + 18.487
R² = 0.9992
σ (MPa) Confinning Stress
Pp (MPa) Pore Pressure
28
27.5
27
26.5
26
25.5
25
24.5
0
2
4
6
8
10
12
14

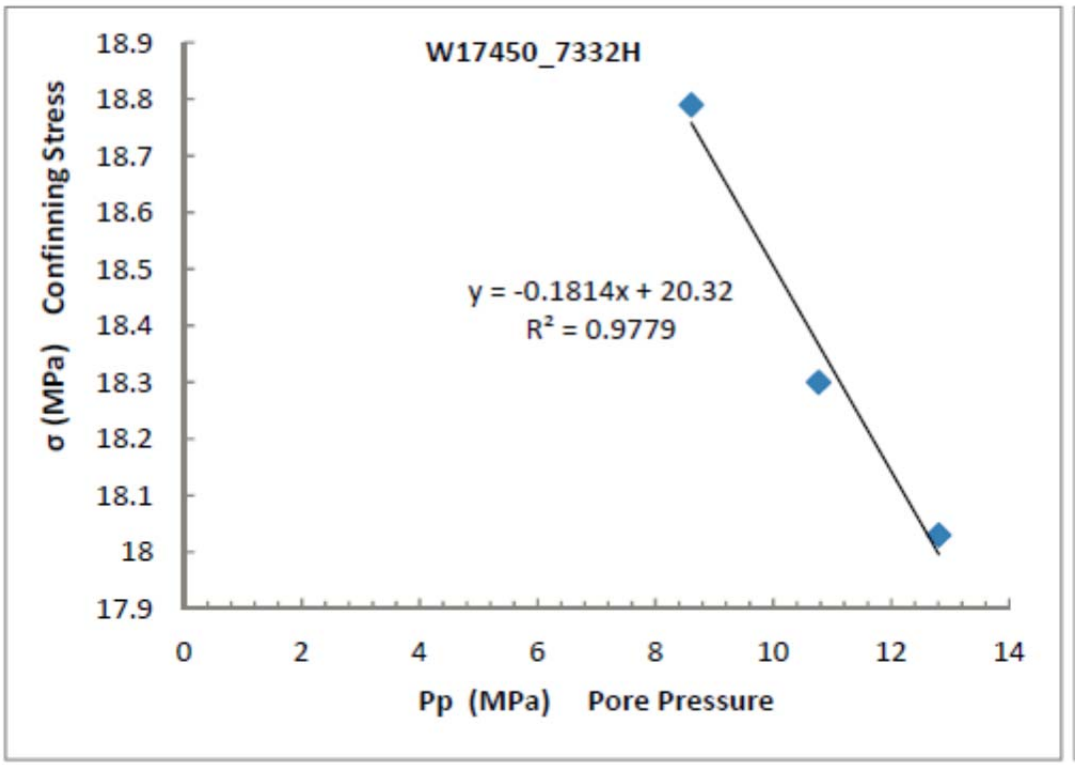
W17450_7332H
y = -0.1814x + 20.32
R² = 0.9779
σ (MPa) Confinning Stress
Pp (MPa) Pore Pressure
18.9
18.8
18.7
18.6
18.5
18.4
18.3
18.2
18.1
18
17.9
0
2
4
6
8
10
12
14

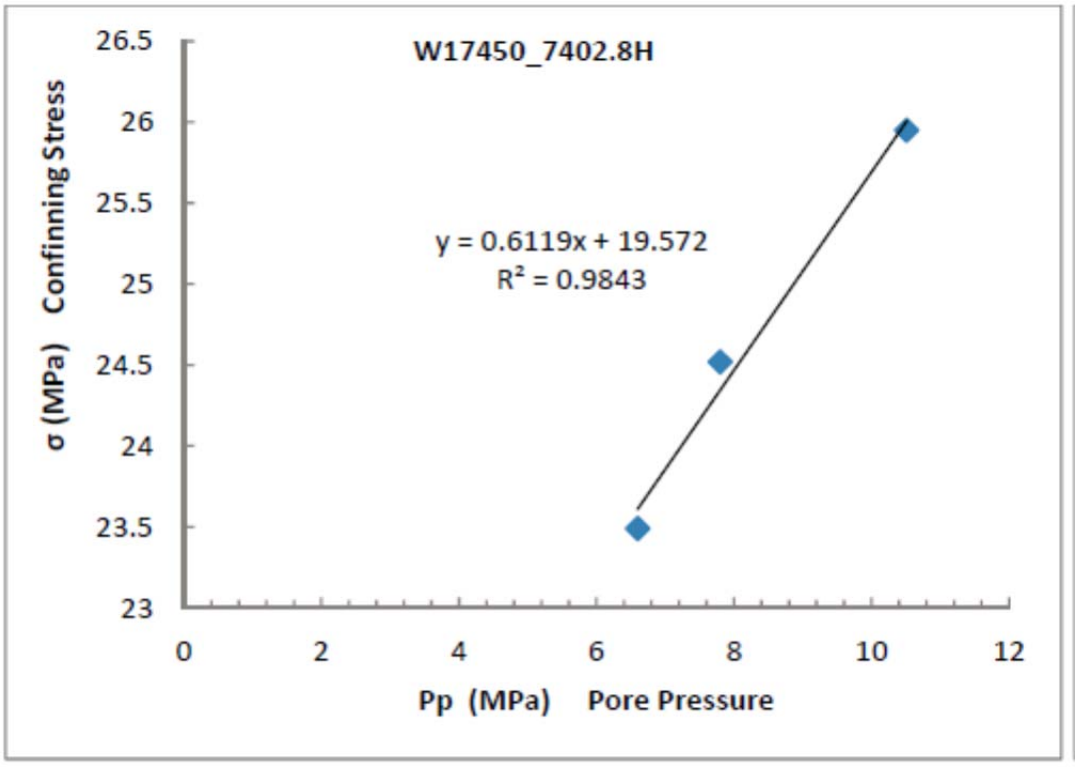
W17450_7402.8H
y = 0.6119x + 19.572
R² = 0.9843
σ (MPa) Confinning Stress
Pp (MPa) Pore Pressure
26.5
26
25.5
25
24.5
24
23.5
23
0
2
4
6
8
10
12

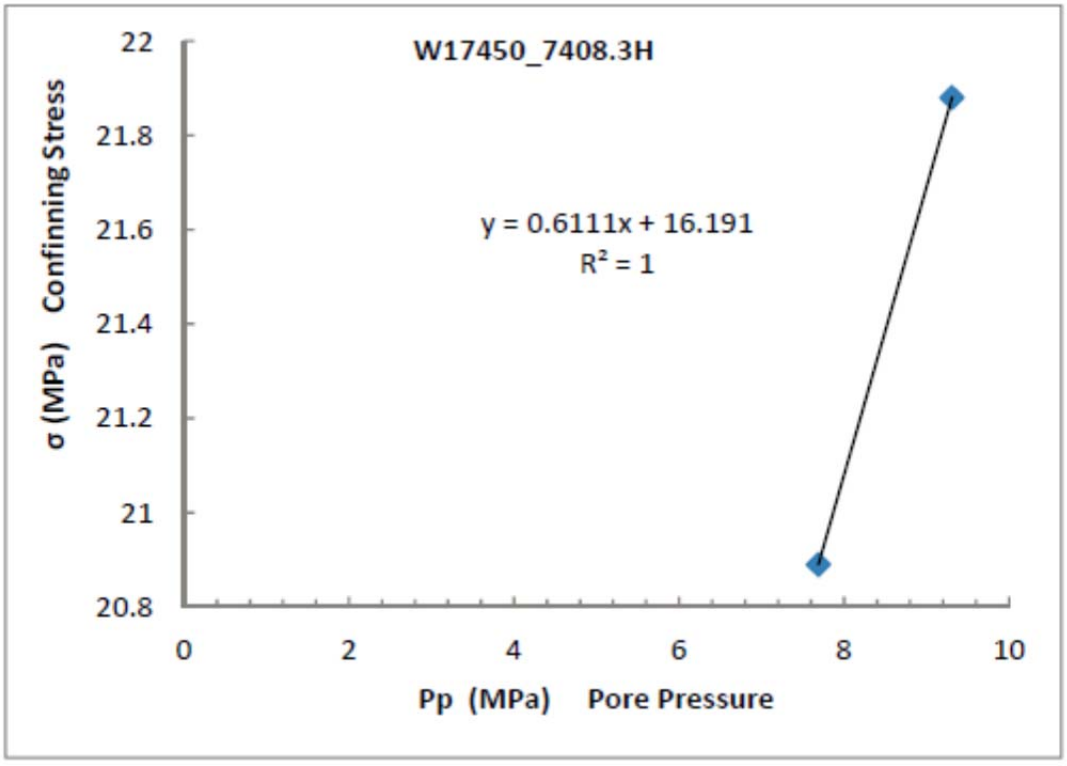
W17450_7408.3H
y = 0.6111x + 16.191
R² = 1
σ (MPa) Confinning Stress
Pp (MPa) Pore Pressure
22
21.8
21.6
21.4
21.2
21
20.8
0
2
4
6
8
10

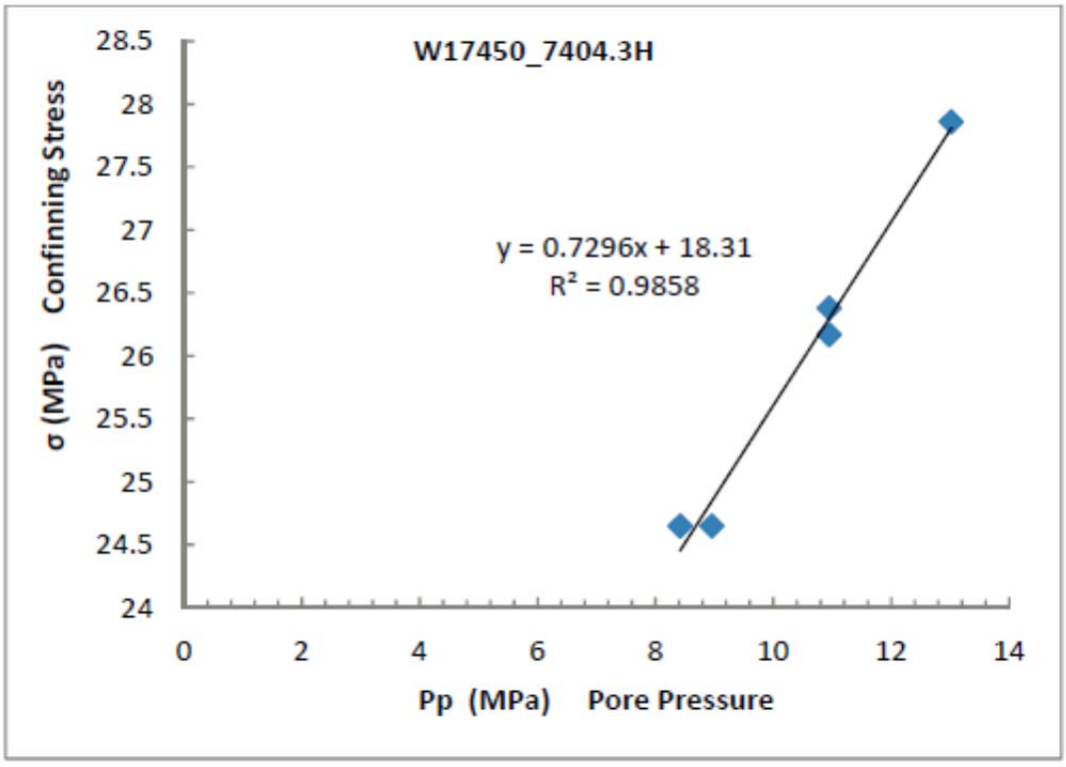
W17450_7404.3H
y = 0.7296x + 18.31
R² = 0.9858
σ (MPa) Confinning Stress
Pp (MPa) Pore Pressure
28.5
28
27.5
27
26.5
26
25.5
25
24.5
24
0
2
4
6
8
10
12
14

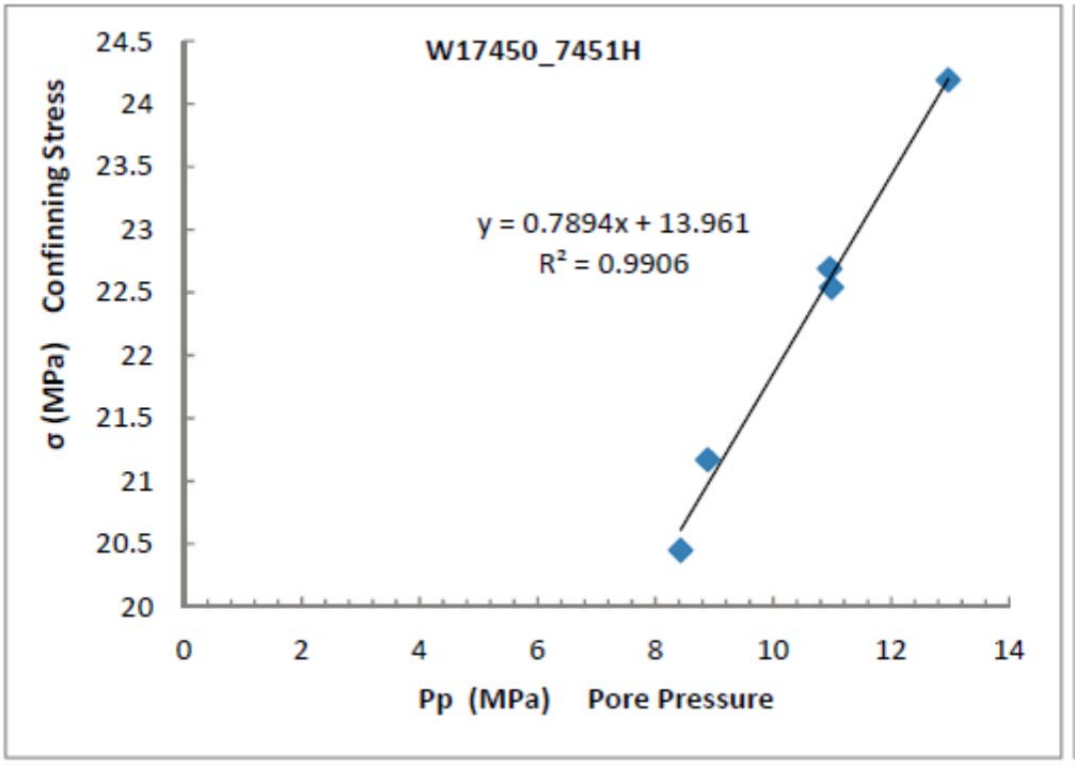
W17450_7451H
y = 0.7894x + 13.961
R² = 0.9906
σ (MPa) Confinning Stress
Pp (MPa) Pore Pressure
24.5
24
23.5
23
22.5
22
21.5
21
20.5
20
0
2
4
6
8
10
12
14

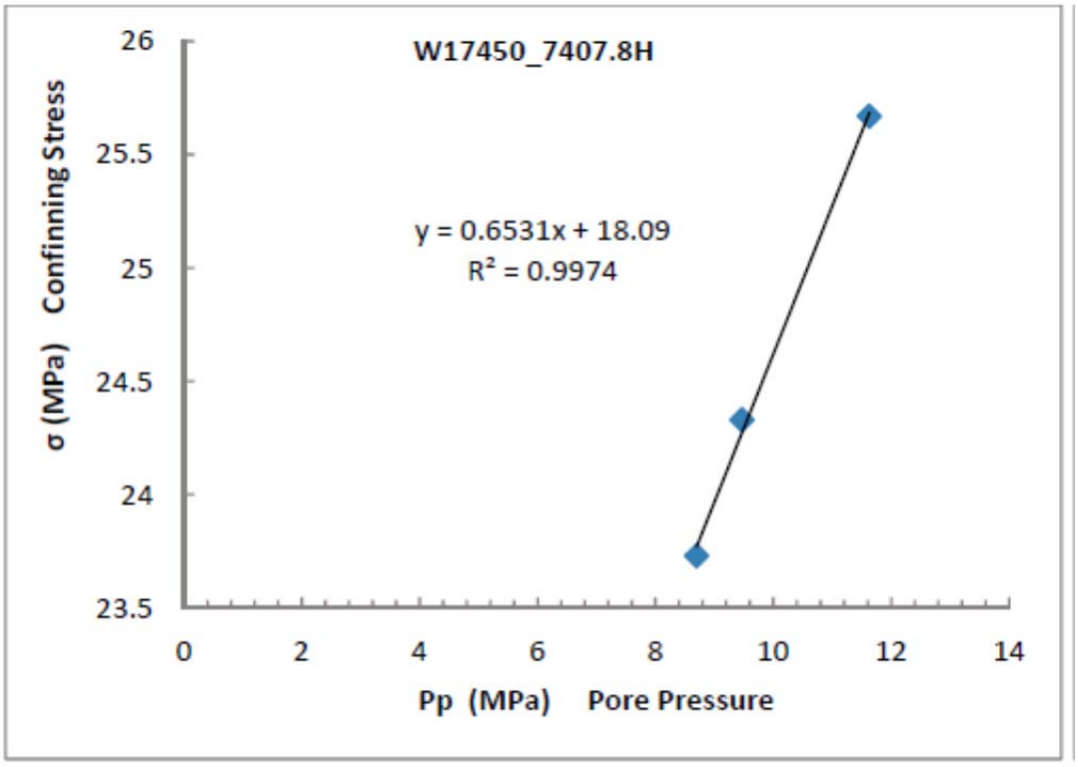
W17450_7407.8H
y = 0.6531x + 18.09
R² = 0.9974
σ (MPa) Confinning Stress
Pp (MPa) Pore Pressure
26
25.5
25
24.5
24
23.5
0
2
4
6
8
10
12
14

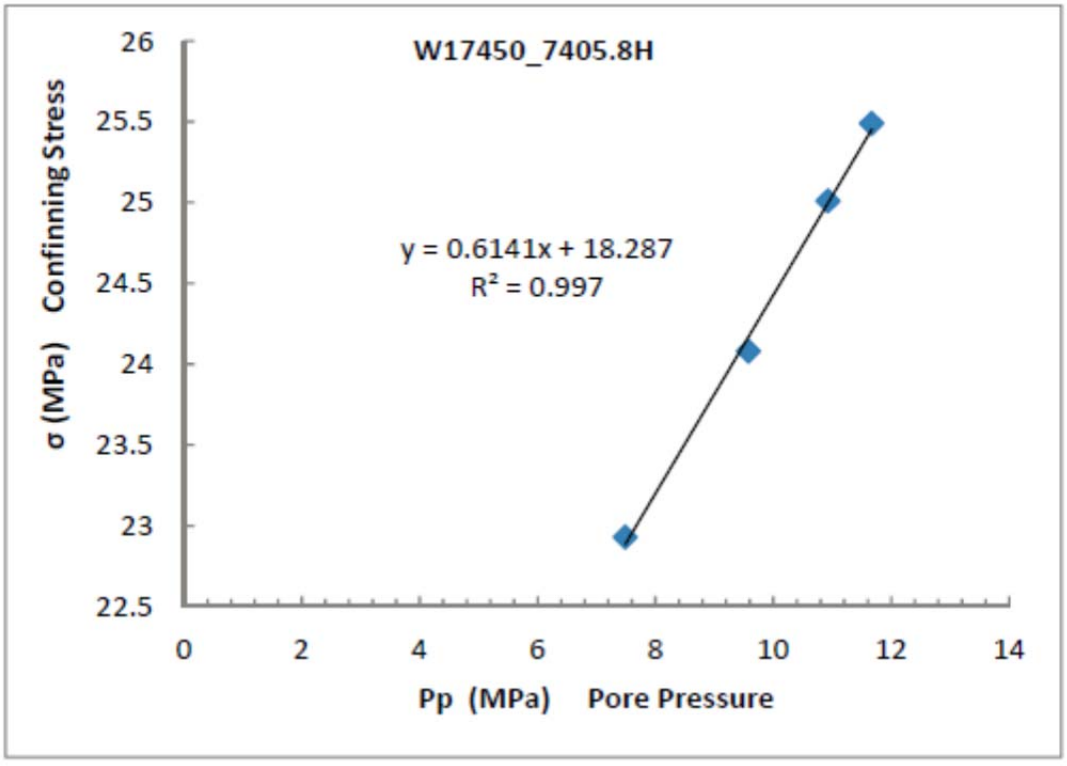
W17450_7405.8H
y = 0.6141x + 18.287
R² = 0.997
σ (MPa) Confinning Stress
Pp (MPa) Pore Pressure
26
25.5
25
24.5
24
23.5
23
22.5
0
2
4
6
8
10
12
14

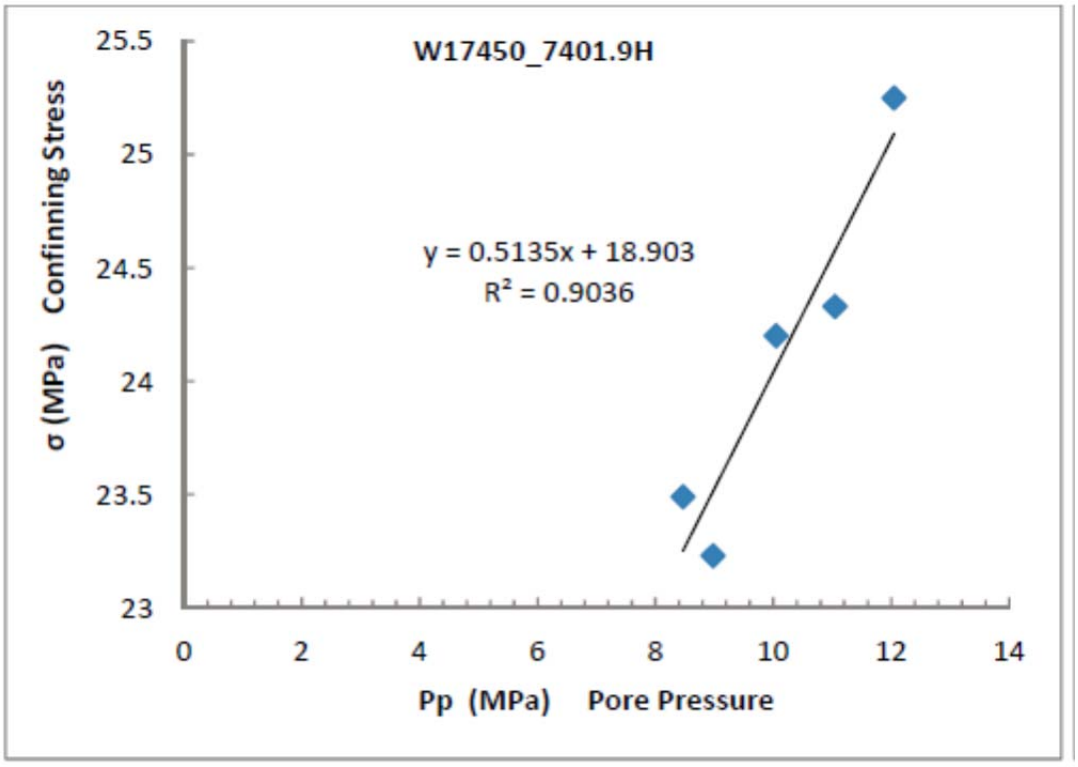
W17450_7401.9H
y = 0.5135x + 18.903
R² = 0.9036
σ (MPa) Confinning Stress
Pp (MPa) Pore Pressure
25.5
25
24.5
24
23.5
23
0
2
4
6
8
10
12
14

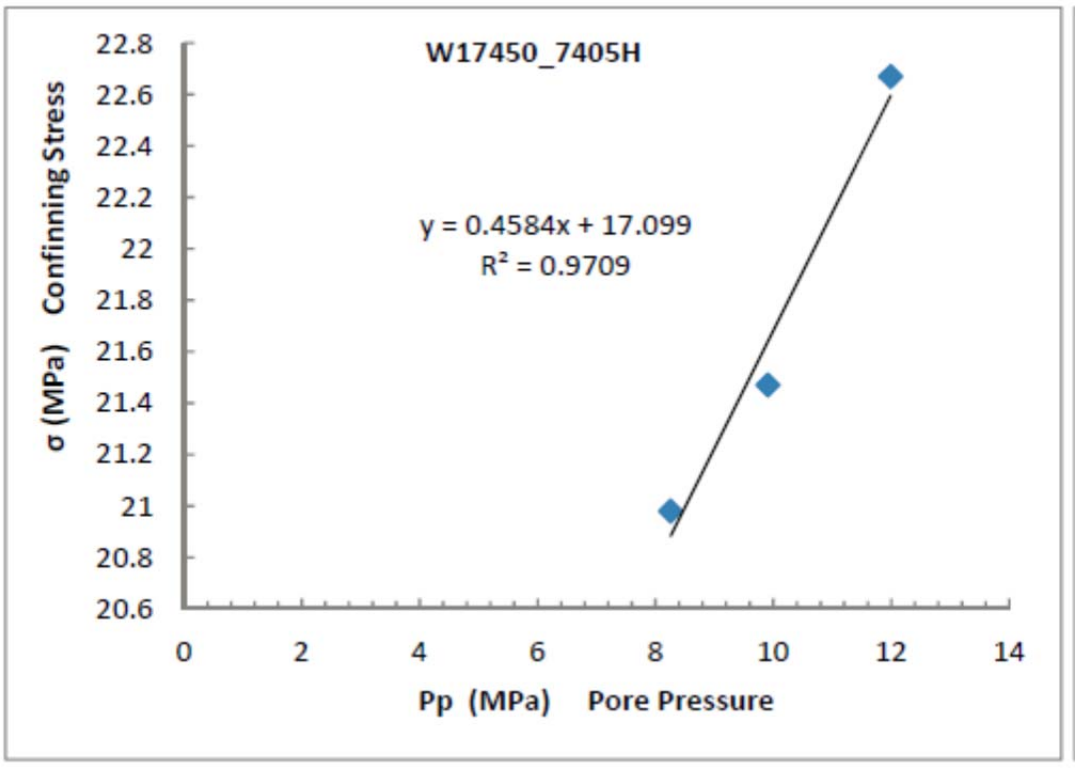
W17450_7405H
y = 0.4584x + 17.099
R² = 0.9709
σ (MPa) Confinning Stress
Pp (MPa) Pore Pressure
22.8
22.6
22.4
22.2
22
21.8
21.6
21.4
21.2
21
20.8
20.6
0
2
4
6
8
10
12
14

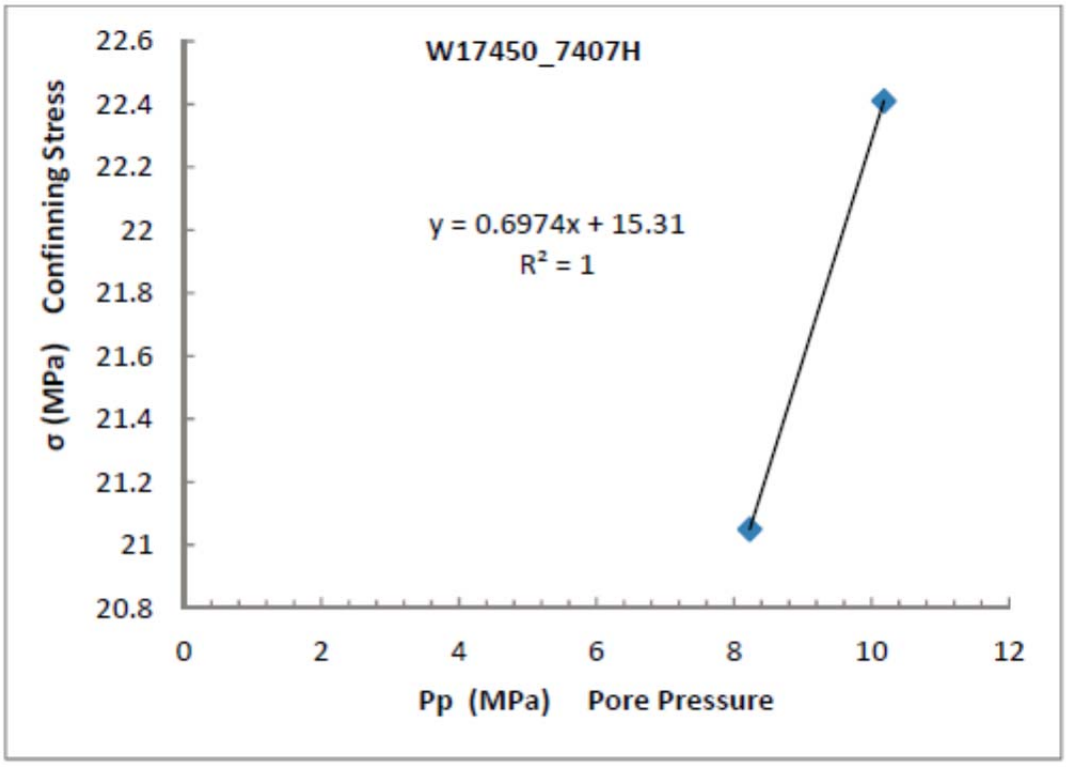
W17450_7407H
y = 0.6974x + 15.31
R² = 1
σ (MPa) Confinning Stress
Pp (MPa) Pore Pressure
22.6
22.4
22.2
22
21.8
21.6
21.4
21.2
21
20.8
0
2
4
6
8
10
12

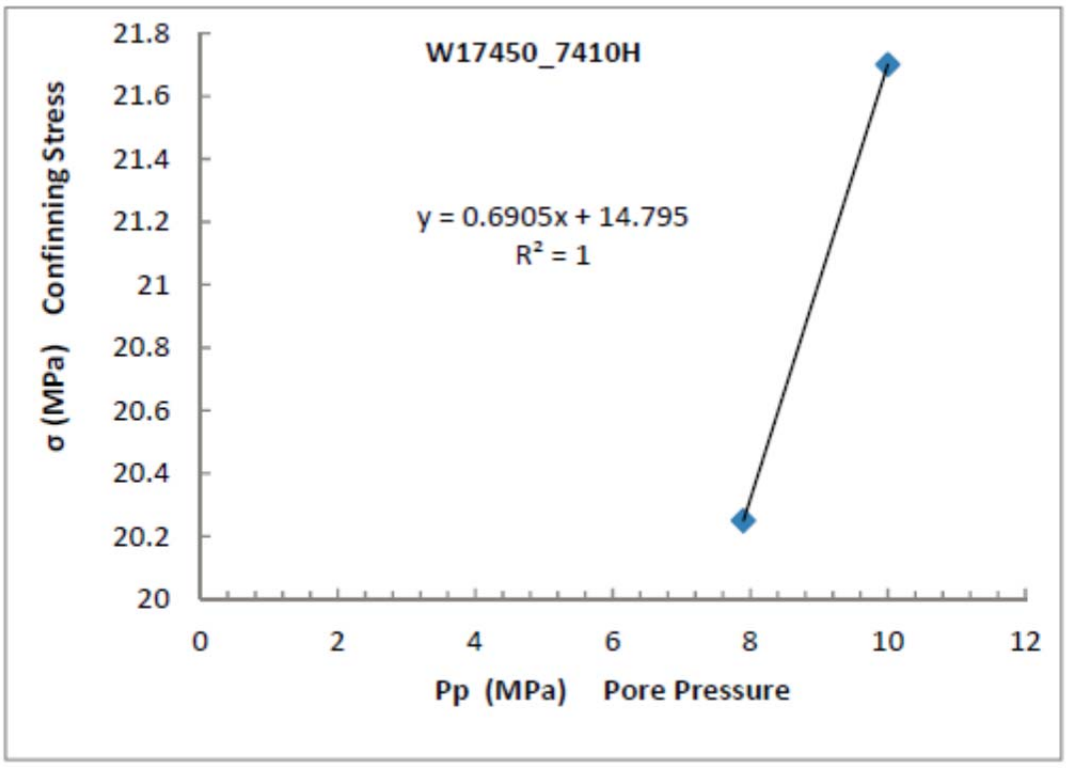
W17450_7410H
y = 0.6905x + 14.795
R² = 1
σ (MPa) Confinning Stress
Pp (MPa) Pore Pressure
21.8
21.6
21.4
21.2
21
20.8
20.6
20.4
20.2
20
0
2
4
6
8
10
12

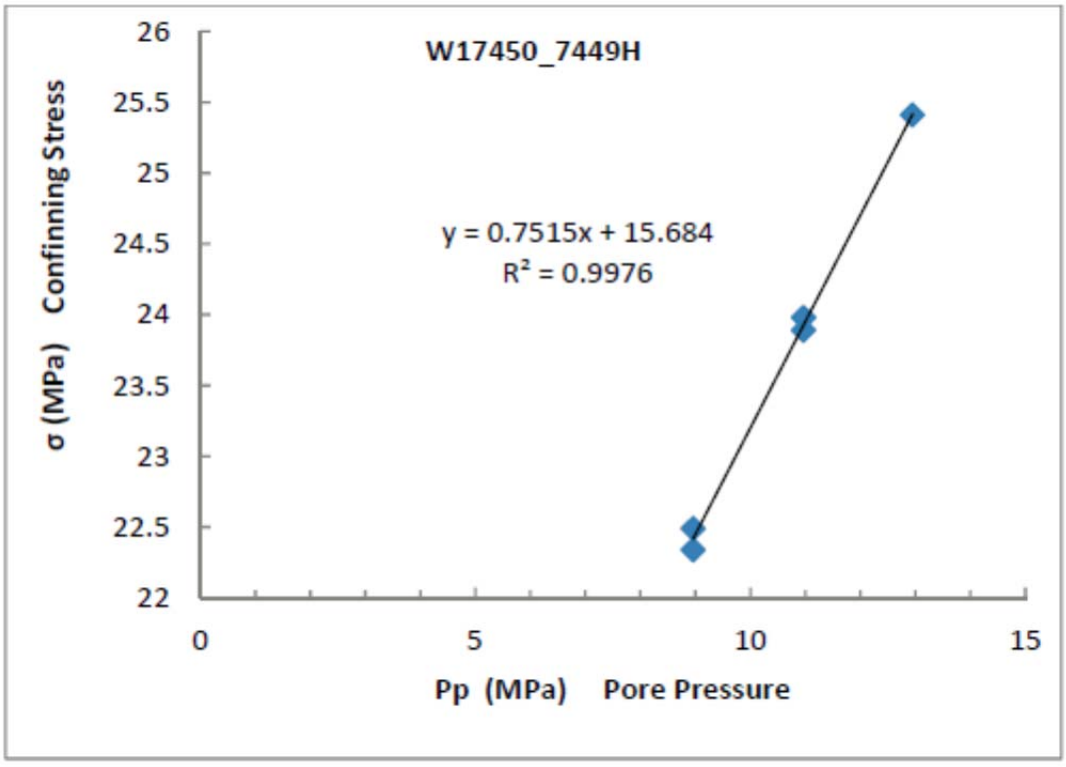
W17450_7449H
y = 0.7515x + 15.684
R² = 0.9976
σ (MPa) Confinning Stress
Pp (MPa) Pore Pressure
26
25.5
25
24.5
24
23.5
23
22.5
22
0
5
10
15

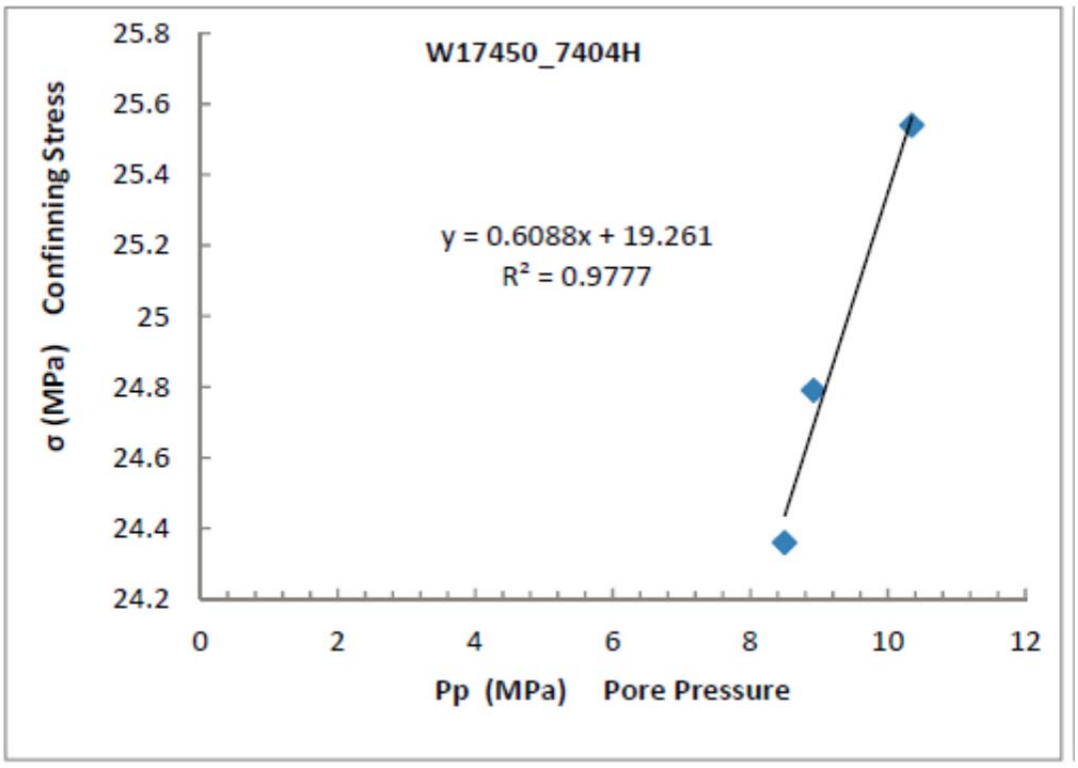
W17450_7404H
y = 0.6088x + 19.261
R² = 0.9777
σ (MPa) Confinning Stress
Pp (MPa) Pore Pressure
25.8
25.6
25.4
25.2
25
24.8
24.6
24.4
24.2
0
2
4
6
8
10
12

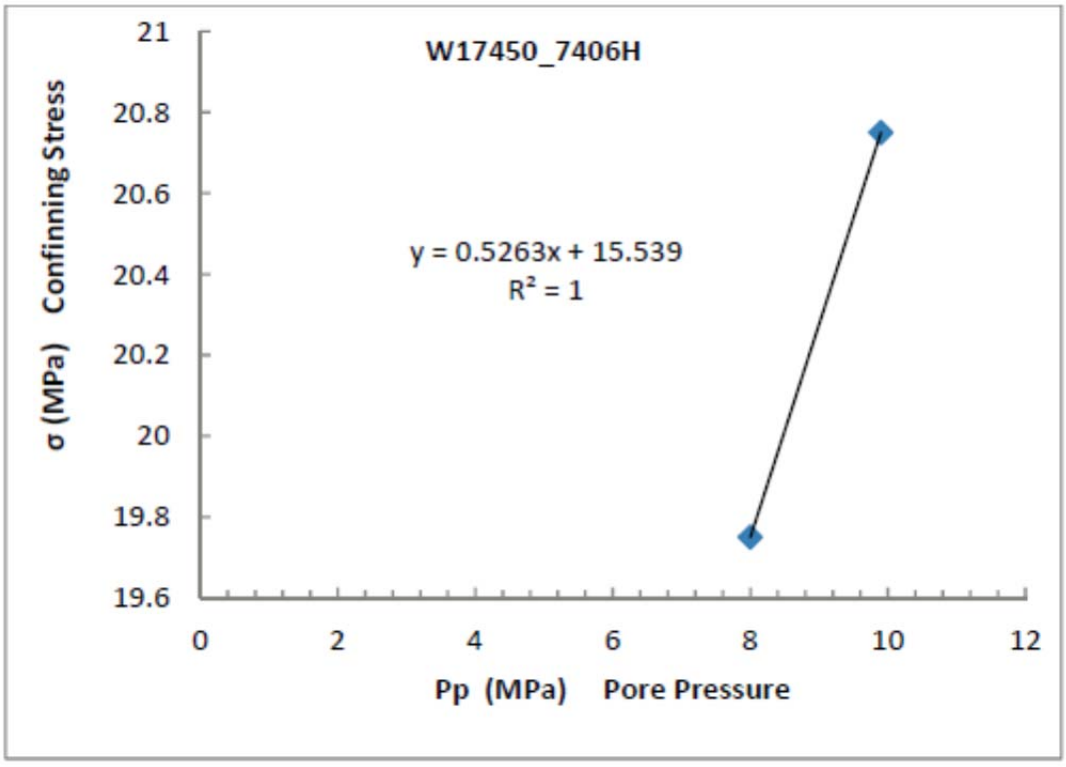
W17450_7406H
y = 0.5263x + 15.539
R² = 1
σ (MPa) Confinning Stress
Pp (MPa) Pore Pressure
21
20.8
20.6
20.4
20.2
20
19.8
19.6
0
2
4
6
8
10
12

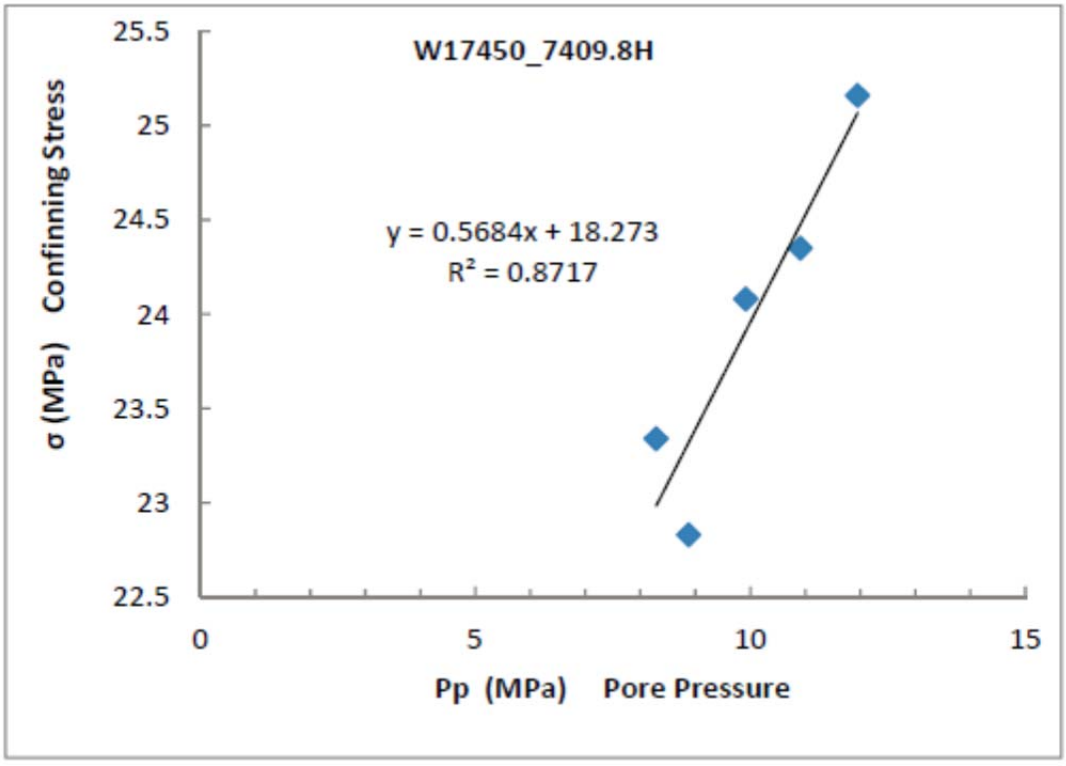
W17450_7409.8H
y = 0.5684x + 18.273
R² = 0.8717
σ (MPa) Confinning Stress
Pp (MPa) Pore Pressure
25.5
25
24.5
24
23.5
23
22.5
0
5
10
15

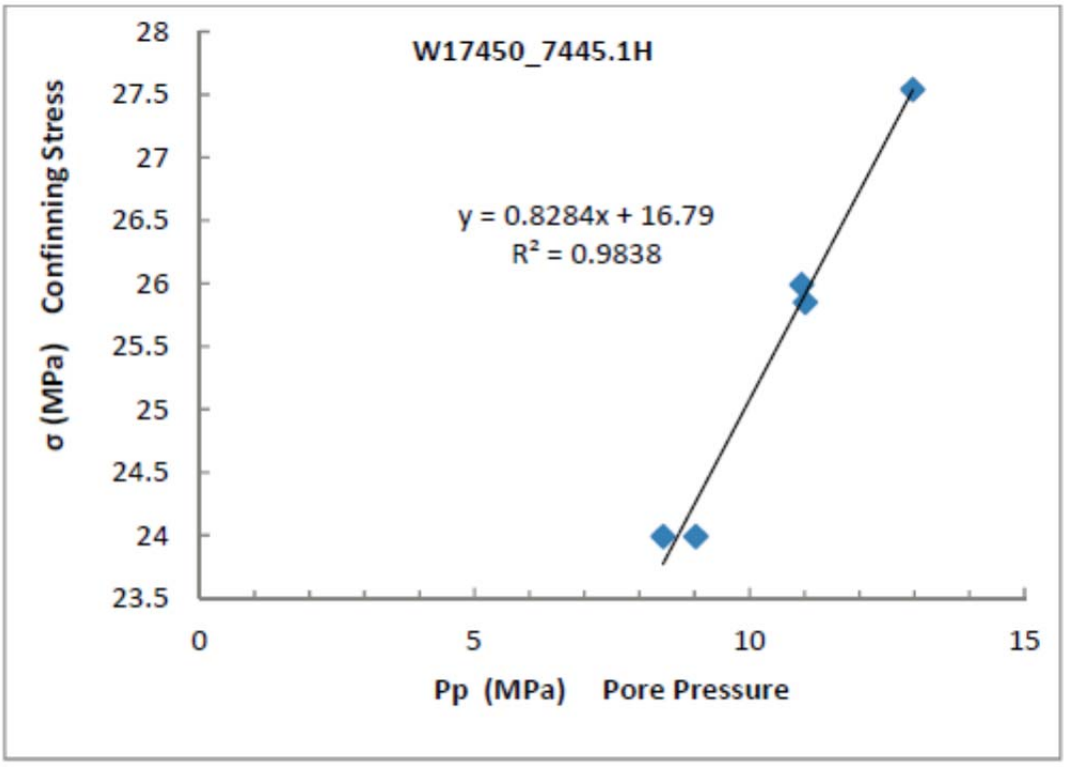
W17450_7445.1H
y = 0.8284x + 16.79
R² = 0.9838
σ (MPa) Confinning Stress
Pp (MPa) Pore Pressure
28
27.5
27
26.5
26
25.5
25
24.5
24
23.5
0
5
10
15

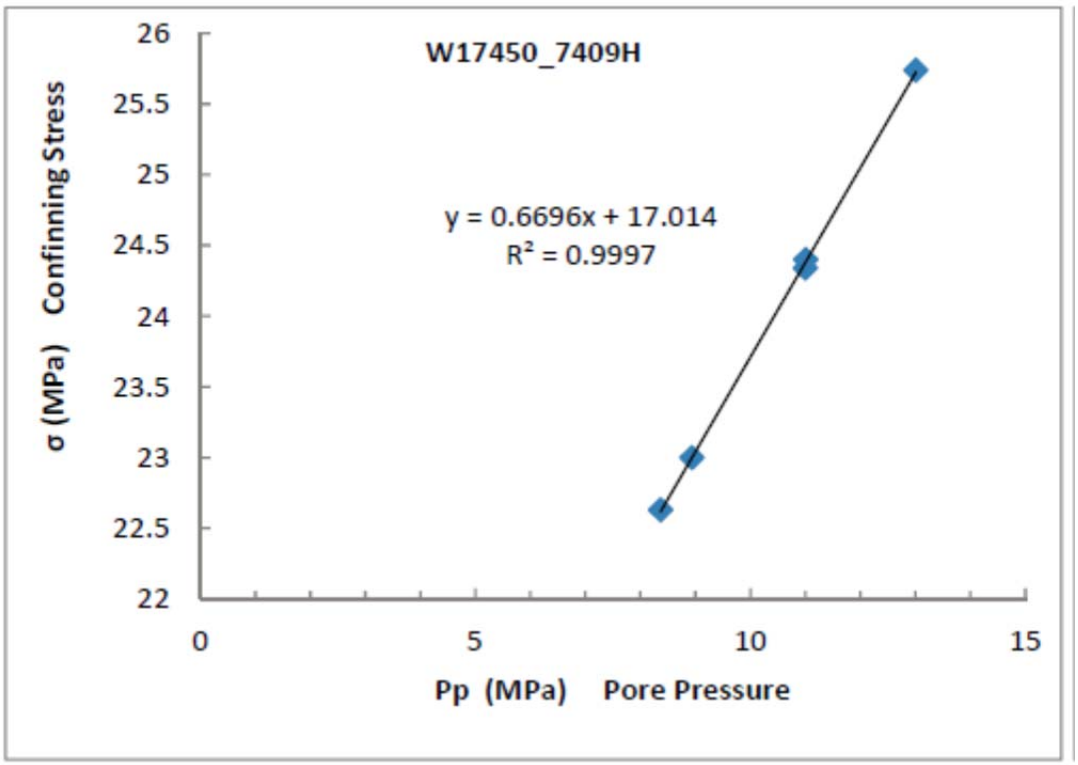
W17450_7409H
y = 0.6696x + 17.014
R² = 0.9997
σ (MPa) Confinning Stress
Pp (MPa) Pore Pressure
26
25.5
25
24.5
24
23.5
23
22.5
22
0
5
10
15

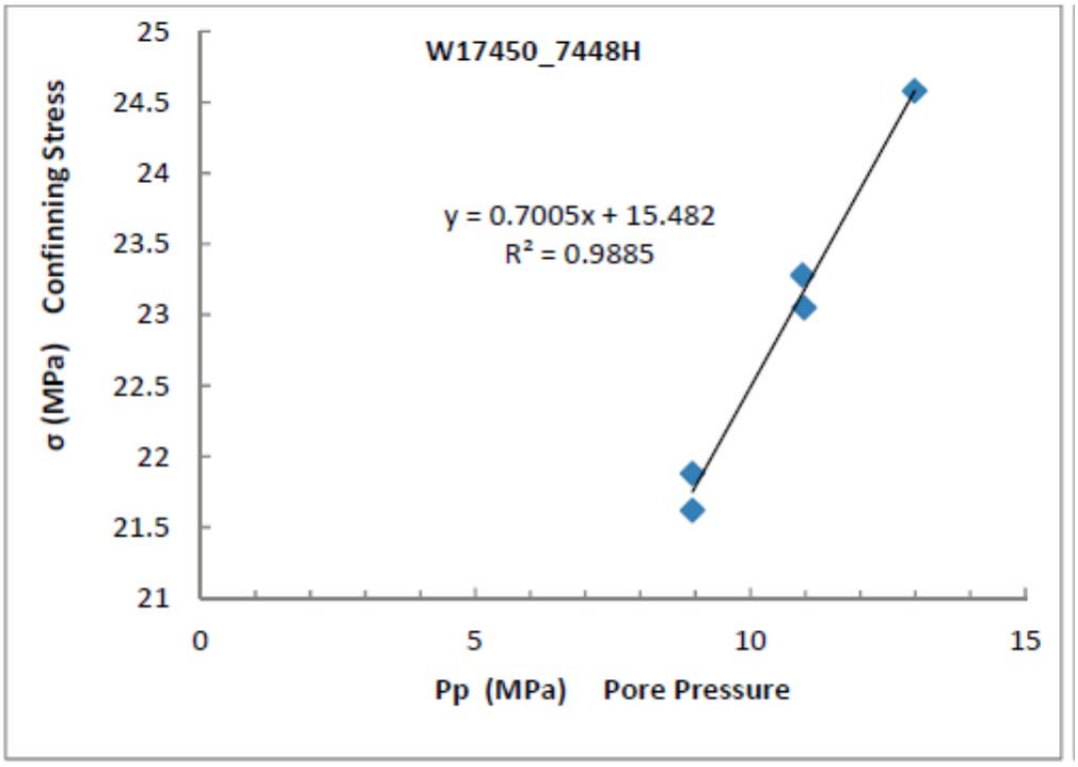
W17450_7448H
y = 0.7005x + 15.482
R² = 0.9885
σ (MPa) Confinning Stress
Pp (MPa) Pore Pressure
25
24.5
24
23.5
23
22.5
22
21.5
21
0
5
10
15

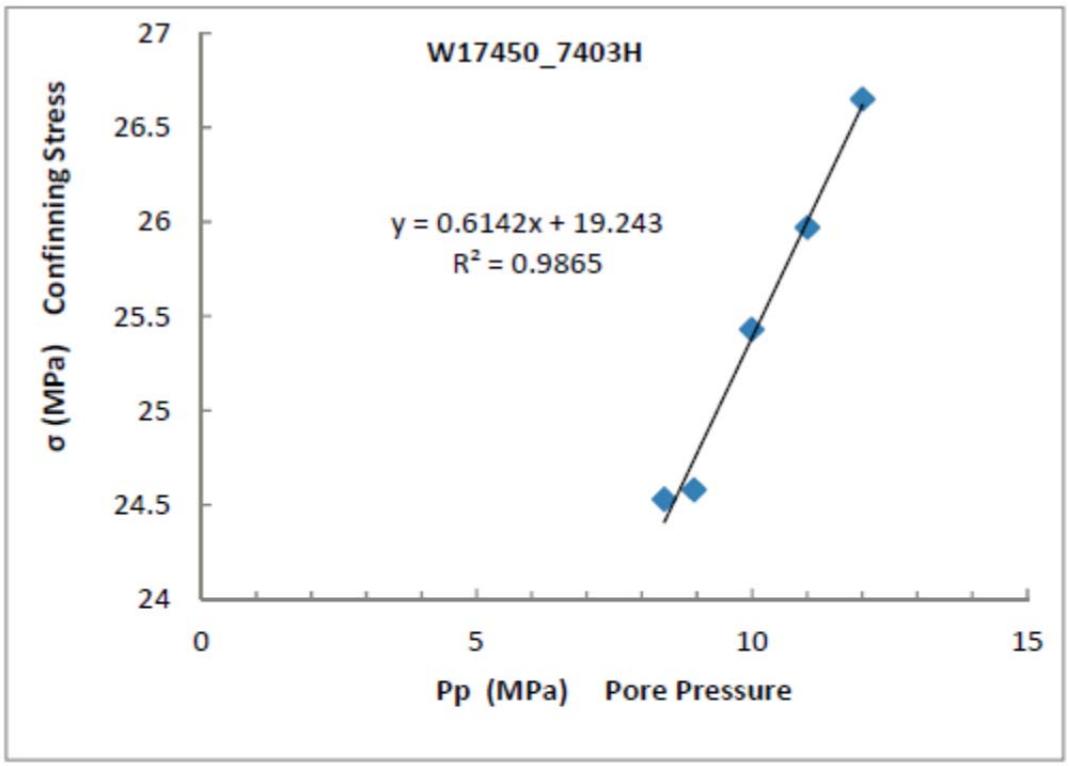
W17450_7403H
y = 0.6142x + 19.243
R² = 0.9865
σ (MPa) Confinning Stress
Pp (MPa) Pore Pressure
27
26.5
26
25.5
25
24.5
24
0
5
10
15

A.7.4 Static Moduli and Poisson's Ratio (Non-destructive)

Uniaxial Stress for File W86-mb-7374H-uniaxial_stress								
Event	Conf	Diff	Temp	E	n	K	G	P
	MPa	MPa	°C	GPa		GPa	GPa	GPa
0	25.5	29.9	26.5	51.96	0.181	27.16	22.00	56.49
1	15.4	15.8	25.4	49.80	0.200	27.71	20.74	55.37
2	5.4	10.7	24.0	46.63	0.216	27.33	19.18	52.90

Uniaxial Stress for File w86-mb-7350H-uniaxial_stress								
Event	Conf	Diff	Temp	E	n	K	G	P
	MPa	MPa	°C	GPa		GPa	GPa	GPa
0	25.5	30.4	28.9	73.86	0.281	56.22	28.83	94.66
1	15.4	16.3	29.2	60.43	0.290	47.90	23.43	79.14
2	5.4	11.6	29.1	52.86	0.292	42.29	20.46	69.58

Uniaxial Stress for File w86-mb-7355.9H-uniaxial_stress								
Event	Conf	Diff	Temp	E	n	K	G	P
	MPa	MPa	°C	GPa		GPa	GPa	GPa
0	25.4	27.4	25.9	67.29	0.130	30.28	29.79	70.00
1	15.3	12.4	25.1	60.90	0.100	25.36	27.69	62.28
2	5.3	8.6	20.6	51.94	0.092	21.20	23.79	52.92

Uniaxial Stress for File w86-mb-7355V-uniaxial_stress								
Event	Conf	Diff	Temp	E	n	K	G	P
	MPa	MPa	°C	GPa		GPa	GPa	GPa
0	25.4	28.6	26.8	54.10	0.162	26.70	23.28	57.73
1	15.3	13.7	24.3	51.91	0.125	23.06	23.08	53.83
2	5.3	9.0	22.2	43.00	0.090	17.48	19.73	43.78

Uniaxial Stress for File w86-mb-7369H-uniaxial_stress								
Event	Conf	Diff	Temp	E	n	K	G	P
	MPa	MPa	°C	GPa		GPa	GPa	GPa
0	25.2	27.8	24.6	67.09	0.271	48.92	26.38	84.10
1	25.3	13.3	25.3	69.79	0.234	43.79	28.27	81.48
2	25.2	8.2	25.8	67.77	0.228	41.60	27.58	78.38
3	15.3	13.7	24.8	67.79	0.225	41.08	27.67	77.97
4	5.3	9.0	23.2	63.12	0.154	30.39	27.36	66.86

Uniaxial Stress for File w86-mb-7380H90-uniaxial_stress								
Event	Conf	Diff	Temp	E	n	K	G	P
	MPa	MPa	°C	GPa		GPa	GPa	GPa
0	25.4	28.2	25.1	52.73	0.219	31.30	21.63	60.14
1	15.3	13.3	24.3	49.53	0.162	24.45	21.30	52.86
2	5.3	9.4	23.5	46.50	0.118	20.27	20.80	48.01

Uniaxial Stress for File w86-mb-7393.1H90-uniaxil_stress								
Event	Conf	Diff	Temp	E	n	K	G	P
	MPa	MPa	°C	GPa		GPa	GPa	GPa
0	25.4	27.8	33.2	56.78	0.169	28.59	24.29	60.97
1	15.3	13.7	27.9	60.70	0.148	28.71	26.44	63.97
2	5.3	9.4	23.0	55.43	0.124	24.54	24.67	57.43

Uniaxial Stress for File w86-mb-7397V-uniaxial_stress								
Event	Conf	Diff	Temp	E	n	K	G	P
	MPa	MPa	°C	GPa		GPa	GPa	GPa
0	25.3	27.8	26.6	73.50	0.249	48.87	29.42	88.09
1	15.3	13.3	26.0	64.82	0.205	36.60	26.90	72.46
2	5.3	8.6	18.9	56.90	0.196	31.22	23.78	62.93

Uniaxial Stress for File w86-mb-7403.8V-Uniaxial_stress								
Event	Conf	Diff	Temp	E	n	K	G	P
	MPa	MPa	°C	GPa		GPa	GPa	GPa
0	25.4	28.6	27.8	61.90	0.204	34.88	25.70	69.14
1	15.4	15.0	27.5	64.47	0.210	36.99	26.65	72.52
2	5.4	10.7	21.8	61.89	0.214	36.02	25.50	70.01

Uniaxial Stress for File W17450-7313-uniaxial-stress									
Event	Conf	Pore	Diff	Temp	E	n	K	G	P
	MPa	MPa	MPa	°C	GPa		GPa	GPa	GPa
0	30.1	-0.2	20.5	28.2	71.11	0.251	47.68	28.41	85.56
1	30.1	-0.2	24.0	28.1	86.67	0.264	61.11	34.29	106.83

Uniaxial Stress for File W17450-7320-uniaxial-stress									
Event	Conf	Pore	Diff	Temp	E	n	K	G	P
	MPa	MPa	MPa	°C	GPa		GPa	GPa	GPa
0	30.1	-0.2	14.6	32.6	53.81	0.337	55.13	20.12	81.95
1	30.0	-0.2	20.5	33.1	68.34	0.324	64.76	25.81	99.17
2	30.0	-0.2	24.4	33.3	70.32	0.316	63.71	26.72	99.33

Uniaxial Stress for File W17450-7327-uniaxial-stress									
Event	Conf	Pore	Diff	Temp	E	n	K	G	P
	MPa	MPa	MPa	°C	GPa		GPa	GPa	GPa
0	50.2	-0.2	39.7	26.5	74.46	0.253	50.15	29.72	89.78
1	50.2	-0.2	44.9	26.1	76.64	0.258	52.71	30.47	93.34

Uniaxial Stress for File W17450-7328.8-uniaxial-stress									
Event	Conf	Pore	Diff	Temp	E	n	K	G	P
	MPa	MPa	MPa	°C	GPa		GPa	GPa	GPa
0	30.3	-0.2	20.5	36.7	86.43	0.239	55.18	34.88	101.68
1	30.3	-0.2	25.2	36.5	92.61	0.288	72.93	35.94	120.86

Uniaxial Stress for File W17450-7330-uniaxial-stress									
Event	Conf	Pore	Diff	Temp	E	n	K	G	P
	MPa	MPa	MPa	°C	GPa		GPa	GPa	GPa
0	30.2	-0.2	15.4	24.7	82.49	0.214	48.12	33.97	93.41
1	30.1	-0.2	18.8	24.2	80.60	0.229	49.64	32.78	93.34
2	30.1	-0.2	24.4	24.3	79.05	0.244	51.39	31.78	93.77

Uniaxial Stress for File W17450-7332-uniaxial-stress									
Event	Conf	Pore	Diff	Temp	E	n	K	G	P
	MPa	MPa	MPa	°C	GPa		GPa	GPa	GPa
0	50.1	-0.2	41.5	32.4	159.11	0.628	-207.73	48.88	-142.56

Uniaxial Stress for File W17450-7353-uniaxial-stress									
Event	Conf	Pore	Diff	Temp	E	n	K	G	P
	MPa	MPa	MPa	°C	GPa		GPa	GPa	GPa
0	30.3	-0.2	15.4	36.3	67.15	0.184	35.40	28.36	73.21
1	30.3	-0.2	21.0	36.2	63.95	0.189	34.24	26.90	70.10

Uniaxial Stress for File W17450-7354-uniaxial-stress									
Event	Conf	Pore	Diff	Temp	E	n	K	G	P
	MPa	MPa	MPa	°C	GPa		GPa	GPa	GPa
0	30.0	-0.2	20.1	33.7	80.14	0.106	33.94	36.22	82.23
1	50.1	-0.2	29.9	34.1	69.55	0.044	25.43	33.30	69.83
2	50.1	-0.2	35.5	33.7	75.16	0.109	32.07	33.87	77.24

Uniaxial Stress for File W17450-7354.5-uniaxial-stress									
Event	Conf	Pore	Diff	Temp	E	n	K	G	P
	MPa	MPa	MPa	°C	GPa		GPa	GPa	GPa
0	50.1	-0.2	25.2	35.0	62.34	0.152	29.85	27.06	65.93
1	50.0	-0.2	29.5	34.6	65.12	0.142	30.35	28.50	68.35

Uniaxial Stress for File W17450-7402.8-uniaxial-stress									
Event	Conf	Pore	Diff	Temp	E	n	K	G	P
	MPa	MPa	MPa	°C	GPa		GPa	GPa	GPa
0	30.1	-0.2	19.7	33.1	51.94	0.165	25.81	22.30	55.54
1	30.1	-0.2	24.8	33.1	51.66	0.215	30.19	21.26	58.54

Uniaxial Stress for File W17450-7404-uniaxial-stress									
Event	Conf	Pore	Diff	Temp	E	n	K	G	P
	MPa	MPa	MPa	°C	GPa		GPa	GPa	GPa
0	30.2	-0.2	15.0	31.8	53.96	0.143	25.17	23.61	56.65
1	30.2	-0.2	20.1	31.9	52.22	0.159	25.54	22.52	55.57
2	30.3	-0.2	25.2	31.9	53.77	0.155	25.97	23.28	57.01

Uniaxial Stress for File W17450-7404.3-uniaxial-stress									
Event	Conf	Pore	Diff	Temp	E	n	K	G	P
	MPa	MPa	MPa	°C	GPa		GPa	GPa	GPa
0	30.1	-0.2	20.1	31.1	70.03	0.144	32.76	30.62	73.58
1	30.1	-0.2	25.2	31.7	56.81	0.191	30.67	23.84	62.46

Uniaxial Stress for File W17450-7407.8-uniaxial-stress									
Event	Conf	Pore	Diff	Temp	E	n	K	G	P
	MPa	MPa	MPa	°C	GPa		GPa	GPa	GPa
0	30.1	-0.2	19.3	27.9	41.48	0.475	281.40	14.06	300.14
1	30.1	-0.2	25.2	27.7	49.13	0.360	58.41	18.07	82.50

Uniaxial Stress for File W17450-7408.3-uniaxial-stress									
Event	Conf	Pore	Diff	Temp	E	n	K	G	P
	MPa	MPa	MPa	°C	GPa		GPa	GPa	GPa
0	30.0	-0.2	21.0	26.7	36.49	0.336	37.11	13.66	55.32
1	30.1	-0.2	25.2	26.5	46.13	0.278	34.59	18.05	58.66

Uniaxial Stress for File W17450-7409-uniaxial-stress									
Event	Conf	Pore	Diff	Temp	E	n	K	G	P
	MPa	MPa	MPa	°C	GPa		GPa	GPa	GPa
0	30.1	-0.2	15.0	33.4	113.83	0.350	126.68	42.15	182.88
1	30.1	-0.2	20.1	33.2	116.86	0.334	117.12	43.81	175.53
2	30.1	-0.2	24.8	33.3	117.21	0.313	104.62	44.63	164.12

Uniaxial Stress for File W17450-7409.8-uniaxial-stress									
Event	Conf	Pore	Diff	Temp	E	n	K	G	P
	MPa	MPa	MPa	°C	GPa		GPa	GPa	GPa
0	30.2	-0.2	15.0	30.2	62.71	0.149	29.76	27.29	66.15
1	30.2	-0.2	20.5	30.5	69.88	0.153	33.58	30.30	73.98
2	30.2	-0.2	25.7	30.8	69.09	0.157	33.57	29.86	73.38

Uniaxial Stress for File W17450-7410-uniaxial-stress									
Event	Conf	Pore	Diff	Temp	E	n	K	G	P
	MPa	MPa	MPa	°C	GPa		GPa	GPa	GPa
0	50.3	-0.2	29.5	31.7	62.49	0.244	40.70	25.11	74.18
1	50.3	-0.2	35.1	31.7	66.98	0.194	36.52	28.04	73.91

Uniaxial Stress for File W17450-7445.1-uniaxial-stress									
Event	Conf	Pore	Diff	Temp	E	n	K	G	P
	MPa	MPa	MPa	°C	GPa		GPa	GPa	GPa
0	20.2	-0.2	15.8	32.4	45.97	0.057	17.31	21.73	46.29
1	20.2	-0.2	20.5	32.5	53.14	0.106	22.51	24.01	54.52

Uniaxial Stress for File w17450-7321-uniaxial-stress									
Event	Conf	Pore	Diff	Temp	E	n	K	G	P
	MPa	MPa	MPa	°C	GPa		GPa	GPa	GPa
0	40.7	-0.2	20.1	30.1	98.06	0.283	75.35	38.21	126.30
1	50.6	-0.2	23.5	30.1	97.34	0.316	88.13	36.99	137.44
2	30.6	-0.2	18.8	30.0	100.68	0.289	79.49	39.06	131.56

Uniaxial Stress for File w17450-7321.2-uniaxial-stress									
Event	Conf	Pore	Diff	Temp	E	n	K	G	P
	MPa	MPa	MPa	°C	GPa		GPa	GPa	GPa
0	40.5	-0.2	18.4	35.1	76.49	0.279	57.78	29.89	97.64
1	50.5	-0.2	23.1	35.1	80.48	0.209	46.14	33.28	90.51
2	30.4	-0.2	18.4	34.8	83.29	0.299	68.98	32.07	111.74

Uniaxial Stress for File w17450-7326.5-uniaxial-stress									
Event	Conf	Pore	Diff	Temp	E	n	K	G	P
	MPa	MPa	MPa	°C	GPa		GPa	GPa	GPa
0	40.6	-0.2	18.4	31.0	92.29	0.319	84.99	34.98	131.63
1	50.5	-0.2	23.1	31.0	78.94	0.315	71.24	30.01	111.25
2	30.5	-0.2	19.3	30.4	94.40	0.321	87.83	35.73	135.48

Uniaxial Stress for File w17450-7348.8-uniaxial-stress									
Event	Conf	Pore	Diff	Temp	E	n	K	G	P
	MPa	MPa	MPa	°C	GPa		GPa	GPa	GPa
0	40.6	-0.2	28.2	31.6	53.60	0.162	26.47	23.05	57.20
1	50.6	-0.2	33.3	31.5	46.54	0.150	22.16	20.24	49.14
2	30.5	-0.2	24.0	30.9	76.43	0.192	41.32	32.06	84.08

Uniaxial Stress for File w17450-7351-uniaxial-stress									
Event	Conf	Pore	Diff	Temp	E	n	K	G	P
	MPa	MPa	MPa	°C	GPa		GPa	GPa	GPa
0	40.5	-0.2	18.4	34.3	73.63	0.212	42.63	30.37	83.12
1	50.5	-0.2	23.1	34.8	70.89	0.221	42.30	29.04	81.02
2	30.5	-0.2	19.3	34.5	72.20	0.205	40.82	29.95	80.76

Uniaxial Stress for File w17450-7401.9-uniaxial-stress									
Event	Conf	Pore	Diff	Temp	E	n	K	G	P
	MPa	MPa	MPa	°C	GPa		GPa	GPa	GPa
0	40.5	-0.2	18.0	34.1	41.03	0.472	243.27	13.94	261.86
1	50.5	-0.2	22.7	34.2	44.22	0.444	132.22	15.31	152.63
2	30.5	-0.2	18.8	33.9	45.71	0.490	746.25	15.34	766.71

Uniaxial Stress for File w17450-7405.8-uniaxial-stress									
Event	Conf	Pore	Diff	Temp	E	n	K	G	P
	MPa	MPa	MPa	°C	GPa		GPa	GPa	GPa
0	40.5	-0.2	18.4	30.4	120.05	0.498	12925.20	40.06	12978.60
1	50.5	-0.2	22.7	31.2	115.71	0.470	645.74	39.35	698.21
2	30.5	-0.2	18.4	31.1	122.65	0.500	-52549.30	40.87	-52494.80

Uniaxial Stress for File w17450-7449-unixial-stress									
Event	Conf	Pore	Diff	Temp	E	n	K	G	P
	MPa	MPa	MPa	°C	GPa		GPa	GPa	GPa
0	30.5	-0.2	23.5	33.1	70.96	0.232	44.18	28.79	82.57

A.7.5 Uni/Triaxial Compressive Strength, Young's Modulus and Poisson's Ratio

Strength for File w86-mb-7355.9H-strength					
Event	Conf	Temp	E	n	peak_stress
	MPa	°C	GPa		MPa
0	15.4	25.9	73.13	0.704	116.2

Strength for File w86-mb-7355V-strength					
Event	Conf	Temp	E	n	peak_stress
	MPa	°C	GPa		MPa
0	15.1	29.9	32.65	0.246	188.3

Strength for File w86-mb-7380H90-strength					
Event	Conf	Temp	E	n	peak_stress
	MPa	°C	GPa		MPa
0	15.0	29.0	31.31	0.354	198.1

Strength for File w17450-7320-strength						
Event	Conf	Diff	Temp	E	n	peak_stress
	MPa	MPa	°C	GPa		MPa
0	12.9	25.2	24.8	150.22	1.735	53.0
1	12.9	11.6	24.4	123.07	0.006	38.9

Strength for File w17450-7321-strength						
Event	Conf	Diff	Temp	E	n	peak_stress
	MPa	MPa	°C	GPa		MPa
0	6.1	11.6	23.9	56.85	0.689	64.5

Strength for File w17450-7321.2-strength						
Event	Conf	Diff	Temp	E	n	peak_stress
	MPa	MPa	°C	GPa		MPa
0	0.7	32.5	26.0	41.32	0.332	111.5

Strength for File w17450-7323.6-strength						
Event	Conf	Diff	Temp	E	n	peak_stress
	MPa	MPa	°C	GPa		MPa
0	13.2	68.3	26.2	82.45	0.041	79.4

Strength for File w17450-7326.5-strength						
Event	Conf	Diff	Temp	E	n	peak_stress
	MPa	MPa	°C	GPa		MPa
0	6.2	48.7	21.1	71.72	0.372	105.9

Strength for File w17450-7327-strength						
Event	Conf	Diff	Temp	E	n	peak_stress
	MPa	MPa	°C	GPa		MPa
0	0.4	19.3	20.5	183.32	9.455	21.4

Strength for File w17450-7328.8-1-strength						
Event	Conf	Diff	Temp	E	n	peak_stress
	MPa	MPa	°C	GPa		MPa
0	13.1	10.3	24.1	65.13	0.280	171.6

Strength for File w17450-7348.8-strength						
Event	Conf	Diff	Temp	E	n	peak_stress
	MPa	MPa	°C	GPa		MPa
0	6.2	48.3	28.2	62.03	0.270	111.5

Strength for File w17450-7351-strength						
Event	Conf	Diff	Temp	E	n	peak_stress
	MPa	MPa	°C	GPa		MPa
0	0.9	26.5	23.3	73.70	1.170	82.4

Strength for File w17450-7353-strength						
Event	Conf	Diff	Temp	E	n	peak_stress
	MPa	MPa	°C	GPa		MPa
0	13.7	14.1	21.7	50.92	0.266	266.0

Strength for File w17450-7354-strength						
Event	Conf	Diff	Temp	E	n	peak_stress
	MPa	MPa	°C	GPa		MPa
0	6.4	7.3	22.5	64.62	0.285	139.2

Strength for File w17450-7354.5-strength						
Event	Conf	Diff	Temp	E	n	peak_stress
	MPa	MPa	°C	GPa		MPa
0	0.8	15.4	20.1	39.82	0.284	146.5

A.7.6 Mohr's Circle

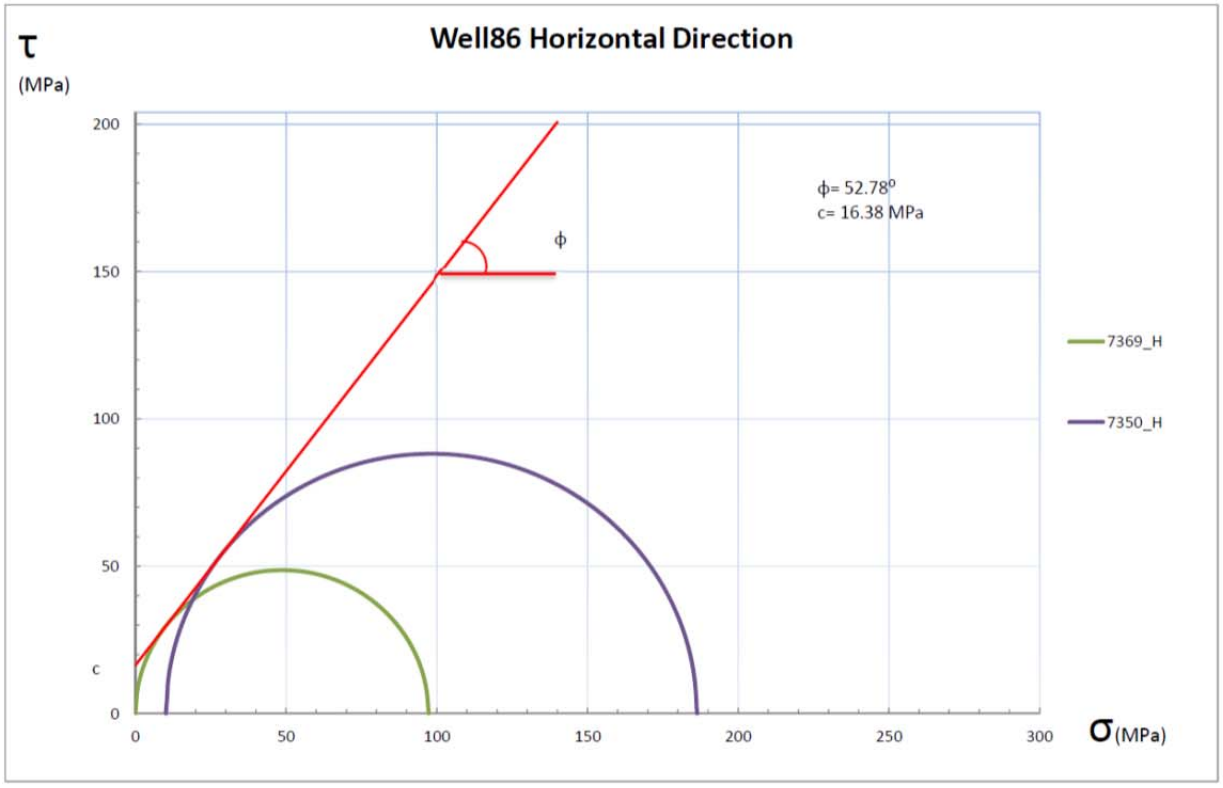

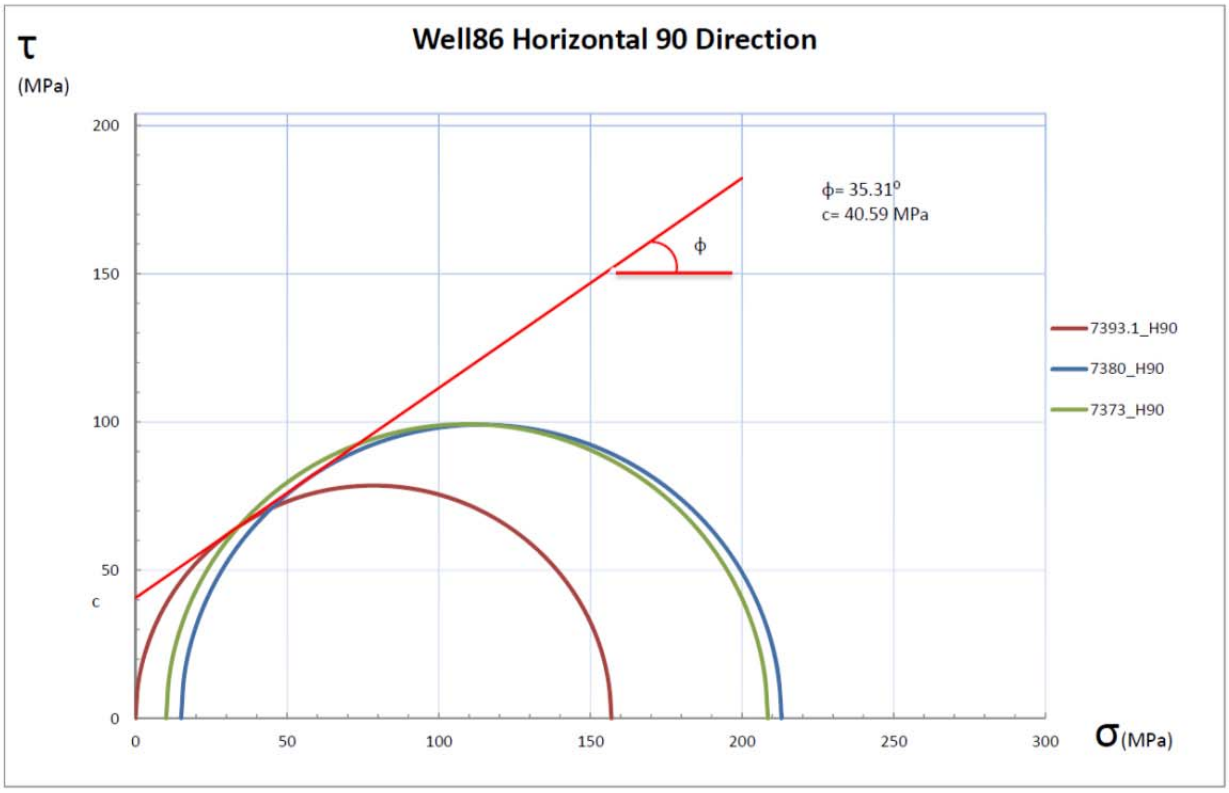

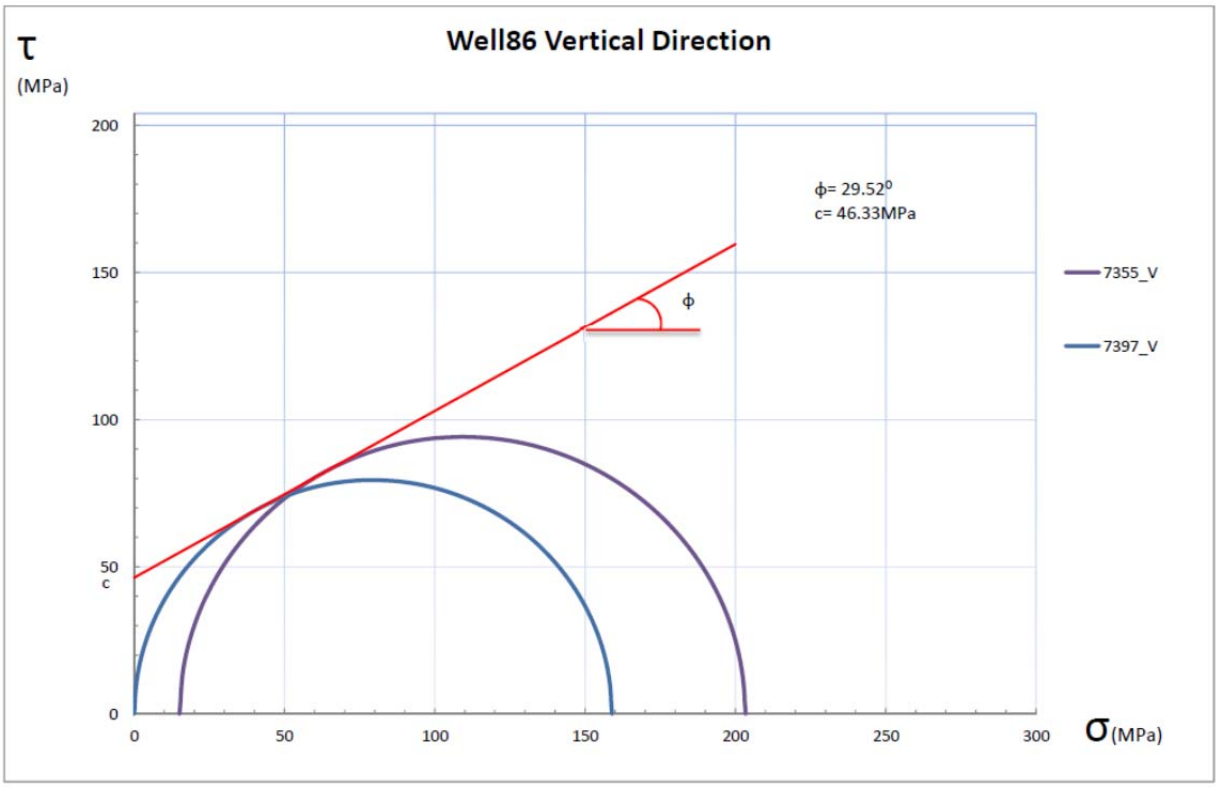
Well86 Vertical Direction
τ
(MPa)
200
150
100
50
c
0
0
50
100
150
200
250
300
σ(MPa)
ϕ= 29.52⁰
c= 46.33MPa
ϕ
7355_V
7397_V

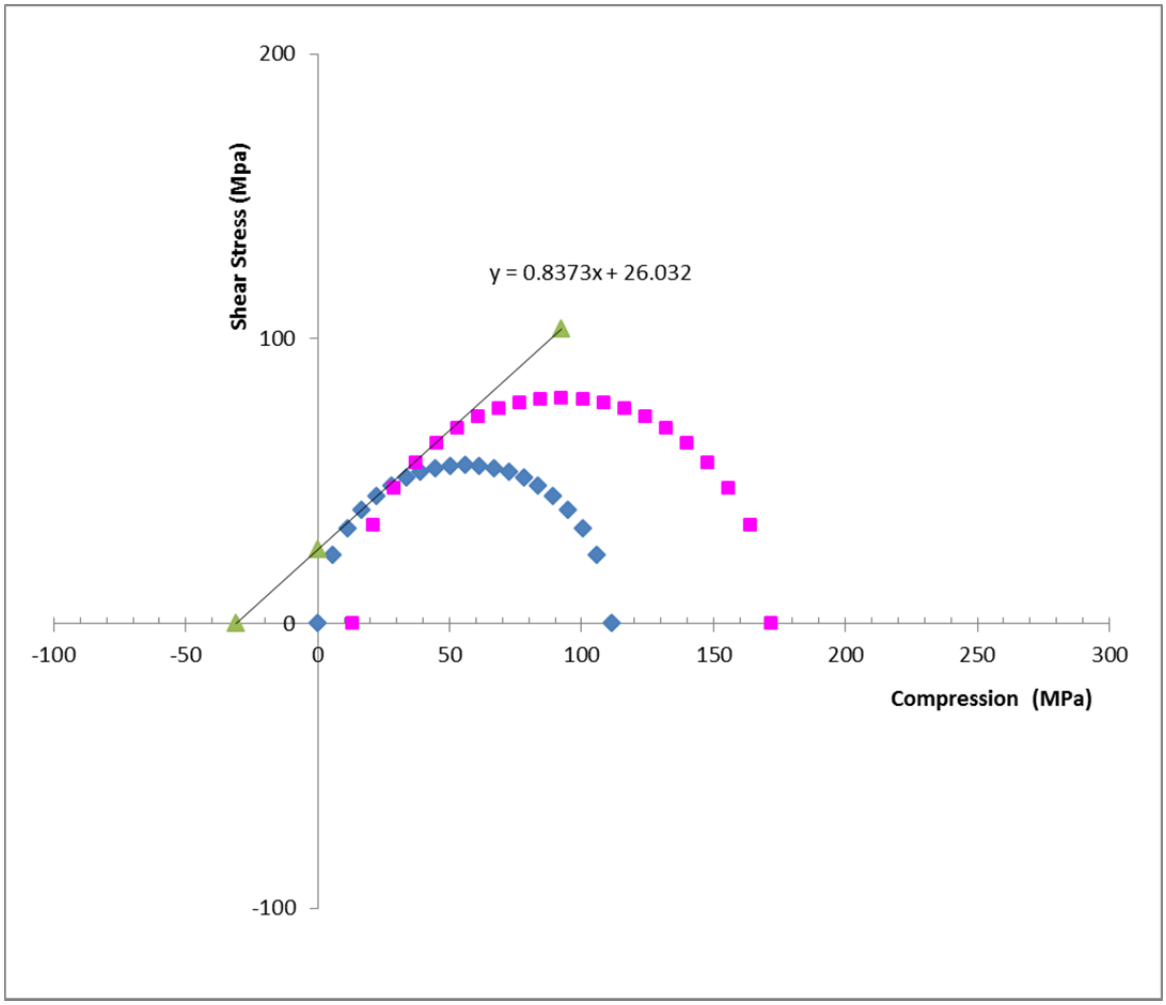
200
100
0
-100
Shear Stress (Mpa)
y = 0.8373x + 26.032
-100
-50
0
50
100
150
200
250
300
Compression (MPa)

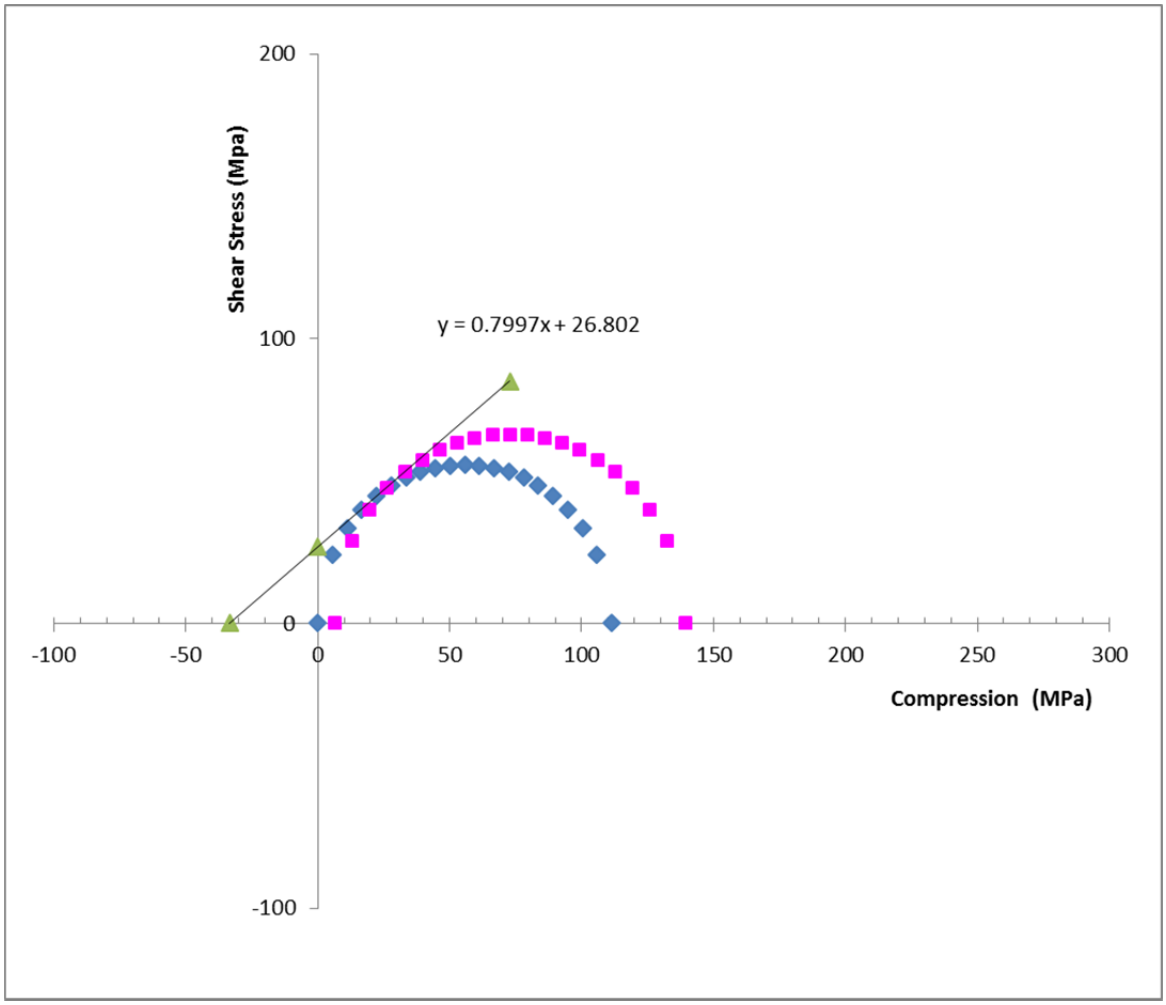
200
100
0
-100
Shear Stress (Mpa)
y = 0.7997x + 26.802
-100
-50
0
50
100
150
200
250
300
Compression (MPa)

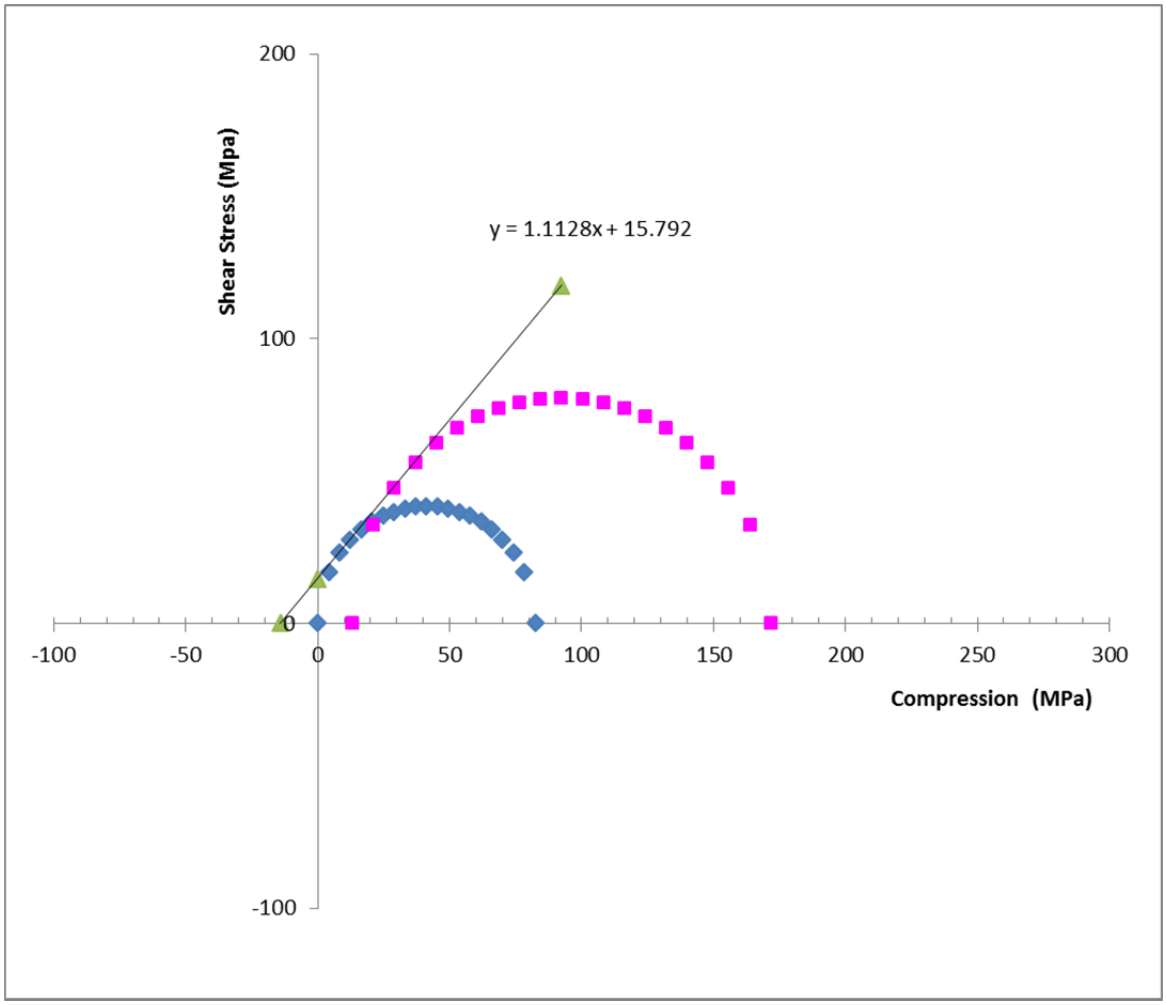
200
100
0
-100
Shear Stress (Mpa)
y = 1.1128x + 15.792
-100
-50
0
50
100
150
200
250
300
Compression (MPa)

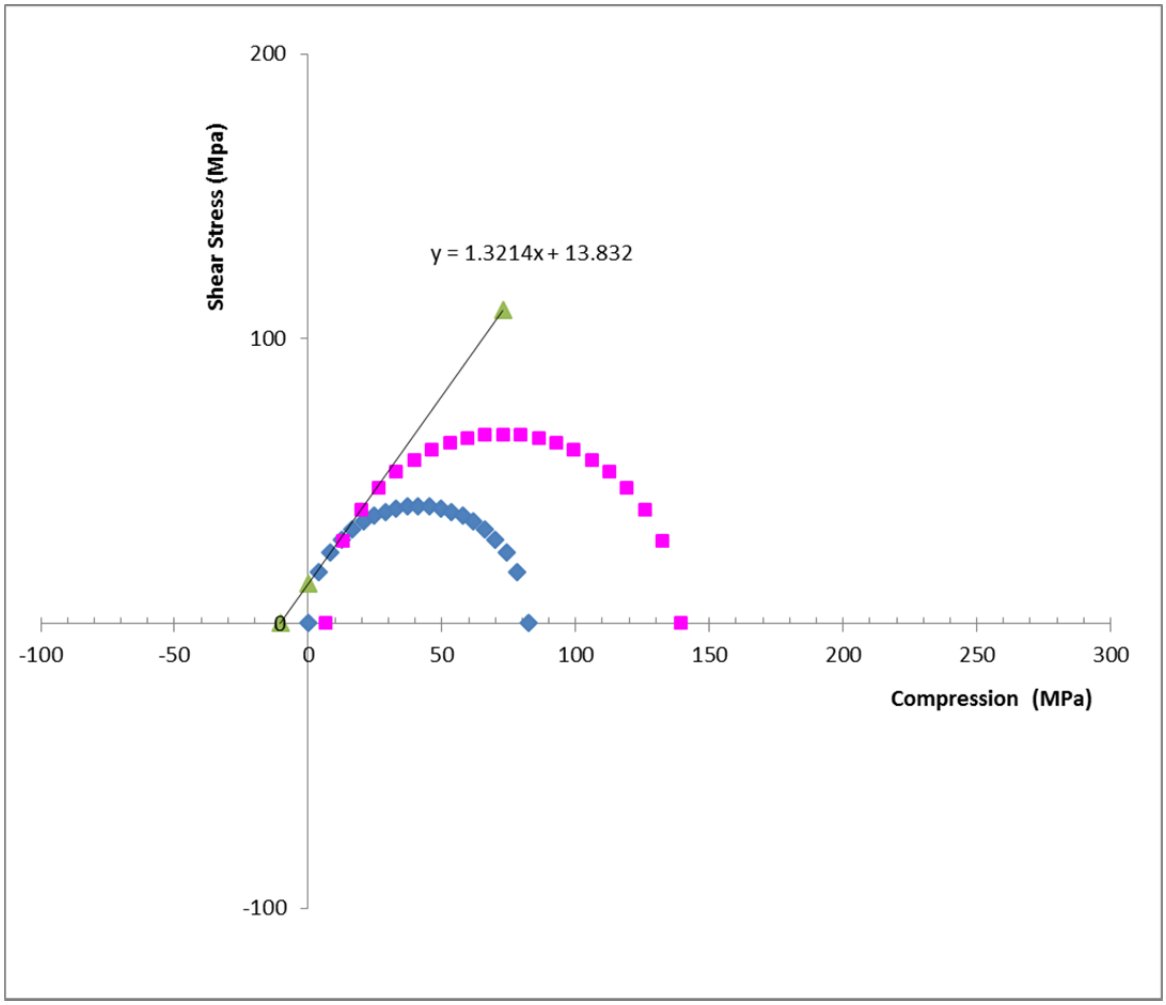
Shear Stress (Mpa)
y = 1.3214x + 13.832
200
100
-100
-100
-50
0
50
100
150
200
250
300
Compression (MPa)

A.8. Well 18 Bakken Samples Testing Results

A.8.1 Permeability

Permeability and Specific Storage for File w16089-8670.2-perm-biot							
Event	Type	Conf	Pore Top	Diff	Temp	Perm	Storage
		MPa	MPa	MPa	°C	μD	m^{-1}
0	multipulse	20.7	7.6	-0.4	21.4	0.0519	1.04e-07
1	multipulse	30.6	7.5	-1.3	28.8	0.0136	7.98e-08
2	multipulse	40.7	7.6	-1.7	31.7	0.00566	1.44e-07
3	multipulse	40.7	7.6	-1.7	32.7	0.269	8.55e-05

Permeability and Specific Storage for File w16089-8672-perm-biot							
Event	Type	Conf	Pore Top	Diff	Temp	Perm	Storage
		MPa	MPa	MPa	°C	μD	m^{-1}
0	multipulse	20.7	7.5	-0.4	23.0	0.0671	8.83e-07
1	multipulse	30.6	7.5	-1.3	23.2	0.0403	7.33e-07
2	multipulse	40.7	7.5	-1.7	26.3	0.0306	4.28e-07
3	multipulse	50.7	7.6	-2.5	25.9	0.0213	4.33e-07

Permeability and Specific Storage for File w16089-8673.2-perm-biot							
Event	Type	Conf	Pore Top	Diff	Temp	Perm	Storage
		MPa	MPa	MPa	°C	μD	m^{-1}
0	aspike	20.7	7.5	-0.8	23.0	1.06	1.20e-12
1	aspike	20.7	7.5	-0.8	23.2	0.689	7.96e-11
2	aspike	30.6	7.5	-1.7	23.4	0.352	1.51e-11
3	aspike	40.7	7.5	-1.3	24.5	0.453	1.34e-11

Permeability and Specific Storage for File w16089-8674-perm-biot							
Event	Type	Conf	Pore Top	Diff	Temp	Perm	Storage
		MPa	MPa	MPa	°C	μD	m^{-1}
0	aspike	20.7	7.6	-0.4	24.8	0.735	1.50e-11
1	aspike	30.6	7.6	-1.7	24.4	0.695	2.74e-07
2	aspike	40.7	7.6	-2.1	24.3	0.609	3.93e-07

Permeability and Specific Storage for File w16089-8677.4-perm							
Event	Type	Conf	Pore Top	Diff	Temp	Perm	Storage
		MPa	MPa	MPa	°C	μD	m^{-1}
0	multipulse	20.7	7.6	-0.8	21.6	0.134	5.27e-07
1	multipulse	30.6	7.6	-1.7	21.7	0.0838	4.68e-07
2	multipulse	40.7	7.6	-1.7	21.9	0.0728	6.24e-07

A.8.2 Sonic Velocity, Dynamic Moduli and Poisson's Ratio

Observed Velocities and Moduli for File w16089-8648.2-velocity									
Event	Conf	Pore	Diff	Temp	V_p	$V_s^{(1)}$	$V_s^{(2)}$	Young's Modulus	Poisson's Ratio
	MPa	MPa	MPa	°C	m/s	m/s	m/s	GPa	
0	10.6	-0.2	1.2	26.9	4233	2688	2501	40.84	0.199
1	20.6	-0.2	0.4	27.7	4484	2786	2609	44.79	0.216
2	30.6	-0.2	-0.3	28.1	4635	2888	2706	48.04	0.214
3	40.6	-0.2	-0.8	28.5	4766	2960	2782	50.68	0.215
4	50.6	-0.2	-0.8	28.9	4853	3011	2834	52.53	0.216

Observed Velocities and Moduli for File w16089-8650.6-velocity									
Event	Conf	Pore	Diff	Temp	V_p	$V_s^{(1)}$	$V_s^{(2)}$	Young's Modulus	Poisson's Ratio
	MPa	MPa	MPa	°C	m/s	m/s	m/s	GPa	
0	10.6	-0.2	1.0	27.6	4136	2640	2640	40.78	0.156
1	20.6	-0.2	0.3	28.0	4319	2732	2735	44.08	0.166
2	30.6	-0.2	0.0	28.7	4764	2813	2815	49.37	0.232
3	40.6	-0.2	-0.6	29.3	4764	2873	2886	50.86	0.212
4	50.6	-0.2	-1.3	29.5	4818	2924	2931	52.36	0.207

Observed Velocities and Moduli for File w16089-8651.4-velocity									
Event	Conf	Pore	Diff	Temp	V_p	$V_s^{(1)}$	$V_s^{(2)}$	Young's Modulus	Poisson's Ratio
	MPa	MPa	MPa	°C	m/s	m/s	m/s	GPa	
0	10.6	-0.2	1.3	26.9	4108	2559	2637	39.85	0.167
1	20.6	-0.2	0.7	27.9	4318	2649	2742	43.41	0.181
2	30.6	-0.2	0.3	28.8	4541	2738	2826	46.98	0.200
3	40.6	-0.2	-0.6	29.2	4709	2805	2889	49.71	0.212
4	50.6	-0.2	-1.1	30.2	4778	2847	2939	51.27	0.211

Observed Velocities and Moduli for File w16089-8655-velocity									
Event	Conf	Pore	Diff	Temp	V_p	$V_s^{(1)}$	$V_s^{(2)}$	Young's Modulus	Poisson's Ratio
	MPa	MPa	MPa	°C	m/s	m/s	m/s	GPa	
0	10.6	-0.2	1.0	29.8	4361	2785	2781	45.50	0.156
1	20.7	-0.2	0.9	30.7	4605	2870	2886	49.63	0.180
2	30.5	-0.2	0.0	31.3	4700	2928	2961	51.84	0.177
3	40.6	-0.2	0.0	31.7	4843	2976	3009	54.19	0.191
4	50.6	-0.2	-0.7	32.0	4913	3000	3030	55.32	0.198

Observed Velocities and Moduli for File w16089-8655.7-velocity									
Event	Conf	Pore	Diff	Temp	V_p	$V_s^{(1)}$	$V_s^{(2)}$	Young's Modulus	Poisson's Ratio
	MPa	MPa	MPa	°C	m/s	m/s	m/s	GPa	
0	10.5	-0.2	1.3	30.3	4491	2783	2776	46.50	0.190
1	20.6	-0.2	1.2	31.3	4711	2884	2859	50.25	0.204
2	30.5	-0.2	0.4	32.0	4782	2952	2931	52.35	0.196
3	40.6	-0.2	0.2	32.0	4931	3000	2970	54.59	0.211
4	50.6	-0.2	-0.4	32.6	5043	3029	2998	56.17	0.222

Observed Velocities and Moduli for File w16089-8657.2-velocity									
Event	Conf	Pore	Diff	Temp	V_p	$V_s^{(1)}$	$V_s^{(2)}$	Young's Modulus	Poisson's Ratio
	MPa	MPa	MPa	°C	m/s	m/s	m/s	GPa	
0	10.6	-0.2	1.6	30.6	4739	2809	2959	51.35	0.206
1	20.6	-0.2	1.3	30.9	4930	2912	3025	54.85	0.216
2	30.5	-0.2	0.4	31.3	5013	2983	3082	57.04	0.211
3	40.6	-0.2	0.2	31.6	5137	3035	3123	59.20	0.220
4	50.6	-0.2	0.0	31.9	5161	3058	3151	60.03	0.216

Observed Velocities and Moduli for File w16089-8657.4-velocity									
Event	Conf	Pore	Diff	Temp	V_p	$V_s^{(1)}$	$V_s^{(2)}$	Young's Modulus	Poisson's Ratio
	MPa	MPa	MPa	°C	m/s	m/s	m/s	GPa	
0	10.6	-0.2	2.0	30.5	4709	2917	2736	49.64	0.218
1	20.6	-0.2	1.3	31.0	4812	2976	2830	52.17	0.214
2	30.6	-0.2	1.0	31.5	4973	3014	2894	54.62	0.227
3	40.6	-0.2	0.2	31.8	5010	3046	2936	55.80	0.223
4	50.6	-0.2	-0.1	32.2	5038	3064	2966	56.61	0.221

Observed Velocities and Moduli for File w16089-8659.4-velocity									
Event	Conf	Pore	Diff	Temp	V_p	$V_s^{(1)}$	$V_s^{(2)}$	Young's Modulus	Poisson's Ratio
	MPa	MPa	MPa	°C	m/s	m/s	m/s	GPa	
0	10.6	-0.2	1.3	27.8	4531	2675	2870	47.07	0.201
1	20.6	-0.2	0.4	28.6	4647	2760	2912	49.36	0.203
2	30.5	-0.2	0.0	29.5	4812	2923	3007	53.53	0.194
3	40.6	-0.2	-0.1	29.8	4946	2981	3060	55.96	0.203
4	50.6	-0.2	-0.6	30.4	4989	3011	3089	57.01	0.202

Observed Velocities and Moduli for File w16089-8660.7-velocity									
Event	Conf	Pore	Diff	Temp	V_p	$V_s^{(1)}$	$V_s^{(2)}$	Young's Modulus	Poisson's Ratio
	MPa	MPa	MPa	°C	m/s	m/s	m/s	GPa	
0	10.6	-0.2	1.3	27.9	4381	2693	2774	44.84	0.181
1	20.6	-0.2	0.4	28.0	4595	2788	2863	48.50	0.196
2	30.6	-0.2	0.0	28.6	4725	2850	2937	51.04	0.200
3	40.6	-0.2	-0.1	29.0	4845	2804	2978	51.95	0.224
4	50.7	-0.2	-0.6	29.2	4893	2850	3006	53.18	0.221

Observed Velocities and Moduli for File w16089-8661.9-velocity									
Event	Conf	Pore	Diff	Temp	V_p	$V_s^{(1)}$	$V_s^{(2)}$	Young's Modulus	Poisson's Ratio
	MPa	MPa	MPa	°C	m/s	m/s	m/s	GPa	
0	10.7	-0.2	1.2	27.4	4567	2668	2843	46.63	0.214
1	20.6	-0.2	0.4	27.8	4715	2777	2921	49.80	0.212
2	30.7	-0.2	0.4	28.5	4836	2882	2985	52.64	0.209
3	40.7	-0.2	-0.4	28.6	4920	2927	3012	54.14	0.213
4	50.7	-0.2	-0.7	28.8	5020	2959	3058	55.86	0.220

Observed Velocities and Moduli for File w16089-8664.2-velocity									
Event	Conf	Pore	Diff	Temp	V_p	$V_s^{(1)}$	$V_s^{(2)}$	Young's Modulus	Poisson's Ratio
	MPa	MPa	MPa	°C	m/s	m/s	m/s	GPa	
0	10.6	-0.2	0.4	25.5	3759	2490	2522	34.95	0.100
1	20.7	-0.2	0.2	26.4	4003	2643	2654	39.42	0.111
2	30.6	-0.2	-0.4	27.2	4232	2746	2755	43.42	0.134
3	40.6	-0.2	-0.8	27.8	4484	2828	2821	47.27	0.171
4	50.7	-0.2	-1.1	28.0	4627	2869	2880	49.58	0.186

Observed Velocities and Moduli for File w16089-8665-velocity									
Event	Conf	Pore	Diff	Temp	V_p	$V_s^{(1)}$	$V_s^{(2)}$	Young's Modulus	Poisson's Ratio
	MPa	MPa	MPa	°C	m/s	m/s	m/s	GPa	
0	10.6	-0.2	0.9	26.0	4174	2693	2726	42.70	0.136
1	20.6	-0.2	0.0	26.3	4445	2803	2851	47.48	0.160
2	30.6	-0.2	-0.6	27.2	4656	2444	2337	38.65	0.321
3	40.7	-0.2	-0.6	27.7	4752	2461	2369	39.59	0.326
4	50.7	-0.2	-1.3	28.1	4819	2515	2402	40.98	0.324

Observed Velocities and Moduli for File w16089-8665.3-velocity									
Event	Conf	Pore	Diff	Temp	V_p	$V_s^{(1)}$	$V_s^{(2)}$	Young's Modulus	Poisson's Ratio
	MPa	MPa	MPa	°C	m/s	m/s	m/s	GPa	
0	10.6	-0.2	1.3	25.2	4406	2791	2826	47.12	0.158
1	20.6	-0.2	0.4	27.3	4499	2856	2878	49.12	0.158
2	30.6	-0.2	0.0	29.2	4676	2912	2928	51.93	0.180
3	40.6	-0.2	-0.7	28.5	4781	2969	2983	54.10	0.184
4	50.7	-0.2	-0.8	29.4	5000	3005	3024	56.95	0.214

Observed Velocities and Moduli for File w16089-8668-velocity									
Event	Conf	Pore	Diff	Temp	V_p	$V_s^{(1)}$	$V_s^{(2)}$	Young's Modulus	Poisson's Ratio
	MPa	MPa	MPa	°C	m/s	m/s	m/s	GPa	
0	10.6	-0.2	1.2	25.6	5124	3004	3006	56.78	0.238
1	20.7	-0.2	0.7	26.6	5248	3048	3021	58.42	0.249
2	30.6	-0.2	0.0	27.6	5336	3070	3052	59.72	0.255
3	40.6	-0.2	-0.7	28.3	5390	3094	3076	60.74	0.256
4	50.6	-0.2	-1.0	28.8	5384	3114	3092	61.21	0.251

Observed Velocities and Moduli for File w16089-8669-velocity									
Event	Conf	Pore	Diff	Temp	V_p	$V_s^{(1)}$	$V_s^{(2)}$	Young's Modulus	Poisson's Ratio
	MPa	MPa	MPa	°C	m/s	m/s	m/s	GPa	
0	10.7	-0.2	1.0	24.6	4580	2730	2862	48.53	0.203
1	20.7	-0.2	0.4	25.1	4688	2820	2976	51.60	0.191
2	30.6	-0.2	-0.4	25.5	4879	2902	3021	54.68	0.208
3	40.7	-0.2	-0.8	27.6	5043	2974	3068	57.46	0.220
4	50.7	-0.2	-0.8	30.9	5086	3004	3099	58.56	0.219

Observed Velocities and Moduli for File w16089-8670.2-velocity									
Event	Conf	Pore	Diff	Temp	V_p	$V_s^{(1)}$	$V_s^{(2)}$	Young's Modulus	Poisson's Ratio
	MPa	MPa	MPa	°C	m/s	m/s	m/s	GPa	
0	10.5	-0.2	0.2	32.1	5572	3108	3162	65.82	0.268
1	10.6	-0.2	0.2	32.1	5518	3074	3180	65.23	0.263
2	10.5	-0.2	0.3	32.2	5412	3041	3127	63.25	0.260
3	10.6	-0.2	0.4	32.3	5311	3091	3127	63.25	0.239
4	10.6	-0.2	0.3	32.3	5412	3091	3253	65.79	0.238
5	10.6	-0.2	0.2	32.4	5361	3074	3180	64.13	0.242
6	20.7	-0.2	0.0	32.9	5572	3142	3234	67.44	0.257
7	30.6	-0.2	-0.8	31.2	5412	3232	3216	67.23	0.225
8	40.6	-0.2	-1.3	31.7	5572	3387	3234	71.01	0.227
9	50.6	-0.2	-2.1	32.1	5628	3347	3253	71.19	0.238

Observed Velocities and Moduli for File w16089-8672-vel									
Event	Conf	Pore	Diff	Temp	V_p	$V_s^{(1)}$	$V_s^{(2)}$	Young's Modulus	Poisson's Ratio
	MPa	MPa	MPa	°C	m/s	m/s	m/s	GPa	
0	10.7	-0.2	0.0	27.4	4929	3019	3066	56.95	0.192
1	20.6	-0.2	-0.8	27.8	4950	3062	3091	57.89	0.185
2	30.7	-0.2	-1.0	28.2	5122	3085	3131	60.24	0.209
3	40.7	-0.2	-1.4	28.9	5065	3099	3153	60.12	0.192
4	50.7	-0.2	-2.1	28.6	5128	3118	3166	61.10	0.199

Observed Velocities and Moduli for File w16089-8673.2-vel									
Event	Conf	Pore	Diff	Temp	V_p	$V_s^{(1)}$	$V_s^{(2)}$	Young's Modulus	Poisson's Ratio
	MPa	MPa	MPa	°C	m/s	m/s	m/s	GPa	
0	10.6	-0.2	0.0	27.9	4808	3004	2818	53.14	0.211
1	20.7	-0.2	-0.6	28.1	4970	3053	2963	56.76	0.211
2	30.6	-0.2	-1.3	28.3	5031	3085	3002	58.13	0.211
3	40.7	-0.2	-2.0	28.3	5105	3122	3029	59.54	0.215
4	50.7	-0.2	-2.3	28.3	5176	3144	3087	61.14	0.216

Observed Velocities and Moduli for File w16089-8674-vel									
Event	Conf	Pore	Diff	Temp	V_p	$V_s^{(1)}$	$V_s^{(2)}$	Young's Modulus	Poisson's Ratio
	MPa	MPa	MPa	°C	m/s	m/s	m/s	GPa	
0	10.7	-0.2	0.2	27.2	4825	3008	3010	55.00	0.182
1	20.7	-0.2	-0.4	27.6	4873	3052	3042	56.26	0.179
2	30.7	-0.2	-1.1	27.9	5071	3080	3071	58.78	0.209
3	40.7	-0.2	-1.3	28.0	5042	3110	3098	59.17	0.195
4	50.7	-0.2	-2.1	28.0	5089	3127	3111	59.96	0.199

Observed Velocities and Moduli for File w16089-8677.4-vel									
Event	Conf	Pore	Diff	Temp	V_p	$V_s^{(1)}$	$V_s^{(2)}$	Young's Modulus	Poisson's Ratio
	MPa	MPa	MPa	°C	m/s	m/s	m/s	GPa	
0	10.7	-0.2	0.3	27.9	4486	2893	2951	48.50	0.132
1	20.7	-0.2	-0.4	28.1	4645	2957	2991	51.18	0.153
2	30.7	-0.2	-0.8	28.4	4753	3002	3042	53.21	0.161
3	40.7	-0.2	-1.7	28.5	4890	3042	3070	55.30	0.180
4	50.7	-0.2	-2.1	28.5	5014	3077	3093	57.11	0.195

A.8.3 Biot's Coefficient

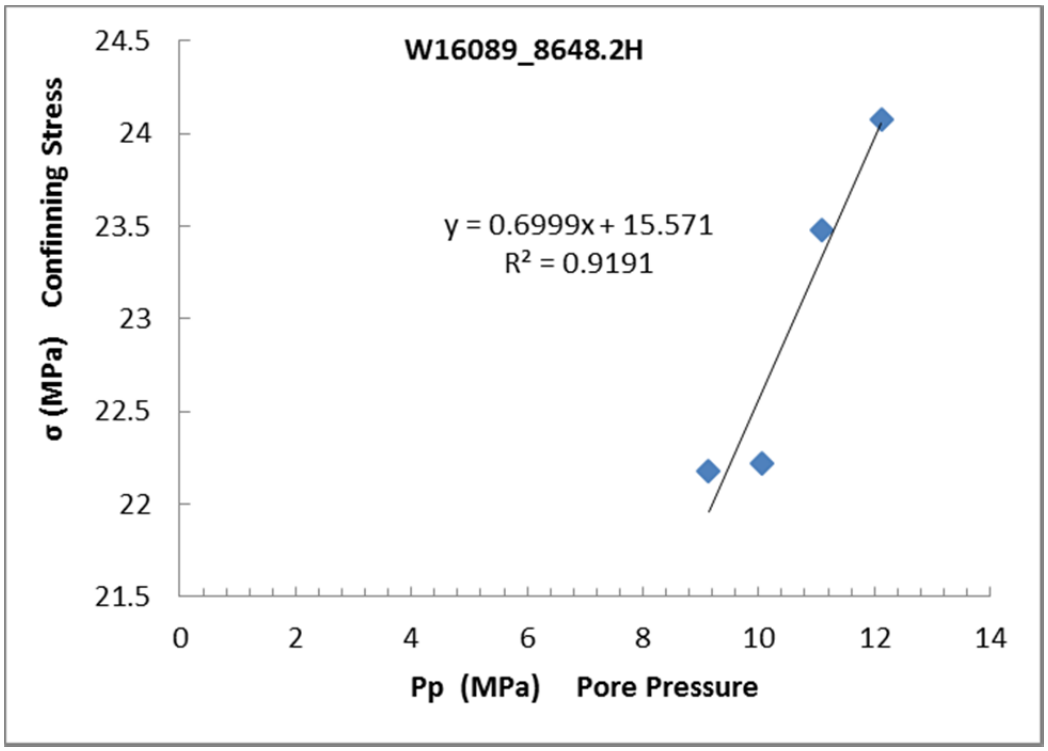

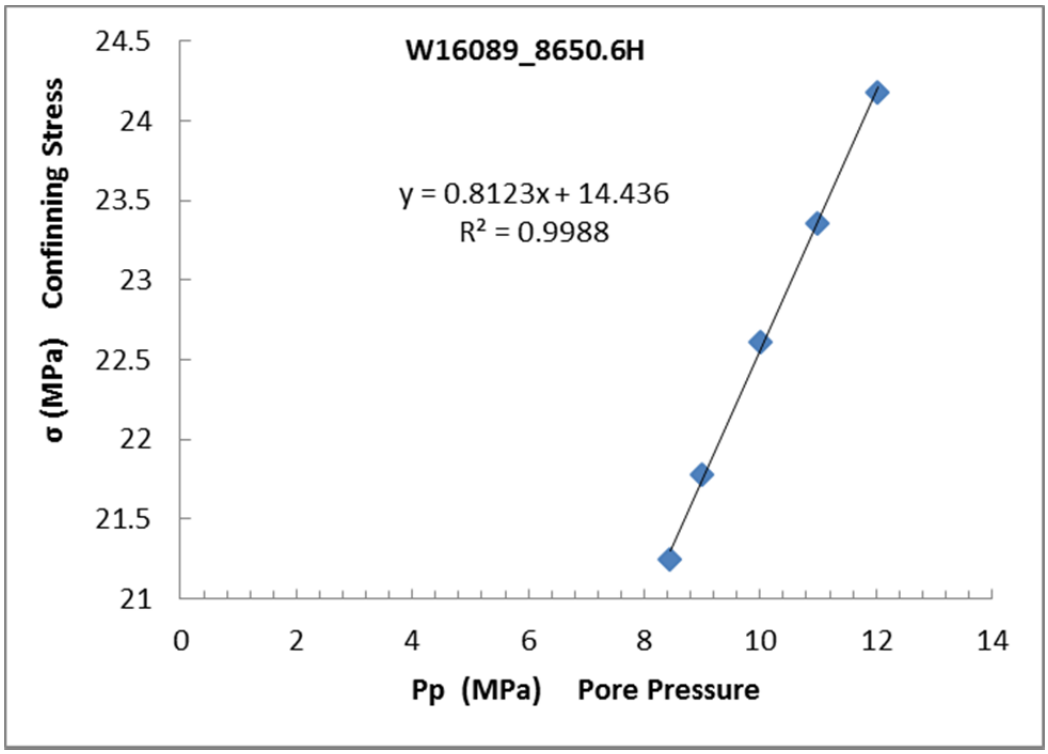

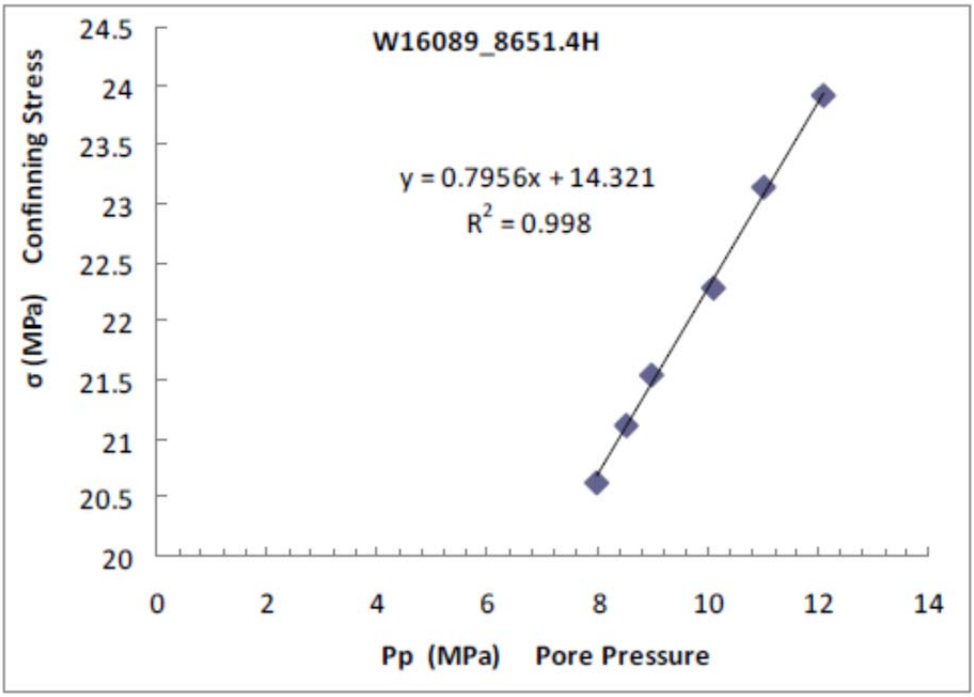
W16089_8651.4H
y = 0.7956x + 14.321
R2 = 0.998
σ (MPa) Confinning Stress
Pp (MPa) Pore Pressure
24.5
24
23.5
23
22.5
22
21.5
21
20.5
20
0
2
4
6
8
10
12
14

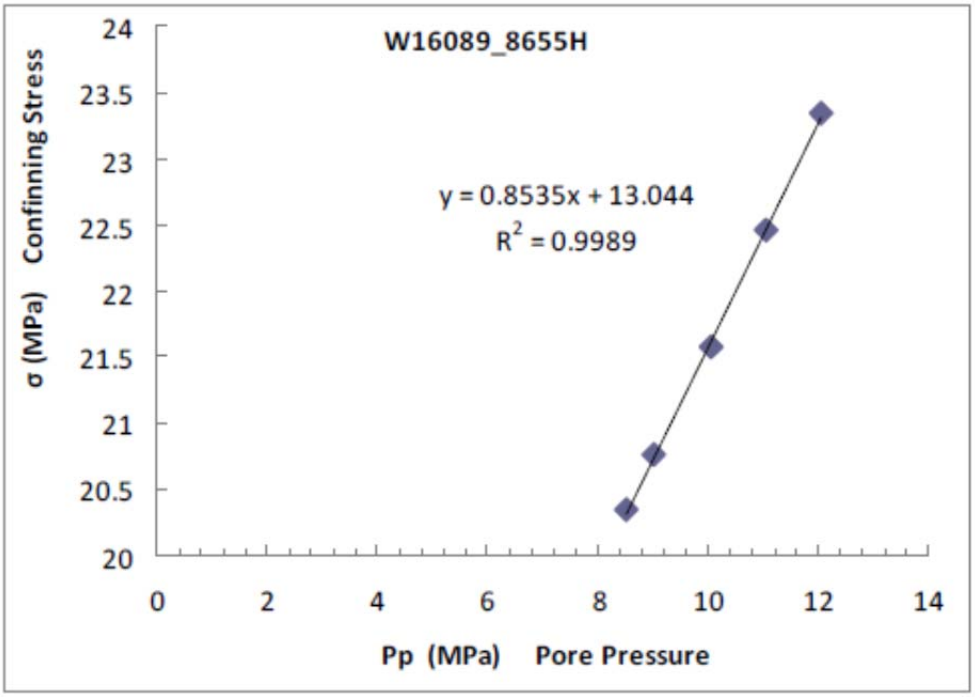
W16089_8655H
y = 0.8535x + 13.044
R2 = 0.9989
σ (MPa) Confinning Stress
Pp (MPa) Pore Pressure
24
23.5
23
22.5
22
21.5
21
20.5
20
0
2
4
6
8
10
12
14

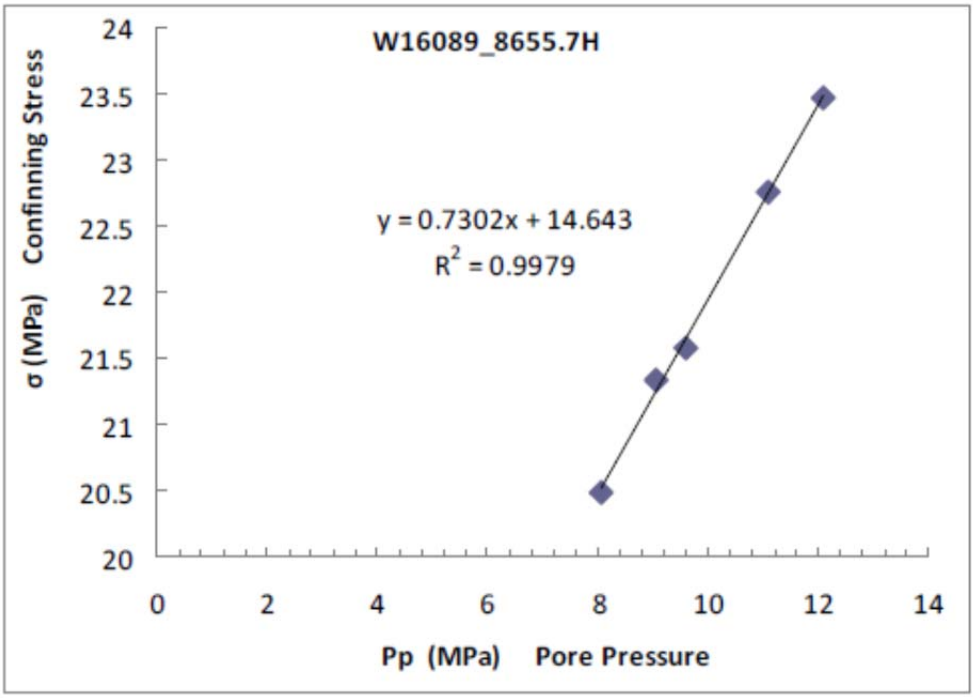
W16089_8655.7H
y = 0.7302x + 14.643
R2 = 0.9979
σ (MPa) Confinning Stress
Pp (MPa) Pore Pressure
24
23.5
23
22.5
22
21.5
21
20.5
20
0
2
4
6
8
10
12
14

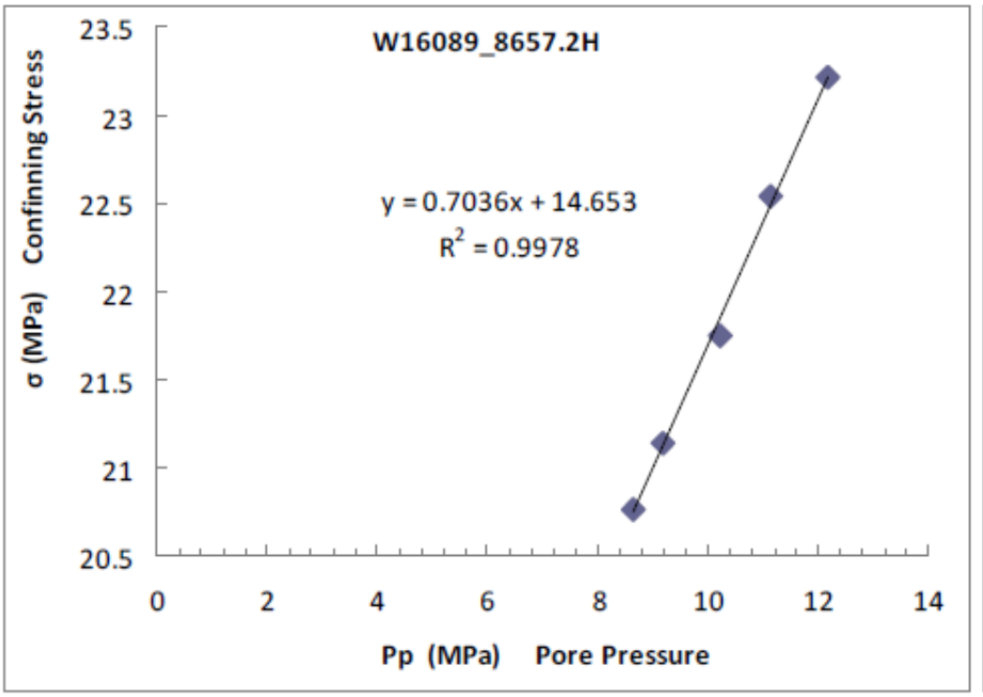
W16089_8657.2H
y = 0.7036x + 14.653
R2 = 0.9978
σ (MPa) Confinning Stress
Pp (MPa) Pore Pressure
23.5
23
22.5
22
21.5
21
20.5
0
2
4
6
8
10
12
14

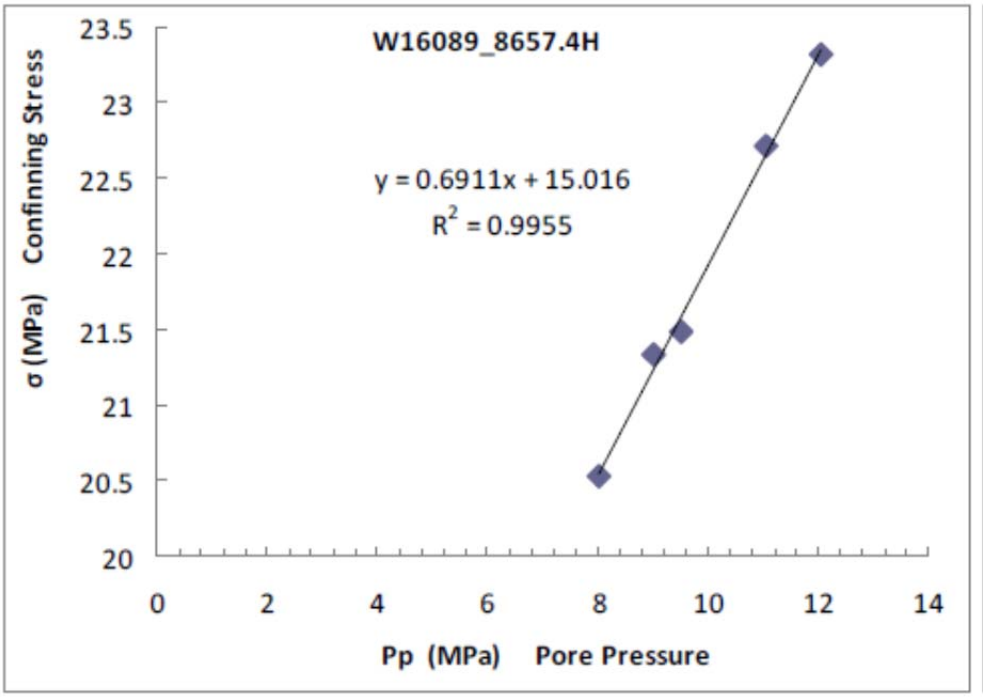
W16089_8657.4H
y = 0.6911x + 15.016
R2 = 0.9955
σ (MPa) Confinning Stress
Pp (MPa) Pore Pressure
23.5
23
22.5
22
21.5
21
20.5
20
0
2
4
6
8
10
12
14

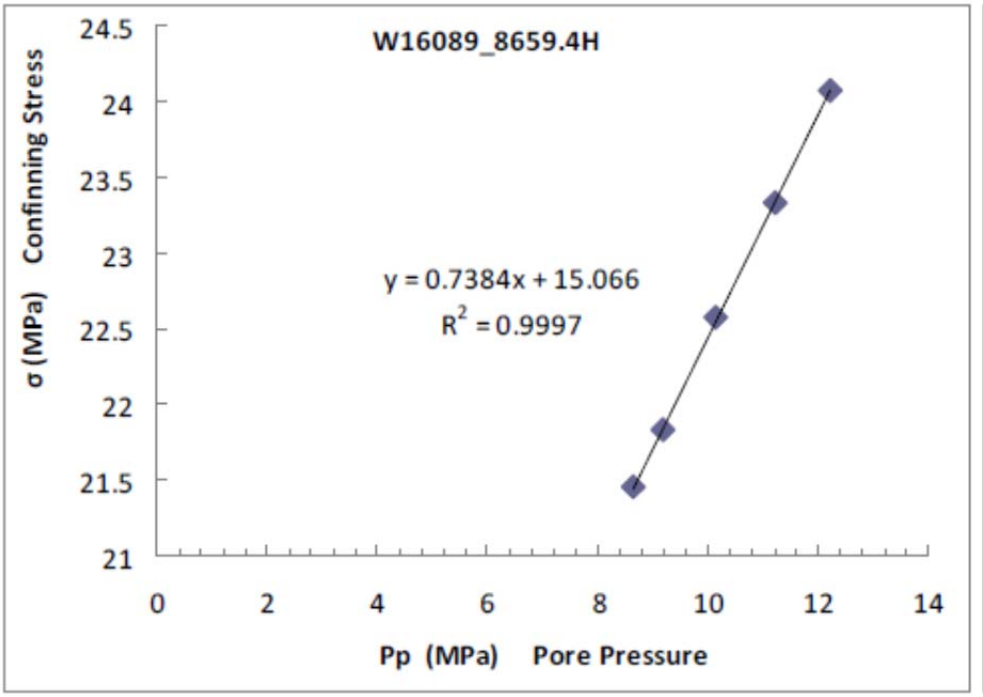
W16089_8659.4H
y = 0.7384x + 15.066
R2 = 0.9997
σ (MPa) Confinning Stress
Pp (MPa) Pore Pressure
24.5
24
23.5
23
22.5
22
21.5
21
0
2
4
6
8
10
12
14

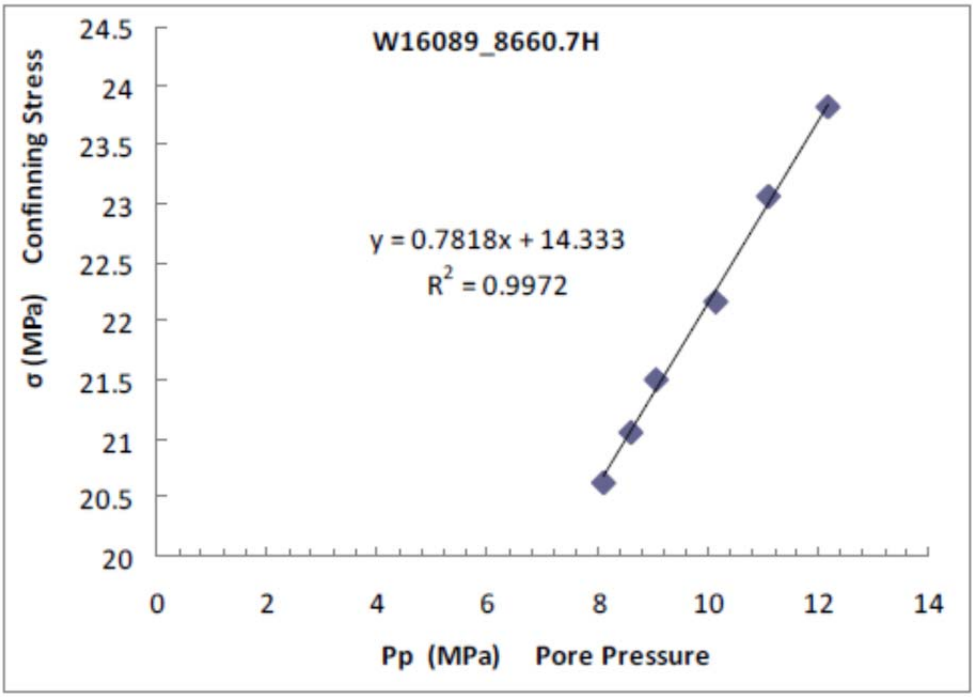
W16089_8660.7H
y = 0.7818x + 14.333
R2 = 0.9972
σ (MPa) Confinning Stress
Pp (MPa) Pore Pressure
24.5
24
23.5
23
22.5
22
21.5
21
20.5
20
0
2
4
6
8
10
12
14

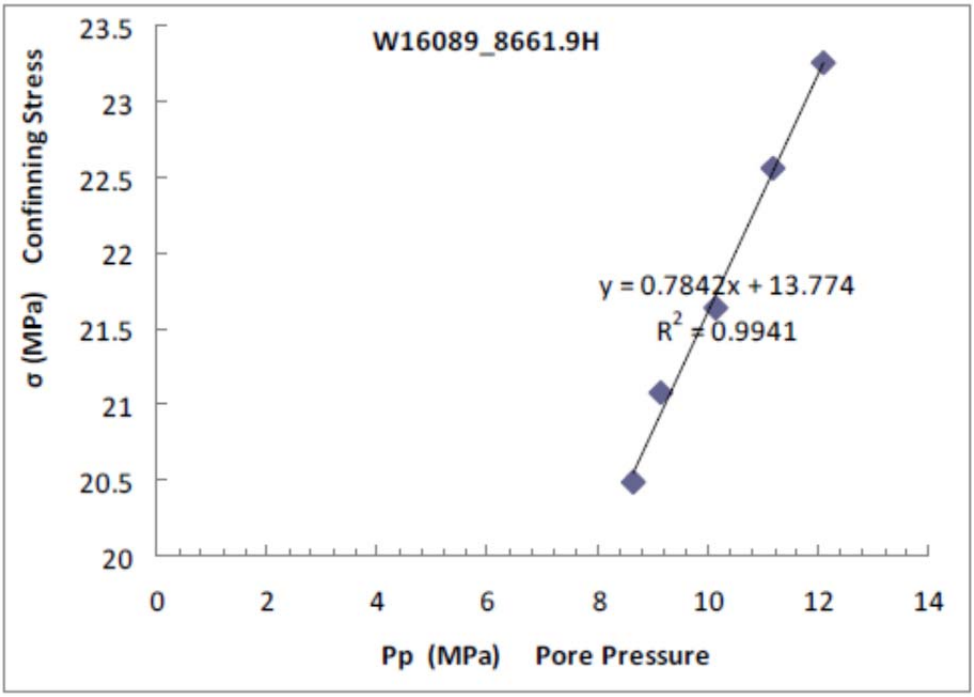
W16089_8661.9H
y = 0.7842x + 13.774
R2 = 0.9941
σ (MPa) Confinning Stress
Pp (MPa) Pore Pressure
23.5
23
22.5
22
21.5
21
20.5
20
0
2
4
6
8
10
12
14

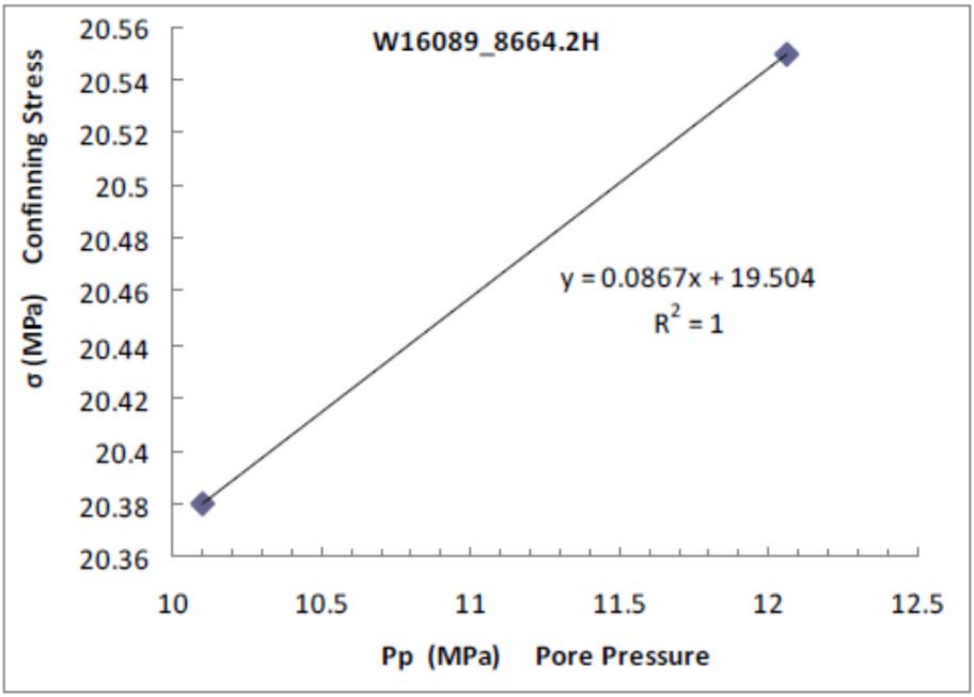
W16089_8664.2H
σ (MPa) Confinning Stress
Pp (MPa) Pore Pressure
y = 0.0867x + 19.504
R2 = 1
20.56
20.54
20.52
20.5
20.48
20.46
20.44
20.42
20.4
20.38
20.36
10
10.5
11
11.5
12
12.5

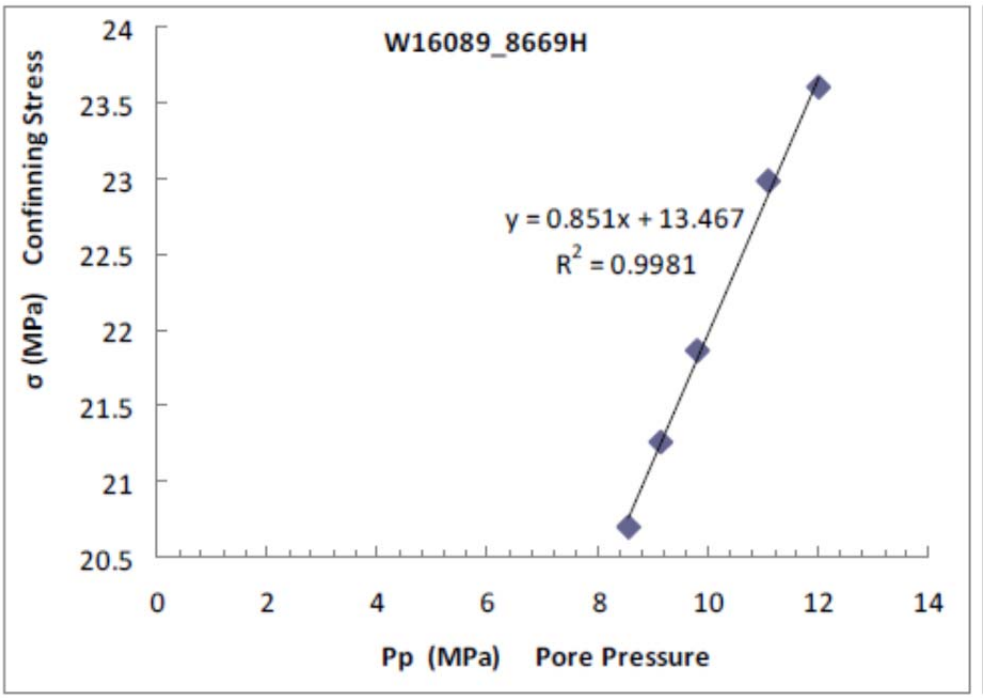
W16089_8669H
σ (MPa) Confinning Stress
Pp (MPa) Pore Pressure
y = 0.851x + 13.467
R2 = 0.9981
24
23.5
23
22.5
22
21.5
21
20.5
0
2
4
6
8
10
12
14

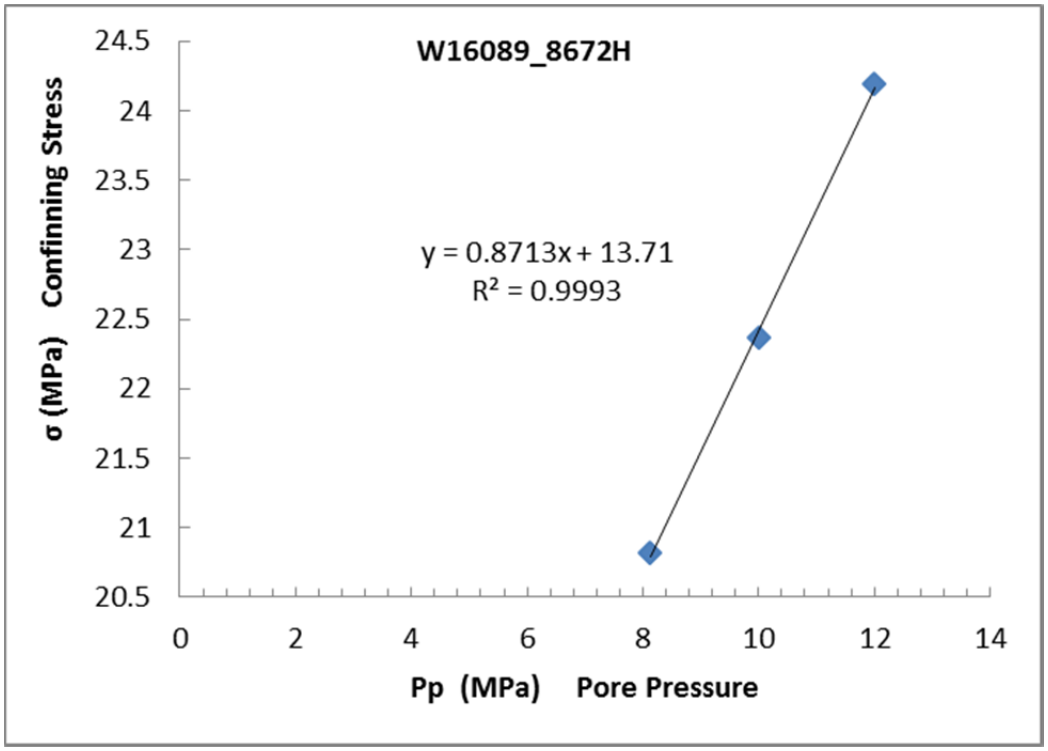
W16089_8672H
y = 0.8713x + 13.71
R² = 0.9993
σ (MPa) Confinning Stress
Pp (MPa) Pore Pressure
24.5
24
23.5
23
22.5
22
21.5
21
20.5
0
2
4
6
8
10
12
14

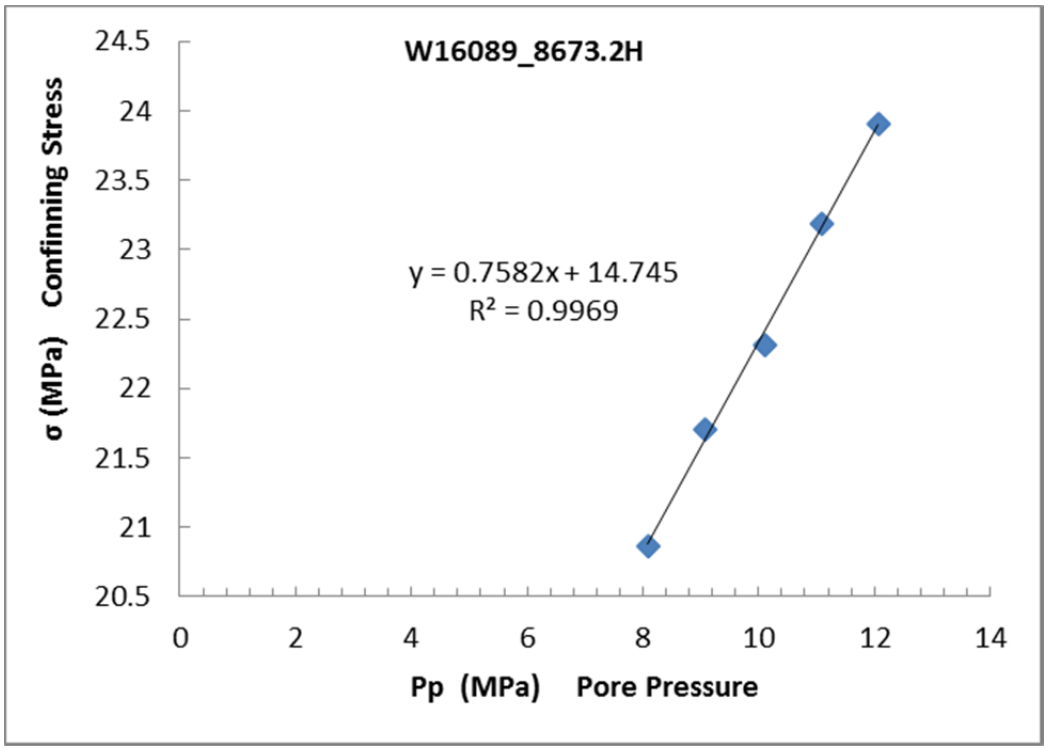
W16089_8673.2H
y = 0.7582x + 14.745
R² = 0.9969
σ (MPa) Confinning Stress
Pp (MPa) Pore Pressure
24.5
24
23.5
23
22.5
22
21.5
21
20.5
0
2
4
6
8
10
12
14

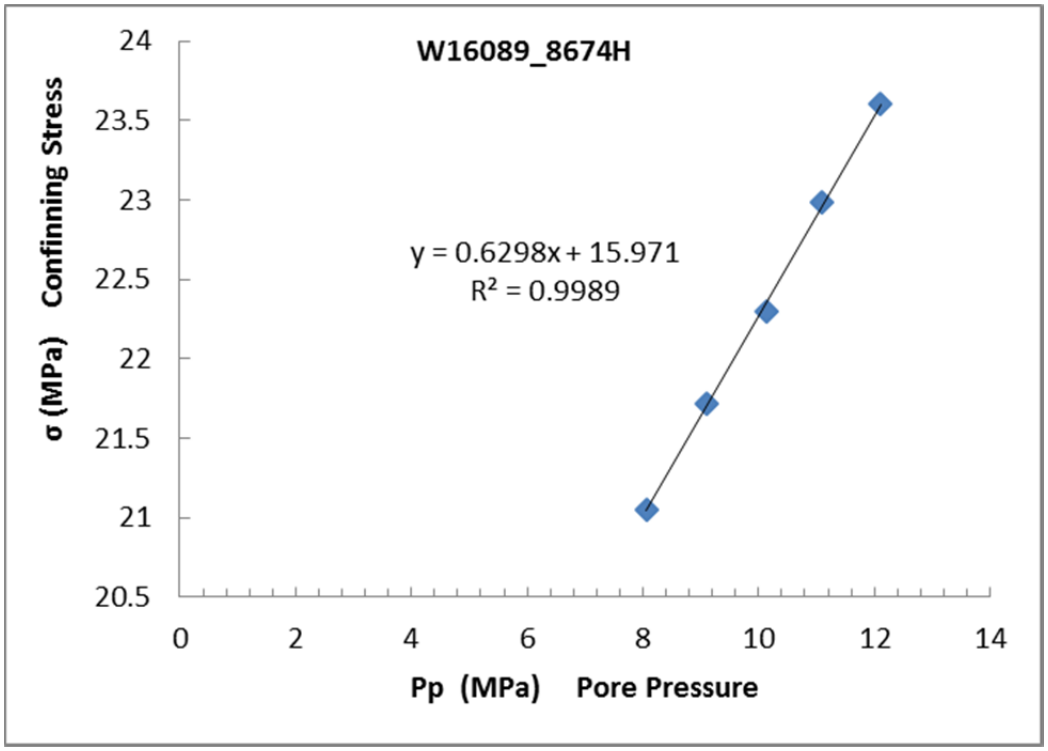

A.8.4 Static Moduli and Poisson's Ratio (Non-destructive)

Uniaxial Stress for File w16089-8648.2-uniaxil-stress									
Event	Conf	Pore	Diff	Temp	E	n	K	G	P
	MPa	MPa	MPa	°C	GPa		GPa	GPa	GPa
0	40.6	-0.2	20.5	29.7	53.44	0.306	45.99	20.45	73.26
1	50.6	-0.2	25.2	29.5	49.06	0.279	36.95	19.18	62.53
2	30.5	-0.2	20.5	27.2	51.96	0.331	51.34	19.51	77.35

Uniaxial Stress for File w16089-8650.6-uniaxial-stress									
Event	Conf	Pore	Diff	Temp	E	n	K	G	P
	MPa	MPa	MPa	°C	GPa		GPa	GPa	GPa
0	40.6	-0.2	19.3	28.4	68.77	0.252	46.26	27.46	82.87
1	50.7	-0.2	24.4	28.8	65.10	0.206	36.90	26.99	72.89
2	30.5	-0.2	19.7	26.5	68.44	0.270	49.64	26.94	85.56

Uniaxial Stress for File w16089-8651.4-uniaxial-stress									
Event	Conf	Pore	Diff	Temp	E	n	K	G	P
	MPa	MPa	MPa	°C	GPa		GPa	GPa	GPa
0	40.5	-0.2	19.3	30.2	59.74	0.185	31.58	25.21	65.20
1	50.5	-0.2	33.3	29.9	59.32	0.189	31.76	24.95	65.02
2	20.5	-0.2	20.1	26.4	53.26	0.169	26.80	22.78	57.18

Uniaxial Stress for File w16089-8655-uniaxial-stress									
Event	Conf	Pore	Diff	Temp	E	n	K	G	P
	MPa	MPa	MPa	°C	GPa		GPa	GPa	GPa
0	40.5	-0.2	24.4	32.1	53.59	0.191	28.95	22.49	58.94
1	30.6	-0.2	20.5	30.2	59.66	0.182	31.23	25.25	64.89

Uniaxial Stress for File w16089-8655.7-uniaxial-stress									
Event	Conf	Pore	Diff	Temp	E	n	K	G	P
	MPa	MPa	MPa	°C	GPa		GPa	GPa	GPa
0	40.7	-0.2	20.1	28.3	107.90	0.394	169.10	38.71	220.72
1	50.7	-0.2	24.8	29.0	103.00	0.356	119.27	37.98	169.91
2	30.6	-0.2	20.1	26.8	106.84	0.392	164.74	38.38	215.91

Uniaxial Stress for File w16089-8657.2-uniaxial-stress									
Event	Conf	Pore	Diff	Temp	E	n	K	G	P
	MPa	MPa	MPa	°C	GPa		GPa	GPa	GPa
0	40.6	-0.2	21.0	28.8	42.11	0.019	14.60	20.66	42.14
1	50.6	-0.2	25.2	28.6	36.71	0.029	12.98	17.85	36.77
2	30.5	-0.2	20.5	25.7	42.33	0.020	14.71	20.74	42.37

Uniaxial Stress for File w16089-8657.4-uniaxial-stress									
Event	Conf	Pore	Diff	Temp	E	n	K	G	P
	MPa	MPa	MPa	°C	GPa		GPa	GPa	GPa
0	40.6	-0.2	19.7	27.6	82.22	0.147	38.84	35.83	86.62
1	50.7	-0.2	24.8	28.1	70.64	0.082	28.15	32.65	71.68
2	30.6	-0.2	20.1	26.1	78.83	0.159	38.51	34.01	83.87

Uniaxial Stress for File w16089-8659.4-uniaxial-stress									
Event	Conf	Pore	Diff	Temp	E	n	K	G	P
	MPa	MPa	MPa	°C	GPa		GPa	GPa	GPa
0	40.6	-0.2	20.5	25.3	128.19	0.091	52.17	58.77	130.54
1	50.6	-0.2	25.2	25.9	129.98	0.069	50.22	60.82	131.31
2	30.5	-0.2	20.5	23.9	124.50	0.109	53.07	56.13	127.91

Uniaxial Stress for File w16089-8660.7-uniaxial-stress									
Event	Conf	Pore	Diff	Temp	E	n	K	G	P
	MPa	MPa	MPa	°C	GPa		GPa	GPa	GPa
0	40.7	-0.2	20.5	22.8	42.02	0.308	36.53	16.06	57.94
1	50.6	-0.2	24.8	23.1	40.24	0.232	25.01	16.34	46.79
2	30.6	-0.2	20.5	21.2	40.93	0.326	39.22	15.43	59.80

Uniaxial Stress for File w16089-8661.9-uniaxial-stress									
Event	Conf	Pore	Diff	Temp	E	n	K	G	P
	MPa	MPa	MPa	°C	GPa		GPa	GPa	GPa
0	40.7	-0.2	20.5	26.8	65.91	0.086	26.54	30.34	67.00
1	50.7	-0.2	25.2	28.4	62.49	0.065	23.93	29.34	63.06
2	30.6	-0.2	20.5	23.7	65.75	0.104	27.69	29.77	67.38

Uniaxial Stress for File w16089-8664.2-unixial-stress									
Event	Conf	Pore	Diff	Temp	E	n	K	G	P
	MPa	MPa	MPa	°C	GPa		GPa	GPa	GPa
0	40.5	-0.2	20.1	31.3	63.57	0.241	40.90	25.61	75.05
1	50.6	-0.2	24.8	31.5	60.36	0.240	38.68	24.34	71.14
2	30.5	-0.2	20.5	24.0	66.36	0.233	41.41	26.91	77.29

Uniaxial Stress for File w16089-8668-uniaxial-stress									
Event	Conf	Pore	Diff	Temp	E	n	K	G	P
	MPa	MPa	MPa	°C	GPa		GPa	GPa	GPa
0	40.7	-0.2	20.1	27.4	70.64	0.172	35.94	30.13	76.11
1	50.7	-0.2	24.8	32.0	57.48	0.182	30.14	24.31	62.55
2	30.6	-0.2	20.1	25.5	70.94	0.179	36.78	30.10	76.91

Uniaxial Stress for File w16089-8669-uniaxial-stress									
Event	Conf	Pore	Diff	Temp	E	n	K	G	P
	MPa	MPa	MPa	°C	GPa		GPa	GPa	GPa
0	40.6	-0.2	19.7	33.3	57.58	0.168	28.90	24.65	61.76
1	50.6	-0.2	24.8	35.2	57.00	0.156	27.61	24.66	60.48
2	30.5	-0.2	20.1	32.4	52.24	0.167	26.12	22.39	55.97

Uniaxial Stress for File w16089-8670.2-uniaxial-stress									
Event	Conf	Pore	Diff	Temp	E	n	K	G	P
	MPa	MPa	MPa	°C	GPa		GPa	GPa	GPa
0	40.7	-0.2	21.8	31.7	77.26	0.129	34.68	34.22	80.32
1	50.7	-0.2	25.7	32.0	70.96	0.123	31.40	31.59	73.51
2	30.7	-0.2	21.8	31.3	64.42	0.140	29.86	28.24	67.51

Uniaxial Stress for File w16089-8672-uniaxial-stress									
Event	Conf	Pore	Diff	Temp	E	n	K	G	P
	MPa	MPa	MPa	°C	GPa		GPa	GPa	GPa
0	40.7	0.4	21.4	28.6	31.66	0.469	168.07	10.78	182.44
1	50.7	0.4	26.1	29.8	32.80	0.446	100.57	11.34	115.69
2	30.7	0.4	19.7	24.8	42.02	0.404	72.76	14.97	92.71

Uniaxial Stress for File w16089-8673.2-uniaxial-stress									
Event	Conf	Pore	Diff	Temp	E	n	K	G	P
	MPa	MPa	MPa	°C	GPa		GPa	GPa	GPa
0	40.6	-0.2	20.5	26.6	81.13	0.305	69.17	31.10	110.63
1	50.7	-0.2	40.2	28.3	76.00	0.243	49.27	30.57	90.03
2	30.6	-0.2	21.0	26.5	84.93	0.330	83.47	31.92	126.03

Uniaxial Stress for File w16089-8674-uniaxial-stress									
Event	Conf	Pore	Diff	Temp	E	n	K	G	P
	MPa	MPa	MPa	°C	GPa		GPa	GPa	GPa
0	40.7	-0.2	21.0	28.5	47.83	0.238	30.39	19.32	56.16
1	50.7	-0.2	29.9	27.7	53.93	0.220	32.08	22.11	61.56
2	30.7	-0.2	21.4	24.5	65.64	0.306	56.33	25.13	89.84

Uniaxial Stress for File w16089-8677.4-uniaxial-stress									
Event	Conf	Pore	Diff	Temp	E	n	K	G	P
	MPa	MPa	MPa	°C	GPa		GPa	GPa	GPa
0	40.7	-0.2	40.6	24.8	106.89	0.004	35.94	53.22	106.89

A.8.5 Uni/Triaxial Compressive Strength, Young's Modulus and Poisson's Ratio

Strength for File w16089-8648.2-strength						
Event	Conf	Diff	Temp	E	n	peak_stress
	MPa	MPa	°C	GPa		MPa
0	15.3	-2.9	22.4	21.25	0.472	92.7

Strength for File w16089-8650.6-strength						
Event	Conf	Diff	Temp	E	n	peak_stress
	MPa	MPa	°C	GPa		MPa
0	8.0	39.3	19.8	34.16	0.313	169.1

Strength for File w16089-8651.4-strength						
Event	Conf	Diff	Temp	E	n	peak_stress
	MPa	MPa	°C	GPa		MPa
0	0.5	20.5	21.7	36.71	0.346	130.7

Strength for File w16089-8655-strength						
Event	Conf	Diff	Temp	E	n	peak_stress
	MPa	MPa	°C	GPa		MPa
0	15.3	4.3	26.3	44.33	0.295	171.2

Strength for File w16089-8655.7-strength						
Event	Conf	Diff	Temp	E	n	peak_stress
	MPa	MPa	°C	GPa		MPa
0	8.1	68.8	36.9	60.15	0.477	175.9

Strength for File w16089-8657.2-strength						
Event	Conf	Diff	Temp	E	n	peak_stress
	MPa	MPa	°C	GPa		MPa
0	0.7	21.0	37.2	44.37	0.038	102.9

Strength for File w16089-8657.4-strength						
Event	Conf	Diff	Temp	E	n	peak_stress
	MPa	MPa	°C	GPa		MPa
0	15.2	15.4	29.5	42.14	0.260	192.6

Strength for File w16089-8659.4-strength						
Event	Conf	Diff	Temp	E	n	peak_stress
	MPa	MPa	°C	GPa		MPa
0	8.4	18.8	36.1	143.69	0.402	147.3

Strength for File w16089-8660.7-strength						
Event	Conf	Diff	Temp	E	n	peak_stress
	MPa	MPa	°C	GPa		MPa
0	0.4	21.8	32.4	32.34	0.516	64.9

Strength for File w16089-8661.9-strength						
Event	Conf	Diff	Temp	E	n	peak_stress
	MPa	MPa	°C	GPa		MPa
0	0.5	-2.5	23.6	55.03	0.188	92.7
1	15.5	26.9	28.5	77.19	0.776	82.4

Strength for File w16089-8664.2-strength						
Event	Conf	Diff	Temp	E	n	peak_stress
	MPa	MPa	°C	GPa		MPa
0	17.7	12.9	39.1	52.91	0.670	92.7

Strength for File w16089-8669-strength						
Event	Conf	Diff	Temp	E	n	peak_stress
	MPa	MPa	°C	GPa		MPa
0	0.8	13.3	38.7	42.14	0.096	124.7

A.8.6 Mohr's Circle

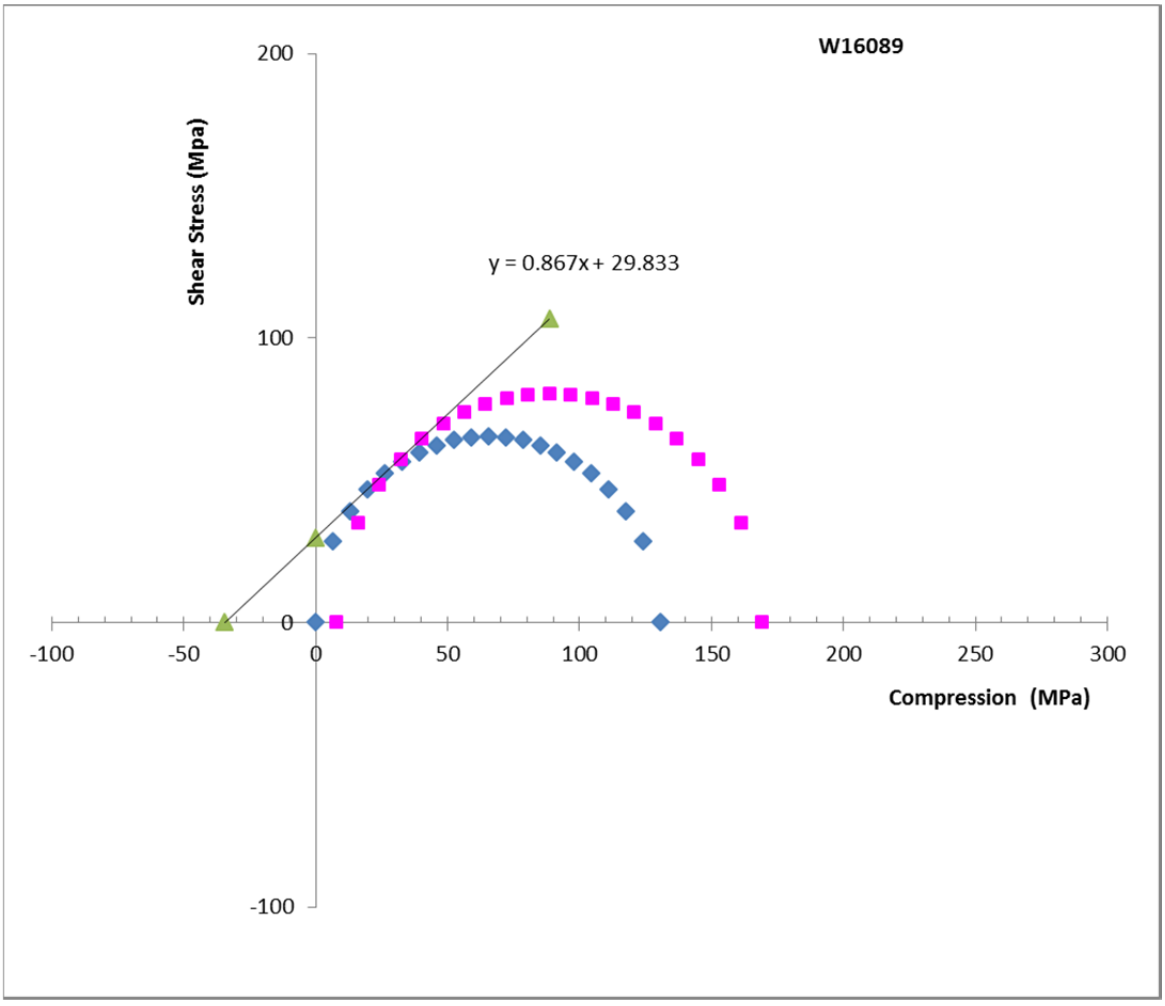

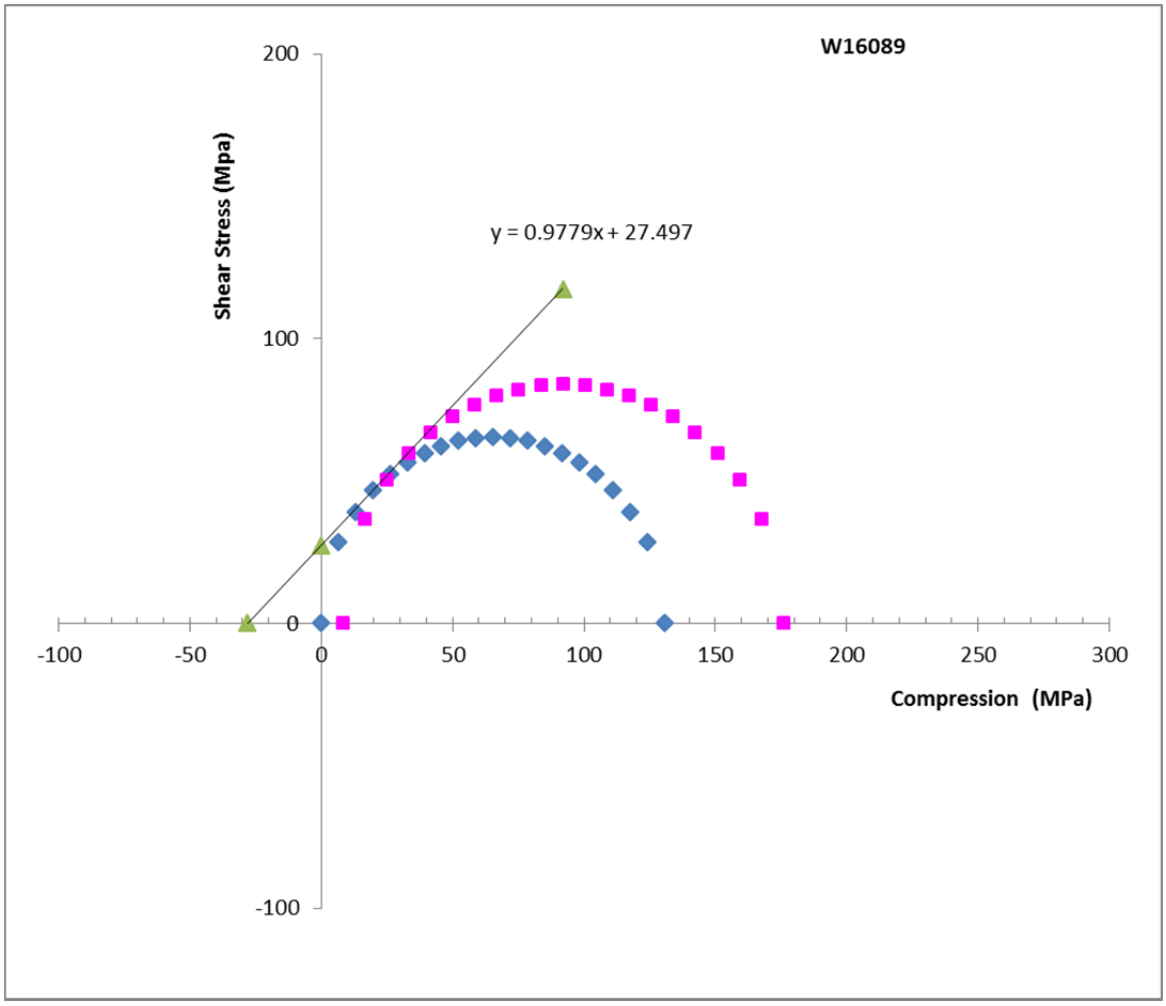
W16089
Shear Stress (Mpa)
y = 0.9779x + 27.497
200
100
0
-100
-100
-50
0
50
100
150
200
250
300
Compression (MPa)

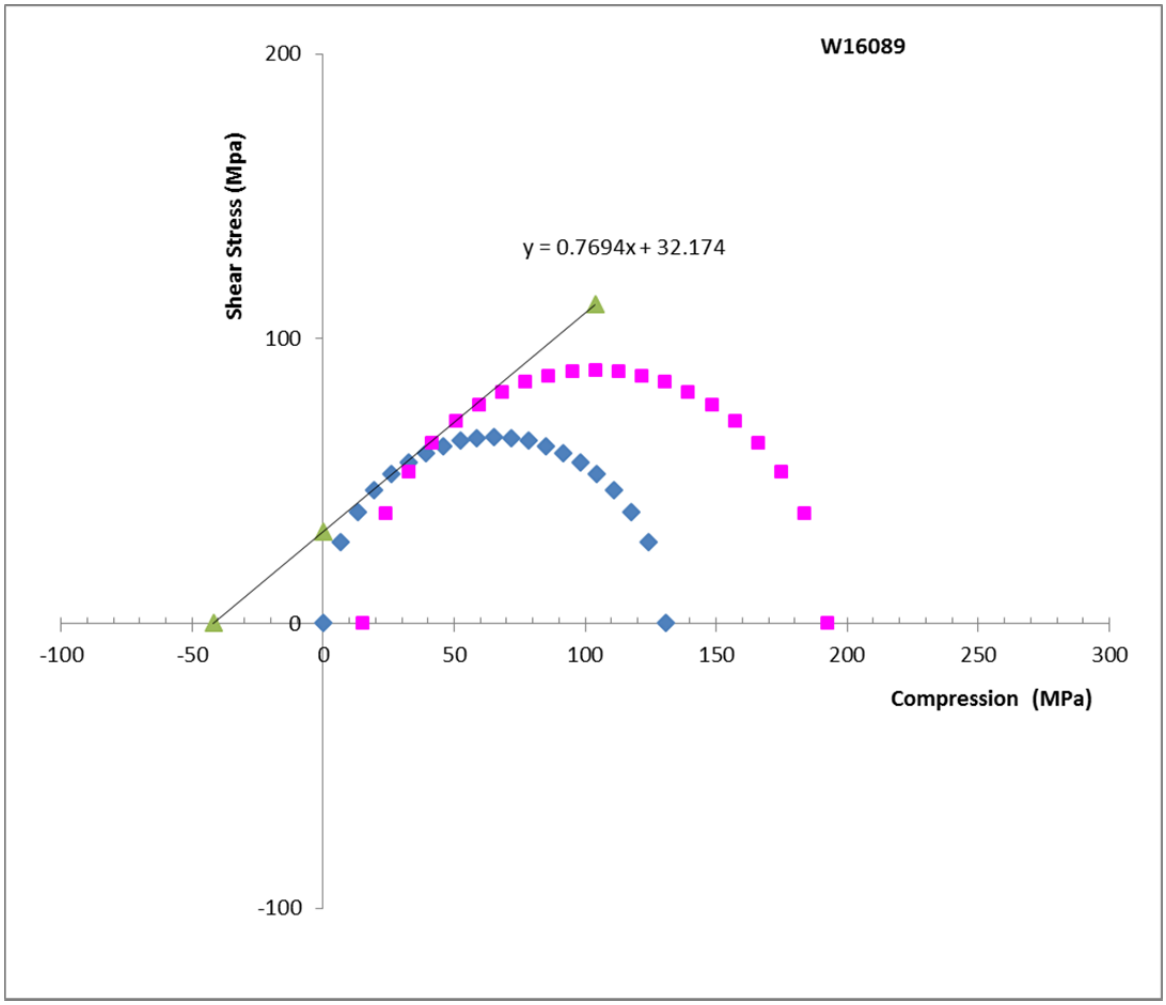
W16089
Shear Stress (Mpa)
y = 0.7694x + 32.174
200
100
0
-100
-100
-50
0
50
100
150
200
250
300
Compression (MPa)

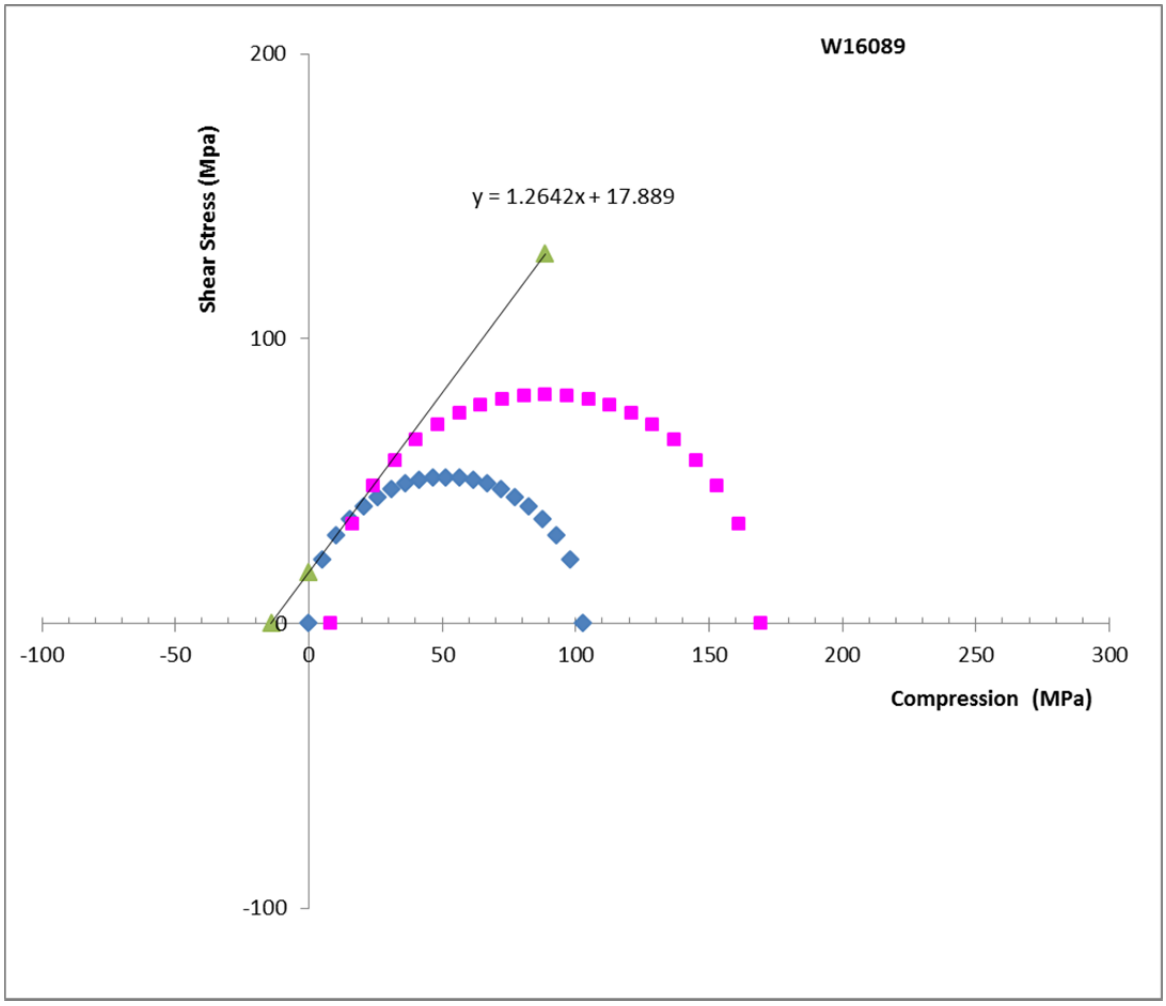
W16089
y = 1.2642x + 17.889
Shear Stress (Mpa)
Compression (MPa)
200
100
0
-100
-100
-50
0
50
100
150
200
250
300

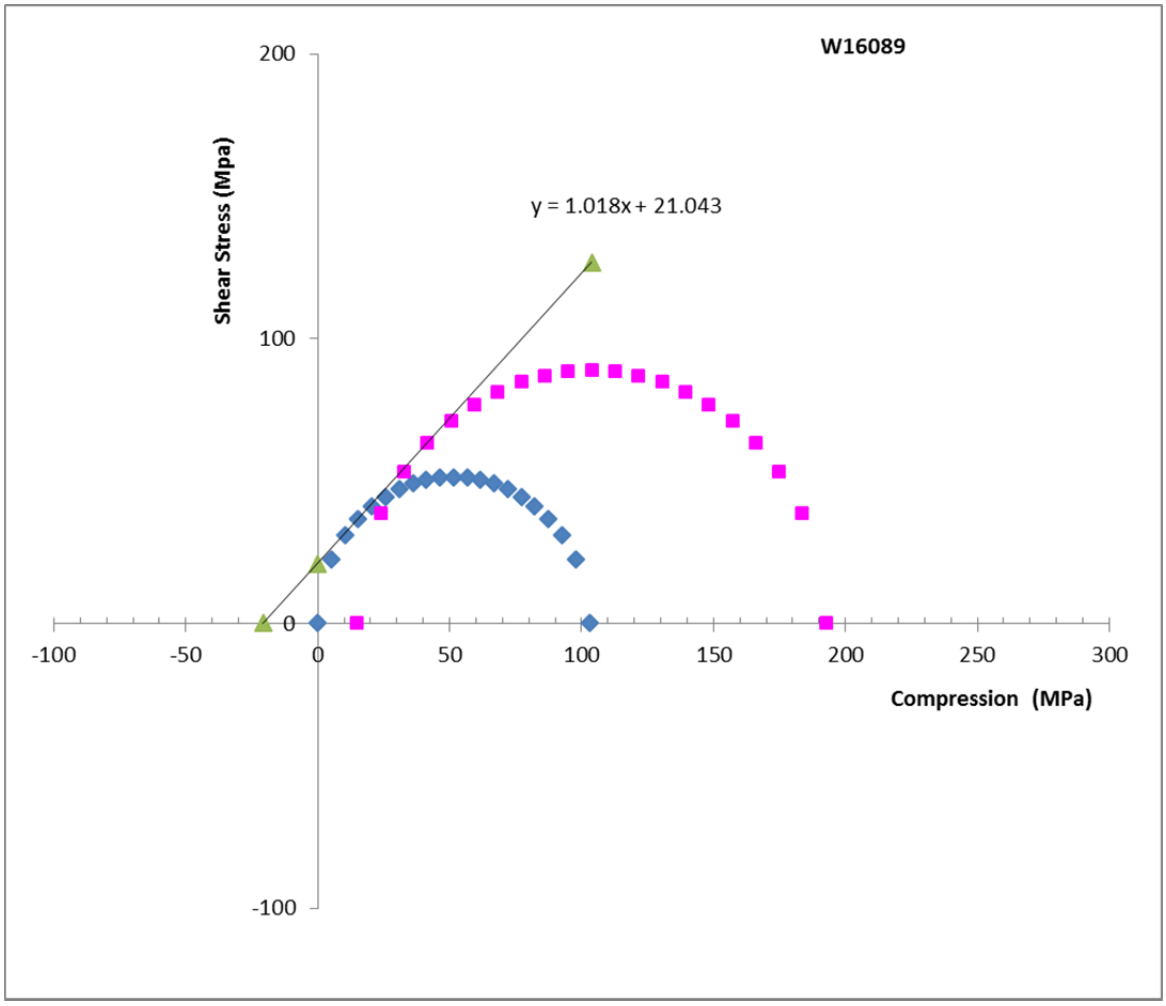
W16089
y = 1.018x + 21.043
Shear Stress (Mpa)
Compression (MPa)
200
100
0
-100
-100
-50
0
50
100
150
200
250
300

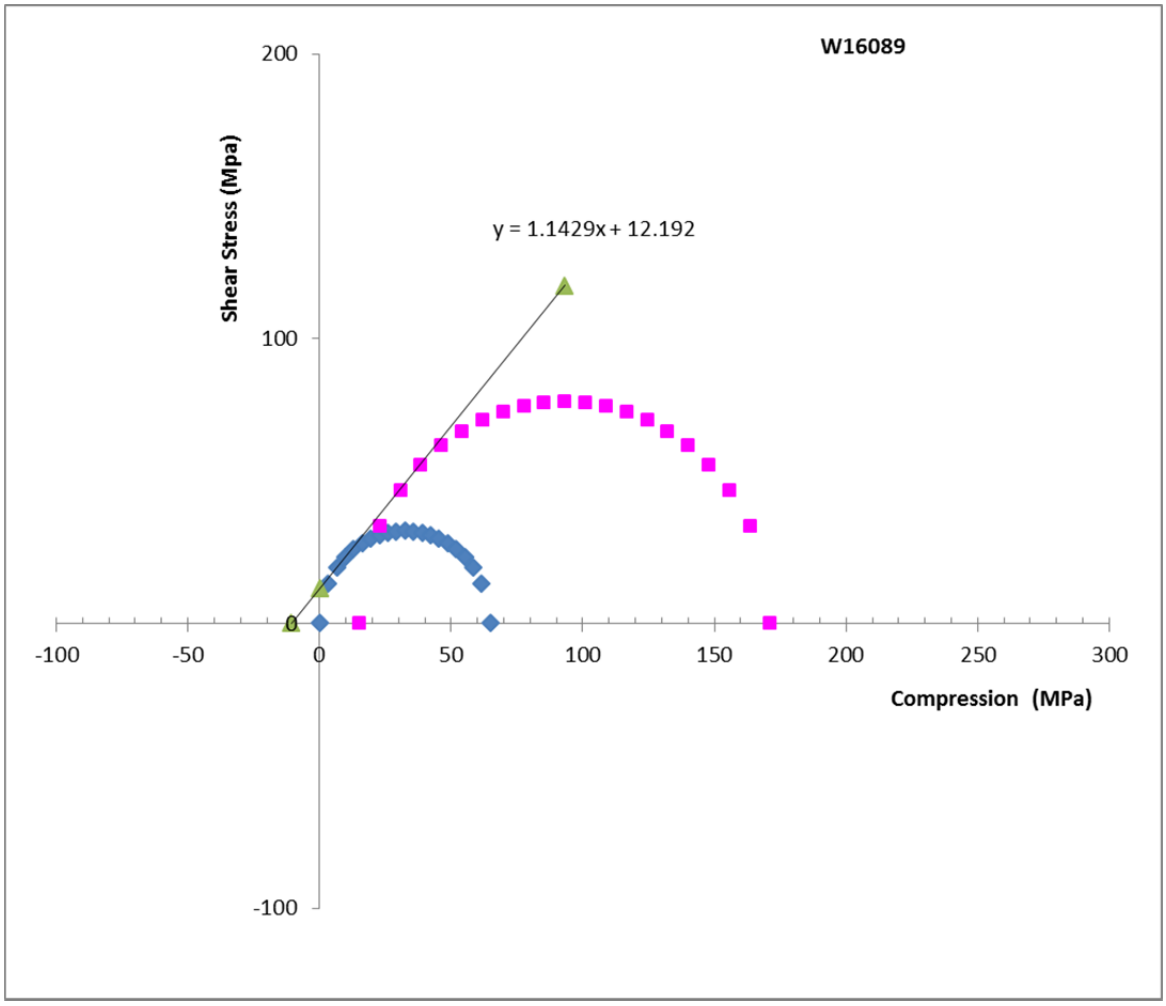
W16089
Shear Stress (Mpa)
y = 1.1429x + 12.192
200
100
0
-100
-100
-50
0
50
100
150
200
250
300
Compression (MPa)

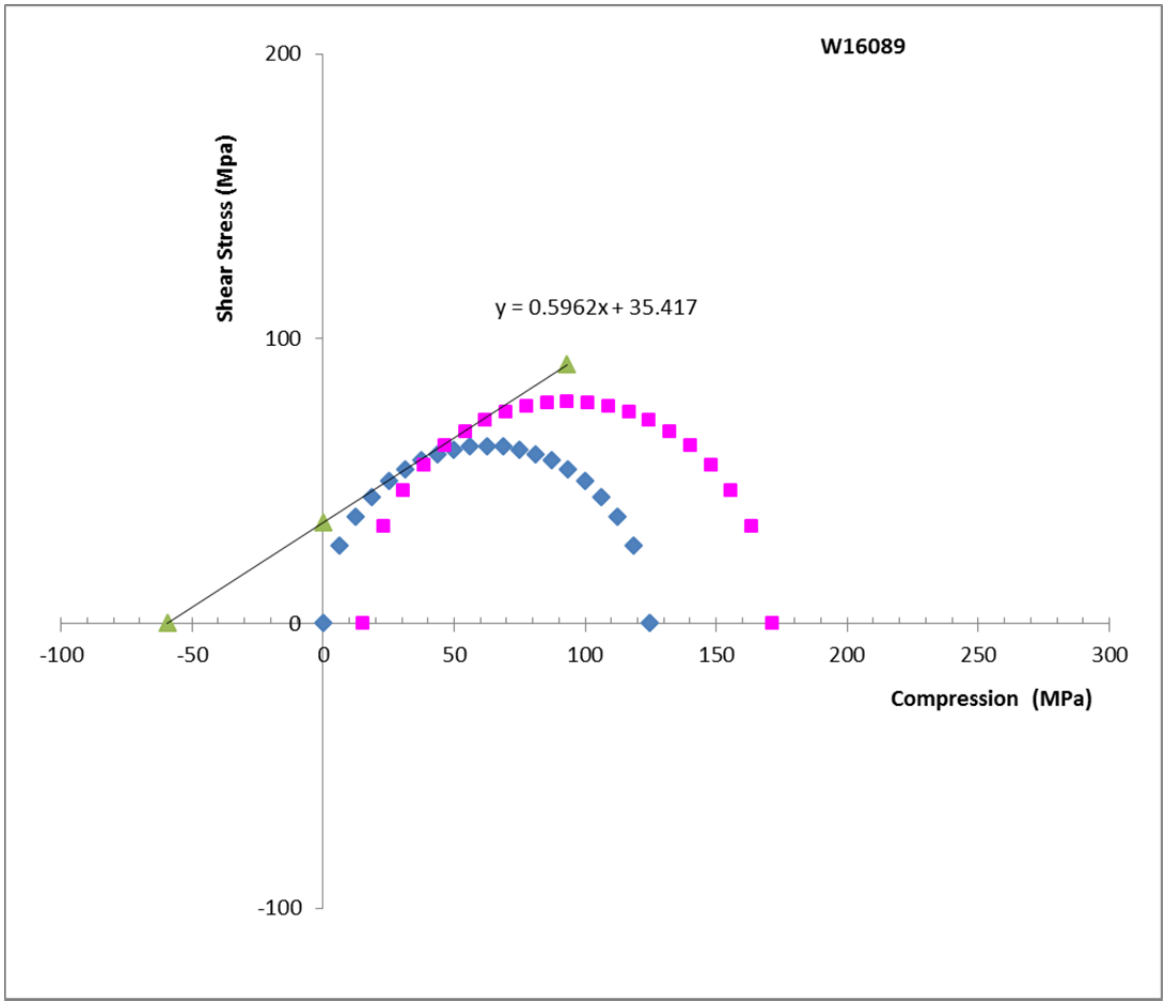
W16089
Shear Stress (Mpa)
y = 0.5962x + 35.417
200
100
0
-100
-100
-50
0
50
100
150
200
250
300
Compression (MPa)